Proceedings of the 7th Graz Brain-Computer Interface Conference 2017

From Vision to Reality

September 18-22, 2017
Graz University of Technology, Austria

Officially endorsed by the BCI Society

Edited by
Gernot R. Müller-Putz, David Steyrl, Selina C. Wriessnegger, Reinhold Scherer

Verlag der Technischen Universität Graz 2017

 DOI: 10.3217/978-3-85125-533-1-00

Verlag der Technischen Universität Graz

http://ub.tugraz.at/Verlag

ISSN 2311-0422

ISBN 978-3-85125-533-1

DOI 10.3217/978-3-85125-533-1

Published by Verlag der TU Graz
Graz University of Technology

 DOI: 10.3217/978-3-85125-533-1-00

Welcome Note

From Vision to Reality

We have chosen our this year's conference title to summarize the current situation of BCI research in a very brief statement. On the one hand, we see that some of our ideas are still visions, far from any applications. Basic research is the state of those visions and we still need to lay the foundation to transform those visions into working systems. On the other hand, we see that first BCI systems come to patients in clinics and that they are used on regular basis. However, it is important to discuss the needs in the BCI field to bring more of our ideas, our visions into reality. Is it research funding? Do we have too few people in the field? Is it too interdisciplinary? Do we need big industry partners? All these questions are vivid and need to be addressed to achieve progress in the field of BCI research. This 7th Graz Brain-Computer Interface Conference (GBCIC2017) offers the opportunity for extensive discussions and exchange of ideas among BCI experts from more than 30 countries. We received more than 100 scientific contributions from roughly 300 authors. The scientific contributions have been peer-reviewed by at least two reviewers and collected in this present open access ebook.

For the Conference itself, we have been able to setup a colorful and multifaceted program. We are very happy that the GBCIC2017 has been officially endorsed by the BCI Society and that we will have an official Meeting of the BCI Society at the Conference. Further, we are lucky that outstanding experts in the field, Dr. A Bolu Ajiboye (Case Western Reserve University, & Louis Stokes Cleveland VA Medical Center, Cleveland, OH, USA), Prof. Benjamin Blankertz (Technische Universität Berlin, Germany), Dr. Fabien Lotte (Inria Bordeaux Sud-Ouest, France), and Dr. Natalie Mrachacz-Kersting (Aalborg University, Denmark), accepted our invitation to present keynote addresses at the Conference. As a special keynote, we present Prof. Fred D. Davis (Texas Tech University, Rawls College of Business, USA). He is a senior researcher in the field of user acceptance of information technology, technology supported decision making, skill acquisition, and NeuroIS. With his talk he will make a link between the BCI field and his research disciplines. Additionally, we have several Satellite Events prior and after the Conference. New in the program: the BCI Science Slam, an event where researchers can present their work in an entertaining way. Finally, we end the GBCIC2017 with a tour to the South Styrian Vineyards, like we did in the past years.

We hope that this conference contributes towards a strong scientific cooperation among our field, and we wish all participants an exciting, stimulating and productive Graz BCI Conference 2017!

Gernot R. Müller-Putz
Conference Chair

Published by Verlag der TU Graz
Graz University of Technology

 DOI: 10.3217/978-3-85125-533-1-00

Editorial Board

Prof. Dr. **Gernot R. Müller-Putz** is head of the Institute of Neural Engineering and its associated Laboratory of Brain-Computer Interfaces. He received his MSc in electrical and biomedical engineering in 2000, his PhD in electrical engineering in 2004 and his habilitation and “venia docendi” in medical informatics from Graz University of Technoloy in 2008. Since 2014 he is full professor for semantic data analysis. He has gained extensive experience in the field of biosignal analysis, brain-computer interface research, EEG-based neuroprosthesis control, communication with BCI in patients with disorders of consciousness, hybrid BCI systems, the human somatosensory system, and BCIs in assistive technology over the past 16 years. He has also managed several national projects (State of Styria) and international projects (Wings for Life, EU Projects) and is currently coordinator of the EU Horizon 2020 project “MoreGrasp”. Furthermore, he organized and hosted six international Brain-Computer Interface Conferences over the last 13 years in Graz. He is review editor of Frontiers in Neuroscience, special section neuroprosthetics, associate editor of IEEE Transactions in Biomedical Engineering and associate editor of the Brain-Computer Interface Journal. In 2014/15 he was guest editor in chief of a special issue of the Proceedings if the IEEE “The Plurality of Human Brain-Computer Interfacing”. He has authored more than 135 peer reviewed publications and more than 100 contributions to conferences which were cited more than 10000 times (h-index 47). Recently he was awarded with an ERC Consolidator Grant “Feel your Reach” from the European Research Council. In May 2017 he received the Ludwig-Guttman Award from the German Medical Spinal Cord Injury Association (DMGP).

David Steyrl is teaching and research assistant at the Institute of Neural Engineering (BCI-Lab), Graz University of Technology, Austria. He received his M.Sc. in electrical engineering with focus on biomedical engineering from Graz University of Technology in 2012. He (co-) authored more than 20 peer-reviewed journal and conference articles. Among others, he is reviewer for Journal of Neural Engineering, IEEE-TBME, IEEE-THMS, and Neuroimage. David Steyrl co-organized two major BCI conferences in Graz and he is founding member of the Graz BCI Racing Team MIRAGE91. His research interests include biosignal processing and machine learning for simultaneous EEG-fMRI and brain-computer interfaces. Currently he is working towards his PhD degree in computer science.

Selina Christin Wriessnegger is assistant professor at the Institute of Neural Engineering (BCI-Lab), Graz University of Technology, Austria. From 2001 to 2005 she was PhD student at the Max-Planck-Institute for Human Cognitive and Brain Sciences and received her PhD from the Ludwig-Maximilians University. During that time, she spent one year in Rome as research assistant at IRCCS (Fondazione Santa Lucia), Laboratory for Human Psychophysiology. From 2005 to 2008 she was university assistant at the Karl-Franzens-University Graz, section neuropsychology. From 2009 until May 2016 she was senior researcher at the Institute of Neural Engineering (BCI-Lab). In 2017 she was visiting professor at SISSA (Scuola Internazionale Superiore di Studi Avanzati), Trieste. Her research interests are subliminal visual information processing, neural correlates of motor imagery, novel applications of BCIs for healthy users, passive BCIs and embodiment of language acquisition.

Reinhold Scherer is associate professor and deputy head of the Institute of Neural Engineering at the Graz University of Technology, Austria. He is member of the Laboratory for Brain-Computer Interfaces (BCI-Lab) at Graz University of Technology and of the Institute for Neurological Rehabilitation and Research at the rehabilitation center Judendorf-Strassengel, Austria. In 2008 he received his PhD in computer science from Graz University of Technology, where, beginning in 2001, he worked on non-invasive electroencephalogram-based (EEG) brain-computer interfacing (BCI). He spend the years from 2008 to 2010 as postdoctoral researcher at the Department for Computer Science & Engineering, University of Washington, Seattle, USA, and was member of the Neural Systems and the Neurobotics Laboratories at the University of Washington.

Published by Verlag der TU Graz
Graz University of Technology

 DOI: 10.3217/978-3-85125-533-1-00

Organizing Committee

Conference Chair

Univ.-Prof. Dipl.-Ing. Dr.techn.
Gernot R. Müller-Putz
Institute of Neural Engineering
Graz University of Technology
Austria
(BCI Society Member)

Papers and Proceedings

Dipl.-Ing.
David Steyrl
Institute of Neural Engineering
Graz University of Technology
Austria

Students Awards

ing. Dr. MSc
Andreea I. Sburlea
Institute of Neural Engineering
Graz University of Technology
Austria

Social Media

MSc
Joana Pereira
Institute of Neural Engineering
Graz University of Technology
Austria
(BCI Society Member)

Advisor

Prof. Dipl.-Biol. Dipl.-Psych. Dr.rer.nat.
Andrea Kübler
Interventionspsychologie am Lehrstuhl für Psychologie I
Universität Würzburg
Germany
(BCI Society Board)

Satellite Events and Sponsoring

Assoc.Prof. Dipl.-Ing. Dr.techn.
Reinhold Scherer
Institute of Neural Engineering
Graz University of Technology
Austria
(BCI Society Member)

Poster Sessions

Ass.Prof. Mag.rer.nat. Dr.phil.
Selina C. Wriessnegger
Institute of Neural Engineering
Graz University of Technology
Austria

Administration

Petra Still
Institute of Neural Engineering
Graz University of Technology
Austria

Advisor

Prof. Dr.
Nicolas F. Ramsey
Brain Center Rudolf Magnus
University Medical Center Utrecht
The Netherlands
(BCI Society President)

Advisor

Assoc.Prof. Dr.
José del R. Millán
Defitech Foundation Chair in Brain-Machine Interface
École polytechnique fédérale de Lausanne EPFL
Switzerland
(BCI Society Board)

Published by Verlag der TU Graz
Graz University of Technology

 DOI: 10.3217/978-3-85125-533-1-00

Additional Local Staff

Local Arrangements

Dipl.-Ing.
Reinmar Kobler
Institute of Neural Engineering
Graz University of Technology
Austria

Program Folder

MSc
Catarina Lopes Dias
Institute of Neural Engineering
Graz University of Technology
Austria

Local Arrangements

Dipl.-Ing.
Patrick Ofner
Institute of Neural Engineering
Graz University of Technology
Austria

Local Arrangements

Dipl.-Ing.
Andreas Pinegger
Institute of Neural Engineering
Graz University of Technology
Austria

Local Arrangements

Dipl.-Ing.
Andreas Schwarz
Institute of Neural Engineering
Graz University of Technology
Austria

Published by Verlag der TU Graz
Graz University of Technology

 DOI: 10.3217/978-3-85125-533-1-00

International Program Committee and Review Board I

We are very grateful to all reviewers for their help, to make this conference a success!

A	
Aarnoutse Erik	University Medical Center Utrecht
Anderson Charles	Colorado State University
B	
Bauernfeind Günther	Medizinische Hochschule Hannover
Bianchi Luigi	University of Rome Tor Vergata
Blankertz Benjamin	Technische Universität Berlin
Brouwer Anne-Marie	TNO Human Factors - Perceptual and Cognitive Systems
Brunner Clemens	University of Graz
C	
Chavarriaga Ricardo	École polytechnique fédérale de Lausanne (EPFL)
Clerc Maureen	INRIA Congedo Marco CNRS
Cohen Ori	Interdisciplinary Center Herzliya
Coyle Damien	University of Ulster
D	
Daly Ian	University of Essex
F	
Faller Josef	Columbia University
Farquhar Jason	Radboud University Nijmegen
Friedman Doron	Interdisciplinary Center Herzliya
G	
Gao Shangkai	Tsinghua University
Grosse-Wentrup Moritz	Max Planck Institute for Intelligent Systems
Guan Cuntai	Nanyang Technological University
Guger Christoph	g.tec Guger Technologies OG
Gutiérrez Dania	Center for Research and Advanced Studies (Cinvestav)
H	
Halder Sebastian	University of Wuerzburg
Hochberg Leigh	Brown University
Huggins Jane	University of Michigan Health System
J	
Jeunet Camille	Inria / École polytechnique fédérale de Lausanne (EPFL)
Jin Jing	East China University of Science and Technology

Published by Verlag der TU Graz
Graz University of Technology

 DOI: 10.3217/978-3-85125-533-1-00

International Program Committee and Review Board II

K

Kanoh Shin'Ichiro	Shibaura Institute of Technology
Kindermans Pieter-Jan	Technische Universität Berlin
Kleih Sonja	University of Würzburg
Kober Silvia	Department of Psychology, University of Graz
Kobler Reinmar	Graz University of Technology
Krusienski Dean	Old Dominion University
Kübler Andrea	Julius Maximilian University of Würzburg

L

Lopes Dias Catarina	Graz University of Technology
Lotte Fabien	INRIA Bordeaux Sud-Ouest

M

Mattia Donatella	Fondazione Santa Lucia, IRCCS
Mattout Jérémie	Lyon Neuroscience Research Center
Milekovic Tomislav	École polytechnique fédérale de Lausanne (EPFL)
Millan José del R.	École polytechnique fédérale de Lausanne (EPFL)
Müller-Putz Gernot R.	Graz University of Technology

N

Nam Chang	North Carolina State University
Nijboer Femke	Leiden University
Nijholt Anton	University of Twente
Noirhomme Quentin	Brain Innovation BV

O

Ofner Patrick	Graz University of Technology

P

Pereira Joana	Graz University of Technology
Pinegger Andreas	Graz University of Technology
Prasad Girijesh	Ulster University

R

Ron-Angevin Ricardo	University of Malaga
Rutkowski Tomasz M.	University of Tokyo

S

Sburlea Andreea I.	Graz University of Technology
Scherer Reinhold	Graz University of Technology
Schwarz Andreas	Graz University of Technology

Published by Verlag der TU Graz
Graz University of Technology

 DOI: 10.3217/978-3-85125-533-1-00

International Program Committee and Review Board III

Silvoni Stefano	Central Institute of Mental Health
Solis-Escalante Teodoro	Delft University of Technology
Sorger Bettina	Dpt. of Cognitive Neuroscience, Maastricht University
Spüler Martin	Eberhard-Karls-University Tübingen
Steyrl David	Graz University of Technology
T	
Tangermann Michael	University of Freiburg
Tonin Luca	Ecole Polytechnique Fédérale de Lausanne (EPFL)
V	
Vansteensel Mariska J	Brain Center Rudolf Magnus, UMC Utrecht
Vidaurre Carmen	Public University of Navarra
Volosyak Ivan	Rhine-Waal University of Applied Sciences
Vuckovic Aleksandra	University of Glasgow
W	
Wriessnegger Selina Christin	Graz University of Technology
Z	
Zander Thorsten	Berlin Institute of Technology
Zhang Yu	East China University of Science and Technology

Published by Verlag der TU Graz
Graz University of Technology

 DOI: 10.3217/978-3-85125-533-1-00

List of Authors I

List of authors in alphabetical order with start pages of their respective contributions.

Published by Verlag der TU Graz
Graz University of Technology

 DOI: 10.3217/978-3-85125-533-1-00

List of Authors II

Published by Verlag der TU Graz
Graz University of Technology

 DOI: 10.3217/978-3-85125-533-1-00

List of Authors III

Published by Verlag der TU Graz
Graz University of Technology

 DOI: 10.3217/978-3-85125-533-1-00

List of Authors IV

Published by Verlag der TU Graz
Graz University of Technology

 DOI: 10.3217/978-3-85125-533-1-00

List of Authors V

Published by Verlag der TU Graz
Graz University of Technology

 DOI: 10.3217/978-3-85125-533-1-00

List of Authors VI

Published by Verlag der TU Graz
Graz University of Technology

 DOI: 10.3217/978-3-85125-533-1-00

List of Authors VII

Published by Verlag der TU Graz
Graz University of Technology

 DOI: 10.3217/978-3-85125-533-1-00

List of Authors VIII

Published by Verlag der TU Graz
Graz University of Technology

 DOI: 10.3217/978-3-85125-533-1-00

List of Authors IX

Published by Verlag der TU Graz
Graz University of Technology

 DOI: 10.3217/978-3-85125-533-1-00

Table of Contents I

All contributions are sorted in alphabetical order based on the name of the first author.

Published by Verlag der TU Graz
Graz University of Technology

Table of Contents II

Published by Verlag der TU Graz
Graz University of Technology

Table of Contents III

Published by Verlag der TU Graz
Graz University of Technology

Table of Contents IV

Published by Verlag der TU Graz
Graz University of Technology

Table of Contents V

Published by Verlag der TU Graz
Graz University of Technology

Table of Contents VI

Published by Verlag der TU Graz
Graz University of Technology

Table of Contents VII

Published by Verlag der TU Graz
Graz University of Technology

Table of Contents VIII

Published by Verlag der TU Graz
Graz University of Technology

Table of Contents IX

Published by Verlag der TU Graz
Graz University of Technology

Table of Contents X

Published by Verlag der TU Graz
Graz University of Technology

 DOI: 10.3217/978-3-85125-533-1-00

Table of Contents XI

Published by Verlag der TU Graz
Graz University of Technology

Proceedings of the
7th Graz Brain-Computer Interface Conference 2017 DOI: 10.3217/978-3-85125-533-1-01

WORKING MEMORY AS A CONTROL SIGNAL IN A FULLY IMPLANTED BRAIN-COMPUTER INTERFACE

E.J. Aarnoutse[1], E.G.M. Pels[1], S. Leinders[1], Z.V. Freudenburg[1], M.P. Branco[1], M.A. van den Boom[1], T. Denison[2], M.J. Vansteensel[1], N.F. Ramsey[1]

[1] Brain Center Rudolf Magnus, Department of Neurology & Neurosurgery, University Medical Center Utrecht, Utrecht, The Netherlands
[2] Department of Neuromodulation, Medtronic, Minneapolis, MN

E-mail: e.j.aarnoutse@umcutrecht.nl

ABSTRACT: Voluntary control of brain activity using working memory can be used to control a BCI. Here we present data on an ALS patient with a fully implanted BCI with ECoG electrodes placed over left dorsolateral prefrontal cortex. This area is a versatile brain region involved in cognition. During several runs of a task where sustained activity in the high frequency band (HFB) is required to control a cursor in the direction of a target, the subject initially reached above chance performance, but in later runs reached performance up to 96%. The subject also performed a task in which a short rise in HFB (click) had to be generated to select an icon in a matrix. The subject was able to generate clicks, although with many false positives. We conclude that both sustained and short activity can be generated with a working memory strategy. The improvement on the cursor control task suggests that the task became more automated.

INTRODUCTION

It has long been established that one can control a Brain-Computer Interface (BCI) with activity from the motor cortex, both with EEG and ECoG signals. The latter signal has a more precise localization and higher amplitude. A demonstration of BCI control with activity from the motor cortex, using ECoG signal, was presented recently by our group: an ALS patient was implanted with a fully implantable BCI with ECoG electrodes on the motor cortex [1]. A rise in high frequency band (HFB) activity during a short attempted movement was used to generate a click. This click was translated to a selection in a spelling program to enable spelling for the patient.

The motor cortex, however, is not the only cortical area which can be controlled voluntarily. We have shown previously that sustained ECoG activity from the dorsolateral prefrontal cortex (dlPFC), an area active during working memory tasks, such as mental calculation, can be used for BCI control [2]. Also, clicks generated from dlPFC were demonstrated in an ECoG study [3].

In addition to the electrodes placed over motor cortex, also electrodes over dlPFC were placed. Two reasons motivated placing electrodes over dlPFC: Primary, it was not known whether the signal over motor cortex would deteriorate as a result of the disease and secondary, the dlPFC is a higher order cortex where training may cause a quicker automatization of BCI control. We here present results on using sustained and short signal changes in dlPFC for BCI control.

MATERALS AND METHODS

BCI implant: The subject is a 60-year-old woman with late stage ALS in a locked-in state. She was implanted in October 2015 with four subdural electrode strips (two on the left motor cortex, two on the left dlPFC; Medtronic LLC, Minneapolis, MN) on the basis of prelocalisation with fMRI. Extension cables were tunneled through the neck and externalized through the abdominal skin. After an electrode selection procedure, during a second surgery three days later, the strips with highest correlation with a screening task (both attempted movement and mental calculation) were connected to an Activa® PC+S amplifier/transmitter device (Medtronic), which was placed infraclavicularly in the thorax. See for more detail on the procedures [1]. The bandpass filtered signal (HFB, center frequency 65 Hz) is received by a unit and send to a computer running custom software, based on the BCI2000 software package, which is capable of presenting real-time visual feedback of the brain signal to the subject.

Tasks: Data was gathered during research sessions twice a week at the home of the subject. Multiple runs of a working memory task were performed during a session, not all sessions contained working memory runs.

Two working memory tasks are presented to the subject: First, a Cursor Control Task for sustained activity which provides feedback on the HFB (Fig. 1). The HFB is translated to velocity in y-direction, in x-direction velocity is a fixed number. Trials lasts 2-6s. The instruction was to move the cursor up by counting backwards in steps of e.g. 7 from a random starting number, in order to reach the upper target at the right and move the cursor down with rest to reach the lower target.

Published by Verlag der TU Graz
Graz University of Technology

 DOI: 10.3217/978-3-85125-533-1-01

Initially, both the random starting number and random step size were displayed at the beginning of each trial. Accuracy is calculated by the number of targets hit divided by the total number of targets, chance level is 50%. Second, a Click Task is presented, where a mole is presented at a random location in a matrix with icons (Fig. 2). First, the rows were highlighted in a stepwise manner and the instruction is to make a click to select the row where the mole icon is. Subsequently, the icons in that row are highlighted and the subject is instructed to select the icon with the mole. Feedback to the user is given with a color change of the highlight with a correct selection and removal of the mole. The next trial starts with the mole in a new random position. The clicks are generated when the power in the HFB exceeds an empirical threshold for 1.2 s.

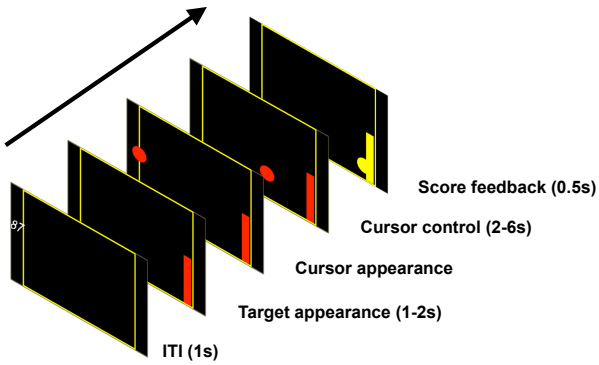

Figure 1. The Cursor Control Task provides feedback to the subject on the dlPFC activity. Note that a random number is given as a starting point for counting backwards.

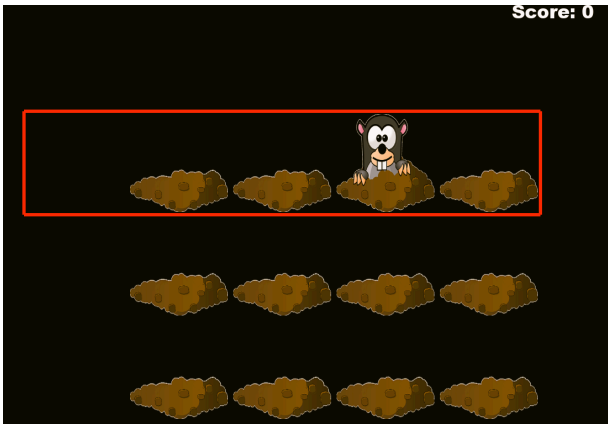

Figure 2. Rows of icons were highlighted sequentially at a fixed pace (red box) during which it could be selected by a click. Individual icons of the selected row were subsequently highlighted and could be selected with a second click. Goal was to select only the mole.

RESULTS

The subject was able to perform the Cursor Control Task with a working memory strategy.
Initially, accuracy was low (60%), but after a few sessions of training an accuracy of 90% was reached (Fig. 3). The subject reported in later sessions that display of a starting number was not needed anymore, thinking of a number already resulted in a higher dlPFC activity. She experimented with this in the sessions 31-40, with lower performance as a result. After returning to the previous strategy, accuracy increased to a maximum of 96%. After session 84 the display of the starting number was not needed anymore. Average accuracy after session 84 was 80.6%.

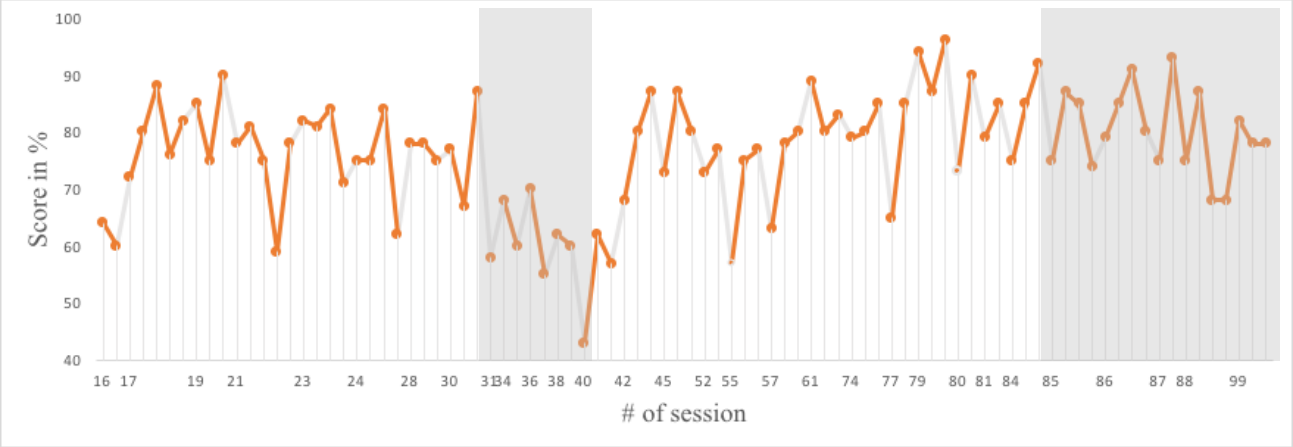

Figure 3. The performance of all runs of the Cursor Control Task with this subject. The lower performance in sessions 31-40 (grey background) can be attributed to a change in mental strategy: no starting numbers for counting backward. After session 84 this strategy without starting numbers (grey background) was used again, but now with high performance.

Published by Verlag der TU Graz
Graz University of Technology

 DOI: 10.3217/978-3-85125-533-1-01

The subject performed 13 runs of the Click Task during 3 sessions. The subject was able to generate a click with a working memory strategy. Accuracy was 63%, with chance level of 50%. The low accuracy can be attributed to the high number of false positives. However, she was able to generate a short rise in HFB (Fig. 4).

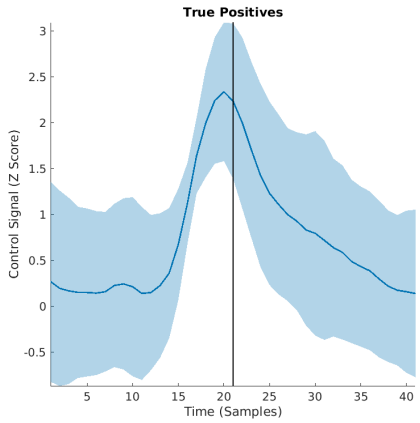

Figure 4. The mean HFB (±SD) activity over runs (after normalization) relative to the time the activity was translated into a true positive click. Samples of HFB are recorded every 200ms. Note a clear rise in HFB 1200ms before the click and 4s fall after the click.

DISCUSSION

The data demonstrate that the subject was able to use a working memory strategy for BCI control. Continuous control in a Cursor Control task was shown before [2]. In this study the subject had the opportunity to perform many more runs than reported before. According to the subject some automatization takes place over time, which correlates to the higher scores, even without a starting number, in later sessions. This is in line with the flexible nature of the dlPFC. In addition, the subject reports that her strategy for generating clicks shifted from actual counting backward to thinking of a number. This may also cause the irregular timing of the working memory clicks and false positives during highlight of the icon just before the mole. Irregular timing in working memory BCI control was found also in a previous study [3]. The number of false positives diminished in one run by a more active rest strategy. With more training we expect improvement, especially on the timing.
Working memory controlled BCI might be more valuable as an addition to motor control, than as a replacement. However, using working memory clicks for spelling might be feasible at a slower speed than motor clicks.

CONCLUSION

A subject with an implanted BCI was able to use a working memory strategy for BCI control, both in a task with sustained activity and in a task with short clicks. Feedback of the subject that she could perform the task without starting numbers suggests that the task becomes more automated.

REFERENCES

[1] Vansteensel MJ, Pels EGM, Bleichner MG, Branco MP, Denison T, Freudenburg ZV, Gosselaar P, Leinders S, Ottens TH, Van Den Boom MA, Van Rijen PC, Aarnoutse EJ, Ramsey NF. 2016. Fully Implanted Brain–Computer Interface in a Locked-in Patient with ALS. New England Journal of Medicine 375 (21): 2060–66. doi:10.1056/NEJMoa1608085.
[2] Vansteensel MJ, Hermes D, Aarnoutse EJ, Bleichner MG, Schalk G, van Rijen PC, Leijten FSS, Ramsey NF. 2010. Brain-Computer Interfacing Based on Cognitive Control. Annals of Neurology 67 (6): 809–16. doi:10.1002/ana.21985.
[3] Aarnoutse, EJ, Vansteensel MJ, Bleichner MG, Freudenburg ZV, Ramsey NF. 2013. “Just a Switch: Timing Characteristics of ECoG-Based Assistive Technology Control.” In Proceedings of the Fifth International Brain-Computer Interface Meeting 2013 Article ID: 007. doi:10.3217/978-3-85125-260-6-7.

Published by Verlag der TU Graz
Graz University of Technology

Proceedings of the
7th Graz Brain-Computer Interface Conference 2017 DOI: 10.3217/978-3-85125-533-1-02

DETECTION OF ATTENTION ALTERATION OF BCI USERS BASED ON EEG ANALYSIS

S. Aliakbaryhosseinabadi[1], E. N. Kamavuako[1], N. Jiang[2], D. Farina[3]
, N. Mrachacz-Kersting[1]

[1] Center of Sensory Motor Interaction, Department of Health and Science Technology, Aalborg, Denmark

[2] Department of System Design Engineering, Faculty of Engineering, University of Waterloo, Canada

[3] Department of Bioengineering, Imperial College London, SW7 2AZ London, UK

E-mail: sal@hst.aau.dk

ABSTRACT: In previous studies we have introduced a brain-computer interface (BCI) system based on movement related cortical potentials (MRCP). The performance of this system was shown to be significantly affected by the users' attention state. In the current study, we analyzed MRCP features (low frequencies) and features extracted at higher frequencies to determine the effect of variations in user's attention on EEG. Attention was modulated by a combination of auditory and visual stimuli that served as external distractors from the main task, which was a simple dorsiflexion. Time and frequency analysis was performed on EEG signals recorded from twenty-eight channels. The amplitude of the peak negativity and the slope of the negative deflection of the MRCP decreased and pre-movement variability increased with the distractors. Moreover, spectral analysis revealed an increment of theta power and alpha power due to attentional shifts. These results have implications for the design of real-life BCI systems, potentially allowing an increased robustness and adaptability with users' conditions.

INTRODUCTION

BCI systems provide a bi-direction interface with the human brain and can be used to modulate neural activity for rehabilitation (1, 2). For this purpose, the user's attention has an impact on the system performance. The effect of attention levels by the user was previously investigated for synchronous BCIs, where a cue was used as a source of information for the task execution (3, 4). However, the performance of asynchronous (self-paced) BCI in relation to attention variations remains unclear.

External stimuli can play the role of attention distractors and therefore drift the attention away from the target task (5, 6). Different types of attention activate various locations of the brain. While visual attention influences the parietal and occipital areas (7), auditory stimuli are directed to temporal and frontal locations (8).

Attention level modulates electroencephalography (EEG) signals. Event-related cortical potentials, steady–state evoked potentials and event-related (de)synchronization have been the most common types of signal modalities for the investigation of attention in BCI (9-11). In our previous work, we used features of the MRCP for detection of attention variations. We showed that temporal features of the MRCP are influenced by attention distractors (3).

In this study, temporal and spectral features of EEG signals were used for detection of attention variations. The main aim of this analysis is to make BCIs more robust for attention detection. Additionally, we aimed to identify which brain locations were more influenced by using each group of features.

MATERALS AND METHODS

Experimental set up

Nine healthy participants (4 females, 5 males) without hearing or visual impairments took part in the experiments. The experimental procedures were approved by the local ethical committee for the region of Northern Jutland (N-2016006).

EEG signals were recorded from twenty-eight channels by using an active EEG electrode system (g.GAMMAcap[2], Austria) and two synchronized g.USBamp amplifier (gTec, GmbH, Austria). EEG channels corresponded to AF3, AFz, Af4, F3, F1, Fz, F2, F4, FC3, FC1, FCz, FC2, FC4, C3, C1, Cz, C2, C4, CP3, CP1, CPz, CP2, CP4, P3, P1, Pz, P2 and P4 of the international 10-20 system. Two electromyography (EMG) electrodes were placed on the tibialis anterior (TA) muscle of the dominant foot to get information about movement execution.

Paradigm and task

Participants were asked to sit on a comfortable chair placed approximately one meter away from a computer screen, which showed the visual oddball task. An auditory oddball was played from a conventional headphone.

The experiment consisted of two phases.

Published by Verlag der TU Graz
Graz University of Technology

 DOI: 10.3217/978-3-85125-533-1-02

Control Level (CL): Participants were asked to perform 60 repetitions of self-paced ankle dorsiflexion divided into two blocks, each with 30 repetitions. They were instructed to perform the movement rapidly and forcefully and to hold the position for approximately 2 s after which they were asked to rest for 5-10 s.
Diverted Attention Level (DAL): participants had to focus on the oddball stimuli and count the number of target sequences while performing the same movements as in the first phase (dual-tasking).
The oddball used in this experiment was a combination of visual and auditory oddballs. For the visual oddball, two Gabor masks with an orientation of 60º and 30º, each with a probability of 25%, were used. For the auditory oddball, two auditory tones with frequencies of 1200 and 1900 Hz (middle and high pitch), each with a probability of 25%, were applied. All stimuli were randomized with an inter-stimulus interval of 1-2 s. Participants were asked to count the number of Gabor 30º followed by the middle pitch sound or the number of high pitch sounds following the Gabor 60º mask.

Signal analysis
The correlation of EMG envelopes in each block was computed to quantify the consistency of movement execution. EMG signals were rectified and low-pass filtered (10 Hz) to extract the envelopes. The correlation between averaged envelopes was calculated among trials of each block. In addition, the movement onsets were computed in each block with using a threshold for EMG signals to provide information about the timing of movement execution.
EEG signals were filtered in the bandwidth [0.05 10] Hz using a 2nd order Butterworth filter. MRCPs were extracted in the time interval [-3 3] s with reference to the movement onset, as estimated from the EMG signals.
Ten temporal features were extracted from the MRCPs: amplitude and timing of the peak negativity (APN and TPN), first derivatives (slopes) for the time intervals [-2 0] s, [-2 -1] s, [-1 0] s, and [0 1]s, and the standard deviations of the signal amplitude in the same time intervals. Figure 1 illustrated these features on a representative case.
Sixteen spectral features were extracted from the spectrogram of EEG signals in the delta [0 3] Hz, theta [4 8] Hz, alpha [8 13] Hz and beta [15 31] Hz bands, and at the four time intervals T1= [-1 -.6] s, T2= [-.8 -.4], T3= [-.6 -.2] s, and T4= [-.4 0] s.

Statistics
Three-way ANOVA was applied to compare the temporal or spectral features among the two attention levels (CL and DAL) and channel placement. The fixed factors were 'attention level' with two states (CL and DAL), 'channel lobe' with six levels (Anterio-frontal, Frontal, Centro-frontal, Central, Centro-parietal and parietal lobes), and 'channel hemisphere' with three levels (Right, midline and left). Wilcoxon matched-pair sign rank test was used to analyze the differences in EMG envelopes between two attention levels. Significant was set to $p<0.05$.

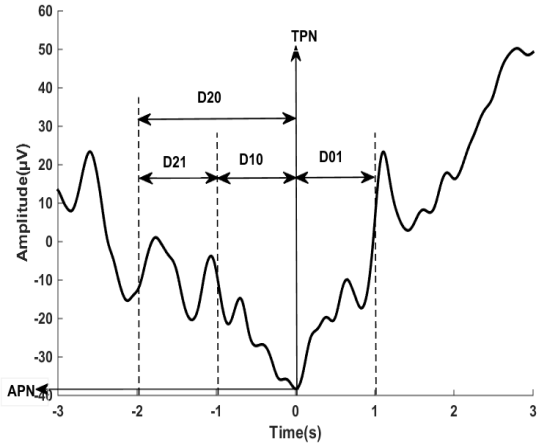

Figure 1: Schematic of temporal features extracted from single-trial MRCPs. 'D' indicates the range of time domains for slope and variability extraction. D21 shows [-2 -1] s, D10 represents [-1 0] s, D20 means [-2 0] s and D01 is for [0 1] s.

RESULTS

EMG Analysis
The EMG envelope and the time interval between movements were not significantly different between CL and DAL ($p>0.05$). The duration between movements was also greater in the diverted attention level (CL: 9.9s, DAL: 11.5s) but not significantly different.

Temporal Features
APN, slope and variability in the range of [1 0] s (S10 and Var10) were significantly different between CL and DAL. Table 1 shows the values for these variables and the associated significance levels based on the three independent factors.
APN and S10 were significantly reduced from CL to DAL (APN: $F_{(1,412)}= 6.4$, $p=0.01$; S10: $F_{(1,412)}= 37.3$, $p<0.001$). Figure 2 illustrates the average MRCP signals across all subjects and each channel for both conditions. Both the MRCP amplitude and slopes were reduced from CL to DAL for most channels.
APN was significantly different between the three channel hemispheres ($F_{(2,412)}= 7.9$, $p<0.001$). The *Bonferroni post-hoc* test revealed that the midline locations were significantly different compared to the right ($p= 0.03$) and left channel placements ($p=0.001$). Var10 was increased significantly from CL to DAL ($F_{(1,412)}= 125.2$, $p<0.001$) although it did not show statistical differences with regards to the channel lobe or channel hemisphere.

Published by Verlag der TU Graz
Graz University of Technology

 DOI: 10.3217/978-3-85125-533-1-02

Table 1: Three temporal features of MRCPs as a function of the three independent factors, with corresponding p values.

	Attention Level			Hemisphere placement				Lobe Placement						
	CL	DAL	P	Left	Midline	Right	P	AF	F	FC	C	CP	P	P
APN	-20.1 µV	-17.2 µV	0.01	-17.8 µV	-21 µV	-19 µV	<.001	-19.6 µV	-19.9 µV	-18.4 µV	-19.8 µV	-18.8 µV	-19.2 µV	0.9
S10	-10.5 µV/s	-4.1 µV/s	<.001	-9.6 µV/s	-9.2 µV/s	-7.5 µV/s	0.2	-9.9 µV/s	-9.1 µV/s	-9.8 µV/s	-9.4 µV/s	-9.9 µV/s	-9.5 µV/s	0.7
Var10	0.013	0.016	<.001	.014	.014	.015	0.4	.015	.014	.015	.014	.014	.014	0.2

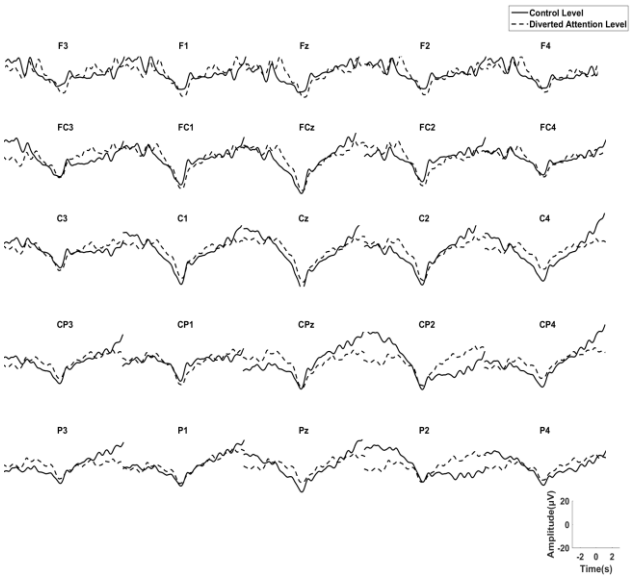

Figure 2: Grand average of the MRCP signals in different channel locations based on the two attention levels. CL is shown as a solid black line and DAL as the dotted black line. Data are the average across all subjects (n=9).

Spectral Features

The alpha and theta range had more variations in specific time windows. Alpha power was increased statistically in T1 ([-1 -.6]) s between the CL and DAL condition ($F_{(1,412)}$= 4.7, p= 0.03). In addition, channel lobe had a significant effect on alpha power distribution in four time intervals (T1[-1 -.6]: $F_{(5,412)}$= 4.6, p<0.001; T2[-8 -.4]: $F_{(5,412)}$= 3.6, p= 0.03; T3[-.6 -.2]: $F_{(5,412)}$= 2.8, p= 0.02; T4[-.4 0]: $F_{(5,412)}$= 3.1, p= 0.009). The *Post-hoc* test revealed that the Parietal and Anterio-Frontal lobe channels led to significantly different features compared to the other lobes.

Theta power was also increased in the time interval [-1 -.6] for CL versus DAL condition ($F_{(1,412)}$= 32.3, p< 0.001). Similar to the alpha power, the factor 'lobe' had a significant effect on theta power distribution (T1[-1 -.6]: $F_{(5,412)}$= 16.8, p<0.001; T2[-.8 -.4]: $F_{(5,412)}$= 15.8, p= 0.03; T3[-6 -.2]: $F_{(5,412)}$= 12.4, p= 0.02; T4[-.4 0]: $F_{(5,412)}$= 9.8, p= 0.009). The factor 'channel hemisphere' revealed a significant effect in T1[-1 -.6] ($F_{(2,412)}$= 6.8, p= 0.001) and T2[-.8 -.4] ($F_{(2,412)}$= 8.3, p< 0.001). The post-hoc test indicated that channels located on the midline led to different features compared to those located in the other two hemispheres. Figure 3 shows the topographic plots of the power distribution in T1 [-1 -.6] for one representative subject. Regarding to all subjects, the signal power increased in the theta and alpha range, particularly in the channels placed on left hemisphere, with attention diversion.

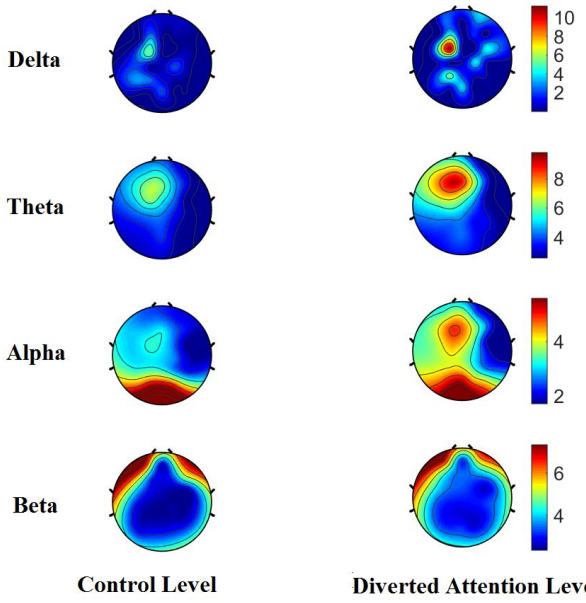

Figure 3: Power distribution in four frequency ranges for T1 [-1 -.6] with respect to the dorsiflexion onset. Data are for n=1.

DISCUSSION

We studied time and frequency features of EEG signals with attention variations. The results suggest that among ten temporal features, the amplitude of peak negativity and pre-movement slope in the late negativity phase before movement onset decrease in DAL by comparison with CL. Our previous studies support that by dividing the attention (dual-tasking), the EEG signal associated to movement preparation is reduced in amplitude and thus detection of movement intention delayed (3). One of the possible reasons for this effect is a reduction of attention to the main task in dual-task conditions in comparison with the single task. Therefore, the majority of attention is diverted to the secondary task and causes a reduced motor cortex excitability for the main

Published by Verlag der TU Graz
Graz University of Technology

 DOI: 10.3217/978-3-85125-533-1-02

movement preparation and execution (12). Nonetheless, the movement execution was not significantly influenced, as quantified by EMG activity.
Moreover, we observed significant increases in theta and alpha power with reduced attention. Although theta power enhancement particularly in the frontal lobe suggests an increment in the working memory or focused attention to the target task, in this study it is presumably due to an increased task demand in the dual-task conditions (13-15). This supports previous studies which revealed an inverse relation between attention demand in multi-tasking and alpha power (16) and the same relation between task demand and alpha power in the frontal, central and parietal lobes (17, 18).

CONCLUSION

For designing robust and reliable BCI systems, it is important to adapt the system to the users' attention variations. Here we demonstrate that attention influences the temporal and spectral features of EEG signals. These results may have potential application in the design of systems for detecting the attention level from EEG features.

REFERENCES

[1] Shende PM, Jabade VS. Literature review of brain computer interface (BCI) using Electroencephalogram signal. Int. Con. Pervasive Computing (ICPC). 2015 ,1-5

[2] Kim T, Kim S, Lee B. Effects of Action Observational Training Plus Brain-Computer Interface-Based Functional Electrical Stimulation on Paretic Arm Motor Recovery in Patient with Stroke: A Randomized Controlled Trial. Occup. Ther. Int. 2016; 23(1):39-47

[3] Aliakbaryhosseinabadi S, Kostic V, Pavlovic A, Radovanovic S, Nlandu Kamavuako E, Jiang N, et al. Influence of attention alternation on movement-related cortical potentials in healthy individuals and stroke patients. Clin. Neurophysiol. 2017;128(1): 165-175

[4] Aliakbaryhosseinabadi S, Jiang N, Petrini L, Farina D, Dremstrup K, Mrachacz-Kersting N. Robustness of movement detection techniques from motor execution: Single trial movement related cortical potential. Neural Engineering (NER), 2015 7th International IEEE/EMBS Conference ; 2015

[5] Hill NJ, Schölkopf B. An online brain–computer interface based on shifting attention to concurrent streams of auditory stimuli. J. Neural Eng. 2012 ;9(2):026011

[6] De Vos M, Gandras K, Debener S. Towards a truly mobile auditory brain–computer interface: Exploring the P300 to take away. Int. J. Psychophysiol. 2014 ;91(1): 46-53

[7] Trojano L, Grossi D, Linden DE, Formisano E, Hacker H, Zanella FE, et al. Matching two imagined clocks: the functional anatomy of spatial analysis in the absence of visual stimulation. Cereb. Cortex. 2000;10(5):473-481

[8] Altmann CF, Bledowski C, Wibral M, Kaiser J. Processing of location and pattern changes of natural sounds in the human auditory cortex. Neuroimage. 2007;35(3):1192-1200

[9] Aftanas LI, Savotina LN, Makhnev VP, Reva NV. Event-related synchronization and desynchronization of EEG during perception of emotional stimuli: association with autonomous nervous system activity. Ross. Fiziol. Zh. Im. I M Sechenova. 2004;90(11):1314-1323

[10] Ilardi SS, Atchley RA, Enloe A, Kwasny K, Garratt G. Disentangling Attentional Biases and Attentional Deficits in Depression: An Event-Related Potential P300 Analysis. Cognit. Ther. Res. 2007;31(2):175-187

[11] Pokorny C, Breitwieser C, Müller-Putz GR. The Role of Transient Target Stimuli in a Steady-State Somatosensory Evoked Potential-Based Brain–Computer Interface Setup. Front. Neurosci. 2016 ;10: 152

[12] Bruckmann S, Hauk D, Roessner V, Resch F, Freitag CM, Kammer T, et al. Cortical inhibition in attention deficit hyperactivity disorder: new insights from the electroencephalographic response to transcranial magnetic stimulation. Brain. 2012;135(7):2215-2230.

[13] Dussault C, Jouanin J, Philippe M, Guezennec C. EEG and ECG changes during simulator operation reflect mental workload and vigilance. Aviat. Space Environ. Med. 2005;76(4):344-351

[14] Smith ME, McEvoy LK, Gevins A. The impact of moderate sleep loss on neurophysiologic signals during working-memory task performance. Sleep. 2002;25(7):784-794

[15] Doppelmayr M, Finkenzeller T, Sauseng P. Frontal midline theta in the pre-shot phase of rifle shooting: Differences between experts and novices. Neuropsychologia. 2008;46(5):1463-1467

Published by Verlag der TU Graz
Graz University of Technology

 DOI: 10.3217/978-3-85125-533-1-02

[16]Fournier LR, Wilson GF, Swain CR. Electrophysiological, behavioral, and subjective indexes of workload when performing multiple tasks: manipulations of task difficulty and training. International journal of psychophysiology. 1999 ;31(2):129-145

[17] Slobounov SM, Fukada K, Simon R, Rearick M, Ray W. Neurophysiological and behavioral indices of time pressure effects on visuomotor task performance. Brain. Res. Cogn. Brain. Res. 2000 ;9(3):287-298

[18] Fairclough SH, Venables L. Prediction of subjective states from psychophysiology: a multivariate approach. Biol. Psychol. 2006;71(1):100-110

Published by Verlag der TU Graz
Graz University of Technology

Proceedings of the
7th Graz Brain-Computer Interface Conference 2017 DOI: 10.3217/978-3-85125-533-1-03

INVESTIGATING WRITTEN TEXT READABILITY FOR PASSIVE BCI BASED NEUROADAPTIVE SPEED READING APPLICATIONS

L.M. Andreessen[1,2], P. Gerjets[3,4,6], D. Meurers[5,6], T.O. Zander[1,2]

[1]Department of Biological Psychology and Neuroergonomics, Technische Universität Berlin, Berlin, Germany

[2] Team PhyPA, Department of Biological Psychology and Neuroergonomics, Technische Universität Berlin, Berlin, Germany

[3] Leibniz-Institut für Wissensmedien, Tübingen, Germany

[4] Department of Psychology, Eberhard-Karls-Universität Tübingen, Tübingen, Germany

[5] Department of Linguistics, Eberhard-Karls-Universität Tübingen, Tübingen, Germany

[6] LEAD Graduate School and Research Network, University of Tübingen, Germany

E-mail: lena.andreessen@gmail.com

ABSTRACT: Rapid serial visual presentation (RSVP) can prove useful as a reading technique when text is presented on small screens. Optimal text presentation speed for text reading depends on the reader himself, context and features of the text. Readability is a measure which estimates the ease with which a reader can understand a written meaningful text.
The presented study investigated whether a passive Brain-Computer Interface (pBCI) can be used to distinguish between texts of distinct levels of readability presented at different presentation speeds. A predictive model was trained on EEG data derived from a cognitive load paradigm. The model was then applied to data collected while participants read easy and difficult texts at a self-adjusted speed and at an increased speed level.
Results suggest that predictions made by the predictive model could be used as an estimate for categorization and adaptation of longer text passages, though its robustness and potential for the use in neuroadaptive reading applications should be further investigated.

INTRODUCTION

Reading is the written form of a language and serves communication and information sharing in societies. Textual information nowadays is distributed as digital media presentations on electronic displays (e.g., monitors, mobile phones, eReaders, etc.) and is accessible in a broad and fast way through advanced communication technology. With decrease in size of mobile devices, smaller screen sizes are a consequence and constitute challenges for the way text material can be presented. Scrolling and paging in text presentation can be bothersome and inconvenient for the reader [1]. Hence new forms of text presentation for mobile devices recently have emerged and are developed.
Rapid serial visual presentation (RSVP) is a popular approach to build a text presentation method appropriate for reading on (very) small displays. In this presentation form, words of a text are presented sequentially one word at a time at a fixed screen location [2]. It was claimed that in contrast to traditional left to right text body reading, texts can be read faster at constant comprehension levels [3]. It is suggested that a reduction of saccades, small and rapid eye movements to fixate the next word, due to a constant fixation point while reading, leads to an increase of overall reading speed in RSVP reading methods [4]. Over the past years claims like these have been subjected to several studies examining RSVP reading effects on text comprehension and reading speed [5, 6]. It emerged that reading comprehension and efficiency depend on nuanced features of the textual information to be read, such as text difficulty, length, and reading speed. Readability is a measure of the ease with which the meaning of a text can be comprehended. Readability ratings traditionally are obtained using readability formulas such as Flesch-Kincaid Grade Level [7] or the Flesch Reading Ease [8]. Most readability formulas are based on a combination of easily countable features such as word length and sentence length.
Recently commercial speed reading applications were made available for RSVP reading on electronic devices. Reading speed in these applications is regulated manually and stays static if the user does not alter it throughout the reading process. Here a less intrusive form of presentation speed regulation would prove useful, especially if features of the read text material, e.g., text readability, differ over time. Then the cognitive load of the reader might change according to different levels of text difficulty.
Passive Brain-Computer Interfaces [pBCIs, 9] are a technology which uses neurophysiological signals to distinguish between different cognitive states [10]. Data recorded by Electroencephalography (EEG) while different cognitive states are evoked in a person, can be used to train a BCI to distinguish between these different

Published by Verlag der TU Graz
Graz University of Technology

 DOI: 10.3217/978-3-85125-533-1-03

states and evaluate new data when it is recorded. This evaluation of a BCI then can be used to generate a signal to change the state of a system. In the process the user does not need to actively generate a signal towards the machine, but her cognitive state is monitored and interpreted continuously. A reader would not be required to pay attention and conscious effort to generate a signal to change e.g. the reading speed appropriate to her current state. Such an automatic adaptation to a user's current cognitive state through the application of a pBCI would be a realization of neuroadaptive technology [11]. This technology enhances the interaction between user and machine as it provides knowledge about the situational user state to the machine. A neuroadaptive reading application could make the reading process more pleasant and efficient. Additionally, the generated information about the user state could be used to generate an assessment of the user's individual text difficulty levels and readability skills. Such a measure detecting the relation between the user's current level of cognitive load and a text of a given level of difficulty could be useful in learning contexts to generate personalized learning content. Here, the pBCI could be utilized to find appropriate learning material which can be optimized to fit the learner's current needs and abilities.

The aim of the presented work was to examine whether a pBCI can be trained to distinguish between different levels of text difficulty while reading with a speed reading application. Moreover, the effects of reading speed on this measure were investigated. As connections to other words become more complex with the position of a word within a sentence, it was also investigated whether this relationship is reflected in the output from the pBCI. Moreover, long sentences should be more difficult to understand than short ones as they are more complex in structure and relations between words. Therefore, is was also investigated whether the average output of the pBCI shows a difference between short and long sentences. The outcomes were interpreted according to their applicability in neuroadaptive technologies.

MATERALS AND METHODS

Participants: Eight participants, five female, took part in the experiment. The mean age was 29 years (*SD* = 3.2 years). All participants had normal or corrected-to-normal vision and their native language was German. Prior to the experiment participants gave their written informed consent to participate in the study and were paid thirty euros as expense allowance.

Speed Reading Application: The speed reading application applied in this study was Spritz. The Spritz Application programming interface (API) was provided by Spritz™ (spritzinc.com/) for the use in this study. Together with Psychophysics Toolbox extensions [12] the experimental paradigm was computed in MATLAB.

Stimuli: Texts used in the investigation were extracted from the GEO/GEOlino Corpus [13]. The corpus is a collection of 1066 German texts taken from the German magazine GEO, which covers topics related to nature, culture and science, and the magazine GEOlino, which deals with similar topics, but is targeted at children aged between 8 and 14 years. The texts from GEO therefore are generally more complex than those from the GEOlino magazine. Six texts were chosen from each magazine, all covering similar topics about animals and their habits. Overall the average number of words per text was 493 (*SD* = 34.6 words). GEO texts had an average word count of 472 words (*SD* = 23.1 words) and GEOlino texts of 514 words (*SD* = 31.7 words). GEO texts had an average Flesch reading ease index of 45.1 (*SD* = 2.4), which is equivalent to difficult texts on college level. The Flesch-Kincaid grade level of GEO texts was 10.9 (*SD* = .29). For GEOlino texts, the average Flesch reading ease index was 62 (*SD* = 1.38) which corresponds to a readability suitable for 13 to 15 years old students. These texts had an average Flesch-Kincaid grade level of 7.9 (*SD* = .24).

EEG system and software: During the experiment brain activity was recorded from 64 active Ag/AgCl electrodes (ActiCap, Brain Products, Munich, Germany) applied to an elastic cap according to the extended international 10/20 positioning system. The ground electrode was placed at position AFz and the reference at FCz. All electrodes were connected to a BrainAmp amplifier (Brain Products GmbH, Munich, Germany), which was connected to a laptop through a universal serial bus (USB) 2.0. Electrode impedances were kept below 5 kΩ. Data was recorded using the BrainVision Recorder, BrainVision RDA (Brain Products GmbH, Munich, Germany) and LabRecorder [14]. The sampling rate was set to 500 Hz. The experimental paradigms were run in SNAP [15] and in MATLAB, using the Psychophysics Toolbox extensions. Data was analyzed with the MATLAB embedded EEGLAB toolbox [16]. For classification and BCI model application the open source toolbox BCILAB [17] was used.

Pre-test: Six participants took part in a pre-test to examine whether an increase of 40 percent in text presentation speed would lead to an increase of perceived workload. The participants' mean age was 27.2 years (*SD* = 3.8 years), five were male, all had normal or corrected-to-normal vision and their native language was German. Participants read the twelve texts in blocks of three at a self-adjusted reading speed with the speed reading application. Half of the texts from each difficulty class (easy vs. difficult) were presented at a self-adjusted speed plus 40 percent. After each block, participants filled out a Raw-Task Load Index (RTLX) [18], a modified version of NASA-TLX [19], a standardized questionnaire assessing perceived workload on a Likert scale along six dimensions. A two-way repeated measures ANOVA revealed a significant main effect of presentation speed, $F(1,5) = 6.758$, $p = .048$. Workload of texts presented in normal speed was rated lower ($M = 45.7$, $SD = 16.9$) than for texts represented with 40 percent increase in speed ($M = 53.58$, $SD = 17.1$). There was no significant main effect of text difficulty, $F(1,5) = 1.371$, $p = .294$. The interaction of the factors was also not significant, $F(1,5) = 0.255$, $p = 0.635$. From these results, it was concluded that an increase of individual reading speed by 40 percent

Published by Verlag der TU Graz
Graz University of Technology

 DOI: 10.3217/978-3-85125-533-1-03

was sufficient to increase the subjective workload for participants while reading the texts later used in the main study.

Experimental procedure: In the main experiment, participants first completed an experimental paradigm, which was applied to induce two different levels of cognitive load [20]. This so-called 'sparkles' paradigm was developed by Team PhyPA (TU Berlin) [21]. In several experiments the classifier trained on the data obtained from this paradigm was tested while participants completed not only arithmetic assignments, as during data collection, but tasks from other task domains. It was used, e.g., while the participant verbally described a complex context or solved anagrams, where the classifier could reliably distinguish between phases of high and low workload. Due to its applicability to multiple domains the classifier can be seen as a form of task-independent classifier for cognitive load.

During half of the paradigm the participant saw colorful spots moving around slowly on an otherwise black screen. In this phase, the participant was supposed to relax and simply focus on watching the spots flying around with eyes open. This part of the paradigm was supposed to induce low workload. To induce higher workload, from time to time an arithmetic subtraction assignment appeared at the center of the screen. At its appearance the participant was supposed to silently subtract the number standing on the right side (range between 6 and 20) iteratively from the number on the left (range between 200 and 1200). After some time, the arithmetic assignment disappeared again, whereat the participant stopped subtracting and turned towards watching the spots again. Overall 40 trials of low or high induced workload were performed with a length of 10 seconds per trial.

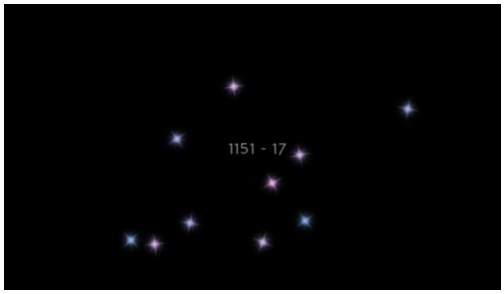

Figure 1: Screenshot of the workload ('sparkles') paradigm. The arithmetic assignment is presented in the center of the screen. Colorful dots are moving around the black background at a slow pace.

After completion of the workload paradigm participants familiarized with the speed-reading application. They read passages of a German novel and incrementally adjusted the presentation speed to a level they felt comfortable reading with.

Then participants read all twelve texts in blocks of three. All texts of a block were either easy or difficult texts and presented in the self-adjusted reading speed or with an increase of 40 percent (as determined in the pre-study). After each text, participants answered three questions regarding literal text comprehension. Under each question four possible answers were displayed, of which one was the right choice. If, e.g., the text had read 'The warm sun hatches the eggs in the sand', the question could have been: 'Who hatches the eggs of the turtle?', then of the possible answers a) the father, b) a cormorant c) the sun and d) the mother, c) would have been the right choice. Participants selected their answer by key press. Each participant answered 3x12 literal comprehension questions, a total of 36 questions.

After each of the four text blocks participants were handed a RTLX questionnaire to assess subjective ratings of perceived workload. Overall each participant completed the RTLX four times.

Analyses: Individually adjusted presentation rates were averaged over participants from the pre- and main study. Ratings collected in the RTLX questionnaire were converted to workload scores according to NASA-TLX procedures. The workload scores of all eight participants were subjected to a two-way repeated measures ANOVA with the within-subject factors presentation speed (normal vs. plus 40 percent) and text difficulty (easy vs. difficult). The numbers of correct answers to literal text comprehension questions of each participant within each of the four text blocks were added. These scores per block then were subjected to a two-way repeated measures ANOVA with within-subject factors presentation speed (normal vs. plus 40 percent) and text difficulty (easy vs. normal).

Due to a recording software problem, only data from seven of the eight participants was used for classification. For feature extraction, a filter bank common spatial patterns (fbCSPs) approach [22] was used. Two frequency band (4-7, expected increase with increasing workload and 7-13, expected decrease with increasing workload) Hz was selected and epochs of 5 seconds length starting at stimulus were extracted. Linear discriminant analysis (LDA) regularized by shrinkage [23] was used as a classifier and a (5x5)-fold cross-validation was employed.

For each participant, the individual predictive model trained on data from the workload paradigm was applied to text reading data. The BCILAB built-in function onl-simulate was used to apply the predictive model to the raw data from all twelve texts, resulting in a predictive value between 0 and 1 for each word of a text. An output with a value of 0 would indicate low load and a value of 1 high load.

Predicted values from each predictive model were subjected to permutation tests with 50000 permutations per test. All predictions from one group of texts according to text difficulty (easy vs. difficult) and presentation speed (normal vs. fast) were tested within and between the two factors. Tests were one-tailed as the assumptions were that easy texts should result in lower predictive values than difficult texts. Also within one text difficulty category, predictions of texts presented at normal speed were expected be lower than predictions of texts presented at an increased speed. Easy texts

Published by Verlag der TU Graz
Graz University of Technology

 DOI: 10.3217/978-3-85125-533-1-03

presented at normal speed were assumed to have lower predictive values than difficult text which were presented fast. Finally, for predictions in easy texts which were presented fast against predictions from difficult texts presented at normal speed, no assumption regarding difficulty was made.
It was further assumed that longer sentences would have an overall higher difficulty as word relations within a longer sentence regularly become more complex in structure than in short sentences. To test if this assumption was manifested in the predictions made by the applied predictive models, predictions within each sentence were averaged. The averaged predictive values alongside with the word count of the respective sentences were subjected to linear regression analysis. Regression analysis was performed once for all sentences of easy texts presented in normal speed and again for sentences from difficult texts presented at normal speed. Moreover, it was performed for all participants together and again for each individual participant.
Another assumption was that predictive values could reflect an increase of complexity of relations towards a word caused by an increase of the word's position within a sentence. To test this assumption words and their predicted values were sorted by their position within sentences. All predictive values for the occurred sentence positions were subjected to a linear regression analysis. Again, the analysis was only performed for easy and difficult texts presented at normal presentation speed, for each participant and also for data from all subjects together.

RESULTS

Individually adjusted presentation rates from the overall 13 participants of the pre-test and the main experiment ranged between 175 and 600 words per minute (wpm). The average adjusted reading speed was 308 wpm (*SD* = 130 wpm).
The two-way repeated measures ANOVA performed on ratings from the RTLX questionnaire from the eight participants revealed significance for the main factor text difficulty, F (1,7) = 8.75, p = .021. Difficult texts (M = 68.4, SD = 26.2) received higher ratings than easy texts (M = 59.1, SD = 18.4). Results for the main factor presentation speed were significant as well, F (1,7) = 11.10, p = .012. Texts presented at the normal (M = 56.4, SD = 17.3) self-adjusted reading speed received lower RTLX ratings than texts presented with a speed increase of 40 percent (M = 71.1, SD = 25.7). The interaction effect was not significant, F (1,7) = 1.22, p = .306.
The ANOVA performed on correct answers given to literal text comprehension questions revealed neither significant main effects, nor an interaction effect of significance, all *ps* > .258. On average participants answered 6.2 (SD = .48) questions out of nine per text block correctly. An average of 6.9 (SD = 1.96) correct answers was given for easy texts and 6.0 (SD = 1.31) for difficult texts presented at normal speed. For texts blocks with an increased presentation speed, questions on easy texts were answered 5.8 (SD = 1.28) times correctly and difficult texts 6.25 (SD = 1.67) times.
The average cross validation error rate was 23.7 percent (SD = 6.7 percent). See Table 1 for individual classification errors.

Table 1: Classification results of the workload paradigm. Obtained error rates (*ER*) in percent and standard deviations (*SD*) are reported.

participant	*ER* (*SD*)
1	14.1 (3.2)
2	28.5 (14.7)
3	14.8 (4.9)
4	14.5 (2.5)
5	44.3 (7.8)
6	18.9 (4.1)
8	8.3 (1.5)
average	**20.5 (5.5)**

Almost all performed permutation tests were highly significant (all *ps* < .0001). Only for the test of predictions in easy texts which were presented fast against predictions from difficult texts presented at normal speed, results were not significant (p = .961). It must be noted though that absolute values of observed differences between classes (M = -.077, SD = .032) were smaller in all tests than variances within classes (M = .086, SD = .008). Effect sizes therefore were small to medium (M = .266, SD = .116).
For linear regressions, no significant equations were found for average word predictions in sentences with different length. Analysis results were neither significant for data from all participants taken together (all *ps* > .632) nor on subject level (all *ps* > .072).
No significant regression equation was found when data of all seven participants was collapsed for analysis performed on predictions for word positions within a sentence, all *ps* > .053. On single subject level, four regression analyses were significant. Half of the slopes for significant equations were negative while the other was positive, ranging between -.003 and .006.

DISCUSSION

Individually adjusted text presentation rates showed a strong variation and an average of 308 wpm. The strong individual variation in adjusted speeds might be caused by differences in preference for the RSVP reading method, as some participants may have felt unconfident with the new reading technique, while others felt more comfortable using it. Such strong variations in preference with speed reading applications were shown before [24]. The average adjusted speed of 308 wpm lies above the average speed for traditional reading, which lies between 250 and 300 wpm [25]. This effect of faster reading with speed reading applications is found in most literature on speed reading applications. Results from the RTLX revealed that perceived load was higher for difficult texts than for easy texts. Cognitive load was also higher for

Published by Verlag der TU Graz
Graz University of Technology

 DOI: 10.3217/978-3-85125-533-1-03

texts presented with an increased reading speed than when presented at an individually adjusted speed. Since no differences in literal comprehension emerged between different text difficulties and presentation speeds, it can be concluded that an increased presentation speed did not lead to less comprehension. On average two thirds of questions within one text block were answered correctly. It could have been possible that too high reading speeds would lead to an overextension of participants who become less attentive to understanding the text as a consequence. However, this was not the case and results from literal comprehension questions indicate that participants read all variations of texts attentively at similar levels of literal comprehension.

pBCI classification for cross validation on data from the workload paradigm was on average around 20% and hence acceptable. Permutation tests performed on predictions made by the predictive model showed that difficult texts had significantly higher predictive values than easy texts. Moreover, predictions for texts presented with an increase of 40 percent in reading speed had significantly higher values than texts shown at the individually adjusted speed. However, effect sizes for all tests were very small, as prediction variances within text and speed groups were higher than the observed differences between groups in the permutation tests. The results obtained from permutation tests of predictive suggest that that the cognitive load classifier could be used to distinguish overall difficulty differences between longer passages of texts. This applies for difficulty changes induced by presentation speed and text readability level.

It was assumed that averaged prediction values of words within a sentence would increase with a rise of sentence length due to rising structural complexity of word relations. In regression analysis, no significant equations were found. The results suggest that classifiers trained on the cognitive load paradigm are not suitable to reflect possible effects of higher structural complexity in longer sentences. Predictions from the predictive models therefore cannot be used as an estimate of single sentence difficulty.

Regarding the position of a word within a sentence it was assumed that words appearing later in a sentence would receive higher predictive values. Regression analysis of predictions was only significant on single subject level. Several significant equations were found, but half of the slopes were positive while the others were negative. These ambiguous results indicate that predictions derived from the predictive models trained in this study are not suitable as predictors for single word difficulty based on the complexity of relations the word stands in.

Altogether results showed that the trained BCI models were not applicable for measuring single word or sentence difficulty within texts. Only when all predictions for whole texts are regarded together, the predicted values can be used to distinguish between levels of readability and reading speed. RTLX had shown that perceived workload was higher for difficult texts as well as for reading at increased presentation rates. Results suggest that predictions made for broader text passages contain and reflect this information. For much shorter passages, like single sentences or even single words, immediate changes seem to be absent or are not detectable by the model employed in this study.

CONCLUSION

Broader changes of activity in frequency bands employed in the workload classifier were found to correspond to differences in text readability and presentation speed. Such changes are detectable when single word predictions made for larger text passages are examined together. These results add text readability and presentation speed in RSVP reading to the domains where the task-independent workload classifier can distinguish between levels of cognitive load.

Complex texts also contain many easy words which may prevent classification on sentence or word level, as long as linguistic information about word difficulty is not accessible for integration to the classifier. The results suggest though that the effects on cognitive load are highly responsive and that the employed predictive model is sensitive enough to detect these changes.

For future research the robustness and potential for application of the classifier to full texts should be examined further. The predictive model should be applied to a larger variety of text material of different readability level and text length. The predictive model trained in this study could already be used as an estimate for user modelling in educational practice, e.g., in online tutoring systems, to choose appropriate texts as learning material matching the learner's individual readability level. In speed reading it could also be used to modify the presentation speed after a sufficient amount of text has been read. The presentation speed could then be de- or increased according to classifier output.

To obtain more fine-tuned information about difficulty levels of single sentences or texts, other measures than investigated in this study need to be found. A neuroadaptive system capable of detecting levels of text readability in real time on a word by word basis could perform text simplification [26]. It would be able to individually adapt to its user to improve reading comprehension, which could be well applied in future learning scenarios. Speed reading applications are seen as especially suitable for reading short texts on mobile devices with small screens [27]. Oblinger and Oblinger [28] describe the so-called net generation, who grew up using mobile devices, are used to instant information access and not reading large amounts of text. Moreover, mobile computer-supported collaborative learning is regarded as a promising approach to support and facilitate learning interactions between students [29]. Neuroadaptive features on the side of technology and devices would be a further enrichment to such approaches to future learning.

Published by Verlag der TU Graz
Graz University of Technology

 DOI: 10.3217/978-3-85125-533-1-03

REFERENCES

[1] Hedin, B., (2006). Mobile Message Services Using Text, Audio or Video for Improving the Learning Infrastructure in Higher Education. Int'l J. Emerging Technologies in Learning, vol. 1, no. 1.

[2] Forster, K.L., (1970).Visual Perception of Rapidly Presented Word Sequences of Varying Complexity. Perception and Psychophysics, vol.8, no. 4, pp. 215–221.

[3] Potter, M. C. (1984). Rapid serial visual presentation (RSVP): A method for studying language processing. New Methods in Reading Comprehension Research.

[4] Rubin, G. S., & Turano, K. (1992). Reading without saccadic eye movements. Vision research, 32(5), 895-902.

[5] Masson, M. E. (1983). Conceptual processing of text during skimming and rapid sequential reading. Memory & Cognition, 11(3), 262-274.

[6] Kang, T. J., & Muter, P. (1989). Reading dynamically displayed text. Behaviour & information technology, 8(1), 33-42.

[7] Kincaid, J. P., Fishburne Jr, R. P., Rogers, R. L., & Chissom, B. S. (1975). Derivation of new readability formulas (automated readability index, fog count and flesch reading ease formula) for navy enlisted personnel (No. RBR-8-75). Naval Technical Training Command Millington TN Research Branch.

[8] Flesch, R. (1948). A new readability yardstick. Journal of applied psychology, 32(3), 221.

[9] Zander, T. O., & Kothe, C. A. (2011). "Towards passive brain-computer interfaces: applying brain-computer interface technology to human machine systems in general." Journal of Neural Engineering, 8(2), 025005.

[10] Brouwer, A. M., Zander, T. O., & van Erp, J. B. (2015). Using neurophysiological signals that reflect cognitive or affective state. Frontiers Media SA.

[11] Zander, T. O., Krol, L. R., Birbaumer, N. P., & Gramann, K. (2016). Neuroadaptive technology enables implicit cursor control based on medial prefrontal cortex activity. Proceedings of the National Academy of Sciences, 201605155.

[12] Brainard, D. H. (1997). The Psychophysics Toolbox, Spatial Vision 10:433-436.

[13] Hancke, J., Vajjala, S., & Meurers, D. (2012). Readability Classification for German using Lexical, Syntactic, and Morphological Features. In COLING 2012: Technical Papers (pp. 1063-1080).

[14] Delorme, A., Kothe, C., Vankov, A., Bigdely-Shamlo, N., Oostenveld, R., Zander, T. O., & Makeig, S. (2010). MATLAB-based tools for BCI research. In Brain-Computer Interfaces (pp. 241-259). Springer London.

[15] Iversen, J.R., Makeig, S. (2013). MEG/EEG Data Analysis Using EEGLAB.

[16] Delorme, A., & Makeig, S. (2004). EEGLAB: an open source toolbox for analysis of single-trial EEG dynamics including independent component analysis. Journal of neuroscience methods, 134, 9-21.

[17] Kothe, C. A., & Makeig, S. (2013). BCILAB: a platform for brain–computer interface development. Journal of neural engineering, 10(5), 056014.

[18] Hart, S. G. (2006). NASA-task load index (NASA-TLX); 20 years later. In Proceedings of the human factors and ergonomics society annual meeting (Vol. 50, No. 9, pp. 904-908). Sage Publications.

[19] Hart, S. G., & Staveland, L. E. (1988). Development of NASA-TLX (Task Load Index): Results of empirical and theoretical research. Advances in psychology, 52, 139-183.

[20] Krol, L.R., Freytag, S.C., Fleck, M., Gramann, K., & Zander, T.O. (n.n). A Task-Independent Workload Classifier for Neuroadaptive Technology: Preliminary Data. IEEE International Conference on Systems, Man and Cybernetics. Budapest, Hungary, Oct. 9-12, 2016.

[21] Team PhyPA: Brain-Computer Interfacing for Everyday Human-Computer Interaction Thorsten O. Zander, Laurens R. Krol Periodica Polytechnica Electrical Engineering and Computer Science, in review

[22] Ang, K. K., Chin, Z. Y., Zhang, H., & Guan, C. (2008, June). Filter bank common spatial pattern (FBCSP) in brain-computer interface. In Neural Networks, 2008. IJCNN 2008.(IEEE World Congress on Computational Intelligence). IEEE International Joint Conference on (pp. 2390-2397). IEEE.

[23] Blankertz, B., Lemm, S., Treder, M., Haufe, S., & Müller, K. R. (2011). Single-trial analysis and classification of ERP components—a tutorial. NeuroImage, 56(2), 814-825.

[24] Hedin, B., & Lindgren, E. (2007). A comparison of presentation methods for reading on mobile phones. IEEE Distributed Systems Online, 8(6), 2-2.

[25] Carver, R. (1990). Reading rate: A review of research and theory. San Diego: Academic Press.

[26] Crossley, S. A., Allen, D. B., & McNamara, D. S. (2011). Text readability and intuitive simplification: A comparison of readability formulas. Reading in a foreign language, 23(1), 86.

[27] Öquist, G. & Goldstein, M., (2002). Towards an Improved Readability on Mobile Devices: Evaluating Adaptive Rapid Serial Visual Presentation. Proc. 4th Int'l Symp. Human Computer Interaction with Mobile Devices (Mobile HCI), LNCS 2411, Fabio Paterno, ed., Springer, pp. 225–240.

[28] Oblinger, D., & Oblinger, J. (2005). Is it age or IT: First steps toward understanding the net generation. Educating the net generation, 2(1-2), 20.

[29] Naismith, L., Lonsdale, P., Vavoula, G. N., & Sharples, M. (2004). Mobile technologies and learning.

Published by Verlag der TU Graz
Graz University of Technology

Proceedings of the
7th Graz Brain-Computer Interface Conference 2017 DOI: 10.3217/978-3-85125-533-1-04

ELECTROENCEPHALOGRAPHY (EEG)-DERIVED MARKERS TO MEASURE COMPONENTS OF ATTENTION PROCESSING

A. Anzolin[1,2], L. Astolfi[1,2], J. Toppi[1,2], A. Riccio[2], F. Pichiorri[2], F. Cincotti[1,2], D. Mattia[2]

[1] Dept. of Computer, Control, and Management Engineering, Sapienza University of Rome, Italy
[2] IRCCS Fondazione Santa Lucia Hospital, Rome, Italy

E-mail: anzolin@dis.uniroma1.it

ABSTRACT: Although extensively studied for decades, attention system remains an interesting challenge in neuroscience field. The Attention Network Task (ANT) has been developed to provide a measure of the efficiency for the three attention components identified in the Posner's theoretical model: alerting, orienting and executive control. Here we propose a study on 15 healthy subjects who performed the ANT. We combined advanced methods for connectivity estimation on electroencephalographic (EEG) signals and graph theory with the aim to identify neuro-physiological indices describing the most important features of the three networks correlated with behavioral performances. Our results provided a set of band-specific connectivity indices able to follow the behavioral task performances among subjects for each attention component as defined in the ANT paradigm. Extracted EEG-based indices could be employed in future clinical applications to support the behavioral assessment or to evaluate the influence of specific attention deficits on Brain Computer Interface (BCI) performance and/or the effects of BCI training in cognitive rehabilitation applications.

INTRODUCTION

Attention is fundamental for human cognitive processing. As such, it includes a wide class of processes related with the ability of a subject to interact with the external environment. According to Posner's theoretical model [1], this is possible through a sustained state of alertness (alerting), the selection of the important information in a noisy context (orienting) and the ability to control a situation and solve conflicts (executive control). When the complex mechanism at the basis of attention is altered, e.g. following a stroke event, consequences may affect a wide range of behavioural and social aspects. Several neuroimaging and neurophysiological studies have employed the so-called Attention Network Task (ANT), a behavioural task which allows to disentangle the three components (alerting, orienting and executive control) as described by Fan et al. in [2]. The available evidences indicate that the three attention components are independent [3], involve different anatomical areas (functional magnetic resonance imaging, fMRI, studies) [4] and each of them has a distinct oscillatory activity and time course (EEG study) [5].

In this study, we applied modern methodologies for effective connectivity estimation and graph theory approaches with the aim to define stable and reliable descriptors of the dynamic brain circuits underpinning the attentional components in terms of directed relationships between the brain areas and their frequency content. Currently available brain connectivity studies on attention are based on structural networks (anatomical connectivity) [6] or functional networks extracted from fMRI data [7]. We were interested in extracting markers of the brain circuits elicited by the ANT performed by healthy volunteers while recording high density EEG (hdEEG) and thus, exploiting its high temporal resolution, low invasiveness and cost-effective. To this purpose we explore whether connectivity-based indices would correlate with behavioural data in order to strengthen their relevance as measure of attention processing for future applications. [8], [9].

MATERIALS AND METHODS

Experimental Design: Data (60 EEG channels + 4 EOG channels, reference at linked mastoids and ground at Fpz, Brain Products) were recorded from 15 healthy volunteers (10 female, age 27.2 ± 2.5) during the execution of the ANT [5] (Fig.1). They had no history of neurological or psychiatric disorders. The experimental protocol was approved by the local Ethical Committee. Participants were seated in front of a computer screen; a row of 5 black arrows pointing left or right was presented in the middle part of the screen. Subjects were asked to indicate the direction of the central arrow (target stimulus) as quickly and accurately as possible with the left arrow keyboard or the right arrow keyboard button according to the direction of the target, using their right hand. Trials were defined as *Congruent* if the 4 lateral *flankers* and the central arrow had the same direction, *Incongruent* if the flankers pointed at the opposite direction. In addition there were three cue (an asterisk sign) conditions: *No cue*, *Center cue* (in the center of the screen for alerting), and *Spatial cue* (at the target location, above or below a fixation cross, for alerting plus orienting) [3]. The timeline of the paradigm is showed in Fig.1. The contrast between the different experimental conditions (72 trials each condition) allowed to extract the three attention components: i) *Center cue* and *No cue* conditions define the alerting, ii) *Spatial cue* and *Center*

Published by Verlag der TU Graz
Graz University of Technology

 DOI: 10.3217/978-3-85125-533-1-04

cue the orienting, iii) *Incongruent* and *Congruent* the executive control.

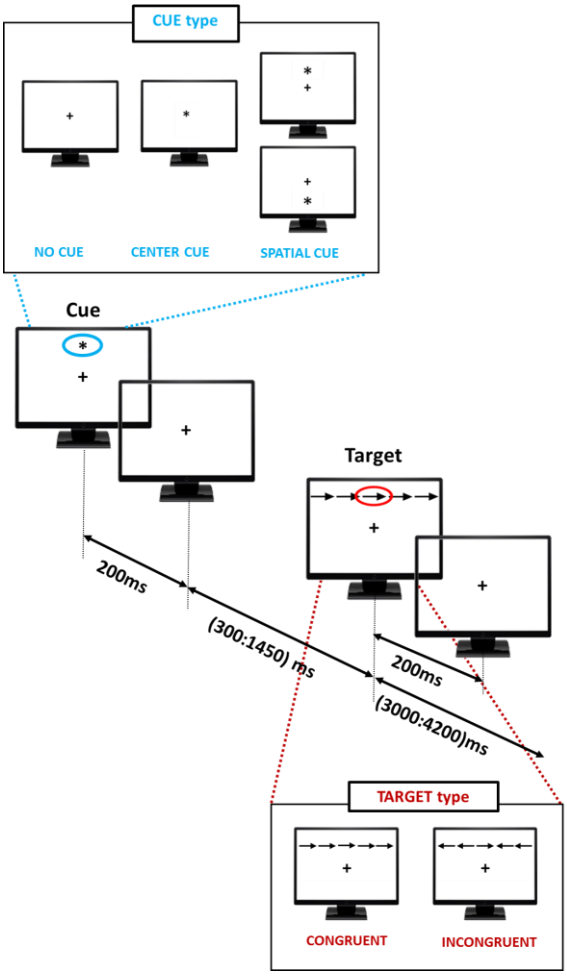

Figure 1: Timeline of the ANT paradigm. In each trial, a cue (asterisk) may appear for 200 ms in the center of the screen (center cue condition) or in the semi-space in which the target will appear (spatial cue). After a variable duration (300–1450ms), the target and the flankers (congruent or incongruent) are presented. The participant indicate the direction of the central arrow within a time window of 2000 ms. The target and flankers disappear after the response is made.

Behavioral Data: As behavioral index for each attention component we used the efficiency measure introduced in [2]. Alerting efficiency (Eff_{Al}), orienting efficiency (Eff_{Or}) and executive control efficiency (Eff_{EC}) are defined as the difference between the mean reaction times (RT) in specific experimental conditions:

$$Eff_{Al} = RT_{No} - RT_{Center} \quad (1)$$

$$Eff_{Or} = RT_{Center} - RT_{Spatial} \quad (2)$$

$$Eff_{EC} = RT_{Incong} - RT_{Cong} \quad (3)$$

EEG Data Analysis and Connectivity Estimation: EEG scalp data were band-pass filtered in the range [1-45] Hz and ocular artifacts were removed through Independent Component Analysis (fast-ICA algorithm). EOG channels were also included in the ICA decomposition. Signals were segmented in different time windows defined as [0 - 500] ms according to the *cue* onset and [0-400] ms according to the *target* onset. Residual artifacts were removed by means of a semi-automatic procedure based on a threshold criterion (±80 μV). Connectivity patterns were estimated through Partial Directed Coherence (PDC) [10] and averaged in four frequency bands (Theta, Alpha, Beta and Gamma) defined according to the Individual Alpha Frequency (IAF) [11]. We obtained a network for each frequency band, each experimental condition and each subject. A statistical comparison (unpaired t-test, $p<0.05$, False Discovery Rate, FDR, correction) was performed between appropriate conditions (according to ANT theory) in order to isolate the networks associated with each of the three attention components. In particular, we compared: i) *center cue* vs *no cue* for alerting, ii) *spatial cue* vs *center cue* for orienting and iii) *congruent* vs *incongruent* for executive control. Graph theory indices were extracted from the networks underlying the three attention components with the aim to synthetize their main global and local properties. In this study, we adopted the following indices:

Global Indices to describe the general properties of the entire network [12]:

- Clustering: to measure the tendency of the network to segregate the information in subnetworks;
- Path Length: to measure efficiency of the communication between the nodes on the basis of the shortest paths between them.

Local Indices: to quantify the involvement of a specific sub-network and/or investigating the relation between different sub-networks. In particular as sub-networks we considered left (Fp1, AF7, AF3, F7, F5, F3, F1, FT7, FC5, FC3, FC1, T7, C5, C3, C1, TP7, CP5, CP3, CP1, P7, P5, P3, P1, PO7, PO3, O1) and right (Fp2, AF4, AF8, F2, F4, F6, F8, FC2, FC4, FC6, FT8, C2, C4, C6, T8, CP2, CP4, CP6, TP8, P2, P4, P6, P8, PO4, PO8, O2) hemispheres, anterior (Fp1, Fp2, AF7, AF3, AFz, AF4, AF8, F7, F5, F3, F1, Fz, F2, F4, F6, F8, FT7, FC5, FC3, FC1, FCz, FC2, FC4, FC6, FT8) and posterior (TP7, CP5, CP3, CP1, CPz, CP2, CP4, CP6, TP8, P7, P5, P3, P1, Pz, P2, P4, P6, P8, PO7, PO3, POz, PO4, PO8, O1, Oz, O2) areas [13]. We computed the following indices:

- Density: to quantify the percentage of existing connections with respect to the totality of possible links. It has been adapted as in the following formula to quantify the percentage of connections relative to a specific area:

$$sub - Density = \frac{n_{subnet}}{n_{TOT}}$$

  Where n_{subnet} is the number of existing links connecting only the nodes (electrodes) belonging to the considered subnetwork and n_{TOT} is the number of all the existing connection of the entire circuit.
- Divisibility - Modularity: to measure the level of interaction between subnetworks in terms of inter

Published by Verlag der TU Graz
Graz University of Technology

 DOI: 10.3217/978-3-85125-533-1-04

(divisibility) and intra (modularity) connections: strict interconnection or isolation [14].

- Influence: to measure a prevalence in the direction of inter-connections linking two spatial regions [13].

Connectivity indices extracted for each attention component were then correlated with the relative behavioral parameters (Eff_{Al}, Eff_{Or}, Eff_{EC}) by means of Pearson's correlation ($p<0.05$). FDR correction was applied to take into account errors due to multiple correlations.

RESULTS

Results are reported separately for each component of the ANT paradigm.

Alerting: as shown in Figure 2, we found significant negative correlations between the efficiency Eff_{Al} and i) the path length index in beta band (Fig. 2, panel a) and ii) the left/right influence index in theta band (Fig. 2, panel b). Such correlations pointed out a relation between the behavioral performances and the speed in the exchange of information between network nodes in the alerting phase (low path length) in beta band. Moreover, an efficient alerting is associated to a communication between the two hemispheres in theta band with a prevalence of the information flows directed from right to left (negative values for left/right influence).

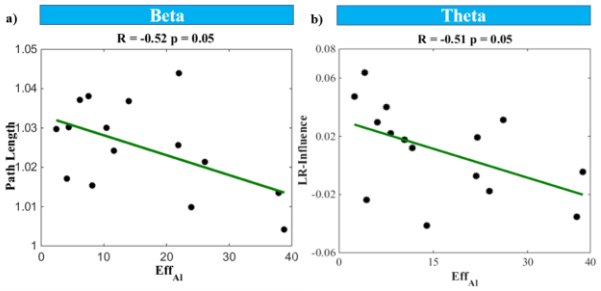

Figure 2. Alerting: statistical correlations between the efficiency Eff_{Al} (y-axis) and the connectivity indices (x-axis): path length in beta band (panel a) and left/right influence in theta band (panel b). As in all figures, dots correspond to the values obtained for each of the 15 subjects involved in the study. The green line represents the linear fitting computed on the data. The associated values of correlation (R) and significance (p) are reported on the top of the figure.

Orienting: as shown in Figure 3, a positive correlation was found between the efficiency Eff_{Or} and i) the right density (Fig. 3, panel a) and ii) the left/right divisibility (Fig.3, panel b) in the theta band.

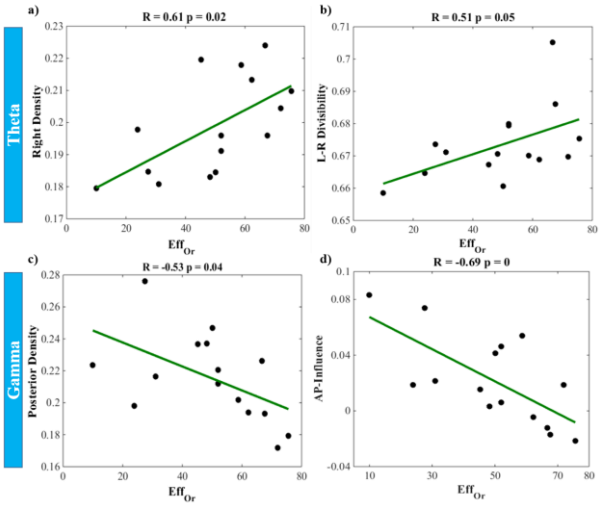

Figure 3. Orienting: statistical correlations between the efficiency Eff_{Or} (y-axis) and the connectivity indices (x-axis) right density (panel a) and Left/Right Divisibility (panel b) in theta band, posterior density (panel c) and Anterior/Posterior Influence (panel d) in gamma band.

In particular, such results pointed out how an efficient orienting process is associated to a strong segregation of the information flows within the right hemispheres (high right density) and a low integration of the two hemispheres (high left/right divisibility) in theta band. Furthermore, we found that the parameter Eff_{Or} negatively correlated with the posterior density index (Fig.3, panel c) and the anterior/posterior influence index (Fig.3, panel d) in the gamma band.
This indicates that an efficient orienting process is associated to a low involvement of the posterior scalp regions (low posterior density) and to the establishment of a communication between anterior and posterior regions with a prevalent direction from posterior to anterior.

Executive Control: Figure 4 shows a significant positive correlation between executive control efficiency Eff_{EC} and both the Path Length (Fig.4, panel a) and the Clustering indices (Fig.4, panel b) in the gamma band. Significant correlations were also found between efficiency Eff_{EC} and left/right divisibility (Fig.4, panel c), left/right modularity (data not shown; R=0.53, p=0.05) and left/right influence indices (Fig.4, panel d) in the alpha band. In particular such results indicated how a reduction in the time required for solving the conflict (low Eff_{EC}) is associated to a high communication speed between the electrodes (low path length) and to a less tendency of the network to create clusters (low clustering). Moreover, an efficient (i.e. correlated with high behavioural performance) executive control is explained by a high integration of the two hemispheres (low left/right divisibility) with information flows directed from right to left (negative values of left/right influence).

Published by Verlag der TU Graz
Graz University of Technology

 DOI: 10.3217/978-3-85125-533-1-04

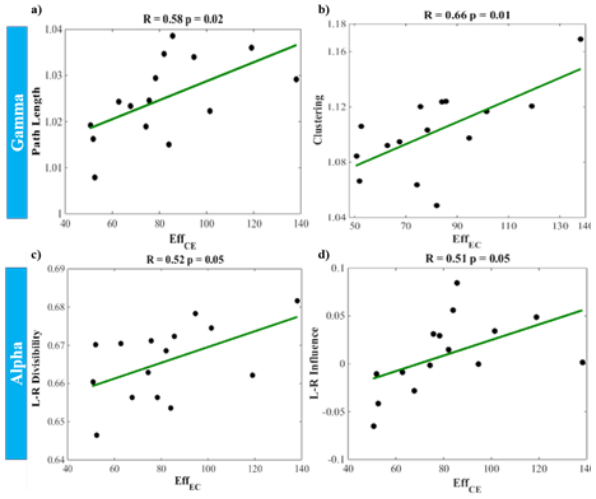

Figure 4. Executive control: statistical correlations between the efficiency Eff_{EC} (y-axis) and the connectivity indices (x-axis) -Path Length (panel a) and Clustering (panel b) in gamma band -Left/Right Divisibility (panel c) and Left/Right Influence (panel d) in alpha band.

DISCUSSION

In the present study, we used advanced techniques for EEG signals processing to extract the cortical connectivity patterns (causal relationship between scalp areas) associated with the 3 attention components as elicited by the ANT paradigm (i.e. alerting, orienting and executive control) performed by healthy subjects. Some indices, derived from the graph theory, allowed the quantitative description of the relevant local and global properties of the 3 different causal connectivity networks in specific EEG frequency bands as they correlated with the behavioural performance (i.e. correlated with Eff_{Al}, Eff_{Or}, Eff_{EC}). According to our findings, the estimated *alerting* network was described mainly by a negative relationship between the behavioral efficiency (Eff_{Al}) and Path Length index in the beta band, (ie, the higher efficiency the shorter Path Length) and the left/right Influence index in the theta band (ie, the higher efficiency the higher interhemispheric connection from right-to-left; negative values for left-right influence index).

The phasic alerting improves the speed of target response by changing the internal state of preparation for perceiving a (visual) stimulus [5]. Our results indicate that an efficient alerting function (higher speed to target response) is associated with a global network organization characterized by a shorter average Path Length which corresponds to a high efficiency information transfer [15]. As yet, the entire network appears to be characterized by a prevalent exchange of information directed from right to left hemisphere. Such prevalence might reflect the role of the right hemisphere to sustain alertness that was already stressed in previous studies in which lesions of the right frontal and parietal areas were associated to reduced ability in maintaining the alert state [16]. The above discussed index modulation occurred in beta and theta band, respectively. This finding is in line with previous EEG evidence of a relationship between these frequency oscillations and the alerting function [5].

The efficiency of the *orienting* function was in our study, described by a set of network indices which correlated with behavioral performance (Eff_{Or}). First, we found that the higher performance efficiency the higher right Density and left-right Divisibility in the theta band. In addition, higher orienting efficiency also correlated to both lower posterior Density and anterior/posterior Influence (prevalence for post-to-ant) in the gamma oscillations. Together, these results indicate a prevalent role of the right hemisphere versus the left (higher connectivity density) and poor communication between hemispheres (higher divisibility). About the frontal and parietal areas, results indicate a prevalence of connections from posterior to anterior areas (higher anterior/posterior influence and lower posterior density). This is in line with previous evidence of the (right) parietal and frontal areas involved in orienting function which enables for the selection of specific information from a number of sensory inputs [3],[16][4]. The above discussed index modulation occurred in the theta and gamma frequency oscillations that may be in line with the evidence in favour of the contribution of the theta oscillation to long-range communications for cognitive processing by phase-locking to high gamma power (Fries, 2015).

Finally, an efficient *conflict* resolution (ie, *executive control*) was described mainly by a positive relationship between the behavioral efficiency (Eff_{EC}) and both the Clustering and Path Length indices in the gamma band, (ie, the lower time to solve the conflict (low Eff_{EC}) the lower tendency to clustering and shorter Path Length) and both the left/right Divisibility and Influence indices in the alpha band (i.e., the higher efficiency the higher interhemispheric connection with a prevalent right-to-left direction flow; negative values for left-right influence index). Altogether these results reflect the highly integrative nature of the conflict processing which requires more integration than segregation of information flow which are originated from several partially overlapping networks [18].

Future studies conducted at cortical and subcortical level (i.e. using source localization techniques like sLoreta [19]) should clarify the effective brain networks properties and their relationship with the currently available knowledge on anatomical and functional connectivity of attention networks. Such further step mightvalidate the proposed indices as neuro-physiological correlates of attention components for future applications.

CONCLUSION

Advanced EEG signals elaboration based on time-varying connectivity estimation and graph theory were applied to extract direct and weighted connectivity patterns elicited by the ANT paradigm at scalp level. Correlation results pointed out a set of EEG-based indices able to synthetically describe each of the three

Published by Verlag der TU Graz
Graz University of Technology

 DOI: 10.3217/978-3-85125-533-1-04

attention components in the different frequency bands and to follow the variations in the corresponding behavioural measures. Such preliminary results could be used in the near future to: i) support the neuropsychological assessment in healthy subject and people with attention impairments; ii) clarify the role of specific attention components in BCI contexts (P300- and SMR-based BCI) and eventually improve the design of BCIs targeting attention rehabilitation; iii) increase the knowledge on attention brain networks elicited by the ANT paradigm. Altogether, our findings at the scalp level might have a strong impact on several clinical/non clinical applications related to the BCI field.

REFERENCES

[1] M. I. Posner and S. E. Petersen, "The attention system of the human brain," *Annu. Rev. Neurosci.*, vol. 13, pp. 25–42, 1990.

[2] J. Fan, B. D. McCandliss, T. Sommer, A. Raz, and M. I. Posner, "Testing the efficiency and independence of attentional networks," *J. Cogn. Neurosci.*, vol. 14, no. 3, pp. 340–347, Apr. 2002.

[3] J. Fan, B. D. McCandliss, J. Fossella, J. I. Flombaum, and M. I. Posner, "The activation of attentional networks," *NeuroImage*, vol. 26, no. 2, pp. 471–479, Jun. 2005.

[4] M. Corbetta and G. L. Shulman, "Control of goal-directed and stimulus-driven attention in the brain," *Nat. Rev. Neurosci.*, vol. 3, no. 3, pp. 201–215, Mar. 2002.

[5] J. Fan *et al.*, "The Relation of Brain Oscillations to Attentional Networks," *J. Neurosci.*, vol. 27, no. 23, pp. 6197–6206, Jun. 2007.

[6] M. Xiao *et al.*, "Attention Performance Measured by Attention Network Test Is Correlated with Global and Regional Efficiency of Structural Brain Networks," *Front. Behav. Neurosci.*, vol. 10, Oct. 2016.

[7] S. Markett *et al.*, "Assessing the function of the fronto-parietal attention network: insights from resting-state fMRI and the attentional network test," *Hum. Brain Mapp.*, vol. 35, no. 4, pp. 1700–1709, Apr. 2014.

[8] M. Rubinov and O. Sporns, "Complex network measures of brain connectivity: uses and interpretations," *Neuroimage*, vol. 52, no. 3, pp. 1059–1069, Sep. 2010.

[9] L. A. Baccalá and K. Sameshima, "Partial directed coherence: a new concept in neural structure determination," *Biol. Cybern.*, vol. 84, pp. 463–474, May 2001.

[10] L. A. Baccalá and K. Sameshima, "Partial directed coherence: a new concept in neural structure determination," *Biol. Cybern.*, vol. 84, no. 6, pp. 463–474, Jun. 2001.

[11] P. Sauseng, W. Klimesch, W. Gruber, M. Doppelmayr, W. Stadler, and M. Schabus, "The interplay between theta and alpha oscillations in the human electroencephalogram reflects the transfer of information between memory systems," *Neurosci. Lett.*, vol. 324, no. 2, pp. 121–124, May 2002.

[12] M. Rubinov and O. Sporns, "Complex network measures of brain connectivity: Uses and interpretations," *NeuroImage*, vol. 52, no. 3, pp. 1059–1069, Sep. 2010.

[13] J. Toppi *et al.*, "Describing relevant indices from the resting state electrophysiological networks," *Conf. Proc. Annu. Int. Conf. IEEE Eng. Med. Biol. Soc. IEEE Eng. Med. Biol. Soc. Annu. Conf.*, vol. 2012, pp. 2547–2550, 2012.

[14] M. E. J. Newman, "Finding community structure in networks using the eigenvectors of matrices," *Phys. Rev. E*, vol. 74, no. 3, Sep. 2006.

[15] V. Latora and M. Marchiori, "Efficient Behavior of Small-World Networks," *Phys. Rev. Lett.*, vol. 87, no. 19, Oct. 2001.

[16] W. Sturm and K. Willmes, "On the functional neuroanatomy of intrinsic and phasic alertness," *NeuroImage*, vol. 14, no. 1 Pt 2, pp. S76-84, Jul. 2001.

[17] M. Corbetta, "Frontoparietal cortical networks for directing attention and the eye to visual locations: Identical, independent, or overlapping neural systems?," *Proc. Natl. Acad. Sci. U. S. A.*, vol. 95, no. 3, pp. 831–838, Feb. 1998.

[18] J. Fan *et al.*, "Testing the behavioral interaction and integration of attentional networks," *Brain Cogn.*, vol. 70, no. 2, pp. 209–220, Jul. 2009.

[19] R. D. Pascual-Marqui, "Standardized low-resolution brain electromagnetic tomography (sLORETA): technical details," *Methods Find. Exp. Clin. Pharmacol.*, vol. 24 Suppl D, pp. 5–12, 2002.

Published by Verlag der TU Graz
Graz University of Technology

Proceedings of the
7th Graz Brain-Computer Interface Conference 2017 DOI: 10.3217/978-3-85125-533-1-05

STEADY STATE VISUAL EVOKED POTENTIALS AT THE BOUNDARIES OF VISUAL PERCEPTION

G. Berumen[1], T. Tsoneva[2,3]

[1]University of Twente, Enschede, The Netherlands
[2]Philips Research Europe, Eindhoven, The Netherlands
[3]Radboud University, Nijmegen, The Netherlands

E-mail: tsvetomira.tsoneva@philips.com

ABSTRACT: Steady-state visual evoked potentials (SSVEP) are electrical brain responses that oscillate at the same frequency, or harmonics, of rapid repetitive visual stimulation (RVS). SSVEP are widely used in practice, however, the exposure to RVS is associated with discomfort and safety risks. Those negative effects can be overcome by understanding how properties of the stimulation, such as frequency and modulation depth (MD) affect the SSVEP.
In order to explore whether SSVEP can be elicited by barely perceptible RVS and potentially safer stimulation, we used MDs around the visual perception thresholds (VPT), the lowest threshold at which people perceive RVS. SSVEP were detected only for frequencies higher than 19 Hz with MDs close to the VPT. In addition, an increase in MD was associated with an increase in the amplitude of SSVEP. These findings can help designing a quasi-imperceptible stimulation able to elicit SSVEP, reducing the discomfort associated to with the RVS.

INTRODUCTION

Steady-state visual evoked potentials (SSVEP) are electrical brain responses associated with the stimulation of the retina by rapid repetitive visual stimulation (RVS), also known as flicker [1]. SSVEP are oscillatory responses at the same frequency, or harmonics, as that of the driving stimulation [2]. SSVEP have a very stable amplitude and phase over time and are most prominent over parieto-occipital cortical areas [3]. SSVEP have a high signal to noise ratio [4] and are not very susceptible to artifacts and noise contamination [5, 6].
SSVEP are largely used in research and practical applications. In cognitive neuroscience, they are used to estimate the propagation of brain activity during a cognitive task [7]. In clinical settings, SSVEP are used as a diagnostic tool to study pathological brain dynamics [8]. However, the main application of SSVEP is in brain-computer interfaces (BCI). SSVEP are used to establish a direct communication between a brain and a computer without the need of muscular intervention [9] by identifying the frequency of the RVS [10] in the EEG recorded from a participant scalp.
One of the main disadvantages of SSVEP is the discomfort and safety issues associated with the prolonged exposure to RVS. Epileptic seizures [11] and migraines [12] are examples of side effects associated to continuous exposure to flickering light. Among various characteristics of the RVS, people are very sensitive to its frequency and modulation depth (MD). MD is a measure of light contrast that quantifies the relation between the spread and sum of two luminances during periodic oscillations [13]. For a time-varying luminance, MD is an indication of the ratio between the average light level and the amount of change in the light. The equation to calculate MD can be found below:

$$MD = \frac{L_{max} - L_{min}}{L_{max} + L_{min}} * 100 \quad (1)$$

where:

MD = modulation depth

L_{max} = maximum luminance

L_{min} = minimum luminance

The relationship between MD, frequency and visual perception of RVS has been described by the contrast sensitivity curve (CSC) [14]. The curve defines the visual perception thresholds (VPT): the lowest MD for a particular frequency at which people perceive RVS as discontinuous for at least 50% of the attempts. In recent years an updated version of the CSC, using the entire visual field and controlling for adaptation was created [13] (Fig. 1).

Contrary to the vast volume of research on visual perception there is little known about the effect of the frequency and MD of the stimulation on SSVEP. There is not a CSC describing the lowest MD necessary to elicit SSVEP at different frequencies. If there is a relationship between frequency, MD and SSVEP strength as in visual perception research, the MD of the RVS can be adjusted at different frequencies to reduce discomfort.

Published by Verlag der TU Graz
Graz University of Technology

 DOI: 10.3217/978-3-85125-533-1-05

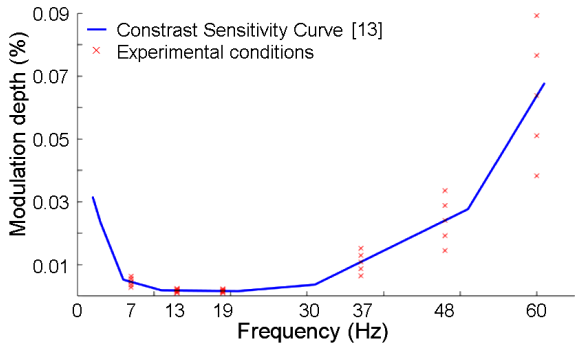

Figure 1: Contrast sensitivity curve (CSC) [13], and the experimental conditions in the current study.

To our knowledge, there are only two studies that have investigated the effect of frequency and MD on SSVEP [15, 16]. One study used RVS with frequencies from 8 to 48 Hz at MDs relative to the VPT described by the first version of the CSC [14]. They found SSVEP for frequencies higher than 24 Hz and MDs below the VPT [15]. In another study, five frequencies from 6 to 60 Hz at five absolute MDs from 0.002 to 0.026 were used. They found SSVEP only for the frequencies 24 and 32 Hz at MD starting at 0.008 and for 40 Hz at MD starting at 0.002 [16].
In this study, we aim to investigate the effect of frequency and MD on the SSVEP response and to find the lowest MDs necessary to elicit SSVEP for frequencies in the range of the CSC (1 to 70 Hz). For this purpose we employed the full field CSC described in [13] (see also Fig. 1). Furthermore, to get a better resolution, we expanded the sampling area around the VPT, compared to the previous two studies, and included conditions (i.e. frequency-MD pairs) that were not tested earlier.

MATERIALS AND METHODS

Participants: Twenty-four healthy volunteers with normal or corrected to normal vision were included in the study: 17 males and 7 females (mean age = 26.4; SD = 6.0). Participants were recruited among the Philips employee population at High Tech Campus, Eindhoven. Before the study, participants signed a written consent letter. The research protocol was approved by the Philips Research Ethics committee board.

Experimental task: The flicker perception task consisted of 300 trials. A trial started with 3 seconds of continuous light, followed by a beep, and 3 seconds of RVS, followed by 2 beeps, and another period of continuous light that continued until the participant provided a response (Fig. 2). Participants were instructed to look with their eyes open at a fixation cross in the middle of a white wall in front of them, where the light was projected (Fig. 3). They were asked to indicate whether or not they perceive flicker by pressing a “yes” and “no” button on a number pad.
The trials were presented randomly in three blocks of 100 trials. Each block lasted approximately 14 minutes and was followed by a break of a variable duration (3-10 minutes). A full session had a duration of approximately one hour and fifteen minutes. The EEG was continuously recorded while the participants performed the task.

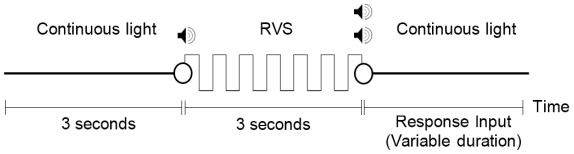

Figure 2: Structure of a trial in the flicker perception task. *Note.* RVS = Repetitive visual stimulation.

Stimuli: The RVS consisted of 30 distinct square waveforms (6 frequency x 5 MDs) that were repeated 10 times each. These conditions were created from the combination of 6 frequencies - 7, 13, 19, 37, 48 and 60 Hz - and 5 MDs selected as a proportion of the corresponding VPT of each frequency - 0.6x, 0.8x, 1.0x, 1.2x, and 1.4x. The experimental conditions are visualized in Figure 1. The light stimulation was delivered via two LEDs panels with a size of 57.5 cm x 57.5 cm suspended at a height of 2.5 m. The light stimulation was reflected on a white wall covering and area of approximately 210 cm x 360 cm (vertically x horizontally). Participants were seated at a distance of 70 cm with a visual angle of 137°. The average light luminance level was 1000 Lux and the color temperature was 4000 K.

Data acquisition: EEG data was recorded from 32 scalp sites using an elastic cap and a BioSemi^{TM} ActiveTwo signal acquisition system. Common Mode Sense Active and Driven Right Leg passive electrodes were used as ground and reference electrodes respectively. Offset values were maintained below 20 kΩ, and the sampling rate was at 2048 Hz. The onset of RVS was recorded using a photodiode placed at a distance of approximately 70 cm to the wall. The photodiode recorded the variations of the light reflected on the wall, and those variations were used to identify the start and the end of the trials in the EEG.

Data pre-processing: EEG signals were notch filtered at power-line frequency (50Hz) and then re-sampled at 256 Hz. Then, the signals were high-pass filtered at 2 Hz and blinks were removed by Independent Component Analysis [17]. After that, signals were re-referenced to a

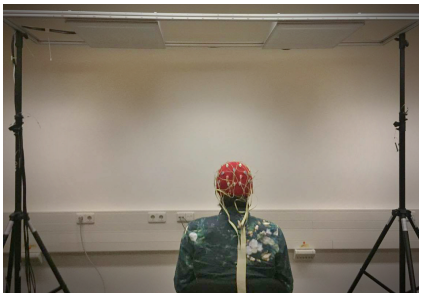

Figure 3: The experimental setup. The picture depicts a participant wearing and EEG cap and the LED panels.

Published by Verlag der TU Graz
Graz University of Technology

 DOI: 10.3217/978-3-85125-533-1-05

common average reference excluding T7 and T8 channels. Finally, the data was separated into non-overlapping epochs of 3 seconds, starting at stimulus onset (during stimulation epochs) and 3 seconds before stimulus onset (before stimulation epochs, baseline). The procedures were conducted using EEGLAB [18] and custom-made MATLAB scripts.

RESULTS

Behavioral responses: We calculated the rates at which people perceive RVS as discontinuous by averaging across all participants the number of "yes" responses per condition. We sought the lowest MDs at which participants perceive RVS as discontinuous in at least 50 percent of the conditions. The perception rate of 0.5 was reached in for frequencies 7 Hz and 60 Hz at MD 0.8x VPT and for frequencies 37 Hz and 48 Hz at MD 0.6x VPT. The 0.5 perception rate was not reached for frequencies 13 and 19 Hz. All the conditions had an increase in perception rates with an increase of MD.

SSVEP analysis: Power spectral density (PSD) of the EEG signal was estimated to measure the strength of the SSVEP. PSD is a measure of the power of a signal in the frequency domain and it was obtained by the use of fast Fourier transform (FFT). The FFT was applied on segments of the length of 256 samples (1 second) and an overlap of 128 samples (0.5 seconds) separately for epochs before and during stimulation (see Fig. 4). Characteristic peaks during stimulation at the frequency of stimulation were observed at 37, 48 and 60 Hz starting from MD 0.6x VPT, and were higher for higher MDs. Furthermore, during stimulation there was a decrease in power around the alpha frequency band (8-12 Hz) compared with the baseline.

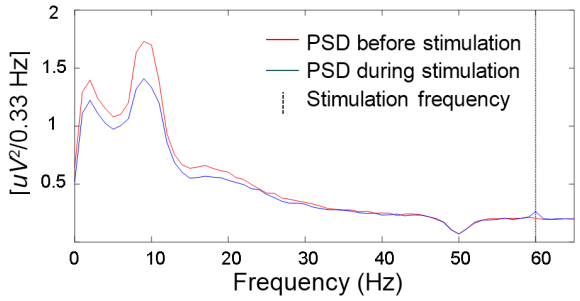

Figure 4: Power spectrum density for a condition (60 Hz and MD 1.4x VPT) at channel Pz.

To get a more objective estimation of the power change due to the RVS, PSD during stimulation was compared with PSD in the absence of flicker, before stimulus onset. To do so for each stimulation epoch we calculated a Z_{score} by subtracting the log PSD mean over all baseline epochs and dividing by the baseline log PSD standard deviation as shown in Equation 2. Positive Z_{scores} are an indication of higher power during stimulation, and they were observed for frequencies 37, 48 and 60 Hz for MDs even below 1.0x VPT (Fig. 5). Overall, Z_{scores} were larger for higher frequencies and for higher MDs.

$$Z_{score} = \frac{x - \mu}{\sigma} \tag{2}$$

where:

x = log PSD during a stimulation epoch

μ = log PSD mean baseline

σ = log PSD standard deviation baseline

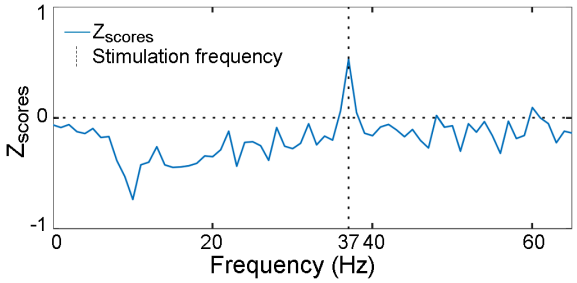

Figure 5: Z_{scores} for a condition (37 Hz and MD 1.2x VPT) at channel Pz.

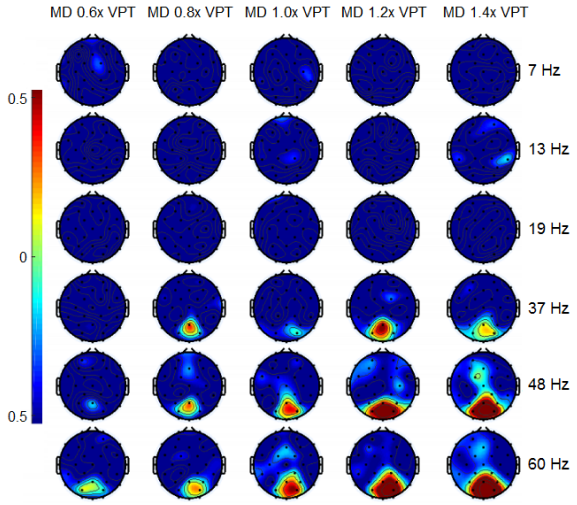

Figure 6: Spatial distribution of Z_{scores} for all the conditions. The color bar located at the left represents the Z_{scores}.

The spatial representation of the Z_{scores} can be observed in the topographic maps of the scalp in Fig. 6. The higher scores were observed in parietal (Pz) and occipital (O1, Oz, and O2) channels. The scores were higher for the higher frequencies and MDs. Frontal and temporal sites did not show significant changes associated with an increase of frequency or MD. Channel Pz displayed very consistent results across the different conditions and analyses, and we selected it for results visualization.
To better estimate the thresholds at which we can distinguish an SSVEP response from the absence of such with sufficient confidence, we selected the Z_{scores} defined by an equal probability of type I and type II errors (equal

Published by Verlag der TU Graz
Graz University of Technology

 DOI: 10.3217/978-3-85125-533-1-05

error rate, EER). The EER finds the point at which the probability of both types error is equal. The lower the EER the higher the accuracy of the measurement. The three lower frequencies 7, 13 and 19 Hz have EERs at chance level. An increase in MD was not associated with either an increase or decrease in the EER values for all the frequencies (Fig. 7).

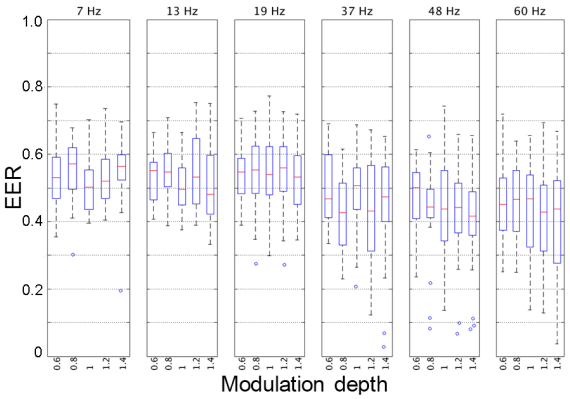

Figure 7: EER distribution at channel Pz. The box edges are the 25th and 75th percentiles. Outliers are plotted by small blue circles. Modulation depths are relative to the VPT (e.g. 0.6x VPT).

Z_{scores} and EER values were combined into a new metric ZEER: Z_{scores} at the EER. ZEER measure the strength of SSVEP, a weak SSVEP response reflected on a low Z_{scores} can be boosted by the EER in case the distribution of the samples before and during stimulation has a small overlap. On the contrary, a strong SSVEP response based on a high Z_{score} can be reduced if there is a big overlap in the distributions before and during stimulation. The ZEER were computed according to the Eq. 3.

$$\begin{aligned} if \quad EER \geq 0.5 \quad or \quad Z \leq 0 \\ then \quad Z_{EER} = 0 \end{aligned} \qquad (3)$$

$$\begin{aligned} if \quad EER \leq 0.5 \quad or \quad Z \geq 0 \\ then \quad Z_{EER} = Z * (1\text{–}EER) \end{aligned}$$

where:

EER = Equal Error Rate

$Z = Z_{score}$

ZEER = Z_{score} at the EER

Sensitivity curves estimation for SSVEP: We used two methods to create estimations of CSC for SSVEP, a curve containing the lowest MDs necessary to elicit SSVEP. The absolute modulation depth method (AMD) finds the lowest MD for which the ZEER is greater than zero in at least 50% of the trials . ZEER values greater than zero in at least 50 percent of the trials for a condition are an indication that SSVEP responses were elicited for that condition (see Table 1). These thresholds were found for frequencies 37, 48 and 60 Hz for MDs starting at 0.6x the VPT, and for frequency 13 Hz for MD starting at 1.0x VPT.

Table 1: Percentage (%) of ZEER scores with values greater than 0 at Pz channel.

	Frequency					
MD	7	13	19	37	48	60
0.6	37	35	36	42	48	50
0.8	33	33	38	57	52	54
1.0	45	41	37	48	51	54
1.2	37	32	31	56	55	56
1.4	36	40	37	53	53	58

Note. Gray cells indicate the lowest MD at which ZEER scores were greater than 0 in at least 50 percent of the trials.

The psychometric method (PM) makes use of a psychometric function. This method models the observed data, ZEER values, with a non-linear square regression model to estimate the coefficients of the nonlinear regression function and with that estimate the exact MD at which the SSVEP could be elicited in at least 50% of the conditions.

$$L(x;\alpha,\beta) = \frac{1}{1+e^{\frac{\alpha-x}{\beta}}} \qquad (4)$$

where:

definition range: $x \in (-\infty, +\infty)$

parameter set: $\theta = (\alpha, \beta)$

with:

$\alpha \in (-\infty, +\infty)$: position parameter

$\beta > 0$: spread parameter

AMD and PM curves together with the CSC from literature [13] can be observed in Fig. 8. Both SSVEP sensitivity curves had a similar shape and MD thresholds lower than the CSC. The MD thresholds estimated by the Psychometric method were lower than the AMD method. Furthermore, contrary to the AMD method, PM allows us to estimate the MD thresholds even for lower frequencies, e.g. 7 and 13 Hz. Those values appeared way above the MDs around the CSC. Based on our data, we could not estimate a threshold for frequency 19 Hz.

DISCUSSION

SSVEP were elicited for the highest frequencies (37, 48, and 60 Hz) for MDs below the VPT, e.g. 0.8x VPT. Consistent with visual perception research, we found out that the relationship between frequency and MD involves an increase in MD with an increase in frequency: higher MDs are required for SSVEP detection at higher frequencies. For instance, the lowest MD that elicited SSVEP at 60 Hz is more than double the lowest MD that elicited

Published by Verlag der TU Graz
Graz University of Technology

 DOI: 10.3217/978-3-85125-533-1-05

SSVEP at 48 Hz. In addition, the estimated contrast sensitivity curve for SSVEP has a similar shape to the CSC. Both curves show an increase of MD with an increase in frequency and this increase is particularly large for frequencies greater than 40 Hz.
SSVEP were not found for the three lowest frequencies at any MD. According to the PM, the MD thresholds for low frequencies lie much higher than the CSC. For instance, the estimated MD threshold at 7 Hz is around ten times higher than the VPT. This might be because at these frequencies the MDs covered by our choice of conditions were in general very low. This range also falls very close to the alpha band, which is known to desynchronize during visual processing [19].
The behavioral responses in our study were aligned with with existing research. The MD at which participants were able to perceive the flicker were around the CSC [13], and an increase in MD was associated with a higher perception rate. This suggests that our task was appropriate to evaluate perception of RVS.

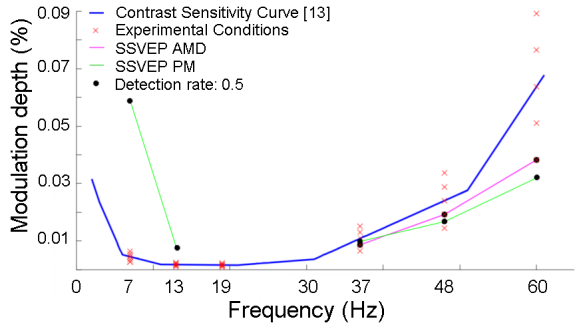

Figure 8: Contrast sensitivity curve (CSC)[13] and the SSVEP-AMD and SSVEP-PM sensitivity curves. Black dots indicate the MD at which SSVEP reaches 50% detection rate.

CONCLUSION

In this paper we studied the effect of stimulation properties, such as frequency and MD, around human visual perception thresholds on the SSVEP response. We were able to elicit SSVEP around the VPT but only for high frequencies. SSVEP were detected close or below to the behavioral CSC found in the literature, i.e by a quasi-imperceptible RVS. We estimated a contrast sensitivity curve based on SSVEP using two different methods. The shape of the estimated SSVEP contrast sensitivity curves is very similar to the behavioral CSC. Such sensitivity curve will help the development of a more diverse variety of stimuli, using more frequencies and MDs. This would increase the conditions that could be used to elicit distinct SSVEP and decrease the discomfort and the risk of photo-induced epilepsy caused by the RVS.

REFERENCES

[1] Regan D. Steady-state evoked potentials. JOSA. 1977;67(11):1475-1489.

[2] Regan D. Methods for recording Steady-State Evoked Potentials. In: Regan D. (Ed.) Human Brain Electrophysiology: Evoked Potentials and Evoked Magnetic Fields in Science and Medicine. Elsevier Science Publishing Co., Inc., New York 1989, pp. 70-111.

[3] Regan D. Some characteristics of average steady-state and transient responses evoked by modulated light. Electroencephalography and clinical neurophysiology. 1966;20(3):238-48.

[4] Norcia AM, Appelbaum LG, Ales JM, Cottereau BR, Rossion B. The steady-state visual evoked potential in vision research: a review. Journal of vision. 2015;15(6):1-46.

[5] Perlstein WM, Cole MA, Larson M, Kelly K, Seignourel P, Keil A. Steady-state visual evoked potentials reveal frontally-mediated working memory activity in humans. Neuroscience letters. 2003;342(3):191-5.

[6] Gray M, Kemp AH, Silberstein RB, Nathan PJ. Cortical neurophysiology of anticipatory anxiety: an investigation utilizing steady state probe topography (SSPT). Neuroimage. 2003;20(2):975-86.

[7] Morgan ST, Hansen JC, Hillyard SA. Selective attention to stimulus location modulates the steady-state visual evoked potential. Proceedings of the National Academy of Sciences. 1996;93(10):4770-4.

[8] Sartucci F, Borghetti D, Bocci T, Murri L, Orsini P, Porciatti V, Origlia N, Domenici L. Dysfunction of the magnocellular stream in Alzheimer's disease evaluated by pattern electroretinograms and visual evoked potentials. Brain research bulletin. 2010;82(3):169-76.

[9] Van Erp JB, Lotte F, Tangermann M. Brain-computer interfaces: beyond medical applications. Computer-IEEE Computer Society. 2012;45(4):26-34.

[10] Bi L, Fan XA, Liu Y. EEG-based brain-controlled mobile robots: a survey. IEEE Transactions on Human-Machine Systems. 2013;43(2):161-76.

[11] RS Fisher, G Harding, G Erba, GL Barkley, A Wilkins. Photic-and Pattern-induced Seizures: A Review for the Epilepsy Foundation of America Working Group. Epilepsia. 2005;46(9):1426-41.

[12] J Vanagaite, JA Pareja, O Støren, LR White, T Sanc, LJ Stovner. Light-induced discomfort and pain in migraine. Cephalalgia. 1997;17(7):733-41.

[13] Perz M, Sekulovski D, Vogels I, Flicker perception. Technical Report. Eindhoven, NB: Philips Research Europe. 2011.

[14] Kelly DH. Visual Responses to Time-Dependent Stimuli.* I. Amplitude Sensitivity Measurements. JOSA. 1961;51(4):422-9.

[15] Tsoneva T, Garcia-Molina G, van de Sant J, Farquhar J. Eliciting steady state visual evoked potentials near the visual perception threshold. In Neural Engineering (NER), 6th International IEEE/EMBS Conference, San Diego, USA, 2013, 93-96.

[16] Tsoneva T, Garcia-Molina G, Lazo M, Sekulovski D. New Metric to Characterize SSVEPs at the Edge of

Published by Verlag der TU Graz
Graz University of Technology

 DOI: 10.3217/978-3-85125-533-1-05

Perception. 36th International IEEE/EMBS Conference, Chicago, USA, 2014.
[17] Hyvärinen A, Karhunen J, Oja E. What is Independent Component Analysis? In: Hyvärinen A, Karhunen J, Oja E, editors. Independent component analysis. New York, NY: John Wiley Sons; 2004, pp. 146-164.
[18] Delorme A, Makeig S. EEGLAB: an open source toolbox for analysis of single-trial EEG dynamics including independent component analysis. Journal of neuroscience methods. 2004;134(1):9-21.

[19] Tsoneva T, Garcia-Molina G, Desain P. Neural dynamics during repetitive visual stimulation. Journal of neural engineering. 2015;12(6):066017.

Published by Verlag der TU Graz
Graz University of Technology

Proceedings of the
7th Graz Brain-Computer Interface Conference 2017 DOI: 10.3217/978-3-85125-533-1-06

BRAIN-COMPUTER INTERFACING WITH EMOTION-INDUCING IMAGERY: A PILOT STUDY

A. D. Bigirimana[1, 2], N. Siddique[1], D. Coyle[1]

[1] Intelligent Systems Research Centre, Ulster University, Derry, UK
[2] College of Science and Technology, University of Rwanda, Huye, Rwanda

E-mail: Bigirimana-a@ulster.ac.uk

ABSTRACT: Using neural correlates of intentionally induced human emotions may offer alternative imagery strategies to control brain-computer interface (BCI) applications. In this paper, self-induced emotions, i.e., emotions induced by participants performing sad or happy related emotional imagery, are compared to motor imagery (MI) in a two-class electroencephalogram (EEG)-based BCI. The BCI setup includes a multistage signal-processing framework allowing online continuous feedback presentation in a game involving one-dimensional control of game character. From seven participants, the highest online classification accuracies are 90% for emotion-inducing imagery (EII) and 80% for MI. Offline and online results analysis showed no significant differences in MI and EII performance. The results suggest that EII may be suitable for intentional control in BCI paradigms and offer a viable alternative for some BCI users.

INTRODUCTION

Brain-computer interfaces (BCIs) offer means to communicate and control computer-based applications without movement, including entertainment [1], [2] (e.g. BCI games), rehabilitation [3] and assistive technologies. BCIs are built around decoding the person's intent by direct measurement of brain activity [4], usually measured through electroencephalography (EEG). One of the challenges in BCI is that there are limited options for control strategies available to the users: some strategies, e.g., motor imagery, are challenging for some users and require training [5], [6], and other strategies (evoked potentials) often require gaze control and are dependent on external stimuli. As a non-negligible portion of subjects have been shown to be unable to learn how to control a motor imagery (MI) BCI [5], within a limited duration of training there is a need for investigation of alternative imagery strategies for such users.

Emotion is being investigated as a potential BCI control strategy. The differences observed in brain responses to different emotional stimuli or recall of emotional events may enable a multi-class BCI [7]. Positive emotions (e.g., happy, joy) are associated with less relative alpha power in left frontal cortical regions than the right, whereas for negative emotions (e.g., sad, disgust) less relative alpha power is observed in the right frontal cortical area [8], [9], and similar hemispheric asymmetry activation was reported in functional imaging [10]. Besides the differences in brain activity associated with different emotions, for emotion to be useful in active independent BCIs, where the user issues a command as opposed to waiting on a stimulus to evoke a brain response, the BCI user is required to imagine or recall emotional situations. Chanel et al. [11] reported an accuracy of 71.3% in two-class classification of self-induced emotion, in their study, the participants were self-paced in the task of self-inducing emotion. In similar study, Chanel et al [12] achieved an accuracy of 63% in a three-class (negative emotion, positive emotion, and neutral) and 80% for two-class classification. In their study, the participants were asked to recall emotional events in an 8 s trial. Furthermore, Iacoviello et al. [13] achieved a classification accuracy of 90.2% for imagery induced by remembering unpleasing odor versus relaxed state. Sitaram et al. [14], in fMRI-based study, presented performance feedback to participants who were recalling sad, happy, and disgust emotions, and achieved an accuracy of 60% in a three-class classification with feedback presentation. Only a few of previous work have applied emotion-inducing imagery with real or pseudo-real time feedback presentation. In a typical BCI system, the user should be provided with interaction feedback.

In the preliminary study on EII [15], participants controlled a video game character using sad and happy imageries, and their performance suggested that the use of emotion-inducing imageries in BCI should be investigated. Here, imageries of self-induced emotional states are investigated as an alternative to MI, using a standard MI BCI paradigm and setup with healthy human participants. Performance results of imageries induced by sad versus happy events compared to results of left versus right hand movement imageries during the one-dimensional control of a video game character are reported.

MATERIALS AND METHODS

Participants: Seven healthy volunteering participants (1 female and 6 men, mean age 29, SD = 6) were recruited at Ulster University. Each participant, individually participated in one EEG recording session,

Published by Verlag der TU Graz
Graz University of Technology

 DOI: 10.3217/978-3-85125-533-1-06

and after the session the participant was asked, in an informal interview, what he/she thought about his/her performance in task execution during the session. Six of the participants had previously participated in at least one motor imagery BCI study, and one of these six participants was known to have a good performance in MI. The remaining participant was participating in active BCI paradigm for the first time. All the seven participants had not previously participated in EII BCI training prior to the study.

Experimental Setup: Each EEG recording session included four runs: two EII runs and two motor imagery runs. Each type of imagery consisted of one training run and one online feedback run as shown in Fig. 1. The order of runs was randomized between participants i.e., either EII or MI was performed in the first two runs. The recording session utilized a computer game paradigm called NeuroSensi, in which a light, representing a neuronal spike, traversed the left or right graphical axon (see Fig. 2) on the computer screen, cued the participant to perform one of two imageries i.e., left versus right hand movement, or sad versus happy emotion-inducing imagery. In feedback runs, the game objective was to collect the spike by moving the game character (a graphical representation of neuron's cell body and dendrites as shown in Fig. 2). Points are awarded for moving the game character in the right direction and positioning the character as close as possible to the axon when the spike reached the end of the axon. Additional points are awarded for collecting more than three spikes consecutively without failure. These bonus points are accompanied with background neurons firing and propagating several spikes for about 1 s (after task execution). The continuous feedback, i.e., movement of the game character, was controlled by the BCI. Each run included 60 trials randomly ordered for two class tasks, 30 trials for each class. Before starting EII runs, the participant was instructed to identify two mnemonic or fictitious emotional events: one event he/she thought would make him/her happy and another events that would make him/her sad. To avoid possible emotional stress into the participants, they were instructed to refrain from using extremely sad events. During EII training runs, participants were asked to imagine or recall the sad event when the spike was cued on the left axon, and to imagine or recall the happy event when the cue appeared on the right hand side axon. In the case of motor imagery tasks, the participant was asked to imagine right hand movement when the cue was on right, and left hand movement when the cue appeared on the left side.

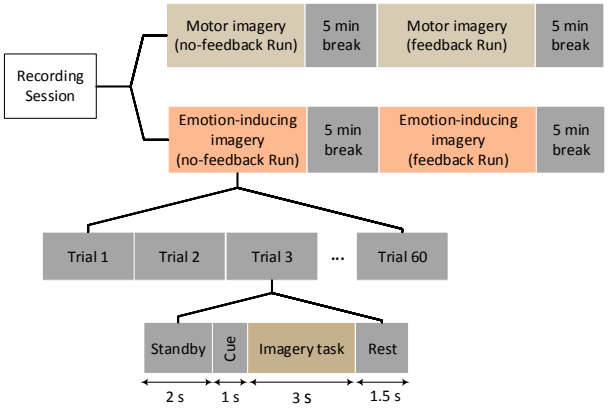

Figure 1. The structure of recording session. Each recording session had 4 runs of imagery tasks, each run with 60 trials (see details in text).

EEG data were sampled at 125 Hz from 16 channels (Fp1, Fp2, F3, Fz, F4, T7, C3, Cz, C4, T8, P3, Pz, P4, PO7, PO8, and Oz) setup in 10-20 system. EEG data were visually inspected for strong artefacts (e.g., eye-blinks) and then processed through a multistage signal processing framework which includes neural-time-series-prediction-preprocessing (NTSPP), spectral filtering (SF) in subject specific frequency bands and common spatial patterns (CSP) as previously used in [1], [16]. This signal processing framework is illustrated in Fig. 3.

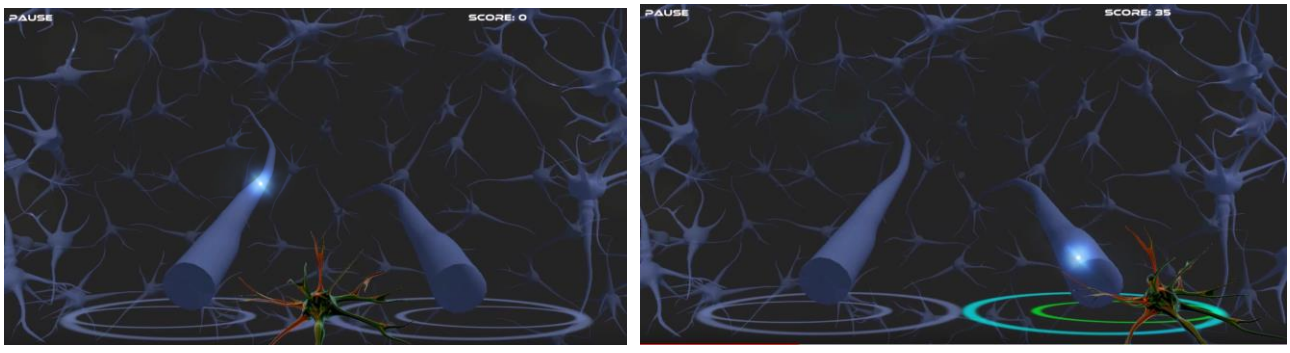

Figure 2. The screenshots of the BCI game used in cueing and feedback presentation. The neuron character is fixed in the middle of the two axons during no-feedback run (screenshot on the left), and it moves horizontally to collect the spike during the feedback run (screenshot on the right).

Published by Verlag der TU Graz
Graz University of Technology

 DOI: 10.3217/978-3-85125-533-1-06

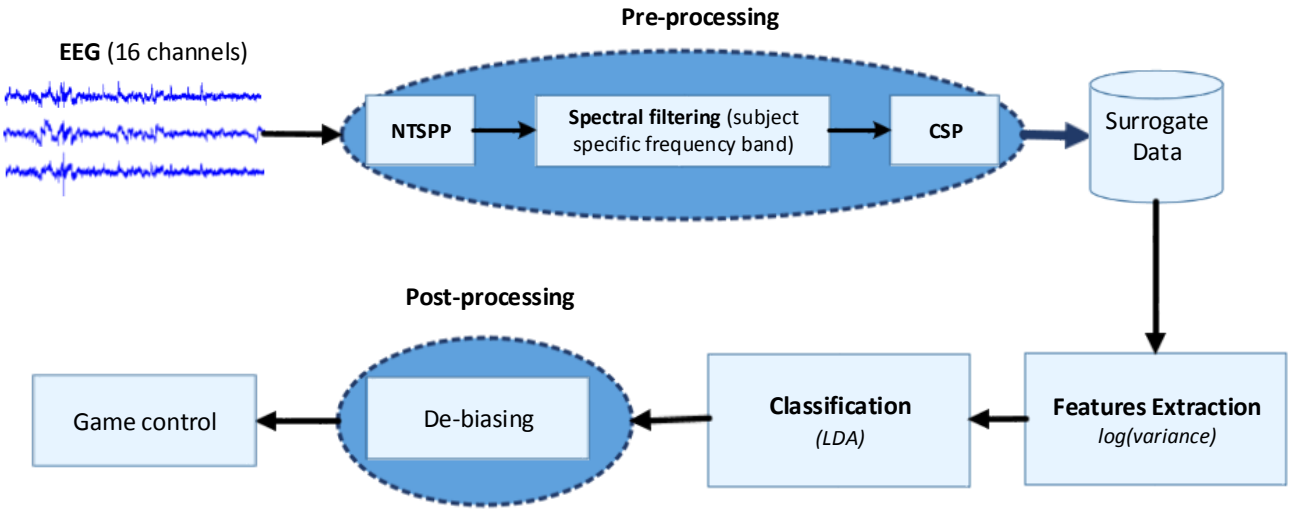

Figure 3. BCI setup used to preprocess EEG, extract and classify EEG features correlating to imageries; in the feedback session, the classifier's output is de-biased to adapt the feedback.

Time-Series-Prediction: In the NTSPP framework different prediction networks are trained to specialize in predicting future samples of different EEG signals. Due to network specialization, features extracted from the predicted signals are more separable and thus easier to classify. The number of time-series available and the number of classes governs the number of specialized predictor networks and the resultant number of predicted time-series from which to extract features

$$P = M \times C \tag{1}$$

where P is the number of networks (which is equal to number of predicted time-series), M is the number of EEG channels and C is the number of classes. For prediction,

$$\hat{x}_{ci}(t+\pi) = f_{ci}\left\langle x_i(t),\ldots,x_i(t-(\Delta-1)\tau)\right\rangle \tag{2}$$

where t is the current time instant, Δ is the embedding dimension and τ is the time delay, π is the prediction horizon, f_{ci} is the prediction model trained on the i^{th} EEG channel, x_i, i=1,..,M, for class c, c =1,..C, and $\hat{x}_{ci}$ is the predicted time series produced for channel i by the predictor for class c. NTSPP adapts to each subject autonomously using self-organizing fuzzy neural networks (SOFNN) [17].

Spectral Filtering: Prior to the calculation of the spatial filters, X can be preprocessed with NTSPP and/or spectrally filtered in specific frequency bands. The bands are selected autonomously in the offline data processing stage using a heuristic search and are subsequently used to band pass filter the data before CSP is applied. The search space is every possible band size in the 8 - 28Hz range. The high frequencies are not considered since they are likely to be contaminated with scalp electromyogram (EMG) [18], especially in the case of frowning associated with emotion-inducing tasks. These bands encompass the alpha, beta bands which are altered during sensorimotor processing [17], [19], [20] and for emotional state detection these bands or sub-bands within these bands are often used [21], [22].

Common Spatial Patterns (CSP): CSP is used to maximize the ratio of class-conditional variances of EEG sources. CSP is applied by pooled estimates of the covariance matrices, Σ_1 and Σ_2, for two classes, as follows:

$$\Sigma_c = \frac{1}{I_c}\sum_{i=1}^{I_c} X_i X_i^t \quad (c \in \{1,2\}) \tag{3}$$

where I_c is the number of trials for class c and X_i is the $M \times N$ matrices containing the i^{th} windowed segment of trial i; N is the window length and M is the number of EEG channels – when CSP is used in conjunction with NTSPP, M=P as per (1). The two covariance matrices, Σ_1 and Σ_2, are simultaneously diagonalized such that the Eigenvalues sum to 1. This is achieved by calculating the generalized eigenvectors W:

$$\Sigma_1 W = (\Sigma_1 + \Sigma_2) W D \tag{4}$$

where the diagonal matrix D contains the Eigenvalue of Σ_1 and the column vectors of W are the filters for the CSP projections. With this projection matrix the decomposition mapping of the windowed trials X is given as

$$E = WX \tag{5}$$

Features Extraction and Classification: Features, $\bar{\omega}$, are derived from the log-variance of preprocessed/surrogate signals within a 2 second sliding window:

$$\bar{\omega} = \log(\mathrm{var}(E)) \tag{6}$$

The dimensionality of $\bar{\omega}$ depends on the number of surrogate signals used from E. The common practice is to use several (between 2 and 6) eigenvectors from both ends of the eigenvector spectrum, i.e., the columns of W. Using NTSPP the dimensionality of X can increase significantly. CSP, can be used to reduce the

Published by Verlag der TU Graz
Graz University of Technology

 DOI: 10.3217/978-3-85125-533-1-06

dimensionality therefore combining NTSPP with CSP leads to increased separability while maintaining a tractable dimensionality [16]. Linear discriminant analysis (LDA) is used to classify the features at the rate of the sampling interval.

An inner-outer cross-validation (CV), with 5 outer folds, is performed to find the optimal subject-specific frequency. In the outer fold, NTSPP is trained on up to 10 trials randomly selected from each class (2 seconds of event related data from each trial). The trained networks then predict all the data from the training folds to produce a surrogate set of trials containing only EEG predictions. The 4 training folds from the outer splits are then split into 5 folds on which an inner 5-fold cross validation is performed for best subject specific frequency selection. After the subject specific frequency band selection, NTSPP-SF-CSP is then applied on the outer fold training set, where a feature set is extracted. The LDA classifier is trained at every time point across the trials and tested for that point on the outer test folds. The average across the five-folds is used to identify the optimal number of CSPs (between 1-3 from each side of W) and the final time point of maximum separation which are then used to setup the final classifier using all the training data, to be deployed online. The Fig. 3 illustrates the BCI setup used in this study.

In the online processing, the classifier's output translation to the game character movement was de-biased to account for class bias behaviour and improve feedback stability. This de-biasing was carried out by continuous removal of the mean from the continuous classifier output, where the mean was calculated with a 35s window on the most recent classifier output.

Additionally, EEG dynamics throughout tasks execution were also explored through event-related (de)synchronization (ERD/S) analysis. The ERD/S was computed as power change respective to the baseline power as in [23] within the subject's selected frequency band after applying independent components analysis and wavelet transform on the data for further artefacts removal [24].

RESULTS

Offline cross-validation classification accuracy (CA) for each run, along with online single-trial CA results for feedback runs, online results, and sample results from event-related (de)synchronization analysis are reported in Fig. 4, Fig. 5, Fig. 6, and Fig. 7 respectively. Wilcoxon signed rank tests showed no significant differences between EII and MI ($p > 0.05$), although the EII training accuracies exceed the MI accuracies for most of the participants. ERD/S analysis showed EII tasks separability in the temporal and frontal channels; this can be seen in sample topographic maps for subject 2 in Fig. 7. The online classification results in Fig. 5 show decrease in accuracies for most of the participants compared to what was achieved in offline analysis for the feedback run. However, in each of the considered BCI strategies, there was one participant who achieved good online performance: one experienced participant achieved 81% in MI and another achieved 90% in EII online performance. The performance in the remaining participants is 64.18 ± 4.75% and 62.09 ± 2.03% for EII and MI respectively.

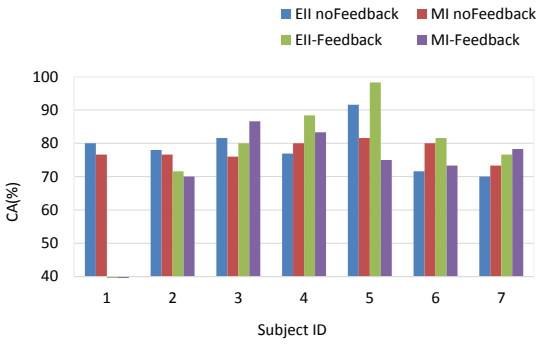

Figure 4. The LOOCV classification accuracy for feedback and no-feedback runs. There were no feedback runs for subject 1.

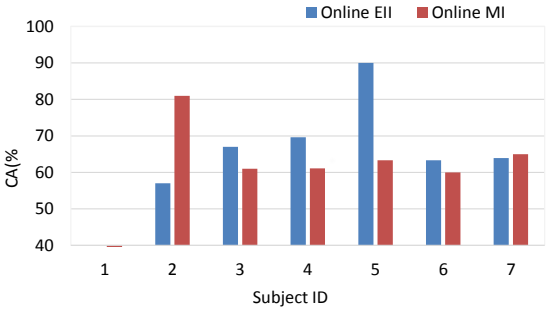

Figure 5. Online task classification accuracies for emotion inducing imagery and motor imagery during feedback runs. Note that there were no feedback runs for subject 1.

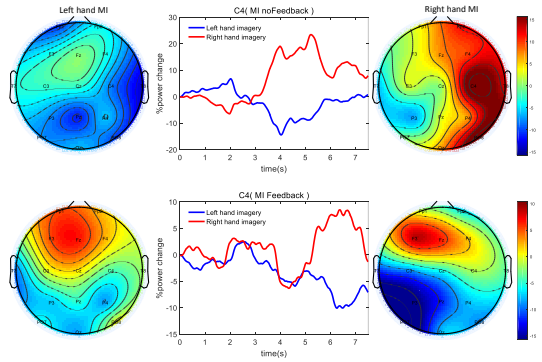

Figure 6. Topographic maps of band power changes (ERD/S) in [8–13] Hz band during motor imagery task execution for subject 2, and time-course ERD/S observed from channel C4.

Published by Verlag der TU Graz
Graz University of Technology

 DOI: 10.3217/978-3-85125-533-1-06

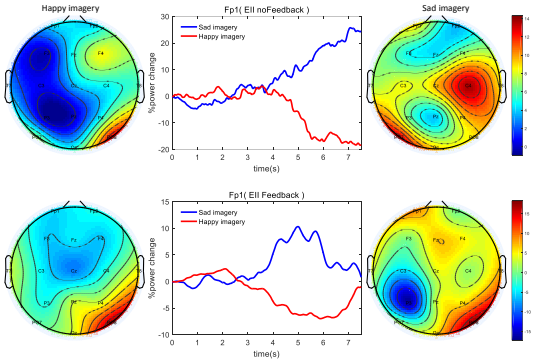

Figure 7. Topographic maps of band power changes in [8–20] Hz band during emotion inducing tasks execution for subject 2, and and time-course ERD/S from channel Fp1.

DISCUSSION

The objective of this pilot study was to investigate the discriminability of EEG during emotion inducing imagery, to investigate if emotion-inducing imageries could be used to control a video game using a BCI and to compare performances of EII with the extensively studied motor imagery based control strategies. The results suggest that emotions, which normally influence the way we live [25], may be intentionally modulated and actively translated in a BCI control paradigm. Consequently, the study shows some of the first evidence to support the use of emotion inducing imagery as a replacement to motor imagery. This study was based on one off-line training session and online training session for both MI and EII. Although participants were limited by the amount of training, their classification accuracies exceed chance level which was 50%. It usually requires several training sessions to achieve good accuracy in motor imagery performance, so further validation with multiple sessions training and on a larger sample of participants is required to determine if emotion imagery could be used by BCI users who do not perform well with motor imagery. Subject 2 who achieved high online performance in MI is familiar with motor imagery based BCI and had achieved good accuracies in the past. The participant with highest accuracy in online EII (subject 5) reported in the post-session interview that meditation practice was the key technique used in executing tasks for EII; meditation has been shown to improve BCI performance [26], [27]. Subject 2 also reported regular meditation practice.

Two participants showed acceptable online performance, whereas for the other participants' online performance is diminished with respect to the calibration run (the run without feedback). Even though a reduction in accuracy was observed in the online runs, the baseline accuracy (1 s before cue) were significantly lower that the peak accuracy during the task execution ($p < 0.05$) for all the participants indicating that above chance performance was achieved. In addition, as this is single session and participants experienced on-screen feedback for the first time (except subject 2) along with distractors in the games (game score updates and bonus firing spikes), this likely had an impact on participants' concentration, cognitive load [28] and maintaining focus and consistency between the runs. With additional sessions the BCI and participants' performance may be more robust.

CONCLUSION

Emotion induced by imagining fictional events or recalling mnemonic emotional events with a continuous feedback in a BCI setup was investigated in this preliminary study, using a setup normally used for motor imagery. The comparison between online control of a game in single session with either motor imagery and emotion-inducing imagery showed that the performance difference is insignificant, suggesting that emotion-inducing imagery may be used as an alternative to motor imagery. The reported results are from seven participants, each with one EEG recording session, so more analysis with a larger sample of participants and multiple training sessions is currently being carried out to thoroughly compare motor imagery and emotion inducing imagery BCI. Besides validating the comparison, there is a need to assess the effect of multiple training sessions on EII performance.

REFERENCES

[1] Coyle D, Garcia J, Satti AR, and McGinnity TM. EEG-based continuous control of a game using a 3 channel motor imagery BCI: BCI game. Proc. IEEE CCMB'11, Paris, France, 2011, pp. 1-7

[2] Ahn M, Lee M, Choi J, Jun SC. A review of brain-computer interface games and an opinion survey from researchers, developers and users. Sensors 2014;14(8):14601-14633

[3] Prasad G, Herman P, Coyle D, McDonough S, Crosbie J. Using Motor Imagery Based Brain-Computer Interface for Post-stroke Rehabilitation. Proc. IEEE EMBS'09, Minnesota, USA, 2009, 251-255

[4] Wolpaw JR, Winter Wolpaw E. Brain–Computer Interfaces: Something New under the Sun. In: Wolpaw J, Winter Wolpaw E (Ed.) Brain–Computer Interfaces Principles and Practice. Oxford University Press 2012, pp. 3-12

[5] Blankertz B, Sannelli C, Halder S, Hammer EM, Kübler A, Müller KR, et al. Neurophysiological predictor of SMR-based BCI performance. Neuroimage 2010;51(4):1303-1309

[6] Ahn, M, Cho, H, Ahn, S, Jun, S C. High Theta and Low Alpha Powers May Be Indicative of BCI-Illiteracy in Motor Imagery. PLoS One 2013;8(11):e80886

[7] Makeig S, Leslie G, Mullen T, Sarma D, Bigdely-Shamlo N, Kothe C. First Demonstration of a Musical Emotion BCI. Proc. ACII'11, Memphis, USA, 2011, 487–496

Published by Verlag der TU Graz
Graz University of Technology

 DOI: 10.3217/978-3-85125-533-1-06

[8] Davidson RJ, Ekman P, Saron CD, Senulis LA, Friesen WV. Approach-withdrawal and cerebral asymmetry: emotional expression and brain physiology. I. Pers. Soc. Psychol. 1990;58(2):330-341

[9] Allen JJ, Harmon-Jones E, Cavender JH. Manipulation of frontal EEG asymmetry through biofeedback alters self-reported emotional responses and facial EMG. Psychophysiology 2001 Jul;38(4):685-693

[10] Canli T. Hemispheric Asymmetry in the Experience of Emotion: A Perspective from Functional Imaging. Neuroscientist 1999;5:201-207

[11] Kothe CA, Makeig S, Onton JA. Emotion recognition from EEG during self-paced emotional imagery. Proc. ACII'13, Geneva, Switzerland, 2013, 855-858

[12] Chanel G, Kierkels JJM, Soleymani M, Pun T. Short-term emotion assessment in a recall paradigm. Int. J. Hum. Comput. Stud. 2009;67(8):607-627

[13] Iacoviello D, Petracca A, Spezialetti M, Placidi G. A real-time classification algorithm for EEG-based BCI driven by self-induced emotions. Comput. Methods Programs Biomed. 2015:122(3):293-303

[14] Sitaram R, Lee S, Ruiz S, Rana M, Veit R, Birbaumer N. Real-time support vector classification and feedback of multiple emotional brain states. Neuroimage 2011;56(2):753-765

[15] Bigirimana AD, Siddique N, Coyle D. Emotion Imagery BCI. Proc. BCI Meeting 2016, Pacific Grove, USA, 2016, 125-125.

[16] Coyle D. Neural network based auto association and time-series prediction for biosignal processing in brain-computer interfaces. IEEE Comput. Intell. Mag. 2009;4(4):47-59

[17] Coyle D, Prasad G, McGinnity TM. Faster self-organizing fuzzy neural network training and a hyperparameter analysis for a brain-computer interface. IEEE Trans. Syst. Man, Cybern. Part B Cybern. 2009;39(6):1458-1471

[18] Whitham EM, Pope KJ, Fitzgibbon SP, Lewis T, Clark CR, Loveless S, et al. Scalp electrical recording during paralysis: Quantitative evidence that EEG frequencies above 20 Hz are contaminated by EMG. Clin. Neurophysiol. 2007;118(8):1877-1888

[19] Pfurtscheller G, Neuper C, Schlögl A, and Lugger K. Separability of EEG signals recorded during right and left motor imagery using adaptive autorregresive parameters. IEEE Trans. Rehab. Eng. 1998;6(3):316-324

[20] Johnston SJ, Boehm SG, Healy D, Goebel R, Linden DEJ. Neurofeedback: A promising tool for the self-regulation of emotion networks. Neuroimage 2010;49(1);1066-1072

[21] Kim, M-K, Kim, M, Oh, E, and Kim, S-P. A Review on the Computational Methods for Emotional State Estimation from the Human EEG. Comput. Math. Methods Med. 2013;13:573734

[22] Mauss IB, Robinson M. Measures of emotion: A review. Cogn. Emot. 2009;23(2):209-237

[23] Pfurtscheller G, Da Silva FL. Event-related EEG/MEG synchronization and desynchronization: basic principles. Clin. Neurophysiol. 1999,110(11):1842-1857

[24] Bigirimana AD, Siddique N, Coyle D. A Hybrid ICA - Wavelet Transform for Automated Artefact Removal in EEG-based Emotion Recognition. Proc. IEEE SMC'16, Budapest, Hungary, 2016, 4429 - 4434

[25] Giorgetta C, Grecucci A, Bonini N, Coricelli G, Demarchi G, Braun C, et al. Waves of regret: A meg study of emotion and decision-making. Neuropsychologia, 2013;51(1):38-51

[26] Eskandari P, Erfanian A. Improving the performance of brain-computer interface through meditation practicing. Proc. IEEE EMBS'08, Vancouver, Canada, 2008, 662-665

[27] Tan LF, Dienes Z, Jansari A, Goh SY. Effect of mindfulness meditation on brain-computer interface performance. Conscious. Cogn. 2014;23(1):12-21

[28] Jong T. Cognitive load theory, educational research, and instructional design: Some food for thought. Instr. Sci. 2010;38:105-134

Published by Verlag der TU Graz
Graz University of Technology

Proceedings of the
7th Graz Brain-Computer Interface Conference 2017 DOI: 10.3217/978-3-85125-533-1-07

ADAPTIVE SPATIAL FILTERING: INCREASING THE EFFECTIVENESS OF MOTOR IMAGERY BASED BCI

Bartosz Binias[1]

[1]Data Mining Group, Institute of Automatic Control, Silesian University of Technology, Gliwice, Poland

E-mail: Bartosz.Binias@polsl.pl

ABSTRACT: In this article a novel approach to spatial filtering of electroencephalographic (EEG) signals – Adaptive Spatial Filtering (ASF) is proposed. The goal of ASF is to enhance the components of EEG signals that are specific to the spatial location of analyzed electrode, while at the same time to reduce the influence of components originating from distant sources of brain's bioelectrical activity. For that purpose an approach is utilized, where electrodes uncorrelated with analyzed electrode are used as noise input for the multichannel Adaptive Noise Cancelling algorithm. Proposed method is evaluated and compared with most popular approaches to spatial filtering: Common Spatial Patterns and its Filter Bank extension. Influence of compared algorithms on the classification accuracy of motor imagery tasks is tested on the data from 'Dataset IVa' provided for the 'BCI Competition III' and 'EEG Motor Movement/Imagery Dataset' provided by the BCI2000 group. During all performed tests ASF outperformed reference methods achieving 94%, 84% and 82% mean classification accuracies.

INTRODUCTION

Interpretation of the electroencephalographic (EEG) data often involves speculation about the possible locations of the sources inside the brain that are responsible for the observed activity on the scalp [1]. Since it is difficult to interpret recorded EEG signals in terms of the site of the underlying neuronal process, determining the relationship between different signals recorded at various scalp locations is required. It is desirable to eliminate or account for the possible linear relation resulting from the volume conduction [2]. This relation can be represented in a form of weighted combination of some or all measurement channels inside a defined neighbourhood of the channel of interest. Such approach is often related to as *spatial filtering*. It has gained a great popularity for EEG processing problems in Brain-Computer Interface (BCI) applications [3, 4]. In theory, use of spatial filters should either lead to decomposition of the EEG data into components containing activity related to specific sources or elimination of the overlapping signals originating from sources other than those in the direct neighbourhood of the measurement electrode. The Common Spatial Pattern (CSP) method represents one of the most popular approaches to the spatial filtering. Is is a technique used for the analysis of multichannel EEG recordings with two classes of different EEG phenomena present [3]. For that purpose it provides the set of spatial filters in form of the transformation matrix. One of the drawbacks of the CSP is that it's performance is highly dependent on the selected frequency bandwidth in which signals are analyzed. Thus, the theoretical assumption that the analysed signals have been bandpass filtered to the most discriminative frequency range for both classes [3]. An effective solution to this problem was presented as the Filter Bank CSP (FBCSP) [5]. In this method the EEG signals are first bandpass filtered into few frequency subbands. Then, the CSP algorithm is applied independently to each subband. Since its introduction, FBCSP has become a state-of-art approach for the spatial filtering of EEG signals containing motor imagery related tasks [5, 6].

In this article use of the Adaptive Noise Cancelling (ANC) techniques for the elimination of source overlapping effects from EEG recordings presented as a novel algorithm - the Adaptive Spatial Filtering (ASF) is being examined. The general idea of the proposed approach is based on the assumption that signal measured by each electrode consists not only of component that contains information specific to the location of that electrode, but also of unwanted ones that originate from sources closer to other electrodes available in the experiment. Therefore, signals recorded by these distant electrodes can be used as a noise reference for any multichannel algorithm of adaptive filtering. In theory, signal achieved as a result of such filtering will be free from the influence of electrical sources that are distant from the analysed electrode. At the same time, this decoupled recording will be a reliable representation of the neuronal activity occurring in the close localization of the measurement point. Use of adaptive filters is a known practice in the processing of EEG signals. Such algorithms are widely used for the removal and correction of artifacts that, due to their amplitude and shape, are clearly distinguishable from the background EEG activity (e.g. eye blinks, muscular artifacts, electrode movement) [7]. In these classical applications some additional reference recording of noise signal (i.e. electrooculogram) must be provided for the adaptation algorithm. Since such signal is not always available, a focus of researchers have been already drawn to

Published by Verlag der TU Graz
Graz University of Technology

 DOI: 10.3217/978-3-85125-533-1-07

the problem of utilizing EEG recordings for that purpose [7]. However, to the best knowledge of the Author of this article no research has ever been conducted on the use of such approach for the problem of elimination of source overlapping in EEG.

MATERIALS

Dataset IVa: One of two datasets used for the evaluation of proposed method was the 'Dataset IVa' provided for the 'BCI Competition III' organized by the Berlin Brain-Computer Interface group which took place in 2005 [4, 8]. All available signals were recorded using BrainAmp amplifiers with 118 EEG channels with 1000 Hz sampling frequency and 16 bit accuracy, band-pass filtered to the $0.05 \div 200$ Hz range and then downsampled to 100 Hz. The measurement electrodes were positioned with regard to the extended *10-20* montage system. Data was recorded from five healthy subjects denoted as *aa, al, av, aw, ay*. For each subject 280 trials of either right hand or foot movement imagination were available. Visual cues indicated for 3.5 s which of the motor action the subject should imagine [4]. Detailed information about used dataset can be found in [8].

EEG Motor Movement/Imagery Dataset: Second dataset used in this research was 'EEG Motor Movement/Imagery Dataset' (EEGMMI) provided by the BCI2000 group [9] and contributed to the PhysioNet platform [10]. Signals were recorded using 64 electrodes placed accordingly to the *10-10* montage system with $160Hz$ sampling frequency. The EEGMMI consists of data recorded from 109 subjects. Each of whom was asked to perform specific tasks organized in the following sessions (either 7 or 8 repetitions per task): right vs. left hand movement, imagination of right vs. left hand movement, both hands vs. feet movement and imagination of both hands vs. feet movement. Each session was repeated 3 times and lasted approximately 2 minutes. As a result between 21 and 24 trials per class were obtained. Duration of one trial was about 4-s long. In this research only sessions with tasks involving motor imagery were used. Additionally, since this work is focused on the two class problems, sessions involving Left vs. Right hand motor imagery were treated separately from the Hands vs. Feet sessions. As a result, two different validation experiments could be performed on the EEGMMI dataset.

Validation and parameter tuning: To test the proposed ASF algorithm the following validation procedure was performed. For 'Dataset IVa' all trials were divided into two sets depending on their class membership. Then trials in each set were sorted chronologically. 70% of consequent trials from each class were used to create a set used for the classifier training and parameter tuning purposes. The remaining samples formed a test set, which was used only once, to evaluate algorithm's accuracy. Both sets were designed in way so that both classes were represented equally. In order to assure that the results achieved during the experiment are statistically meaningful such validation was repeated 7 times. The new folds were created by selecting consecutive 70% of trials beginning from a different trial each time. These starting trials were evenly distributed across all examples, so that the best data coverage was provided. Consistency of the data was achieved by implementing the circular buffer idea in cases where the length of the training window exceeded the total data length. Organization of sessions in the EEGMMI dataset allowed to approach the problem of creating the data folds in a slightly different way. Since there were 3 repetitions of both Left vs. Right and Hands vs. Feet sessions (each containing $7 - 8$ trials per class) a more natural division was possible. In this research one complete session of specific motor imagery tasks was used as an independent test set, while remaining two sessions containing the same mental actions were used for training and parameter tuning purposes. That way it was ensured that both classes will be represented by a similar amount of examples. Additionally, such way of dividing data guarantees that trials used for testing were recorded during the same time window and that both test and train examples maintain some kind on continuity. Described validation procedures implemented for both datasets allow to take into consideration not only the order of samples from each trial but also the chronological order of the trials. Proposed approach resembles a real life case where training trials for the BCI calibration are recorded consequently during specified time frame. Such examples will share some common characteristics, that might differ for trials recorded in later stages (i.e. during the operation of the system). The resemblance of the proposed procedure of data partitioning to the real applications is a significant advantage over random choice of trials or individual samples. For most of the spatial filtering approaches presented in the METHODS section to perform on a satisfactory level, some parameters need to be properly selected. The method of parameter tuning used in this work requires that the data dedicated for training purposes is divided accordingly to the procedure described for the 'Dataset IV' earlier in this section. As a result two subsets of the training set are created, which will be referred to as subtraining and subtest. Then, the EEG signals are processed with the different values of the tuned parameter of specific spatial filtering method, the classifier is trained on a subtraining dataset and the accuracy on the subtest set is obtained. This is repeated 7 times and the parameter which achieved the highest median accuracy is selected for the specific validation session. It must be noted that the training data of the current validation session remains uninvolved in the parameter tuning process. Since Author of this article prioritize the research on the real-time BCI applications, instead of classifying each trial as a whole, the classifier output was provided for every sample tagged as containing imagination of motor movement and belonging to the assumed region of interest. Due to the nature of the experiment, the reaction time of the subject could potentially become a variable in the process of evaluation of system's accuracy. Since such influence

Published by Verlag der TU Graz
Graz University of Technology

 DOI: 10.3217/978-3-85125-533-1-07

is an uncontrollable factor, it is desirable to diminish or remove it's impact on the results. In this research, this problem was avoided by selecting and classifying only samples that appear after 0.5 s from the moment tagged as a start of the trial.

METHODS

Adaptive Spatial Filtering: The idea behind the Adaptive Spatial Filtering of EEG signals proposed in this work stems from the concept of Adaptive Noise Cancelling [11]. In this methodology an auxiliary (reference) input from at least one sensor is used in process of the elimination or attenuation of the noise present in the primary input s. Let us assume that the analyzed signal s consists of two additive components d_0 and n_0. Therefore, it can be represented as $s = d_0 + n_0$, where d_0 denotes the desired part of the s and n_0 is a noise that is not correlated with d_0. Additionally, present is an auxiliary signal n which also is not correlated with d_0, but in some unknown way correlates with the noise n_0. Such signals are often called reference and should be recorded at noise field locations where the signal of interest d_0 is weak [11]. Providing more than just one reference input to the ANC algorithm can improve it's performance in scenarios where one source of noise is present [11]. Moreover, if there are many sources of noise coming from different locations, increased number of auxiliary signals recorded by specific sensors can be very effective [11]. In such cases n will consist of N signals recorded by different sensors at varying locations. This can be noted as $n = \{n_1, n_2, \ldots, n_N\}$. For applications where $N > 1$ the algorithm is often referred to as Mutichannel Adaptive Noise Canceller. If each of the input reference signal components n_k ($k = 1, \ldots, N$) could be transformed (filtered) so that the their summed output $y = \sum_{k=1}^{N} y_k$ would resemble the unknown noise component n_0 it could then be subtracted from the analyzed signal s. Assuming that the signal n_k after the transformation is denoted as a y_k, described operation can be presented as in Eq. 1. As a result the estimate of uncorrupted desired signal $e \simeq d_0$ will be achieved. Signal e can also be treated as the error of adaptation.

$$e = d_0 + n_0 - y \tag{1}$$

In an ANC applications said transformation of recorded noise input n is realized by an adaptive filtering. An adaptive filter automatically adjusts its own impulse response through an algorithm that responds to an error signal e [11]. If $n_k(t) \in \mathbb{R}^M$ is a segment of signal n_k a time index t consisting of M discrete samples with indexed $[t - M + 1, \ldots, t - 1, t]$, then the output of a adaptive filter at discrete moment t can be calculated as in Eq. 2.

$$y_k(t) = n_k(t)^T w_k(t) \tag{2}$$

The coefficients $w_k(t) \in \mathbb{R}^M$ of the filter are being adjusted individually for every input with each new sample. The adaptive algorithm used for that in this work is the Normalized Least Mean Squares (NLMS). If algorithm's error at index t is denoted as $e(t) \in \mathbb{R}$ and calculated accordingly to the Eq. 1, then the formula for updating the filter coefficients for $t + 1$ sample is presented in Eq. 3.

$$w_k(t + 1) = w_k(t) + \mu(t)e(t)n_k(t) \tag{3}$$

The NLMS guarantees a better stability than the classical Least Mean Square algorithm thanks to the normalisation of the fixed adaptation step μ_0 with the power of input [12]. The purpose of γ parameter is to prevent situations where the denominator of that expression approaches 0.

$$\mu(t) = \frac{\mu_0}{\gamma + n_k^T(t)n_k(i)} \tag{4}$$

It should be particularly emphasized that the described Multichannel ANC algorithm satisfies all the causality requirements and therefore is suitable for the real time applications. The block diagram of the described algorithm is presented in Fig. 1.

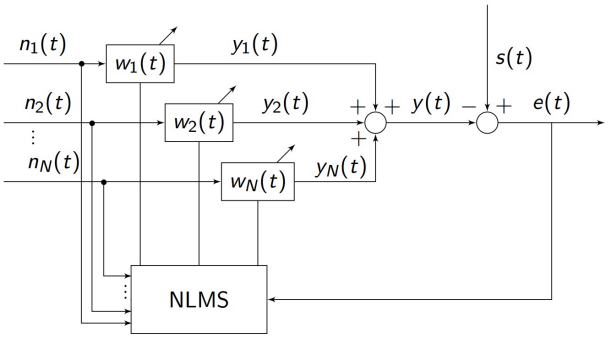

Figure 1: Block diagram of a Multichannel ANC filter.

The general idea of proposed ASF approach is based on the assumption that signal recorded by each electrode consists of desired component which contains information specific to the location of that electrode and unwanted, noise that originates from sources closer to other electrodes available in the experiment. Additionally, undefined measurement noise and artifacts (i.e. muscular) are in some way present in all recordings measured by all electrodes. With simplification it can be assumed that as the distance of the electrical signal from its bioelectrical source increases, its amplitude decreases [2]. However, it must be emphasized that said assumption does not state that activity originating from the source closest to the electrode will be the strongest one present in the raw EEG recording [13]. Nevertheless, the introduced assumption leads to an observation, that for the electrode labeled ch signals recorded by electrodes from some subset electrode labels $L_{ch} = \{L \setminus ch\}$ can be used as a noise reference for the multichannel ANC algorithm described earlier in this section. In this scenario, L denotes the set of all electrode labels that are available in the experiment. In

Published by Verlag der TU Graz
Graz University of Technology

 DOI: 10.3217/978-3-85125-533-1-07

theory, signal achieved as a result of such adaptive filtering would be free from the influence of electrical activity of sources that are distant from the analysed electrode ch. At the same, this decoupled recording will be a reliable representation of the neuronal activity occurring in the direct localization of the measurement point. To guarantee a satisfactory performance of the ASF, a proper selection of the subset of electrodes used as the multichannel noise reference must be ensured. According to the basic principles of the ANC algorithms, signals used for that purpose cannot be correlated with the filtered signal [11]. Therefore, for the analyzed electrode $ch \in L$ adaptation is performed only on the subset of electrodes L_{ch} for which the Pearson's correlation coefficient $r(ch, l)$ ($\forall_{l \in L}$) with signal from ch is lower than some user-defined parameter T_r. To maintain the compatibility with previously introduced symbols, in this scenario, the secondary input to the Multichannel ANC filter n will be composed of signals recorded by the electrodes whose labels belong to the subset L_{ch}. Therefore, proposed ASF algorithm requires for a few parameters to be specified, such as the number of filter coefficients M, initial adaptation step μ_0, parameter γ and the Pearson's correlation threshold used for selecting the reference electrodes T_r. During the experiments performed for the purpose of this work, the following, exemplary parameters were chosen for both datasets: $M = 3$, $\gamma = 0.01$, $T_r = 0.6$. To ensure the improved stability and effectiveness of the ASF algorithm the μ_0 was selected individually form the set of values $\mu_0 = \{0.0001, 0.0005, 0.001, 0.005, 0.01\}$ for each test with respect to the parameter selection approach described in the MATERIALS section of this article. During the experiment the ASF algorithm was applied to the raw EEG data. The subset of electrodes used as the reference L_{ch} was selected individually for each analysed electrode. The Pearson's correlation values $r(ch, l)$ were calculated only on the basis of time segments containing the interesting brain activity (i.e. during motor imagery periods) from training sessions. Therefore, L_{ch} was not updated after the training stage. The signal power features were extracted directly form the filtered data. All of them were passed to the classification algorithm (no feature selection stage was implemented). No artifact correction or bandpass filtering was applied for the additional processing of the EEG signals.

Reference methods: The influence of the proposed ASF algorithm on the accuracy of classifying various mental activity tasks was compared with three classical approaches. First method used as the reference during the comparison does not involve any spatial filtering and will be referred to as the *basic* approach. Here, the raw data is only bandpass filtered to the frequency range from 8 to $30Hz$. This specific band was selected as it is often associated with brain activity related to the planning of movement [3, 14]. The bandpower features are then extracted directly from the filtered data. No additional steps like feature/channel selection are used in this approach. The Common Spatial Pattern method is a technique used for the analysis of multichannel EEG recordings with two classes of different EEG phenomena present [3]. As a result of CSP the variance of the transformed signals is maximized for examples from one class, while at the same it is minimized for the other class. For that purpose it provides the set of optimal spatial filters in form of the transformation matrix. In general, only a few pairs of filters from both ends of eigenvalue spectrum carrying a discriminant information are used [3]. Therefore, a feature selection step is often required in order to maximize the effectiveness of CSP decomposition. In this work, the best number form between 1 and 8 of the consecutive CSP filter pairs were selected for each subject and each validation session during parameter tuning stage. Since performance of the CSP method is highly dependent on the selection of frequency bandwidth in which signals are analyzed, they were bandpass filtered to the frequency range from 8 to $30Hz$ befor the applying CSP. Third method used for the comparison in this research is the FBSCP [5]. In this method the recorded EEG signal is first bandpass filtered into B, small and consequent frequency subbands. In this research the same $B = 9$ subbands as in the original paper of FBCSP were selected: $[4-8]$ Hz, $[8-12]$ Hz, $[12-16]$ Hz, $[16-20]$ Hz, $[20-24]$ Hz, $[24-28]$ Hz, $[28-32]$ Hz, $[32-36]$ Hz, $[36-40]$ Hz [5]. After filtering, the CSP algorithm is applied independently to each frequency band. Then, for each CSP transformation a $C = 3$ pairs of filters were selected and bandpower features were calculated for each sample. As a result $F_0 = 2 \times C \times B = 54$ features were extracted for each time index in the region of interest. To avoid overfitting of the classifier to the training data, the FBCSP requires for the feature selection step to be performed. Authors of this method have validated it with multiple feature selection algorithms [5]. According to the results of the mentioned study, the Mutual Information-based Best Individual Feature (MIBIF) method works very effectively with the FBCSP. Based on the MIBIF only F_1 best features from the original subset of F_0 is chosen for the further analysis. In this work the number F_1 was selected individually for each subject and each validation session from the subset $F_1 \in \{1, 2, 3, 4, 5\}$ during the parameter tuning stage. It must be noted that due to the pairing of the CSP features, the corresponding feature from the pair had to be additionally included if it was not selected by the MIBIF algorithm.

All spectral filtering operations in this research were performed with the Finite Impulse Response (FIR) filter of order 364. Coefficients of the used filters were designed using the Kaiser window. Linear phase characteristics of the FIR filters make them ideally suited for the processing of biomedical signals. On the other hand, the delay introduced by such filtering may significantly influence the quality of the BCI systems in terms of real-time performance. Since the focus of this research was mostly placed on the evaluation of the proposed spatial filtering method it was decided that the filter's delay should be neglected. Therefore, the zero-phase filtering was applied

Published by Verlag der TU Graz
Graz University of Technology

 DOI: 10.3217/978-3-85125-533-1-07

during offline processing. This was achieved by a recursive filtering of the original signal both forward and backward in time [15]. As a result, a perfect frequency filtering could be assumed in the performed experiment. This operation was applied to all of the reference methods used in the experiment. It must be noted that such approach favours slightly these approaches as in the normal scenario their output would be delayed resulting in worse classification accuracy and generally decreased performance of the BCI system.

Machine learning: The characteristics of the signals achieved after their processing were described by the logarithm of their power in specific frequency ranges. To ensure the causality of the feature extraction step only the analysed time index and those that precede it were taken into consideration. In this research the 0.5 s-long time window was used. The features were extracted for every sample during each trial and provided as an input to the Linear Discriminant Analysis (LDA) classifier. This simple classifier has been successfully used in many BCI systems and has generally produced a satisfactory results [16]. One of the main motivations for the choice of LDA classifier in this experiment was it's simplicity and transparency in data processing. Thanks to these features, the participation of the classification algorithm in the feature engineering process has been restricted. Thanks to that, the results achieved in this research will not be biased by the quality of cooperation between spatial filtering algorithm and classifier in extracting features of the data.

RESULTS

In Tab. 1 presented are the mean accuracies obtained after 7 cross-validations performed for each subject from the Dataset IVa. For each sessions used in this test the best set of parameters was selected for each method. This was achieved with accordance to the parameter tuning approach described in the METHODS section of this work.

Table 1: Dataset IVa - mean accuracies

Method	Avg	aa	al	av	aw	ay
ASF	0.94	0.93	0.95	0.89	0.96	0.96
FBCSP	0.81	0.78	0.92	0.66	0.86	0.84
CSP	0.79	0.71	0.90	0.67	0.85	0.84
basic	0.70	0.62	0.82	0.57	0.71	0.76

A more informative summary of the experiment performed on the Dataset IVa can be found in Tab. 2. The statistics used for the description of the achieved results were the first quartile Q_1, mean value, third quartile Q_3 and standard deviation σ calculated from the accuracies of all tests performed on all subjects for each method. Therefore a more complex and profound overview of the experiment was achieved.

Table 2 - Dataset IVa - statistics

Method	Q_1	Mean	Q_3	σ
ASF	0.88	0.94	1.00	0.08
FBCSP	0.74	0.81	0.87	0.10
CSP	0.71	0.79	0.86	0.09
basic	0.62	0.70	0.77	0.10

Since the EEGMMI dataset contains a large number of subjects it was decided to omit the presentation of the average accuracies achieved for each of them. Instead, in Tab. 3 the statistics calculated for Hand vs. Foot classification task are shown. Likewise, same summary for Left vs. Right hand discrimination task is presented in Tab. 4. Values contained in both of these tables were obtained analogously to those presented in Tab. 2.

Table 3: EEGMMI (Hand vs Foot) - statistics

Method	Q_1	Mean	Q_3	σ
ASF	0.78	0.84	0.90	0.08
FBCSP	0.54	0.63	0.69	0.11
CSP	0.58	0.66	0.74	0.11
basic	0.54	0.60	0.63	0.09

Table 4: EEGMMI (Left vs Right) - statistics

Method	Q_1	Mean	Q_3	σ
ASF	0.76	0.82	0.89	0.10
FBCSP	0.52	0.57	0.60	0.08
CSP	0.55	0.62	0.66	0.10
basic	0.51	0.56	0.60	0.08

DISCUSSION

Proposed in this work ASF algorithm significantly outperforms classical spatial filtering methods like CSP and FBCSP during tests performed on two class motor imagery-based BCI datasets. Statistics calculated for the distributions of the achieved accuracies presented in Tab. 2- 4 allow further assessment of the ASF performance. It can be observed that for all three datasets the mean accuracies of ASF are higher than for the reference methods. Additionally, in all cases first quartile Q_1 of ASF is higher than third quartile Q_3 of other methods tested in this work. Although FBCSP and CSP achieved expected mean accuracies on the Dataset IVa their performance on the EEGMMI dataset is unsatisfactory. This might be explained by a relatively small number of training trials for each validation session which ranged from 14 to 16 per class. As a result the number of training examples provided for the CSP and its Filter Bank modification might be too small for them to achieve their full potential. Training BCI systems with a limited number of trials is a known problem which has been discussed in the literature [4].
The tests to which the ASF and reference methods were subjected to can be considered to be demanding not only due to the high number of repetitions performed for each dataset. The goal of providing the output for each sample is generally considered to be more a more difficult task

Published by Verlag der TU Graz
Graz University of Technology

 DOI: 10.3217/978-3-85125-533-1-07

than the classification of the whole trial [6]. However, since ASF was designed for the real-time BCI applications such approach to testing was necessary.
It must be noted that the due to their nature the adaptive filters and ANC algorithms (such as ASF) are susceptible to instabilities [12]. Therefore, selecting the proper adaptation step during the parameter tuning stage of the ASF method was very important. The issue of stability of the adaptive filtering algorithms used with the ASF method should be a subject of further research. Due to the preliminary character of this work the tuning of the channel correlation threshold T_r was omitted in this work. This shows that tuning of this parameter is not necessary for the ASF to achieve a high level results. Nevertheless, some future work must be devoted to the analysis of the influence of this parameter on the effectiveness of ASF, as it has the potential to additionally improve its performance.

CONCLUSION

In this article a novel approach to spatial filtering of EEG signals the Adaptive Spatial Filtering is proposed. The algorithm has proved to significantly outperform the classic reference methods for two class BCI problems. The fact that the ASF does not require providing the number of classes present in the experiment is a great advantage over CSP-based approaches. As a result it can be easily used with the multiclass problems without the need of implementing strategies like *One vs. One* or *One vs. All*. Additionally, adaptive properties of the algorithm make it insusceptible to the changes of the EEG characteristics which occurs with the passing of the experiment time. Author of this work believes that the introduction of the ASF algorithm can lead to an advancement in the usable BCI technology capable of operating in the real time. Future research regarding the ASF algorithm will focus on its application to multiclass BCI problems. Additionally, its performance with limited electrode configurations (i.e. International *10-20* Standard) and with feedback BCI systems will be evaluated.

ACKNOWLEDGEMENTS

This work was supported by Silesian University of Technology grant no. 02/010/BKM16/0047/31.

REFERENCES

[1] Koles ZJ. Trends in EEG source localization. Electroencephalography and Clinical Neurophysiology. 1998;106(2):127—137.
[2] Holsheimer J, Feenstra BWA. Volume conduction and EEG measurements within the brain: a quantitative approach to the influence of electrical spread on the linear relationship of activity measured at different locations. Electroencephalography and Clinical Neurophysiology. 1977;43(1):52-58.
[3] Blankertz B, Tomioka R, Lemm S, Kawanabe M, Müller KR. Optimizing spatial filters for robust EEG single-trial analysis. IEEE Signal Processing Magazine. 2008;25(1):41-56.
[4] Blankertz B, Müller KR, Krusienski DJ, Schalk G, Wolpaw JR, Schlögl A, et al. The BCI competition III: Validating alternative approaches to actual BCI problems. IEEE Transactions on Neural Systems and Rehabilitation Engineering. 2006;14(2):153—159.
[5] Ang KK, Chin ZY, Zhang H, Guan C. Filter bank common spatial pattern (FBCSP) in Brain-Computer Interface, in IEEE International Joint Conference on Neural Networks, Hong Kong, China, 2008, 2390—2397.
[6] Tangermann M, Müller KR, Aertsen A, Birbaumer N, Braun C, Brunner C. Review of the BCI Competition IV. Frontiers in Neuroscience. 2012;6:55.
[7] Binias B, Palus H, Jaskot K. Real-Time Detection and Filtering of Eye Blink Related Artifacts for Brain-Computer Interface Applications. In: Gruca A, Brachman A, Kozielski S, Czachórski T (Ed.). Advances in Intelligent Systems and Computing. Springer International Publishing, Kocierz, Poland 2015, pp. 281-290.
[8] Dornhege G, Blankertz B, Curio G, Müller KR. Boosting bit rates in noninvasive EEG single-trial classifications by feature combination and multiclass paradigms. IEEE Transactions on Biomedical Engineering. 2004; 51(6):993-1002.
[9] Schalk G, McFarland DJ, Hinterberger T, Birbaumer N, Wolpaw JR. BCI2000: A General-Purpose Brain-Computer Interface (BCI) System. IEEE Transactions on Biomedical Engineering. 2004;51(6):1034-1043.
[10] Goldberger AL, Amaral LAN, Glass L, Hausdorff JM, Ivanov PCh, Mark RG, et al. PhysioBank, PhysioToolkit, and PhysioNet: Components of a New Research Resource for Complex Physiologic Signals. Circulation. 2000;101(23): 215-220.
[11] Widrow B, Glover JR, McCool JM, Kaunitz J, Williams CS, Hearn RH, et al. Adaptive noise cancelling: Principles and applications. Proceedings of the IEEE. 1975;63(12): 1692-1716.
[12] Haykin SO. Adaptive Filter Theory, Prentice Hall (2001).
[13] Nunez PL, Srinivasan R, Westdorp AF, Wijesinghe RS, Ranjith S, Tucker DM, et al. EEG coherency: I: statistics, reference electrode, volume conduction, Laplacians, cortical imaging, and interpretation at multiple scales. Electroencephalography and Clinical Neurophysiology. 1997;103(5):499-515.
[14] Pfurtscheller G, Lopes da Silva FH. Event-related EEG/MEG synchronization and desynchronization: basic principles. Clinical Neurophysiology. 1999;110(11): 1842-1857.
[15] Smith JO. Introduction to digital filters: with audio applications, W3K Publishing, http://books.w3k.org/ (2007).
[16] Lotte F, Congedo M, Lécuyer A, Lamarche F. A review of classification algorithms for EEG-based Brain–Computer Interfaces. Journal of Neural Engineering. 2007;4.

Published by Verlag der TU Graz
Graz University of Technology

Proceedings of the
7th Graz Brain-Computer Interface Conference 2017 DOI: 10.3217/978-3-85125-533-1-08

CONTROLLING FALSE POSITIVES ON A BCI IMPLANT FOR COMMUNICATION

M. P. Branco[1], Z. V. Freudenburg[1], E. G. M. Pels[1], S. Leinders[1], M. A. van den Boom[1], T. Denison[2], M. J. Vansteensel[1], E. J. Aarnoutse[1] and N. F. Ramsey[1]

[1] Brain Center Rudolf Magnus, University Medical Center Utrecht, Department of Neurology and Neurosurgery, Section Brain Function and Plasticity, Utrecht, The Netherlands
[2] Neuromodulation Core Technology, Medtronic, Minneapolis

E-mail: N.F.Ramsey@umcutrecht.nl

ABSTRACT:

A fully implanted Brain-computer Interface was recently applied in a locked-in patient allowing for a one-dimensional control of a spelling board on a computer. The patient attempts to move her hand in order to generate a 'click', which is used to select letters. The optimal parameters to generate an accurate click were estimated from a cursor control task where the control signal was used to control the y-velocity of a cursor on the screen. However, the set of parameters used for the cursor control task was not accurate enough to be used for clicks. In order improve accuracy, three filters were designed to add features, smooth and z-transform the signal before conversion to a click, in order to provide a more reliable communication channel that has less false positive events.

INTRODUCTION

People with severe paralysis who have lost the ability to communicate have only limited options to regain this ability. Since the 1990's Brain-Computer Interfacing (BCI) has been proposed as an assistant technology to reestablish this lost communication [1]. For optimal usability in daily life at the homes of the target population, such a system should be accurate and intelligent (i.e., it incorporates smart decoding algorithms that dynamically adjust to e.g. slow signal changes), fully implantable (i.e., permanently available and invisible), safe, stable, easy and comfortable to use [2]. However, even though technology advances fast, many of these requirements have not been met so far.

Recently, a fully implantable BCI communication system [3] (Utrecht NeuroProsthesis, UNP, Figure 1) was implemented, which translates neuronal activity elicited upon attempted hand movements into a binary control signal for selection of characters in spelling software running in 'switch-scanning mode', where so-called 'brain-clicks' can be used to select characters, or groups of characters, that are highlighted automatically and sequentially by the computer. The UNP system was implanted in a locked-in patient with late stage Amyotrophic Lateral Sclerosis, with a four-electrode strip covering the hand sensorimotor cortex. The bipolar pair to use for BCI control was chosen based on the highest correlation to a motor localizer task, where the patient alternated between trials of attempted hand movement and rest. The patient gave informed consent to this study, which was approved by the ethics committee at the University Medical Center Utrecht in accordance with the 2013 provisions of the Declaration of Helsinki.

Extraction of good parameters

A standard Cursor Control task (CCT, in BCI2000 [4]) was used to estimate the optimal signal processing parameters for a one-dimensional continuous control signal. In this task the subject controlled the y-velocity of a ball on the screen (Figure 2), while the ball moved at constant speed on the x-direction in attempt to hit one of two targets displayed on the right hand side of the screen. The subject attempted to move her hand to move the ball up and relaxed to move it down.

Across several months the average CCT performance using high-frequency broadband power (80±2.5 Hz) was 90.73±6.42 % (N=70 runs), which is significantly above chance (50%, $p<0.01$). However, the high performance with this continuous signal did not predict performance using the same electrode pair and frequency band for a binary signal (above or below a fixed threshold) to generate brain-clicks. The threshold was initially based on the midpoint between the averaged high-frequency band power during the active and during the inactive states. This resulted in a lower than expected performance during spelling and a need for frequent calibration. Errors were mainly unintended clicks (false positives), although misses also occurred.

Hence, we were interested in investigating how the continuous brain signal could be translated optimally into brain-clicks that were usable for high accuracy spelling, with a low false positive rate and without compromising the sensitivity to intended actions. Two hypotheses based on the acquired signals were defined:

1) Many false positives (FPs) were caused by the noisy and spiky morphology of the signal, hence smoothing of the signals would decrease the FPs;
2) The power signal was not stable over time, hence

Published by Verlag der TU Graz
Graz University of Technology

 DOI: 10.3217/978-3-85125-533-1-08

normalization of the signal would improve performance.

Figure 1: Utrecht NeuroProthesis (UNP) fully implanted brain-computer interface system.

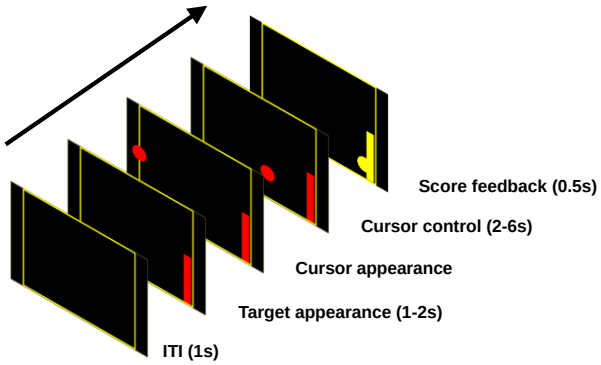

Figure 2: CCT design as implemented in BCI2000. The ball moves towards the target at constant speed while the subject controls the y-velocity of the ball towards the target.

MATERALS AND METHODS

General description of the system

The UNP system (Figure 1) consists of four 4-electrode ECoG strips, from which one strip is placed over the hand region of primary motor cortex. The subcutaneous amplifier and transmitter device, placed subclavicularly, transmits power signals to an antenna attached to the clothing, every 200ms (5 Hz) for one bipolar pair. As a first step to improve the reliable conversion of continuous brain activity into a 'brain-click' control signal, instead of only using the high-frequency band, we used a filter (linear classifier filter) that summed two frequency bands (Low Frequency Band, LFB, 20±2.5Hz, weight -1; and High Frequency Band, HFB, 80±2.5 Hz, weight +1) of the same bipolar pair (F_{HFB} - F_{LFB}). For more details about the motivation behind this filter see [3]. The resulting control signal was then thresholded through a threshold filter and converted into a binary signal, where 1 represents the samples above the threshold and 0 otherwise (Figure 3). Finally, this binary signal was converted into a click signal in the click translator filter, which defined a click when more than 5 samples (1 s) exceeded the threshold (Figure 3). The click was then sent to a spelling program where rows of characters, or individual characters, could be selected with a brain-click (Figure 4). Additionally, in order to address the two hypotheses, we tested and implemented two additional filters.

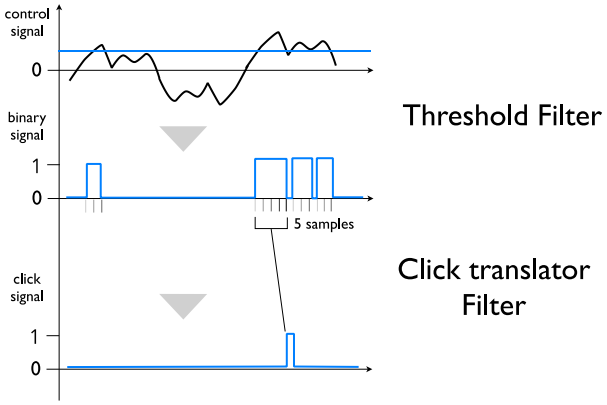

Figure 3: The threshold filter converts the control signal (F_{HFB} - F_{LFB}) into a binary signal, whereas the click translator filter converts the binary signal in a click signal.

Figure 4: Spelling program used during online research runs to spell 5 or 7-letter words. The computer automatically highlights each row or item sequently, looping from top to bottom and left to right, respectively. Each row of characters, or individual characters, can be selected with a brain-click.

Addressing hypothesis 1: The Smoothing filter

To tackle the problem of noisy and spiky signals intrinsic to neuronal recordings, a smoothing filter was designed to smooth each feature signal (F_{LFB} and F_{HFB}) independently (Figure 5). In the design of real-time feedback BCI systems the use of future samples to

Published by Verlag der TU Graz
Graz University of Technology

 DOI: 10.3217/978-3-85125-533-1-08

smooth the signal is not possible. Therefore the smoothing function here implemented averages each incoming sample with the previous 5 samples (i.e., 1.2 s smoothing window).

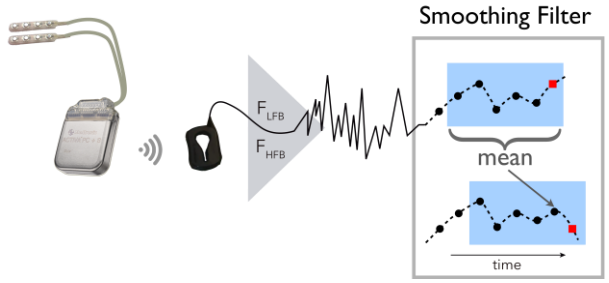

Figure 5: Smoothing filter averages each incoming sample (red square) with the previous 5 samples (black circles). The smoothing filter is applied to each feature signal (F_{LFB} and F_{HFB}) independently.

Addressing hypothesis 2: The Z-Transform filter
Another property of the signal that is crucial for accurate performance is the stability of the signal over long periods of time, i.e., the minimization of slow amplitude trends of the signal. A constant signal amplitude allows for the use of constant parameters, such as the threshold, across sessions. For that, normalization to a z-score can be used to diminish signal variability. Furthermore, when adding two different feature signals, their separate z-transformation allows for a straightforward combination for the signals (weights -1 for LFB and +1 for HFB, see [3] for more details). Hence, a z-transform filter (Figure 6) was implemented, by subtracting each incoming sample (of each feature signal F_{LFB} and F_{HFB}) with the mean of a 30 s calibration window and dividing it by the standard deviation of the same window.

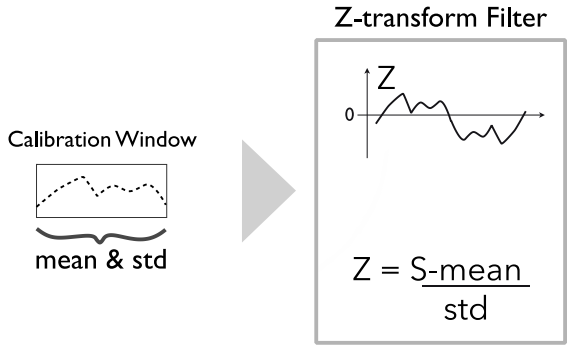

Figure 6: The z-transform filter subtracts from each incoming sample (S) the mean of a 30s calibration window and divides the resulting value by the standard deviation (std) of the calibration window.

Hypotheses testing
Click-performance during online copy-spelling runs (see Figure 4 for an explanation of the speller application) was compared before and after the filter implementation, which also includes the addition of the LFB feature. An overview of the implemented filters can be found in Figure 7.
Performance was assessed by means of false positive (FP) rate and true positive (TP) rate of the online runs. The patient performed a total of 35 copy-spelling runs before (words with 7 letters) and 69 after filter implementation (words with 5 letters). The number of FP, TP, true negatives and false negatives were determined automatically from the data recorded during online runs and visually inspected by two independent observers. Please note that no offline (post-hoc) processing was applied to the recorded data.

RESULTS

For comparison of click-performance before and after the filter implementation the FP rate and true positive (TP) rate during online runs (where the patient was asked to spell dictated words) were computed. Notably, we observed that many events classified as FPs were in fact intended clicks that were slightly too early or too late in time. For this reason a FP-rate-corrected was calculated, which did not include these timing mistakes. Timing mistakes were identified and marked by visual inspection of all runs performed by two independent observers.

Performance before filter implementation
There were on average 2.06 FP/min (N=35 7-letter words), yielding a FP rate of approximately 9%, a FP rate-corrected of 6% and a true positive (TP) rate of 84% (Figure 8).

Performance after filter implementation
Regarding the smoothing filter, the optimal smoothing window (number of samples used to average each incoming sample) was optimized together with the threshold via a heat map (see supplementary material in [3] for more details), where the highest performance region was mapped in a two-dimensional matrix. For that the offline classification accuracy of recorded runs replayed with different smoothing window and threshold was computed. Within the hotspot, multiple sets of parameters were chosen and tested by the patient (compromise between effort and accuracy of the system) and the optimal ones (1.2s smoothing window and 0.85 threshold) were used for spelling [3]. This resulted in a score of 1.02 FP/min (N=69, 5-letter words), and a significant decrease in FP-rate and FP rate-corrected to 7% and 2%, respectively ($p<0.001$). True positive rate (TPR) also decreased significantly ($p<0.05$) to 76% (Figure 8), mainly due to an increase of False Negatives (FNs, i.e. a miss to click), which the user prefers over FPs because they do not require spelling correction (back-space).

Published by Verlag der TU Graz
Graz University of Technology

 DOI: 10.3217/978-3-85125-533-1-08

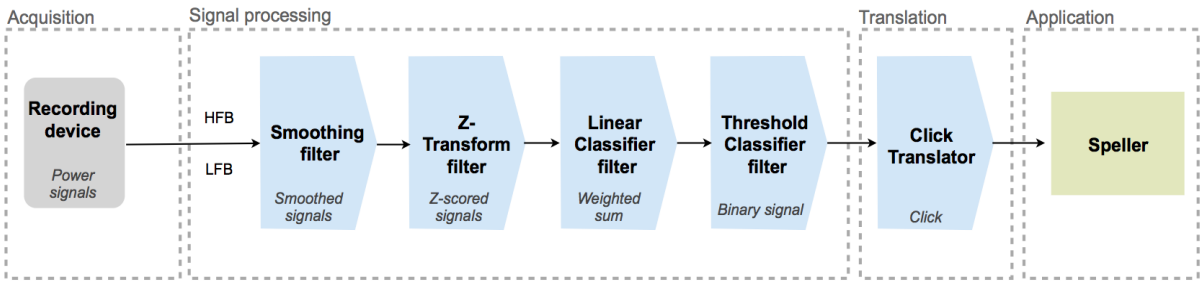

Figure 7: Filter pipeline implemented on the BCI2000 platform. The recording unit (gray block) streams power signals every 200 ms. Two frequency bands, LFB and HFB, are recorded, smoothed, z-transformed and summed (linear threshold classifier) with -1 and 1 weights, respectively. The resulting control signal is then thresholded and converted into a click. The latter was used to select rows or itens on a spelling program. Figure adapted from [3].

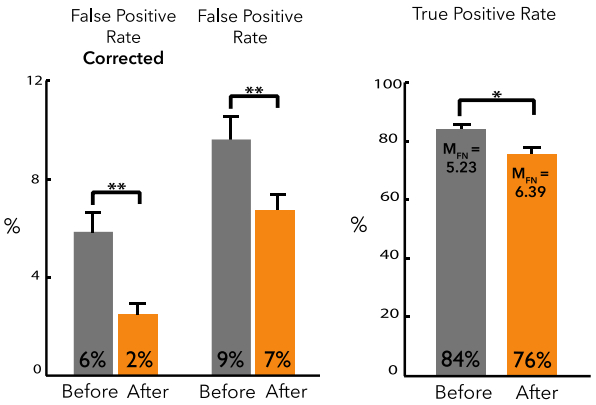

Figure 8: FP rate and FP rate-corrected before and after the filter implementation. True positive rate before and after filter implementation, where mean FN is indicated as M_{FN}. **p<0.001; *p<0.05.

DISCUSSION AND CONCLUSION

In our previous article [3], we demonstrated for the first time that a fully implanted BCI (UNP system) could be used to control a spelling program on a computer by converting brain activity into a one-dimensional 'click'. Here we address in more detail than in our previous publication, the filter pipeline implemented to convert the continuous brain signal to binary brain-clicks, for control of a spelling program on a computer. As a first approach the settings used to produce a click were derived from the optimal settings of a standard Cursor Control task. However, this set of parameters was sub-optimal for a reliable click production. Besides implementing a filter that combines two feature signals with a certain weight (F_{HFB} - F_{LFB}), the motivation for which can be found in [3], we implemented two filters to overcome the unstable characteristics of the signal: a smoothing filter and a z-transform filter. Combined, these three filters allowed for a more stable signal and a significant improvement of the performance of the system. The FP rate and FP rate-corrected for timing mistakes were significantly reduced after filter implementation. At the same time, the TP rate also reduced, mainly because of the increase in FN, which the patient preferred over FPs, because they do not require spelling correction.

Finally, one note for the calibration window used for the z-transform filter. After actual implementation, this calibration window was recorded for multiple runs and the mean and standard deviation across runs showed to be consistent. These values were then used for z-transformation, without need for repeated calibration and without a continuous adaption. Due to the normalization of the signal, the combination of feature signals with different amplitude ranges (i.e., F_{LFB} and F_{HFB}) was possible, and allowed for the setting of a constant threshold (to convert the control signal into a click) for over 9 months. During this period, user satisfaction of the UNP system was high or very high on all items of a modified QUEST2.0 user satisfaction questionnaire and the user used the system at home for communication without any technical staff present.

REFERENCES

[1] Daly JJ and Wolpaw JR. "Brain–computer interfaces in neurological rehabilitation." *The Lancet Neurology* 7.11 (2008): 1032-1043.

[2] Huggins JE, Wren PA, and Gruis KL. "What would brain-computer interface users want? Opinions and priorities of potential users with amyotrophic lateral sclerosis." *Amyotrophic lateral sclerosis* 12.5 (2011): 318-324.

[3] Vansteensel MJ, Pels EG, Bleichner MG, Branco MP, Denison T, Freudenburg ZV, Gosselaar P, Leinders S, Ottens TH, Van Den Boom MA, Van Rijen PC. Fully implanted brain–computer interface in a locked-in patient with ALS. *New England Journal of Medicine*. 2016 Nov 24; 375(21):2060-6.

[4] Schalk G, McFarland DJ, Hinterberger T, Birbaumer N, and Wolpaw JR. BCI2000: a general-purpose brain-computer interface (BCI) system. *IEEE Transactions on biomedical engineering* (2004), *51*(6), 1034-1043.

Published by Verlag der TU Graz
Graz University of Technology

Proceedings of the
7th Graz Brain-Computer Interface Conference 2017 DOI: 10.3217/978-3-85125-533-1-09

EVALUATION OF AN SSVEP AND EYE GAZE HYBRID BCI

C. P. Brennan, P. J. McCullagh, G. Lightbody, L. Galway

Faculty of Computing and Engineering, Ulster University, UK.

E-mail: Brennan-C15@email.ulster.ac.uk

ABSTRACT: An evaluation of a *hybrid* Brain-Computer Interface that combines input modalities of Steady State Visual Evoked Potential (SSVEP) and eye gaze is provided. Thirty volunteers participated and all but one could use the BCI, eye-tracker and hybrid system. The *hybrid* BCI was compared with SSVEP alone for navigating to four domotic tasks issued via a graphical user interface. Mean performance metrics of *Accuracy (Acc.*), *Efficiency (Eff.)* and Information Transfer Rate (ITR) all improved (mean *Acc*. = 93.3% to 99.84%, mean *Eff*. = 89.56% to 99.74%, mean ITR = 23.78 to 24.41 bpm). While the absolute improvements are small, better performance may contribute to user acceptability, as the eye-gaze component adds minimal additional user effort to the interaction yet provides control that is more robust.

INTRODUCTION

The electroencephalogram (EEG) provides a recording of electrical activity within the brain. As complex as this activity is there are methods to extract meaningful information from the brain waves. By developing certain paradigms intentional modulation of brain activity can be established and used as a mechanism for communication and control. Known as Brain-Computer Interfaces (BCI), this technology has been explored extensively for over two decades as a mechanism to provide an input modality to a computing system that does not require the involvement of peripheral nerves and muscles [1]. Recording normally takes place under controlled laboratory conditions; in more recent years there has been an objective to extend the technology to users in the community, placing more emphasis on reliability, robustness and ease of use. Reliance on EEG features only is one of the key attributes with BCI systems, particularly important for users who have lost peripheral movement including eye gaze. However, BCI is recognized as a difficult assistive technology to establish for a user as successful deployment requires substantial tailoring to the user's needs and individuality within their EEG.

In contrast, for potential users with residual eye movement, eye-gaze technology has been deployed as an effective assistive technology, albeit with its own challenges in terms of attaining robust decision making. In particular, eye trackers have been used to navigate on-screen commands; when a decision or action needs confirmed, features such as 'dwell-time' may be used to activate the classification.

Combining active eye-gaze technology with BCI can bridge the gap between the two systems [2][3][4], creating a *hybrid* BCI (*h*BCI) system. BCI paradigms lend themselves to performing this confirmation or 'switch' operation [5][6], providing complementary intentional control for the user. In some cases, the searching activity, can be employed to items and locations within the user's physical environment, and this information provides a context to the decision to be made by the BCI system [7]. Meena *et al.*, 2015 [8], proposed a *h*BCI combining motor imagery (using the event related desynchronization component) with eye tracking, aspiring to increase the number of available command choices. The eye gaze is used to detect (search for) the spatially located device, while the BCI (motor imagery) is used to select.

Additionally, eye tracking has been used to provide the selection of 'on-screen' icons, with a BCI component confirming a choice. Galway *et al.*, presented eye tracking selection of directional arrows to gain navigation through a Graphical User Interface (GUI) for control of domestic appliances [9]. The arrow icons flash to initiate Steady State Visual Evoked Potential (SSVEP) responses and thus perform the switch operation to activate the desired movement through the GUI or to activate a command on an external device.

Kalika *et al*. [10] combined a P300 speller with eye tracking. Instead of a sequential search and select protocol, complementary inputs were combined and a Bayesian classifier enhanced the accuracy of selecting a character in the speller. Dong *et al.* [11] used a similar approach to combine motor imagery with eye gaze. Évain *et al.*, [12] combined eye gaze and SSVEP inputs to enhance classification accuracy and demonstrated a speed up in operation and performance over existing BCI systems.

In this paper, we provide an evaluation of an *h*BCI, which combines input modalities of SSVEP and eye gaze, and uses a similar signal processing approach as [13]. The aim was to evaluate the performance and usability of SSVEP for healthy participants and indicate improvements, that *h*BCI offers. The SSVEP paradigm provides a natural and intuitive procedure to collaborate with an eye-tracking algorithm. Users interacted with an existing menu system [9], which provided navigation of a virtual smart home, on a desktop computer. They were required to observe and fixate on the navigation icon they wished to select; as the icons were collocated with frequency-modulated stimuli, the technique for interaction does not change from a user perspective.

Published by Verlag der TU Graz
Graz University of Technology

 DOI: 10.3217/978-3-85125-533-1-09

MATERALS AND METHODS

Ethical approval was granted by the Ulster University Research Ethics Committee (UUREC ethics number REC/16/0053). Thirty healthy volunteers (16 males and 14 females), from staff and students at Ulster University and members of the public over the age of 18 years participated. Participant age ranged from 21-73 years, average 37.6 (SD 14.73). Exclusion criteria prevented volunteers from participating if they were sensitive to flickering lights, had substantial problems with left-right discrimination, and hearing or visual impairments, which could not be corrected. Prior to beginning, participants undertook a practice run to familiarize themselves with the control paradigm and the GUI of the menu system. The assessment required participants to complete tasks to initiate domotic control, multimedia playback, communication, and free control of a smart-home environment. Participants completed a pre-questionnaire to indicate expertise and their perceived level of tiredness/arousal and a post-questionnaire to provide some qualitative feedback.

Setup time ranged between 4-26 mins, (average 13m:53s, SD 5m:35s) and total experiment time ranged from 50 mins to 2 hours and 29 mins, dependent on the number of sessions that the participant completed, (average 1 hour and 25mins, SD 20m:07s). From the 30 participants, 12 had prior experience with eye tracking technology, nine had prior experience with SSVEP BCI, and 28 were experienced computer users. Eight participants required vision correction; six of which removed their glasses for the duration of the experiment to account for reflections, which may have adversely affected eye tracking performance.

The experimental setup comprised dual LCD displays (refresh rate 60 Hz), an EyeTribe eye tracker, g.USBamp, g.LADYbird passive electrodes, g.GAMMAcap, and a Raspberry Pi home-automation server (for interaction with external devices such as lights). The experiment was controlled by monitor one and participants were required to interact with the GUI displayed on monitor two. Participants were seated approximately 70 cm from this monitor. The EyeTribe Tracker was utilized to record gaze at a sampling rate of 60Hz, with a latency of <20 ms. The device was calibrated on 9 points and with an accuracy in the range 0.5 – 1 degree. On-screen gaze coordinates were derived from the EyeTribe application programming interface.

For SSVEP generation, four unique flickering stimuli (6.67 Hz, 7.5 Hz, 8.57 Hz, 12 Hz) were presented by modulating pixels on screen (rather than through external LEDs, which was adopted in previous studies). The four stimulation areas were set at the default size of 150 x 150 pixels and by focusing attention on flickering stimuli, users could traverse through the menu structure by issuing a succession of *left*, *right*, *up*, and *down* commands. The *down* command selected an item or navigated to a lower level in the hierarchical structure, and the *up* command returned to the previous (higher) level. In addition, spoken feedback was provided after each command to reinforce the user experience by confirming the command. The four stimulators were surrounded by a 250 x 250-pixel border, representing the maximum size that each stimulator could increase to without classification occurring. As an additional method of feedback, the stimulators were designed to grow dynamically in relation to the SSVEP amplitude of the respective frequency. This design was for two reasons: 1) it provides user feedback allowing participants to know when they have issued a command; and 2) larger stimuli produce a greater SSVEP response. In the second case, real-time SSVEP visualization relating to the power estimation of the relevant frequency, decreases the time to select, as the response becomes increasingly more prominent in the EEG due to the increasing size of the stimuli; it is a positive feedback loop.

Feature detection and command translation were based on signal processing methods realized by Volosyak *et al.* [13]. The SSVEP signal detection and classification process utilized the Minimum Energy Combination (MEC) method to create a spatial filter and enhance the SSVEP response while reducing ambient signals and other interference [13]. The system was designed to automatically determine the best spatial filter for each participant at each frequency. The manifestation of each frequency in the EEG was detected by spatial filtering, power estimation, and a statistical probability method, which enhanced the quality of signal and separated channel-specific features. Furthermore, an adaptive windowing technique was employed in order to determine a suitable window length based on online performance. Stimuli induced frequencies and harmonics were estimated in the recorded EEG. When this estimation exceeded a predefined threshold, as determined during calibration, a directional vote (i.e. $SSVEP_E$ *left*, *right*, *up*, *down* or *no-control state*) was transmitted to the data fusion component of the menu system, as illustrated in Fig. 1.

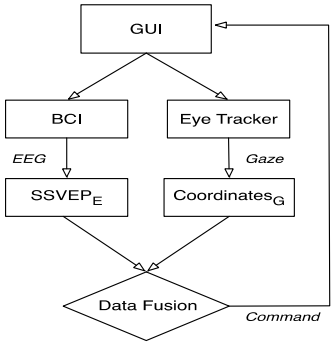

Figure 1: Conjunction-based collaborative decision making process data flow

In collaboration with the directional vote, coordinates of the participant's gaze ($Coordinates_G$) were used to ascertain an overall command and concurrently transmitted to the Data Fusion component. Employing the conjunction of the estimated location derived from the participant's gaze point and the directional vote, agreement of the intended command would occur if the

Published by Verlag der TU Graz
Graz University of Technology

 DOI: 10.3217/978-3-85125-533-1-09

conjunction was found to be true. Figure 2 illustrates the partitioning scheme utilized by the Data Fusion component, which partitioned the overall GUI along the horizontal, vertical and diagonal axes, centered on the origin of the GUI, such that gaze coordinates were easily mapped to specific quadrants surrounding the SSVEP navigation icons.

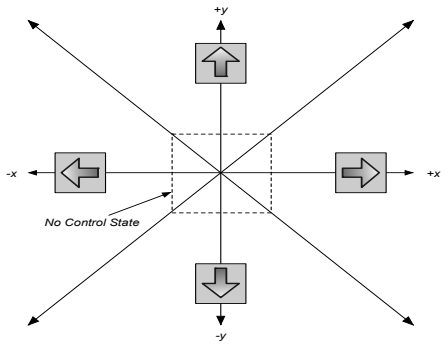

Figure 2: *h*BCI user interface partitioning scheme showing partitioning of screen along x, y and diagonal axes, placement of SSVEP navigation icon stimuli and no control state

In addition, a no-control state within a predefined area centered on the origin of the GUI was used in order to permit the participants to view the currently active menu icon, which would appear in the center of the bespoke menu system. Accordingly, gaze coordinates were not acquired when the participant's gaze was within the bounds of this zone, thus preventing the possibility of erroneous commands being issued by the Data Fusion module whenever the participant was regarding the active menu icon. Directional decisions were calculated as follows:

$$F(x,y) = \begin{cases} \xi_L \Delta, if & \phi_1 \wedge \neg\left(y-\left(\frac{x}{2}\right)<0\right) \vee \phi_3 \wedge \neg\left(y-\left(\frac{x}{2}\right)>0\right) \wedge \left(y+\left(\frac{x}{2}\right)-\alpha>0\right) \\ \xi_R \Delta, if & \phi_2 \wedge \neg\left(y-\left(\frac{x}{2}\right)<0\right) \wedge \left(y+\left(\frac{x}{2}\right)-\alpha<0\right) \vee \phi_4 \wedge \neg\left(y+\left(\frac{x}{2}\right)-\alpha>0 \wedge y-\left(\frac{x}{2}\right)>0\right) \\ \xi_U \Delta, if & \phi_1 \wedge \left(y-\left(\frac{x}{2}\right)<0\right) \vee \phi_2 \wedge \left(y-\left(\frac{x}{2}\right)<0 \wedge y+\left(\frac{x}{2}\right)-\alpha<0\right) \\ \xi_D \Delta, if & \phi_3 \wedge \left(y-\left(\frac{x}{2}\right)>0\right) \wedge \left(y+\left(\frac{x}{2}\right)-\alpha>0\right) \vee \phi_4 \wedge \left(y+\left(\frac{x}{2}\right)-\alpha>0 \wedge y-\left(\frac{x}{2}\right)>0\right) \end{cases}$$

where F is a function of x and y, α is the horizontal resolution divided by two, β is the vertical resolution divided by two, and ϕ_1, ϕ_2, ϕ_3, and ϕ_4 are quadrants one, two, three, and four, respectively, and $\xi_L, \xi_R, \xi_U,$ and ξ_D are the eye tracking vote for *left*, *right*, *up*, and *down*, respectively. Upon successful command determination, the resulting command is transmitted by the Data Fusion component to the GUI resulting in continued traversal of the menu structure.

Participants were instructed to complete four tasks, controlling the GUI-based menu system, to traverse a hierarchal-menu structure and activate features and functions of a smart-home environment. The instructions, issued by trained-research staff, requested that participants navigate the menu structure executing four-way control, e.g. *left*, *right*, *up*, and *down* commands. The first task required participants to interact with smart home lighting in the dining room. The second task asked if they could select a specified video for playback on the television set and subsequently end playback when requested. The third task required users to navigate to the talk menu and communicate using predefined iconography and auditory feedback to indicate hunger (e.g., to a potential companion). The fourth task required users to freely navigate the interface to complete a predetermined goal (in this case to go to the kitchen, find the extractor fan, and turn it off), without receiving a predefined set of instructed commands and therefore permitting users to initiate different command sequences to reach the goal. Fig. 3 gives a representative example of task one, whereby participants were instructed to issue a minimum of 13 commands to traverse the hierarchal-menu structure and control room lighting. For the particulars of the individual tasks, please see [9].

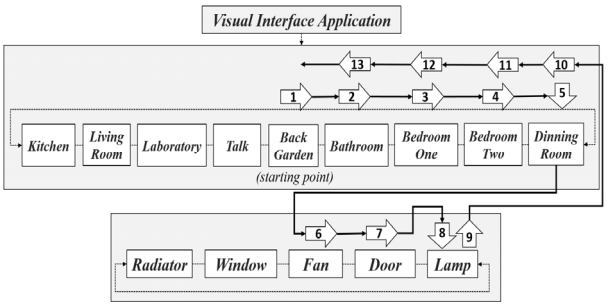

Figure 3: The minimum commands to successfully traverse the hierarchal-menu structure and complete tasks two.

In the case of an erroneous command (due to user error or misclassification), participants were instructed to rectify the mistake by issuing an additional command when required, which for subsequent analysis was considered as a 'correct' selection. In certain circumstances, however, rectifying commands were not required, e.g. when a false-positive '*up*' command was issued at the highest level of the hierarchy. Such commands did not initiate traversal of the menu structure and therefore did not require rectification. Each task was associated with a critical path (i.e. the minimum number of compulsory commands for successful completion). When completing the tasks, the total time for task completion, and the number of correct, incorrect, and rectified commands were recorded. Performance metrics for accuracy of target detection (*Acc.),* efficiency of the interaction (*Eff.*) and Information Transfer Rate (ITR) were computed offline.

In some situations, the accuracy value provides a misimpression of participant performance. Due to the structure of the tasks, false-positive commands are often succeeded by a command to rectify the mistake, which is defined as an additional correct command. The result from specific participants who issued several false-positive commands suggests performance is of a higher level than in reality. For this reason, *Efficiency*, as defined by Volosyak *et al.* [15], is calculated as follows:

$$Efficiency = \frac{C_{min}}{C_{total}} * 100$$

where C_{min} is the minimum number of compulsory

Published by Verlag der TU Graz
Graz University of Technology

 DOI: 10.3217/978-3-85125-533-1-09

commands (13 for Task 1 in our interface layout) and C_{total} is the total number of detected commands. ITR was calculated as defined by Wolpaw *et al.* in [1] and formularized as follows:

$$ITR = \left(log_2 M + P log_2 P + (1-P) log_2 \left[\frac{1-P}{M-1}\right]\right) * \left(\frac{60}{T}\right)$$

where M is the number of choices, P is the accuracy of target detections, and T (in seconds/selection) is the average time for a selection.

RESULTS

The experimental results, summarized in Fig. 4, provide an analysis of the individual accuracies, efficiencies, and ITRs as well as the averages across all participants. Furthermore, these results contrast the performance of SSVEP alone with *h*BCI, conveying a mean accuracy increase from 93.3% to 99.84%, mean efficiency improvement of 89.56% to 99.7%, and indeed an ITR improvement of 23.78 bpm to 24.41 bpm. The latter may be surprising as the eye tracker may be expected to somewhat dampen the responsiveness of the interaction (whether correct or incorrect), and contrast with the findings of Vilimek *et al.* in [16]. A paired t-test indicated that participants performed better using *h*BCI than BCI alone in terms of accuracy and efficiency with a significance of $p < .001$. This finding indicates that there is a statistical significant difference between the two conditions that is not attributable to chance, and likely due to the independent variable manipulation. A further paired t-test provided an analysis of the bit rates contrasting BCI-only and *h*BCI indicating a significance of $p > 0.10$. This finding suggests that there is no statistical significant difference between these two metrics, and hence the difference of the means, in this case, is likely owing to chance.

To compare these results with eye tracking-only please see the previous study in which the same tasks were employed to assess the performance of eye tracking alone on healthy volunteers (N=12), indicating an average accuracy, efficiency and ITR of 88.88%, 81.20% and 41.16 bpm, respectively.

DISCUSSION

This research indicates that the *h*BCI outperforms SSVEP-based BCI alone across all considered metrics, *Acc*., *Eff*. and ITR. Hence we believe that the *h*BCI is potentially more robust. This could go some way to addressing BCI acceptability outside the laboratory and, therefore, the additional cost and complexity of eye tracking can be readily justified. Indeed, the hardware cost in this case (a couple of hundred Euro) is minimal when compared to the BCI component as high spatial accuracy is not needed. Eye tracking is limited by false-positive selections, however, which is often referred to as the 'Midas Touch' problem [18] (i.e. selecting everything unintentionally), while SSVEP performance is not robust enough for critical applications, e.g. false-positive selections in smart environments are known to produce intolerable events in the local environment, such as lights flashing on and off, doors opening and closing, security alarms triggering etc. Therefore, the integration of both modalities as an *h*BCI has been demonstrated to improve the performance up to a level unobtainable by either modality on its own.

An analysis of the post-questionnaire responses from the 30 participants, conveyed that five preferred BCI alone, 19 preferred the *h*BCI, and six had no preference. Multiple participants stated the *h*BCI improved confidence during interaction and one user in particular stated *"the hybrid demonstrates a potential for more complex tasks"*. Other users substantiated this claim by mentioning that the *h*BCI seemingly offered enhanced robustness. A small subset of the participants contradicted these findings, however, by suggesting that SSVEP was superior as a sole input modality. In some exceptional circumstances, for example, when participant 28 achieved remarkable performance using BCI alone (*Acc. 100%, Eff. 100%, ITR 36.37 bpm*), the *h*BCI merely slowed the interaction (*Acc. 100%, Eff. 100%, ITR 33.31 bpm).* Likewise, participant 6 who also preferred SSVEP alone, achieved *Acc. 95.54%, Eff. 93.88%, and ITR 23.36 bpm* utilising BCI-only. Their qualitative feedback was somewhat surprising considering their performance improved for the *h*BCI (*Acc. 100%, Eff. 100%, ITR 21.91 bpm)* for both accuracy and efficacy, albeit with a slight reduction in ITR. While such a finding is inherently subjective, this participant was apparently more tolerant to errors than to an increase in time per selection, even if it meant 100% accuracy of target detection. Participant 8, who did not achieve 100% *h*BCI accuracy and efficacy, expressed that they found *"the hBCI control restrictive due to the fixed nature of the hardware"*. This participant highlights a known restriction of eye tracking technology whereby calibration enforces users to remain stationary; for example, adjusting the seated positioning is known to produce erratic screen-based coordinates.

The only volunteer who failed to complete the tasks, Participant 11, suffered from macular degeneration, a medical condition affecting the central field of vision, and would have been screened out if they had informed research staff prior to running the experiment. The result was labelled 'inconclusive' and excluded from subsequent numerical calculations. However, it reinforces that there will always be people that the BCI will not work with. Our intention is to assess the performance of people with brain dysfunction in the future and this will obviously pose additional challenges.

A quantitative analysis comparing SSVEP with *h*BCI is represented in Fig. 3 (A) and (B). From 30 participants, 29 completed the tasks successfully. Of those 29, only three failed to achieve 100% *Acc.* and *Eff.* and yet their

Published by Verlag der TU Graz
Graz University of Technology

 DOI: 10.3217/978-3-85125-533-1-09

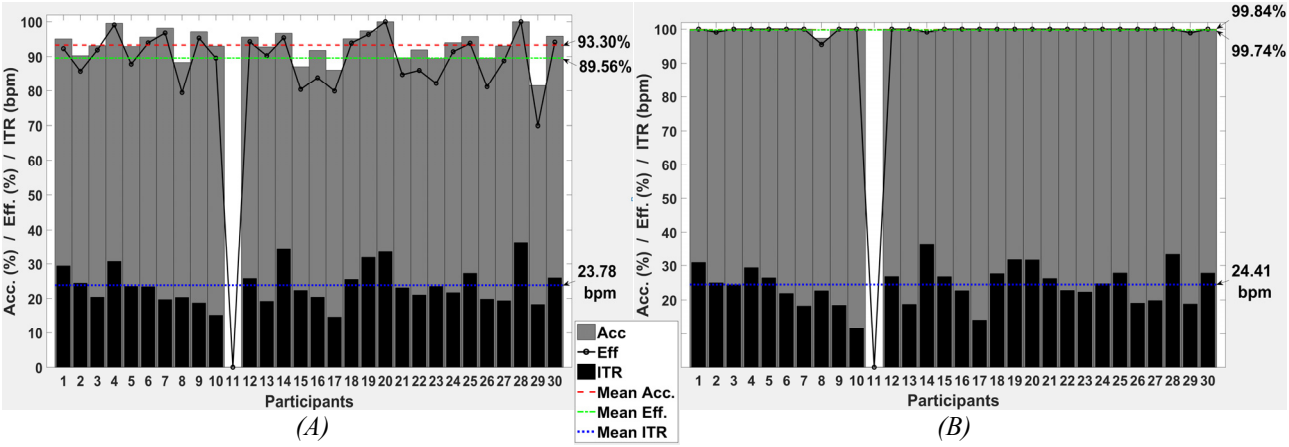

Figure 4: Data collected from 30 healthy participants. (A) The results from SSVEP-only achieved a mean *Acc. 93.3%, Eff. 89.56%,* and ITR *23.78* bpm. (B) The results from the *h*BCI (SSVEP + Eye Tracking) achieved a mean *Acc. 99.84%, Eff. 99.74%*, and ITR *24.41* bpm.

performance still increased significantly in contrast with SSVEP-only. In some cases, the ITR may have dropped moderately from SSVEP control to the *h*BCI. As mentioned previously, and contradictory to prior research [16], the average bit rate improved for *h*BCI interaction. This is likely due to the ITR calculation, which is satisfied with three variables: 1) accuracy of target detection; 2) number of choices; and 3) time per selection. A system that returns perfect accuracy can account for an increased time per selection and return a higher bit rate when compared with less accurate systems that have a decreased time per selection. In an eye-gaze collaborative BCI this tradeoff is related to the dwell time of eye tracking decisions. Optimal parameters in the eye tracking algorithm will ensure interaction speed does not diminish to a level that reduces bit rate. An offline analysis of the data for a representative participant confirms this finding. Fig. 5 provides further interpretation of *h*BCI task one for a representative participant, confirming the eye tracker voted first on 12 of the 13 selections. For the most part, the eye tracker was not limiting performance, but for one of the selections, the *up* selection, the BCI had to wait for the eye tracker to agree before a selection could be issued, which increased the total time for task completion. A common assumption, may suggest this should indicate the BCI-only version will return a higher ITR, but in certain cases this is incorrect. The *h*BCI still manages to outperform the BCI alone in terms of information throughput, if it issues slower selections with greater accuracy. Comparison of the result of BCI alone and *h*BCI for Participant 2 when completing task one confirms this to be the case. From period 45-48 seconds, it is clear the BCI was confident that the participant was attempting to issue an *up* selection but the eye tracker slowed performance, and yet the *h*BCI still exceeded the bit rate of BCI alone. This is particularly interesting as it suggests that refining the hybrid system may further improve performance. A softer decision process allowing selection based on confidence level of singular modalities would likely improve the system as an assistive technology. Allowing decisions from one modality to surpass the other, however, prevents the assessment of individual components from a research perspective, e.g. eye tracking decisions that do not interact with BCI cannot be considered as an *h*BCI process, since decisions do not necessarily rely on activity from the brain.

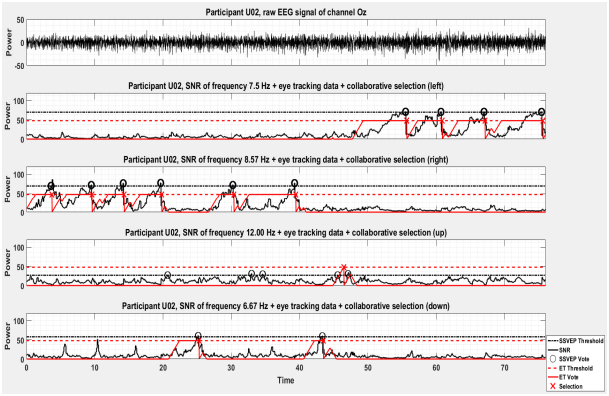

Figure 5: BCI, eye tracking, and collaborative selections for Participant 2 completing task one using the *h*BCI.

Moreover, a comparative analysis of BCI and *h*BCI *must* always consider the same number of choices in the ITR calculations. The BCIs discussed herein have four choices, the SSVEP stimuli for *left* (7.5 Hz), *right* (8.57 Hz), *up* (12 Hz) and *down* (6.67 Hz) selections. Each of these choices is reinforced with eye tracking decisions but the number of choices in the ITR calculation does not increase. In a hybrid design, the number of choices could potentially increase significantly. For example, a single frequency for SSVEP detection could be employed and 12 choices added to an interface. Each choice would be selectable via the user gaze and a BCI component. In this form the hybrid utilizes BCI as a *switch,* but unfortunately the ITR cannot consider 12/13 choices. Doing so would provide a misimpression of performance and instead the ITR should be calculated using a single choice.

Published by Verlag der TU Graz
Graz University of Technology

 DOI: 10.3217/978-3-85125-533-1-09

CONCLUSION

The SSVEP paradigm provided a natural and intuitive procedure to collaborate with an eye tracking algorithm. Users were required to observe and fixate on the icon they wished to select, and if icons were also collocated with SSVEP stimuli, then the technique for interaction would not change at all from a user perspective. For the *h*BCI mean performance metrics of *Acc., Eff.* and ITR all improved. While the absolute improvements are small, they may contribute to user acceptability, as the eye gaze component adds minimal additional user effort to the interaction. BCI offers enormous hope for assisting communication/interaction for people with neurological disease. Further significant advances have been made in recent years. The hybrid discussed in this paper increased the performance metrics under study and generally the perceived robustness by the volunteers. Set up by an experienced user is still required, particularly regarding the thresholds to achieve best performance. Analysis of the eye tracking data and the collaborative decision process provides insight, showing that metrics can be further improved. This level of detail can also be used to quickly screen out people for whom the technology is inappropriate.

REFERENCES

[1] Wolpaw JR, Birbaumer N, McFarland DJ, Pfurtscheller G, and aughan TM, Brain-computer interfaces for communication and control, Clinical Neurophysiology 2002, 113:(6):767-791

[2] Brunner C, Birbaumer N, Blankertz B, Guger C, Kübler A, Mattia D, Millán J , Miralles F, Nijholt A, Opisso E, Ramsey N, Salomon P, Müller-Putz GR. BNCI Horizon 2020: towards a roadmap for the BCI community. BCI Journal, 2015.

[3] Pfurtscheller G, Allison BZ, Brunner C, Bauernfeind G, Solis-Escalante T, Scherer R, Zander TO, Mueller-Putz G, Neuper C, and Birbaumer N, The hybrid BCI. Frontiers in neuroscience, 2010.

[4] Allison BZ, Jin J, Zhang Y and Wang X, Brain-Computer Interfaces (2014): A four-choicehybrid P300/SSVEP BCI for improved accuracy, Brain-Computer Interfaces.

[5] Zander, T., Gaertner, M., Kothe, C. and Vilimek, R. (2010) 'Combining Eye Gaze Input With a Brain–Computer Interface for Touchless Human–Computer Interaction', International Journal of Human-Computer Interaction, 27(1), pp. 38–51.

[6] Amiri, S., Rabbi, A., Azinfar, L. and Fazel-Rezai, R. (2013) 'A Review of P300, SSVEP, and Hybrid P300/SSVEP Brain- Computer Interface Systems', Brain-Computer Interface Systems - Recent Progress and Future Prospects, 2013, pp. 1–8.

[7] Valbuena, D., Volosyak, I., Malechka, T. and Gräser, A. (2011) 'A novel EEG acquisition system for Brain Computer Interfaces', Journal of Bioelectromagnetism, 13(2), pp. 74–75

[8] Meena, Y. K., Cecotti, H., Wong-Lin, K. and Prasad, G. (2015) 'Towards increasing the number of commands in a hybrid brain-computer interface with combination of gaze and motor imagery', *Proceedings of the Annual International Conference of the IEEE Engineering in Medicine and Biology Society, EMBS*, 2015–Novem, pp. 506–509.

[9] Galway, L., Brennan, C., McCullagh, P. and Lightbody, G. (2015) 'BCI and Eye Gaze: Collaboration at the Interface', pp. 199–210.

[10] Kalika, D., Collins, L., Caves, K. and Throckmorton, C. (2016) 'Fusion of P300 and Eye Tracker Data for Spelling Using BCI2000', in Proceedings of the 6th International Brain-Computer Interface Meeting, organized by the BCI Society, p. 27.

[11] Dong, X., Wang, H., Chen, Z. and Shi, B. E. (2015) 'Hybrid Brain Computer Interface via Bayesian Integration of EEG and Eye Gaze', 7th Annual International IEEE EMBS Conference on Neural Engineering, 1, pp. 22–24.

[12] Évain, A., Argelaguet, F., Casiez, G., Roussel, N. and Lécuyer, A. (2016) 'Design and evaluation of fusion approach for combining brain and gaze inputs for target selection', Frontiers in Neuroscience, 10(OCT). doi: 10.3389/fnins.2016.00454.

[13] Volosyak I, "SSVEP-based Bremen-BCI interface--boosting information transfer rates.," J. Neural Eng., vol. 8, no. 3, 2011

[14] Mulvenna, Maurice, Gaye Lightbody, Eileen Thomson, Paul McCullagh, Melanie Ware, and Suzanne Martin. "Realistic expectations with brain computer interfaces." Journal of Assistive Technologies 6, no. 4 (2012): 233-244.

[15] I. Volosyak, H. Cecotti, D. Valbuena, A. Graser, and A. Gräser, "Evaluation of the Bremen SSVEP based BCI in real world conditions," in 2009 IEEE International Conference on Rehabilitation Robotics, ICORR 2009, pp. 322–331.

[16] R. Vilimek and T. O. Zander, "BC(eye): Combining Eye-Gaze Input with Brain-Computer Interaction," in Proceedings of the 5th International on Conference Universal Access in Human-Computer Interaction, C. Stephanidis, Ed. San Diego, CA: Springer-Verlag, 2009, pp. 593–602.

[17] C. Brennan, P. Mccullagh, L. Galway, and G. Lightbody, "The hybrid BCI: Closing the Performance Gap between Standard Input Devices and the BCI," in EEG-based Brain-Computer Interfaces for Healthcare Applications, I. Volosyak, Ed. Kleve, Germany: Shaker Verlag, 2016, pp. 37–52.

[18] R. J. K. Jacob, "What you look at is what you get: eye movement-based interaction techniques," in *Proceedings of the SIGCHI conference on Human factors in computing systems Empowering people - CHI '90*, 1990, vol. 23, no. 5, pp. 11–18.

Published by Verlag der TU Graz
Graz University of Technology

Proceedings of the
7th Graz Brain-Computer Interface Conference 2017 DOI: 10.3217/978-3-85125-533-1-10

SIGVIEWER – CURRENT STATUS AND RECENT DEVELOPMENTS

C. Brunner[1], Y. Lin[2], P. Sajda[3], J. Faller[3]

[1]Institute of Psychology, University of Graz, Austria
[2]Manhattan School of Music, NY, USA
[3]Laboratory for Intelligent Imaging and Neural Computing, Columbia University, NY, USA

E-mail: clemens.brunner@uni-graz.at

ABSTRACT: SigViewer is an open source cross-platform biosignal viewer designed to visualize and annotate biomedical data streams. It supports a wide variety of file formats, including BDF, EDF, GDF, CNT, BrainVision, and BCI2000. Recently, support for loading multi-stream XDF data has been added. Besides visualizing raw data, SigViewer supports loading, displaying, creating, and editing events that can be used to annotate specific segments within a signal. Other useful tools include offset removal, computation of event-related potentials, and calculation of power spectral densities. To our knowledge, SigViewer is the only open source cross-platform multi-format biosignal viewer currently available that supports XDF files. Furthermore, SigViewer is completely free in that it does not depend on any proprietary software such as e. g. MATLAB. SigViewer is actively maintained and widely used across the globe (as measured by the monthly downloads). Filtering data in the frequency domain before visualization to e. g. remove line noise or excessive drift is one of the next planned features for a future release.

INTRODUCTION

Inspecting and visualizing raw biophysiological data such as EEG (electroencephalography), EOG (electrooculography) or ECG (electrocardiography) remains one of the first steps in any processing pipeline. Visualization can help in assessing general data quality, which includes detecting segments contaminated with artifacts, identifying noisy or completely bad channels, and inspecting events co-registered with the data.
Most available visualization tools are either tied to specific hardware, restricted to a small number of file formats, limited to a specific operating system, depend on proprietary programming environments, do not feature a fully featured GUI, and/or need to be purchased (i. e. are neither free nor open source). Relevant open source tools that focus on EEG/MEG analysis and ship with a visualization component include the MATLAB-based toolboxes EEGLAB [1], FieldTrip [2], Brainstorm [3], Biosig [4] (does not have a GUI[1]), and the Python package MNE [5] (does not have a GUI). Commercial tools include the MATLAB-based g.BSanalyze[2] as well as BrainVision Analyzer[3].
In contrast, SigViewer [6,7] is free, open source, cross-platform, supports many different file formats, and is written in standard-compliant C++ using the GUI toolkit Qt[4]. Development of SigViewer started some 10 years ago as a software project at Graz University of Technology, Austria. A first public version was uploaded to a dedicated SourceForge.net repository[5] in May 2010. The initial design goals of SigViewer can be summarized as follows (note that they are still valid today for the most recent release):

1. SigViewer should be cross-platform (i. e. it needs to run on Windows, Mac OS X, and Linux) with a native look-and-feel.

2. Visualization and interaction should be fast and responsive.

3. SigViewer should be completely free and open source (that is, all components required to build and run SigViewer should be available as open source). This specifically excludes MATLAB as a development environment, which many alternative viewers are based on.

An important use case for SigViewer is post-hoc manual signal inspection with the aim to identify and mark continuous artifact segments within the data. In a typical workflow, once artifact segments have been selected with SigViewer, they can be exported and thus integrated in any subsequent data analysis pipeline. Figure 1 illustrates this use case with SigViewer's main window displaying three EEG channels and one ECG channel, together with different events shown as rectangular areas in varying colors. Conveniently, these segments can be exported to a file for reuse in other stages of the processing pipeline.

[1]Graphical User Interface
[2]http://www.gtec.at/Products/Software/g.BSanalyze-Specs-Features
[3]http://www.brainproducts.com/productdetails.php?id=17
[4]https://www.qt.io/
[5]http://sigviewer.sourceforge.net/

Published by Verlag der TU Graz
Graz University of Technology

 DOI: 10.3217/978-3-85125-533-1-10

FEATURES

SigViewer uses *libbiosig* from the BioSig project[6] to support various file formats. Specifically, SigViewer provides read access for the following file types: BDF (Biosemi), EDF (European Data Format), GDF (General Data Format), CNT (Neuroscan), EEG/VHDR/VMRK (BrainVision), and DAT (BCI2000). Recently, support for XDF (Extensible Data Format) has been added. Other file formats supported by *libbiosig*[7] may work but are not fully tested yet; official support for these formats may be added at a later stage.

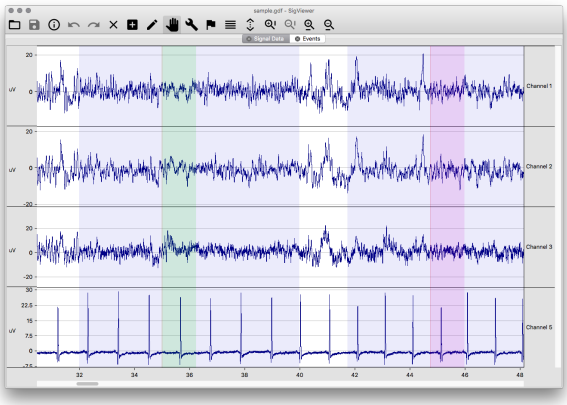

Figure 1: SigViewer running on Mac OS X.

After an initial search for global minimum and maximum values on a per-channel basis (required for auto-scaling the data), SigViewer renders the signal traces and events contained in the loaded file. Smooth and rapid scrolling through the file is supported, in contrast to many viewers which feature only page-wise (and thus relatively slow) navigation through a file.
In addition to visualizing the signals contained in a file, a list of events is automatically generated in a separate tab. Selected events can be deleted from this list.
Events can also be visualized, edited, and created within the main signal view. Events are marked with colored areas ranging from event onset to event offset. Multiple events occurring at the same time can be discerned by either assigning custom colors and/or alpha (transparency) levels. Events with duration zero are drawn as vertical lines. Events can be selected and edited graphically, which includes deleting and changing both the onset and offset as well as the event type. New events can be created by dragging the mouse pointer over the desired time range. Events can also be exported for use in other applications.
Basic meta information about the data can be displayed in a dedicated dialog window, which depends on the file type. Possible displayed fields include file type, recording time, patient ID, number of events, sample rate, channel labels, data types, physical dimensions of the recorded signals, and so on.

In addition to these visualization features, SigViewer also supports simple signal processing operations. Currently, power spectral densities as well as event-related potentials can be computed for selected channels. Both tools operate on (and thus require) selected event types in order to compute averages.

RECENT DEVELOPMENTS

The latest stable release is 0.5.2, which has been available for almost four years. It can be downloaded from the old SourceForge project website, but the project has since moved to a new GitHub repository[8]. The latest source code, issues, pull requests, and new releases will only be available on the new GitHub website. The old SourceForge page will remain online until further notice.

Since this version, development has focused on adding support for XDF files. Other minor changes include switching to the latest version of the Qt library (from version 4 to version 5) and replacing all icons with a more modern monochromatic icon set.

XDF files are flexible XML-based containers that store multiple data streams with different sample rates and data types[9]. This makes XDF an ideal format for multimodal data, which combines different modalities such as EEG, eye tracking, motion capturing, and joystick and mouse tracking into multiple synchronized data streams. To import XDF files, SigViewer uses the dedicated library *libxdf*, which handles all necessary conversions required to reshape the data contained in an XDF file to a format that SigViewer can process. Specifically, *libxdf* resamples all data streams to a common sample rate, which can be set by the user (see Figure 2). For this purpose, SigViewer presents a dialog window when opening an XDF file, which shows all streams contained in the file with their sample rates and a suggested common sample rate. Irregular streams (that is, streams without a constant sample rate) are linearly interpolated for visualization. Streams containing strings are treated as events (and are therefore listed in the event table as well as plotted over the signals).

Another new feature is detrending of signals, which is often required for EEG signals that were recorded without a highpass filter. This works for many recordings, but a more general solution using highpass frequency filters is necessary for signals exhibiting a significant amount of non-constant low-frequency activity.

[6] http://biosig.sourceforge.net/
[7] http://pub.ist.ac.at/~schloegl/biosig/TESTED
[8] https://github.com/cbrnr/sigviewer
[9] https://github.com/sccn/xdf

Published by Verlag der TU Graz
Graz University of Technology

 DOI: 10.3217/978-3-85125-533-1-10

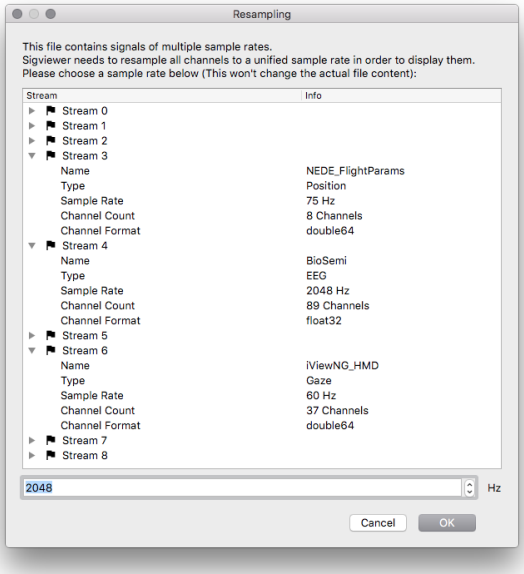

Figure 2: Resampling dialog window for XDF files.

There are two ways to save events for XDF files; events are either stored in a new XDF file or appended to an existing XDF file. Another recent change regarding events is that SigViewer now exports event to plain-text CSV (comma separated values) files for all supported file formats. Previously, it was only possible to export to binary EVT files (which are essentially GDF files without signals). Such binary files are not straightforward to open, whereas CSV files can be opened with any plain-text editor (or imported and analyzed with more specialized software like Microsoft Excel, LibreOffice Calc, R, and Python/Pandas). Table 1 shows how such an exported CSV file might look like (note that -1 in the channel column means that an event is associated with all channels).

Table 1: Exported events example (names abbreviated).

position	duration	channel	type	name
767	2048	-1	768	Start
767	2048	-1	786	Cross
1535	0	-1	785	Beep
1535	320	-1	769	class1
1791	768	-1	781	Feedback
...	...	...	...	...

BUILDING SIGVIEWER

Building SigViewer is straightforward and completely relies on open source tools. However, the exact steps vary depending on which operating system is used. SigViewer runs on Windows, Mac OS X, and Linux. Official builds are available for Windows 10, Mac OS X (macOS) 10.9–10.12, and recent Debian/Ubuntu/Arch Linux distributions. Older versions of these three platforms may work, but are neither fully tested nor officially supported.

The source code of SigViewer is cross-platform, that is, it works on all operating systems mentioned before without further modifications. A prerequisite for building SigViewer is therefore a folder with the source code, which can be downloaded from the GitHub project site (e. g. via downloading a zipped file or cloning the repository).

On Windows, Qt 5.8 needs to be downloaded and installed together with the included MinGW 5.3 toolchain. External dependencies must be copied to the *external* folder within SigViewer's source folder. At the time of writing, *libbiosig* is a required dependency, but building it on Windows is somewhat involved. Therefore, pre-built binaries of this library are available on the old SourceForge repository[10]. The contents of this zipped file needs to be extracted into the SigViewer source folder, which automatically creates the required *external* folder structure. Next, SigViewer is ready to be compiled. The easiest way is to open the source tree with Qt Creator (the file *sigviewer.pro* needs to be opened). After selecting *Qt 5.8 MinGW 5.3* as the toolkit, the project can be built as a release by selecting *Build – Build Project "sigviewer"*. This creates an executable in the *bin/release* folder.

On macOS, XCode (available from the App Store) and the Command Line Tools (these can be installed by running `xcode-select --install` in a terminal) are required. The source of the external dependency *libbiosig* can be downloaded from the project website (this requires at least version 1.8.4b). In the *Makefile*, the following lines need to be adapted: lines 199 and 207 need to be commented out, and 10.7 needs to be changed to 10.9 in lines 148 and 151. Furthermore, the program *gawk* is required, which can be installed via Homebrew[11] or by downloading a pre-built binary such as the one available from Rudix[12]. Then, `make libbiosig.a` can be executed in a terminal. This creates the file *libbiosig.a*, which needs to be copied to SigViewer's source into *external/lib*. Similarly, the files *biosig.h* and *gdftime.h* need to be copied to *external/include*. After that, `qmake` can be run in a terminal within the SigViewer source tree, followed by `make`. This creates the app in the *bin/release* folder.

The procedure on Linux is almost identical to the one described for macOS. The only difference concerns the way required dependencies are installed. We recommend to use the native package manager to install a GNU toolchain with *g++*, *gawk*, and Qt 5.

Since details in this process can change rapidly with ongoing development, the most recent instructions on how to build SigViewer can be found on the project website. Note that we provide pre-built binary packages of SigViewer for Windows, macOS, and Linux for users who wish to skip the build process.

[10] `https://sourceforge.net/projects/sigviewer/files/0.5.2/external-0.5.2-win32.zip/download`
[11] `http://brew.sh/`
[12] `http://rudix.org/packages/gawk.html`

Published by Verlag der TU Graz
Graz University of Technology

 DOI: 10.3217/978-3-85125-533-1-10

DISCUSSION

SigViewer is an actively maintained open source viewer for biosignals. The number of monthly downloads is around 250 on average and around 20,000 in total according to the download statistics available from SourceForge (see Figure 3 for the monthly downloads over the past six and a half years). Given that these downloads are for a version that was released almost four years ago, we expect these numbers to increase when the new version with support for XDF is released.

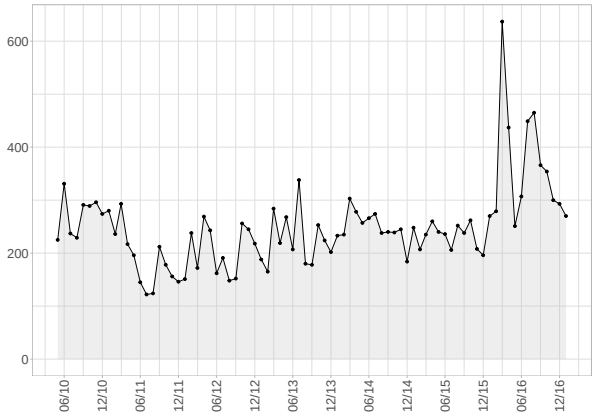

Figure 3: Monthly downloads from SourceForge. The total number of downloads since project upload until 2017-01-31 is 20079, and the average number of monthly downloads is 248.

Planned enhancements for the near future include adding support for spectral filters (highpass, lowpass, notch) to improve visualization of signals with known noise characteristics such as large low-frequency drifts or 50/60 Hz power line noise. Other future efforts will be directed to refactoring parts of the code base, for example to create a more suitable header structure for meta information (which facilitates displaying multi-rate streams without the need for resampling), to implement a hierarchical buffer which stores the signals in different resolutions for rapid visualization in different zoom levels, and to implement a more modular file reader interface.

CONCLUSION

We have added several useful features to SigViewer, most notably support for visualizing multi-stream XDF files. Continued development ensures that SigViewer will remain a valuable tool for inspecting raw biomedical data, which is an important stage in any signal processing pipeline including brain-computer interface (BCI) research.

ACKNOWLEDGMENTS

The authors declare that there is no conflict of interest. We would like to thank Thomas Brunner for starting development on SigViewer, for continued discussions on current issues, and for providing many helpful comments for this manuscript. In addition, we would like to thank Christoph Eibel for his contributions to SigViewer as part of his master's thesis.

REFERENCES

[1] Delorme A, Makeig S. EEGLAB: an open source toolbox for analysis of single-trial EEG dynamics. J. Neurosci. Meth. 2004;134:9–21.
[2] Oostenveld R, Fries P, Maris E, Schoffelen J-M. FieldTrip: Open Source Software for Advanced Analysis of MEG, EEG, and Invasive Electrophysiological Data. Comp. Intell. Neurosci. 2011;2011:156869.
[3] Tadel F, Baillet S, Mosher JC, Pantazis D, Leahy RM. Brainstorm: A User-Friendly Application for MEG/EEG Analysis. Comp. Intell. Neurosci. 2011;2011:879716
[4] Schlögl A, Brunner C. BioSig: A Free and Open Source Software Library for BCI Research. IEEE Comput. 2008;41(10):44–50.
[5] Gramfort A, Luessi M, Larson E, Engemann D, Strohmeier D, Brodbeck C, Parkkonen L, Hämäläinen M. MNE software for processing MEG and EEG data. Neuroimage 2014;86:446–460.
[6] Brunner C, Schlögl A, Pfurtscheller G. SigViewer – an open source viewing and scoring program for biomedical signals, in Proc. 4th International Brain-Computer Interface Workshop and Training Course 2008, 396.
[7] Brunner C, Breitwieser C, Müller-Putz GR. SigViewer and SignalServer – open source software projects for biosignal analysis. Biomed. Eng./Biomed. Tech. 2013;58(S1).

Published by Verlag der TU Graz
Graz University of Technology

Proceedings of the
7th Graz Brain-Computer Interface Conference 2017 DOI: 10.3217/978-3-85125-533-1-11

INCREASING STROKE PATIENTS MOTOR IMAGERY CLASSIFICATION BY SELECTING FEATURES WITH PARTICLE SWARM OPTIMISATION

J. Cantillo-Negrete[1], R.I. Carino-Escobar[1], P. Carrillo-Mora[2], J. Gutierrez-Martinez[1]

[1] Division of Medical Engineering Research, Instituto Nacional de Rehabilitación, Mexico City, Mexico

[2] Division of Neurosciences, Instituto Nacional de Rehabilitación, Mexico City, Mexico

E-mail: jcantillo@inr.gob.mx

ABSTRACT: Motor Imagery based Brain-Computer Interfaces (BCI) have shown potential for the rehabilitation of stroke patients. In order to make BCI systems available in the clinical environment new processing stages that increase the number of patients that can use these systems must be developed. This work presents a novel processing stage for BCI systems using the Filter Bank Common Spatial Patterns algorithm for feature extraction and Particle Swarm Optimisation for feature selection. The proposed BCI's processing stage performance was evaluated with electroencephalography data of six stroke patients, which performed motor imagery of their paralysed hand. Offline tests reached average classification accuracies of 75±8 %. For 4 out of 6 patients, the proposed method showed a statistically significant higher performance ($p<0.05$) than the Common Spatial Pattern method. Therefore, although a higher sample is needed to confirm the observations, it is possible to significantly improve hand motor imagery classification by selecting filter bank common spatial patterns features with particle swarm optimization.

INTRODUCTION

Stroke is the first cause of disability worldwide [1]. Approximately 400 patients receive neurorehabilitation therapy for stroke sequelae each year in the National Institute of Rehabilitation, located in Mexico City. Loss of motor function (known as hemiparesis) is one of the most disabling consequences of stroke, which usually affects both upper and lower limbs from one side of the body.

Assistive technologies such as Brain-Computer Interfaces (BCI) provide an artificial communication channel between the brain and an external device such as a robotic orthosis [2, 3]. BCI systems based on motor imagery (MI) of affected limbs have shown great potential as a tool for brain plasticity enhancement [4, 5]. MI is a mental rehearsal of movements of a limb, for example the hand or foot, without muscle activation [6, 7, 8]. MI elicits distinctive patterns in the electrical activity of the sensory-motor cortex, mainly in the frequency bands known as mu (8-13 Hz) and beta (14-30 Hz) [6, 9]. A MI-based BCI system is comprised of four stages: acquisition, pre-processing, feature extraction and classification. Most BCI acquire electroencephalography (EEG) since is a non-invasive technique, has a good time resolution and is easy to accept by patients. Linear Discriminant Analysis (LDA) is the most used classification technique reported in BCI publications [10, 11]. One of the most effective feature extraction methods is the Common Spatial Patterns (CSP) algorithm, which computes a set of spatial filters that optimally differentiate two classes of MI. To achieve good classification performances using the CSP algorithm, the temporal filtering of the EEG signal must be performed on a specific frequency band, usually this band is comprised by the mu and beta frequency range. Two other parameters that need to be set up are the time interval from which features are going to be extracted, and the subset of spatial filters involved in the feature extraction process [12].

The performance of CSP can be enhanced by selecting subject-specific parameters. Therefore, modifications to the original CSP method have been proposed to include this aspect. One of such modifications is known as Filter Bank Common Spatial Patterns (FBCSP); this method performs an automatic frequency band selection for temporal filtering of the EEG [13]. FBCSP algorithm employs a filter bank that decomposes the EEG into 9 different frequency bands covering the range of 4 to 40 Hz. Each of these 9 frequency bands is spatially filtered using the CSP algorithm; afterwards the extracted features for each band are selected with either the Mutual Information-based Best Individual Feature (MIBIF) or the Mutual Information-based Rough Set Reduction (MIRSR) algorithms. Classification is performed only with the selected features [13,14]. Feature selection is an important stage of the FBCSP algorithm, since it lowers the number of frequency bands needed for MI classification, and at the same time increases the classification performance of the BCI system. Feature selection is in fact an optimisation problem, and therefore artificial intelligence techniques, such as Particle Swarm Optimisation (PSO), could be used for finding a solution for it. PSO was originally proposed by Shi and Eberhart, inspired by the social behaviour of bird flocks

Published by Verlag der TU Graz
Graz University of Technology

 DOI: 10.3217/978-3-85125-533-1-11

while searching for food. PSO performs a search in the space of the problem, with the aid of a population (called swarm) of individuals (called particles). Each particle executes a search based on its current position and velocity in the search space. In each iteration (called generations), the position and velocity of the particles are updated according to their best previous position (local search) and the best position of the swarm (global search) [15]. To the author's knowledge, there are few studies that describe the use of PSO as a feature selection algorithm for BCI systems [16,17].
In this work, a novel signal processing stage comprised of FBCSP for feature extraction, PSO for feature selection and LDA for classification was implemented as part of a BCI system. The proposed algorithm was evaluated offline with data of patients with subcortical stroke diagnosis.

MATERIALS AND METHODS

Participants: The sample for this study comprised 6 patients diagnosed with stroke (Mean = 55.8 ± 12 years). In order to be considered for inclusion in the study, patients had to have a first stroke event of subcortical localisation, confirmed by a neurologist by means of neuroimaging studies (Magnetic Resonance or Computed Tomography); total or partial paresis of one of their hands; without clinical history of any other previous neurological or psychiatric diseases; right handed; with normal or corrected to normal vision and, with a normal performance in the subscales of digit detection and visual detection of the neuropsychological test NEUROPSI (this test has been validated for Spanish-speaking populations) [18]. The subscales evaluate the ability to follow instructions and concentrate in repetitive tasks. Subcortical stroke patients were selected since their brain damage does not involve the brain cortex and, therefore, they were less likely to present significant cognition impairments. Patients' data are shown in Tab. 1.

Table 1: Clinical and Demographic data of patients

Patient	Age	Gender	Hemiparesis	Evolution
1	50	Male	Right	7 months
2	57	Female	Right	36 months
3	58	Male	Left	2 months
4	79	Female	Left	1 month
5	46	Male	Left	3 months
6	45	Male	Left	3 months

EEG acquisition: A g.USBamp biosignal amplifier from g.tec was used for EEG acquisition. EEG was acquired with 24-bits of resolution and sampling rate of 256 Hz. Active EEG electrodes were used for acquisition, with 11 electrodes placed over the scalp of the patients, in positions C3, C4, Cz, T3, T4, F3, F4, Fz, P3, P4 and Pz of the international 10-20 system. Ground placement was set in the AFz position, and the reference electrode was placed in the right earlobe. To verify that no real movements were elicited during MI, Electromyography (EMG) was recorded from the deep flexor and superficial muscles of the fingers of both hands. For each patient, four recording sessions were performed in consecutive days, with 120 trials recorded in total. Recordings were performed in 4 days to avoid patients' exhaustion, and all trials recorded per patient were included in the analysis. Patients were instructed to sit in a comfortable armchair, with a computer monitor placed at 150 cm in front of them. Visual cues shown in the monitor directed the patients to perform both rest with eyes open and MI from their paralysed hand. EEG acquisition was performed using a similar strategy as the one followed by the Graz paradigm [19]. Fig. 1 shows that the rest interval of the trials lasted 3 s and the MI interval lasted 5 s.

Implementation of the FBCSP+PSO algorithm: A one-second length window was extracted from 1.5 s to 2.5 s to obtain the rest information for each trial. Another window of one-second length was extracted from the 3.5 to 4.5 s time interval of each trial, to obtain the MI information of the trials, as observed in Fig. 1. These time windows were selected based on previous studies which show that differentiation between MI and REST classes is higher in these time intervals [20]. The FBCSP algorithm encompassed the processing stage of the BCI system, and PSO was used for feature selection (named FBCSP+PSO). A diagram of the algorithm's implementation is shown in Fig. 2.

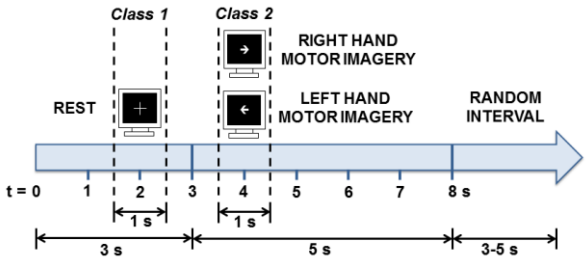

Figure 1: Illustration of the experimental paradigm. Dotted lines show the time windows extracted from EEG signals.

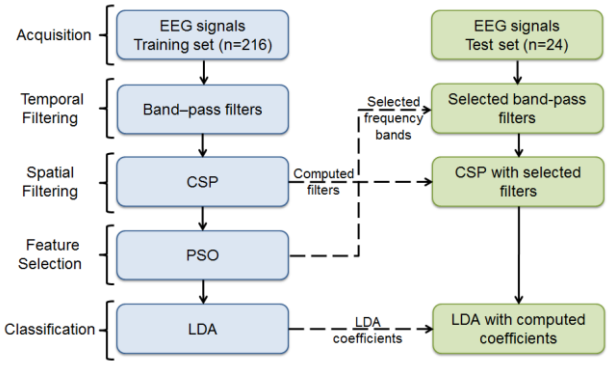

Figure 2: Diagram of FBCSP+PSO implementation

Published by Verlag der TU Graz
Graz University of Technology

 DOI: 10.3217/978-3-85125-533-1-11

EEG data were filtered in order to obtain 6 frequency sub-bands, each 4 Hz broad, and with 1 Hz of overlapping in order to avoid loss of information. Encompassing both alpha and beta frequency bands as follows: 8-12 Hz, 12-16 Hz, 16-20 Hz, 20-24 Hz, 24-28 Hz and 28-32 Hz. A 60 Hz band-stop filter was also applied to the EEG signals. All filters were FIR filters of 20th order, selected for their linear phase features.

For the EEG data filtered in each sub-band, spatial filters were computed with the CSP algorithm. CSP performs a linear transformation on the EEG data, in order to obtain features whose variances are optimal for classification of two classes of MI, in a specific frequency band. Details of the CSP implementation can be found in the works of Blankertz et al. [21], and Ramoser et al. [22]. Spatial filters were computed using the MATLAB command $W = eig\,(S1, S1 + S2)$ as suggested in the above-mentioned works. W is the matrix containing the spatial filters, $S1$ and $S2$ are the covariance matrices of MI and rest computed from the EEG data of each filtered frequency sub-band. In the implementation of the original CSP, only the first and last m columns of the W matrix (m is generally 2) are used to generate the feature vector used for classification. With the goal of having a greater chance of finding the optimal sub-band for each patient, in this work all possible features were extracted with CSP. The feature vector generated for each trial i is comprised as follows:

$$f_i = [f_{1,i}, f_{2,i}, f_{3,i}, f_{4,i}, f_{5,i}, f_{6,i}] \quad (1)$$

Therefore, CSP features computed for the training set comprised by nt trials are:

$$F_{Train} = [f_1; f_2; f_3; f_4; \dots; f_{nt}], \qquad F_{Train} \in \mathbb{R}^{nt \times 66} \quad (2)$$

Where 66 are the 6 frequency band features f extracted for each of the 11 recorded electrodes. For feature selection, PSO was used for selecting a subset of features from F_{Train} in order to decrease both the classification error and the number of selected features. PSO was computed by solving two equations:

$$v_i^{n+1} = w \cdot v_i^n + c_1 \cdot r_1 \cdot (PBest_i^n - x_i^n) + c_2 \cdot r_2 \cdot (GBest_g^n - x_i^n) \quad (3)$$

$$x_i^{n+1} = x_i^n + v_i^{n+1} \quad (4)$$

Where x_i^{n+1} and v_i^{n+1} are the position and velocity of the ith particle of the nth generation. For PSO implementation 50 particles and 50 generations were used. w is the inertial weight of PSO which linearly descends from 1 to 0 as generations of PSO are computed. c_1 and c_2 are positive constants set to 1. r_1 and r_2 have random values between 0 and 1, which coupled to c_1 and c_2 set the local and global search properties of PSO. $PBest_i^n$ is the best position reached by the ith particle in the nth generation. $GBest_g^n$ is the best position (g) reached by the entire swarm in the nth generation. The maximum position value that a particle could reach was 1 and the minimum was 0. Maximum speed of each particle was set to 1 and minimum speed to 0. In this work, the search space of PSO was $1xD$, where D equals 66, and was comprised of the 66 features that can be selected from the FBCSP algorithm. Each computed solution with PSO is a subset of the selected features. Solution values are in the range from 0 to 1. If the value of an element of the solution was higher or equal to 0.5, then the corresponding feature was selected. The original CSP algorithm states that selected features must be paired, so complementary features of the selected ones were also included, in case they were not originally selected by PSO. Selected features from the training set were used for designing an LDA classifier. PSO fitness value was computed with the following equation:

$$value = (err \times 2) + (nselec/66) \quad (5)$$

Where err is the computed classification error from the training set. $nselec$ is the number of selected features. Variables err and $nselec/66$ have values ranging from 0 to 1. Both parameters err and $nselec/66$ are summed, so that PSO can perform a reduction of both classification error and the number of features used for classification. The value err is multiplied by 2, so that the optimization priority of PSO is the reduction of the classification error over the selection of a lower number of features. The stop criteria used for PSO was either achieving 0% of classification error, or 50 generations. Fig. 3 shows a block diagram depicting the implemented PSO algorithm.

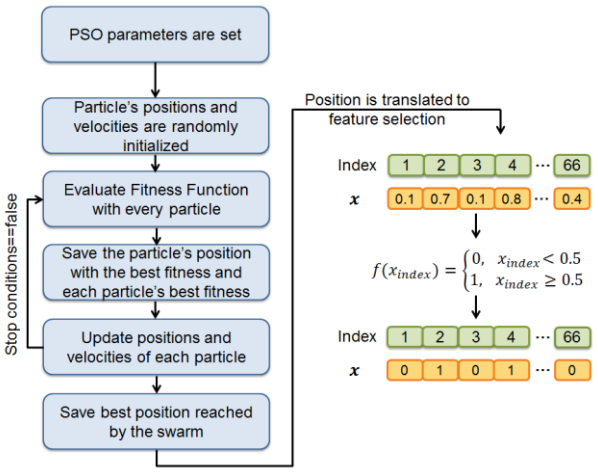

Figure 3: Block diagram describing the implementation of the PSO algorithm

With the final selected features (x) and the training set, a LDA classifier was designed, which was later evaluated with the testing set. Features selected with PSO in the training stage were the same as the ones used for the testing stage of the classifiers. LDA

Published by Verlag der TU Graz
Graz University of Technology

 DOI: 10.3217/978-3-85125-533-1-11

performance was measured by computing the percentage of classification accuracy (%CA).

Cross-Validation: A stratified cross-validation of 10x10-Fold was used in order to avoid bias in the computation of %CA. Classifiers were tested using totally different datasets than the ones used for training. For each fold and repetition, the FBCSP+PSO algorithm was calculated. The 100 values of %CA obtained from this procedure were used to compute the average %CA for each patient.

For comparison purposes, the performance of the FBCSP+PSO method was compared with that of the original CSP using the same training and test subsets, and applied to a frequency band of 8 to 32 Hz.

Statistical Analysis: In order to assess the reliability of the BCI system, both %CA and the practical level of chance were computed. The practical level of chance for each experiment was not 50%, since its value needs to be computed by means of a confidence interval as explained by Muller-Putz et al. [23]. Practical level of chance was computed with a binomial distribution using a 95% confidence interval, with 120 trials encompassing the data of each class. The computed %CA were compared with the practical level of chance in order to assess if a patient could control the BCI system.

A paired t-test (α=0.05) was performed for comparing the %CA obtained with the proposed FBCSP+PSO method, and the original CSP (with a frequency band ranging from 8-32 Hz).

Computational cost: The averaged execution time of the proposed algorithm's training stage for each patient's cross validation was used to estimate its computational cost. All computations were performed in a PC with a 2.5GHz Core i7 processor and 12GB of RAM.

RESULTS

Tab. 2 shows the number of selected features by the FBCSP+PSO algorithm for each patient. This number is the mode from the 100 values computed from the 10x10-Fold cross-validation with the train set. On average, for each patient, 10 features were selected by PSO. The most selected frequency band for all experiment's repetitions is also shown: for 5 of the 6 patients it was from 8 to 12 Hz, which comprises the mu rhythm, while for the other patient the selected frequency sub-band was 12 to 16 Hz. Tab. 3 shows the %CA obtained with FBCSP+PSO and the ones obtained with CSP with a frequency band from 8 to 32 Hz are shown. These percentages are the offline MI and rest recognition capabilities of the BCI.

It is important to remember that the number of selected features with the CSP algorithm was always 4 ($2\times m$). An asterisk (*) was used to indicate if a statistically significant difference ($p<0.05$) was found between both methods. FBCSP+PSO showed better performance than CSP for the 6 patients. For 4 of the 6 patients, differences were statistically significant.

Table 2: Feature selection performed with PSO. SD refers to standard deviation.

Patient	FBCSP+PSO	
	Features	Frequency Band (Hz)
1	10	8-12
2	8	12-16
3	8	8-12
4	10	8-12
5	10	8-12
6	12	8-12
Mean(SD)	10(2)	-

Table 3: Performances of FBCSP+PSO and CSP. An asterisk (*) means that statistically significant differences ($p<0.05$) were found between both methods. SD refers to standard deviation.

Patient	FBCSP+PSO % Classification accuracy (SD)	CSP % Classification accuracy (SD)
1	83 (2)	82 (1)
2	85 (2)	84 (1)
3	68 (2)*	66 (1)
4	65 (3)*	58 (2)
5	76 (2)*	69 (1)
6	74 (2)*	63 (1)
Mean(SD)	75(8)	70(10)

The average computational cost of FBCSP-PSO training stage across all patients was 3.6 s (SD=0.04 s).

DISCUSSION

The presented novel processing stage was comprised by the FBCSP algorithm for feature extraction and PSO for feature selection. Test results were compared to those from the original CSP algorithm with a frequency band from 8 to 32 Hz. The proposed method was designed in order to increase the BCI's MI classification performance of the paralysed hand of stroke patients. Offline performances of the proposed processing algorithm achieved better performances than the original CSP. It is important to mention that for 4 out of 6 patients, these performance differences were statistically significant. These results are different from the ones presented by Ang et al., who performed an offline evaluation of the FBCSP that employed the MIRSR feature selection algorithm. They performed their test with a public database comprised of 9 healthy subjects. In their work, it is shown that FBCSP using the MIRSR algorithm had better performances for 6 out of 9 subjects than CSP (using a 7 to 35 Hz band), but none of the performance differences were statistically significant [14]. Therefore, the FBCSP+PSO method seems to be a better option for automatic frequency band selection of each patient.

The average offline performance computed for each patient is similar to the one reported by Ang et al. in a study which analysed the performance of 46 stroke

Published by Verlag der TU Graz
Graz University of Technology

 DOI: 10.3217/978-3-85125-533-1-11

patients which achieved an average of 74% of correct classification. In order to acquire MI from the patients' paralysed hands, authors recorded 27 EEG channels. The processing stage comprised the FBCSP using MIBIF as feature selection algorithm [24]. In the present work, similar offline performances were obtained, however only 11 EEG channels were recorded. PSO is an optimisation method for which extensive research has been conducted in order to ensure better convergence and to reduce stagnation of the search space. The heuristic nature of PSO implies that the method performance will not be limited by statistical features of the search space, since the method does not need to compute inverse matrices or other computations which often present restrictions, especially for high dimensional search spaces. Consequently, PSO can be easily adapted for feature selection in MI-based BCI with setups involving a high number of EEG electrodes; however, one of the main disadvantages of PSO optimisation is the high computational cost required for its training phase. In this work, computational cost was not an issue since a relative low number of EEG channels were recorded and processed. Offline performances of the BCI system show that PSO implementation for feature selection of FBCSP allows this method to have better performances than CSP. This performance is achieved by setting a multi-objective optimisation for the PSO algorithm, which is computationally efficient since it only required computing the LDA performance and the number of selected features. It is important to mention that, in order to achieve better performances, higher importance was given to the LDA's classification performance than to the number of selected features in the fitness function.

One of the limitations of the present study was that scalp location of the selected features was not analysed. However, all the recorded electrodes were placed over the sensorimotor cortex and, therefore, in an online BCI aimed for neurorehabilitation no maladaptive changes during neural re-organization would be elicited by the feedback.

CONCLUSION

This work presents a novel processing stage for BCI systems. The proposed processing stage comprised of FBCSP+PSO combined with LDA showed good performances for classification of MI from the paralysed hand of stroke patients. PSO as a selection algorithm for FBCSP features allows reducing the problem's dimensionality and achieving better classification performances, compared to those obtained if only the original CSP is used. The next developing stage of the system will be to perform tests involving direct EEG acquisition from patients. An online implementation of the proposed algorithm must be assessed to further confirm its feasibility for stroke patients' rehabilitation.

ACKNOWLEDGEMENTS

The authors would like to thank the National Council of Science and Technology (CONACYT) from Mexico for funding under the grant number SALUD-2015-2-262061. The authors would also like to thank the patients for their participation in this study.

REFERENCES

[1] Mozaffarian D, Benjamin EJ, Go AS, Arnett DK, Cushman M, Ferranti S, et al. Heart Disease and Stroke Statistics-2015 Update A report from the American Heart Association. Circulation. 2015; 131: 29-322

[2] Pfurtscheller G, Guger C, Muller G, Krausz G, Neuper C. Brain oscillations control hand orthosis in a tetraplegic. Neurosci. Lett. 2000;292(3)

[3] King CE, Dave KR, Wang PT, Mizuta M, Reinkensmeyer DJ, Do AH, et al. Performance Assessment of a Brain-Computer Interface Driven Hand Orthosis. Ann Biomed Eng. 2014;40(10): 2095-2105

[4] Mihara M, Hattori N, Hatakenaka M, Yagura H, Kawano T, Hino T, et al. Near-infrared spectroscopy-mediated neurofeedback enhances efficacy of motor imagery-based training in poststroke victims: a pilor study. Stroke. 2013;44: 1091-1098

[5] Mrachacz-Kersting N, Jiang N, Stevenson AJT, Niazi IK, Kostic V, Pavlovic A, et al. Efficient neuroplasticity induction in chronic stroke patients by an associative brain-computer interface. J Neurophysiol. 2016;115: 1410-1421

[6] Pfurtscheller G, Silva L. Event-related EEG/MEG synchronization and desynchronization: basic principles. Clin. Neurophysiol. 1999;110(11): 1842-1857

[7] Zimmermann-Schlatter A, Schuster C, Puhan M, Siekierka E, Steurer J. Efficacy of motor imagery in post-stroke rehabilitation: a systematic review. J Neuroeng Rehabil. 2008;5:8

[8] Pfurtscheller G, Brunner C, Schlogl A, Lopez da Silva FH. Mu rhythm (de)synchronization and EEG single-trial classification of different motor imagery tasks. Neuroimage. 2006; 31(1): 153-159

[9] Andrew C, Pfurtscheller G. On the existence of different alpha band rhythms in the hand area of man. Neurosci Lett. 1997;222(2): 103-106

[10] Muller J, Pfurtscheller G, Flyvbjergc H. Designing optimal spatial filters for single trial EEG classification in a movement task. Clin Neurophysiol. 1999;110(5): 787-798.

[11] Ye J, Xiong T. Computational and Theoretical Analysis of Null Space and Orthogonal Linear Discriminant Analysis. J. Mach. Learn. Res. 2006;7: 1183-1204

[12] Blankertz B, Tomioka R, Lemm S, Kawanabe M, Müller KR. Optimizing spatial filters for robust EEG

Published by Verlag der TU Graz
Graz University of Technology

 DOI: 10.3217/978-3-85125-533-1-11

single-trial analysis. IEEE Signal Proc Mag. 2008; 25:41–56.
[13] Ang KK, Chin ZY, Zhang H, Guan C. Filter Bank Common Spatial Pattern (FBCSP), in Brain-Computer Interface, IEEE IJCNN, Hong Kong, China, 2008, 2390-2397
[14] Ang KK, Chin ZY, Wang H, Guan C, Zhang H. Filter Bank Common Spatial Pattern algorithm on BCI competition IV Datasets 2a and 2b. Front. Nerosci. 2012; 6(39): 1-9
[15] Shi Y, Eberhart RC. A modified particle swarm optimizer, in proc. of the IEEE international Conference on Evolutionary Computation, Anchorage, United States, 1998, 69-73.
[16] Wei Q, Wei Z. Binary particle swarm optimization for frequency band selection in motor imagery based brain-computer interfaces. Bio-med Mater. Eng. 2015;26: 1523-1532
[17] Atyabi A, Luerssen MH, Powers D. PSO-based dimension reduction of EEG recordings: Implications for subject transfer in BCI. Neurocomputing. 2013;119: 319-331.
[18] Ostrosky-Solis F, Gómez-Pérez E, Ardila A, Rosselli M, Matute E, Pineda D. Batería Neuropsicolófica NEUROPSI Atención y memoria, 6 a 85 años de edad. Bookstore, Mexico.
[19] Pfurtscheller G, Neuper C. Motor imagery and direct brain-computer communication. P. IEEE. 2001;7: 1123:1134.
[20] Cantillo-Negrete J, Gutiérrez-Martínez J, Flores-Rodriguez TB, Cariño-Escobar RI, Elías-Viñas D. Characterization of electrical brain activity related to hand motor imafery in healthy subjects. Rev. Invest. Clin. 2014;66 Suppl 1: 111-121
[21] Blankertz B, Tomioka R, Lemm S, Kawanabe M, Müller KR. Optimizing spatial filters for robust EEG single-trial analysis. IEEE Signal Proc. Mag. 2008;25: 41-56
[22] Ramoser H, Muller-Gerking J, Pfurtscheller G. Optimal spatial filtering of single trial EEG during imagined hand movement. IEEE T Biom-med Eng. 2000;8(4): 441-446
[23] Müller-Putz JR, Scherer R, Brunner C, Leeb R, Pfurtscheller G. Better than random? A closer look on BCI results. Int. J. Bioelectromagn. 2008;10: 52-55
[24] Ang KK, Guan C, Chua KS, Ang BT, Kuah CW, Wang C. A Large Clinical Study on the Ability of Stroke Patients to Use an EEG-based Motor Imagery Brain-Computer Interface. Clin EEG Neurosci. 2011;42(4): 252-258

Published by Verlag der TU Graz
Graz University of Technology

Proceedings of the
7th Graz Brain-Computer Interface Conference 2017 DOI: 10.3217/978-3-85125-533-1-12

CLOSED-LOOP DEEP BRAIN STIMULATION SYSTEM FOR AN ANIMAL MODEL OF PARKINSON'S DISEASE: A PILOT STUDY

S. Castaño-Candamil[1*], S. Mottaghi[2*], V.A. Coenen[3], U.G. Hofmann[2], M. Tangermann[1]

[1]Brain State Decoding Lab, BrainLinks-BrainTools, University of Freiburg, Germany
[2]Neuroelectronic Systems, University Medical Center Freiburg, Germany
[3]Stereotactic and Functional Neurosurgery, University Medical Center Freiburg, Germany

[*]E-mail: sebastian.castano@blbt.uni-freiburg.de, soheil.mottaghi@uniklinik-freiburg.de.

ABSTRACT: Deep Brain Stimulation (DBS) is a standard clinical tool for treating refractory stages of Parkinson's Disease (PD). While current chronic DBS systems apply constant stimulation patterns, improved clinical effects are expected from adaptive DBS (aDBS) systems, which stimulate only when required, and for which single-trial methods developed in the field of BCI may prove fruitful. The development of aDBS systems requires (among others) two key ingredients: neural markers informative about the state of the patient's motor system, and algorithmic control strategies which translate the observed markers into stimulation patterns. While both start to be investigated in human patients, animal models of PD may drive aDBS research forward at substantially higher speed and lower risks. In this regard, we present a prototype setup of a closed-loop aDBS system. It enables online recording, signal analysis and stimulation for a rodent model of PD. Our preliminary analyses show that the system – in accordance to the literature – is able to evoke spectral power changes of cortical and subcortical LFPs, and thus provides the experimental basis to systematically investigate informative markers and control strategies.

INTRODUCTION

Deep brain stimulation (DBS) of the subthalamic nucleus (STN) has become a standard therapy for treating refractory stages of Parkinson's disease (PD) [1]. Clinical applications of DBS usually rely on open-loop technology, which means that the stimulation is uninterruptedly delivered, disregarding the motor state of the patient or his/her related brain activity signatures, also called neural markers (NM). This type of DBS is termed continuous DBS (cDBS). Despite proven clinical benefits, cDBS systems are energetically inefficient, leading to a reduced battery life, and are also known to cause side effects like tolerance to treatment [2], [3], [4] which may be related to the continuous stimulation. In recent years, first closed-loop adaptive DBS (aDBS) systems have been presented in research environments [5], [6], [3]. They pursue the goal to provide stimulation on-demand only, for example, by reducing or stopping stimulation during periods of inactivity or when the motor performance of the patient does not require it. The envisioned effect of aDBS is an improvement of the PD symptoms which is at least comparable to that of a cDBS approach, while simultaneously minimizing the energy input to the brain. Determining when and how to deliver stimulation in closed-loop aDBS systems could directly be based upon the observed motor ability of the patient. For practical reasons, however, current approaches try to replace the behavioral measurements by NMs which describe the current motor state of the patient. Such NMs can be extracted from local field potentials (LFPs) recorded via electrodes which habe been implanted in the STN for delivery of the DBS pulses [7], [8]. Although the identification of PD-relevant NMs has been studied in recent years, the high intersubject variability of the signal features makes the characterization of such NMs a difficult task [9], [10], [11]. In addition, the development of closed-loop control algorithms poses a great challenge as (a) non-stationarities govern the dynamics of measured brain activity, (b) artifacts of biological and non-biological origin are contained in the data, (c) the amount of labeled data per patient to learn from is limited. Further studies on investigating the mechanisms of the DBS [12] and on the optimization of stimulation parameters [13], are additional examples of the efforts done in this regard. Along these lines, several studies on closed loop DBS in both computational and experimental neuroscience — such as by [14], [15] and [16] — have been published, where the development of systems that can record, analyze and stimulate in an online closed-loop scenario seemed key to scientific progress. The development of such systems can be addressed using an experimental setup based on animal models, as introduced in [17], [18], [19]. The 6-hydroxydopamine (6-OHDA) PD rat model is an example of a neurotoxic model. It makes use of 6-OHDA injected into the substantia nigra pars compacta (SNC), medial forebrain bundle (MFB), or the caudate-putamen complex CPu [20] to generate Parkisonian-like biomarkers and behavior. In the present work,

[*]Both authors have contributed equally to this study

Published by Verlag der TU Graz
Graz University of Technology

 DOI: 10.3217/978-3-85125-533-1-12

we introduce our initial work on a novel closed-loop DBS stimulation system that allows recording, analysis and stimulation of cortical and subcortical structures in hemi-Parkinsonian rats, which has not been reported so far in the literature. We also present preliminary results on the spectral effects evoked by DBS when applied to the STN of 6-OHDA PD rats.

METHODS

Animal Preparation

Stereotactic surgery was carried out for high precision lesioning and electrode implantation. All protocols were approved by the Animal Care Committee of the University of Freiburg (permit G-15/31). Female Sprague-Dawley rats (300-320g) received inhalation anaesthesia with isoflorane. A freshly prepared 6-hydroxydopamine according to [21], kept in the dark and on ice, was injected unilaterally into the ventrolateral CPu. The flow rate of the injection was 0.5 μl/min and the injection was carried out for 10 min using a micropefusion pump.

Four weeks after the operation, a rotational test was carried out on each rat. Each animal was habituated to the test environment for around 30 minutes. Then, the animal was taken out, subcutaneously administrated with apomorphine to evaluate the success of the lesioning operation with drug-induced rotation, as explained in [21]. The animals were placed back in the experiment environment and the rotation was measured for 40 minutes. The animals showing drug-induced rotation (PD rats from now on) were chosen for the electrode implantation surgery.

The week after, electrodes implantation surgery was carried out on 6 PD rats. Two electrodes were implanted in two different regions of the brain. One tetrode in the subthalamic nucleus (STN) with four contacts (two stimulation and two recording), made from 50μm micro wires (Science Products GmbH, Germany) and a bitrode with two recording contacts in the motor cortex with the same micro wires. Two anchors were placed on the rat's skull as reference and ground contacts, respectively. After a week of recovery the closed loop experiment was executed.

Signal Acquisition

The stimulation device used in this study was designed and built in the Neuroelectronic System group (NES STiM) of the University Medical Center Freiburg, Germany [22],[23]. An Alphalab SnR (Alphaomega Co., Israel) recording device was utilized to capture the LFPs of the rat's brain during the experiment. The schematic of the closed loop setup is depicted in Fig. 1. The signals were recorded at 1395 Hz sampling frequency. For the offline analysis, a frequency filter with a pass band of 0.7-90 Hz was applied before signals were downsampled to 250 Hz.

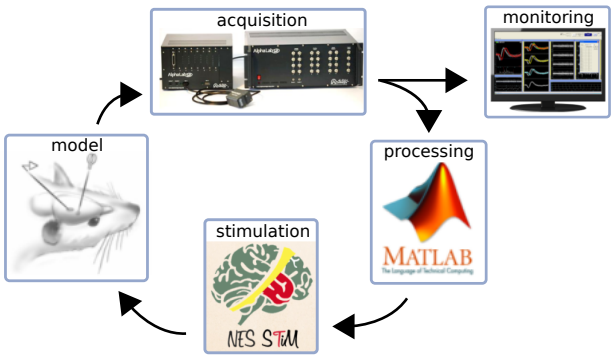

Figure 1. Schematic of the closed loop utilized in this study. The signal of local field potentials (LFPs) is captured using an Alphalab SnR device and streamed out for visualization and into Matlab. Analysis of the acquired signals, as well as the stimulation control was performed online.

Experimental Design

The timeline of one experimental session is depicted in Figure 2. Each rat was recorded for 10 mins after being placed in the experimental environment (pre-stimulation phase), followed by a stimulation phase of 10 min duration. Prior to the subcutaneous injection of apomorphine and directly after it, the LFP baseline activity was recorded for 10 s each. During the following 10 minutes, closed loop DBS stimulation was carried out (stimulation phase). In this stage, the stimulation onset was triggered when the power of the beta band (13-25 Hz) activity averaged across channels surpassed a threshold defined as the median of the power recorded in the post-injection baseline interval. Once the stimulation was triggered, it was delivered with constant intensity for one minute. For later offline analysis of the simulation effect, two time intervals of LFP signals of 10 s duration each were extracted from the stimulation-free periods directly before and after the stimulation. After a washout period of 60 s, the threshold criterion became active again and the next stimulation block could be delivered. Within the 10 min stimulation phase, an average of 4.6 stimulation blocks were delivered per animal.

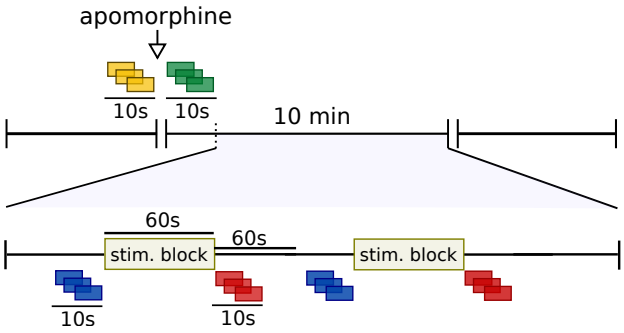

Figure 2. Schematic of the recording sessions with a depiction of the segments analyzed: baseline prior to apomorphine delivery ●, baseline following apomorphine delivery ●, pre-stimulation ●, post-stimulation ●.

Published by Verlag der TU Graz
Graz University of Technology

 DOI: 10.3217/978-3-85125-533-1-12

Segments analyzed: Recorded signals were analyzed under two different setups.

1) To determine the effects of DBS in the spectra of the motor cortex and the STN, signals before and after each stimulation interval were analyzed. The 10 s of data before and after DBS stimulation were segmented using 2 s rectangular windows with 90% overlap. Pre-stimulation and post-stimulation spectra were compared using the Wilcoxon rank-sum test to determine the statistical significance of observed differences. For reference, the spectra of two baseline recordings were also computed, i.e., 10 s segments immediately before and after apomorphine delivery, but prior to any DBS stimulation. Refer to Figure 2 for an schematic representation.
2) To analyze potential washout effects of the apomorphine, as well as cumulative effects caused by repeated delivery of DBS periods over 10 minutes, the 10 s segments of data collected before each DBS stimulation (windowed as described above) were correlated with the timestamp (time since apomorphine delivery) of each window using the Spearman's rank correlation.

In all scenarios, PSD of the signals was computed using a multitaper estimate with a multitaper windowing bandwidth of 4 Hz. The frequency components around 30 Hz were disregarded in the analysis due to a hardware-related artifact in that frequency band.

RESULTS

Effects of DBS onto the spectrum

Figure 3 depicts spectra of all animals, four recording locations and the four conditions: baseline prior (yellow) and after (green) apomorphine, and the average of the spectra prior (blue) and after (red) each DBS stimulation block, according to the setup shown in Figure 2. It is observed, that the administration of apomorphine causes an increment in the signal power particularly in the low frequency range. This phenomenon can be observed in all the channels for subjects 2, 3, 4 and 6. DBS effects are assessed by comparing pre and post segments of each simulation block (blue vs. red). Various, subject-specific effects were observed: For subject 1 synchronization of activity in the 5-10 Hz range was observed (mainly visible in channels m1, m2, and stn1). Subject 2 shows a contrary effect upon stimulation, where power in the low frequency range decreases, as observed in m2 and stn2. An even stronger power decrement can be observed in the beta band (around 15 Hz) of this subject, particularly evident in channels m2, stn1, and stn2. Subject 3 shows a much more smooth spectrum, with no specific frequency peaks standing out from the background in either conditions, except for a low frequency desynchronization present in stn2 and a beta band synchronization detected in stn1. Subject 4 shows a behavior similar to subject 1, presenting power decrease in the lower part of the frequency spectrum for m2, stn1, and stn2. Subject 5 shows the smallest spectral changes caused by DBS stimulation, with a subtle power decrement of the alpha-range component in channel m2. Similarly to subject 3, power spectra of subject 6 do not show any evident frequency components standing out from the background, with the effects of the stimulation decreasing the signal energy of the entire analyzed spectrum.

Effects of time in PSD

Spearman's rank correlation between the energy of each of the frequency bins and the corresponding timestamp are provided in Figure 4. Subject 1 shows rather heterogeneous changes in the spectra of m1 and m2, however both stn1 and stn2 show a clear desynchronization (marked in blue) in the lower frequency range. Subject 3 shows a consistent power decrement in the lower part of the spectrum for m1 and m2, and a generalized increment of the power (marked in red) in stn2. Subjects 4 and 5 show a generalized decrease in the signal energy along time. It is worth pointing out that for subject 4, alpha band was stable for m1, m2 and stn1, whereas beta was stable only for m1 and m2. On the other hand, the time-related desychronization for subject 5 is present in the whole spectrum, although a stronger desynchronization in stn1 beta band can also be observed. Finally, subject 3 reveals a weak power decrement in the lower part of the spectrum for m2, having stn1 the contrary effect. Channel stn2 presents a power decrement, which is homogeneous across the spectrum.

DISCUSSION

In this contribution, we presented (1) a closed loop aDBS system allowing acquisition, analysis and stimulation of subcortical and cortical structures of PD animal models and (2) preliminary results on the individual effects observed upon DBS on spectral characteristics of LFP signals.

i Our system provides a suitable platform for acquisition of subcortical and cortical signals in an online scenario. Although, the real-time requirements of the system have not been defined, its modular construction allows for a flexible setup, that is easy to customize. As future work, the exact temporal characteristics of the system will be assessed.
ii DBS-evoked cortical and subcortical desynchronization and synchronization effects in alpha and beta bands have been observed. As the effects varied between animals, relevant NMs should be determined individually for each subject. This finding underlines the potential benefit of data-driven approaches for driving aDBS methods forward.
iii We have shown that the experimental setup divided in pre-, during, and post-stimulation phases is appropriate to carry out the intended analysis.
iv Temporal structure of the spectral features confirms the existence of non-stationary dynamics. While in

Published by Verlag der TU Graz
Graz University of Technology

 DOI: 10.3217/978-3-85125-533-1-12

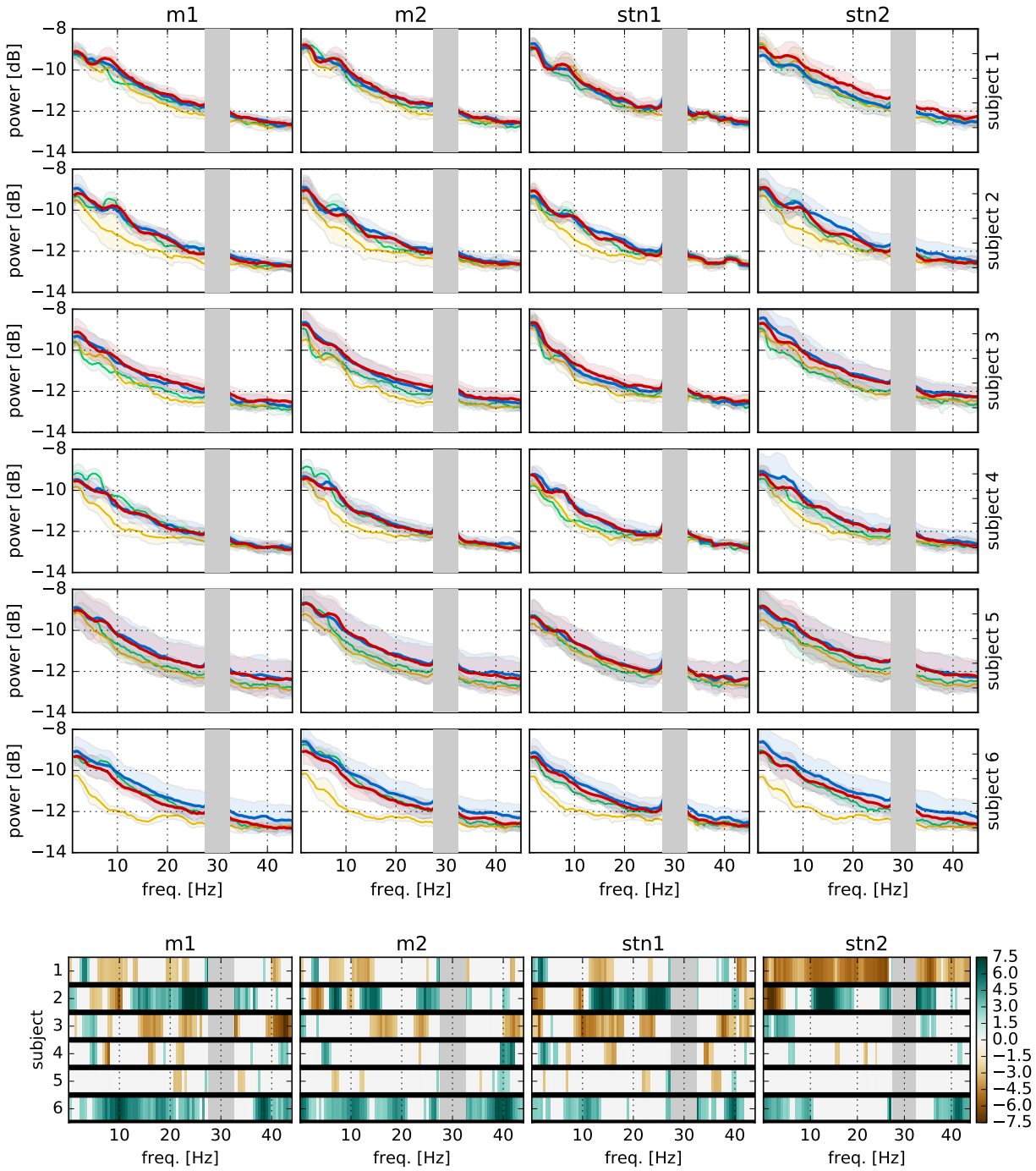

Figure 3. **Top**: spectra of recorded channels displaying DBS- and apomorphine-evoked changes: baseline prior to apomorphine ●, and baseline following apomorphine ●, pre-stimulation block ●, post-stimulation block ●. **Bottom**: Graded scores of the ranksum test are provided in green to brown colors. They compare pre- ● vs. post-stimulation ● spectra. In both figures, gray areas mark the spectral band affected by a technical artifact.

our setup, it could not be determined, if this non-stationarity is caused by repeated DBS or by the washout of the apomorphin, the results strongly indicate, that non-stationarities must be considered in analyses and aDBS systems.

ACKNOWLEDGEMENTS

This work is supported by the BrainLinks-BrainTools Cluster of Excellence funded by the German Research Foundation (DGF, grant number EXC 1086).

Published by Verlag der TU Graz
Graz University of Technology

 DOI: 10.3217/978-3-85125-533-1-12

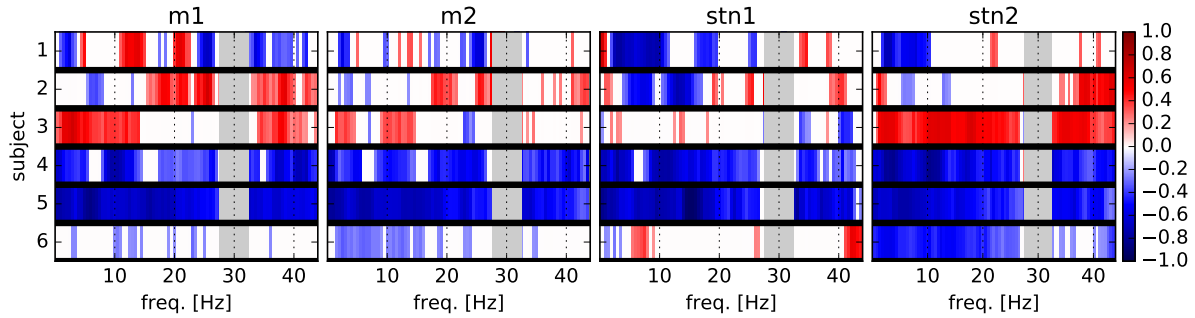

Figure 4. Correlation of power spectrum with time. Red means that the power of the corresponding frequency bin increased during the stimulation phase, whereas blue signals a decrease in power. For each bin, correlations are colored if the p-value of the correlation was > 0.02. Statistical tests were not corrected for multiple testing.

REFERENCES

[1] Günther Deuschl, Carmen Schade-Brittinger, Paul Krack, Jens Volkmann, Helmut Schäfer, Kai Bötzel, Christine Daniels, Angela Deutschländer, Ulrich Dillmann, Wilhelm Eisner, Doreen Gruber, Wolfgang Hamel, Jan Herzog, Rüdiger Hilker, Stephan Klebe, Manja Kloß, Jan Koy, Martin Krause, Andreas Kupsch, Delia Lorenz, Stefan Lorenzl, H. Maximilian Mehdorn, Jean Richard Moringlane, Wolfgang Oertel, Marcus O. Pinsker, Heinz Reichmann, Alexander Reuß, Gerd-Helge Schneider, Alfons Schnitzler, Ulrich Steude, Volker Sturm, Lars Timmermann, Volker Tronnier, Thomas Trottenberg, Lars Wojtecki, Elisabeth Wolf, Werner Poewe, and Jürgen Voges. A randomized trial of deep-brain stimulation for Parkinson's disease. *New England Journal of Medicine*, 355(9):896–908, 2006. PMID: 16943402.

[2] Simon Little, Elina Tripoliti, Martijn Beudel, Alek Pogosyan, Hayriye Cagnan, Damian Herz, Sven Bestmann, Tipu Aziz, Binith Cheeran, Ludvic Zrinzo, Marwan Hariz, Jonathan Hyam, Patricia Limousin, Tom Foltynie, and Peter Brown. Adaptive deep brain stimulation for Parkinson's disease demonstrates reduced speech side effects compared to conventional stimulation in the acute setting. *Journal of Neurology, Neurosurgery & Psychiatry*, pages jnnp–2016, 2016.

[3] Simon Little, Alex Pogosyan, Spencer Neal, Baltazar Zavala, Ludvic Zrinzo, Marwan Hariz, Thomas Foltynie, Patricia Limousin, Keyoumars Ashkan, James FitzGerald, Alexander L. Green, Tipu Z. Aziz, and Peter Brown. Adaptive deep brain stimulation in advanced Parkinson disease. *Annals of Neurology*, 74(3):449–457, 2013.

[4] Romain Carron, Antoine Chaillet, Anton Filipchuk, William Pasillas-Lepine, and Constance Hammond. Closing the loop of deep brain stimulation. *Frontiers in Systems Neuroscience*, 7(112), 2013.

[5] Robert Leeb, Aleksander Sobolewski, Inaki Iturrate, Ricardo Chavarriaga, Iulia Peciu-Florianu, Etienne Pralong, Francois Vingerhoets, Jocelyne Bloch, and José del R Millán. First steps towards adaptive deep brain stimulation in Parkinson's disease. In *Proceedings of the 6th International Brain-Computer Interface Meeting*, 2016.

[6] Simon Little, Martijn Beudel, Ludvic Zrinzo, Thomas Foltynie, Patricia Limousin, Marwan Hariz, Spencer Neal, Binith Cheeran, Hayriye Cagnan, James Gratwicke, Tipu Z Aziz, Alex Pogosyan, and Peter Brown. Bilateral adaptive deep brain stimulation is effective in Parkinson's disease. *Journal of Neurology, Neurosurgery & Psychiatry*, pages jnnp–2015, 2015.

[7] Zack Blumenfeld and Helen Brontë-Stewart. High frequency deep brain stimulation and neural rhythms in Parkinson's disease. *Neuropsychology review*, 25(4):384–397, 2015.

[8] Simon Little and Peter Brown. What brain signals are suitable for feedback control of deep brain stimulation in Parkinson's disease? *Annals of the New York Academy of Sciences*, 1265(1):9–24, 2012.

[9] Diane Whitmer, Camille de Solages, Bruce C Hill, Hong Yu, Jaimie M Henderson, and Helen Bronte-Stewart. High frequency deep brain stimulation attenuates subthalamic and cortical rhythms in Parkinson's disease. *Frontiers in Human Neuroscience*, 6(155), 2012.

[10] Andrea A. Kühn and Jens Volkmann. Innovations in deep brain stimulation methodology. *Movement Disorders*, 32(1):11–19, 2017.

[11] Luke A. Johnson, Shane D. Nebeck, Abirami Muralidharan, Matthew D. Johnson, Kenneth B. Baker, and Jerrold L. Vitek. Closed-loop deep brain stimulation effects on Parkinsonian motor symptoms in a non-human primate - is beta enough? *Brain Stimulation*, 9(6):892–896, 2016.

[12] Karl Nowak, Eilhard Mix, Jan Gimsa, Ulf Strauss, Kiran Kumar Sriperumbudur, Reiner Benecke, and Ulrike Gimsa. Optimizing a rodent model of Parkinson's disease for exploring the effects and mechanisms of deep brain stimulation. *Parkinson's*

Published by Verlag der TU Graz
Graz University of Technology

 DOI: 10.3217/978-3-85125-533-1-12

Disease, page 414682, 2011.

[13] Amorn Wongsarnpigoon and Warren M Grill. Energy-efficient waveform shapes for neural stimulation revealed with genetic algorithm. *Journal of neural engineering*, 7(4):46009, 2010.

[14] Georgios Detorakis, Antoine Chaillet, Stéphane Palfi, and Suhan Senova. Closed-loop stimulation of a delayed neural fields model of Parkinsonian STN-GPe network: a theoretical and computational study. *Frontiers in Neuroscience*, 9:237, 2015.

[15] Hemmings Wu, Hartwin Ghekiere, Dorien Beeckmans, Tim Tambuyzer, Kris van Kuyck, Jean-Marie Aerts, and Bart Nuttin. Conceptualization and validation of an open-source closed-loop deep brain stimulation system in rat. *Scientific Reports*, 4:9921, 2015.

[16] Gian Nicola Angotzi, Fabio Boi, Stefano Zordan, Andrea Bonfanti, and Alessandro Vato. A programmable closed-loop recording and stimulating wireless system for behaving small laboratory animals. *Scientific Reports*, 4:5963, 2014.

[17] Yasin Temel, Veerle Visser-Vandewalle, Brenda Aendekerk, Bart Rutten, Sonny Tan, Bart Scholtissen, Christoph Schmitz, Arjan Blokland, and Harry W.M. Steinbusch. Acute and separate modulation of motor and cognitive performance in parkinsonian rats by bilateral stimulation of the subthalamic nucleus. *Experimental Neurology*, 193(1):43 – 52, 2005.

[18] Yasin Temel, Chunyan Cao, Rinske Vlamings, Arjan Blokland, Hatice Ozen, Harry W. Steinbusch, Kimmo A. Michelsen, Stephan von Hörsten, Christoph Schmitz, and Veerle Visser-Vandewalle. Motor and cognitive improvement by deep brain stimulation in a transgenic rat model of Huntington's disease. *Neuroscience letters*, 406(1):138–141, 2006.

[19] Kim Tieu. A guide to neurotoxic animal models of Parkinsons disease. *Cold Spring Harbor perspectives in medicine*, 1(1):a009316, 2011.

[20] Ronald Deumens, Arjan Blokland, and Jos Prickaerts. Modeling Parkinson's disease in rats: an evaluation of 6-OHDA lesions of the nigrostriatal pathway. *Experimental neurology*, 175(2):303–317, 2002.

[21] Ronald Deumens, Arjan Blokland, and Jos Prickaerts. Modeling Parkinson's disease in rats: An evaluation of 6-OHDA lesions of the nigrostriatal pathway. *Experimental Neurology*, 175(2):303 – 317, 2002.

[22] Soheil Mottaghi, Richard Pinnell, and Ulrich G. Hofmann. 16-bit high-voltage digital charge-control electrical stimulator. *World Congress on Medical Physics and Biomedical Engineering*, pages 1208–1212, 2015.

[23] Soheil Mottaghi and Ulrich G. Hofmann. Dynamically adjusted, scalable electrical stimulator for exciteable tissue. *7th International IEEE/EMBS Conference on Neural Engineering (NER)*, pages 288–291, 2015.

Published by Verlag der TU Graz
Graz University of Technology

Proceedings of the
7th Graz Brain-Computer Interface Conference 2017 DOI: 10.3217/978-3-85125-533-1-13

SUBSPACE DECOMPOSITION IN THE FREQUENCY DOMAIN

S. Castaño-Candamil[1] and M. Tangermann[1]

[1]Brain State Decoding Lab, BrainLinks-BrainTools Cluster of Excellence
Department of Computer Science
University of Freiburg, Germany
E-mail: sebastian.castano@blbt.uni-freiburg.de

ABSTRACT: Measuring brain activity with non invasive techniques as EEG and MEG allows to detect oscillatory sources related to neural processes. Covariance-based spatial filters determined by linear subspace methods allow to extract narrow band sources whose band power correlates with a given target variable in single trial. Since knowledge about the frequency band of interest usually is unknown, filterbank strategies are commonly used. They rely on time domain filtering of the signals to predefined frequency bands. We suggest that the implementation can be optimized by computing the covariance matrices directly in the frequency domain, thus rendering the iterative time-domain filtering unnecessary. Our contribution shows that the implementation in the frequency domain is computationally more efficient than the classic approach. We evaluated the novel approach in the context of source power comodulation (SPoC) and give indications, how it can be extended to other subspace methods such as common spatial patterns (CSP) [1].

INTRODUCTION

Measuring electrical oscillatory activity of the brain by using electroencephalography (EEG) provides functional information about the underlying neural processes [2]. Extraction and analysis techniques of such oscillatory components have been developed in the context of brain-computer interfaces (BCI) [3], [4] and neuroscience [5]. As low signal-to-noise ratio (SNR) and volume conduction impedes the EEG analysis, spatial de-mixing approaches are widely used in order to extract oscillatory subspace components. For this purpose, unsupervised techniques are widely used, with independent component analysis (ICA) [6], [7] being most prominent in the field. With specific prior knowledge, however, more specialized methods like spatio-spectral decomposition (SSD) [8] or slow feature analysis [9] may prove valuable. If discrete labels are available, however, then a supervised method like common spatial patterns (CSP) [1] can improve the subspace representation, as the spatial decomposition can be guided by the label information. CSP is applicable when discrete labels are given (e.g. class labels in a motor imagery task, hits vs. misses in a perception task). CSP determines the projecting components based on channel-space covariance matrices, that maximize the contrast of oscillatory activity between conditions.

In other paradigms, the additional information is provided in the form of continuous labels rather than discrete class labels. A regression approach – like Source Power Comodulation (SPoC), introduced by Dähne et al. – is able to exploit these continuous labels in order to extract spatial components [10], [11]. Both supervised covariance-based subspace methods, CSP and SPoC, have been designed to extract oscillatory components whose band-power is informative. However, while CSP expects discrete two-class labels and maximizes contrast, SPoC requires a continuous target signal and identifies spatial components, which co-modulate in their power with this known continuous univariate target signal. For applications of SPoC on neural signals please refer to [12], [10], [11], [13].

Choosing a suitable frequency band is a critical hyperparameter for these methods, since they require a narrow band frequency filter to be applied to the data prior to starting the search for subspace components [14], [15]. If knowledge about expected informative frequency bands is not available, a generic filter bank approach can be used, as proposed by Ang et al. for CSP [16]. It runs CSP separately on several versions of the data, each one pre-filtered to a different frequency band. Finally, the outcomes of the bands are merged, e.g. by a subsequent feature selection or regression step as proposed by Nove et al. [17].

Typically, filterbank strategies are implemented by filtering the signals in the time domain. However, since trial-wise stationarity of the signals is assumed for most applications, the explicit representation of the temporal dynamics within a trial may actually not be necessary.

In this regard, we propose the implementation of a more computationally efficient filter-bank approach for subspace methods that is based on the calculation of a stationary frequency domain representation of the data. We present results of a study carried out in the context of SPoC for real EEG data.

METHODS

Forward Model of EEG Generation

Let $\boldsymbol{X} \in \mathbb{R}^{N_c \times N_t}$ be a multivariate signal describing data of brain activity measured in the EEG sensor space, where N_t is the number of time samples and N_c the number of sensors. Furthermore, let $\boldsymbol{S} \in \mathbb{R}^{N_s \times N_t}$ describe the time course of N_s neural sources, where

Published by Verlag der TU Graz
Graz University of Technology

 DOI: 10.3217/978-3-85125-533-1-13

N_s describes the number of hidden neural sources considered. We assume a linear generative model, which maps the source space to the sensor space as follows:

$$\boldsymbol{X} = \boldsymbol{A}\,\boldsymbol{S} + \boldsymbol{E}\,. \tag{1}$$

In this model, matrix $\boldsymbol{A} \in \mathbb{R}^{N_c \times N_s}$ describes the projection of the sources to the sensor space, where the columns of $\boldsymbol{A}$, $\boldsymbol{a} \in \mathbb{R}^{N_c}$, are referred to as *spatial patterns*. Furthermore, the matrix $\boldsymbol{E}$ contains spatially and temporally uncorrelated noise to model measurement noise.

An estimation of the time course of a source component $\hat{\boldsymbol{s}}$ can be extracted from the measurements by applying a *spatial filter* $\boldsymbol{w} \in \mathbb{R}^{N_c}$, which projects the data from sensor space into source space. Thus we have $\hat{\boldsymbol{s}} = \boldsymbol{w}^\top \boldsymbol{X}$. For many problems, such a spatial filter $\boldsymbol{w}$ is not known a priori and must be estimated from the data. However, once a spatial filter (or an entire set thereof, denoted by $\boldsymbol{W} \in \mathbb{R}^{N_c \times N_s}$, where each column $\boldsymbol{w}$ represents a single spatial filter) has been obtained, an estimate of the corresponding spatial patterns can be obtained via $\hat{\boldsymbol{A}} = \boldsymbol{C}\boldsymbol{W}\left(\boldsymbol{W}^\top \boldsymbol{C}\boldsymbol{W}\right)^{-1}$, where $\boldsymbol{C} \in \mathbb{R}^{N_c \times N_c}$ denotes the spatial covariance matrix of the data. See [18] for further details on the relation between spatial filters and spatial patterns.

Source Power Co-Modulation — SPoC

The multivariate analysis method called source power co-modulation (SPoC) by Dähne and colleagues [10] utilizes a supervised regression approach in order to estimate a set of spatial filters $\boldsymbol{W}$. The method assumes that the recorded data $\boldsymbol{X}$ has been pre-filtered to a narrow frequency band, which contains the oscillatory source of interest.

Based on data of multiple epochs e, a filter $\boldsymbol{w}$ is optimized such that the power of an epoch $\Theta_x(e) = \mathrm{var}[\hat{\boldsymbol{s}}](e)$ of the spatially filtered data $\hat{\boldsymbol{s}} = \boldsymbol{w}^\top \boldsymbol{X}$, maximally covaries with a known, epoch-wise defined univariate target variable $z(e)$. For the sake of simplicity in the notation, $\hat{\boldsymbol{s}}$ will be noted as $\boldsymbol{s}$, hereafter.

It can be shown that solving such an optimization problem is equivalent to solving the generalized eigenvalue problem [10]

$$\boldsymbol{C}_z \boldsymbol{W} = \boldsymbol{\Lambda}\boldsymbol{C}\boldsymbol{W} \tag{2}$$

where $\boldsymbol{C}_z = \langle \boldsymbol{C}(e) z(e) \rangle$ and $\boldsymbol{C} = \langle \boldsymbol{C}(e) \rangle$. $\langle \boldsymbol{C}(e) \rangle$ and $\langle \boldsymbol{C}(e) z(e) \rangle$ provide the (z-weighted) covariance of $\boldsymbol{X}$, averaged across epochs e: $\boldsymbol{C}(e) = \boldsymbol{X}(e)\boldsymbol{X}(e)^\mathsf{T}$. Matrix $\boldsymbol{\Lambda} \in \mathbb{R}^{N_c \times N_c}$ contains the corresponding eigenvalues in the main diagonal.

Given a spatial filter $\boldsymbol{w}_{tr}$ determined on training data tr, the true target variable $\boldsymbol{z} = [z(1) \ldots z(N_e)]^\top$ can subsequently be approximated/estimated as $\hat{\boldsymbol{z}}$ on a single-trial basis for unseen test data (te) epochs $\boldsymbol{X}_{te}$ via $\hat{z}(e) = \mathrm{var}[\boldsymbol{w}_{tr}^\top \boldsymbol{X}_{te}(e)]$. While in most scenarios a small number of filters is utilized, we limit our analysis for the reminder of this contribution to the one spatial filter $\boldsymbol{w}$ which corresponds to the biggest eigenvalue of the aforementioned decomposition.

Filterbank SPoC

Until now, we have assumed that the target frequency band is known. Unfortunately, this is typically not true, thus exploring the full available spectrum is necessary. SPoC can then be extended by using the filterbank concept proposed by Ang and colleagues for the filterbank CSP algorithm [16]. Here, a set of N_{filt} frequency bands are defined, for which the subspace decomposition method is applied separately. In the context of SPoC, this approach shall be termed filterbank SPoC (**FB-SPoC**) hereafter. FB-SPoC results in a set of N_{filt} different estimations of $\hat{\boldsymbol{z}}$. We define these intermediate band-wise estimations $\hat{\boldsymbol{z}}_i$. To obtain a final $\hat{\boldsymbol{z}}$, a linear model combining all the estimations of the target variables can be applied:

$$\widehat{z}(e) = \sum_{i}^{N_{filt}} \beta_i \widehat{z}_i(e) \tag{3}$$

where the weights $\boldsymbol{\beta}$ are determined by solving the optimization problem:

$$\arg\max_{\boldsymbol{\beta}} ||\widehat{\boldsymbol{z}} - \boldsymbol{z}||_2^2 + \lambda ||\boldsymbol{\beta}||_p^2. \tag{4}$$

In Eq. 4, λ is a positive real-valued regularization parameter and p defines the type of regularization applied to the model, with $p = 2$ corresponding to the classic Tikhonov regularization and $p = 1$ a sparseness promoting prior, termed LASSO.

Computation of Covariance Matrices in the Frequency Domain

In implementations of filterbanks for different algorithms (as CSP, spatio-spectral decomposition [8], among others), data initially is bandpass filtered in the time domain using IIR or FIR filters. Thus, the computational cost grows linearly with the number of bands.

However, since the aforementioned methods are based on the computation of the covariance matrix of the signal, which is assumed to be stationary in the analyzed epochs, the actual computation of such covariance matrices could alternatively be executed directly in the frequency domain. According to the Plancherel theorem [19], the dot product of two signals in the time domain is equal to the inner product of their frequency representation. Consequently, the covariance matrix $\boldsymbol{C}$ may be computed for a specific frequency band f as

$$\boldsymbol{C}_{i,j}^f = \mathrm{re}(< \mathcal{X}_i^f, \mathcal{X}_j^f >) \tag{5}$$

where $\mathrm{re}(\cdot)$ is the real part of the argument, $\mathcal{X}_i$ are the coefficients of the Fourier transform of channel i in $\boldsymbol{X}$, and superindex f indexes the frequency bin corresponding to frequency bands of interest. The intuition behind neglecting the imaginary part of the dot product is that it provides information about the mean phase difference between the considered distributions,

Published by Verlag der TU Graz
Graz University of Technology

 DOI: 10.3217/978-3-85125-533-1-13

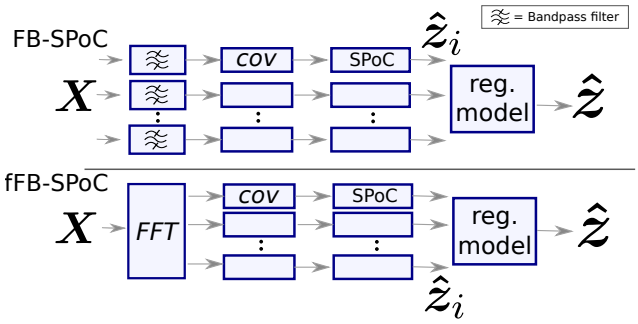

Figure 1. Schematic representation of the filter bank strategy applied to SPoC, FB-SPoC, compared to the proposed approach of computing the covariance matrix directly in the frequency domain (fFB-SPoC).

therefore it does not contribute to the co-varying power information provided by the covariance matrix.

Computing the covariance matrix in the frequency domain requires a single calculation of the fourier transform of $\boldsymbol{X}$, and this computational effort is independent of the number of frequency bands included in the filter bank. Furthermore, a single copy of the signal is required in memory, whereas for time domain filter bank approaches, N_{filt} versions of it are necessary. Thus, the frequency domain representation optimizes memory access operations and allows cheaper caching in hierarchical memory architectures. The proposed approach of computing FB-SPoC using the frequency representation of data $\boldsymbol{X}$ is termed **fFB-SPoC** hereafter. Figure 1 shows a schematic representation of the implementation differences between FB-SPoC and fFB-SPoC

EXPERIMENTAL SETUP

The proposed approaches, FB-SPoC and fFB-SPoC, were tested using real EEG data. Signals were recorded from 64 passive Ag/AgCl electrodes (EasyCap / BrainAmp DC amplifiers) placed according to the 10-20 system and referenced against the nose. Data were recorded while performing an auditory oddball experiment with an interstimulus onset of 1 s. Information about the paradigm was not used in the subsequent analysis. Signals were sampled at 1 kHz, then a band-pass filter with a cut-off frequency of 0.7-90 Hz and a notch filter at 50 Hz were applied to the data. Afterwards, it was downsampled to 250 Hz.

A target source $\boldsymbol{s}$, which would serve as the ground truth source in a following simulation, was determined by projecting the preprocessed EEG data onto a single source. The corresponding filter $\boldsymbol{v}$ for this purpose was chosen pseudo-randomly. The projected signal was then filtered to the alpha band ($8 - 12$ Hz) and its envelope was extracted via the Hilbert transform.

The final dataset for running performance comparisons was obtained by segmenting the EEG and the ground truth target source $\boldsymbol{s}$ data into 1 s windows with 50 % overlap. The ground truth target variable $z(e)$ for each epoch e was defined as the average of the envelope of the target source $\boldsymbol{s}$ for that epoch.

Performance Metrics

In order to quantitatively assess the performance of the considered methods, the following performance metrics were considered:

Correlation – corr: This metric evaluates the quality of the final regression model. More precisely, it describes the correlation between the target variable estimated by the regression model $\hat{\boldsymbol{z}}$ and the true modulating signal (target variable) $\boldsymbol{z}$. A higher absolute value suggests a better estimation.

Best Band Correlation – corr: This metric evaluates the quality of estimation for the best performing frequency band. More precisely, it describes the correlation between the target variable estimated by the best filter $\hat{\boldsymbol{z}}_i$ and the true modulating signal (target variable) $\boldsymbol{z}$. A higher absolute value suggests a better estimation.

Earth Mover's Distance – emd: This metric can be used to characterize the most important frequency band. It measures the dissimilarity between the estimated and the true spatial pattern $\hat{\boldsymbol{a}}$ and $\boldsymbol{a}$ within a single frequency band. The lower the value of emd, the more accurate the estimation. As fFB-SPoC and FB-SPoC yield one pattern per frequency band, emd is calculated in the frequency band achieving the highest $corr$ performance.

Angle Between Patterns – angle: Analogous to emd, this metric describes the angle between the estimated and true spatial patterns $\hat{\boldsymbol{a}}$ and $\boldsymbol{a}$. The lower the value of $angle$, the more accurate the estimation. Since FB-SPoC and fFB-SPoC yield patterns corresponding to more than one frequency band, emd is calculated using the pattern related to the most relevant frequency band, according to the $corr$ achieved.

Elapsed Time – et: Computational cost is compared in terms of walltime required to compute the final estimation of $\hat{\boldsymbol{z}}$.

Parameter Sensitivity Analysis

The aforementioned metrics are assessed in a parameter sensitivity analysis. For this, a random search was performed, where the parameter space is defined by (1) the number of bands in the filter bank, (2) the type of spacing (grid) between passing bands of the filter bank and their corresponding width, which can be linearly or logarithmically spaced, and (3) the regularization type for the regression model in Eq. 4. Random search of the parameter space was performed using the random-search tool provided by the publicly available sequential model-based algorithm configuration (SMAC) toolbox[1] [20], whereas the parameters sensitivity analysis was performed using functional ANOVA (FANOVA)[2] [21]

[1] http://www.cs.ubc.ca/labs/beta/Projects/SMAC/
[2] https://github.com/automl/fanova

Published by Verlag der TU Graz
Graz University of Technology

 DOI: 10.3217/978-3-85125-533-1-13

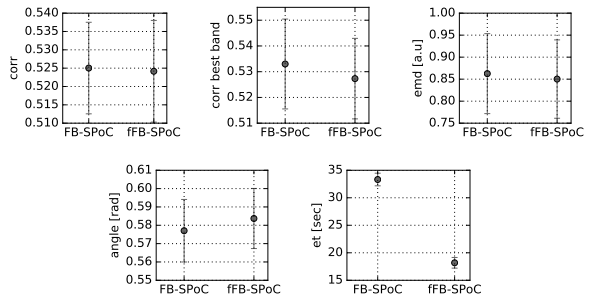

Figure 2. Marginalized performance of FB-SPoC and fFB-SPoC for the considered metrics.

RESULTS

FB-SPoC vs fFB-SPoC: Overall Performance

Figure 2 shows the marginalized performance of FB-SPoC and fFB-SPoC as computed with FANOVA. As expected, correlation values achieved and the spatial accuracy of the spatial patterns (as assessed by emd and angle), are not significantly different for the considered methods. On the other hand, marginalized walltime was significantly lower for fFB-SPoC compared to FB-SPoC.

FB-SPoC vs fFB-SPoC: Parameter Sensitivity Analysis

Figure 3 shows marginalized effects of different configurations of the parameter space uppon the performance, both for FB-SPoC and fFB-SPoC.

The number of frequency bands is the parameter that had the greatest impact on the correlation achieved. The grid type used for the definition of the filter bands plays a less critical role, with the linear model showing a small advantage over the logarithmic grid. The regularization method of the regression model did not affect the performance in terms of the marginalized correlation.

The effects of the parameter configuration upon emd and angle are very similar. Comparably to the effects upon the correlation metrics, the number of bands used in the filter bank is the parameter that has the strongest impact upon the spatial patterns, where as the grid type and the regression model do not seem to be critical.

For both, the accuracy of the target variable (corr) and the spatial pattern estimation, the optimal number of frequency bands for the considered scenario are approximately 5 bands. Using more than 5 bands does not improve the performance, according to any of the considered measures.

Finally, the bottom row of Figure 3 demonstrates the computational advantages of fFB-SPoC, where the walltime required increases at a much slower rate than for FB-SPoC. It is worth mentioning that between 1 and 3 bands, the metric et grows with the same rate for both algorithms.

DISCUSSION

In this contribution, we extended the use of a filterbank approach to the context of source power co-modulation analysis, SPoC. Furthermore, we propose to perform the covariance matrix calculation in the frequency domain to speed-up the computation of filterbank-based subspace techniques.

i A filterbank strategy for SPoC is a suitable approach to estimate target variables that co-modulate with the power of hidden neural sources. The proposed approaches are specially valuable in scenarios where the frequency band of interest is not known and, consequently, a full exploration of the available spectrum is necessary. Such applications have already been reported in the literature, for example [13], [12].

ii Under the realistic scenario considered, the number of frequency bands is the most important hyperparameter considering the high final correlation with the target variable and a good reconstruction of the true spatial pattern $\boldsymbol{a}$. This might be explained by the fact that a coarse segmentation of the frequency spectrum leads to mixing of informative and noisy frequency bands into the same filters, thus degrading the performance. This is also observed in the variance of the performance itself — a sudden reduction of the variance is observed once the number of frequency bands becomes greater than five. It is important to point out that the optimal number of frequency bands should be defined individually and for each application scenario, since the width of the informative frequency band of the target source and its location within the spectrum is not known a priori.

iii For our data, where no label noise was involved, the grid type and regression model had little influence. Similarly to the number of frequency bands, the grid type is likely to be application-dependent. The regression model, on the other hand, is likely to be independent of the frequency characteristics of the target neural source, but may be sensitive to the level of noise contained in its labels. In future work, we will investigate the interaction of label noise noise with different regression models.

iv We have also shown that the computation of the covariance matrix using the frequency representation of the EEG data is a suitable approach for filter bank strategies. The computational advantage is not only caused by the single-time computation of the FFT compared to the N_{filt}-many (sequential) time-domain filtering steps. It also affects the calculation of the covariance matrix itself, which has quadratic runtime. When computed in the time domain, each of the entries of the covariance matrix $\boldsymbol{C}$ corresponds to the dot product of two time series, each with length N. In contrast, when computed in the frequency domain, each entry of $\boldsymbol{C}$ corresponds to the dot product of two vectors containing a subset of M frequency bins obtained after the Fourier transform, with typically $N >> M$. It is important to point out that the covariance is computed simul-

Published by Verlag der TU Graz
Graz University of Technology

 DOI: 10.3217/978-3-85125-533-1-13

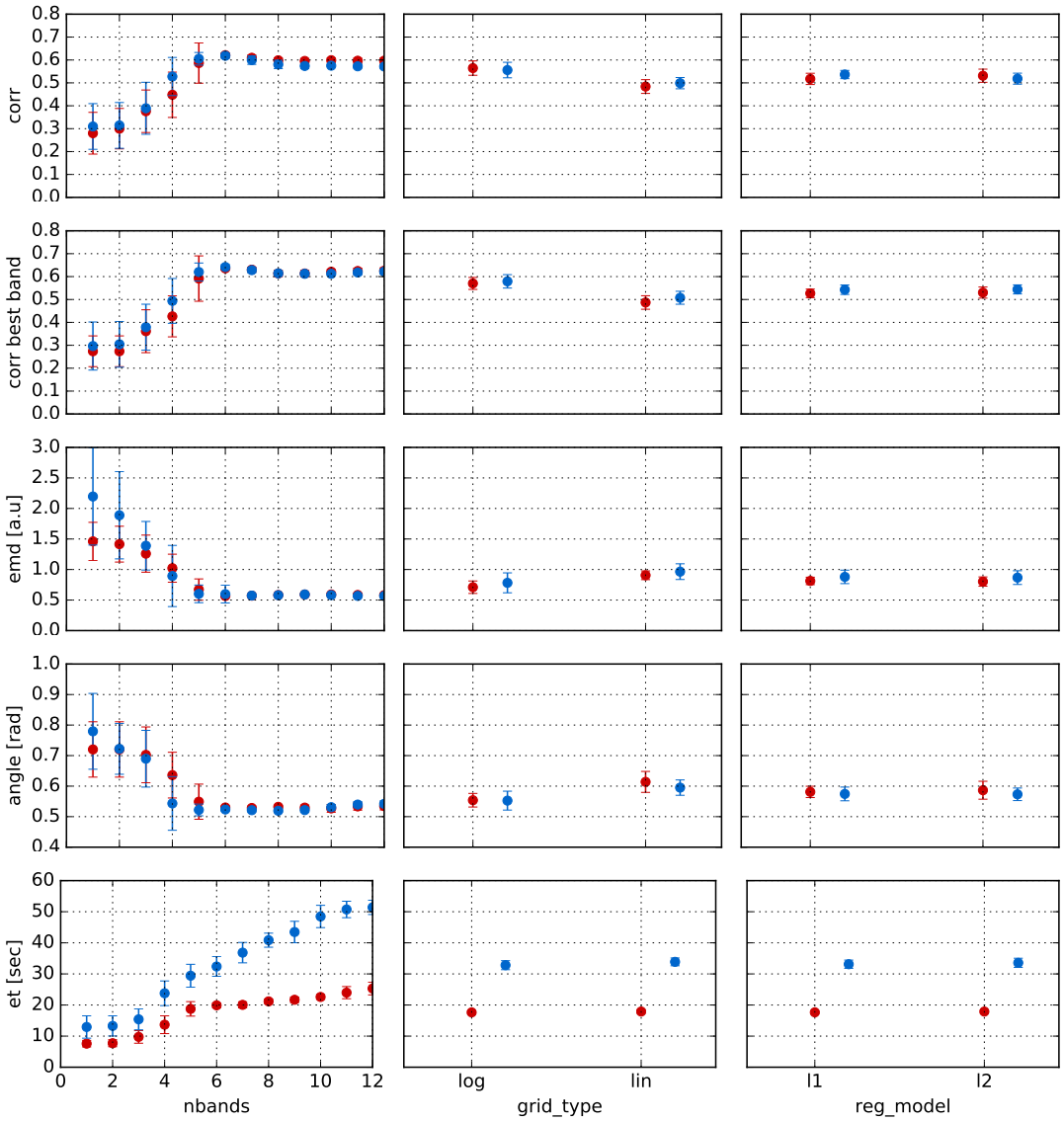

Figure 3. Marginalized parameter sensitivity analysis comparing FB-SPoC ● and fFB-SPoC ●, in terms of the considered performance measures.

taneously on the entire subset of M frequency bins in a single step, and not for each bin individually.

v The main limitation of the frequency-domain filterbank approach is the coarse granularity of the frequency bands considered. Their resolution is limited by the number of frequency bins resulting from the Fourier transformation, while filters in the time domain can be defined in high precision.

vi Another limitation of applying SPoC in the frequency domain is the smaller number of SPoC components which can be derived per frequency band. Specifically, the rank of the covariance matrix is limited by the number of frequency bins contained in the analyzed band. However, this limitation may not be a relevant one in practice, as a full rank SPoC decomposition often is not required and usually only the first-ranked, most informative components are used.

vii Finally, the proposed frequency domain approach for filterbank analysis should easily extend to other covariance-based subspace methods such as CSP or SSD.

ACKNOWLEDGEMENTS

This work is supported by the BrainLinks-BrainTools Cluster of Excellence funded by the German Research Foundation (DGF, grant number EXC 1086). Special thanks to Sven Dähne for the code of SPoC and fruitful discussions. We also acknowledge support by the state of Baden-Württemberg through bwHPC and the German Research Foundation (DFG) through grant no INST 39/963-1 FUGG. Finally, we want to thank Katharina Eggensperger for providing software wrappers for SMAC, which we have made heavy use of in our analyses.

Published by Verlag der TU Graz
Graz University of Technology

 DOI: 10.3217/978-3-85125-533-1-13

REFERENCES

[1] Steven Lemm, Benjamin Blankertz, Gabriel Curio, and K.-R. Müller. Spatio-spectral filters for improving the classification of single trial EEG. *Biomedical Engineering, IEEE*, 52(9):1541–1548, 2005.

[2] György Buzsáki and Andreas Draguhn. Neuronal oscillations in cortical networks. *Science*, 304(5679):1926–1929, 2004.

[3] Jan B. F. van Erp, Fabien Lotte, and Michael Tangermann. Brain-computer interfaces: Beyond medical applications. *Computer*, 45(4):26–34, 2012.

[4] Johannes Höhne, Elisa Holz, Pit Staiger-Sälzer, Klaus-Robert Müller, Andrea Kübler, and Michael Tangermann. Motor imagery for severely motor-impaired patients: Evidence for brain-computer interfacing as superior control solution. *PLoS ONE*, 9(8):e104854, 08 2014.

[5] Ole Jensen, Ali Bahramisharif, Robert Oostenveld, Stefan Klanke, Avgis Hadjipapas, Yuka O Okazaki, and Marcel AJ van Gerven. Using brain–computer interfaces and brain-state dependent stimulation as tools in cognitive neuroscience. *Frontiers in Psychology*, 2:100, 2011.

[6] Scott Makeig, Anthony J. Bell, Tzyy ping Jung, and Terrence J. Sejnowski. Independent component analysis of electroencephalographic data. In *in Advances in Neural Information Processing Systems*, pages 145–151. MIT Press, 1996.

[7] Aapo Hyvärinen and Erkki Oja. Independent component analysis: Algorithms and applications. *Neural networks*, 13(4-5):411–430, May 2000.

[8] Stefan Haufe, Sven Dähne, and Vadim V Nikulin. Dimensionality reduction for the analysis of brain oscillations. *NeuroImage*, 101:583–597, 2014.

[9] Sven Dähne, Johannes Höhne, Martijn Schreuder, and Michael Tangermann. Slow feature analysis-a tool for extraction of discriminating event-related potentials in brain-computer interfaces. In *International Conference on Artificial Neural Networks*, pages 36–43. Springer, 2011.

[10] Sven Dähne, Frank C. Meinecke, Stefan Haufe, Johannes Höhne, Michael Tangermann, Klaus-Robert Müller, and Vadim V. Nikulin. SPoC: A novel framework for relating the amplitude of neuronal oscillations to behaviorally relevant parameters. *NeuroImage*, 86(0):111 – 122, 2014.

[11] Sven Dähne, Vadim V. Nikulin, David Ramírez, Peter J. Schreier, Klaus-Robert Müller, and Stefan Haufe. Finding brain oscillations with power dependencies in neuroimaging data. *NeuroImage*, 96:334–348, 2014.

[12] Andreas Meinel, Sebastián Castaño-Candamil, Sven Dähne, Janine Reis, and Michael Tangermann. EEG band power predicts single-trial reaction time in a hand motor task. In *Proc. Int. IEEE Conf. on Neural Eng. (NER)*, pages 182–185, Montpellier, France, April 2015. IEEE.

[13] Andreas Meinel, Sebastián Castaño-Candamil, Janine Reis, and Michael Tangermann. Pre-trial EEG-based single-trial motor performance prediction to enhance neuroergonomics for a hand force task. *Frontiers in Human Neuroscience*, 10(170), 2016.

[14] Benjamin Blankertz, Klaus-Robert Müller, Dean Krusienski, Gerwin Schalk, Jonathan R. Wolpaw, Alois Schlögl, Gert Pfurtscheller, José del R. Millán, Michael Schröder, and Niels Birbaumer. The BCI competition III: Validating alternative approaches to actual BCI problems. *IEEE Transactions on Neural Systemas and Rehabilitation Engineering*, 14:153–159, 2006.

[15] Michael Tangermann, Klaus-Robert Müller, Ad Aertsen, Niels Birbaumer, Christoph Braun, Clemens Brunner, Robert Leeb, Carsten Mehring, Kai J Miller, Gernot Müller-Putz, Guido Nolte, Gert Pfurtscheller, Hubert Preissl, Gerwin Schalk, Alois Schlögl, Carmen Vidaurre, Stephan Waldert, and Benjamin Blankertz. Review of the BCI competition IV. *Frontiers in Neuroscience*, 6(55), 2012.

[16] Kai Keng Ang, Zheng Yang Chin, Haihong Zhang, and Cuntai Guan. Filter bank common spatial pattern (FBCSP) in brain-computer interface. In *Neural Networks, 2008. IJCNN 2008. (IEEE World Congress on Computational Intelligence). IEEE International Joint Conference on*, pages 2390–2397, 2008.

[17] Quadrianto Novi, Cuntai Guan, Tran Huy Dat, and Ping Xue. Sub-band common spatial pattern (SBCSP) for brain-computer interface. In *Neural Engineering, 2007. CNE '07. 3rd International IEEE/EMBS Conference on*, pages 204–207, May 2007.

[18] Stefan Haufe, Frank Meinecke, Kai Görgen, Sven Dähne, John-Dylan Haynes, Benjamin Blankertz, and Felix Bießmann. On the interpretation of weight vectors of linear models in multivariate neuroimaging. *NeuroImage*, 87(0):96 – 110, 2014.

[19] Michel Plancherel and Mittag Leffler. Contribution à l'étude de la représentation d'une fonction arbitraire par des intégrales définies. *Rendiconti del Circolo Matematico di Palermo (1884-1940)*, 30(1):289–335, 1910.

[20] Frank Hutter, Holger Hoos, and Kevin Leyton-Brown. Sequential model-based optimization for general algorithm configuration. In *Proc. of LION-5*, page 507–523, 2011.

[21] Frank Hutter, Holger Hoos, and Kevin Leyton-Brown. An efficient approach for assessing hyperparameter importance. In *Proceedings of International Conference on Machine Learning 2014 (ICML 2014)*, pages 754–762, June 2014.

Published by Verlag der TU Graz
Graz University of Technology

Proceedings of the
7th Graz Brain-Computer Interface Conference 2017 DOI: 10.3217/978-3-85125-533-1-14

BRAIN COMPUTER INTERFACE BASED COMMUNICATION IN THE COMPLETELY LOCKED-IN STATE

U. Chaudhary[1,2], A. Rana[1], A. Malekshahi[1], S. Silvoni[3], N. Birbaumer[1,2]

[1] Institute of Medical Psychology and Behavioral Neurobiology, University of Tuebingen
[2] Wyss Center for Bio and Neuroengineering, Genéva, Switzerland
[3] Department of Cognitive and Clinical Neuroscience, Central Institute of Mental Health, Mannheim, Germany

E-mail: niels.birbaumer@uni-tuebingen.de; chaudharyujwal@gmail.com

ABSTRACT: Patients in completely locked-in state (CLIS) are unable to communicate with the external world because of complete paralysis of the motor system. Brain computer interface (BCI) aims to restore communication in CLIS patient by bypassing the dysfunctional motor system. Electroencephalography (EEG) based BCI has been used successfully in patient in Locked-in state (LIS), but once the patient transition in CLIS EEG-BCI fails to provide communication. Recently we reported the first single case report of functional near infrared spectroscopy (fNIRS) based auditory BCI control by an ALS patient in CLIS. Here we report fNIRS-BCI based communication in four ALS patients in CLIS, two of them in permanent completely locked-in state (CLIS) and two entering the CLIS without reliable means of communication. Patients learned to answer personal questions with known answers and open questions all requiring a "yes" or "no" thinking using fronto-central oxygenation changes measured with fNIRS. Online fNIRS classification of personal questions with known answers and open questions, using linear support vector machine (SVM), resulted in an above-chance-level correct response rate over 70%. Electroencephalographic (EEG) oscillations and electro-oculographic (EOG) signals did not exceed the chance-level threshold for correct communication despite occasional differences between the physiological signals representing a "yes" or "no" response.

INTRODUCTION

Amyotrophic lateral sclerosis is a progressive motor disease of unknown etiology resulting eventually in a complete paralysis of the motor system but affecting sensory or cognitive functions to a minor degree [1]. There is no treatment available; patients have to decide to accept artificial respiration and feeding after the disease destroys respiratory and bulbar functions or to die of respiratory or related problems. If they opt for life and accept artificial respiration, the disease progresses until the patient loses control of the last muscular response, usually the eye muscles. If rudimentary voluntary control of at least one muscle is present, the syndrome is called locked-in state (LIS) [2]; ultimately as the disease progresses most of the ALS patients lose the control of all the muscles, the resulting condition is called completely locked-in state (CLIS) [2]. Patients in CLIS are unable to communicate with the external world because all assistive communication aids are based on some remaining motor control; hence there is a vital need for an assistive technology to help patients in CLIS to communicate their needs and feelings to their family members/caregivers. Brain computer interface (BCI) represents a promising strategy to establish communication with paralyzed ALS patients, as it does not need muscle control. BCI research includes invasive (implantable electrodes on or in the neocortex) and noninvasive means (including electroencephalography (EEG), magnetoencephalography (MEG), functional magnetic resonance imaging (fMRI), and near-infrared spectroscopy (NIRS)) to record brain activity for conveying the user's intent to devices such as simple word-processing programs. Non-invasive methods have been utilized more frequent than invasive methods for people with disabilities (such as those with ALS) [3-7].
For these conditions (LIS and CLIS) Brain-Computer-Interfaces were developed and tested extensively since the first publication of Birbaumer et al (1999) [8] of two LIS patients suffering from ALS. Patients select letters or words after learning self-regulation of the particular brain signal or by focusing their attention to the desired letter or a letter-matrix (Farwell & Donchin) [9] and the attention related brain signals allow the selection of desired letter. While healthy people and ALS patients up to the LIS showed successful BCI control and communication [10], completely paralyzed ALS patients in CLIS did not learn sufficient BCI control for brain communication (Kuebler & Birbaumer, 2008) [11]. A single case report by Gallegos Ayala et al., 2014 [12] suggested that a CLIS patient with ALS could achieve BCI-control and "yes" - "no" communication to simple questions with known positive answers or negative answers and some open questions over an extensive time period. NIRS was used to measure and classify cortical oxygenation and deoxygenation following the questions. The BCI methodology used in this report departed radically from the previous BCI-

Published by Verlag der TU Graz
Graz University of Technology

 DOI: 10.3217/978-3-85125-533-1-14

procedures: a more "reflexive" mode based on learning principles of classical conditioning to simple questions was used to train the classifier separating "yes" and "no" thinking of answers by the patient and instead of neuroelectric recording (EEG) functional NIRS (fNIRS) was used.
Hence, an extensive study was performed on four ALS patients in CLIS to train them to communicate "yes" and "no". The fNIRS based BCI was employed successfully to train patients to regulate their fronto-central brain regions in response to auditorily presented questions. After training a classifier separating "yes" from "no" answer for several days the patients were given feedback of their affirmative or negative response to questions with known answers and open questions over weeks [13].

MATERIAL AND METHOD

The Internal Review Board of the Medical Faculty of the University of Tubingen approved the experiment reported in this study and the patients' legal representative gave informed consent for the study with permission to publish the results and show the face of patients in the publication. The study was in full compliance with the ethical practice of Medical Faculty of the University of Tubingen. The clinical trial registration number is ClinicalTrials.gov Identifier: NCT02980380.

Patient
Patient F (Female, 68 years old, completely locked-in state) was diagnosed with bulbar sporadic ALS in May 2007, as locked-in in 2009, and as completely locked-in May 2010, based on the diagnosis of experienced neurologists. She has been artificially ventilated since September 2007, fed through a percutaneous endoscopic gastrostomy tube since October 2007, and is in home care. No communication with eye movements, other muscles, or assistive communication devices was possible since 2010.
Patient G (Female, 76 years old, CLIS) was diagnosed with bulbar ALS in 2010. She lost speech and capability to walk by 2011. She has been fed through a percutaneous endoscopic gastrostomy tube since September 2011, artificially ventilated since March 2012, and is in home care. She started using assistive communication devices employing one finger for communication in Feb 2013. Later she was diagnosed with degeneration of vision due to cornea defects in Sept 2013. After the failure of the finger communication device an attempt was made to communicate using eye tracking in early 2014. She stopped communicating with the eye in Aug. 2014 before the BCI was introduced and an attempt was made to communicate with the subtle twitch of eye lid which was not reliable. The husband and caretaker declared no communication with her since August 2014.
Patient B (Male, 61 years old, CLIS) was diagnosed with non-bulbar ALS in May 2011. He has been artificially ventilated since August 2011, fed through a percutaneous endoscopic gastrostomy tube since October 2011, and is in home care. He started communicating with a speech device in his throat from Dec. 2011 which ultimately failed and he started using MyTobii eye-tracking device in April 2012. He was able to communicate with MyTobii until Dec 2013 after which the family members attempted to communicate by training him to move his eyes to the right to answer "yes" and left to answer "no", but the response was variable. No communications was possible since August 2014.
Patient (Female, 24 years old, locked-in state on the verge of CLIS) was diagnosed of juvenile ALS in Dec 2012. She was completely paralyzed within half a year after diagnosis and has been artificially ventilated since March 2013, fed through a percutaneous endoscopic gastrostomy tube since April 2013, and is in home care. She was able to communicate with eye-tracking from early 2013 to Aug 2014 but was unable to use the eye-tracking device after the loss of eye control in Aug 2014. After August 2014 family members were able to communicate with her by training her to move her eyes right to answer "yes" and left to answer "no" questions until Dec 2014. In Jan 2015 eye control was completely lost and she tried to answer yes by twitching the right corner of her mouth and that too varied considerably.

Instrumentation
A continuous wave (CW) based NIRS system, NIRSPORT (NIRX), which performs dual-wavelength (760 nm & 850 nm) CW near-infrared spectroscopic measurement at a sampling rate of 6.25 Hz, was used. The NIRS optodes were placed on the fronto central brain region.
During the BCI sessions the EEG was also recorded with a multi-channel EEG amplifier (Brain Amp DC, Brain Products) from ten Ag/AgCl passive electrodes mounted on the same cap. Six electrodes were used to acquire EEG signals based on the international 10-10 system and the selected channels were FC5, FC1, FC6, CP5, CP1 and CP6 while four electrodes were used to acquire the vertical and horizontal EOG. The signals were bandpass filtered using an FIR filter with a passband of 0.5 – 35 Hz. The EOG was filtered with different filters (3.5 Hz, 10 Hz, and 30 Hz) but none of the filters led to significant differences of neurophysiological patterns related either to the ocular activity or to their SVM-classification accuracies. Each channel was referenced to an electrode on the right mastoid and grounded to the electrode placed on the Fz location of the cap. Electrodes impedances were kept below 10 kΩ and the EEG signal was sampled at 500 Hz. During all BCI sessions the spontaneous EEG was visually controlled by one of the authors (NB or BX) to avoid longer periods of slow wave sleep. A BCI session was initiated only if the EEG was free of high amplitude slow activity below 3.5Hz.

Experiment Procedures

Published by Verlag der TU Graz
Graz University of Technology

 DOI: 10.3217/978-3-85125-533-1-14

An auditory based paradigm was employed to a) train patients on questions with known answers, b) give feedback on questions with known answers and c) answer open questions. Known questions are personal questions with known "yes" and "no" answer. Patients were asked to think yes or no and if possible also to use their previously successful eye movements. Open questions are general questions related to quality of life and questions of caretakers whose answer can only be known by the patient. The BCI study started with training sessions during which the patients were instructed to listen to 20 personal questions (with known answers) consisting of 10 true and 10 semantically equivalent false sentences, presented in random order. Patients were asked to think "ja, ja, …" (German for "yes") and "nein, nein, …" (German for "no") for 15 seconds, during the inter stimulus interval (ISI), until they heard the next sentence, as shown in Fig1. After the end of each training session the NIRS feature necessary to differentiate between "yes" and "no" answers during ISI was extracted and classified. If the classification accuracies across at least 3 consecutive training sessions were greater than 65% - 70% the patients were given online feedback after each question. During the online feedback sessions again the patients were presented the same sentences as described above but now at the end of the 15 sec answering period they were given auditory feedback, whether their answer was recognized as "yes" or "no". If the accuracy of online feedback was greater than 70% we presented the patient with open questions during which he/she was always given the auditory feedback of his/her answer. The validity of answers to open questions can only be estimated by a) face validity (i.e. questions of pain in the presence of an open wound), b) stability over time and c) external validity estimated by family members and caretakers and d) internal validity between questions (i.e. the concordance between the answers to semantically equivalent questions (e.g., "Berlin is the capital of France" and "Berlin is the capital of Germany"). Tab. 1 enumerates the total number of training, feedback and open questions sessions performed by each patient.

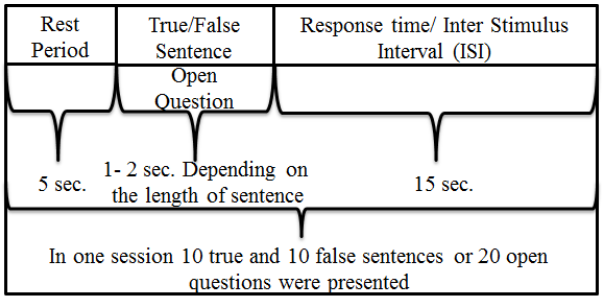

Figure 1: The auditory brain computer interface paradigm used for communication in CLIS patient.

Patient W received no open questions because of low classification accuracy which we and the parents attributed to her emotionality distracting her from concentrating on the responses due to the short time period of adaptation to the CLIS.

Table 1: Lists the total number of training, feedback, open question sessions performed by each patient

Patient / Sessions	Training Sessions	Feedback Sessions	Open Questions Sessions
Patient F	51	7	2
Patient G	51	6	2
Patient B	40	4	2
Patient W	16	4	0

Data Acquisition and Analysis

The schematic depicting the acquisition and analysis of NIRS and EEG data during the BCI sessions is shown in Figure 2. The NIRS data acquired online throughout all the sessions was normalized, filtered using a bandpass filter of 0.01 Hz – 0.3 Hz and processed using Modified Beer Lambert's law, as described in Cope et al. (1987) [14] and Chaudhary et al. (2011) [15], to calculate the relative change in concentration of oxy (O_2Hb) and deoxy hemoglobin (RHb). The relative change in O_2Hb, with respect to the baseline, calculated online during each training session was used to train a model and check the cross-validation classification accuracy. The offline classification procedure used the mean of relative change in O_2Hb across each channel as input feature to train a 5-fold linear support vector machine (SVM) classifier [16]. The SVM [16] model interpolates the data corresponding to true and false sentences' ISI in a two-dimensional space such that the two categories are divided by a hyperplane and the gap between them is as wide as possible.

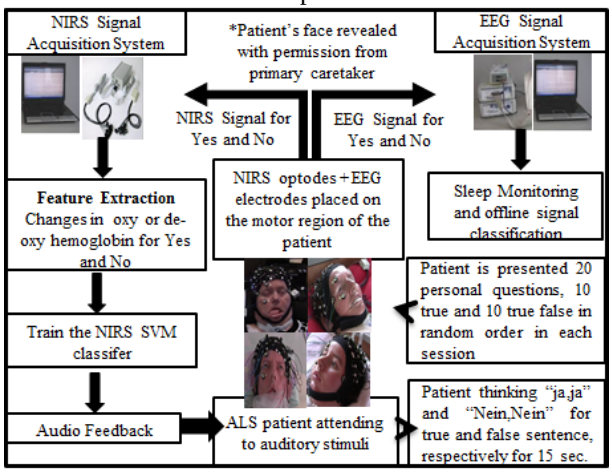

Figure 2: The setup and flow diagram of the brain computer interface for communication in ALS patients.

Firstly a model space was determined and the input feature, extracted from the recorded and processed NIRS signal, i.e., the relative change in O_2Hb, was mapped onto the model space to determine the side of the hyperplane the input feature fell on. For the NIRS signal the mean of the relative change in O_2Hb across all the channels was used as input feature to map onto

Published by Verlag der TU Graz
Graz University of Technology

 DOI: 10.3217/978-3-85125-533-1-14

model space, while for EEG and EOG signals temporal and power spectral features were used. The relative change in O_2Hb, EEG and EOG data acquired during BCI sessions from Patient F, G, B and W were processed off-line separately for each patient to determine:

1) The statistical difference in the particular physiological signal (O_2Hb, EEG and EOG) during the ISI of true (yes) and false (no) sentences.

T-tests between the averaged ISI of true and false sentences were performed to ascertain the significant difference, if any, between "yes" and "no" thinking. The t-test analysis was performed across all the channels in a session and for all the sessions of acquired O_2Hb, EEG and EOG signals. Furthermore t-test was also performed between the ISI of all the 10 true sentences and all the 10 false sentences across different channels in a session averaged over many sessions varying slightly between patients.

2) Classification accuracy, using SVM as described above, of O_2Hb, EEG and EOG signals across each session between the true and false sentences' ISI.

The shapes of the relative change in O_2Hb and EOG during ISI corresponding to true and false sentences from all the sessions were plotted in Figure 3 and Figure 5 respectively, while the power spectrum of the EEG signal, calculated using Welch's method [17], during the same ISIs is plotted in Figure 4.

RESULT

The t-test analysis performed using the relative change in O_2Hb showed a significant difference between the true and false sentences' ISI across all patients (not shown here). While, the same analysis performed using the EEG and EOG data across all the training sessions showed no significant differences ($p > 0.05$) between the true and false sentences' ISI across each. The relative change in O_2Hb in five channels over the fronto-central brain region of Patient F, G, B and W during the true and false sentence ISI is shown in Figure 3. Figure 3 illustrates that the shape of the change in O_2Hb during true sentence ISI is qualitatively different from false sentence ISI. Figure 3 also illustrates that the shape of the change in O_2Hb during a true or a false sentence ISI is not consistent between the patients even though within each patient the shape of the change in O_2Hb is stable. Figures 4 illustrates the power spectrum density (PSD) of EEG oscillations, in the frequency band 0 to 10 Hz, during the true and false sentence ISI from patient F, G, B and W respectively. The PSD of EEG signal shows that there was no significant difference between the true and false sentences ISI across all patients. The eye movements (vertical or horizontal, patients were free to use any direction) of patient F, G, B and W while they were performing the "ja (yes)" or "nein (no)" thinking task is shown in Figure 5. It illustrates that there was no significant difference in the eye movements between the true and false sentences ISI for all patients, confirmed by the t-test: Figures 6, 7, 8 and 9 depicts the SVM classification across all the sessions using the change in (a) O_2Hb, (b) EEG and (c) EOG in Patient F, G, B and W; respectively.

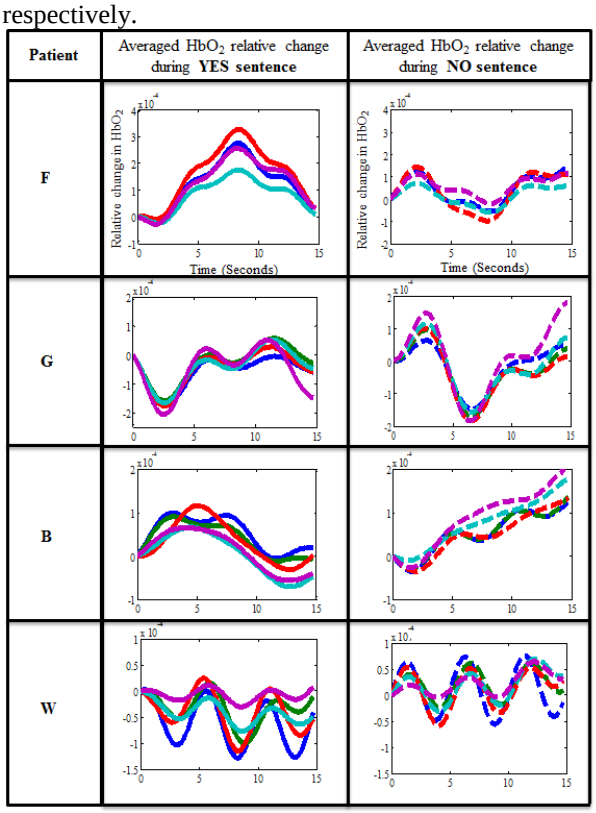

Figure 3: The averaged relative change in O_2Hb across 5 out of 20 channels corresponding to **YES and NO sentence** inter-stimulus interval (ISI) in Patient **F, G, B** and **W**. In each subplot; five different colored trace corresponds to relative change in HbO_2 across five different channels, x-axis is time in seconds and y-axis is relative change in HbO_2.

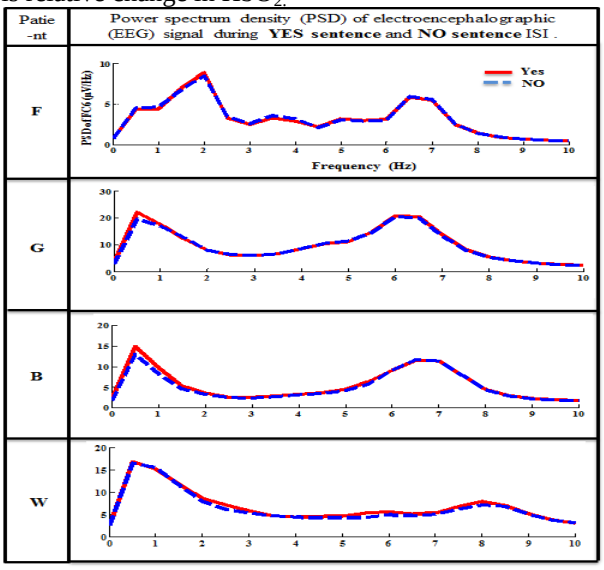

Figure 4: Power spectrum density (PSD) of electroencephalographic (EEG) signal corresponding to **YES** (red solid trace) and **NO** (blue dashed trace) sentence ISI acquired from channel FC6 in Patient **F, G, B** and **W**.

Published by Verlag der TU Graz
Graz University of Technology

 DOI: 10.3217/978-3-85125-533-1-14

A 65% cut off was used to define whether the classification accuracy was above or below the acceptable level [18].

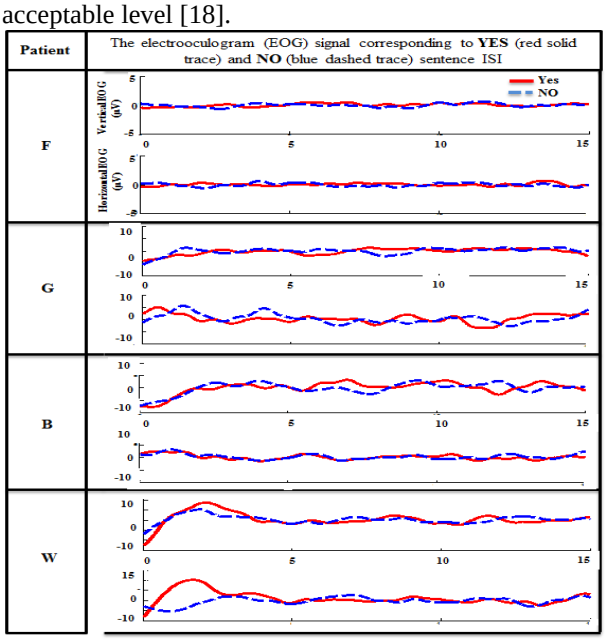

Figure 5: The electrooculogram (EOG) signal corresponding to **YES** (red solid trace) and **NO** (blue dashed trace) sentence ISI in Patient **F, G, B** and **W**. In each subplot x-axis is time in second and y-axis is EOG in micro volt (μV).

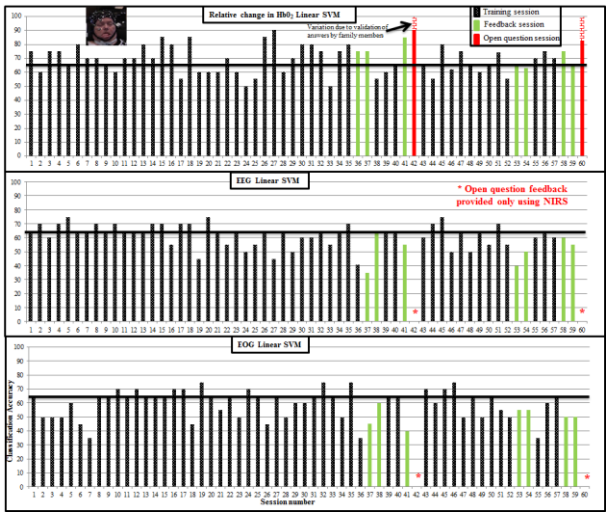

Figure 6 – ***Patient F***: Linear support vector machine (SVM) classification accuracy across all sessions 1) Training (bar plot in spotted black), 2) Feedback (bar plot in solid green) and 3) Open question (bar plot in solid red) obtained using **a)** Relative change in HbO_2, **b)** EEG and **c)** EOG data. In each histogram plot x-axis is the number of sessions and y-axis is classification accuracy. The black horizontal line represents the 65% classification accuracy.

The SVM results illustrates that highest classification accuracy was achieved using the change in O_2Hb for which more than 75% of the sessions yielded greater than 65% classification accuracy for all the patients with an average classification accuracy of 70%.

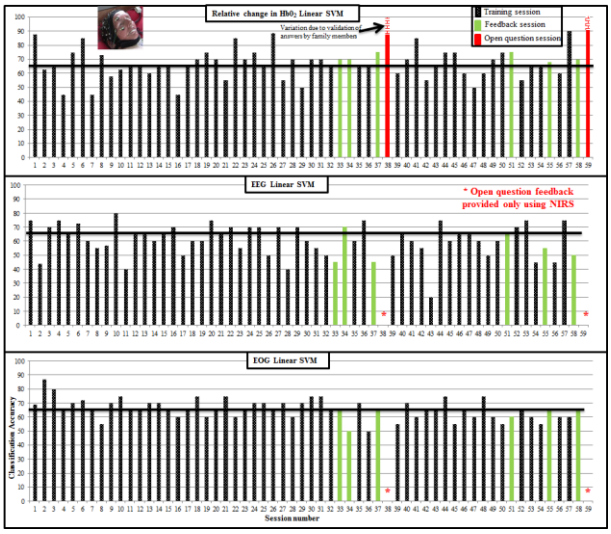

Figure 7 – ***Patient G***: The description of Figure is same as described in Figure 6.

Figure 8 – ***Patient B***: The description of Figure is same as described in Figure 6.

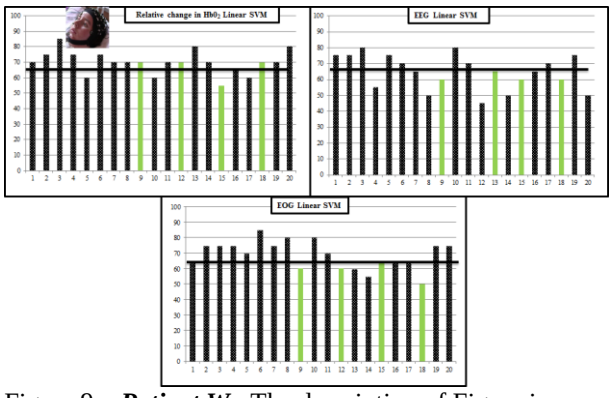

Figure 9 – ***Patient W***: The description of Figure is same as described in Figure 6.

While the SVM classification accuracy obtained using EEG and EOG data only few sessions yielded greater than 65% classification accuracy across all patients. Classification results using fNIRS for open question in

Published by Verlag der TU Graz
Graz University of Technology

 DOI: 10.3217/978-3-85125-533-1-14

patients F, B and G, using the criteria for correctness described above in paragraph 2.3 ranged between 75-90% "correct". Patient W with 24 years of age suffering from juvenile ALS with an extremely rapid disease progression (2 years from diagnosis to CLIS) was not asked open questions at that early stage but continue to train the BCI at present.

DISCUSSION AND CONCLUSION

All in all, 4 patients in CLIS communicated with fronto-cortical oxygenation based BCI with an average correct response rate of 70% over a period of several weeks. Correct response rate for open questions as estimated by relatives exceeded even 75% in 3 of the 4 patients. Patient W, 24 years with juvenile ALS (completely locked-in within 2 years after diagnosis) is still in an emotional labile state which prevented us from asking her the difficult to validate open questions at the time of this study. Patient F, G and B answered open questions containing quality of life estimation with a yes response indicating a positive attitude towards the present situation and life in general as found in larger samples of ALS patients [19]. Correct classification of "yes" and "no" answers given mentally through fNIRS exceeded classification of EEG oscillations from 0-10 Hz (EEG frequencies in advanced ALS rarely show high frequencies) and vertical and horizontal EOG classification. However, despite the absence of reliable eye communication in all patients as the inclusion criteria in the study, EOG classification often was above chance despite the inability of the social environment to perceive them and eye tracker's failure to use them for communication [10]**.** If replicated with ALS patients in CLIS, these positive results could indicate the first step towards abolition of complete locked-in states at least for ALS.

ACKNOWLEDEGMENT:

We acknowledge the participation of all our patients because of them we have been able to shed light on the use of BCI in CLIS - ALS patients. All the researchers who were the part of team at different stage of the research as well as our funding sources Deutsche Forschungsgemeinschaft (DFG, Kosellek), DFG BI 195/77-1, BMBF 16SV7701 CoMiCon, Stiftung Volkswagenwerk (VW), Brain Products, Gilching and German Center of Diabetes Research (DZD) at Univ. Tübingen, Eva and Horst Köhler Stiftung, Baden-Württernberg-Stiftung, LUMINOUS-EU H2020 (68674), and Wyss center Bio and Neuroengineering, Genéva.

REFERENCES:

[1] Norris FH. Amyotrophic lateral sclerosis: The clinical disorder. In R. A. Smith (Ed), Handbook of Amyotrophic Lateral Sclerosis. New York: Marcel Dekker; 1992.

[2] Birbaumer N. Breaking the silence: Brain–computer interfaces (BCI) for communication and motor control. Psychophysiol. 2006; 43(6):517–32.

[3] Chaudhary U, Birbaumer N, Curado MR. Brain-Machine Interface (BMI) in paralysis. Annals of Physical and Rehabilitation Medicine 2015; 58(1):9–13.

[4] van Gerven M, Farquhar J, Schaefer Ret al. The brain computer interface cycle.J. Neur. Eng. 2009; 6(4):1–10.

[5] Birbaumer N and Cohen LG. Brain-computer interfaces: communication and restoration of movement in paralysis. J Physiol 2007;579(3):621–36.

[6] Birbaumer N, Murguialday AR, Cohen L. Brain computer interface in paralysis. Curr. Opin. Neurol. 2008;21(6):634–8.

[7] Chaudhary U, Birbaumer N, Ramos-Murguialday A. Brain–computer interfaces for communication and rehabilitation. Nat. Rev. Neurol. 2016;12(9):513–25.

[8] Birbaumer N, Ghanayim N, Hinterberger T, et al.A spelling device for the paralyzed. Nature 1999; 398(6725):297–298.

[9] Farwell, LA and Donchin E. Talking off the top of your head: toward a mental prosthesis utilizing event-related brain potentials. Electroencephalogr. Clin. Neurophysiol. 1988;70(6):512–23.

[10] De Massari D, Ruf CA, Furdea A et al. Brain communication in the locked-in state.Brain 2013;136(6):1989–2000.

[11] Kuebler A and Birbaumer N. Brain–computer interfaces and communication in paralysis: Extinction of goal directed thinking in completely paralysed patients? Clin.Neurophysiol. 2008;119(11):2658–66.

[12] Gallegos-Ayala G, Furdea A, Takano K, et al. Brain communication in a completely locked-in patient using bedside near-infrared spectroscopy. Neurology.2014;82(21):1930-1932.

[13] Chaudhary U, Xia B, Silvoni S, Cohen LG, Birbaumer N. Brain-Computer Interface-Based Communication in the Completely Locked-in State. PLoS Biol. 2017;15(1):e1002593.

[14] Cope M, Delpy DT, Reynolds EOR, et al. Methods of quantitating cerebral near infrared spectroscopy data. Adv. Exp. Med. Biol. 1987;222(July):183–189.

[15] Chaudhary U, Hall M, DeCerce J, et al. Frontal activation and connectivity using near-infrared spectroscopy: Verbal fluency language study. Brain Res. Bull. 2011;84(3):197–205.

[16] Vapnik, V., Golowich, S. and Smola, A. Support vector method for function approximation, regression estimation, and signal processing. Advances in Neural Information Processing Systems, 1996;9:281–287.

[17] Harris, F.J. "On the use of Windows for Harmonic Analysis with the Discrete Fourier Transform." Proceedings of the IEEE. Vol. 66 (January 1978).

[18] Müller-Putz G, Scherer R, Brunner C, Leeb R, Pfurtscheller G. Better than random: a closer look on BCI results. International Journal of Bioelectromagnetism. 2008; 10(1): 52-55.

[19] Lulé D, Ehlich B, Lang D, Sorg S, Heimrath J, Kübler A, et al. Quality of life in fatal disease: The flawed judgement of the social environment. J Neurol. 2013;260(11):2836–43.

Published by Verlag der TU Graz
Graz University of Technology

Proceedings of the
7th Graz Brain-Computer Interface Conference 2017 DOI: 10.3217/978-3-85125-533-1-15

MINDFULNESS BASED STRESS REDUCTION IMPROVES TACTILE SELECTIVE ATTENTION BCI ACCURACY

Mei Lin Chen, Lin Yao, Ning Jiang

Department of Systems Design Engineering, Faculty of Engineering, University of Waterloo, Waterloo, Canada

E-mail: ning.jiang@uwaterloo.ca

ABSTRACT:
Brain-computer interfaces (BCI) control is a mentally tasking activity that requires the user's concentrated attentional efforts. We hypothesized that mindfulness-based exercises, such as a 20-minutes Mindfulness-Based Stress Reduction training session (MBSR), can help to improve BCI performance. This pilot experiment demonstrated a BCI accuracy improvement after four subjects engaged in a 20-minute MBSR intervention session. The average BCI performance of the four subjects before the session was 67.42% and after the session was 78.94%, resulting in a performance increase of 11.52%. Three of the four subjects were considered BCI-illiterate (<70% accuracy) in the pre-MBSR session, and all three subject's accuracies were improved to >70% in the post-MBSR session. Moreover, an enhanced event related desynchronization in the alpha frequency band was found in post-MBSR intervention. These results demonstrate promising potential for using mindfulness-based exercises to improve BCI accuracy.

INTRODUCTION

Brain-computer interface (BCI) uses brain activity alone to control external devices or to communicate with the external world [1]. It provides a non-muscular channel of communication for severely disabled individuals who are totally paralyzed or 'locked in' by neurological disorders, such as amyotrophic lateral sclerosis, stroke, or spinal cord injury [1]. An electroencephalogram (EEG) based BCI measures brain activity through non-invasive electrodes at the scalp surface. One of the biggest challenges in BCI is for users to produce consistent and reliable EEG patterns, which can be significantly affected by the user's mental state [2]. Stress, anxiety, fatigue, frustration, and loss of concentration may cause an unstable mental state which may in turn cause inconsistent EEG patterns to be produced. Even distraction during the experiment such as feedback presented by the BCI (i.e. in game control) can modify the user's global mental state and hence their EEG, introducing noise to the system [3].

Researchers have been attempting to apply different signal processing techniques to improve its signal-to-noise input signal to increase the accuracy and classification of EEG-based BCI. Some studies trained the users through extensive neuro-/biofeedback training [4], [5]. Nevertheless, the inconsistencies in EEG due to mental state changes still remains to be a great challenge in EEG-based BCIs, whereas 15~30% of the users cannot usefully control a BCI, which is termed the 'BCI-illiteracy phenomenon' [6].

It is suggested that psychological parameters such as high attention span, sustained focus and concentration could yield better BCI performance, as BCI-control requires a substantial amount of focused attention [7]. In event-related desynchronization (ERD) based BCI, attention plays a significant role, with high attention correlating with to a significantly higher ERD value compared to lower attention [8]. Mindfulness based interventions have also been shown to lead to an increased level of attention, self-reported mindfulness and improvements in psychological functioning [9]. By providing participants who do not succeed in BCI control with such intervention to increase their oscillatory activation (ERD), it may lead to more accurate and consistent BCI performance and hence overcome the problematic 'BCI-illiteracy phenomenon' [7]. Previous research on meditation-based intervention and BCI accuracy demonstrated a 12-week meditation intervention program to significantly increase a group of 23 participants' baseline accuracy from 58% to 64% [2]. This finding motivated us to investigate whether a shorter session of mindfulness-based intervention can lead to a similar effect of increasing BCI accuracy.

The mindfulness-based intervention we will be investigating is a 20 minute standard Mindfulness-Based Stress Reduction (MBSR), which have shown to be able to increase mindfulness and well-being, while decreasing stress and improving psychological wellbeing [10], [11]. It has been proposed that the mechanisms responsible for positive changes following MBSR involve attentional improvements, the cultivation of a nonjudgmental attitude, and an intention to be present in the present task. This current study aims to examine the effect of mindfulness-based training on the ability to control a tactile BCI using selective sensation (SS) [12], [13], and to improve the performance accuracy for poorly performing BCI subjects.

Published by Verlag der TU Graz
Graz University of Technology

 DOI: 10.3217/978-3-85125-533-1-15

MATERALS AND METHODS

Subjects

A total of four healthy subjects participated in this experiment (all male, all right handed, age 20~25, mean age 22.75 ± 2.22 yr). All subjects had no prior experience with EEG. The study was approved by the Ethics Committee of the University of Waterloo, in Waterloo Canada. All subjects signed an informed consent form prior to participation.

Experiment Paradigm

In order to discriminate the subject's active attention to the sensations on respective hands, a vibration stimulation is provided to the subject's respective wrist to help direct their attention. This task of paying attention to either the left or the right hand is termed tactile selective sensation (SS); SS-L for left hand and SS-R for right hand.

Fig. 1 illustrates the experiment paradigm. The subject was seated on a comfortable armchair 1 meter in front of the display screen, with their forearms and hands resting on the armrest. They are instructed to limit all physical movements (i.e. facial, arm) and limit eye blinks to a minimum. During the experiment, a randomized series of one of two visual cues that correspond to the above SS task were displayed on the screen; a left-pointing red bar indicates the SS-L task and a right-pointing red bar indicates the SS-R task. After 3 runs of 40 trials (120 trials total), the subject is asked to complete a 20-minute guided sitting MBSR session. After the MBSR session, the subject repeats 3 runs of 40 trials of SS (another 120 trials total).

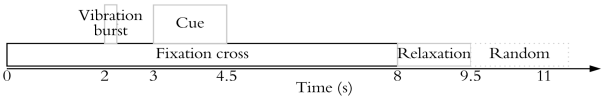

Figure 1. An illustration of the experiment protocol.

MBSR Training Session

During the 20-min MBSR training session, participants were guided through a 'body-scan' by the voice recording of a trained instructor. The participants were asked to sit quietly while focusing on the flow of their breath, with their eyes closed, and to adopt a nonjudgmental mentality while becoming aware of their thoughts, senses, and feelings. They were taught to calm down their mind by remaining focused on their breath, in performing the 'body scan'. This brings awareness to the physical sensations throughout the whole body while nonjudgmentally allowing discursive thoughts to simply pass [2]. The link to this 20-min guided sitting meditation MBSR mp3 audio file can be found here[1].

EEG recording and Sensory Stimulation

A 32-channel wireless g.Nautilus EEG system from g.tech Australia was used to record EEG signals. The electrodes were placed according to the extended 10/20 system, with the reference and ground placed on the right earlobe and forehead, respectively. A hardware notch filter of 60Hz was applied to the raw signals, which were digitally stamped at 250Hz. All EEG data were recorded, stored, and processed offline.

Mechanical stimulation was applied to the wrists. Linear resonant actuators (10 mm, C10-100, Precision Microdrives Ltd., typical normalized amplitude 1.4 G) were used for producing vibrotactile stimulation. The stimulation device produced a 23-Hz sine wave for the left wrist, and 27-Hz sine wave for the right wrist. Both stimuli were modulated with a 175-Hz sine carrier wave.

Algorithms and performance evaluation

The EEG data was manually corrected for artifacts using EEGLAB toolbox [14]. The trials that were affected by artifacts such as swallowing and physical movement (either in baseline or task line interval), were excluded in the analysis.

A fourth-order Butterworth filter of [8 26] Hz was applied to the raw EEG signals before the CSP spatial filtering. A 10×10 fold cross-validation was utilized to evaluate the BCI performance.

RESULTS AND DISCUSSION

Tactile BCI performance improved with MBSR

The BCI performance before and after the MBSR intervention is shown in Fig. 2, with a mean performance accuracy of 67.42% before MBSR and 78.94% after – an average improvement of 11.52%. This method demonstrated a clear benefit for poor-performing subjects (subject 1, 2, and 3 had <70% accuracy before MBSR). For example, subject 1 had a dramatic improvement from 55.50% before the 20-minute MBSR session to 77.5% after the session, a 22% improvement.

This increase in BCI accuracy is consistent with another BCI study on the effect of a 12-week meditation training

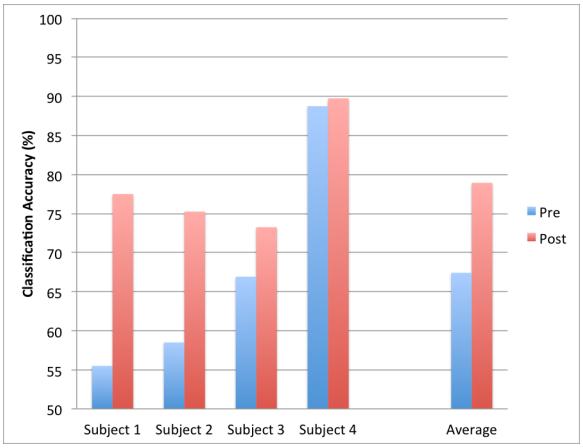

Figure 2. BCI performance before and after the MBSR training. The blue bar indicates BCI performance prior to the MBSR session; and the red bar indicates BCI performance after the MBSR session.

Published by Verlag der TU Graz
Graz University of Technology

 DOI: 10.3217/978-3-85125-533-1-15

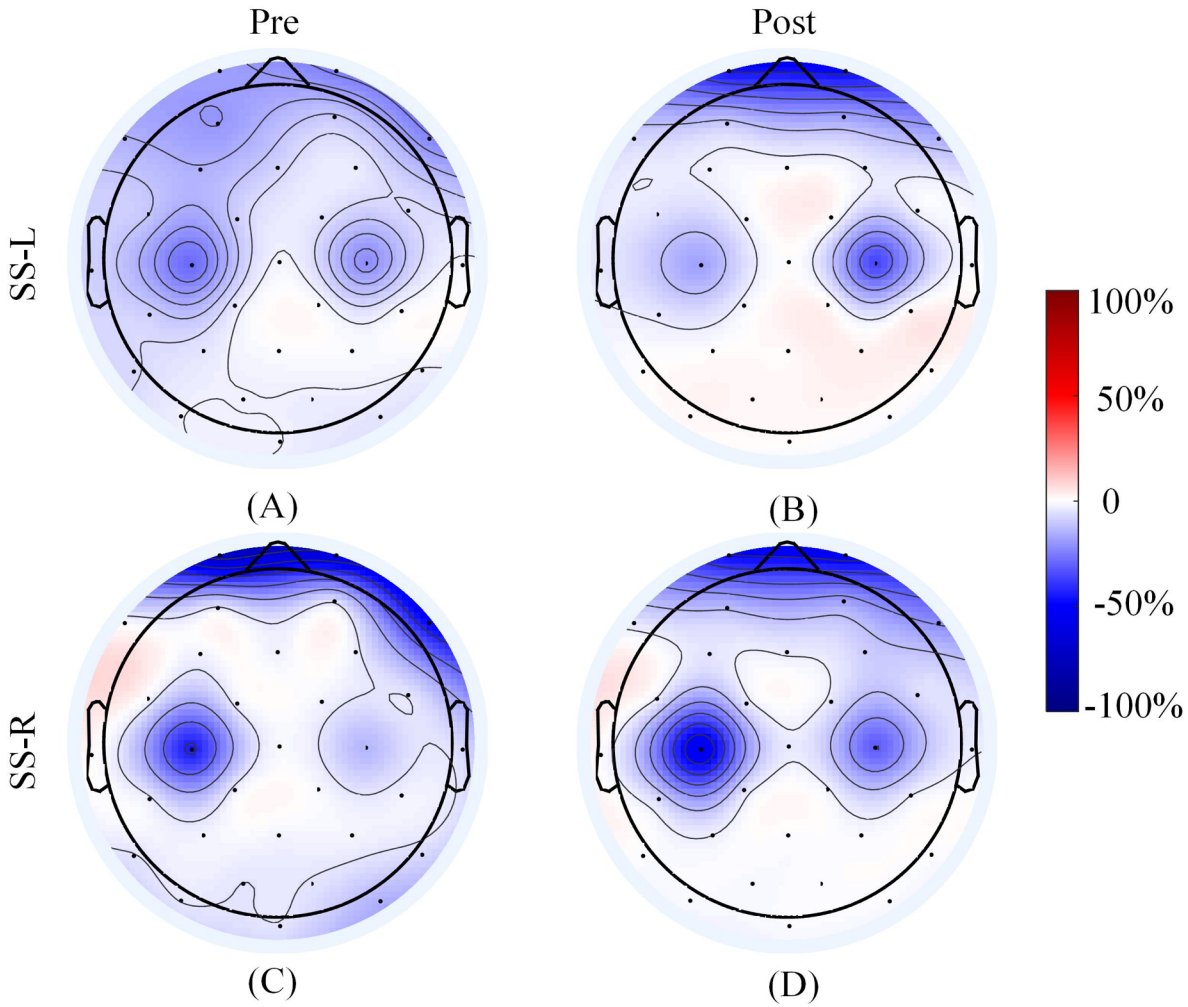

Figure 3. Cortical activation distribution across the scalp (ERD within the [8 13] Hz alpha frequency band). (A) ERD topolot of the SS-L task in Pre-MBSR session. (B) ERD topolot of the SS-L task in Post-MBSR session. (C) ERD topolot of the SS-R task in Pre-MBSR session. (D) ERD topolot of the SS-R task in Post-MBSR session. The colour bar indicates the ERD/ERS value.

program that resulted in an accuracy increase from 58% to 64% – a significant increase of 6% in a group of 23 subjects [2]. This study utilized motor imagery for BCI control [2].

The ERD cortical distribution before and after the MBSR intervention with respect to different SS tasks can be seen from a representative subject (subject 1 in Fig. 3 demonstrate an increased ERD activation between 8 to 13 Hz of the frequency band. This could be one of the factors underlying the increase in classification discrimination.

The effect of learning should also be taken into consideration, as the subjects will become increasingly familiar with the BCI system controls with practice and this may lead to an increase in BCI accuracy. Therefore, a control group should be implemented with future research.

CONCLUSION

Focused tactile selective attention was required in tactile BCIs, in which the subjects were instructed to focus their attention either to the vibration stimulation on either the left or right hand. The 20 minute MBSR based training session may have improved attention which in turn improved the subject's BCI performance.

In this study, we demonstrated that a 20 minute MBSR guided sitting meditation program can help improve BCI performance, accompanied by an enhanced ERD activation. Further research needs to be done on to understand the underlying physiological mechanism for the changes observed and to incorporate MBSR into a training paradigm to maximize the effect of MBSR in improving BCI performance and user compliance.

Published by Verlag der TU Graz
Graz University of Technology

 DOI: 10.3217/978-3-85125-533-1-15

REFERENCES

[1] L. F. Nicolas-Alonso and J. Gomez-Gil, "Brain computer interfaces, a review," *Sensors*, vol. 12, no. 2, pp. 1211–1279, 2012.

[2] L. F. Tan, Z. Dienes, A. Jansari, and S. Y. Goh, "Effect of mindfulness meditation on brain-computer interface performance," *Conscious. Cogn.*, vol. 23, no. 1, pp. 12–21, 2014.

[3] A. Nijholt, B. Reuderink, and D. O. Bos, "Turning shortcomings into challenges: Brain-computer interfaces for games," *Entertain. Comput.*, vol. 9 LNICST, no. 2, pp. 153–168, 2009.

[4] D. C. Hammond, "What is Neurofeedback: An Update," *J. Neurother.*, vol. 15, no. 4, pp. 305–336, 2011.

[5] H. J. Hwang, K. Kwon, and C. H. Im, "Neurofeedback-based motor imagery training for brain-computer interface (BCI)," *J. Neurosci. Methods*, vol. 179, no. 1, pp. 150–156, 2009.

[6] C. Vidaurre and B. Blankertz, "Towards a Cure for BCI Illiteracy," *Brain Topogr.*, vol. 23, no. 2, pp. 194–198, Jun. 2010.

[7] E. M. Hammer, S. Halder, B. Blankertz, C. Sannelli, T. Dickhaus, S. Kleih, K. R. Müller, and A. Kübler, "Psychological predictors of SMR-BCI performance," *Biol. Psychol.*, vol. 89, no. 1, pp. 80–86, 2012.

[8] K. Dujardin, P. Derambure, L. Defebvre, J. L. Bourriez, J. M. Jacquesson, and J. D. Guieu, "Evaluation of event-related desynchronization (ERD) during a recognition task: effect of attention," *Electroencephalogr. Clin. Neurophysiol.*, vol. 86, no. 5, pp. 353–356, 1993.

[9] S. E. Sauer-Zavala, E. C. Walsh, T. A. Eisenlohr-Moul, and E. L. B. Lykins, "Comparing Mindfulness-Based Intervention Strategies: Differential Effects of Sitting Meditation, Body Scan, and Mindful Yoga," *Mindfulness (N. Y).*, vol. 4, no. 4, pp. 383–388, 2013.

[10] J. Carmody and R. A. Baer, "Relationships between mindfulness practice and levels of mindfulness, medical and psychological symptoms and well-being in a mindfulness-based stress reduction program," *J. Behav. Med.*, vol. 31, no. 1, pp. 23–33, 2008.

[11] C. G. Jensen, S. Vangkilde, V. Frokjaer, and S. G. Hasselbalch, "Mindfulness training affects attention—Or is it attentional effort?," *J. Exp. Psychol. Gen.*, vol. 141, no. 1, pp. 106–123, 2012.

[12] L. Yao, J. Meng, D. Zhang, X. Sheng, and X. Zhu, "Selective Sensation Based Brain-Computer Interface via Mechanical Vibrotactile Stimulation," *PLoS One*, vol. 8, no. 6, 2013.

[13] L. Yao, X. Sheng, D. Zhang, N. Jiang, D. Farina, and X. Zhu, "A BCI System based on Somatosensory Attentional Orientation," *IEEE Trans. Neural Syst. Rehabil. Eng.*, vol. 4320, no. c, pp. 1–1, 2016.

[14] A. Delorme, T. Mullen, C. Kothe, N. Bigdely-Shamlo, Z. Akalin, A. V. Acar1, and S. Makeig, "EEGLAB, MPT, NetSIFT, NFT, BCILAB, and ERICA: New tools for advanced EEG/MEG processing," *Comput. Intell. Neurosci.*, vol. 2011, p. 130714, 2011.

Published by Verlag der TU Graz
Graz University of Technology

Proceedings of the
7th Graz Brain-Computer Interface Conference 2017 DOI: 10.3217/978-3-85125-533-1-16

DIMENSIONALITY REDUCTION FOR BCI CLASSIFICATION USING RIEMANNIAN GEOMETRY

P. L. C. Rodrigues[1], F. Bouchard[1], M. Congedo[1], C. Jutten[1]

[1]GIPSA-lab, CNRS, University Grenoble Alpes, Grenoble Institute of Technology, Grenoble, France

E-mail: pedro-luiz.coelho-rodrigues@gipsa-lab.fr

ABSTRACT: In the past few years, there has been an increasing interest among the Brain-Computer Interface research community in classification algorithms that respect the intrinsic geometry of covariance matrices. These methods are based on concepts of Riemannian geometry and, despite demonstrating good performances on several occasions, do not scale well when the number of electrodes increases. In this paper, we evaluate two methods for reducing the dimension of the covariance matrices in a geometry-aware fashion. Our results on three different datasets show that it is possible to considerably reduce the dimension of covariance matrices without losing classification power.

INTRODUCTION

In recent years a new trend of algorithms using concepts from Riemannian geometry have demonstrated remarkable performance on classification of BCI signals, often superior to the current state of the art. As shown in a recent literature survey [1], such results gave rise to a new generation of Brain-Computer Interface (BCI) systems that is becoming each year more popular among the research community.

In BCI classification we are given a dataset containing short-time recordings of EEG, each associated to a condition (or class). The goal is to train an algorithm on an ensemble of trials with known labels and use it to correctly classify a set with unknown labels. The usual approach is to select certain features describing the trials and use statistical models to classify them [3]. A useful feature one may consider when working with EEG signals is their spatial covariance matrix, since different classes are expected to have different patterns of correlation between electrodes. The core idea behind algorithms using Riemannian geometry is to manipulate covariance matrices in the manifold of symmetric positive-definite (SPD) matrices and use them directly as features in a classifier that respects their intrinsic geometry.

The computational complexity of algorithms based on this premise is of concern for high-density EEG data. This happens because Riemannian algorithms rely on eigendecompositions, whose number of operations is on the order of n^3, where n is the number of electrodes. Also, due to very low eigenvalues in the spectrum of high-dimensional covariance matrices (mainly associated to noise), logarithmic maps used by Riemannian algorithms may encounter numerical difficulties. Furthermore, classifiers using high-dimensional covariance matrices as features are prone to overfitting because of the curse of dimensionality and the limited number of trials usually available in BCI datasets [3].

Fortunately, the very nature of EEG recordings allows us to consider only a subspace of the data without losing much information. This is possible because of the strong statistical correlation between signals recorded from close positions and the small number of independent sources that are active during brain activity. By exploring this redundancy, we can reduce the dimensions of spatial covariance matrices and use Riemannian geometric algorithms more efficiently.

The literature of dimensionality reduction (DR) is very rich and many methods already exist. Some are general-purpose algorithms, like principal component analysis (PCA) and multi-dimensional scaling (MDS), others are specific to the analysis of EEG signals, such as common spatial patterns (CSP). However, none of these alternatives take into account the intrinsic geometry of the covariance matrices to reduce their dimensions in a principled manner.

Recently, in the computer vision literature, Ref. [4] presented two geometry-aware methods for reducing the dimensions of SPD matrices, a supervised and an unsupervised approach. Both algorithms are based on the theory of optimization on manifolds [7] and demonstrated good results on image and video databases. Shortly after, Ref. [5] applied the unsupervised dimensionality reduction described in [4] to datasets of Motor Imagery (MI) BCI and obtained encouraging results.

In this work, we apply both algorithms given in [4] to the context of BCI signals. We extend the results from [5] by considering datasets with several subjects and test the algorithms not only on MI but also on the P300 paradigm. We examine the sensitivity of the classification algorithms to the choice of the reduced dimension and investigate the conditions in which a DR would be advisable or not. This paper continues with a section on Materials and Methods, where we give a brief presentation of concepts of Riemannian geometry and an overview of methods for geometry-aware dimensionality reduction. We also present the datasets and the classification pipelines used for assessing the quality of each dimensionality re-

Published by Verlag der TU Graz
Graz University of Technology

 DOI: 10.3217/978-3-85125-533-1-16

duction proposal. We continue with a section of Results and Discussion and leave final comments to the Conclusions section.

MATERIALS AND METHODS

This section begins with a brief introduction to concepts of Riemannian geometry on SPD matrices. Then, we cast dimensionality reduction as an optimization problem and consider two cost functions encoding different criteria. Finally, we describe the datasets in which we applied our classification pipelines.

We denote by $X_k \in \mathbb{R}^{n\times T}$ the recording of T samples on n electrodes of the k^{th} trial in an ensemble of K trials and y_k the class associated to X_k. The spatial covariance matrix C_k of X_k is a $n \times n$ matrix estimated using

$$C_k = \frac{1}{T-1} X_k X_k^T. \tag{1}$$

Riemannian geometry of SPD matrices: Given enough samples, a covariance matrix estimated with (1) is symmetric positive definite (SPD), which means that all of its eigenvalues are strictly positive. Matrices with such property form a manifold $\mathcal{M}$, a set of points with the property that the neighborhood of each $\boldsymbol{x} \in \mathcal{M}$ can be mapped to an Euclidean space, also known as its tangent space $T_{\boldsymbol{x}}\mathcal{M}$. When associated to a metric, $\mathcal{M}$ becomes a Riemannian manifold and fundamental geometric notions are naturally defined, such as geodesics (shortest curve joining two points), distance between two points (length of the geodesic connecting them), the center of mass of a set of points, etc.

We denote the manifold of SPD matrices by $\mathcal{S}_n^{++}$ and endow it with the affine-invariant Riemannian metric. This metric induces a distance between any two matrices, as [6]

$$\delta(C_i, C_j) = \| \log(C_i^{-1/2} C_j C_i^{-1/2}) \|_F, \tag{2}$$

offering a more appropriate distance in the SPD space as compared to the Euclidean distance. In fact, it is possible to show that $\mathcal{S}_n^{++}$ is a manifold with nonpositive curvature [6], so concepts from Euclidean geometry do not necessarily apply. For instance, the sum of angles in a triangle is different than 180 degrees (see Figure 1).

The center of mass M according to distance (2) of a set of covariance matrices $\{C_1, \ldots, C_K\}$ is defined as [1]

$$M = \underset{M\in\mathcal{S}_n^{++}}{\operatorname{argmin}} \sum_{k=1}^{K} \delta^2(M, C_k). \tag{3}$$

Note that M is the point in the manifold minimizing the dispersion (variance) of the set of matrices. When $n = 1$ (C_k is a strictly positive scalar), M corresponds to the geometric mean of the C_k's.

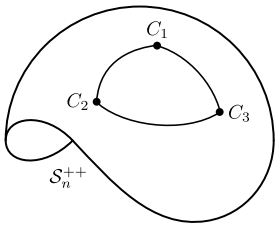

Figure 1: The manifold $\mathcal{S}_n^{++}$ is portrayed as a surface with nonpositive curvature. The distance between any two elements is the length of the geodesic.

This explains why many researchers adopt the term "geometric mean" to refer to the center of mass of a set of covariance matrices. The geometric mean of two SPD matrices is the half-way point of the geodesic that connects them. For $K > 2$, there is no closed form solution for M, so one has to resort to iterative algorithms [2]. The above definitions suffice for the intents of this paper. The interested reader will find a thorough treatment of the subject in the book of R. Bhatia [6].

Dimensionality reduction: Our approach for dimensionality reduction determines a map that takes a set of matrices $\{C_k\}$ in $\mathcal{S}_n^{++}$ to a new set $\{C_k^{\downarrow}\}$ in $\mathcal{S}_p^{++}$ ($p < n$) and keeps a maximum amount of information (under some criterium) from the original matrices. To do so, we search for a p-dimensional subspace of $\mathbb{R}^n$ containing the most relevant features spanned by the columns of the original C_k's. This subspace is represented by a matrix $W \in \mathbb{R}^{n\times p}$ whose columns form a basis for the subspace. We use W to select linear combinations of electrodes in X_k via

$$X_k^{\downarrow} = W^T X_k,$$

which is the same as calculating

$$C_k^{\downarrow} = W^T C_k W \in \mathbb{R}^{p\times p}. \tag{4}$$

Without loss of generality, we impose W to be an orthonormal matrix. Note that because W is full rank the dimension-reduced matrices are guaranteed to be positive definite.

The procedure for choosing W is cast as an optimization problem,

$$\begin{aligned} &\text{minimize} && \mathcal{L}(W), \\ &\text{subject to} && W^T W = \mathbf{I}_p, \end{aligned} \tag{5}$$

where $\mathcal{L}$ is a loss function that encodes the criteria for reducing the dimension of the covariance matrices. One possible criterium is that of making sure that the distances of points C_k to a given "landmark" L do not change very much for the dimension-reduced matrices in $\mathcal{S}_p^{++}$. This can be written formally as

$$\mathcal{L}_u(W) = \sum_{k=1}^{K} \Big(\delta^2(C_k, L) - \delta^2(W^T C_k W, W^T L W) \Big).$$

If we choose L to be the geometric mean of the set of matrices $\mathbb{C}$, the loss function $\mathcal{L}_u$ is the one proposed in [4].

Published by Verlag der TU Graz
Graz University of Technology

 DOI: 10.3217/978-3-85125-533-1-16

Note that $\mathcal{L}_u$ is based on an unsupervised criterium, since it does not assume knowledge of the labels y_k of each covariance matrix. In the supervised case, W can be chosen to enforce the separability of classes in the reduced-dimension manifold, as in the function

$$\mathcal{L}_s(W) = \sum_{i=1}^{K}\sum_{j=1}^{K} A_{ij}\delta^2(W^T C_i W, W^T C_j W),$$

where the A_{ij}'s encode a measure of affinity between matrices C_i and C_j, so that

$$A_{ij} = g_w(C_i, C_j) - g_b(C_i, C_j),$$

with

$$g_w(C_i, C_j) = \begin{cases} 1, & \text{if } C_i \in \mathcal{N}_w(C_j) \text{ or } C_j \in \mathcal{N}_w(C_i) \\ 0, & \text{otherwise} \end{cases},$$

and

$$g_b(C_i, C_j) = \begin{cases} 1, & \text{if } C_i \in \mathcal{N}_b(C_j) \text{ or } C_j \in \mathcal{N}_b(C_i) \\ 0, & \text{otherwise} \end{cases},$$

where $\mathcal{N}_w(C_i)$ is the set of n_w nearest neighbours of C_i with the same label as y_i and $\mathcal{N}_b(C_i)$ contains the n_b nearest neighbours whose labels are different from y_i. With this definition, $\mathcal{L}_s$ tries to preserve the distances between each pair of matrices in the dimension-reduced space while at the same time enhancing the class separability: for large positive values of A_{ij} (within class) the dimension-reduced matrices are encouraged to come closer to one another, while for small negative values (between classes) their distances tend to increase. Figure 2 illustrates the two aforementioned criteria.

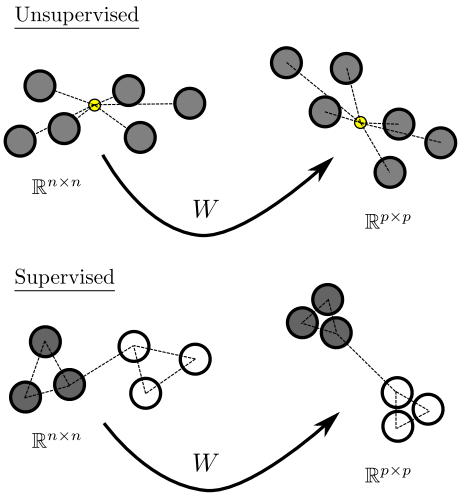

Figure 2: Illustration of the priorities for each type of dimensionality reduction. In the unsupervised case, the distances to a landmark point are preserved, while for the supervised approach the intra-class distances decrease and the inter-class distances tend to augment.

We should mention that the computational cost for calculating $\mathcal{L}_u$ and $\mathcal{L}_s$ is not comparable. In the unsupervised case the number of operations increases linearly with K since all distances are calculated with respect to a single landmark. In the supervised algorithm the number of operations scales quadratically with K, a rather problematic aspect when working with large datasets.
Problem (5) has a special structure and can be solved as an optimization problem on manifolds, a branch of applied mathematics with a considerable amount of recent research [7] and excellent computational tools available online, such as the Python package `pymanopt` [9] used in this work. In particular, we use a version of the conjugate gradient algorithm adapted for manifold optimization and solved (5) considering the W matrices as elements of a Grassmann manifold. We will not delve into more the details of these procedures, but the interested reader will find more information in [4] and [7].

Classification pipeline: We classify each trial X_k via the minimum distance to mean (MDM) algorithm. It determines the geometric mean of the covariance matrices in each class of the training set and then assigns to each matrix in the test set the class to which the distance to the mean is the smallest [8].
We compare three different pipelines for classification:

MDM: No dimensionality reduction (DR) and classification using the MDM algorithm.

unsDR + MDM: Unsupervised DR with $\mathcal{L}_u$ as cost function and landmark L fixed to the geometric mean of the dataset. Classification using MDM.

supDR + MDM: Supervised DR with $\mathcal{L}_s$ as cost function, n_w always fixed to the minimum number of elements in each class and n_b chosen via cross-validation. Classification using MDM.

The performance of each pipeline is assessed via a 10-fold cross-validation procedure and compared by their AUC (area under the receiver operating characteristic curve).

Datasets: We carried out our analysis on three datasets, two from MI experiments and one using the P300 paradigm. The first MI database comes from the BCI Competition III – Dataset IV [10] and contains recordings from 5 subjects with 118 electrodes. We applied our classification pipelines on 140 trials corresponding to tasks of left and right imagined hand movements (70 for each class). The second MI database is available at the Physionet website [11] and comprises recordings on 64 electrodes from 109 subjects. We only used the data from tasks of imagined hands and feet movement, which corresponds to approximately 44 trials per subject (22 for each class). The P300 dataset comes from experiments performed in our laboratory on the P300-based game Brain Invaders [12]. We used data from 32 electrodes on 38 subjects with 720 trials each (120 target and 600 non-target).

Published by Verlag der TU Graz
Graz University of Technology

 DOI: 10.3217/978-3-85125-533-1-16

The data from each BCI paradigm were processed differently. For MI we filtered the EEG signals in the 8-30 Hz band and considered each trial as a segment from 0.5 to 2.5s after each trial onset. We estimated the spatial covariance matrices using (1). For the P300 data we used filters from 1 to 20 Hz and considered each epoch with a duration of one second and starting just after a flash. We used the approach described in [13] to estimate a special form of covariance matrices capturing signals of interest in event-related potentials.

RESULTS AND DISCUSSION

This section describes the analysis on each dataset and discuss the obtained results.

BCI III-IV: We began our investigations on a dataset where dimensionality reduction is of major concern, because of its 118×118 covariance matrices. We compared the classification pipelines with different values of p, the dimension of the reduced covariance matrices, and n_b, the number of neighbors considered in $\mathcal{N}_b(C_i)$ for the supervised DR. The three values of p were chosen in the following way: obtain the geometric mean M of the covariances of the dataset (all classes together) and compute its eigenvalue decomposition. Sort the eigenvalues in decreasing order and select the values of p for which their cumulative sum equals to at least 80%, 95% and 99% of their total sum. For the BCI III-IV dataset this corresponds to p = 4, 12, and 32, respectively.
The results in Figure 3 show that for $p = 32$ the AUC of pipelines with dimensionality reduction were at least equivalent to those using all 118 available electrodes. This can be explained by the low-dimensional structure of the subspace spanned by the columns of the spatial covariance matrices. Consequently, most of the variance of these matrices is associated to their first few principal vectors. In contrast, reducing the dimensions to $p = 4$ degrades the classification performance on most subjects, a consequence of the loss of discriminatory features in the reduced matrices. Figure 3 also indicates that the parameter n_b of supervised DR does not seem to have much influence over the scores of the pipelines.

Physionet: In this second dataset we tested the performance of classification pipelines on a wide range of individuals. Having data from so many subjects allows us to observe certain patterns and make general conclusions that would be difficult otherwise. Figure 4 displays the results on three subjects for multiple values of n_b and fixed $p = 24$. For certain choices of n_b the score with supervised DR was higher than the other pipelines, but in general we did not observe any considerable improvement. In fact, one could include a grid-search step to the pipeline with supervised DR for choosing the best value of n_b for each subject. However, this would lead to a considerable increase in processing time, since the quadratic scaling of supervised DR makes it a quite expensive operation by itself. With this in mind, we fixed $n_b = 10$ in all of the following analysis, accepting the compromise that it might not be the optimal value for all subjects.

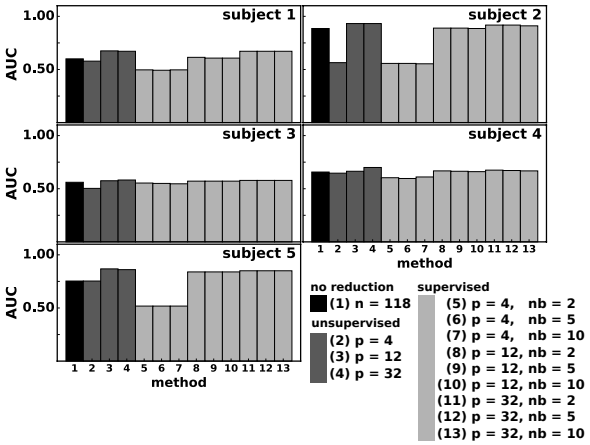

Figure 3: AUC of the classification pipelines on five subjects from dataset BCI III-IV. We considered pipelines with $p \in \{4, 12, 32\}$. For the supervised DR we fixed $n_w = 70$ and varied n_b in $\{2, 5, 10\}$.

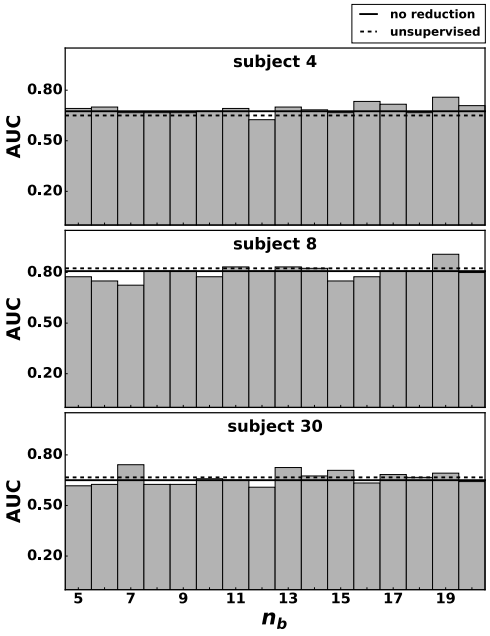

Figure 4: AUC of the classification pipelines with supervised DR on three subjects from the Physionet database. We considered multiple values of n_b and fixed $n_w = 22$ and $p = 24$. Horizontal lines correspond to AUCs of pipelines with no dimensionality reduction and unsupervised DR.

Figure 5 compares the performances of the classification pipelines on all subjects for different values of p and fixed $n_b = 10$. The curves in each plot correspond to the AUC of each pipeline in decreasing order. We observe the same behavior as before: on most subjects, when the dimension of the reduced matrices (e.g. $p = 4$) is small, the AUC of the pipeline with full matrices (64×64) is higher as compared to both dimensionality reduction methods. The score of all pipelines become close to one another when p increases. Another important observation from Figure 5 is that the classification performance of the

Published by Verlag der TU Graz
Graz University of Technology

 DOI: 10.3217/978-3-85125-533-1-16

pipelines varies smoothly with the choices of the dimension p of the reduced covariances. This is of great practical value because it demonstrates that we do not need to choose a precise p for attaining good results; there exists a certain range where all choices are equivalent.

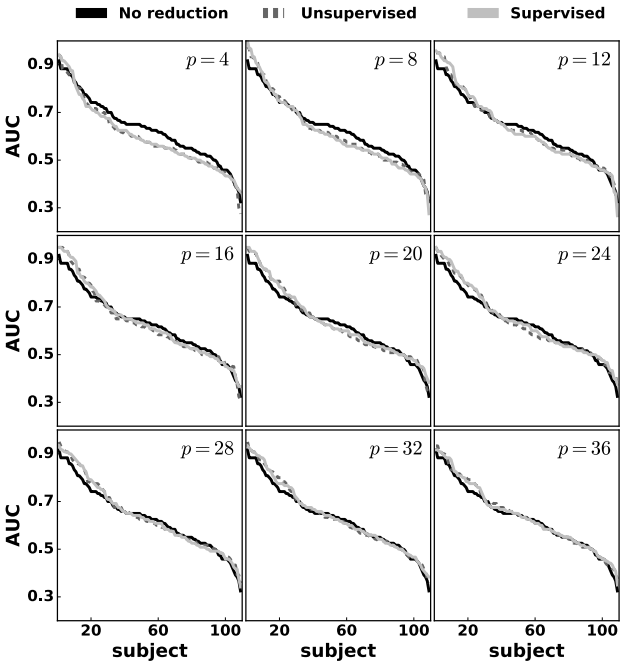

Figure 5: AUC scores in decreasing order for classifications on all subjects from the Physionet database. We fixed $n_b = 10$ and $n_w = 22$, and considered the values of p indicated in the figure.

P300: The results for our investigations of the P300 dataset are displayed in Figure 6. We compare once again the classification performance of a pipeline without dimensionality reduction (64×64 matrices) to classifiers using either an unsupervised or a supervised approach. We did all analysis with fixed $n_b = 10$ and considered multiple values of p. We observed the same behavior as before for the performance of dimensionality reduction algorithms: when p is too small the pipelines with DR are clearly inferior, as seen for $p = 8$, whereas for higher p the performances are all very similar.
The computing time for supervised DR in the P300 paradigm was excessively high, mainly because of the large number of trials in the dataset. We tried using a smaller set of trials, but in this case the classification performance of all pipelines were lower. In fact, usually P300 BCI systems are expected to improve their performance when more trials are available, so having a dimensionality reduction step that does not scale well with their number is problematic.

Comparing all pipelines: Besides investigating the conditions in which a dimensionality reduction would be useful or not, we tested whether any of the methods had a globally superior performance on the P300 and Physionet datasets. In theory, we expect the supervised approach to have better results because of the extra information it has concerning the labels of each covariance matrix. To test this hypothesis, we rearranged the results from Figures 5 and 6 into the plots in Figure 7, where each axis contains the AUC of a different pair of pipelines.

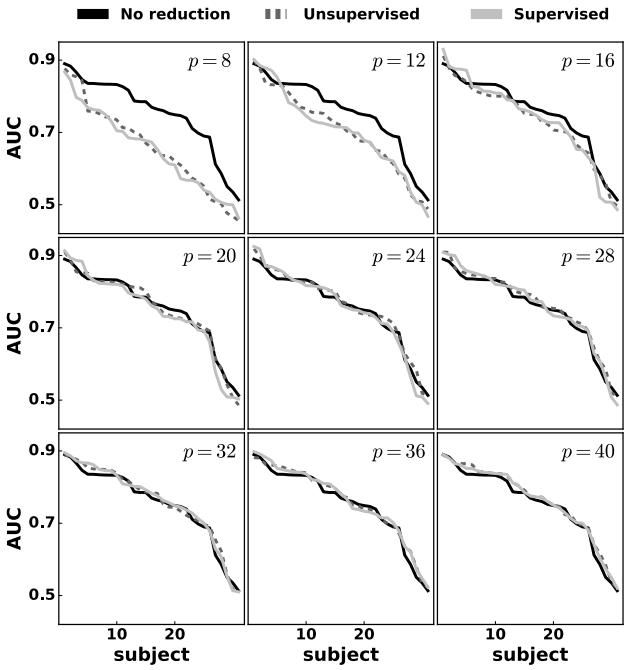

Figure 6: AUC values in decreasing order for the three pipelines applied to all subjects from the P300 database. We fixed $n_b = 10$ and $n_w = 120$, and considered the values of p indicated in the figure.

We estimated regression lines with intercept fixed to the origin for each plot and used a F-statistic to test if we could reject the hypothesis of its slope being equal to one. None of the statistical tests rejected the null hypothesis with type I error fixed to 5%, meaning that nothing can be said about one pipeline being consistently better than the others. This result indicates that the extra information used by the supervised DR is not enough for improving its classification power. It also means that adding a dimensionality reduction step to a classification pipeline does not harm its performance, a very useful fact that alleviates the computational burden of processing high-dimensional features using Riemannian geometry.

CONCLUSION

In this work, we evaluated two methods for reducing the dimension of positive-definite matrices and compared their scores in classification tasks on different BCI datasets. We observed that reducing too much the dimension discards important information from the original high-dimensional space and degrades the classification performance. Also, the choice of p showed a smooth influence over the scores of the classification pipelines, a

Published by Verlag der TU Graz
Graz University of Technology

 DOI: 10.3217/978-3-85125-533-1-16

very useful result in practice.
Our statistical tests did not reject the hypothesis of each pair of pipelines having equivalent performances, indicating that it is possible to reduce the dimensions of a spatial covariance matrix without losing classification performance. We should point out that we probably did not obtain better results for the supervised DR because we did not use a grid search for choosing the best n_b on each subject. However, if we had included this step the algorithm would have become impractical, because of the computational power that minimizing the loss function $\mathcal{L}_s$ demands.

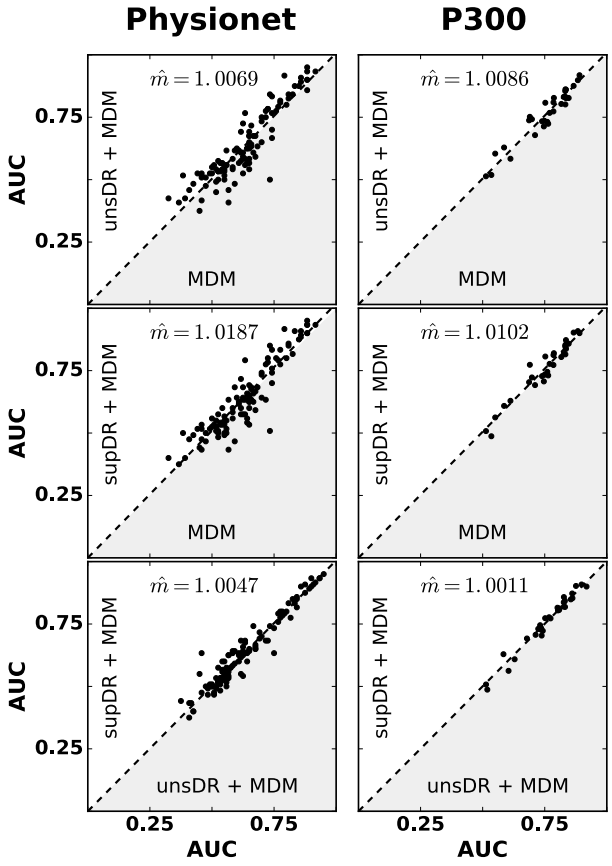

Figure 7: Scatter plots with the AUC scores of each pair of pipelines in the axis. We used only the results for $p = 24$ on both datasets. Coefficient $\hat{m}$ is the slope of a regression line with intercept fixed at the origin.

In comparison to [5], our investigations on BCI signals were more thorough. We explored the effects of the choice for the reduced covariance matrices, used a dataset containing many more subjects and a BCI paradigm that had not been considered until now. In future work, we intend to explore new options for performing supervised DR. The approach proposed by [4] does not scale well for large datasets and we believe that there are better alternatives. Also, we would like to explore more deeply the effects of reducing the dimensions of covariance matrices, not only in terms of classification power but as a general problem in Riemannian geometry. Finally, we should extend our comparisons to other proposals available in the literature for reducing the dimension of EEG signals.

AKNOWLEDGEMENTS

This work was partly supported by the ERC grant CHESS (2012-ERC-AdG-320684).

REFERENCES

[1] Congedo, M., Barachant A., Bhatia R., Riemannian Geometry for EEG-based Brain Computer Interfaces; a primer and a review. Brain Computer Interfaces. 2017. In press.
[2] Congedo, M., Barachant, A., Koopaei, E. Fixed Point Algorithms for Estimating Power Means of Positive Definite Matrices, IEEE Transactions in Signal Processing. 2017. In press.
[3] Lotte, F., Congedo, M., Lecuyer, A., Lamarche, F., Arnaldi, B., A review of classification algorithms for EEG-based brain–computer interfaces, Journal of Neural Engineering. 2007;4(2):1741-2560.
[4] Harandi, M, Salzmann, M., Hartley, R., Dimensionality Reduction on SPD Manifolds: The Emergence of Geometry-Aware Methods, preprint arXiv:1605.06182.
[5] Horev, I. and Yger, F., Masashi S., Geometry-Aware Principal Component Analysis for Symmetric Positive Definite Matrices, in Proceedings of the 7th ACML, Hong Kong, 2015, 1–16.
[6] Bhatia, R. Positive Definite Matrices, Princeton University Press, Princeton, United States (2009).
[7] Absil, P.-A., Mahony, R., Sepulchre, R. Optimization Algorithms on Matrix Manifolds, Princeton University Press, Princeton, United States (2008).
[8] Barachant, A., Bonnet, S., Congedo, M., Jutten, C., Multiclass Brain-Computer Interface Classification by Riemannian Geometry, IEEE Transactions on Biomedical Engineering. 2012;59(4):920-928.
[9] Townsend, J., Koep, N., Weichwald, S., Pymanopt: A Python Toolbox for Manifold Optimization using Automatic Differentiation, preprint arXiv:1603.03236
[10] Schlogl, A., Lee, F., Bischof H., Pfurtscheller, G., Characterization of Four-Class Motor Imagery EEG Data for the BCI-Competition 2005, Journal of Neural Engineering. 2005;2(4):L14-L22.
[11] Schalk, G., McFarland, D. J., Hinterberger, T., Birbaumer N., Wolpaw, J. R., BCI2000: A general-purpose brain-computer interface (BCI) system, IEEE Transactions on Biomedical Engineering. 2004;51(6):1034-1043.
[12] Congedo, M., et al., "Brain Invaders": a prototype of an open-source P300-based video game working with the OpenViBE platform, in Proc. 5th International BCI Conference, Graz, Austria, 2011, 280-283.
[13] Barachant, A. and Congedo, M., A plug & play P300 BCI using information geometry, preprint arXiv: 1409.0107

Published by Verlag der TU Graz
Graz University of Technology

Proceedings of the
7th Graz Brain-Computer Interface Conference 2017 DOI: 10.3217/978-3-85125-533-1-17

REAL-TIME FMRI CONTROL OF A HUMANOID ROBOT USING TWO BRAIN NETWORKS SIMULTANEOUSLY: A PILOT STUDY

Ori Cohen[1,2], François Keith[3], Moshe Koppel[2], Abderrahmane Kheddar[4,5], Rafael Malach[6], and Doron Friedman[1]

[1]The Interdisciplinary Center, Herzliya 46150, Israel
[2]Bar-Ilan University, Ramat-Gan 52900, Israel
[3]CEA-Saclay, France
[4]CNRS-UM LIRMM, 161 rue Ada 34095 Montpellier Cedex 5, France
[5]CNRS-AIST Joint Robotics Laboratory, UMI3218, 305-8568 Tsukuba, Japan
[6]Weizmann Institute of Science, Department of Neurobiology, Rehovot 76100, Israel

E-mail: doronf@idc.ac.il, orioric@gmail.com

ABSTRACT: We have previously shown that real-time fMRI, despite the low temporal resolution of the BOLD signal, can be used for BCI navigation, using motor-imagery and -execution. Here we leverage the superior spatial resolution of fMRI to implement a BCI paradigm going beyond a single brain network for control, while retaining an intuitive mapping between brain activity and BCI functionality. The experiments simulate non-trivial navigation and item selection tasks by a subject teleoperating an HRP-4 humanoid-robot. Motor actions are mapped into simple navigation commands inside a room and visual attention is mapped to direct the robot's arm toward one of three objects placed on a table. When the correct item has been selected, the subject navigates the robot toward the experimenter in order to simulate the delivery of the object. We describe a method based on two parallel classifiers, with four and three classes (independent of the first four), offline and real-time classification results from a single-subject pilot, performing several times.

INTRODUCTION

This research is part of a thread of studies aimed at dissolving the boundary between the human body and a surrogate robotic representation in a physical reality. The subject is expected to act as if the robotic body is his own body, and our aim was to provide the subject with an intuitive thought-based control of this surrogate representation. The subject was located in Israel and the robot was located in France; this geographic split was only made due to the availability of the facilities.

Electroencephalogram (EEG)-based brain-computer interface (BCI) for device control, despite much recent progress, is still mostly based on three paradigms (with some variants): motor imagery, P300, and steady state visually evoked potential (SSVEP). Our overarching goal in this research is to leverage the superior spatial resolution of blood-oxygen-dependent-signal (BOLD) in order to explore novel BCI control paradigms based on multiple brain systems simultaneously, such that we map different types of mental patterns to relevant functional goals, approximating a realistic task. Specifically, in this study we allow the subject to navigate using three motor classes, to select one of three objects using the visual system, and a null class.

There have been several studies including EEG-based BCI control of avatars [1, 2, 3] and teleoperation of a humanoid robot [4, 5], including studies with spinal cord injured people [6]. We have demonstrated teleoperating a humanoid robot using motor imagery and execution with real-time functional magnetic resonance imaging (fMRI) [7, 8], and others have demonstrated navigating a robot using covert visuospatial attention [9]. In this pilot study we aim going beyond these studies, using two different brain systems simultaneously.

MATERIALS

fMRI scans were performed on a 3T Trio Magnetom Siemens scanner as described in [7, 10], with a repetition time (TR) of 2000ms. Our system includes a tool for whole brain classification of raw data in real-time as described in [11]. Visual feedback is provided by a mirror, placed 11cm from the eyes of the subject and 97.5cm from a screen, which results in a total distance of 108.5cm from the screen to the eyes of the subject.

We used the vision system framework (VSF)[1] to acquire, transcode and transmit the video stream between the scanner (in Israel) and the robot (in France) with minimum latency.

METHODS

We created a complete software suite for running a wide range of real-time fMRI studies, which is able to process

[1]https://github.com/LIRMM-Beziers/visionsystem

Published by Verlag der TU Graz
Graz University of Technology

 DOI: 10.3217/978-3-85125-533-1-17

both brain data arriving in real time from the fMRI scanner and pre-recorded fMRI data [11]. It supports various experimental protocols, includes several analysis methods, is integrated with the Unity3D game engine for virtual environment feedback, and can interface with other external devices. Our tool is efficient in terms of processing, can be configured for a wide range of experimental protocols and was previously tested in several types of real-time fMRI BCI experiments. It is based on statistical machine learning classification of subjects' brain state in real time, based on whole brain activity.

Figure 1: Sample stimuli for testing the visual category task. From left to right the categories are: faces, tools and houses.

Training and applying classifiers in real-time requires that learning be executed faster than is generally done in the application of machine learning to fMRI. Our system is optimized for memory usage, processing speed, and classification speed using feature reduction, feature selection, and redundant data reduction. The system uses pre-recorded raw brain data for the purpose of learning a classifier using Platt's sequential minimal optimization (SMO) version of the support vector machine (SVM) learning algorithm [12]. The system culls empty voxels and the subject's eyes and corrects nonlinear non-homogeneous drifts. For classification and feature selection we use Weka, which is a collection of machine learning algorithms [13]. For feature selection we use the information gain (IG) measure to select the most relevant voxels [14]. The filtered dataset is passed into Weka's [15] implementation of multiclass [16] SVM [12], using default parameters. The result of the training phase is an SVM classifier model that can classify previously unseen vectors. The system automatically verifies that the model classifies the training data with perfect accuracy ("test on train" for sanity check) and displays the selected voxels.

In the real-time classification stage, the subjects perform a task and the system classifies their intentions in real time. The system classifies a brain scan every time resolution unit (TR), which in this case is 2 seconds. It uses the filtering and normalization methods as in the training stage and select the same voxels based on the IG filtering performed at model training. The data is then passed into the trained SMO model, and the classification result is then transmitted to the external application using a user datagram protocol (UDP). The classification process takes approximately 50 milliseconds. Before moving to a free choice task the subject undergoes a cue-based part of the study, the task is similar to training but feedback is provided based on real time classification.

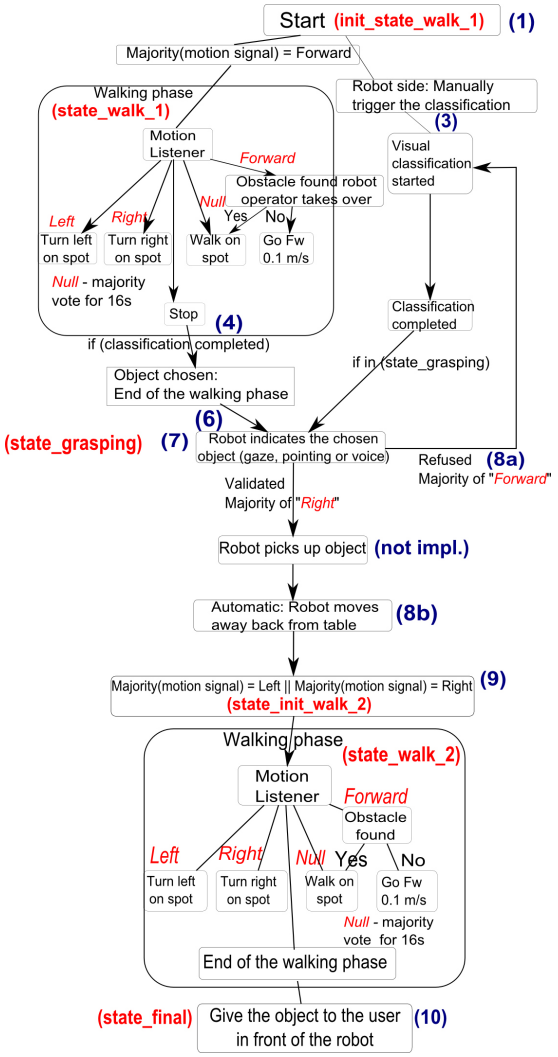

Figure 2: The HRP-4 humanoid robot's state-machine protocol for the visual-motor task.

The subject (female, 31) underwent several training sessions for each classification task: i) motor execution (4 sessions) – moving left fingers, right fingers, toes, and a null (rest) class; ii) motor imagery (4 sessions) – imagining left hand, right hand, feet, and a null class; and iii) visual categories (5 sessions) – viewing images of houses, faces and tools. The motor execution classifier was trained 3 months prior to this experiment, the motor imagery classifier was trained 2.5 months prior and the visual categories classifier was trained 24 days prior.

Each motor training session included 40 events from each category, i.e., for four training sessions there are 160 labelled samples; all details are as in [10]. For visual classification training is done using a block design – a sequence of images from the same category is flashed, one per second, for 12 seconds, followed by a duration of six seconds during which the category images were painted in white to allow the signal to return to baseline. The subject

Published by Verlag der TU Graz
Graz University of Technology

 DOI: 10.3217/978-3-85125-533-1-17

was trained with 36 image sequences for each category, i.e., for five training sessions there were 180 samples. In test sessions each stimulus includes three images from the three categories simultaneously, and the target category is indicated by a fixation dot (Fig. 1). The subject carried out three such test runs, with 30 stimuli in each session (10 from each category).

The motivation behind the visual paradigm is to allow the subject to select one of several objects by visual attention, even if the multiple objects are seen together. Our processing pipeline assures that information from the areas surrounding the eyes is pruned prior to being fed into the machine learning system [11]. Thus, we expect that the machine learning system can classify this task by decoding, in real time, the activity of the well-known visual areas in the cortex, corresponding to the visual categories of faces, tools, and houses. Such decoding in real time and as part of a BCI task has never been attempted to our knowledge, and the task is especially challenging given that the training and testing of the algorithm are not done in the same conditions – the training is based on a single image display and the testing is based on three images shown simultaneously. The goal in this paradigm is to move towards new naturalistic BCI paradigms, such that training is done in controlled conditions, and the model can be applied in real time, in naturalistic conditions, which may be different than those available for training. In our case, we expect the classifier to be trained separately over different object categories, whereas the free choice task includes multiple object categories at the same time.

The experiment and the robot's control were based on a predefined state machine (Fig. 2). The task included several stages, including navigation and object selection (see Fig. 3 and companion video[2]). The robot was placed in a fixed orientation. First, the subject steered the robot towards a table, by passing an obstacle chair and by utilizing all four motor commands in order to reach the table (Fig. 4, 3). The subject was instructed to guide the robot around the chair and then turn towards the printed sign as seen in 4(b) (on the right). The subject had to read, through the eyes of the robot, the instructions from the sign with the target object to select. After seeing the instruction, the subject was expected to navigate towards a table, eventually stopping in front of it. On top of the table we placed three objects: a (toy) doll's head, a (toy) house, and a tool (either a hammer or a tea cup). Prior to the experiment, the subject was instructed that in order to select an object she had to rotate towards the sign to learn about the target object, and from that moment she had to focus her attention to the target physical object on the table at all times and study it, including while walking to table, until it is selected. For example, if the experimenter revealed the word "face" then the subject had to focus attention to the head's eyes, nose and chin, i.e., pay attention to the features of the object. If the word "tool" is revealed, then the subject had to imagine herself using that tool.

After walking the path, the subject was expected to stop within grasping distance from the objects. Once the subject reached the table the steering was deactivated, the robot stood still and the robot's left hand was pointed toward one of the items on the table. The item was selected by a majority vote from the classification at times 0-16 seconds following the instruction from the experiment (8 TRs). The 16 seconds delay was based on the optimal classification time as determined in offline evaluation. If a majority vote did not take place (i.e., a draw) the classification continued until there was a decision.

Following the classification, the subject had to indicate whether she agrees with the selection or not using motor categories. The subject used either motor execution or motor imagery (in different runs), as follows: feet – try again, right hand – activate a grasp motion. If the motor action was classified as null, then the subject received feedback indicating her to repeat the motor action. The subject repeated this step until she was satisfied with the category that was selected. Immediately after the subject activated the grasp motion by selecting the category, the robot takes a few steps backward away from the table. Only then the system is re-activated the steering and the subject was allowed to control the robot and navigate it towards the experimenter.

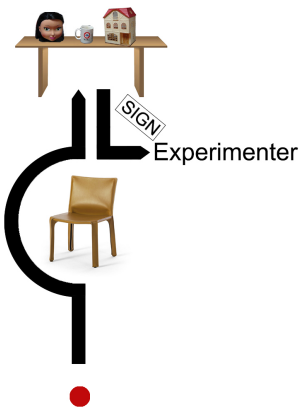

Figure 3: A schematic drawing of the intended walking path inside the room. The red dot indicates the robot's fixed position. The path goes around the chair rotating towards the sign, and then towards the table that has the three category items placed on top. Following the visual task, the path continues toward the experimenter.

During the task our system ran two classifiers in parallel: motor (motor execution or motor imagery) and visual categories, the former with four categories and the latter

[2] http://y2u.be/eYSb9Q5PcP8

Published by Verlag der TU Graz
Graz University of Technology

 DOI: 10.3217/978-3-85125-533-1-17

with three. The subject teleoperated the robot using all seven classes: left, right, forward, null class, house, face and tool. The longest run was 12 minutes. For each run the subject was assigned with a different target category (face, house, or tool). During the navigation part of the experiment, the flow of high level commands (forward, left, right, null, face, tool, house) was sent to the robot through a user UDP connection with a latency of 100-150 milliseconds using the VSF.

RESULTS

Throughout the experiment we used three classifier models: motor execution, motor imagery, and visual categories. A combination of motor execution and visual categories was used on the first day of the experiment, and a combination of motor imagery and visual categories on the second day. Estimating accuracy for the free choice is difficult, so we provide offline evaluation of the classification models.

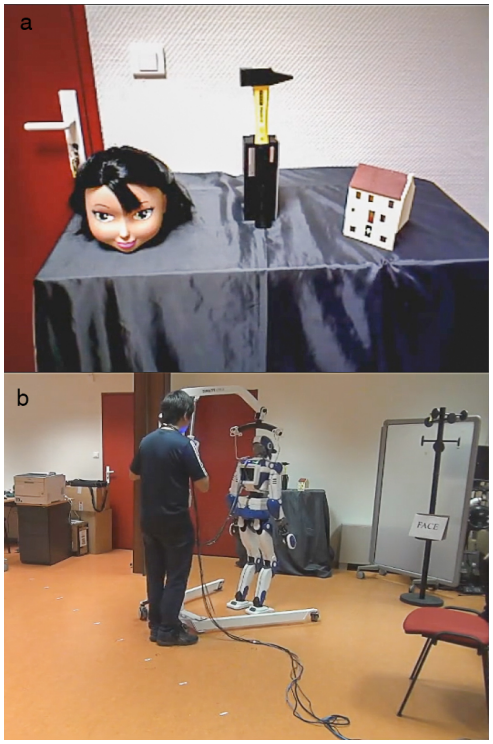

Figure 4: The HRP-4 humanoid robot during a visual-motor task, standing in front of three objects. Top: the target objects as seen from the robot camera by the subject, bottom: the robot performing the task, escorted by an experimenter for robot safety.

Offline analysis of the motor classifier is based on a single training session (Fig. 5). As expected, a cue-based session with real time feedback using the same classifier yields similar results. More real-time data is required to assess the difference in accuracy in TR3. The motor execution classifier was trained and tested three months prior to this real-time experiment and test. Similarly, single-run motor imagery classification accuracy results can be seen in Fig. 6; we note that the pre-recorded and real-time tests were done 3 & 2.5 months apart, respectively.

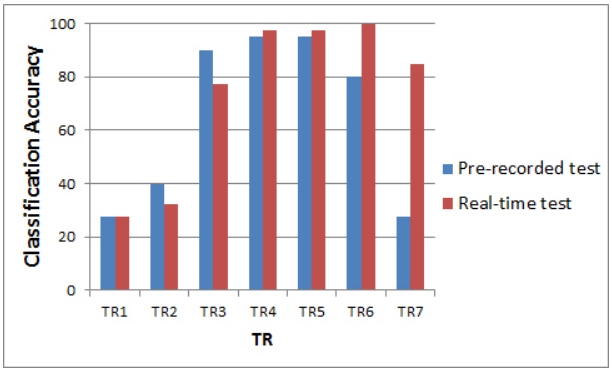

Figure 5: Motor execution cue-base classification accuracy comparison between a single pre-recorded and a single real-time run.

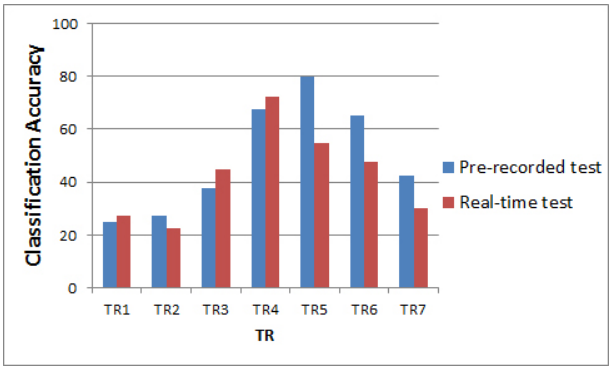

Figure 6: Motor imagery cue-base classification accuracy comparison between a single pre-recorded and a single real-time run.

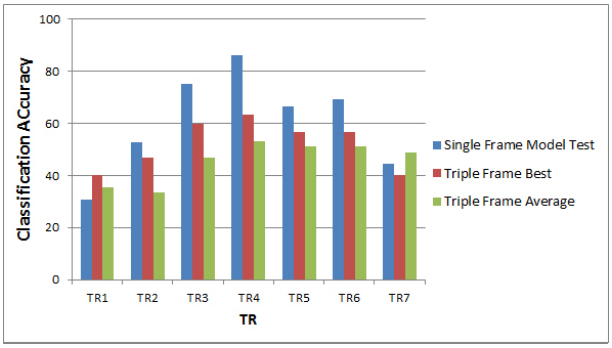

Figure 7: Cue-base classification accuracy, comparing single and triple frame (best run and average).

Offline analysis of the visual classifier was performed as follows. A single model was trained on five sessions – overall 180 stimuli, each including one category. The model was then tested in two conditions: i) another run of 36 stimuli with one image displayed on screen, and ii) a

Published by Verlag der TU Graz
Graz University of Technology

 DOI: 10.3217/978-3-85125-533-1-17

run of 36 stimuli, each comprising of all three categories displayed on the screen simultaneously. Fig. 7 presents the results, indicating that while both methods perform significantly better than chance (33%), testing on a single image is superior to testing on three parallel images.

A qualitative assessment of the subject's performance can be provided for the free choice task. In the motor execution experiment the subject performed the navigation part successfully in all four experimental sessions. In the motor imagery experiments the subject failed to stop the robot near the table and was only successful in the third session.

Thus, our subject had five attempts at the visual task: four in the motor execution conditions and one in the motor imagery condition. The subject succeeded in all cases, but only in the second attempt (in all of the motor execution sessions) or in the fourth attempt (in the motor imagery session).

The classification seemed to be skewed towards the face category. Fig. 8(A) shows several red dots that correspond to a successful classification of the "face" command in each time point during 8 TRs. However, when the subject was instructed to focus on one of the two other categories (house or tool) there was category rivalry between the classes. Fig. 8(B) is a rivalry example that show a fluctuation between "face" and "house". When category rivalry occurs, it prolongs the classification stage and it is harder to get a majority vote. In other words, without rivalry there are less classification attempts and a majority vote occurs quickly.

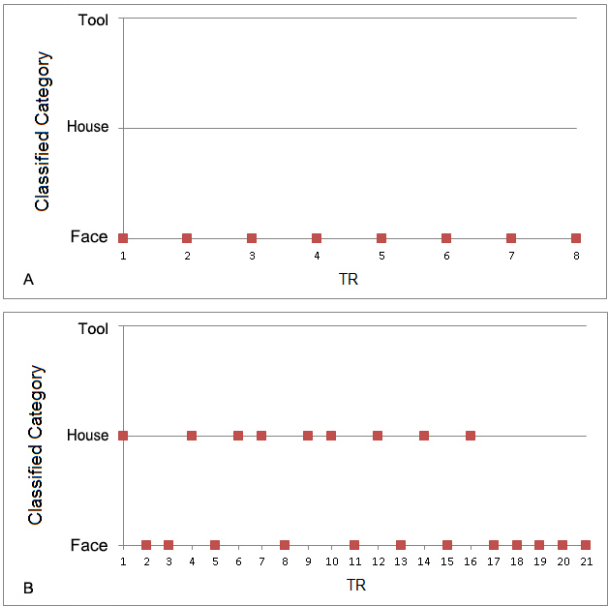

Figure 8: Visual categories real-time classification examples. The subject was instructed to focus on a) face, b) house.

DISCUSSION

We have developed a novel paradigm, based on simultaneous classification of both motor and visual brain networks, and have evaluated it in the context of a complex navigation and object-selection task, involving teleoperating of a humanoid robot. The pilot study with one subject serves to demonstrate that our system is fully operable, and provides a preliminary evaluation of the paradigm. Our results indicate that the task can be performed, although motor imagery and visual classification are challenging. Specifically, further work is required to refine the visual paradigm. Our offline evaluation results suggest that training subjects on simultaneous images (in the same fashion as the actual task) may be more appropriate.

ACKNOWLEDGEMENTS

This research was supported by the European Union FP7 Integrated Project VERE (No 657295), `www.vereproject.eu`. We would like to thank the subject for her participation, and the Weizmann Institute fMRI scanner staff Edna Furman-Haran, Nachum Stern and Fanny Attar for their help in this experiment.

REFERENCES

[1] C Kapeller, C Hintermüller, and C Guger. Augmented control of an avatar using an SSVEP based BCI. In *Proceedings of the 3rd Augmented Human International Conference*, page 27. ACM, 2012.

[2] J Faller, G Müller-Putz, D Schmalstieg, and G Pfurtscheller. An application framework for controlling an avatar in a desktop-based virtual environment via a software SSVEP brain–computer interface. *Presence: teleoperators and virtual environments*, 19(1):25–34, 2010.

[3] D Friedman, R Leeb, L Dikovsky, M Reiner, G Pfurtscheller, and M Slater. Controlling a virtual body by thought in a highly-immersive virtual environment. *GRAPP 2007*, pages 83–90, 2007.

[4] P Gergondet, S Druon, A Kheddar, C Hintermüller, C Guger, and M Slater. Using brain-computer interface to steer a humanoid robot. In *Robotics and Biomimetics (ROBIO), 2011 IEEE International Conference on*, pages 192–197. IEEE, 2011.

[5] E Tidoni, P Gergondet, A Kheddar, and S M Aglioti. Audio-visual feedback improves the BCI performance in the navigational control of a humanoid robot. *Frontiers in neurorobotics*, 8:20, 2014.

[6] E Tidoni, P Gergondet, G Fusco, A Kheddar, and S M Aglioti. The role of audio-visual feedback in a thought-based control of a humanoid robot: A BCI study in healthy and spinal cord injured people. *IEEE Transactions on Neural Systems and Rehabilitation Engineering*, 2016.

[7] O Cohen, S Druon, S Lengagne, A Mendelsohn, R Malach, A Kheddar, and D Friedman. fMRI robotic embodiment: A pilot study. In *Biomedical Robotics and*

Published by Verlag der TU Graz
Graz University of Technology

 DOI: 10.3217/978-3-85125-533-1-17

Biomechatronics (BioRob), 2012 4th IEEE RAS EMBS International Conference on, pages 314–319, June 2012.

[8] O Cohen, S Druon, S Lengagne, A Mendelsohn, R Malach, A Kheddar, and D Friedman. fMRI-based robotic embodiment: Controlling a humanoid robot by thought using real-time fMRI. *PRESENCE: Teleoperators and Virtual Environments*, 23(3):229–241, 2014.

[9] P Andersson, J PW Pluim, M A Viergever, and N F Ramsey. Navigation of a telepresence robot via covert visuospatial attention and real-time fMRI. *Brain topography*, 26(1):177–185, 2013.

[10] O Cohen, M Koppel, R Malach, and D Friedman. Controlling an avatar by thought using real-time fMRI. *Journal of Neural Engineering*, 11(3):035006, 2014.

[11] O Cohen, M Ramot, R Malach, M Koppel, and D Friedman. A generic machine-learning tool for online whole brain classification from fMRI. In *The 6th International Brain-Computer Interface Conference*, 2014.

[12] J Platt. Sequential minimal optimization: A fast algorithm for training support vector machines. 1998.

[13] M Hall, E Frank, G Holmes, B Pfahringer, P Reutemann, and I H Witten. The weka data mining software: An update. *ACM SIGKDD explorations newsletter*, 11(1):10–18, 2009.

[14] J R Quinlan. Induction of decision trees. *Machine Learning*, 1(1):81–106, 1986.

[15] I H Witten, E Frank, and A M Hall. *Data Mining: Practical machine learning tools and techniques, 3rd Edition*. Morgan Kaufmann, 2011.

[16] T Hastie and R Tibshirani. Classification by pairwise coupling. In I.M. Jordan, J.M. Kearns, and A.S. Solla, editors, *Advances in Neural Information Processing Systems*, volume 10. MIT Press, 1998.

Published by Verlag der TU Graz
Graz University of Technology

Proceedings of the
7th Graz Brain-Computer Interface Conference 2017 DOI: 10.3217/978-3-85125-533-1-18

SPATIAL FILTERS SELECTION TOWARDS A REHABILITATION BCI

E. Colamarino[1,2], F. Pichiorri[2], D. Mattia[2], F. Cincotti[1,2]

[1] Department of Computer, Control, and Management Engineering Antonio Ruberti, Sapienza University of Rome, Rome, Italy

[2] Neuroelectrical Imaging and BCI Lab, Fondazione Santa Lucia IRCCS, Rome, Italy

E-mail: cincotti@dis.uniroma1.it

ABSTRACT: Introducing BCI technology in supporting motor imagery (MI) training has revealed the rehabilitative potential of MI, contributing to significantly better motor functional outcomes in stroke patients. To provide the most accurate and personalized feedback during the treatment, several stages of the electroencephalographic signal processing have to be optimized, including spatial filtering.
This study focuses on data-independent approaches to optimize spatial filtering step.
Specific aims were: i) assessment of spatial filters' performance in relation to the hand and foot scalp areas; ii) evaluation of simultaneous use of multiple spatial filters; iii) minimization of the number of electrodes needed for training.
Our findings indicate that different spatial filters showed different performance related to the scalp areas considered. The simultaneous use of EEG signals conditioned with different spatial filters could either improve classification performance or, at same level of performance could lead to a reduction of the number of electrodes needed for successive training, thus improving usability of BCIs in clinical rehabilitation context.

INTRODUCTION

Brain-computer interface (BCI) technology allows people with severe motor disabilities to use their brain activity (e.g. the electroencephalographic, EEG, signals) to control external devices, thereby bypassing their impaired neuromuscular system, or receive a feedback related with their cognitive processes [1]. One of the most recent and promising BCI applications regards post-stroke functional motor rehabilitation [2]. For instance, the introduction of BCI technology in assisting the motor imagery (MI) practice has been demonstrated to uncover the rehabilitative potential of MI, contributing to significantly better hand motor functional outcomes [3]. In order to facilitate the practice of voluntary covert and /or overt access to the affected hand, patients received a discrete feedback that should be the faithful representation of the brain activity (congruent with the affected hand).
To bridge the gap between research-oriented methodology in BCI design and the usability of a system in the clinical realm requires efforts towards BCI signal processing procedures (feature extraction and translation) that would optimize the balance between system accuracy and usability. This study focuses on the process of feature extraction and more specifically on its spatial filtering step.
Spatial filters are generally designed to enhance sensitivity to particular brain sources, improve source localization and/or suppress artifacts. Most commonly, spatial filters are a linear combination (i.e. weighted sums) of channels. There are several approaches for determining the set of spatial filter weights. These approaches fall into two major classes: data-independent and data-dependent spatial filters [4]. According to the review [5] of signal processing methods used in BCI studies, the surface Laplacian, the common spatial pattern, the common average reference and the independent component analysis are the most employed filters. For sensorimotor rhythms-based BCIs, the common average reference and Laplacian methods are superior to the ear reference method because they enhance the focal activity from the local sources and reduce the widely distributed activity [6]. Furthermore, concerning the two variations of the Laplacian filter, i.e. the large and the small Laplacian, it appears that they are the best filters in prediction and source identification, respectively [7].
This study approached the spatial filtering step by hypothesizing that filtering the EEG data with a different data-independent spatial filters would return a better rendering of the scalp areas of interest to allow for a more suitable *physiologically informed* feature extraction. As such, this procedure would best lead to a reinforcement of individual *correct* EEG patterns during BCI training [3] and, thus, maximize target prediction in the rehabilitation training.
In this view the specific study aims were: (a) to compare performances of different spatial filters as a function of the scalp areas relevant for hand or foot executed motor tasks (i.e. areas of interest), (b) to compare performances of gold standard filters, e.g. Laplacian filters, versus those obtained by pooling information (EEG features) coming from different spatial filters, (e.g. two kinds of bipolar filters), (c) to evaluate the impact of number of electrodes needed in those spatial filters which showed similar classification performance.
Confirming the main hypothesis, we might suggest that the a priori (defined one time, before starting the analysis) choice of just one spatial filter at the start of the

Published by Verlag der TU Graz
Graz University of Technology

 DOI: 10.3217/978-3-85125-533-1-18

BCI signal processing is not optimal.
Common average reference (CAR), surface Laplacian (LAP) and bipolar filters, the latter commonly used in the EEG clinical field but not in sensorimotor rhythms-based BCI, were explored in this preliminary study on an EEG data set, acquired at IRCCS Fondazione Santa Lucia, that does not include stroke patients.

METHODS

Subjects: Forty subjects (seven of them with severe motor disabilities due to traumatic spinal cord lesion or progressive neurodegenerative disorders) participated in the study. Each subject gave written informed consent prior to inclusion. The study was approved by the Fondazione Santa Lucia (Rome) ethics committee.

Experimental protocol: The protocol consisted of two main parts: the screening session and some training (weekly) sessions. During the initial screening session, subjects were comfortably seated on a reclining chair (or, when necessary, on a wheelchair) in a dimly lit room. The session was divided in 12 runs (30 trials each one). Each trial began with a target appearing on a side of the screen (up/down, i.e., vertical, or left/right, i.e., horizontal). The trial lasted 5.8 seconds, with the inter trial interval of 1.8 seconds. Subjects were instructed to execute (first run) and imagine (second run) movements of their hands (opening and closing) or feet (flexion) upon the appearance on the screen of top or bottom target, respectively. When the targets appeared on the left or right side of the screen subjects were invited to move (third run) or to imagine (forth run) their left or right hand (opening and closing) upon the appearance of the target in the correspondent side. This sequence was repeated three times for a total of 12 runs. Subjects were instructed to minimize muscular, electrooculographic and blink activity. In the screening session, subjects were not provided with any feedback (any representation of their brain activity).

Experimental setup: Scalp EEG potentials were collected from 58, 59 or 61 positions assembled on an electrode cap (according to an extension of the 10-20 International System) and amplified by a commercial EEG system (BrainAmp, Brain Products GmbH, Germany) which sampled signals at 200 samples/s (per channels). Electrical reference has been provided by both ear lobes. The BCI system was realized using the BCI2000 [8] software system.

Signal processing and feature extraction: Using Matlab, EEG signals were band-pass filtered (0.1-70 Hz) with a forth order Butterworth filter and notch filtered at 50 Hz. The conventional ear reference, the common average reference (CAR), two different Laplacian derivations (small and large) [6] and two simple bipolar methods were considered in the study. In the bipolar methods (applied via software) each voltage difference was computed between two channels, longitudinally subtracting e.g. FCz from Fz and transversely subtracting e.g. Cz from C1.
EEG data recorded and filtered with each spatial filter considered were divided into epochs 1 second long. The spectral analysis was performed on EEG data epochs corresponding to task employing the Maximum Entropy method (16^{th} order model) with a resolution of 2 Hz and considering no overlapped epochs. All possible features in a reasonable range (i.e., 0-36 Hz in 2 Hz bins) were extracted and analysed. A feature vector (spectral amplitude at each bin for each channel) was extracted from each epoch.

Data analysis: Consistently with the aims of the study two analysis were planned.
For the aim (a) just vertical runs, corresponding to the movement execution of hands or feet, were analysed. Hands opening/closing and feet flexion engage separate areas of the sensorimotor strip, different about anatomical and functional point of view.
Basing on the sensorimotor rhythms, the analysis was constrained to features belonging to the sensorimotor strip (FC, C and CP channels) in the range from 7 Hz to 31 Hz. The hands area was defined as the area containing derivations coming from FC, C and CP electrodes in all their even and odd positions (bilateral area); the feet area was defined as the area containing derivations coming from electrodes placed on the mid-line, e.g. FCz, according to the 10-20 International System.
Features belonging to those areas, first separately considered, i.e., hands area, feet area, and then in the combined manner, hands and feet areas, were the input for the stepwise regression which identifies the optimal subset of predictor variables (i.e. the features in this case) and assigns weights to them in order to build an effective regression model to evaluate the relationship between the predictors and the dependent variable (here equivalent to subject's movement intention). The maximum number of features to be selected by the stepwise regression algorithm was set, for all feature domain, to 8 because of results obtained in a preliminary study. The latter aimed to compute the optimal number of features from which the mean (among tasks and subjects) classification performance does not grow in a significant way. We concluded that increasing the number of features, from eight to largest values, does not significantly increase the performance values.
In order to compare performances of the six spatial filters considered, after the features translation step in which a linear classifier is used to predict if the epoch examined belonged to hands movement trials or feet movement trials, the Area Under Curve (AUC) of Receiver Operating Characteristic (ROC) curve was assessed using a 15-fold cross-validation design.
For the aim (b) both vertical and horizontal runs were analysed, allowing selection algorithm (stepwise) to choose features from both areas, hands and feet areas in combined manner for vertical runs and left and right hand areas in combined manner for horizontal runs. This analysis included six feature domains each one extracted from EEG signals pre-processed with one of six filters earlier defined and a new feature domain containing all (in sensorimotor strip and frequencies) features computed from EEG signals pre-processed by

Published by Verlag der TU Graz
Graz University of Technology

 DOI: 10.3217/978-3-85125-533-1-18

longitudinal and transversal bipolar filters. The feature dimensionality reduction (stepwise regression), the classification (linear classifier) and the computation of performance index (AUC of ROC curve) followed the stages as proposed for (a).
For the aim (c) three representative subjects for which different spatial filters showed (for each subject) in (b) the same classification performances were identified. The number of electrodes needed to realize the hardware montage containing the eight (as earlier defined) optimal features was computed for each spatial filters.

Statistical analysis: To investigate the performances of different spatial filters in relation to the scalp areas, AUC values (in movement execution runs) were analysed by repeated measures two factors analysis of variance (ANOVA). The filter factor had six levels (the six filters earlier listed), the area factor had three levels (hands area, feet area, hand &feet area).
To the aim (b), for each task (vertical and horizontal task) AUC values were analysed by repeated measures two factors ANOVA in which filter factor had seven levels (6 filters listed earlier and the new filter obtained combining longitudinal and transversal bipolar filters) and modality factor two levels, the movement execution and imagination. Horizontal and vertical runs were studied separately.
The Tukey HSF post hoc analysis was conducted to assess pairwise differences. If not indicated otherwise, all results are presented as mean ± SE (standard error). For all statistical analysis, threshold for statistical significance was set to $p < 0.05$.

RESULTS

Spatial filters and scalp areas relation: The repeated measures two factors ANOVA of the AUC values revealed a significant effect of both filter ($F=28.72$, $p < 0.01$) and area ($F=52.43$, $p < 0.01$) factors and a significant area –filter interaction ($F=9.59$, $p < 0.01$). Figure 1 shows statistical analysis output and post-hoc tests result. The results are consistent with the findings in [6]: common average reference and large Laplacian methods are significantly superior to the ear-reference method.

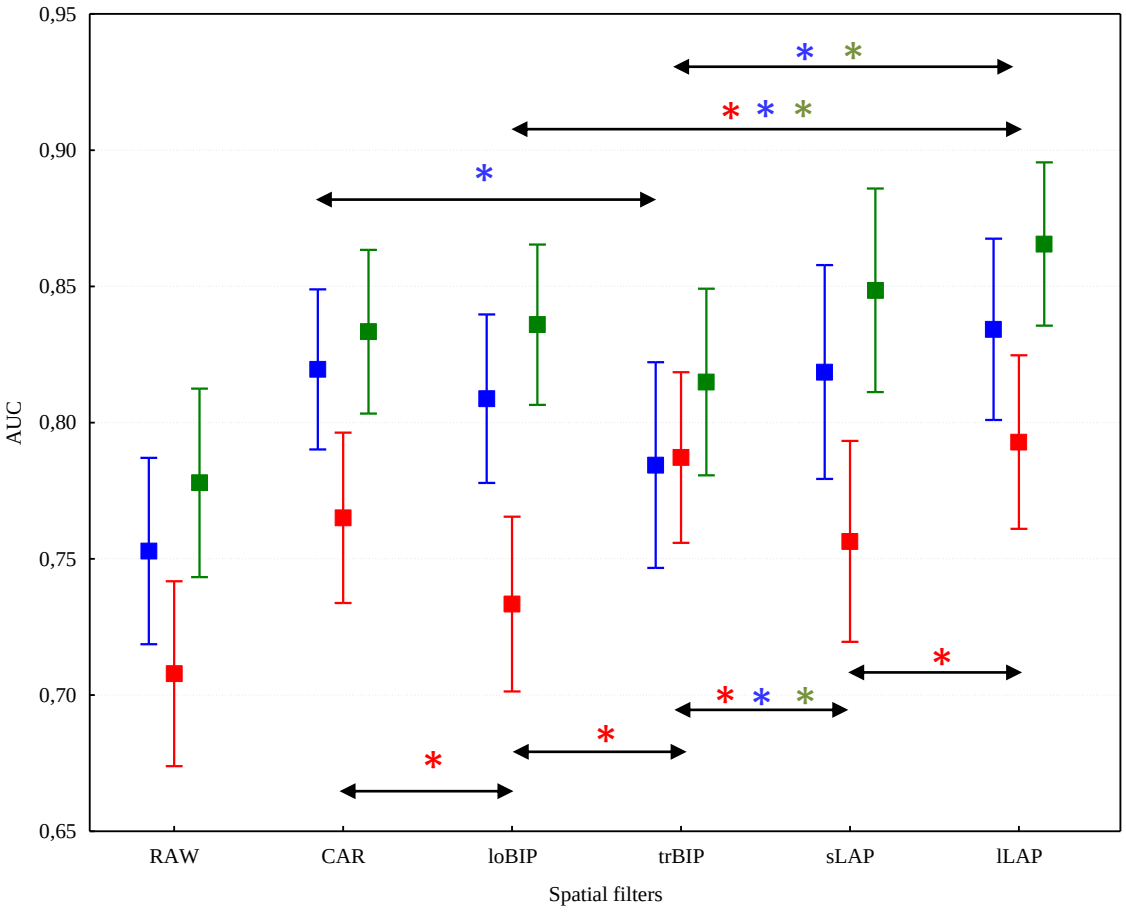

Fig. 1. Classification performance (AUC values of ROC curve) presented as mean ± SE (standard error) evaluated in movement execution vertical runs (hands opening/closing and feet flexion tasks) using features selected (by stepwise regression algorithm) from hands area (in blue), feet area (in red), both areas (in green) on EEG data no filtered (RAW), filtered with common average reference (CAR), longitudinal bipolar (loBIP) and transversal bipolar (trBIP) filters, surface Laplacian in its derivation small (sLAP) and large (lLAP). The symbol * shows the significant differences ($p<0.05$) pointed out by the Tukey HSF post hoc test. The colour of the symbol expresses the area in which this difference is significant. Although figure does not report the comparison between RAW and others filters, post-hoc tests confirm findings in McFarland et al., 1997.

Published by Verlag der TU Graz
Graz University of Technology

 DOI: 10.3217/978-3-85125-533-1-18

Table 1: List of the eight features selected (by stepwise algorithm) in the features domains obtained from EEG data filtered with small surface Laplacian (sLAP) and using both longitudinal and transversal bipolar filter feature domains (long + trans BIP, simultaneous use of multiple spatial filters). No statistical differences for this pair of filters from the previous analysis. Three representative subjects (S01, S02, S03) were considered for the comparison (results in table from movement execution of vertical runs, hand opening/closing and feet flexion). The AUC values, for each subject, are the same for both filters (sLAP and long+trans BIP). Channels positions are conformed with 10-20 International System. Each channel indicated in sLAP is the central electrode of the difference (e.g., C3 is the central electrode: the surface Laplacian involved its neighbours C1, C5, FC3, CP3).

	S01				S02				S03			
	sLAP chan – freq (Hz)		long + trans BIP chan – freq (Hz)		sLAP chan – freq (Hz)		long + trans BIP chan – freq (Hz)		sLAP chan – freq (Hz)		long + trans BIP chan – freq (Hz)	
1	C3	11	FC3-C3	11	CP4	11	FC4-C4	11	C4	13	FC3-C3	13
2	Cz	27	Cz-C2	13	CPz	25	CP4-P4	25	CP3	13	C2-C4	13
3	C4	13	Cz-CPz	29	C4	25	CPz-Cz	25	Cz	25	F5-FC5	17
4	C4	21	CPz-Pz	21	C3	13	C1-Cz	11	C6	11	TP7-CP5	27
5	Cz	21	FC3-C3	17	C2	29	CP3-P3	27	FC5	29	FC6-C6	13
6	FC3	31	FC1-C1	11	FC3	15	CP1-CPz	25	C3	13	C1-Cz	25
7	FC2	25	FC4-C4	21	CP4	25	FC4-C4	25	CP3	15	FC4-FC6	31
8	CP6	13	C1-Cz	11	Cz	27	F5-FC5	19	C6	27	CPz-CP2	29
Number of electrodes need to realize this hardware montage	21		10		22		12		22		15	

Simultaneous use of multiple spatial filters: The repeated measures two factors ANOVA of the AUC values revealed a significant effect of both filter ($F=22.13$, $p < 0.01$) and modality ($F=46.72$, $p < 0.01$) factors and a significant modality –filter interaction ($F=2.79$, $p < 0.05$). The post-hoc Tukey HSF test confirms findings in [6] about differences existing between apply and not apply spatial filters on EEG data. The tests disclose pairwise differences ($p < 0.01$) between the common average reference (mean=0.83) and the large surface Laplacian (mean=0.87), the longitudinal bipolar filter (mean=0.83) and the large surface Laplacian (mean=0.87), the transversal bipolar filter (mean=0.81) and the small surface Laplacian (mean=0.85), the transversal bipolar filter (mean=0.81) and the large surface Laplacian (mean=0.87) and, above all, between the transversal bipolar filter (mean=0.81) and the simultaneous use of longitudinal and transversal bipolar filters (mean=0.87). No significant differences were seen between performances obtained using features extracted from the new domain and those from the two variations (small and large) of the surface Laplacian filter.

Minimization of number of electrodes: Table 1 shows the comparison between the features selected from the new domain (longitudinal and transversal bipolar filters) and the small surface Laplacian domain for three subjects for which classification performance is the same for both domains.

DISCUSSION

Feature extraction and feature selection are crucial steps to ensure an optimal BCI system performance. When applying BCI to support clinical rehabilitation it is mandatory to comply with quality of EEG patterns reinforced via BCI training to promote post-stroke (good) plasticity leading to a better motor outcome. Yet, deployment of BCI systems with high level of usability enables the actual transfer of this technology in routine clinical usage.

In this study the spatial filters commonly used in BCI control were compared with filters commonly used in EEG clinical application (e.g., bipolar filters) in order to allow for a *handy* feature selection but still taking into account the physiological requirements specific for this BCI application.

Here, the relation between performances shown by several (BCI and clinical gold standard) spatial filters and sensorimotor strip areas, engaged in different tasks, was investigated. Considering scalp areas separately (i.e., hands area and feet area) highlights interesting differences (e.g., from longitudinal and transversal bipolar in the feet area) that do not emerge considering features in the sensorimotor strip altogether.

Our findings indicate that the comparison between the transversal bipolar and the small surface Laplacian filters showed different performances in the three scalp areas of interest analyzed. In particular, we found better performance for transversal bipolar filter in the foot area and for small surface Laplacian in the hand area. The identification of a best spatial filter is, therefore, related to the scalp area (its anatomical and functional properties) of interest and thus, improving performance can be pursued using specific filters for specific areas.

Further analysis will be oriented to investigate the reason why transversal bipolar filter shows better performance in the feet area.

In addition, these findings require a consolidation by exploring their use with other motor tasks (different from hand opening/closing and feet flexion, analyzed in this preliminary study) and/or imagined movements.

Furthermore, the integration of features information as in this case from longitudinal and transversal bipolar filters, led to an improvement of performance with respect to

Published by Verlag der TU Graz
Graz University of Technology

 DOI: 10.3217/978-3-85125-533-1-18

considering each domain individually. Specifically, no differences were found between the performance obtained with the ***integration approach*** and those obtained with the surface Laplacian filters (i.e., the gold standard when scalp areas were considered all together). Moreover, comparing the number of electrodes needed to realize the hardware montage containing just the appropriate features for the rehabilitation (both in case of features selected from integrated approach and surface Laplacian filter), We suggest that the use of a new integrated approach for feature extraction and selection might enhance the usability of the BCI technology in the field of rehabilitation.
The next step to ultimately promote this approach to rehabilitation applications would be to analyze BCI data collected from stroke patients.

CONCLUSION

Different spatial filters show different performance in relation to the scalp areas of interest, suggesting that potentially useful information for optimal feature extraction in BCI contexts can be obtained taking into account neurophysiological aspects. This could be particularly relevant in the context of rehabilitation applications. Furthermore, to consider features from more than one feature domain improves classification performance and, comparing filters at same performance level, allows to reduce the number of electrodes, improving the usability of BCI technology. For these reasons, we suggest that the a priori choice of one spatial filter might not be optimal for BCI rehabilitation applications.

ACKNOWLEDGEMENTS

This work was funded in part by the Sapienza University of Rome - Progetti di Ateneo 2015 (C26A15N8LZ).

REFERENCES

[1] Daly JJ and Wolpaw JR. Brain-computer interfaces in neurological rehabilitation. The Lancet Neurology 2008; 7(11) pp. 1032-1043.

[2] Cincotti F, Pichiorri F, Arico P, Aloise F, Leotta F, de Vico Fallani F et al. EEG-Based Brain-Computer Interface to Support Post-Stroke Motor Rehabilitation of the Upper Limb. Proceedings of the Annual International Conference of the IEEE Engineering in Medicine and Biology Society, EMBS, 2012, 4112–15.

[3] Pichiorri F, Morone G, Petti M, Toppi J, Pisotta I, Molinari M et al. Brain-computer interface boosts motor imagery practice during stroke recovery. Annals of Neurology 2015; 77 (5): 851–65.

[4] Wolpaw J and Wolpaw EW. Brain-Computer Interfaces: Principles and Practice. Oxford, 2012.

[5] Bashashati A, Fatourechi M, Ward RK, Birch GE. A survey of signal processing algorithms in brain-computer interfaces based on electrical brain signals. Journal of Neural Engineering 2007; 4(2): R32-R57.

[6] McFarland DJ, McCane LM, David SV and Wolpaw JR. Spatial Filter Selection for EEG-Based Communication. Electroencephalography and Clinical Neurophysiology 1997; 103 (3): 386–94.

[7] McFarland DJ. The advantages of the surface Laplacian in brain-computer interface research. International Journal of Psychophysiology 2015; 97: 271-276.

[8] Schalk G, McFarland DJ, Hinterberger T, Birbaumer N and Wolpaw JR. BCI2000: A General-Purpose Brain-Computer Interface (BCI) System. IEEE Transactions on Biomedical Engineering 2004; 51 (6): 1034–43.

Published by Verlag der TU Graz
Graz University of Technology

Proceedings of the
7th Graz Brain-Computer Interface Conference 2017 DOI: 10.3217/978-3-85125-533-1-19

GUIDER: A GUI FOR SEMIAUTOMATIC, PHYSIOLOGICALLY DRIVEN EEG FEATURE SELECTION FOR A REHABILITATION BCI

E. Colamarino[1,2], F. Pichiorri[2], F. Schettini[2], M. Martinoia[1], D. Mattia[2], F. Cincotti[1,2]

[1] Department of Computer, Control, and Management Engineering Antonio Ruberti, Sapienza University of Rome, Rome, Italy

[2] Neuroelectrical Imaging and BCI Lab, Fondazione Santa Lucia IRCCS, Rome, Italy

E-mail: emma.colamarino@uniroma1.it

ABSTRACT: GUIDER is a graphical user interface developed in MATLAB software environment to identify electroencephalography (EEG)-based brain computer interface (BCI) control features for a rehabilitation application (i.e. post-stroke motor imagery training). In this context, GUIDER aims to combine physiological and machine learning approaches. Indeed, GUIDER allows therapists to set parameters and constraints according to the rehabilitation principles (e.g. affected hemisphere, sensorimotor relevant frequencies) and foresees an automatic method to select the features among the defined subset. As a proof of concept, we compared offline performances between manual, just based on operator's expertise and experience, and GUIDER semiautomatic features selection on BCI data collected from stroke patients during BCI-supported motor imagery training. Preliminary results suggest that this semiautomatic approach could be successfully applied to support the human selection reducing operator dependent variability in view of future multi-centric clinical trials.

INTRODUCTION

Brain-computer interfaces (BCIs) collect the neurophysiological correlates of the brain activity (e.g. the electroencephalogram, EEG) and process them with the aim of controlling external devices, bypassing the neuromuscular system, or providing the user with a feedback of specific processes occurring in the brain [1]. A growing application field of this technology regards rehabilitation and more specifically the improvement of motor recovery in stroke patients [2]. In this context EEG-based BCIs monitor the modulation of brain activity induced by e.g. the imagination of movement. In fact, motor imagery (MI) practice elicits event-related desynchronization that occurs within EEG frequency bands (alpha and beta) and primarily over the scalp in sensorimotor cortical regions contralateral to the imagined part of the body. The introduction of BCI technology in assisting MI practice has been demonstrated to uncover the rehabilitative potential of MI, contributing to significantly better motor functional outcomes [3]. In order to reinforce a specific pattern, related to correct MI, appropriate choosing of BCI control parameters (EEG features) is needed. In [3], BCI features, channels and frequencies, were identified according to a "manual" procedure (following EEG data analysis from the screening session). Namely, neurologists and/or therapists identify the features taking into account neurophysiological evidence and rehabilitation principles and basing on the visualization of matrices obtained from the statistical comparison between two conditions (task and rest). This procedure is highly dependent on the operator and is not suitable for the majority of therapists because it requires experience for visualizing patterns of desynchronization in that form.

With the aim to reduce the variability of this procedure in view of a wider employ of the BCI-based rehabilitation in stroke (e.g. for a multi-centric clinical trial), this study proposes the application of an algorithm to automatically choose EEG features.

As reported in [4], the genetic algorithm, the principal component analysis, the distinctive sensitive learning vector quantization and the sequential floating forward selection are the most common features selection methods used in BCI studies, especially the last one in sensorimotor rhythms-based BCI. In the same context, McFarland [5] proposed a stepwise multiple regression procedure to periodically update the features used to control cursor movement across training sessions. According to the stepwise algorithm, the feature that most reduces the residual variance (i.e., the variance not accounted for by target location) and does so with p-value less than 0.01 is added to the model. Additional features are then added in the same way. After each new addition, a backward stepwise regression removes any variables for which p-value is greater than 0.01. This process continues until no further features satisfy the addition/removal criteria.

As previously mentioned, the identification of "appropriate" control features, consistent with rehabilitation principles in terms of frequencies and areas, is a milestone in rehabilitation protocols supported by BCI technology. For this reason, this study proposes the application of the method in [5], as automatic method, suggesting an essential improvement for the rehabilitative field: the inclusion of the operator, neurologist and/or therapist and his neurophysiological

Published by Verlag der TU Graz
Graz University of Technology

 DOI: 10.3217/978-3-85125-533-1-19

knowledge, in the features selection procedure. With this in mind and in view of a wider employ of the BCI-based rehabilitation in stroke, a user-friendly graphical interface was developed to guide the operator in the feature selection procedure and give him the possibility to define some constraints in which the automatic method has to run. In the overview [6] of publicly available software platforms for BCIs, the presented tool might match needs of rehabilitation BCI researchers orientated to a translational approach, from machine learning to physiology and vice-versa.

METHODS

Description and operating procedure: GUIDER is a graphical user interface (GUI) for semiautomatic and physiologically driven EEG features selection. It was designed and developed in MATLAB R2015a (The MathWorks, Inc., Natick, Massachusetts, USA) and runs until MATLAB R2011a. GUIDER allows users to interact with BCI data through a graphic interface without needing to use MATLAB syntax. Calling GUIDER in the MATLAB command window launches the first screen (Fig. 1) of the tool.

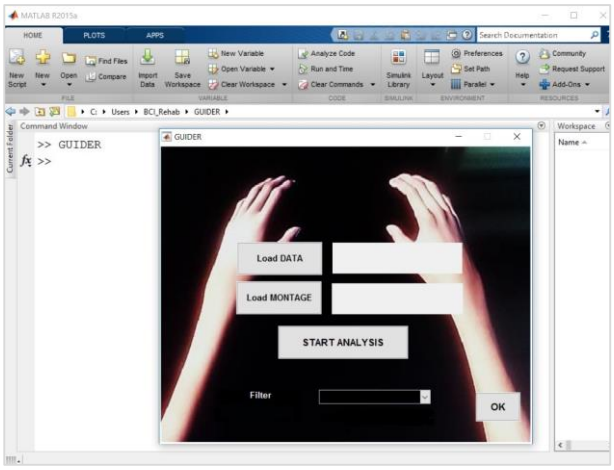

Figure 1: MATLAB main window and typical screen shot of GUIDER (right side).

The buttons “Load DATA” and “Load MONTAGE” allow importing BCI data (GUIDER supports several file formats) and montage files, respectively. More than one data file could be processed: files are concatenated.
The “START ANALYSIS” button launches the following modules,
(a) data conditioning module which applies spatial and frequency filtering,
(b) feature extraction module which employs methods to estimate the signal spectrum,
(c) statistical analysis module in which comparison tests of two conditions, i.e., two tasks, task vs rest, are implemented,
(d) visualization module that gives output a matrix, channels and bins, where the statistical comparison index value of any feature is shown in a colour tint. A colour bar shows the colour range.

At the end of these analyses, the user visualizes pattern of desynchronization in the form of statistical index matrices, each one obtained using a different spatial filtering [7], e.g., common average reference (CAR), bipolar filters, surface Laplacian filters (other filtering options can be implemented). The pop-up menu in the bottom part of GUIDER main window allows the choice of filtering option (how many and which filters). At this point, the operator is required to define topographical and spectral constraints taking into account neurophysiological evidence and rehabilitation principles. This step may be guided by GUIDER or manual (Fig. 2). According to the first modality, the operator checks which hemisphere and channels to include in the analysis. In the manual modality, instead, operator selects rectangular areas in the statistical matrix after inserting the number of areas of interest in the edit-text box in GUIDER. The “OK” button closes all figures and opens the figures of statistical matrices, according to the number and the type of filtering earlier chosen, allowing the user to select rectangular areas accordingly (Fig. 3).
The values of features belonging to the areas selected manually or by the guided modality, are the inputs for the features selection algorithm: the stepwise regression (SW). This algorithm identifies an optimal subset of predictor variables (i.e. the features) and assigns weights to them in order to build an effective regression model to evaluate the relationship between the predictors and the dependent variable (here equivalent to subject’s intention). During each iteration, the algorithm adds or removes a feature from the classification model in order to obtain a combination of features ensuring a good classification performance. GUIDER implements it using the MATLAB ® function stepwisefit.m.
The optimal features and their weights are saved both as text file and external parameter file.

Proof-of-Concept: EEG dataset from three patients (subacute stroke patients with right-sided lesions, involved in previous studies at IRCCS Fondazione Santa Lucia, [3] for an extended description) were used to compare semiautomatic and manual procedure in terms of both features selection (channels and frequencies) and classification performance. Screening session’s data of each patient were analysed to identify the control features. Patients were instructed by the therapist to perform the movement (grasping and finger extension) imagination of their affected hand. During the initial screening session EEG signals were collected from 61 electrodes according to an extension of the 10–20 International System with 200 Hz as sampling frequency; scalp signals were referenced to the linked-ear signal. Each run consisted of 15 trials related to motor imagery task (grasping and finger extension) and 15 trials of baseline rest (9s each). Trials were randomly presented within a run. For each trial, we analysed the 4 epochs corresponding to the 4 seconds during which the patients performed the MI task. In the screening session, the subjects were not provided with any feedback of their brain activity.

Published by Verlag der TU Graz
Graz University of Technology

 DOI: 10.3217/978-3-85125-533-1-19

To compare the procedures, the number of features automatically identified (in the constraints imposed by operator using GUIDER) is coherent with the number of features manually selected just by observing the statistical index matrix. These two control features drive the visual feedback to therapist and patient during the training sessions. In the training session the patients sat in a chair/wheelchair and their hands were covered by a white sheet on which a dedicated software projected a realistic visual representation of the patient's hands. The therapist instructed the patients to imagine the movement (grasping and finger extension) of the affected hand and they received a feedback when the trial was successful. The feedback consisted in the replication of the imagined movement by the virtual hand.

Data Analysis: The spectral analysis was performed on EEG data epochs (1s long) corresponding to MI task. The Maximum Entropy Method (16th order model) was employed to estimate amplitude spectrum with a resolution of 2 Hz and considering not overlapped epochs. All possible features in a reasonable range (i.e., 0-36 Hz in 2 Hz bins) were extracted and analysed. A feature vector, spectral amplitude at each bin for each channel, was extracted from each epoch. For each feature a contrast was performed to assess statistically significant modulation induced on a specific feature. To this aim, the coefficient of determination R-square, i.e., the proportion of the total variance on the feature samples accounted for by target position, was computed for each feature (dependent variable).

Validation: In order to compare the classification performance achieved with both human and semiautomatic selection, Area Under Curve (AUC) of Receiver Operating Characteristic (ROC) curve was assessed in auto-validation and cross-validation condition: screening data (previously exploited to obtain the control features and weights) and training data were used as testing dataset, respectively. Separately, outputs of the stepwise regression and the weights assigned by neurologists and/or therapists (conventionally, each one of -0.5) were the input of a linear classifier for the computation of the score used to calculate AUC values.

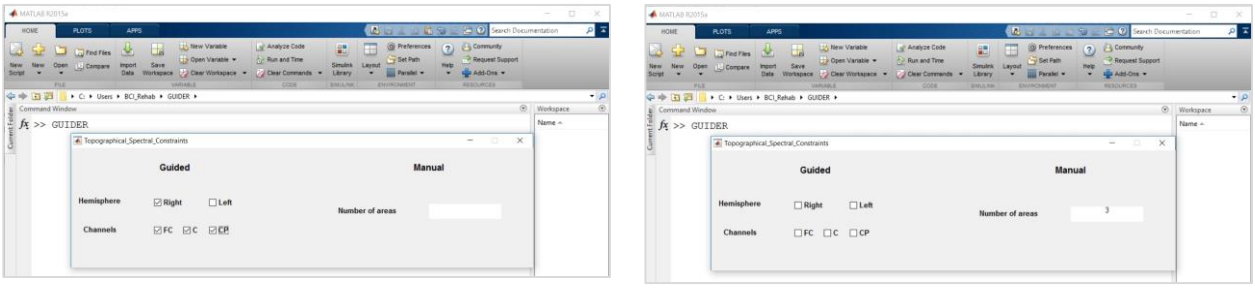

Figure 2: Screen shot of the window for the definition of topographical and spectral constraints. In the left side, guided procedure: the operator just checks the hemisphere and channels (in the sensorimotor area) to include in the analysis. In the right side, manual procedure: the operator just writes in the box the number of rectangular areas he would to select in the statistical matrix that it will following open.

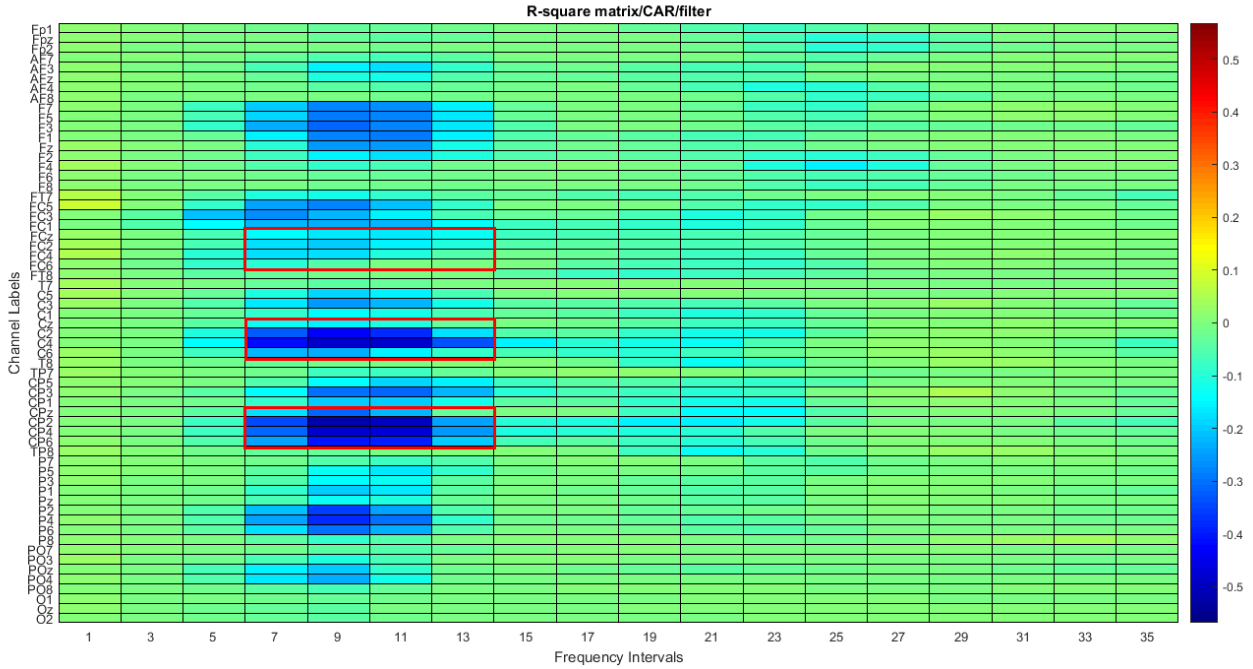

Figure 3: R-square matrix (channels and frequency intervals) obtained from EEG data analysis collected during the screening session and filtered using the filter chosen in GUIDER pop-up menu (e.g. CAR). The red rectangular areas (e.g. three areas as those written in Figure 2 right panel) are those selected by the operator (according neurophysiological evidence and rehabilitation principles) for the features selection using the GUIDER manual procedure.

Published by Verlag der TU Graz
Graz University of Technology

 DOI: 10.3217/978-3-85125-533-1-19

RESULTS

Figure 4 shows the graphic output of the GUIDER operating procedure until topographical and spectral constraints definition. It displays for Subject 1 (S01) the R-square values of all features (61 channels and 18 frequency bins) after the filtering selection (in this case, CAR). The relevant control features selected, just based on R-square matrix visualization, by an expert neurophysiologist are reported in Table 1 for all three patients. The same operator, using the areas selection procedure in GUIDER, selected some rectangular areas: three for S01, from FCz to FC6, from Cz to C6, from CPz to CP6, all ranged from the forth and to the seventh bin in the R-square matrix. Two optimal, coherent with the number of features selected just based on R-square matrix visualization, features identified by the stepwise algorithm in those areas are in Table 1.
The classification performance (AUC) in both auto-validation and cross-validation condition using the features identified in manual and semiautomatic (GUIDER) procedure are summarized in Table 2.

Table 1: Control features identified during BCI tasks at the screening session (for three subjects with right-sided lesions) by an expert neurophysiologist (manual procedure) and by the semiautomatic procedure implemented by GUIDER. For each feature EEG channel and frequency are reported (for each procedure) in the left and right columns, respectively.

Subject	Control feature	Manual procedure		GUIDER procedure	
S01	1	CP4	9 Hz	CP2	9 Hz
	2	C4	9 Hz	C4	11 Hz
S02	1	C2	21 Hz	C2	21 Hz
	2	CP2	23 Hz	Cz	25 Hz
S03	1	C4	19 Hz	C4	19 Hz
	2	CP4	19 Hz	CPz	21 Hz

Table 2: AUC values computed in auto-validation condition (namely, on data previously exploited to obtain the control features and weights) and in cross-validation condition (data from a rehabilitation training session used as testing dataset) for manual and semiautomatic procedure.

Subject	Validation (V)	Manual procedure	GUIDER procedure
S01	Auto-V	0.91	0.94
	Cross-V	0.88	0.88
S02	Auto-V	0.76	0.79
	Cross-V	0.74	0.74
S03	Auto-V	0.75	0.82
	Cross-V	0.70	0.65

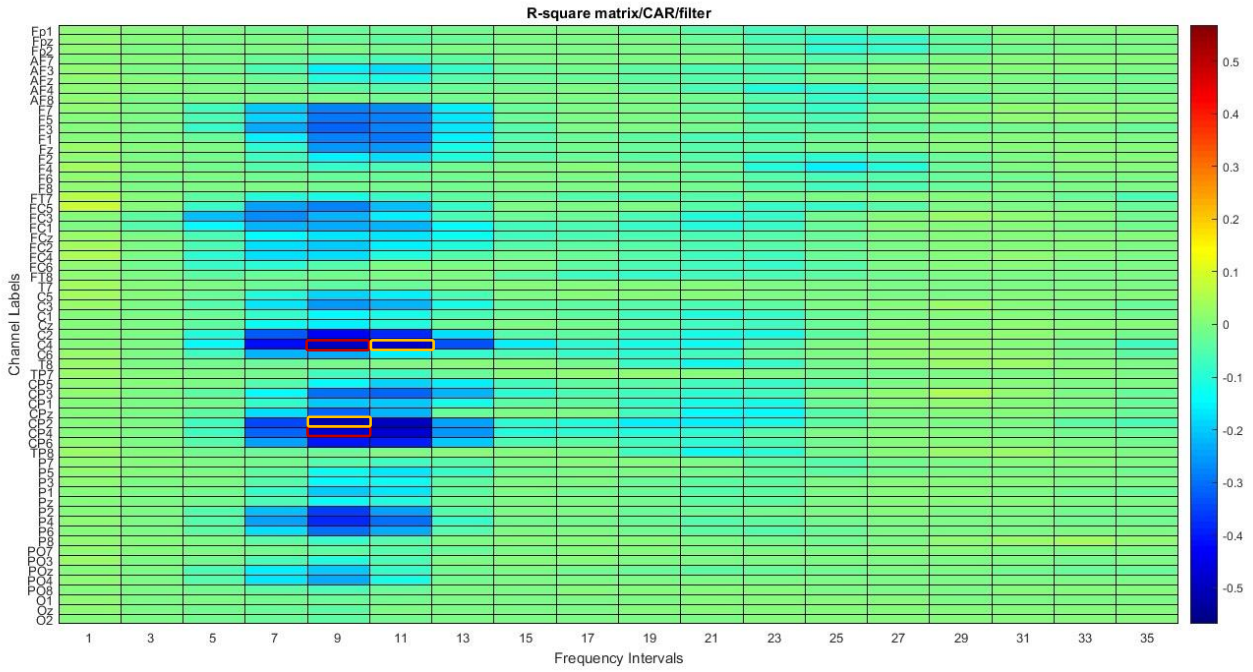

Figure 4: R-square matrix (channels and frequency intervals) obtained from EEG data analysis collected during the screening session from a subacute stroke patient with right-sided lesions (S01). The red (channels CP4 and C4 at 9 Hz) and yellow rectangles (channels CP2 and C4 at 9 Hz and 11 Hz, respectively) are features selected (for the rehabilitation training phase) by an expert neurologist and by GUIDER, respectively.

Published by Verlag der TU Graz
Graz University of Technology

 DOI: 10.3217/978-3-85125-533-1-19

DISCUSSION

Identifying the optimal control features is a milestone in rehabilitation protocols supported by BCI technology. In contrast to other fields of application where optimal cursor control is pursued, in a rehabilitation context the aim is also to reinforce the appropriate sensorimotor activation in terms of both topographic and spectral characteristics. Therefore, the feature selection procedure requires knowledge coming of neurophysiology and rehabilitation principles as well as expertise in visualizing pattern of desynchronization in the form of statistical index matrices. The manual procedure is highly dependent on the operator and is currently restricted to researchers with experience in the BCI field. Therefore, the aim of GUIDER is twofold: first, to reduce the intra- and inter- operator variability of feature selection supporting the procedure with a semiautomatic method but without giving up to neurophysiological principles that characterize the rehabilitation; second, to facilitate this procedure for therapists without experience with BCIs.

GUIDER could be a (user-friendly) tool to support even non-expert operators in the reproducible identification of control features, since it considers both neurophysiological and machine learning approaches.

However, in view of a wider employ of GUIDER, several limitations must be addressed in the near future. First, although involved operators anecdotally considered GUIDER a user-friendly tool, the needs of the target group in terms of usability haven't been evaluated yet according to the user centered design approach. Second, the implementation in MATLAB environment, which is subjected to licensing issue, will be considered and overtaken as a next step.

The preliminary results suggest that the features identified by GUIDER are close to those chosen by experienced operators (manual procedure): e.g., CP4 vs CP2 at the same frequency and the same channel (C4) at neighboring bins (9 Hz and 11 Hz) for Subject 01. Furthermore, both procedure's outputs are congruent with the physiological evidences. Also in terms of classification performance, the procedures give indices (values of AUC) comparable in cross-validation condition and higher in the GUIDER application that in manual procedure in auto-validation. Hence, the choices of neurologists could be reproducible by a semiautomatic method that includes the operator and his neurophysiological knowledge in the procedure.

CONCLUSION

The introduction of GUIDER and its application in a BCI rehabilitation context suggest that it is feasible to support the operators during the procedure of features selection with a user-friendly tool. GUIDER employs a semiautomatic method and takes into account neurophysiological evidence and rehabilitation principles. Performances are as good as manual selection, and GUIDER allows reproducibility of the procedure. The latter is a prerequisite for planning large multi-centric clinical trials, including a larger number of patients with several different operators, ensuring the comparability of BCI results among centers and thus increasing the generalizability of the results.

ACKNOWLEDGEMENTS

This work was funded in part by the Sapienza University of Rome - Progetti di Ateneo 2015 (C26A15N8LZ).

REFERENCES

[1] Wolpaw J and Wolpaw EW. Brain-Computer Interfaces: Principles and Practice. Oxford, 2012.

[2] Cincotti F, Pichiorri F, Arico P, Aloise F, Leotta F, de Vico Fallani F et al. EEG-Based Brain-Computer Interface to Support Post-Stroke Motor Rehabilitation of the Upper Limb. Proceedings of the Annual International Conference of the IEEE Engineering in Medicine and Biology Society, EMBS, 2012, 4112–15.

[3] Pichiorri F, Morone G, Petti M, Toppi J, Pisotta I, Molinari M et al. Brain-computer interface boosts motor imagery practice during stroke recovery. Annals of Neurology 2015; 77 (5): 851–65.

[4] Bashashati A, Fatourechi M, Ward RK, Birch GE. A survey of signal processing algorithms in brain-computer interfaces based on electrical brain signals. Journal of Neural Engineering 2007; 4(2): R32-R57.

[5] McFarland DJ, Sarnacki WA, Wolpaw JR. Electroencephalographic (EEG) control of three-dimensional movement. Journal of Neural Engineering 2010; 7(3).

[6] Brunner C, Andreoni G, Bianchi L, Blankertz C, Breitwieser S, Kanoh S et al. BCI Software Platforms. In: Towards practical Brain-Computer Interfaces. Springer, 2013.

[7] McFarland DJ, McCane LM, David SV and Wolpaw JR. Spatial Filter Selection for EEG-Based Communication. Electroencephalography and Clinical Neurophysiology 1997; 103 (3): 386–94.

Published by Verlag der TU Graz
Graz University of Technology

Proceedings of the
7th Graz Brain-Computer Interface Conference 2017 DOI: 10.3217/978-3-85125-533-1-20

TIME TO RELAX: NO EFFECTS TO THE STRESS RESPONSE AFTER SHORT-TERM USE OF A BRAIN-COMPUTER INTERFACE

A.W. Cole[1], B.E. Riecke[1], A.N. Antle[1]
[1] Interactive Arts and Technology, Simon Fraser University, Vancouver, Canada

E-mail: miac@sfu.ca

ABSTRACT: Chronic stress is a significant contributor to emotional distress and a myriad of health issues. Some coping mechanisms for stress and anxiety often have significant barriers preventing people from seeking a remedy. A new home-based treatment method using a brain-computer interface provides people with visual feedback of their affective state. This study compared EEG and Sham Neurofeedback to find if short-term use of a brain-computer interface had any effect on stress. We found EEG Neurofeedback, in the short-term, does not significantly reduce an individual's physiological or psychological stress response to an event-based stressor. One explanation is the participant's self-reported feelings of control of the on-screen object showed no significant differences between groups, which may potentially highlight a design issue in neurofeedback games. Next steps will be to reconfigure the immediate feedback loop to enhance the responsiveness of the application to better match the reported relaxation score from the headset.

INTRODUCTION

Chronic exposure to stress has significant psychological and physiological effects on human beings. Long-term exposure to stress impairs people's cognitive abilities for simple tasks like memorizing a list of words [1], inhibits academic performance in undergraduate students [2], increases the likelihood to engage in procrastination behaviours [3], and can even effect a person's overall health [4]. While stress falls on continuum between positive and negative, the primary focus of this study is the human response to an event that creates a negative or distress response in the brain [5]. Negative stressors are generally unpleasant events and can exceed an individual's coping abilities, resulting in anxiety. For most people, stress is a temporary state that can be easily overcome, but regular exposure to lower-level stress events over time increases the risk of mental and physical health issues [6], largely because the stress response doesn't dissipate immediately following the stressful event. The stressful response can persist in the body and the mind long after the event is over [7], especially if there is no recovery period between events [8]. Without proper intervention, many people experiencing repeated short-term stress events may be subjected to the ill effects of chronic stress and significantly limit their career opportunities due to the typical avoidance strategies enacted by people who suffer from anxiety [9].

Stress and Coping Mechanisms: When faced with a stressful event that exceeds a person's coping ability, some people attend in-person therapy sessions to reduce anxiety [5], [9], [10]. In-person therapy is designed to increase an individual's ability to self-regulate or control their response to stressful emotions [5], [9], [11]. These studies are based on self-reported claims and exclude physiological health markers, thus can only make claims regarding the individual's perception of health versus triangulating the data with physiological health markers, making it difficult to ascertain long-term health benefits. The therapies used in these studies require the active presence of a therapist, which reduces the immediacy of the response and requires active scheduling on behalf of the client. The therapies also don't address new technologies and behaviours that engage individuals, like video games [12]. The negative effects of stress motivate research into developing effective coping strategies through interdisciplinary inquiry. Revised coping mechanisms can borrow from neuroscience, psychology, and technology to establish more immediate mechanisms for reducing the response to predictable stress events (e.g., a public speech, an exam, etc.), incorporate a continuous biometric measure to determine whether or not the treatment is working and implement the motivational elements of game play. If a method can be found to mitigate the effects of predictable stress events and people are motivated to prepare in advance of a difficult conversation, an exam, or a public speech could mean a shift in the approach to therapeutic practices.

Brain-Computer Interfaces: Brain-computer interfaces may be a potential solution to reducing a person's response to stress in the short-term. Several studies have already determined certain brainwaves (EEG) are an effective measure of stress [13], and today, consumer grade EEG devices are becoming increasingly popular. But consumer grade EEG devices in the health and psychology domain is not yet validated and still needs exploration [14].

Amongst today's growing number of brain-computer interfaces, we reviewed two systems that currently address stress and anxiety in a scholarly way: Mindlight and Brainball. Both Mindlight and Brainball use an EEG headset as the main input device to an application. Mindlight is a PC-based game that uses an individual's attentional (beta waves) and relaxation (alpha waves) EEG scores as a means to interact with elements in a game-like environment (e.g., increased attention will turn on a light) [15]. Brainball is a real-world game that

Published by Verlag der TU Graz
Graz University of Technology

 DOI: 10.3217/978-3-85125-533-1-20

dynamically moves a physical ball across a table based on the user's neural activity [16]. Mindlight and Brainball depend on a single game to address multiple concerns (attention and stress) and are dependent on a PC-based windows platform or physical objects respectively, limiting its deployment potential. The Mind-full application, on the other hand, is an Android-based system with three 2D games that address different concerns: (1)a warm-up game using a pinwheel, (2) a meditation game using a paraglider visual, and (3) an attention game using stones with an inuksuk visual (i.e., digital representation of a human-made stone landmark). Each game animates an on-screen object (pinwheel, paraglider, or stone) based on the EEG scores of the user and changes the action of the on-screen object based on whether the individual's EEG scores are above or below a predefined threshold of 40. The visualization of neurofeedback in Mind-Full is intended for users to (a) better understand their current affective state by relating the position of the on-screen object to their relaxation levels and (b) over time, learn to self-regulate their stress-related emotions. The hope is with continued use of the device people will develop the ability to self-induce a state of relaxation without the support of any devices. To date both Mindlight and Mind-Full have demonstrated a reduction in anxiety with consistent long-term use [15], [17] but in neither case has a study been completed regarding the effects of short-term use. Brainball did demonstrate a reduction in stress in the short-term, but used a galvanic skin response to measure stress instead of the EEG device and had a limited number of participants [16]. No literature has been found that approaches any type of therapeutic practice from a short-term perspective, which is likely due to the embedded concepts established in psychology regarding habit development and reinforced learning [18]. By incorporating new elements into the therapeutic approach to stress reduction, like gameplay and neurofeedback, researchers have an opportunity to explore all potential uses of EEG Neurofeedback as a therapeutic tool.

The goal of this study was to further explore the potential uses for consumer grade EEG devices and the practical applications for positively altering a person's response to stress in the short-term. Should short-term use of an EEG neurofeedback device reduce the response to stress means that people can use the device in preparation for known event-based stressors (e.g., public speaking event). This study compared EEG neurofeedback with sham neurofeedback to understand if short-term use of a brain-computer interface can reduce the physiological or psychological stress response to an event-based stressor.

Hypotheses: Participants actively controlling an on-screen object using an EEG-based game, Mind-full, will:

H1: have a higher average of relaxation scores during a stressful event as compared to participants who receive sham neurofeedback in the video condition.

H2: self-report increased feelings of relaxation after a stressful event as compared to participants who receive sham neurofeedback in the video condition.

H3: self-report greater feelings of control regarding the on-screen object as compared to participants who receive sham neurofeedback in the video condition.

MATERIALS AND METHODS

Participants: 24 students volunteered for this study, but 1 participant's data was excluded from the analysis due to incomplete data. As such all associated data from the participant is removed. Participants (N = 23) were female (n = 15) and male (n = 8) undergraduate (n = 21) and graduate students (n = 2) from Simon Fraser University between the ages of 18 and 25 (M = 22.1). Participants were recruited via the University research participant system, SONA, as well as through individual undergraduate classes. Each participant was randomly allocated to one of two groups: the video group (n = 9) and the EEG neurofeedback group (n = 14). Each participant was given a choice of compensation in the form of a $15 gift card or course credit. The university's ethics board approved the study and each participant, prior to the start of the experiment, signed an online informed consent form.

Procedure: Participants were randomly allocated to either the EEG Neurofeedback or Video condition with sham neurofeedback, a video recording of someone else playing the Mind-full game. Each participant wore an EEG headset (Neurosky Mindwave Mobile) paired via Bluetooth to a Samsung Galaxy tablet running the Mind-full application throughout the entire session. The EEG headset consists of two pieces: an ear clip to ground the signal and a dry EEG sensor positioned at Fp1; above the left eyebrow on the forehead [19]. The EEG sensor outputs 12 bit raw brainwaves (3 – 100 Hz) with a sampling rate of 512 Hz and EEG power spectrums (gamma, delta, alpha, beta, and theta) every second. This study used Neurosky's proprietary eSense meter, meditation (relaxation is used to differentiate between the event and the EEG data score), which combines raw data from different brainwaves (emphasizes alpha) and converts it into a single

Figure 1 - Participant using the EEG Headset with Mind-Full's Meditation (relaxation) application.

Published by Verlag der TU Graz
Graz University of Technology

 DOI: 10.3217/978-3-85125-533-1-20

relaxation score, which updates the tablet every second. A minor delay between the headset and the tablet is estimated to be approximately 16.7 ms. Participants were seated in a chair in a standard-sized office with the tablet mounted on a black frame about 30 cm away from the participant for optimal hands-free viewing (Figure 1). Each participant was asked to focus on two separate games in the experiment: (1) a Baseline practice event, in which participants were asked to relax while watching imagery of a rotating pinwheel and (2) a Meditation event, in which participants were asked to relax while watching imagery of a paraglider gently landing on the earth's surface (Fig 2). Each participant was given access to an internet-enabled MacBook Pro laptop for online surveys as well as a black pen and paper surveys throughout the course of the experiment.

Figure 2 - Mind-full Paraglider App

Figure 1 - Image of the two 2 x 3 independent measures design

A 2 (EEG Neurofeedback, Video) x 3 (Baseline, Meditation, Stress) independent measures experimental design was conducted (Fig 3). An independent measures design was selected due to the potential for a learning effect between conditions. The EEG Neurofeedback condition presented the participant with actual visual feedback of their neural activity, essentially connecting the animation of the on-screen object with their neural activity. The video condition was a representation of neurofeedback and presented the participant with an exact replica of the EEG Neurofeedback games withholding only the ability to control the object on-screen based on the neural activity of the user; instead the participant watched a pre-recorded video of the game, referred to as 'sham' neurofeedback. All participants were exposed to three events: (1) a 3-minute Baseline event that level set the data based on personal differences in neural activity, (2) a 10-minute Meditation event that captured the participant's neural activity in a meditative state, and (3) a 3 to 5 minute Stress event containing a math test. The math test was selected as a stressful event based on assessments of math anxiety and findings from a previous EEG study [20]–[22]. Self-report data was collected in-between each of the events, creating a second 2 (EEG Neurofeedback, Video) x 3 (Baseline, Meditation, Stress) independent measures experimental design. At the end of the session, each participant was asked to rate how much control they felt over the on-screen object.

Measures: The dependent variables are (1) continuous EEG data and (2) validated Stress-Trait Anxiety Inventory (STAI-6) to measure each participant's response to the three pre-determined events. EEG data is based on Neurosky's eSense meter parameters[1] and measured on a scale of 0 to 100, with scores between 0 and 40 classified as a non-relaxed state and scores between 41 and 100 as a neutral or relaxed state. The STAI-6 scales are on a scale of 0 to 4, with 0 being relaxed, and 4 being stressed. The STAI-6 has been documented as being both reliable and valid measure of stress [23]. Participants spent about the same amount of time in each activity in the EEG neurofeedback (M = 14:54) and video condition (M = 13:23). One self-reported question regarding the participant's feeling of control was asked at the end of the study in which participants were asked to estimate how much control they felt they had of the on-screen object from 0% to 100%.

RESULTS

This study aimed to discover if people have a reduced response to a stress event after they've actively controlled an on-screen object via a brain-computer interface for 10-minutes. Using two 2 X 3 independent measures ANOVA measuring both continuous EEG data (results per second) as well as self-report scales, this study found no significant differences between those who were actively controlling the object on screen in the EEG neurofeedback condition and those who were watching a video containing sham neurofeedback.

H1: Participants actively controlling an on-screen object using an EEG-based game, Mind-full, will have a higher average of relaxation scores during a stressful event as compared to as compared to participants who receive sham neurofeedback in the video condition.

We hypothesized participants receiving EEG neurofeedback would show higher relaxation scores after being exposed to a stress event. Shapiro-Wilks test indicate non-normal distribution (ps < .01), however since a factorial ANOVA was run, it will compensate for the non-normal distribution. The Levene's Test for unequal variances was not violated (*ps* > .32), but Mauchly's test indicated the assumption of sphericity had been violated $\chi^2(2) = 13.64$, $p = .01$, therefore a Greenhouse-Geisser correction was applied for within

[1] http://developer.neurosky.com/docs/doku.php?id=esenses_tm

Published by Verlag der TU Graz
Graz University of Technology

 DOI: 10.3217/978-3-85125-533-1-20

subject data. A 2 x 3 ANOVA showed a significant difference between the event types $F(1.33) = 5.33$, $p = .02$, η_p^2, = .20. The large effect size of .20 indicates a large difference in the magnitude or size between the events. Post-hoc analysis consisted of pairwise comparisons and found differences between the stress event ($M = 48.61$, $SD = 2.07$) and the main Meditation event ($M = 55.75$, $SD = 1.32$), $p = .002$, as well as between the Stress event and the Baseline event ($M = 56.36$, $SD = 1.20$), $p = .031$ (see Fig 4 for between group means). There was not a significant main effect between the EEG Neurofeedback ($M = 54.36$, $SD = 1.59$) and Video Condition ($M = 53.07$, $SD = 1.27$), $F(1) = .41$, $p = .53$, η_p^2, = .02. There was no significant interaction effect between Event type and Condition, $F(1.33) = 2.01$, $p = .16$, η_p^2, = .09, indicating no differences between the EEG neurofeedback and Video conditions between events. Thus, the first hypothesis is not supported. While both groups showed decreased relaxation scores during the stress event as compared to the Meditation or Baseline event, there were no significant differences between the EEG neurofeedback and Video conditions.

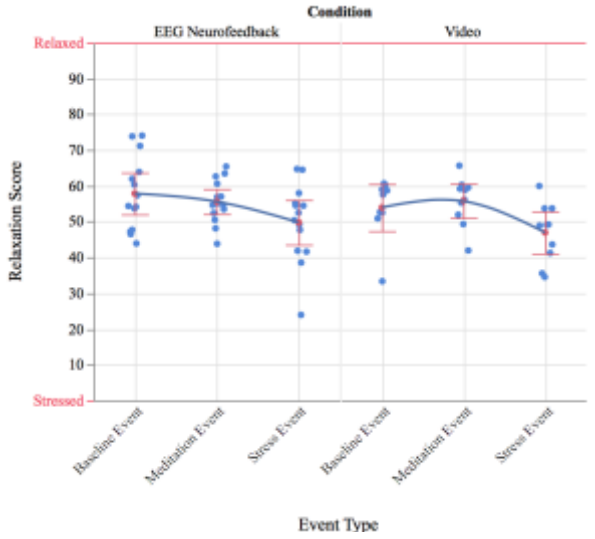

Figure 4 - Mean of EEG data by type of event, separated by video and EEG neurofeedback conditions (95% CI). The blue dots represent the mean score of individual participants.

H2: People actively controlling an on-screen object though an EEG neurofeedback device will self-report increased feelings of relaxation after a stressful event as compared to participants as compared to participants who receive sham neurofeedback in the video condition.

We hypothesized participants receiving EEG neurofeedback would self-report feeling more relaxed as compared to participants receiving sham neurofeedback. Shapiro-Wilks test indicates a normal distribution for all instances ($ps > .25$) except in the 3rd STAI-6 survey in the control group ($p = .02$). Levene's test did not suggest unequal variances for the STAI-6 ($p > .10$) and Mauchly's test indicated no violation in sphericity $\chi^2(2) = 2.13$, $p = .345$. The validated stress scale, STAI-6 ($\alpha = .88$), was considered reliable. A 2x3 ANOVA showed no main effect of conditions on STAI-6, as there were no significant differences between the EEG Neurofeedback ($M = 1.83$, $SD = .16$) and Video conditions ($M = 1.72$, $SD = 13$), $F(1) = .32$, $p = .58$, $\eta_p^2 = .02$. There were no significant differences in the STAI-6 self-report surveys between the 1st survey baseline ($M = 1.77$, $SD = .56$), 2nd survey pre-test ($M = 1.71$, $SD = .51$) and 3rd survey post-test ($M = 1.85$, $SD = .52$), $F(2) = .44$, $p = .65$, $\eta_p^2 = .02$ (see Fig 5 for between group means). There were no significant differences in the interaction between the event and the type of group, $F(2) = 1.61$, $p = .21$, η_p^2, = .07. Thus, the second hypothesis is not supported. There were no significant differences found between the self-reported surveys.

H3: People actively controlling an on-screen object using an EEG-based game, Mind-full, will report greater feelings of control regarding the on-screen object as compared to participants as who receive sham neurofeedback in the video condition.

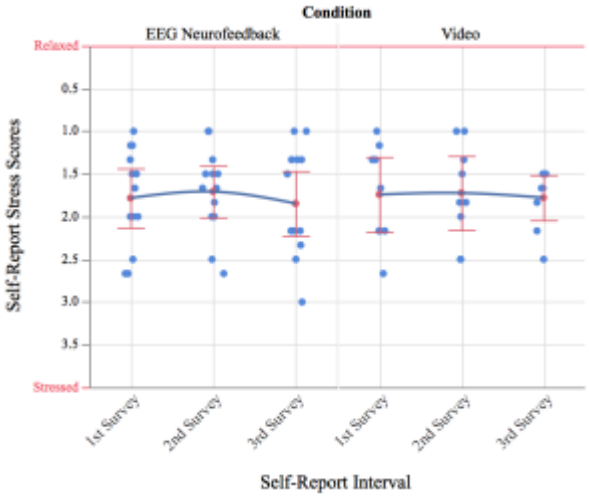

Figure 5 - Mean of Self-Report Surveys by type of event, separated by video and EEG neurofeedback conditions (95% CI). The blue dots represent the mean score of individual participants.

We hypothesized participants receiving EEG neurofeedback would indicate a greater feeling control of the on-screen object. Four participant's data was excluded due to missing data, leaving 12 participants in the EEG Neurofeedback and 7 participants in the video condition. Shapiro-Wilks test revealed a normal distribution ($ps > .25$) and Levene's test for unequal variances was not violated ($p = .83$). A pooled t-test was run and found no significant differences between the EEG neurofeedback ($M = 44.2$, $SD = .27$) and Video condition ($M = 47.1$, $SD = .29$), $t(17) = .22$, $p = .83$, $\eta_p^2 = .003$ (Fig 6). Thus, the third hypothesis is not supported and participants in the EEG condition did not report greater feelings of control compared to participants in the sham (video) condition.

Published by Verlag der TU Graz
Graz University of Technology

 DOI: 10.3217/978-3-85125-533-1-20

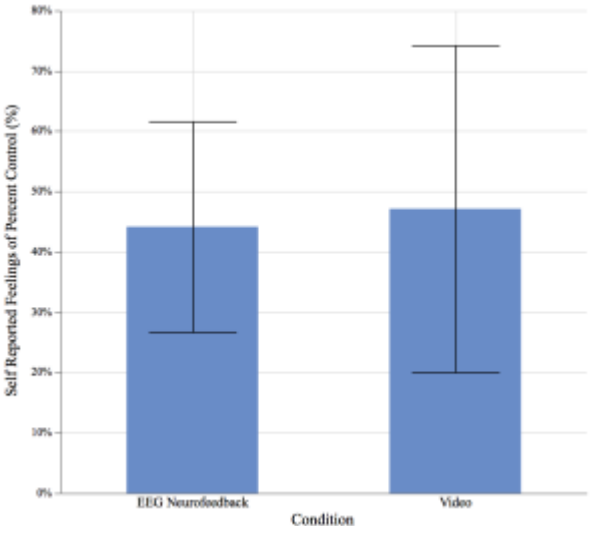

Figure 6 - Mean of self-reported feelings of control of on-screen object in percent by condition (95% CI)

DISCUSSION

This study aimed to discover if people had a reduced response to a stress event (e.g., demonstrated higher EEG relaxation scores) after they've actively controlled an on-screen object via a brain-computer interface for 10-minutes. We found no significant differences between EEG Neurofeedback and video-watching conditions in either the physiological or psychological measures to an event-based stressor.

One possible reason could be that the use of EEG Neurofeedback in the short-term (10 minutes) is insufficient time to train the brain to respond differently to a negative stimulus, as there is no literature studying the short-term effects of brain-computer interfaces on the stress response. In pre- and post- test studies, EEG neurofeedback devices appear to help people learn to self-regulate emotions after 8 weeks of use [17]. But in comparative studies in which there is both EEG neurofeedback and video (sham) neurofeedback, there are no significant differences between the sham and EEG neurofeedback conditions. For example, Mindlight reported that while there was a difference between pre- and post- tests, no differences were found between the treatment and control groups [15], which may suggest that neurofeedback games may be a support mechanism to help people remember to practice meditation skills instead of actively working to retrain the brain.

There is potential that studies using consumer grade EEG devices with Neurosky's proprietary eSense meter may not be an accurate measure of relaxation, however, the math test used in this study did report a significant difference between events, as well as in a previous study [22], indicating the eSense meter is picking up some significant changes in neural activity. It should also be noted that the Neurosky headset may register facial activity (e.g., eye blinks) [24], which may limit the findings of this study, despite Neurosky's claims that the device accommodates for facial movements in its algorithms.

The other possible explanation may be the perceived immediacy of feedback. Both the EEG Neurofeedback and Video group had approximately the same amount of time in relaxation with the only difference being that the EEG Neurofeedback group had active control of the on-screen object. We expected the Video condition with sham neurofeedback to report a lack of control of the on-screen object, and were surprised to find no significant differences between the EEG Neurofeedback and Video (sham) condition. Currently the Mind-full application reports on whether or not the user is above or below a specific threshold of 40, and does not provide immediate feedback to changes in the affective state; users experience a delay between their neural activity and the response from the on-screen object (e.g., object position). For example, the user's relaxation score has to be below 40 to send the paraglider upwards and above 40 to let the paraglider land, which means the user is not aware of the immediate changes to their affective state. Software design guidelines purport the need for users to receive immediate feedback when they perform an action, which may point to an important element that is missing from the user experience design: immediate feedback. Immediate feedback is a critical communication element between the user and the system [25], [26] that impacts an individual's feeling of control over the system. If a sense of control is a factor in neurofeedback games, improving the feedback mechanisms within the application could make short-term use a possibility. The next step will be to reconfigure the immediate feedback loop to enhance the responsiveness of the Mind-full game application to better match the reported relaxation score from the headset.

If feasible, the next study would test the effects of the design change to the system and investigate if the feeling of control is a factor in EEG Neurofeedback systems and short-term use. This study would use an concurrent parallel mixed methods independent measures design with one tablet application with improved immediate feedback (e.g., intervals of 20), one tablet application that utilizes the current parameters (0-40 and 40-100), and a control (video) condition with sham neurofeedback to test the individual feelings of control. A similar stress test would be used to measure their response to stress, followed by a brief interview to understand the participant's perspective on the feeling of control and collect any additional game feedback.

ACKNOWLEDGEMENTS

Dr. Riecke, Dr. Antle, and Emily Cramer provided feedback on the study design. Dr. Antle provided $15 gift cards for each participant. Elgin McLaren for organizing the headsets and recruiting participants

Published by Verlag der TU Graz
Graz University of Technology

 DOI: 10.3217/978-3-85125-533-1-20

REFERENCES

[1] S. Kuhlmann, "Impaired Memory Retrieval after Psychosocial Stress in Healthy Young Men," *J. Neurosci.*, vol. 25, no. 11, pp. 2977–2982, Mar. 2005.

[2] American College Health Association, "National College Health Assessment Spring 2015 Reference Group Executive Summary." 2015.

[3] L. J. Solomon and E. D. Rothblum, "Academic procrastination: Frequency and cognitive-behavioral correlates," *J. Couns. Psychol.*, vol. 31, no. 4, pp. 503–509, Oct. 1984.

[4] H. Selye, *Stress in Health and Disease*. Butterworth-Heinemann, 2013.

[5] S. E. Hobfoll, R. Schwarzer, and K. K. Chon, "Disentangling the stress labyrinth: Interpreting the meaning of the term stress as it is studied in health context," *Anxiety Stress Coping*, vol. 11, no. 3, pp. 181–212, Jul. 1998.

[6] B. A. van der Kolk, "The Compulsion to Repeat the Trauma: Re-enactment, Re-Victimization, and Masochism," *Psychiatr. Clin. North Am.*, vol. 12, no. 2, pp. 389–411, 1989.

[7] A. Baum, "Stress, intrusive imagery, and chronic distress," *Health Psychol.*, vol. 9, no. 6, pp. 653–675, 1990.

[8] R. A. Dienstbier, "Arousal and physiological toughness: Implications for mental and physical health," *Psychol. Rev.*, vol. 96, no. 1, pp. 84–100, Jan. 1989.

[9] S. Folkman, R. S. Lazarus, C. Dunkel-Schetter, A. DeLongis, and R. J. Gruen, "Dynamics of a stressful encounter: cognitive appraisal, coping, and encounter outcomes.," *J. Pers. Soc. Psychol.*, vol. 50, no. 5, p. 992, 1986.

[10] B. J. Fisak, D. Richard, and A. Mann, "The Prevention of Child and Adolescent Anxiety: A Meta-analytic Review," *Prev. Sci.*, vol. 12, no. 3, pp. 255–268, Sep. 2011.

[11] C. J. Holahan and R. H. Moos, "Personal and contextual determinants of coping strategies," *J. Pers. Soc. Psychol.*, vol. 52, no. 5, pp. 946–955, 1987.

[12] T. Baranowski, R. Buday, D. I. Thompson, and J. Baranowski, "Playing for Real," *Am. J. Prev. Med.*, vol. 34, no. 1, p. 74–82.e10, Jan. 2008.

[13] J. F. Alonso, S. Romero, M. R. Ballester, R. M. Antonijoan, and M. A. Mañanas, "Stress assessment based on EEG univariate features and functional connectivity measures," *Physiol. Meas.*, vol. 36, no. 7, pp. 1351–1365, Jul. 2015.

[14] R. T. Thibault and A. Raz, "When can neurofeedback join the clinical armamentarium?," *Lancet Psychiatry*, vol. 3, no. 6, pp. 497–498, Jun. 2016.

[15] E. A. Schoneveld, M. Malmberg, A. Lichtwarck-Aschoff, G. P. Verheijen, R. C. M. E. Engels, and I. Granic, "A neurofeedback video game (MindLight) to prevent anxiety in children: A randomized controlled trial," *Comput. Hum. Behav.*, vol. 63, pp. 321–333, Oct. 2016.

[16] S. I. Hjelm and C. Browall, "Brainball-using brain activity for cool competition," in *Proceedings of NordiCHI*, 2000, vol. 7, p. 9.

[17] A. N. Antle, L. Chesick, A. Levisohn, S. K. Sridharan, and P. Tan, "Using neurofeedback to teach self-regulation to children living in poverty," 2015, pp. 119–128.

[18] W. Wood and D. Rünger, "Psychology of Habit," *Annu. Rev. Psychol.*, vol. 67, no. 1, pp. 289–314, Jan. 2016.

[19] B. Hamadicharef *et al.*, "Learning EEG-based spectral-spatial patterns for attention level measurement," in *Circuits and Systems, 2009. ISCAS 2009. IEEE International Symposium on*, 2009, pp. 1465–1468.

[20] M. H. Ashcraft, "Math anxiety: Personal, educational, and cognitive consequences," *Curr. Dir. Psychol. Sci.*, vol. 11, no. 5, pp. 181–185, 2002.

[21] J. Liew, H. C. Lench, G. Kao, Y.-C. Yeh, and O. Kwok, "Avoidance temperament and social-evaluative threat in college students' math performance: a mediation model of math and test anxiety," *Anxiety Stress Coping*, vol. 27, no. 6, pp. 650–661, Nov. 2014.

[22] S. K. Sridharan, "Investigating Methods to Pre-process and Analyze NF Data to Identify Change in Relaxation and Attention across Sessions," Simon Fraser University, Surrey, British Columbia, 2017.

[23] Tluczek A, Henriques JB, and Brown RL, "Support for the reliability and validity of a six-item state anxiety scale derived from the State-Trait Anxiety Inventory," *J. Nurs. Meas.*, vol. 17, no. 1, pp. 19–28, Spring 2009.

[24] W. Lidwell, K. Holden, and J. Butler, *Universal Principles of Design, Revised and Updated: 125 Ways to Enhance Usability, Influence Perception, Increase Appeal, Make Better Design Decisions, and Teach Through Design*. Rockport Publishers, 2010.

[25] R. B. Miller, "Response Time in Man-computer Conversational Transactions," in *Proceedings of the December 9-11, 1968, Fall Joint Computer Conference, Part I*, New York, NY, USA, 1968, pp. 267–277.

[26] R. Maskeliunas, R. Damasevicius, I. Martisius, and M. Vasiljevas, "Consumer-grade EEG devices: are they usable for control tasks?," *PeerJ*, vol. 4, Mar. 2016.

Published by Verlag der TU Graz
Graz University of Technology

Proceedings of the
7th Graz Brain-Computer Interface Conference 2017 DOI: 10.3217/978-3-85125-533-1-21

SENSORY THRESHOLD ELECTRICAL STIMULATION ENHANCES CLASSIFICATION OF MOTOR IMAGERY

T. Corbet[1], I. Iturrate[1], M. Pereira[1], S. Perdikis[1], J.d.R. Millán [1]

[1] Chair in Brain-Machine Interface (CNBI), Center for Neuroprosthetics (CNP), Ecole Polytechique Fédérale de Lausanne (EPFL), Genève, Switzerland;

E-mail: tiffany.corbet@epfl.ch

ABSTRACT: Non-invasive brain-machine interfaces (BMI) based on motor imagery (MI) of body limbs have been largely studied. However, a non-negligible percentage of users do not produce sufficient discriminable MI brain patterns. It has been suggested that this limitation could be explained by the non-congruency of the delivered feedback with the attended MI task. Following this theory, we propose for the first time the use of sensory threshold neuromuscular electrical stimulation (St-NMES) during MI task to enhance kinesthetic strategies. We hypothesized that St-NMES would foster subjects MI performance without any EEG artefactual contamination by NMES. In this offline study, five naïve healthy subjects were recorded over two different days using either a visual or St-NMES guidance during MI or resting exercises. Results showed how, St-NMES led to enhanced MI discriminability and classification accuracy. Our findings indicate that St-NMES is a promising support for future online MI-BCI performances.

INTRODUCTION

Perirolandic μ and β rhythms modulations in response to motor actions, are a common input control signal for brain-machine interfaces (BMI) for healthy and paralyzed users [13, 2]. In particular, motor imagery (MI) is among the most common tasks to control devices via a BMI. MI is defined as a mental representation of body actions based on internal sensation of movement [10, 17]. However, in practice it can be very challenging for some subjects, especially naïve ones, to generate discriminable MI brain patterns [10]. A possible explanation to this large inter-subject performance variability is that the strategy used to perform MI plays a key role in the accuracy of MI production. It has been proven that the most efficient strategy to perform MI is based on kinesthetic imagery (internally feeling the movement) preferred over visual imagery (internally visualizing the movement) [17]. Indeed, contrary to visual imagery, only kinesthetic imagery activates sensorimotor brain networks, which are similarly observed during motor imagery and motor execution [17, 7, 8]. Thus, the difference between these two kinds of imagery is crucial to improve BMI efficiency, as pointed out by previous works. In particular, several studies already remarked the importance of emphasized users' kinesthetic experiences instead of visual representations during MI [6, 12]. However, despite it is currently well known that we have to brief users how to perform kinesthetic imagery, BMI remains poorly reliable and users' performance is still limited. Furthermore, most BMI systems are currently based on a visual feedback, although other types of feedback could possibly be more effective to help subject perform kinesthetic MI. The choice of the feedback modality could then have an important impact on the accuracy of the BMI.

Instead of simply delivering the outcome of the movement imagery as is common use for visual feedback, one possible solution is the use of somatosensory afferences in order to deliver kinesthetic information and to help subjects to focus on the sensation of the movement. Recent studies have already implemented continuous somatosensory feedback, such as robotic orthosis, vibrotactile stimulation or neuromuscular-electrical stimulation (NMES) to improve MI performance. Among them, Vukelić et al. showed that subjects were able to better modulate β oscillatory rhythms with a proprioceptive feedback delivered by a robotic orthosis [18]. Reynolds et al. demonstrated that NMES during MI induces a larger desynchronization of the sensorimotor rhythm compared to motor imagery supported only by visual feedback [15]. However, the main drawback of the proposed approaches is that the use of somatosensory feedbacks alone (such as passive movement of the joint [18], muscular contraction [15] and even vibrotactile stimulation [5, 6, 9] may also activate similar sensorimotor networks [4, 11, 1], even without any voluntary motor imagery performed by the subject. Thus, it is not yet clear how to provide such rich kinesthetic feedback for online experiments or kinesthetic guidance for offline MI tasks, without interfering with the voluntary modulation of brain activity, limiting their usability for online applications.

In this paper we propose a novel guidance modality to guide subjects during MI performance, based on sensory threshold neuromuscular electrical stimulation (St-NMES). This stimulation conveys natural proprioception by depolarizing sensory and motor nerves, yet without eliciting muscular contraction [15]. The purpose of this offline study is to understand the possible impact of this new approach on MI classification compared to a standard visual guidance. We hypothesize that St-NMES guidance does not interfere with EEG detected brain

Published by Verlag der TU Graz
Graz University of Technology

 DOI: 10.3217/978-3-85125-533-1-21

patterns, fosters MI and enhances the discriminability of EEG patterns during MI.

MATERALS AND METHODS

Experimental design

Five right-handed healthy subjects (2 females, age 25.6 ±1.67) naïve in motor imagery practice, took part voluntarily in the experiment. The study was approved by an internal ethical protocol and participants gave their written informed consent before participation.

The experiment (Fig. 1) was composed of two days of recordings during which all subjects were asked to perform continuous kinesthetic motor imagery (MI) of closing their dominant hand (day 1: n = 60 trials, day 2: n = 40 trials) or a resting task (same amount of trials). For both days subjects randomly started with one guidance modality (St-NMES or visual guidance) then with the other one (visual or St-NMES guidance). During the second day, a control condition was also recorded during which subjects received St-NMES whereas no MI was performed. For all 3 conditions (St-NMES, visual, control) each trial started with the preparation cue (3s), then a cue indicating the type of trial (MI or rest, 1s), followed by the task (MI or resting, 4s) and finished with the appearance of the stop cue. Inter-trial intervals lasted between 3 and 4.5 s.

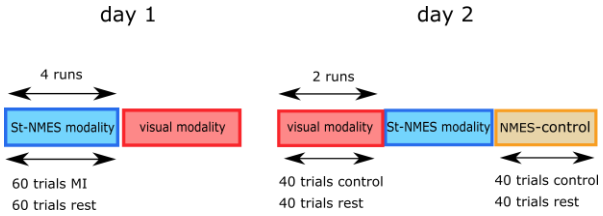

Figure 1: Schema of the experimental design. The order of the guidance modality was randomized across subjects.

St-NMES guidance modality

NMES electrodes were placed on the *Flexor digitorum superficialis* muscle at the anterior face of the forearm. Amplitude of the sensory threshold stimulation (St-NMES) was fixed for each subject before each recording (but keeping the same for both days), and was on average 5±1 mA. With sensory threshold stimulation subjects felt tingling sensation in their palm and forearm but they did not elicit any muscular contraction. The frequency of stimulation was fixed to 30 Hz for all subjects. Subjects received sensory threshold NMES during the MI task and control trials. No stimulation was delivered during resting trials. No visual guidance was provided during the St-NMES condition.

Visual guidance modality

We compared our new approach to the standardly used cursor paradigm moving in a screen for MI [3] [14] [20]. Subjects were instructed to perform kinesthetic MI while seeing a bar going up (for MI trials) or going down (for resting trials).

EEG acquisition and trials extraction

EEG signal was recorded at 512 Hz using a gHiAmp system (gTec, Austria) from 60 channels equally distributed over the scalp following the 10/10 International System. EEG was filtered within the [1,100] Hz (zero-phase Butterworth 4th order), re-referenced to linked ears, then common-averaged referenced. Noisy channels (detected post-experiment by visual inspection) were manually replaced by the mean of the orthogonal neighboring channels. Trials were epoched and concatenated per condition (St-NMES, visual, control), and composed of a baseline from [-3s 0s] and a task time window [1s 5s]. Trials with a filtered EEG signal above 100 µV were considered artefactual and discarded.

Features analysis

We evaluated the discriminability of MI EEG patterns with both guidance modalities (St-NMES, visual) with single-sample classification. First, power spectral density (PSD) for the 16 channels covering the sensorimotor regions (Fz, FCz-1-3-2-4, Cz-1-3-2-4 and Cpz-1-3-2-4) were computed using the Welch method with 5 internal Hanning windows of 500ms (75% overlap). We extracted all the features from µ and β frequency bands for all channels, then fed them to principal component analysis (PCA). We evaluated the accuracy of each guidance modality (St-NMES vs rest, visual vs rest) using a linear discriminant analysis (LDA) as a function of the number of components retained from PCA (from 1 to 20). Each classifier was trained with data from day 1 and tested with data from day 2.

Additionally, we investigated the impact of guidance modality by plotting the first two principal components extracted from 4 pairs of tasks: St-NMES MI vs rest; visual MI vs rest; visual MI vs St-NMES MI; and St-NMES MI vs control.

Classification analysis

We further evaluated the LDA classification performance from the following pairs of tasks St-NMES-MI vs rest, visual-MI vs rest, and control vs rest. Every classifier was trained with data from day 1 using the first 8 principal components (optimal number of features, see below) and tested with data from day 2. For the control condition the classifier was trained with data from St-NMES-MI vs rest from day 1 and tested with the control data from day 2. Statistical significance of classification was defined from a binomial cumulative distribution assuming equal priors (p=0.5) and the number of trials available (n = 80) leading to a chance level of 0.60.

The impact of the guidance modality during the training phase of the classifier on the final accuracy was assessed by comparing accuracies of classifiers with equivalent guidance between the training and testing set to different guidance (e.g. training with St-NMES and testing with St-NMES versus training with visual guidance and testing with St-NMES guidance).

Published by Verlag der TU Graz
Graz University of Technology

 DOI: 10.3217/978-3-85125-533-1-21

RESULTS

Features analysis

Figure 2 shows the classification accuracy of MI compared to rest as a function of the number of selected features. We chose to use eight features as no discernable improvement was observed with more features. The averaged mean of accuracy across subjects was higher for the St-NMES (0.78±0.1) compared to the visual modality (0.69±0.1). Despite this improvement was not significant (Wilcoxon ranksum test, *p=0.31*), the power of the statistical analysis was low (0.5) and more subjects will be needed to draw further conclusions.

Representative cases

Figure 3 shows the representative case of one subject (s1) with larger discriminability with St-NMES compared to visual guidance; and another example of a subject (s3) who had low performances with both guidance modalities. S1 showed discriminable MI patterns with St-NMES guidance but not with visual guidance. The discriminable EEG patterns were induced by MI performance and not by the device itself, since the control condition, where the subject received St-NMES without performing MI, was poorly discriminable from rest. On the other hand, s3 showed no clear dissociation between distributions during St-NMES and poorly separable EEG patterns during the visual condition.

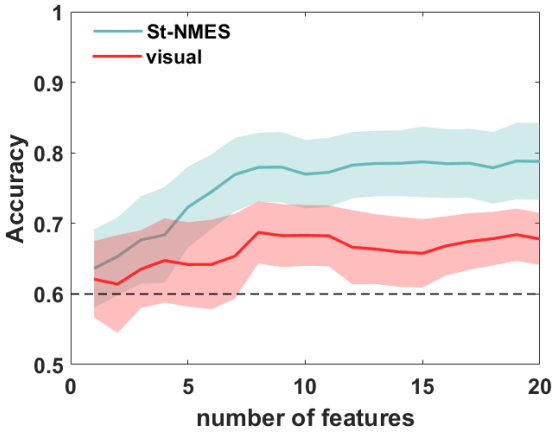

Figure 2: Classification accuracy between MI and rest as a function of the number of features selected, for both guidance modalities. The line (shade) represents the mean (standard error of the mean) of accuracy across subjects. The dashed line represents the chance level estimated at 0.60.

Classification accuracy

Figure 4 represents the accuracies of each subjects for each guidance modality (St-NMES and visual) as well as the classification of a possible bias induced by the St-NMES itself (control). On average, the accuracy for the St-NMES guidance was higher than for the visual guidance (accuracies: 0.78 and 0.69, respectively). Importantly, the control condition showed no significant classification of the St-NMES itself compared to rest

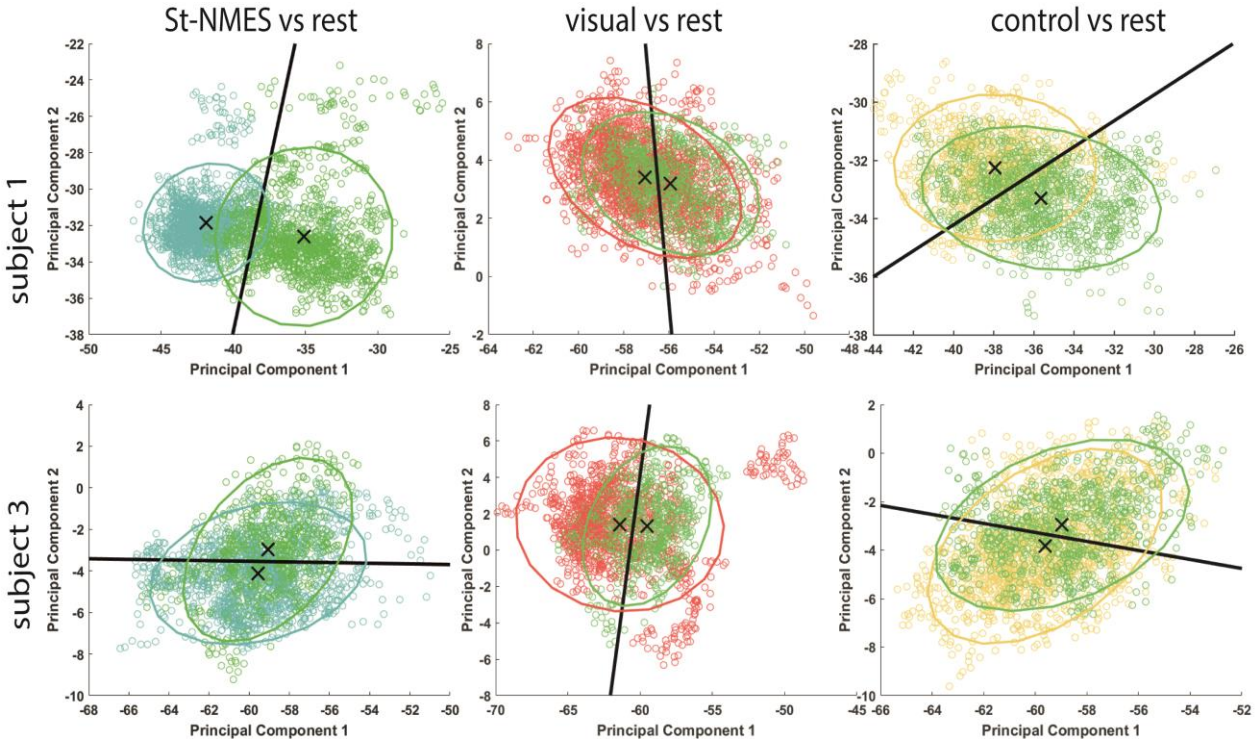

Figure 3: PCA analysis between the 4 pairs of tasks St-NMES (blue), visual (red), rest (green) and control (yellow). Representation of the two first principal components of each pairs of tasks. Each dot represent a sample. The ellipsoids represent the covariance matrix of the distriutions and the cross the mean of the distribution. The black line represents the hyperplane computed from an LDA classifier.

Published by Verlag der TU Graz
Graz University of Technology

 DOI: 10.3217/978-3-85125-533-1-21

(accuracy: 0.59). For 3 subjects over 5 (s1, s4 and s5) the accuracy increased with the St-NMES compared to the visual guidance by 35%, 27% and 26% respectively.
One subject (s2) had similar accuracy with both modalities (St-NMES: 0.84, visual: 0.85), and one subject (s3) had better accuracy with the visual modality (St-NMES: 0.61, visual: 0.69). Importantly, for every subjects except subject 1, the St-NMES itself (control condition) did not induce significant detectable EEG artefacts. In the case of subject 1, the St-NMES induced some discriminable patterns, but they did not explain completely the results obtained during MI with St-NMES.

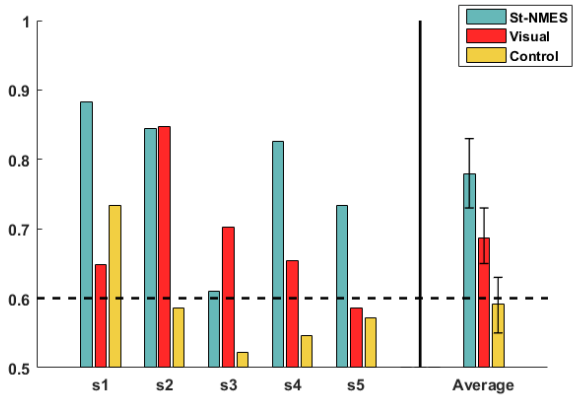

Figure 4: Classification accuracies for each individual subject according to the guidance modality and the control condition. The averaged accuracy across subjects (with the standard error of the mean) is represented on the right part of the figure. The dashed line highlights the chance level.

Impact of the guidance modality of the training data set on classification accuracy
Previous classification analyses were based on equivalent guidance modalities between the training data set and the testing data set. However, as illustrated in Figure 5, the guidance of the training set had an impact on the classification accuracies. Indeed, if the guidance modality of the training data set was different than the testing set the accuracy was decreased (St-NMES—St-NMES: 0.78±0.1, visual—St-NMES: 0.69±0.1 and visual—visual: 0.69±0.1, St-NMES—visual: 0.61±0.1).

DISCUSSION

In this work we show that St-NMES guidance enhanced discriminability of MI pattern and substantially increased classification accuracy without interfering with the recorded EEG signal. EEG pattern during MI were probably enhanced and stronger with the support of the St-NMES which led to a better classification. A plausible explanation of the obtained results is that St-NMES helped subjects to emphasize and focus on kinesthetic imagery.

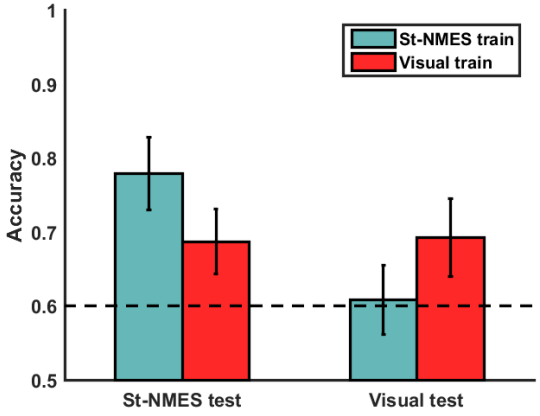

Figure 5: Classification accuracy based on the testing data set according to the guidance modality of the training data set. The dashed line represents the chance level.

As described in the literature kinesthetic imagery activates sensorimotor brain regions similarly to motor execution [15, 8]. Moreover, it is known that MI is based on body representation and on the internal focus of sensation of movement. Thus, we believe that our somatosensory support delivered by St-NMES guided subjects to bring their attention toward the feeling of the limb movement and less on the outcome of the task. On the contrary, the standard visual guidance did not deliver information through somatosensory afferences, which may make less natural for subjects to focus on the sensation of the movement. As a result, subjects may have performed suboptimal strategy during MI based on visual guidance. Our results could be explained then by more accurate kinesthetic focus which induced more discriminable EEG patterns.
Moreover, it has been shown that in the absence of somatosensory feedback, novice subjects were spontaneously less able to produce kinesthetic imagery [19], which can explain the lack of BMI reliability and accuracy [16, 6]. Our study shows that a somatosensory guidance appeared to be more suitable to support MI tasks and it could improve BMI classification. Importantly, our results show that the increase of classification accuracy was not due to a bias induced by the stimulation but by an improvement in MI task. Indeed, St-NMES during rest did not provide detectable sensorimotor network activations.
The representative cases highlighted further elucidated the differences in accuracy obtained. S1 was barely able to modulate sensorimotor rhythms modulations with visual guidance (accuracy: 0.65), but able to perform accurate MI with St-NMES (accuracy: 0.88). As a result, no discriminable patterns were obtained with visual guidance whereas St-NMES guided the user to generate more discriminable brain patterns. Our explanation is that the visual guidance and the instructions of the task were insufficient to guide our subject to perform

Published by Verlag der TU Graz
Graz University of Technology

 DOI: 10.3217/978-3-85125-533-1-21

appropriate MI strategy. In fact, this subject reported that it was easier to focus with St-NMES because he knew where to focus his attention (behavioral questionnaire, results not shown). However, for subject 3 no discriminable EEG pattern could be discerned during MI task even during St-NMES condition. Further studies will have to investigate the reasons of this remaining limitation.

Our results are in line with current opinions on motor imagery performance. Neuper et al. [12] already pointed the importance of emphasizing kinesthetic imagery to improve single trial EEG classification. Moreover, other studies also showed that a somatosensory feedback such as a robotic orthosis [18], vibrotactile stimulation [1, 6] or NMES [15] improves BMI classification and may induce stronger MI neural correlates. In this study, we also showed that results are only due to subjects' improvement and not biased by the feedback alone. On the contrary, a continuous robotic feedback which induces a passive movement of the joint may induce similar EEG patterns and thus, the detected EEG brain pattern will be biased by the passive movement and not due to an accurate MI. In a similar context, Chatterjee et al. [5] also proved that vibrotactile stimulation induces a significant bias in BMI MI features, and other studies showed that NMES eliciting muscular contraction cannot be used as a continuous feedback since it activates similar brain networks [11].

In sum, these results show that the choice of the guidance modality can have a significant impact on the induced EEG features and classification accuracy. Thus, future BMIs may benefit from the use of a continuous feedback that does not induce undesirable brain activations but that help subject to perform MI. Perhaps logically, this feedback should remain the same throughout the entirety of the sessions as results have shown that the transferability from one feedback to another leads to suboptimal performances.

CONCLUSION

MI-based BMI systems have become an interesting tool to induce motor recovery and motor learning. However, its applicability remains limited for an important amount of subjects. In this work, we propose a new kind of continuous guidance, St-NMES that has the potential to face some BMI limitations by delivering feedback congruent with the kinesthetic effort of the task without biasing the EEG recordings. Further analysis and online experiments will shed light on the applicability of the proposed feedback for online BMIs.

REFERENCES

[1] Ahn,S, Ahn M, Cho H, Jun SC. Achieving a hybrid brain–computer interface with tactile selective attention and motor imagery. J. Neural Eng. 2014; 11(6): 1741-2552

[2] Birbaumer N, Cohen LG. Brain-computer interfaces: Communication and restoration of movement in paralysis. The Journal of Physiology 2007; 579(3): 621-636

[3] Carlson T and Millán JdR. Brain-Controlled Wheelchairs: A Robotic Architecture. IEEE Robotics &Automation Magazine, 2013, 65-73

[4] Cassim F, Monaca C, Szurhaj W, Bourriez JL, Defebvre L, Derambure P, et al. Does post-movement beta synchronization reflect an idling motor cortex? Neuroreport. 2001; 12(17): 3859-63

[5] Chatterjee A, Aggarwal V, Ramos A, Acharya S, Thakor, NV. A brain-computer interface with vibrotactile biofeedback for haptic information. J. Neuroeng. Rehabi. 2007; 4(1): 1-12

[6] Cincotti F, Kauhanen L, Aloise F, Palomäki T, Caporusso N, Jyänki P, et al. Vibrotactile Feedback for Brain-Computer Interface Operation. Comput. Intell. Neurosc. 2007; 2007: 1-12

[7] Guillot A, Collet C, Nguyen V, Malouin, F, Richards C, Doyon J. Brain activity during visual versus kinesthetic imagery: An fMRI study. Hum. Brain. Mapp. 2009; 30(7): 2157-2172

[8] Hétu S, Grégoire M, Saimpont A, Coll MP, Eugène F, Michon, PE, et al. The neural network of motor imagery: An ALE meta-analysis. Neurosci. Biobehav. Rev. 2013; 37(5): 930-949

[9] Leeb R, Gwak K, Kim DS, Millán JdR. Freeing the visual channel by exploiting vibrotactile BCI feedback, in Proc. IEEE EMBC 35th, Osaka, Japan, 2013, 3093-3095

[10] Milton J, Small S, Solodkin A. Imaging motor imagery: Methodological issues related to expertise. Methods 2008; 45(4): 336-341

[11] Müller GR, Neuper C, Rupp R, Keinrath C, Gerner HJ, Pfurtscheller G. Event-related beta EEG changes during wrist movements induced by functional electrical stimulation of forearm muscles in man. Neurosci. Lett. 2003; 340(2): 143-147

[12] Neuper C, Scherer R, Reiner M, Pfurtscheller G. Imagery of motor actions: Differential effects of kinesthetic and visual-motor mode of imagery in single-trial EEG. Cogn. Brain Res. 2005; 25(3):668-677

[13] Pfurtscheller G, Lopes da Silva FH. Handbook of Electroencephalography and Clinical Neurophysiology – Event-related desynchronization, Elsevier, Amsterdam, Netherlands (1999)

Published by Verlag der TU Graz
Graz University of Technology

 DOI: 10.3217/978-3-85125-533-1-21

[14] Pfurtscheller G, Brunnera C, Schlögla A, Lopes da Silva FH. Mu rhythm (de)synchronization and EEG single-trial classification of different motor imagery tasks. NeuroImage 2006; 31(1): 153-159

[15] Reynolds C, Osuagwu BA, Vuckovi A. Influence of motor imagination on cortical activation during functional electrical stimulation. Clinical Neurophysiology. 2015; 126(7): 1360-1369

[16] Sakurada T, Hirai M, Watanabe E. Optimization of a motor learning attention-directing strategy based on an individual's motor imagery ability. Exp. Brain Res. 2016; 234(1): 301-311

[17] Solodkin A, Hlustik P, Chen EE, Small SL. Fine Modulation in Network Activation during Motor Execution and Motor Imagery. Cereb. Cortex 2004; 14(11): 1047-3211

[18] Vukelić M, Gharabaghi A. Oscillatory entrainment of the motor cortical network during motor imagery is modulated by the feedback modality. NeuroImage 2015; 111: 1-11

[19] Wei G, Luo J. Sport expert's motor imagery: Functional imaging of professional. Brain Res. 2010; 1341:52-62

[20] Wolpaw, J.R. and McFarland, D.J. Control of a twodimensional movement signal by a noninvasive brain–computer interface in humans. Proc. Natl. Acad. Sci. U.S.A, 2004, 17849–17854

Published by Verlag der TU Graz
Graz University of Technology

Proceedings of the
7th Graz Brain-Computer Interface Conference 2017 DOI: 10.3217/978-3-85125-533-1-22

Affective Brain Computer Music Interfacing: A Case Study Of Use By An Individual With Huntington's Disease

I. Daly[1], A.K. Ho[5,6], J. Marcon[4] F. Hwang[2], D. Williams[3], A. Kirke[3], E. Miranda[3], S. J. Nasuto[2]

[1]Brain-Computer Interfaces Laboratory, School of Computer Science and Electronic Engineering, University of Essex, Colchester, CO4 3SQ, UK
[2]Brain Embodiment Lab, Biomedical Engineering Section, School of Biological Sciences, University of Reading, Reading, RG6 6AY, UK
[3]Interdisciplinary Centre for Music Research, University of Plymouth, Plymouth, Devon, PL8 4AA, UK
[4]Ecole Polytechnique Grenoble, University Grenoble Alps, BP 5314 place du conseil nacional de la resistance, 38041 Grenoble Cedex 9, France
[5]School of Psychology and Clinical Language Sciences, University of Reading, UK
[6]Royal Berkshire NHS Foundation Trust, UK

E-mail: i.daly@essex.ac.uk

ABSTRACT: An affective brain-computer music interface (aBCMI), developed for use as an aid to music therapy, is trialled in a case study with an individual with Huntington's disease. The aBCMI aims to detect a users current affective state and modulate music generated and played to that user in order to manipulate their affective state in a way that has potential therapeutic benefits. We have previously demonstrated the efficacy of this aBCMI on a population of healthy participants but it is unclear whether it could work with individuals with Huntington's.
Our case study demonstrates that there is some potential for aBCMI systems to be used by individuals with Huntington's disease. However, we also highlight some key challenges that need to be overcome in adapting aBCMI systems to this user group. Specifically, we identify a need for more robust measures of ground truths of affective states to allow the aBCMI to be trained with this user group.

INTRODUCTION

Brain-computer music interfaces (BCMIs) provide a method for allowing a user to interact with music via modulations of their brain activity and without the need for movement [17, 11, 10]. We have previously described and presented an evaluation of an affective BCMI (aBCMI) that was able to identify an individual's current affective state from their neural and physiological activity and use this to modulate music played to the individual [7, 8].
We previously demonstrated the ability of this system to modulate the affective states of a cohort of healthy individuals in a manner that has potential applications for music therapy. Specifically, we were able to use our aBCMI to increase felt valence (happiness), decrease felt stress (increase valence and decrease arousal), and decrease felt arousal (calm) reported by our participants [8]. Our aBCMI system was developed with intended applications in music therapy for individuals with a range of different neurological, psychological, or physiological conditions. One example application area is in the treatment of affective changes resulting from Huntington's disease. Huntington's disease is a progressive disorder of the central nervous system that causes damage to the brain and, over a period of typically 10-12 years leads to increased difficulties with movement, cognition and behavior. It also leads to disruption of an individual's ability to effective regulate their affective states. Therefore, there is potential utility in providing an aBCMI system to individuals with Huntington's disease [1].
Huntington's disease affects approximately between 7 to 12 in 100,000 people and there is currently no cure available [13]. Early symptoms of Huntington's disease can include change to personality, mood swings, cognitive processing, and fidgety movement [14].
To begin to explore whether a physiologically informed affective music therapy could be beneficial for individuals with Huntington's disease, we provided our aBCMI system to one individual with Huntington's disease as a case study. We had the following objectives in this study.

1. To determine if is it possible to deploy the aBCMI with an individual with Huntington's disease.
2. To explore how affective state reporting and detection may differ for this individual.
3. To determine whether we could accurately identify affective states from an individual with Huntington's disease.
4. To determine whether we could modulate affective states for this individual.

Published by Verlag der TU Graz
Graz University of Technology

 DOI: 10.3217/978-3-85125-533-1-22

MATERIALS AND METHODS

Patient: We recruited one individual with genetically confirmed Huntington's disease (male, 43 years old), who was at a very early stage of the disease.
Our participant received £20.00 (GBP) for each of the sessions attended. The study was given a favorable ethical opinion according to the research ethics procedures of the School of Systems Engineering, University of Reading.

Brain-computer music interface: The aBCMI includes 4 stages: (1) data measurement, (2) affective state detection, (3) case based reasoning, and (4) music generation. These are illustrated in Figure 1.

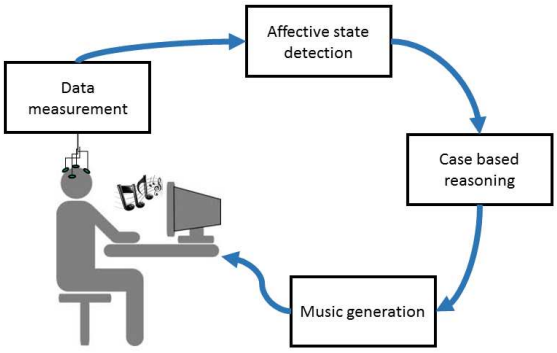

Figure 1: A schematic diagram of our aBCMI.

Data measurement: The data measured included electroencephalogram (EEG), electrocardiogram (ECG), galvanic skin response (GSR), blood pulse oximetry data, and head movement data recorded via an accelerometer. All data was recorded at a sample rate of 1,000 Hz via a BrainAmp EEG amplifier and ExG amplifier (BrainProducts, Germany).
EEG was recorded from 32 channels positioned according to the international 10/20 system for EEG electrode placement. The reference channel was placed at electrode FCz and the ground electrode was placed at position AFz. The impedances on all the channels throughout the study was less than 10 kΩ.
The ECG was recorded from the ventral positions on the participant's left and right wrists. GSR was recorded from the ventral medial phalanx positions of the participant's index and middle fingers on the left hand. The blood pulse oximetry information was recorded from the participant's left thumb with a pulse oximeter. Finally, the participant's head movement was recorded with an accelerometer placed at position CPz.

Affective state detection: Affective state detection was performed by first selecting features that were most frequently associated with changes in affective states and then classified via a combination of support vector machines (SVMs).
Features were extracted from the EEG by first segmenting the EEG into spatial regions depending on the region of the scalp the EEG was recorded from. Specifically, the EEG was subdivided into ten spatial regions, which are listed in Table 1.

Table 1: Spatial regions of EEG features.

Region	Channels
Whole head	All channels
Frontal	FP1, FP2, F7, F3, F4, F8
Central	C3, Cz, C4, CP5, CP6, CP1, CP2
Parietal	P7, P3, Pz, P4, P8, POz
Occipital	O1, O2
Left temporal	FT9, T7, TP9
Right temporal	FT10, T8, TP10
Midline	Fz, Cz, Pz, POz
Left hemisphere	FP1, F7, F3, FT9, FC5, FC1, T7, C3, TP9, CP5, CP1, P7, P3, O1
Right hemisphere	FP2, F4, F8, FC2, FC6, FT10, C4, T8, CP2, CP6, TP10, P4, P8, O2

Features were then subdivided further into 10 frequency bands. Specifically, the EEG within each spatial region was filtered into the delta (1-4 Hz), slow theta (4-5.5 Hz), fast theta (5.5-7 Hz), total theta (4-7 Hz), slow alpha (8-10 Hz), fast alpha (10-12 Hz), total alpha (8-12 Hz), sigma (12-14 Hz), beta (14-30 Hz), and gamma (30-45 Hz) frequency bands.

From the physiological signals the mean peak-to-peak interval time was extracted from the ECG and the blood pulse oximeter. Additionally, the mean amplitude of the GSR within a 1 s window was extracted and baseline corrected against the previous 1 s of data.

This resulted in a set of 103 candidate features. A subset of these features was then selected via a stepwise linear discriminant analysis approach. Features were iteratively added and removed from a linear regression model relating features (independent variables) to the participant's reported affective state over different trials (the dependent variable). This process continued until the addition or subtraction of further features did not significantly improve the fit of the regression further. The remaining set of features were then taken as the selected features for use in classifying affective states via a set of SVMs during online use of the aBCMI. Further details of this approach are reported in [4].

Case based reasoning: The case based reasoning system was used to identify the specific musical modulations that are most effective at modulating our participant's affective state in the desired direction during each trial. Specifically, case based reasoning was used to build a rule set that determines, for a given current affective state experienced by the participant and a target final affective state that we want them to be moved to, what is the best set of modulations of the music generator that should be applied.

The rule set of the case based reasoning system was trained from the participant's responses to the music played during a series of 3 training sessions. Each trial in these runs included different modulations to the music generator. The participant's felt affective states were

Published by Verlag der TU Graz
Graz University of Technology

 DOI: 10.3217/978-3-85125-533-1-22

recorded throughout the trial and used to determine the relationships between the music manipulations and the participant's felt affective states.

Music generator: A music generator was used to produce the music stimuli use throughout this study for both the offline training sessions and the online testing sessions. This allowed a very large amount of varying musical stimuli to be produced for the experiments, preventing well known effects of repeated listening on an individual's affective state [9]. An affectively driven algorithmic composition system was used to generate the music used in this study. This system has been previously described in [15, 16] and validated in [5].

Experiments: We attempted to train our aBCMI system to identify affective states and modulate music to achieve 4 key goals related to music therapy. Specifically, we attempted to use the aBCMI to achieve the following.

1. Make the participant happier: increase their reported valence.
2. Calm the participant: reduce reported arousal.
3. Reduce stress in the participant: simultaneously increase valence and decrease arousal.
4. Excite the participant: increase reported arousal.

The experiments were split over 4 sessions conducted over a 2 week period. The first three sessions were offline training sessions in which the participant was played a series of pieces of generated music intended to induce a range of different affective states. The affective state detector and case based reasoning system were trained based on the data from these sessions. Finally, the fourth session was an online session in which the aBCMI was used to attempt to achieve each of the four goals listed above.

Each training session contained 4 runs and was split into 18 trials per run (72 trials per session). In each trial the participant first observed a fixation cross for 2 s and then listened to music for 40 s. Each piece of music was generated to attempt to modulate the affective state of the participant from one of nine discrete regions on the valence arousal circumplex (high, neutral, and low valence and arousal tuples) to a new position on the circumplex. Specifically, the first 20 s of the music attempted to induce the first affective state and the next 20 s attempted to induce the second affective state.

While listening to the music the participant was instructed to report their currently felt affective state at each moment in time via the use of the, joystick controlled, FEELTRACE interface [3]. Before using the interface the system was explained to the participant via a written document, a power-point presentation, a video, and verbally. The participant was also given the opportunity to run through a practice session with the interface.

Between trials a distraction task was used to minimize serial effects of changes in affective states between trials. Specifically, the participant was asked to listen to a series of beep tones, one of which was at a higher pitch and occurred 20 % of the time and other occurred 80 % of the time. The tones were played in random order and the participant was asked to count the number of high pitch tones they heard.

The online session consisted of 6 runs, each of which contained 10 trials. In this session the aBCMI attempted to move the participant from a current affective state to a target affective state as described above. The affective state detector and the case based reasoning system were used to determine which modulations of the music generator were to be applied in each trial. The trial structure was the same as the training sessions.

Evaluation: The success of the aBCMI was measured by whether it was able to modulate our participant's affective state in the desired way significantly more often than chance during the online testing session. This was determined by inspecting the FEELTRACE reports provided by the participant during the online session. A first order polynomial function was fitted to these complete (40 s) traces over each trial and the angle of the resulting line was measured. The distribution of these angles was evaluated to determine if it differed significantly from a standard normal distribution (mean = 0, standard deviation = 1) via a Kolmogorov-Smirnov test. Specifically, if the distribution of these angles did not differ significantly from a standard normal distribution this would indicate that the participant's affective state had not been significantly altered by the aBCMI.

Furthermore, in cases where the distribution of the angles of the FEELTRACE reports was observed to differ significantly from chance the mean angle of the reports was inspected to determine whether it was moving in the correct direction for a particular goal. For example, for trials in which the aBCMI was attempting to increase the valence felt by the participant the FEELTRACE report of valence is expected to increase significantly over the course of the trial.

RESULTS

The aBCMI was able to significantly increase the participant's reported valence during trials in which the goal of the system was to make the participant happier ($p < 0.01$, ks-test, average of 17 trials per participant). This is illustrated in Figure 2.

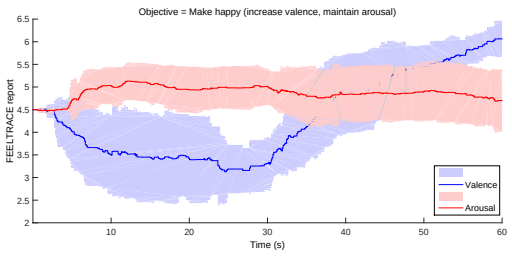

Figure 2: The participant's reported mean FEELTRACE responses over trials during the online session while us-

Published by Verlag der TU Graz
Graz University of Technology

 DOI: 10.3217/978-3-85125-533-1-22

ing the aBCMI to attempt to increase the valence.

Additionally, the affective state detection system was observed to be able to correctly identify the participant's felt valence in 43.8 % of the trials ($p < 0.001$) and the participant's felt arousal in 50.8 % of the trials ($p = 0.007$). These classification results, and their statistical significance, were calculated using methods first described in our earlier work [6].
However, unlike in the cohort of healthy participants reported in [8], the aBCMI was not able to successfully calm our participant. Specifically, no significant change in arousal was noted. Additionally, the aBCMI was not able to de-stress the participant, although it is worth noting that a non-significant trend of increased valence (illustrated in Figure 3) was observed during trials for which the goal was to reduce the stress of the participant. Finally, the aBCMI was not able to excite the participant. A significant increase in valence was noted during these trials but no significant change in arousal (the intended outcome of this goal) was noted.

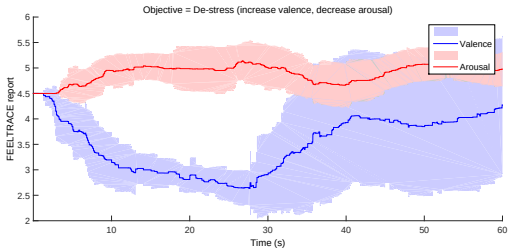

Figure 3: The participant's reported mean FEELTRACE responses over trials during the online session while using the aBCMI to attempt to de-stress (increase valence and reduce arousal).

DISCUSSION

It is not, of course, possible to draw general population wide conclusions from a single case study. Nonetheless, a number of observations may be drawn which should be considered when developing aBCMIs (and other types of affective BCIs) for use by individuals with Huntington's disease.
First, the aBCMI was able to correctly increase our participant's reported valence during trials in the online session in which the goal was to make our participant feel happier. This suggests that there is some potential for this aBCMI to be useful for at least some individuals with Huntington's disease.
Second, it is important to note that our participant had some difficulty using the 2-dimensional, joystick controlled, FEELTRACE interface to report their affective states. Although our participant was carefully briefed on what was meant by "valence" and "arousal" and how to use FEELTRACE, they had difficulty with simultaneously reporting their valence and arousal. For example, when the music attempted to first convey a neutral affective state (in terms of both valence and arousal) followed by a high valence and high arousal affective state we observed that our participant would only report an increase in valence.
In cases where only the arousal of the music changed, the participant used the FEELTRACE interface to report an increase in arousal. However, in cases where both the music's valence and arousal changed our participant reported only the change in valence. Upon careful questioning our participant reported that they felt a change in both the experienced valence and arousal while listening to the music. However, these were not reflected in his FEELTRACE report.
It may be the case that the use of FEELTRACE to report felt affect via continuously controlling a joystick is effecting the participant's affective state. Continuous use of the joystick requires a degree of concentration, and this is likely to distract from conscious awareness of the current felt affective state. However, FEELTRACE is used continuously for all affective states, thus, this effect is likely to be uniform over all affective states.
It may also be the case that, as a construct, arousal is more complex and less amenable to immediate self reporting than valence. Thus, it may have been harder for our participant to make judgments on their arousal and, consequently, their responses tended not to differ from the default middle range of the reporting space.
This suggests that FEELTRACE may not always be the most suitable tool for obtaining a ground truth measure of felt affective states. Alternative tools, such as GTRACE, which allows independent reporting of valence and arousal [2], and an alternative training process, which doesn't include any trials in which both valence and arousal are simultaneously changed, may be needed in these cases.
It is important to note that there is no completely agreed upon method to measure affective state from the individual [12]. Subjective measurements (such as FEELTRACE) and objective measures (such as physiological measurements) are both subject to error. The inaccuracy in reporting may also, in part, explain the relatively lower performance of the aBCMI with this participant compared to our previous cohort of healthy participants [8]. If we are not always able to obtain an accurate ground truth measure of changes in valence and arousal this is going to lead to lower classification accuracies in the affective state detection system and lower performance during the aBCMI's online session.
Third, we did not observe noticeable signal quality problems with our participant. Some individuals with Huntington's disease exhibit difficulties with movement and fidgeting, which may lead to increased amounts of artefact in the observed EEG. However, this was not observed to be the case in our study. Nonetheless, in general robust artefact removal methods are needed to assist with acquiring good quality EEG signals from such patient groups.
Finally, our case study suggests that there may be some

Published by Verlag der TU Graz
Graz University of Technology

 DOI: 10.3217/978-3-85125-533-1-22

potential for our aBCMI as a tool to aid with some aspects of therapy for individuals with Huntington's disease. However, a number of adjustments may need to be made to the aBCMI in order for it to be more useful for this population (for example by replacing the FEELTRACE interface with a more appropriate measure of the ground truth of the individuals affective state, such as GTRACE, for training the system). Further research in this area is needed.

Acknowledgments

This work was supported by the EPSRC grants (EP/J003077/1 and EP/J002135/1).

References

[1] G. Bates, S.J. Tabrizi, and L. Jones. *Huntington's Disease - Google Books*. Oxford University Press, Oxford, 2014.

[2] R. Cowie and G. Mckeown. Statistical analysis of data from initial labelled database and recommendations for an economical coding scheme. *SEMAIN Report D6b*, 2010.

[3] Roddy Cowie, Ellen Douglas-Cowie, Susie Savvidou, Edelle McMahon, Martin Sawey, and Marc Schröder. 'FEELTRACE': An Instrument For Recording Perceived Emotion In Real Time. In *Proceedings of the ISCA Workshop on Speech and Emotion*, pages 19–24, 2000.

[4] I. Daly, A. Malik, J. Weaver, F. Hwang, S.J. Nasuto, D. Williams, A. Kirke, and E. Miranda. Identifying music-induced emotions from EEG for use in brain-computer music interfacing. In *6th Affective Computing and Intelligent Interaction*, 2015.

[5] I. Daly, A. Malik, J. Weaver, F. Hwang, S.J. Nasuto, D. Williams, A. Kirke, and E. Miranda. Towards Human-Computer Music Interaction: Evaluation of an Affectively-Driven Music Generator via Galvanic Skin Response Measures. In *7th Computer Science and Electronc Engineering Conference*, 2015.

[6] I. Daly, D. Williams, A. Kirke, J. Weaver, A. Malik, F. Hwang, E.R. Miranda, and S.J. Nasuto. Affective Brain-Computer Music Interfacing. *Journal of Neural Engineering*, accepted, 2015.

[7] I. Daly, D. Williams, A. Kirke, J. Weaver, A. Malik, F. Hwang, M. Wairagkar, E. Miranda, and S.J. Nasuto. An Affective Brain-computer music Interface. In *Proceedings of the 6th International Brain-Computer Interface Meeting, organized by the BCI Society*, 2016.

[8] Ian Daly, Duncan Williams, Alexis Kirke, James Weaver, Asad Malik, Faustina Hwang, Eduardo Miranda, and Slawomir J Nasuto. Affective brain–computer music interfacing. *Journal of Neural Engineering*, 13(4):046022, aug 2016.

[9] R.J. Larsen. Toward a Science of Mood Regulation. *Psychological Inquiry*, 11(3):129–141, 2000.

[10] Scott Makeig, Grace Leslie, Tim Mullen, Devpratim Sarma, Nima Bigdely-Shamlo, and Christian Kothe. First Demonstration of a Musical Emotion BCI. pages 487–496. Springer Berlin Heidelberg, 2011.

[11] E R Miranda. Brain-computer music interface for generative music.

[12] Robert. Plutchik and Henry. Kellerman. *The Measurement of emotions*. 2013.

[13] S A Pridmore. The prevalence of Huntington's disease in Tasmania. *The Medical journal of Australia*, 153(3):133–4, aug 1990.

[14] Sarah J Tabrizi, Rachael I Scahill, Gail Owen, Alexandra Durr, Blair R Leavitt, Raymund A Roos, Beth Borowsky, Bernhard Landwehrmeyer, Chris Frost, Hans Johnson, David Craufurd, Ralf Reilmann, Julie C Stout, Douglas R Langbehn, and TRACK-HD Investigators. Predictors of phenotypic progression and disease onset in premanifest and early-stage Huntington's disease in the TRACK-HD study: analysis of 36-month observational data. *The Lancet Neurology*, 12(7):637–649, jul 2013.

[15] D. Williams, A. Kirke, E.R. Miranda, I. Daly, J. Hallowell, F. Hwang, A. Malik, E. Roesch, J. Weaver, and S.J. Nasuto. Affective calibration of a computer aided composition system by listener evaluation. In *Proceedings of the Ninth Triennial Conference of the European Society for the Cognitive Sciences of Music (ESCOM2015)*, 2015.

[16] Duncan Williams, Slawomir Nasuto, Alexis Kirke, Eduardo Miranda, Ian Daly, James Hallowell, James Weaver, Asad Malik, Etienne Roesch, and Faustina Hwang. Investigating Perceived Emotional Correlates of Rhythmic Density in Algorithmic Music Composition. *ACM Transactions on Applied Perception*, 12(3):1–21, jun 2015.

[17] Jonathan R Wolpaw, Niels Birbaumer, Dennis J McFarland, Gert Pfurtscheller, and Theresa M Vaughan. Brain-computer interfaces for communication and control. *Clin Neurophysiol*, 113:767–791, jun 2002.

Published by Verlag der TU Graz
Graz University of Technology

Proceedings of the
7th Graz Brain-Computer Interface Conference 2017 DOI: 10.3217/978-3-85125-533-1-23

IMPROVING INFORMATION TRANSFER RATE IN ACTIVE BCIS

V. R. de Sa[1]

[1]Cognitive Science, UC San Diego, La Jolla, CA, United States

E-mail: desa@ucsd.edu

ABSTRACT: We consider the case of a noisy binary EEG-based brain-computer interface where a human attempts to generate two discriminable control signals but the received signals are noisy and the optimal classification boundary (or decoder) is not known or changing. In such situations, it is common for the computer to accumulate evidence over time before performing an action. Intermediate feedback can be given to inform the user of the current decoding along the way. Under these conditions we have shown via Markov chain analysis that the information transfer rate is higher when the user and computer attach the responsive (to the intermediate feedback) meanings of "continue/good" and "change-direction/bad" to the two classes of noisy signals they generate instead of direct commands "left" and "right". In this paper, we analyze the first step of these systems and show that when there is not yet a computer-interpreted response to respond to, the "right/left" commands are most informative and that a system where a first "right/left" step is combined with future "good/bad" interactive commands gives the highest information transfer rate. Finally we show that this hybrid approach can be seen as a natural game-like interface.

INTRODUCTION

We consider the case of a human-controlled interface to a computer where the received signals are noisy and not perfectly classifiable. Such signals arise in EEG-based brain-computer interfaces (BCIs) but could also arise in other noisy interfaces such as gesture recognition or speech recognition in noisy environments or in some clinical populations. For this paper, we restrict analyis to the binary control case, where humans are trying to generate one of two signals as is commonly used in motor-imagery EEG-based brain computer interfaces.

For concreteness, we consider the scenario of a user using an EEG-based motor-imagery brain-computer interface with the goal of selecting one of two targets on the right and left of the screen. Subjects require a certain level of selection accuracy (e.g. 70% [5]) for performance to be considered acceptable, and there are applications where it is costly to output the wrong answer [11]. For these reasons, it is common to accumulate evidence, and feedback can be given to the subject over time. A common method is to have the cursor move a step every processing window (processing windows are usually 500ms to 1 second long). The number of steps between the two target endpoints can be varied to trade off accuracy and selection speed or can be set to optimize information transfer rate (ITR) for a given discriminability between the distributions of signals for the two classes [2]. In text and figures below, we refer to the number of possible cursor positions (NCP) which is equal to twice the number of steps from the center to a target plus one.

While EEG signals are high dimensional, after standard signal processing [9, 1, 7] the signals are reduced to a lower dimensional space, and it is common to approximate them as Normal/Gaussian distributions and use simple linear classifiers in this projected space [10, 9, 8]. Once a classifier is defined, the critical variable for classification, is the side of the classification boundary (or more generally the signed perpendicular distance from the classification boundary). This is represented as the (single-step) one-dimensional probability distributions diagrammed on the right side of Figures 1, 2, 3, and 8. and given by the blue dashed curves in Figures 4, 6, 7.

In any noisy machine learning problem with finite data, a classifier will not be able to find the exact optimal classification boundary between the distributions. In problems with non-stationary data such as EEG [3, 10], this issue is especially true. In these cases, we have shown that by changing the meaning of the single-step signals generated by the humans, the information transfer rate can be increased by changing the meanings of the two signals that the user generates to “continue” and “change direction” instead of “left” or “right” [2]. What this means is that the same signals that the user generates are given different semantics in the communication strategy. So for example, right hand imagery could be used to mean “change direction (I am disatisfied with the current movement)” and left hand imagery used to signal “continue (I am satisfied with the current movement direction)”. This changes the communication protocol from direct commands to interactive commands that respond to the current interpretation as reflected by the feedback of the cursor movement. We have shown that when a control signal is used “that depends intimately on what has already been transmitted, interpreted, and received”, a much more robust communication system results [2]. In particular the information transfer rate is demonstrably higher with the interactive communication system than with the standard direct communication system when the classification boundary is not in the optimal position. As in [2], we will refer to the direct method of controlling with “move right” and “move left” signals as an R/L control system and the interactive method of con-

Published by Verlag der TU Graz
Graz University of Technology

 DOI: 10.3217/978-3-85125-533-1-23

trolling with “change-direction/bad/**D**issatisfaction” and “continue/good/**S**atisfaction” as a D/S control system.

We examine the mathematics for single step systems (where a target is reached in one step or NCP=3), and based on this analysis propose a new hybrid approach, where the starting cursor direction is fixed and known but D/S commands are used. We show that in this case the first step is equivalent to a “Right/Left” commanded step, and the system makes less processing demand of the user and results in a higher information transfer rate than the previously proposed D/S method in [2] using random start direction.

METHODS

The standard R/L method of control where the user generates one signal (e.g. right hand motor imagery) to mean “Move the cursor to the Right” and another discriminable signal (e.g. left hand motor imagery) to mean “Move the cursor to the Left” can be shown to be modeled by a Markov chain as shown in Figure 1 [2] whereas the interactive D/S method of control that uses the same underlying signals of right and left hand motor imagery can be modeled by a Markov chain shown in Figure 2. In this case, the state of the system contains the position and cursor direction information.

If the system does not use multiple steps to reach the goal (in other words, if NCP=3. See Figures 1,2,3), then the interactive nature does not come into play. We can still consider how a D/S control system might work in a one-step system. In a D/S system the cursor would appear moving in one direction (or simply appear as an arrow instead of a circular cursor, and the user would generate a "continue" (if they like that direction) or "change direction" (if they don’t) signal which would influence the one and only step. It might seem that the most natural method would be to have the initial cursor direction be drawn randomly from right/left as in [2] (and shown in Figure 2 by the 0.5 probabilities for each possible starting state). In this case, the accuracies are actually the same as a function of the classification boundary for the D/S and R/L system. However the error-rates when considered separately for the left and right classes can be quite different as the boundary is moved from the crossing points of the distributions. In the R/L system, if the boundary is offset so "Right" is output more than it should be, the error rate for the Left class will be higher than the error rate for the right class. This is shown in Figure 4.

However for the D/S system, if the classification boundary is not at the crossing point of the distributions, it will be more likely to output "continue" or "change-direction". If, the start direction (to which continue or change-direction are responded to) is chosen randomly and the two classes have equal prior probabilities, then the error-rate for the left and right classes will be equal, as whatever happens to the left class when the cursor starts in the left direction will be matched by what happens to the right class when the cursor starts in the right direction and what happens to the left class when the cursor starts in the right direction will be matched by what happens to the right class when the cursor starts in the left direction. This can be seen in Figure 4.

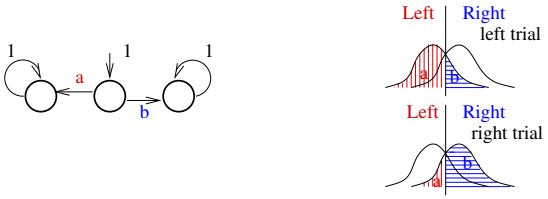

Figure 1: This figure shows the Markov chain model for the R/L control method for one step (NCP=3).

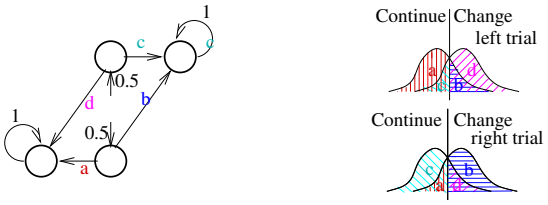

Figure 2: This figure shows the Markov chain model for the original D/S control method for one step (NCP=3) with random start direction (RS). Notice that this model is different from the Markov chain for the one step R/L control method.

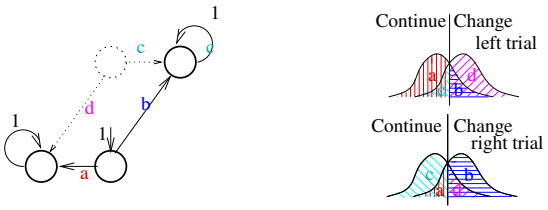

Figure 3: This figure shows the Markov chain model for the D/S control method with one step (NCP=3) and constant left direction start (CS). The node and connections with dashed lines represents states and transitions that are not possible but are possible in the random start model. Note how this Markov chain is equivalent to that of the one step R/L control method with transition probabilities given only by a and b.

Note, however, that if the cursor always starts in the left direction, the one-step D/S method of control is equivalent to the R/L method of control (with continue equivalent to left and change-direction equivalent to right). (This is shown in Figure 3). (Similarly if the cursor always starts in the right direction, the one-step D/S method of control is equivalent to the R/L method with continue equivalent to right and change-direction equivalent to left.)

The number of steps (one in this case) are the same for either starting strategy with the D/S method, but because the accuracies are different for the two classes for the R/L control and the D/S (random start), the information transfer rate (ITR) ends up being different for the two systems. As our classification rates can differ for the right and left classes, we use the general equation for computing the ITR.

Published by Verlag der TU Graz
Graz University of Technology

 DOI: 10.3217/978-3-85125-533-1-23

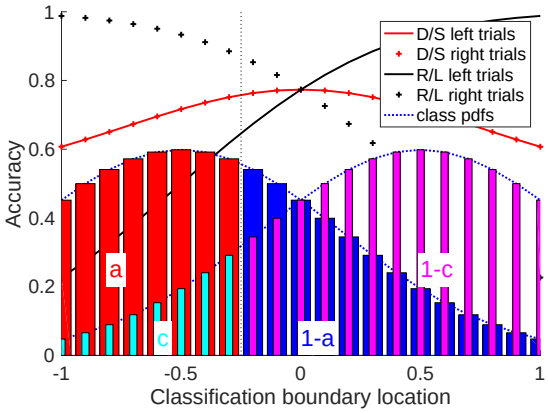

Figure 4: This figure shows the probability distributions for two classes (bottom) and the error rate for the left and right classes as a function of the classification boundary (top). Note that with the R/L control method the error rate is different for right and left trials whereas for the D/S control system with random start direction, the error rates are the same for the two classes as discussed in the text. At the possible classification boundary given by the dotted vertical line, the R/L control accuracy for the left class is 61.8% and the accuracy for the right class is 88.5%. The accuracy for both left and right classes for the D/S control (random-start) is the average of these two (75.14%) Also shown in the bottom of the figure are the variables used in the mathematical analysis of the one-step system. Note that b and c will change as a function of the classification boundary.

$$ITR = \left(\sum_{j=1}^{C} -p(y_j)\log_2(p(y_j)) + \sum_{i=1}^{C}\sum_{j=1}^{C} p(x_i)p(y_j|x_i)log_2(p(y_j|x_i)) \right) /T$$

where $p(y_j) = \sum_{i=1}^{C} p(x_i)p(y_j|x_i)$ and x_i represents intended class i and y_j represents decoded class j. (For our example $C = 2$). T is the total time (including overhead/set up time) for the full trial to select either target.
Figure 6 shows by analysis of the Markov chain model [2] that for the one-step system, the ITR is better for the R/L (and equivalent D/S same-start) control than the D/S random start method. We now prove this mathematically. For the purposes of the proof we will consider the probabilities under the pdfs given by the distributions in Figure 4. For R/L control the class on the left corresponds to "Left trials" and the class on the right "Right trials" and thus for R/L control $P(y_1|x_1) = a, P(y_1|x_2) = c, P(y_2|x_1) = 1-a, P(y_2|x_2) = 1-c$. For the one-step D/S system with random start (RS) the distributions actually represent the "Continue" and "Change Direction" distributions. In order to determine $P(\text{"Left"}|left)$ we must compute the expected value over both right and left start directions. If the cursor starts right, then the accuracy is given by the area under the change direction distribution on the correct side of the boundary (i.e. $1-c$). If the cursor starts moving left, then the accuracy is given by the area under the continue distribution on the correct side of the boundary (i.e. b). So for equal probability of each starting direction $P(\text{"Left"}|left) = .5a + .5(1-c)$. Likewise $P(\text{"Right"}|right) = .5a + .5(1-c)$. That is the error rates are equal for the right and left classes and equal to $\frac{c+(1-a)}{2}$.

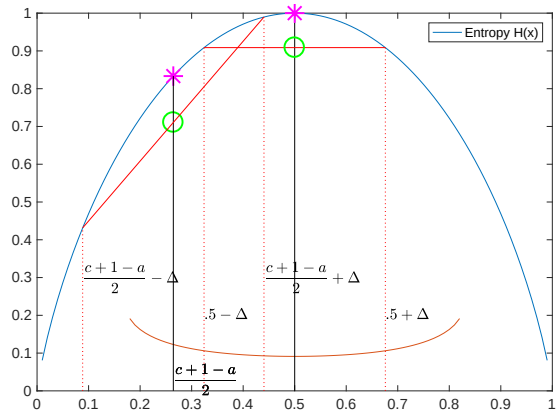

Figure 5: Graphical view of the entities in IT_{RS} and IT_{CS}. The magenta asterisks show $H(x)$ and the Green circles show $G(x,\Delta)$ where $\Delta = \frac{1-a-c}{2}$. IT_{RS} Subtracts the lower magenta asterisk from the higher one (at x=.5). IT_{CS} subtracts the lower green circle from the higher one (at x=.5). As $H(x) - G(x,\Delta)$ (the difference between the magenta asterisks and the green circles (a subset is shown by the red curve near the bottom of the Figure)) has a minimum at 0.5 on $(0,1)$, $IT_{CS} \geq IT_{RS}$. When $\Delta = 0$ $(c = 1-a)$, $IT_{CS} = IT_{RS}$.

$$\begin{aligned} IT_{RS} = & \sum_{j=1}^{2} -p(y_j)log_2(p(y_j)) \\ & + \sum_{i=1}^{2}\sum_{j=1}^{2} p(x_i)p(y_j|x_i)log_2(p(y_j|x_i)) \\ = & H(.5) - H\left(\frac{c+1-a}{2}\right) \end{aligned}$$

where $H(p) = -p\log_2(p) - (1-p)\log_2(1-p)$ is the discrete entropy function for a Bernoulli random variable with probability of one class given by p (and probability of the other class given by $(1-p)$).

For the one-step D/S system with consistent left start (CS) similarly assuming equal number of class 1 and class 2 patterns, the error rates are different for the right and left classes (and are identical to an R/L system) and are respectively given by $1-a$ and c we have:

Published by Verlag der TU Graz
Graz University of Technology

 DOI: 10.3217/978-3-85125-533-1-23

$$
\begin{aligned}
IT_{CS} &= \sum_{j=1}^{2} -p(y_j)log_2(p(y_j)) \\
&\quad + \sum_{i=1}^{2}\sum_{j=1}^{2} p(x_i)p(y_j|x_i)log_2(p(y_j|x_i)) \\
&= -\left(\frac{a+c}{2}\right) * \log_2\left(\frac{a+c}{2}\right) \\
&\quad -\left(1-\frac{a+c}{2}\right) * \log_2\left(1-\frac{a+c}{2}\right) \\
&\quad + .5(1-a)log_2(1-a) + .5(a)log_2(a) \\
&\quad + .5(c)log_2(c) + .5(1-c) * log_2(1-c) \\
&= H\left(\frac{a+c}{2}\right) - .5H(a) - .5H(c) \\
&= .5H(.5 - \frac{1-a-c}{2}) + .5H(.5 + \frac{1-a-c}{2}) \\
&\quad - .5H(\frac{1-a+c}{2} + \frac{1-a-c}{2}) \\
&\quad - .5H(\frac{1-a+c}{2} - \frac{1-a-c}{2}) \\
&= G\left(.5, \frac{1-a-c}{2}\right) - G\left(\frac{c+1-a}{2}, \frac{1-a-c}{2}\right)
\end{aligned}
$$

where we define

$$G(p,\Delta) = \frac{H(p+\Delta)+H(p-\Delta)}{2}$$

for $\Delta = \frac{1-a-c}{2}$ and we use $H(x) = H(1-x)$ for $x \in (0,1)$. If we compare the IT_{CS} with consistent start to the IT_{RS} with random start,

$$
\begin{aligned}
IT_{RS} - IT_{CS} &= H(.5) - G\left(.5, \frac{1-a-c}{2}\right) - \\
&H\left(\frac{c+1-a}{2}\right) + G\left(\frac{c+1-a}{2}, \frac{1-a-c}{2}\right)
\end{aligned}
$$

To see whether IT_{CS} is larger or smaller than IT_{RS} we check how $H(x) - G(x,\Delta)$ varies as a function of x. Looking at the first derivative of the function. $H(x) - G(x,\Delta)$, we have

$$
\begin{aligned}
\frac{d(H(p) - G(p,\Delta))}{dp} &= -\log_2(p) - 1 + \log_2(1-p) + 1 \\
&\quad - .5(-\log_2(p+\Delta) + \log_2(1-(p+\Delta))) \\
&\quad - .5(-\log_2(p-\Delta) + \log_2(1-(p-\Delta)))
\end{aligned}
$$

which equals 0 at $p = .5$.
The second derivative:

$$
\begin{aligned}
\frac{d^2(H(p) - G(p,\Delta))}{dp^2} &= -\frac{1}{p} - \frac{1}{1-p} + \frac{.5}{(p+\Delta)} \\
&+ \frac{.5}{(1-p-\Delta)} + \frac{.5}{(p-\Delta)} + \frac{.5}{(1-p+\Delta)} > 0
\end{aligned}
$$

is positive for $p \in (0,1)$ and $\Delta = \frac{1-a-c}{2}$ by the concavity (Jensen's inequality [4]) of $\frac{1}{x}$. Therefore $H(x) - G(x,\Delta)$ where $\Delta = \frac{1-a-c}{2}$ has its minimum for $x \in (0,1)$ at $x = 0.5$ and therefore $IT_{RS} \leq IT_{CS}$ (and equality only when $c = 1-a$ at the optimal crossing point). That is more information is transferred in the single step system using the standard R/L control method and consistent start D/S method than the random start D/S method. Note that by symmetry, the direction of the start does not matter; it just matters that it always starts in the same direction.

Following the results of [2] showing that in the multi-step case, an interactive D/S control method is preferable to the standard R/L control method for improved ITR in the presence of noise, the one-step result showing that the consistent start D/S control (equivalent to R/L control on the first step) is better than the random start D/S control might be somewhat surprising, but the reason for improved performance of interactive commands in the multi-step D/S systems is because the user is responding to the computer's classification error. However in the one-step systems, the user response is to a randomly generated direction, not the result of the computer's interpretation of the user's command, and so does not provide the benefit of revealing the computer's bias.

As the first step in a multi-step system (NCP>3) is equivalent to a one-step system we conclude that for multi-step systems it is also better to start with a consistent direction. For reasons discussed below, we will consider the start direction to be left. This new suggested control strategy is shown in Figure 8. The ITR curves computed from the Markov chain analysis [2] for chains with NCP=7 are shown in Figure 7. The plots show that there is an ITR benefit to having a consistent start direction, though the effect is less with the models with more NCPs as should be expected with a change that only changes the first step. The difference is larger on the side when "continue" is more likely to be output (on the right side of the figure) as that is when fewer steps are taken, and an effect from the first step will have a greater effect.

DISCUSSION

While for systems with larger NCPs the ITR difference is not large between the random-start and same-start D/S systems, there are also other human factors considerations. When the original D/S control method was introduced, there was a concern that the control system would require more time for the user to process each step as they would need time to determine whether to give a "change" or "continue" command [2]. Thinking about each step compared to constantly generating a "right" or "left" command requires more processing and is less automatic. However, starting the cursor movement in the same direction allows the user responses to be more automatic. For instance if the user knows that the cursor will always start moving left and the change direction command is given by right hand motor imagery, then for right targets, the user will start with right motor imagery and will continue right im-

  Published by Verlag der TU Graz
Graz University of Technology

 DOI: 10.3217/978-3-85125-533-1-23

agery until the cursor changes direction at which point they will switch to left hand motor imagery (see Figure 9). In this way, the user feels like they are pushing the cursor (moving the hand that the cursor is moving away from). If the subject desires the left target, he will start with left motor imagery and again only change imagery when the cursor changes direction. In this mode (left target), the user feels like they are trying to bat the target back and forth (moving the hand that the cursor is moving towards). The user does not need to think about which hand is continue or change direction, they simply have to start with the motor imagery of the hand in the desired direction (e.g. left hand imagery for left target) and change whenever the cursor changes direction.

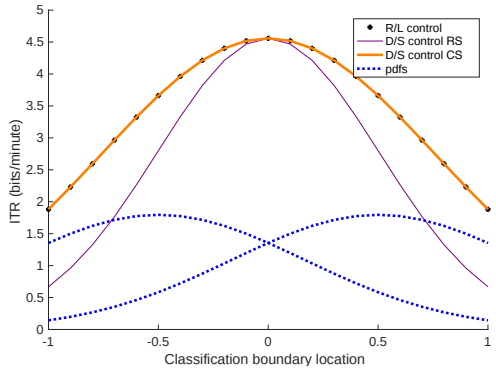

Figure 6: This figure shows the probability distributions for two classes and the information transfer rate for the R/L and D/S (random start (RS) and left/consistent start (CS)) control methods with NCP=3 (the one-step systems). Note the R/L and D/S left start curves are on top of each other.

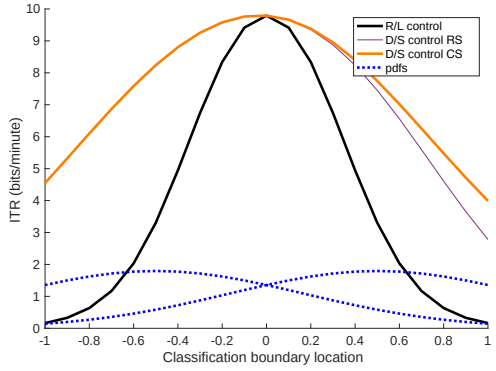

Figure 7: This figure shows the probability distributions for two classes and the information transfer rate for the R/L and D/S (random start (RS) and left/consistent start (CS)) control methods with NCP=7. The orange curve shows the results with D/S control with consistent left-moving start. The thin purple line, gives the result for D/S control with random start direction, and the thick black line shows the result using the standard R/L paradigm.

The idea behind the interactive communication method is to allow a user to compensate for inaccuracies or biases in the classification boundary that are inevitable with noisy and non-stationary systems. This is similar to the idea used in [11] where Wolpaw and colleagues required users to activate two commands on opposite sides of a possibly biased classification boundary. Notice in the multi-step D/S control method, the forces pushing the cursor in each direction are caused by transitions from each side of the classification boundary (e.g. a and d cause transitions in the same direction as do b and c in Figures 2, 3, and 8.)

It is also similar to the way that humans naturally change to a more interactive style when giving directions to a non-native speaker. If the person does not understand, we don't repeat the same sentences but attempt to give the same instructions with different words. We also monitor understanding and change our directions to react to their understanding. Some HCI systems have a feature like this; when performing a risky computer operation that may have been incorrectly activated (e.g. delete a file), the interface does not ask you to press the same button that was originally (possibly mistakenly pressed), but to respond to "Are you sure? (Yes/No)."

There are other practical advantages to the D/S control system for many modalities of signal generation. In EEG, for example, emotional, error, and frustration, responses are combined with any signal the user is actively trying to generate. Frustration with loss of control has been shown to induce non-stationarity in EEG [3]. It has been shown that some of these signals are in the same frequency bands as the signals to be actively detected and are difficult to separate [6]. By using the D/S control method, these unconscious signals actually add to the discriminability of the signals rather than subtracting from them. This may also be true in gesture-based systems where a person who is happy with the progress may make more animated, or otherwise somewhat different, moves than when unhappy. Similarly in speech-based systems, affect is generally reflected in people's speech signals.

We see this work as important for considering the human and computer as cooperative agents. While the human may be limited by the discriminability of the signals they can generate and the computer is limited in its ability to learn the best classification boundary (given finite data), the two together can have greater information transfer (from human to computer) by changing the semantics of the signals the human generates.

CONCLUSIONS

To conclude, we have analyzed the first step and revealed that the direct R/L control is better for this first step (where the feedback is random and can't provide the computer's interpretation of the user's signal). Through incorporation of this knowledge to restrict the intial cursor direction in a D/S system, we have further improved the information transfer rate of the D/S interactive control method over the standard direct R/L control method. At the same time, this change reduces the real-time processing requirements of the user and reduces the task to a more reactive task requiring less conscious effort. The change in how the first step is handled maintains the other advantage of the D/S in-

Published by Verlag der TU Graz
Graz University of Technology

 DOI: 10.3217/978-3-85125-533-1-23

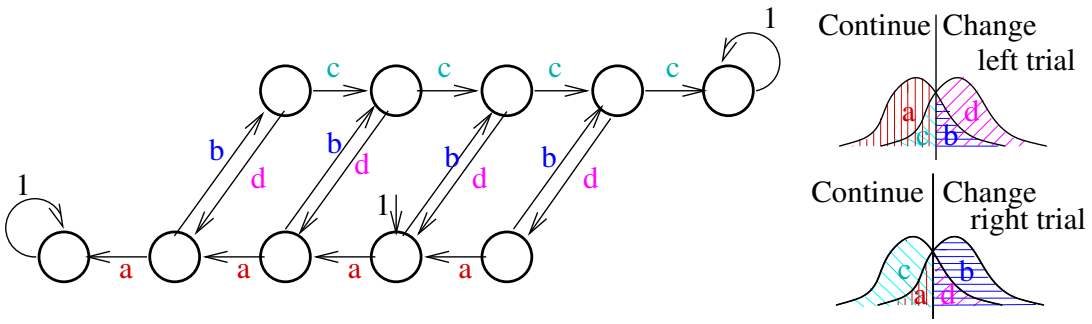

Figure 8: This Figure shows the Markov chain model for the new proposed D/S control method with constant left start direction.

teractive control strategy: changes in emotion/frustration help the classification instead of distracting from it.

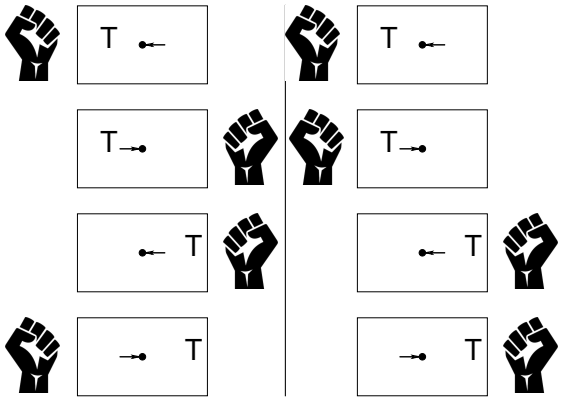

Figure 9: This figure shows the commands a user would use after specific cursor movements with the D/S control method (LEFT) and R/L control method (RIGHT). The hand icon on the right/left side of the drawn screen represents right/left-hand motor imagery. The T represents the desired target location/direction and the arrow represents the direction of the last cursor movement. Note that with the D/S control the user changes command when the cursor changes direction and that right hand targets can be viewed/felt as the user performing a pushing behavior giving the imagery of the hand that the cursor is moving away from (as if to push it away). When the user desires the left hand target, the user performs a batting back and forth behavior where they perform imagery of the hand that the cursor is moving towards (as if to bat it back).

ACKNOWLEDGMENTS

This work is supported by NSF grants IIS 1219200, SMA 1041755, IIS 1528214, and UCSD FISP G2171.

REFERENCES

[1] B. Blankertz, R. Tomioka, S. Lemm, M. Kawanabe, and K.-R. Muller. Optimizing spatial filters for robust EEG single-trial analysis. *Signal Processing Magazine, IEEE*, 25(1):41–56, 2008.

[2] V. de Sa. An interactive control strategy is more robust to non-optimal classification boundaries. In *Proceedings of ICMI'12*, pages 579–586, 2012.

[3] S. Jatzev, T. Zander, M. DeFlilippis, C. Kothe, S. Welke, and M. Roetting. Examining causes for non-stationarities: The loss of controllability is a factor which induces non-stationarities. In *In Proc. of the 4th Int. BCI Workshop & Training Course*. Graz University of Technology Publishing House, 2008.

[4] J. Jensen. Sur les fonctions convexes et les inegalites entre les valeurs moyennes. *Acta Mathematica*, 30:175–193, 1906.

[5] A. Kübler, N. Neumann, J. Kaiser, B. Kotchoubey, T. Hinterberger, and N. P. Birbaumer. Brain-computer communication: self-regulation of slow cortical potentials for verbal communication. *Archives of physical medicine and rehabilitation*, 82(11):1533–1539, 2001.

[6] M. Mousavi, A. S. Koerner, Q. Zhang, E. Noh, and V. R. de Sa. Improving motor imagery BCI with user response to feedback. *Brain-Computer Interfaces*, 2017.

[7] J. Müller-Gerking, G. Pfurtscheller, and H. Flyvbjerg. Designing optimal spatial filters for single-trial EEG classification in a movement task. *J Clin Neurophysiol*, 110(5):787–98, May 1999.

[8] E. Noh and V. de Sa. Discriminative dimensionality reduction for analyzing EEG data. In *Proceedings of the 36th Annual Meeting of the Cognitive Science Society*, pages 1090–1095, 2014.

[9] G. Pfurtscheller, C. Brunner, A. Schlögl, and F. L. da Silva. Mu rhythm (de)synchonization and EEG single-trial classification of different motor imagery tasks. *Neuroimage*, 31:153–159, 2006.

[10] P. Shenoy, M. Krauledat, B. Blankertz, R. Rao, and K.-R. Müller. Towards adaptive classification for BCI. *J Neural Eng*, 3:R13–R23, 2006.

[11] J. R. Wolpaw, H. Ramoser, D. J. McFarland, and G. Pfurtscheller. EEG-based communication: improved accuracy by response verification. *IEEE transactions on Rehabilitation Engineering*, 6(3):326–333, 1998.

Published by Verlag der TU Graz
Graz University of Technology

Proceedings of the
7th Graz Brain-Computer Interface Conference 2017 DOI: 10.3217/978-3-85125-533-1-24

TOWARDS A NON-INVASIVE SYSTEM FOR TRANS-HUMERAL AMPUTEE MOTION RESTORATION

J. Fernandez-Vargas[1], K. Kita[1,2] and W. Yu[1,2]

[1] Graduate School of Engineering, Chiba University, Chiba, Japan
[2] Center for Frontier Medical Engineering, Chiba University, Chiba, Japan

E-mail: jacobofv@chiba-u.jp

ABSTRACT: There are very few studies that try to solve the motion reconstruction problem, and those few studies focused on rehabilitation of amputee patients. In this paper, we will discuss the major problems in the field and propose possible solutions for them using a rehabilitation perspective considering long-term, real-world applications. In addition, we performed a preliminary study with five subjects using electroencephalography and electromyography, a virtual avatar to obtain the position of the hand, and a set of motions containing a wide range of motions. Among the participants, we obtained a mean correlation value between the real and reconstructed motion that was equal to 0.834. This result exceeds the average in the field, suggesting that our solutions are appropriate to solve the current problems.

INTRODUCTION

Brain Computer Interfaces (BCI) have been used for amputee rehabilitation for many years. It has been especially useful for motion reconstruction problems. Motion reconstruction is the problem of reconstructing or predicting the dynamics of an extremity using bio-signals. Motion reconstruction is important for motion analysis and motor function assessment. In the case of amputees, motion reconstruction can be used to build a prosthetic device that substitutes the original limb using intuitive motions. The motion reconstruction problem can be classified by the extremity reconstructed by the system. In general, the distal part of the extremity (hand or foot) is comparatively easier to reconstruct than the proximally amputated part (arm or leg), because most of the motion related muscles are still present in the distal amputation. This makes it possible to use electromyography (EMG) signals for the reconstruction. There is also a large difference between reconstructing upper limb or lower limb movements. In the case of the leg, the dynamics are well known, and the prostheses are simpler since they reconstruct fewer degrees of freedom. For these reasons, motion reconstruction of the proximally amputated upper limb is the most complex reconstruction. There are two different types of upper limb proximal amputations: trans-humeral and shoulder disarticulation. We focused our study on trans-humeral amputations that, by definition, demonstrate conservation of the *deltoidus* muscle. A full prosthesis is needed to reconstruct every degree of freedom in the arm, including the elbow, wrist, and fingers. Since the shoulder has a few motion-related muscles that help control the hand, it is not possible to reconstruct the hand's position using only EMG. Thus, BCI is also needed. Concerning the aforementioned limitations, we need to add the limitations that are produced from using the system for rehabilitation. For instance, the system must be able to work in real time, including preprocessing of bio-signals. Also, the accuracy required to build a prosthetic device that is needed for daily life is higher than the accuracy required for normal applications.

Due to the complexity of the task, a simplification is used most of the time. Most commonly, only the position of the hand is reconstructed [1], [2]. We used this simplification as well in this study. Most of the studies that try to solve this problem use a neuroscientific approach, i.e., the main purpose is to determine the brain's function during motion execution using electroencephalography (EEG). For this reason, we considered it necessary to create a roadmap regarding the problems and the challenges that we must confront to solve it, always keeping in mind the rehabilitation perspective.

In this paper, we present the major problems that the motion reconstruction field faces when applied to rehabilitation, providing possible solutions that can be applied to real-world environments. We divided the system into six parts that are necessary to implement a rehabilitation system. These parts are very similar to those that compose any BCI system. For each part, we provide our analysis of how important the changes are to make the technology available under real-world conditions for trans-humeral amputees.

1. Acquisition system: which signals are used as input for the predictor. The changes needed are not important.
2. Training signal: which signal is used as output for the predictor. The changes needed are critical.
3. Evaluation: the fitness value used for evaluating the system. The changes needed are of high importance.
4. Task: which motion is performed during the training session. The changes needed are of medium importance.
5. Preprocessing: the filters and transformations applied to the signals and the features extracted from them. There are no changes needed.
6. Predictor: the architecture used for reconstructing the signal. There are no changes needed.

Published by Verlag der TU Graz
Graz University of Technology

 DOI: 10.3217/978-3-85125-533-1-24

We excluded from our analysis the preprocessing and the predictor parts for two reasons. First, both parts are too complex to analyse in just one paper, even individually. The second and more important reason, is that they do not present problems as important as the other parts. Furthermore, these two parts have been revised the most in the literature.

In addition, we performed an experiment implementing the proposed solutions for the acquisition system, the training system, and the task. The preliminary results are presented and discussed to analyse each one of the parts.

MATERALS AND METHODS

In each subsection, we present one of the mentioned parts along with our proposed solution and their implementation.

Subjects

Five healthy right-handed subjects (3 males, 2 females, mean age 28, range 22-40) participated in the experiment. Permission from the Ethics Committee of the Graduate School of Engineering, Chiba University was obtained. All subjects participated voluntarily and gave informed consent without receiving any incentives. Participants were informed that they could stop the experiment at any time.

Acquisition Systems

The first decision we made was which system we used for acquiring the data. When applied to prosthetics, there are two main constraints: the system must be non-invasive and it must be portable. The most common solution, taking into consideration the constraints, is to use EEG. The use of EEG itself does not present a problem. In the BCI community, it is considered one of the best non-invasive methods to read brain signals. Additionally, near-infrared spectroscopy is becoming more common in BCI studies due to its higher spatial resolution and robustness against artefacts [3]. The major drawback of this technology is the lower resolution time compared to that of EEG. Both technologies can be used together to complement each other [4]. Nevertheless, EEG has rarely been combined with other technologies in motion reconstruction studies. Usually, EMG is not used for motion reconstruction. In the cases that used EMG [5], the goal was to control wearable systems and the electrodes were positioned all along the arm to get better results. In the case of trans-humeral amputees, this would be impossible. Nonetheless, EMG provides a signal highly correlated with motion, is more localised than EEG, and is also less noisy. We also recognise that both systems complement each other.

In our experiment, we used an EEG cap (BioSemi ActiveTwo) with 16 active electrodes at 2048 Hz. We decided to place the electrodes in an asymmetric setup to better cover the contralateral motor area. The locations for the electrodes were Fz, F2, F4, FC2, FC4, FC6, Cz, C2, C4, C6, CPz, CP6, Pz, and P2. We covered a wide area since there is no consensus regarding which areas (other than the motor area) contribute to reconstruction of motion [1], [6]–[9].

In addition, we included four surface EMG electrodes (Delsys Trigno Wireless EMG) with a sample rate of 2000 Hz. We placed two on the *trapezius*, one on the *deltoidus*, and one on the *pectoralis major*. The locations were identical to our previous study [9]. We placed the electrodes in the shoulder area to consider the rehabilitation goals.

Training Signal

To train the systems, we paired the acquired bio-signals with the desired position of the hand. Most studies use a motion tracking system. Motion tracking systems use cameras to detect the position of the hand by using, for example, reflective devices. This kind of system tracks the position of the subject's hand precisely in a 3D space. However, this approach cannot be used with amputee patients since there is no hand to track.

There are two possible solutions: either use a virtual avatar, i.e. the subject looks at a virtual avatar moving the arm while he/she repeats the motion; or use a surrogate system in which the motion tracking device is placed in the trainer's hand and the subject repeats the motion of the trainer.

We decided to use the first approach, since this method confirms that the motion is always the same, since the position data comes from a virtual avatar that has a predefined motion compared to a human that may slightly vary the position for each iteration. In addition, implementing a system such as this would be easier, since there is no need for a specialized trainer and it can be used whenever the subject wants. The drawback of this approach is that it adds inherent error, because the position of the avatar and the real position cannot be the same. Thus, the subject's motion cannot achieve a perfect correlation with the avatar's motion.

Task

Regarding which motion the subject should perform to train the system, there was little discussion as it is not considered an important part of the experimental design. The most common task used is the centre-out motion, which consists of moving the hand between a centre position to a set of surrounding positions, because it is easy to perform for the subject and has been used in neuroscience experiments for many years. We considered that these motions were not the best for a rehabilitation approach, so we decided to create a new set of motions. We thought that the motions should cover two aspects: wide variation of motions and *useful* motions that are required for daily life.

Considering this, we included six motions in our training set. The first three were generic motions that covered motions in both shoulder and elbow joints. They included shoulder flexion-extension, shoulder abduction-adduction and elbow flexion-extension. The other three motions included reaching motions at three different positions: right middle height, centre upper height, and left lower height. In our experiment, the motion was

Published by Verlag der TU Graz
Graz University of Technology

 DOI: 10.3217/978-3-85125-533-1-24

performed with the left arm.
For each motion, there were two phases: training and execution. During the training phase, the subjects could watch an animation as many times as they wanted. They could change the perspective freely to obtain a clear view of the motion. Also, they were asked to practice the motion and not only to watch the motion. The execution phase started when the subjects indicated that they were ready. During this phase, they had to perform the trained motion 10 times. They could also start each of the 10 repetitions by pressing a button on a handheld controller.

Preprocessing

During EEG recordings, movement of muscles can generate noise in the electrodes [10]. If the preprocessing is not performed correctly, this can result in poor results. Here, we have decided not to discuss this issue.
In this experiment, the EEG signal was divided into windows of 1 s with 93.75% overlap. This resulted in 16 different windows per second. Then we downsampled the signal to 10 Hz, using each of the points as a feature. This is similar to a process proposed by Bradberry et al. [1] and followed by Ofner et al. [2]. There is, however, discrepancy in the field about the validity of this method. The main argument against it is that the arm motion creates artefacts in the low frequency band, and the system uses those artefacts for reconstruction and not EEG data [10]. Still, there is an important argument against this statement. In every study that has analysed the relevance of each electrode for reconstruction, those located in the contralateral area have shown (especially in the motor area) better results. If the artefacts from the arm movements were so strong (or important for the reconstruction), a larger effect would be shown on the lateral area (since it is closer to the source of the artefact) or a uniform distribution over the scalp would be observed (compared to a more focused distribution on the motor cortex area). Nevertheless, these concerns are important and should be addressed in depth.
For EMG, we also divided the signal in 1 s windows with 93.75% overlap. Then, we calculated seven features from the time domain. The seven features were integrated EMG, modified mean absolute value 2, mean absolute value slope, simple square integral, zero crossing, slope sign change, and Wilson amplitude. For more information regarding the features, please refer to Phinyomark et al. [11] Please also see Fernandez-Vargas et al., [9] in which we provide an analysis on why these features were selected with additional information about them. Finally, for calculating the output for each window, we took the mean for each of the three position coordinates (x, y, and z) used a sliding window of 0.0625 s (1/16 s) without overlapping. This position corresponded to the avatar's hand and was acquired at a variable rate of ~60 Hz.

Predictor

Excluding the preprocessing, the predictor is probably the component with the highest variability across studies. The most common predictor is the linear regression [1], [2], [12], [13]. This predictor creates a linear regression model using features of EEG as input and the position of the hand as output. One of the advantages of this method is that it is easy to interpret the results. Other options include the particle filter model [12], the kernel ridge regression method [13], or artificial neural networks [9]. For this study, we decided to use the linear regression approach for the EEG data because of its wide use, simplicity, and overall accuracy. For the EMG data, an artificial neural network was selected as previously published [9]. Then, the result of both predictors was used as input for a second linear regression. Additionally, to this second linear regression we used the previous two reconstructed points as input, and we refer to these two points in this report as temporal data.

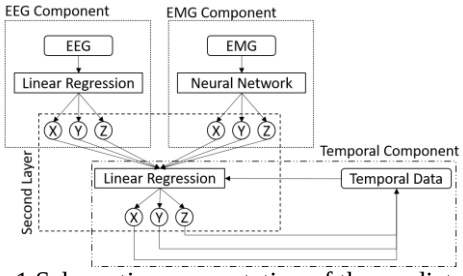

Figure 1 Schematic representation of the predictor. Each component is marked with a rectangular shape to indicate the data that belong to that component.

With this configuration, we divided the predictor into four different components: EEG, EMG, second layer, and temporal. EEG and EMG components correspond to the predictors that used only the EEG and EMG data, respectively. The second layer is the predictor that used the output of both previous components as input. Finally, the temporal component uses the previously reconstructed points. The actual predictor, represented in Figure **1**, uses as input for the second layer the output of the EEG component, the EMG component, and the temporal data at the same time. Nonetheless, the *second layer* term refers to the result obtained when using only the data from the EEG and EMG components, whereas the "temporal" term refers to the result when the temporal data was added.

Evaluation

In each study, the correlation value (CV) between the real position and the reconstructed position was used as the fitness value. In general, this approach is well accepted, despite its possible problems.
The main problem is that the CV is calculated only with data obtained during the training session. Even if the task contains a wide range of motions, those motions will be repeated several times. Thus, the training, test, and validation sets will be similar, which could result in a lack of generalisation of the system. This is usually intended since, in general, we want to train the system with data that is similar to the data that we are going to use in the future. However, in this specific case, the problem is that the set of motions that the arm can perform is too large to train them all. If we were to use those systems in a real environment, the result would be

Published by Verlag der TU Graz
Graz University of Technology

 DOI: 10.3217/978-3-85125-533-1-24

worse than what we would expect by only considering the CV. In brief, any system excels at reconstructing motions similar to those that were used for training it. However, we cannot know how the system behaves with radically different movements. Since we cannot train the system with all possible arm motions, we need to calculate the quality of the system when presented with unexpected motions.

As a solution, we propose to use a time related feature, which can be calculated after training the system. For example, the subject uses the trained system to move a virtual avatar or prosthetic device to perform a set of motions different from those included in the training task. The time to complete those motions would be used as the fitness value. Unfortunately, we were not able to implement this approach in our study; consequently, we used the CV as the fitness value.

For training the system, we used a 10-fold leave-one-out cross validation procedure, and 9 out of the 10 repetitions of each motion then used the remaining motion as validation. This process was repeated 10 times, rotating which repetition was left for validation. The final CV was calculated as the mean of the obtained CV for each repetition.

RESULTS

Table 1 shows the results obtained during the experiment for every component of the system. In addition, we performed a permutation test to calculate the chance level, i.e., we calculated the obtained CV for the EEG component using random EEG data from the motion task. As a result, we obtained a CV <0.001.

In three cases, the EMG component obtained better results than the EEG component. Nonetheless, in every case, the second layer was better than any of the other two components. In addition, the temporal component was also always better than the second layer.

The correlations between the second layer and each component were EMG-second layer 0.905, *p-value* 0.035; EEG-second layer -0.75, *p-value* 0.145; temporal-second layer 0.687, *p-value* 0.2.

Finally, Figure 2 presents the reconstruction of the system for subject #3. Note that the CV for this reconstruction was 0.789, which was below the mean CV for subject #3. As was explained before, the mean CV for every subject was obtained through a 10-fold validation process. This means that there were 10 different reconstructions with slightly different CVs among them.

Table 1 Component CV and the mean CV of all subjects.

#	*EMG*	*EEG*	*2nd Layer*	*Temporal*
1	0.672	0.584	0.747	0.870
2	0.125	0.676	0.679	0.810
3	0.350	0.693	0.716	0.794
4	0.784	0.576	0.811	0.856
5	0.621	0.586	0.732	0.838
Mean	***0.510***	***0.623***	***0.737***	***0.834***

DISCUSSION

Acquisition System

The results obtained in this study show that the combined use of EEG and EMG provides an improved result in terms of CV compared to using only one of the systems. This also indicates that EEG and EMG contain different information regarding the position of the hand. Notably, the variation of the CV of the EMG component is much larger than the CV of the EEG component. This suggests that the EEG component is more robust than the EMG component. This result is counterintuitive, since EEGs signal are noisier than EMG signals. In addition to the fact that the overall CV appears to correlate with EMG accuracy, it would be very important to study the reason for this. Also, results obtained in this study using only the EEG component are above average in the field, even using only 16 electrodes compared to the common 32-64 used in most studies.

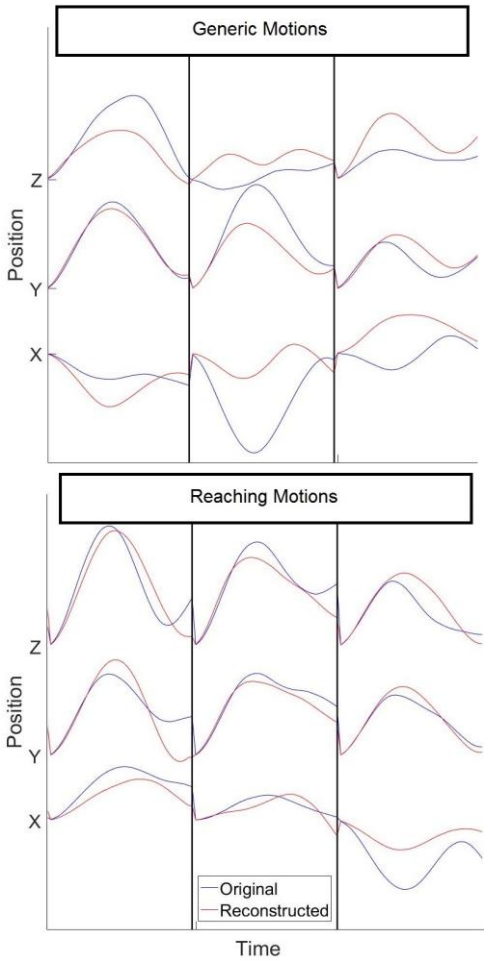

Figure 2 Motion reconstructed from subject #3. Each line corresponds to one dimension. The position has no real-world dimensions since it corresponds to the position of the avatar's hand in the virtual world. The vertical thick lines divide each one of the six reconstructed motions that correspond to the motion described in the subsection "Task".

Published by Verlag der TU Graz
Graz University of Technology

 DOI: 10.3217/978-3-85125-533-1-24

Table 2 Problems and solutions summary

Section	Common Approach	Disadvantages	Importance	Proposed Solution	Expected Impact	Implemented
Acquisition System	Only EEG	Noisy signal, difficult to analyse	Low	Adding EMG and temporal data	Great accuracy improvement	Yes
Training Signal	Motion Tracking	Cannot be used by amputees	Critical	Using virtual avatar	Accuracy decrease	Yes
Evaluation	CV	May not represent the system's real accuracy	High	Post-training measurement	Better system evaluation	No
Task	Centre out movement	Is not a daily life movement	Medium	Using general and reaching movements	More general predictor	Yes

This means that placing the electrodes on the contralateral motor area provides results that are similar to using more electrodes over the whole scalp. This result suggests that it possible to create cheaper systems for real-world applications. An additional advantage of using fewer numbers of electrodes is that the preparation time is shorter.

Training signal

The most important solution that we implemented is the use of the virtual avatar for recording the training signal.

The results obtained from the EEG component in this study are similar to those obtained in [1], [2], [6], [12], [13]. In addition, compared with our previously published results [9], the temporal component had a better result. Nonetheless, with these preliminary results, we do not have enough evidence to properly compare with other studies. We will perform more experiments to make a proper comparison in the future.

Task

We consider that the reaching motions are the most important motions that the system should be able to reconstruct, because those motions are the most useful for amputee patients. Figure 2 shows that the reconstructions for reaching motions are more accurate than the reconstructions for the generic motions. Thus, if we only consider the accuracy of the reaching motions, the selected task is appropriate for the problem. Nonetheless, we should investigate what effect the different training sets have on the overall and specific accuracies.

Predictor

Table 1 shows that adding more layers to the predictor and temporal data increases the accuracy in every case. In short, more complex predictors increase the CV. In our opinion, the predictor should be even more complex, with different parts predicting specific movement components. As an example, Figure 2 shows that the motion for the shoulder abduction-adduction has the biggest error, especially in the "*x*" dimension. To improve the accuracy of the system, we could add an additional layer that classifies the motion into subgroups. Then, once we know the subtype of motion, we could use the EEG and EMG data as input for different specific predictors. This could also be useful if we want to reconstruct wrist motions without moving other parts of the arm.

CONCLUSION

We identified four problems that the motion reconstruction field faces from the rehabilitation perspective (Table 2). Out of the four problems, we implemented a solution for three of them and obtained preliminary results that suggest that these are valid solutions, especially for the training signal and the acquisition system. However, there are still many problems to solve. We consider the problem of the evaluation method to be one of the most important problems that the field is currently facing.

REFERENCES

[1] T. J. Bradberry, R. J. Gentili, and J. L. Contreras-Vidal, "Reconstructing three-dimensional hand movements from noninvasive electroencephalographic signals.," *J. Neurosci.*, vol. 30, no. 9, pp. 3432–7, 2010.

[2] P. Ofner and G. R. Muller-Putz, "Decoding of velocities and positions of 3D arm movement from EEG," *Proc. Annu. Int. Conf. IEEE Eng. Med. Biol. Soc. EMBS*, pp. 6406–6409, Aug. 2012.

[3] S. Coyle, T. Ward, C. Markham, and G. McDarby, "On the suitability of near-infrared (NIR) systems for next-generation brain–computer interfaces," *Physiol. Meas.*, vol. 25, no. 4, pp. 815–822, Aug. 2004.

[4] V. Kaiser *et al.*, "Cortical effects of user

Published by Verlag der TU Graz
Graz University of Technology

 DOI: 10.3217/978-3-85125-533-1-24

training in a motor imagery based brain–computer interface measured by fNIRS and EEG," *Neuroimage*, vol. 85, pp. 432–444, 2014.

[5] K. Kiguchi and Y. Hayashi, "Motion Estimation Based on EMG and EEG Signals to Control Wearable Robots," *2013 IEEE Int. Conf. Syst. Man, Cybern.*, pp. 4213–4218, 2013.

[6] J. Lv, Y. Li, and Z. Gu, "Decoding hand movement velocity from electroencephalogram signals during a drawing task," *Biomed. Eng. Online*, vol. 9:64, 2010.

[7] J.-M. Schoffelen, J. Poort, R. Oostenveld, and P. Fries, "Selective movement preparation is subserved by selective increases in corticomuscular gamma-band coherence," *J. Neurosci.*, vol. 31, no. 18, pp. 6750–6758, 2011.

[8] S. Waldert *et al.*, "Hand movement direction decoded from MEG and EEG," *J. Neurosci.*, vol. 28, no. 4, pp. 1000–1008, 2008.

[9] J. Fernandez-Vargas, K. Kita, and W. Yu, "Real-time Hand Motion Reconstruction System for Trans-Humeral Amputees Using EEG and EMG," *Front. Robot. AI*, vol. 3, no. August, p. 50, 2016.

[10] T. Castermans, M. Duvinage, G. Cheron, and T. Dutoit, "About the cortical origin of the low-delta and high-gamma rhythms observed in EEG signals during treadmill walking," 2014.

[11] A. Phinyomark, S. Hirunviriya, C. Limsakul, and P. Phukpattaranont, "Evaluation of EMG feature extraction for hand movement recognition based on Euclidean distance and standard deviation," *Electr. Eng. Comput. Telecommun. Inf. Technol. (ECTI-CON), 2010 Int. Conf.*, pp. 856–860, 2010.

[12] J. Zhang, J. Wei, B. Wang, J. Hong, and J. Wang, "Nonlinear EEG decoding based on a particle filter model.," *Biomed Res. Int.*, vol. 2014, p. 159486, 2014.

[13] J.-H. Kim, F. Bieβmann, and S.-W. Lee, "Reconstruction of hand movements from EEG signals based on non-linear regression," in *2014 International Winter Workshop on Brain-Computer Interface (BCI)*, 2014, pp. 1–3.

Published by Verlag der TU Graz
Graz University of Technology

Proceedings of the
7th Graz Brain-Computer Interface Conference 2017 DOI: 10.3217/978-3-85125-533-1-25

BAYESIAN REGRESSION FOR ARTIFACT CORRECTION IN ELECTROENCEPHALOGRAPHY

Karl-Heinz Fiebig[1], Vinay Jayaram[3], Thomas Hesse[2], Alexander Blank[1], Jan Peters[1,3], Moritz Grosse-Wentrup[3]

[1]Autonomous Systems Labs, Technische Universität Darmstadt, Darmstadt, Germany
[2]Institute for Mechatronic Systems in Mechanical Engineering, Technische Universität Darmstadt, Darmstadt, Germany
[3]Department Empirical Inference, Max Planck Institute for Intelligent Systems, Tübingen, Germany

E-mail: karl-heinz.fiebig@stud.tu-darmstadt.de

ABSTRACT: Many brain-computer interfaces (BCIs) measure brain activity using electroencephalography (EEG). Unfortunately, EEG is highly sensitive to artifacts originating from non-neural sources, requiring procedures to remove the artifactual contamination from the signal. This work presents a probabilistic interpretation for artifact correction that unifies session transfer of linear models and calibration to upcoming sessions. A linear artifact correction model is derived within a Bayesian multi-task learning (MTL) framework, which captures influences of artifact sources on EEG channels across different sessions to correct for artifacts in new sessions or calibrate with session-specific data. The new model was evaluated with a cross-correlation analysis on a real world EEG data set. We show that the new model matches state-of-the-art correlation reduction abilities, but ultimately converges to a simple group mean model for the experimental data set. This observation leaves the proposed MTL approach open for a more detailed investigations of artifact tasks.

INTRODUCTION

As opposed to artifact-computer interfaces, a brain-computer interface (BCI) relies on decoding signals of neural origin. Unfortunately, electroencephalography (EEG) based BCIs are very prone to contamination with non-neural noise sources. On the one hand, such artifacts may deteriorate the signal-to-noise ratio and decrease BCI performance. On the other hand, the performance may misleadingly increase due to exploitation of artifact patterns in the learning process. Hence, reducing the effect of artifacts is a key requirement for BCIs in order to reliably decode brain activity from EEG signals.

Many successful techniques to enhance the signal-to-noise ratio in EEG signals have been proposed for BCIs over the last decades. However, advanced methods like beamforming [1], Independent Component Analysis [8] or Common Spatial Patterns [2] often require manual selection of components by an expert for optimal performance. While hybrid approaches have been reported to work well [9], computing filters in the first place is also prone to noise and may miss signals of interest in favor of artifacts. It may therefore be advantageous to correct the signal from known artifact sources before applying further techniques. A popular method is the correction of electrooculographic (EOG) artifacts caused by eye movements and blinks using linear regression. This technique aims to learn the influence of EOG electrodes on EEG and subtracts EOG artifacts from the EEG signals. Note that EOG electrodes may accidentally capture brain activity from the frontal area, which is then unwantedly removed in the process. Influence coefficients are usually determined by regressing the observed EEG signal [10, 11, 12]. It has been found that averaging over coefficients from different signal segments, trials or subjects may increase performance of the artifact correction [13, 14]. However, approaches based on calibration data from the upcoming session or time based re-calculation of the coefficients were also suggested [3, 15]. These findings motivate a common framework in order to exploit stability of transfer models while still retaining the ability to calibrate regression models with new data.

In this work, a theoretical framework is presented that unifies the combination of influence coefficients from different sessions and the adaptation with new artifacts. The artifact correction problem is put into a probabilistic interpretation and approached within a Bayesian multi-task learning (MTL) framework that is already used to decode brain activity [4, 5, 16]. The presented algorithm is able to learn a matrix Gaussian prior distribution over artifact influences from different signal segments, sessions and subjects. The trained prior can be either used to directly correct artifacts in new sessions or be calibrated with new artifacts.

The remainder of this paper is organized as follows. The method section introduces a probabilistic interpretation for artifact correction and restates the problem with an equivalent formulation in order to derive a closed form solution. It is then shown how the new model can be immediately used for artifact correction and later on adapted with calibration data. Afterwards, the experimental setup

Published by Verlag der TU Graz
Graz University of Technology

 DOI: 10.3217/978-3-85125-533-1-25

and the evaluation of the new model against current artifact regression models is described. The results section shows that the new model operates on lower correlation levels in comparison with other models. However, the MTL algorithm is found to train a simple group mean over influence coefficients for the artifacts in the data set. Finally, this paper elaborates on the results with a discussion and concludes with a short summary and future work on the proposed framework.

METHODS

In this paper, scalars are denoted with lowercase, vectors with bold lowercase, matrices with upper case and sets with calligraphic uppercase letters.

Probabilistic Artifact Regression: In accordance with the literature, we assume that an EEG measurement sample $\boldsymbol{y} \in \mathbb{R}^k$ from k channels can be modeled with $\boldsymbol{y} = \boldsymbol{s} + W\boldsymbol{n}$, where $\boldsymbol{s} \in \mathbb{R}^k$ are the EEG signals, $\boldsymbol{n} \in \mathbb{R}^m$ are the artifact sources as measured by m artifact channels and $W \in \mathbb{R}^{k\times m}$ is the weighting matrix. W explains the influence of the m artifact sources on each of the k EEG channels. However, the signal that is observed at the recording sites is additionally contaminated by noise contributions arising from other sources that we do not keep track of. We therefore extend the model to $\boldsymbol{y} = \boldsymbol{s} + W\boldsymbol{n} + \boldsymbol{\varepsilon}$, where $\boldsymbol{\varepsilon} \in \mathbb{R}^k$ represents the signal contribution from other noise. This model can be put into a probabilistic relation by assuming that the noise is distributed according to a zero-mean Gaussian $\boldsymbol{\varepsilon} \sim \mathcal{N}\left(\mathbf{0}, \sigma^2 I_k\right)$ with some variance σ^2, where $I_k \in \mathbb{R}^{k\times k}$ denotes the identity matrix in k dimensions. An observed EEG sample $\boldsymbol{y}$ is then drawn from a Gaussian distribution

$$\boldsymbol{y} \sim \mathcal{N}\left(\boldsymbol{s} + W\boldsymbol{n}, \sigma^2 I_k\right), \tag{1}$$

centered at the linear model output and deviating according to some noise encoded in σ^2.

Multi-task Learning with Artifacts: The weight matrix W is usually determined by linear regression on an artifactual data set in order to find the influences of artifact sources on EEG channels. However, these influences may vary across subjects, sessions and trials. We therefore regard the regression problem for an artifact as an individual task and denote the gathered data set of q tasks with $\mathcal{T} = \left\{\mathcal{D}^{(t)}\right\}_{t=1}^{q}$. Each task data set $\mathcal{D}^{(t)} \in \mathcal{T}$ takes the form

$$\mathcal{D}^{(t)} = \left\{\left(\boldsymbol{n}_i^{(t)}, \boldsymbol{y}_i^{(t)}\right)\right\}_{i=1}^{n_t} \subset \mathbb{R}^m \times \mathbb{R}^k \tag{2}$$

consisting of a single artifact contaminated segment with n_t EEG samples $\boldsymbol{y}_i^{(t)}$ measured at k channels and artifact samples $\boldsymbol{n}_i^{(t)}$ recorded at m channels. Each data set $\mathcal{D}^{(t)} \in \mathcal{T}$ is associated with a linear regression model defined by its weight matrix $W^{(t)} \in \mathbb{R}^{k\times m}$. We denote the set of weight matrices with $\mathcal{W} = \left\{W^{(t)}\right\}_{t=1}^{q}$. Following the Bayesian MTL framework presented in [16], we can state a data *likelihood* from the probabilistic interpretation in (1) and introduce a *prior* distribution over the weight matrices. The prior aims to capture commonalities in the influence of artifact sources to EEG channels across artifacts. In particular, we assume a matrix Gaussian distribution $p(W) = \mathcal{MN}\left(W \mid M_W, \Sigma_{r;W}, \Sigma_{c;W}\right)$ as prior model, where $M_W \in \mathbb{R}^{k\times m}$ is the mean weight matrix, $\Sigma_{r;W} \in \mathbb{R}^{k\times k}$ is the row covariance matrix that captures correlations in the influence between the EEG channels and $\Sigma_{c;W}$ is the column covariance capturing correlations between the artifact channels. Unfortunately, pulling everything together to state a *posterior* objective does not yield a closed form solution. However, the relation between matrix and multi-variate Gaussians is exploited in the next section in order to obtain an analytic solution for MTL artifact regression.

Bayesian Kronecker Regression: While the MTL approach using a matrix Gaussian prior does not derive in closed form, the problem can be restated into a form that yields an analytic solution. First, note that the matrix Gaussian $\mathcal{MN}\left(W \mid M_W, \Sigma_{r;W}, \Sigma_{c;W}\right)$ is equivalent to a multi-variate Gaussian of the form $\mathcal{N}\left(\mathrm{vec}\left(W\right) \mid \mathrm{vec}\left(M_W\right), \Sigma_{c;W} \otimes \Sigma_{r;W}\right)$, where $\mathrm{vec} : \mathbb{R}^{k\times m} \to \mathbb{R}^{km}$ is the vectorization of a matrix stacking the columns into a column vector and $\otimes : \mathbb{R}^{k\times m} \times \mathbb{R}^{k\times m} \to \mathbb{R}^{km\times km}$ is the Kronecker product of two matrices [6]. Hence, instead of targeting the weight matrix W itself, the vectorized version $\mathrm{vec}\left(W\right)$ of the weights can be optimized. In fact, the model stated in (1) is equivalent to a Kronecker formulation of the form

$$\boldsymbol{y} \sim \mathcal{N}\left(\boldsymbol{s} + \left(\boldsymbol{n}^T \otimes I_k\right)\mathrm{vec}\left(W\right), \sigma^2 I_k\right). \tag{3}$$

It turns out that by assuming that the source $\boldsymbol{s}$ and noise signal $\boldsymbol{n}$ are independent, the artifact regression problem in this formulation is directly solvable by the MTL algorithm from [16]. Hence, the maximum a-posteriori (MAP) estimate of a task weight matrix $W \in \mathcal{W}$ for task t is given by

$$\mathrm{vec}\left(W\right) = \left(\Sigma_{\otimes}\sum_{i=1}^{n_t} {N_i^{(t)}}^T N_i^{(t)} + \sigma^2 I_{km}\right)^{-1} \left(\Sigma_{\otimes}\sum_{i=1}^{n_t} {N_i^{(t)}}^T \boldsymbol{y}_i^{(t)} + \sigma^2 \mathrm{vec}\left(M_W\right)\right), \tag{4}$$

where $N_i^{(t)} = {\boldsymbol{n}_i^{(t)}}^T \otimes I_k$ and $\Sigma_{\otimes} := \Sigma_{c;W} \otimes \Sigma_{r;W}$. Applying the iterative learning algorithm from [16] trains the parameters of the multi-variate Gaussian prior, i.e. the vectorized mean $\mathrm{vec}\left(M_W\right)$ and Kronecker covariance matrix $\Sigma_{\otimes}$. The original weight matrix W can be easily restored from the Kronecker model by reshaping the vectorized weights accordingly $W = \mathrm{unvec}\left(\mathrm{vec}\left(W\right)\right)$. The original row and column covariance matrices $\Sigma_{r;W}$ and $\Sigma_{c;W}$, respectively, may be obtained from the unvectorized weights using expectation maximization algorithms [17]. An algorithm to obtain the matrix Gaussian parameters is outlined in Algorithm 1.

Published by Verlag der TU Graz
Graz University of Technology

 DOI: 10.3217/978-3-85125-533-1-25

Calibration-Free Correction: A prior model $\mathcal{MN}(M_W, \Sigma_{r;W}, \Sigma_{c;W})$ encodes shared characteristics across artifact regression models. In fact, the mean weight matrix M_W can be used to parameterize a matrix regression model $\boldsymbol{y} = \boldsymbol{s} + M_W\boldsymbol{n}$. A sample $(\boldsymbol{y}, \boldsymbol{n}) \in \mathbb{R}^k \times \mathbb{R}^m$ from a new session can be therefore immediately corrected by computing

$$\boldsymbol{s} = \boldsymbol{y} - M_W\boldsymbol{n} \tag{5}$$

and using $\boldsymbol{s}$ as the artifact-free sample. This correction is based on the commonalities found across artifact influences in different sessions or subjects. Hence, in contrast to the group mean approach, the MTL algorithm additionally updates the prior mean in dependency to the covariance relations.

Model Adaptation: The Bayesian setting of the MTL model proposed in this work allows for a natural adaptation to calibration data. If a calibration data set $\mathcal{D}^{(*)}$ becomes available, an adapted weight matrix $W^{(*)}$ can be inferred using the MAP estimate from (4) on the data set $\mathcal{D}^{(*)}$. The prior then acts as a regularizer towards the shared structure that is controlled by the variance factor σ^2. The correction procedure then follows (5) where we replace the prior mean M_W with the adapted weights $W^{(*)}$. The adaptation is also eligible for calibration in which new artifacts are obtained in an online setting, e.g. by thresholding techniques [18] or the Riemannian Potato [7].

Experimental Setup: We performed an evaluation of the model on real EEG signals recorded from five subjects with four to five sessions. Each subject sat on a comfortable chair in front of a screen and began the session with a five minute resting state recording (eyes open, fixating a cross on the screen). The subject then performed five to 13 runs of mental imagery with nine trials per run. As we are only interested in the artifacts of the recordings, the exact design of the imagery experiment is of no further interest in this work (however, details on the data set can be requested from the authors).

Brain activity during the experiment was recorded using EEG with 128 electrodes positioned according to the extended 10-20 system (referenced at TPP10h). The signals were sampled at 500Hz using actiCHamp amplifiers [1] and active electrodes.

The recorded EEG signals were divided into training and test segments. The five minute resting state recording was used to extract EOG blinking artifacts for model training. Each training segment consisted of a one second window containing an EOG blink artifact in the center that was automatically extracted by variance thresholding. In absence of explicitly placed EOG channels in the recordings, the artifacts were measured at two frontal electrodes (Fp1 and Fp2) designated to act as sources for EOG artifacts that measure eye blinks. The data from the experimental runs were then used as test signals for a cross-correlation evaluation between artifact sources and EEG

[1] BrainProducts GmbH, Gilching, Germany

Algorithm 1: Multi-task Kronecker Regression

Data: Training sets $\mathcal{T}$ as described in (2)
Result: Matrix-variate Gaussian prior $\mathcal{MN}(M_W, \Sigma_{r;W}, \Sigma_{c;W})$

Initialize $M_W = \mathbf{0}$, $\Sigma_{r;W} = I_k$, $\Sigma_{c;W} = I_m$;
Initialize $\mathcal{W} = \{W^{(t)}\}_{t=1}^{q}$ with $W^{(t)} = \mathbf{0}$;
Set $\Sigma_{\otimes} = \Sigma_{c;W} \otimes \Sigma_{r;W}$;
for $\mathcal{D}^{(t)} \in \mathcal{T}$ **do**
  for $\left(\boldsymbol{n}_i^{(t)}, \boldsymbol{y}^{(t)}\right) \in \mathcal{D}^{(t)}$ **do**
    Compute $N_i^{(t)} = {\boldsymbol{n}_i^{(t)}}^T \otimes I_k$
while M_W *and* $\Sigma_{\otimes}$ *not converged* **do**
  for $W^{(t)} \in \mathcal{W}$ **do**
    Train $\mathrm{vec}\left(W^{(t)}\right)$ using (4) ;
    Restore $W^{(t)} := \mathrm{unvec}\left(\mathrm{vec}\left(W^{(t)}\right)\right)$;
  Update M_W with the sample mean of the weights in $\mathcal{W}$;
  Update $\Sigma_{\otimes}$ with the sample covariance of the vectorized weights in $\mathcal{W}$;
Estimate $\Sigma_{r;W}$ and $\Sigma_{c;W}$ from $\mathcal{W}$ [17];

channels. Each test segment consisted of a four second window where the subject was either in an imagery phase (with rare eye blinks and little noise) or a pause phase (with more frequent eye blinks and more noise). In summary, the models were only trained from contaminated EEG samples, while the test segments consisted of artifact-free as well as contaminated samples. All signals were preprocessed with a common average reference and band-passed in 1-40Hz (Butterworth, order 4).

We based our evaluation on the assumption that EEG source signals are uncorrelated to artifact signals [13]. Accordingly, correction models with lower correlation between artifact and EEG were considered better. We compared the MTL regression model for artifact correction presented in this work against no correction, standard linear regression and a group mean of weight matrices. The MTL prior and group mean are transfer models and were trained from artifacts of the training segments of all subjects, but excluding the subject that was evaluated. The MTL prior model (MTL Reg (P)) was trained using Algorithm 1. The group mean model (Mean Reg) was constructed by averaging over the weight matrices trained from individual artifacts. The standard regression (Std Reg (A)) and adapted MTL regression (MTL Reg (A)) were calibrated models trained from the artifacts in the same session that was been evaluated.

The test segments were corrected with the models and the Pearson correlation coefficient between the time series of an artifact source and the cleaned EEG signals were computed. This procedure resulted in 125 normalized cross-correlation values for a total of 360 test segments (resulting in a total of 45000 correlations per artifact source). The correlation coefficients were pooled and compared according to their absolute total correlation, density

Published by Verlag der TU Graz
Graz University of Technology

 DOI: 10.3217/978-3-85125-533-1-25

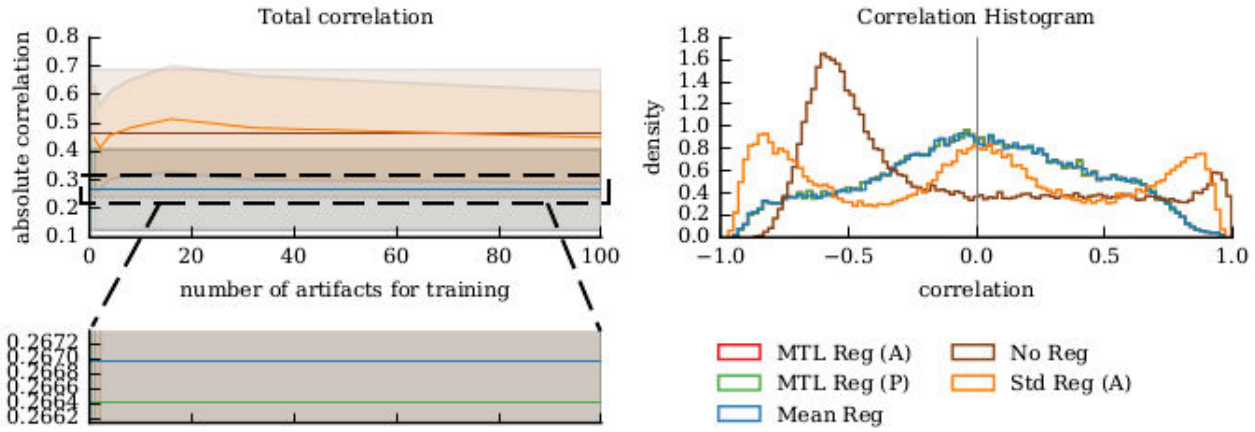

Figure 1: Correlation analysis between EOG electrode and the EEG channels. The Pearson correlation coefficient between EOG channel Fp1 and the 125 EEG channels were computed over all 360 test segments. The top and bottom left plot show the mean (solid lines) and standard deviation (shaded areas) of the total absolute correlation of each model. The bottom left plot rescaled the y-axis to highlight the differences between the transfer models. The histogram on the right shows the density distribution of the correlation coefficients for each model.

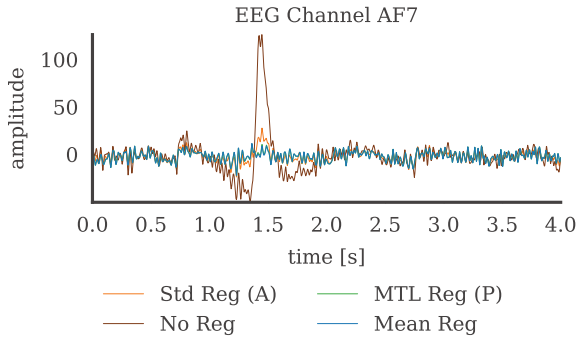

Figure 2: An exemplary comparison of the artifact correction models on a preprocessed EEG time series of four seconds recorded at channel AF7. The signal was bandpassed between 1 and 40Hz and contains an EOG blink artifact at 1.5 seconds. All artifact correction methods visibly attenuate the deflection and follow the original signal in the segments where no artifact occurs.

distribution and topographic relations. In the following section, we only present the results for EOG channel Fp1 and omit Fp2, as both channels showed identical behavior.

RESULTS

We first compared the performance of each model in terms of total correlation. Therefore, the mean correlation values over all 360 test segments was taken at each EEG electrode. Then, the mean and standard deviation of the absolute correlations were computed across all channels. The results for the different models are shown in Figure 1 (top left and bottom left). The calibrated models (suffixed by (A)) were trained on an increasing number of artifacts from the calibration session. The standard regression approach (orange) shows similar total correlation as opposed to not performing any regression at all (brown). The MTL and mean regression models show equal performance by decreasing the total correlation and variance compared to both, no and standard regression. The bottom left plot scales towards the MTL models and the mean regression. Here, the MTL prior (green) and adapted model (red) have minimally lower correlation than the mean model (blue). The MTL adaptation performance is equal to the MTL prior and does not change with more session-specific artifacts to train on.

The top right plot of Figure 1 shows the density distribution of the correlations in a histogram. Performing no regression at all (brown) exhibits a clear peak at negative correlations and a smaller at the positive tail. Standard regression (orange) also has modes at the positive and negative tails, but induces another peak around zero. The MTL models (red and green) and mean regression (blue) are again indistinguishable and centered with most correlation values around zero. Hence, the transfer models are able to keep more correlation values closer to zero than standard or no regression.

The topographic relations of the cross-correlations are depicted in Figure 3. The topographies show the correlation difference on each electrode between the two models pairs in a row and column. Red areas are positive differences indicating that the row model has lower correlation than the column model. Likewise, blue areas are negative differences and indicate that the row model has higher correlation than the column model. Performing regression lowers correlations mainly at the very frontal and occipital region. The transfer models (Mean Reg, MTL Reg (P) and MTL Reg (A)) yield reduced occipital and parietal correlations compared to standard regression (Std Reg (A)). While topographic differences between the MTL models compared to mean regression are present, there are no clear brain regions where one model outper-

Published by Verlag der TU Graz
Graz University of Technology

 DOI: 10.3217/978-3-85125-533-1-25

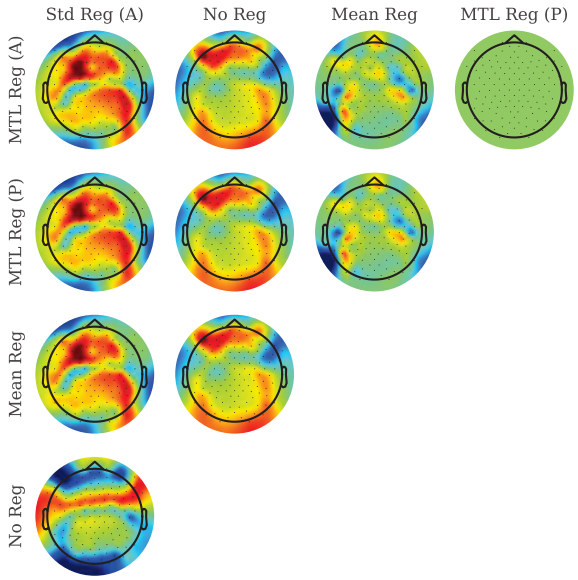

Figure 3: Topographies of the correlation difference between two models for artifact source Fp1 and the EEG channels. Red regions are positive differences and state the the row-model induces a lower correlation at that region than the column-model. Likewise, blue regions are negative differences and imply a lower correlation of the column-model compared to the row-model. Notable differences emerge for EEG channels near the frontal artifact sources (associated with No Reg) and for the frontal and occipital areas (associated with regression).

forms the other. The MTL prior model (MTL Reg (P)) and its calibrated version (MTL Reg (A)) show no differences at all.
Finally, Figure 2 shows an example of an EEG times series from a four second test segment at the frontal electrode AF7. An eye blink occurred at 1.5 seconds and after the preprocessing it is still clearly visible without EOG regression (green). Standard regression (blue) manages to reduce the amplitude, but the deflection is still visible. The transfer models (red and purple) manage to even further reduce the amplitude and seem to have visually corrected the artifact well. The corrected signals follow the original signal before and after the artifact occurred.

DISCUSSION

The results suggest that the group mean and MTL models outperform standard regression in terms of reducing correlation between artifact sources and EEG channels. In fact, standard correction seems to perform worse at some EEG channels with a varying total correlation, similar to the uncorrected signal and high negative and positive correlation modes. The differences seem to also occur at relevant brain regions within the frontal and parietal areas. A possible explanation may be that the standard regression is able to regress out artifacts well, but corrupts the signal at some channels when there is no artifact present. The transfer methods on the other hand account for variability in the artifacts, resulting in more stable regression models. These results agree with findings that group means may outperform individual regression models [13, 14].

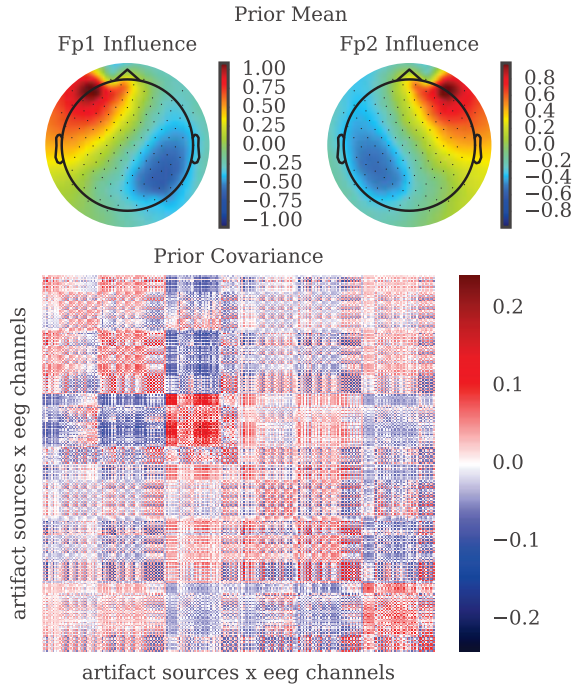

Figure 4: Visualization of the matrix Gaussian prior parameters trained by the MTL algorithm. The top two plots show topographies of the learned weights associated with the corresponding artifact source Fp1 or Fp2 on each channel. In both cases, the influence gradually decreases with increasing distance to the artifact source. The bottom plot shows a heatmap of the prior covariance matrix in Kronecker form that was estimated from the vectorized form with the standard sample covariance. The covariance matrix shows spatial block structures captured across artifacts from different subjects and sessions.

Notice that the group mean is a special case of the MTL learning algorithm where only a single prior update is performed. This equivalence led to our expectation that the MTL prior will perform at least as good as the group mean. Moreover, as the prior was used to regularize adaptation with session-specific calibration data, we expected to further increase performance as opposed to using the plain prior or group mean. Unfortunately, the MTL prior and adaptation have trained the same weights and there are only minimal differences between the MTL and group mean model. The neglectable difference in total correlation and density distribution indicate that MTL and group mean essentially trained the same weights. This conclusion is supported by the lack of correlation differences at clear brain regions shown in the topographic maps. We analyzed the MTL training process and found that the prior quickly converges within a few iterations. A possible explanation for the quick convergence may arise from the rather low dimensionality of the feature

Published by Verlag der TU Graz
Graz University of Technology

 DOI: 10.3217/978-3-85125-533-1-25

space compared to the large amount of data points for training. Hence, the resulting MAP estimates are mainly based on the data likelihood and do not need to rely much on the prior regularization. It is further worth noticing that the MTL adaptation process to calibrate with session specific artifacts does not increase performance over the MTL prior. The covariance prior was also analyzed and showed structure captured across artifacts (see Figure 4), which implies general spatial feature directions for training. However, the captured structure did not seem to be of relevance in case of EOG artifacts, as the final prior ultimately converge to the group mean and could not be improved through calibration. A solution to this problem may have been to not only consider eye blinks, but further horizontal and vertical saccades.

CONCLUSION

This work presented a probabilistic interpretation of artifact correction that unifies inter-subject linear models and session-specific calibration. The introduced method combines influence distributions of artifact sources on EEG channels within a Bayesian MTL framework in which individual artifacts across sessions and subjects constitute the tasks. However, the final model ultimately converges to a group mean of the weight matrices, implicating that there was no additional session-specific structure across EOG artifacts that further improved performance of the model. The MTL framework has already proven to work well in the case where tasks have few data points compared to the feature dimensionality. In this sense, promising follow up work is the evaluation of this approach for other tasks, artifacts and data sets that may contain exploitable structure across artifact tasks. Further promising future work may investigate and interpret the influence structure captured by the covariance matrix. Such an analysis is likely to give further insights into the behavior of artifacts across sessions or subjects and may aid the development of new models for artifact correction or regression techniques on EEG signals.

ACKNOWLEDGEMENTS

We thank the Athena-Minerva Team for providing the data set used in this work. We further thank Natalie Faber and Daniel Tanneberg for discussions on the topic and the reviewers for their valuable feedback.

REFERENCES

(Conference proceeding)
[1] Grosse-Wentrup M, Liefhold C, Gramann K, Buss M. Beamforming in noninvasive brain–computer interfaces, IEEE Transactions on Biomedical Engineering, 2009, 56(4):1209–1219.
[2] Lotte F, Guan C. Regularizing common spatial patterns to improve BCI designs: unified theory and new algorithms, IEEE Transactions on biomedical Engineering, 2011, 58(2):355–362.
[3] Van Vliet M. Effectiveness of Automatic EOG Regression, University of Twente, Netherlands, 2006.
[4] Alamgir M, Grosse-Wentrup M, Altun Y. Multitask Learning for Brain-Computer Interfaces, AISTA, 2010, 9(5):17–24.
[5] Fiebig KH, Jayaram V, Peters J, Grosse-Wentrup M. Multi-task logistic regression in brain-computer interfaces, Proceedings of the IEEE International Conference on Systems, Man, and Cybernetics (SMC 2016), 2016.
[6] Stegle O, Lippert C, Mooij JM, Lawrence ND, Borgwardt KM. Efficient inference in matrix-variate Gaussian models with\ iid observation noise, Advances in Neural Information Processing Systems 24, 2011, 630–638.
[7] Barachant A, Andreev A, Congedo M. The Riemannian Potato: an automatic and adaptive artifact detection method for online experiments using Riemannian geometry, TOBI Workshop lV, 2013, 19–20.
(Journal)
[8] Hyvärinen A, Oja E. Independent component analysis: algorithms and applications, Neural networks, 2000, 13(4):411–430.
[9] Klados MA, Papadelis C, Braun C, Bamidis PD. REG-ICA: a hybrid methodology combining blind source separation and regression techniques for the rejection of ocular artifacts, Biomedical Signal Processing and Control, 2011, 6(3):291–300.
[10] Wallstrom GL, Kass RE, Miller A, Cohn JF, Fox NA. Automatic correction of ocular artifacts in the EEG: a comparison of regression-based and component-based method, International journal of psychophysiology, 2004, 53(2):105–119.
[11] Croft RJ, Chandler JS, Barry RJ, Cooper NR, Clarke AR. EOG correction: a comparison of four methods, Psychophysiology, 2005, 42(1):16–24.
[12] Fatourechi M, Bashashati A, Ward RK, Birch GE. EMG and EOG artifacts in brain computer interface systems: A survey, Clinical neurophysiology, 2007, 118(3):480–494.
[13] Verleger R, Gasser T, Möcks J. Correction of EOG Artifacts in Event-Related Potentials of the EEG: Aspects of Reliability and Validity, Psychophysiology, 1982, 19(4):472–480.
[14] Gasser T, Sroka L, Möcks J. The correction of EOG artifacts by frequency dependent and frequency independent methods, Psychophysiology, 1986, 23(6):704–712.
[15] Schlögl A, Keinrath C, Zimmermann D, Scherer R, Leeb R, Pfurtscheller G. A fully automated correction method of EOG artifacts in EEG recordings, Clinical neurophysiology, 2007, 118(1):98–104.
[16] Jayaram V, Alamgir M, Altun Y, Schölkopf B, Grosse-Wentrup M. Transfer learning in brain-computer interfaces, IEEE Computational Intelligence Magazine, 2016, 11(1):20–31.
[17] Dutilleul P. The MLE algorithm for the matrix normal distribution, Journal of statistical computation and simulation, 1999, 64(2):105–123.
[18] Nolan H, Whelan R, Reilly RB. FASTER: fully automated statistical thresholding for EEG artifact rejection, 2010, 192(1):152–162.

Published by Verlag der TU Graz
Graz University of Technology

Proceedings of the
7th Graz Brain-Computer Interface Conference 2017 DOI: 10.3217/978-3-85125-533-1-26

ERP-BASED BCI TRAINING FOR CHILDREN WITH ADHD: MOTIVATIONS AND TRIAL DESIGN

M. Fouillen[1,2], E. Maby[1,2], L. Le Carrer[1,2,3], V. Herbillon[1,2,3], J. Mattout[1,2]

[1] Brain Dynamics and Cognition Team, Lyon Neuroscience Research Center, INSERM U1028-CNRS, UMR5292, 69000 Lyon, France

[2] University Lyon 1, 69000 Lyon, France

[3] Hospices Civils de Lyon, 69000 Lyon, France

E-mail: melodie.fouillen@inserm.fr

ABSTRACT: Neurofeedback is a promising treatment for children with ADHD. However, although several studies have investigated its efficacy, the effectiveness of current approaches is still debated. This might be partly due to the biomarkers that are used and might not be enough specific of ADHD core symptoms. We here motivate the evaluation of P300-based BCI training as an alternative. We review the arguments in favor of this approach and reveal the design of an ongoing randomized and controlled clinical trial. Essentially, the P300 EEG evoked response is affected in ADHD. It does reflect selective attention and action selection. It is modulated by successful pharmacological intervention in ADHD. And it can be used in BCI for training purposes, through varied and engaging games. Interestingly, these games enable the use of precise instructions as well as multi-level feedbacks to favor learning. Finally, this new type of Neurofeedback allows for instantiating a highly specific control condition that is compatible with a double-blind design.

INTRODUCTION

Attention-Deficit/Hyperactivity Disorder (ADHD) is a common neurodevelopmental disorder, affecting 3-5% of children. ADHD refers to a variable cluster of inattention, hyperactivity and impulsivity symptoms. It is also associated with impaired social skills, poor school performance and even accidents or substance use [1]. The predominant treatment for these children is pharmacological, with dopaminergic stimulant medication. The long-term effects of these treatments remain unclear, and close to 30% of children with ADHD do not fully respond to them. Moreover, some adverse effects of psychostimulants have been reported such as a decreased appetite and insomnia [2]. Hence a substantial number of parents are quite reluctant to give these drugs to their children. Additional, complimentary or alternative non-pharmacological interventions are therefore needed. In this paper, we briefly review the converging arguments supporting the hypothesis that P300-BCI based training of attention could potentially be effective in children with ADHD. We also describe the main aspects of a double blind design that we just initiated to evaluate its efficacy. Results of such a heavy longitudinal study will only be available after months, but discussing its theoretical grounds and practical aspects should already be useful to many readers in the field.

CLASSICAL NEUROFEEDBACK IN ADHD

One attractive and non-pharmacological alternative is EEG-based Neurofeedback. The aim of this technique is to enable the patient to learn how to modulate his own brain activity through operant or classical conditioning. By providing positive reinforcement when changes in brain activity are made in the desired direction, the subject can learn how to self-regulate her neuronal activity and normalize it [3]. It is expected that repeated practice will relief the patient of the main symptoms. ADHD is by far the disorder that is most targeted by Neurofeedback treatments today.

Three main types of Neurofeedback protocols are typically used. They all rest on the modulation of an endogenous, spontaneous and continuous measure of some brain signals.

The first application of Neurofeedback in hyperkinetic children aimed at training the sensory-motor rhythm (SMR) between 12 and 14Hz. This was motivated by the relationship between this rhythm and the process of motor inhibition. An increase in SMR amplitude would be associated with a decrease of ADHD symptoms [4].

Besides, several quantitative EEG (QEEG) studies found excess power in the theta band (4–8 Hz) and diminished power in the beta band (13-30) in ADHD children compared to healthy children of the same age [5]. This led to proposing the online training of the theta/beta ratio (TBR) to reduce the activity in the theta band while increasing the one in the beta band [6].

Finally, a very slow component of the EEG known as the contingent negative variation (CNV) has been found to be reduced in ADHD children. This component is characterized by a negative shift of the signal, in anticipation of an expected event. Its reduction in ADHD children would reflect an impairment of self-regulation abilities [7]. To improve control on this component,

Published by Verlag der TU Graz
Graz University of Technology

 DOI: 10.3217/978-3-85125-533-1-26

Neurofeedback training protocol targeting Slow Cortical Potentials (SCP) are carried out. SCPs are broadly assume to reflect the regulation of cortical excitability. With SCP training, children seem to become able to regulate their brain potentials and to produce more negative SCPs (i.e. CNV) [8].

Five meta-analysis have assessed the effectiveness of Neurofeedback. The first one showed that this technique has a large effect on inattention and impulsivity and a medium size effect on hyperactivity [9]. All of the fifteen studies reported in this analysis did include a control condition but only a few of them were randomized trials. When including only the randomized studies, the effect on hyperactivity appeared to be reduced. Sonuga-Barke et al., 2013 [10], analyzed 8 randomized controlled trials (RCTs) and reported a significant effect of Neurofeedback when evaluation was based on "probably not blind assessments", i.e., scores from raters closest to the therapeutic setting (e.g. parents), while they simply concluded to a trend when evaluation was based on "probably blinded assessments", i.e. scores from placebo controlled trials or made by adults likely to be blind to treatment allocation.

More recently, another meta-analysis based on 5 RCTs reported a significant effect of Neurofeedback on attention, when comparing it to semi-active or placebo conditions and when evaluated based on both "probably blinded" and "probably not blinded" assessments. An effect on hyperactivity/impulsivity was also found but only for "probably not blinded" assessments [11].

Finally, a last meta-analysis based on 13 RCTs [12] yielded a similar conclusion, namely that Neurofeedback training had a significant effect on inattention, hyperactivity and impulsivity as well as on the total score of the ADHD rating scale (ADHD-RS) but only with most proximal raters, not with probably blinded raters.

Despite the growing number of studies and meta-analysis assessing the effect of Neurofeedback in ADHD children, the effectiveness of current treatments remains debated, calling for more studies and as well as new methods [13]–[16]. Studies that are included in these meta-analyses are in fact hard to compare with each other. First because different biomarkers are targeted by the Neurofeedback training (TBR, SMR or SCP). Also, because sample sizes are quite different between studies. Finally, different controlled groups are used. Semi-active conditions refer to treatments with no expected clinical benefit (e.g. EMG-based Biofeedback). They aim at controlling for the non-specific effect of Neurofeedback such as the interaction between the therapist and the children. Then active conditions aim at comparing the effect of Neurofeedback with another therapy (e.g. pharmacological intervention or behavioral therapy). Finally, rare placebo controlled studies have also been performed in order to control for all the nonspecific effects of Neurofeedback treatments. They can allow for a double-blind design but have proven difficult to instantiate. All these different control conditions between studies may have contributed to the heterogeneity of the results.

Importantly, it has recently been questioned whether the above exploited biomarkers are specific enough of the targeted deficits. In particular, recent studies have reported an excessive TBR for a subgroup of ADHD children only [17]. Ogrim, Kropotov, & Hestad, 2012 [18] found a significant increase of the TBR in 25.8% of ADHD patients, but also in 2.6% of healthy controls. Moreover, it has been shown that lots of cognitive processes elicit an increase in frontal-midline theta power [19], such as working memory or episodic memory. It has also been shown that sustained internalized attention or meditation can yield an increase of frontal-midline theta power. More recently, it has been reported that the up-regulation of frontal-midline theta power facilitates memory updating and mental set shifting in healthy subjects [20]. Hence and contrary to the rational of TBR training, a correlation was observed between an improvement in the control of attentional resources and an increase in theta power. Finally and in line with those findings, the increase of TBR found in ADHD children seems to be more important when the children are engaged in a task, suggesting that this increase may simply reflect a compensatory mechanism [21]. The same authors suggested that TBR Neurofeedback "*may not produce the best possible therapeutic effect as far as executive control functions are concerned*". These findings raise the question of whether current training protocols rely on the appropriate neurophysiological targets.

ERP-BASED NEUROFEEDBACK

Over the past two decades, electrophysiology has been used increasingly to investigate differences in cortical activity between children with and without ADHD. An often occulted research stream investigating deficits in children with ADHD has used Evoked-Related Potentials (ERPs) and several ERP components have proven altered [22]. The most consistent report is the reduction in amplitude of the P300 component, both in auditory [23] and visual tasks [24]. The P300 is a large positive complex that reaches its peak at approximately 300 milliseconds after stimulus onset. It is in fact made of two subcomponents, a frontal P3a reflecting attentional capture by some external stimulation, followed by a parietal P3b elicited by the voluntary orientation of attention [25]. The amplitude of the P300 grows with the amount of attentional resources engaged in processing the external event [26]. This biomarker has never been used in Neurofeedback protocols for ADHD children so far. In contrast, it is very much used online for the control of Brain-Computer Interface (BCI) applications such as the well-known P300-speller [27]. The P300-speller aims at enabling Locked-in people to communicate by spelling a text on a computer screen. It is based on the principle of the visual oddball paradigm. The user must pay attention to a specific item on the screen while groups of items are lit up in a pseudo-random fashion. Every time the target letter is lit up, the brain produces a P300.

Published by Verlag der TU Graz
Graz University of Technology

 DOI: 10.3217/978-3-85125-533-1-26

Conversly, no P300 will be produced for non-target letters. This way, but only if the user performs the task as requested, the computer can detect the target letter to be spelled. This selection process based on the orientation of spatial attention can be used in different settings, beyond spelling applications, such as in games for instance [28]. Interestingly, a few studies have investigated the effect of training on performances in P300-based BCIs. This was done on healthy adults [29]–[31], or adults with motor impairments [32]. Although the training were quite short, and included only a few participants with no control group, results suggested that performances can indeed be improved with practice. This corroborates our own informal observations on a several volunteers who did practice with the P300-speller a lot in our lab. Since a good performance in P300-based BCI involves being able to selectively pay attention to the target, it appears very well suited for training children with ADHD who show difficulties in both sustaining focused attention (towards a target) and avoiding being distracted (by a non-relevant stimulation).

P300 AND ADHD

Overall, the P300 amplitude has been suggested to quantify the degree of engaged attentional resources in processing a particular stimulus [26]. Importantly, it has been shown that children with ADHD have a reduced P300 amplitude which can be up-regulated by Methylphenidate (MPH) intake . Sawada et al., 2010 [33] have shown an increase of P300 amplitude after intake of osmotic-release MPH in ADHD children. Seifert et al., 2003 [34] have found that after the intake of MPH, ADHD children had no more P300 amplitude difference compared to control children. Moreover, two studies have shown an increase of the P300 amplitude following the intake of MPH but also a concomitant improvement of behavioral measures of attention in a Stroop [34] or a CPT task [35]. Yan-ling & Xu, 2013 [35] have found that good performers (i.e. children who improved their behavior after taking MPH), showed no difference of P300 amplitude compared to control children. On the contrary, poor performers (i.e. children who did not significantly improve their behavior), still showed a significantly reduced P300 compared to control children. To conclude, P300 is a specific neurophysiological marker of selective attention which, in one hand, is affected in ADHD children and, in the other hand, can evolve positively along with behavioral symptoms.

P300-BASED NEUROFEEDBACK FOR ADHD CHILDREN

All the above arguments speak quite strongly in favor of attempting to design a Neurofeedback like training that would yield an improvement of the P300 in ADHD children. If successful, we would then expect that this non-pharmacological treatment would yield a concomitant improvement of behavioral symptoms.
However, since the P300 is a transient neurophysiological marker that is evoked by an external stimulation, this calls for drastically different Neurofeedback interfaces compared to classical trainings based on endogenous and continuous signals.
Interestingly, P300-based BCI games have already been designed [28], [36]. They have shown that various and particularly engaging and entertaining games can be easily designed thanks to the transient and reactive nature of the targeted signal. These games typically involve an opponent and require from the user to develop a strategy (see for instance the well-known Connect 4, Space invader or Battleship). The mental effort needed to derive a strategy is independent from the one that has to be made to focus attention and send the proper neurophysiological command, but it certainly contributes to the engagement of the user and should thus favor the learning. This aspect is usually absent from classical Neurofeedback interfaces. Moreover, those games naturally instantiate an interaction where a clear instruction can be given to the user (e.g. to focus its gaze on the targeted screen location and to count the number of times it is lit up). Hence the user can easily infer the causal relationship between a successful attentional effort and a successful outcome in the game (having selected the desired location on screen).

A DOUBLE BLIND RCT

To demonstrate the effectiveness and specificity of Neurofeedback, it is important to conduct double blind, controlled and randomized studies. Interestingly, ERP-based training as we propose makes this requirement from evidence-based medicine attainable.

In our study, 60 children diagnosed with ADHD (aged between 8-17 years) will be recruited. 30 will be assigned following a randomized minimization procedure, to a P300-based Neurofeedback (group A, n = 15) or to an active control group (group B, n=15). 30 other children will be assigned to a third and passive control group (Group C). Children in groups A and B will undergo 30 individual training sessions at a rate of 2 sessions per week. Each session will last an hour, including at least 30 minutes of Neurofeedback training. During these training sessions, children will be offered to play various P300-based video games to keep up their motivation. All these games are based on the same principle as the well-known visual P300-speller. Importantly though, an eye tracking system will be used to know which target the child is aiming at. This eye-tracking system will be useful for two reasons. First, by indicating to us what the target is, we will be able to assess the child's accuracy in controlling the BCI over trials and sessions. Second, in active control group B, it will replace the BCI control so that the interaction with the game will only be based on gaze direction and will not depend upon the attentional effort. Importantly, this active control is thus identical to the P300-based condition in every aspect, except for the signal that will be accounted for to control the interface. Precisely, gaze location on the screen will be monitored

Published by Verlag der TU Graz
Graz University of Technology

 DOI: 10.3217/978-3-85125-533-1-26

online for both groups. In group A, selection will be based on the most attended location, while in group B, selection will be based on the most looked-at location. In group A, although the most attend location also corresponds to the one that was mostly looked-at, the control will only be efficient with attentional effort. In contrast, children in group B will be able to control the BCI game by simply looking at the targeted location, no matter how they master their attentional control.
This specific control condition further enables a double-blind comparison of treatments A and B. Indeed, neither the children and the parents, nor the therapists will know if the children are controlling the interface with their EEG signals or with their gaze.
For our recruitment, we will privilege children who are not under medication. However, a few children under medication will also be included inevitably, so that can meet our objectives in terms of inclusion. Children under medication will be asked not to take their drugs on days of training and evaluation. Indeed, the P300 can be up-regulated by MPH intake, suggesting that being trained while under medication would not be useful. To control for a putative interaction of medication and training, children under medication will be randomized between the two groups.
The feasibility of this blind approach was assessed during a preliminary testing with about 30 healthy children who underwent a single session where they blindly switched from one type of control to the other in blocks. This way, we can control for all the non-specific effects of the Neurofeedback training. Children in both groups will receive exactly the same number of training sessions, they will enjoy the same games and receive the same instructions and support.

Unlike classical BCI protocols, children will not have to perform any calibration prior to using the interface. Instead, template signals derived from the above mentioned 30 healthy children will be used. Classificaiton based on these template signals operate in the space of covariance matrices, using Riemannian geometry [37]. Making use of a template from healthy subjects has a twofold advantage. First, it eschews the need for a cumbersome calibration stage at the beginning of each Neurofeedback session. Second, since ADHD children typically exhibit a reduced P300 amplitude, it is more sensible to use template signals derived from a healthy population as model signals to be achieved by the patients with training.

For the quantitative and qualitative evaluation of the treatment, four evaluation sessions will be performed by each child: one prior to any training, one after half the number of training sessions (i.e. 15), one at the end of the training (after the 30 sessions), and a final one two months after the end of the training, as a follow-up measure. During those sessions, children will undergo several paper-pencil and computerized tests in order to evaluate the evolution of their ADHD symptoms. Parents will also complete some questionnaires to evaluate the evolution of the symptoms and the quality of life of their child.

Children included in the passive control group (group C) are only going to carry out these four evaluation sessions.

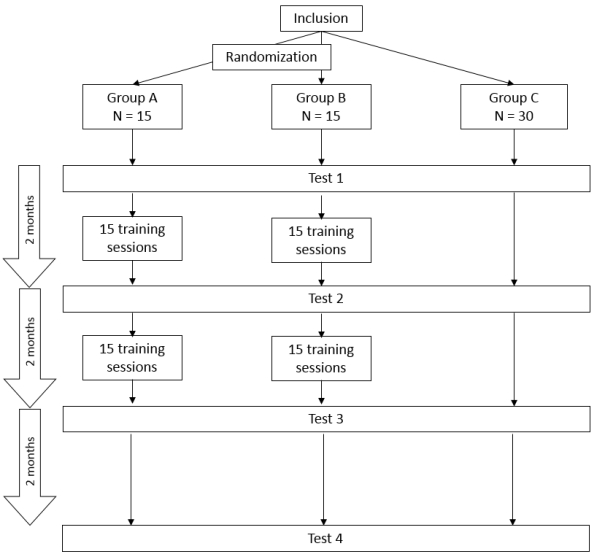

Figure 1: flow chart of the RCT design for the evaluation of a P300-bsed BCI training for ADHD children.

AKNOLEGEMENTS
This clinical evaluation is part of the project “Mind Your Brain”. This project is conducted by four partners: the Lyon Neuroscience Research Center, the Hospices Civils de Lyon, Black sheep studio and Mensia technologies. It is funded by the *Banque publique d’investissement* (BPI-France) and *Region Ile-de-France*.
Mélodie Fouillen held a doctoral fellowship from *Région Rhônes-Alpes*.

REFERENCES

[1] E. Cormier, “Attention deficit/hyperactivity disorder: a review and update.,” *J. Pediatr. Nurs.*, vol. 23, no. 5, pp. 345–57, Jun. 2008.
[2] N. Lofthouse, L. E. Arnold, S. Hersch, E. Hurt, and R. DeBeus, “A Review of Neurofeedback Treatment for Pediatric ADHD,” *J. Atten. Disord.*, vol. 16, no. 5, pp. 351–372, Jul. 2012.
[3] L. H. Sherlin *et al.*, “Neurofeedback and Basic Learning Theory: Implications for Research and Practice,” *J. Neurother.*, vol. 15, no. 4, pp. 292–304, Oct. 2011.
[4] M. Shouse and J. Lubar, “Operant-Conditioning of Eeg Rhythms and Ritalin in the Treatment of Hyperkinesis,” *Biofeedback Self-Regul.*, vol. 4, no. 4, pp. 299–312, 1979.
[5] H. Heinrich, K. Busch, P. Studer, K. Erbe, G. H. Moll, and O. Kratz, “EEG spectral analysis of attention in ADHD: implications for neurofeedback training?,” *Front. Hum. Neurosci.*, vol. 8, p. 611, 2014.

Published by Verlag der TU Graz
Graz University of Technology

 DOI: 10.3217/978-3-85125-533-1-26

[6] H. Gevensleben *et al.*, "Is neurofeedback an efficacious treatment for ADHD? A randomised controlled clinical trial," *J. Child Psychol. Psychiatry*, vol. 50, no. 7, pp. 780–789, Jul. 2009.

[7] H. Heinrich, H. Gevensleben, F. J. Freisleder, G. H. Moll, and A. Rothenberger, "Training of slow cortical potentials in attention-deficit/hyperactivity disorder: Evidence for positive behavioral and neurophysiological effects," *Biol. Psychiatry*, vol. 55, no. 7, pp. 772–775, Apr. 2004.

[8] H. Gevensleben *et al.*, "Neurofeedback of slow cortical potentials: neural mechanisms and feasibility of a placebo-controlled design in healthy adults," *Front. Hum. Neurosci.*, vol. 8, p. 990, Dec. 2014.

[9] M. Arns, S. de Ridder, U. Strehl, M. Breteler, and A. Coenen, "Efficacy of Neurofeedback Treatment in ADHD: the Effects on Inattention, Impulsivity and Hyperactivity: a Meta-Analysis," *Clin. Eeg Neurosci.*, vol. 40, no. 3, pp. 180–189, Jul. 2009.

[10] E. J. Sonuga-Barke *et al.*, "Nonpharmacological interventions for ADHD: systematic review and meta-analyses of randomized controlled trials of dietary and psychological treatments," *Am J Psychiatry*, vol. 170, no. 3, pp. 275–89, 2013.

[11] J. A. Micoulaud-Franchi, P. A. Geoffroy, G. Fond, R. Lopez, S. Bioulac, and P. Philip, "EEG neurofeedback treatments in children with ADHD: an updated meta-analysis of randomized controlled trials," *Front Hum Neurosci*, vol. 8, p. 906, 2014.

[12] S. Cortese *et al.*, "Neurofeedback for Attention-Deficit/Hyperactivity Disorder: Meta-Analysis of Clinical and Neuropsychological Outcomes From Randomized Controlled Trials," *J. Am. Acad. Child Adolesc. Psychiatry*, vol. 55, no. 6, pp. 444–455, Jun. 2016.

[13] M. Arns and U. Strehl, "Evidence for Efficacy of Neurofeedback in ADHD?," *Am. J. Psychiatry*, vol. 170, no. 7, pp. 799–800, Jul. 2013.

[14] E. J. S. Sonuga-Barke *et al.*, "Evidence for Efficacy of Neurofeedback in ADHD? Response," *Am. J. Psychiatry*, vol. 170, no. 7, pp. 800–802, Jul. 2013.

[15] J.-A. Micoulaud-Franchi, F. Salvo, S. Bioulac, and T. Fovet, "Neurofeedback in Attention-Deficit/Hyperactivity Disorder: Efficacy," *J. Am. Acad. Child Adolesc. Psychiatry*, vol. 55, no. 12, pp. 1091–1092, Dec. 2016.

[16] S. Cortese *et al.*, "The European ADHD Guidelines Group replies:," *J. Am. Acad. Child Adolesc. Psychiatry*, vol. 55, no. 12, pp. 1092–1093, Dec. 2016.

[17] S. K. Loo and S. Makeig, "Clinical Utility of EEG in Attention-Deficit/Hyperactivity Disorder: A Research Update," *Neurotherapeutics*, vol. 9, no. 3, pp. 569–587, Jul. 2012.

[18] G. Ogrim, J. Kropotov, and K. Hestad, "The quantitative EEG theta/beta ratio in attention deficit/hyperactivity disorder and normal controls: Sensitivity, specificity, and behavioral correlates," *Psychiatry Res.*, vol. 198, no. 3, pp. 482–488, Aug. 2012.

[19] D. J. Mitchell, N. McNaughton, D. Flanagan, and I. J. Kirk, "Frontal-midline theta from the perspective of hippocampal 'theta,'" *Prog. Neurobiol.*, vol. 86, no. 3, pp. 156–185, Nov. 2008.

[20] S. Enriquez-Geppert, R. J. Huster, C. Figge, and C. S. Herrmann, "Self-regulation of frontal-midline theta facilitates memory updating and mental set shifting," *Front. Behav. Neurosci.*, vol. 8, p. 420, Dec. 2014.

[21] A. Bluschke, V. Roessner, and C. Beste, "Editorial Perspective: How to optimise frequency band neurofeedback for ADHD," *J. Child Psychol. Psychiatry*, vol. 57, no. 4, pp. 457–461, Apr. 2016.

[22] S. J. Johnstone, R. J. Barry, and A. R. Clarke, "Ten years on: A follow-up review of ERP research in attention-deficit/hyperactivity disorder," *Clin. Neurophysiol.*, vol. 124, no. 4, pp. 644–657, Apr. 2013.

[23] M. Senderecka, A. Grabowska, K. Gerc, J. Szewczyk, and R. Chmylak, "Event-related potentials in children with attention deficit hyperactivity disorder: An investigation using an auditory oddball task," *Int. J. Psychophysiol.*, vol. 85, no. 1, pp. 106–115, Jul. 2012.

[24] M. Doehnert, D. Brandeis, G. Schneider, R. Drechsler, and H.-C. Steinhausen, "A neurophysiological marker of impaired preparation in an 11-year follow-up study of attention-deficit/hyperactivity disorder (ADHD)," *J. Child Psychol. Psychiatry*, vol. 54, no. 3, pp. 260–270, Mar. 2013.

[25] J. Polich, "Updating P300: an integrative theory of P3a and P3b," *Clin Neurophysiol*, vol. 118, no. 10, pp. 2128–48, 2007.

[26] R. J. Johnson, "The amplitude of the P300 component of the event-related potential: Review and synthesis," *Adv. Psychophysiol.*, vol. 3, pp. 69–137, Jan. 1988.

[27] J. Mattout, M. Perrin, O. Bertrand, and E. Maby, "Improving BCI performance through co-adaptation: Applications to the P300-speller," *Ann. Phys. Rehabil. Med.*, vol. 58, no. 1, pp. 23–28, Feb. 2015.

[28] E. Maby, M. Perrin, O. Bertrand, G. Sanchez, and J. Mattout, "BCI Could Make Old Two-Player Games Even More Fun: A Proof of Concept with 'Connect Four,'" *Adv. Hum.-Comput. Interact.*, vol. 2012, p. 8, 2012.

[29] E. Baykara *et al.*, "Effects of training and motivation on auditory P300 brain-computer

Published by Verlag der TU Graz
Graz University of Technology

 DOI: 10.3217/978-3-85125-533-1-26

interface performance," *Clin. Neurophysiol.*, vol. 127, no. 1, pp. 379–387, Jan. 2016.

[30] J. D. Jacoby, M. Tory, and J. Tanaka, "Evoked response potential training on a consumer EEG headset," in *2015 IEEE Pacific Rim Conference on Communications, Computers and Signal Processing (PACRIM)*, 2015, pp. 485–490.

[31] S. Halder, K. Takano, H. Ora, A. Onishi, K. Utsumi, and K. Kansaku, "An Evaluation of Training with an Auditory P300 Brain-Computer Interface for the Japanese Hiragana Syllabary," *Front. Neurosci.*, vol. 10, p. 446, Sep. 2016.

[32] S. Halder, I. Käthner, and A. Kübler, "Training leads to increased auditory brain–computer interface performance of end-users with motor impairments," *Clin. Neurophysiol.*, vol. 127, no. 2, pp. 1288–1296, Feb. 2016.

[33] M. Sawada *et al.*, "Effects of osmotic-release methylphenidate in attention-deficit/hyperactivity disorder as measured by event-related potentials," *Psychiatry Clin. Neurosci.*, vol. 64, no. 5, pp. 491–498, 2010.

[34] J. Seifert, P. Scheuerpflug, K. E. Zillessen, A. Fallgatter, and A. Warnke, "Electrophysiological investigation of the effectiveness of methylphenidate in children with and without ADHD," *J. Neural Transm.*, vol. 110, no. 7, pp. 821–829, Jul. 2003.

[35] R. Yan-ling and D. Xu, "Effects of Methylphenidate in Children with Attention Deficit Hyperactivity Disorder: A Comparison of Behavioral Results and Event–Related Potentials," in *Attention Deficit Hyperactivity Disorder in Children and Adolescents*, S. Banerjee, Ed. InTech, 2013.

[36] M. Congedo *et al.*, ""Brain Invaders": a prototype of an open-source P300- based video game working with the OpenViBE platform," in *5th International Brain-Computer Interface Conference 2011 (BCI 2011)*, Graz, Austria, 2011, pp. 280–283.

[37] A. Barachant and M. Congedo, "A Plug&Play P300 BCI Using Information Geometry," *ArXiv14090107 Cs Stat*, Aug. 2014.

Published by Verlag der TU Graz
Graz University of Technology

Proceedings of the
7th Graz Brain-Computer Interface Conference 2017 DOI: 10.3217/978-3-85125-533-1-27

THE SPECTRAL CONTROL FEATURES OF A BIPOLAR ECOG BCI IMPLANTOVER PRIMARY HAND MOTOR CORTEX

Z.V. Freudenburg[1], M.P. Branco[1], S. Leinders[1], E.G.M. Pels[1], M.A. Van Den Boom[1], T. Denison[2], M.J. Vansteensel[1], E.J. Aarnoutse[1], N.F. Ramsey[1]

[1] University Medical Center Utrecht, Brain Center Rudolf Magnus, Utrecht, The Netherlands
[2] Department of Neuromodulation, Medtronic, Minneapolis, MN

E-mail: Z.V.Freudenburg@umcutrecht.nl

ABSTRACT: Both Low Frequency Band (LFB) and High Frequency Band (HFB) features of the electrocorticography (ECoG) signal have been described and explored in the context of BCI. In literature, HFB power is emerging as a dominant control feature. However, the recently published Utrecht Neural Prosthesis (UNP) showed that HFB power from a bipolar electrode pair over the hand motor area alone was not good enough for stable high performance click-based BCI control [1]. Instead, a combination of LFB and HFB signals was optimal for click-based control. Here, we explore the spectral features that make up the LFB and HFB features of the bipolar ECoG signal used in the UNP. We demonstrate that the LFB of the bipolar signal is a combination of mu and low and high beta rhythms with independent functional and temporal characteristics.

INTRODUCTION

For continuous real-life use of a BCI implant, the standards of performance are much higher than those needed for proof of concept in a controlled lab setting. Optimal neural control signals in real-life use can differ significantly from those established for short experiments in the lab given the requirement for reliable and robust decoding for daily use.

The Utrecht Neural Prosthesis (UNP) is a fully implanted communication BCI based on bi-polar electrocorticography (ECoG) signals recorded from the primary motor cortex (subdural Resume II electrodes, Investigational Activa® PC+S and Nexus System, Medtronic). We recently demonstrated that a subject with late-stage ALS is able to use the UNP system to generate reliable brief neural events to control a spelling device at home [1].

Initial tests with a standard BCI cursor control task [2] showed high performance using the High Frequency Band (HFB) signal that has been most commonly used in human ECoG BCI studies [1, 3-7]. The HFB signal has been shown to be ubiquitous to human neocortex [8] and has been associated with increased asynchronous neural activity in the cortical tissue directly underneath an ECoG electrode [8-11].

However, in the case of the UNP it was also demonstrated that reliable click-based spelling control was dependent on a combination of the HFB signal and a Low Frequency Band (LFB) signal, the spectral range of which (indicate frequency band we use in LFB) is consistent with that of the classic LFB spectral feature of motor cortex reported in ECoG literature [6, 12]. The LFB signal overlaps the mu-band (6-12 Hz) motor rhythm often used in EEG-based motor BCI [13], in addition to other oscillatory features commonly reported in EEG and ECoG literature such as the theta (4-7Hz) [14], and beta (12-30Hz) [15] bands.

A number of factors make the UNP control signal unique among human BCI systems. First, the chronic use click-based control requires precise control of the timing of control features derived from cognitive tasks. Second, the UNP has a bi-polar ECoG signal source (as opposed to the generally reported Common Average Referenced (CAR) signals). Third, the signals are gathered from a subject with late stage ALS, who has been paralyzed for years. Hence, in this work we explored the temporal and spectral characteristics of the UNP control signal to gain a better understanding of the underlying neural features that compose the bipolar control signal.

MATERALS AND METHODS

UNP ECoG signal: The primary control signal of the UNP device is recorded using a bi-polar electrode pair implanted over the 'hand knob' within the primary motor cortex of a subject suffering from late-stage ALS. (see Fig. 1 in [1]). Each electrode was 4 mm in diameter and the center-to-center separation was 1 cm. The cognitive strategy used to control the UNP signal is attempted movement of the contralateral hand. In addition to the online control mode of the UNP device, in which analog filtered spectral amplitude signal is relayed to the receiving tablet at 5Hz (see [1] Methods for details), non-filtered 'raw' time domain signals can be transmitted at 200Hz. This work uses off-line analysis of the time domain signal recorded during several types of research tasks. This raw signal is used to compute Event-Related Potential (ERP) responses, time-locked to cued attempted hand movements, in addition to time-locked responses in the frequency domain (see sections *Spectral analysis* and *Spectral band analysis*).

Attempted hand movement screening task: Signal

Published by Verlag der TU Graz
Graz University of Technology

 DOI: 10.3217/978-3-85125-533-1-27

properties during repetitive attempted hand movements were assessed using time domain data from a screening task in which the subject was cued to make repetitive attempted hand moments or relax for periods of 15s each. In total 46 runs consisting of either 10 (17 runs) or 3 (29 runs) alternated rest and attempted movement trials were used.

Short activation feedback task: In addition data from a task that cue the user to make brief 1s attempted hand movements was analyzed. This task also provided feedback to the user using the UNP control signal to control the vertical position of ball centered on the screen while alternating blocks of sky and grass scrolled from right to left across the top and bottom of the screen respectively. The blocks of sky were timed so that they took 1s to move pass the ball. The subject was instructed to make brief attempted hand movements to hold the ball at the top of the screen during the sky blocks and rest to allow the ball to reach the bottom of the screen during the grass blocks.

2-Target BCI control task: The signal properties during successful online BCI control were evaluated using time domain signal data from a subset of runs of a standard 2-target BCI control task (see [2] for details). In short, the subject was instructed to use attempted hand movements to control the vertical position of a ball moving at a constant speed from the left towards either an upper or lower target on the right of a screen. The task was administered using the BCI200 software package [ref] and used elevated power in the HFB (60-90Hz) to drive the ball up and relaxation (inducing a decrease in HFB power) to drive the ball down. A 1s cue, indicating either the top or bottom target, was presented before the ball appeared and began to move for a 2-4s period towards the right. Task performance was high (95%) for 2 runs with 3s movement periods.

Spectral analysis: The amplitude for each frequency bin from 1 to 90Hz (in steps of 1Hz) was computed offline for every time sample of each time domain data file using the real component of the convolution with a complex Gabor wavelet (span 4 cycles at full width half maximum) [16].

Spectral band analysis: In order to access the contributions of known distinct spectral bands to the UNP control signal, the Delta (1-4Hz), Theta (5-7Hz) Mu (8-12Hz), Low Beta (13-20Hz), and High Beta (21-31Hz) in addition to the HFB (41-90Hz) were analyzed. Each band's amplitude trace was computed for the duration of each data set by summing the mean normalized 1Hz bin amplitude traces over the above ranges. The amplitude trace of each band was then z-score normalized.

RESULTS

The bi-polar spectral profile for attempted hand movements during the screening task closely matched the classic ECoG spectral profile for M1 activity [6, 12] (Fig. 1). The range of 1-4Hz and 41 to 90Hz showed an attempted movement related increase in amplitude. A decrease in amplitude during attempted movement compared to relaxation was seen from 9 to 34 Hz. While the magnitude of the HFB increase is relatively uniform after 50 Hz, the LFB decrease shows a trough centered at 25 Hz and approximately covering the high Beta (21-31Hz) range.

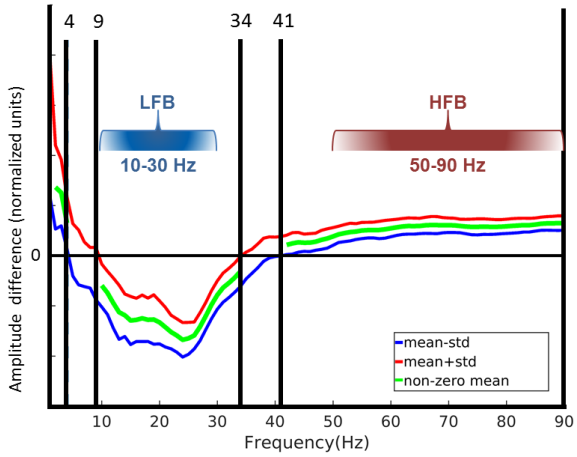

Figure 1: Attempted hand movement vs. rest condition spectral contrast. The classically reported HFB and LFB ranges [6, 12] are indicated with the red and blue highlights respectively. The mean + 1 standard deviation and mean – 1 standard deviation spectral contrast (attempted hand – rest condition) profiles (over trials and runs) are plotted in red and blue respectively. The green trace indicates the regions of the mean profile that are 1 std above or below 0.

Inspection of the mean spectrogram of the attempted movement and rest periods of the screening task (Fig. 2) shows that the decrease in High Beta amplitude parallels the increase in HFB and Delta band amplitude, which starts at attempted movement onset and continues until offset. In addition, a relative increase in amplitude in the High Beta range during the duration of the rest condition parallels the general decrease in the HFB and Delta ranges that begin at approximately 2s after the rest cue. However, it can also be seen in Fig. 2 that the lower portion of the LFB (9-20Hz) which consists of the mu and Low Beta bands has a pronounced initial drop in amplitude in the period after attempted movement onset (compared to the period prior to the offset). Furthermore, this lower LFB range shows a very pronounced increase (referred to hereafter as a rebound) in amplitude just after attempted movement offset. This rebound last for 3-4 seconds and does not continue for the duration of the rest periods. Strikingly, the rebound not only includes a peak in High Beta amplitude in the first 2s after attempted movement offset, it is accompanied by increased HFB amplitudes during the beginning of the rebound period.

Published by Verlag der TU Graz
Graz University of Technology

 DOI: 10.3217/978-3-85125-533-1-27

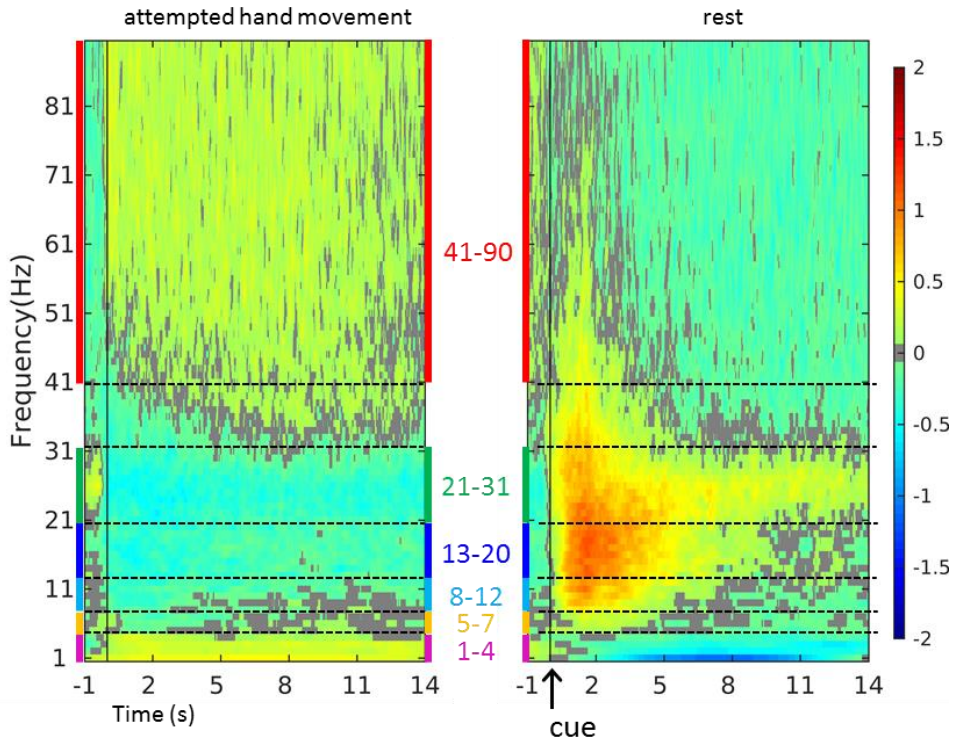

Figure 2: Mean attempted hand movement and rest condition responses. A) Mean spectrograms for -1 to 14s periods centered on movement onset (left) and offset (right) cues (note: trials were 15s, meaning that last 1s of each trial is analogous to the -1 to 0 second periods in plots). The colors indicate positive (yellow to red) and negative (turquoise to blue) mean z-scores. In addition the HFB, High Beta, Low Beta, Mu, Theta, and Delta bands are highlighted in red, green, blue, cyan, orange, and magenta respectively.

Fig. 3 depicts the temporal response patterns of the separate frequency bands (colored traces) to a series of short impulse like attempted hand movements made in the context of visual feedback (see section: *Short activation closed loop feedback task*). As with the repetitive attempted hand movements, a clear increase in HFB power (red trace) with a parallel decrease in High Beta (green trace) power can. Likely due to the anticipation facilitated by the feedback the coupled HFB and High Beta response starts approximately 1s before the cue. In addition, the same decoupling between the Mu/ Low Beta bands on the one hand, and the High Beta band on the other, that is seen in the sustained movement response, is seen in the short attempted movement response. Notably, the Low Beta band trace increases past zero and begins the rebound period just before the offset cue. This rebound period is also seen to continue to increase till past the cessation of the HFB increase and High Beta decrease. However, the short attempted movements also reveal that the Mu band response has a later negative peak and subsequent later rebound onset than the Low Beta band. The Theta band has a similarly timed decrease in amplitude as that of the Mu band, but does not show a post offset rebound.

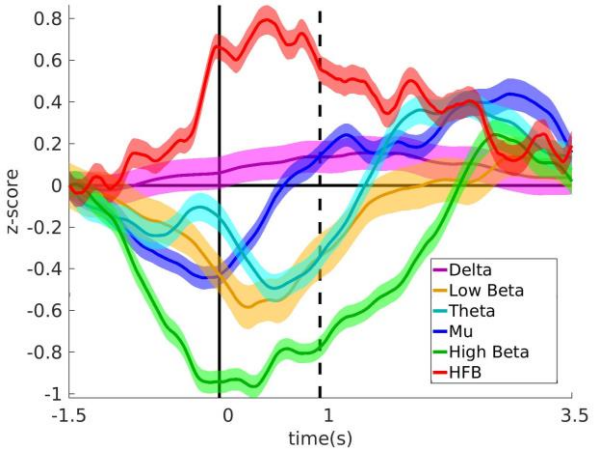

Figure 3: Spectral band responses to brief attempted hand movements during a feedback task. The mean z-scored traces and standard error margins (indicated by the shaded regions) are plotted (see legend for color indications) for the period of -1.5s to 3.5 time-locked to the onset of the sky blocks in the Short activation feedback task (see section *Short activation feedback task*).

Given the separate temporal profiles of individual bands, it is interesting to consider the full range (1-90Hz) spectral response to the traditional 2-Target BCI control

Published by Verlag der TU Graz
Graz University of Technology

 DOI: 10.3217/978-3-85125-533-1-27

task (Fig.4). As expected, the HFB increase used to drive the feedback is well timed to the up trials' movement cue (vertical black line, left plot). Again this HFB increase is paralleled by a High Beta band decrease and a broad spectrum rebound after the target feedback cue which includes the Mu and Low Beta bands.
However, the expected lack of HFB increase during the down trials (right plot) is not coupled by an increase in High Beta band amplitude. In fact, the High Beta band shows a decrease in amplitude coupled by a marked increase in the Low Beta band towards the end of the down trials. Furthermore, the rebound in amplitude seen after target feedback offset in the up trails is much diminished after the down trials. Another interesting features is the increase in Mu band amplitude just before and around the down trail movement cues which is clearly not present in the up trials.

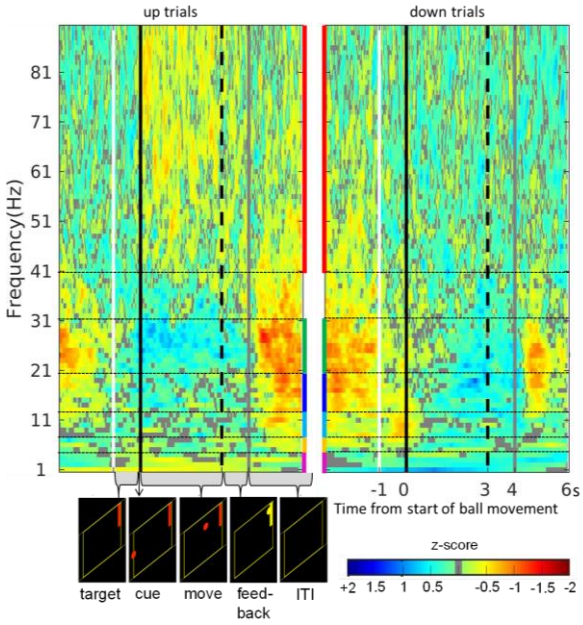

Figure 4: Mean up (attempted hand movement) on the left and down (rest) condition spectrograms on the right. The colors indicate positive (yellow to red) and negative (turquoise to blue) mean z-scores. The visual feedback corresponding to the successive periods of the task are depicted under the x-axis of the left plot. See Fig. 3 for explanation of color colored highlights.

DISCUSSION

The bi-polar signal used with the UNP has 3 main distinguishable frequency bands. A 41-90Hz HFB which is well matched to the traditional HFB [6], and a 9-34 Hz LFB (matched to the traditional LFB [6]) that is made up of distinguishable Mu/Low Beta and High Beta band features.
The results presented here indicate that the HFB is likely a segregate for the broadband component of the ECoG signal described by Miller et al. [8-9]. Since the HFB has been linked to synaptic mechanisms and irregular firing of single neurons [9-12] bi-polar referencing should only serve to strengthen its presence as a functional feature. If there is an increase broad band activity in one of the two neural populations under electrode pair then an increase in the differential bi-polar signal will be observed. In addition, due to the irregular or asynchronous nature of the broad band feature in the raw potential signal, if there is ab increase in both neural populations then the broad band (and hence HFB) component of the differential signal will be even further increased in amplitude. However, this does lead to more possible functional variance since two neuronal populations that are on a scale at which they are likely to be functionally independent [17] are reflected in the signal. This could have advantages and disadvantages. One advantage is the possibility for more distinct functional states. However, this also implies that larger range of cognitive tasks could affect the signal and lead to false positives in simple single click based system like the UNP.
We also show that LFB is clearly present in the bi-polar signal. Since this range has traditionally been associated with synchronized neural population oscillation effects [18] and the LFB has been reported to be anatomically broader than the 1 cm separation of the electrode pair [6, 12], it could be expected that synchronized suppression of the neural populations under the electrodes could lead to the LFB amplitude responses being subtracted out of the differential signal. However, the results presented here suggest that either the LFB is not synchronized across the covered populations or that a large enough phase shift in this range between the two populations exists to prevent this. This concept is exemplified by considering the subtractions of two signals with equal amplitude oscillations at the same frequency that are exactly out of phase. In this situation the amplitude of the differential signal would be doubled.
In addition the LFB band can be divided into distinct oscillatory bands with distinct temporal function

Published by Verlag der TU Graz
Graz University of Technology

 DOI: 10.3217/978-3-85125-533-1-27

response patterns. The High Beta (21-31Hz) component of the LFB shows task suppression consistent with hypothesized release of inhibition during cortical processing associated with the motor Mu rhythm [18]. On the other hand, the Mu/Low Beta component is also suppressed during attempted movement, but is not directly anti correlated with HFB. The rebound affect that has been reported for the Beta band [15] is most prominent in this range.

CONCLUSION

In addition to a clearly present HFB component, a multi-faceted LFB component made up of distinct High Beta and Mu/Low Beta components is present in the to the bi-polar signal. This LFB component is not only suppressed during attempted movements, it also shows a large post neural activation rebound affect. The combination of these effects helps improve robustness of HFB feature and leads to the stable single cognitive event features [1].

REFERENCES

[1] Vansteensel MJ, Pels EGM , Bleichner MG, Branco MP, Denison T, Freudenburg ZV, Gosselaar P, Leinders S, Ottens TH, Van Den Boom MA, Van Rijen PC, Aarnoutse EJ, Ramsey NF. Fully Implanted Brain-Computer Interface in a Locked-In Patient with ALS. N Engl J Med 2016;375(21): 2060-66

[2] Schalk G, McFrland DJ, Hinterberger T, Birbaumer N, Wolpaw JR. BCI2000: a general-purpose brain-computer interface (BCI) system. IEEE Trans Biomed Eng 2004;51: 1034-43.

[3] Buzsáki G, Wang XJ. Mechanisms of Gamma Oscillations. Annu Rev Neurosci 2012; 35: 203–25.

[4] Leuthardt E, Miller K, Anderson N, Schalk G, Dowling J, Miller J, Moran D, Ojemann J. Electrocorticographic freuquency alteration mapping: a clinical technique for mapping the motor cortex. Neurosurgery 2007; 60: 260.

[5] Leuthardt, E, Schalk, G, Wolpaw, J, Ojemann, J, Moran D. A brain-computer interface using electrocorticographic signals in humans. J Neural Eng 2004; 1: 63.

[6] Miller KJ, Schalk G, Fetz EE, den Nijs M, Ojemann JG, Rao RPN. Cortical activity during motor execution, motor, imagery, and imagery-based online feedback. PNAS 2010;107(9): 4430-35.

[7] Vansteensel M, Bleichner M, Freudenburg Z, Hermes D, Aarnoutse E, Leijten F, Ferrier C, Jansma J, Ramsey N,. Spatiotemporal characteristics of electrocortical brain activity during mental calculation. Hum Brain Mapp 2014;35: 5903–20.

[8] Miller KJ, Honey CJ, Hermes D, Rao RPN, Nijs M, Ojemann JG. Broadband changes in the cortical surface potential track activation of functionally diverse neuronal populations. NeuroImage 2014;85: 711-20.

[9] Miller K, Sorensen L, Ojemann J, Nijs M. Power-Law Scaling in the Brain Surface Electric Potential. PLoS Computational Biology 2009;5(12).

[10] Hermes D, Miller K., Vansteensel M, Aarnoutse E, Leijten F, Ramsey N. Neurophysiologic correlates of fMRI in human motor cortex. Hum Brain Mapp 2012; 33: 1689–99.

[11] Hermes D, Siero J, Aarnoutse E, Leijten F, Petridou N, Ramsey N. Dissociation between Neuronal Activity in Sensorimotor Cortex and Hand Movement Revealed as a Function of Movement Rate. J Neurosci 2012; 32: 9736–44.

[12] Miller KJ, Leuthardt E, Schalk G, Rao RPN, Anderson N, Moran D, Miller J, Ojemann JG. Spectral changes in cortical surface potentials during motor movement. J. Neurosci. 2007; 27(9): 2424-32.

[13] Wolpaw J, Wolpaw EW. Brain-Computer Interfaces: Principles and Practice. Oxford University Press, Oxford, England (2012)

[14] Canolty RT, Edwards E, Dalal SS, Soltani M, Nagarajan SS, Kirsch HE, Berger MS, Barbaro NM, Knight RT. High gamma power is phase-locked to theta oscillations in human neocortex, Science 2006, 313(5793), 1626-28

[15] Miller K, Hermes D, Honey C, Hebb A, Ramsey NF, Knight RT, Ojemann J, Fetz E. Human motor cortical activity is selectively phase-entrained on underlying rhythms. PLoS Comp Bio 2012; 8(9).

[16] Bruns A. Fourier-, Hilbert- and wavelet-based signal analysis: are they really different approaches? J Neurosci Methods 2004;137.

[17] Leuthardt EC, Schalk G, Roland J, Rouse A, Moran DW. Evolution of brain-computer interfaces: going beyond classic motor physiology. Neurosurg Focus. 2009; 27(1).

[18] Amzica F, da Silva FL, Schomer DL. Basic Principles, Clinical Applications, and Related Fields. Lippincott Williams & Wilkins, Philadelphia, Pa, USA (2010)

Published by Verlag der TU Graz
Graz University of Technology

Proceedings of the
7th Graz Brain-Computer Interface Conference 2017 DOI: 10.3217/978-3-85125-533-1-28

OPTIMAL TRANSPORT APPLIED TO TRANSFER LEARNING FOR P300 DETECTION

N.T.H. Gayraud[1], A. Rakotomamonjy[2], M. Clerc[1]

[1]Université Côte d'Azur, Inria, France
[2]Rouen University, France

E-mail: nathalie.gayraud@inria.fr

ABSTRACT: Brain Computer Interfaces suffer from considerable cross-session and cross-subject variability, which makes it hard for classification methods to generalize. We introduce a transfer learning method based on regularized discrete optimal transport with class labels in the interest of enhancing the generalization capacity of state-of-the-art classification methods. We demonstrate the potential of this approach by applying it to offline cross-subject transfer learning for the P300-Speller paradigm. We also simulate an online experiment to assess the feasibility of our method. Results show that our method is comparable to -and sometimes even outperforms- session-dependent classification.

INTRODUCTION

Brain Computer Interfaces (BCI) are a means of communication that connect a human brain and a machine, bypassing any other neurological output. In particular, during a non-invasive EEG-based BCI session, neurophysiological signals are acquired, processed, and transformed into commands, for which the user receives some form of feedback. Due to the very low Signal to Noise Ratio (SNR) non-invasive EEG-based BCI suffer from, advanced signal processing and machine learning techniques need to be employed for the intermediate steps [1].
EEG signals also suffer from a high amount of session-to-session and subject-to-subject variability, whose sources are diverse [2]. It can be due to the use of different acquisition means, to varying conditions during the day of the acquisition, to neurophysiological differences between one user and another, or to the fact that mental states and levels of concentration change from one session to another. Therefore, the classifier used to label mental tasks needs to be trained before every use, a task commonly referred to as calibration. Furthermore, because variability can occur within a session, the BCI may need to be recalibrated during its use. Calibration can last several minutes depending on the subject; it lists high among the reasons why the use of BCI is still not widespread.
The design of a robust transfer learning classification algorithm has been a subject of broad interest in the BCI community. The first attempts towards zero-training BCI are made for the Motor Imagery paradigm. Some of these methods rely on recovering spatial filters to project the samples onto a space where a pre-trained classifier will generalize well [3, 4], others on the use of adaptive or ensemble methods [5, 6]. The latter are also used in cross-session and cross-subject classification for P300-based BCI [7, 8], along with approaches under the Riemannian framework [9].
This work handles transfer learning classification by treating cross-session and cross-subject variability as a unsupervised domain adaptation problem. Recent works by Courty et al. [10] propose a solution based on regularized optimal transport to tackle the problem of classifying unlabeled test data that belong to a different domain from which the training data is drawn. Transportation theory applications to BCI have been researched under a mostly theoretical framework in the works of Ma et al. [11] towards generalizing the Posterior Matching Scheme to arbitrarily many dimensions.
Our contribution is a methodological framework based on regularized optimal transport with class labels which can be used for transfer learning alongside existing classifiers. In this paper, it is assessed through offline cross-subject experiments under the P300-Speller paradigm.
In the following sections, we first describe the problem formally and introduce notations. We proceed by describing our method, the dataset used in the experiments, and the experiments themselves. Then, we present our results and discuss them. Finally, we give our conclusions and propose future extensions.

MATERIALS AND METHODS

Transfer learning as a domain adaptation problem

Let $\mathbf{S} = \{(x_i, y_i)\}_{i=1}^{N}$ be the set of data acquired during a BCI session, that is, the set of N extracted feature vectors $\mathbf{X} = \{x\}_{i=1}^{N} \subset \mathbb{R}^d$ of dimension d coupled with the corresponding labels $\mathbf{Y} = \{y\}_{i=1}^{N}$. Furthermore, let $\mathbf{P}(x) \in \mathcal{P}(\Omega)$ denote the probability distribution from which the samples in $\mathbf{X}$ are drawn, where $\Omega \in \mathbb{R}^d$ is a measurable space of dimension d and $\mathcal{P}(\Omega)$ the set of all probability measures over the domain Ω.
We denote by $\mathbf{S}^e$ an existing session for which the labels are available, and by $\mathbf{S}^n$ a new session for which they are unknown. We seek to train a classifier to recover the unknown labels $\mathbf{Y}^n$. However, as a result of cross-session and cross-subject variability, most classifiers do

Published by Verlag der TU Graz
Graz University of Technology

 DOI: 10.3217/978-3-85125-533-1-28

not give accurate results about $\mathbf{Y}^n$ when trained on $\mathbf{S}^e$. This effect can be modeled as a domain adaptation problem, known as covariate shift [2]: while the conditional probability distributions $\mathbf{P}(y|x^e)$ and $\mathbf{P}(y|x^n)$ are equal, the same does not hold for the probability distributions of $\mathbf{P}(x^e) \in \mathcal{P}(\Omega^e)$ and $\mathbf{P}(x^n) \in \mathcal{P}(\Omega^n)$. Assuming that a transformation causes the drift between domains Ω_n and Ω_e, we propose to recover a transport plan to map the new features onto the domain of the existing features (Ω_e) using Optimal Transportation (OT) theory.

Regularized discrete OT with class labels

OT theory studies a problem known as the Monge-Kantorovic transportation problem [12]. This problem can be intuitively understood as the search for the optimal way to transport mass between two probability distributions. The optimization criterion is the minimization of a transportation cost; typically, the cost function represents some metric between the random variables of each distribution. Also, constraints may be imposed so that the mass is preserved during the transport. Since we only have a fixed number of samples from each set, the discrete adaptation of the OT problem boils down to matching empirical measures μ_e, μ_n of $\mathbf{P}(x^e)$ and $\mathbf{P}(x^n)$.

We can now formally define regularized discrete OT with class labels in the following way: consider the estimated empirical marginal distributions $\mu_e = \sum_{i=1}^{N_e} p_i \delta_{x_i^e}$ and $\mu_n = \sum_{i=1}^{N_n} p_i \delta_{x_i^n}$ of the samples in $\{x_i^e\}_{i=1}^{N_e} = \mathbf{X}^e$ and $\{x_i^n\}_{i=1}^{N_n} = \mathbf{X}^n$, where δ_{x_i} is the Dirac function at $x_i \in \mathbb{R}^d$ and p_i is the probability mass associated to the i^{th} sample, $\sum_{i=1}^{N} p_i = 1$. We look for a probabilistic coupling $\gamma_0 \in \mathcal{B}$ satisfying the following minimization problem:

$$\gamma_0 = \underset{\gamma \in \mathcal{B}}{\operatorname{argmin}} \langle \gamma, \mathbf{C} \rangle_{\mathbf{F}} + \lambda \mathbf{R}_s(\gamma) + \eta \mathbf{R}_c(\gamma) \qquad (1)$$

where $\langle \cdot \rangle_{\mathbf{F}}$ is the Frobenius dot product, and $\mathcal{B}$ is the set of all probabilistic couplings between μ_e and μ_n, $\mathcal{B} = \left\{ \gamma \in (\mathbb{R}^+)^{N_e \times N_n} \mid \gamma \mathbf{1}_{N_n} = m_e, \gamma^{\mathbf{T}} \mathbf{1}_{N_e} = m_n \right\}$ where $\mathbf{1}_d$ denotes a d-dimensional vector of ones and $m \in \mathbb{R}^N$ denotes a vector of probabilities, each probability associated to a point in feature set $\mathbf{X}$.

The first term of equation 1 is the discrete adaptation of the Kantorovic formulation of the OT problem [13]. $\mathbf{C}$ is the cost function matrix, whose elements correspond to a metric between two points, $\mathbf{c}_{ij} = d(x_i^e, x_j^n)$, $x_i^e \in \mathbf{X}^e, x_j^n \in \mathbf{X}^n$; it can be intuitively understood as the effort required to move a probability mass from x_i^e to x_j^n. In this work, the metric we use is the squared Euclidean distance $d(x_i^e, x_j^n) = \|x_i^e - x_j^n\|_2^2$, as it guarantees the existence of a unique coupling [12]. When the squared euclidean distance is used as the cost function, the first term leads to a sparse version of γ_0

The second term regularizes γ_0 by its entropy [14]:

$$\mathbf{R}_s(\gamma) = \lambda \sum_{i,j} \gamma(i,j) \log \gamma(i,j) \qquad (2)$$

This allows for smoother variants of γ_0, whose sparsity gradually decreases as λ increases, and renders the transport more robust to noise. Moreover, $\mathbf{R}_s(\gamma)$ can also be interpreted as a Kullback-Leibler divergence between γ and a uniform joint probability $\gamma_u = \frac{1}{N_e N_n}$, which allows for the use of a computationally efficient algorithm based on Sinkhorn-Knopp's scaling matrix approach [15].

The third term is a regularizer, proposed by Courty et al. [10], based on group sparsity which makes use of the available class labels of session $\mathbf{S}^e$:

$$\mathbf{R}_c(\gamma) = \sum_j \sum_{cl} \|\gamma(\mathcal{I}_{cl}, j)\|_2 \qquad (3)$$

where $\mathcal{I}_{cl}$ denotes the set of indices belonging to class $cl \in \{Target, Nontarget\}$. In this way, the j-th element $x_j^n \in \mathbf{X}^n$ will not be coupled with elements from $\mathbf{X}^e$ that belong to different classes.

OT applied to P300-based BCI

Based on the previous formulation of the OT problem, we propose a transfer-learning method whose three main steps are (a) feature extraction, (b) transportation of the new features to the domain of the existing set and (c) label prediction. The pipeline of our method is illustrated in Fig. 1.

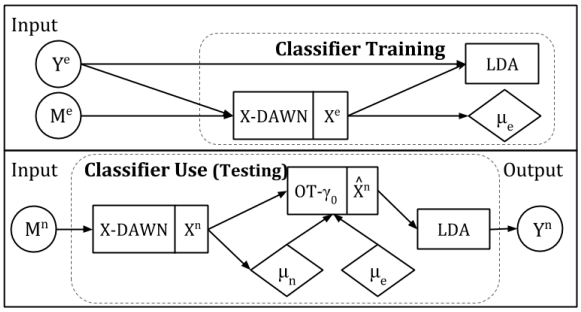

Figure 1: Pipeline of the method. During the training process, an existing set $\mathbf{M}^e$ is given as input along with the corresponding labels $\mathbf{Y}^e$. Then, (a) the X-DAWN spatial filters are learned and (b) the extracted features $\mathbf{X}^e$ are used to estimate μ_e and train the LDA classifier. When a new set $\mathbf{M}^n$ is given as input to the trained classifier, (a) the trained X-DAWN filters are used to extract features $\mathbf{X}^n$, (b) μ_n and γ_0 are estimated, and (c) $\hat{\mathbf{X}}^n$ is computed and given as input to the LDA classifier, which estimates $\mathbf{Y}^n$.

Let $m(t) \in \mathbb{R}^C$ be a measurement extracted from a downsampled EEG signal over C electrodes at time t during a P300-Speller session. After pre-processing, $M_i \in \mathbb{R}^{C \times T}$ denotes the i^{th} trial whose columns are T consecutive measurements. From $\{M_i\}_{i=1}^{N_e} = \mathbf{M}^e$ and the corresponding labels $\mathbf{Y}^e$, we learn spatial filters using the X-DAWN algorithm [16], and project each M_i onto the first N_f X-DAWN filters, yielding feature vectors $x_i \in \mathbb{R}^{N_f \times T}$.

We proceed by computing γ_0 according to equation (1) and use it to map $\mathbf{X}^n$ onto $\mathbf{\Omega}^e$ by computing a transformation based on barycentric mapping [10],

$$\hat{\mathbf{X}}^n = \operatorname{diag}(\gamma_0^\top \mathbf{1}_{N_e})^{-1} \gamma_0^\top \mathbf{X}_e \qquad (4)$$

Published by Verlag der TU Graz
Graz University of Technology

 DOI: 10.3217/978-3-85125-533-1-28

Each $x^n \in \mathbf{X}^n$ will thus be mapped onto the weighted barycenter of the features of $\mathbf{X}^e$ that it was coupled with. In the end, a Linear Discriminant Analysis (LDA) classifier is trained on $\mathbf{S}^e$, and used to predict the labels $\{y_i^n\}_{i=1}^{N_n} = \mathbf{Y}^n$ that correspond to $\{\hat{\mathbf{x}}_i^n\}_{i=1}^{N_n} = \hat{\mathbf{X}}^n$.

Dataset Description

The first dataset used in our experiments, Dataset A, consists of EEG signals recorded during P300-Speller sessions that were conducted by adult patients suffering from Amyotrophic Lateral Sclerosis. The experiment took place in the premises of the Nice University hospital, and had been approved by the local ethics committee CPP Sud Méditerrannée [17]. Each subject participated in three free-spelling sessions, each one preceded by a calibration session. In this paper, we use the calibration sessions of 12 randomly selected patients. In each session there are in total 200 trials in the $Target$ class (considered to contain the elicited P300 component) and 1000 trials in the $Nontarget$ class.

Dataset B includes EEG signals from four healthy subjects, which were recorded during P300-speller sessions conducted in the premises of Inria Sophia-Antipolis Mediterranée. Each subject participated in two free-spelling sessions, each one preceded by a calibration session. Again, we only include the calibration sessions, each one containing 66 trials in the $Target$ class and 330 trials in the $Nontarget$ class.

In both datasets, a Refa-8 amplifier (ANT) with 12 electrodes (Fz,C3,Cz,C4,P7,P3,Pz,P4,P8,O1,Oz,O2) was used for the recording. The EEG signals are filtered with a 5th order Butterworth filter between 1 and 15Hz. Each signal is then downsampled from 256 Hz to 64Hz and separated into trials $M_i \in \mathbb{R}^{C\times T}$, where $C = 12$ and $T = 32$ to account for a 0.5s epoch starting at the time of the flash.

Cross-subject experiments

To demonstrate the potential of our approach, we initially conduct two offline experiments using Dataset A, the difference between them lying in the composition of the training (existing) set. In both cases, the labels associated to the testing (new) set are not taken into consideration during the experiment, and are only used for evaluation purposes.

In the first experiment we assess the generalization capacity of our classifier in *pairwise transfer learning* experiments. For each experiment, the training set consists of a single session, that is, a set $\mathbf{M}_i^e$ of trials along with the corresponding labels in $\mathbf{Y}_i^e$ and the test set is $\mathbf{M}_j^n$, where $i, j \in I = \{A1, A2, ..., A12\}$ denote the subject index, and $i \neq j$. The cardinality of each set is $N_e = N_n = 1200$.

For the second experiment, we evaluate the performance of our classification method when trained with a larger training set by performing *Leave-One-Out transfer learning*. As the test session contains data from a single session, $\mathbf{X}_{j\in I}^n$, here, the training set consists of the entire dataset but session j. Hence, $\mathbf{M}^e = \bigcup_{i\in I_j^-} \mathbf{M}_i$ and $\mathbf{Y}^e = \bigcup_{i\in I_j^-} \mathbf{Y}_i$, where $I_j^- = I - \{j\}$ denotes the set of indices of all subjects except subject j. In this setting, $N_e = 13200$ and $N_n = 1200$.

Since the size of the training set is prohibitively large to allow for the fast computation of γ_0, we use an ensemble classifier method known as Bootstrap Aggregating (BA) or Bagging. Introduced by Breiman in 1996 [18], BA has often been used in BCI [19, 20] to enhance classification results. The pipeline of our method combined to BA is illustrated in Fig. 2. Initially, BA creates k subsets of length l, called bootstraps, by sampling the training set uniformly and with replacement. We train an instance of our classifier for each bootstrap. During testing, each instance produces a prediction; all of the predictions are aggregated via a voting scheme, that is, a majority vote, to produce the final result.

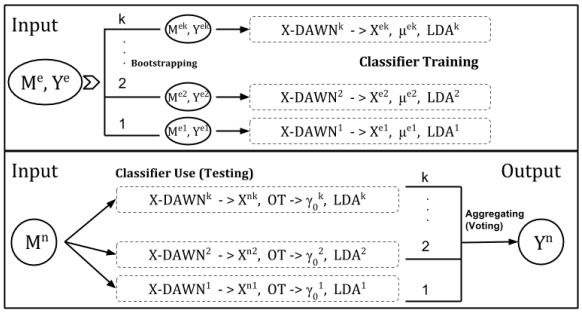

Figure 2: Pipeline of our method with BA. Initially, BA creates k subsets from the training set. Then, an instance of our classifier is trained for each subset. During testing, the new set $\mathbf{M}^n$ is given as input to each instance. All instances produce a prediction, and all predictions are aggregated via voting to produce the final result.

Finally, we simulate one online experiment per session in Dataset B, using the pairwise transfer learning classifier from dataset A that produced the best performance. The simulation proceeds in the following way: every $N_F = 36$ trials, the feature vector set is extracted from $\{M_i\}_{i=1}^{N_F} = \mathbf{M}^n$, the transport map between $\mathbf{X}^e$ and $\{x_i\}_{i=1}^{N_F} = \mathbf{X}^n$ is computed, and $\{y_i\}_{i=1}^{N_F} = \mathbf{Y}^n$ is generated from the mapped set $\{\hat{x}_i\}_{i=1}^{N_F} = \hat{\mathbf{X}}^n$. Note that we keep the chronological ordering of the trials within each test session.

For all experiments, we use the first and last two X-DAWN filters during feature extraction, resulting in a total of $N_f \times T = 128$ extracted features. The best values for the OT regularization terms are searched and selected in $\lambda, \eta \in \{0.01, 0.1, 1, 10, 100\}$. For classifiers using the BA method, $k = 20$ bootstraps of length $l = 500$ were used, and we drew the same number of elements from each class to remedy the issue of class imbalance.

RESULTS

We introduce this section by illustrating an example of a transport between two pairs of sessions. Then, we report

Published by Verlag der TU Graz
Graz University of Technology

 DOI: 10.3217/978-3-85125-533-1-28

Table 1: Pairwise transfer learning. Columns display the average AUC value and standard deviation over 11 experiments where the classifier is trained with the corresponding existing session; the last column is the average over 132 experiments. The first row shows the results obtained by XD+LDA, while the second row shows the results from XD+OT+LDA.

Existing Session	A1	A2	A3	A4	A5	A6	A7	A8	A9	A10	A11	A12	**Avg.**
XD+LDA	0.535 $\pm$ 0.05	0.562 $\pm$ 0.07	0.598 $\pm$ 0.09	0.600 $\pm$ 0.07	0.591 $\pm$ 0.10	0.595 $\pm$ 0.08	0.570 $\pm$ 0.06	0.578 $\pm$ 0.06	0.516 $\pm$ 0.02	0.566 $\pm$ 0.07	0.553 $\pm$ 0.06	0.526 $\pm$ 0.02	**0.566** $\pm$ **0.03**
XD+OT+LDA	0.627 $\pm$ 0.07	0.539 $\pm$ 0.02	0.567 $\pm$ 0.06	0.548 $\pm$ 0.04	0.611 $\pm$ 0.11	0.598 $\pm$ 0.07	0.560 $\pm$ 0.06	0.490 $\pm$ 0.17	0.518 $\pm$ 0.01	0.551 $\pm$ 0.04	0.583 $\pm$ 0.05	0.585 $\pm$ 0.06	**0.565** $\pm$ **0.04**

Table 2: Leave-One-Out transfer learning. Columns display the AUC score when the classifier is trained with all of dataset A except for the corresponding new session. The last column is the average and standard deviation over 11 experiments. The first two rows show results obtained whithout OT; in the first row, the BA method is not used either. The third row displays the results when both BA and OT are used. The last row shows the AUC score of the Session-Dependent (SD) classifier of each session in dataset A.

New Session	A1	A2	A3	A4	A5	A6	A7	A8	A9	A10	A11	A12	**Avg.**
XD+LDA	0.804	0.500	0.529	0.567	0.528	0.593	0.577	0.506	0.525	0.689	0.690	0.721	**0.602** $\pm$ **0.099**
BA+XD+LDA	0.778	0.535	0.720	0.808	0.623	0.698	0.739	0.596	0.521	0.696	0.673	0.809	**0.683** $\pm$ **0.098**
BA+XD+OT+LDA	0.779	0.529	0.835	0.790	0.732	0.541	0.802	0.608	0.673	0.740	0.655	0.809	**0.708** $\pm$ **0.106**
SD Classifier	0.724	0.593	0.709	0.713	0.648	0.624	0.692	0.658	0.548	0.694	0.702	0.781	**0.673** $\pm$ **0.063**

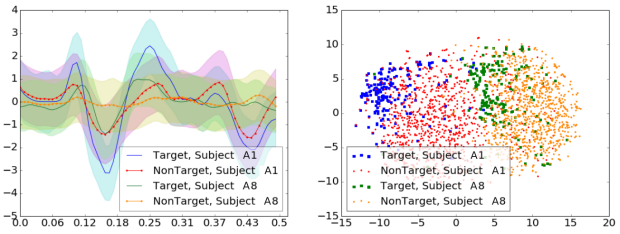

(a) $\mathbf{X}^e_{A1}$ and $\mathbf{X}^n_{A8}$, before transport.

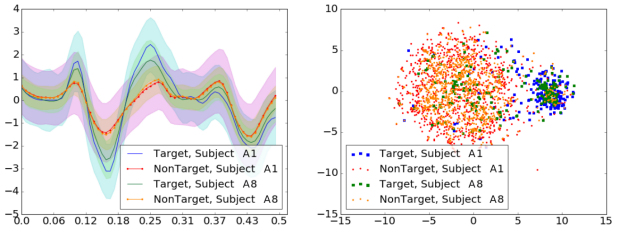

(b) $\mathbf{X}^e_{A1}$ and $\mathbf{X}^n_{A8}$, after transport.

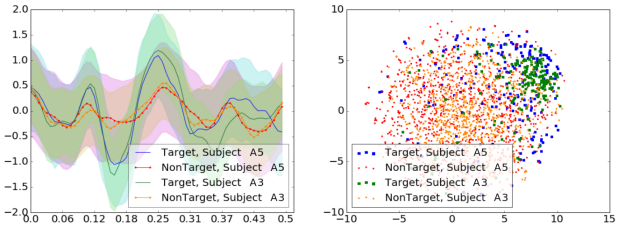

(c) $\mathbf{X}^e_{A5}$ and $\mathbf{X}^n_{A3}$, before transport.

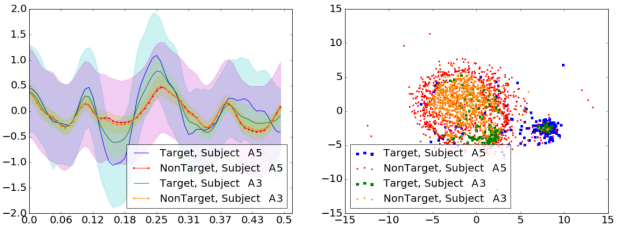

(d) $\mathbf{X}^e_{A5}$ and $\mathbf{X}^n_{A3}$, after transport.

Figure 3: Examples of the barycentric mapping induced by γ_0 for pairs of sessions. On the left we see the average response and standard deviation of the first X-DAWN filter projection for the $Target$ and $Nontarget$ classes. On the right side, we see the 2D projection of the features, projected using t-SNE.

the experimental results of our method, which we refer to as XD+OT+LDA. Motivated by the high level of imbalance between the $Target$ and $Nontarget$ class, we use the Area Under the receiver operating characteristic Curve (AUC) as our performance metric.

We display two examples of the estimated optimal transport in Fig. 3. In the first, the training and testing feature vector sets are $\mathbf{X}^e_{A1}$ and $\mathbf{X}^n_{A8}$ respectively, while in the second, $\mathbf{X}^e_{A5}$ and $\mathbf{X}^n_{A3}$. Fig. 3a and 3c show the original datasets, while Fig. 3b and 3d illustrate the outcome after computing $\hat{\mathbf{X}}^n_{A8}$ and $\hat{\mathbf{X}}^n_{A3}$. On the right side, we display a 2D projection of the features using t-distributed stochastic neighbor embedding (t-SNE) [21]. On the left side, we can observe the average response and standard deviation of the first X-DAWN filter, estimated on $\mathbf{X}^e_{A1(A5)}$, for both sessions and both classes. By looking closely at Fig. 3b and 3d, we can see that the transport causes a decrease in the variance of the response, for both the $Target$ and $Nontarget$ classes.

Pairwise Transfer Learning

The results of pairwise transfer learning can be seen on Tab. 1. To evaluate the performance of our method, we compare it to the performance of an XD+LDA classifier, i.e. an LDA classifier and X-DAWN features trained on $\mathbf{M}^e_{i\in I}$, $\mathbf{Y}^e_{i\in I}$, where no transport takes place. For each training session, we display the average AUC score and the standard deviation of the 11 experiments conducted with its corresponding classifier, where each one of the remaining session was used as the test session, $\mathbf{M}^n_{j\in I}, j \neq i$. At first glance, the two methods seem to perform equally well, yielding an average score of ~ 0.56. We note however that the best performance overall is the one of our method when trained with session S^e_{A1}, which is equal to 0.627.

Leave-One-Out Transfer Learning

On Tab. 2, we display the results of Leave-One-Out transfer learning; for each test session $\mathbf{M}^n_{j\in I}$, we trained a BA+XD+OT+LDA classifier (a combination of the BA ensemble method and our method, where each bootstrap is used to train an XD+OT+LDA classifier), using the union of the remaining sessions. For comparison pur-

Published by Verlag der TU Graz
Graz University of Technology

 DOI: 10.3217/978-3-85125-533-1-28

poses, we show the corresponding results of two additional transfer learning classifiers: a classifier without OT, in which BA is used to enhance the performance of an XD+LDA classifier, and those of an XD+LDA classifier, where neither BA nor OT are used. Finally, the performance of the session-dependent (SD) LDA classifier trained on X-DAWN features, computed after 5-fold cross-validation, is also displayed at the bottom.

Our findings demonstrate that merely using the BA method produces better results than the simple XD+LDA classifier. The average score of the BA+XD+LDA classification method is equal to 0.683, while the average performance of the session-dependent classifiers is 0.673. On top of that, when we use OT, we boost the performance even more producing an average performance equal to 0.708.

Online Simulation

After obtaining the results from pairwise transfer learning and observing that the XD+OT+LDA classifier trained with $\mathbf{M}^e_{A1}$,$\mathbf{Y}^e_{A1}$ generated the best performance, we used it to simulate an online experiment using each one of the four sessions $\{B1, B2, B3, B4\}$ in Dataset B as the test session (Sim 1). A label set $\mathbf{Y}^{n_i}$ was produced every $N_F = N_n = 36$ trials; since each test set contains 396 trials, a total of 11 label sets $\mathbf{Y}^{n_i}$, $i \in 1, \cdots, 11$, were generated in the course of each experiment. For each simulation, we report on Tab. 3 the average AUC and standard deviation over all label sets $\mathbf{Y}^{n_i}$. We compare it to an analogous online simulation using the XD+LDA classifier trained with $\mathbf{M}^e_{A4}$,$\mathbf{Y}^e_{A4}$, which generated the best score in pairwise transfer leaning among all XD+LDA classifiers (Sim 2). The AUC scores for the session specific classifiers of each test session, computed after 5-fold cross-validation, are also reported.

Table 3. Results from the online simulations. Sim 1 is the simulation where the XD+OT+LDA classifier is trained with Dataset A session $A1$, while Sim 2 is the simulation where the XD+LDA classifier is trained with Dataset A session $A4$.

Test Sess.	B1	B2	B3	B4	**Avg.**
Sim 2	0.66 ± 0.11	0.60 ± 0.07	0.76 ± 0.14	0.86 ± 0.09	$\mathbf{0.72 \pm 0.11}$
Sim 1	0.78 ± 0.12	0.71 ± 0.14	0.77 ± 0.10	0.69 ± 0.10	$\mathbf{0.74 \pm 0.04}$
SD cl.	0.78	0.80	0.68	0.85	**0.77**

We can see that, 3 times out of 4, our best pairwise transfer learning classifier outperforms the best pairwise transfer learning XD+LDA classifier. For subject P3, both classifiers score better than the session-dependent classifier.

Computation time

Regarding the complexity of our method, the average computation time needed to compute each transport map in pairwise transfer learning is equal to $\sim$8 sec, compared to $\sim$35 sec for Leave-One-Out transfer learning. Since the test sets are much smaller in the online simulation, the average computation time is $\sim$0.86 seconds per test set. All experiments were conducted on a computer with a 2.8 GHz Intel i7 processor and 8 GB of RAM.

DISCUSSION

The results presented in the previous section are strong indicators that the OT approach can effectively enhance transfer learning.

Regarding the mapping itself, the examples illustrated on Fig. 3 give us some insight on the process and how it acts on the components of the EEG signal. We see that, after the transport, the average values of the first X-DAWN component of $Target$ and $Nontarget$ class match quite well, especially for the $Nontarget$ class. However, due to the presence of a much larger number of $Nontarget$ class elements in the training set, it appears that samples whose elicited P300 component is weak are drawn to the training $Nontarget$ class barycenter. Our decision to select an equal number of elements in each class to generate the bootstraps for the BA method finds its motivation in this observation.

Another product of barycentric mapping is the observed decrease in the variance of the responses of the X-DAWN filters, seen on Fig. 3b and 3d. This is a consequence of the choices for parameter η and λ. For high values, the "new" data points tend to be drawn to the mean of each class in the existing set. Lower parameters generate a larger variance in each mapped class; however, they also reduce the separability of the classes in the mapped feature vector set.

Despite the fact that pairwise transfer learning did not produce conclusive result in favor of OT, our method generated the two highest AUC scores. Concerning Leave-One-Out transfer learning, we remark that the high level of variability in the training set, due to the fact that it contains trials from many different subjects, actually affects the average prediction accuracy in a positive way. Moreover, the use of the BA method induces a general improvement in prediction accuracy, and leads to even better results when OT-based mapping is used. However, it increases the computational time, since the computational cost of computing γ_0 depends on the size of the number of elements in each set.

Fortunately, the computational time of ≤ 1 sec for each small 36-trial set in the online simulation is low enough to allow for a fast online implementation. Our findings during online simulations show that our method outperforms the state-of-the-art classification method. These observations encourage us to continue our research towards the implementation of a zero-training OT-based classifier.

CONCLUSION

In this work, we have demonstrated that Discrete Regularized OT can be used in cross-subject transfer learning to improve the generalization capacities of existing P300-based classification methods. The results obtained by OT-based classifiers indicate that our method has the potential to cancel the need for calibration.

Nevertheless, we are most interested in understanding why some sets seem to contain more information than others. In future works, we would investigate which are the characteristics that qualify a good "map-to" candi-

Published by Verlag der TU Graz
Graz University of Technology

 DOI: 10.3217/978-3-85125-533-1-28

date. Subsequently, instead of using one specific session, or a number of bootstraps generated from specific sessions, we would be using a number of prototypical training sets that carry these characteristics. In that case, the voting scheme could be bypassed by session-dependent selection of one of these subsets with respect to a metric, such as the Kullback-Leibler divergence or the Information Geometry derived Riemannian distance.
While in this paper we concentrate on cross-subject transfer learning, this work can be extended to cross-session transfer learning or even be used to improve classification results within a session classifier. Finally, we are also interested in using this approach under Motor Imagery BCI paradigms.

ACKNOWLEDGEMENTS

The Nice University Hospital is acknowledged for providing the dataset used in this paper. We would also like to thank Rémi Flamary for letting us use his toolbox, Python Optimal Transport (POT).

REFERENCES

[1] Clerc M, Bougrain L, Lotte F. Brain-Computer Interfaces 1, Part 2, Wiley-ISTE (2016).

[2] Clerc M, Daucé E, Mattout J. Adaptive Methods in Machine Learning. In: Clerc M, Bougrain L, and Lotte F. Brain-Computer Interfaces 1. Wiley-ISTE, 2016, pp. 209-232.

[3] Krauledat M, Tangermann M, Blankertz B, Müller KR. Towards zero training for brain-computer interfacing. PloS one. 2008;3(8):e2967.

[4] Reuderink B, Farquhar J, Poel M, Nijholt A. A subject-independent brain-computer interface based on smoothed, second-order baselining, in Proc. IEEE EMBC, 2011, Boston, MA, USA, 2011, 4600-4604.

[5] Blankertz B, Dornhege G, Krauledat M, Müller KR, Curio G. The non-invasive Berlin brain–computer interface: fast acquisition of effective performance in untrained subjects. NeuroImage. 2007;37(2):539-550.

[6] Fazli S, Popescu M, Danóczy M, Blankertz B, Müller KR, Grozea C. Subject-independent mental state classification in single trials. Neural networks. 2009;22(9):1305-1312.

[7] Rakotomamonjy A, Guigue V. BCI competition III: dataset II-ensemble of SVMs for BCI P300 speller. IEEE transactions on biomedical engineering. 2008;55(3):1147-1154.

[8] Lu S, Guan C, Zhang H. Unsupervised brain computer interface based on intersubject information and online adaptation. IEEE Transactions on Neural Systems and Rehabilitation Engineering. 2009;17(2):135-145.

[9] Barachant A, Congedo M. A plug&play p300 bci using information geometry. arXiv preprint. 2004;arXiv:1409.0107.

[10] Courty N, Flamary R, Tuia D, Rakotomamonjy A. Optimal transport for Domain adaptation. IEEE Transactions on Pattern Analysis and Machine Intelligence. 2016.

[11] Ma R, Coleman TP. Generalizing the posterior matching scheme to higher dimensions via optimal transportation, in Proc. 49th Annual Allerton Conference on Communication, Control, and Computing , IEEE, 2011 , Allerton, IL, USA 96-102.

[12] Villani C. Optimal transport: old and new, Springer Science & Business Media, (2008).

[13] Kantorovitch L. On the translocation of masses. Management Science. 1958;5(1):1-4.

[14] Cuturi M. Sinkhorn distances: Lightspeed computation of optimal transport, in Proc. Advances in Neural Information Processing Systems, 2013, 2292-2300.

[15] Knight PA. The Sinkhorn–Knopp algorithm: convergence and applications. SIAM Journal on Matrix Analysis and Applications. 2008;30(1):261-275.

[16] Rivet B, Souloumiac A, Attina V, Gibert G. xDAWN algorithm to enhance evoked potentials: application to brain–computer interface. IEEE Transactions on Biomedical Engineering. 2009;56(8):2035-2043.

[17] Clerc M, Mattout J, Maby E, Devlaminck D, Papadopoulo T, Guy V, Desnuelle C. Verbal communication through brain computer interfaces, in Proc. Interspeech-14th Annual Conference of the International Speech Communication Association, 2013.

[18] Breiman L. Bagging predictors. Machine learning. 1996;24(2):123-140.

[19] Sun S, Zhang C, Zhang D. An experimental evaluation of ensemble methods for EEG signal classification. Pattern Recognition Letters. 2007;28(15):2157-2163.

[20] Blankertz B, Dornhege G, Müller KR, Schalk G, Krusienski D, Wolpaw JR, et al. Results of the BCI Competition III, in Proc. BCI Meeting, 2005.

[21] van der Maaten L, Hinton G. Visualizing data using t-SNE. Journal of Machine Learning Research. 2008;9(Nov):2579-2605.

Published by Verlag der TU Graz
Graz University of Technology

Proceedings of the
7th Graz Brain-Computer Interface Conference 2017 DOI: 10.3217/978-3-85125-533-1-29

HOW MANY ELECTRODES ARE NEEDED FOR MULTI-TARGET SSVEP-BCI CONTROL: EXPLORING THE MINIMUM NUMBER OF SIGNAL ELECTRODES FOR CCA AND MEC

F. W. Gembler[1], P. R. Stawicki[1], I. Volosyak[1]

[1]Rhine-Waal University of Applied Sciences, 47533 Kleve, Germany

E-mail: ivan.volosyak@hochschule-rhein-waal.de

ABSTRACT:
As the SSVEP paradigm (based on steady state visual evoked potentials) requires EEG-measurement, high number of EEG electrodes might be impractical in daily life scenarios because of the time consuming electrode montage. Reducing the number of signal electrodes can shorten preparation time but might compromise signal quality.
This paper explores the number of signal electrodes required to achieve sufficient control over multi-target SSVEP-based BCI systems.
In this respect, two of the most commonly used multi-channel classification methods, the minimum energy combination method (MEC) and the canonical correlation analysis (CCA), are investigated.
Data from six healthy subjects recorded during a copy spelling experiment using eight signal electrodes were analyzed off-line. A spelling interface with 30 flickering targets was used. Results for all possible channel combinations were evaluated, revealing that already three electrode channels are sufficient for reliable BCI control.

INTRODUCTION

Brain-computer interface (BCI) describes a field of technologies providing hope for the severely impaired as brain activity patterns are translated into output commands, allowing control of external devices without using any muscle activity [1]. Among other brain signals that can be utilized for spelling devices are so called Steady-State Visual Evoked Potentials (SSVEPs), which are evoked in the visual and parietal cortexes when gazing at a flickering visual stimulus [2]. Typically, SSVEPs are recorded noninvasively by electroencephalography (EEG). The graphical user interface (GUI) usually presents a set of stimuli flickering with distinct frequencies. If the user focuses on a particular stimulus, the corresponding frequency can be found in the recorded EEG.
Two established SSVEP signal detection methods are the minimum energy combination (MEC) method, an approach based on principal component analysis [3], and the canonical correlation analysis (CCA), a method of extracting similarities between two data sets [4]. One of the major challenges of EEG-based BCIs is posed by the considerable preparation time that is necessary to get ready for the EEG signal acquisition: Usually various signal electrodes are placed at the occipital areas, at the back of the head, which are usually covered with hair. For each of these electrodes electrolytic gel needs to be applied to assure low impedances; usually thresholds below 10 $k\Omega$ are required, depending on the type of electrodes used. A proper preparation can only be done by experienced personal. After use of the BCI-system the hair of the BCI users needs to be washed.
Several studies aiming to circumvent parts of the issues accompanying the EEG preparation procedure have been conducted. Some articles focus on the avoidance of electrolytic electrode gel. Water-based electrodes, for instance, could simplify daily setup and cleanup [5]. Dry-contact electrodes do not require any skin preparation or usage of gel at all [7]. However, the signal-to-noise ratio (SNR) might be considerably lower with these electrodes. Mihajlović et al. compared SSVEP-based BCI performance using dry, water and gel electrode setup[6]. By comparing the raw signal obtained within different EEG channels they found that the severity of noise contribution was higher for dry setup than for water-based setup, and for the water-based than the gel setup. Average classification accuracies across six participants were 63% for dry, 88% for water-based and 96% for gel electrodes.
Other research groups focus on a more practical electrode placement. E.g. Hsu et al. compared the amplitude-frequency characteristics of occipital and frontal SSVEPs; although the latter could be an alternative choice in design of SSVEP-based BCIs, the amplitudes and SNRs of occipital SSVEPs were significantly larger [8]. Similarly, Wang et al. employed EEG signals collected from non-hair-bearing areas such as the neck and ears for their SSVEP-BCI system [9]. While results from their high-density EEG recording (256 electrodes) demonstrated that

Published by Verlag der TU Graz
Graz University of Technology

 DOI: 10.3217/978-3-85125-533-1-29

SSVEPs are detectable with behind-the-ear electrode montage, SSVEPs acquired from occipital area were the strongest.
Another approach is to reduce the number of used electrodes in order to shorten the preparation time. Several articles investigated the impact of the number and location of electrode channels. Müller-Putz et al. investigated how the classification accuracy of a 4-class BCI can be improved by localizing individual EEG recording positions [10]. In a study with ten subjects, Friman et al. systematically excluded electrodes from offline analysis and stated that the MEC benefits from more electrodes because of the additional information gained about the nuisance signal [3]. Lin et al. also observed that using more channels for the CCA approach might improve recognition accuracy [4].
The presented paper further investigates the minimum number of signal electrodes for multi-target SSVEP-based BCI applications. In this respect, a spelling performance with a 30-target spelling application was evaluated. All possible channel combinations were evaluated off-line and ranked according to detection accuracy. In addition, the SSVEP response detection obtained with the MEC were compared with results obtained later off-line using CCA. The paper is organized as follows: the second section describes the experimental setup, and introduces the tested spelling application and used classification methods. The results are presented in the third section, followed by discussion and conclusion.

MATERIALS AND METHODS

Participants: BCI performance of six healthy volunteer subjects (two female, mean age 23.8 years) is evaluated in this paper. All participants were recruited from the Rhine-Waal University campus in Kleve. This research was approved by the ethical commitee of the medical faculty of the University Duisburg-Essen; the experiment was conducted in accordance with the Declaration of Helsinki. Before participation, subjects gave written informed consent. Participant information was not directly linked to experiment data, but stored pseudonymously. The EEG recording was conducted in a typical laboratory room with good light conditions and little background noise. Participation was not linked with a financial reward.

Hardware: Participants were seated on a comfortable chair in front of a computer monitor (BenQ XL2420T, resolution: 1920×1080 pixels, vertical refresh rate: 120 Hz) at a distance of about 60 cm. The used computer system operated on Microsoft Windows 7 Enterprise running on an Intel processor (Intel Core i7, 3.40 GHz).
Ag/AgCl electrodes were used to acquire the signals from the surface of the scalp for the EEG recording.

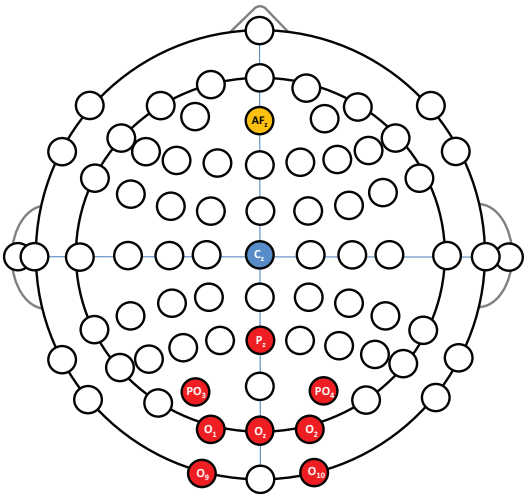

Figure 1: Signal electrodes used in the on-line experiment. Eight signal electrodes were placed at $P_Z, PO_3, PO_4, O_1, O_2, O_Z, O_9$ and O_{10}. Ground was placed over AF_Z, the reference electrode over C_Z.

Electrode placement in accordance with the international 10-20 system was applied. The ground electrode was placed over AF_Z, the reference electrode over C_Z, and the eight signal electrodes were placed at $P_Z, PO_3, PO_4, O_1, O_2, O_Z, O_9$ and O_{10} (see also Fig. 1). In order to assure high signal quality, standard abrasive electrode gel was applied between the electrodes and the scalp to bring impedances below 5 $k\Omega$. A g.USBamp (Guger Technologies, Graz, Austria) EEG amplifier was utilized with a sampling frequency of 128 Hz. An analogue band pass filter (between 2 and 30 Hz) and a notch filter (around 50 Hz) were applied.

Signal Acquisition: The MEC [2, 3] was used for on-line SSVEP signal classification. This method creates a set of channels (a weighted combination of the electrode signals) that minimize the nuisance signals. For EEG detection, we consider N_t samples of EEG data. The sampled EEG signal data from N_y electrodes can be written as $N_t \times N_y$ matrix

$$Y = X_f A + B. \tag{1}$$

The $N_t \times 2N_h$ model matrix X_f associated with the N_h harmonics of a stimulus frequency f is defined by

$$X_f(t, 2k-1) = sin(2\pi k f t) \tag{2}$$
$$X_f(t, 2k) = cos(2\pi k f t) \tag{3}$$

for $k = 1, \ldots, N_h$. The matrix A contains the amplitudes for the expected sinusoids and B contains the information that cannot be attributed to the SSVEP response. The noise and nuisance signal can be estimated by removing the SSVEP components from the signal. In this respect, the signal Y is projected

Published by Verlag der TU Graz
Graz University of Technology

 DOI: 10.3217/978-3-85125-533-1-29

on the orthogonal complement of the SSVEP model matrix,

$$\tilde{Y} = Y - X_f(X_f^T X_f)^{(-1)} X_f^T Y. \quad (4)$$

As $B \approx \tilde{Y}$, an optimal weight combination for the electrode signals can then be found by calculating the eigenvectors of $\tilde{Y}^T\tilde{Y}$ (please refer to [2] for more details). The calculated SSVEP power estimations $\hat{P}_f$ of the frequency f in the spatially filtered signals were then normalized into probabilities,

$$p_f = \frac{\hat{P}_f}{\sum_{j=1}^{N_f} \hat{P}_j}. \quad (5)$$

For the implemented application, power estimations for $N_f = 30$ frequencies, considering $N_h = 2$ harmonics, were evaluated.

The CCA approach, on the other hand, works on two variable sets (see e. g [4]). Here, one set was chosen to be the electrode signals Y, and the other was the SSVEP model matrix X_f associated with the $N_h = 2$ harmonics of a specific stimulation frequency f. CCA was applied for each of the 30 stimulation frequencies; weighted vectors a and b such that the linear combinations $x_f = X_f^T a$ and $y = Y^T b$ are maximally correlated were found by solving

$$\max_{a,b} \rho_f = \frac{E[x_f^T y]}{\sqrt{E[x_f^T x_f]E[y^T y]}}. \quad (6)$$

The maximum canonical correlation ρ_f was calculated for each frequency f; the frequency associated with the highest correlation value determined the output command.

The on-line experiment was conducted using the MEC. The classification was performed on the basis of the hardware synchronization of the EEG amplifier (g.USBamp). EEG data were transferred block-wise to the computer. Each block consisted of 13 samples (101.5625 ms with the sampling rate of 128 Hz). Block-wise increasing classification time window were used (refer to [2] for more details). If a particular stimulation frequency had the highest probability, exceeded a certain predefined threshold and the classification time window exceeded 20 blocks (approximately 2 seconds), the corresponding command was classified. After each classification the flickering stopped for approximately 914 ms (9 blocks).

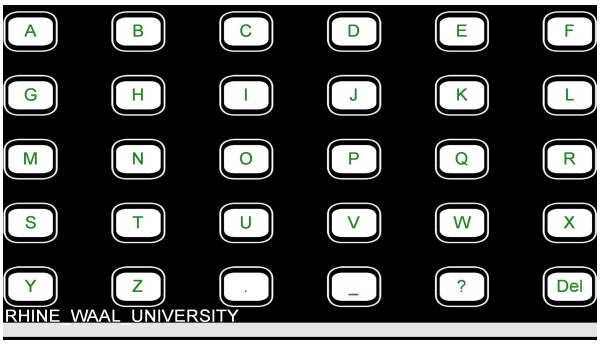

Figure 2: Graphical user interface used in the on-line experiment. The spelling task was to write "RHINE WAAL UNIVERSITY" (name of our University). In total, 30 frequencies between 6.1 Hz and 11.7 Hz flickered simultaneously.

During this gaze shifting period, the targets did not flicker and the user changed his or her focus to another target unhindered (please also refer to [2] for more details).

Software: The spelling interface displayed 30 selectable buttons representing the alphabet plus additional characters (see Fig. 2). Each button flickered with a specific frequency. The button sizes varied between 130×90 and 170×120 pixels in relation to the SSVEP amplitude during the experiment as described in [2]. Each button was outlined by a frame which determined the maximum size a box could reach. Additionally, to increase user friendliness, command classifications were followed by an audio feedback.
To implement the 30 stimulation frequencies a frame-based stimulus approximation was used (see e. g [12, 11]). Frequencies between 6.1 and 11.7 Hz (logarithmic distributed resolution, as suggested in [13]) were implemented. This range was used in previous studies as well, as it avoids overlapping in the 2-nd harmonics frequencies while still allowing a sufficient difference between frequencies [14].

Experimental Setup: After signing the consent form, each participant was prepared for the EEG recording. Then participants went through a short familiarization run, spelling short words such as "KLEVE", "BCI" or "BRAIN". Thereafter, participants were instructed to write the phrase "RHINE WAAL UNIVERSITY". Spelling errors were corrected via the "delete" button. The entire session took on average roughly 30 minutes.

RESULTS

For the evaluation of the BCI performance we considered the command accuracy P (the number of correct command classifications divided by the total number of classified commands C_n) as well as the commonly

Published by Verlag der TU Graz
Graz University of Technology

 DOI: 10.3217/978-3-85125-533-1-29

Table 1: Results from the analysis of the copy spelling task with different numbers of channels. Average accuracies [%] and ITRs [bpm] over all participants for the best channel configurations are provided for CCA and MEC. Additionally, the amount of combinations surpassing accuracy thresholds of 90% and 70% are listed. The last column displays the mean accuracy over all combinations with the given number of electrodes.

Electrodes		Acc. (ITR) of the best combination		Combinations acc. >90%		Combinations acc. >70%		Mean acc. (ITR) over all combinations	
No.	Best combination	CCA	MEC	CCA	MEC	CCA	MEC	CCA	MEC
1	O_Z	48 (15)	48 (15)	0/8	0/8	0/8	0/8	38 (10)	38 (10)
2	O_Z,O_{10}	67 (25)	66 (24)	0/28	0/28	0/28	0/28	54 (17)	49 (15)
3	P_Z,O_Z,O_{10}	84 (34)	87 (37)	0/56	0/56	20/56	12/56	67 (24)	63 (22)
4	P_Z,PO_4,O_Z,O_9	93 (41)	93 (41)	4/70	5/70	55/70	55/70	77 (30)	76 (29)
5	P_Z,PO_4,O_Z,O_2,O_9	96 (42)	97 (43)	18/56	22/56	55/56	55/56	85 (35)	85 (35)
6	P_Z,PO_4,O_1,O_Z,O_2,O_9	98 (45)	99 (45)	19/28	19/28	28/28	28/28	91 (39)	92 (40)
7	P_Z,PO_3,O_1,O_Z,O_2,O_9,O_{10}	99 (45)	100 (46)	7/8	7/8	8/8	8/8	96 (42)	97 (43)
8	P_Z,PO_3,PO_4,O_1,O_Z,O_2,O_9,O_{10}	98 (45)	100 (46)	1/1	1/1	1/1	1/1	99 (45)	100 (46)

used information transfer rate (ITR) in bits/min (see e. g [1]). The number of bits per trial B is given by

$$B = \log_2 N + P \log_2 P + (1-P) \log_2 \left[\frac{1-P}{N-1} \right],$$

where N represents the overall number of possible outputs ($N = 30$, given by the number of targets). To obtain ITR in bits per minute, B is multiplied by the number of command classifications per minute.
In the on-line experiment the MEC with eight signal electrodes was utilized. All participants completed the copy spelling task without any errors achieving a mean ITR of 45.9 bpm.
For the off-line analysis the recorded electrode signals were re-evaluated and channel combinations were ranked according to detection accuracy using the MEC as well as the CCA. The time windows for the off-line classifications were determined by the on-line performance.
In order to investigate to what extend classification accuracy drops with fewer electrodes, channels were excluded systematically. E. g, to examine detection accuracy using only five channels, the off-line analyses was carried out with all $\binom{8}{5} = 56$ options to choose five out of eight recorded signals. All possible combinations composed of the eight recorded signals were evaluated using the numerical computing environment MATLAB. Electrode combinations were ranked according to the accuracies achieved in the simulated experiment. Results based on the off-line analysis are provided in Table 1, Fig. 3 and Fig. 4.

DISCUSSION

In the following we want to summarize and discuss the most relevant results from the off-line analysis.
As also observed by Müller-Putz et al., optimal recording channels differ between subjects, but some electrodes tended to be important in a larger number of subjects [10]. All participants, achieved peak performance with all eight channels. As expected, the accuracy generally increases if a higher number of channels is used. But some of the combinations using less than four electrodes worked surprisingly well. With the channel combination P_Z,O_Z,O_{10} average accuracies above 85% were achieved.

The results obtained with single electrodes show that for most participants the O_Z electrode yielded highest accuracies, followed by O_1 and O_2 (see Fig. 3). The relevance of the P_Z electrode for multiple channel combinations can also be seen in Tab 1. The best electrode combinations using three electrodes or more all included P_Z. Further, the analysis of combinations using seven electrodes (all but one of the electrode signals) showed that the combination excluding P_Z was by far the weakest. While the average of all combinations using seven electrodes was above 95%, the combination excluding P_Z yielded less than 85% accuracy. Interestingly, one participant, subject 2, reached 100% accuracy with channel P_Z alone.

Though electrodes O_9 and O_{10} yielded lowest accuracies of all single electrodes, all of the highest ranked combinations (with more than one electrode) included either O_9 or O_{10} (see Tab. 1).

This findings might be interesting for the design of, optically more pleasing and more practical EEG-caps. For example, signal electrodes could be implemented in the side and back straps of typical head mounted displays (HMDs) used for virtual reality (VR) simulations in respect to the aforementioned locations; some articles already tested the SSVEP method successfully in a VR HMD (see e. g [15]).

In general, results achieved with CCA and MEC are relatively equivalent. There seems to be no difference between the methods for different time windows (see Fig. 4). This is consistent with previous findings by Cecotti et al. [16]. The optimal electrode combinations between the methods differed only slightly.

Published by Verlag der TU Graz
Graz University of Technology

 DOI: 10.3217/978-3-85125-533-1-29

It is worth noting that the mean accuracy over all combinations with less than three electrodes was slightly higher with the CCA. For combinations with four electrodes or more the mean for the MEC was slightly better (see Tab. 1).

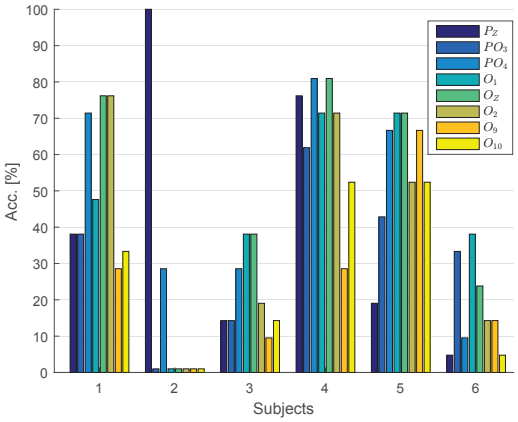

Figure 3: MEC detection accuracies for individual channels. The entire experiment was re-evaluated off-line for each single electrode.

The increased channel number could be more relevant for the MEC, as it might lead to a more precise estimation of the noise and nuisance signals due to the additional information gained.
Fig. 4 also addresses the importance of classification time window length. A dynamic time window with minimal length of roughly 2 seconds was used, a rather typical value throughout BCI literature (see also [16]). It should be noted though, that some studies reported good results with smaller time windows as well [2, 11].
Note that we tested these two methods in a rather standard form and they usually could be improved in several ways. Training sessions to choose electrode scalp path as suggested by Lin et al. could improve the CCA. Instead of sinusoidal reference signals, EEG training data could be incorporated in the CCA templates, reflecting natural SSVEP features (see e. g [17]). While the MEC does not require additional training, a user specific calibration could enhance accuracies as well [18, 19]. Longer test sessions with a broader population including participants of the target group (severly disapled people) are required to further investigate results under conditions that are as realistic as possible.

CONCLUSION

The effect of channel selection of two multi channel SSVEP detection methods (MEC and CCA) was investigated. Though both methods benefit from a larger number of electrodes, presumably because of the additional information gained about the nuisance signal, some electrode configurations using a lower amount of channels yielded good results.

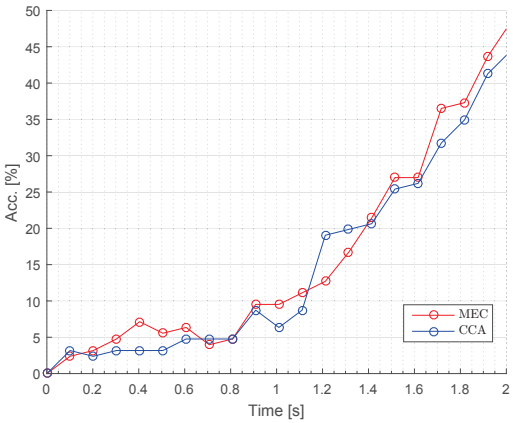

Figure 4: Comparison of MEC and CCA. The grand average accuracy achieved using all eight recorded signals is displayed as a function of the classification blocks for both MEC and CCA. Dynamic classification windows with a minimum length of roughly 2 seconds were used in the on-line experiment. Chance level in target identification was 3.33%.

For both methods the minimum number of channels required to achieve classification accuracies above 70% was three. Especially the channel combination P_Z,O_Z,O_{10} yielded good results for both methods which might be relevant for the design of practical EEG-caps. Optimal channel sets all included the P_Z electrode.
The comparison of mean classification accuracies show no significant difference between the CCA and MEC. Further improvement of the detection could allow a greater reduction of electrode channels and simplify the setup.

ACKNOWLEDGEMENT

This research was supported by the European Fund for Regional Development under Grant GE-1-1-047. The authors thank the participants and student assistants for their help during the study.

REFERENCES

[1] J. Wolpaw, N. Birbaumer, D. McFarland, G. Pfurtscheller, and T. Vaughan. Brain-computer interfaces for communication and control. Clin. Neurophysiol., vol. 113, pp. 767–791, 2002.

[2] I. Volosyak. SSVEP-based Bremen-BCI interface – boosting information transfer rates. J. Neural Eng., vol. 8, no. 3, p. 036020, 2011.

Published by Verlag der TU Graz
Graz University of Technology

 DOI: 10.3217/978-3-85125-533-1-29

[3] O. Friman, I. Volosyak, and A. Gräser. Multiple Channel Detection of Steady-State Visual Evoked Potentials for Brain-Computer Interfaces. IEEE Trans. Biomed. Eng., vol. 54, no. 4, pp. 742–750, 2007.

[4] Z. Lin, C. Zhang, W. Wu, and X. Gao. Frequency recognition based on canonical correlation analysis for SSVEP-based BCIs. IEEE Transactions on Biomedical Engineering, vol. 53, no. 12, pp. 2610–2614, 2006.

[5] I. Volosyak, D. Valbuena, T. Malechka, J. Peuscher, and A. Gräser. Brain-Computer Interface using Water-based Electrodes. J. Neural Eng., vol. 7, p. 066007, 2010.

[6] V. Mihajlović, G. Garcia-Molina, J. Peuscher. Dry and water-based EEG electrodes in SSVEP-based BCI applications, in: International Joint Conference on Biomedical Engineering Systems and Technologies. pp. 23–40. Springer (2012)

[7] Y. M. Chi, Y.-T. Wang, Y. Wang, C. Maier, T.-P. Jung, and G. Cauwenberghs. Dry and non-contact EEG sensors for mobile brain–computer interfaces. IEEE Transactions on Neural Systems and Rehabilitation Engineering, vol. 20, no. 2, pp. 228–235, 2012.

[8] H. Hsu, I. Lee, H. Tsai, H. Chang, K. Shyu, C. Hsu, H. Chang, T. Yeh, C. Chang, and P. Lee. Evaluate the feasibility of using frontal SSVEP to implement an SSVEP-based BCI in young, elderly and ALS groups. Neural Systems and Rehabilitation Engineering, IEEE Transactions on, vol. PP, no. 99, pp. 1–1, 2015.

[9] Y.-T. Wang, Y. Wang, C.-K. Cheng, and T.-P. Jung. Measuring steady-state visual evoked potentials from non-hair-bearing areas, in 2012 Annual International Conference of the IEEE Engineering in Medicine and Biology Society, pp. 1806–1809, IEEE, 2012.

[10] G. R. Müller-Putz, E. Eder, S. C. Wriessnegger, and G. Pfurtscheller. Comparison of DFT and lock-in amplifier features and search for optimal electrode positions in SSVEP-based BCI. Journal of neuroscience methods, vol. 168, no. 1, pp. 174–181, 2008.

[11] X. Chen, Y. Wang, M. Nakanishi, T.-P. Jung, and X. Gao. Hybrid frequency and phase coding for a high-speed SSVEP-based BCI speller, in Engineering in Medicine and Biology Society (EMBC), 2014 36th Annual International Conference of the IEEE, pp. 3993–3996, 2014.

[12] Y. Wang, Y.-T. Wang, and T.-P. Jung. Visual stimulus design for high-rate SSVEP BCI. *Electronics letters*, vol. 46, no. 15, pp. 1057–1058, 2010.

[13] P. Stawicki, F. Gembler, and I. Volosyak. Evaluation of Suitable Frequency Differences in SSVEP-Based BCIs, in Symbiotic Interaction, pp. 159–165, Springer, 2015.

[14] F. Gembler, P. Stawicki, and I. Volosyak. Exploring the possibilities and limitations of multitarget SSVEP-based BCI applications, in Engineering in Medicine and Biology Society (EMBC), 2016 IEEE 38th Annual International Conference of the, pp. 1488–1491, IEEE, 2016.

[15] B. Koo and S. Choi. SSVEP response on Oculus Rift, in Brain-Computer Interface (BCI), 2015 3rd International Winter Conference on, pp. 1–4, IEEE, 2015.

[16] H. Cecotti and D. Coyle. Calibration-less detection of steady-state visual evoked potentials-comparisons and combinations of methods, in 2014 International Joint Conference on Neural Networks (IJCNN), pp. 4050–4055, IEEE, 2014.

[17] H. Wang, Y. Zhang, N. R. Waytowich, D. J. Krusienski, G. Zhou, J. Jin, X. Wang, and A. Cichocki. Discriminative Feature Extraction via Multivariate Linear Regression for SSVEP-Based BCI. IEEE Transactions on Neural Systems and Rehabilitation Engineering, vol. 24, no. 5, pp. 532–541, 2016.

[18] F. Gembler, P. Stawicki, and I. Volosyak. Autonomous Parameter Adjustment for SSVEP-based BCIs with a Novel BCI Wizard. Frontiers in neuroscience, vol. 9, 2015.

[19] P. Stawicki, F. Gembler, and I. Volosyak. Driving a semi-autonomous mobile robotic car controlled by a SSVEP-based BCI. Computational Intelligence and Neuroscience, Hindawi, vol. 2016, no. 5, 2016.

Published by Verlag der TU Graz
Graz University of Technology

Proceedings of the
7th Graz Brain-Computer Interface Conference 2017 DOI: 10.3217/978-3-85125-533-1-30

INVESTIGATING MUSIC IMAGERY AS A COGNITIVE PARADIGM FOR LOW-COST BRAIN-COMPUTER INTERFACES

L. Großberger[1], M. R. Hohmann[1], J. Peters[1,2], M. Grosse-Wentrup[1]

[1]Max Planck Institute for Intelligent Systems, Department for Empirical Inference, 72076 Tübingen, Germany
[2]Intelligent Autonomous Systems, Technische Universität Darmstadt, 64289 Darmstadt, Germany

lukas.grossberger@tuebingen.mpg.de

ABSTRACT: Many current brain-computer interfaces (BCIs) rely on motor imagery or oculomotor paradigms to transfer information, yet these functions are impaired in people that suffer from late stage Amyotrophic Lateral Sclerosis (ALS). Additionally, patients have limited access to cutting-edge BCI technology for home-use because the necessary, medical grade equipment is expensive and difficult to setup.
We addressed both issues with the current study. First, we devised a novel paradigm that relies on music imagery and mental subtraction. We argue that these are motor-independent abilities that can be reliably executed, without the need for subject training. We find that both tasks can be distinguished after only one experimental session with a 124-channel EEG system, from the band-power in the theta (4-8 Hz) and alpha (8-13 Hz) range. Second, we tested our paradigm in combination with a low-cost EEG system to show that it can be used to develop accessible BCIs for patients in the future.

INTRODUCTION

Background For patients suffering from paralysis, brain-computer interfaces (BCIs) offer the possibility of renewed communication [1, 2, 3]. This is of great importance for people who suffer from amyotrophic lateral sclerosis (ALS), a motor-neuron disease that renders patients completely locked-in during its final stage [4]. However, BCIs for ALS patients suffer from two limitations: The usability of existing paradigms varies greatly, and the required technology is expensive and difficult to set up.
In the final stages of their disease, ALS patients are unable to use most current BCIs that rely on motor-imagery or oculomotor control [5], as these functions decay during disease progression [1, 6]. Recently, efforts have been made to combine motor imagery with higher cognitive tasks including spatial navigation, meditation, mental calculation to improve BCI usage for people with motor-disabilities [7, 8]. Hohmann et al. [9, 12] devised a self-paced strategy that relies on positive self-referential thoughts to modulate activity in the Default-Mode Network (DMN) as an alternative to motor-based strategies. However, it was argued that repeatedly recalling a positive memory may induce fatigue which limits the performance of the BCI over longer time-periods.

Current Work We propose music imagery as another motor-independent task for BCI control. Music imagery fulfils three important criteria: First, it targets a cognitive process that should be immediately accessible to everyone. Second, it is unrelated to motor imagery. And third, it is self-paced and stimulus-independent and should therefore remain accessible to completely paralysed patients. We argue that music imagery is a more concrete task than self-referential thought generation and it may therefore be easier to execute it repeatedly. Music imagery has been found to modulate parietal alpha, similar to positive self-referential thoughts [10].
Based on Hohmann et al. [12], we choose mental subtraction as the opposing task. Mental subtraction is related to an increase in prefrontal theta and a decrease in parietal alpha [13]. With music imagery and mental subtraction we introduce an easy-to-use two-class paradigm that can be performed without the need for motor-abilities.
BCIs are only accessible to patients if they are affordable and easy to set up. To investigate the portability of our paradigm, we tested our paradigm on a low-cost EEG system, in addition to our recordings with a conventional high-density EEG system.

MATERIALS AND METHODS

Experimental Paradigm We conducted a study with 10 healthy subjects that were seated in a chair approx. 1.25 meters away from a 17" LCD screen with a refresh rate of 60 Hz and a resolution of 1280x1024 px. For each trial the instructions were presented in white font on a black background. Between instructions we presented a fixation cross in the middle of the screen.
After the resting phase we recorded two experimental phases, where we employed the high-density EEG and the low-cost EEG for recording. Each experimental phase consisted of two blocks with a brief intermission that each contained 10 trials for the mental subtraction task and 10 for the music imagery task, in randomized order. The order of those two phases was counterbalanced between subjects.
For the music imagery condition, participants were asked to “imagine a favourite song”. In the mental subtraction

Published by Verlag der TU Graz
Graz University of Technology

 DOI: 10.3217/978-3-85125-533-1-30

task they were asked to "continuously subtract X from Y" until the end of the trial, where X was a single-digit number and Y was a three-digit number. We excluded 1, 2 and 5 for the single digit number and restricted the range of the three digit number to the interval between $[800, 999]$. Each trial took 35 seconds and began with 5 ± 0.50 seconds pause, after which the instructions were displayed on screen as well as given acoustically by a text-to-speech engine (CereProc Ltd., Edinburgh, United Kingdom). The respective task then had to be executed continuously for the whole trial.

Experimental Data The study was conducted at the Max Planck Institute for Intelligent Systems in Tübingen, Germany. Ten healthy subjects (five male and five female, mean age 24.6 ± 3.6 years) were recruited from the local community and received 12 Euro per hour for their participation. Half of the subjects had previous experience with EEG studies. The experimenter informed them about the procedure with standardised instructions. All participants signed a consent form in advance to confirm their voluntary participation. For the high-density system, a 124-channel EEG was employed. Recordings were conducted at a sampling rate of 500 Hz using actiCAP active electrodes and a BrainAmp amplifier (BrainProducts GmbH, Gilching, Germany). Electrodes were placed according to the 10-5 system with the left mastoid electrode as the initial reference. For the low-cost system, a 14-channel EPOC+ portable EEG system (EMOTIV, San Francisco, U.S.A.) was employed. Recordings were conducted at a sampling rate of 128 Hz. OpenViBE [14] was used to record and store the EEG data. Because of technical issues we excluded the recorded low-cost device data for the first three subjects .

Data Analysis The analysis was performed offline.
To differentiate between the patterns of neural activity related to music imagery and mental subtraction we computed per-trial θ-bandpower features between 4 and 8 Hz as well as α-bandpower features between 8 and 13 Hz for all channels. For each subject the feature matrix contains $trials \times features$, which is one alpha and theta value per channel per trial, so a $40 \times (2 * 124)$ matrix for the high-density system (124 electrodes), and a $40 \times (2 * 14)$ matrix for the low-cost system (14 electrodes). The number of features is twice the number of electrodes since for each electrode there are two bandpower values associated.
We used a transfer learning method by Jayaram et al. [15] to account for variation across subjects and the issues arising from large feature spaces. This method fits a linear regression model for each subject individually but penalises deviations in the regression weights from a Gaussian prior distribution. We evaluated the classification performance on one subject in a 10-fold cross-validation procedure, after learning a prior on all others as follows. Afterwards we tested the $H_0 : Accuracies_{BrainAmp} \neq Accuracies_{EPOC+}$ by a paired Student's T-Test.
To investigate the meaningfulness of the weights learned by the transfer learning framework, we multiplied the learned weights with the feature covariance matrix [16]. The resulting matrix can be visualized as a topography map where each value represents the importance the classifier has assigned to this channel based on the modulation by the cognitive strategy.

RESULTS

We achieved a mean classification accuracy of 85% with the high-density system and 77% with the low-cost system (Fig. 1). The paired Student's T-Test yields a significant difference between the classification accuracies from subjects S4 to S10 of the BrainAmp ($M = 0.84, SD = 0.17$) compared to the EPOC+ ($M = 0.77, SD = 0.18$); $t(6) = -2.83,\ p = 0.03$.

After multiplying the weights learned by the transfer learning framework with the feature covariance, we obtained the relevance-map of all 124 features for both the theta and alpha frequency-band (Figure 2).

The channel with the largest weight for the alpha features is PO1 and for the theta features is AFF1. Figure 3 shows the modulation in the power spectrum for both tasks at both of those channels from the BrainAmp recordings.

DISCUSSION

We investigated whether the neural activity during music imagery and mental subtraction could be discriminated without prior subject-training. We found that we can classify both tasks with a mean accuracy of 85% for the high-density EEG system, and 77% for a low-cost EEG system. Additionally, we observed high classification weights for frontal electrodes for the theta band-power features and parietal ones for alpha.
Our results are consistent with previous publications that show frontal activation during a mental subtraction task [17, 18] and parietal activity in the alpha band for music imagery [11]. Therefore the spatial patterns of the relevant features for classification (Figure 2) are in line with our hypotheses and previous research of both tasks.
All except one subject reported the tasks to be very easy. Only subject S4 reported both tasks to be "boring", which might have lead them to not participating very actively over the course of the experiment, causing the decrease in performance as depicted in Fig. 1.
The performance of the low-cost system was significantly lower than the performance of the full-sized system. This may have been caused by the smaller amount of channels, the lesser quality of the electrodes, or non-optimal positioning of the sensors for this paradigm. However, on both the high-density and the low-cost system, we achieved classification performances above 70%, which is considered to be the threshold for building a meaningful communication device. Therefore, we argue that our

Published by Verlag der TU Graz
Graz University of Technology

 DOI: 10.3217/978-3-85125-533-1-30

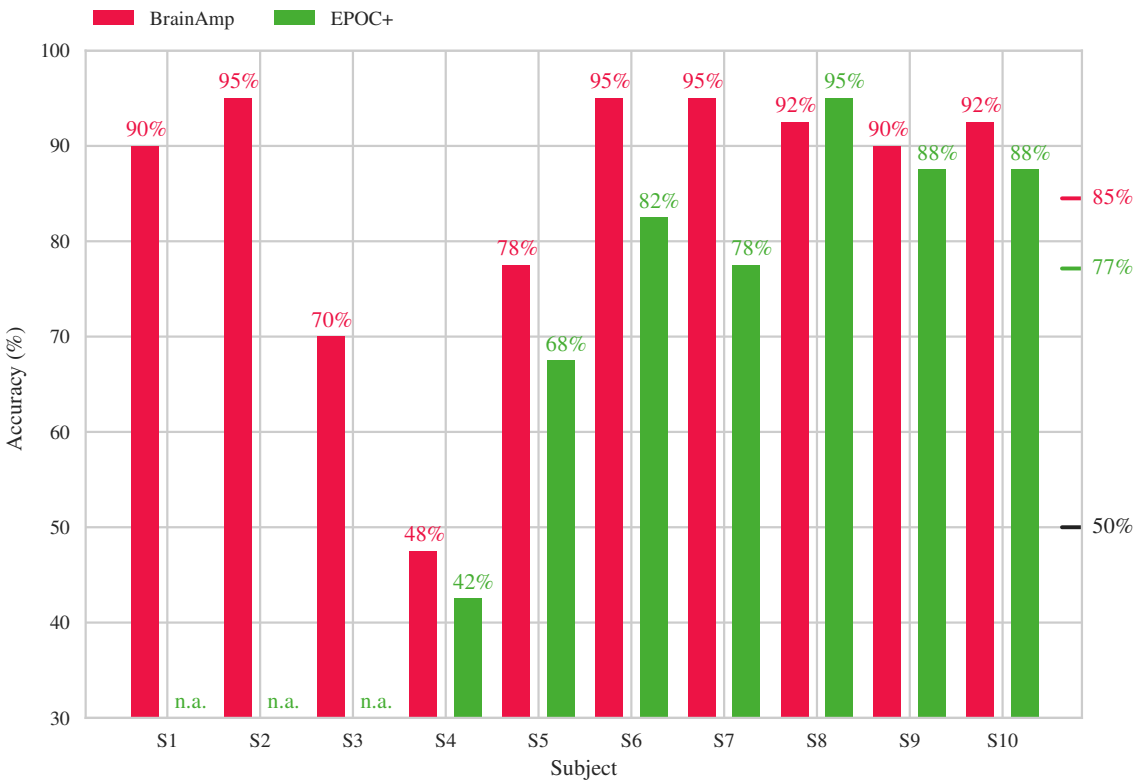

Figure 1: Classification accuracies for both devices (BrainAmp & EPOC+) for all ten individual subjects (S1-S10) in case of the brain amp and the reduced subject set (S4-S10) for the EPOC+. The mean classification accuracy across subjects is 85% for the BrainAmp and 77% for the EPOC+. Chance level (50%) as well as both mean accuracies are indicated with a solid tick on the right of the plot and are labeled accordingly.

results motivate further studies that focus on the development of low-cost EEG devices with better electrode placement with respect to the presented paradigm, or a higher signal quality.

Asking subjects to imagine their favorite song is hard to control, as songs vary in their genre, complexity, the presence of lyrics, and personal relevance. The large variability could have affected the classification performance. To get a better understanding of the effects, it would be interesting to combine this EEG approach with an imaging method like fMRI. This could provide some insight in the related brain-networks which might be for example the dorsal attention network as Scherer et al. [7] hypothesize.

Most importantly, an online BCI study with ALS-patients in all stages of the disease is very important to investigate the feasibility of this cognitive paradigm.

CONCLUSION

We find the neural activity elicited by music imagery and mental subtraction to be distinguishable after only one experimental session. We believe, that our work can be used as a foundation for future development of reliable and accessible systems for paralyzed patients to communicate throughout the whole progress of their disease.

ACKNOWLEDGEMENTS

We especially thank Bernd Battes for the technical support on the hardware and Theresa Emde for her assistance during data collection.

REFERENCES

[1] Niels Birbaumer. Breaking the silence: Brain–computer interfaces (BCI) for communication and motor control. *Psychophysiology*, 43(6):517–532, nov 2006. doi: 10.1111/j.1469-8986.2006.00456.x.

[2] Rajesh P N Rao. *Brain-Computer Interfacing*. Cambridge University Press, New York, 2013. doi: 10.1017/CBO9781139032803.

[3] Moritz Grosse-Wentrup and Bernhard Schölkopf. A brain-computer interface based on self-regulation of gamma-oscillations in the superior parietal cortex. *Journal of Neural Engineering*, 11(5):056015, 2014. doi: 10.1088/1741-2560/11/5/056015.

[4] Kuninobu Nihei, Ann C. McKee, and Neil W. Kowall. Patterns of neuronal degeneration in the

Published by Verlag der TU Graz
Graz University of Technology

 DOI: 10.3217/978-3-85125-533-1-30

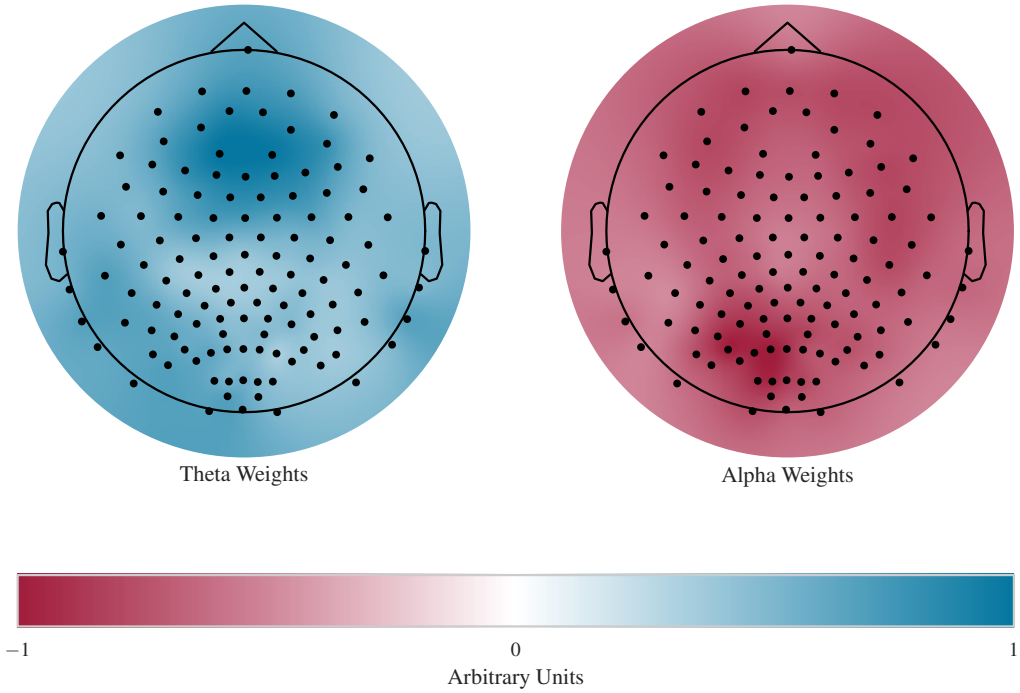

Figure 2: Topography of the weights of the transfer learning classifier based on the BrainAmp recordings. A larger weight represents stronger relevance for the classification. The weights for the theta features are plotted on the left and on the right the weights for the alpha features can be seen.

motor cortex of amyotrophic lateral sclerosis patients. *Acta Neuropathologica*, 86:55–64, 1993. doi: 10.1007/BF00454899.

[5] Mauro Marchetti and Konstantinos Priftis. Brain–computer interfaces in amyotrophic lateral sclerosis: A metanalysis. *Clinical Neurophysiology*, 126(6):1255–1263, jun 2015. doi: 10.1016/j.clinph.2014.09.017.

[6] Peter Brunner, S. Joshi, S. Briskin, Jonathan R. Wolpaw, H. Bischof, and Gerwin Schalk. Does the 'P300' speller depend on eye gaze? *Journal of Neural Engineering*, 7(5):056013, oct 2010. doi: 10.1088/1741-2560/7/5/056013.

[7] Reinhold Scherer, Josef Faller, Elisabeth V C Friedrich, Eloy Opisso, Ursula Costa, Andrea Kübler, et al. Individually adapted imagery improves brain-computer interface performance in end-users with disability. *PLoS ONE*, 10(5):1–14, 2015. doi: 10.1371/journal.pone.0123727.

[8] Elisabeth V.C. Friedrich, Reinhold Scherer, and Christa Neuper. The effect of distinct mental strategies on classification performance for brain–computer interfaces. *International Journal of Psychophysiology*, 84(1):86–94, apr 2012. doi: 10.1016/j.ijpsycho.2012.01.014.

[9] Matthias R Hohmann, Tatiana Fomina, Vinay Jayaram, Natalie Widmann, Christian Förster, Jennifer Müller vom Hagen, et al. A Cognitive Brain-Computer Interface for Patients with Amyotrophic Lateral Sclerosis. *Proceedings of the 2015 IEEE International Conference on Systems, Man, and Cybernetics (SMC2015)*, 2015. doi: 10.1109/SMC.2015.553.

[10] Yan Mu and Shihui Han. Neural oscillations involved in self-referential processing. *Neuroimage*, 53(2):757–768, 2010.

[11] Rebecca S. Schaefer, Rutger J. Vlek, and Peter Desain. Music perception and imagery in EEG: Alpha band effects of task and stimulus. *International Journal of Psychophysiology*, 82(3):254–259, 2011. doi: 10.1016/j.ijpsycho.2011.09.007.

[12] MR Hohmann, T Fomina, V Jayaram, C Förster, J Just, M Synofzik, et al. An improved cognitive brain-computer interface for patients with amyotrophic lateral sclerosis. 2016.

[13] Bert De Smedt, Roland H Grabner, and Bettina Studer. Oscillatory eeg correlates of arithmetic strategy use in addition and subtraction. *Experimental brain research*, 195(4):635–642, 2009.

[14] Yann Renard, Fabien Lotte, Guillaume Gibert, Marco Congedo, Emmanuel Maby, Vincent Delannoy, et al. Openvibe: An open-source software platform to design, test, and use brain–computer interfaces in real and virtual environments. *Presence*, 19 (1):35–53, 2010.

Published by Verlag der TU Graz
Graz University of Technology

 DOI: 10.3217/978-3-85125-533-1-30

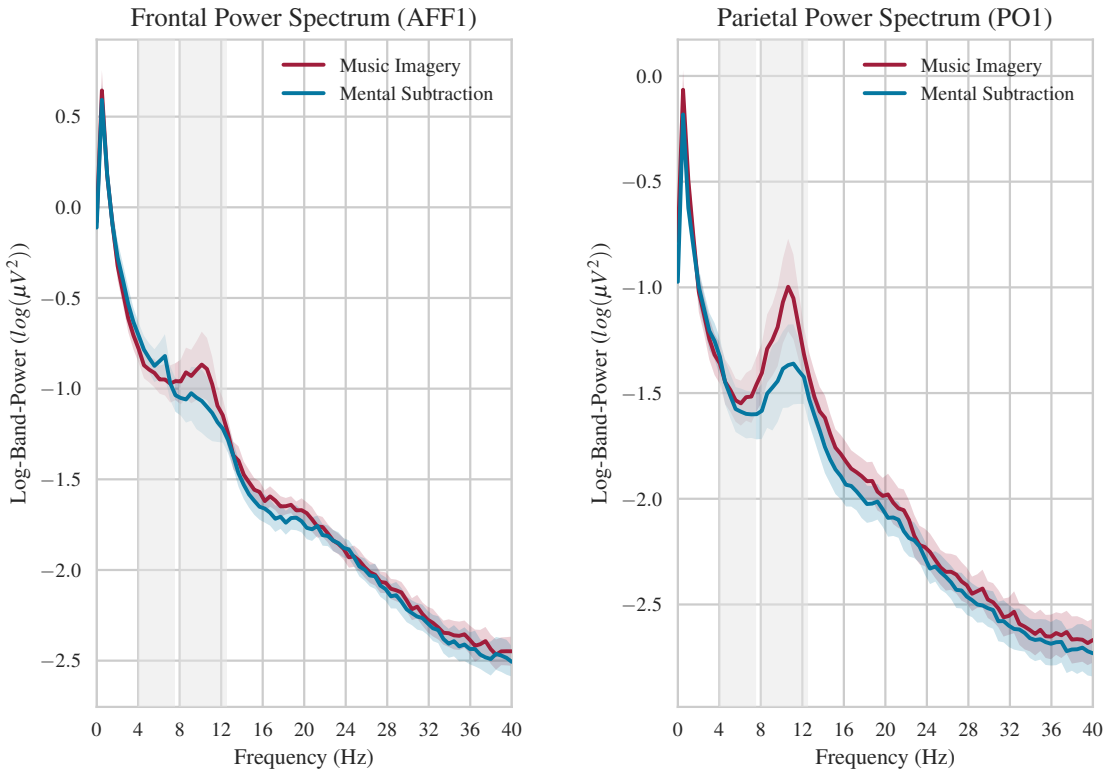

Figure 3: Average power spectral density with a single standard deviation across all 10 subjects for the BrainAmp at the two electrodes with the highest classification weights (AFF1, PO1).

[15] Vinay Jayaram, Morteza Alamgir, Yasemin Altun, Bernhard Schölkopf, and Moritz Grosse-Wentrup. Transfer Learning in Brain-Computer Interfaces. *IEEE Computational Intelligence Magazine*, 11(1): 20–31, feb 2016. doi: 10.1109/MCI.2015.2501545.

[16] Stefan Haufe, Frank Meinecke, Kai Görgen, Sven Dähne, John-Dylan Haynes, Benjamin Blankertz, et al. On the interpretation of weight vectors of linear models in multivariate neuroimaging. *NeuroImage*, 87:96–110, feb 2014. doi: 10.1016/j.neuroimage.2013.10.067.

[17] F Chochon, L Cohen, P F van de Moortele, and S Dehaene. Differential contributions of the left and right inferior parietal lobules to number processing. *Journal of Cognitive Neuroscience*, 11(6):617–30, nov 1999.

[18] Thalía Harmony, Thalía Fernández, Juan Silva, Jorge Bosch, Pedro Valdés, Antonio Fernández-Bouzas, et al. Do specific EEG frequencies indicate different processes during mental calculation? *Neuroscience Letters*, 266(1):25–8, apr 1999. doi: 10.1016/S0304-3940(99)00244-X.

Published by Verlag der TU Graz
Graz University of Technology

Proceedings of the
7th Graz Brain-Computer Interface Conference 2017 DOI: 10.3217/978-3-85125-533-1-31

CLOSING ONE'S EYES AFFECTS AMPLITUDE MODULATION BUT NOT FREQUENCY MODULATION IN A COGNITIVE BCI

M. Görner[1], B. Schölkopf[2], M. Grosse-Wentrup[2]

[1]Computer Science Department, University of Tübingen, Germany
[2]Max Planck Institute for Intelligent Systems, Tübingen, Germany

E-mail: moritzgw@tuebingen.mpg.de

ABSTRACT: Cognitive brain-computer interfaces (BCIs) are an auspicious alternative to BCIs based on motor tasks for severely paralyzed patients, e.g., those in late-stages of amyotrophic lateral sclerosis. These patients, however, are often not able to volitionally control their eye lids: Undeliberate eye opening and closing affects modulation of theta- and alpha-rhythms, which impairs decoding performance in cognitive BCIs. Here, we demonstrate on EEG data recorded from nine healthy subjects that a cognitive BCI based on task-induced modulation of the frequency of the parietal alpha-rhythm is more robust to eye lid movements than a BCI based on amplitude modulation. Specifically, we instructed subjects to either open or close their eyes while performing cognitive tasks, and show that closing their eyes decreases decoding performance relative to the eyes-open condition for amplitude modulation but not for frequency modulation features. This insight has important consequences for the design of cognitive BCIs for severely paralyzed patients.

INTRODUCTION

Humans' capability to interact with the environment – whether via motion, sensation or communication – relies on the precise control of muscles. Several diseases may impair the capabilities of control. Temporary or partially reversible disturbances up to a complete degeneration of the necessary structures in the central nervous system can be the consequence in which case the (complete) locked-in state ((C)LIS) is the inevitable final condition of the patient [1].

In this condition the only remaining devices for communication are brain-computer interfaces (BCIs). Most of the well-established designs, however, trigger neural activity in brain areas that are impaired in some of these patients [2]. Amyotrophic lateral sclerosis (ALS) is characterized by a creeping degeneration of the upper and lower motor neurons impairing motor control already at the central level and hence neural activity therein [3, 4]. As well, long-lasting paralysis as a consequence of disorders on lower levels of motor control may likewise affect processing in central regions due to neuroplastic changes that result from omitted afferent projections [5–7]. It is apparent that under these circumstances motor imagery based BCIs are likely to be compromised. Because P300 speller systems [8] indirectly require motor control to shift the visual attention, they are, however, likewise affected. The degeneration of neurons in central sensorimotor areas may eventually impair the ability of oculomotor control [9] completing the locked-in state [10] and impeding the use of BCIs that directly or indirectly involve motor areas [11].

For these patients another class of BCIs, one that lacks any involvement of the very areas, is necessary in order to have a chance of establishing communication. Cognitive tasks that involve the imagination of goals of movements [12], language processing [13], working memory [14–16] and internal self-referential attention [17, 18] share this characteristic and have been shown to provide neural modulations useful as control signals. The big advantage of the cognitive strategy over another sensorimotor free approach – learning volitional control over certain neural activities through neurofeedback training [19, 20] – is that it can be used intuitively. Tasks like mental calculation, the imagination of words or remembering one's own past are convenient, under precise conscious control and feasible without training.

Functional MRI studies indeed suggest that performing tasks of this kind induces modulations of large-scale cortical networks which exhibit correspondent alterations in the ECoG and EEG signal [16, 21, 22]. Topographies show the involvement of frontal and parietal regions in line with networks related to higher cognitive functions like working memory, attention and self-referential thinking [14, 23, 24].

Despite this encouraging perspective, online communication with a CLIS patient using any of these tasks in an EEG- or even in a less artifactual ECoG-based BCI has failed to date [11]. A potential cause is directly related to the impairment and eventual complete loss of volitional eye(lid) movements once the CLIS state is entered [9, 10]. In this condition erratic and undeliberate eye closing and opening is likely to occur. Given the vast differences in the electrophysiological patterns resulting from closed and open eyes, it may likely be that classification accuracies based

Published by Verlag der TU Graz
Graz University of Technology

 DOI: 10.3217/978-3-85125-533-1-31

on these signals do not remain unscathed.
The most prominent electrophysiological change that accompanies eyes closed periods is the power increase in the alpha band of the EEG in occipital visual areas [25]. More elaborate investigations revealed, however, that the power of all of the common EEG frequency bands in virtually all brain regions is modulated and that a restriction of functional effects to visual processing is unlikely [26]. Specifically, Geller et al. found that besides alpha's up-modulation in occipital regions it is likewise affected in parietal regions and that a spatially diffuse low-frequency power increase (delta to beta) is accompanied by a high-frequency (gamma) decrease in some areas [27]. This indicates effects on large-scale cortical networks whose modulation is intended by cognitive BCIs.
The specific paradigm under investigation in the present study utilizes activation and deactivation of the default mode network (DMN) triggered by self-referential thinking and mental calculation [18]. The DMN is a prominent example of a large-scale cortical network whose discovery is directly associated with the recording of brain activity during closed eyes conditions (EC) [24]. Since the common feature used for classification in BCIs is task-induced amplitude modulation (AM), the aforementioned may pose a significant problem for cognitive BCIs aiming to establish communication with patients lacking control over their eyelids. In that light, an interference between modulations induced by cognitive tasks and an EC-induced activation appears to be likely.
Recently, another property of the EEG signal was described to be similarly informative as AM in the context of BCIs. Jayaram et al. found that task-induced shifts of the pronounced peaks in the power spectra of EEG signals (FM) can be used to predict task conditions in motor imagery as well as in cognitive BCIs [28]. This finding provides a promising perspective for the design of communication systems for severely paralyzed patients. Here we test to what extend AM and FM based classification in a cognitive BCI is affected by the EC condition and whether this condition leads to structural differences of the task-induced AM compared to the open eyes condition (EO).

MATERIALS AND METHODS

Experimental Paradigm: The mental tasks performed by the participants were identical to those described in [18]. The experiment was composed according to a randomized block design. Each block consisted of $10+10$ randomized trials in which participants had to either memorize a personal positive experience or perform a mental subtraction task (trial-conditions). In total, four of these blocks had to be completed. During two of them participants were asked to keep their eyes open and during the other two to keep them closed (block-conditions). The order of block-conditions was randomized for each participant. Each trial started with the instruction to either recall a positive memory or successively subtract a given one-digit number from a given three-digit number. Trial length without instruction time was 35 s. Instructions were presented both visually and vocally on a computer screen and via headphones. Before each trial, a 5 s pause separated it from the preceding one. Experiments always began with 2×5 min of consecutive resting state recording, one in EO and the other in EC condition. During these participants were asked to relax and let their mind wander at will. Following, the experimental blocks began between which participants were allowed to have a break if desired.

Data Acquisition: The study was conducted at the Max Planck Institute for Intelligent Systems in Tübingen. Ten healthy subjects (5 female, 5 male) with a mean age of 26 ± 3 years participated and received an allowance of 12 € per hour. Before the start of the experiment participants had to fill out a consent and a questionnaire asking personal data, former experience with the use of BCIs, the presence of neurological disorders, drug abuse and level of fatigue. The experiment started after a detailed explanation of the task and a demonstration of the stimuli. Participants were seated in a chair at a distance of 1.25 m to the screen and asked to remain as still as possible and to minimize eye blinks during trials.
EEG was recorded at a sampling frequency of 500 Hz using actiCAP active electrodes (124 channels) and the BrainAmp amplifier (BrainProducts GmbH, Gilching, Germany). Electrodes were mounted according to the extended 10-20 system with the left mastoid electrode as the initial reference and the AFz-electrode as ground. Before data analysis, recordings were re-referenced to common average. Data streams were digitized and stored via OpenViBE [29], stimuli were implemented using a custom BCI GUI. After each experiment behavioral questions were asked to rate the perceived difficulty of performing the tasks in the different conditions on a scale between 1 and 10.

Data Analysis: Preprocessing of the data included band-pass filtering between 0.1 Hz to 45 Hz. Visual inspection lead to exclusion of one participant due to an abnormal shape of the power spectrum. No further artifact reduction was performed since the frequency band of interest is largely robust against the main sources of EEG artifacts [30]. Bandpower modulation and frequency modulation for each channel and trial were computed for the common alpha band (8 Hz to 13 Hz). The former via FFT and the latter according to the method described in [28]. This method relies on the analytic signal which is obtained through the Hilbert transform and provides

Published by Verlag der TU Graz
Graz University of Technology

 DOI: 10.3217/978-3-85125-533-1-31

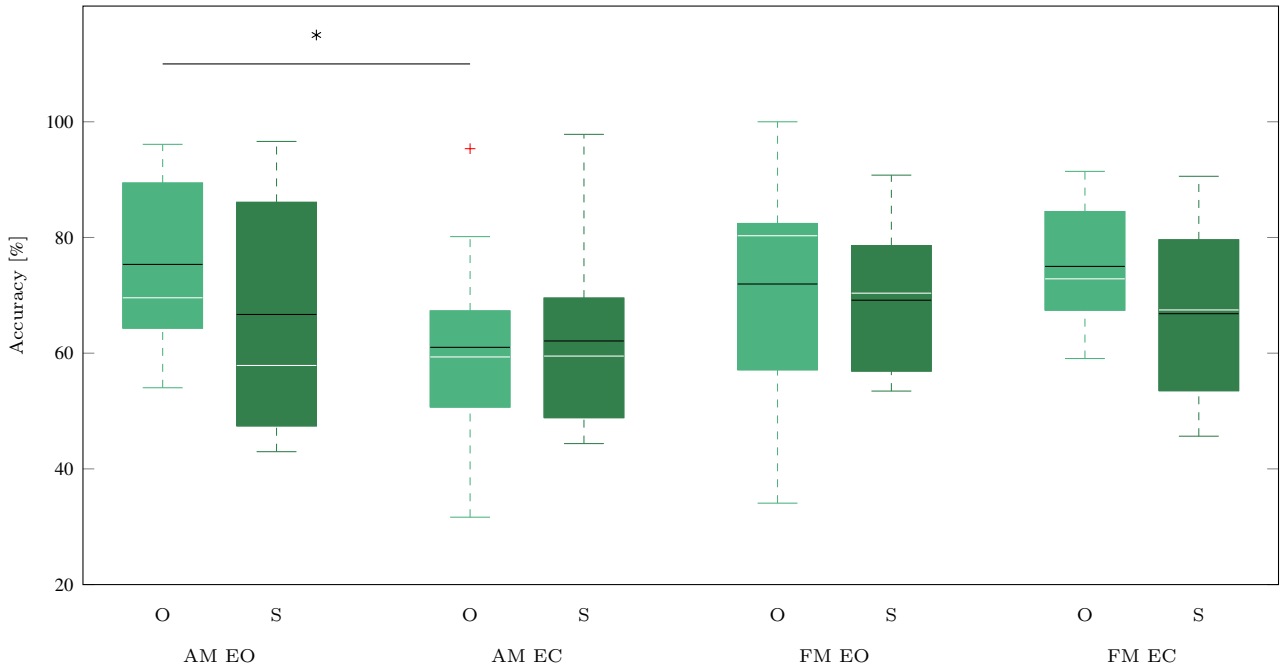

Figure 1: Distributions of the performance across participants for the different features (AM/FM), block- (EO/EC) and classification-conditions (O/S). Black lines mark the mean and white the median accuracy. Difference between AM EO O and AM EC O is significant ($p_{median} = 0.038$).

phase information. Derivation of the instantaneous phase with respect to time yields the instantaneous frequency. To obtain the location of a trial's alpha peak its data was band-pass filtered between the alpha band and the median of each data point's estimate used as the instantaneous frequency of that trial. Linear discriminant analysis was used for classification. According to the paradigm's underlying hypothesis concerning the involved brain areas, classification was based on channel Pz and channel Fz providing a two dimensional feature space. Classification accuracy of each participant and condition was computed by 100 repetitions of 10-fold cross validated LDA (random split). Mean values across repetitions are reported. To test the significance of classification against chance level permutation tests were used, i.e. class labels were randomly permuted 1000 times and for each iteration the classification accuracy was calculated again. The fraction of values greater than or equal to the original accuracy constitutes the p-value. An analog procedure was used to test the differences between conditions. Here the difference between the means across participants of two conditions was used as test statistic and its value was calculated 1000 times by randomly splitting the combined set of accuracies into sets of equal size. The fraction of differences greater or equal to the original difference constitutes the p-value. Permutation tests were calculated for each of the LDA repetitions separately yielding distributions of p-values for each comparison whose median value is the reported.

To further probe the differences between the block-conditions the classification accuracies obtained by using the condition's own classifier, i.e., training and prediction based on the same data set (O condition), and the accuracies obtained by swapping the classifier (S condition), i.e., training on the EC data and predicting EO data and vice versa, were compared. Perceived difficulties of the tasks in different conditions were compared using the non parametric Wilcoxon rank sum test.

RESULTS

Average performance across participants of all conditions was significantly above the chance level of 50 % (p-values not reported here). Fig. 1 shows the accuracy distributions across participants for each block- and classification-condition based on AM and FM within the alpha band at channels Pz and Fz.

Table 1: Mean (top) and median (bottom) accuracies across participants separated by trial- and block-condition in correspondence with Fig. 1 (values in [%]).

AM EO		AM EC		FM EO		FM EC	
O	S	O	S	O	S	O	S
75.3	66.7	61	62.1	72	69.2	75	66.8
69.6	57.9	59.4	59.5	80.3	70.4	72.9	67.5

Published by Verlag der TU Graz
Graz University of Technology

 DOI: 10.3217/978-3-85125-533-1-31

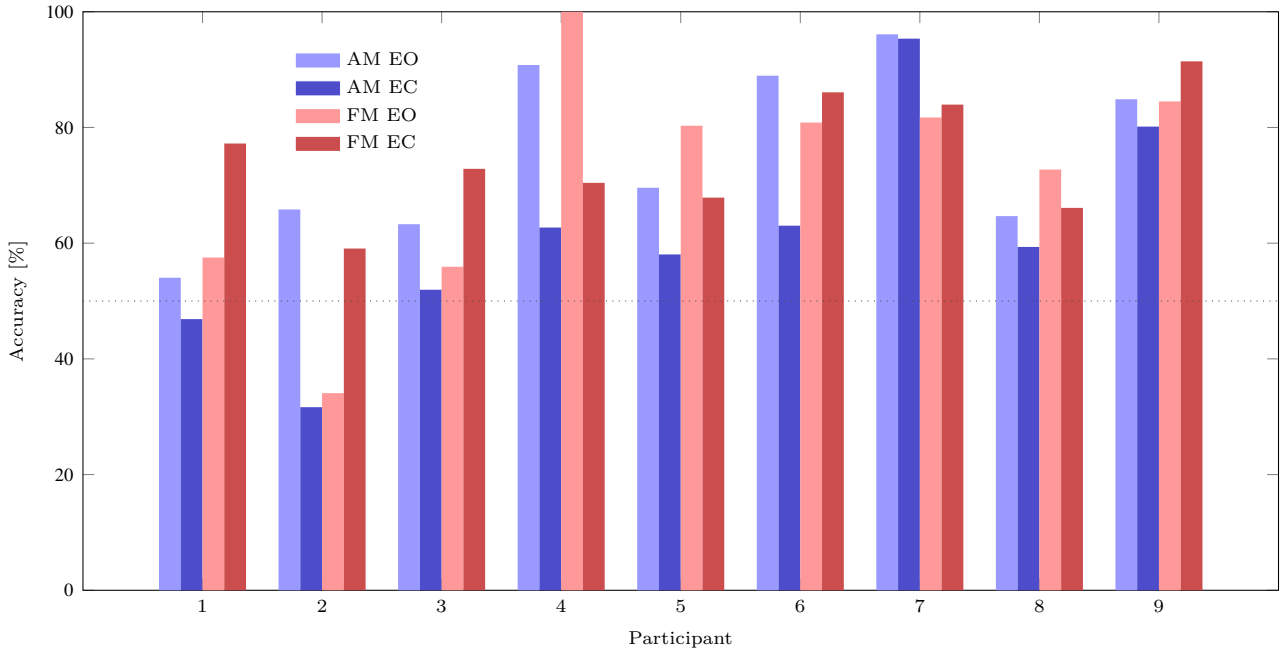

Figure 2: Individual performances separated by feature and block-condition. Dashed line marks chance level. AM EO: amplitude modulation in the eyes open condition. AM EC: amplitude modulation in the eyes closed condition. FM EO: frequency modulation in the eyes open condition. FM EC: frequency modulation in the eyes closed condition.

Tab. 1 shows the corresponding mean (top) and median (bottom) values. A significant difference between the EO and the EC condition was observed if classification was based on the AM feature in the O classification-condition (72 of the 100 p-values obtained by LDA iterations were smaller or equal to 0.05, $p_{median} = 0.038$). No significant differences were found neither between block-conditions if classification was based on the FM feature nor between the O and S classification-conditions of both features. Importantly, classification performance based on FM is on average roughly the same as based on AM, though, considering the individual accuracies shown in Fig. 2, the feature which performs better varies from participant to participant.
Analysis of the behavioral data suggested no difference in the perceived difficulty of performing the memory or the mental calculation task in EO or EC conditions ($p_{Memory} = 0.53$, $p_{Calculation} = 0.85$).

DISCUSSION

We could show that discriminability between trials with mnemonic content and those without based on AM in the common alpha range significantly drops in the EC condition compared to the EO condition. This is not the case for classification based on FM; here distinguishability between trial-conditions is roughly the same in the EO and the EC condition. Furthermore, classification based on FM meets the level of the well established AM, concerning the median values FM even exceeded AM by more than 10 %, proving it to be a very promising feature for the use in BCIs. Although our initial hypothesis that a classifier trained on trials of the EC condition but applied to EO data performs significantly worse than the condition's own classifier was not met, results still indicate a downswing and, in addition, that the downswing is stronger for AM than for FM (comparing AM EO O/AM EO S and FM EO O/FM EO S in Fig. 1). If significant, this effect would have been evidence for the hypothesis that task related AM exhibits diverging structures in the two block-conditions impairing the classifier and contributing to the failure of current BCI systems to establish communication with patients lacking control over their eyelid movements.
From another perspective, though, the fact that the classifier trained on EC data performed better if applied to EO data than if applied to EC data itself sheds new light on the issue. It suggests that training the LDA model on either EO or EC data resulted in a similarly oriented decision boundary and, hence, that orientation of the task-induced AM in the EC condition was preserved but less pronounced in comparison with the EO condition.
Another possible explanation for the accuracy drop from AM EO to AM EC is that it is more difficult to concentrate on the cognitive tasks during EC periods causing a weaker modulation of the neural activity. The rational behind this explanation is that closing one's eyes might increase the likeliness

Published by Verlag der TU Graz
Graz University of Technology

 DOI: 10.3217/978-3-85125-533-1-31

of mind-wandering and/or effects of fatigue leading to a weaker involvement with the tasks. However, probing the ratings of perceived difficulty to that effect suggests no difference between block-conditions. Furthermore, in the case of a behavioral cause the accuracy drop in the EC condition should likewise be observable if classifying the FM feature. Taken together, these arguments speak in favor of a genuine effect within the alpha band caused by an interference of the EC related up-modulation and the task-induced modulations.

The strong up-modulation of the alpha band during EC periods is a result of a corresponding synchronization of neural activity. A straightforward explanation for the observed drop is, hence, that alpha synchrony is largely saturated during the EC condition and that modulation atop triggered by the cognitive task is therefore less effective. This is in line with the hypothesis that the orientation of the modulation is preserved in the EC condition but less pronounced. An interference of that kind is supported by fMRI studies suggesting effects of EC periods on the topology of large-scale networks [31,32]. Xu et al. report that the EC condition leads to a higher global processing efficiency compared to EO and relate this to an activation of the "introceptive" network which includes the DMN. Including the assumed correlates of DMN activation in the EEG [17,33] these findings provide neurophysiological evidence.

In light of this argumentation it remains unclear why classification is not impaired if based on FM. Assuming the activation of the DMN along with EC as well as along with self-referential thinking and further that this activation reflects in an alpha power increase in either case it may be expected that FM would suffer the same fate. Nonetheless our results indicate a dissociation between AM and FM which can be explained by three settings. First, there is one neural network whose activity is likewise triggered by the EC condition and by the task but unlike AM task-induced FM is effective atop EC-induced effects. Second, there is one neural network but FM is only induced by the tasks and not by closing and opening the eyes, or third, there are two distinct neural networks involved one of which features AM and the other FM. Considering a study by Thuraisingham et al. the second option can likely be rejected. Estimating the instantaneous frequency of EEG recordings during EO and EC conditions via an Hilbert-Huang transform they were able to distinguish with an high level of accuracy between those two conditions [34]. This points to the significance of our results. As in contrast to AM, the task-induced FM withstands the block-condition related FM described by Thuraisingham et al. – whether because of the involvement of two distinct neural networks or whether effective modulations atop the EC-induced modulation –, FM should be among the routinely considered features when designing communication systems for severely paralyzed patients.

CONCLUSION

Frequency modulation appears to be a more consistent feature than amplitude modulation across eyes open and eyes closed periods in a cognitive BCI that relies on modulations of parietal alpha rhythms. This property might help to improve BCI systems for patients who lost control over oculomotor functions.

ACKNOWLEDGMENTS

Special thanks to Bernd Battes for his help with preparing the experiments.

REFERENCES

[1] León-Carrión J, van Eeckhout P, Domínguez-Morales MDR, The locked-in syndrome: a syndrome looking for a therapy. Brain injury 2002; 16(7):571–582.

[2] Wolpaw JR, Birbaumer N, McFarland DJ, Pfurtscheller G, Vaughan TM, Brain-computer interfaces for communication and control. Clinical neurophysiology : official journal of the International Federation of Clinical Neurophysiology 2002; 113(6):767–91.

[3] Nihei K, Mckee AC, Kowau NW, Patterns of neuronal degeneration in the motor cortex of amyotrophic lateral sclerosis patients. Acta Neuropathologica 1993;86:55–64.

[4] Chou SM, Norris FH, Amyotrophic lateral sclerosis: Lower motor neuron disease spreading to upper motor neurons. Muscle & Nerve 1993; 16(8):864–869.

[5] Cramer SC, Lastra L, Lacourse MG, Cohen MJ, Brain motor system function after chronic, complete spinal cord injury. Brain 2005;128(12):2941–2950.

[6] Lacourse MG, Cohen MJ, Lawrence KE, Romero DH, Cortical potentials during imagined movements in individuals with chronic spinal cord injuries. Behavioural brain research 1999;104(1-2):73–88.

[7] Müller-Putz GR, Zimmermann D, Graimann B, Nestinger K, Korisek G, Pfurtscheller G, Event-related beta EEG-changes during passive and attempted foot movements in paraplegic patients. Brain Research 2007;1137(1):84–91.

[8] Farwell LA, Donchin E, Talking off the top of your head: toward a mental prosthesis utilizing event-related brain potentials. Electroencephalography and Clinical Neurophysiology 1988; 70(6):510–523.

[9] Sharma R, Hicks S, Berna CM, Kennard C, Talbot K, Turner MR, Oculomotor dysfunction in amy-

Published by Verlag der TU Graz
Graz University of Technology

 DOI: 10.3217/978-3-85125-533-1-31

otrophic lateral sclerosis: a comprehensive review. Archives of neurology 2011;68(7):857–861.
[10] Murguialday AR, Hill J, Bensch M, Martens S, Halder S, Nijboer F, et al., Transition from the locked in to the completely locked-in state: A physiological analysis. Clinical Neurophysiology 2011; 122(5):925–933.
[11] Marchetti M, Priftis K, Brain-computer interfaces in amyotrophic lateral sclerosis: A metanalysis. Clinical Neurophysiology : Official Journal of the International Federation of Clinical Neurophysiology 2015;126(6):1255–63.
[12] Musallam S, Corneil B, Greger B, Scherberger H, Andersen R, Cognitive Control Signals for Neural Prosthetics. Science 2004;305(July):258–263.
[13] Leuthardt EC, Schalk G, Wolpaw JR, Ojemann JG, Moran DW, A brain-computer interface using electrocorticographic signals in humans. Journal of neural engineering 2004;1(2):63–71.
[14] Ramsey NF, Heuvel MPVD, Kho KH, Leijten FSS, Towards Human BCI Applications Based on Cognitive Brain Systems: An Investigation of Neural Signals Recorded From the Dorsolateral Prefrontal Cortex. IEEE Transactions on Neural Systems and Rehabilitation Engineering 2006;14(2):214–217.
[15] Friedrich EVC, Scherer R, Neuper C, The effect of distinct mental strategies on classification performance for brain-computer interfaces. International Journal of Psychophysiology 2012;84(1):86–94.
[16] Vansteensel MJ, Hermes D, Aarnoutse EJ, Bleichner MG, Schalk G, Van Rijen PC, et al., Brain-computer interfacing based on cognitive control. Annals of Neurology 2010;67(6):809–816.
[17] Hohmann MR, Fomina T, Jayaram V, Widmann N, Förster C, Müller vom Hagen J, et al., A Cognitive Brain-Computer Interface for Patients with Amyotrophic Lateral Sclerosis, in 2015 IEEE International Conference on Systems, Man, and Cybernetics, pp. 3187–3191.
[18] Hohmann MR, Fomina T, Jayaram V, Widmann N, Förster C, Müller vom Hagen J, et al., An Improved Cognitive Brain-Computer Interface for Patients with Amyotrophic Lateral Sclerosis, in Proceedings of the 6th International Brain-Computer Interface Meeting, p. 44.
[19] Birbaumer N, Ghanayim N, Hinterberger T, Iversen I, Kotchoubey B, Kübler A, et al., A spelling device for the paralysed. Nature 1999; 398(6725):297–298.
[20] Grosse-Wentrup M, Schölkopf B, A brain-computer interface based on self-regulation of gamma-oscillations in the superior parietal cortex. Journal of neural engineering 2014;11(5):056015.
[21] Chen ACN, Feng W, Zhao H, Yin Y, Wang P, EEG default mode network in the human brain: Spectral regional field powers. NeuroImage 2008; 41(2):561–574.
[22] Vansteensel MJ, Bleichner MG, Freudenburg ZV, Hermes D, Aarnoutse EJ, Leijten FSS, et al., Spatiotemporal characteristics of electrocortical brain activity during mental calculation. Human Brain Mapping 2014;35(12):5903–5920.
[23] Andreasen NC, O'Leary DS, Cizadlo T, Arndt S, Rezai K, Watkins GL, et al., Remembering the past: Two facets of episodic memory explored with positron emission tomography. American Journal of Psychiatry 1995;152(11):1576–1585.
[24] Raichle ME, MacLeod AM, Snyder AZ, Powers WJ, Gusnard DA, Shulman GL, A default mode of brain function. Proceedings of the National Academy of Sciences 2001;98(2):676–682.
[25] Berger H, Über das Elektrenkephalogramm des Menschen. Archiv für Psychiatrie 1929;87.
[26] Barry RJ, Clarke AR, Johnstone SJ, Magee CA, Rushby JA, EEG differences between eyes-closed and eyes-open resting conditions. Clinical Neurophysiology 2007;118:2765–2773.
[27] Geller AS, Burke JF, Sperling MR, Sharan AD, Litt B, Baltuch GH, et al., Eye closure causes widespread low-frequency power increase and focal gamma attenuation in the human electrocorticogram. Clinical Neurophysiology 2014; 125(9):1764–1773.
[28] Jayaram V, Schölkopf B, Grosse-Wentrup M, Task-Induced Frequency Modulation Features for Brain-Computer Interfacing. Journal of neural engineering (under review) 2017;.
[29] Renard Y, Lotte F, Gibert G, Congedo M, Maby E, Delannoy V, et al., OpenViBE: An Open-Source Software Platform to Design, Test and Use Brain-Computer Interfaces in Real and Virtual Environments. Presence : teleoperators and virtual environments 2010;19(1).
[30] Klass DW, The Continuing Challenge of Artifacts in the EEG. American Journal of Electroneurodiagnostic Technology 1995;35:239–269.
[31] Xu P, Huang R, Wang J, Van Dam NT, Xie T, Dong Z, et al., Different topological organization of human brain functional networks with eyes open versus eyes closed. NeuroImage 2014;90:246–255.
[32] Zhang D, Liang B, Wu X, Wang Z, Xu P, Chang S, et al., Directionality of large-scale resting-state brain networks during eyes open and eyes closed conditions. Frontiers in Human Neuroscience 2015; 9(February):Article 81.
[33] Mo J, Liu Y, Huang H, Ding M, Coupling between Visual Alpha Oscillations and Default Mode Activity. Neuroimage 2013;68:112–118.
[34] Thuraisingham RA, Tran Y, Craig A, Nguyen H, Frequency analysis of eyes open and eyes closed EEG signals using the Hilbert-Huang Transform, in 2012 Annual International Conference of the IEEE Engineering in Medicine and Biology Society, 1, pp. 2865–2868.

Published by Verlag der TU Graz
Graz University of Technology

Proceedings of the
7th Graz Brain-Computer Interface Conference 2017 DOI: 10.3217/978-3-85125-533-1-32

TACTILE BRAIN-COMPUTER INTERFACE CONTROL OF A MOBILE PLATFORM IN A REAL WORLD ENVIRONMENT USING A LOW-COST ELECTROENCEPHALOGRAPHY HEADSET

S. Halder[1], J. Räderscheidt[1], R. Heß[2], D. Eck[2], K. Schilling[2], A. Kübler[1]

[1]Institute of Psychology, University of Würzburg, Würzburg, Germany
[2]Institute of Computer Science, University of Würzburg, Würzburg, Germany

E-mail: sebastian.halder@uni-wuerzburg.de

ABSTRACT: We used a brain-computer interface (BCI) system controlled with event-related potentials (ERPs) evoked by tactile stimulation to control a mobile platform.

Eight tactile stimulators were attached in four pairs to the arms, legs and back of the participants (N=12). The electroencephalogram (EEG) was recorded via a modified Emotiv headset. All participants were trained in the laboratory, then four participants controlled the mobile platform in an outdoor environment.

Inside the laboratory the participants achieved average accuracies of 72%. Outside four participants achieved average accuracies of 61% (range 52-88%).

Technical problems with the responses of the mobile platform and high outside temperatures prevented higher levels of control with the mobile platform. A mobile platform better suited for the discrete control implemented with the BCI or a different control scheme will be needed for future experiments. Nevertheless, subjects were able to control the mobile platform with tactile ERPs using low-cost EEG equipment in a real world environment.

INTRODUCTION

Since the first demonstration of Farwell and Donchin that the visual P300 event-related potential (ERP) component of the electroencephalogram (EEG) can be used to control a brain-computer interface (BCI) the usefulness of this method for communication has been shown in numerous studies, also with persons with severe motor impairments [1, 2]. Another application in which assistive technologies, such as BCIs, have the potential to improve the quality of life of persons with disabilities is personal mobility. Control of mobile platforms with BCIs has been shown mostly using motor imagery (see e.g. [3]). The disadvantage of this approach is that control over more than two classes is difficult to obtain without a long training period. A potential alternative are P300 BCIs that do not rely on visual stimulation and thus leave the visual channel unoccupied to observe the environment [4]. In studies using a simulated wheelchair tactile evoked ERPs were shown to be a viable control method with four classes [5]. In the current study we used a modified Emotive headset (see [6]) to control a physical mobile platform [7, 8, 9] in an outdoor environment using the same setup as in [5].

MATERIALS AND METHODS

We recruited twelve healthy participants (six female, average age 23.4 SD 3.4, range 20-32) without a history of neurological or psychological disorders. Participants signed informed consent and were compensated with € 8 per hour. None of the participants had experience with tactile P300 BCIs, six of the participants had experience with visual P300 BCIs.

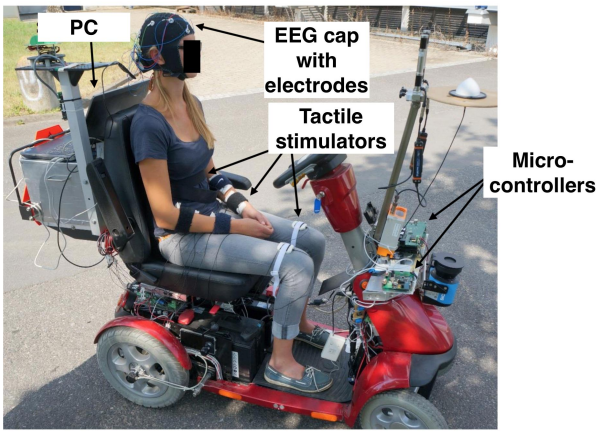

Figure 1: Setup used to control the mobile platform. The control PC received the EEG data from the modified Emotiv headset, classified the data and sent commands to the microcontrollers that controlled the mobile platform. Eight tactile stimulators were attached two to the left arm, two to the right arm, two to the left leg and right leg and two to the back.

Eight tactile stimulators (C2 Tactors, Engineering Acoustics Inc., Casselberry, USA) were attached in pairs, as suggested in [5], to the arms, legs and back of the participants (see Figure 1). To steer to the left the participants attended to the stimulators on the left arm, to steer to

Published by Verlag der TU Graz
Graz University of Technology

 DOI: 10.3217/978-3-85125-533-1-32

the right the participants had to attend to the stimulators on the right arm, to move forward to the stimulators on the legs and to move backwards to the stimulators on the back. The stimulators were placed at least 10 cm apart. The stimulus duration was set to 250 ms with a frequency of 250 Hz and an inter-stimulus interval of 375 ms. For one selection each pair of stimulators was activated ten times. Between selections there was a pause of five seconds to give the participants enough time to choose the next command to attend to. Participants were seated in a comfortable chair in a quiet room and received verbal feedback on the selected direction.

For calibration each of the four directions had to be chosen twice (eight selections) in one run. A total of three runs were performed for calibration (24 selections). Based on this calibration data a classifier was trained using stepwise linear discriminant analysis (SWLDA; forward $p < 0.1$, backward $p > 0.15$, 60 features). The data was segmented into 800 ms epochs and subsampled to 16 samples.

After calibration the participants were asked to perform another two runs with a total of twelve selections (the participants were asked to "copy" a specific sequence of twelve commands) and a third run in which they had to plan a route and choose the appropriate commands themselves (the participants were asked to "drive" the mobile platform from a starting to an an end point shown to them on a piece of paper).

Four participants with over 90% accuracy in the previously described tasks participated in a second experiment in which the physical mobile platform was controlled. The calibration for this task was performed in a large hall in which also other activities were taking place. Thus the environment was noisy. The driving task was performed outside. Outside it was quiet except during the experiment of participant six (construction noise). The participants performed the same calibration task as in the previous experiment while seated in a chair and selected five commands to confirm that the calibration was successful. Participant three was chronologically the first participant to perform the driving task (participant twelve the second, participant two the third and participant six the last). Due to a higher amount of noise when operating the BCI in the hall where the calibration was performed a 9 Hz low-pass filter was activated for all participants after participant three. Then the participants were asked to move outside to the start position of the route that was to be navigated with the mobile platform. While the mobile platform was controlled with the BCI one of the experiment supervisors held an emergency stop button. The last two participants first controlled the mobile platform with a keyboard to gain familiarity with the behaviour of the mobile platform and the route. From the starting position the participants drove around a patch of grass and back to the starting position. If this was not accomplished with 60 commands the experiment was aborted. The optimal path needed 36 correct selections. The mobile platform was configured to change the angle of the steering wheels if the left or right command was chosen. Choosing forward or backward would move the mobile platform in the corresponding direction for approximately one meter.

Leave one-run-out cross validation accuracy was calculated for the four participants that performed both sessions (training and driving) also using SWLDA. ERP analysis was also performed on the calibration data because this is the only data with target markers in the second session (the driving task was performed without predefined selections).

The EEG was recorded using 14 passive Ag-AgCl electrodes placed in plastic holders in an elastic EEG cap (Easycap GmbH, Herrsching, Germany). The electrodes were positioned at Fp1, Fp2, F3, Fz, F4, C3, Cz, C4, P3, Pz, P4, PO7, Oz and PO8 with the ground at AFz and the reference on the right mastoid. The amplifier was a modified version of an Emotiv EPOC headset (EMOTIV Inc, San Francisco, California, USA), for a description see [6]. The amplifier was connected via bluetooth to BCI2000 [10]. The output of the classifier was sent to the mobile platform via a python script. The EEG was sampled with 128 Hz, notch filtered at 50 Hz and additionally bandpassfiltered from 0.1-30 Hz (for the driving experiment of participants two, six and twelve this was set to 0.1-9 Hz).

RESULTS

While performing the training in the laboratory the averaged accuracy of the twelve participants during the selection task with predefined commands was 72.2%. Two participants reached 100% and eight participants accuracies over 70%. The accuracy decreased to an average of 55% during the task in which the participants had to plan the route themselves. Five participants achieved accuracies of 70%. Participants two (average accuracy both tasks 80%), three (86.7%), six (75.2%) and twelve (100%) took part in the second session to control the mobile platform in an outdoor environment. For a summary of the accuracy of all participants see Figure 2. The dependency of the accuracy on the number of stimulus repetitions for the four participants that performed both training and driving is shown in Figure 3. Only participant twelve would have been able to control the mobile platform with a lower number of stimulus repetitions.

The participants needed between 36 and 57 minutes to make 60 selections (the maximum until the experiment was aborted) on the outside course. None of the participants reached the end point of the course. During the experiment conducted with participants two, three and six the outside temperatures were around 30 degrees Celsius and the sun was shining. The first participant of the outside driving task (participant three) expressed that the sun did not bother her, nonetheless the subsequent participants were shielded with an umbrella. During the experiment with participant twelve the sun was behind clouds. Participant two performed 65% of the selections as intended. The experiment was interrupted once to correct

Published by Verlag der TU Graz
Graz University of Technology

 DOI: 10.3217/978-3-85125-533-1-32

the angle of the steering wheel.

Participant three performed 65% of the selections as intended and the emergency button had to be pressed twice to prevent collisions with the sidewalk. Twice the mobile platform did not move backwards even though the correct command was selected.

Participant six performed 52% of the selections as intended. A possible negative influence may have been construction noise 100 m away from where the experiment was conducted.

Participant twelve performed 88% of the commands as intended. The mobile platform had to be reset during the task due to the battery indicator erroneously showing a charge state of 0%. Twice the emergency button had to be used to prevent collisions. Five selections of the command move to right direction were not executed by the mobile platform. After a second reset the problem was resolved.

ERP data of the target responses in the calibration data of the four participants that performed the outdoor driving task is shown in Figure 5.

All participants said they found the control of the mobile platform to be intuitive and felt to be in control during the experiment. The particularly enjoyed the realistic setting. All participants expressed their frustration about the mobile platform not always executing the selected command.

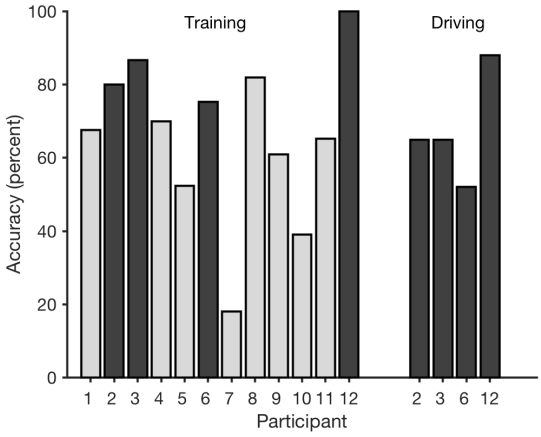

Figure 2: Online accuracies of the participants during the training task (left group of bars) and during the driving task (right group of bars). Participants selected for the driving task are shown in dark gray. Accuracy is the average of all tasks excluding calibration.

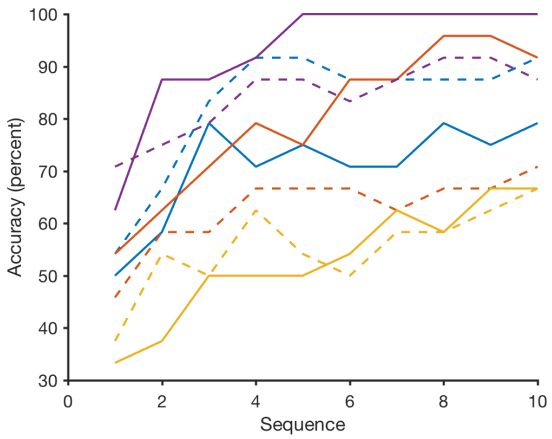

Figure 3: Offline accuracies of the participants that performed training (dashed line; session one) and driving (continuous line; session two) tasks. The accuracies were calculated using the calibration data. Accuracy is shown per sequence (i.e. the number of stimulus repetitions; higher number of repetitions increase the signal to noise ratio of the ERP compared to the background EEG but also increase selection times). Participant two in blue, participant three in red, participant six in yellow and participant twelve in purple.

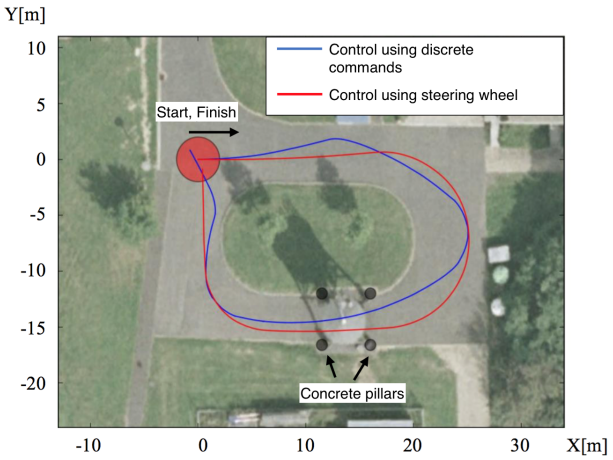

Figure 4: The area where the outdoor experiment was conducted. Participants started at the location indicated by the red circle. The paths shown are an exemplary path using the steering wheel of the mobile platform (red) and a path using keyboard control to give discrete commands analogous to the BCI experiment (blue). Trajectory data during the BCI experiment is not avaliable. The satellite image was obtained from Google Maps.

Published by Verlag der TU Graz
Graz University of Technology

 DOI: 10.3217/978-3-85125-533-1-32

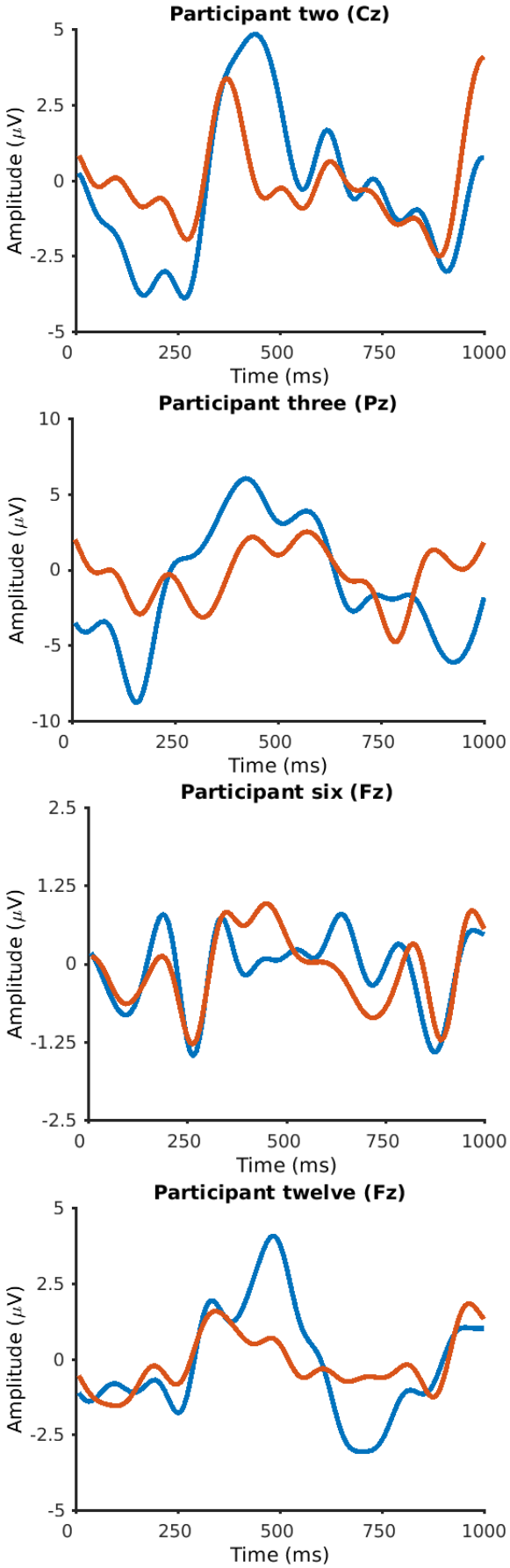

Figure 5: Exemplary event-related potentials based on the calibration data from session one of the four participants that performed the outdoor experiment in session two. The blue line shows the the target response, the red line the non-target response. Note that amplitude scales and channel location differ between participants.

DISCUSSION

With 72% the average accuracies across all twelve participants would have been sufficient to control the BCI. Task difficulty appears to have had an effect on performance in our sample as the accuracy decreased to 55% when the participants had to plan the path themselves. Considering the EEG hardware that was used the 62% average accuracy the four participants that performed the outdoor driving task achieved are comparable to the 69% in a binary choice task also using the modified Emotiv and conducted outdoors that was reported in [6]. The stimulation unit that was used in the current study was also used for control of a virtual wheelchair inside the laboratory and the accuracies were higher with on average 85% [5]. In the current study, the EEG recordings showed a lot of noise in the environment of the hall where the calibration for the driving task was conducted in the second session and the low-pass filter was reduced to 9 Hz for three of the four participants in this session. It is uncertain whether such problems may have been avoided with another amplifier as other studies using a similar paradigm were conducted in a lab environment [5].

Distractions in the form of additional tasks or the environment as well as fatigue have a detrimental effect on BCI performance [11]. High temperatures may have had a detrimental effect on the outdoor performance of participants two, three and six. Nonetheless, an ideal BCI should function under any condition and BCIs should be evaluated under different environmental conditions outside of the laboratory. To deal with changes in the environment, adaptations to the signal processing used in the BCI may be necessary [12]. Additionally, the signal processing methods used in the current publication may benefit from being updated to the approaches outlines in e.g. in [13].

In its current form the mobile platform we used for the experiments is not well suited for BCI control. Sometimes commands were not executed, in particular if there was a slight slope, which had a frustrating effect on the participants. There may have also been an effect of friction as sometimes the steering angle could not be set. It has to be considered that driving short distances of about one meter with low speeds is not optimal for the motor of the mobile platform.

CONCLUSION

We were able to show that low-cost EEG hardware can be used to control a mobile platform using tactile ERPs an a real world driving task. The mobile platform must

Published by Verlag der TU Graz
Graz University of Technology

 DOI: 10.3217/978-3-85125-533-1-32

be adapted to react precisely to the discrete commands issued with a ERP BCI. Environmental influences are a key component for this type of experiment. Even if they have a negative impact on the performance of the BCI should only be protected against to the extent as not to cause any discomfort for the user. To summarize, we were able to show that BCI control of the mobile platform with tactile stimulation is possible and important steps for future research were determined.

REFERENCES

[1] Farwell, L. and Donchin, E. "Talking off the top of your head: toward a mental prosthesis utilizing event-related brain potentials". In: *Electroencephalogr Clin Neurophysiol* 70 (1988), pp. 510–523.

[2] Nijboer, F. et al. "A P300-based brain-computer interface for people with amyotrophic lateral sclerosis". In: *Clin Neurophysiol* 119.8 (Aug. 2008), pp. 1909–16. DOI: 10.1016/j.clinph.2008.03.034.

[3] Leeb, R. et al. "Self-paced (asynchronous) BCI control of a wheelchair in virtual environments: a case study with a tetraplegic". In: *Comput Intell Neurosci* (2007), p. 79642. DOI: 10.1155/2007/79642.

[4] Riccio, A. et al. "Eye-gaze independent EEG-based brain-computer interfaces for communication". In: *J Neural Eng* 9.4 (Aug. 2012), p. 045001. DOI: 10.1088/1741-2560/9/4/045001.

[5] Kaufmann, T., Herweg, A., and Kübler, A. "Toward brain-computer interface based wheelchair control utilizing tactually-evoked event-related potentials". In: *J Neuroeng Rehabil* 11.1 (2014), p. 7. DOI: 10.1186/1743-0003-11-7.

[6] Debener, S. et al. "How about taking a low-cost, small, and wireless EEG for a walk?" In: *Psychophysiology* 49.11 (Nov. 2012), pp. 1449–53. DOI: 10.1111/j.1469-8986.2012.01471.x.

[7] Schilling, K. "Robotic and telematic assistant technologies to support aging people". In: *Instrumentation, Communications, Information Technology, and Biomedical Engineering (ICICI-BME), 2009 International Conference on*. IEEE. 2009, pp. 1–3.

[8] Eck, D. et al. "Mobility assistance for older people". In: *Applied Bionics and Biomechanics* 9.1 (2012), pp. 69–83.

[9] Eck, D. et al. "Evaluation of a Drive Assistance Function for older Adults". In: *IFAC Proceedings Volumes* 45.4 (2012), pp. 176–181.

[10] Schalk, G. et al. "BCI2000: a general-purpose brain-computer interface (BCI) system." eng. In: *IEEE Trans Biomed Eng* 51.6 (2004), pp. 1034–1043. ISSN: 0018-9294 (Print). DOI: 10.1109/TBME.2004.827072.

[11] Käthner, I. et al. "Effects of mental workload and fatigue on the P300, alpha and theta band power during operation of an ERP (P300) brain-computer interface". In: *Biol Psychol* 102 (Oct. 2014), pp. 118–29. DOI: 10.1016/j.biopsycho.2014.07.014.

[12] Brandl, S. et al. "Brain-computer interfacing under distraction: an evaluation study". In: *J Neural Eng* 13.5 (Oct. 2016), p. 056012. DOI: 10.1088/1741-2560/13/5/056012.

[13] Farquhar, J. and Hill, N. J. "Interactions between pre-processing and classification methods for event-related-potential classification: best-practice guidelines for brain-computer interfacing". In: *Neuroinformatics* 11.2 (Apr. 2013), pp. 175–92. DOI: 10.1007/s12021-012-9171-0.

Published by Verlag der TU Graz
Graz University of Technology

Proceedings of the
7th Graz Brain-Computer Interface Conference 2017 DOI: 10.3217/978-3-85125-533-1-33

P300 SPELLER IMPLEMENTATION USING WEB DEVELOPMENT LANGUAGES

R.E.S. Harnarinesingh[1] and C.S. Syan[2]

[1] Department of Electrical and Computer Engineering, The University of the West Indies, St. Augustine, Trinidad

[2] Department of Mechanical and Manufacturing Engineering, The University of the West Indies, St. Augustine, Trinidad

E-mail: randy.harnarinesingh@sta.uwi.edu

ABSTRACT: Brain-computer Interface (BCI) applications present significant assistive potential for disabled individuals. BCI software is typically implemented on desktop and laptop computers. Mobile platforms such as smartphones and tablets however possess comparable processing power to desktops and laptops. Recent studies have investigated BCI implementation using mobile phones [1, 2]. However, the programs developed in these studies are intended for specific platforms and recoding is required to implemented the programs on other mobile devices.
This paper investigates the implementation of the P300 Speller Paradigm using web development languages. This provides an avenue for universal implementation of the paradigm without the need for recoding for specific platforms. The developed paradigm was tested to ensure that the temporal properties of the paradigm complied with the required timed delays. The testing showed a maximum mean error of 5.17ms and standard deviation of 11.23ms for 100ms temporal segments. This work demonstrates that web languages are a promising avenue for the implementation of BCI paradigms. However, modalities for increasing timing compliance will be explored. Further work will also investigate incorporating data collection and signal processing into the developed program to implementing training and testing sessions for full BCI implementation.

INTRODUCTION

Brain-Computer Interfaces (BCIs) allow user control of external devices using inherent brain activity. BCI paradigms require users to perform tasks which represent commands for external devices. For example, some paradigms can require users to gaze at a left arrow to issue motive commands to a driven wheelchair [3]. BCIs are responsible for recording the raw brain activity and processing the signals to interpret the subject command. This involves multiple hardware and software stages and the anatomy of the standard BCI is presented in Fig. 1.

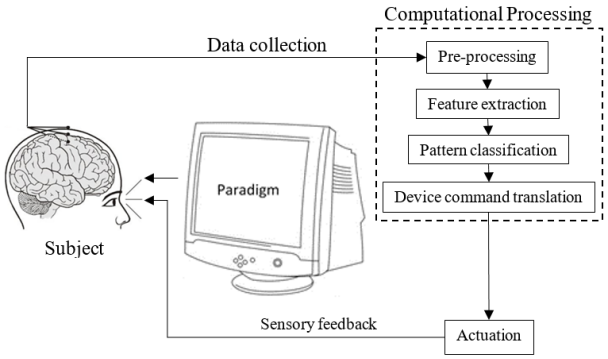

Figure 1: Anatomy of the standard BCI.

BCIs can be implemented using a host of paradigms. These paradigms include the P300 Speller [4], Steady State Visually Evoked Potentials (SSVEP) [5], Slow Cortical Potentials (SCP) [6] and Motor Imagery (MI) [7]. BCIs have been employed for a host of assistive applications such as wheelchair navigation [8] and keyboard control [9].

BCIs are typically implemented on desktop and laptop computers. Mobile platforms such as smartphones and tablets however possess comparable processing power to desktop and laptop machines whilst being smaller and more affordable. Recent studies have investigated BCI implementation using cell phones [1, 2].

These studies however implemented programs on select phone models using device specific software libraries and operating systems. This presents a hurdle to implementing the developed programs on other mobile platforms since code would have to be rewritten to be compatible on other devices.

This paper investigates the feasibility of implementing the P300 Speller Paradigm using web development languages. The expression of the P300 Speller in web development languages allows for implementation on all devices with web browsers regardless of operating systems. These devices include desktops, laptops, tablets and smartphones. This work however treats with the presentation aspects only.

Published by Verlag der TU Graz
Graz University of Technology

 DOI: 10.3217/978-3-85125-533-1-33

MATERIALS AND METHODS

The development, testing and analysis was performed on a Dell Inspiron17R laptop with an Intel® Core™ i7-4500U CPU clocked at 1.8GHz with 8.00GB of Random Access Memory (RAM). The browser used for laptop testing was Google Chrome Version 55.0.2883.87m. The mobile phone used for testing was the Digicel DL1 manufactured by TCL.

P300 SPELLER DEVELOPMENT

This section provides background on the P300 Speller Paradigm as well as details of the implementation of the P300 Speller using web development languages.

P300 SPELLER PARADIGM

The seminal work on P300-based BCIs was done by Farwell and Donchin [10]. Various modifications to the P300 Speller have since been implemented such as alterations to the paradigm character set and stimulus delivery patterns.

The P300 Speller Paradigm itself is an oddball paradigm in which rare target stimuli are presented amongst frequently delivered non-target stimuli [11]. The Speller Paradigm requires subjects to view a single matrix element during the randomly ordered flashing of all matrix elements [12]. When a matrix element the subject is focusing on is flashed, the P300 response is evoked and the detection of the P300 is used to identify user focus [13]. The P300 Speller has been used for a host of practical BCI applications [8].

WEB DEVELOPMENT LANGUAGES

The sequential operation of the P300 Speller is embodied in the flow chart of Fig. 2. This flow chart represents the specific case of 100ms flash time and Inter-Stimulus Interval (ISI).

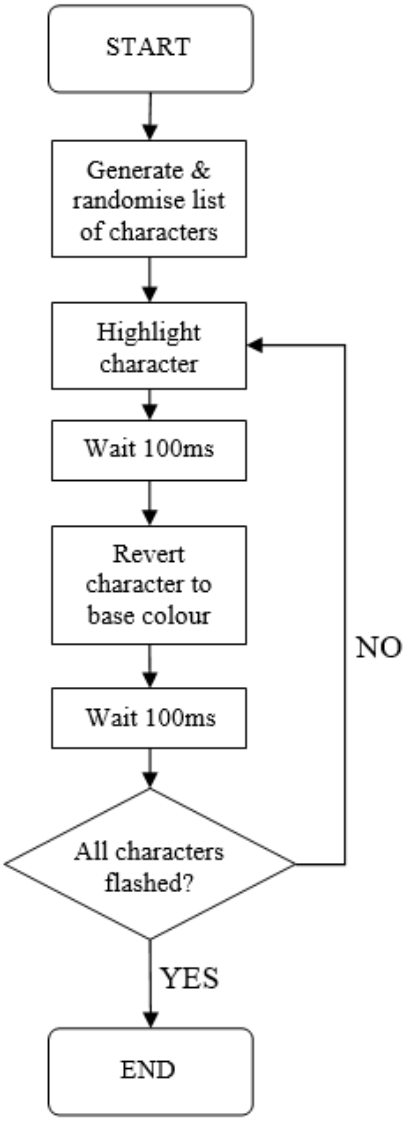

Figure 2: P300 Speller Paradigm Flow Chart

There are 3 main client-side programming languages that are used to implement webpages. They are Hyper Text Markup Language (HTML) [14], Cascading Style Sheets (CSS) [15] and JavaScript (JS) [16]. There are also server-side programming languages that are utilized in live websites. However, the P300 Speller developed in this work is intended to be used offline without the need for an active internet connection. This work therefore does not involve server-side programming languages.

The client-side languages each perform different functions as it relates to webpages. Some of their functions are pictured in Fig. 3.

Published by Verlag der TU Graz
Graz University of Technology

 DOI: 10.3217/978-3-85125-533-1-33

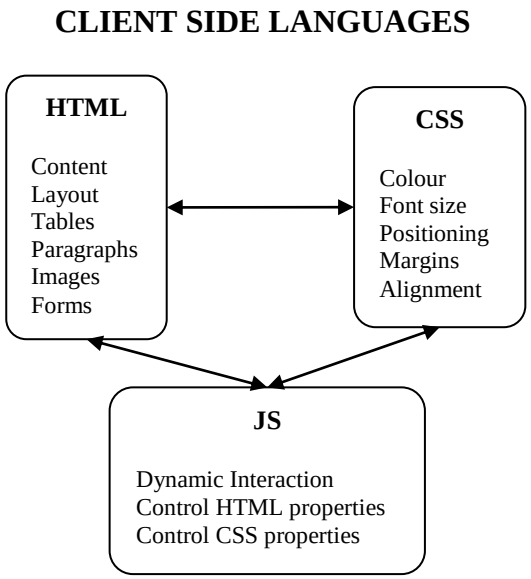

Figure 3: Functions of client side programming languages

There are some elements of the P300 Speller that do not vary with time. These time-static elements such as background colour and button positions can be realized using HTML and CSS. However, it can be seen from Fig. 2. that the P300 Speller also has time-dynamic elements such as element colour changes and timing delays. The only client-side language capable of expressing time-dynamic behaviour is JS. This work also uses JQuery [17] which is a JS Library capable of shorthand coding conventions.

PROGRAM IMPLEMENTATION

This section presents some code snippets and technical information regarding the developed program. The P300 Speller was implemented using HTML, CSS and JS.

The matrix of P300 Speller elements was realised as a table in HTML as shown in Fig. 4. The HTML code for the first row of Speller element is presented below. The remaining 5 rows denoted by the vertical ellipsis are identical to tow 1 besides the text and HTML ids.

```
<table>
    <tr>
        <td id="A">A</td>
        <td id="B">B</td>
        <td id="C">C</td>
        <td id="D">D</td>
        <td id="E">E</td>
        <td id="F">F</td>
    </tr>
                    ⋮
</table>
```

Figure 4: P300 Speller Paradigm HTML code snippet

Each element of the P300 Speller matrix was given a unique id label in HTML. This was done to enable easy targeting by the CSS for character flashing. The CSS code snippet that defines the margins and background-foreground colour for the P300 elements is presented in Fig. 5.

```
table {
    color: white;
    background-color: black !important;
    margin-left: auto;
    margin-right: auto;
}

td {
    width:120px;
    height:120px;
    font-size:6em;
    text-align: center;
    font-family: Arial;
}
```

Figure 5: P300 Speller Paradigm CSS code snippet

The JS code snippet that was responsible for the time dynamic aspects of the P300 Speller Paradigm is showed in Fig. 6.

```
function flash() {
    i=0;
    if(i<c) {
        var flash_index = new_chars[i];
        light_unlit(flash_index,1);

        setTimeout(
            function() {
                light_unlit(flash_index,0);
                setTimeout(flash,ISI);
            }
        ,flash_time);
    }
    i++;
}
```

Figure 6: P300 Speller Paradigm JS code snippet

The ‘new_chars’ variable with length ‘c’ is defined outside of the function and contains the total list of characters to be flashed based on the number of trials. The “light_unlit” function flashes a P300 matrix element if the second function input is ‘1’ and reverts the element base colour to white if the second input is ‘0’.

The JS language does not contain a standard delay function that halts code execution for a predefined period. The paradigm timing is therefore implemented using the “setTimeout” JS function. The “setTimeout” function waits for a certain time before running some specified code. Recursion is then employed to ensure

Published by Verlag der TU Graz
Graz University of Technology

 DOI: 10.3217/978-3-85125-533-1-33

that the code progresses to highlight and then revert character colours until the total character set is flashed.

The developed P300 Speller as viewed on a laptop is shown in Fig. 7.

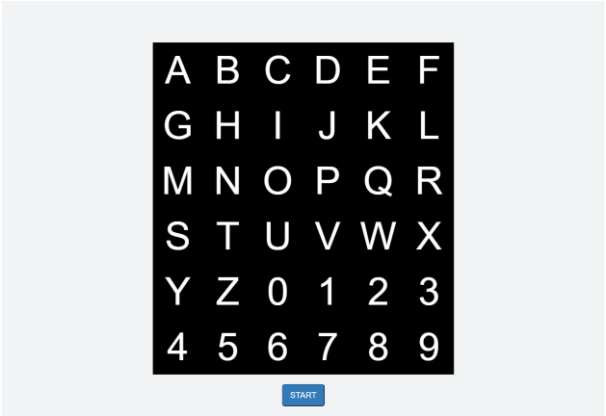

Figure 7: P300 Speller on Laptop Chrome Browser

A mobile version of P300 Speller was also developed and is viewed in Fig. 8. This is a modified P300 Speller with a smaller command matrix intended for better viewing on a mobile platform. The commands are tailored for the control of a vehicular platform which is a common P300-based BCI application.

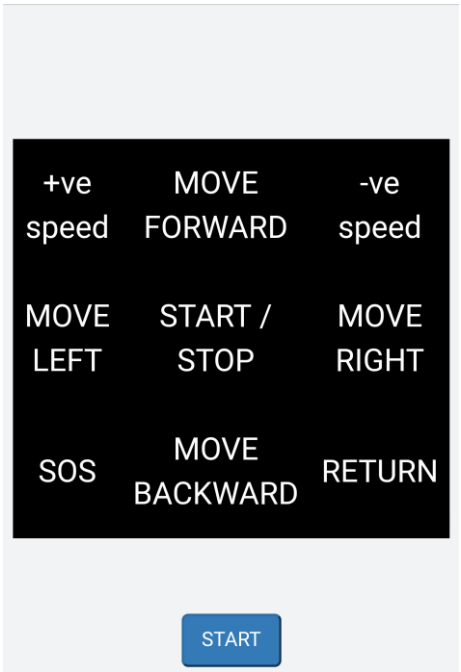

Figure 8: P300 Speller on Android Chrome Browser

RESULTS

The developed paradigm was executed on the Google Chrome Browser for Windows. The paradigm also successfully ran on Internet Explorer and Mozilla Firefox however Chrome was preferred due to previous author experience with the browser. A scaled down P300 Speller was also developed for Chrome on Android to highlight the feasibility of the program for mobile platforms.

The developed program accurately implemented the stimulus sequencing required of the P300 Speller. However, stimulus flash times and ISIs were obtained to determine compliance with the stimulus timing requirements. The PC monitor was therefore recorded using a software screen recorder which ran concurrently with the paradigm. The recording was done at 60 frames per second (fps) which coincides with the screen refresh rate. The recorded videos were then imported into MATLAB and decomposed into individual frames which were analysed to determine the stimulus flash times and ISI.

Fig. 9 and Fig. 10 presents examples of the image processing that was done to determine where a stimulus was flashing or base colour. The technique used utilised the non-flashing case as a subtractive reference image. The result image for subtraction from the non-flashing case is therefore a blank image output. The result for subtraction from the screen capture of the flashing case is a non-zero image. The latter result was therefore discriminated against the former using a basic RGB intensity count feature.

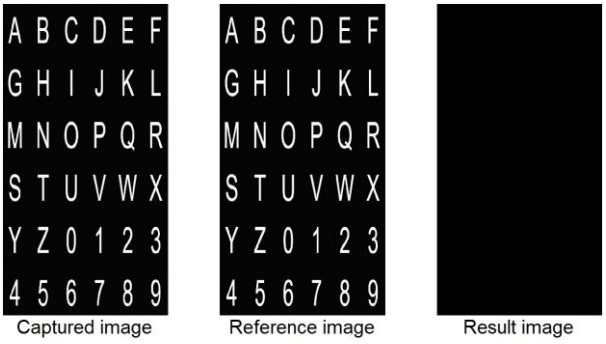

Figure 9: Image subtraction for ISI period

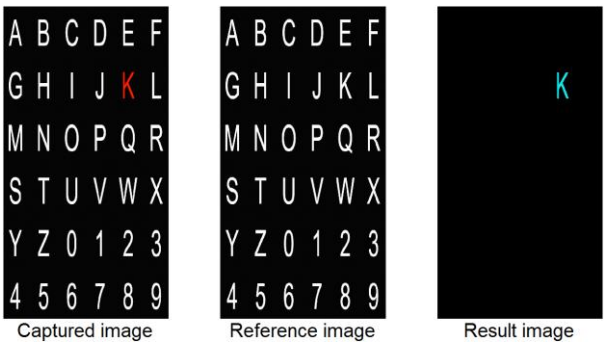

Figure 10: Image subtraction for stimulus highlight

Published by Verlag der TU Graz
Graz University of Technology

 DOI: 10.3217/978-3-85125-533-1-33

The P300 Speller was run for 5 trials which entailed 180 individual character flashes. The frame analysis therefore testing two main timed elements: (1) 180 flash times and (2) 179 ISIs. The flash times and ISIs were collected for each session. This was repeated for 30 experiments in total and the average times were obtained.

Fig. 11 presents the histogram of stimulus highlight times in terms of number of frames for a single session. Fig. 12 shows a histogram of ISIs for a representative session. It is worth noting that 6 frames are equivalent to the programmed time of 100ms.

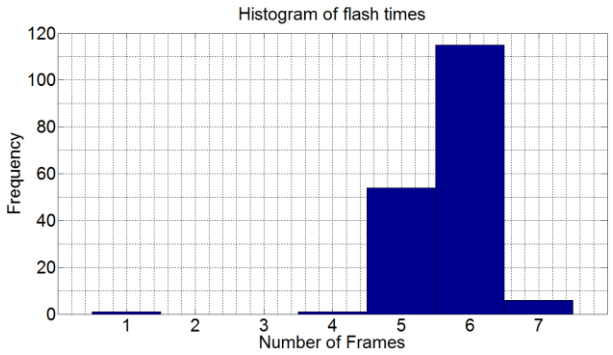

Figure 11: Histogram of stimulus flash times

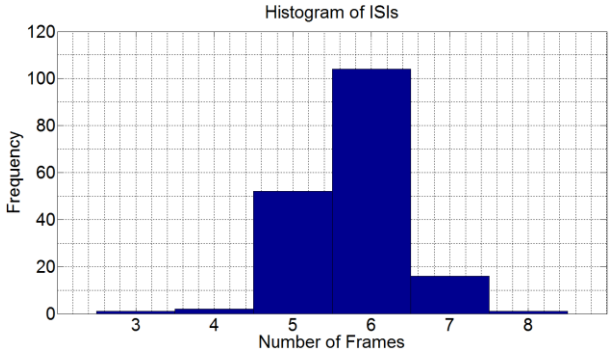

Figure 12: Histogram of ISIs

The global mean and standard deviation of stimulus flash times and ISIs across all testing sessions are presented in Table 2.

Table 2: Programmed and actual timings for P300 Speller

Feature	Programmed Timing	Mean observed time	Error	
			Mean	SD
Flash Time	100ms	94.83ms	5.17ms	10.65ms
ISI	100ms	96.17ms	3.83ms	11.23ms

DISCUSSION

This work investigated the implementation of the P300 Speller using web development languages. The developed paradigm was executed on both laptop and Android variants of the Google Chrome browser. The paradigm was captured and analysed to determine the compliance of the programmed timing delays. This was useful in evaluating time skew due to computational overheads and determining if time skew was significant. The results revealed that the actual flash times and ISIs deviated at most 5.17ms from the programmed time. These timing errors are expected in any time-based BCI paradigm. However, their magnitudes in this work were not detrimental to the success of the paradigm.

The successful implementation of the P300 Speller using web development languages provides a useful proof of concept for BCI implementation in a web browser. In addition, the advent of Android compatible EEG headsets [18] provides a pathway for full implementation of a BCI using mobile platforms such as smartphones and tablets.

There are also benefits to coding the P300 Speller in web development languages such as HTML/CSS/JS instead of device standard languages such as C++ and Java. Web pages can be executed on all modern devices with a web browser. This averts the requirement for any special library or virtual runtime and promises universal execution. This allows the benefit of a single program which can run on every operating system that implements a web browser without considerations for library and hardware constraints.

CONCLUSION & FUTURE WORK

This paper investigated the implementation of the P300 Speller Paradigm using web development languages. The results demonstrate that the developed paradigm complied with the timing delays required of the P300 Speller. The paradigm was executed successfully on both a laptop and Android smartphone. This paper therefore provided an important proof of concept for web browser based BCI paradigm presentation.

However, there are possible avenues of future work. The developed paradigm must be integrated to data collecting and signal processing elements to allow for a full BCI implementation that included training and testing sessions. Virtual PC COM ports provide an avenue for this integration. This would allow for the communication of data between JS and data collection programs in MATLAB for example. In addition, the user interface can be improved to allow for selectable parameters. This can be further expanded to allow for a testbed based approach.

Published by Verlag der TU Graz
Graz University of Technology

 DOI: 10.3217/978-3-85125-533-1-33

REFERENCES

[1] Wang Y-T, Wang Y, Jung T-P. A cell-phone-based brain–computer interface for communication in daily life. Journal of neural engineering. 2011;8(2):025018

[2] Campbell A, Choudhury T, Hu S, Lu H, Mukerjee MK, Rabbi M, Raizada RD. NeuroPhone: brain-mobile phone interface using a wireless EEG headset, in Proc. Proceedings of the second ACM SIGCOMM workshop on Networking, systems, and applications on mobile handhelds, 2010, 3-8

[3] Pires G, Castelo-Branco M, Nunes U. Visual P300-based BCI to steer a wheelchair: A Bayesian approach, in Proc. 30th Annual International Conference of the IEEE Engineering in Medicine and Biology Society, 658-661

[4] Krusienski DJ, Sellers EW, Mcfarland DJ, Vaughan TM, Wolpaw JR. Toward enhanced P300 speller performance. Journal of Neuroscience Methods. 2008;167(1):15-21

[5] Zhu D, Bieger J, Molina GG, Aarts RM. A survey of stimulation methods used in SSVEP-based BCIs. Computational intelligence and neuroscience. 2010;2010(1):1-13

[6] Hinterberger T, Weiskopf N, Veit R, Wilhelm B, Betta E, Birbaumer N. An EEG-driven brain-computer interface combined with functional magnetic resonance imaging (fMRI). IEEE transactions on biomedical engineering. 2004;51(6):971-974

[7] Scherer R, Lee F, Schlogl A, Leeb R, Bischof H, Pfurtscheller G. Toward Self-Paced Brain-Computer Communication: Navigation Through Virtual Worlds. IEEE transactions on biomedical engineering. 2008;55(2):675-682

[8] Iturrate IÃ, Antelis JM, Kubler A, Minguez J. A noninvasive brain-actuated wheelchair based on a P300 neurophysiological protocol and automated navigation. IEEE Transactions on Robotics. 2009;25(3):614-627

[9] Scherer R, Muller GR, Neuper C, Graimann B, Pfurtscheller G. An asynchronously controlled EEG-based virtual keyboard: improvement of the spelling rate. IEEE transactions on biomedical engineering. 2004;51(6):979-984

[10] Farwell LA, Donchin E. Talking off the top of your head: toward a mental prosthesis utilizing event-related brain potentials. Electroencephalography and clinical Neurophysiology. 1988;70(6):510-523

[11] Garcia-Larrea L, Lukaszewicz AC, Mauguiere F. Revisiting the oddball paradigm. Non-target vs neutral stimuli and the evaluation of ERP attentional effects. Neuropsychologia. 1992;30(8):723-741

[12] Segalowitz SJ, Barnes KL. The reliability of ERP components in the auditory oddball paradigm. Psychophysiology. 1993;30(5):451-459

[13] Guger C, Daban S, Sellers E, Holzner C, Krausz G, Carabalona R, Gramatica F, Edlinger G. How many people are able to control a P300-based brain-computer interface (BCI)? Neuroscience letters. 2009;462(1):94-98

[14] Frain B. Responsive web design with HTML5 and CSS3, Packt Publishing Ltd, (2012)

[15] Lie HW, Bos B. Cascading style sheets: Designing for the web, Portable Documents, Addison-Wesley Professional, (2005)

[16] Flanagan D. JavaScript: the definitive guide, O'Reilly Media, Inc., (2006)

[17] De Volder K. JQuery: A generic code browser with a declarative configuration language, in Proc. International Symposium on Practical Aspects of Declarative Languages, 2006, 88-102

[18] Duvinage M, Castermans T, Dutoit T, Petieau M, Hoellinger T, Saedeleer CD, Seetharaman K, Cheron G. A P300-based quantitative comparison between the Emotiv Epoc headset and a medical EEG device. Biomedical Engineering. 2012;765(1):2012-2764

Published by Verlag der TU Graz
Graz University of Technology

Proceedings of the
7th Graz Brain-Computer Interface Conference 2017 DOI: 10.3217/978-3-85125-533-1-34

A PLEASANT AUDITORY BRAIN COMPUTER INTERFACE USING NATURAL ENVIRONMENT SOUNDS

Minqiang Huang[1], Ian Daly[2], Xingyu Wang[1], Jing Jin[1]

[1] Key Laboratory of Advanced Control and Optimization for Chemical Processes, Ministry of Education, East China University of Science and Technology, Shanghai, P.R. China
[2] University of Essex, Wivenhoe Park, Colchester, Essex, CO4 3SQ, UK

E-mail: jinjingat@gmail.com, xywang@ecust.edu.cn

ABSTRACT: An auditory brain computer interface system which utilizes pleasant water-drop sounds is proposed in this study. The purpose of this study is to explore the property of the paradigm which uses water-drops as stimuli. The results show that the water-drop paradigm can improve the user friendness and get robust performance in items of online classification accuracy. The group average online accuracy is 73.33% which is acceptable.

INTRODUCTION

Brain computer interfaces (BCIs) can provide a new path to communicate with the external world for people who have lost the ability to control their muscles (such as individuals with amyotrophic lateral sclerosis (ALS)) [1]. The P300 event-related potential is a large positive component appearing at about 300 ms after a rare task-related event happened [1]. A single-modal BCI based on the P300 can be categorized into one of three groups according its modality of stimulation: visual BCI, auditory BCI or tactile BCI [2]. Our research mainly focuses on the auditory P300 BCI paradigm in this study. For people who cannot rely on visual BCIs, auditory BCIs can provide another way for them to improve their quality of life. Among the proposed works related to auditory BCIs, the acoustic stimuli used have included beeps with different frequencies, Arabic Numbers or animal vocalization [2-4]. As one kind of environmental sound which can be heard often, water drops have not been explored as stimuli in an auditory BCI system.

In this study, water drops are chosen as stimuli. Water drops are natural environmental sounds. The positive effect of using natural sounds as stimuli for auditory BCIs has been discussed in Höhne et al's work [5]. Among the existed auditory paradigms for BCIs using natural sounds as stimuli, water drop sounds remain unexploited. The use of water drops is mentioned in research related to how to reduce the noise in the environments and this research showed that water sounds are the best sounds with which to mask the environment noises and reduce the annoyance of people [6]. It should be taken into consideration that the environment of BCI usage might not be as quiet as in the lab. Hence, the water drops have its special advantage compared with other kind of sounds in the auditory paradigm. In this study, the potential of water drop sounds as auditory stimuli materials are investigated. A hypothesis that the auditory BCI system using water drops as stimuli can get good performance in terms of both accuracy and user friendness is investigated.

MATERALS AND METHODS

Stimuli

Three water-drop sounds are extracted from a music work (Fragile Hope (WANDER/WONDER, Balam Acab). The criterion of selecting the water-drop sounds is to make sure that each water drop sounded different but not obtrusive.

All the audio files are edited with Adobe Audition CS6 5.0. A pair of earphones (Sennheiser CX200) is used to play sounds. Direction cues (left, middle, and right) are added to the water-drops to decrease the difficulty of the tasks. To maximize the difference between directions, the right sound channel of the left water drops is muted and the left sound channel of the right water drop is muted. The details of the stimuli in both paradigms are shown in the Fig.1. All the stimuli lasted 200 ms, and the inter-stimulus interval (ISI) is 350 ms. The minimum TTI (Target to Target Interval) is 900 ms. In this study, the target stimulus indicated that one of the stimuli which is asked the participant to focus on and the non-target stimuli are the ignored stimuli. The probability of the target stimulus appearing is 1/3. All the stimuli are played in a pseudorandom order that the same stimulus would not appear consecutively to avoid the double-flashing effect. Although the probability of the target stimuli is fairly high, the long TTI can evoke high quality ERPs.

Published by Verlag der TU Graz
Graz University of Technology

 DOI: 10.3217/978-3-85125-533-1-34

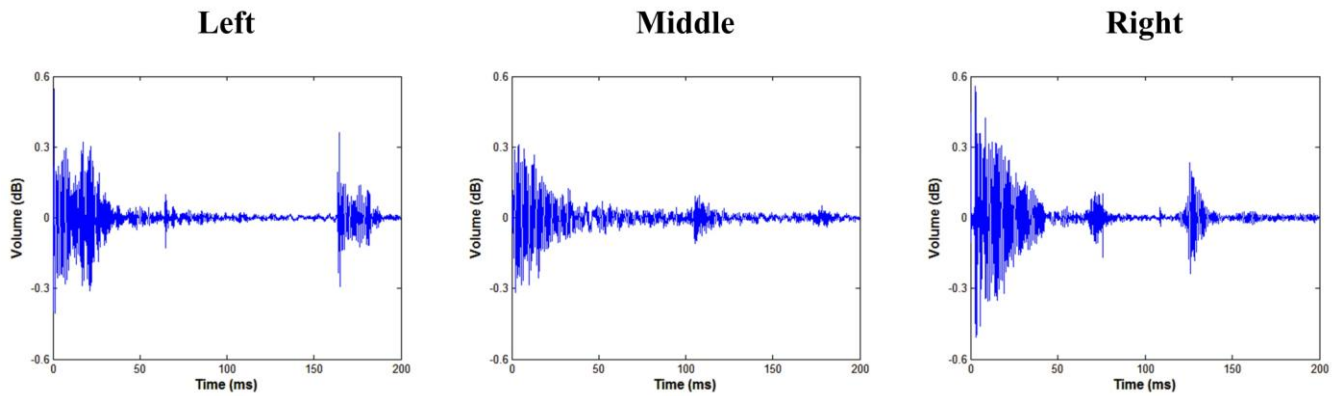

Figure1: The acoustic waveforms of the auditory stimuli.

Experiment set up

EEG data is recorded from 15 channels of a 64-channel 'g.EEGcap' EEG cap (Guger Technologies, Graz, Austria). The electrode positions used are F3, Fz, F4, T7, C3, Cz, C4, T8, CP3, CPz, CP4, P3, Pz, P4, and Oz from the international 10-20 system. The right earlobe is used as the reference and FPz is used as the ground. A 16-channel 'g.USBamp' amplifier (Guger Technologies, Graz, Austria) with a 512 Hz sampling rate is used to measure the EEG. The data is band pass filtered between 0.1-100 Hz and the notch-filter is applied at 50 Hz.
Ten healthy students (21-26 years old, mean 23.8) participated in this study. Six of them had attended BCI experiments before. The participants are asked to keep their eyes open and focus on a fixed point on the screen. They are also asked to avoid eye blinking and other body movements during the experiments. The volume of system is adjusted to a suitable level according to each participant's demand. In the offline experiments, three sessions are conducted. Each session contains five runs; each run had sixteen trials; each trial contained three sub-trials (one stimulus). Before each run, an audio cue would prompt participant the target stimulus. When participants finished one run, the offline training data of one target is collected. When participants finished one session, they had a short rest for 3 minutes. After the offline experiments, online experiments are executed. The online task had 36 given target-selections to complete. An adaptive method, proposed by Jin et al, is used in the online experiments [7]. In this study, it needed ~7 iterations for most participants to finish one target-selection. The whole online task lasted about 10 minutes.

Feature extraction and classification

A third order Butterworth band pass filter between 0.1 and 30 Hz is used to filter the raw EEG data. The filtered EEG data is downsampled from 512 Hz to 64 Hz and 1000 ms of data after each stimulus is extracted. The size of the feature vector is 15×64 (15 channels by 64 time points).
The classification algorithm in this study is Bayesian linear discriminant analysis (BLDA). BLDA has better performance on classification accuracies and lower risk of over-fitting when deal with high dimension data than Fisher's discriminant analysis (FLDA) [8].

RESULT

Online accuracy results of each participant are shown in Tab. 1. The grand average amplitudes of ERPs across ten participants are presented in the Fig.2 (A). The topographic maps of average amplitudes of the P300 and N400 are shown in Fig. 2 (B).

Table 1: The average online accuracy of each participant.

Participant	Online accuracy (%)
S1	75
S2	63.89
S3	80.56
S4	69.44
S5	80.56
S6	88.89
S7	66.67
S8	69.44
S9	69.44
S10	69.44
Avg	73.33

DISCUSSION

The goal of this study is to explore the property of water-drops as auditory stimuli and the results show that water-drops sounds can be reliable auditory materials for auditory BCI systems.

ERPs

The grand average ERP amplitude of targets and non-targets across all participants at electrodes Fz, Cz, CPz, and Pz are shown in Fig.2 (A). Obviously, the target amplitudes are different from the non-target amplitudes. No clear N1 component and N2 component are found in the early period between 0-200 ms. P300 and late negative components are the key potentials that are used to distinguish the target amplitudes from the non-target amplitudes. The spatial distributions of P300 and late negative components are presented in the Fig 2 (B).

Published by Verlag der TU Graz
Graz University of Technology

 DOI: 10.3217/978-3-85125-533-1-34

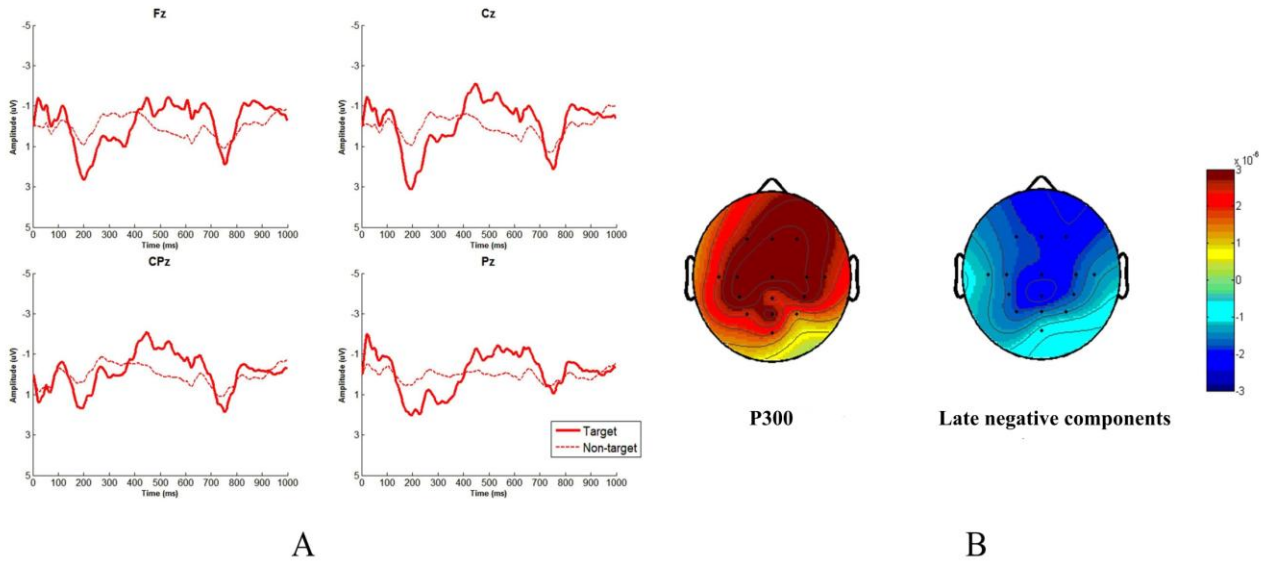

Figure 2: (A) The grand average amplitude of ERPs across ten participants at Fz, Cz, CPz, and Pz. (B) The topographic maps of average amplitudes of P300 and N400.

Online accuracy

As shown in the Table 1, the group average online accuracy is above 70%, which is considered by some to be the minimum value to meet the communication needs of BCI users [9]. Compared with other works [8, 10-12], this accuracy is in the middle level. The mental fatigue increases during the online task that explores the performance of this BCI system in a long-term usage. A phenomenon, observed in most participants, is that during the online period, the accuracy would decrease after finishing some targets and then increase after a short time (the time varies with individuals). The jitter of the accuracy might be caused by the level of fatigue when the participants are executing the task.

CONCLUSION

This paper proposed an auditory BCI paradigm with water-drops as stimuli and verified its utility. The online results shown that this paradigm could be a reliable choice for auditory BCI systems to provide a better experience for users. The future work is to increase the classes of this paradigm and optimize the water drops to get higher performance on classification accuracy while retaining the pleasant user experience.

ACKNOWLEDGMENTS

This work is supported in part by the Grant National Natural Science Foundation of China, under Grant No. 91420302 and 61573142. This work is also supported by the Fundamental Research Funds for the Central Universities (WH1516018) and Shanghai Chenguang Program under Grant 14CG31.

REFERENCES

[1] Farwell LA, Donchin E. Talking off the top of your head: toward a mental prosthesis utilizing event-related brain potentials. Electreon. Clin neuro1988;70(6):510-523.
[2] Schreuder M, Blankertz B, Tangermann M. A New Auditory Multi-Class Brain-Computer Interface Paradigm: Spatial Hearing as an Informative Cue. PloS one 2010;5(4): e9813.
[3] Baykara E, Ruf C, Fioravanti C, Käthner I, Simon N, Kleih S, Kübler A, Halder S. Effects of training and motivation on auditory P300 brain–computer interface performance. Clin. Neurophysiol. 2016;127(1):379-387.
[4] Kübler A, Furdea A, Halder S, Hammer EM, Nijboer F, Kotchoubey B. A brain-computer interface controlled auditory event-related potential (p300) spelling system for locked-in patients. Ann. NY. Acad. Sci. 2009;1157(1):90-100.
[5] Höhne J. Natural stimuli improve auditory BCIs with respect to ergonomics and performance. J. Neural. Eng. 2012;9(4):045003.
[6] Jeon JY, Lee PJ, You J, Kang J. Perceptual assessment of quality of urban soundscapes with combined noise sources and water sounds. J. Acoust. Soc. Am. 2010;127(3):1357-1366.
[7] Jin J, Allison BZ, Sellers EW, Brunner C, Horki P, Wang X, et al. An adaptive P300-based control system. J. Neural. Eng. 2011; 8(3):036006.
[8] Hoffmann U, Vesin JM, Ebrahimi T, Diserens K. An efficient P300-based brain-computer interface for disabled subjects. J. Neurosci. Meth. 2008;167(1):115–125.
[9] Kübler A, Kotchoubey B, Kaiser J, Wolpaw JR, Birbaumer N. Brain–computer communication: Unlocking the locked in. Psychol. Bull. 2001;127(3):358.
[10] Zhou S, Allison BZ, Kübler A, Cichocki A, Xingyu

Published by Verlag der TU Graz
Graz University of Technology

 DOI: 10.3217/978-3-85125-533-1-34

W, Jin J. Effects of background music on objective and subjective performance measures in an auditory BCI. Front. Comput. Neurosci. 2016;10:105.

[11] Lopez-Gordo MA, Fernandez E, Romero S, Pelayo F, Prieto A. An auditory brain–computer interface evoked by natural speech. J. Neural. Eng. 2012;9(3):408-417.

[12] Klobassa DS, Vaughan TP, Schwartz NE, Wolpaw JR, Neuper C, Sellers EW. Toward a high-throughput auditory P300-based brain–computer interface. Clin. Neurophysiol. 2009;120(7):1252-1261.

Published by Verlag der TU Graz
Graz University of Technology

Proceedings of the
7th Graz Brain-Computer Interface Conference 2017 DOI: 10.3217/978-3-85125-533-1-35

IMPROVING LEARNING FROM LABEL PROPORTIONS BY REDUCING THE FEATURE DIMENSIONALITY

D. Hübner[1], P.-J. Kindermans[2], T. Verhoeven[3], M. Tangermann[1]

[1] University of Freiburg, Dept. Computer Science,
Excellence Cluster BrainLinks-BrainTools, Freiburg, Germany
[2]Machine Learning Group, Berlin Institute of Technology, Berlin, Germany
[3]Electronics and Information Systems, Ghent University, Ghent, Belgium

E-mail: david.huebner@blbt.uni-freiburg.de, michael.tangermann@blbt.uni-freiburg.de

ABSTRACT: Learning from label proportions (LLP) is a recently introduced unsupervised classification method for event-related potential (ERP) based brain-computer interfaces. It estimates the target and non-target means of brain signal epochs based on a known proportion of these classes in different subsets of the data, which can be generated by interleaving different stimulus sequences, e.g., in a visual ERP speller. In contrast to other unsupervised methods, estimations obtained by LLP have the theoretical property of converging to the correct class means. However, the convergence is rather slow. In this paper, we investigate the effect of varying EEG channel numbers as a simple form of regularization onto the performance of LLP classifiers by offline analyses. We found that reduced channel sets can outperform the full set both in terms of single event classification rate and symbol selection accuracy. This is especially pronounced in the initial learning phase. These findings suggest that LLP classification can be significantly improved by reducing the feature dimensionality.

INTRODUCTION

One of the fundamental tasks in brain-computer interfaces (BCI) is to tune the decoder to reliably detect a user's intention. This is a challenging problem because signals do not only differ between subjects, but also between sessions for the same subjects. While some information can be transferred from other subjects or sessions [1–3], a portion of task-specific information remains unknown prior to the start of each session. Hence, the traditional approach is to conduct a calibration session before going into the online application. While this generally works well, some problems are associated with it, namely that it requires additional time, that wrongly labelled data may be recorded when the user incorrectly follows the instructions and that the effect of feedback is not present during the calibration session, possibly leading to different data distributions between calibration and online use of the system [4].

To overcome these problems and avoid calibration sessions, unsupervised methods have been introduced to the BCI communities which can learn from scratch without requiring label informations. They have the additional benefit of continuously learning during a session, thus adapting to possible non-stationarities in the data. One example is the expectation-maximization (EM) algorithm by Kindermans et al. [5] which is applicable for BCI paradigms that use event-related potentials (ERPs) of the electroencephalogram (EEG). It optimizes a likelihood function given a probabilistic model of the data. While it generally works well in practice, it relies on a good random initialisation and has no guarantee to converge to the right solution. As an alternative unsupervised learning method, we recently introduced *learning from label proportions* (LLP) to the BCI community [6]. This method estimates the average responses to target and non-target stimuli based on ERP data. It exploits known proportions of target and non-target stimuli contained in different subsets of the data, but does not require the labels for each stimulus. In contrast to the EM approach, LLP is guaranteed to converge to the correct class means (and thus, to the corresponding decoder) given sufficient amount of data. It also has the advantages of being easy to implement, has extremely short runtime and is deterministic. However, the convergence is often slower as for the EM-algorithm. Further details on LLP are provided in the method section.

An important argument against unsupervised learning is, that these methods go through an initial learning phase in which the feedback is relatively unreliable. The major reason of this effect is the limited amount of (unlabelled) training data in this initial phase, in combination with the high dimensionality of the feature space leading to a difficult unsupervised learning problem. In this paper, we re-analyse data from a previous experiment to answer the question whether a reduced number of channels, corresponding to a reduced number of features, can improve the performance of LLP and shorten this initial ramp-up phase.

MATERIALS AND METHODS

Learning from Label Proportions

For classification, we used the recently introduced learn-

Published by Verlag der TU Graz
Graz University of Technology

 DOI: 10.3217/978-3-85125-533-1-35

ing from label proportions (LLP) for ERP data [6] which is based on the work of Quadrianto and colleagues [7]. The main idea is to tune the stimulus presentation of a visual ERP-BCI paradigm such that the prerequisites of LLP are satisfied – in this way, the experimental paradigm and decoder are very closely linked and should be seen as a whole and not as independent steps. In order to enable LLP to estimate the target and non-target class means, it is necessary that the recorded visual ERP responses consist of at least two subsets, and that one of the sets has a higher target proportion than the other. Additionally, these proportions have to be known.

The way we created two different subsets is by randomly interleaving two sequences in each single trial (i.e. spelling one character) of a visual speller. In each highlighting event of the first sequence, 12 characters are highlighted, while an event of the second sequence only highlights 3 or 4 characters resulting in average of $3.\overline{5}$ highlighted characters per event. Because there is a total of 32 selectable characters, this leads to an average target ratio of $12/32 = 3/8$ and $3.\overline{5}/32 = 2/18$ for the first and second sequence respectively.

By manipulating the stimulus presentation in that fashion, we can write the average responses of the two sequences $\boldsymbol{\mu}_1$ and $\boldsymbol{\mu}_2$ as a combination of target $\boldsymbol{\mu}_+$ and non-target responses $\boldsymbol{\mu}_-$, therefore utilizing our knowledge about the average proportions.

$$\begin{cases} \boldsymbol{\mu}_1 = \frac{3}{8}\boldsymbol{\mu}_+ + \frac{5}{8}\boldsymbol{\mu}_- \\ \boldsymbol{\mu}_2 = \frac{2}{18}\boldsymbol{\mu}_+ + \frac{16}{18}\boldsymbol{\mu}_- \end{cases} \tag{1}$$

As we are interested in the mean target and non-target ERP responses, we solve the equations for $\boldsymbol{\mu}_+$ and $\boldsymbol{\mu}_-$ which yields the following two equations.

$$\begin{cases} \boldsymbol{\mu}_+ = 3.37\,\boldsymbol{\mu}_1 - 2.37\,\boldsymbol{\mu}_2 \\ \boldsymbol{\mu}_- = -0.42\,\boldsymbol{\mu}_1 + 1.42\,\boldsymbol{\mu}_2 \end{cases} \tag{2}$$

Two steps are necessary to obtain an estimate of the average target and non-target ERP responses. In a first step, the sequence means ($\hat{\boldsymbol{\mu}}_1$ and $\hat{\boldsymbol{\mu}}_2$) are estimated. In a second step, these estimates are plugged into the equation set 2. Given independent and identically distributed (IID) data points, the estimated sequence means will converge to their true value, such that the true class means can be obtained in the limit.

An implicit assumption of LLP in this formulation is the *homogeneity assumption*, which states that the average target and non-target responses have to be the same in both subsets. The first precautionary measure to accomplish this is to randomize the order of events from both sequences within each single trial. This should guarantee that the target-to-target interval (TTI) does not depend on the sequence, which seems like a desirable characteristic given the known influence of target-to-target intervals onto e.g. the P300 amplitude [8]. The second precautionary measure we propose is to match the overall visual stimulus intensity between both sequences. It is expressed by the overall number of symbols highlighted on the screen in one point in time. To reach a balanced setting, the traditional P300-spelling matrix was extended by 10 additional blank/hash symbols ('#'). These are included only in the second highlighting sequence and should never be attended by the subject, thus they never serve as targets. This simple trick ensures that events of both sequences have the same number of highlighted symbols per event while having the predefined target and non-target ratios. An example is depicted in Fig. 1. Apart from these manipulations, the sequences were generated in a pseudo-random manner using a heuristic approach designed by Verhoeven et al. [9] with the goal to minimize double flashes and adjacency distractions. We previously showed that the homogeneity assumption holds for the data generated in the above way [6].

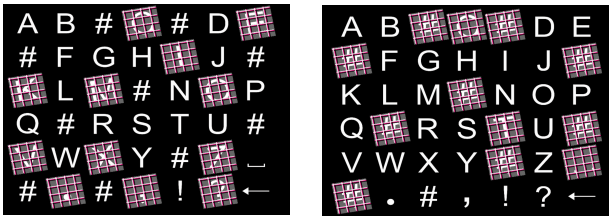

Fig. 1: **Examples of pseudo-randomized highlighting events** of sequence 1 (left) and sequence 2 (right). Sequence 1 never highlights '#' symbols, while sequence highlights 8-9 '#' symbols per event.

Classification

Given estimates of the class means, several classifier approaches are possible. It was previously observed that the ERP responses for targets and non-targets closely follow a multivariate normal distribution with the same covariance matrix [10]. Based on this assumption, linear discriminant analysis (LDA) classifier have shown to be very competitive in ERP-BCI paradigms [11]. These are linear classifiers looking for the best projection $\boldsymbol{w}$ such that samples $\boldsymbol{x}$ are assigned to the target class if $\boldsymbol{w} \cdot \boldsymbol{x} \geq 0$ and to the non-target class otherwise. It is known that the optimal projection can be found solely by knowing the shared covariance matrix $\boldsymbol{\Sigma}$ and the class-wise means $\boldsymbol{\mu}_+$ and $\boldsymbol{\mu}_-$ in the following way [10]:

$$\mathbf{w} = \boldsymbol{\Sigma}^{-1}\left(\boldsymbol{\mu}_+ - \boldsymbol{\mu}_-\right).$$

In the formulation of Blankertz et al. [10], the class-wise covariance matrix is used as $\boldsymbol{\Sigma}$. However, one can show that the pooled covariance matrix, i.e. the covariance computed on the complete data-set, leads to a projection which has the same orientation, but is scaled differently [12]. As no label information are used for the pooled covariance estimation, we can replace the class-wise covariance matrix by the pooled covariance matrix and still obtain the same classifier — if the means are

Published by Verlag der TU Graz
Graz University of Technology

 DOI: 10.3217/978-3-85125-533-1-35

correctly estimated. In addition, it was shown that regularizing the estimated covariance matrix towards an identity matrix leads to better performance. Hence, we adopt the covariance-shrinkage by Ledoit & Wolf as proposed in [10]. In summary, data is classified by combining the mean estimations derived from LLP with the regularized pooled covariance in order to obtain a linear classifier.

To compare the LLP-approach to a traditional classifier, we included a supervised classifier into our comparisons. Again, we used a LDA classifier with regularized covariance matrix [10], which is precisely the same model as described above, only that the class-wise means and covariances are estimated using the sample statistics based on the label information. As supervised classifiers are much more prone to overfitting than unsupervised approaches, we estimated the generalization performance on increasing data sets in a chronological 5-fold cross-validation.

Data

The data used in this work was previously described in our paper on LLP [6]. A short summary is given here. In an online copy spelling tasks, thirteen subjects (5 female, average age: 26 years) spelled three times the same sentence of 63 symbols. The stimulus onset asynchrony (SOA) was 250 ms. To spell an individual symbol, a train of 68 highlighting events were presented. This train is the result of randomly interleaving 32 events of sequence 1 and 36 events of sequence 2, which had been generated as described before. A very salient highlighting method proposed by Tangermann et al. [13] using a combination of brightness enhancement, rotation, enlargement and a trichromatic grid overlay was used. EEG signals were recorded at 1 KHz sampling rate with 31 passive Ag/AgCl electrodes (EasyCap) placed on the head according to the extended 10-20 system. The reference was placed on the nose. After a baseline correction of each EEG epoch, the ERP features were extracted as the average potential values in the six intervals [50, 120], [121, 200], [201, 280], [281, 380], [381, 530] and [531, 700] ms. Outlier epochs were not removed at any time during the data processing, however, visual inspection ensured, that classification was not performed based on eye movement artefacts.

The data of all 13 subjects is freely available online at: `http://doi.org/10.5281/zenodo.192684`.

Performance Measures

The selection accuracy is the percentage of characters intended to spell by a user and that were decoded correctly by the BCI system. As the selection accuracy is only based on 63 symbols per sentence, it is quite a noisy performance metric. It can be evaluated online by reporting the actual performance observed during the experiment, but it can also be estimated by a post-hoc offline analysis.

For the latter, we decided to simulate the experiment several times and on different subsets of the data. Within each sentence, the classifier was restarted multiple times to obtain a better estimate of the selection accuracy. A total of 7 classifiers were simulated per sentence, and each classifier was trained on data of 21 characters: The first one used the characters 1-21, the second one used characters 8-28, . . ., and the last one used the characters 43-68. Finally, these spelling accuracies were averaged across the classifiers, subjects and experimental blocks.

We also looked at how well single targets (attended highlighting events) can be discriminated from non-targets (not-attended highlighting events). This was quantified by the area under the curve (AUC) of the classifier outputs as a threshold-independent and robust performance metric. The AUC values range between 0 % and 100 %, with a theoretical chance level of 50 %. An AUC value of 100 % indicates perfect separation between the two classes, i.e. the classifier can correctly tell for each highlighting event whether it was attended or not. To compute these values in this paper, we simulated an online experiment with different number of channels where the LLP classifier was retrained after each character. The performance was then computed on the complete data-set up to that point by using the given label information. Please note that overfitting is not a problem in this context, because the classifiers do not use the label information for training.

Channel Selection

To determine the importance of an EEG channel in isolation, it is a common strategy to estimate its informative content with respect to the target vs. non-target classification task. We estimated this by assessing univariate informative content expressed by the AUC between the target and non-target features derived from the same six intervals as mentioned before. This was computed for each subject and channel. The AUC values were rescaled to have a theoretical chance level of 0 by applying the following formula:

$$\mathrm{AUC}_{\mathrm{rescaled}} = |(\mathrm{AUC}_{\mathrm{regular}} - 0.5) \cdot 2|$$

These values were then averaged across all subjects and intervals to obtain one relevance score per channel. Unlike in wrapper methods for channel selection [14], this simple and fast relevance score does not grasp informative content of a channel which is only expressed in combination with other channels.

RESULTS

Channels sorted according to their descending importance are shown in Fig. 2. One can observe that the occipital channels *O1* and *O2* have the highest importance which is in accordance with our expectations for a visual ERP experiment [6] that should elicit class-discriminative visual ERP components for electrodes located over the

Published by Verlag der TU Graz
Graz University of Technology

 DOI: 10.3217/978-3-85125-533-1-35

occipital cortex. The five next top-ranked channels are mostly located over the centro-parietal cortex, showing a slight lateralization to the right hemisphere.

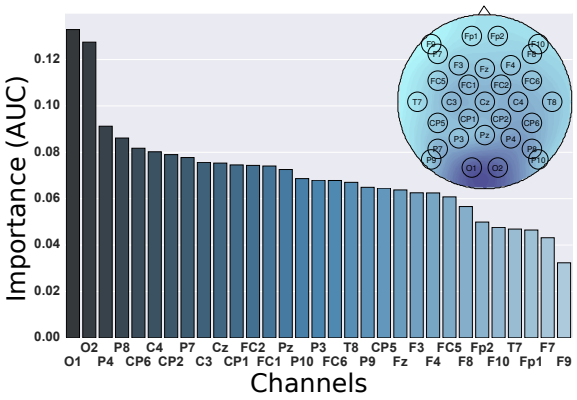

Fig. 2: **Channels sorted according to their importance.** The y-axis shows the averaged AUC value across all 13 subjects for each channel.

According to these results, we selected the n first-ranked channels for $n \in \{3, 5, 10, 31\}$ to run offline experiments with classifiers trained on smaller channel subsets. In the simulation with growing amounts of data, the classifiers were retrained after each additional character and directly applied to classify the current character. The target vs. non-target LLP performances reported in Fig. 3 overall reflect a growing amount of information provided by larger and larger training data sets. Interestingly, a reduced number of 10 channels outperforms the complete set of 31 channels, even if the full amount of data is used. The difference between channel subsets and the full channel set is especially pronounced, when data from only few epochs is available, which corresponds to the early stages of a spelling session. With more and more training data available, the configuration with 10 channels remains on top, while 5 and 31 channels are close behind. The configuration with 3 channels falls back by a good margin.

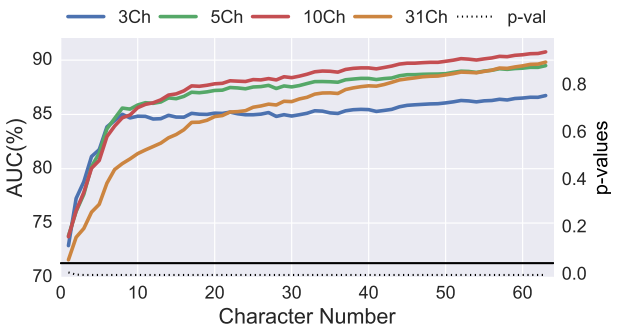

Fig. 3: **Average simulated LLP classification accuracy** in dependence of the number of channels and training points. Per trial, the p-value of a Wilcoxon signed-rank test is given, comparing the results of 31 channels and 10 channels.

When looking at the selection accuracy in the initial ramp-up phase of LLP in Fig. 4, a similar behaviour is observable. Again, the full set of channels is outperformed by a reduced number of channels. Around 70 % of the characters are already classified correctly from the third character on, when using a reduced channel number. This corresponds to less than a minute of training time. After a bit more than 2 minutes of training time, the selection accuracy already exceeds 80 % for the configuration with 5 or 10 channels.

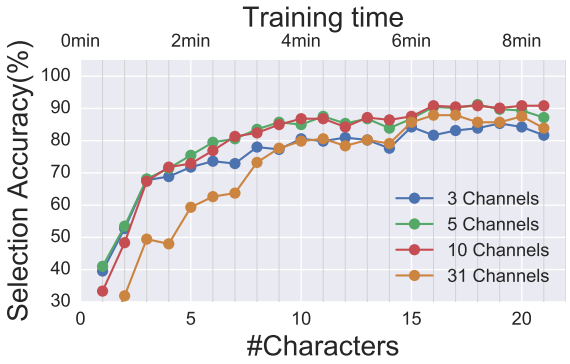

Fig. 4: **Average simulated LLP selection accuracy** as a function of training time / amount of data points and channels.

Finally, we ran a simulation of a supervised shrinkage-LDA classifier to compare the effect of reduced channel subsets with those observed for LLP. Fig. 5 shows that 10 channels significantly outperform 31 channels when few data is available. However, the supervised classifier is able to learn much quicker and utilize the additional information from all channels leading to significantly better performance when data of more than 15 characters is available.

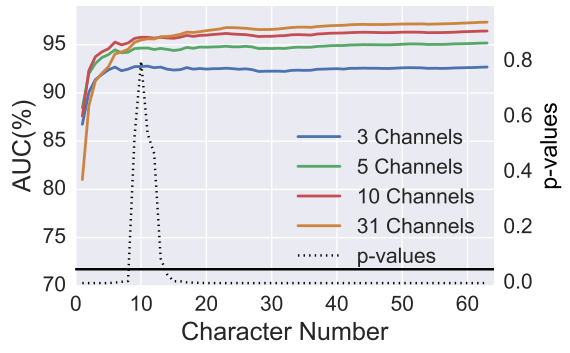

Fig. 5: **Average simulated supervised single epoch accuracy** as a function of training time / data points and channels. For each character, the complete data up to that point was divided in 5 chronological parts and a cross-validation was applied. The p-values show the outcome of a Wilcoxon signed-rank test between the configurations with 31 and 10 channels.

Published by Verlag der TU Graz
Graz University of Technology

 DOI: 10.3217/978-3-85125-533-1-35

DISCUSSION

In theory, more information is contained in the complete channel set. Reducing the number of channels corresponds to a reduced model complexity and less free parameters and effectively regularizes the learning problem, which can be a beneficial strategy for smaller data sets. In accordance with this reduced complexity, the LLP was able to learn the essential characteristics in our simulations much faster with reduced channel sets. The best performance could be achieved with 10 channels. While this is an expected outcome, it is interesting that LLP could not reach a superior performance for the full channel set despite the full amount of data provided. To explain this, one hypothesis is that even when a lot of data is available, a reduced number of channels, which are highly correlated to the control task, could facilitate the learning of LLP in comparison to using more channels which are potentially polluted by task-irrelevant features, including noise. The alternative hypothesis is that our experiment has just not delivered a sufficient amount of data in order to make the 31 channel LLP outperform the smaller subsets. Looking at the results from the supervised classification, one can see a similar behaviour in the early stage, but the configuration with 31 channels quickly rises to the top.

The similarity of the behaviour is in accordance with our theoretical considerations in [6], where we introduced the term *noise amplification factor* (NAF). It measures how much more data is necessary for LLP to reach the same accuracy in the class mean estimation compared to the supervised case. This NAF metric depends on the target and non-target ratios of each sequence and can be influenced by designing the experimental paradigm. For the sequences used in this data-set, the NAF was around 20. We observe that – with growing data – the unsupervised LLP behaves like a slowed-down supervised method. This is expressed by a qualitatively similar behaviour of the curves, as they display the same order of intersection points in Figures 3 and 5 with growing data set sizes. Observing this similarity in the behaviour of the LLP and the supervised methods supports the second hypothesis that the LLP configuration with 31 channels will eventually outperform the smaller channel sets when a sufficient amount of data is available.

We cannot directly observe a slowing factor of 20, which would correspond to the NAF. One of the causes is that the performance of these classifiers is not only dependent on the quality of the estimated class means, but also on the quality of the estimated covariance matrix.

Realizing the slow ramp-up behaviour of LLP with large channel sets, a possible mitigation strategy is to start with a low number of channels and incrementally increase the number of channels and features over time. A similar approach was already proposed for motor imagery data classification [15, 16]. By developing new adaptive feature selection methods, other unsupervised methods, e.g. the MIX method [17], which is the combination of LLP and an expectation-maximization algorithm, could also benefit.

CONCLUSION

By re-analysing data from 13 subjects performing a copy-spelling task, we showed that the unsupervised LLP classifier can be significantly improved by simply reducing the number of utilized features. Interestingly, this is not only the case during the initial ramp-up, but even during a later stage of the experiment when more data is available. In contrast, a supervised classifier only benefits from a reduction of features in the early stage. This behaviour of the unsupervised LLP method can be understood by considering it as a slowed-down version of the supervised algorithm with the same guaranteed convergence. Future work will go towards the development of adaptive feature selection method for unsupervised classifiers utilizing the observations made in this paper.

ACKNOWLEDGEMENTS

DH and MT gratefully acknowledge the support by BrainLinks-BrainTools Cluster of Excellence funded by the German Research Foundation (DFG), grant number EXC 1086. PJK thanks for the support from the European Union's Horizon 2020 research and innovation programme under the Marie Sklodowska-Curie grant agreement NO 657679. TV gratefully acknowledges the support by the special research fund (BOF) from Ghent University. The authors also acknowledge support by the state of Baden-Württemberg through bwHPCand the German Research Foundation (DFG) through grant no INST 39/963-1 FUGG.

REFERENCES

[1] Lu S, Guan C, and Zhang H. Unsupervised brain computer interface based on intersubject information and online adaptation. *IEEE Transactions on Neural Systems and Rehabilitation Engineering*, 17(2):135–145, 2009.

[2] Fazli S, Popescu F, Danóczy M, Blankertz B, Müller K-R, and Grozea C. Subject-independent mental state classification in single trials. *Neural networks: The Official Journal of the International Neural Network Society*, 22(9):1305–1312, Jun 2009.

[3] Jayaram V, Alamgir M, Altun Y, Schölkopf B, and Grosse-Wentrup M. Transfer learning in brain-

Published by Verlag der TU Graz
Graz University of Technology

 DOI: 10.3217/978-3-85125-533-1-35

computer interfaces. *IEEE Computational Intelligence Magazine*, 11(1):20–31, 2016.

[4] Vidaurre C, Kawanabe M, von Bünau P, Blankertz B, and Müller K-R. Toward unsupervised adaptation of LDA for brain–computer interfaces. *IEEE Transactions on Biomedical Engineering*, 58(3):587–597, 2011.

[5] Kindermans P-J, Verstraeten D, and Schrauwen B. A bayesian model for exploiting application constraints to enable unsupervised training of a P300-based BCI. *PLOS ONE*, 7(4):e33758, 2012.

[6] Hübner D, Verhoeven T, Schmid K, Müller K-R, Tangermann M, and Kindermans P-J. Learning from label proportions in brain-computer interfaces: online unsupervised learning with guarantees. *PLOS ONE*, 12(4):e0175856, 2017.

[7] Quadrianto N, Smola A J, Caetano T S, and Le Q V. Estimating labels from label proportions. *Journal of Machine Learning Research*, 10(Oct):2349–2374, 2009.

[8] Gonsalvez C-J and Polich J. P300 amplitude is determined by target-to-target interval. *Psychophysiology*, 39(3):388–396, 2002.

[9] Verhoeven T, Buteneers P, Wiersema J, Dambre J, and Kindermans P-J. Towards a symbiotic brain–computer interface: exploring the application–decoder interaction. *Journal of Neural Engineering*, 12(6):066027, 2015.

[10] Blankertz B, Lemm S, Treder M, Haufe S, and Müller K-R. Single-trial analysis and classification of ERP components, a tutorial. *NeuroImage*, 56(2):814 – 825, 2011.

[11] Lotte F, Congedo M, Lécuyer A, Lamarche F, and Arnaldi B. A review of classification algorithms for EEG-based brain–computer interfaces. *Journal of Neural Engineering*, 4(2):R1, 2007.

[12] Bishop C. M. Pattern recognition. *Machine Learning*, 128:1–58, 2006.

[13] Tangermann M, Schreuder M, Dähne S, Höhne J, Regler S, Ramsay A, Quek M, Williamson J, and Murray-Smith R. Optimized stimulation events for a visual ERP BCI. *Int. J. Bioelectromagn*, 13(3):119–120, 2011.

[14] Schröder M, Lal T. N, Hinterberger T, Bogdan M, Hill N J, Birbaumer N, Rosenstiel W, and Schölkopf B. Robust EEG channel selection across subjects for brain computer interfaces. *Eurasip Journal of Applied Signal Processing*, 19:3103–3112, 2005.

[15] Vidaurre C and Blankertz B. Towards a cure for BCI illiteracy. *Brain Topography*, 23(2):194–198, 2010.

[16] Sannelli C, Vidaurre C, Müller K-R, and Blankertz B. CSP patches: an ensemble of optimized spatial filters. an evaluation study. *Journal of Neural Engineering*, 8(2):025012, 2011.

[17] Verhoeven T, Hübner D, Tangermann M, Müller K-R, Dambre J, and Kindermans P-J. Improving zero-training brain-computer interfaces by mixing model estimators. *Journal of Neural Engineering*, 14(3):036021, 2017.

Published by Verlag der TU Graz
Graz University of Technology

Proceedings of the
7th Graz Brain-Computer Interface Conference 2017 DOI: 10.3217/978-3-85125-533-1-36

CHALLENGING THE ASSUMPTION THAT AUDITORY EVENT-RELATED POTENTIALS ARE INDEPENDENT AND IDENTICALLY DISTRIBUTED

D. Hübner, M. Tangermann

University of Freiburg, Dept. Computer Science,
Excellence Cluster BrainLinks-BrainTools, Freiburg, Germany

E-mail: david.huebner@blbt.uni-freiburg.de

ABSTRACT: The majority of brain-computer interface classifiers assumes that repeated events elicit brain potential responses which follow the same class-wise distributions. A few adaptive classifiers can deal with violations of this assumption and compensate for non-stationarities occurring on time scales of minutes to hours. This work reports on non-stationarities observed on much shorter time scales. An electroencephalogram study was conducted with elderly subjects ($N = 20$) using an auditory event-related potential paradigm with bisyllabic words as stimuli and a stimulus onset asynchrony of 250 ms. The collected data reveals three effects within a single sequence of 90 stimuli: (1) habituation: the duration of the ongoing sequence negatively correlates with the P300 amplitude, (2) outliers: stimuli at the start and end of each sequence have a special structure, and (3) order effects: longer target-to-target intervals lead to higher P300 amplitudes. Observing that the performance of linear discriminant analysis, a widely used classifier, suffers from these effects, we propose several mitigation strategies.

INTRODUCTION

The centrepiece of a Brain-Computer Interface (BCI) is the decoder which translates brain signals into meaningful control commands, e.g., to spell text without using muscular pathways [1]. One of the most widely used brain signal features in the electroencephalogram (EEG) are so-called *event-related potentials* (ERPs), transient potential responses elicited by events such as visual or auditory stimuli. In a ERP-based BCI, the decoder is deciding for each stimulus whether it was attended (*target stimulus*) or not (*non-target stimulus*). Generally, this is achieved by training a classification model on calibration data under the assumption of stationarity, i.e. that both, the (labelled) calibration data and any data recorded during online use share the same distribution. For instance, in ERPs, a common assumption is that both classes – targets and non-targets – are multivariate Gaussian distributions which share the same covariance [2].

Even though it is well-known that the distribution of brain signal features can change over the course of a session [3–5] or between calibration phase of a BCI and its online use [5, 6], many classifiers assume that all data points are independent and identically distributed (IID) [2]. Adaptive classifiers exist which can continuously adapt to changing distributions and may not even require label information [3, 7]. However, this adaptation of classifiers typically happens on time scales of minutes to hours. For shorter time scales, adaptive approaches are not feasible if they require the tracking of distributions in order to achieve the adaptive behaviour. In this work, we focus on non-stationarities and violations of the independence assumption in the data distribution, which take place on very short time scales. We systematically analyse (1) the effect of habituation, (2) effects of stimuli at the beginning and the end of a stimulation sequence and (3) order effects, specifically the influence of target-to-target distances. All of them are investigated within the time frame of a single sequence of 90 stimuli, which typically lasts only a few seconds in ERP-BCI paradigms. While these three aspects have been reported in the literature, existing studies either lack a connection to BCIs, have used very long interstimulus durations or have covered only a single aspect of the overall problem [8–14].

The *habituation* effect describes how the repeated presentation of a stimulus affects the ERP response. In two studies [8, 9], Polich and colleagues have studied the habituation of the P300 amplitude in an auditory oddball task – which is to discriminate a high tone from a low tone – with a relatively long stimulus onset asynchrony (SOA) of 1.2 s and 2 s, respectively, which clearly are beyond the fast SOA values utilized in current ERP-BCI paradigms. In the first study [8] it was found that the P300 amplitude decreased only slightly over repeated stimulus presentations, and it was reported to remain constant in the second study [9]. For another oddball study by Murphy and colleagues (SOA=1.2 s−1.6 s) a decrease in amplitude was reported as long as the length of each stimulus sequence was unpredictable for the subjects [10].

The second aspect of our study is the response to stimuli which are located at the beginning and end of

Published by Verlag der TU Graz
Graz University of Technology

 DOI: 10.3217/978-3-85125-533-1-36

each sequence. From the literature, it is known that brain responses to novelty (P3a ERP component) are different from responses to infrequent, task-relevant stimuli (P3b) in latency, peak position and peak amplitude [11]. We suspected to see outlier responses in the form of P3a ERP components at the beginning and end of the stimulus sequence while observing a P3b within the running sequence.

Third and lastly, we focused on how the target-to-target interval (TTI) influences the brain responses. The TTI is defined as the time between the onset of the current and of the preceding target stimulus. Based on the literature, we assumed that longer TTI values yield stronger P300 responses (see [12] for a review). In addition, it has been reported that longer TTIs yield higher amplitudes of the early negativity (with a latency of approx. 150 ms post stimulus onset) in an auditory oddball task with TTI values ranging from 1 to 16 s [13], which is again beyond the TTI range used in current BCI paradigms. Specifically, the first target was found to have a much higher P300 amplitude [14]. Taken together, a confirmation of these three effects in the context of realistic BCI stimulus conditions would clearly violate the assumption that each stimulus elicits an independent and identically distributed brain response and would leave room for improving the classification approach in BCI. So far, only a few attempts have been undertaken to realize this improvement. Citi and colleagues suggested a weighting of the classifier outputs depending on their TTI [12]. A contribution by Martens et al. suggested training one classifier for each TTI [15]. However, both of these studies only focused on TTI, neglecting the other two effects.

The goal of this work is to conduct a comprehensive analysis of violations of the IID assumption under realistic SOA conditions (250 ms) and by using bisyllabic words as stimuli which are more complex and realistic compared to traditional oddball tones. The results are discussed in the context of BCI classifiers for which we will propose possible enhancement strategies.

MATERIALS AND METHODS

An EEG study with $N = 20$ normal hearing subjects (10 female, mean age 60.20 yrs, SD 8.04 yrs) was conducted. It was approved by the Ethics Committee of the University Medical Center Freiburg, and subjects expressed written informed consent prior to participation. EEG signals from 63 passive Ag/AgCl electrodes (EasyCap) were recorded, which were placed approximately equidistantly according to the extended 10–20 system. Impedances were kept below 20 kΩ, and channels were referenced against the nose. The signals were registered by multichannel EEG amplifiers (BrainAmp DC, Brain Products) at a sampling rate of 1 kHz.

Subjects were seated within a ring of 6 loudspeakers (AMUSE paradigm, [16]). Six bisyllabic German words (Drucker, Flasche, Glocke, Knöpfe, Stempel, Trichter; length=300 ms) were chosen as stimuli by the following constraints: Words should have similiar frequency in the German language, should be unambiguous and represent objects which can be depicted. They were played with a 1:1 relation between words and loudspeakers and had an SOA of 250 ms. We define a *trial* as a series of 90 word stimuli. In total, 36 trials were recorded per subject, each consisting of 15 target- and 75 non-target stimuli. The target word/direction was cued at the start of each trial and changed between trials. Within each trail, we grouped 6 consecutive stimuli as one *iteration*, yielding 15 iterations per trial. A target occurred once per iteration. The exact sequences were pseudo-randomized over iterations such that between 2 and 10 non-target stimuli appeared between two targets. The complete stimulus sequence of a single trial took $90 \cdot 0.25\,s = 22.5\,s$ to play.

Data was analysed offline. A third order bidirectional Chebyshev Type II bandpass filter between 0.5 and 12 Hz was applied and data was downsampled to 100 Hz. Eye artefacts were projected out using bipolar EOG recordings [17]. We extracted signal epochs from $[-250, 1000]$ ms relative to each stimulus onset. They were corrected for baseline drifts observed in the interval $[-250, 0]$ ms. Epochs in which the difference between maximum and minimum exceeded 60 μV were treated as outliers and excluded from further analysis. In total, 9.41% of target epochs and 9.03% of non-target epochs were excluded.

Classification was performed using a shrinkage-regularized linear discriminant analysis (*shrinkage-LDA*), a commonly used classification model for ERP signals in BCI [2]. For all 63 channels and 9 intervals per channel located between 100 ms and 1000 ms post stimulus, the average amplitude was computed and used as features for classification, resulting in a 567-dimensional feature vector per epoch.

RESULTS

Overall, the observed ERP responses revealed three kinds of violations of the IID assumption within the course of a single trial (90 stimuli).

First, *habituation* of the target P300 amplitude was observed over the trial duration of 22.5 s. On the grand average view (see Fig. 1) the habituation was expressed by a decreased target response in the central channel 'Cz' from 2.8 μV in the first iteration to only 0.8 μV in the second to last iteration. Fitting a

Published by Verlag der TU Graz
Graz University of Technology

 DOI: 10.3217/978-3-85125-533-1-36

linear regression model yielded a significant influence of the iteration number ($p = 2.28e-08, r = 0.31$):

$$\text{Amp} = 2.49\mu V - 0.17\mu V \cdot \text{Iteration\#}.$$

We chose 580 ms for the evaluation, as the maximum of the grand average target response was located at this latency. The value of the second to last iteration was reported, because ERP responses in the last iteration were subject to another effect which is described in the next paragraph.

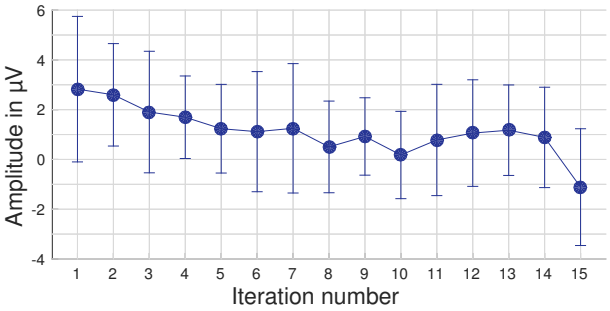

Fig. 1: **Grand average (N=20) target amplitude in Cz at 580 ms post stimulus as a function of the iteration number**. Error bars show the standard deviation across subjects.

This leads to the second type of observed non-stationary behaviour, expressed by the different responses to the first and last stimuli within a sequence. For both, the masking effect due to (missing) neighbouring stimuli is different from stimuli in the middle of a sequence. This effect is visualized via the observed grand average non-target ERP responses in Fig. 2. The top plot reveals strong amplitudes in frontal to central channels, which represent a P1-N2-P3a complex for the average first non-target ERP response. These responses are strongly reduced for stimuli played in the middle of the sequence as shown by depicting an average non-target response observed at the 45th position of sequences (middle plot). The response to the last non-target (bottom plot) shows relatively strong amplitudes after approx. 400 ms, which could indicate an ERP response upon the non-event of a missing 91st stimulus.

The third effect is the influence of the TTI onto the P300 amplitude. We could replicate results from the literature showing a decreased P300 amplitude with shorter distances between two targets, see Fig. 3. This is a clear violation of the independence assumption of target epochs and also shows that the distributions are not identical. The negative peak at around 200 ms was not affected systematically by the TTI. This is especially interesting, as this ERP component shows a class-discriminative amplitude difference between target and non-target stimuli in auditory paradigms [16, 18–20]. The P300 was practically non-existent for a TTI of 750 ms (brown line), which corresponds to exactly two non-target stimuli between target stimuli.

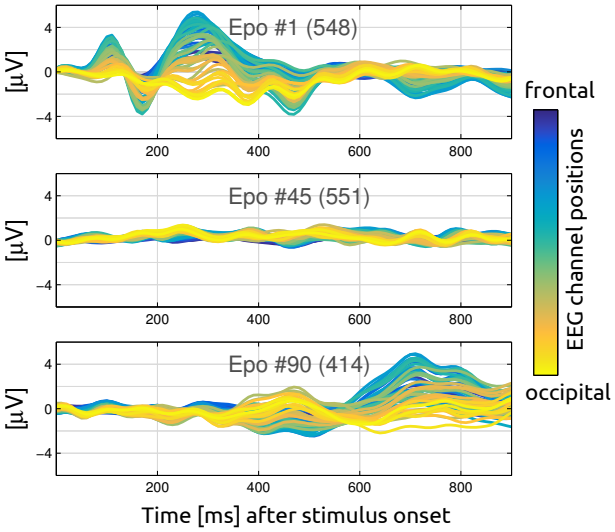

Fig. 2: **Grand average non-target ERP responses for epochs at the beginning (top), the middle (center) and the end of a stimulus sequence (bottom).** Each line depicts the ERP response of one EEG channel, with frontal to occipital channels coloured in blue to yellow. Numbers in parentheses correspond to the number of averaged epochs, with differences caused by artefact removal.

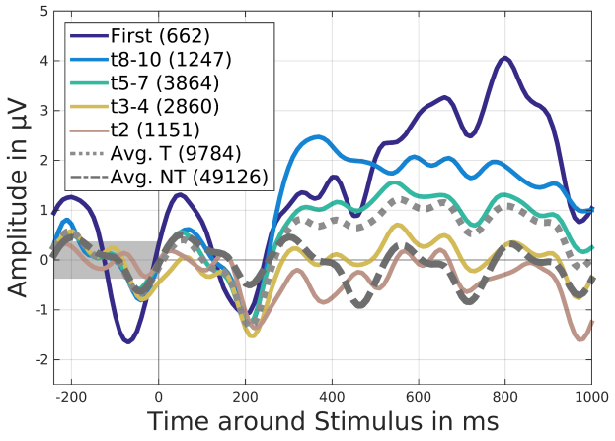

Fig. 3: **Grand average target amplitudes in channel Cz** sorted by the number of non-target stimuli appearing prior to the target stimulus, e.g., t5-7 indicates that since the last target stimulus a number of five to seven non-target stimuli had been played before the next target stimulus was presented. *First*: First epoch per trial, t: Number of preceding non-targets of each target. T and NT: average target and non-target responses over all possible TTIs. Numbers provided in parentheses indicate the number of averaged epochs.

The effect of the TTI upon the classifier has been described previously by Citi et al. [12] for a visual

Published by Verlag der TU Graz
Graz University of Technology

 DOI: 10.3217/978-3-85125-533-1-36

paradigm. We show how the two other effects, habituation and stimulus position, can affect the classifier performance as well. We chose to test a regularized LDA classifier [2], as a state-of-the-art classifier in BCI. The classifier was rescaled such that the mean target and non-target classifier outputs of the training data are mapped to $+1$ and -1. The classifier performance was estimated by 5-fold chronological crossvalidation, an approach in which the epochs are divided in 5 consecutive blocks, from which 4 blocks are always used for training and one for testing the classifier. Classifier outputs of all test epochs were sorted according to their positions within the sequence of 90 stimuli, averaged over all trials and subjects and plotted in Fig. 4.

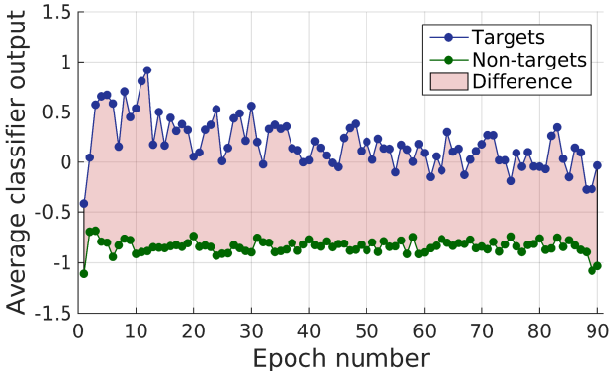

Fig. 4: **Grand average classifier outputs** for target- and non-target epochs plotted as a function of their position within a trial's sequence.

It can be observed, that the non-target classifier outputs for this unseen test data remain relatively stable around -0.85 over the trial, while the target outputs decrease over the duration of a trial's sequence. In addition, target epochs located at the first sequence position may appear as outliers, as their classifier outputs are similar to those of non-target epochs. These two effects show that the discriminatory power of the classifier suffers especially in the beginning and with the ongoing length of a trial.

DISCUSSION

We showed how the stimulus position within a sequence and the preceding stimuli can influence the ERP responses, and that these effects lead to systematic variations during a single sequence of 90 stimuli. Most findings were coherent with the literature. However, we observed no changes in the amplitude of the early negativity as a function of the TTI which was previously reported in [13]. We also found that habituation was more pronounced than previously reported in the literature. We observed a reduction in mean amplitude from 2.8 μV to 0.8 μV corresponding to a drop of 71 %. In contrast, Polich et al. [9] observed no difference in amplitude values for any ERP component as a function of the epoch number. In a second study by Polich [8], a significant decrease was found, however it was rather weak and concluded to be "more spurious than real". Concerning TTI, we observed almost a complete extinction of the P300 response for short TTIs. This is also surprising as an auditory oddball experiment by Höhne et al. [18] showed P300 components for SOA values as short as 125 ms.

We believe that three effects contribute to these observations: (1) Using words instead of simple tones can lead to delayed ERP responses [21], (2) the short SOA of 250 ms may reduce the amplitude of ERP responses [18] and (3) elderly subjects have been reported to show weaker and later P300 amplitudes [22] compared to many BCI offline studies performed with young subjects.

Not surprisingly, we found indications, that an LDA classifier, which assumes IID data points, is suffering from these effects. In the following, we propose different mitigation strategies to overcome these non-stationarities and improve current classifiers.

Adjusting the stimulus order

An easy-to-implement solution is to change the order of stimuli. Instead of allowing for a wide range of TTIs, it might be beneficial to limit them to a narrow range of possibilities, e.g., 4-7 non-targets between two targets in our paradigm. Following the observations of Tangermann et al. [23], it may not even be necessary to retain uncertainty in the sequence. To some extent, this concept is already implemented by the pseudo-randomization of the stimuli order, which at least avoids the subsequent highlighting of the same symbol in visual speller and is used by many groups [24–26].

Weighting individual epoch

Citi et al. proposed an approach in which classifier outputs of each epoch were weighted according to their TTI [12]. To select a target at the end of a trial, this approach should give a higher relevance to more informative epochs. This approach could also be used to deal with the special brain responses in the beginning and end of each trial, e.g., by reducing their influence. A downside of this approach is that it does not actually solve the underlying problem of the violation of the IID assumption, but rather fights the symptoms of bad classifier outputs for some epochs.

Training of sub-classifiers

In contrast, Martens and colleagues outlined an approach in which an individual classifier is trained for each TTI [15]. They showed that specifically those

Published by Verlag der TU Graz
Graz University of Technology

 DOI: 10.3217/978-3-85125-533-1-36

targets with small TTI can benefit. Considering a bias-variance trade-off, this approach will have a smaller bias, as the individual classifiers are able to capture the characteristics of the epoch-wise brain responses and their dependency on TTI more accurately. However, it will have a larger variance as fewer data points can be used to train each of these individual classifiers.

A similar idea was previously applied in another context by Höhne et al. [27], who observed that ERP responses vary for each of the individual stimuli due to different stimulus properties, e.g., length, pitch or loudness. They exploited this observation by creating individual LDA classifiers for each of the stimuli which give higher weight to the mean estimation of that specific stimuli and thus, reduce the influence of the other stimuli on the mean estimation. Their results show that this approach can improve performance in auditory ERP data and could be easily transferred to deal with habituation or TTI effects.

Adding additional features

The TTI and epoch number can be given as additional features to the classifier enabling it to learn dependencies on those parameters as well and thus, to partly overcome independence violations and non-stationarities in the data. However, one has to be careful whether the classifier model is suited for discrete features or not. Linear discriminant analysis (LDA), for example, assumes multivariate normally distributed features and may perform suboptimally with discrete features.

Data correction

To account for the observation that the first epochs are not influenced from preceding epochs and that they include a novelty P3a, one could add a template of an average non-target and remove a template of a P3a to those ERP responses. The templates could be learned based on data from the same or other subjects. A similar procedure may mitigate the problems observed for epochs at the end of a trial.

CONCLUSION

We showed three different effects – habituation, outlier effects of first and last stimuli, and effects based on the target-to-target interval – which influence the event-related potential responses within a single sequence of 90 stimuli. They clearly violate the assumption that brain responses to single stimuli are class-wise independent and identically distributed (IID). We showed how the decoding performance of a state-of-the-art classifier, regularized linear discriminant analysis, varies within a sequence of 90 stimuli as a result of this violation. To overcome this loss in discriminatory power, we proposed several mitigation strategies, partly by modifying the stimulus presentation and partly by changing the data processing and classification. The next step will be to implement and compare these strategies to ultimately enhance the decoding quality in ERP-based BCIs.

ACKNOWLEDGEMENTS

The authors gratefully acknowledge the support by BrainLinks-BrainTools Cluster of Excellence funded by the German Research Foundation (DFG), grant number EXC 1086 and by the state of Baden-Württemberg through bwHPC and the German Research Foundation (DFG) through grant no INST 39/963-1 FUGG. The authors would also like to thank Simone Denzer for her involvement in recording the data. We also thank the reviewer for their helpful feedback.

REFERENCES

[1] Farwell L A and Donchin E. Talking off the top of your head: toward a mental prosthesis utilizing event-related brain potentials. *Electroencephalography and Clinical Neurophysiology*, 70(6):510–523, 1988.

[2] Blankertz B, Lemm S, Treder M, Haufe S, and Müller K-R. Single-trial analysis and classification of ERP components, a tutorial. *NeuroImage*, 56(2):814 – 825, 2011.

[3] Vidaurre C, Kawanabe M, von Bünau P, Blankertz B, and Müller K-R. Toward unsupervised adaptation of LDA for brain–computer interfaces. *IEEE Transactions on Biomedical Engineering*, 58(3):587–597, 2011.

[4] Kindermans P-J, Schreuder M, Schrauwen B, Müller K-R, and Tangermann M. True zero-training brain-computer interfacing–an online study. *PLOS ONE*, 9(7):e102504, 2014.

[5] Shenoy P, Krauledat M, Blankertz B, Rao R P, and Müller K-R. Towards adaptive classification for BCI. *Journal of Neural Engineering*, 3(1):R13, 2006.

[6] Blankertz B, Dornhege G, Krauledat M, Müller K-R, and Curio G. The non-invasive Berlin brain–computer interface: fast acquisition of effective performance in untrained subjects. *NeuroImage*, 37(2):539–550, 2007.

Published by Verlag der TU Graz
Graz University of Technology

 DOI: 10.3217/978-3-85125-533-1-36

[7] Hübner D, Verhoeven T, Schmid K, Müller K-R, Tangermann M, and Kindermans P.-J. Learning from label proportions in brain-computer interfaces: online unsupervised learning with guarantees. *PLOS ONE*, 12(4):e0175856, 2017.

[8] Polich J. P300 development from auditory stimuli. *Psychophysiology*, 23(5):590–597, 1986.

[9] Polich J. Habituation of P300 from auditory stimuli. *Psychobiology*, 17(1):19–28, 1989.

[10] Murphy T I and Segalowitz S J. Eliminating the P300 rebound in short oddball paradigms. *International Journal of Psychophysiology*, 53(3):233–238, 2004.

[11] Polich J. Updating P300: an integrative theory of P3a and P3b. *Clinical Neurophysiology*, 118(10):2128–2148, 2007.

[12] Citi L, Poli R, and Cinel C. Documenting, modelling and exploiting P300 amplitude changes due to variable target delays in Donchin's speller. *Journal of Neural Engineering*, 7(5):056006, 2010.

[13] Gonsalvez C J, Barry R J, Rushby J A, and Polich J. Target-to-target interval, intensity, and P300 from an auditory single-stimulus task. *Psychophysiology*, 44(2):245–250, 2007.

[14] Ganin I, Shishkin S, Kochetova A, and Kaplan A Y. P300-based brain-computer interface: The effect of the stimulus position in a stimulus train. *Human Physiology*, 38(2):121–128, 2012.

[15] Martens S, Hill N, Farquhar J, and Schölkopf B. Impact of target-to-target interval on classification performance in the P300 speller. In *Applied Neuroscience Conference*, 2007.

[16] Schreuder M, Blankertz B, and Tangermann M. A new auditory multi-class brain-computer interface paradigm: spatial hearing as an informative cue. *PLOS ONE*, 5(4):e9813, 2010.

[17] Parra L C, Spence C D, Gerson A D, and Sajda P. Recipes for the linear analysis of EEG. *NeuroImage*, 28(2):326–341, 2005.

[18] Höhne J and Tangermann M. How stimulation speed affects event-related potentials and BCI performance. In *2012 Annual International Conference of the IEEE Engineering in Medicine and Biology Society*, pages 1802–1805. IEEE, 2012.

[19] Höhne J, Schreuder M, Blankertz B, and Tangermann M. A novel 9-class auditory ERP paradigm driving a predictive text entry system. *Frontiers in Neuroscience*, 5:99, 2011.

[20] Gao S, Wang Y, Gao X, and Hong B. Visual and auditory brain–computer interfaces. *IEEE Transactions on Biomedical Engineering*, 61(5):1436–1447, 2014.

[21] Tangermann M, Schnorr N, and Musso M. Towards aphasia rehabilitation with BCI. In *Proceedings of the 6th International Brain-Computer Interface Conference*, pages 65–68. Verlag der Technischen Universität Graz, 2014.

[22] van Dinteren R, Arns M, Jongsma M L, and Kessels R P. P300 development across the lifespan: a systematic review and meta-analysis. *PLOS ONE*, 9(2):e87347, 2014.

[23] Tangermann M, Höhne J, Stecher H, and Schreuder M. No surprise-fixed sequence event-related potentials for brain-computer interfaces. In *Engineering in Medicine and Biology Society (EMBC), 2012 Annual International Conference of the IEEE*, pages 2501–2504. IEEE, 2012.

[24] Townsend G, LaPallo B, Boulay C, Krusienski D, Frye G, Hauser C, Schwartz N, Vaughan T, Wolpaw J, and Sellers E. A novel P300-based brain–computer interface stimulus presentation paradigm: moving beyond rows and columns. *Clinical Neurophysiology*, 121(7):1109–1120, 2010.

[25] Tangermann M, Schreuder M, Dähne S, Höhne J, Regler S, Ramsay A, Quek M, Williamson J, and Murray-Smith R. Optimized stimulation events for a visual ERP BCI. *Int. J. Bioelectromagn*, 13(3):119–120, 2011.

[26] Verhoeven T, Buteneers P, Wiersema J, Dambre J, and Kindermans P-J. Towards a symbiotic brain–computer interface: exploring the application–decoder interaction. *Journal of Neural Engineering*, 12(6):066027, 2015.

[27] Höhne J, Blankertz B, Müller K-R, and Bartz D. Mean shrinkage improves the classification of ERP signals by exploiting additional label information. In *Pattern Recognition in Neuroimaging, 2014 International Workshop on Pattern Recognition in Neuroimaging*, pages 1–4. IEEE, 2014.

Published by Verlag der TU Graz
Graz University of Technology

Proceedings of the
7th Graz Brain-Computer Interface Conference 2017 DOI: 10.3217/978-3-85125-533-1-37

MIXING TWO UNSUPERVISED ESTIMATORS FOR EVENT-RELATED POTENTIAL DECODING: AN ONLINE EVALUATION

D. Hübner[1], T. Verhoeven[2], P.-J. Kindermans[3], M. Tangermann[1]

[1] Brain State Decoding Lab, Cluster of Excellence BrainLinks-BrainTools, Dept. of Computer Science, Albert-Ludwigs-University, Freiburg, Germany
[2] Electronics and Information Systems, Ghent University, Ghent, Belgium
[3] Machine Learning Group, Berlin Institute of Technology, Berlin, Germany

E-mail: david.huebner@blbt.uni-freiburg.de, michael.tangermann@blbt.uni-freiburg.de

ABSTRACT

An ideal decoder in brain-computer interfaces (BCIs) would not require any calibration period and instead start with the actual online application right away. While we cannot reach this goal yet, two novel unsupervised classification methods for BCIs based on event-related potentials (ERPs) of the electroencephalogram (EEG) have recently been proposed which do not require a calibration session. The first method estimates the projection weights of the classifier heuristically using an expectation-maximization approach, while the second utilizes slight changes of the ERP paradigm and deterministically learns from label proportions. As both unsupervised methods have pros and cons, we propose to combine their strengths in a novel MIX approach. Under realistic unlabelled conditions, we compare the online performances of the mixed and the two original methods, finding that for our data recorded during visual spelling with 6 subjects, the mixed approach reveals strong performance gains. Users got perfect selection accuracy after an average of only 2 minutes of online usage.

INTRODUCTION

In Brain-Computer Interfaces (BCI) based on event-related potentials (ERP), the user is presented with a predefined set of different control commands. For example in the original P300-speller [1], a BCI for spelling text, these options are symbols of the alphabet highlighted on a screen. The user is asked to focus on the symbol that he or she wants to spell. When this target symbol is highlighted, the brain of the user elicits a different brain response compared to the case when other non-target symbols are highlighted. The decoder in the BCI has the task to classify the recorded ERP responses as target or non-target and subsequently detect the desired symbol. In this way, the user can spell words symbol by symbol, solely by attending to the symbols on the screen.

To discriminate between target and non-target responses in the brain, machine learning (ML) techniques are often used [2, 3]. With ML, previously recorded ERPs are used by the classifier to learn how to discriminate between the two classes of responses. Newly recorded ERPs are then processed by this classifier to assign them to one of these classes. A common ML technique used in BCIs is linear discriminant analysis (LDA), which searches for a one-dimensional projection $\boldsymbol{x} \cdot \boldsymbol{w}$ of the ERP response signal features $\boldsymbol{x}$ in order to assign the target label t_+ to the response when $\boldsymbol{x} \cdot \boldsymbol{w} \geq 0$ and label t_- otherwise.

It was shown that ERP-BCI data follows a Gaussian distributed with class-wise means $\boldsymbol{\mu}_+$ and $\boldsymbol{\mu}_-$, and shared covariance matrix $\boldsymbol{\Sigma}_s$ [4]. Under this assumption, the optimal projection $\boldsymbol{w}^*$ in LDA can be computed as following [4]:

$$\boldsymbol{w}^* \quad = \boldsymbol{\Sigma}_s^{-1} \left(\boldsymbol{\mu}_+ - \boldsymbol{\mu}_- \right). \tag{1}$$

Training the classifier comes down to estimating the values of the class-wise mean responses $\boldsymbol{\mu}_+$, $\boldsymbol{\mu}_-$ and the shared covariance $\boldsymbol{\Sigma}_s$. In a traditional supervised scenario, labelled data would be collected during a calibration session on which these three quantities can directly be estimated by using the sample statistics. In unsupervised learning, no label information are present which makes it a more challenging learning problem.

It can be shown that if the means are estimated correctly, then replacing the shared covariance by the pooled covariance $\boldsymbol{\Sigma}$, i.e. the covariance computed on all data disregarding label information, leads to the same direction of the projection $\boldsymbol{w}$. This follows from the equivalence of least square regression with rescaled outputs and LDA [5]. No label information are needed to estimate the pooled covariance matrix.

In BCI systems, the data is usually high dimensional and the amount of data recorded during calibration is low. It was shown that this makes the estimation of the covariance matrix less accurate [4] This can be compensated for by introducing a regularization term to obtain the (shrinkage)-regularized covariance matrix $\boldsymbol{\Sigma}_R$

$$\boldsymbol{\Sigma}_R = (1 - \lambda)\boldsymbol{\Sigma} + \lambda \boldsymbol{I} \tag{2}$$

where $\boldsymbol{I}$ is the identity matrix and λ is the regularization parameter.

Published by Verlag der TU Graz
Graz University of Technology

 DOI: 10.3217/978-3-85125-533-1-37

The learning problem in the unsupervised case now boils down to estimating the class means $\boldsymbol{\mu}_+$ and $\boldsymbol{\mu}_-$ and the shrinkage parameter λ. Everything else can be computed without using label information.

To compute the class means, we recently proposed to combine two unsupervised methods [6]. The first method is an expectation-maximization (EM) algorithm which estimates the class means to maximize the likelihood of the recorded data [7]. It is a heuristic which relies on a good random initialisation to obtain accurate class estimates.

The second method is based on the learning from label proportions (LLP) concept [8]. In this approach, the train of stimuli is divided in two interleaved sequences with different proportions of targets and non-targets. The average response in these two sequences is calculated and used together with the known proportional composition, to set up two linear equations. The two unknowns are the class means. Solving the linear problem provides an estimate of these class means. We presented the application of the LLP method in BCI recently [9]. In contrast to the EM method, there is no variance in the result as there are no randomly initialized parameters in this method. Furthermore, the estimation of the mean ERP response is guaranteed to converge to the true solution as more data is recorded [9]. This convergence slowly leads to an increasing classification performance.

Two different options have been previously used to compute the regularization parameter λ. An analytical formula for λ has been presented by Ledoit and Wolf [10], see Blankertz et al. for an application in BCI [4]. Another approach directly optimized λ as part of the EM-algorithm [11].

The EM-means and LLP method for unsupervised ERP classification clearly show complementary strengths and weaknesses [6]. We proposed to exploit the different strengths by combining their individual mean estimations in a data-driven fashion. This resulted in a third method which we call MIX. We previously evaluated this approach by comparing LLP, EM and MIX by simulating an online experiment on existing visual ERP data [6]. In this previous study all three classifier used the analytic formula by Ledoit and Wolf for computing λ. To have comparable results to the original EM-method, we used the direct regularization of the EM-method in this current study, while both other methods use the analytic formula to find regularization parameter λ. The following table shows an overview of the three different methods used in this paper.

Table 1: Overview of classification methods

Method	Mean estimation	λ estimation
LLP	Using known proportions	Ledoit&Wolf
EM	Maximizing data likelihood	Direct (EM)
MIX	Combining LLP and EM	Ledoit&Wolf

Previous simulations showed that the MIX method significantly outperformed both other methods [6]. However, as simulation on previously recorded data are possibly prone to overfitting, this work presents the first online evaluation of the MIX method with 6 subjects and its comparison with the LLP and EM algorithm. The goal of this work is to compare the three methods under equal conditions on unlabelled and unseen data. With this comparison, we hope to contribute further to the integration of unsupervised classification methods in calibrationless BCIs and as such to improve the usability of these systems.

MATERIALS AND METHODS

The MIX model

In the MIX method, the estimation of the class-wise means is proposed as a mixing of the estimation found with the LLP and EM method:

$$\hat{\boldsymbol{\mu}}(\gamma) = (1-\gamma)\hat{\boldsymbol{\mu}}_{EM} + \gamma\hat{\boldsymbol{\mu}}_{LLP} \tag{3}$$

where $\hat{\boldsymbol{\mu}}$ denotes the new estimator of the mean target or non-target response, $\hat{\boldsymbol{\mu}}_{EM}$ and $\hat{\boldsymbol{\mu}}_{LLP}$ denote existing estimators and $\gamma \in [0, 1]$ is the mixing coefficient, indicating the weight given to each estimator. See our previous work about LLP [9] and the EM-algorithm [7] for more details about these two unsupervised classification methods.

To minimize the expected mean squared error between the estimator value $\hat{\boldsymbol{\mu}}$ and the unknown true parameter value $\boldsymbol{\mu}$, we proposed an analytical solution for the mixing coefficient γ^* [6]:

$$\gamma^* = \frac{1}{2}\left(\frac{\sum_d Var\left[\hat{\boldsymbol{\mu}}_{EM,d}\right] - \sum_d Var\left[\hat{\boldsymbol{\mu}}_{LLP,d}\right]}{\|\hat{\boldsymbol{\mu}}_{EM} - \hat{\boldsymbol{\mu}}_{LLP}\|^2} + 1\right) \tag{4}$$

Here, $Var\left[\hat{\boldsymbol{\mu}}_{(\cdot),d}\right]$ denotes the variance on the estimation of the d$^{\text{th}}$ entry of the estimated mean $\hat{\boldsymbol{\mu}}$. This variance is a measure for the uncertainty on the estimated value. The higher the uncertainty on the output of the EM method, the higher the weight given to the output of the LLP method in the MIX method and vice versa.

Implementation

In practice, the original EM algorithm and the one used in the mean estimation of the MIX method are different in terms of the number of parallel initialisations. It is known that the EM-algorithm requires a good random initialisation and therefore, it profits from many parallel initialisations. A number of 5 was used before in the EM algorithm [11]. In contrast, the MIX method in our previous paper only used 1 initialisation of the EM algorithm [6]. We keep these values to make the results comparable.

Published by Verlag der TU Graz
Graz University of Technology

 DOI: 10.3217/978-3-85125-533-1-37

Experiment

Six healthy subjects (3 female, aged 22-31) performed a visual copy-spelling task. The EEG study was approved by the Ethics Committee of the University Medical Center Freiburg and the subjects gave informed written consent prior to the beginning of the session. They were compensated with 8 Euros per hour. The experiment was almost identical with the one described in [9]. A short overview is provided here. Each subject was asked to spell the 35 characters: "FRANZY JAGT IM TAXI DURCH DAS " three times. Each time, a different classifier (MIX, LLP, or EM) was trained from scratch such that each subject used each classifier exactly once. With 6 subjects, each possible order of the three different classifiers was used once to reduce order effects, see Fig. 1 for a schematic overview.

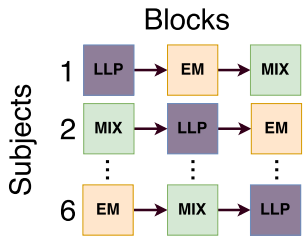

Figure 1: **Experimental structure.** Each subject performed three copy-spelling blocks with each of the three classifiers in varying order. Each block consisted of 35 characters.

The classifiers were retrained after each character utilizing the complete data set up to that point. Label information were not used for the training of the classifiers at any point in time, they were solely used to assess the performance. To spell one character, a train of 68 highlighting events with a stimulus onset asynchrony (SOA) of 250 ms was presented. An example of a highlighting event is shown in Fig. 2. Classifier outputs for each highlighting event and symbol were summed up and the symbol with the highest sum was selected and shown to the user.

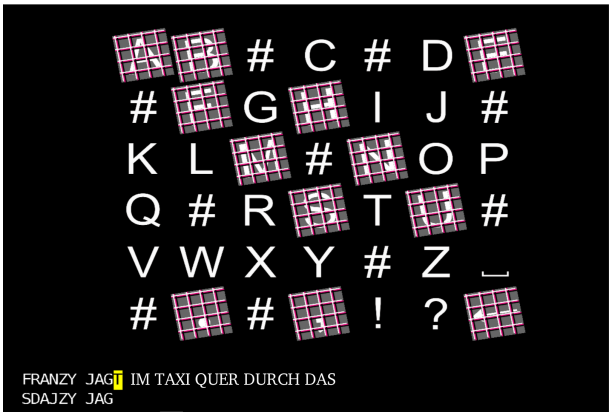

Figure 2: **Spelling Interface.** The '#' symbols serve as visual blanks, meaning that they are always non-targets, and are part of the LLP decoding strategy.

EEG and Feature Extraction

EEG signals from 31 passive Ag/AgCl electrodes (EasyCap) were recorded, which were placed approximately equidistantly according to the extended 10–20 system, and whose impedances were kept below 20 kΩ. All channels were referenced to the nose. The signals were registered by multichannel EEG amplifiers (BrainAmp DC, Brain Products) at a sampling rate of 1 kHz. The data was then bandpass filtered between 0.5 and 8 Hz and downsampled to 100 Hz. Epochs were windowed to [-200, 700] ms relative to the stimulus onset and corrected for baseline shifts observed in the interval [-200, 0] ms. Per channel, the mean amplitudes of six intervals ([50, 120], [121, 200], [201, 280], [281, 380], [381, 530] and [531, 700] ms) were finally computed as features. This resulted in a total of $6 \cdot 31 = 186$ features.

Performance estimations

Two performance metrics were used to evaluate the performance of the three different classifier during the online experiment. First, we looked at how well single targets could be discriminated from non-targets. This was assessed in terms of area under the curve (AUC) as a threshold-independent robust performance measure. The AUC values can range between 0 and 1, with a theoretical chance level of 0.5. An AUC value of 1 indicates perfect separation between the two classes, i.e. the classifier can correctly tell for each single stimulus whether it was attended or not. To compute this score during the online experiment, the unsupervised classifiers were retrained after each character and applied to the complete previous data up to the current point of the experiment. The given label information were then used to compute the AUC. Please note that overfitting is not a problem in this context, because the classifiers do not use the label information for training.

Second, we looked at the selection accuracy, i.e. to which percentage a user could spell the intended characters. To obtain more robust estimates, this metric was evaluated on sub-blocks of 5 trials, i.e. on characters 1-5, on characters 6-10, and so on.

In addition, we performed an offline analysis after the experiment to assess the overall quality of the data and to judge whether there is an interaction between classification method and classification performance. This was done by training and testing a supervised shrinkage-LDA classifier [4] in a 5-fold chronological cross-validation. This is the same classification method as described before – only that all quantities are estimated with the (supervised) sample statistics. The offline analysis was done individually for each subject and block.

RESULTS

First, we assessed the quality of the data of the online re-

Published by Verlag der TU Graz
Graz University of Technology

 DOI: 10.3217/978-3-85125-533-1-37

cordings by looking at the grand average ERP response shown in Fig. 3. A strong early negativity with a peak around 160 ms in the occipital area is observable in target responses while the non-targets only have a very weak rhythmic response. Furthermore, a central positivity exists for targets, which is however smaller in amplitude and more washed out than the early negativity. The strongest class discriminant information comes from the early visual component. This is in accordance with earlier studies using the same highlighting scheme [9, 12].

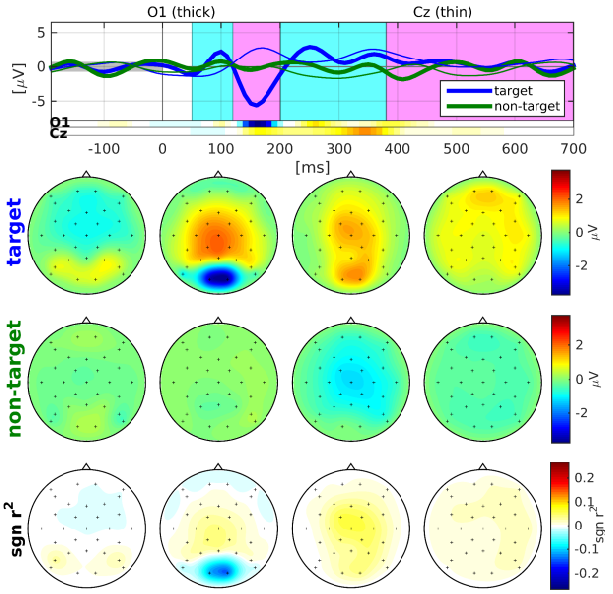

Figure 3: **Grand average (N=6) ERP plot. Top row**: Average responses evoked by visual target (blue) and non-target (green) stimuli in the occipital channel O1 (thick) and the central channel Cz (thin). The signed r^2 values for channels O1 and Cz over time are provided by two horizontal colour bars with the same scale as in bottom row scalp plot. **Middle rows**: Scalp plots visualising the spatial distribution of mean target and non-target responses within four selected time intervals marked by blue/pink shading. **Bottom row**: Scalp plots with signed r^2 values indicate spatial areas with high class-discriminative information.

Classifier influence on the data quality

To quantify the quality of the ERP responses and judge whether there is an interaction between classification method and performance, a supervised classifier was applied in an offline analysis after the experiment. The resulting target vs. non-target AUC performances were sorted according to the classifier used in each block and are shown in Fig. 4. One can see that the quality of the data is very high with all subjects having an AUC above 95 %. This is most likely due to the high saliency of the optimized stimuli [12]. In addition, a paired t-test between the supervised classification values of the three methods showed no significant differences. Hence, we cannot reject the null hypothesis that there is no interaction between classifier and performance. This means that we observed no effect of the feedback on the user performance probably due to the small sample size. Other studies did observe this effect [13, 14].

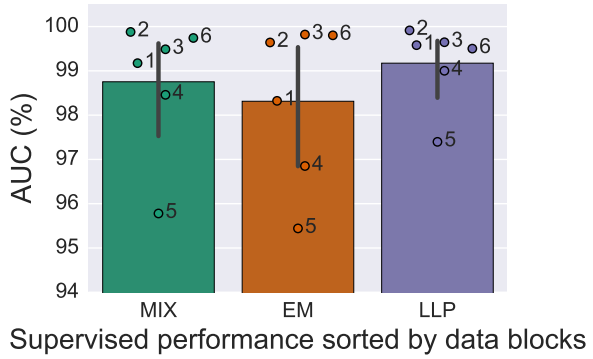

Figure 4: **Supervised offline cross-validation performance sorted by the classification method used per data block.** Bars show the mean ± std of the supervised performances for each sentence sorted according to the decoding method. Individual dots and numbers indicate the subject numbers. MIX = Mixing method, EM = Expectation-maximization, LLP = Learning from label proportions.

Next, we compared the performance of the three different classifiers in the online experiment. Fig. 5 shows the average and individual AUC performances for all subjects over time. While LLP starts at relatively high level and slowly improves over time, the EM algorithm behaves dichotomous: depending on its initialisation, it can either achieve a very high performance early on or it can fail to improve over a prolonged time period. The MIX method combines the strengths of both decoders by starting on a relatively high level and quickly finding a very good projection with almost perfect decoding performance by utilizing the complementary information of the LLP.

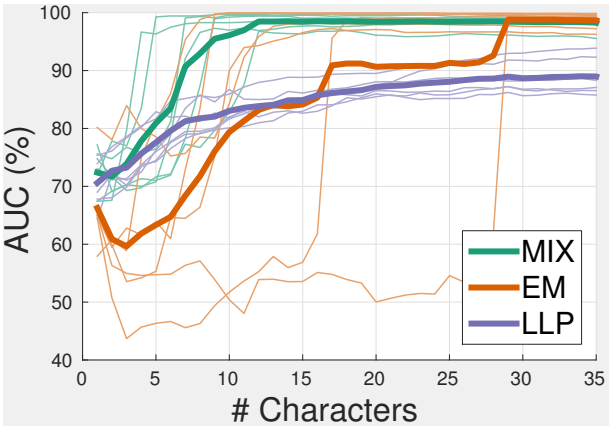

Figure 5: **Online decoding performance over time.** The y-axis shows the AUC of separating target from non-target epochs for each decoder. Thick line depicts the average performance while thin lines show results for each individual subject.

Published by Verlag der TU Graz
Graz University of Technology

 DOI: 10.3217/978-3-85125-533-1-37

Another way of looking at the decoding performance is by considering the number of correct character selections. One can see in Fig. 6 that the MIX method slightly outperforms the LLP and that both these methods outperform the EM-method by a big margin. This is due to the two sentences in which the EM-algorithm found the right projection only relatively late, see again Fig. 5.

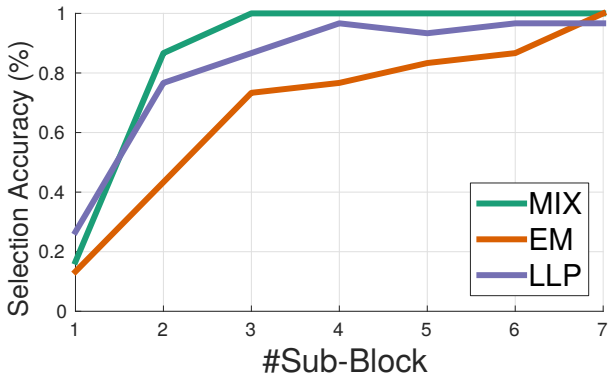

Figure 6: **Online character selection accuracy for each decoder.** The y-axis shows the percentage of correctly classified characters for sub-blocks of 5 characters each.

When looking at the correctly and incorrectly spelled characters of all three methods for each subject in Fig. 7, similar results are visible. After a short learning phase of 2-8 characters corresponding to an average of around 2 minutes of training time, users gain perfect control with the MIX method. Depending on the initialisation, the user can get very good control with the EM-algorithm at an earlier or later stage of the experiment. The LLP determines many characters correctly already after a few trials, but fails to display a very high reliability in the later stage.

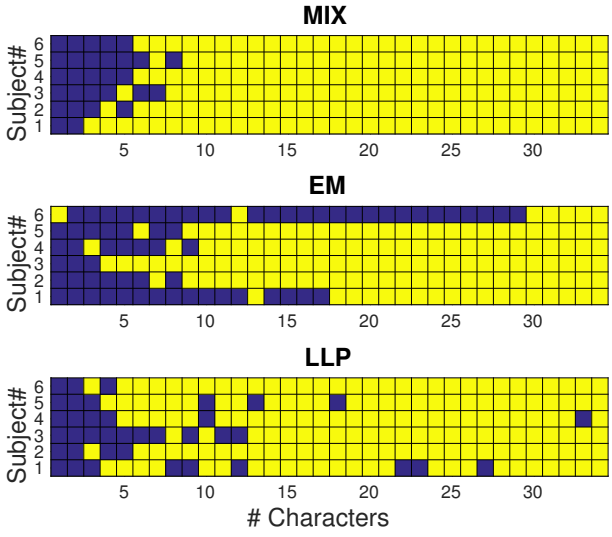

Figure 7: **Correctly (yellow) and incorrectly (blue) spelled characters of all three methods in the online experiment.**

DISCUSSION

The goal of this study was to show that the unsupervised MIX method can work in an online scenario and compare it to the EM and LLP method. We found that the MIX method could quickly and reliably decode the users' intention for all 6 subjects clearly outperforming both other methods. Remarkably, we observed almost perfect single epoch classification accuracy, meaning that the classifier could assign almost each highlighting event correctly as being attended or not. Here, the unsupervised classifier also profited from the very salient highlighting scheme.

On the other hand, spelling speed was not the focus of this work. Indeed, it was rather low with around 2.4 characters per minute after the initial training phase. This is due the high and constant number of 68 epochs per trial and long SOA of 250 ms. A moderate single epoch classification accuracy is already sufficient to correctly decode most characters with 68 highlighting events per characters. Hence, the additional performance in the MIX method is only slightly rewarded in terms of spelling speed or accuracy in this set-up. However, it could easily be boosted by implementing dynamic stopping [15], where the classifier stops a trial when he reaches a predefined certainty threshold.

Results from the online study showed that an average of around 2 minutes of online training time is sufficient to obtain perfect control over the BCI with the MIX method. Remarkably, this result was achieved without prior calibration or transfer learning. And even the data from the initial training phase can be corrected, when a more advanced classifier from a later stage of the experiment is re-applied to the initial data. In this way, initial mistakes due to limited data can be post-hoc corrected in unsupervised classifiers [11]. Hence, a potential user could directly start spelling with this MIX method when trusting the re-analysis.

CONCLUSION

The online ERP study showed that the MIX method is combining the strength of the probabilistic EM algorithm and the deterministic LLP approach. This opens the door for short ramp-up times combined with a very high reliability. Further desirable properties like the lack of calibration phase, the continuous learning, the guaranteed convergence and the possible post-hoc analysis, make this method an attractive alternative to traditional supervised methods. Future work will go towards increasing the usability of the system by increasing the information transfer per time. This can be achieved by implementing an SOA reduction, dynamic stopping, transfer learning, adaptive channel selection and using language models.

Published by Verlag der TU Graz
Graz University of Technology

 DOI: 10.3217/978-3-85125-533-1-37

ACKNOWLEDGEMENT

DH and MT gratefully acknowledge the support by BrainLinks-BrainTools Cluster of Excellence funded by the German Research Foundation (DFG), grant number EXC 1086. PJK has received funding from the European Union's Horizon 2020 research and innovation programme under the Marie Sklodowska-Curie grant agreement NO 657679. TV is supported by the special research fund (BOF) from Ghent University.

REFERENCES

[1] Farwell L. A and Donchin E. Talking off the top of your head: toward a mental prosthesis utilizing event-related brain potentials. *Electroencephalography and Clinical Neurophysiology*, 70(6):510–523, 1988.

[2] Lotte F, Congedo M, Lécuyer A, Lamarche F, and Arnaldi B. A review of classification algorithms for EEG-based brain–computer interfaces. *Journal of Neural Engineering*, 4(2):R1, 2007.

[3] Müller K-R, Tangermann M, Dornhege G, Krauledat M, Curio G, and Blankertz B. Machine learning for real-time single-trial EEG-analysis: from brain–computer interfacing to mental state monitoring. *Journal of Neuroscience Methods*, 167(1):82–90, 2008.

[4] Blankertz B, Lemm S, Treder M, Haufe S, and Müller K-R. Single-trial analysis and classification of ERP components, a tutorial. *NeuroImage*, 56(2):814 – 825, 2011.

[5] Bishop C. M. Pattern recognition. *Machine Learning*, 128:1–58, 2006.

[6] Verhoeven T, Hübner D, Tangermann M, Müller K-R, Dambre J, and Kindermans P.-J. Improving zero-training brain-computer interfaces by mixing model estimators. *Journal of Neural Engineering*, 14(3):036021, 2017.

[7] Kindermans P-J, Verstraeten D, and Schrauwen B. A bayesian model for exploiting application constraints to enable unsupervised training of a P300-based BCI. *PLOS ONE*, 7(4):e33758, 2012.

[8] Quadrianto N, Smola A. J, Caetano T. S., and Le Q. V. Estimating labels from label proportions. *Journal of Machine Learning Research*, 10(Oct):2349–2374, 2009.

[9] Hübner D, Verhoeven T, Schmid K, Müller K-R, Tangermann M, and Kindermans P.-J. Learning from label proportions in brain-computer interfaces: online unsupervised learning with guarantees. *PLOS ONE*, 12(4):e0175856, 2017.

[10] Ledoit O and Wolf M. A well-conditioned estimator for large-dimensional covariance matrices. *Journal of Multivariate Analysis*, 88(2):365–411, 2004.

[11] Kindermans P.-J, Schreuder M, Schrauwen B, Müller K-R, and Tangermann M. True zero-training brain-computer interfacing–an online study. *PLOS ONE*, 9(7):e102504, 2014.

[12] Tangermann M, Schreuder M, Dähne S, Höhne J, Regler S, Ramsay A, Quek M, Williamson J, and Murray-Smith R. Optimized stimulation events for a visual ERP BCI. *Int. J. Bioelectromagn*, 13(3):119–120, 2011.

[13] Lotte F, Larrue F, and Mühl C. Flaws in current human training protocols for spontaneous brain-computer interfaces: lessons learned from instructional design. *Frontiers in Human Neuroscience*, 2013.

[14] Barbero Á and Grosse-Wentrup M. Biased feedback in brain-computer interfaces. *Journal of NeuroEngineering and Rehabilitation*, 7(1):34, 2010.

[15] Schreuder M, Höhne J, Blankertz B, Haufe S, Dickhaus T, and Tangermann M. Optimizing event-related potential based brain–computer interfaces: a systematic evaluation of dynamic stopping methods. *Journal of Neural Engineering*, 10(3):036025, 2013.

Published by Verlag der TU Graz
Graz University of Technology

Proceedings of the
7th Graz Brain-Computer Interface Conference 2017 DOI: 10.3217/978-3-85125-533-1-38

PRELIMINARY RESULTS OF TESTING A BCI-CONTROLLED FES SYSTEM FOR POST-STROKE REHABILITATION

D.C. Irimia[1,3], M.S. Poboroniuc[3], R. Ortner[1], B.Z. Allison[2], C. Guger[1,2]

[1] g.tec Medical Engineering GmbH, Schiedlberg, Austria
[2] Guger Technologies OG, Graz, Austria
[3] "Gheorghe Asachi" Technical University of Iasi, Romania

E-mail: irimia@gtec.at

ABSTRACT: This work presents the recoveriX system, a hardware and software platform specially designed for stroke rehabilitation, as well as the preliminary results of testing it within clinical environment. Three patients with motor impairments due to stroke participated to the current study. In every session, the patients had to imagine 120 left and 120 right hand movements. The electroencephalogram (EEG) data was analyzed with Common Spatial Patterns (CSP) and linear discriminant analysis (LDA). The feedback was provided in form of an extending bar on the screen. During the trials where the correct imagination was classified, the FES was activated to move the corresponding hand. All patients were able to achieve high accuracies, even above 95% in at least one session, and all exhibited improvements in motor function. These first results showed that the stroke patients can control the motor-imagery BCI system with high accuracy and reflect the efficacy of combining movement imagination, the bar feedback and the real hand movements.

INTRODUCTION

Motor imagery-based brain-computer interface (BCI) have been used to assist people with motor disabilities since many years. The BCI systems extract commands in real-time, commands which can be used to control cursors or external devices like robots or neurostimulators. In the last few years, the control of functional electrical stimulation (FES) devices, termed as neurostimulators, became very interesting for post-stroke rehabilitation. A patient can use the movement imagery to induce real-time movements of specific limb segments.

In the last decade, a new field of application for motor imagery (MI) –based BCI proved to be of great interest. Many publications provide evidence that using MI-based BCIs can induce neural plasticity and thus serve as an important tool to enhance the rehabilitation outcome in stroke patients [1-4]. In here, MI is used to introduce closed-loop feedback within conventional motor rehabilitation therapy. This approach pairs each user's MI with stimulation and feedback, such as activation of a FES stimulator, avatar movement, and/or auditory feedback indicating successful task completion [5].

FES is a rapidly developing technology having the potential to restore the body motor functions. For example, FES has been used to restore hand grasp and release in people with tetraplegia [6] and standing and stepping in people with paraplegia [7]. The feasibility of integrating a non-invasive BCI system with a FES device eliciting foot dorsiflexion by means of surface electrode over the tibial anterior muscle has been investigated in [8]. Five healthy subjects performed 10 trials of idling and repetitive foot dorsiflexion to trigger BCI-FES controlled dorsiflexion of the contralateral foot. The epochs of BCI-FES controlled foot dorsiflexion were highly correlated with those of voluntary foot dorsiflexion (correlation coefficient between 0.59 and 0.77) with latencies ranging from 1.4 s to 3.1s. The classification of the mental states was based on a linear Bayesian classifier. Moreover, all subjects managed to achieve a 100% BCI-FES response (no omissions), and one subject had a single false alarm.

Daly et al. [9] tested a combined BCI and FES system on a patient presenting stroke-related dyscoordination of isolated index finger joint extension of the metacarpal phalangeal joint. The experiment took into account trials in which the user attempted to move a finger and alternate that with relaxation, as well as trials in which the finger movement has been imagined. The BCI2000 software has been used to process the recorded EEG signals. In the first session the patient exhibited highly accurate control of brain signal for attempted movement (97%), imagined movement (83%), and some difficulties with attempted relaxation (65%). During the session number six, control of relaxation improved to more than 80%. In three weeks time, meaning a total of nine sessions, it has been concluded that the patient's volitional isolated index finger extension has been improved.

In [10], Rüdiger Rupp and colleagues made an overview of neuroprosthesis for the upper extremity in individuals with spinal cord injury and its control with noninvasive BCIs.

In this paper we introduce the recoveriX system, a complete new hardware and software platform that can record, analyze and utilize EEG activity in real time to "close the loop" in stroke rehabilitation. Fig. 1 presents a schematic illustration of the conceptual approach used in

Published by Verlag der TU Graz
Graz University of Technology

 DOI: 10.3217/978-3-85125-533-1-38

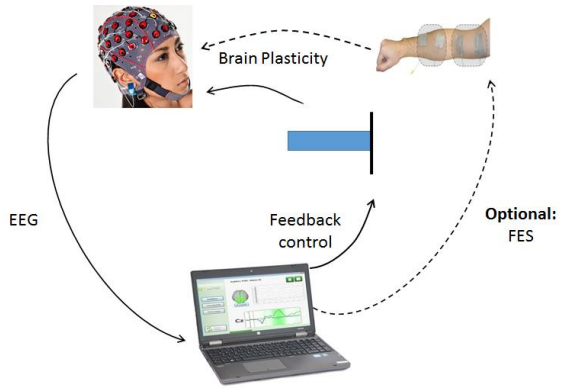

Figure 1: The schematic view of the recoveriX system.

recoveriX. The user imagines or performs specific movements, such as wrist dorsiflexion. The resulting EEG activity is detected through electrodes positioned in an electrode cap, then sent to an amplifier.
After the signals are amplified and digitalized, they are sent to a computer which manages the data analysis and presentation of feedback. Like in conventional therapy, the recoveriX users are instructed to perform motor imagery and receive feedback (specifically, visual feedback on a monitor and through FES stimulation). Unlike conventional therapy, RecoveriX users also wear an EEG cap that monitors MI that influences the feedback. The key element is the real-time connection between brain activity and feedback. recoveriX provides feedback only when the user correctly imagines the left or right hands movement. Thus, unlike conventional therapy, the feedback is always paired with the brain activity.
This paper presents further details about our system, experimental procedures, results from three patients clinical trials, and future research directions. Many of our future research directions will be addressed within the new RecoveriX project, an SME Instrument active from 2016-2018.

MATERALS AND METHODS

Subjects: Three patients participated in this study, as all of them experienced a sylvian ischemic stroke. Subject 1 is a 61 years old woman, right-handed, who suffered a stroke that left her with difficulties in moving the right hand. One month after the stroke, she participated in 24 recoveriX training sessions. Subject 2 (male, 69 years, right handed) joined our study 4 months after suffering a stroke. At that time, he was not able to perform any kind of movements with the right hand fingers. He performed 22 training sessions with our system. Due to personal problems, patient P2 had to leave the hospital 2 days earlier than planned, therefore missing the last 2 training sessions. The third subject (male, 64 years, right handed) joined our study three months after the stroke and performed 24 training sessions with recoveriX. At the time he started the training, he was able to perform only some limited movements with the left arm.
All three patients were recorded in an open room at the Rehabilitation Hospital of Iasi. The patients were not placed in an anechoic chamber to reduce noise that might affect the EEG, and none of the equipment was placed in a shielded area. During the period the patients attended the recoveriX training session, they performed also conventional rehabilitation therapy consisting of passive movements helped by a physiotherapist.
Data acquisition and experimental paradigm: the EEG data were recorded using a g.HIamp device (g.tec medical engineering GmbH, Austria) with a sampling frequency of 256 Hz and digitally filtered with a 0.5-30Hz 8th order bandpass Butterworth filter. The electrode cap had 45 active electrodes (g.LADYbird, g.tec medical engineering GmbH, Austria) arranged according to the 10-20 International System. Fig. 2 shows the recoveriX system mounted on a patient (left) and the electrode displacement on the scalp (right). The data classification was done using common spatial patterns (CSP) and a linear discriminant analysis (LDA) classifier. The study was approved by the institutional review board of the Rehabilitation Hospital of Iasi, the ethical approval has been granted, and all patients signed an informed consent before the start of the study.
The patients were seated in a comfortable chair in front of a computer monitor that presented cues and feedback (see Fig.2) with FES pads positioned over the forearm of each upper limbs to induce wrist extension and fingers opening. The FES stimulation was provided through an 8-channel neurostimulator (MOTIONSTIM8, Krauth+Timmermann GmbH, Germany). For all patients, the first session was a training session, where each subject got trained regarding the correct motor imagery taks (in all three cases, hand opening), and then conducted two practice runs for getting familiar with the experience of electrical stimulation and visual feedback. During all subsequent sessions, after setting up the system, each patient performed six runs each lasting about 6 minutes. Each run contained 40 8-seconds trials with a randomly chosen inter-trial time interval between 1 to 2 seconds. Each MI trial started with the display of a cross in the center of the monitor. After 2 seconds, a beep informed the user about the upcoming cue. The patients were instructed to start imagining the movement of either left or right hand when an arrow pointing to the left or right side was presented as a cue. After the cue dissapearance, the users began to receive visual and proprioceptive feedback. The visual feedback consisted of a blue bar starting in the center of the monitor and exending to the rignt or left side, according to the classified MI. The patients had to continue imagining the hand opening and closing movements for 4 seconds after the cue, until the visual feedback presentation ended. The neurostimulator induced the fingers and wrist extension of the coresponding hand only if the classified MI was the one dictated by the cue.
Motor assessment: we assessed the motor improvement for patients 1 and 3 using the 9-hole PEG test. In this game, the user has to fill 9 holes of a wooden board with

Published by Verlag der TU Graz
Graz University of Technology

 DOI: 10.3217/978-3-85125-533-1-38

Figure 2: The recoveriX system mounted on a patient (left) and the EEG electrode positions over the scalp (right).

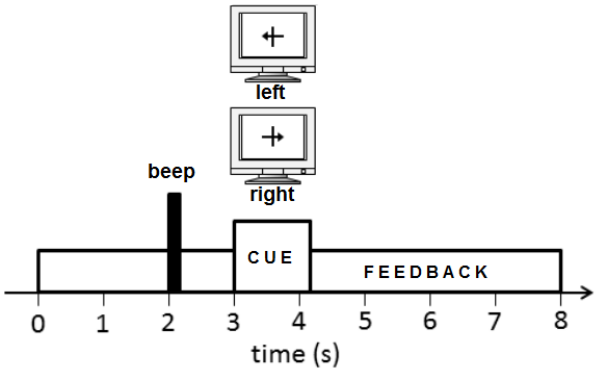

Figure 3. The time course of a single trial.

sticks placed on the table, and then to put the sticks back on the table one by one. The test has to be performed for both hands and the time for accomplishing the task and the number of dropped sticks are counted, representing the score for that evaluation.

The muscle contraction by FES was sufficient enough to cause movement of the affected hand for all patients.

The feedback period lasted four seconds. The time course of a single trial is presented in Fig. 3.

Feature extraction and classification: The CSP method is very well known for discrimination of two motor imagery tasks [11] and was firstly used for extracting abnormal components from clinical EEG [12]. By applying the simultaneous diagonalization of two covariance matrices, one is able to construct new time series that maximize the variance for one task, while minimizing it for the other one.

Considering N channels of EEG for each right and left trial X, the CSP method outputs an N x N projection matrix. This resulting matrix reflects the subject specific activation patterns of the data during motor imagery of left or right hand in this study. The decomposition of a trial can be written as:

$$Z=W\cdot X \qquad (1)$$

This transformation projects the variance of X onto the rows of Z and results in N new time series. The columns of W-1 are a set of CSPs and can be considered as time-invariant EEG source distributions.

Due to the definition of W, the variance for a left movement imagination is largest in the first row of Z and decreases with the increasing number of the subsequent rows. The opposite is the case for a trial with right motor imagery. For classification of the left and right trials, the variances have to be extracted as reliable features of the newly designed N time series. However, it is not necessary to calculate the variances of all N time series. The method provides a dimensionality reduction of the EEG. Mueller-Gerking and colleagues [13] showed that the optimal number of common spatial patterns is four. Following their results, after building the projection matrix W from an artifact corrected training set X, only the first and last two rows (p=4) of W are used to process new input data X. Then the variance (VARp) of the resulting four time series is calculated for a time window T. After normalizing and log-transforming four feature vectors are obtained (2). These four features are used as input for a linear discriminant analysis (Fisher's LDA [14]) classifier which categorizes the MI as left-hand or right-hand movement.

$$f_p = \log\left(\frac{VAR_p}{\sum_{p=1}^{4} VAR_p}\right) \qquad (2)$$

Using the training data recorded during runs 1 to 4, 5 sets of spatial filters and classifiers were calculated from two seconds time windows shifted in time with a 0.5 seconds Hamming window based on the data from the time interval from 4 to 8 seconds in each trial. The classifier with the highest ten-fold cross validated accuracy [15] was chosen to provide the visual and FES feedback while recording runs 5 and 6. These last two runs were used to calculate the online accuracy of the chosen classifier for the current session. The classifier calculated in the previous session was used to provide the feedback while recording the first 4 runs.

RESULTS

Figure 4 presents the BCI control accuracy for all three patients based on the online results. All three patients started with accuracies above 80%. Patient P1 reached an average accuracy of 90.5% over all sessions, while patient P2 reached 85.4% and patient P3 87.1%. Each patient attained accuracy above 96.2% in at least one session. There are sessions were the accuracies were low for all patients. These lower scores are highly correlated with each patient's degree of tiredness, emotional state or other health conditions during that day. Patient 1 reported that she could not sleep during the night before the session 16, when she achieved the lowest accuracy. Patient 2 got a cold and coughed a lot during sessions 15 and 16.

Table 1 presents the score of the 9-hole PEG test for patients P1 and P3, for the paretic and for the healthy hand. For patient P1, the evaluation was performed before starting the first recoveriX training session and the results were considered as baseline for the subsequent evaluations, which were done once at each 3 sessions of training. P3 patient's condition didn't allowed him to perform the 9-hole PEG test before and during the first 6

Published by Verlag der TU Graz
Graz University of Technology

 DOI: 10.3217/978-3-85125-533-1-38

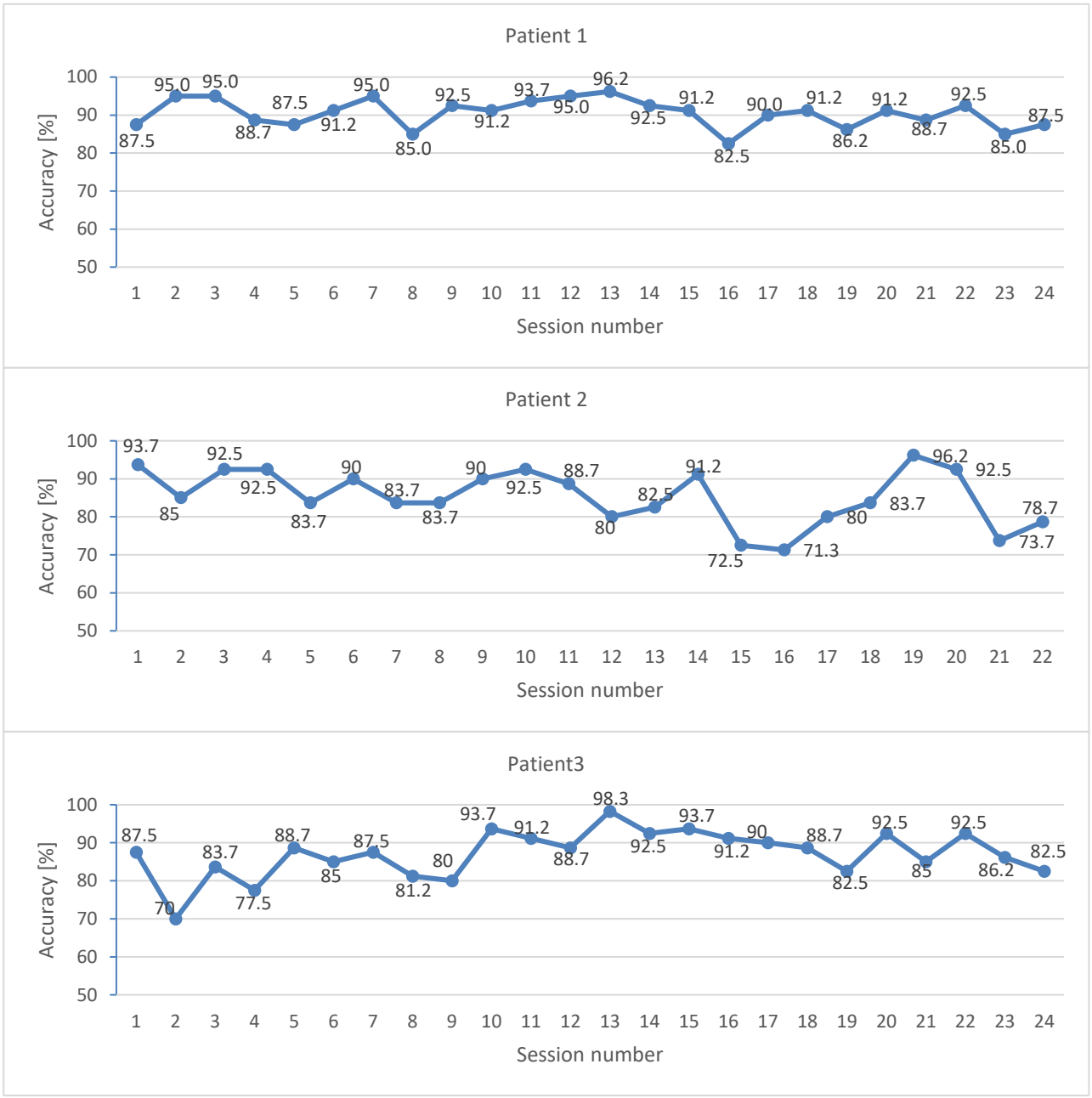

Figure 4. The online accuracy plots of the three patients across the training sessions with the recoveriX system.

Figure 5. The snapshots with the moves that patient P2 was able to do after 22 sessions of training with recoveriX.

Published by Verlag der TU Graz
Graz University of Technology

 DOI: 10.3217/978-3-85125-533-1-38

Table 1: The results of the 9-hole PEG test for patients P1 and P3

Sessions	Time [s] / dropped PEGs			
	Paretic hand		Healthy hand	
	P1	P3	P1	P3
0	65 / -	-	31 / -	-
3	54 / -	-	32 / -	-
6	45 / -	-	32 / -	-
9	42 / -	90 / 1	31 / -	26 / -
12	42 / -	77 / -	31 / -	26 / -
15	38 / -	94 / -	29 / -	26 / -
18	34 / -	60 / -	29 / -	25 / -
21	30 / -	61 / -	29 / -	25 / -
24	30 / -	52 / -	29 / -	26 / -
Time improve-ment [sec]	35	38	2	0

training sessions. After 9 sessions of training, the motor functions of his left hand improved, and he was able perform the test for the first time. In his case, the results of the evaluation after the 9th session were considered as baselines for the next evaluations.

The last line of Tab.1 presents the time improvements of each hand for patients 1 and 3. Both patients improved the time exercise of the paretic hands with 35 seconds, respectively 38 seconds, and the time exercise for the healthy hands remained relatively constant. After the last training session, P1 managed to perform the test with the paretic hand in 30 seconds, almost the same time as with the healthy hand.

Patient 2 could not perform the 9-hole PEG test during the study. He started to move the thumb after the 12th session, and during the last sessions of training he started to perform small range voluntary movements also with the other fingers. Fig. 5 presents two snapshots taken while patient 2 performed voluntary movements with his right hand after the last session of training.

DISCUSSION

Results discussion: Before starting this study, we supposed that patients will have difficulties in achieving high accuracies. These first results showed the opposite. This may occur because these patients are highly motivated to participate in a study to improve their motor functions. All patients reported that they were eager to come back for further recoveriX sessions especially after they seen the first functional improvements. The high accuracy, coupled with rewarding feedback, also motivated the patients to perform the motor imagery effectively. In addition to motivating patients, the blue bar feedback is important to maintain patients' attention. A feedback is also provided by the FES system that actively moves the hand as long as the person imagines the movement. This activates tactile and proprioceptive systems that feed back to the sensorimotor system. The BCI system is able to manage this feedback, and the CSP and LDA algorithms can adapt to changes in each user's brain activity. Even though motor improvements were reported after the last training session for all three patients, in this early stage of the study we do not exclude the possibility that the motor improvements were due spontaneous remission or due to concomitant physiotherapy. This crucial point will be better discussed after testing the system on a higher group of patients and the results compared with the ones of a control group, as planned. Anyway, even though a control group is missing the feedback from the clinicians has been a positive one and according to their experience dealing with patients in the same condition, the recoveriX system has certain potential to induce voluntary hand movement in stroke patients.

Future research directions: This paper validates the recoveriX approach from a technical perspective by demonstrating that, at least with the three patients using the prototype system presented here, our system can function in real-world settings. Up to now we found that the participants to our study had sometimes difficulties with the bar feedback when the classification was incorrect, because it was hard to associate the corresponding movement with the feedback. Therefore, one of our future development directions involve improved immersive software to present feedback and maximize the patients' engagement by replacing the graphically simple feedback with more advanced environments such as different views of an avatar whose movements attempt to mimic the movements that the user imagines [16]. At the beginning of each trial, the left or right hand moves for 1 second, which triggers the patient to start the corresponding movement imagery. When the BCI system correctly classifies the activity, then the avatar hand movement is prolonged and the FES is triggered. When the classification is wrong, then the avatar and the FES are temporarily inactive. Apart of the avatar feedback, we are also exploring improved hardware. In this work the experiments were performed using 45 channels wired electrode cap with gel electrodes. Recently, we developed a wireless version of the system using only 16 gel electrodes overlying over the motor areas. The new amplifier is lightweight (only 70 grams), placed on the back side of the electrode cap

Figure 6. The experimental setup with avatar feedback and FES.

Published by Verlag der TU Graz
Graz University of Technology

 DOI: 10.3217/978-3-85125-533-1-38

and transmits wireless, in real time, the recorded data to the laptop/PC.
The FES device will be replaced by our new g.Estim neurostimulator developed mainly for BCI applications. Fig. 6 illustrates the future setup of the system, using the avatar, wireless EEG cap and the new neurostimulator.

ACKNOWLEDGEMENTS

The study was funded by the EC projects VERE and recoveriX.

REFERENCES

[1]Ang K. K., Guan C., , Chua K. S. G., Ang B. T., Kuah C., Wang C., et al. A clinical study of motor imagery-based brain-computer interface for upper limb robotic rehabilitation, Conf Proc IEEE Eng Med Biol Soc., 2009, vol. 2009, 5981-4.

[2] Shindo K., , Kawashima K., Ushiba J., Ota N., Ito M., Ota T., et al. Effects of neurofeedback training with an electroencephalogram-based brain-computer interface for hand paralysis in patients with chronic stroke: a preliminary case series study. J Rehabil Med, 2011, 43(10), 951-957.

[3] Grosse-Wentrup M., Mattia D., Oweiss K., Using brain–computer interfaces to induce neural plasticity and restore function. J Neural Eng., 2011, 8(2), 025004.

[4] Pichiorri F, Morone G, Petti M, Toppi J, Pisotta I, Molinari M, Paolucci S, Inghilleri M, Astolfi L, Cincotti F, Mattia D. Brain-computer interface boosts motor imagery practice during stroke recovery. Ann Neurol. 2015 May;77(5):851-65.

[5] Sabathiel N., Irimia D.C., Allison B.Z., Guger C., Edlinger G. Paired Associative Stimulation with Brain-Computer Interfaces: A New Paradigm for Stroke Rehabilitation. In: Schmorrow D., Fidopiastis C. (Ed) Foundations of Augmented Cognition: Neuroergonomics and Operational Neuroscience. AC 2016. Lecture Notes in Computer Science, vol 9743. Springer, Cham.

[6] Munih M., Ichie M. Current status and future prospects for upper and lower extremity motor system neuroprosthesis. Neuromodulation: Technology at the Neural Interface, 2001, (4), 176-186.

[7] Poboroniuc M.S., Wood D.E., Riener R., Donaldson N.N. A New Controller for FES-Assisted Sitting Down in Paraplegia. Advances in Electrical and Computer Engineering, 2010. (10-4), 9-16.

[8] Do A.H., Wang P.T., King C.E., Abiri A., Nenadic Z. Brain-Computer Interface controlled functional electrical stimulation system for ankle movement. 2011, Journal of NeuroEng. and Rehabilitation, 8:49.

[9] Daly J.J., Cheng R., Rogers J., Litinas K., Hrovat K, Dohring M. Feasibility of a new application of noninvasive brain-computer interface (BCI): A case study of training for recovery of volitional motor control after stroke. J. of Neurologic Physical Therapy, 2009, 33, 203-2011.

[10] Rupp R., Rohm M., Schneiders M., Kreilinger A., Muller-Putz G.R. Functional rehabilitation of the paralyzed upper extremity after spinal cord injury by noninvasive hybrid neuroprostheses, Proc. Of the IEEE, 2015, 103(6), pp. 954-968.

[11] Blankertz B., Tomioka R., Lemm S., Kawanabe M., Müller K.-R. Optimizing Spatial Filters for Robust EEG Single-Trial Analysis. IEEE Signal Processing Magazine, 2008, 25, 41-56.

[12] Koles Z. The quantitative extraction and topographic mapping of the abnormal components in the clinical EEG. Electroencephalogr. Clin. Neurophysiol., 1991, 79(6), pp. 440-447.

[13] Mueller-Gerking J., Pfurtscheller G., Flyvbjerg H., Designing optimal spatial filters for single-trial EEG classification in a movement task. Clin Neurophysiol, 1999, 110, pp. 787-798.

[14] Lemm S., Blankertz B., Dickhaus T., Müller K-R. Introduction to Machine Learning for Brain Imaging. NeuroImage, 2011, 56(2), 387–399.

[15] Naseer N., Hong M.J., Hong K.-S. Online binary decision decoding using functional near-infrared spectroscopy for development of a brain-computer interface. Experimental Brain Research. 2014, 232(2), 555-564.

[16] Guger G., Edlinger G. Methods for non-invasive EEG detection. In: Farina D., Jensen W., Akay M. (Ed.). Introduction to neural engineering for motor rehabilitation. John Wiley & Sons, 2013, pp. 137-154.

Published by Verlag der TU Graz
Graz University of Technology

Proceedings of the
7th Graz Brain-Computer Interface Conference 2017 DOI: 10.3217/978-3-85125-533-1-39

DECODING OF WALKING INTENTION UNDER LOWER LIMB EXOSKELETON ENVIRONMENT USING MRCP FEATURE

J. -H. Jeong, N. -S. Kwak, M. -H. Lee, S. -W. Lee

Department of Brain and Cognitive Engineering, Korea University, Seoul, Republic of Korea

E-mail: sw.lee@korea.ac.kr

ABSTRACT: In brain-machine interface (BMI) researches, a fast and accurate detection of user intention is an important research issue for an efficient human-machine interaction. Among electroencephalography (EEG)-based BMI paradigms, a movement-related cortical potential (MRCP) could be useful to recognize user intention due to its characteristics of spontaneity and low latency. Therefore, in our study, we propose a MRCP feature selection method for decoding user intention under the powered exoskeleton environment. We combined two spectral features that were extracted from readiness potential (RP) and movement-monitoring potential (MMP) sections, respectively. In each MRCP section, we estimated optimal frequency bands for the discriminative feature using a nested cross-validation. Five healthy subjects who were wearing the exoskeleton performed a self-initiated walking task. Our results showed the grand averaged classification accuracy of 87.6%. To our best knowledge, we first validated a single-trial analysis using the MRCP data acquired from self-initiated exoskeleton walking. Our experimental results present that the proposed MRCP-based exoskeleton control system is becoming more feasible for real-world applications.

INTRODUCTION

Brain-machine interface (BMI) is a communication system between users and machines, in which users can control the external devices through conveying user's intention without direct manipulation or the activations of peripheral nerve system [1]. The BMI techniques have commonly used electroencephalography (EEG) signals to recognize user intention for controlling external devices such as wheelchairs, robot arms, or robotic exoskeleton [2, 3]. Recently, EEG-based BMI has been developed for not only healthy people but also the patients with paralysis or nerve damage in neuro-rehabilitation [4].

Movement-related cortical potential (MRCP) is one of the representative slow cortical potential (SCP) components, which is measured by a slow decrease in the EEG amplitude over primary motor cortex (M1) during a motor task in human. Also, it is a spontaneous potential which is generated by execution or imagination of either cue-based movement paradigm known as a contingent negative variation (CNV) or self-paced movement paradigm. MRCP comprises two main components that are readiness potential (RP) and movement-monitoring potential (MMP). RP is a negative cortical potential which has two fundamental parts before the movement onset. Negative slope, called 'early bereitschaftspotential (BP)', begins about $(1 \sim 2)$s before voluntary movement onset. About 1s before the movement onset, steeper negative slope is called 'late BP' or 'motor potential (MP)' (Fig. 1). In contrast, MMP is a positive cortical potential which reflected an outcome of the motor process. After the movement onset, the MMP generated as an increase deflection for returning to initiate state (Fig. 1). MRCP reflects the stepwise process of movement preparation/planning and execution [5]. It could be a useful feature for an intuitive assistive robot control due to its advantages of spontaneous potential and early detection of user intention based on a single-trial. MRCP researches have been investigated to amyotrophic lateral sclerosis (ALS), stroke, and paralysis patients for rehabilitation with assistive robots as well as to the normal person for controlling BMI-based external devices [6].

Therefore, the researchers in previous studies decoded user's movement intention from MRCP in the various experiment paradigm (e.g. self-paced arm movement (reaching task) [7], executed and imagined foot movement (foot dorsiflexion) [8], self-initiated walking [9]). They have applied MRCP decoding system to BMI-based rehabilitation for inducing patient's brain plasticity effectively. These studies have utilized different EEG data acquisition techniques with different electrode montage, brain signal enhancement technologies, and some of them presented an usefulness of EEG data acquired in the real-time BCI. They verified that their approaches could be useful for accurate detection or classification of user intention from MRCP. Also, various machine learning approaches were applied for a single-trial MRCP analysis [10, 11].

However, MRCP-based BMI systems have a low performance to recognize movement intention in the single-trial basis. The system performance to detect user intention still requires more stable accuracy for efficient and reliable BMI system. Also, the current MRCP-based detection systems are difficult to apply in asynchronous BMI system. Because the MRCP is primarily extracted from the narrow frequency ranges (i.e. the SCP ([0.1-1] Hz and delta ([1-4] Hz) band, etc.) for all subjects.

Published by Verlag der TU Graz
Graz University of Technology

 DOI: 10.3217/978-3-85125-533-1-39

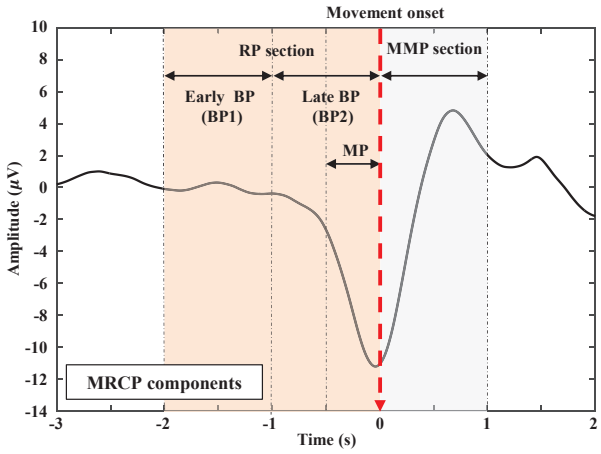

Figure 1: Representation of MRCP amplitude fluctuation at Cz electrode. Movement onset is defined at the time point 0s. The MRCP comprises RP and MMP sections. (In RP section, (-2 ∼ -1)s is early BP, (-1 ∼ 0)s is late BP, (-0.5 ∼ 0)s is motor potential (MP), and after movement onset, (0 ∼ 1)s is MMP section).

For these reasons, we hypothesized that the MRCP detection performance would be improved using the subject-dependent MRCP feature selection method. We approached in two main perspectives. In spectral-domain perspective, we extracted the optimal frequency band by nested cross-validation based on classification accuracy across each filter bank. In temporal-domain perspective, we approached that motor-cortical fluctuations in EEG have different frequency power in the pre-movement state (RP section) and after the movement onset (MMP section) during the MRCP evoked time. We also designed an exoskeleton control system for acquiring the MRCP data under the real-world exoskeleton environment. Hence, we propose a subject-dependent MRCP feature selection method for the accurate detection of user intention on the single-trial basis.

MATERIALS AND METHODS

A. Experimental protocols: Fig. 2 shows our designed experiment system for acquiring MRCP data under a lower limb exoskeleton walking environment.
First, we used the lower limb exoskeleton (REX, Rex Bionics Ltd) module. The exoskeleton has various functions; self-balancing, self-supporting, and programmed motions (e.g. walking, turning, sitting, standing, and shuffling). It allows a person to move by joystick or wireless interface [12]. In our experiment, the exoskeleton was controlled by electromyogram (EMG) signal which generated from muscle movements. We used a wireless EEG and EMG module (MOVE, BrainProduct GmbH). The EEG and EMG signals were transmitted to the recording program (BrainVision Recorder, BrainProduct GmbH) simultaneously. The signal amplifier was located on the right arm of the exoskeleton. The EEG module was used for decoding the user's walking intention from MRCP. The EMG module was used for acquiring the electrical signals by muscle movements from the right leg. The EMG module detected the movement onset triggers that generated when the EMG activity exceeded a pre-defined threshold value.
Five healthy subjects without any neurological or physical disorder history participated in the experiments (aged 26-29, five males). The EEG data were acquired using 32 Ag/AgCl electrodes (Fp1, Fz, F3, F7, C1, FC5, FC1, C3, T7, CPz, CP5, CP1, Pz, P3, P7, O1, Oz, O2, P4, P8, CP6, CP2, Cz, C4, T8, C2, FC6, FC2, F4, F8, Fp2, and POz) following 10/20 international systems. The ground electrode was mounted on FPz and reference electrodes

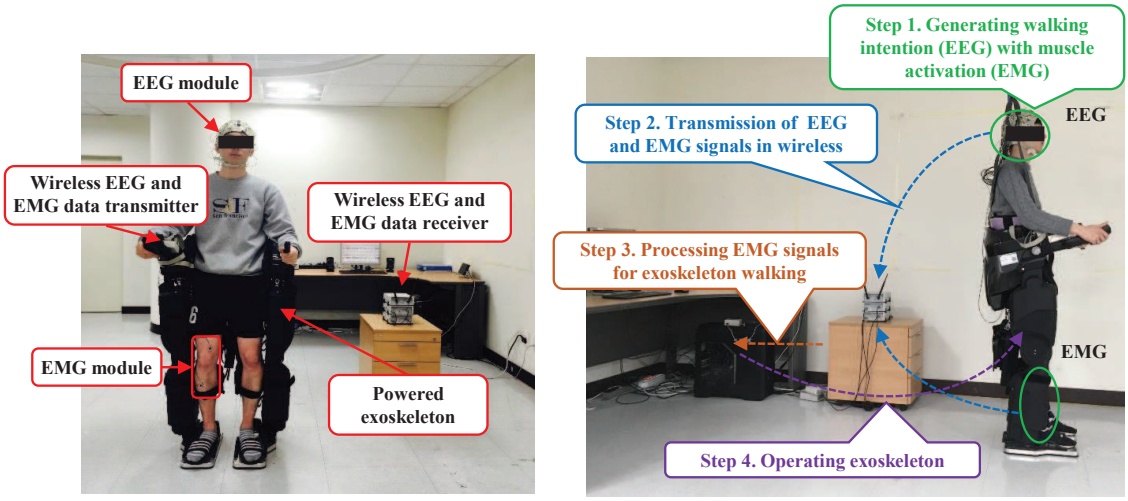

Figure 2: Experimental modules (left) and protocols (right) for MRCP data acquisition under lower limb exoskeleton environment. The subjects performed the self-initiated exoskeleton walking task during the experiment. The exoskeleton is controlled by the EMG activation.

Published by Verlag der TU Graz
Graz University of Technology

 DOI: 10.3217/978-3-85125-533-1-39

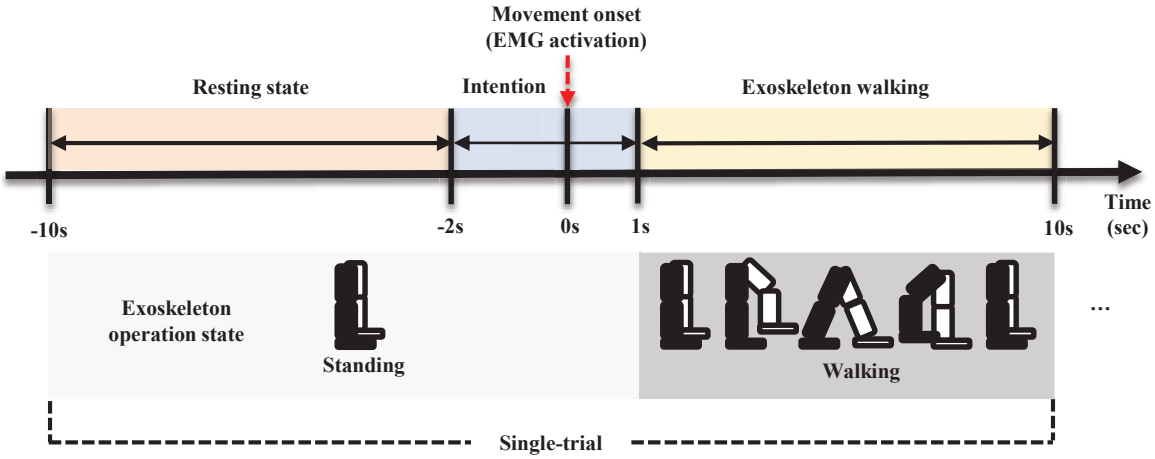

Figure 3: Experimental paradigm. After the experiment starts, the subjects performed self-initiated walking whenever they intended to walk in 50 trials. The lower limb exoskeleton is operated walking task for 8s (movement onset triggers were marked). After one-step exoskeleton walking, the resting state was given for 8s (the resting triggers were marked).

on FCz. All impedance of electrodes were maintained below 10kΩ. The sampling frequency rate was 1000Hz. A notch filter frequency rate was 60Hz for reducing DC power supply noise.

The EMG data were recorded using two bipolar Ag/AgCl electrodes on the tibialis anterior (TA) and biceps femoris (BF) muscles of the right leg. These muscles were selected because of fast muscle activation in walking [8]. The EMG data were preprocessed using 2s sliding window size with a 100ms shift. The data filtered by a zero-phase Butterworth fourth-order band-pass filter at [0.05-60] Hz and were rectified using the absolute value of filtered EMG data and calculated the moving average of the EMG amplitudes window size in an online manner.

B. Experimental paradigm: In exoskeleton walking task, the subjects performed the self-initiated exoskeleton walking when they intended to walk. The lower limb exoskeleton was operated by the movement onset trigger which was generated by EMG activation. (Note that the experiments were conducted by self-paced walking, not a cue-based instruction) The exoskeleton operated for 9s as one-step walking. After one step had been performed, the resting state was given to the subject for 10s. The subjects were asked to relax the muscle because the muscle tension could affect contamination of EMG signal. This experiment process is a single-trial of the entire experiment paradigm. The subjects performed the self-paced exoskeleton walking over 50 trials (Fig. 3).

C. Data processing: The acquired EEG and EMG data were processed using a BBCI toolbox [13]. First, we composed the frequency filter bank for extracting subject-dependent optimal frequency band. The frequency filter bank was comprised by thirty different frequency bands such as [0.05-1,2, ...10] Hz, [0.1-1,2, ...10] Hz, and [0.5-1,2, ...10] Hz. The EEG data were randomly selected 80% of the trials as training set and use remaining 20% as test set for applying the principle of nested cross-validation to design the framework of signal processing (Fig. 4). In the inner loop (blue line), we selected subject-dependent optimal frequency bands based on the MRCP classification accuracies using training set, which is band-pass filtered using the frequency filter bank according to each RP and MMP section. After the inner loop step, the selected frequency bands were updated as band pass filter parameter for the outer loop (red dashed line). In the outer loop, the MRCP detection performance was calculated using selected subject-dependent frequency band with test set.

More in detail, in the inner loop, the acquired EEG data were pre-processed by 2nd Butterworth band-pass filter according to each frequency band at the filter bank and down-sampled from 1000Hz to 100Hz. The filtered data were then spatially filtered using large Laplacian filter to maximize spatial distribution for the poor spatial resolution [15]. The large Laplacian filter was applied at C1, C2, CPz, and Cz channels, respectively, using the surrogate 8 channels. We did not apply the artifact rejection techniques because the subject who wearing the exoskeleton maintained the standing state only (Fig. 3). The spatially filtered data were segmented from (-6 $\sim$ 4)s by the movement onset. The epoched data were divided into RP section (-2 $\sim$ 0)s and MMP section (0 $\sim$ 1)s respectively (Fig. 1). The data of RP and MMP sections were defined as “walking intention state” class. The data in the interval of (-5 $\sim$ -2)s were defined as “resting state” class. Each class consisted of the data which is filtered by each frequency band. Especially, in the resting state, we also divided the epoched data as (-5 $\sim$ -3)s and (-3 $\sim$ -2)s. The data for each interval applied the same frequency band used for filtering the RP and MMP section, respectively.

Before the extracted the RP and MMP features, the epoched data were computed the correlation coefficient signed r-square values between walking intention and

Published by Verlag der TU Graz
Graz University of Technology

 DOI: 10.3217/978-3-85125-533-1-39

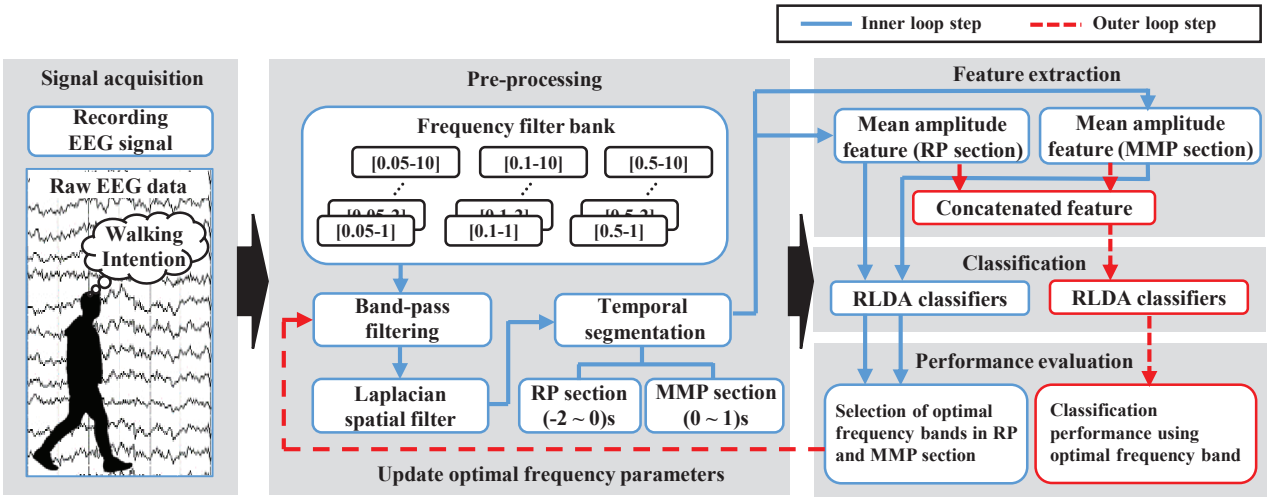

Figure 4: The flowchart of the subject-dependent MRCP feature selection for decoding of walking intention

resting state classes for detecting statistically significant time intervals for each channel. In the RP section, the signed r square values showed relatively high values between walking intention and resting state at Cz, C1, C2, and CPz channels. In the MMP section, the signed r square values showed relatively high values at Cz, C1, C2, FC1, and FC2 channels (Fig. 5). Specifically, the signed r square value showed significant discriminant values between classes at Cz, C1, C2, CPz, CP1, CP2 channels nearby motor cortex compared to other channels. Therefore, Cz, C1, C2, and CPz channels were selected for extracting MRCP features.

For extracting MRCP feature, we extracted mean amplitude feature in the 0.2s intervals at all classes (walking intention and resting state) from epoched data.

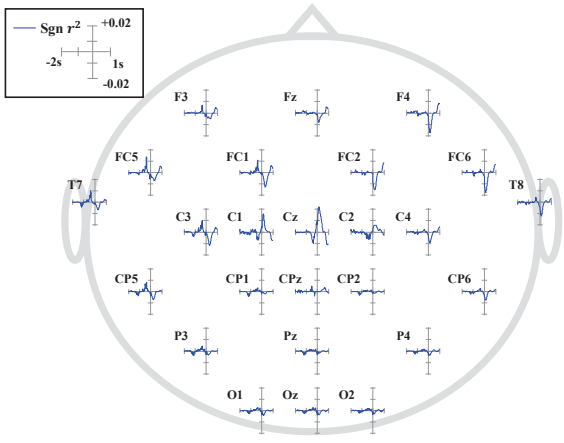

Figure 5: Topographic plots of signed r-square values between walking intention and resting state classes at subject E. The signed r-square represented the relatively discriminant degree between classes in each channel.

The extracted features composed 15 × 4 matrix (feature vector × channel). The features were classified as walking intention and resting state classes using regularized linear discriminant analysis (RLDA). The RLDA is one of the methods to simple classification modeled with normal distribution in each class samples. In our data processing, the RLDA was used as a classifier to detect walking intention depending on each frequency band. 10-fold cross validation was applied for evaluating of MRCP detection performance.

Therefore, through the inner loop, we obtained thirty MRCP classification accuracies using the frequency filter bank depending on RP and MMP section, respectively. The subject-dependent optimal frequency bands were selected to have the best classification accuracy at each RP and MMP section.

In the outer loop, the selected frequency bands for each section were updated to band-pass filter parameter in the pre-processing step. The raw EEG data were band-pass filtered using the updated frequency bands.The EEG data processing step of the outer loop is processed the same way as in the inner loop (i.e. down-sampled frequency rate 1000 Hz to 100 Hz, applying large Laplacian spatial filter, channel selection, time segmentation, extraction of mean amplitude feature). The processed RP and MMP features were concatenated for comprising either walking intention class or resting class. Finally, the RLDA classifier was used as detection of user's walking intention from subject-dependent MRCP feature. The MRCP detection performance was evaluated using test set.

Through the proposed method, we obtained the subject-dependent frequency parameter for robust MRCP detection system.

RESULTS

Tab. 1 shows the selected frequency bands in each RP and MMP section across subjects and the results of MRCP classification accuracy based on a single-trial analysis. The grand average classification accuracy is 87.61% across five subjects. Through this results, we observed that the frequency bands were extracted discrimi-

Published by Verlag der TU Graz
Graz University of Technology

 DOI: 10.3217/978-3-85125-533-1-39

natively for each RP and MMP section. Also, the optimal frequency bands were different in each subject.
Fig. 6 shows the significant MRCP patterns which were observed in self-initiated exoskeleton walking task. The actual movement onset (0s) were set when the EMG signals exceeded pre-defined threshold amplitude. The averaged MRCP patterns are indicated from (-2 $\sim$ 1)s at Cz electrode in subject C and E. The MRCP were baseline corrected from (-2 $\sim$ -1.5)s by the movement onset time. The black line indicates the MRCP patterns filtered by the selected frequency bands in subject C and E. In subject C, the MRCP features were filtered by [0.1-1] Hz and [0.05-9] Hz across RP and MMP section, respectively. Also, in subject E, the MRCP features were filtered by [0.1-10] Hz and [0.5-2] Hz across sections. The steeper negative slope indicates from (-1 $\sim$ 0)s (RP section) and, after movement onset, the positive slope indicates from (0 $\sim$ 1)s (MMP section).

Table 1: Selected frequency bands and classification accuracies of MRCP for each subject

Subject	Selected frequency band [Hz]		Performance (%)
	RP section	MMP section	
Sub A	[0.5-10]	[0.1-7]	94.12
Sub B	[0.5-4]	[0.5-2]	75.22
Sub C	[0.1-1]	[0.05-9]	85.29
Sub D	[0.5-3]	[0.5-9]	86.36
Sub E	[0.1-10]	[0.5-2]	97.06
Average			87.61 $\pm$ 8.5

Scalp topographies are plotted to show the spatial distribution of MRCP patterns (Fig. 6). The time interval separated into three sections to observe the specific time-spatial changes of MRCP patterns. As we mentioned (Fig. 1), the time interval of (-2 $\sim$ -1)s is 'early BP' in the RP section, (-1 $\sim$ 0)s is 'late BP' in RP section. (0 $\sim$ 1)s is MMP section. Scalp topographies in the RP section (-2 $\sim$ 0)s appeared gradually negative distribution in the central and post-central area. Especially, in the range of (-1 $\sim$ 0)s, the scalp topography shows significant the negative distribution relatively nearby motor cortex in Cz, CPz, C1, and C2 channels. After the movement onset in MMP sections (0 $\sim$ 1)s, the intensity of the spatial distribution was observed returning from negative to initial distribution.
Therefore, we confirmed that the scalp topography in 'late BP' section shows the relatively more negative spatial distribution compared to 'early BP' section. Also, scalp topographies in MMP section shows certainly positive spatial distribution.

DISCUSSION

In this paper, we propose a subject-dependent MRCP feature selection method for robust detection of user's walking intention on the single-trial basis. Also, we designed a single-trial MRCP acquisition system under the lower limb exoskeleton environment. Due to our designed system, we could obtain the EEG signals with respect to walking intention from MRCP feature with the self-initiated exoskeleton walking.
Through the proposed method, we have observed that movement intention can be decoded above chance level using optimal frequency bands for each subject compared to different EEG frequency bands (i.e. SCP, delta bands, etc.).
Regarding system performance, we used a systematic ap-

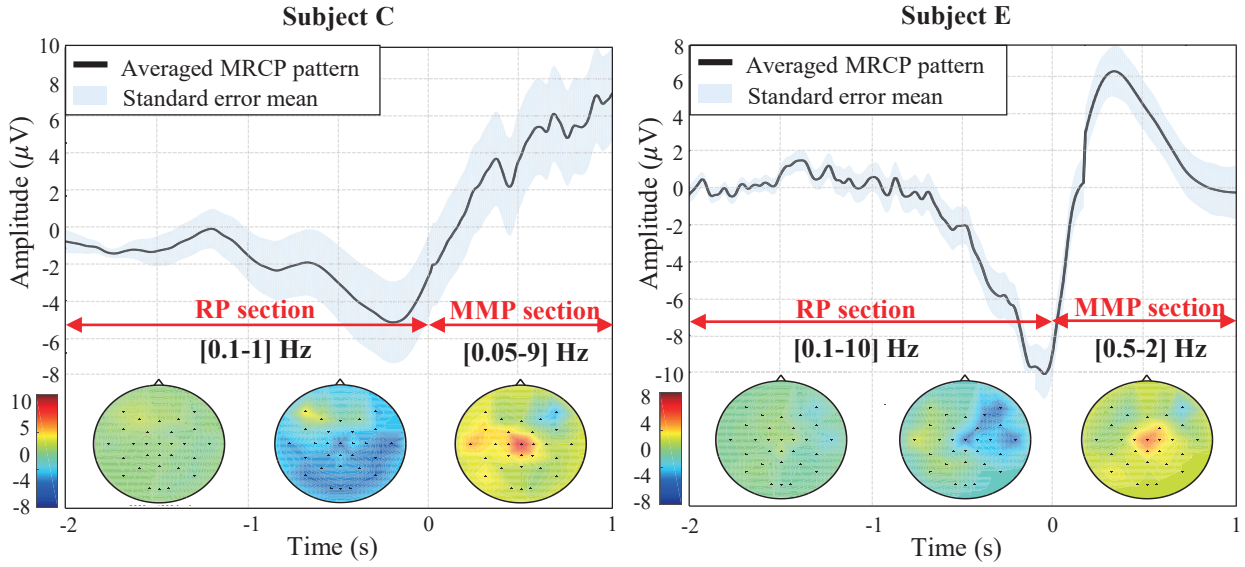

Figure 6: Time-amplitude representation of averaged MRCP filtered by selected frequency bands at channel Cz in subject C and E. Representation of scalp topographies from MRCP using selected frequency bands in each section.

Published by Verlag der TU Graz
Graz University of Technology

 DOI: 10.3217/978-3-85125-533-1-39

proach for detecting the onset of self-initiated exoskeleton walking to extract user's walking intention. Outcome of the proposed method showed that subject-dependent EEG features are also important to detect the movement intention from MRCP. Also, we validated that subject-dependent optimal frequency parameter could improve the performance of MRCP detection system compared to the heuristic frequency bands.
Our current study, however, focused on applying to stroke patients or lower limb discomfort people who are able to extract EMG signal for the real world application control or gait rehabilitation. Hence, we have developed our system can be applied in the online environment without EMG. We have implemented a 3s sliding window which can filter in real-time with an optimal RP frequency band of 2s and an optimal MMP frequency band of 1s.

CONCLUSION

In the context of BMI-based real world application control or gait rehabilitation, the robust detection of movement intention is an essential and critical issue for the development of self-initiated BMI control systems. Fast and accurate detection of self-initiated movement intention using MRCP has raised hope for rehabilitation scenarios in which neural plasticity and brain function recovery implicitly.
In our study, we proposed the subject-dependent MRCP feature selection method for robust MRCP detection based on a single-trial. The result showed that grand-averaged classification accuracy is 87.6 $\pm$ 8% using the single-trial MRCP data acquired from the self-initiated exoskeleton walking task in the ambulatory environment. In our method, the temporal intervals of MRCP are divided into two sections of RP (-2 $\sim$ 0)s and MMP (0 $\sim$ 1)s. The optimal frequency band has validated from each temporal interval independently. We firstly report that the RP and MMP component have different optimal frequency ranges, and it highly depends on the individual subject. Our data were acquired by healthy subjects whose wearing the lower limb exoskeleton.
Our study still needs to demonstrate the possibility of applying to the stroke patients or the lower limb discomfort people for the online system. Hence, future work will target to devote the robustness of our method with those people, and prove the possibility of MRCP-based exoskeleton system as a real-world application.

ACKNOWLEDGEMENT

This research was supported by the MSIP(Ministry of Science, ICT and Future Planning), Korea, under the "SW Starlab" (IITP-2015-1107) supervised by the IITP(Institute for Information & communications Technology Promotion).

REFERENCES

[1] Wolpaw JR, Birbaumer N, McFarland DJ, Pfurtscheller G, Vaughan TM. Brain–computer interfaces for communication and control. Clinical Neurophysiology, 2002;113(6):767-791.
[2] Kim KT, Suk HI, Lee SW. Commanding a brain-controlled wheelchair using steady-state somatosensory evoked potentials. IEEE Transactions on Neural Systems and Rehabilitation Engineering, 2016;Accepted.
[3] Do AH, Wang PT, King CE, Chun SN, Nenadic Z. Brain-computer interface controlled robotic gait orthosis. Journal of NeuroEngineering and Rehabilitation, 2013;10(1):111.
[4] Venkatakrishna A, Francisco GE, Contreras-Vidal JL. Applications of brain–machine interface systems in stroke recovery and rehabilitation. Current Physical Medicine and Rehabilitation Reports, 2014;2(2):93-105.
[5] Shibasaki H, Hallett M. What is the Bereitschaftspotential? Clinical Neurophysiology, 2006;117(11):2341-2356.
[6] Blank AA, French JA, Pehlivan AU, O'Malley MK. Current trends in robot-assisted upper-limb stroke rehabilitation: promoting patient engagement in therapy. Current Physical Medicine and Rehabilitation Reports, 2014;2(3):184-195.
[7] Lew EY, Chavarriaga R, Silvoni S, Millán JDR. Single trial prediction of self-paced reaching directions from EEG signals. Frontiers in Neuroscience, 2014;8(222):166-178.
[8] Jochumsen M, Niazi IK, Mrachacz-Kersting N, Farina D, Dremstrup K. Detection and classification of movement-related cortical potentials associated with task force and speed. Journal of Neural Engineering, 2013;10(5):056015.
[9] Sburlea AI, Montesano L, Minguez J. Continuous detection of the self-initiated walking pre-movement state from EEG correlates without session-to-session recalibration. Journal of Neural Engineering, 2015;12(3):036007.
[10] Jochumsen M et al. Comparison of spatial filters and features for the detection and classification of movement-related cortical potentials in healthy individuals and stroke patients. Journal of Neural Engineering, 2015;12(5):056003.
[11] Xu R, Jiang N, Lin C, Mrachacz-Kersting N, Dremstrup K, Farina D. Enhanced low-latency detection of motor intention from EEG for closed-loop brain-computer interface applications. IEEE Transactions on Biomedical Engineering, 2014;61(2):288-296.
[12] Kwak NS, Müller KR, Lee SW. A lower limb exoskeleton control system based on steady state visual evoked potentials. Journal of Neural Engineering, 2015;12(5):056009.
[13] Blankertz B et al. The Berlin brain–computer interface: non-medical uses of BCI technology. Frontiers in Neuroscience, 2010;4:198.
[14] Niazi IK et al. Detection of movement intention from single-trial movement-related cortical potentials. Journal of Neural Engineering, 2011;8(6):066009.

Published by Verlag der TU Graz
Graz University of Technology

Proceedings of the
7th Graz Brain-Computer Interface Conference 2017 DOI: 10.3217/978-3-85125-533-1-40

TOWARDS A COGNITIVE MODEL OF MI-BCI USER TRAINING

C. Jeunet[1,2], B. N'Kaoua[1], F. Lotte[2]

[1]Handicap Activity Cognition Health Lab, University of Bordeaux, France
[2]Potioc Project-Team, Inria / CNRS / University of Bordeaux, Bordeaux, France

E-mail: camille.jeunet@inria.fr

ABSTRACT: Mental-Imagery based Brain-Computer Interfaces (MI-BCIs) enable users to control applications using their brain activity alone, by realising mental-imagery tasks. Although promising, MI-BCIs remain barely used outside laboratories, notably due to the difficulties users encounter when attempting to control them. We claim that understanding and improving the user-training process could greatly improve users' MI-BCI control abilities. Yet, to better understand the training process, we need a model of the factors impacting MI-BCI performance. In other words, we need to understand which traits and states impact MI-BCI performance, how these factors interact and how to influence them to improve this performance. Such a model would enable us to design adapted and adaptive training protocols, to guide neurophysiological analyses or design informed classifiers, among others. In this paper we propose a theoretical model of MI-BCI tasks, which is the first step towards the design of this full cognitive and computational model.

INTRODUCTION

Mental-Imagery based Brain-Computer Interfaces (MI-BCIs) enable users to control an application using their brain activity alone, through the realisation of mental imagery tasks. For instance, using MI-BCIs, paralysed patients can control a wheelchair by imagining left/right hand movements to make the wheelchair turn left/right, respectively [33]. Although very promising for a wide range of applications, MI-BCIs remain barely used outside laboratories, in particular due to the difficulties users encounter when attempting to control them. Indeed, 10 to 30% of users are unable to control MI-BCIs [3].

Two main factors have been identified to explain the low reliability of MI-BCIs. The first, which has been extensively investigated, concerns brain signal processing, current classification algorithms being still imperfect [3]. On the other hand, the potential role of user-training in MI-BCI performance requires much further investigation. Controlling an MI-BCI requires the acquisition of specific skills, and particularly the ability to generate stable and distinct MI brain activity patterns [21]. An appropriate training procedure is required in order to acquire these skills and an inefficient training protocol could consequently be partly responsible for users' modest performances. Yet, although current training protocols are theoretically inappropriate for skill-acquisition, rather little research is done towards their improvement [10]. We claim that understanding and improving the user-training process could greatly improve MI-BCI performance.

In [11], we reviewed the available literature on MI-BCI training protocols, which gave rise to several guidelines for the design of MI-BCI training protocols. For instance, regarding the *instructions*, it appears promising to explicitly specify the object of the training process. Furthermore, we should provide *training tasks* that are specific to each user. Then, visual *feedback* with emotional connotations seems to increase user motivation levels and, consequently, performance, although formal comparisons with non-emotional feedback are missing. Finally, it has been shown that gamifying the *training environment* increases motivation, and consequently performance.

These guidelines show that several promising avenues regarding the training protocols have been explored. Unfortunately, such studies remain scarce and, critically, their results are rarely taken into account by the BCI community. By building on theories in disciplines such as psychology and instructional design, it is possible to suggest new approaches for further improving user performance. However, being able to do so requires to understand the MI-BCI training process, and how it is impacted by users' specificities, in order to adapt the training protocols to their individual profiles. In order to reach a better understanding of the training process, we need a model of the factors impacting MI-BCI skill acquisition. In other words, we need to understand which users' traits and states impact MI-BCI performance, how these factors do interact and how to influence them through the experimental design or specific cognitive training procedures in order to improve MI-BCI performance. Such a model is called a *Cognitive Model*. Busemeyer and Diederich describe cognitive models as models which aim to scientifically explain one or more cognitive processes or how these processes interact [7]. Three main features characterise cognitive models: (1) their goal: they aim to explain cognitive processes scientifically, (2) their format: they are described in a formal language, (3) their background: they are derived from basic principles of cognition [7]. Cognitive models guarantee the production of logically valid predictions, they allow precise quantitative predictions to be made and they enable generalisation [7].

In the context of BCIs, developing a cognitive model is

Published by Verlag der TU Graz
Graz University of Technology

 DOI: 10.3217/978-3-85125-533-1-40

a huge challenge due to the complexity and imperfection of BCI systems. Indeed, BCIs suffer from many limitations, independent from human learning aspects, that could explain users' modest performance. For instance, the sensors are often very sensitive to noise and do not enable the recording of high quality brain signals while the signal processing algorithms sometimes fail to recognise the correct mental command. But it is also a huge challenge due to the lack of literature on the topic and to the complexity and cost associated with BCI experiments that are necessary to increase the quantity of experimental data. Nonetheless, as stated earlier, a cognitive model would enable to reach a better understanding of the MI-BCI user-training process, and consequently to design adapted and adaptive training protocols. Additionally, it would enable us to guide neurophysiological analyses by targeting the cognitive and neurophysiological processes involved in the task. Finally, it would make it possible to design classifiers robust to variabilities, i.e., able to adapt to the model factors. To summarise, building such a model, by gathering the work done by the whole BCI community, could potentially lead to substantial improvements in MI-BCI reliability and acceptability.

Different steps are required to build a cognitive model [7]. First, building a cognitive model requires a formal description of the cognitive process(es) to be described based on conceptual theories. Next, since the conceptual theories are most likely incomplete, *ad hoc* assumptions should be made to complete the formal description of the targeted cognitive process(es). Third, the parameters of the model, e.g., the probabilities associated with each element of the model, should be determined. Then, the predictions made by the model should be compared to empirical data. Finally, this process should be iterated to constrain and improve the relevance of the model.

In this paper, we propose to do the first step of this process: the formal description of the cognitive processes involved. Therefore, in a first section, we will introduce briefly the different factors depicted in the literature as influencing MI-BCI performance. Then, we will describe the first step of the cognitive model. Finally, we will propose future work that will aim at completing the model.

FACTORS IMPACTING MI-BCI PERFORMANCE

In [12] we proposed a literature survey dedicated to the description of the factors impacting MI-BCI performance, also called predictors. It has to be noted that we used the classification accuracy as a measure of performance, as most current MI-BCI studies do. This survey enabled us to classify most of the predictors into three categories representing higher-level cognitive concepts:

Category 1 - The user-technology relationship & the notion of control: indeed, it appears that people who apprehend the use of technologies (and more specifically the use of BCIs) and who do not feel in control, experience more trouble controlling BCIs. This category gathers different concepts such as self-efficacy, mastery confidence, sense of agency, computer anxiety or self-reliance.

Category 2 - Attention: this category includes both attentional abilities (trait) and attention level (state). The latter can fluctuate with respect to different parameters such as mood or motivation. Both these aspects of attention have been repeatedly suggested to be predictors of BCI performance, and more generally of learning performance.

Category 3 - Spatial Abilities: many predictors depicted in the literature are related to motor abilities (e.g., 2-hand coordination) or to the ability to produce mental images (e.g., kinaesthetic imagination). These predictors can be gathered under the label of "spatial abilities", which are described as the ability to produce, manipulate and transform mental images [28].

As explained in [12], the involvement of *Category 1* predictors can be explained by the fact BCI users were naïve [1], while the involvement of *Category 2* and *Category 3* predictors is relevant with the Ackerman model [2]. Indeed, this model states that inter-individual differences of performance in early stages of training are due to differences in attentional (*Category 2* predictors) and task-specific (*Category 3*) abilities. Interestingly enough, this model was already used by Neumann and Birbaumer to interpret BCI performances in 2003 [20].

COGNITIVE MODEL - STEP #1: DESCRIPTION OF THE COGNITIVE PROCESSES

While our survey in [12] enabled us to gather the BCI performance predictors into 3 categories, it lacks a global view of the relationships between these factors, of how they interact to impact MI-BCI performance and of how they can be influenced by external factors. We propose to fill this lack in this section. It should be noted that we only considered the factors that are supposed to impact performance based on the MI-BCI literature: thus, several relevant factors, that have not yet been studied by the BCI community, are likely to be missing. They will be investigated in the second phase of the construction of this model. Also, since we are dealing with a model, it is of course only a simplified representation of the complex cognitive processes underlying MI-BCI tasks that will require formal validation, testing and updating in the future.

To provide a formal description of the cognitive processes leading to good BCI performances, two steps had to be completed. First, we described both the intrinsic factors (i.e., users' states and traits) which impact performance as well as the connections between these factors. Then, the extrinsic elements impacting the users' states/traits, and consequently their performance, as well as the nature of this impact was formalised. These extrinsic elements include design artefacts and different cognitive activities or exercises. The next paragraphs are dedicated to the description of both these stages.

Stage 1 - Building a Model of the Intrinsic Factors Influencing MI-BCI Performance

The intrinsic factors included in this model correspond

Published by Verlag der TU Graz
Graz University of Technology

 DOI: 10.3217/978-3-85125-533-1-40

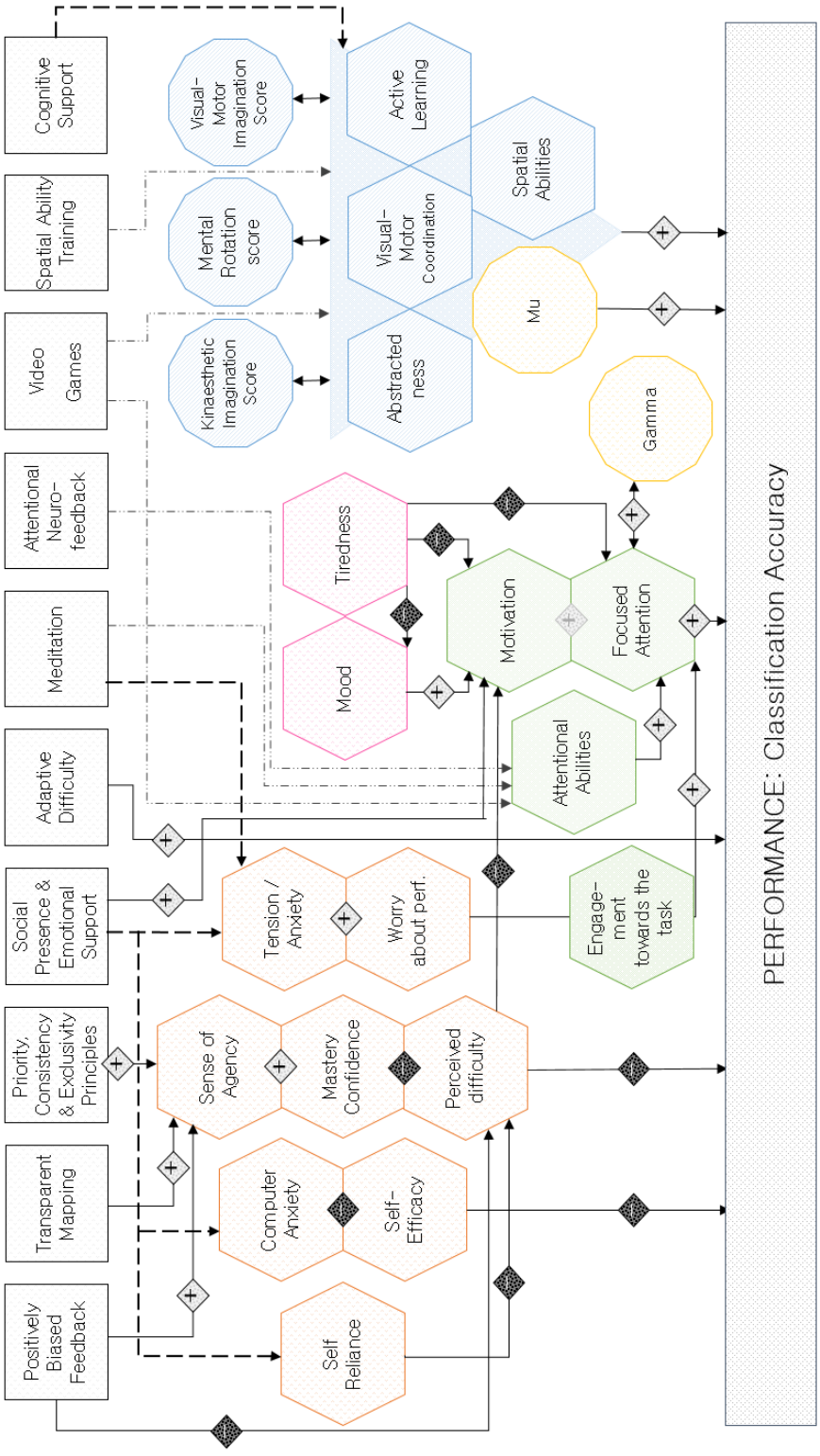

Figure 1: This network gathers the factors impacting MI-BCI performance, according to the literature and the extrinsic elements that can influence these factors. The factors are represented by hexagons. The circles represent ways to measure these factors: they are either neurophysiological markers or psychometric test scores. Moreover, vertically juxtaposed hexagons as well as unidirectional arrows represent causal relationships (if factor A is above factor B, then factor A influences factor B). The plus and minus signs indicate if the causal relationship between 2 factors is positive or negative. Concerning the links with extrinsic factors, solid lines represent a "direct influence on user state", dashed lines correspond to a "Help for users with a specific profile" while dash-dot lines represent extrinsic factors that can "Improve abilities".

Published by Verlag der TU Graz
Graz University of Technology

 DOI: 10.3217/978-3-85125-533-1-40

on the one hand to users' cognitive and motivational states and on the other hand to users' traits, i.e., personality traits and malleable cognitive abilities that can be trained. All these factors are represented as hexagons in the model, see Figure 1. The circles represent ways to measure these factors: they are either neurophysiological markers or psychometric test scores. Moreover, the plus and minus signs indicate if the causal relationship between 2 factors is positive or negative. Subsequently, we briefly describe all the factors included in the model. For more information about these factors or the studies that revealed their relationship with MI-BCI performance, please refer to our review of performance predictors in [12]. This first model can be divided into 3 main parts, corresponding to the 3 categories of predictors mentioned earlier. On the left of the model we can find the factors related to the user-technology relationship (in orange), in the middle, those related to attention (in green) and to mood (in pink) and on the right, the factors related to the ability to perform an MI-task (in blue). All these factors can modulate the user's ability, at a given moment in time, to perform a MI task and to reach good performance. Each of these blocks is described more precisely in the following paragraphs.

Factors pertaining to the user-technology relationship are gathered on the left of Figure 1. Users showing low self-reliance traits, according to the 16-PF5 test [8], tend to perceive the task as more difficult [19]. Moreover, the phenomenon of computer anxiety, that is to say the apprehension of the user towards BCI use, has been shown to reduce users' self-efficacy [29], which in turn will induce a higher perceived difficulty [6] and a decrease in performance. On the other hand, by reducing computer anxiety, and consequently improving self-efficacy, it is possible to improve users' engagement towards the task and thus their motivation and performance [1]. This can be explained by the fact that self-efficient users do not consider difficulty as a threat but as a challenge which encourages them to persevere to reach good performance [1]. In order to reduce computer anxiety, the sense of agency should be improved. Besides, a high sense of agency will also increase the feeling of mastery of the system and consequently reduce perceived difficulty, increase motivation and performance [31]. Finally, tense(anxious) users tend to have lower performances which is notably due to the fact they devote a lot of resources to off-task considerations (such as worrying about their performance) and thus have fewer resources to allocate to focusing attention on the task [6]. To summarise, in order to enable users to reach good performance, training protocols should enable them to experience a high sense of agency and a low level of computer anxiety. Also, protocols should be adapted to non self-reliant and highly tense users so that their personality does not hinder their progress.

Tiredness has a negative impact on motivation, focused attention and mood. However, a good mood positively affects motivation and performance [25]. Then, the block in the middle comprises factors related to attention. We have previously shown that engagement towards the task as well as motivation are modulated by the user-technology relationship and by users' state (mood and tiredness). Motivation as well as general attentional abilities will determine how much focused attention is dedicated to the MI-BCI task. The more resources are allocated to the task, the better the performance. One neurophysiological predictor has been shown to correlate with attention state: the central gamma power (in attentional networks related to executive control - [9]).

Finally, on the right of the model the elements represent the various factors that have been suggested to be related to the ability to perform MI tasks. Indeed, abstractedness abilities correspond to the ability to produce mental images [8]. Also, visual-motor coordination is one aspect of spatial abilities. Finally, active learners prefer "learning by doing" [16] and might thus be more prone to producing kinaesthetic mental images, which have been shown to be more efficient than visual ones [22]. These abilities can be measured by different scores such as the Kinaesthetic Imagination score, the Visual-Motor Imagination Score [32] or the Mental Rotation Score [30] (the latter correlating with BCI performance [13, 10]). Moreover, the mu rhythm could enable, to a certain extent, to measure the ability to perform motor-imagery. Indeed, [4] have shown that a high mu amplitude at rest correlates with motor-imagery based BCI performance.

Stage 2 - A First Attempt at a Cognitive Model of the Task

Once all the intrinsic factors had been integrated into a network, we added the extrinsic elements that can be seen as levers to optimise users' performance, see Figure 1. These extrinsic elements are mainly based on theoretical hypotheses. Their impact on the users' states, traits and performance are yet to be quantified. Thus, although these links make sense from a theoretical point of view, they should still be considered with caution. These extrinsic elements are of two kinds: design artefacts and cognitive activities. We determined three types of links between the extrinsic elements and the intrinsic factors: *"Direct influence on user state"* (solid lines): this link connects extrinsic elements in the "design artefacts" category to intrinsic states (mainly). These extrinsic factors are suggested to influence the user's state and, consequently, are likely to have a direct impact on performance. For instance, proposing a positively biased feedback has been suggested to improve (novice) users' sense of agency [17]. *"Help for users with a specific profile"* (dashed lines): this link connects extrinsic elements to traits; they indicate that these extrinsic elements could help users who have a specific profile to improve their performance. For instance, proposing an emotional support has been suggested to benefit highly tense users [26]. *"Improved abilities"* (dash-dot lines): finally, this link connects extrinsic elements in the "cognitive activities" category to abilities that could be improved thanks to these activities. For instance, attentional neurofeedback has been suggested to improve attentional abilities [34].

Published by Verlag der TU Graz
Graz University of Technology

 DOI: 10.3217/978-3-85125-533-1-40

The extrinsic elements related to the experimental design that theoretically impact users' state are listed hereafter. First, providing novice users with a positively biased feedback [17] is thought to improve their sense of agency and consequently decrease perceived difficulty and increase their motivation. Then a transparent mapping as well as the priority, consistency and exclusivity principles [31] all aim to improve users' sense of agency. Moreover, providing users with emotional support and social presence could improve their motivation [26]. Emotional support can be provided as smileys or avatars, but not only. It is also important not to forget the role of the therapist/researcher/experimenter, notably concerning: (1) the demystification of the BCI technology to reduce a priori computer anxiety, through scientific mediation and communication with the media, (2) the writing of informed-consent forms and explanations, that should be clear and informative, and provide an objective estimation of the benefit on risk balance and enable to regulate any form of hope that may be generated [24], and (3) the social presence and trust relationship with the user, which are essential in facilitating the learning process [15]. Finally, adapting the difficulty and proposing progressive difficulty has also been suggested to improve performance [33]. On the other hand, meditation, emotional support and social presence have been suggested to help highly tense and non-autonomous users [27]; while cognitive support (i.e., guidance to find a good strategy) could help users to produce mental-images that the system can recognise efficiently. Finally, the last type of links (dash-dot links) connects cognitive activities/exercises to the specific abilities they could benefit. Indeed, video-games, meditation and attentional neurofeedback have been suggested to improve attentional abilities [5]; while video-games and spatial-ability exercises may improve the ability to create mental-images.

FUTURE WORK

The model proposed comprises intrinsic factors impacting BCI performance, their relationships, as well as extrinsic factors that can be manipulated to modulate BCI performance. This model has been built based on the BCI and skill acquisition literature. As such, it represents the first phase in the development of a cognitive model [7], here for MI-BCI tasks. The next phases will consist first in making assumptions about the missing factors that should be included. For instance, our model includes factors also present in the ARCS (Attention Relevance Confidence and Satisfaction) model [14], notably attention and confidence, but relevance and satisfaction are missing. Yet, they may prove meaningful as well for MI-BCI. Then, with all the factors and their relationships identified, we will have to computationally implement this model, e.g., using a Bayesian network, and thus to determine its parameters (i.e., the probabilities for each factor and the weights -impact- of each factor on the BCI performance). Ideally, this could be estimated from data. Finally, we will have to assess this computational model based on unseen BCI experiments data. It will also be worth considering alternative performance metrics, beyond classification accuracy [18]. This could indeed bring additional insights about MI processes.

CONCLUSION

In order to bring BCIs out of the lab, both their reliability and usability should be enhanced. To this end, all their components should be considered: EEG caps should be both reliable and aesthetic [23]; algorithms should enable the improvement of BCI robustness and reduction of the calibration time [35]; the user training should be improved [12]. In this paper, we focused on this last axis. Indeed, we have provided the first theoretical cognitive model of MI-BCI performance. This is the first step towards a full model of MI-BCI tasks, which appears necessary to fully understand and then improve MI-BCI user training approaches, as well as to inform MI-BCI signal processing tools. In the future, we are going to try to complement this model with additional relevant factors, start first computational implementations of it and collect additional data to make that implementation possible. We hope other BCI researchers could join us in that endeavour to contribute to make the full model a reality.

Acknowledgments: This work was supported by the IdEx Bordeaux and the French National Research Agency with the REBEL project and grant ANR-15-CE23-0013-01.

REFERENCES

[1] N. Achim and A. Al Kassim. Computer usage: The impact of computer anxiety and computer self-efficacy. *Procedia-Social and Behavioral Sciences*, 172:701–708, 2015.

[2] P. L. Ackerman. Determinants of individual differences during skill acquisition: cognitive abilities and information processing. *Journal of experimental psychology: General*, 117(3):288, 1988.

[3] B. Allison and C. Neuper. Could anyone use a BCI? In D. Tan and A. Nijholt, editors, *Brain-Computer Interfaces*, pages 35–54. Springer London, 2010.

[4] B. Blankertz, C. Sannelli, S. Halder, E. Hammer, A. Kübler, K.-R. Müller, G. Curio, and T. Dickhaus. Neurophysiological predictor of SMR-based BCI performance. *Neuroimage*, 51(4):1303–09, 2010.

[5] T. Brandmeyer and A. Delorme. Meditation and neurofeedback. *Frontiers in psychology*, 4, 2013.

[6] M. J. Brosnan. The impact of computer anxiety and self-efficacy upon performance. *Journal of computer assisted learning*, 14(3):223–234, 1998.

[7] J. R. Busemeyer and A. Diederich. *Cognitive modeling*. Sage, 2010.

Published by Verlag der TU Graz
Graz University of Technology

 DOI: 10.3217/978-3-85125-533-1-40

[8] R. B. Cattell and H. E. Cattell. Personality structure and the new fifth edition of the 16pf. *Educational and Psychological Measurement*, 55:926–37, 1995.

[9] M. Grosse-Wentrup. What are the causes of performance variation in brain-computer interfacing? *International Journal of Bioelectromagnetism*, 2011.

[10] C. Jeunet, E. Jahanpour, and F. Lotte. Why standard brain-computer interface (BCI) training protocols should be changed: an experimental study. *Journal of neural engineering*, 13(3):036024, 2016.

[11] C. Jeunet, F. Lotte, and B. N'Kaoua. *Brain-Computer Interfaces 1: Foundations and Methods*, chapter Human Learning for Brain–Computer Interfaces, pages 233–250. Wiley Online Library, 2016.

[12] C. Jeunet, B. N'Kaoua, and F. Lotte. Advances in user-training for mental-imagery-based BCI control: Psychological and cognitive factors and their neural correlates. *Progress in brain research*, 2016.

[13] C. Jeunet, B. N'Kaoua, S. Subramanian, M. Hachet, and F. Lotte. Predicting mental imagery-based BCI performance from personality, cognitive profile and neurophysiological patterns. *PLOS ONE*, 10(12):e0143962, 2015.

[14] J. M. Keller. *Motivational design for learning and performance: The ARCS model approach*. Springer, 2010.

[15] S. Kleih, T. Kaufmann, E. Hammer, I. Pisotta, F. Pichiorri, A. Riccio, D. Mattia, and A. Kübler. Motivation and SMR-BCI: fear of failure affects BCI performance. In *Proc. Int. BCI Meeting*, 2013.

[16] D. A. Kolb. *Learning style inventory*. McBer and Company, 1999.

[17] A. Kübler, N. Neumann, J. Kaiser, B. Kotchoubey, T. Hinterberger, and N. Birbaumer. Brain-computer communication: self-regulation of slow cortical potentials for verbal communication. *Arch Phys Med Rehabil*, 82:1533–39, 2001.

[18] F. Lotte and C. Jeunet. Online classification accuracy is a poor metric to strudy mental imagery based BCI user learning: an experimental demonstration and new metrics. *accepted - Int. BCI Conf.*, 2017.

[19] M. Miserandino. Children who do well in school: Individual differences in perceived competence and autonomy in above-average children. *Journal of Educational Psychology*, 88(2):203, 1996.

[20] N. Neumann and N. Birbaumer. Predictors of successful self control during brain-computer communication. *Journal of Neurology, Neurosurgery & Psychiatry*, 74(8):1117–1121, 2003.

[21] C. Neuper and G. Pfurtscheller. *Brain-Computer Interfaces*, chapter Neurofeedback Training for BCI Control, pages 65–78. 2010.

[22] C. Neuper, R. Scherer, M. Reiner, and G. Pfurtscheller. Imagery of motor actions: differential effects of kinesthetic and visual-motor mode of imagery in single-trial EEG. *Brain Res Cogn Brain Res.*, 25(3):668–677, 2005.

[23] F. Nijboer. Technology transfer of brain-computer interfaces as assistive technology: Barriers and opportunities. *Annals of physical and rehabilitation medicine*, 58(1):35–38, 2015.

[24] F. Nijboer, J. Clausen, B. Z. Allison, and P. Haselager. The asilomar survey: Stakeholders' opinions on ethical issues related to brain-computer interfacing. *Neuroethics*, 6(3):541–578, 2013.

[25] F. Nijboer, A. Furdea, I. Gunst, J. Mellinger, D. MacFarland, N. Birbaumer, and A. Kübler. An auditory brain-computer interface. *Journal of Neuroscience Methods*, 167(1):43–50, 2007.

[26] R. Nkambou, J. Bourdeau, and R. Mizoguchi. *Advances in intelligent tutoring systems*, volume 308. Springer, 2010.

[27] L. Pillette, C. Jeunet, B. Mansencal, B. N'Kaoua, R. N'Kambou, and F. Lotte. PEANUT: Personalised emotional agent for neurotechnology user-training. In *submitted*, 2017.

[28] S. E. Poltrock and P. Brown. Individual differences in visual imagery and spatial ability. *Intelligence*, 8(2):93–138, 1984.

[29] A. Simsek. The relationship between computer anxiety and computer self-efficacy. *Contemporary Educational Technology*, 2(3):177–187, 2011.

[30] S. G. Vandenberg and A. R. Kuse. Mental rotations, a group test of three-dimensional spatial visualization. *Percept Mot Skills*, 47:599–604, 1978.

[31] R. Vlek, J.-P. van Acken, E. Beursken, L. Roijendijk, and P. Haselager. BCI and a user's judgment of agency. In *Brain-Computer-Interfaces in their ethical, social and cultural contexts*, pages 193–202. Springer, 2014.

[32] A. Vuckovic and B. A. Osuagwu. Using a motor imagery questionnaire to estimate the performance of a brain–computer interface based on object oriented motor imagery. *Clinical Neurophysiology*, 124(8):1586–1595, 2013.

[33] J. Wolpaw and E. Wolpaw. *Brain-computer interfaces: principles and practice*. Oxford Press, 2012.

[34] T. Zander, B. Battes, B. Schoelkopf, and M. Grosse-Wentrup. Towards neurofeedback for improving visual attention. In *Proc Int BCI Meeting*, 2013.

[35] T. O. Zander, K. Ihme, M. Gärtner, and M. Rötting. A public data hub for benchmarking common brain–computer interface algorithms. *Journal of neural engineering*, 8(2):025021, 2011.

Published by Verlag der TU Graz
Graz University of Technology

Proceedings of the
7th Graz Brain-Computer Interface Conference 2017 DOI: 10.3217/978-3-85125-533-1-41

FEATURE EXTRACTION OF EVENT RELATED POTENTIAL BASED ON TIME AND FREQUENCY DOMAIN ANALYSIS

G. Kaur[1], N. K. Roma[1], B. Bhattacharya[1], P. Sircar[1]

[1]Indian Institute of Technology Kanpur, U.P., India

E-mail: gagank@iitk.ac.in

ABSTRACT: The event related potential is traditionally obtained in time domain by computing ensemble average. However, due to non-stationarity and poor localization of these signals, this may result in erroneous feature extraction. In this present study, a standard database is considered to elucidate this problem. It is shown that a frequency domain decomposition followed by the estimation of spectral distance by measures like Itakura-Saito distance may partially resolve the problem. However, recognizing the contribution of endogenous and exogenous inputs to each event related potential, it is further argued that a Wavelet Packet Decomposition may be more useful since each signal in the frequency domain can be further decomposed into five characteristic domains (delta, theta, alpha, beta, and gamma) and based on the feasibility of contributions from each domain a better feature extraction will be possible.

INTRODUCTION

Oddball paradigm is an experimental standard used in several studies to elicit event related potential (ERP) and analyze its subcomponents. In this paradigm, a visual stimulus is presented where a sequence of random elements are displayed with a high likelihood (80-90%), non-target stimuli and is interjected by a low likelihood (5-20%), the "oddball" stimuli, which might vary in duration and intensity [1].

The salience associated with stimulus ensures the occurrence of P300; more the event has an element of surprise to it, stronger is the response. Hence the stimulus should be designed in such a way that the desired event be randomly positioned and infrequently presented among a series of non-target events. The present study focuses on an enhanced component of ERP, the P3b observed at the parietal region; commonly known as the P300. It occurs around 300ms +/- 100ms after the onset of target stimulus. The amplitude of P300 varies directly with the relevance of the eliciting events and inversely with the probability of the stimuli [2].

The ERP waveform has the observable peaks and troughs; however, it has also the unobservable latent components. It is these latent components that give measure of neuronal response to visual stimulation task, the peaks are a summation of latent components. The latency, amplitude and duration of latent components vary across trials. Once the ensemble averaging over multiple trials is done, nothing can be ascertained about the behaviour of these components.Given this, latency and amplitude may not be sufficient measures to compare two ERPs [3].Additionally,ERP phase can also shift across trials,which would imply, that the signal to noise ratio will deteriorate after ensemble averaging. Using the well-known time-frequency inverse relation; it is hypothesized that a large shift in time latency will depict as a small variation in the frequency of ERP component. Thus, irrespective of shift in phase; using frequency as the feature could determine presence of P3b-ERP. To further argue the choice of frequency as a probable feature in a practical system, one may assume a small window of samples taken after each run. Within this window the amplitude and phase are non-deterministic whereas frequency is a deterministic parameter.While state of the art algorithms are well equipped to analyze deterministic signals, it is still challenging to investigate the non-deterministic signals.For some time, wavelet transforms have been used to observe ERPs by choosing appropriate mother wavelets and manipulation of bases functions gives a closer look at the wave shapes. This approach helps with choice of filters to be used, extraction of single trial ERP, breaking down ERP response into various frequency bands, detection of overlapping peaks[4]. [5] Another study discusses which single channel wavelet transform to auditory evoked potentials in cats. It also draws attention to limitations of sole reliance on amplitude and latency and highlights ability of wavelet transform to identify ERP components and effects of various experimental conditions on properties of these components. [6]This study used simulated EEG data generated using Gabor logons and chirped signals. To extract P300, time frequency transformation using morlet wavelet and reduced interference distribution (RID) are fed as inputs to principal component analysis (PCA). It reduced three dimensional data to two dimensional vectors which further retrieved P300 ERP. Wavelet analysis indicated that appreciable theta activity was related to the more novel non-target stimuli; primarily target component delta coefficients were affected by the discrimination difficulty variable. In the present study, it is proposed that a frequency domain analysis be followed after the time domain ensemble averaging. Further the ERP be decomposed and visualized in terms of basic brain rhythms using wavelet packet decomposition.

Published by Verlag der TU Graz
Graz University of Technology

 DOI: 10.3217/978-3-85125-533-1-41

MATERIALS AND METHODS

The present study uses P300 speller dataset from BCI competition III webpage with due acknowledgement [7].In the beginning, an ensemble average of a single trial, corresponding to a target is obtained; the spectral components of the signal are extracted, using DFT.Following this, the spectral components of all ensuing trials are computed. Subsequently, using some of the spectral distance measure techniques, the spectral distances between the initial trial and each of the subsequent trials are computed. It is assumed that if a threshold for each of these spectral distances is selected, and then target and non-target may be differentiated.

The input EEG signal is sampled at 240Hz.There are 85 epochs, each having a target character. Also an epoch contains 7794 samples, but for the purpose of ERP retrieval, individual trails are extracted from within each epoch. Each trial has 240 samples. The process of extracting samples from epochs can potentially corrupt the original signal by introducing noise. To avoid this, appropriate window functions are applied to the signal while deducting samples. Windows are selected so that the signal smoothly approaches zero at both ends.

The fast Fourier transform algorithm has been be used for ensemble average of each trial, i.e. 240 samples taken over 1000ms while DFT is designed for signal extending from 0 to ∞. For such a case, nothing can be known about the signal behavior outside the measured interval and the Fourier transform makes an implicit assumption; that the signal is repetitive. This assumption leads to discontinuities that are not really present in signal. Since sharp discontinuities have broad frequency spectra, this will cause frequency spectra to spread out. Consequently, the signal energy which should be concentrated only at one frequency instead leaks into other frequencies. This will lower the signal to noise ratio. Secondly, the spectral leakage from a large signal component may be severe enough to mask other smaller signals at different frequencies.

Thus, the signal is multiplied within the measurement-time, by some function that smoothly reduces the signal to zero at the end points; hence, avoiding the discontinuities altogether and curtailing the spectral leakage. Further it is expected to reduce the contribution of each frequency to one DFT bin.

The basic discrete Fourier transform (DFT) synthesis and analysis equations are

$$X[k] = \sum_{n=0}^{N-1} x[n] e^{jk\Omega_o n}, 0 \leq k \leq N-1 \qquad (1)$$

$$x[n] = \frac{1}{N} \sum_{k=0}^{N-1} X[k] e^{-jk\Omega_o n}, 0 \leq n \leq N-1 \qquad (2)$$

$X[k]$ and $x[n]$ are periodic sequences in frequency and time domains respectively. $X[k]$ is equal to samples of periodic fourier transform $X(e^{j\omega})$. $X[k]$ will be the transform of a periodic extension of $x[n]$ for n outside the interval $0 \leq n \leq N-1$. In defining DFT representation, we are recognizing that we are interested in values of $x[n]$ only in the interval $0 \leq n \leq N-1$ because $x[n]$ is really zero outside this interval. k represents discrete instances in frequency, n represents the number of samples in time, N the period, j represents $\sqrt{-1}$, Ω_o represents discrete frequency [8].

Distance measure is a common technique used to measure difference between a model/estimate(s) and its observations.The spectral distances are computed using second order properties of signal. Current study uses asymmetric and symmetric distance measures to gauge target and non-target ERP responses.

The Itakura-saito distance measure is defined as

$$D_{IS}(P(w_k), \widehat{P}(w_k)) = \frac{1}{N} \sum_{k=0}^{N-1} \frac{|X[k]|^2}{\left|\widehat{X}[k]\right|^2} - \frac{1}{N} \sum_{k=0}^{N-1} \left[\log \frac{|X[k]|^2}{\left|\widehat{X}[k]\right|^2} - 1 \right] \qquad (3)$$

where $k = 0, 1, ..., N-1$ and $P(w_k) = |X[k]|^2$

It is a measure of difference between original spectrum (template P300 in present context) $P(w)$ and a typical observation that can be considered as an approximation $\widehat{P}(w)$ of that spectrum. It is intended to reflect structural dissimilarity. Further Itakura-Saito distance is a Bregman divergence which is not a true metric since it fails to meet the symmetry and inequality axioms.

Spectral distances between two spectral densities $P(w_m)$ and $\widehat{P}(w_m)$ can be measured using L_q norm of the difference between them, depicted as;

$$D(P(w_m), \widehat{P}(w_m)) = \left\| P(w_m) - \widehat{P}(w_m) \right\|_q \qquad (4)$$

Such distances satisfy triangular inequality and symmetry property and are thus true distances [9].

A spectral distance measure D can be symmetrized by extending D_{IS} as shown:

$$D_{cosh} = \frac{1}{N} \sum_{m=1}^{N} \left[\frac{P(w_m)}{\widehat{P}(w_m)} - \log \frac{P(w_m)}{\widehat{P}(w_m)} + \frac{\widehat{P}(w_m)}{P(w_m)} \right] - \frac{1}{N} \sum_{m=1}^{N} \left[\log \frac{\widehat{P}(w_m)}{P(w_m)} - 2 \right] \qquad (5)$$

One of the main spectral deviation measures is log spectral, defined by L_q norm of difference between log of spectra $D = \left\| \log \frac{P(w_m)}{\widehat{P}(w_m)} \right\|_q$ where $q = 2$ for root mean square (rms) or the mean quadratic distance given below:

$$D_{rms} = \frac{1}{2N} \sum_{m=1}^{N} \left[\log \frac{P(w_m)}{\widehat{P}(w_m)} \right]^2 \qquad (6)$$

Published by Verlag der TU Graz
Graz University of Technology

 DOI: 10.3217/978-3-85125-533-1-41

Given a signal, the wavelet packet decomposition filters the signal into equal low-frequency and high-frequency subspaces. Present study uses MATLAB software for wavelet packet decomposition. Averaged trials from individual epochs were the input signals and decomposition into the lower frequencies was repeated till level 5. Daubechies wavelet of order 8 was used as the mother wavelet. The outcome was signals divided into delta, theta, alpha, beta, gamma activity.

RESULTS AND DISCUSSION

Ensemble averaging is one of the most popular time domain methods for extraction of ERP signatures. During the course of present investigation, it was found that this signature makes significant departure from its known pattern across trials. Fig. 1-3,are manifestations of the same. Fig. 1-3 are time domain ensemble average of target and non-target responses at frontal (Fz), Parietal (Pz) and occipital (Oz) electrodes, taken over duration of one second. In Figures 1 and 2, the target responses peaks at nearly 450 ms though the peaks begin to appear around 200 ms, modulated by a higher frequency noise. Both patterns closely match upto an expected ERP. It has to be noted though that they are not same, because, while what appeared at Pz correspond to P3b component, the response to rare target, in an oddball paradigm. The response at Fz is directing to P3a component which corresponds to non-target [10]. This distinction is important to make, in order to choose the right channel for analysis.

A marked departure from the said pattern can be seen in Fig. 3, which is a time domain ensemble average of target responses computed over central midline at the occipital lobe. Contrary to the norm, there is rather a dip spreading across 250-380 ms. One possible explanation could be that the ERP response is getting superimposed by a more prominent activity at the occipital lobe [11]. It is imperative to recognize the patterns associated with non-target responses. Ideally a non-target stimulus does not elicit the endogenous ERP component, specifically peak around 300ms. For example, the non-target in Figures 1 and 2 depicts compliance to the rule, while in Fig. 3, it does not. An small unanticipated peak appears between 300-400ms. A classifier such as PCA which is not able to handle jitters will not be able to make the system very much efficient with such responses in given signal. The present study proposes to compute spectral distances between two spectra. One is a fixed spectrum, that of a template or estimated ERP. The other is a dynamic spectrum which changes with each trial; in other words, spectrum of each subsequent trials. Itakura-Saito reveals the spectral distances between the two. The procedure to compute Itakura-Saito distance is as follows: 1- The first input is estimated and its spectrum is computed as follows: The grand average of responses to target stimuli for a single channel is taken.

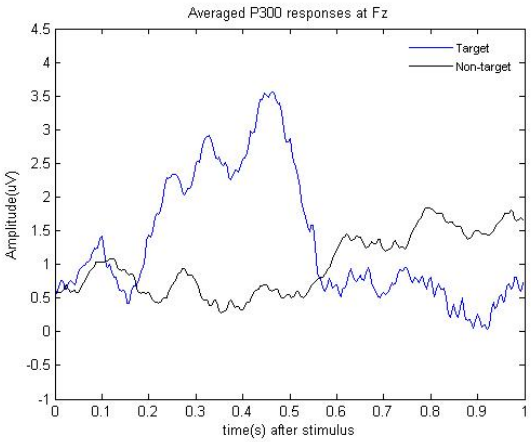

Figure 1: Target(T) and Non-Target(NT) responses at Fz.

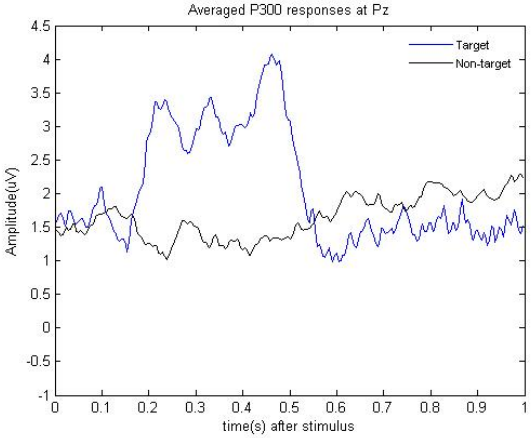

Figure 2: Target(T) and Non-Target(NT) responses at Pz.

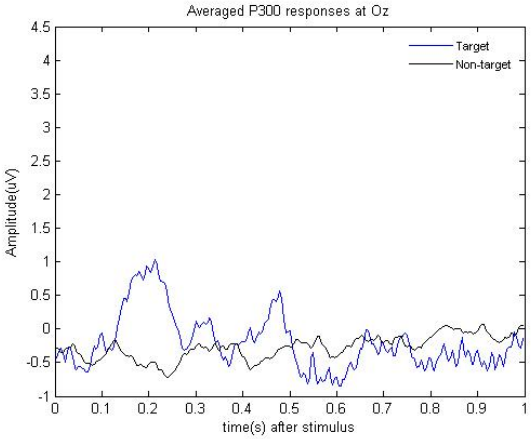

Figure 3: Target(T) and Non-Target(NT) responses at Oz.

To avoid high frequency noise modulation an appropriate window function is applied right before it is mapped onto the frequency domain using DFT. The spectral components thus retrieved are considered as desired markers of an ERP.

Published by Verlag der TU Graz
Graz University of Technology

 DOI: 10.3217/978-3-85125-533-1-41

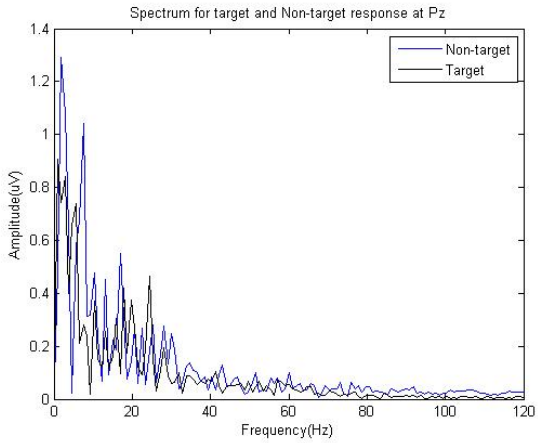

Figure 4a Frequency spectrum for target and non-target responses at Pz.

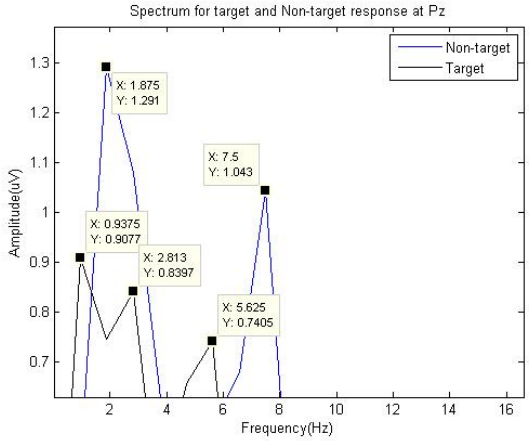

Fig 4b Closer look at frequency spectrum for target and non-target responses at Pz.

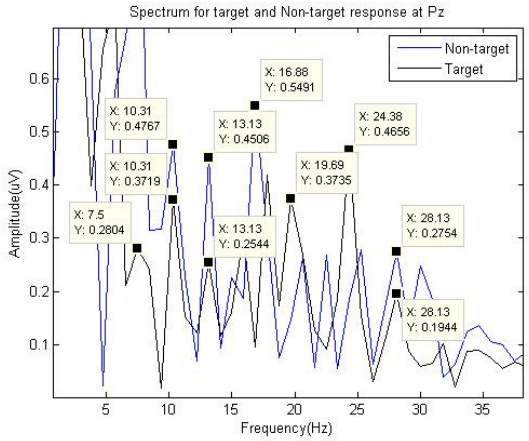

Fig 4c Closer look at frequency spectrum for target and non-target responses at Pz.

2- The template evaluated in earlier step is compared with respect to spectral components of each subsequent trial. These spectral components are computed in a similar fashion as described in the above step.

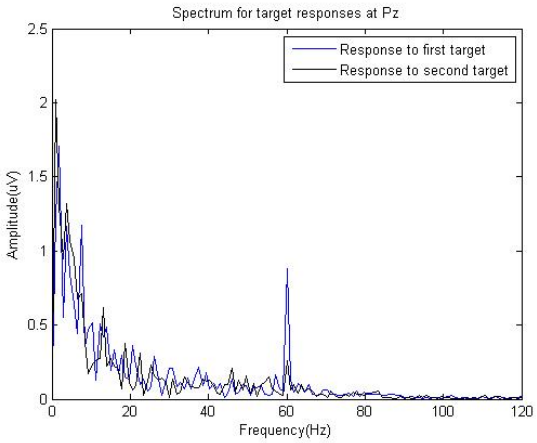

Figure 5a: Frequency spectrum for two target responses at Pz.

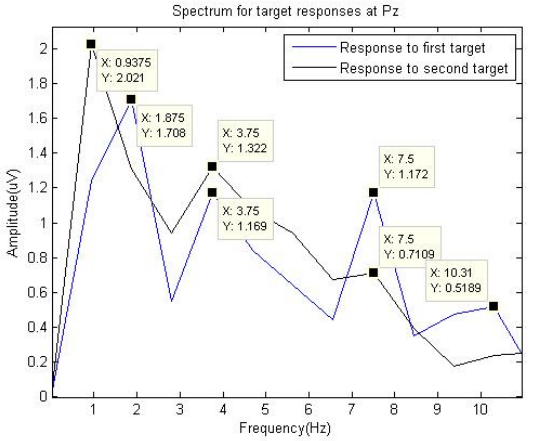

Figure 5b: Closer look at frequency spectrum for two target responses at Pz.

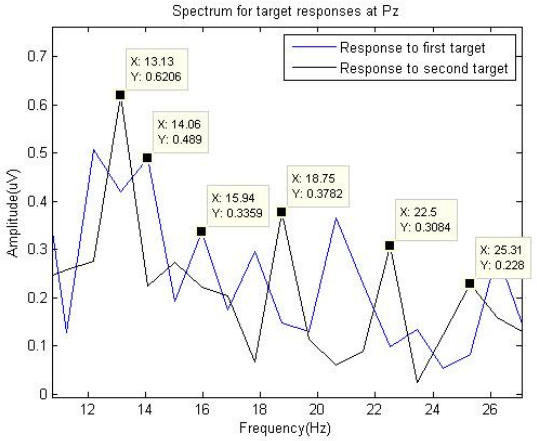

Figure 5c: Closer look at frequency spectrum for two target responses at Pz.

3- The Power spectra for estimated spectra as well as of individual trials are computed to evaluate the Itakura-Saito distance as described in equation (3). The Itakura-Saito distances was measured between, a target and a non-target, as well as, between two targets and following interesting observation were made. Ideally the frequency components while attending to the target and non-target

Published by Verlag der TU Graz
Graz University of Technology

 DOI: 10.3217/978-3-85125-533-1-41

stimulus should differ, as attention to a target stimulus should elicit ERP response containing peak component at 300ms after stimulus onset. It was observed that both target and non-target responses had overlapping frequency components, to a certain degree Figures 4,5. Frequency spectrum of target responses between two trials is shown in Fig.5a-c, again while some components are overlapping; a disparity can also be observed. It can be explained by going back to jitter effects between trials in time domain.

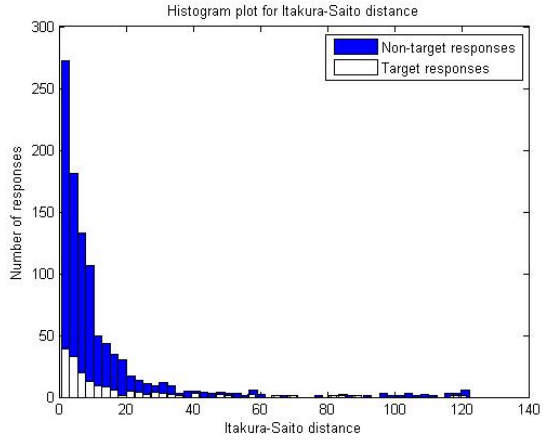

Figure 6: Itakura-Saito distance measure between the response corresponding to target stimuli and the non-target stimuli.

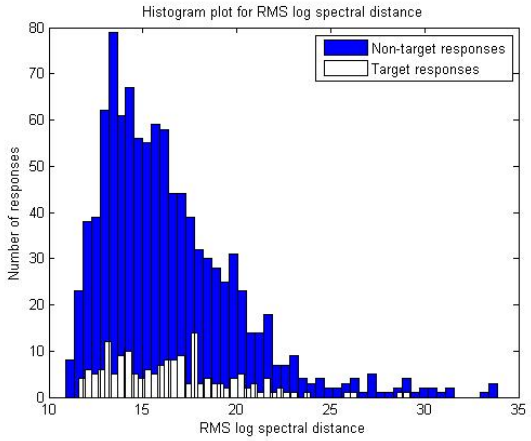

Figure 7: RMS Log Spectral distance measure between the response corresponding to target stimuli and the non-target stimuli.

Given the non-stationary nature of EEG signals, and presence of both endogenous and exogenous components in the ERP response these manifestations are hard to deal with by a simple mapping from time to frequency domain. This ambiguity calls for a more specific decomposition of the ERP. The overlap in frequency components of both targets and non-targets demands that the endogenous component, which is unique to target response be separated.

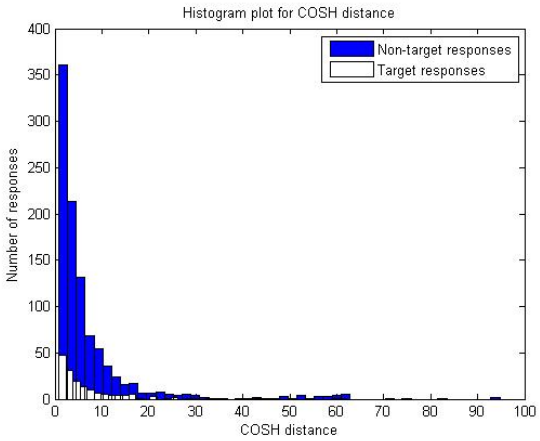

Figure 8: COSH distance measure between the response corresponding to target stimuli and the non-target stimuli.

In order to achieve this, wavelet packet decomposition (WPD) could be carried out, using an appropriate basis function. This shall be explained later in this section. If a standard pattern manifests every time an ERP is elicited, a measurement of spectral distance between a template target spectrum and response of subsequent ERP trials will be able to classify between target and non-target. Fig. 6-8 illustrate spectral distance measures between targets and non-targets for which, Pz channel is selected. At first, an asymmetric spectral distance measure is computed using Itakura-Saito distance. This distance is calculated between estimated spectrum and individual trials. The range of Itakura–Saito distance lies within 0-120 units which are divided in 50 bins. 87.5% of Nontarget and 81.1% of target responses falls within 0-25 units. This shows that high percent of both target and non-target stimuli lie in the same range and hence results in poor detection of target responses. It also depicts the generalization of our said observation for Fig. 4 and 5 across all trials. As the detection of target responses in Itakura-Saito became intricate, symmetric spectral distance measures were attempted. Here, RMS log spectral and COSH spectral distances were computed and their outcomes are shown in Fig. 7 and 8. In Fig. 7, RMS log spectral distance varies between 11- 22 units which is divided into 50 bins. 92.5% of nontarget and 94.7% of target stimuli falls within above range. It is observed that the responses are broadly distributed over a large range of distance. In Fig. 8, 91.5% of non-target and 88.2% of target responses are between 0-20 units of COSH distances. Consequently, the differentiation of target stimuli from non-target becomes obscure in both symmetric as well as asymmetric spectral distance measure methods. At this juncture, instead of looking at the ERP as a whole, wavelet packet decomposition was used to separate the ERP to lower frequency bands. After wavelet packets decomposition, an ERP could be visualized in terms of delta, theta, alpha, and beta rhythms. Fig. 9 shows decomposition of target and non-target activity at Pz.

Published by Verlag der TU Graz
Graz University of Technology

 DOI: 10.3217/978-3-85125-533-1-41

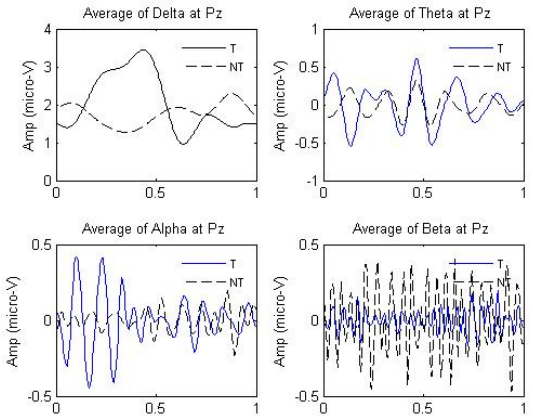

Figure 9: Average Delta, Theta, Alpha and Beta activities at Pz, corresponding to Target(T) and Non-Target(NT) responses.

As ERP is not a single response but rather a coagulation of exogenous and endogenous responses to the visual stimulation; coming from a highly non-linear system, the human brain. Decomposing ERP into multiple frequency bands rather than visualizing it as a whole shall be more befitting approach, to extract the endogenous P3b response to target stimuli.In present work when target and non-target responses were decomposed into multiple frequency bands using wavelet packet decomposition, Fig. 9. The delta rhythm associated with target has higher amplitude than for non-target. Theta activity is known to increase with increasing memory load; a slightly higher theta activity was observed for target responses. Alpha activity for target stimulus had higher amplitude compared to non-target when observed at Pz. The alpha activity is associated with idle state of brain region under consideration. But this statement would be an oversimplification given the fact that, different areas of brain possess their unique alpha activity. Parietal alpha power is known to increase as task load increases. There is a marked difference between beta activity of target and non-target. Such can be considered as a feature which can be used for classification between targets and non-targets. By keeping these results as basis, we will continue to take on a more thorough investigation on ERP components and identify more features for robust target classification.

CONCLUSION

The present study summoned up the non-stationary nature of event related potentials. On that premise, a scrutiny of common approaches for extraction of event related potentials from raw EEG data was instigated. The limitations of those approaches were accounted and the study proceeded to computation of spectral distance measures expecting to mark distinction between target and non-target ERP responses.

ACKNOWLEDGEMENTS

This work used BCI competition-III dataset provided by Wadsworth Center, NYS Department of Health (Jonathan R. Wolpaw, Gerwin Schalk, Dean Krusienski). The authors are thankful to Professor K.S. Venkatesh for providing time, space and resources for discussions and critical reviews.

REFERENCES

[1] Pfurtscheller G, Lopes da Silva FH. Handbook of Electroencephalography and Clinical Neurophysiology – Event-related desynchronization, Elsevier, Amsterdam, Netherlands (1999).Steven J. Luck, An Introduction to the Event-Related Potential Technique, Massachusetts Institute of Technology (2005).

[2] Neal R. Swerdlow (Ed.), Behavioral Neurobiology of Schizophrenia and Its Treatment. Springer-Verlag Berlin Heidelberg, April 2010 pp. 287.

[3] Luck, S. J. Ten Simple Rules for Designing and Interpreting ERP Experiments. In: Handy, TC (Ed.) Event-Related Potentials: A Methods Handbook.(2004), pp.20-30.

[4] Samar VJ, Swartz KP, Raghuveer MR. Multiresolution analysis of event-related potentials by wavelet decomposition. Brain and cognition. 1995 Apr 30;27(3):398-438.

[5] Raz J, Dickerson L, Turetsky B. A wavelet packet model of evoked potentials. Brain and Language. 1999 Jan 31;66(1):61-88.

[6] Bernat EM, Williams WJ, Gehring WJ. Decomposing ERP time–frequency energy using PCA. Clinical Neurophysiology. 2005;116(6):1314-34.

[7] G.Schalk, Dean Krusienski, 'BCI Competition III Challenge 2004', Wadsworth BCI Dataset (P300 Evoked Potentials), Data Acquired Using BCI2000's P3 Speller Paradigm.

[8] Alan V. Oppenheim and Ronald W. Schafer. The discrete Fourier Transform. In:Discrete-Time Signal Processing (3rd ed.). Prentice Hall Press, Upper Saddle River, NJ, USA, 2009, pp.669.

[9] Basseville M., Distance measures for signal processing and pattern recognition. Signal Processing. 1989 Dec 1;18(4):349-69.

[10] Polich J. Updating P300: an integrative theory of P3a and P3b. Clinical Neurophysiology. 2007 Oct 31;118(10):2128-48.

[11] Juri D. Kropotov, Beta Rhythms. In: Kropotov JD.Quantitative EEG, event-related potentials and neurotherapy. Academic Press; 2010 Jul 28.

Published by Verlag der TU Graz
Graz University of Technology

Proceedings of the
7th Graz Brain-Computer Interface Conference 2017 DOI: 10.3217/978-3-85125-533-1-42

RESTING EEG-BASED SUBJECT IDENTIFICATION SYSTEM: A PRACTICAL SCENARIO FOR OFFLINE ANALYSIS

D. Kim, K. Kim

School of Electrical Engineering and Computer Science, Gwangju Institute of Science and Technology, Gwangju, South Korea

E-mail: {dhkim518, kskim}@gist.ac.kr

ABSTRACT: Rapid advancements in brain-computer interfaces (BCIs) have fostered the wide-spread application of biometric systems built on electroencephalography (EEG) measurements in recent years. While current subject identification approaches exhibit high performance, most efforts rely on limited number of EEG recording runs to validate the feasibility and practical usability of EEG-based biometric systems. For a realistic system however, quantitative assessment over long time series is essential due to the intrinsic non-stationary behaviour of EEG signals. In this work, we propose a more practical scenario of the resting EEG-based subject identification system for off-line analysis using public dataset. Moreover, we implement a subject recognition system based on widely-adopted functional connectivity measures. The system is applied to assess performance variations under consecutive EEG recording runs over time. We also provide a simple approach to overcome the performance degradation and eventually, raise several issues as potential future works relating EEG-based systems.

INTRODUCTION

In spite of copious research in BCI technology and its applications in neuroscience and cognitive psychology, it is only recently that the possibility of EEG measurement utilization in biometric systems has emerged [1-3]. Unlike existing technologies that use fingerprints, speech, iris, and facial features as identifiers for human authentication, EEG signal stands out as a unique physiological biometric that is robust against forgery and falsification.

Various paradigms have been proposed for biometric systems based on event-related potentials (ERP) [4,5] or specific tasks related mental states [6]. Since these brainwaves are evoked after a specific time onset, the system is possible to utilize the temporal characteristics of brain signals. Nonetheless, EEG in resting state manifest beneficial advantages regarding user-friendliness in that it does not require additional stimulatory devices and any conditions/ instructions for subjects. In addition, the high potentials of biometric systems based on resting state EEG should not be undermined as these resting state signals differ considerably among subjects [7].

State-of-art studies of brain functional connectivity modulated by resting state networks have advanced our understanding of human brain functions. The traits of functional connectivity are reported to fully exploit physiological information and represent functionally coupled brain regions thus, serving as appropriate tools for EEG-based biometric systems yielding high performance.

Although a number of works based on various functional connectivity measures have been reported [8,9], the system performance were validated within a limited scenario comprising of only a single run of EEG recordings. In particular, researchers have confirmed the potential usability and feasibility of such systems by applying their proposed methodologies on divided non-overlapping EEG segments resulting from the one recording run. In the realm of practical adoption however, such biometric systems should be able to operate successfully in the presence of discontinuous signal inputs as well. Especially, the performance and reliability of these systems should be scrutinized prior to realization since EEG signals have inherent non-stationary characteristics due to various physical and mental drifts.

In this study, we mainly focus on a subject identification system among the various biometric-related topics. Given an input EEG signal, the identification system is required to find and recognize the correct subject label from a database containing various EEG information of several subjects as depicted in Fig. 1. We aim to propose a more realistic and practical scenario of an EEG-based subject identification system for off-line analysis using publicly available dataset. The proposed scenario allows us to determine whether a novel approach would perform reliably as we treat discontinuous trials over time. We then implement the wll-known EEG-based biometric system exploiting the functional connectivity measures and validate it for the proposed scenario. Furthermore, we present a simple approach to enhance the performance of the system and highlight certain issues to be considered as future work.

METHODS

In this section, we describe the approaches undertaken. Our main focus is to investigate and comprehend the performance variation of subject identification incurred by non-stationary EEG signals as the recording runs are processed gradually. Simulations are conducted using public

Published by Verlag der TU Graz
Graz University of Technology

 DOI: 10.3217/978-3-85125-533-1-42

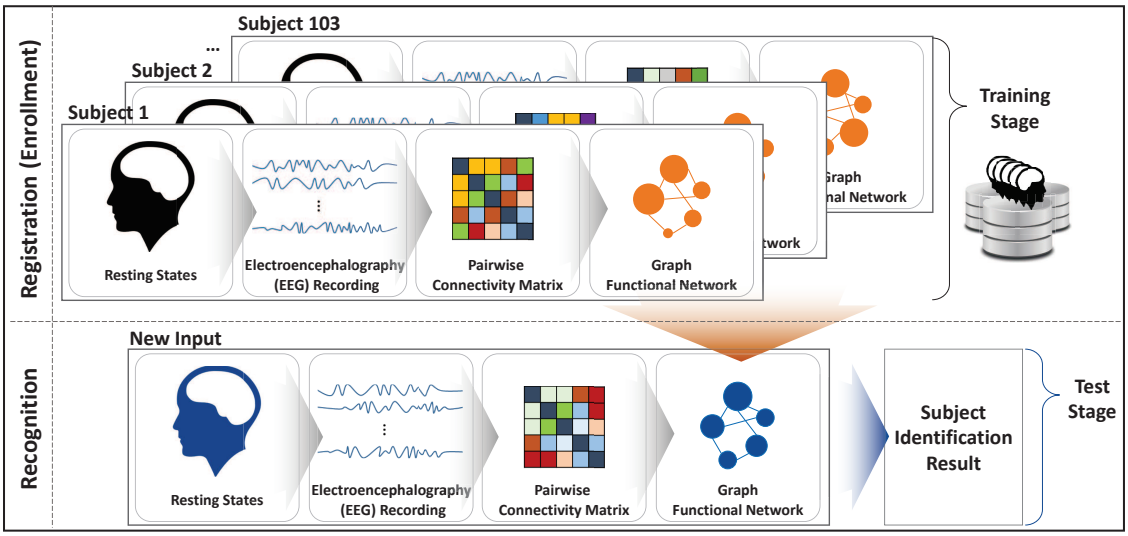

Figure 1: Schematic diagram of electroencephalography-based subject identification system.

dataset and the accuracy assessed under different spectral bands using two prominent feature extraction methods for multiple test runs over time.

A. Dataset

The publicly available "Physionet EEG Motor Movement/Imagery Dataset" acquired by BCI2000 system from 109 subjects was used in our study [10,11]. The EEG signals were recorded from 64 scalp electrodes at the international 10-10 locations and 160 Hz sampling rate was used. The dataset consists of two baseline tasks (eye-open resting state and eye-closed resting state) and twelve motor movement (MM)/ motor imagery (MI) tasks. In our study, we used the twelve MM/I dataset were used, of which the first run was designated as the training data for an enrolment stage and the remaining eleven runs as consecutive testing data for the recognition stage of the performance evaluation process. By excluding subjects with less than fifteen conducted MM/I trials from the dataset, our experiment was finally carried out for a reduced set of 103 subjects.

B. Pre-processing

In the signal pre-processing phase, the dataset was epoched to a range of -4 to 0 seconds with respect to the instructing MM/I target onset. We assumed that the EEG signal in this time period corresponds to the resting states awaiting the cue instruction. Since each subject produced fifteen trials, the fifteen resting state epochs prior to the MM/I trials are extracted in each run. The non-overlapping epochs of 4 seconds were treated as separate trials in the subject identification system.

The extracted epochs were band pass filtered separately to account for the effects of EEG spectral bands. The six different frequency bands that were considered are delta (0.5-4 Hz), theta (4-8 Hz), alpha (8-13 Hz), beta (13-30 Hz), gamma (30-50 Hz), and the complete range (0.5-50 Hz). The accuracy results were analysed and presented in terms of the spectral ranges of the EEG signals.

C. Feature Extraction

Based on recently reported methods for biometric subject identification, we applied widely-used brain connectivity analysis schemes on the EEG signals. We now describe the methods to obtain inter-channel connectivity.

- **Inter-channel relation measures:** We calculated two of the most widely-used brain functional connectivity metrics namely, inter-channel Pearson's correlation coefficient (COR) [12], and inter-channel phase lag index (PLI) [9,13]. The inter-channel COR reveals the strength of the linear relation of pairwise channels by magnitude as it varies from -1 to 1. It measures linear correlation in the time domain between two signals at zero lag. On the other hand, the PLI measure discards phase distributions that center around 0 mod π, in order to be robust against the presence of common sources. The PLI calculates the asymmetry of the distribution of phase differences between two signals varying from 0 to 1, and serves significant in volume conduction and active reference problems.

- **Eigenvalue centrality (EC):** Indicators of centrality represent the most important nodes within a graph in the context of network analysis. One such measure is EC which is used to characterize connectivity and has evidently shown high accuracy performances for brain connectivity-based biometrics [9]. We computed EC for the inter-channel Pearson's correlation coefficient, and phase lag index which are structured as 64×64 matrices (the number of channels is 64). The EC result of each matrix was used as a feature vector. The functional connectivity with EC approach with respect to PLI showed high performance in literature [9].

D. Feature Classification

Published by Verlag der TU Graz
Graz University of Technology

 DOI: 10.3217/978-3-85125-533-1-42

For off-line analysis of the biometric system, dataset composed of twelve runs from 103 subjects were used. By labelling each individual as a distinct class, the system can be treated as a multi-class classification problem with 103 classes. The fifteen epochs in the first MM/I run from all subjects were allocated to training trials, while the remaining eleven runs (consisting of fifteen epochs each) were assessed in a consecutive manner.

As mentioned earlier, the inter-channel COR and PLI-based ECs were computed for each spectral band of the resting state EEG signals. Using the feature vectors extracted by EC, we then calculated the Euclidean distance for the classification process. The subject label showing the minimum Euclidean distance between the training dataset and test trial were then compared for every single test trial of the 103 subjects. We treated the fifteen epochs of all subjects in each test run as fifteen sets composed by 103 subjects' single epoch. In every test run (a total of eleven test runs), the classification procedure was repeated fifteen times for a sequence of 103 subjects' trials. The accuracy was calculated by classifying the epoch out of all the subjects. Finally, we computed a mean and a standard deviation of the accuracies in each test run.

RESULTS

Simulations results for performance variation with consecutive multiple runs with respect to different spectral ranges and functional connectivity measures are provided in this section.

Fig. 2 illustrates the performance variations plots for consecutive test runs at six different spectral bands. In each run, fifteen trials from 103 subjects were tested to identify the correct subject label. The accuracy was calculated based on the number of correct subject identification results, and represented as the mean and standard deviation from the fifteen repeated recognition results in every run. In general, the resting EEG states in beta (13-30 Hz) and gamma (30-50 Hz) bands showed relatively higher accuracy compared to the other spectral bands. Our results are in accordance with the existing works that have reported high classification rates in these two bands [9]. Although the COR-based approach resulted in better performance as compared to its PLI counterpart in most spectral bands, the PLI-based functional connectivity feature shows highest accuracy in the gamma spectrum. However, the performance of this approach in the gamma band also decreased to $57.67 \pm 3.8\%$ over time in the worst case.

The classification matrices of eleven test runs using the PLI-based approach in the gamma band are shown in Fig. 3. Each matrix represents the estimated results for each subject given the actual labels of subject indexes. Therefore, the diagonal of each matrix shows the result of correct classification, whereas the remaining elements correspond to the mis-classification results. We observe that with increase in the number of test runs, the number of mis-classified subjects also gradually increases. For sake of comparison, we reproduced the optimistic identification results ($> 90\%$) reported by the authors in [9] by implementing the same signal processing procedure (band pass filter, PLI, EC, and Euclidean distance-based classification) and evaluated the system performance for our proposed scenario.

Apart from obtaining high accuracy in several runs, we also account for reliable and persistent performance over long time series as important assessment measures in our scenario. To improve the performance over time, we included the mean values of various combinations of the training dataset as additional features for classification. Since the EEG signals are non-stationary, even a small number of training sets may possess non-stationary traits. Hence, calculating the mean values from several EEG segments would de-noise and reduce variations of the training sets. We repeated the same simulation process after adding training features made by taking the sum of three consecutive trials, sum of five consecutive trials, and sum of all the trials. Fig. 4 displays performance variation in gamma bands for the added features. Through such simple addition of enhanced features, the PLI-based performance of the worst case ($57.67 \pm 3.8\%$) improved to $61.93 \pm 3.12\%$ (around 4.2% accuracy improvement). We observe that understanding the stationary features can be a possible solution to overcome performance degradation over time.

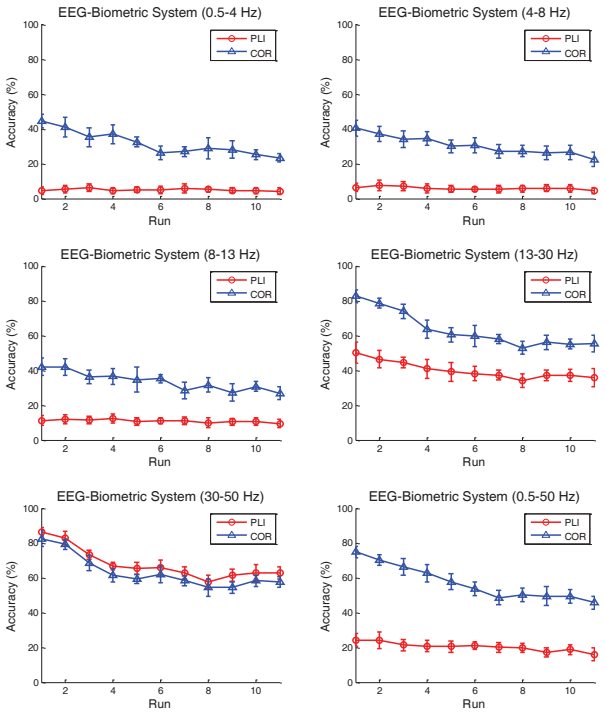

Figure 2: Performance evaluation of consecutive test runs using phase lag index (PLI) and Pearson's correlation coefficient (COR)-based approaches in six different spectral bands.

Published by Verlag der TU Graz
Graz University of Technology

 DOI: 10.3217/978-3-85125-533-1-42

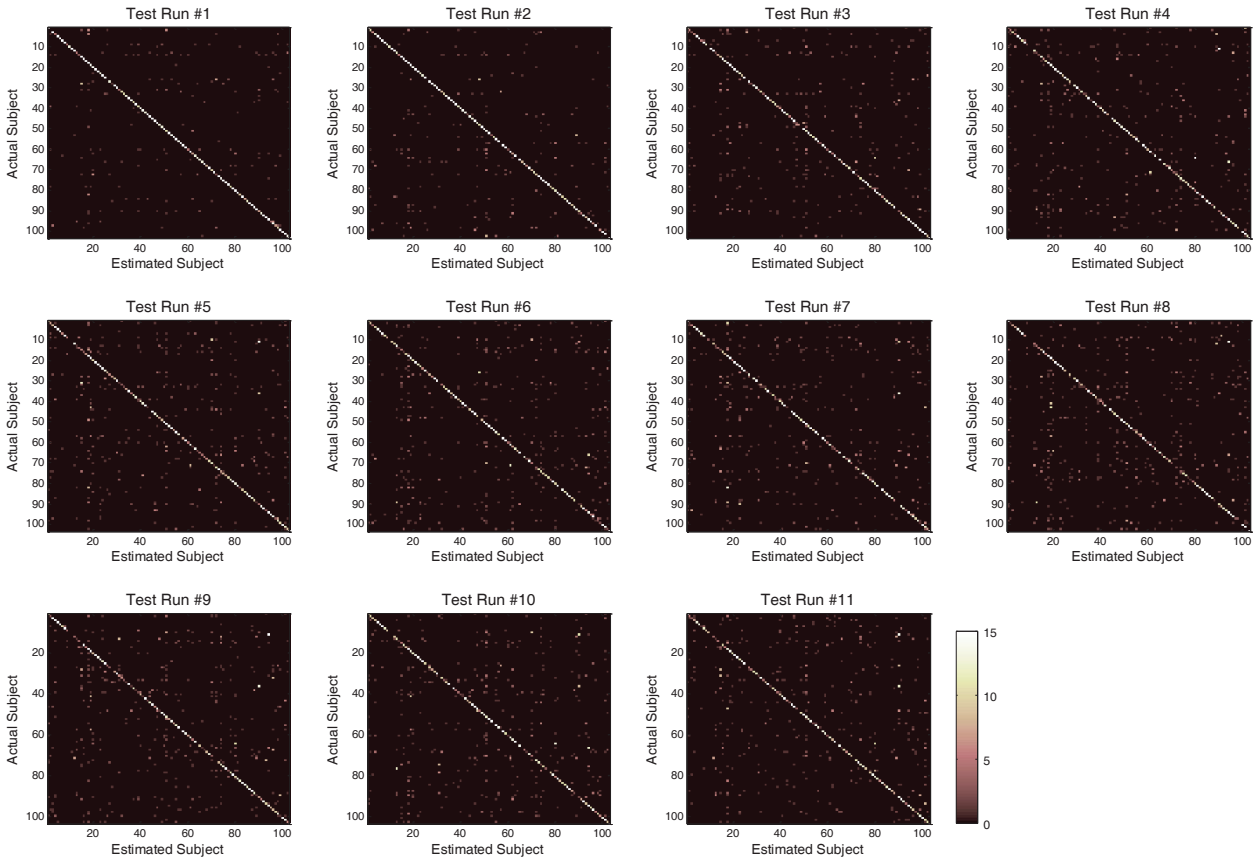

Figure 3: Classification matrices of eleven test runs in gamma band ($30 - 50$ Hz) where phase lag index-based approach is applied.

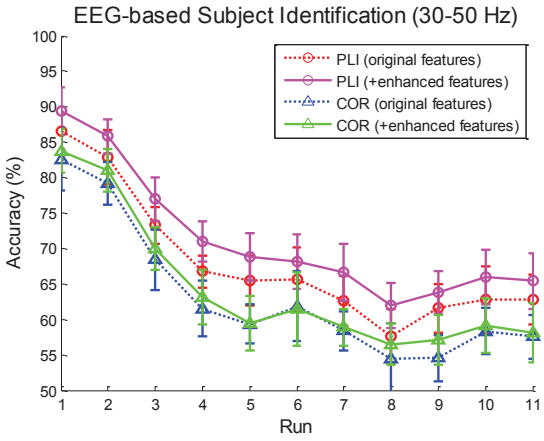

Figure 4: Performance comparison of consecutive test runs using phase lag index (PLI) and Pearson's correlation coefficient (COR)-based approaches in gamma band and comparison with enhanced feature sets.

DISCUSSION

As EEG signals exhibit non-stationary characteristics, BCI features vary from training to testing stages during a BCI experiment. Through off-line analysis, we confirmed that the EEG-based biometric system requires a novel methodology to ensure stable operation over time. One possible approach to enhance the permanence of such biometric systems is the development of signal processing techniques to identify stationary traits hidden in the EEG signals of individual subjects and improve accuracy via a simple averaging approach. One of the issues concerning data processing is to find a unique feature appearing individually and a common feature prominent in all the subjects. The distinct stationary signal features extracted using machine learning and pattern recognition techniques eventually result in the enhanced performance of the biometric subject identification system.

Not only would the stationary traits of EEG sources from training dataset (feature extraction step) enhance the performance, but also would the proper classifier derived by training dataset (classification step). Although linear classification based on Euclidean distance measure was adopted in the our simulation environment, other forms of non-linear classifiers have potentials to strengthen the robustness and improve the reliable accuracy over long runs. Particularly, approaches built on deep neural networks that find and learn the features directly from the data would serve more efficient when handling large volumes of data.

Another appealing approach would be designing an adaptive experimental paradigm for biometric system protocols. Though we assumed the EEG signals before instructing target onset as the resting state, subjects may

Published by Verlag der TU Graz
Graz University of Technology

 DOI: 10.3217/978-3-85125-533-1-42

reveal different mental states, for instance, expecting the next instruction, being affected by the surrounding environment, feeling exhausted due to long experimentation time. The protocol design to maintain stationary mental states between training and test stage would therefore, enhance the biometric system.

CONCLUSION AND FUTURE WORKS

In this paper, we demonstrated the performance evaluation of an EEG-based subject identification system for a more practical scenario via off-line analysis. We implemented the well-known functional connectivity measures for the biometric system which showed high performance in single run recording data. We further applied the state-of-art biometric system to consecutive runs over time and observed the accuracy degradation, and consequently, highly emphasized on prominent issues regarding the necessity of the realistic scenario for rational and reliable evaluation of the practical EEG-based subject identification system. Finally, We discussed possible approaches to overcome current limitations and provided research guidelines for follow-up in future works.
We expect the EEG based biometric system would be spread to be accessed gradually from limited environments requiring an advanced security (such as banks, military or companies) to personal usages. To be the practical application, the longitudinal studies exploring uniqueness and distinctiveness of the brainwaves are fundamentally required.

ACKNOWLEDGEMENT

This research was supported by the Brain Research Program through the National Research Foundation (NRF) of Korea funded by the Ministry of Science, ICT & Future Planning (NRF-2016M3C7A1905477), and partly by the “Basic Research Projects in High-tech Industrial Technology” Project provided by GIST.

REFERENCES

[1] DelPozo-Banos M, Travieso CM, Weidemann CT, Alonso JB. EEG biometric identification: a thorough exploration of the time-frequency domain. J. Neural Eng. 2015;12(5):056019.

[2] DelPozo-Banos M, Alonso JB, Ticay-Rivas JR, Travieso CM. Electroencephalogram subject identification: A review. Expert Syst. Appl. 2014;41(15):6537-6554.

[3] Campisi P, La Rocca D. Brain waves for automatic biometric-based user recognition. IEEE Trans. Inf. Forensics Secur. 2014;9(5):782-800.

[4] Palaniappan R, Mandic DP. Biometrics from brain electrical activity: A machine learning approach. IEEE Trans. Pattern Anal. Mach. Intell. 2007;29(4):738-742.

[5] Ruiz-Blondet MV, Jin Z, Laszlo S. Cerebre: A novel method for very high accuracy event-related potential biometric identification. IEEE Trans. Inf. Forensics Secur. 2016;11(7):1618-1629.

[6] Yang S, Deravi F, Hoque S. Task sensitivity in EEG biometric recognition. Pattern Anal. Appl. 2016:1-13.

[7] Laufs H et al. Electroencephalographic signatures of attentional and cognitive default modes in spontaneous brain activity fluctuations at rest. PNAS, 2003;100(19):11053-11058.

[8] La Rocca D et al. Human brain distinctiveness based on EEG spectral coherence connectivity. IEEE Trans. Biomed. Eng. 2014;61(9):2406-2412.

[9] Fraschini M, Hillebrand A, Demuru M, Didaci L, Marcialis GL. An EEG-based biometric system using eigenvector centrality in resting state brain networks. IEEE Signal Process Lett. 2015;22(6):666-670.

[10] Goldberger AL et al. PhysioBank, PhysioToolkit, and PhysioNet: Components of a New Research Resource for Complex Physiologic Signals. Circulation. 2000;101(23):e215-e220.

[11] Schalk G, McFarland DJ, Hinterberger T, Birbaumer N, Wolpaw JR. BCI2000: A General-Purpose Brain-Computer Interface (BCI) System. IEEE Trans. Biomed. Eng. 2004;51(6):1034-1043.

[12] Riera A, Soria-Frisch A, Caparrini M, Grau C, Ruffini G. Unobtrusive biometric system based on electroencephalogram analysis. EURASIP J. Adv. Signal Process. 2008;2008:18.

[13] Stam CJ, Nolte G, Daffertshofer A. Phase lag index: assessment of functional connectivity from multi channel EEG and MEG with diminished bias from common sources. Hum. Brain Mapp. 2007;28(11):1178-1193.

Published by Verlag der TU Graz
Graz University of Technology

Proceedings of the
7th Graz Brain-Computer Interface Conference 2017 DOI: 10.3217/978-3-85125-533-1-43

APHASIA REHABILITATION AFTER STROKE – WHY P300 BRAIN-COMPUTER INTERFACE (BCI) TRAINING MAY BE BENEFICIAL

S.C. Kleih[1]

[1] Institute of Psychology, University of Würzburg, Würzburg, Germany

E-mail: sonja.kleih@uni-wuerzburg.de

ABSTRACT: This paper suggests a theoretical background for the hypothesis of P300 BCI based cognitive rehabilitation training to be a successful intervention for post-stroke aphasia [1].

POST-STROKE APHASIA

Up to 30% of all stroke survivors are affected by language comprehension or language production deficits [2]. In case of Broca aphasia, lesions affect the opercular and triangular areas of the inferior frontal gyrus, the Broca language area as well as tempoparietal regions and related neuronal circuits [e.g. 3]. While language comprehension is intact, self-expression is limited or impossible. In some cases, phonemes or words can be produced, however, communication with the environment still is challenging. Traditional speech therapy, as provided by the healthcare system, includes, among others, articulation training, slowing of speech rate, prosody training, face muscle, lip and tongue control training and use of compensatory strategies [e.g. 4]. Best results for speech therapy were found for patients in the subacute phase and for patients with language comprehension as compared to language production deficits [5], which is why alternative approaches are urgently needed for this latter group. Chronic cases are numerous, as up to 50% of all patients do not fully recover [6]. Inability to communicate negatively affects relationships [7] and may even lead to depression [8].

BCI BASED POST-STROKE REHABILITATION

BCI based rehabilitation interventions were suggested as treatments for stroke survivors. This line of research was mainly focused on motor rehabilitation [e.g. 9; 10; 11; 12; 13]. Often, motor imagery based BCI interventions were used to increase neuronal plasticity of perilesional areas and clinically relevant improvements were obtained [10].

More recently, also cognitive rehabilitation after stroke was investigated by applying BCI based neurofeedback paradigms to people after stroke with cognitive impairment such as attention deficits [14] or deficits in memory functioning [15]. A BCI based rehabilitation training improving attention capacities might also be beneficial for patients diagnosed with motor aphasia as a link between attention allocation ability and language production was suggested [16].

ATTENTION AND APHASIA

In their theory, Hula and McNeil [16] suggested a link between attention and aphasia. They state parallel processing to be based on intact neuronal network functioning throughout the cortex. Disruption of the network (by e.g. stroke) might therefore lead to loss of the ability to process information simultaneously, and thus, the ability to produce language. Their idea is supported by findings in patients with motor aphasia that show successful communication in case task complexity was decreased [17]. If the ability to produce language would be lost only due to anatomical damage, task complexity reduction would not be helpful for patients with aphasia.

Interestingly, there is also an anatomical overlap between areas that are known to play a major role in language production and those that are hypothesized to be included in the generation of the P300 amplitude. While the P300 can still be detected in patients with motor aphasia [18], its amplitude is reduced [19]. Integrity of the temporoparietal junction was emphasized as a pre-requisite not only for language production but also for P300 generation. Therefore, P300 based training could support the activation of this temporoparietal region and thereby activate areas that are involved in language production.

A BCI based rehabilitation method for aphasia patients based on an auditory BCI was already suggested [20]. This approach is based on the above-mentioned assumption of a link between aphasia symptoms and attention; however, possible brain anatomical overlap was not discussed [20]. In their study, the authors presented sentences. Participants chose the correct last word to finalize presented sentences by allocating attention to one of several words that were presented. This procedure allows for closing the language loop of trying to produce a word and receiving the sensory feedback that this effort led to the intended word production. While this approach is very interesting, it requires the participant to be able to keep in mind the sentence to be finalized while choosing the last word. Further, a participant with aphasia must be able to

Published by Verlag der TU Graz
Graz University of Technology

 DOI: 10.3217/978-3-85125-533-1-43

understand the spoken sentence in the presented speed to decide which is the appropriate word to finalize the sentence. These issues can be adjusted to individual needs of patients and a first feasibility test in a stroke patient were successful [21]. However, when using a visual P300 BCI paradigm in which words and sentences can be spelled, the user might be more directly engaged in working with language material and train communicational skills by attempting to read the spelled words or messages.

THE VISUAL P300 SPELLING PARADIGM

The P300 signal on which the P300 speller [22] is based varies depending on the amount of attention allocated to the task at hand [23]. Therefore, it can be used as an indicator of the attention level and might be trainable with time ([1], see figure 1). Additionally, language can be produced by using the spelling paradigm, which might support neuronal plasticity of perilesional sites, but also increase the motivation of participants. Psychological well-being is an indicator for rehabilitation success [24]. Kleih and colleagues found first results to be promising when training patients diagnosed with Broca aphasia. All patients could use the P300 spelling paradigm, even though individual adjustments were necessary. These individual adjustments such as supporting the patient to use the speller matrix, should only be used in the beginning to familiarize the end-user with the paradigm. In the course of the training, the end-user should be enabled to use the P300 speller as described.

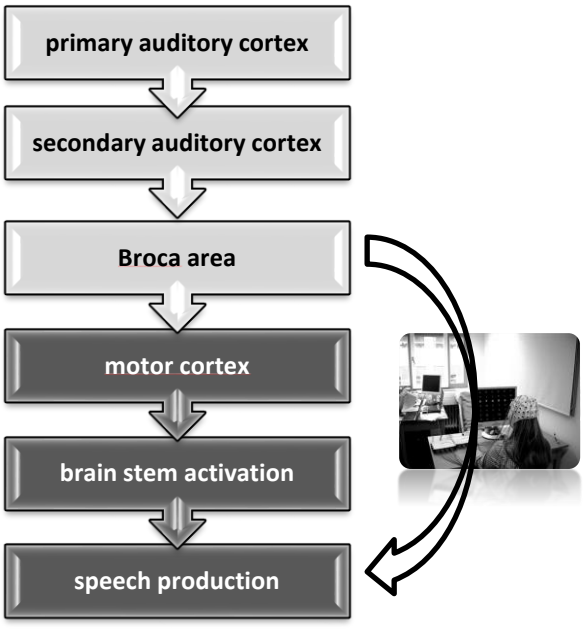

Figure 1. People with Broca aphasia can still perceive language (light grey boxes). Language production is prevented (dark grey boxes). By using a P300 BCI training, usual pathways can be circumvented while training the ability to focus attention.

INTERVENTION SPECIFICITY

Concerning aphasia subtypes, a distinction between different forms of aphasia, such as Broca, Wernicke, transcortical and anomic and according brain lesions is required for the here presented approach to be successful. An activation of brain regions involved in language production and attention allocation was hypothesized to support Broca aphasia rehabilitation after stroke. In case the lesion is not located in the described areas, only the effect of using the P300 BCI as an attention training could be investigated. As brain regions affected by a lesion might be large, overlapping and very heterogeneous between patients, it might be difficult to judge whether a patient is a possible training candidate.

CONCLUSION

P300 based BCI may support post-stroke rehabilitation in patients with aphasia. It should be further investigated how it can be best adapted to the end-user, i.e clinicians and patients alike, following the user-centred design [25]. Questions to be answered are for example: how much training is necessary? Does the increase of the P300 amplitude correlate with regaining of speech function? And, does this type of intervention yield superior results as compared to traditional speech therapy approaches which, from a technical point of view, are easier to apply? These questions are to be addressed by future research to judge the usefulness of the here presented approach.

REFERENCES

[1] Kleih SC, Gottschalt G, Teichlein E, Weilbach FX. Toward a P300 Based Brain-Computer Interface for Aphasia Rehabilitation after Stroke: Presentation of Theoretical Considerations and a Pilot Feasibility Study. Front Hum Neurosci. 2016;10(547): doi.org/10.3389/fnhum.2016.00547

[2] Flowers HL, Silver FL, Fang J, Rochon E, Martino R. The incidence, co-occurrence and predictors of dysphagia, dysarthria and aphasia after first-ever acute ischemic stroke. J Commun Disord 2013; 46: 238–248. doi: 10.1016/j.jcomdis.2013.04.001

[3] Berndt R, Caramazza A. How “regular” is sentence comprehension in Broca’s aphasia? It depends on how you select the patients. Brain Lang 1999; 67: 242–247. doi: 10.1006/brln.1999.2130

[4] Palmer R, Enderby P. Methods of speech therapy treatment for stable dysarthria: A review. Adv Speech Lang Path, 2007;9(2): 140-153.

[5] Robey RR. The efficacy of treatment for aphasic persons: a meta-analysis. Brain Lang 1994; 47: 582–608. doi: 10.1006/brln.1994.1060.

[6] Hartje, W., and Poeck, K. (2000). Klinische Neuropsychologie. Stuttgart: Georg Thieme Verlag.

[7] Visser-Meily A, Post M, Schepers V, Lindeman E.

Published by Verlag der TU Graz
Graz University of Technology

 DOI: 10.3217/978-3-85125-533-1-43

Spouses' quality of life 1 year after stroke: Prediction at the start of clinical rehabilitation. Cerebrovasc dis, 2005;20:443-448.

[8] Gainotti G. Emotional, psychological and psychosocial problems of aphasic patients: an introduction. Aphasiology 1997;11:635–650. doi: 10.1080/02687039708249412

[9] Morone G, Pisotta I, Picchiori F, Kleih S, Paolucci S, Molinari M. Proof of principle of a brain-computer interface approach to support poststroke arm rehabilitation in hospitalized patients: design, acceptability and usability. Arch. Phys. Med. Rehabil,201596:S71–S78. doi:10.1016/j.apmr.2014.05.026

[10] Pichiorri F, Morone G, Petti M, Toppi J, Pisotta I, Molinari M, Paolucci S, Inghilleri M, Astolfi L, Cincotti F, Mattia D. Brain–computer interface boosts motor imagery practice during stroke recovery. Annals of neurology, 2015;77(5):851-65.

[11] Ang KK, Guan C. Brain-computer interface in stroke rehabilitation. J Comp Sci and Eng, 2013;7(2): 139-146.

[12] Daly J., Cheng R, Rogers J, Litinas K, Hrovat K, Dohring M. Feasibility of a new application of noninvasive brain computer interface (BCI): a case study of training for recovery of volitional motor control after stroke. J Neurol Phys Ther, 2009; 33(4):203-211.

[13] Buch E, Weber C, Cohen LG, Braun C, Dimyan M A, Ard T, Birbaumer N. Think to move: a neuromagnetic brain-computer interface (BCI) system for chronic stroke. Stroke,2008;39(3):910-917.

[14] Kleih SC, Real R, Erlbeck H, Kübler A. Treating attention deficits in chronic stroke patients using Slow Cortical Potential (SCP) Neurofeedback. In: G. Müller-Putz, J. E. Huggins & D. Steryl (Eds.). Proceedings of the Sixth International Brain-Computer Interface Meeting: BCI Past, Present, and Future, 2016; Asilomar Conference Grounds, Monterey, CA, USA, May 30- June 03., p. 211. doi:10.3217/978-3-85125-467-9-211.

[15] Kober SE, Schweiger D, Witte M, Reichert JL, Grieshofer P, Neuper C, Wood G. Specific effects of EEG based neurofeedback training on memory functions in post-stroke victims. J Neuroeng and Rehab, 2015; 12(1):107.

[16] Hula WD, McNeil M. Models of attention and dual-task performance as explanatory constructs in aphasia. Semin Speech Lang *2008;* 29:169–187. doi: 10.1055/s-0028-1082882

[17] Murray LL. Review attention and aphasia: theory, research and clinical implications. Aphasiology 1999; 13: 91–111. doi: 10.1080/026870399402226

[18] Knight RT, Scabini D. Anatomic bases of event-related potentials and their relationship to novelty detection in humans. J Clin Neurophysiol 1998;15: 3–13. doi: 10.1097/00004691-199801000-00003

[19] Hagoort P, Brown CM, Swaab TY. Lexical—semantic event-related potential effects in patients with left hemisphere lesions and aphasia and patients with right hemisphere lesions without aphasia. Brain,1996;119:627–649.doi: 10.1093/brain/119.2.627

[20] Tangermann M, Schnorr N, Musso, M. Towards Aphasia Rehabilitation with BCI (2014). In: G. Müller-Putz, G. Bauernfeind, C. Brunner, D. Steryl, S. Wriessnegger & R. Scherer (Eds.). Proceedings of the 6th International Brain-Computer Interface Conference, Technical University of Graz, Graz, Austria, Sept. 16-19.

[21] Musso, M., Bambadian, A., Denzer, S., Umarova, R, Hübner, D. & Tangermann, M. (2016). A novel BCI based rehabilitation approach for aphasia rehabilitation. In: G. Müller-Putz, J.E. Huggins, & D. Steyrl (Eds.). Proceedings of the 6th International Brain-Computer Interface Meeting: BCI Past, Present, and Future. Asilomar Conference Center, Pacific Grove, California, USA, May, 30 – June 3, p. 104.

[22] Farwell LA, Donchin E. Talking off the top of your head: toward a mental prosthesis utilizing event-related brain potentials. Electroencephalogr Clin Neurophysiol 1988;70:510–523. doi: 10.1016/0013-4694(88)90149-6

[23] Johnson R. For distinguished early career contribution to psychophysiology: award address, 1985: a triarchic model of P300 amplitude. Psychophysiology 1986;23: 367–384. doi: 10.1111/j.1469-8986.1986.tb00649.x

[24] Lyubomirsky S, King L, Diener E. The benefits of frequent positive affect: Does happiness lead to success? Psych Bull, 2005;131(6):803-855.

[25] Kübler A, Holz EM, Riccio A, Zickler C, Kaufmann T, Kleih SC et al.. The user-centered design as novel perspective for evaluating the usability of BCI-controlled applications. PLoS One 2014;9:e112392: doi: 10.1371/journal.pone.0112392

Published by Verlag der TU Graz
Graz University of Technology

Proceedings of the
7th Graz Brain-Computer Interface Conference 2017 DOI: 10.3217/978-3-85125-533-1-44

A COMPARISON OF OCULAR ARTIFACT REMOVAL METHODS FOR BLOCK DESIGN BASED ELECTROENCEPHALOGRAPHY EXPERIMENTS

R. J. Kobler[1], A. I. Sburlea[1], G. R. Müller-Putz[1]

[1]Institute of Neural Engineering, Graz University of Technology, Graz, Austria

E-mail: gernot.mueller@tugraz.at

ABSTRACT: Eye movements and their contribution to electroencephalographic (EEG) recordings as ocular artifacts (OAs) are well studied. Yet their existence is typically regarded as impeding analysis. A widely accepted bypass is artifact avoidance. OA processing is often reduced to rejecting contaminated data. To overcome loss of data and restriction of behavior, research groups have proposed various correction methods. State of the art approaches are data driven and typically require OAs to be uncorrelated with brain activity. This does not necessarily hold for visuomotor tasks. To prevent correlated signals, we examined a two block approach. In a first block, subjects performed saccades and blinks, according to a visually guided paradigm. We then fitted 5 artifact removal algorithms to this data. To test their stationarity regarding artifact attenuation and preservation of brain activity, we recorded a second block one hour later. We found that saccades and blinks could still be attenuated to chance level, while brain activity during rest trials could be retained.

INTRODUCTION

In the last two decades extensive research on the neural encoding of upper limb movement kinematics has been carried out [1]. Experiments on kinematics decoding typically comprise visuomotor (VM) tasks [2–4]. Such tasks inherently involve visual feedback e.g. the distance between a target and an end-effector. Naturally, subjects would foveate between or track objects of interest [5]. This is typically avoided in laboratory conditions by instructing subjects to fixate their gaze to an arbitrary fixation point and reduce blinking to a minimum [2, 3, 6].

We want to emphasize that solely removing frontal channels from the analysis, while allowing eye movements is not sufficient to attenuate ocular artifacts (OAs) [4]. Central and parietal channels would nonetheless exhibit high correlations with saccade directions [7].

If the protocol allows saccades and blinks, literature typically separates between three independent types of artifacts [7, 8]. (1) Corneo-retinal dipole (CRD) artifacts cause signal changes that depend on eyeball rotation size and direction [7]. (2) Eyelid artifacts emerge from blinks, eyelid saccades and post-saccadic eyelid movements [7]. They elicit a large potential and are generated by the eyelid, whose displacement changes the impedance between positively charged cornea and extraocular skin [8]. (3) The saccadic spike potential (SP) is most prominent on periorbital electrodes and believed to result from contraction of extra-ocular muscles [8].

In future, we plan to apply the methods developed here on decoding kinematics from continuous visuomotor tasks. Previous studies consistently reported significant decoding information in low frequency components ($<$2 Hz) [2, 3, 6, 9]. We therefore focus on CRD and eyelid movements, since SP artifacts emerge in a frequency range $>$20Hz [8].

An alternative strategy to OA avoidance is correction. Literature provides numerous offline correction methods. For a recent review see [10]. Most common methods are either source estimation [7, 11, 12] or regression based [13] or a hybrid variant [14]. They all assume a linear mixing model:

$$\mathbf{x}(t) = \mathbf{A}\mathbf{s}(t) = \mathbf{A}^{(b)}\mathbf{s}^{(b)}(t) + \mathbf{A}^{(a)}\mathbf{s}^{(a)}(t) \qquad (1)$$

with the scalp recordings $\mathbf{x}(t)$ at time t being a mixture of sources $\mathbf{s}(t)$. The mixing matrix $\mathbf{A}$ is unknown. It can be separated into mixing coefficients $\mathbf{A}^{(b)}$ for brain sources $\mathbf{s}^{(b)}(t)$ and $\mathbf{A}^{(a)}$ for artifact sources $\mathbf{s}^{(a)}(t)$.

Cortical control of an end-effector requires online removal of OAs. One approach is to use adaptive algorithms to iteratively estimate $\mathbf{A}^{(b)}$ [14]. An advantage is that they can track changes of mixing coefficients due to i.e. a changing electrode scalp interface. However, they assume uncorrelated brain activity and artifacts [10]. This does not necessarily hold true for VM tasks. An alternative correction approach proposed in [13] is to use a block based experimental design. In the first block subjects perform voluntary eye artifacts. Thereupon a correction model is learned and applied online in the main block, during which subjects perform the actual task. Here time invariant mixing coefficients are assumed. Consequently, artifacts and brain activity can be correlated during the actual experiment. If the correlated brain activity contributes negligibly to the estimated eye artifact signals, only the artifact fraction is removed.

To our knowledge literature lacks a thorough comparison of how the previously listed correction approaches perform on the described block design. We selected five representatives and assessed their artifact correction performance on held out data. The algorithms are briefly outlined in the remainder of this section.

Published by Verlag der TU Graz
Graz University of Technology

 DOI: 10.3217/978-3-85125-533-1-44

EYE-REG: A regression based algorithm originally proposed for block design [13]. It requires designated EOG channels to compute vertical and horizontal estimates of eye artifact source signal $\hat{\mathbf{s}}^{(a)}(t)$. The model, defined in equation 1, can be rewritten as

$$\mathbf{x}(t) = \mathbf{A}^{(a)}\mathbf{s}^{(a)}(t) + \mathbf{n}(t) \quad (2)$$

with the brain activity considered as noise $\mathbf{n}(t)$. The authors used the least squares solution to calculate an estimate $\hat{\mathbf{A}}^{(a)}$. The cleaned channels $\mathbf{x}_c(t)$ are then:

$$\mathbf{x}_c(t) = \mathbf{x}(t) - \hat{\mathbf{A}}^{(a)}\hat{\mathbf{s}}^{(a)}(t) \quad (3)$$

If the empiric estimates $\hat{\mathbf{A}}^{(a)}$ and $\hat{\mathbf{s}}^{(a)}$ are close to the unknowns, we can recover the brain activity by inserting equation 2 in 3:

$$\mathbf{x}_c(t) = \mathbf{A}^{(a)}\mathbf{s}^{(a)}(t) + \mathbf{n}(t) - \hat{\mathbf{A}}^{(a)}\hat{\mathbf{s}}^{(a)}(t) \approx \mathbf{n}(t) \quad (4)$$

MARA[1]*:* Multiple Artifact Rejection Algorithm (MARA) is an independent component analysis (ICA) based algorithm [12]. ICA is used to estimate an unmixing matrix $\mathbf{V}$ that transforms equation 1 into:

$$\hat{\mathbf{s}}(t) = \mathbf{V}\mathbf{x}(t) = \mathbf{V}\mathbf{A}\mathbf{s}(t) \approx \mathbf{s}(t) \quad (5)$$

and recovers independent components (ICs) $\hat{\mathbf{s}}(t)$. *MARA* then applies a plug-and-play classifier to identify artifactual ICs and rejects them [12].

EYE-EEG[1]*:* Here, artifactual ICs are rejected based on a variance ratio metric [7]. An IC's variance is computed during designated saccade and fixation periods[2]. If their ratio exceeds a threshold, the IC is rejected. In [7] an eye tracker was employed to detect saccades and fixations.

REGICA[1]*:* Regression-ICA is a hybrid method [14]. The authors showed that artifactual ICs carry more ocular and less brain activity than scalp channels. Hence, they proposed to apply regression to artifactual ICs only.

EYE-SUB[1]*:* Artifact subspace subtraction is another approach to correct equation 1 for eye artifacts. Instead of using fixed linear combinations of EOG channels, like for regression, an artifact unmixing matrix $\mathbf{V}^{(a)}$ is computed. It recovers an estimate of the eye artifact signals $\hat{\mathbf{s}}^{(a)}(t)$:

$$\hat{\mathbf{s}}^{(a)}(t) = \mathbf{V}^{(a)}\mathbf{x}(t) \quad (6)$$

In combination with an estimated artifact mixing matrix $\hat{\mathbf{A}}^{(a)}$ equation 3 transforms to:

$$\mathbf{x}_c(t) = \mathbf{x}(t) - \hat{\mathbf{A}}^{(a)}\hat{\mathbf{s}}^{(a)}(t) = (\mathbf{I} - \hat{\mathbf{A}}^{(a)}\mathbf{V}^{(a)})\mathbf{x}(t) \quad (7)$$

The columns of $\hat{\mathbf{A}}^{(a)}$ are computed by finding the subspace which is maximally different between two conditions e.g. up vs. down saccades [11].

[1] We used the publicly available eeg-lab extension. Available online: https://sccn.ucsd.edu/wiki/EEGLAB_Extensions

[2] Fixations are defined as periods during which no eye movements happen [7].

MATERIALS AND METHODS

Participants: Five persons, aged 23.6±3.9 years, participated in this study. Three of them were female. All subjects had corrected to normal vision. They had already participated at least once in an EEG experiment before. All signed an informed consent after they were instructed about purpose and procedure of the study. The experimental procedure conformed to the declaration of Helsinki and was approved by the local ethics committee.

Stimulus Presentation: Subjects were seated in a shielded room at 1.4m distance to a computer screen (NEC Multisync 27" IPS TFT, 60Hz refresh rate, FullHD resolution). Stimuli were restricted to a square of 0.32 m x 0.32 m around the center of the screen ($\sim$13° x 13° visual angle).

Data Acquisition: EEG and EOG were recorded with a 64 channel ActiCap system connected to a BrainAmp amplifier. It sampled the data at a rate of 1 kHz and applied a first order highpass filter with a cutoff frequency of 0.016 Hz. 58 electrodes were placed at frontal, central, parietal and occipital sites according to the extended 10-20 system. The remaining 6 electrodes were placed on the outer canthi, infra and superior orbital to the left and right eye respectively. Ground and reference were placed on AFz and the right mastoid, respectively.

Experimental Procedure: The paradigm is illustrated in Figure 1. It defines four conditions. REST: subjects were instructed to fixate a blue sphere for 10 s. HORZ/VERT: the sphere moved on a continuous horizontal/vertical trajectory. Subjects were directed to accurately follow it with their gaze. BLINK: The sphere's vertical diameter shrunk 8 times for 0.5 s instructing subjects to blink once each time.

We decided to implement a visually guided paradigm to have control over saccades and blinks. It simplifies splitting the data into corresponding epochs. An eye tracker, originally required by *EYE-EEG*, was not necessary either. Figure 5 (right) illustrates the accordance of the stimulus with subject behavior (EOG derivatives).

The recording time was divided into 3 blocks. The first and last followed the presented paradigm. Both consisted of 27 trials (9 REST, 6 HORZ, 6 VERT and 6 BLINK). The choice of 27 trials and their partition was motivated by the requirements of the algorithms. Recordings of the middle block, lasting roughly 60 minutes, followed a different paradigm and will be published elsewhere.

Preprocessing: The EEG data was first downsampled to 250 Hz. To attenuate 50 Hz line noise, a 2$^{\text{nd}}$ order Butterworth bandstop filter was applied. Slow drifts were removed by a zero-phase 4$^{\text{th}}$ order Butterworth highpass filter with 0.4 Hz cutoff frequency.

We visually inspected the data for bad channels and flagged 1 to 3 channels across subjects. They were spherically interpolated. We then extracted epochs of 7 s starting 1 s after cue presentation and rejected 1.7±1.2 trials per block by visual inspection.

Three of the five algorithms, that we compare, process

Published by Verlag der TU Graz
Graz University of Technology

 DOI: 10.3217/978-3-85125-533-1-44

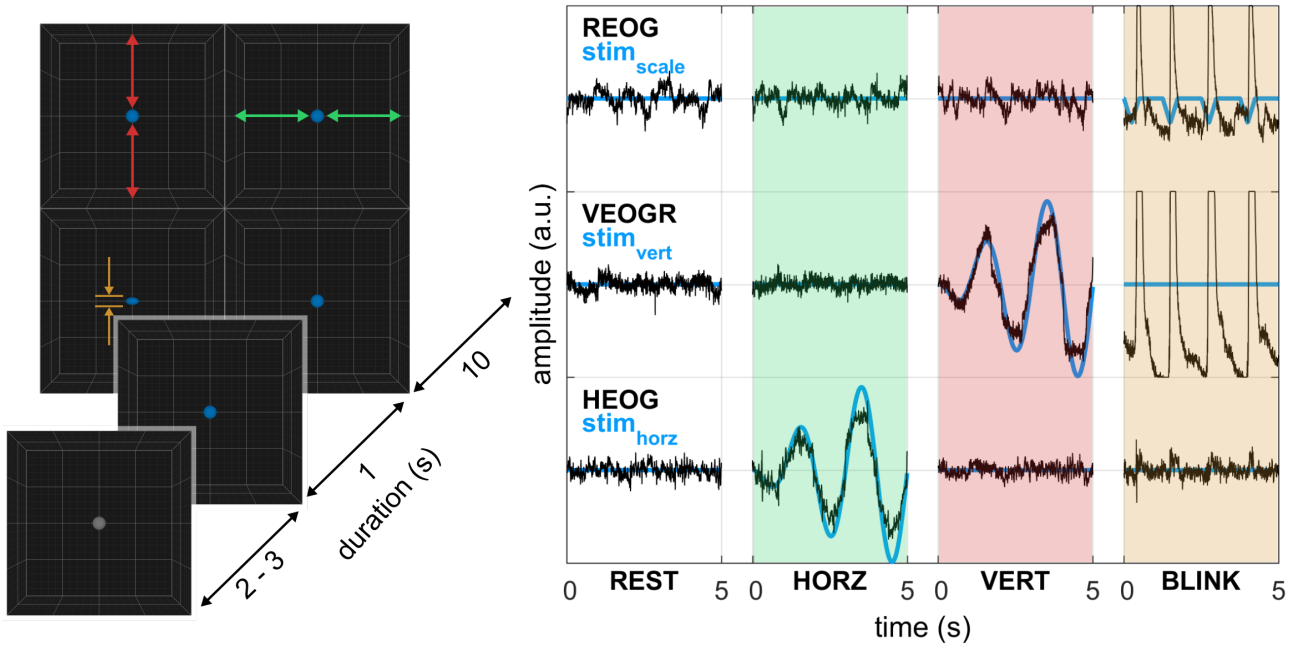

Figure 1: Experimental task. **(left)** The visual stimuli consisted of a 3D grid and a sphere, located in the center of the screen. Every trial started with a break lasting 2 to 3 seconds (uniformly distributed). Thereupon the sphere color changed to blue. After 1 s a condition dependent pattern was presented for 10 s. **(right)** First 5 s of the condition dependent patterns (blue). REST: the sphere remained in the center of the screen. HORZ: it moved along the horizontal plane according to a windowed sinusoid with a frequency of 0.5 Hz. VERT: the same movement but along the vertical plane. BLINK: the vertical diameter of the sphere changed, instructing the subject to blink. Additionally horizontal, vertical and radial EOG derivatives for selected trials of subject 1 are plotted (black).

the data in IC space. Before computing ICA we applied principal component analysis (PCA) on the 64 EEG/EOG channels and retained components explaining 99.9% of the variance. We then applied the extended Infomax algorithm to compute the unmixing matrix $\mathbf{V}$ of equation 5. The regression based algorithms require EOG components as artifact sources $\hat{\mathbf{s}}^{(a)}(t)$. The horizontal EOG (HEOG) derivative was computed as the difference between right and left outer canthi, vertical EOG left/right (VEOGL/R) as the difference between left/right superior and inferior electrode, and the radial EOG (REOG) component as the average of all six EOG electrodes.

Fixation, saccade and blink detection: EYE-EEG required separating the data into fixation and saccade periods. Since we asked subjects to avoid eye movements during REST condition, we used REST trials as fixation periods. For saccade detection the HEOG and VEOG[3] component were first lowpass filtered (zero-phase Butterworth, 2nd order, 20 Hz cutoff frequency). Horizontal/vertical saccade periods were extracted from HORZ/VERT condition trials if the absolute value of the H/VEOG component was above 10 µV for at least 200 ms. The sign was also used to split the data into left/right and up/down saccades.
Blink detection is also based on the lowpass filtered VEOG component. Samples during BLINK trials were set to be blink related if the VEOG amplitude was above 200 µV. The limits of these periods were expanded by 75 ms to include blink on- and offset.

[3]VEOG is the arithmetic mean of VEOGR and VEOGL.

EYE-REG: In [13] the authors argue to omit the REOG component, since it also captures considerable brain activity. We, therefore, used only HEOG and VEOGL/R as predictor variables for multiple linear regression.

EYE-SUB: First, penalized logistic regression (PLR) [11] with a regularization factor of 10^{-3} was applied to compute four artifact source signals $\hat{\mathbf{s}}^{(a)}(t)$ (4x1) that have a maximum magnitude difference between either left/right, up/down, blink/up or blink/down conditions. Similar to the regression approach, given $\hat{\mathbf{s}}^{(a)}(t)$, $\hat{\mathbf{A}}^{(a)}$ (64x4) can be computed by the pseudo inverse. The rest data was used to estimate a noise covariance matrix $\mathbf{R}_n$ (64x64). Considering $\mathbf{R}_n$, the unmixing matrix $\mathbf{V}^{(a)}$ (4x64) can be calculated by the regularized weighted least squares solution [11]:

$$\mathbf{V}^{(a)} = \left(\hat{\mathbf{A}}^{(a)T}\mathbf{R}_n\hat{\mathbf{A}}^{(a)} + \mathbf{\Lambda}\right)^{-1}\hat{\mathbf{A}}^{(a)T}\mathbf{R}_n \quad (8)$$

with $\mathbf{\Lambda} = \lambda\mathbf{I}$ and regularization factor $\lambda = 10^{-4}$.

EYE-EEG: Similar to the original paper we set the threshold for the variance ratio to 1.1 [7].

REGICA: Precomputed ICs were flagged using the correlation between each IC and HEOG, VEOG with a threshold of 0.2. Multiple linear regression was applied to flagged ICs only. We used H/V/REOG as predictor variables.

Evaluation: All algorithms were fitted to the first block of data i.e. computation of ICA, regression weights and fitting of hyper parameters. The second block was solely employed for testing.

Published by Verlag der TU Graz
Graz University of Technology

 DOI: 10.3217/978-3-85125-533-1-44

To assess artifact attenuation, we computed absolute values of Pearson correlation coefficients $|r|$ between EOG derivatives and each EEG channel. HEOG was used for HORZ, VEOG for VERT and blink periods during BLINK condition, respectively. Bootstrapping was applied to estimate chance level for $|r|$. Thus, we first merged the test trials of all subjects. We then randomly sampled 5 trials[4] of e.g. HORZ condition and computed $|r|$ with EEG channels of 5 random REST trials. The shuffling was repeated 5000 times for each condition. This yielded a 95%-quantile of 0.11 in every of the three conditions.

Preservation of neural activity was assessed twofold. Firstly, through computing the root mean squared error (RMSE) between cleaned $\mathbf{x}_c$ and uncleaned $\mathbf{x}$ signals during REST condition trials [14].

$$RMSE(k) = \sqrt{\frac{1}{N_s}\sum_{n}^{N_s}\left(x[k,n] - x_c[k,n]\right)^2} \qquad (9)$$

with k being the channel index and N_s the total number of samples in the test set.

Secondly, by computing the ratio between power spectral density of cleaned (Pxx_c) and uncleaned (Pxx) signals

$$Pxx_{ratio}(k,f) = \frac{Pxx_c(k,f)}{Pxx(k,f)} \qquad (10)$$

for each EEG channel k and frequency bin f [13]. We applied Welch's method to estimate the power spectral density for each trial and averaged across a subject's test trials.

RESULTS

Figure 2 depicts grand average topoplots of the 58 EEG channels after correction. The plots summarize mean test set performance for each metric and algorithm. The first row represents the uncorrected EEG. We observed typical eye artifact patterns for HORZ, VERT and BLINK conditions. Table 1 complements Figure 2. It lists mean and standard deviation across subjects for frontal, central and parietal channel groups.

Regarding the RMSE during REST, all algorithms exhibit a gradient from pre-frontal to occipital regions. *MARA* and *EYE-EEG* removed most activity, whereas *EYE-REG* and *EYE-SUB* achieve lowest RMSE across channel groups.

Figure 2 and Table 1 also summarize the absolute correlation $|r|$ between EEG channels and EOG derivatives after correction. One can clearly see that *MARA* could not identify ICs related to horizontal and vertical eye movements. This results in correlation values of up to 0.28 for frontal regions, which are clearly above the estimated chance level (0.11). The topoplots of the other algorithms show consistent attenuation of horizontal eye movements over scalp regions. Concerning vertical eye movements,

[4] Average number of trials in a subject's test set after rejection.

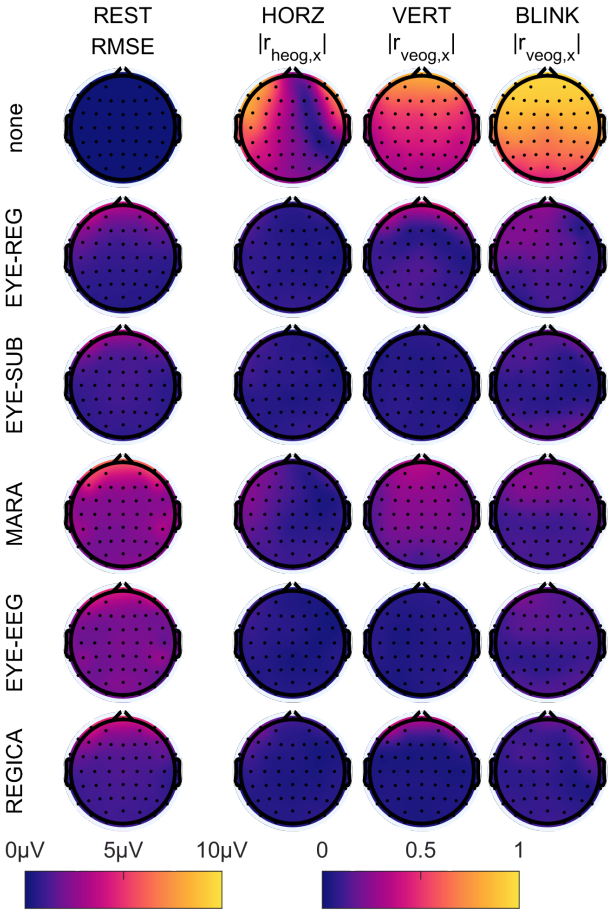

Figure 2: Topoplots (58 EEG channels) summarizing the average test set performance of the algorithms across subjects. (left) RMSE between corrected and uncorrected signal during REST condition, (right) absolute correlation $|r|$ with HEOG/VEOG/VEOG during HORZ/VERT/BLINK conditions.

EYE-SUB, *EYE-EEG* and *REGICA* could attenuate the correlation to similar levels as for horizontal ones. We also found that *EYE-SUB* and *REGICA* could attenuate blinks to chance level for frontal/central and parietal regions.

For visualization purposes, subsequent Figures show only the four algorithms that could attenuate artifact correlations to chance level, namely, *EYE-REG*, *EYE-SUB*, *EYE-EEG* and *REGICA*.

To estimate their performance decrease, we calculated group level means for train and test set. Figure 3 displays them for the average EEG channel. The barplots indicate mean and 95%-confidence interval for each condition and its associated metric. Non-overlapping train and test set confidence intervals, indicate a significant difference. The absolute correlation $|r|$ increased significantly for *EYE-SUB* (HORZ) and *EYE-EEG* (HORZ and BLINK).

The power spectral density ratio Pxx_{ratio} between corrected and uncorrected EEG revealed further differences across algorithms. Group level mean and its 95%-confidence interval are depicted in Figure 4 for frontal, central and parietal regions. *EYE-SUB* had its mean clos-

Published by Verlag der TU Graz
Graz University of Technology

 DOI: 10.3217/978-3-85125-533-1-44

Table 1: Group level summary of performance metrics for frontal, central and parietal channel groups on the test set. Mean and standard deviation across subjects are stated per metric. The lowest value per metric and channel group is highlighted.

Condition	REST	HORZ	VERT	BLINK
Metric	RMSE	$\|r\|$	$\|r\|$	$\|r\|$
Unit	μV	-	-	-
Frontal (F3, Fz, F4)				
EYE-REG	1.8±0.5	0.06±0.04	0.11±0.07	0.19±0.15
EYE-SUB	**1.4±0.1**	0.08±0.03	**0.06±0.04**	0.11±0.08
MARA	3.1±1.0	0.12±0.13	0.28±0.25	0.23±0.08
EYE-EEG	2.3±0.4	**0.06±0.02**	0.06±0.05	0.15±0.09
REGICA	2.0±0.2	0.07±0.02	0.07±0.04	**0.10±0.04**
Central (C3, Cz, C4)				
EYE-REG	**1.0±0.4**	0.06±0.04	0.10±0.04	0.16±0.10
EYE-SUB	1.1±0.4	0.07±0.05	0.06±0.04	0.08±0.05
MARA	2.5±1.0	0.10±0.13	0.24±0.22	0.14±0.09
EYE-EEG	2.2±0.9	**0.05±0.02**	0.05±0.02	0.12±0.07
REGICA	1.3±0.3	0.05±0.03	**0.04±0.03**	**0.08±0.04**
Parietal (P3, Pz, P4)				
EYE-REG	**0.7±0.2**	0.07±0.04	0.12±0.06	0.12±0.06
EYE-SUB	1.0±0.4	0.06±0.04	0.07±0.04	0.10±0.08
MARA	2.2±1.0	0.10±0.13	0.20±0.21	0.12±0.03
EYE-EEG	2.1±0.8	**0.04±0.02**	0.06±0.04	0.10±0.08
REGICA	1.2±0.4	0.05±0.02	**0.04±0.03**	**0.09±0.03**

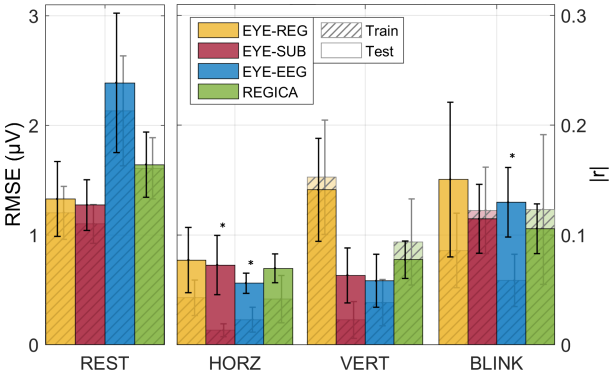

Figure 3: Algorithm performance on the average EEG channel for train (dashed) and test (solid) set. Mean and 95%-confidence interval across subjects are plotted for RMSE (left) and absolute correlation $|r|$ (right). Significant differences between train and test set are marked by *.

est to an ideal ratio of 1 and least variability of the mean across frequencies. *EYE-EEG* showed similar behavior for frontal, but larger attenuation in delta/theta frequency bands for central and parietal areas. *EYE-REG* resulted in largest mean attenuation in frontal areas, closely followed by *REGICA*. This improved considerably for central and posterior areas. We could also observe a larger variance of *REGICA* for the beta frequency band. It peaked in frontal channels.

DISCUSSION

In this work we compared five ocular artifact (OA) removal algorithms with regard to their applicability in a two step block design. We first trained the algorithms on a 5 min block of recordings. We then assessed their

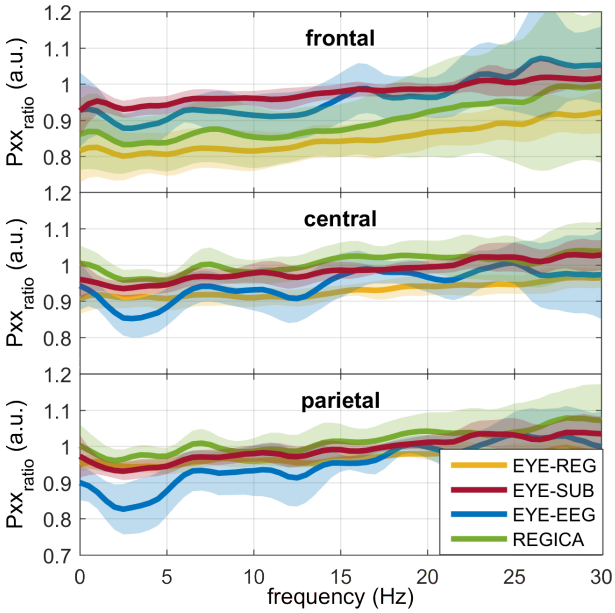

Figure 4: Mean and 95%-confidence interval of the group level power spectral density ratio Pxx_{ratio} for frontal (F3/z/4), central (C3/z/4) and parietal (P3/z/4) channels during REST condition. An ideal algorithm would yield a ratio of 1 for all frequencies.

OA removal quality on a test block recorded 60 minutes later. This approach implies a constant mixing matrix $\mathbf{A}^{(a)}$ for artifact sources. Our results, mainly Table 1 and Figure 3, give evidence that it is a reasonable assumption. We found that correlations for saccades and blinks could be attenuated to chance level, even 60 minutes after training. We emphasize that the difference between train and test set, displayed in Figure 3, captures not only the difference in time but also whether the data was used for parameter estimation. Therefore, we can not rule out if a significant difference was due to changing scalp projections or over-fitting on the train data.

As already pointed out in the introduction, allowing eye movements while only removing frontal channels is insufficient. Average correlations of up to 0.5 for uncorrected central and parietal channels (Figure 2) demonstrate the necessity for correction.

Regarding the algorithms, *MARA*, which did not rely on any label information, achieved lowest performance. While *EYE-SUB*, which required most information (annotated saccade and blink events), could attenuate artifacts to chance level and maintain low RMSE during REST condition. *REGICA* and *EYE-EEG* showed a tendency to achieve better attenuation for saccades and blinks in central and posterior areas but also to remove more brain activity.

The visually guided paradigm allowed us to control artifact occurrence. This simplified an automated annotation of artifact types (e.g. up/down saccades). In general, all algorithms tested here can be applied online. After artifact rejection and model calibration, which takes around 5 minutes, the correction process itself involves only matrix multiplications.

Published by Verlag der TU Graz
Graz University of Technology

 DOI: 10.3217/978-3-85125-533-1-44

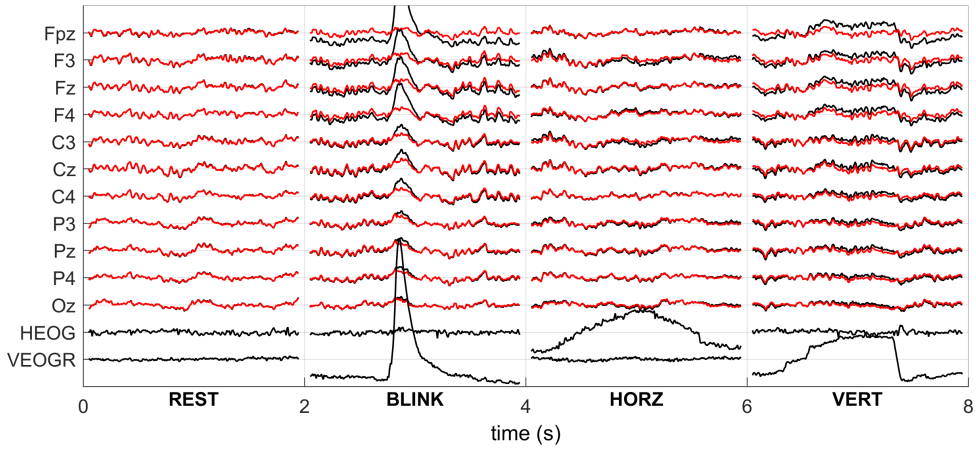

Figure 5: Representative examples in time domain for 2 s windows of selected trials. Displayed are 11 channels before (black) and after correction with *EYE-SUB* (red).

CONCLUSION

Based on the average performance on the test set, we found that *MARA* is not suitable for the investigated block design. Our results indicate, that artifact subspace subtraction (*EYE-SUB*) could achieve the best trade-off between attenuating eye artifacts and maintaining rest brain activity. Figure 5 depicts the difference between corrected and uncorrected EEG for representative trials and channels.

To complement our findings, we plan to analyze the effect on a kinematics decoder. This is a necessary step, since a significant performance drop was reported for a linear decoder after correction for OAs [6]. This demonstrates that eye artifacts were correlated with the dependent variables (x/y/z velocities). Our block design accounts for such a scenario, which encourages further research in this direction.

ACKNOWLEDGMENTS

This work was supported by the ERC Consolidator Grant 681231 ”Feel Your Reach”.

REFERENCES

[1] Müller-Putz GR, Schwarz A, Pereira J, *et al.* From classic motor imagery to complex movement intention decoding: The noninvasive Graz-BCI approach. In: Progress in Brain Research, 2016, vol. 228, 39–70.

[2] Bradberry TJ, Gentili RJ, Contreras-Vidal JL. Reconstructing Three-Dimensional Hand Movements from Noninvasive Electroencephalographic Signals. Journal of Neuroscience. 2010;30(9):3432–3437.

[3] Ofner P, Müller-Putz GR. Using a noninvasive decoding method to classify rhythmic movement imaginations of the arm in two planes. IEEE Transactions on Biomedical Engineering. 2015;62(3):972–981.

[4] Úbeda A, Azoín J, Chavarriaga R, *et al.* Evaluating decoding performance of upper limb imagined trajectories during center-out reaching tasks. In 2016 IEEE International Conference on Systems, Man, and Cybernetics. 2016, 252–257.

[5] Sailer U, Flanagan JR, Johansson RS. Eye–Hand Coordination during Learning of a Novel Visuomotor Task. Journal of Neuroscience. 2005;25(39):8833–8842.

[6] Kim JH, Bießmann F, Lee SW. Decoding three-dimensional trajectory of executed and imagined arm movements from electroencephalogram signals. IEEE Transactions on Neural Systems and Rehabilitation Engineering. 2015;23(5):867–876.

[7] Plöchl M, Ossandón JP, König P. Combining EEG and eye tracking: identification, characterization, and correction of eye movement artifacts in electroencephalographic data. Frontiers in Human Neuroscience. 2012;6(October):278.

[8] Keren AS, Yuval-Greenberg S, Deouell LY. Saccadic spike potentials in gamma-band EEG: Characterization, detection and suppression. NeuroImage. 2010;49(3):2248–2263.

[9] Waldert S, Preissl H, Demandt E, *et al.* Hand movement direction decoded from MEG and EEG. Journal of Neuroscience. 2008;28(4):1000–8.

[10] Urigüen JA, Garcia-Zapirain B. EEG artifact removal-state-of-the-art and guidelines. Journal of Neural Engineering. 2015;12(3):31001.

[11] Parra LC, Spence CD, Gerson AD, *et al.* Recipes for the linear analysis of EEG. NeuroImage. 2005;28(2):326–341.

[12] Winkler I, Brandl S, Horn F, *et al.* Robust artifactual independent component classification for BCI practitioners. Journal of Neural Engineering. 2014;11(3):035013.

[13] Schlögl A, Keinrath C, Zimmermann D, *et al.* A fully automated correction method of EOG artifacts in EEG recordings. Clinical neurophysiology. 2007;118(1):98–104.

[14] Klados MA, Papadelis C, Braun C, *et al.* REG-ICA: A hybrid methodology combining Blind Source Separation and regression techniques for the rejection of ocular artifacts. Biomedical Signal Processing and Control. 2011;6(3):291–300.

Published by Verlag der TU Graz
Graz University of Technology

Proceedings of the
7th Graz Brain-Computer Interface Conference 2017 DOI: 10.3217/978-3-85125-533-1-45

DECODING HAZARDOUS EVENTS IN DRIVING VIDEOS

H. Kolkhorst[1], W. Burgard[1], M. Tangermann[1]

[1]Cluster of Excellence BrainLinks-BrainTools
Department of Computer Science
University of Freiburg, Freiburg, Germany

E-mail: kolkhorst@informatik.uni-freiburg.de

ABSTRACT: Decoding the human brain state with BCI methods can be seen as a building block for human-machine interaction, providing a noisy but objective, low-latency information channel including human reactions to the environment. Specifically in the context of autonomous driving, human judgement is relevant in high-level scene understanding. Despite advances in computer vision and scene understanding, it is still challenging to go from the detection of traffic events to the detection of hazards.
We present a preliminary study on hazard perception, implemented in the context of natural driving videos. These have been augmented with artificial events to create potentially hazardous driving situations. We decode brain signals from electroencephalography (EEG) in order to classify single events into hazardous and non-hazardous ones. We find that event-related responses can be discriminated and the classification of events yields an AUC of 0.79. We see these results as a step towards incorporating EEG feedback into more complex, real-world tasks.

INTRODUCTION

Humans can hardly compete with machines in purely computational tasks. Though the progress in machine learning and artificial intelligence in general has led to computers outperforming humans in difficult tasks such as playing the game of Go, it is still challenging to provide adequate interaction policies between humans and machines. This challenge is faced in application areas in which machines and humans both are actors, such as in collaborative manipulation tasks with robot arms or autonomous cars sharing the road with humans. Robots often require a high amount of adaptation to the human user, specifically by learning from her or him. In the following, we will focus on the driving domain, where many challenges in the interaction between intelligent vehicles and humans (be it as passengers, drivers or pedestrians) arise [1].
When considering complex (e.g., residential) driving environments, it is not sufficient to consider humans in the scene merely as (dynamic) *obstacles*. Rather, it is desirable to have a task-specific label for these obstacles, such as the respective hazardousness.

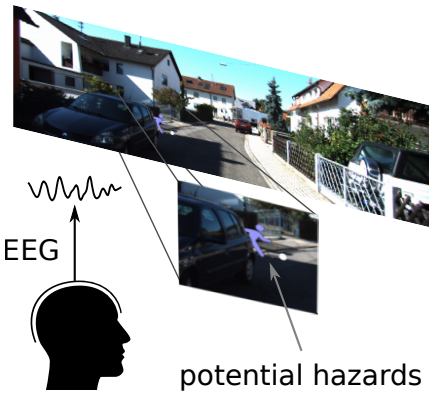

Figure 1: Experimental Paradigm: Recordings of driving scenes have been augmented with potentially hazardous events (artificial pictograms). The resulting videos are shown to the subjects while brain signals are recorded using electroencephalography.

We propose to utilize electroencephalography-based signals (EEG) to gather human feedback about the environment in a passive way. Alternative approaches to incorporating human teaching input, such as learning from demonstrations, can also be valuable tools [2]. However the situation- and context-dependence of preferred behavior (e.g., whether a situation should be treated as hazardous or not) suggests to instead gather feedback from the human, while she or he is acting within the target environment or within a reasonable approximation thereof. EEG signals, as opposed to behavioral feedback like button presses, offer the advantages of being non-intrusive and having a low latency. Additionally, brain-computer interfaces (BCIs) provide an unbiased feedback channel that corresponds to the subject's *individual* scene perception.
As the low signal-to-noise ratio of EEG poses practical challenges, it may be reasonable to seek for a balanced trade-off between a constrained lab environment and the final application environment to run experiments. Therefore, in this study we investigate passive viewing behavior of humans in continuous driving videos as a step towards monitoring humans as passengers in cars, with a possible application in the area of autonomous driving.

Published by Verlag der TU Graz
Graz University of Technology

 DOI: 10.3217/978-3-85125-533-1-45

As illustrated in Figure 1, we use videos of natural driving scenes as stimulus material and augment them with realistic salient pictograms of hazardous and non-hazardous events. With this, we focus on the domain-specific meaning (hazardousness) of the event rather than on the sole detection of an event (as in an oddball setting).
In the context of this paper, events are considered as hazardous when they would be dangerous (to the pedestrian or the driver), are hard to predict and, most importantly, require special attention or reaction by the (robot) driver (e.g., more defensive behavior or slowing down). As an example, a child or a pedestrian walking on the sidewalk would be considered as non-hazardous whereas a child running from occlusion onto the street (c.f, Figure 1) would be hazardous. While we focus on hazardousness here, we view it merely as an example for a high-level semantic scene information.

RELATED WORK

Substantial prior work addresses scene understanding for intelligent vehicles in the presence of humans (c.f., the survey by Ohn-Bar and Trivedi [1]). As a relevant example, Møgelmose et al. [3] present an integrated approach on pedestrian detection, tracking and hazard inference. For the latter, they leverage map data (proximity to street) to assign hazardousness to pedestrians. However, as also discussed in the following section, the mere presence of humans in the vicinity of the car does not necessarily imply a hazard.
Utilizing BCIs in the context of human-machine interaction, substantial previous work has been performed on decoding user state from brain signals for improved user experience or performance. For example, workload or drowsiness can be detected from EEG in different task settings [4], [5] and can be used to adapt tasks based on the decoded user state [6].
At the intersection of BCI research and, both simulated and real, driving, several works have addressed the utility of brain responses for human-machine interaction. Haufe et al. [7] investigated using brain signals in early detection of emergency braking. They report that using event-related potentials for detection of braking signals is feasible both in simulation and real-world driving, whereas oscillatory signals do not provide complementary information. Khaliliardali et al. [8] focused on the anticipation and prediction of the type of driver's actions in an automotive go/no-go paradigm. Zhang et al. [9] investigated the response to directional cues presented by driving assistant systems and classified whether these correspond to the user's intention based on error-related brain activity.
Whereas the subject's desired reaction to a stimulus is immediately clear in the first two studies or only requires a comparison with a street sign in the third, in this paper we consider a more unconstrained stimulus setting in which both the context and partly the movement of stimuli is relevant for the class assignment of an event as a step towards more ecological validity [10].

Figure 2: Exemplary events from the stimulus material. The top row consists of events that have been labeled as hazardous, whereas events in the center and bottom row are labeled as non-hazardous. Only half of the actual width of the video frame is displayed for layout purposes.

MATERIALS AND METHODS

Five healthy subjects participated in the study by watching natural video sequences of traffic scenes. All subjects gave their written informed consent and the study has been approved by the Ethics Committee of the University Medical Center Freiburg.

Experimental Design: The stimulus material consists of video sequences based on actual car recordings from the KITTI dataset [11] with a resolution of 1242x375 px. Parts of the sequences were edited by inserting events with pictograms in order to introduce potential hazards. A selection of exemplary events is depicted in Figure 2. The pictograms introduced in the natural scenes are generally salient and easily discoverable. However, a substantial portion of events consists of pictograms appearing from occlusion (both with or without prior appearances in the scene). The appearance of a pictogram from occlusion does not automatically imply that it is a hazard, which needs to be inferred from the context instead.
Different types of pictograms (such as children, pedestrians, cyclists) and different colors are used. However, the type of pictogram or color does also *not* imply the class label, i.e., hazardousness of the event (c.f., the color distribution by event class in Figure 3). Similarly, events in close proximity to the car can be both hazardous or non-hazardous (e.g., a child running close to the curb compared to a pedestrian with a dog in Figure 2).
In total, each subject watched 240 scenes (videos) of 20 s each. The total of 240 scenes is grouped into blocks of 12 scenes. Each block is balanced between scenes in simple (e.g., highways) and complex (e.g., residential) environments.

Published by Verlag der TU Graz
Graz University of Technology

 DOI: 10.3217/978-3-85125-533-1-45

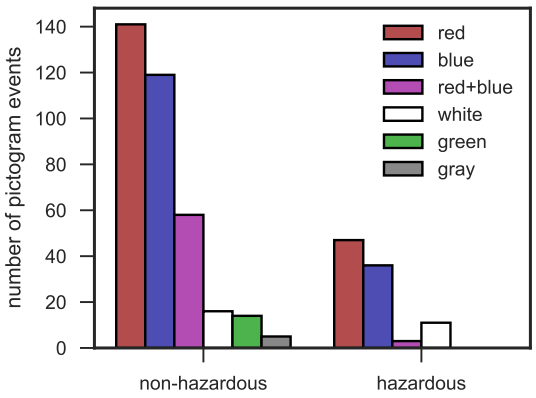

Figure 3: Event counts from a full experiment session, grouped by stimulus color and class label. The "red+blue" group consists of stimuli consisting of multiple participants (e.g., mother and child). It is apparent that the assignment of an event to a class cannot be performed solely based on stimulus type or stimulus color.

Embedded in these scenes are 262 unique events, out of which a portion was repeated over the course of the experiment, resulting in a total of 450 events in an experiment session. Out of all events in an experiment session, 97 are labeled as hazardous and 353 as non-hazardous.

During the experiment, subjects were seated approximately 80 cm in front of a 24 inch monitor, where videos were presented at 10 frames per second (corresponding to the recording rate of the source material). Subjects were instructed that they should assume being passengers in an autonomous vehicle and that they should press a button (in their right hand) in case of hazardous situations. Pressing the button could be seen as relaying the desire to drive more defensively to the vehicle. During the experiment, however, the videos continued normally, disregarding the button press.

EEG signals were recorded from 63 passive Ag/AgCl electrodes (EasyCap), which were positioned according to the extended 10-20 system and referenced against the nose. Impedances were kept below 20 kΩ. The signals were registered by multichannel EEG amplifiers (BrainAmp DC, Brain Products) at a sampling rate of 1 kHz.

Data Analysis: The recorded data was analyzed offline. It has been bandpass-filtered from 1.1 Hz to 15 Hz and downsampled to 100 Hz. Subsequently, the continuous recording has been divided into one segment per event. Each segment has a duration of 1200 ms, consisting of 200 ms preceding the first frame containing the pictogram and 1000 ms succeeding it. Note however that due to occlusions the pictogram is often not yet fully visible in the first frame of its appearance.

Before subsequent processing steps, channels whose variance was smaller than 0.5 for more than 10 % of the segments were rejected.

Additionally, segments that violated either a min-max threshold of 70 µV at frontal electrodes or whose variance was excessively large were rejected as artifactual. For base correction, the mean amplitude of the first 200 ms (corresponding to the duration of the two video frames preceding the pictogram) is subtracted from the signal.

Each segment was labeled as hazardous or non-hazardous (c.f., Figure 2). We use annotated class labels instead of using the behavioral button response of subjects to have constant class distributions and therefore better comparability across subjects.

As features for classification, mean voltages in 100 ms windows from 100 ms to 900 ms after the first visible pictogram frame were used. Both single time intervals and cumulative time intervals (i.e., concatenating the channel means of the interval with all preceding ones) were used as feature vectors (see Figure 5 for the used intervals).

Analyzing each subject individually, we train and evaluate classifiers in a chronological 5-fold cross-validation. Classification was performed by regularized linear discriminant analysis (with analytic determination of the shrinkage parameter). Classification results are reported as the area under the receiver operating characteristic (AUC). Assigning predictions at random would result in a chance-level AUC of 0.5.

RESULTS

Participants gave qualitative feedback that the events labeled as hazardous were perceived as such, and subjects pressed the button in 74 % of hazardous events. Based on the rejection policies described in the previous section, 12 % of all epochs were rejected. Rejection rates were similar for both classes such that the original class distribution was preserved.

We observed event-related responses to both hazardous and non-hazardous events with peak amplitudes around 600 ms after the first (partial) appearance of a potentially hazardous stimulus. Spatially, we observed a predominantly non-lateralized response throughout the subjects. Central and parietal electrodes offer highest discriminative information between hazardous and non-hazardous events for four of the five subjects.

Figure 4 visualizes data of a subject with average decoding results. Both hazardous and non-hazardous events show event-related potentials compared to baseline intervals taken from video segments at least 5 s from each annotated event. However, hazardous events elicit a stronger response. This is most prominent from 500 ms to 800 ms after the event's first video frame, as depicted by the color bars representing the channel-wise discriminatory information between hazardous and non-hazardous events.

Using eight time intervals within the range of 100 ms to 900 ms after the first visible frame of the event, classification yielded a mean AUC of 0.79 over all subjects, with a minimum AUC of 0.75 and a maximum of 0.87 across the five subjects.

Published by Verlag der TU Graz
Graz University of Technology

 DOI: 10.3217/978-3-85125-533-1-45

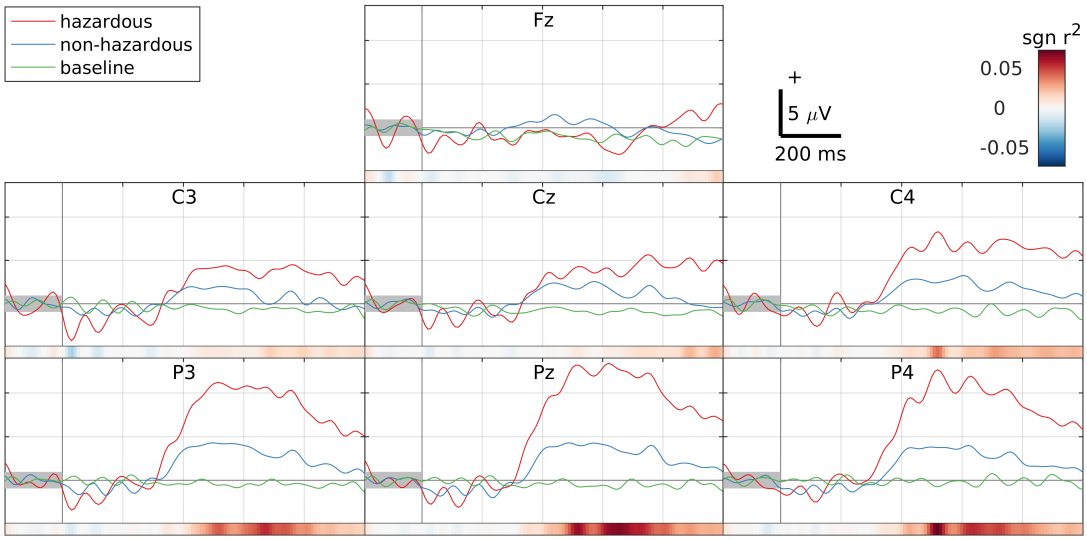

Figure 4: Event-related responses of an exemplary subject (with average classification quality) at seven electrodes. Lines show the mean voltage at the given electrode over all hazardous, non-hazardous events or baseline segments, respectively ($N = 79, 297, 315$). Baseline segments are extracted from parts of scenes that are separated by at least $5\,\mathrm{s}$ from other events. The mean of the first $200\,\mathrm{ms}$ of the interval (i.e., before the appearance of the pictogram) has been subtracted from each channel. The colorbars depict the signed r^2 value between hazardous and non-hazardous events.

Focusing on the features' influence on single-trial decoding quality (see Figure 5), one can see that classifiers trained on features from $300\,\mathrm{ms}$ to $400\,\mathrm{ms}$ after onset show the first reasonable performance (AUC of 0.66). The best single time windows have latencies of $500\,\mathrm{ms}$ to $600\,\mathrm{ms}$ and $600\,\mathrm{ms}$ to $700\,\mathrm{ms}$ after onset. Cumulatively using all time windows up to a given point, we see gains until $800\,\mathrm{ms}$ after the event.

DISCUSSION

We find that distinguishing between hazardous and non-hazardous events is possible with a reasonably good quality for all five subjects (minimum AUC of 0.75). Although results need to be supported by more subjects, the observation that discriminative information from the first $600\,\mathrm{ms}$ already result in a mean AUC of 0.76 suggests the possibility for close-to-realtime utilization as an information source in online systems.

For this study we did not perform exhaustive feature engineering or hyperparameter optimization, but rather focused on obtaining a realistic decoding result using "best practice" methods in order to evaluate the feasibility of distinguishing between high-level event classes. It appears reasonable to expect that better decoding results are possible by, e.g., adapting time intervals or spatial filters to individual subjects.

On a cursory glance, the question might arise whether the results just resemble a "classical" P300 effect in an oddball scenario. We argue that this is not the case since we aim to distinguish between two different types of events (hazardous and non-hazardous) which are both similarly (un)expected. Observed effects are not based on the sole occurrence of an event compared to a baseline stimulus.

Despite the smaller amount of hazardous events compared to non-hazardous ones (since traffic scenes should maintain some degree of realism), both classes are "odd" events that differ strongly from regular parts of the scenes (also in their brain response, as depicted by the baseline class in Figure 4). Hence, rather than discriminating rare *unexpected* events from regular ones, our classes distinguish between the *contextual meaning* of an event. Furthermore, due to the priming of participants (e.g., by pedestrians appearing before occlusions) and some repetitions in the later course of the experiments, we argue that the sole occurrence of (both classes of) events is not always unexpected.

The comparatively high latency of the event-related response could be attributed to the fact that stimuli are still partly occluded at time $0\,\mathrm{s}$. Additionally, it has to be noted that the decision whether a pictogram is hazardous could not always be made immediately at its appearance since movement with respect to the scenes is critical for judging the event. Alongside the different latencies after which participants noticed the pictograms, these differences between time-alignment of events could potentially be mitigated by relying on fixation-related potentials [12]. Nevertheless, these latencies are common to both classes so we expect only minor influence upon the quality of classification.

Since subjects performed button presses during the experiment, the question arises whether the decoding results might be solely based on the motor activity of the subject. However, this appears to not be the case since there is not a clear lateralization of the response as would be expected from a single-handed motor activity. Additionally, artifact rejection should diminish the effects of muscular artifacts in the analyzed signal.

Published by Verlag der TU Graz
Graz University of Technology

 DOI: 10.3217/978-3-85125-533-1-45

As the preceding paragraphs suggest, the complex set of stimuli might lead to several effects that might be considered confounders in the context of the classification. As discussed above for a selection of important candidates, we aimed to either control for these or check that they did not heavily affect the results. More importantly, we would like to stress that real-world use cases of BCIs most likely also implicate substantial confounders to the main task and in the light of ecological validity of BCI studies, these have to be dealt with in the analysis rather than solely by restricting the experiment.

While we focus on hazardous and non-hazardous events in the context of the paper, these labels should be considered as representatives of semantic classes that can easily and "intuitively" be distinguished by humans whereas it is challenging to infer them from alternative sensor data.

Regarding the applicability of the performed experiments to real-world driving, we want to discuss two major impediments of the current setup. First, the experiments are limited to video-based stimuli in a laboratory setting and events have been artificially introduced into the scenes. While this has been motivated by having repeatable experiments with material that is similar in quality, style and salience of stimuli, there is still an apparent mismatch with car recordings in real traffic. Regarding the signal quality, an automotive environment including abrupt movement is certainly a more difficult recording environment. However, such an environment can also be expected to create a much higher immersion than the laboratory setting, which might also transfer to more distinct subject reactions. Additionally, it is reasonable to expect some generalization to a car setting since the stimulus material is comparatively realistic and a transfer across similar ERP-based tasks has been shown to be feasible [13].

A second constraint of the presented analysis is the assumption of having temporal alignments for the potentially hazardous candidate events. However, in the context of autonomous driving it is reasonable to assume that additional sensor equipment (such as cameras or laser scanners) are able to detect candidate events (e.g., the appearance of dynamic obstacles or identification of pedestrians [1]).

Generally, we find that the combination of BCI-based monitoring in the context of autonomous machines promises to be especially helpful in the generation of labels from humans with high temporal resolution. During development of systems, this can be utilized to directly associate training data from other modalities with continuous human feedback, e.g., to evaluate the compliance of the machine to the human's requirements. Additionally, due to the potentially subject-specific but unbiased nature of responses, BCIs can become building blocks for adapting complex systems to individual users, e.g., by optimizing parameters based on the *perceived* hazardousness.

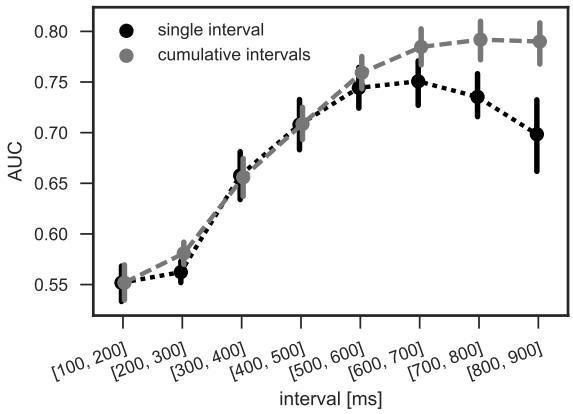

Figure 5: Classification results on different time intervals relative to the event's first visible video frame. Each point represents the mean AUC over all subjects along with a bootstrapped $68\,\%$ confidence interval. The dotted line represents classification results on the respective $100\,\mathrm{ms}$ interval whereas the dashed one shows results based on including all time preceding intervals as features.

CONCLUSION

In order to investigate the discriminability between different high-level semantic events in complex environments with passive BCIs, we describe preliminary experiments with five subjects on distinguishing hazardous and non-hazardous appearances of pictograms in natural driving videos. We find that the event-related responses differ not only compared to baseline stimuli but also between classes. Single-event classification yields a mean AUC of 0.79, suggesting that reasonable discrimination is possible in the context of complex realistic baseline stimuli.
We view these results as a step towards utilization of BCIs as a monitoring and feedback channel of human scene understanding and assessment for improved human-machine interaction.

ACKNOWLEDGMENT

This work was (partly) supported by BrainLinks-BrainTools, Cluster of Excellence funded by the German Research Foundation (DFG, grant number EXC 1086). Additional support was received from the German Research Foundation through grant INST 39/963-1 FUGG and from the Ministry of Science, Research and the Arts of Baden-Württemberg for the project ZAFH-AAL (Az: 32-7545.24-9/18/1) and for bwHPC.

REFERENCES

[1] Ohn-Bar E and Trivedi M. M. Looking at Humans in the Age of Self-Driving and Highly Automated Vehicles. *IEEE Transactions on Intelligent Vehicles*, 1(1):90–104, March 2016.

[2] Bestick A, Bajcsy R, and Dragan A. D. Implicitly Assisting Humans to Choose Good Grasps in Robot to Human Handovers. In *International Symposium on Experimental Robotics (ISER)*, Tokyo, Japan, 2016.

Published by Verlag der TU Graz
Graz University of Technology

 DOI: 10.3217/978-3-85125-533-1-45

[3] Møgelmose A, Trivedi M. M, and Moeslund T. B. Trajectory analysis and prediction for improved pedestrian safety: Integrated framework and evaluations. In *2015 IEEE Intelligent Vehicles Symposium (IV)*, pages 330–335, June 2015. 00000.

[4] Brouwer A.-M, Hogervorst M. A, van Erp J. B. F, Heffelaar T, Zimmerman P. H, and Oostenveld R. Estimating workload using EEG spectral power and ERPs in the n-back task. *J Neural Eng*, 9(4):045008, August 2012.

[5] Borghini G, Astolfi L, Vecchiato G, Mattia D, and Babiloni F. Measuring neurophysiological signals in aircraft pilots and car drivers for the assessment of mental workload, fatigue and drowsiness. *Neuroscience & Biobehavioral Reviews*, 44:58–75, July 2014.

[6] Schultze-Kraft M, Dähne S, Gugler M, Curio G, and Blankertz B. Unsupervised classification of operator workload from brain signals. *J Neural Eng*, 13(3):036008, 2016.

[7] Haufe S, Kim J.-W, Kim I.-H, Sonnleitner A, Schrauf M, Curio G, and Blankertz B. Electrophysiology-based detection of emergency braking intention in real-world driving. *J Neural Eng*, 11(5):056011, October 2014.

[8] Khaliliardali Z, Chavarriaga R, Gheorghe L. A, and Millán J. d. R. Action prediction based on anticipatory brain potentials during simulated driving. *J Neural Eng*, 12(6):066006, 2015.

[9] Zhang H, Chavarriaga R, Khaliliardali Z, Gheorghe L, Iturrate I, and Millán J. d. R. EEG-based decoding of error-related brain activity in a real-world driving task. *J Neural Eng*, 12(6):066028, 2015.

[10] Brouwer A.-M, Zander T. O, van Erp J. B. F, Korteling J. E, and Bronkhorst A. W. Using neurophysiological signals that reflect cognitive or affective state: Six recommendations to avoid common pitfalls. *Frontiers in Neuroscience*, 9, April 2015. 00005.

[11] Geiger A, Lenz P, Stiller C, and Urtasun R. Vision meets Robotics: The KITTI Dataset. *The International Journal of Robotics Research*, page 0278364913491297, August 2013.

[12] Finke A, Essig K, Marchioro G, and Ritter H. Toward FRP-Based Brain-Machine Interfaces—Single-Trial Classification of Fixation-Related Potentials. *PLOS ONE*, 11(1):e0146848, January 2016.

[13] Wenzel M. A, Almeida I, and Blankertz B. Is Neural Activity Detected by ERP-Based Brain-Computer Interfaces Task Specific? *PLOS ONE*, 11(10):e0165556, October 2016.

Published by Verlag der TU Graz
Graz University of Technology

Proceedings of the
7th Graz Brain-Computer Interface Conference 2017 DOI: 10.3217/978-3-85125-533-1-46

PASSIVE BCI-BASED NEUROADAPTIVE SYSTEMS

L.R. Krol[1], T.O. Zander[1]

[1] Team PhyPA, Biological Psychology and Neuroergonomics, Technische Universität Berlin, Berlin, Germany

E-mail: lrkrol@gmail.com

ABSTRACT: Passive brain-computer interfaces have been formally introduced and defined almost a decade ago, and have gained considerable attention since then. Here, we provide a new perspective on this field. We refer to *neuroadaptive* systems, and identify a key aspect with regards to which various passive BCI-based systems differ from each other: *interactivity*. With increased interactivity, the systems become increasingly responsive, autonomous, and capable to adapt to the user. We give an overview of four separate categories of interactivity using examples of past and current research. This categorisation of passive BCI-based neuroadaptive systems helps identify and pinpoint relevant human-computer interaction aspects and possibilities for future neuroadaptive technology and research.

INTRODUCTION

The term and concept of *passive BCI* was formally introduced at the 4th Graz BCI Conference in 2008 [1]. Although at that point, with hindsight, a number of previous works could be said to have already made use of passive BCI, e.g. [2-5], it was in the year 2008 that it was highlighted by two research groups, independently of each other, as a promising research endeavour of its own. BCI methodology that, up until then, was primarily aimed at clinical applications for direct communication and control, they argued, could also be used to provide *implicit input* [6-7] to a system to the benefit of any ongoing human-computer interaction without placing any additional demands on the user.

To that end, a passive BCI system [8] derives its output from automatic, involuntary, spontaneous brain activity, interpreted in the given context [9]. The brain activity in question is not expressly or voluntarily modulated in order to make use of the BCI system, but rather reflects aspects of the naturally present cognitive or affective state of the user. The system takes this context-sensitive interpretation of the user's state as implicit input, enabling it to adapt and support the user with their task.

This is contrasted with *active* BCI, where brain activity is consciously and purposefully modulated to achieve explicit BCI-based communication or control, and with *reactive* BCI, where the signal itself is not generated voluntarily, but its external elicitation is made possible by voluntary attention shifts [8]. For example, an active BCI may rely on imagined movements of the left and right hands to steer a prosthesis to the left or right [10], and a reactive BCI may use the evoked potentials resulting from presented stimuli to detect which stimulus was attended to [11].

The concept of passive BCI was ultimately included in the 2012 standard work on BCI [12], although the term "passive" was criticised for lacking a neuroscientific definition. Indeed both the concept and the terminology assume a perspective centred on the user experience, with the user remaining passive (i.e., undertaking no explicit actions) with respect to the BCI.

However, indeed care should be taken when presuming that user actions and mental states can be readily categorised as either "voluntary" (re/active BCI) or "spontaneous" (passive BCI). For example, the user's knowledge of the supposedly passive BCI system may still lead to certain voluntary changes in activity; or, a supposedly active BCI system may take into account brain activity that is not fully voluntarily modulated.

From the user-centred perspective, a thought experiment can clarify the issue. If the same user behaviour and brain activity would be observed if the user was not aware of their influence over a system, then we can say that this is "natural" behaviour and activity that in that moment does not depend on the presence of the system. In this article, when referring to passive BCI systems, we refer to systems that are—or can be—based on such natural brain activity.

Regardless, however, of these definitory issues, the concept of using BCI methodology to provide computer systems with a measure of its user's mental state as implicit input has endured and received increasing attention over the past decade.

The BCI Society categorises BCI systems based on the intended function of the output. They recognise five categories of applications: BCI systems can *replace*, *restore*, *enhance*, *supplement*, or *improve* the user's natural output [12-13]. The BNCI Horizon 2020 roadmap for the BCI community [13] lists a total of six future applications for the two categories *improve* and *enhance*, five of which rely on passive BCI as defined here. The category *supplement* is not included in the roadmap, but, as mentioned by Wolpaw and Wolpaw [12], this, too, is partially the domain of passive BCI.

Since its inception around a decade ago, passive BCI applications have thus come to represent a relatively large and promising area of BCI research.

Published by Verlag der TU Graz
Graz University of Technology

 DOI: 10.3217/978-3-85125-533-1-46

Among passive BCIs themselves, however, a further categorisation is possible. Whilst already focusing on the user's behaviour to define the scope of passive BCI, we propose to also focus on the BCI's behaviour, rather than its consequences. By focusing on the system's behaviour rather than its intended function, a clearer and more formal emphasis is placed on how the two adaptive agents (i.e. the human and the computer) cooperate and interact with each other. In BCI applications for communication and control (i.e. replace, restore), the intended division of labour between man and machine, and the feedback given from machine to man, is relatively clear. In passive BCI systems however, as they are intended to be unobtrusive and inconspicuous, the machine's influence can manifest in a number of different ways, with different implications for the human-machine system as a whole. It is important to take this into account when designing such systems.

We identify four categories of systems, listed ordinally by increasing degree of *interactivity*. Interactivity denotes "the ability of a computer to respond to a user's input" (Oxford English Dictionary, Oxford University Press, 2016). By the proposed measure, most past and current research into passive BCI as well as suggested future applications, including all those mentioned in the BCI roadmap, provide relatively little interactivity and fall into the lower categories. We found only two recent examples for the final identified category. We believe that a lot can be gained by focusing on increased interactivity when designing new passive BCI systems.

This categorisation suggests a new way to think about passive BCI systems, and highlights BCI-based opportunities for increased human-computer synergy. A more detailed review and discussion of these categories can be found in our contributed chapter for the BCI Handbook (in press), of which this conference submission is a summary aimed more at current BCI researchers.

The following four sections will describe one category each: mental state assessment, open-loop adaptation, closed-loop adaptation, and automated adaptation. The paper concludes with a discussion and outlook.

MENTAL STATE ASSESSMENT

The first category encompasses systems the sole purpose of which is the measurement of mental states, without providing any feedback. Because feedback is lacking, these are not BCI systems, nor is there any interactivity. This category of *mental state assessment* [14-15] is still included, however, to serve as a theoretical zero point on the interactivity scale, and because mental state assessment does provide the basis for all higher systems.

The measurement and quantification of mental states can be helpful and informative by itself in various fields where no interactivity is required. Instead, user state information is gathered to be analysed and studied afterwards, to answer different questions.

For example, mental state assessment based on BCI methodology is being used in the field of *neuroergonomics*, "the study of brain and behaviour at work" [16]. One mental state that is highly relevant to ergonomics and human factors research is the state of high workload [17]. Whilst there are disagreements as to its precise definition and measurement in theory [18], BCI can offer a data-driven approach based on reference measurements. For example, Gevins and Smith [19] simulated controlled working conditions of three different load levels. Based on differences they found in frontal theta and parietal alpha, they constructed a cognitive workload index that could then be used to analyse other, less controlled recordings.

Using such pre-calibrated indices, mental state assessment can be used, for example, to compare alternative graphical user interface designs with respect to the workload they induce. See [20] for a review.

Such an approach has a number of advantages compared to traditional methods to obtain information, such as questionnaires. Brain activity provides a continuous source of data, and its recording does not interfere with the state that is measured. The method can be individually calibrated, side-stepping intersubjective reference issues as well as conceptual conflicts. Certain mental states may not even be possible to ascertain otherwise.

All this, however, hinges on the ecological validity of the recordings and corresponding interpretations. Special care must be taken to validate the measurements, ideally cross-context. See e.g. [21-22] for a discussion of pitfalls and lessons learned in mental state assessment research, which also applies to (passive) BCI research more generally.

OPEN-LOOP ADAPTATION

Interactivity denotes the computer's ability to respond to a user's input. In the case of passive BCI applications, this input is the *implicit input* [6-7] gathered by the system by analysing the user's natural brain activity in real time. In BCI terminology, the system's response to this interpreted input is generally termed *feedback* [12], denoting an action and/or piece of information resulting from the input that is subsequently "fed back to" (i.e. perceived by) the user.

As mentioned above, passive BCI systems can be unobtrusive and inconspicuous, and their responses to user input may thus be similarly hidden. It is for this reason that we refer to *adaptation* as a more generic term for the system's response to input. Traditional feedback—e.g. a cursor moving on a screen or a prosthetic limb moving—can be one form of such adaptation, but, as this categorisation will also highlight, the nature of passive BCI enables other meaningful types of adaptations as well. When adaptation is based on (natural) brain activity, we refer to these systems as *neuroadaptive* [23].

Published by Verlag der TU Graz
Graz University of Technology

 DOI: 10.3217/978-3-85125-533-1-46

It is through the system's adaptations in response to user input that different levels of interactivity can be achieved. The first level of interactivity—the second category overall—consists of *open-loop adaptations*. Systems from this category of applications apply mental state assessment to obtain a measure of a mental state on-line, and respond to certain states with specific pre-programmed actions in an open-loop fashion.

"Open loop" refers to the absence of any direct or intended coupling of the adaptation back to the input.

For example, in the above example of a workload index, open-loop adaptation could be used to assess the load level in real time, and give a warning every time a certain threshold is exceeded [24].

Prominent in the literature is the use of the error-related negativity as indicative of the mental state "error perception" [25]. Once the system learns that its user perceived an error, the system adapts, for example by correcting the error in case of a binary decision [3]. Note that such input corrections can also *induce* errors, rather than correcting them, when the initial mental state was not correctly detected.

Other examples include the detection of an "intention to interact" mental state to replace an explicit selection command in hybrid gaze/BCI systems [26-27]. Once such an intention is detected upon fixating an interactive on-screen element, a "mouse click" can be automatically executed.

In a gaming context, Van de Laar et al. [28] showed how, once a certain threshold of "relaxation" (versus "tension") is passed, the user's in-game character would switch from one set of abilities to another.

Open-loop adaptive systems, based on passive BCI, use a measurement of the user's state as implicit input. The user states of interest can be transient, such as error perception, or more constant and continuous ones such as moods or workload. As such, the former ones need to be clearly linked to the context (e.g., *what* was perceived to be in error?) for the adaptation to be effective [9]. This implicit input can then be used as a basis to execute timely adaptations. Continuous mental states are better suited to control an application's mode.

As mentioned above, it is important to validate that the mental state that is intended to be measured is indeed the one that is measured. Real-time adaptation in response to these measurements can provide an indirect validation that at least the system *functions* as intended.

Open-loop adaptation reflects simple stimulus-response logic: single, independent state detections result in single, fixed actions. More interactivity can be achieved when the system's adaptations have an influence that reaches beyond the single responses, affecting further input and future actions; for example, when interactive applications exhibit closed-loop control, discussed next.

CLOSED-LOOP ADAPTATION

In closed-loop systems, the system's output is fed back to the system as new input, or otherwise influences the next input cycle. In our present context, the ultimate source of input is the human user, and the input given to the adaptive system constitutes a measure of their mental state. In a closed-loop passive-BCI system, the initiated adaptation must thus influence the mental state that is being measured. Closed-loop adaptive systems apply mental state assessment to obtain a measure of a mental state on-line, and adapt to certain states—or changes in states—by means of actions that influence that same mental state.

The adaptations can be either discrete or continuous. For example, sounding an alarm bell to call to attention someone who has been detected to doze off is a discrete countermeasure, aimed at promoting the state being monitored: vigilance.

Kirchner [29] used a sequence of discrete events of increasing saliency: if an initial alarm was not perceived (as detected by the passive BCI), the alarm was repeated with a higher intensity.

Continuous adaptation can provide a more fine-grained approach. For example, *adaptive automation* [30] attempts to match task demands to the current capacity of the user, in real time. When workload increases, certain tasks are automated in order to keep the user in a productive state of engagement. As more capacity becomes available again, task control is gradually handed back to the user, keeping the equilibrium.

For example, Kohlmorgen et al. [31] implemented a form of passive BCI-based adaptive automation in the car. During highway driving, one of the participants' tasks would be automatically suspended and unsuspended depending on measured workload levels.

Similarly, Yuksel et al. [32] demonstrated closed-loop adaptation of educational material. The pacing of the learning process was adjusted dynamically in real time in order to sustain the student's performance, based on a measure of workload.

In a gaming context, [33] applied the concept of closed-loop adaptation to Tetris, adjusting the game's speed in order to maintain a level of optimal engagement.

These examples show how closed-loop feedback mechanisms can increase interactivity and human-computer synergy. The system's adaptations enable it to respond purposefully, as well evaluate the effect of each adaptation, such that the system obtains a qualitative participation in the ongoing interaction. The system not merely adapts to given input, but influences the next input and with that, its next adaptation. The implicit input is now part of a more interactive *implicit dialogue* between a user and the system.

Closed-loop systems go beyond open-loop systems by influencing the next interaction cycle. They can thus have a continuous, dynamic effect on their users and the interaction as a whole. The logic of a single closed loop, however, is still a limited one, usually reflecting the limited amount of input gathered by the system. Coupling adaptation directly to a limited range of input necessarily limits the range of the adaptation. By

Published by Verlag der TU Graz
Graz University of Technology

 DOI: 10.3217/978-3-85125-533-1-46

distancing the adaptation itself from the input, a further step can be made beyond closed-loop systems towards increased interactivity, discussed next.

AUTOMATED ADAPTATION

Purely closed-loop systems are restricted by their respective loops in that the adaptations directly follow the input signal. In case of input derived from neurophysiological signals, such as EEG, its bandwidth and dimensionality are generally limited. It gives insight into momentary mental states, but not into likely causes, or appropriate responses. The adaptive systems mentioned thus far are embedded in fixed, known contexts. As such, it is reasonable to assume that, for example, an increase in workload is caused by the task demands of that same environment, and can be counterbalanced by increased automation. These interactive functions however are constrained by this logic that is predetermined by known contexts.

In this next category, the adaptive logic itself is adaptive, such that a system can support its user across different and changing contexts. To that end, the system needs access to context information as well as the user's mental state. By collating and co-registering these, the system can learn its user's behaviour and responses in different scenarios. Based on that, it can then decide how and at what times to give support. Automatically adaptive systems apply mental state assessment alongside other methods of information gathering in order to build a model to represent aspects of the user's cognitive or affective responses. This model then serves as a basis for the system's own autonomous behaviour.

Zander et al. [7, 23] detected error- and satisfaction-related brain activity not in order to immediately correct perceived errors, but to learn, over time, the user's preferences. To that end, the system exhibited different behaviours and registered which system actions led to negative evoked responses and which led to positive ones, depending on the given context.

Specifically, this approach was applied to two-dimensional cursor control. The system moved to the cursor autonomously, whilst registering the evoked responses to the movements in different directions. Over time, the system could learn the pattern behind these responses and as such, learned where the user wanted the cursor to go. Already during the learning process, the system adapted its behaviour to steer the cursor towards the suspected target.

Iturrate et al. [34] demonstrated a similar principle using a robotic arm. Participants observed its movements whilst their error-related responses to certain movements were tracked and remembered. The robotic arm was guided based on the inferred information.

In automated adaptation, the gathering of information is the primary system adaptation in lieu of direct actions, with action to follow only once the system autonomously determines it to be appropriate. The parameters of adaptation are learned automatically by the system itself. This increased autonomy also translates into increased interactivity, as the system learns to respond in different ways even to input that was given in the past, or not even given at all.

DISCUSSION AND OUTLOOK

We propose a categorisation of passive BCI-based *neuroadaptive* systems based on the behaviour of that system in terms of its interactivity.

The category of *mental state assessment* systems represent a base category. These systems provide no interactivity, but by registering natural brain activity that is not influenced by the system itself, they lay the foundation for passive BCI and interactive neuroadaptive systems.

The most basic way to implement interactivity is to enable *open-loop adaptation*, giving systems the ability to respond to given input in an open-loop fashion: simple input-output response logic connects a mental state to a specific action, with no further dependencies between them.

In *closed-loop adaptation*, the system's output influences its upcoming input. The system now purposefully attempts to influence the user's mental state. Interactivity is increased as the system's actions do not merely inform, but purposefully *act upon* the user and thus influence the interaction as a whole.

Automated adaptation, finally, refers to the category of systems that learn to adapt and act autonomously based on (implicit) information gathered previously. Increased interactivity is due to the system's increased autonomy with respect to its adaptations and adaptive strategies.

These three adaptive behaviours are, of course, not mutually exclusive. An automated adaptation system might predict what a user intends to do and execute that action in advance, but then, in an open-loop fashion, undo the action when it is detected that the prediction was in error.

Note also that whether the above error-correction example should be considered open-loop or closed-loop depends on the exact state that is being targeted. Error perception, as a transient state in the form of e.g. an error-related potential, cannot always or necessarily be used as such in closed-loop systems. A more persistent state, perhaps reflecting general dissatisfaction (initially caused by the error), however, *can* be influenced in a closed loop.

It is important in general that researchers and designers pay close attention to exactly define the user state they are targeting. This categorisation also helps in formalising that.

Four out of five future scenarios suggested in the BCI roadmap under the relevant categories fall into the open-loop adaptation category. The one remaining example of passive BCI systems in the BCI roadmap

Published by Verlag der TU Graz
Graz University of Technology

 DOI: 10.3217/978-3-85125-533-1-46

uses closed-loop adaptation.

We would thus encourage researchers to also look further afield. Human-computer synergy can only be achieved by close cooperation between the two agents. Human-human communication is a dynamic, continuous process, and hinges on a shared understanding of the world and informative as well as empathic models of the conversation partner [35]. Human-computer interaction can be improved by mirroring such processes: by dynamic, responsive adaptation, and by having the system learn autonomously how to optimise that behaviour. Passive BCI methodology in particular can help us attain such close human-computer cooperation, as it can give systems access to an individually calibrated, real-time source of subjective and personally relevant information concerning the user.

A formalisation of passive BCI-based neuroadaptive systems helps identify and pinpoint relevant human-computer interaction aspects during the design and development of such systems, and aids the design of and discourse about future neuroadaptive technology.

ACKNOWLEDGEMENTS

Part of this work was supported by the Deutsche Forschungsgemeinschaft (ZA 821/3-1).

REFERENCES

[1] Zander TO, Kothe CA, Welke S, Rötting M. Enhancing human-machine systems with secondary input from passive brain-computer interfaces. In Proc 4th Int Graz, Graz, Austria, 2008, 144-149.

[2] Blankertz B, Schäfer C, Dornhege G, Curio G. Single Trial Detection of EEG Error Potentials: A Tool for Increasing BCI Transmission Rates. In: JR Dorronsoro (Ed.), Artificial Neural Networks – ICANN 2002 (Vol. 2415, pp. 1137–1143). Berlin, Germany: Springer 2002, pp 1137-1143.

[3] Parra LC, Spence CD, Gerson AD, Sajda P. Response error correction—a demonstration of improved human-machine performance using real-time EEG monitoring. IEEE Trans Neural Syst Rehabil Eng, 11(2), 2003, 173–177.

[4] Ferrez PW, Millán JdR. You Are Wrong!—Automatic Detection of Interaction Errors from Brain Waves. In Proc Int Joint Conference on Artificial Intelligence. San Francisco, CA, 2005, 1413–1418

[5] Zander TO, Kothe CA, Jatzev S, Dashuber R, Welke S, De Filippis M, Rötting M. Team PhyPA: Developing applications for brain-computer interaction. In Proc BCI for HCI and Games Workshop at SIGCHI CHI, 2008.

[6] Rötting M, Zander TO, Trösterer S, Dzaack J. Implicit interaction in multimodal human-machine systems. In CM Schlick (Ed.), Industrial engineering and ergonomics, Berlin Heidelberg, Germany: Springer, 2009, pp 523-536.

[7] Zander TO, Brönstrup J, Lorenz R, Krol LR. Towards BCI-based Implicit Control in Human-Computer Interaction. In SH Fairclough, K Gilleade (Eds.), Advances in Physiological Computing, Berlin, Germany: Springer, 2014, pp. 67–90.

[8] Zander TO, Kothe CA. Towards passive brain-computer interfaces: applying brain-computer interface technology to human-machine systems in general. J Neural Eng, 8(2), 2011, 025005.

[9] Zander TO, Jatzev S. Context-aware brain-computer interfaces: exploring the information space of user, technical system and environment. J Neural Eng, 9(1), 2012, 016003.

[10] Wolpaw JR, McFarland, DJ. Brain-computer interface operation of robotic and prosthetic devices. Computer, 41, 2008, 52–56.

[11] Farwell, LA, Donchin, E. Talking off the top of your head: toward a mental prosthesis utilizing event-related brain potentials. Electroencephalography and Clinical Neurophysiology, 70(6), 1988, 510–523.

[12] Wolpaw JR, Wolpaw EW. Brain-computer interfaces: something new under the sun. In Brain-computer interfaces: Principles and practice. Oxford, UK: Oxford University Press, 2012, pp 3-12.

[13] Brunner C, Birbaumer N, Blankertz B, Guger C, Kübler A, Mattia D, Millán JdR, Miralles F, Nijholt A, Opisso E, Ramsey N, Salomon P, Müller-Putz GR. BNCI Horizon 2020: towards a roadmap for the BCI community. BCI Journal, 2015.

[14] Müller KR, Tangermann M, Dornhege G, Krauledat M, Curio G, Blankertz B. Machine learning for real-time single-trial EEG-analysis: From brain-computer interfacing to mental state monitoring. J Neurosci Methods, 167(1), 2008, 82–90.

[15] van Erp JB, Lotte F, Tangermann M. Brain-Computer Interfaces: Beyond Medical Applications. Computer, 45(4), 2012, 26-34.

[16] Parasuraman R. Neuroergonomics: Research and practice. Theoretical Issues in Ergonomics Science, 2003, 4(1–2), 5–20.

[17] Wickens CD, JG Hollands, S Banbury, R Parasuraman. Engineering psychology and human performance. New York, NY: Routledge, 2016.

[18] Young MS, Brookhuis KA, Wickens CD, Hancock PA. State of science: mental workload in ergonomics. Ergonomics, 58(1), 2015, 1–17.

[19] Gevins A, Smith ME. Neurophysiological measures of cognitive workload during human-computer interaction. Theoretical Issues in Ergonomics Science, 4(1–2), 2003, 113–131.

[20] Frey J, Mühl C, Lotte F, Hachet M. Review of the use of electroencephalography as an evaluation

Published by Verlag der TU Graz
Graz University of Technology

 DOI: 10.3217/978-3-85125-533-1-46

method for human-computer interaction. In Proc Int Conference on Physiological Computing Systems. Lisbon, Portugal, 2014, 214–223.

[21] Gerjets P, Walter C, Rosenstiel W, Bogdan M, Zander TO. Cognitive state monitoring and the design of adaptive instruction in digital environments: lessons learned from cognitive workload assessment using a passive brain-computer interface approach. Front Neurosci, 8, 2014, 385.

[22] Brouwer AM, Zander TO, van Erp JBF, Korteling JE, Bronkhorst AW. Using neurophysiological signals that reflect cognitive or affective state: six recommendations to avoid common pitfalls. Front Neurosci, 9, 2015, 136.

[23] Zander TO, Krol LR, Birbaumer NP, Gramann K. Neuroadaptive technology enables implicit cursor control based on medial prefrontal cortex activity. Proc Natl Acad Sci U.S.A. (PNAS), 113(52), 2016, 14898-14903.

[24] Zander TO, Shetty K, Lorenz R, Leff DR, Krol LR, Darzi AW ... Yang GZ. Automated task load detection with electroencephalography: Towards passive brain-computer interfacing in robotic surgery. J Medical Robotics Research, 2(1), 2017, 1-10.

[25] Gehring WJ, Liu Y, Orr JM, Carp J. The error-related negativity (ERN/Ne). In SJ Luck, ES Kappenman (Eds.), Oxford handbook of event-related potential components. New York, NY: Oxford University Press, 2012, pp 231-291.

[26] Protzak J, Ihme K, Zander TO. A passive brain-computer interface for supporting gaze-based human-machine interaction. In C Stephanidis, M Antona (Eds.), Universal Access in Human-Computer Interaction. Design Methods, Tools, and Interaction Techniques for eInclusion (8009). Berlin Heidelberg, Germany: Springer, 2013, pp. 662– 671.

[27] Shishkin SL, Nuzhdin YO, Svirin EP, Trofimov AG, Fedorova AA, Kozyrskiy BL, Velichkovsky BM. EEG negativity in fixations used for gaze-based control: Toward converting intentions into actions with an eye-brain-computer interface. Front Neurosci, 10, 2016, 528.

[28] van de Laar B, Gürkök H, Bos DPO, Poel M, Nijholt A. Experiencing BCI control in a popular computer game. IEEE Trans Comput Intell AI in Games, 5(2), 2013, 176–184.

[29] Kirchner EA, Kim SK, Tabie M, Wöhrle H, Maurus M, Kirchner F. An intelligent man-machine interface—multi-robot control adapted for task engagement based on single-trial detectability of P300. Front Human Neurosci, 10, 2016, 291.

[30] Byrne EA, Parasuraman R. Psychophysiology and adaptive automation. Biological Psychology, 42(3), 1996, 249–268.

[31] Kohlmorgen J, Dornhege G, Braun M, Blankertz B, Curio G, Hagemann K, ... Kincses W. Improving human performance in a real operating environment through real-time mental workload detection. In G Dornhege (Ed.), Toward Brain-Computer Interfacing. Cambridge, MA: MIT Press, 2007, pp 409-422.

[32] Yuksel BF, Oleson KB, Harrison L, Peck EM, Afergan D, Chang R, Jacob RJK. Learn piano with BAch: An adaptive learning interface that adjusts task difficulty based on brain state. In Proc CHI, 2016, 5372-5384.

[33] Ewing KC, Fairclough SH, Gilleade K. Evaluation of an adaptive game that uses EEG measures validated during the design process as inputs to a biocybernetic loop. Front Human Neurosci, 10, 2016, 223.

[34] Iturrate I, Chavarriaga R, Montesano L, Minguez J, Millán JdR. Teaching brain-machine interfaces as an alternative paradigm to neuroprosthetics control. Scientific Reports, 5, 2015, 13893.

[35] Fischer G. User modeling in human-computer interaction. User Modeling and User-Adapted Interaction, 11(1-2), 2001, 65-86.

Published by Verlag der TU Graz
Graz University of Technology

Proceedings of the
7th Graz Brain-Computer Interface Conference 2017 DOI: 10.3217/978-3-85125-533-1-47

ONLINE-CAPABLE CLEANING OF HIGHLY ARTEFACTUAL EEG DATA RECORDED DURING REAL DRIVING

L.R. Krol[1], T.O. Zander[1], M. Jaswa[2], O. Flascher[2], A. Snelting[3], A-M. Brouwer[3]

[1] Zander Laboratories B.V., Amsterdam, Netherlands
[2] DCS Corporation, Alexandria, VA, United States
[3] Netherlands Organization for Applied Scientific Research (TNO), Soesterberg, Netherlands

E-mail: lrkrol@gmail.com

ABSTRACT: With an increased interest to develop brain-computer interface (BCI) applications that can be used in real-world contexts, comes an increased need to deal with the myriad sources of artefacts that interfere with the signal of interest. We present real-world data recorded in a moving car, contaminated with muscle artifacts, mechanical artifacts, and noise produced by the car's electrical systems. We use artifact subspace reconstruction and independent component analysis to rigorously clean and filter the data. We demonstrate that using state-of-the-art methods, it is possible to identify cortical processes even in heavily contaminated data.

INTRODUCTION

A number of current developments in brain-computer interface (BCI) research point towards an increased interest in real-world implementations. We see the development of easy-to-apply, commercial, dry electrode systems [1-3] as well as a number of wireless, mobile solutions for BCI [4-5]. These developments are no longer aimed at neurophysiological research per se, nor limited to support motor-impaired users. Also the ongoing proliferation of passive BCI [6-7], where BCI is used by individuals without disabilities to support ongoing human-computer interaction, indicates an increased interest in applying BCI to real-world scenarios, outside of the experimental laboratory.

At the same time, developments in other areas are showing a clear need for information reflecting a user's cognitive or affective state. As systems become increasingly automated, researchers attempt to make the automated adaptation match the needs and preferences of the individual user. As these may vary between contexts and over time, it is important that this information can be assessed in real time within the given context [8]. Such information can be provided using passive BCI methodology. This can be fed into *neuroadaptive* [9] systems as implicit input [10], enabling them to support their users in a timely and individualized fashion.

One drawback of real-world scenarios is that they cannot be experimentally controlled. For EEG-based BCI in particular, the presence of electromagnetically active sources may interfere with or obscure the signal of interest. On top of that, users of real-world applications tend not to sit motionless for the duration of the activity. Thus, the myoelectric signals produced by the contracting shoulder, neck, and facial muscles contaminate the EEG recording. These movements as well displacements of the equipment itself may also introduce mechanical artifacts in the EEG recording.

We focus here on the real-world use scenario of an autonomously driving car. The use of in-car EEG and BCI have recently been investigated by e.g. [11-14], establishing that state detection is possible, although the signal-to-noise ratio is low due to environmental noise and movement artefacts. Here, we focus on rigorous cleaning methods in order to implement neuroadaptivity in the context of autonomous driving.

There is an increasing prevalence of automated driving systems taking over drivers' tasks. While there are clear benefits to this in terms of comfort and safety, the human driver is more and more disconnected from the activity and left out of the loop. The behavior of current automated driving systems could benefit from additional information concerning the human driver's perspective. That way, the human brain can serve as an additional sensor for the car, allowing the car to adapt to the needs and wishes of human driver. The driver can be implicitly kept in the human-machine interaction loop, and the car can benefit from the continuous, context-sensitive implicit input provided by the passive BCI.

The future car, thus, presents a highly promising but also challenging environment for BCI applications.

In this paper we present real-world, moving-car EEG recordings of drivers confronted with different types of behaviors from the car's adaptive cruise control (ACC) system. We investigate the detectability of elicited neuroelectric responses amidst unrelated myoelectric and electromagnetic noise. To that end, we use state-of-the-art data cleaning and filtering systems that can also be used online. We present event-related potential (ERP) analyses as well as classification accuracies.

MATERALS AND METHODS

Participants 15 participants (6 female) aged 24-60 participated. All possessed a valid driver's license for at least three years. They received a monetary reward for their participation. This study was conducted in accordance with the Army Research Laboratory's IRB requirements (DoDI 3216.02).

Published by Verlag der TU Graz
Graz University of Technology

 DOI: 10.3217/978-3-85125-533-1-47

Experimental Set-Up The experiment was conducted in a modified Toyota Prius, in which a TNO-designed ACC system was installed [15]. The car was driven on the test circuit of the Dienst Wegverkeer Test Centre Lelystad, Netherlands. Other vehicles were present on a larger track surrounding the track but did not interfere with the experimental procedure. The experimenter was present in the backseat of the car during the whole experiment.

We used a 64-channel BioSemi Active-Two to record EEG. We additionally recorded EOG above and below the left eye, ECG, and EMG on the left and right trapezius muscles. Peripheral data is not discussed in this paper (ECG and EOG findings are described [16]). All physiological signals were recorded at a sampling rate of 512 Hz using the same amplifier.

Task and Procedure Participants were told that we are working on automated detection of the driver's desired deceleration settings for an ACC, without requiring the driver to explicitly communicate this desire. We told them that since this is not yet possible, we use a recording of a human voice to represent the desired setting for each trial (i.e. "soft brake please", or "hard brake please"). Participants started with 10 practice trials to get familiar with the task and car dynamics, followed by 300 experimental trials.

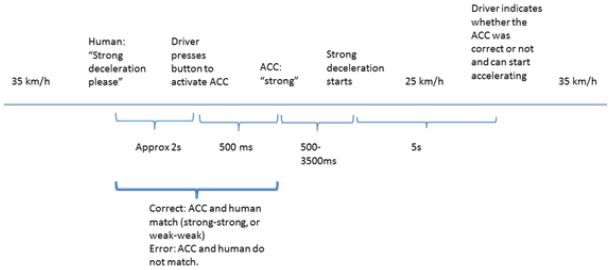

Figure 1: Overview of one trial.

The events constituting one experimental trial are depicted in Figure 1. The car drove at 35 km/h on the track when a human voice indicated the desired deceleration (either soft or hard, in Dutch; 50% chance). The participant pressed down a lever to activate the ACC deceleration. Before executing the deceleration, the ACC announced through a computer voice whether it would decelerate softly or strongly. In 80% of trials, the wish expressed by the human voice was followed (match trial), while in 20% it was not (mismatch trial). A variable time between 0.5 and 3.5 s after the ACC's announcement, the car decelerated to 25 km/h, following either a steep or a shallow velocity profile (i.e. strong or soft deceleration, a maximum deceleration of 3 or 0.7 m/s^2, respectively; total deceleration time of 0.9 or 2.8 s). Following this, the human voice asked the driver to accelerate again. The driver indicated whether the ACC had followed the desired type of deceleration or not, and pushed the lever up to have the ACC accelerate back to 35 km/h.

Data Processing We used EEGLAB [17] for processing. We compare the data after two different processing paths: "standard" and more rigorously ICA-cleaned data.

Standard preprocessed data was first high-pass filtered at 1 Hz using a Hamming windowed sinc finite impulse response filter. Heavily artifact-contaminated channels were then rejected using the `pop_rejchan` function, based first on kurtosis, and then on probability.

ICA-cleaned data received additional, more rigorous processing. First, the data was high-pass filtered as above at 2 Hz. Artifact subspace reconstruction (ASR; [18]) was used to clean the data. ASR uses a section of clean reference data to compute baseline statistics, and then detects subspaces in continuous data that significantly differ from this reference. It reconstructs the contents of the identified sections using a mixing matrix calculated on the reference data. We used those settings that led to the most rigorous cleaning within the recommended range (burst criterion: 3, window criterion: .05).

Infomax independent component analysis (ICA) on CUDA architecture [19] was applied to the ASR-cleaned data. ICA transforms the mixed-source EEG as recorded in sensor space into time series that are statistically maximally independent (independent components; ICs). Under the assumption that signals from different cortical processes and sources as well as artefactual sources are statistically independent from each other, this method thus transforms the data into 'source space'. ICA results in a transformation matrix, i.e. a filter matrix weighting the individual channels in sensor space, to isolate the different source activities. These independent activities can then be identified and subtracted individually.

The resulting transformation matrix was then copied back to the standard preprocessed data. The additional filtering and ASR cleaning was thus only applied in order to obtain a "clean" transformation matrix. Using this matrix, we then removed artefactual ICs from the standard preprocessed data. In the end, we compare standard preprocessed data versus that same data with artefacts removed through ICA.

Artefactual ICs were identified by manual inspection of their scalp projection and frequency spectrum, as per [20]. Artefactual ICs were removed from the data such that only activity remained that could reasonably be assumed to be cortical. In brief, components were not removed only if they clearly fit two main criteria: a) dipolar, not too superficial projection pattern, and b) clear, smooth peaks in the power spectrum at frequencies known to have clear cortical correlates, mostly below 30 Hz, with no high power beyond those frequencies.

The windowed means approach using regularized shrinkage linear discriminant analysis [21], implemented in BCILAB [17], was used for classification. Data was band-pass filtered between 1 and 15 Hz and segmented into six non-overlapping consecutive time windows of 50 ms each, from 0.2 to 0.5 s after the respective event—a time window that, a priori, could be expected to contain relevant responses to the experimental manipulations. We compare the response to the ACC announcing the upcoming braking behavior (match versus mismatch, strong versus soft), as well as to the actual braking. We used a five-fold nested cross-validation to compute classification accuracy estimates.

Published by Verlag der TU Graz
Graz University of Technology

 DOI: 10.3217/978-3-85125-533-1-47

ERP analyses include statistics computed per sample between subjects on the amplitude differences of the two classes, using permutation tests with 1000 permutations.

ASR and ICA cleaning was applied to the whole dataset. Cross-validated BCI performance estimates are calculated based on these cleaned sets as an additional measure of potential differences between the sets.

RESULTS

An average of 4 channels (ranging from 0 to 8) were removed from the initial data. From the on average 60 remaining independent components, an average of 8 (ranging from 2 to 14) ICs were identified as being cortical. All others were removed. See figure 2 for a small but representative selection of ICs that were kept.

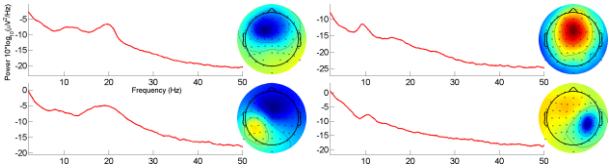

Figure 2: Four ICs that fit the main criteria: spectral speaks in sub-gamma bands and dipolar patterns.

The artefactual noise was not spread evenly across the channels, but was most prominent on parietal and occipital sites. Figure 3 shows grand-average ERPs for the four comparisons. We focus mostly on Oz, a highly contaminated site showing the effect of the ICA cleaning most clearly. To illustrate the vast differences of the noise distribution between the different sites, and the effect on cleaner sites, for one condition, we also present the ERP at the less contaminated electrode Cz. ERPs extracted from standard-preprocessed data are shown on the left; the ICA-cleaned data on the right. Significant differences ($p < 0.05$) are highlighted in grey.

Significant differences can be seen between the peak amplitude around 200 ms in the ICA-cleaned data at electrode Oz comparing the announcement onset of hard versus soft upcoming braking behavior. Also at Oz in ICA-cleaned data, significant differences can be seen around 500 to 600 ms after hard versus soft brake onset. These late differences are most likely due to the experience of the braking itself and not relevant to the driver's mental preparation thereof—thus, we did not update our classification approach to go beyond 500 ms.

Tables 1 to 4 list the individual and mean classification accuracy estimates for the same classifier calibrated on standard-preprocessed data and on ICA-cleaned data for all four comparisons. These results are summarized and discussed in the next section.

CONCLUSION AND DISCUSSION

We have recorded data from 15 participants controlling a moving car. They were confronted with different and sometimes unexpected behavior of the automated driving system, in the form of either strong or soft deceleration. We applied state-of-the-art cleaning and filtering methods in order to investigate the detectability of cortical events amidst the many artifacts produced by the car itself and the participants' movements.

The ICA cleaning of the data was rigid, removing, in one case, all but only two independent components, and in all cases no less than three-fourths of all components. We see, however, that even in this heavily contaminated data it was still possible to identify cortical activity: we see clear event-related potentials reflecting cortical responses to various driving-related events, on electrodes where the original preprocessed signal was completely drowned out by large-amplitude artifacts (e.g. Oz).

Indeed, even given very large-amplitude artifacts (up to 23 µV on Oz), the relatively small cortical signals (<1 µV on that same electrode) could be identified with sufficient sensitivity to allow significant differences to become apparent between the classes.

At less contaminated sites, e.g. electrode Cz, we see that the signal is hardly affected even by such rigorous cleaning. The cortical signals remain intact.

The ERP plots show no significant difference between match and mismatch trials. The experimental set-up likely did not make this distinction sufficiently meaningful to the participant to evoke a clearly discriminable signal. Participants were not instructed to pay attention to this, and were occupied by the primary task of driving, so indeed little effect was expected [22].

Because of this, we also see no general classifiability of match versus mismatch events, nor an improvement in classification accuracy after to ICA cleaning. Given the imbalanced number of classes, chance level is at 68% (±5.2, $\alpha = 0.05$). Neither standard preprocessed nor ICA-cleaned data is classifiable. We do, however, see an increase in the balance of the classes after ICA cleaning (i.e. the true positive divided by the true negative rate).

Comparing hard versus soft trials, chance level here is 49% (±5.6, $\alpha = 0.05$). Time-locked to brake onset, we see a very high classification accuracy of 94% in standard preprocessed data. This decreases significantly after ICA cleaning ($p < 0.01$). This is likely because in the non-cleaned data, strong mechanical and muscular artifacts correlate to these two classes: a steeper braking profile will lead to increased muscular activity and movement. These artifacts are used by the classifier. In the cleaned data, these artifacts are removed and the classifier is only given the activity that was identified to be cortical. This still leads to a classification accuracy of 77%, significantly better than chance.

Time-locked to the onset of the announcement, classification accuracy is 63% without cleaning, and cleaning does not significantly change this ($p = 0.32$). This shows a cortical response to the announcement that is detectable at a single-trial level. The lack of impact on classification accuracy shows that ICA cleaning does not negatively affect these cortical aspects of the data.

The ASR cleaning method can be applied online. Although the precise ICA implementation used here was not online, methods have been developed to calculate ICA transformation matrices online [23]. The two measures on which component selection was based, scalp projection and power spectrum, are thus also available online. It is likely, in fact, that online ICA will give better

Published by Verlag der TU Graz
Graz University of Technology

 DOI: 10.3217/978-3-85125-533-1-47

results as it can be configured to put more weight on current time windows, making it adaptive to the current context. In [23], the selection of which components to keep and which to remove can be done online but must be done manually. However, (semi)automatic component identification is underway [24].

These methods, thus, allow for strong, rigorous cleaning and filtering of data during continuous, online BCI operation. As we have shown here, these state-of-the-art methods are capable of identifying cortical processes even amidst large-amplitude artefacts that would otherwise drown out the signal of interest.

ICA-based cleaning can target artefactual activity specifically, affecting cortical processes only to a minimal degree. This can provide a large advantage for real-world neuroadaptive technology in realistic settings.

ACKNOWLEDGEMENTS

This research was funded by the U.S. Army Research Laboratory and was accomplished under Contract Number W911NF-10-D-0002.

REFERENCES

[1] Zander TO, Lehne M, Ihme K, Jatzev S, Correia J, Kothe CA, … Nijboer F (2011). A dry EEG-system for scientific research and brain-computer interfaces. Front. Neurosci., 5, 53.

[2] Chi YM, Wang YT, Maier C, Jung TP, Cauwenberghs G (2012). Dry and noncontact EEG sensors for mobile brain-computer interfaces. IEEE Trans. Neural. Sys. Rehab. Eng., 20(2), 228-235.

[3] Guger C, Krausz G, Allison BZ, Edlinger G (2012). Comparison of dry and gel based electrodes for P300 brain-computer interfaces. Front. Neurosci., 6, 60.

[4] Debener, S, Minow F., Emkes R., Gandras K, de Vos M (2012). How about taking a low-cost, small, and wireless EEG for a walk? Psychophysiology, 49(11), 1617–1621.

[5] Gargiulo G, Bifulco P, Calvo RA, Cesarelli M, Jin C, van Schaik A (2008). A mobile EEG system with dry electrodes. IEEE Biomed Circuits Syst 273-276.

[6] Zander TO, Kothe, CA (2011). Towards passive brain-computer interfaces: applying brain-computer interface technology to human-machine systems in general. J Neural Eng, 8(2), 025005.

[7] Zander TO, Kothe CA, Welke S, Rötting M (2008). Enhancing human-machine systems with secondary input from passive brain-computer interfaces. In Proc Graz BCI ’08, Graz, Austria, 144–149.

[8] Zander TO, Jatzev S (2012). Context-aware brain-computer interfaces: exploring the information space of user, technical system and environment. J Neural Eng, (1), 016003.

[9] Zander TO, Krol LR, Birbaumer NP, Gramann K (2016). Neuroadaptive technology enables implicit cursor control based on medial prefrontal cortex activity. PNAS, 113(52), 14898-14903.

[10] Zander TO, Brönstrup J, Lorenz R, Krol LR (2014). Towards BCI-based Implicit Control in Human-Computer Interaction. In Fairclough SH, Gilleade K (Eds.), Advances in Physiological Computing (pp. 67–90). Berlin, Germany: Springer.

[11] Zander TO, Andreessen LM, Berg A, Bleuel M, Pawlitzki J, Zawallich L., Krol, LR, Gramann, K (2017). Evaluation of a dry EEG system for application of passive brain-computer interfaces in autonomous driving. Front Human Neurosci, 11, 78.

[12] Haufe S, Kim JW, Kim IH, Sonnleitner A, Schrauf M, Curio G, Blankertz B (2014). Electrophysiology-based detection of emergency braking intention in real-world driving. J Neural Eng, 11(5), 056011.

[13] Lin CT, Wu RC, Liang SF, Chao WH, Chen YJ, Jung TP (2005). EEG-based drowsiness estimation for safety driving using independent component analysis. IEEE Trans Circuits Syst I, 52(12), 2726–2738.

[14] Wang YK, Chen SA, Lin CT. (2014). An EEG-based brain-computer interface for dual task driving detection. Neurocomputing, 129, 85–93.

[15] Ploeg J (2014) Analysis and design of controllers for cooperative and automated driving. PhD Thesis, TU/e, Eindhoven, The Netherlands, 2014.

[16] Brouwer AM, Snelting A, Jaswa M, Flascher O, Krol, LR, Zander, TO (in press). Physiological effects of Adaptive Cruise Control Behaviour in Real Driving. In Proc. IUI’17, Limassol, Cyprus.

[17] Delorme A, Mullen T, Kothe C, Acar ZA, Bigdely-Shamlo N., Vankov A, Makeig, S. (2011). EEGLAB, SIFT, NFT, BCILAB, and ERICA: New Tools for Advanced EEG Processing. Comput Intell Neurosci, 2011, 10:10–10:10.

[18] Mullen T, Kothe C, Chi YM, Ojeda A, Kerth T, Makeig S., ... Jung TP (2013). Real-time modeling and 3D visualization of source dynamics and connectivity using wearable EEG. In Proc. IEEE EMBC ’13, Osaka, Japan.

[19] Raimondo F, Kamienkowski JE, Sigman M, Slezak, DF (2012). CUDAICA: GPU optimization of infomax-ICA EEG analysis. Comput Intell Neurosci., 2012, 2:2–2:2.

[20] Jung TP, Makeig S, Humphries C, Lee TW, McKeown MJ, Iragui V, Sejnowski TJ (2000). Removing electroencephalographic artifacts by blind source separation. Psychophys 37(2), 163-178.

[21] Blankertz B, Lemm S, Treder MS, Haufe S, Müller KR (2011). Single-trial analysis and classification of ERP components. NeuroImage, 56(2), 814–825.

[22] Thurlings ME, van Erp JBF, Brouwer AM, Werkhoven PJ (2013). Controlling a tactile ERP-BCI in a dual-task. IEEE Trans Comput. Intell. AI Games, 5(2).

[23] Hsu SH, Mullen T, Jung TP, Cauwenberghs G. (2014). Online recursive independent component analysis for real-time source separation of high-density EEG. In Proc IEEE EMBC’14, Chicago, US.

[24] Chaumon M, Bishop DV, Busch NA. (2015). A practical guide to the selection of independent components of the electroencephalogram for artifact correction. J Neurosci Methods, 250, 47–63.

Published by Verlag der TU Graz
Graz University of Technology

 DOI: 10.3217/978-3-85125-533-1-47

	Announce match vs. mismatch							
	Standard				ICA			
P	TP	TN	Rat.	Acc.	TP	TN	Rat.	Acc.
1	32	74	0.42	66	44	61	0.72	58
2	25	77	0.33	66	39	74	0.53	67
3	30	74	0.40	66	37	64	0.58	58
4	37	78	0.47	69	48	59	0.82	57
5	32	78	0.41	69	47	73	0.64	67
6	40	76	0.53	69	35	60	0.58	55
7	23	71	0.33	62	33	64	0.52	58
8	25	68	0.37	59	42	59	0.70	56
9	33	70	0.48	62	38	63	0.61	58
10	38	75	0.51	68	43	66	0.65	62
11	30	68	0.44	60	42	56	0.75	53
12	52	85	0.61	78	45	75	0.60	69
13	40	76	0.53	69	43	65	0.66	61
14	30	68	0.44	61	38	59	0.65	55
15	48	79	0.61	72	47	61	0.77	58
	34	74	0.46	66	41	64	0.65	59

Table 1: Classification accuracy estimates for all fifteen participants based on standard-preprocessed data and ICA-cleaned data. Classification distinguished between match versus mismatch trials, time-locked to announcement onset. P = participant number, TP = true positive rate, TN = true negative rate, Rat. = TP/TN, Acc. = combined classification accuracy. Due to class imbalances, chance level is at 68% (±5.2, $\alpha = 0.05$).

	Brake match vs. mismatch							
	Standard				ICA			
P	TP	TN	Rat.	Acc.	TP	TN	Rat.	Acc.
1	16	69	0.23	59	44	65	0.67	61
2	35	72	0.48	65	37	67	0.54	61
3	31	66	0.47	59	36	61	0.60	56
4	39	73	0.54	66	36	57	0.63	53
5	22	67	0.32	58	28	62	0.46	55
6	27	75	0.36	65	37	64	0.57	59
7	22	69	0.32	59	40	59	0.68	55
8	29	74	0.39	65	33	65	0.51	59
9	31	61	0.51	55	36	63	0.57	58
10	17	73	0.23	61	43	70	0.62	64
11	44	73	0.61	67	44	61	0.72	58
12	28	77	0.37	67	50	67	0.75	63
13	33	64	0.52	58	40	61	0.66	56
14	30	64	0.47	57	47	54	0.86	53
15	38	65	0.57	59	31	59	0.53	54
	29	69	0.43	61	39	62	0.62	58

Table 3: As table 1, with classification distinguishing between match versus mismatch trials, time-locked to brake onset.

	Announce hard vs. soft							
	Standard				ICA			
P	TP	TN	Rat.	Acc.	TP	TN	Rat.	Acc.
1	64	61	1.05	63	63	57	1.10	60
2	66	55	1.19	60	66	59	1.13	62
3	47	63	0.75	55	56	59	0.94	57
4	61	59	1.03	60	61	66	0.92	63
5	55	61	0.89	58	52	53	0.99	52
6	57	63	0.89	60	61	59	1.03	60
7	78	74	1.05	76	68	68	1.00	68
8	54	63	0.85	58	62	56	1.10	59
9	49	48	1.01	48	45	55	0.82	50
10	78	69	1.13	74	67	71	0.95	69
11	68	68	1.01	68	58	55	1.06	57
12	72	65	1.10	69	74	67	1.10	71
13	64	73	0.88	68	55	61	0.90	58
14	55	55	0.99	55	62	59	1.06	60
15	59	70	0.85	65	52	55	0.94	54
	62	63	0.98	63	60	60	1.00	60

Table 2: As table 1, with classification distinguishing between hard versus soft brake trials, time-locked to announcement onset. Chance level is at 49% (±5.6, $\alpha = 0.05$).

	Brake hard vs. soft							
	Standard				ICA			
P	TP	TN	Rat.	Acc.	TP	TN	Rat.	Acc.
1	94	85	1.10	89	91	79	1.16	85
2	99	90	1.10	95	79	74	1.07	77
3	87	85	1.02	86	68	69	0.99	69
4	98	93	1.05	96	80	72	1.11	76
5	95	94	1.01	95	65	68	0.96	67
6	99	90	1.10	94	75	77	0.97	76
7	99	96	1.03	98	79	69	1.14	74
8	95	83	1.15	89	67	64	1.05	65
9	99	94	1.05	96	96	90	1.07	93
10	97	90	1.08	94	93	85	1.10	89
11	88	79	1.11	83	88	72	1.22	80
12	100	99	1.01	99	82	76	1.07	79
13	100	98	1.02	99	68	62	1.09	65
14	99	99	1.01	99	75	67	1.13	71
15	99	96	1.04	97	92	79	1.17	85
	97	91	1.06	94	80	73	1.09	77

Table 4: As table 2, with classification distinguishing between hard versus soft trials, time-locked to brake onset.

Published by Verlag der TU Graz
Graz University of Technology

 DOI: 10.3217/978-3-85125-533-1-47

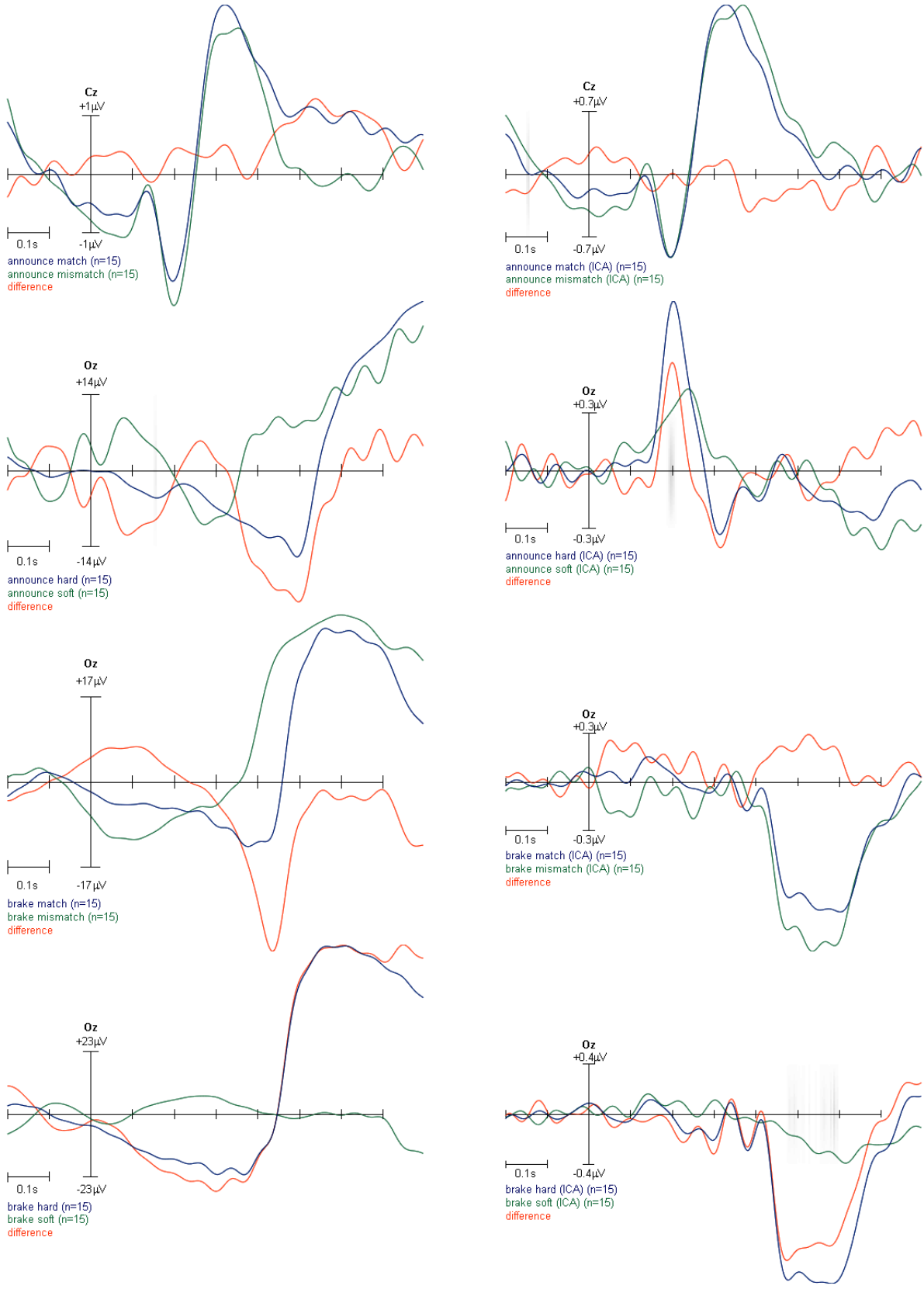

Figure 3: Grand average (n=15) event-related potentials of standard-preprocessed (left) and ICA-cleaned data (right). Top to bottom: ERP at Cz time-locked to the ACC announcement onset of the upcoming braking behavior, match versus mismatch trials; ERP at Oz time-locked to the same, announcing "hard" versus "soft"; ERP at Oz time-locked to the onset of the braking behavior itself, match versus mismatch trials; ERP at Oz time-locked to the same, hard versus soft braking. Significantly different samples are highlighted in grey, modulated by p-values (lower p-value = darker grey).

Published by Verlag der TU Graz
Graz University of Technology

Proceedings of the
7th Graz Brain-Computer Interface Conference 2017 DOI: 10.3217/978-3-85125-533-1-48

NON-STATIONARITY AND INTER-SUBJECT VARIABILITY OF EEG CHARACTERISTICS IN THE CONTEXT OF BCI DEVELOPMENT

T. Krumpe [1], K. Baumgärtner [1], W. Rosenstiel [1], M. Spüler [1]

[1] Department of Computer Engineering, Eberhard Karls University Tübingen, Tübingen, Germany

E-mail: tanja.krumpe@uni-tuebingen.de

ABSTRACT: In a vision of a perfect brain-computer interface (BCI), a user would be able to use the system instantly without the need for a subject-specific calibration, and the performance would remain stable and not deteriorate over time. However, this remains a vision, due to two characteristics of the electroencephalography (EEG) signals: non-stationarity and inter-subject variability. Inter-subject variability describes the fact that the EEG of each person is different and for sufficient BCI communication, the BCI needs to be calibrated separately for each user. Non-stationarity describes a change over time of the EEG signals leading to a decrease in BCI performance with prolonged use. In an approach to better understand these issues, we analyzed the event-related potentials (ERP) and spectral EEG data of 23 subjects in terms of these characteristics. We found that both issues highly affect the data, but we were able to identify a method that nearly eliminates non-stationarity, whereas inter-subject variability remains a major issue that needs to be further addressed.

INTRODUCTION

Using EEG for the signal acquirement in BCI applications is very common and broadly used in research but has some obstacles that prevent a user friendly usage out of the lab. Since scalp EEG recordings represents the summarized activity of a great number of neurons, small changes in the mental state of the user can already make a difference in the overall activity that can be measured. Therefore, training phases before every session are necessary to adapt the system to the current EEG characteristics and mental state of the user in order to guarantee a good performance of the system. Even with long training phases before the start of a session major decrease in performance can occur with increasing time of the session. This will result in a loss of usability and increasing frustration of the subject, which is naturally not desired. Non-stationarity of the signal can be the cause of this, introduced for example by mental changes of the subject (fatigue, disengagement,..) or technical changes (drying electrode gel), leading to differences in the appearance of the trained target signals which in turn leads to a failure of the classifier. Decreasing performance with duration of a session or especially in between offline and online sessions due to a change of the target signal has been observed numerous times. An online, real-time, adaption of the classifier to the upcoming changes in the brain activity is one way to deal with this issue. The classifier is recalibrated by integrating currently recorded data into the already existing data. Supervised [1] as well as unsupervised [2,3] methods have been proposed for the implementation of adaption mechanisms, partly solving this issue. It has also been suggested that the combination of different types of classifiers can reduce the issue of non-stationarity, as they complement each other [4].
Apart from issues within a single session or between online and offline sessions, there are also issues between different subjects that have hardly been solved so far. The issue can be referred to as inter-subject variability which prevents the successful transfer of a previously trained classifier to a new subject, since the differences in EEG signals are usually too big between subjects even though the same task is performed. In some cases normalization methods have been used in order to deal with this variability as for example scaling the data to the mean and standard deviation of a certain number of baseline trials [5]. This can reduce the problem but still cross-subject classification is significantly worse than within subject classification, leaving cross-subject classification an open problem. Other methods like transfer learning, supervised as well as unsupervised, provide the same portion of solution. Information from previously collected trials and subjects can be used to infer knowledge to new and unknown data. Approaches using hierarchical Bayesian models based on Gaussian probability distributions [6,7] or k-Nearest Neighbor approaches [8] for training and optimizing a classifier based on old and new data have been introduced. Almost all approaches are still adaptive since the collection of new and subject specific data is necessary to update the classifier and to integrate subject specific information into the classification approach, therefore persisting the necessity of individual training.

In contrast to this, other approaches were implemented in which researchers used the distinct differences of EEG signals of different subjects during the same task to their advantage. It could be shown that an identification or authentication of a specific subject out of many is possible. Armstrong and colleagues used ERP characteristics [9] and Palaniappan features based on the power spectrum [10] for the authentication of a specific subject which was successfully with almost no errors. This opens up new possibilities for applications using EEG-BCI technology.

Published by Verlag der TU Graz
Graz University of Technology

 DOI: 10.3217/978-3-85125-533-1-48

The aim of the analysis of this paper is to quantify the extent of non-stationarity and inter subject variability in EEG data to better understand these properties. A large dataset from a standard BCI application was chosen for an anew analysis with respect to the mentioned factors. The data set allowed within and between session as well as between subject comparisons which were evaluated with classical correlation and classification measures. The following sections will describe the properties of the chosen dataset, the methods used for quantification of the two stated issues and several approaches to deal with non-stationarity in EEG data.

MATERIALS AND METHODS

Data: A dataset of Spüler and colleagues [11] consisting of EEG recordings of 23 subjects participating in a P300 speller experiment was used for the analysis. The dataset consists of 2 sessions on two different days for each subject. The participants can be divided into three groups according to their age and health status. Group 1 consists of 9 subjects between age 20 - 28, Group 2 of 8 subjects between age 39 - 52 and the third group was a patient group with severe motor impairments consisting of 6 subjects between the age of 36 - 63. The montage was, in standard 10/20 positions, with electrodes at positions F3, Fz, F4, T7, C3, Cz, C4, T8, CP3, CP4, P3, Pz, P4, PO7, PO8, Oz. Ground and reference electrodes were placed at the left and right mastoid, respectively and the signal was sampled at 256 Hz. The P300 speller consisted of a 6x6 matrix in which the 12 rows and columns of symbols were flashed in random order. Each intensification lasted for 62.5 ms and the matrix remained blank for 125 ms between flashes. In one sequence, each row and column were flashed exactly once. One trial contained 2-10 sequences, depending on the subject. This dataset was chosen as it was comparably big and it included two sessions per subject. Therefore, it provided the opportunity to investigate changes across subjects and changes over time within a session as well as across sessions. To that end, inter subject variability as well as non-stationarity can be evaluated and compared within this dataset.

Data processing: For the analysis, ERPs and power spectra of the data were evaluated. The power spectra were calculated for each trial separately with Burgs maximum entropy method [12] (modelorder 16), from 1 to 30 Hz in 1 Hz bin. In contrast to that, ERPs were averaged over several target intensifications, to improve the signal to noise ratio. One ERP in the analysis was calculated by sequentially averaging over 50 target intensifications using a sliding window approach with a step size of 10. This lead to an average number of 237 trials ($\pm$ 49) and 145 ($\pm$ 68) ERPs for session one and 273 trials ($\pm$ 80) and 169 ($\pm$ 68) ERPs for session two.

Inter subject variability: Evaluating the effect of inter-subject variability was done by a classification approach that aimed to assign ERPs and power spectra to the subject they originated from. Two different approaches were tested, one with the aim to identify a subject correctly on the basis of the ERPs (or power spectra) and the other one with the aim to authenticate a subject on the same signals. Since distinct differences between subjects are assumed to be present, a SVM classification approach should be able to separate the data of different subjects according to their differences. For the identification scenario a one vs one classification was implemented in which it is tested how well a subject can be identified within a set of subjects. Therefore, one classifier was trained on one session for each pair of subjects and tested on the second session of all possible pairs. To determine the accuracy a multiclass-classification was performed.
For the authentication scenario a one vs all classification was implemented. One individual classifier was trained for each subject to distinguish between data of the subject itself and the data of all others. Again one session was used for training, the other session used for testing. In this case sensitivity and specificity were used as performance measures to account for the highly unbalanced classes. If the signals of one subject can be extracted from a variety of signals, it validates that the signal of a single subject does stand out and is distinct. It can be seen as an authentication approach since a yes or no decision is made, answering the question if the signal belongs to the person in question.
In consequence both classification approaches reveal a measure to quantify the inter-subject variability within the given dataset. The higher the performance measures the higher the variability between subjects. For both approaches a C-SVM from the libsvm implementation [13] for Matlab was used in a 5-fold cross-validation. The data of all 16 electrodes was used for the classification.

Non-stationarity: To evaluate the non-stationarity of the signal linear regression models were fit to the ERPs (and the power spectra) and the time of their occurrence in the recording (1...n), again in a 5-fold cross-validation. The occurrence in the recording was labeled consecutively with increasing numbers representing the time of appearance. This was done individually for each subject and session. The regression models are evaluated by calculating R^2 values to estimate how well the time of recording can be predicted from the EEG signals. The R^2 value denotes the proportion of variance in the target variable that is explained by the predicted values. Systematic changes over time that can be described by a linear function should lead to a strong correlation, therefore, quantifying non-stationarity to a certain extent. In addition to quantifying non-stationarity, several methods to decrease the influence of non-stationarity were tested and evaluated. The measure for quantification of non-stationarity after the application of the tested approaches remained the same: A fitted linear regression model and its corresponding R^2 values, representing the correlation between actual and predicted time in recording.
(1) First covariate shift adaption was applied to the data. It reduces trial to trial variability in the distribution of spectral power, by normalizing the power with an averag-

Published by Verlag der TU Graz
Graz University of Technology

 DOI: 10.3217/978-3-85125-533-1-48

ing approach shifting over a certain number of preceding trials. The originally proposed window size of w = 15 was used [14].

$$(t) = P(t) - \frac{1}{w}(\sum_{i}^{w} P(t-i)) \quad (1)$$

The hypothesis is that an overall reduced variability might erase the change in signal introduced by non-stationarity.
(2) As a second approach lateral symmetry was calculated on the data for the electrode pairs (F3-F4, T7-T8, C3-C4, Cp3-Cp4, P3-P4, Po7-Po8). It reveals lateral disparities or asymmetries between the two hemispheres and could possibly minimize systematic changes that are present in the signal. Two different ways of calculating the difference were applied. Once the signal of the two electrodes was subtracted before transferring it into the frequency domain, and the other time the signal was subtracted after transferring it to the frequency domain.
(3) As a last approach event related desynchronization or synchronization (ERD/S) was computed by using the difference of the power spectral density of the trial and a time frame of equal size shortly before (pretrial) [15]. The quotient of the difference and the power of the pretrial reveals the ratio of how much the power has changed due to an event by a (de-)synchronization of firing neurons. Again the hope is that this mathematical approach might erase a possibly present systematical change in the signal.

$$ERD/S = \frac{P_{trial} - P_{pretrial}}{P_{pretrial}} \quad (2)$$

RESULTS

Tab. 1 shows the results of the analysis concerning non-stationarity in the data. It includes the R^2 values between the actual time in recording of a trial and the predicted time (with regression methods) for session one. Session two revealed the same trend which is why only the results of one of the two is shown. The individual columns represent the different signals that were used for the analysis, standard ERP and power spectrum and the transformed data according to the four suggested methods. When looking at column two and three it can be seen that the prediction quality is much higher for the spectral density distribution than for the ERPs on average for all subjects. When comparing those two columns to the remaining ones in the table it can also be seen that applying lateral symmetry (difference calculated after) to the data reduces the R^2 value notably, whereas ERD/S reduces it to almost 0. The other two methods have smaller or no notable effects on the correlation with the time of recording. Tab. 2 shows the results of the evaluation of inter-subject variability. It is quantified by the classification performance measured in accuracy or sensitivity and specificity depending on the mode of classification. The table is divided into two parts, each representing one mode of classification. Identifying the signals of an individual subject (across sessions), represented in the left part of the table, works better on the basis of ERPs than on the basis of the spectral density distribution (One vs One). The same observation can be made for the authentication approach (One vs All). The One vs All approach reaches very high specificities (TNR) for both signal types (above 97%), whereas the sensitivity (TPR) is much lower in both cases, but significantly better for ERP than spectral data (0.76 vs 0.49 on average respectively). In both approaches it can be seen that the variance of the performance between subjects is rather high, especially for classification on the spectral data. Both tables reveal that there seem to be differences between the three groups of subjects more or less pronounced throughout the various approaches.

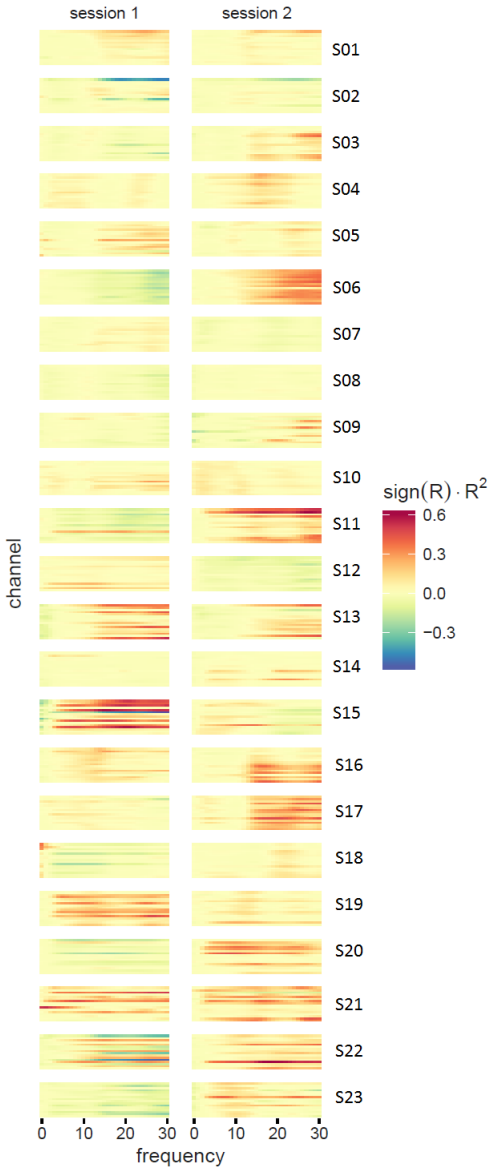

Figure 1: The colors indicate the squared correlation (R^2) between spectral features and the time of recording for each subject and both sessions. Channels from top to bottom: Po8, Oz, Po7, P4, Pz, P3, Cp4, Cp3, T8, C4, Cz, C3, T7, F4, Fz, F3)

Published by Verlag der TU Graz
Graz University of Technology

 DOI: 10.3217/978-3-85125-533-1-48

Table 1: Correlation (R^2) of the actual time and predicted time of each trial in the recording, regression based, for 23 subjects of 3 groups. a) Covariate Shift adaption, b) Lateral symmetry (before), c) Lateral symmetry (after), d) ERD/S

Sub	ERP	Spec	a)	b)	c)	d)
S01	0.20	0.38	0.40	0.38	0.22	0.01
S02	0.37	0.80	0.62	0.82	0.71	0.11
S03	0.37	0.33	0.63	0.20	0.04	0.03
S04	0.20	0.23	0.57	0.72	0.04	0.01
S05	0.30	0.67	0.46	0.60	0.45	0.12
S06	0.29	0.22	0.43	0.29	0.06	0.06
S07	0.50	0.24	0.51	0.35	0.08	0.07
S08	0.20	0.16	0.49	0.31	0.06	0.01
S09	0.21	0.26	0.36	0.10	0.05	0.02
Mean	**0.29**	**0.37**	**0.50**	**0.42**	**0.19**	**0.05**
S10	0.16	0.41	0.46	0.47	0.19	0.01
S11	0.49	0.73	0.36	0.48	0.35	0.02
S12	0.14	0.26	0.20	0.32	0.15	0.03
S13	0.34	0.81	0.62	0.76	0.71	0.04
S14	0.30	0.22	0.66	0.44	0.09	0.06
S15	0.19	0.83	0.32	0.73	0.69	0.07
S16	0.28	0.54	0.35	0.59	0.14	0.02
S17	0.13	0.67	0.43	0.57	0.32	0.04
Mean	**0.25**	**0.56**	**0.42**	**0.55**	**0.33**	**0.04**
S18	0.12	0.85	0.36	0.89	0.75	0.11
S19	0.08	0.81	0.54	0.80	0.58	0.01
S20	0.18	0.78	0.37	0.80	0.76	0.10
S21	0.02	0.74	0.60	0.66	0.77	0.01
S22	0.14	0.89	0.25	0.56	0.87	0.04
S23	0.08	0.60	0.71	0.75	0.55	0.03
Mean	**0.10**	**0.78**	**0.47**	**0.74**	**0.71**	**0.05**
Mean	**0.23**	**0.54**	**0.46**	**0.55**	**0.37**	**0.04**
std	0.13	0.26	0.14	0.22	0.30	0.04

Especially notable are the high R^2 values for spectral data of the patient group in contrast to the other two groups of subjects. Fig. 1 visualizes the analysis of the non-stationarity by plotting the R^2 values for each channel and the respective spectral features of each subject for both sessions. It is included as a showcase to show the variance between and within subjects to highlight the problem statement.

DISCUSSION

The results presented in Tab. 1 and Tab. 2 revealed that non-stationarity and inter-subject variability can be measured and quantified with the proposed methods. Both are highly present in the dataset underlining the importance of awareness of these issues during BCI development. Non-stationarity was assessed by detecting a systematic change of EEG characteristics over time by linear regression methods. It is strongly present in the power spectra of the signal and a little less prominent in the ERP data. Depending on the application, this change in signal might not be a relevant issue, but to ensure the use of valid features that are related to the cognitive process of interest and not to a systematically introduced artifact, this effect needs to be eliminated.

Table 2: Classification performance quantified in accuracy or TPR (sensitivity) and TNR (specificity) in a single-subject approach - training on session 1 - testing on session 2, with a C-SVM and a linear kernel in a 5-fold cross-validation.

	One vs All				One vs One	
Sub	ERP		Spec		ERP	Spec
	TPR	TNR	TPR	TNR	Acc	Acc
S01	0.80	1.00	0.95	0.98	0.99	0.90
S01	0.95	1.00	0.61	0.99	0.99	0.79
S03	0.98	1.00	0.81	0.95	0.99	0.91
S04	0.82	1.00	0.80	0.97	0.97	0.91
S05	0.88	1.00	0.40	0.99	0.85	0.18
S06	0.59	1.00	0.44	0.93	0.65	0.18
S07	0.90	1.00	0.53	0.94	0.85	0.72
S08	0.78	0.98	0.85	0.99	0.91	0.90
S09	0.86	1.00	0.39	0.97	0.96	0.51
Mean	**0.84**	**0.99**	**0.64**	**0.96**	**0.90**	**0.66**
S10	0.67	1.00	0.96	0.99	0.70	0.95
S11	0.75	1.00	0.00	0.99	0.95	0.00
S12	0.85	0.99	0.48	0.95	0.92	0.45
S13	0.86	1.00	0.38	0.97	0.99	0.53
S14	0.97	1.00	0.85	0.99	0.99	0.72
S15	0.25	0.99	0.00	0.96	0.33	0.01
S16	0.63	0.99	0.00	0.96	0.80	0.00
S17	0.94	1.00	0.18	0.98	0.93	0.38
Mean	**0.74**	**0.99**	**0.36**	**0.97**	**0.82**	**0.38**
S18	0.80	1.00	0.66	0.90	0.80	0.88
S19	0.33	0.99	0.22	0.94	0.56	0.24
S20	0.60	0.99	0.01	1.00	0.75	0.00
S21	0.53	1.00	0.26	1.00	0.65	0.27
S22	0.82	0.98	0.59	0.94	0.88	0.70
S23	0.97	1.00	0.89	0.95	0.97	0.94
Mean	**0.67**	**0.99**	**0.44**	**0.95**	**0.77**	**0.51**
Mean	**0.76**	**0.99**	**0.49**	**0.97**	**0.84**	**0.53**
std	0.20	0.01	0.32	0.02	0.17	0.35

Our analysis was able to show that the systematic change over time can be reduced by using the lateral symmetry (R^2 of 0.30), whereas ERD/S can reduce the effect of time to a minimum (R^2 of 0.04) if not eliminate it completely. The systematic change over time affecting ERPs was rather weak. The R^2 value accounted for a squared correlation of 0.23 on average, leading to the assumption that the effect is merely present or can at least not be predicted well with linear regression methods. Non-stationarity therefore seems to be a bigger issue when dealing with frequency-domain than with time-domain features. Interestingly the patient data (subject 18-23) showed a much higher correlation with time in the power spectra than all other subjects did. Nevertheless ERD/S provided a solution for this equally well to subjects with high and also to subjects with low correlation of the power spectra with time of recording. No further universal trends can be derived concerning the different groups of subjects. At this point it needs to be mentioned that the evaluated non-stationarity is linear only, non-linear non-stationarity, which also exists, has not been accounted for in this paper and needs to be addressed further. It can be observed

Published by Verlag der TU Graz
Graz University of Technology

 DOI: 10.3217/978-3-85125-533-1-48

that the variance is in general very high for all evaluated measures between the groups but also within the groups leading over to the topic of inter-subject variability. A first assumption can be made that the inter-subject variability is supposedly very high since a high variance between the R^2 values can be observed. No pattern across subjects is visible, hence for each subject other features provide discriminability. Inter-subject variability was investigated with a classification approach and the achieved performance measures suggest differences between subjects are reflected more strongly in ERPs than in the power spectra. The assignment of the current trial to the correct subject, in a pairwise or overall comparison, can express the stability of the signal across time and sessions or the great variability between subjects. Both are equally valid assumptions that do not exclude each other. The results showed that an assignment of the correct subject based on the ERPs was possible in both classification approaches with good performance values whereas the assignment on the basis of the power spectra worked less well. Since the train and test set were taken from two different sessions it can be assumed that ERPs contain very specific sections that can be identified across sessions. Due to the high performance values it can also be assumed that differences between the subjects must be very distinct, again at least for the ERPs. The performance values therefore suggest, that a biometric use of P300 ERPs could be feasible for an identification as well as an authentication of the subject in question. Regarding the classification on the power spectra it can be said that the variability between subjects must be severe since a high (close to perfect) specificity can be achieved. The rather low sensitivity leads to the assumption that the signal is likely to be not unique enough or too different between sessions that the identification is not viable. This means that an authentication is possible, though with a high rejection rate on the power spectra in this very scenario. Overall it can be said that an authentication on the basis of brain signals is a possibility for future applications as the specificity is very high despite a rather large rejection rate. Since it is desirable with respect to security aspects to rather need several trials to be successfully authenticated, than to grant access to someone that is not allowed to have access, a real world usage seems to be feasible.

CONCLUSION

Non-stationarity in the power spectra of EEG signals can be modeled with linear regression models and almost be eliminated by using ERD/S instead of the plain power signal. Therefore, using ERD/S could prevent a decline in classification performance with increasing time of the experiment or the need of a recalibration during a session. Inter-subject variability was quantified by classification approaches revealing that differences between subject specific ERPs (power spectra) must be very distinct as an authentication of the correct subject to a corresponding signal was possible reliably. It remains a big issue that needs to be further addressed in terms of BCI development, but it can be turned to an advantageous feature when considering subject authentication and identification as an application. It can be suggested that P300 ERPs work as a biometric measure for identifying subjects, whereas the spectral features of a P300 were less suitable for that cause.

REFERENCES

[1] Shenoy, Pradeep, et al. "Towards adaptive classification for BCIPart of the 3rd Neuro-IT and Neuroengineering Summer School Tutorial Series." Journal of neural engineering 3.1 (2006): R13.

[2] Spüler, Martin, Wolfgang Rosenstiel, and Martin Bogdan. "Adaptive SVM-based classification increases performance of a MEG-based Brain-Computer Interface (BCI)." International Conference on Artificial Neural Networks. Springer Berlin Heidelberg, 2012.

[3] Spüler, Martin, Wolfgang Rosenstiel, and Martin Bogdan. "Online adaptation of a c-VEP brain-computer interface (BCI) based on error-related potentials and unsupervised learning." PloS one 7.12 (2012): e51077.

[4] Lotte, Fabien, et al. "A review of classification algorithms for EEG-based brain–computer interfaces." Journal of neural engineering 4.2 (2007): R1.

[5] Spüler, Martin, et al. "EEG-based prediction of cognitive workload induced by arithmetic: a step towards online adaptation in numerical learning." ZDM 2016: 1-12.

[6] Kindermans, Pieter-Jan, et al. "Integrating dynamic stopping, transfer learning and language models in an adaptive zero-training ERP speller." Journal of neural engineering 11(3); 2014: 035005.

[7] Kindermans, Pieter-Jan, et al. "A P300 BCI for the masses: Prior information enables instant unsupervised spelling." Advances in Neural Information Processing Systems. 2012.

[8] Wu, Dongrui, Brent J. Lance, and Thomas D. Parsons. "Collaborative filtering for brain-computer interaction using transfer learning and active class selection." PloS one 8(2); 2013: e56624.

[9] Armstrong, Blair C., et al. "Brainprint: Assessing the uniqueness, collectability, and permanence of a novel method for ERP biometrics." Neurocomputing 166 (2015): 59-67.

[10] Palaniappan, Ramaswamy. "Two-stage biometric authentication method using thought activity brain waves." International Journal of Neural Systems 2009, 18(1) : 59-66.

[11] Spüler M, Bensch, M, Kleih S, Rosenstiel W, Bogdan M, Kübler A. Online use of error-related potentials in healthy users and people with severe motor impairment increases performance of a P300-BCI, Clinical Neurophysiology 2012;123(7): 1328-1337.

[12] Burg, John Parker. The relationship between maximum entropy spectra and maximum likelihood spectra. Geophysics 1972; 37(2):375-376.

[13] Chang, Chih-Chung, and Chih-Jen Lin. LIBSVM: a

Published by Verlag der TU Graz
Graz University of Technology

 DOI: 10.3217/978-3-85125-533-1-48

library for support vector machines. ACM Transactions on Intelligent Systems and Technology (TIST) 2011; 2(3): 27.
[14] Spüler M, Rosenstiel W, and Bogdan M. Principal component based covariate shift adaption to reduce non-stationarity in a MEG-based brain-computer interface. EURASIP Journal on Advances in Signal Processing (2012); 2012(1): 1-7.
[15] Pfurtscheller G, and Aranibar A. Event-related cortical desynchronization detected by power measurements of scalp EEG. Electroencephalography and clinical neurophysiology 1977; 42(6): 817-826.

Published by Verlag der TU Graz
Graz University of Technology

Proceedings of the
7th Graz Brain-Computer Interface Conference 2017 DOI: 10.3217/978-3-85125-533-1-49

The P300 BCI: on its way to end-users?

A. Kübler[1] , K.-R. Müller[2] , C. Guan[3]

[1] Institute of Psychology, University of Würzburg, Würzburg, Germany
[2]Institute of Computer Science, Technical University of Berlin, Berlin, Germany
[3] Nanyang Technological University (NTU), Singapore, Singapore

E-mail: andrea.kuebler@uni-wuerzburg.de

ABSTRACT: Looking at the past 30 years of research into the so-called P300 BCI reveals an almost exponential growth of publications on this topic as indexed in Pubmed. The striking increase has started around 2010 and is currently plateauing at a high rate. Certain aspects of the P300, such as stimulus presentation, feedback modality, classification procedures, or application to be controlled have been intensively investigated. The bulk of studies comprises one session approaches in the laboratory environment with healthy subjects, but patient end-users are increasingly included in studies. However, a lack of long-term studies with end-users in the field is obvious and indicates a translational gap. On the basis of more than 300 studies included, we discuss reasons for this gap and propose remedies; however, this paper presents a coarse overview only and constitutes the basis for a thorough meta-analysis.

INTRODUCTION

The motivation for this overview arose from the observation that a strikingly high amount of manuscripts to be reviewed by the authors do not sufficiently take into account and build upon existing results within the field of the P300 BCI.

The foundations of the P300 BCI were laid with the first description of the P300 by [1] – an event-related potential that could be elicited in a so-called oddball paradigm with rare target and frequent standard stimuli. In 1988 Farwell and Donchin [2] implemented the oddball paradigm in a stimulation set-up to control a BCI. Letters and numbers were presented in a matrix on a monitor. Rows and columns of the matrix were flashed in random order and participants were required to focus attention on the letter to be selected. Focusing of attention was reinforced by asking the participants to count how often the target letter flashed. By this procedure, each letter to be selected becomes a rare target in comparison to all other letters, which turn into standard stimuli. Ever since, this paradigm has been adopted, adapted, changed, and extended in many ways, and reliable target selection in healthy subjects and patients with disease alike has been demonstrated in a plethora of studies. The primary aim of the P300 BCI has been communication and control to replace lost function in patients with severe motor impairment. Only recently have other aspects, such as for rehabilitation after post-stroke aphasia, i.e. to improve lost function (see the BNCI Horizon 2020 website for a categorization of BCI according to their application purpose), gained more attention [e.g., 3].

Despite the many studies aiming at improving different aspects of the P300 BCI such as accuracy, information transfer rate (ITR), or usability, P300 BCIs are not used in daily life by the targeted end-users with disease albeit most studies claim this to be the final goal and motivation for the experiment at hand.

Thus, we face two gaps: (1) a translational gap, which prevents the many positive results arriving at the end-users' home and (2) an awareness gap, i.e. researchers sub-optimally build on the results achieved by the community. Therefore, approaches to the P300-BCI and controlled applications remain idiosyncratic rather than evoking a joint effort toward bridging the translational gap.

In the following we will give a brief overview of the topics covered by P300 BCI related publications (Table 1) and then discuss questions and answers which we consider relevant for the field of the P300 BCI. Those may partially transfer to BCIs with other input signals.

MATERIALS AND METHODS

We used Pubmed as source for our literature search on the P300 BCI. We entered the search terms "Brain" AND "Computer" AND "Interface". This search yielded n=733 hits. Those were then screened for true P300 BCI content and studies in languages other than English were excluded (n=12). Based on the abstracts, studies were then categorized according to the participants included (healthy subjects vs. participants with disease), environment of data collection (laboratory vs. field), number of (daily) sessions (one vs. more than one). Other categories were: "use of existing data sets", "reviews", and "theory and frameworks". During the process of categorization, the category "sample unclear" had to be created because it could not always be derived from the abstract what kind of sample was included.

.

Published by Verlag der TU Graz
Graz University of Technology

 DOI: 10.3217/978-3-85125-533-1-49

RESULTS

A sample of n=366 studies were included for analysis. Figure 1 depicts the number of publications per year. A gap of 12 years is visible between Farwell and Donchin's and subsequent papers. Thus, the next papers follow in 2000. By 2004 the number of publications per year was slowly increasing. Since 2011 it has reached a plateau of around 45 papers per year

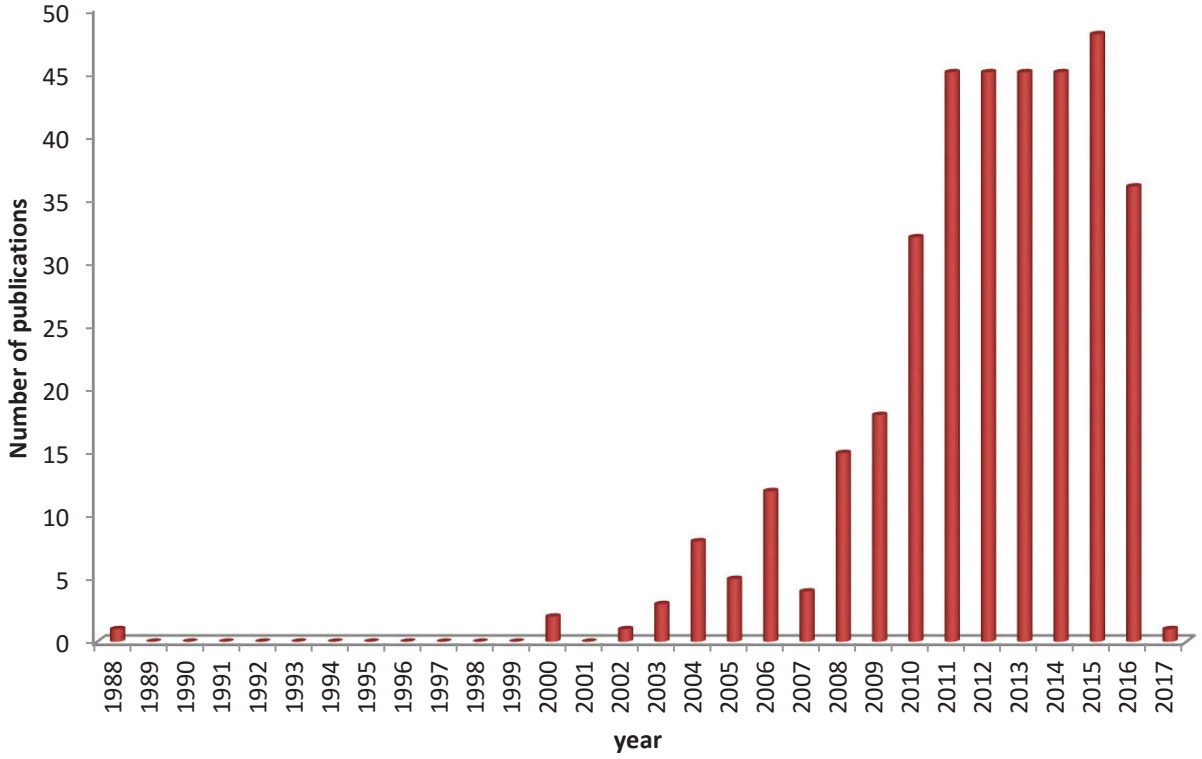

Figure 1: Number of P300 BCI related publications per year. Note, the gap between 1988 and 2000.

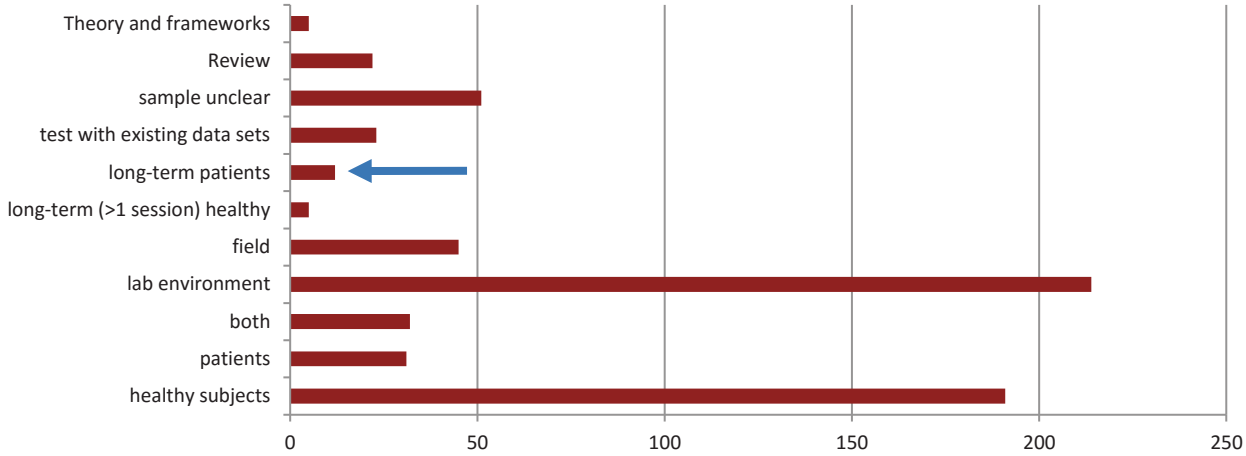

Figure 2: Number of studies (x-axis) per category. It can be clearly seen that the majority of studies was conducted with healthy subjects in the laboratory environment. Studies with patients and in the field are far less in number. The arrow denotes the translational gap.

Most of the studies included healthy subjects and were conducted in the laboratory environment. Patients included were diagnosed with amyotrophic lateral sclerosis (ALS), cerebral palsy, disorders of consciousness (vegetative state, minimally conscious state [MCS], emerging MCS), epilepsy, locked-in syndrome after brain stem stroke, multiple sclerosis, post-stroke aphasia, and spinal cord injury (SCI). Forty-two studies included patients and 32 both healthy participants and patients. If it was not otherwise mentioned, we assumed that the experiment was conducted in the laboratory. Forty-five studies report on data collection in the field. The vast majority of studies report results from one session and only 17 present data from more than one session; of those 12

Published by Verlag der TU Graz
Graz University of Technology

 DOI: 10.3217/978-3-85125-533-1-49

were with patients (see Figure 2). The Table provided an overview of some aspects investigated in P300 BCI related papers. Similar effort was invested in how to best separate target from non-target responses. Analysis of classification procedures and the effect of the different manipulations on accuracy, ITR, and usability were considered beyond the scope of this overview.

Table 1: Topics investigated in P300 BCI publications (a full reference list can be ordered from the first author).

Presentation of stimuli	Stimulation modality, recording, and elicited ERPs	P300 BCI set-up	Psychological variables potentially influencing P300 BCI performance	Predictors of P300-BCI performance	P300-BCI controlled applications
-Matrix size -Matrix colour Moving matrix -Location of stimuli -Luminance -Size of stimuli -Spatial position of stimuli -Character grouping -Flash rate -Flash pattern -Rapid serial visual presentation -Suppressing stimuli -Faces as stimuli (famous, familiar, inverted) -Facial expression modulation -Avoidance of redundant stimuli -Multi-level matrices -Polyphonic music stimuli -Two-stimulus paradigm	-Stimulus modality: visual, auditory, tactual, multimodal -Additional ERPs (N100, MMN, N150, N200, N400, visual evoked potential (VEP), motion-onset VEP) -Error potentials Input signals (EEG, MEG, ECoG, EOG) -Combination of input signals (hybrid: SMR, SSVEP, EMG, eye movement)	-Inter stimulus interval -Length of P300 segment -Number of channels / sensors -Amount of training data -Source of errors -Asynchronous dynamic stopping of stimuli presentation -Mindfulness training -Dictionary predictive spelling -Language models shared control -Auto-calibration and laymen set-up	-Motivation -Emotion -Satisfaction -Empathy -Cognitive performance -Attention -Memory -Workload -Fatigue	-Heart rate variability -Root-mean-square amplitude -Negative peak amplitude of the target ERP -Auditory oddball P300 -Concentration -Working memory -General intelligence	-Spelling -Word presentation -Virtual apartment -Internet surfing -Gaming -Wheelchair control -Brain painting -(Telepresence-) Robot control -Standard assistive technology -Emailing -Prosthesis -Robotic arm -Multimedia player

DISCUSSION

A tremendous amount of work to improve the speed and reliability of the P300 BCI has been done in the past 10 years. By now, basic principles of stimulation, presentation, and classification are known [e.g., 4]. Reasons for the impressive increase in research effort may have been better classification algorithms and more sophisticated ways of presenting the stimuli. For example, the introduction of overlaying faces instead of flashes resulted in a boost of performance of up to one repetition sequence with no decrease in accuracy which stayed at 100% [5].

When looking more closely at the success stories, they are mainly attributed to few studies each belonging to specific research groups. Even within the field of the P300 BCI, successful modifications are only reluctantly or not at all taken up by the community. A positive example is the use of SWLDA

Published by Verlag der TU Graz
Graz University of Technology

 DOI: 10.3217/978-3-85125-533-1-49

for classification. Contrarily, face stimuli were only taken up by few groups and new ways of stimulus presentation are still compared to the classic P300 spelling matrix instead of the most successful presentation mode at any given point in time.

If the field is seriously aiming at bringing BCIs to end-users in the field, be it patients or healthy subjects, researchers have to leave the laboratory and work in exactly this field. The needs and requirements of end-users must be clearly defined and the few available studies indicated that if researchers make this effort, BCIs are indeed an option for communication and control in daily life [6,7].

CONCLUSION

The lack of interaction between research groups and integration of results keeps the P300 BCI below its possibilities. We argue that by now, we have sufficient knowledge for standardization and recommendations beyond which current and future research should not fall behind. This knowledge should be thoroughly applied for the benefit of end-users.

REFERENCES

[1] Squires, K. C., Wickens, C., Squires, N. K., & Donchin, E. (1976). The effect of stimulus sequence on the waveform of the cortical event-related potential. Science, 193(4258), 1142-1146.

[2] Farwell, L. A., & Donchin, E. (1988). Talking off the top of your head: toward a mental prosthesis utilizing event-related brain potentials. Electroencephalogr Clin Neurophysiol, 70(6), 510-523.

[3] Kleih, S. C., Gottschalt, L., Teichlein, E., & Weilbach, F. X. (2016). Toward a P300 based brain-computer interface for aphasia rehabilitation after stroke: presentation of theoretical considerations and a pilot feasibility study. Frontiers in human neuroscience, 10, 547. doi: 10.3389/fnhum.2016.00547

[4] Krusienski, D. J., Sellers, E. W., Cabestaing, F., Bayoudh, S., McFarland, D. J., Vaughan, T. M., & Wolpaw, J. R. (2006). A comparison of classification techniques for the P300 Speller. Journal of Neural Engineering, 3(4), 299-305. doi: 10.1088/1741-2560/3/4/007

[5] Kaufmann, T., Schulz, S. M., Koblitz, A., Renner, G., Wessig, C., & Kübler, A. (2013). Face stimuli effectively prevent brain-computer interface inefficiency in patients with neurodegenerative disease. Clin Neurophysiol, 124(5), 893-900. doi: 10.1016/j.clinph.2012.11.006

[6] Sellers, E. W., Vaughan, T. M., & Wolpaw, J. R. (2010). A brain-computer interface for long-term independent home use. Amyotrophic Lateral Scler, 11(5), 449-455.

[7] Holz, E. M., Botrel, L., Kaufmann, T., & Kubler, A. (2015). Long-term independent brain-computer interface home use improves quality of life of a patient in the locked-in state: a case study. Archives of Physical Medicine and Rehabilitation, 96(3 Suppl), S16-26. doi: 10.1016/j.apmr.2014.03.03

Published by Verlag der TU Graz
Graz University of Technology

Proceedings of the
7th Graz Brain-Computer Interface Conference 2017 DOI: 10.3217/978-3-85125-533-1-50

USING A ONE-DIMENSIONAL CONTROL SIGNAL FOR TWO DIFFERENT OUTPUT COMMANDS IN AN IMPLANTED BCI

S. Leinders[1], E.G.M. Pels[1], M.J. Vansteensel[1], M.P. Branco[1], Z.V. Freudenburg[1], M.A. van den Boom[1], M. Vermaas[2], E.J. Aarnoutse[1], and N.F. Ramsey[1]

[1] Brain Center Rudolf Magnus, University Medical Center Utrecht, Department of Neurology and Neurosurgery, Utrecht, the Netherlands

[2] Donders Centre for Neuroscience, Radboud University Nijmegen, Nijmegen, the Netherlands

E-mail: s.leinders@umcutrecht.nl

ABSTRACT: As part of the Utrecht NeuroProsthesis (UNP) project, a late stage ALS patient has been implanted with a BCI system that allows her to communicate at home. The BCI system converts short, transient changes in brain activity from the motor hand area into ‚brain-clicks', which are used to control spelling software. On request of the participant, we added the option to use the control channel for producing a second output command, giving her the possibility to call for attention at any time. Here, we show that the user is able to produce sustained increases in activity for this purpose and that these signal changes can be clearly distinguished from the transient changes used as ‚brain-clicks'. We conclude that it is possible to use a one-dimensional control signal based on motor hand activity to produce two different output commands.

INTRODUCTION

The Utrecht NeuroProsthesis (*UNP*) project aims to provide locked-in patients with an implanted BCI system for communication, which they can use at home without the presence of research staff. So far, one woman with late stage ALS has been implanted with the UNP system and uses it at home [1]. Although being able to speak one's mind freely (in the case of someone with locked-in syndrome: spell) is a vital aspect of communication, another important component is the ability to call for attention at any moment, for example when there is physical discomfort or pain. On request of our participant, we aimed to implement this additional feature into the UNP system.

The UNP system is a click-based system with one control channel. It converts short and voluntary changes in brain-activity from the motor hand area into ‚brain-clicks', which can be used to navigate through a custom-made interface, called the UNP menu, based on BCI2000 software [1,2]. Within the UNP menu, the user can navigate to and control commercial spelling software (*Communicator 5, Tobii Dynavox*), play brain games, and change settings.

To make sure that the additional feature to call for attention is always available, i.e. from any part of the UNP menu, including the spelling software and the games, a second control signal is required. Earlier observations (see the Supplementary Appendix of the original article [1], Figure S4-D) indicated that the user was able to generate longer periods of increased activity (here referred to as *sustained activity*). We aimed for this sustained activity to activate an escape pop-up menu, containing ‚*call-caregiver'*, ‚*return to main menu'* and ‚*continue'* buttons. After activating the pop-up menu, the user could then use regular clicks to select the different options within the pop-up menu.

Importantly, some key selections within the UNP menu require a 'double click' (i.e. two regular clicks shortly after one another), to prevent accidental selections of menu options that can be difficult to correct (e.g. a settings change). For accurate control of these double clicks *and* the activation of the escape pop-up menu, these two types of neuronal activity profiles need to be clearly distinguishable from one another. Here, we investigated: 1) the optimal duration of the break between double clicks, aimed at minimizing unwanted escape menu pop-ups during double clicks, while keeping double clicks as fast as possible; 2) the optimal duration of the sustained activity for the escape pop-up menu activation.

MATERALS AND METHODS

Participant: Our participant is a sixty year old woman with late stage ALS. She is locked-in and communicates with eye blinks (yes - no), an eye tracker, and/or the UNP system.

Hardware and Data: Data was recorded with the implanted UNP system. Electrocorticography surface electrodes (Resume II ®, Medtronic) are located subdurally on the left M1 hand knob area and leads are subcutaneously tunneled to an implanted amplifier/transmitter device (Activa ® PC+S, Medtronic), which is located subcutaneously under the left clavicle [1]. Brain activity from one bipolar electrode pair was converted into power data over two frequency bands (low frequency band, *LFB:* center frequency 20 Hz; high frequency band, *HFB*: center frequency 80 Hz) in the Activa ® PC+S device and

Published by Verlag der TU Graz
Graz University of Technology

 DOI: 10.3217/978-3-85125-533-1-50

streamed wirelessly at a rate of 5Hz to an antenna connected to a research laptop running BCI2000. To obtain the control signal, both channels were normalized in our BCI2000 filter pipeline, after which the z-scored LFB channel was subtracted from the z-scored HFB channel [1]. All reported data was recorded at our candidate's home.

To allow for a second output command, we implemented a new filter called the escape filter into our existing BCI2000 pipeline. This filter runs in parallel with the regular click filters [1], but settings are set such that it only activates during sustained increases of the control signal. When this filter is activated, the escape menu pops up.

Prior to this escape project (and thus the quantification of escape related sustained activity) our participant already used the escape filter at home. Initial settings were found empirically (i.e. we changed settings online, based on user feedback), using regular click settings as a starting point. In this period before the escape project, the length of escapes (i.e. how long the control signal needs to be above threshold for escape activation) was adjusted several times based on home-use experience. A fixed escape threshold of 0.35 (based on the regular click settings) however always seemed to work well, and was therefore used as the default threshold value in this project. (For more information on determining optimal regular click settings, please see our previous paper [1, Figure S6].)

Validation Task: We used a custom-made BCI2000 task called the MultiClicks task to address our research questions. Task layout was as follows: A cursor was presented at a fixed location at the horizontal and vertical middle of the screen. The background moved from left to right at a fixed pace. Different colours in the background instructed the participant to relax or to produce transient or sustained activity by attempting to tap the fingers of her right hand (Figure 1). More specifically, our candidate attempts flexion of ring finger and thumb until they 'touch' (of course, they do not actually touch because they do not move), and then extension of both fingers. Our participant reports that one such sequence of attempted movement takes approximately one second. Attempted movement is repeated as long as active cue lasts.

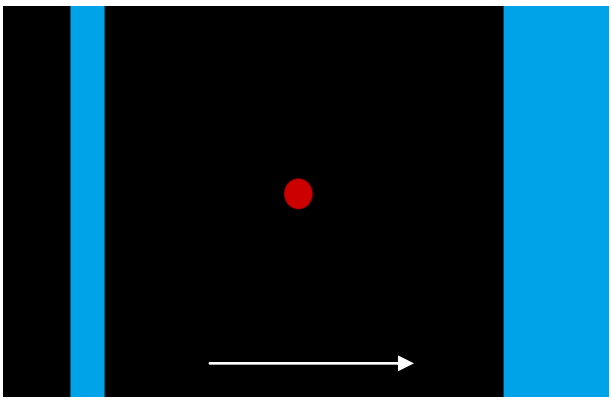

Figure 1: Screenshot of task. The background moved from left to right (direction of arrow) at a fixed pace, while the red cursor remained in the middle of the screen. When the cursor crossed a blue block, the participant was instructed to attempt finger movement. When the cursor crossed a black block, she was instructed to rest. Width of blue and black blocks varied across conditions. From left to right side of screen is 10 seconds.

The MultiClicks task was performed four times in one session with the same set of conditions each time. Conditions comprised single clicks, double clicks, and sustained activity. The break between double clicks ranged from one to five seconds, and the length of the sustained activation condition varied between four and seven seconds (all in steps of one second). To prevent potential false positive escape activations during regular clicks, four seconds was chosen as the shortest escape duration, because we have previously seen that the increase in control signal associated with short active cues of 1 second (required length of regular clicks) can last up to 3 seconds [1, Figure S4-D]. Every condition was presented twice in each run. All runs lasted approximately four minutes and the duration of the inter-trial interval (i.e. rest blocks) was seven seconds. Condition order was randomized. No visual feedback was presented. The subject was instructed to time her mental strategy based on the visual cues, and not to anticipate.

RESULTS

The participant was able to generate broad and sustained peaks in the control signal for up to 7 seconds (the longest period of sustained activity tested, Figure 2). For all durations of sustained activity tested, LFB power decreased shortly before cue onset and increased after cue offset (beta rebound). Moreover, HFB increased sharply at cue onset, and stayed high (although with somewhat more signal variability than LFB) until cue offset. Although the candidate was instructed not to anticipate, there did seem to be some anticipation in brain activity shortly before actual cue onset, especially in the LFB band (Figure 2).

Published by Verlag der TU Graz
Graz University of Technology

 DOI: 10.3217/978-3-85125-533-1-50

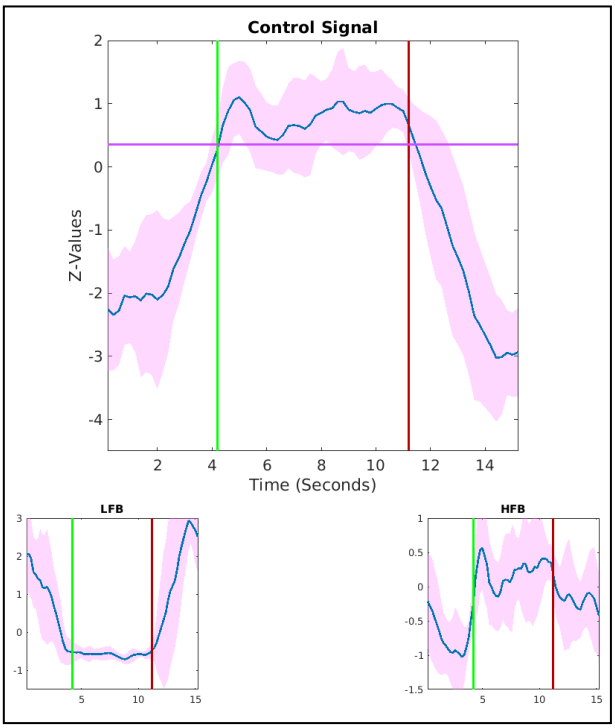

Figure 2: Mean trace (± standard deviation in pink) from the 7 second sustained activity condition, based on all trials from the presented four runs. Top plot: Control signal normally used for clicking (based on both LFB and HFB power, see methods for details). Bottom left: LFB signal. Bottom right: HFB signal. All plots have z-values on the y-axis and time in seconds on the x-axis. Vertical green and red lines indicate cue on- and offset, respectively. The horizontal purple line in the top graph indicates threshold for detecting sustained activity (0.35).

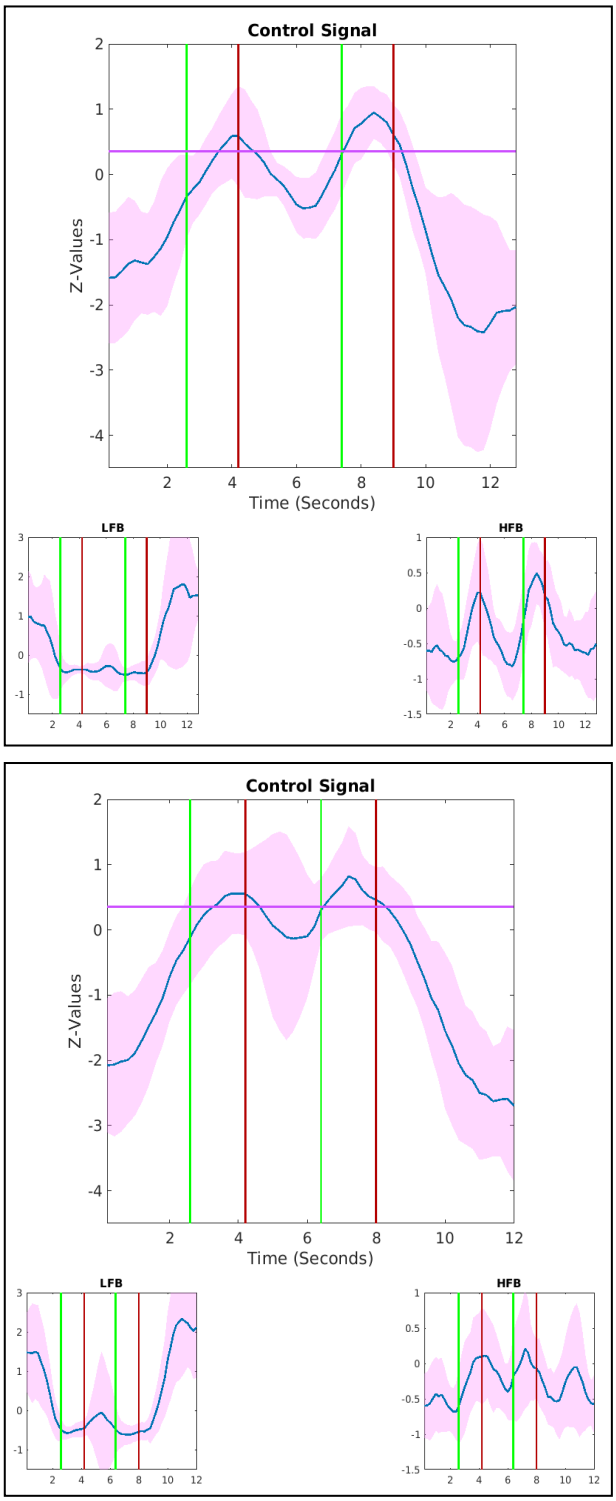

Figure 3: Double click plots with mean trace and standard deviation fill, based on all trials from the presented four runs. Top panel: 3-second break condition. Bottom: 2-second break condition. Both panels contain main plot with control signal, and two subplots with LFB and HFB signal. All plots have z-values on the y-axis and time in seconds on the x-axis. On- and offset of both clicks are plotted (vertical green and red lines, respectively). The horizontal purple lines in the control signal graphs indicate threshold for detecting sustained activity (0.35).

Published by Verlag der TU Graz
Graz University of Technology

 DOI: 10.3217/978-3-85125-533-1-50

With regard to the break between double clicks: The participant was able to generate two separable clicks with intervals of 5, 4 and 3 seconds (Figure 3, top panel). However, a 2 second break between two clicks did not consistently allow a sufficient decrease of the control signal below the threshold (Figure 3, bottom panel). As a result, the control signal of double-click trials with a 2 second break may be mistaken for sustained activity.
Interestingly, the decrease of the control signal between two clicks with 3 second separation could be mostly attributed to a transient decrease in HFB amplitude. In contrast, the LFB signal stays low during both clicks comprising double clicks and also during the break between those clicks, and does not contribute to the separation of the clicks in the 3 second break condition. In the 4 and 5 second break conditions however, LFB increases during the break, contributing to the separation of the two clicks.

DISCUSSION

As part of the UNP project we explored the separability of control signal changes associated with double clicks and sustained activity. From the data we concluded that: 1) the user can produce sustained increases in the control signal for at least seven seconds; 2) the user is able to produce two clearly separable clicks when the break between the clicks is at least three seconds.
The optimal duration of sustained activity required for activating the escape pop-up menu is based on two considerations: 1) the length of sustained activity should be as short as possible, so the user can activate the escape as fast as possible; 2) the length of the sustained activity should be long enough for it to be distinguishable from double clicks, to prevent double clicks without a clear dip between clicks (which is uncharacteristic based on presented data, but possible) from activating the escape pop-up menu.
For the current user we found that 5.6 seconds of sustained activity is feasible. Our user chose this length based on required effort and reliability of escape activation when using a 3 second break strategy during double clicks. Since we fixed these settings during the escape project (December 2016), they have not been changed. Our participant can now reliably activate the escape pop-up menu using a sustained activity length of 5.6 seconds, while minimizing false positive escape menu pop-ups by applying a 3 second break between double-clicks.
Double clicks with an interval of 3, 4 and 5 seconds all showed a clear decrease in the control signal between the two clicks. Since we wanted to optimize speed, we focused on a 3 second break between double clicks for this project. Moreover, our participants‘s home-use settings use a length of 5.6 seconds for sustained activity although she can produce longer sustained activity (up to 7 seconds at least). From these two points we concluded there is a range of usable settings beyond the current settings: we could increase both the sustained activity length and the break in double clicks in case our user is no longer satisfied with her home-use settings in the future. These changes might increase reliability at the cost of speed.
By using a one-dimensional control signal to produce two different types of outputs, we have expanded our implanted BCI’s functionality. Moreover, the MultiClicks task developed for this project can be used with future candidates to determine a range of usable double click and escape settings early on in the UNP project. Because an escape if probably a useful feature for all users, this is an important point. Sustained activity is currently used to activate an escape pop-up menu, which allows our user to select a call-caregiver button as the first option. The other two options in the escape-menu are resuming the current application or quitting to the main menu. Sustained activation could be used for other purposes, depending on a user’s wishes and needs, such as reversing scanning order within spelling software or jumping to a next category or page (this could increase spelling speed).

CONCLUSION

A one-dimensional control signal recorded from a bipolar pair of subdural ECoG electrodes allows for two different types of output commands based on short and sustained activity increases. The newly added sustained activity feature allows our candidate to activate an escape button at any time.

ACKNOWLEDGEMENTS

We would like to thank the participant of our study for her continued and unwavering cooperation and her commitment to the UNP project.

REFERENCES

[1] Vansteensel MJ, Pels EGM, Bleichner MG, Branco MP, Denison T, Freudenburg ZV, et al. Fully Implanted Brain–Computer Interface in a Locked-In Patient with ALS. New England Journal of Medicine. 2016; 375:2060-2066.
[2] Schalk et al., IEEE Trans Biomed Eng, 2004 Mellinger and Schalk, In: Brain-Computer Interfaces. MIT Press, 2007. http://www.bci2000.org

Published by Verlag der TU Graz
Graz University of Technology

Proceedings of the
7th Graz Brain-Computer Interface Conference 2017 DOI: 10.3217/978-3-85125-533-1-51

Can feature selection be used to detect physiological components in P300 based BCI for Amyotrophic lateral sclerosis patients?

L. Bianchi[1], M. Cosmi[1], C. Liti[1], V. Piccialli[1]

[1]DICII, University of Rome Tor Vergata, Rome, Italy

E-mail: chiara.liti@uniroma2.it

ABSTRACT: The detection of brain state changes can dramatically improve the comprehension of cerebral functioning. To reach this aim, machine learning based automatic tools may be extremely useful to correctly classify different brain responses. The performance of these instruments depends on the features and the classification algorithm employed, but also from a good data preprocessing able to improve the poor signal-to-noise ratio [4] of the EEG signal. In this work, we combine data preprocessing with a feature selection based on the filter ReliefF and the linear SVM classifier LibLinear in order to analyse the data deriving from a P300 speller paradigm on patients with Amyotrophic lateral sclerosis (ALS). The purpose of this study is twofold: on the one hand we want to maximize the predictor's performance, but most importantly, we aim at showing how the features ranking can be used to support scientific hypotheses or diagnoses.

INTRODUCTION

In neuroscience, a fundamental theme is the study of brain functioning, for different scopes, such as neurorehabilitation, diagnosis support and brain activity monitoring in general. The detection of brain state changes plays a fundamental role because it can dramatically improve the comprehension of cerebral functioning. Evoked potentials, for example, which are the electrical responses recorded from the brain after specific stimulations, are widely used by researchers and clinicians to support scientific hypotheses [7] or to make diagnoses [8]. Recently, in [1] a feature ranking approach combined with SVM classifier was applied over the EEG signal of nine healthy subjects. The subset of features identified for each subject was physiologically correct. Indeed the filter was able to detect physiological components elicited during the protocol either in space or in latency. In this work we try to use a similar approach over Amyotrophic lateral sclerosis (ALS) patients, even thought the poor signal-to-noise ratio that characterise this kind of electroencephalographic (EEG) signal makes this task more difficult to perform.
The rest of this paper is structured as follows: *Material and Methods* provides a description of the dataset used and of the strategy defined. *Results* shows the outcomes both in terms of predictor's performance and physiological components detection. *Discussion* contains a comparison of the results obtained with the standard strategy and the one proposed in this work. Finally, *Conclusion* contains a brief summary of this work.

MATERIALS AND METHODS

The analysed dataset is the one proposed in [5] that can be downloaded from the BNCI Horizon 2020 database [6] (Dataset 8: P300 speller with ALS patients (008-2014)). The dataset consists of eight patients affected by ALS, and each patient was shown a 6 by 6 matrix containing alphanumeric characters. The user's task was to focus attention on characters in a word that was prescribed by the investigator (i.e., one character at a time). All rows and columns of this matrix were successively and randomly intensified at a rate of 4 Hz. Two out of 12 intensifications contained the desired character (i.e., one particular row and one particular column). Scalp EEG signals were recorded from eight channels according to 10-10 standard (Fz, Cz, Pz, Oz, P3, P4, PO7 and PO8). The EEG signal was digitized at 256 Hz and band-pass filtered between 0.1 and 30 Hz. Participants were required to copy-spell seven predefined words of five characters each (runs), by controlling a P300 matrix speller. Rows and columns on the interface were pseudo-randomly intensified for 125ms, with an inter stimulus interval (ISI) of 125 ms, yielding a 250 ms lag between the appearance of two stimuli (stimulus onset asynchrony, SOA). For each character selection (trial) all rows and columns were intensified 10 times (stimuli repetitions) thus each single item on the interface was intensified 20 times and the total number of flashes was 120. For each channel, 240 samples after stimuli onsets were selected for the analyses. The dataset consisted hence of 4200 instances. Drawing inspiration from [5], we split the dataset by using the first three words as training, and the last four as testing set. We considered four different versions of the dataset:

Single Trial we considered the original dataset, that is 4200 instances with 1921 attributes (240 samples $\times$ 8 channels plus the attribute that represent the row or the column intensified for each trial);

Decimated EEG data were then resampled in the time domain by replacing each sequence of 12 samples with their mean value, yielding 17×8 samples per epoch (eight being the number of channels), which

Published by Verlag der TU Graz
Graz University of Technology

 DOI: 10.3217/978-3-85125-533-1-51

were concatenated in a feature vector of size 137

Decimated 5-averaged EEG data were resampled in the time domain as in the previous dataset version, but also in the instances domain, so that five consecutive instances of the same stimulation class were replaced by one instance of their average; this dataset version was then formed by 840 instances and 137 attributes;

Decimated 10-averaged This version is similar to the previous one, except that averages in the instances domain were computed every 10 consecutive instances of the same stimulation class; this dataset version was then formed by 420 instances and 137 attributes;

The three decimated datasets were obtained by using standard techniques for increasing the signal to noise ratio and hence should represent an improvement over the Single Trial dataset. However, it should be noted that, for online applications, the time necessary to perform a classification increases proportionally to the number of the averaged instances. Following the results described in [1], we use the filter ReliefF for feature selection, see [3]. ReliefF is a robust feature selection filter that can deal with incomplete and noisy data. This method randomly selects an instance R_i, then searches for k of its nearest neighbours from the same class called nearest hits H_j, and also k nearest neighbours from each of the different classes, called nearest misses $M_j(C)$. It updates the quality estimation $W[A]$ for all attributes A according to their values for R_i, hits H_j and misses M_j. Due to the noise of the data we have decided to weight nearest neighbours by their distance.

We tested different SVM based classifiers and the most efficient one was LibLinear described in [2], since it resulted the best on all the datasets, and it is also fast in terms of time for building the model. Liblinear returns an hyperplane $w^T x + b$, that discriminates among the two classes. It is important to stress that we did not use the standard classification function of LibLinear (that is $y(x) = sign(w^T x+b)$), but we exploited the information on the protocol that there is exactly one target element every six instances. Therefore, we assigned the target class to the maximum over the six flashes of $w^T x + b$ both for rows and columns. Whenever this assignment does not correspond to the real target, it results in both a false positive and a false negative.

We compare our results with the standard strategy in BCI (used also in [5]), that is SWLDA. SWLDA uses a stepwise method to perform a multilinear regression of the response values. We used the Matlab implementation with its default setting and with the decision function exploiting the knowledge on the protocol. Therefore, also for this method, we assigned the target class to the maximum over the six flashes of $w^T x+b$ both for rows and columns.

RESULTS

The following tables show, for each patient and for each kind of dataset, the accuracy, the Cohen's $Kappa$, and the true positives rate on the test set (that we recall is the last $4/7$ of the whole dataset), obtained both with SWLDA (default setting, and with the decision function described above) and with our strategy, that is LibLinear combined with the feature selection given by ReliefF.

A01	SWLDA			OUR		
dataset	acc	k	TP	acc	k	TP
orig	0.8145	0.3323	0.4436	0.811	0.320	0.434
dec	0.854	0.475	0.563	0.854	0.475	0.563
5-avg	0.925	0.730	0.775	0.917	0.700	0.750
10-avg	0.958	0.850	0.875	0.958	0.850	0.875

Table 1: Results for Patient A01 on all the datasets

A02	SWLDA			OUR		
dataset	acc	k	TP	acc	k	TP
orig	0.8187	0.3474	0.4561	0.815	0.335	0.446
dec	0.828	0.382	0.485	0.837	0.412	0.510
5-avg	0.938	0.775	0.813	0.933	0.760	0.800
10-avg	0.967	0.880	0.900	0.967	0.880	0.900

Table 2: Results for Patient A02 on all the datasets

A03	SWLDA			OUR		
dataset	acc	k	TP	acc	k	TP
orig	0.8371	0.4135	0.5113	0.836	0.411	0.509
dec	0.869	0.529	0.608	0.873	0.544	0.620
5-avg	0.917	0.700	0.750	0.942	0.790	0.825
10-avg	0.925	0.730	0.775	0.942	0.790	0.825

Table 3: Results for Patient A03 on all the datasets

A04	SWLDA			OUR		
dataset	acc	k	TP	acc	k	TP
orig	0.824	0.365	0.4712	0.835	0.408	0.506
dec	0.856	0.481	0.568	0.843	0.433	0.528
5-avg	0.854	0.475	0.563	0.867	0.520	0.600
10-avg	0.892	0.610	0.675	0.950	0.820	0.850

Table 4: Results for Patient A04 on all the datasets

A05	SWLDA			OUR		
dataset	acc	k	TP	acc	k	TP
orig	0.849	0.456	0.5464	0.832	0.395	0.496
dec	0.850	0.460	0.550	0.863	0.505	0.588
5-avg	0.933	0.760	0.800	0.942	0.790	0.825
10-avg	0.975	0.910	0.925	0.967	0.880	0.900

Table 5: Results for Patient A05 on all the datasets

A06	SWLDA			OUR		
dataset	acc	k	TP	acc	k	TP
orig	0.850	0.459	0.5489	0.835	0.405	0.504
dec	0.881	0.571	0.643	0.878	0.562	0.635
5-avg	0.958	0.850	0.875	0.946	0.805	0.838
10-avg	0.967	0.880	0.900	0.975	0.910	0.925

Table 6: Results for Patient A06 on all the datasets

A07	SWLDA			OUR		
dataset	acc	k	TP	acc	k	TP
orig	0.860	0.495	0.5789	0.830	0.389	0.491
dec	0.873	0.541	0.618	0.863	0.508	0.590
5-avg	0.933	0.760	0.800	0.963	0.865	0.888
10-avg	0.967	0.880	0.900	0.967	0.880	0.900

Table 7: Results for Patient A07 on all the datasets

Published by Verlag der TU Graz
Graz University of Technology

 DOI: 10.3217/978-3-85125-533-1-51

A08	SWLDA			OUR		
dataset	acc	k	TP	acc	k	TP
orig	0.911	0.678	0.7318	0.906	0.663	0.719
dec	0.933	0.757	0.798	0.928	0.7396	0.783
5-avg	0.983	0.940	0.950	0.979	0.925	0.938
10-avg	0.983	0.940	0.950	0.983	0.940	0.950

Table 8: Results for Patient A08 on all the datasets

In order to show the physiological significance of the feature selection that we use, in Figure 1 (patient A02) and Figure 2 (patient A07) are shown the target signals (orange) vs the non target signal (blue) on all the electrodes for patient A02 and patient A07. N200 VEP component can be observed in Fig. 1 on Oz, Po7 and Po8 whereas the P300 component can be observed on both patients in the 400-500 ms range and on Fz and Cz electrodes. Despite the fact that these averages were obtained from a relevant number of trials (300 targets vs 1500 non targets), they appear to be quite different from those known from the literature and from healthy subjects for two main reasons: first of all the EEG signals from these patients have a lower signal to noise ratio, and secondly the responses overlap after each stimulation as they are elicited (every 250ms) before the physiological response in extinguished (usually after no less than 800ms), thus causing some interference.

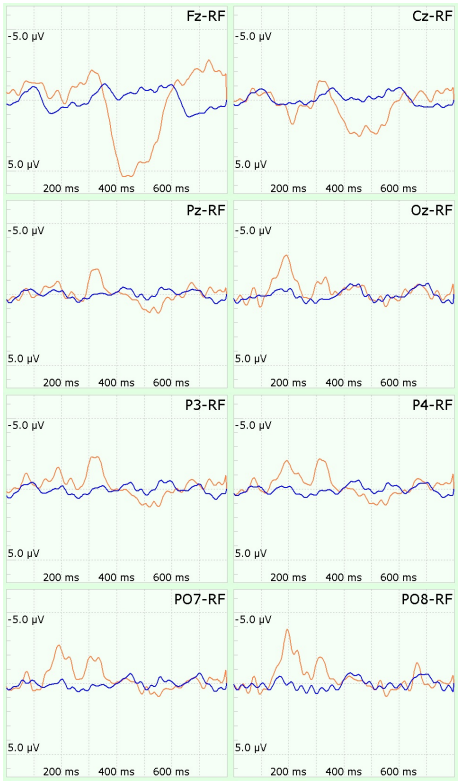

Figure 1: Target (Orange) vs Non-Target (Blue) for Patient A02.

We have selected these two patients because they represent opposite classifiers performance: A02 is among the worst while A07 is one of the best, as shown by the results in Tables 2 and 7.

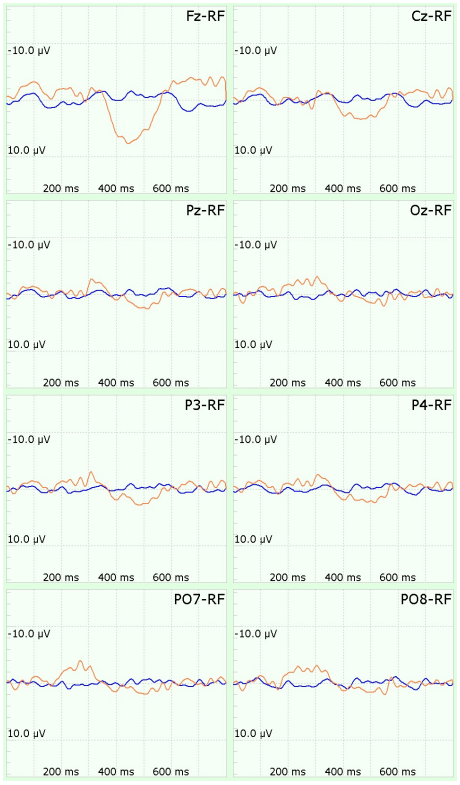

Figure 2: Target (Orange) vs Non-Target (Blue) for Patient A07.

In order to investigate whether the features selected by ReliefF are coherent with the physiological signals represented in Figures 1 and 2, we compared topographic maps (Fig.3, A02; Fig. 4, A07) computed at certain time interval, and according to three different methods:

- on the left we draw the weights chosen by SWLDA for each feature;
- in the center we have the ERPs
- on the right the score computed by ReliefF

In all maps plotted values are relative to 7 distinct time intervals, and averaged across 12 consecutive time samples. SWLDA and ReliefF weights were computed after averaging 10 consecutive instances of the same stimulation class and using 3/7 of the whole dataset. So, 180 instances with 1921 attributes (1920 from the signals and one from the label) were used for training them. Note that each of the 1920 obtained weights are bound to a feature and then to a sample and an electrode. Weights are then reduced after averaging 12 consecutive of them, in order to further increase the signal to noise ratio. Note that this approach preserve time and space information so that each weight is still bound to an electrode and a time (in this case an interval of 12 samples).
From all the possible maps, one for each time interval, a subset of 7 (the most significant ones) is represented in Figures 3 and 4.

Published by Verlag der TU Graz
Graz University of Technology

 DOI: 10.3217/978-3-85125-533-1-51

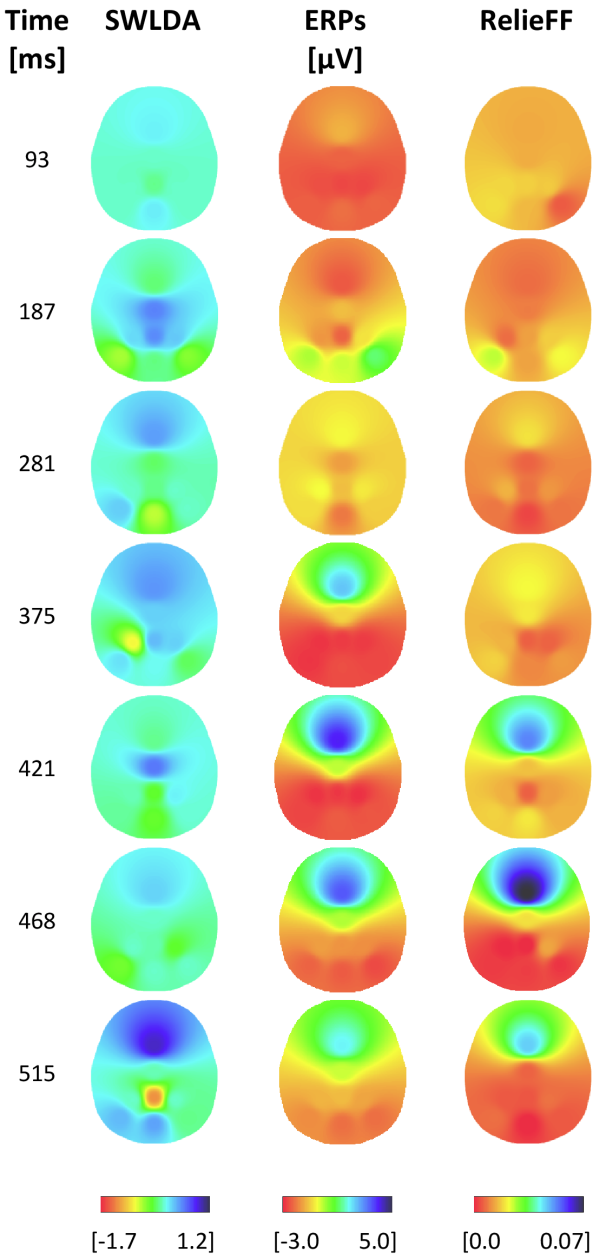

Figure 3: Topographic maps relative to patient A02 computed according to 3 different methods and 7 different time intervals.

From both Figures 3 and 4 it can be seen that maps computed from features selected from ReliefF are very similar to those obtained from the ERPs whereas those computed from SWLDA weights are quite different. This clearly suggests that features selected with our approach are more related to physiological signals than those selected from SWLDA.

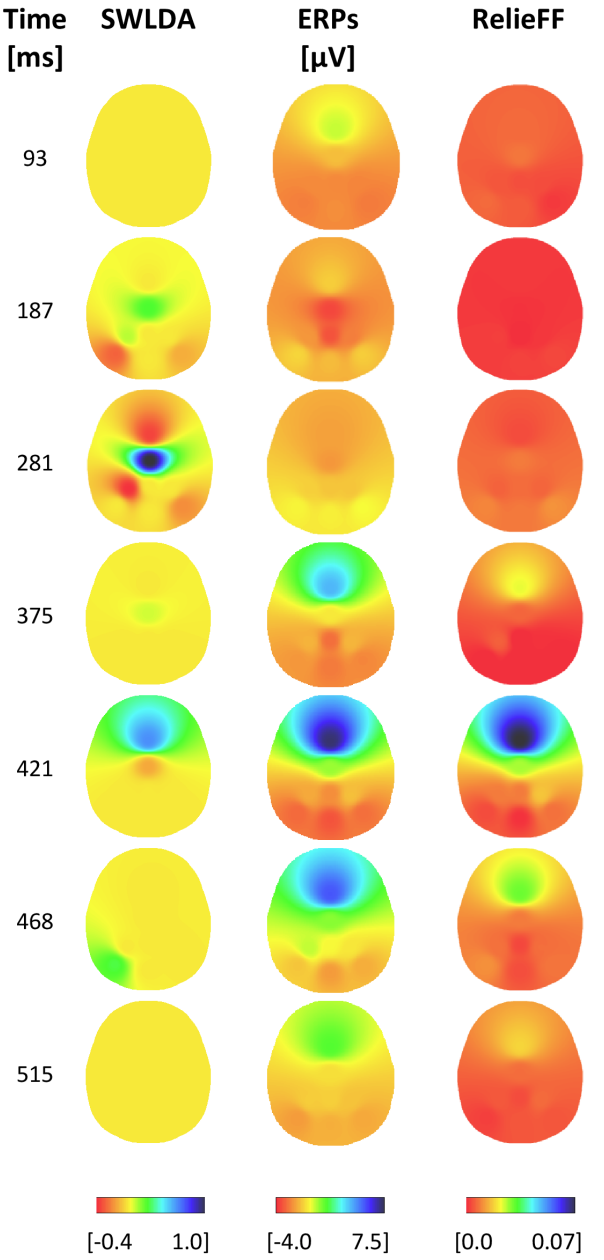

Figure 4: Topographic maps relative patient A07 computed according to 3 different methods and 7 different time intervals.

DISCUSSION

The reported results show how our approach based on ReliefF and LibLinear represents a valid alternative to the widely used SWLDA, since it provides results comparable to SWLDA in terms of accuracy and Cohen?s Kappa, but selecting features that are physiologically relevant while the features selected by SWLDA show scarce correlation with the ERPs. This kind of information might furnish relevant insights to identify which brain areas and when are involved during certain cerebral activities, thus improving the comprehension of brain functioning and furnishing a valuable instrument for supporting scientific hypotheses or diagnoses. It is also clear how the prepro-

Published by Verlag der TU Graz
Graz University of Technology

 DOI: 10.3217/978-3-85125-533-1-51

cessing of the data (especially the averaging of the signal) is effective at improving the performance of the classifier, as shown by the increasing accuracy (and Cohen's Kappa) obtained over the four datasets.

CONCLUSION

The detection of brain state changes translates into classification problems with a huge number of features that make difficult to distinguish those relevant ones for diagnostic use. Therefore, distinguishing significant characteristics not only would improve the predictor's performance, but would also provide a better understanding of the underlying cerebral process that generated the data. From classification point of view, the obtained results show how our approach represents a valid alternative to the standard SWLDA approach. More significantly, as for the feature selection, the performance obtained with our strategy outperforms SWLDA, since it turns out that also in the case of ALS patients, this feature selection filter is particularly robust, and returns a subset of selected feature that is physiologically compatible. Figures 3 and 4 show how ReliefF was able to detect physiological components elicited during the protocol either in space (e.g. Cz, Pz, ...) or in latency (e.g. P300).

REFERENCES

[1]Bianchi L., Liti C. and Piccialli V.. Features Reduction for P300 Spellers. In Proceedings of the Sixth International Brain-Computer In- terface Meeting, May 30-June 3 2016, Asilomar Conference Center, Pacific Grove, California, USA.

[2] Fan R.-E. , Chang K.-W., Hsieh C.-J., Wang X.-R., and Lin C.-J.. LIBLINEAR: A library for large linear classification. Journal of Machine Learning Research 2008;9:1871-1874.

[3] Kononenko, I. Estimating attributes: analysis and extensions of Relief. In De Raedt, L. and Bergadano, F., editors, Machine Learning: ECML-94, 1994, pages 171-s182. Springer Verlag.

[4] Lotte F., Congedo M., Lècuyer A., Lamarche F. and Arnaldi B. A review of classification algorithms for EEG-based brain?computer interfaces Journal of Neural Engineering, 2007; 4(2).

[5] Riccio A, Simione L, Schettini F, Pizzimenti A, Inghilleri M, Olivetti Belardinelli M, Mattia D, Cincotti F. Attention and P300-based BCI performance in people with amyotrophic lateral sclerosis. Frontiers in Human Neuroscience 2013;7:732.

[6] BNCI Horizon 2020. The Future of Brain/Neural Computer Interaction: Horizon 2020 `http://bnci-horizon-2020.eu/database/data-sets`

[7] L. Bianchi, at all. Which physiological components are more suitable for visual ERP based brain computer interface? A preliminary MEG/EEG study. Brain Topography, 23:180-185, 2010

[8] DECODER Project, European ICT program FP7-ICT-2009-04; Grant Agreement 247919

Published by Verlag der TU Graz
Graz University of Technology

Proceedings of the
7th Graz Brain-Computer Interface Conference 2017 DOI: 10.3217/978-3-85125-533-1-52

ERROR-RELATED POTENTIALS WITH MASKED AND UNMASKED ONSET DURING CONTINUOUS CONTROL AND FEEDBACK

C. Lopes Dias[1], A. I. Sburlea[1], G. R. Müller-Putz[1]

[1]Institute of Neural Engineering, Graz University of Technology, Graz, Austria

E-mail: gernot.mueller@tugraz.at

ABSTRACT: Brain-computer interfaces (BCIs) are prone to errors in the decoding of the user's intention, yet the detection of errors can be used to improve the performance of BCIs. We recorded the EEG data of 8 subjects who participated in an experiment to study error-related potentials (ErrPs) with masked and unmasked onset, during a task with continuous control and continuous feedback. The masked ErrPs had a delayed onset and less pronounced peak amplitudes when compared to the unmasked ErrPs. We obtained an average classification rate of 94% for correct trials and of 80% for error trials. The classification rates for masked errors against unmasked errors were at chance level.

INTRODUCTION

Brain-computer interfaces (BCIs) provide control to their users, by recognising their intention from neuronal activity [1]. BCIs are susceptible to errors in the decoding of the user's intention and benefit from the ability to detect what the user perceives as erroneous in order to improve performance. This is possible because the recognition of an error elicits a neuronal response that is associated with a coarse differentiation between favorable and unfavorable outcomes [2] and that can be measured using various techniques, e.g. electroencephalography (EEG). The electrophysiological signature of error detection is named error-related potential (ErrP) and is obtained by subtracting the averaged electrophysiological trace following correct events from the averaged trace following erroneous events.

Different types of ErrPs have been described in literature [3]: response ErrPs occur in speeded response time tasks in which subjects are asked to respond as quickly as possible to a stimulus; observation ErrPs occur when subjects observe an error being committed by an external agent; feedback ErrPs occur when subjects receive the information that the action they performed was not correct; and interaction ErrPs occur in the context of BCIs, when users believe that the command they issued was misinterpreted by the interface.

In BCIs that are controlled in a discrete way, the occurrence of interaction ErrPs is well established [4, 5]. In this context, interaction ErrPs can be detected on a single-trial basis [5, 6, 7]. This enables their real-time detection, either with the aim of correcting erroneous actions of the BCI [8] or with the aim of reducing the possibility of the error reappearing [9, 10].

BCIs that operate in a continuous way have gained attention in the last years because they offer a more natural interaction between user and interface [11, 12, 13]. This has prompted the study of interaction ErrPs during the use of BCIs with continuous control or feedback. Kreilinger et al. [14, 15] investigated the occurrence of interaction ErrPs in a BCI using simultaneously continuous and discrete feedback. Spüler et al. [16] studied interaction ErrPs in a task with continuous control and continuous feedback, given through a cursor, without any additional discrete feedback.

The study of asynchronous detection of ErrPs during continuous movement is still in the early stages. Spüler et al. introduced the asynchronous detection of interaction ErrPs [16]. In the context of an observation task, Omedes et al. asynchronously detected observation ErrPs with sudden and gradually unfolding errors [17, 18]. In the case of gradually unfolding errors, the moment of the error onset was not evident to the observer.

In the current work, we investigate interaction ErrPs with masked and unmasked onset, during a task with continuous control and continuous, jittered and non-jittered, feedback. We consider as unmasked the errors that occur during trials without jittered feedback and as masked the errors that occur during trials with jittered feedback. We hypothesize that masked ErrPs occur later than unmasked ErrPs, when time-locked to the error onset.

MATERIALS AND METHODS

Hardware and data acquisition: EEG data were recorded at 1000 Hz using BrainAmp amplifiers and an actiCap system (Brain Products, Munich, Germany) with 61 active electrodes. The electrodes were placed at positions Fp1, Fp2, AF3, AF4, F7, F5, F3, F1, Fz, F2, F4, F6, F8, FT7, FC5, FC3, FC1, FCz, FC2, FC4, FC6, FT8, T7, C5, C3, C1, Cz, C2, C4, C6, T8, TP9, TP7, CP5, CP3, CP1, CPz, CP2, CP4, CP6, TP8, TP10, P7, P5, P3, P1, Pz, P2, P4, P6, P8, PO9, PO7, PO3, POz, PO4, PO8, PO10, O1, Oz, and O2. The ground electrode was placed at position AFz and the reference electrode was placed on the right mastoid.

Published by Verlag der TU Graz
Graz University of Technology

 DOI: 10.3217/978-3-85125-533-1-52

Experiment overview: Eight subjects, 5 male, with ages between 19 and 27, participated in the experiment after reading and signing an informed consent form. The experiment consisted of 12 blocks with 30 trials each. Each trial lasted on average 4.6 s. Between the trials, subjects were given 2.5 s to rest. Between the blocks, subjects were allowed to rest for as long as they needed. One third of the trials of each block were randomly assigned as *error trials*, described below. Half of the blocks, randomly selected, consisted of trials with *jittered feedback*, also described below.

Trial and task description: In the beginning of each trial, 4 equally spaced squares were displayed on the upper part of a computer's screen, at the same distance from its centre. One of the squares was randomly chosen to be the target and colored yellow, whilst the others were blue. On the lower part of the screen was a red circle, which represented the cursor (see Fig. 1).

The task consisted in moving the cursor from its initial position to the target with a joystick. The joystick's displacement from its resting position controlled the direction of the cursor's displacement, which moved at constant velocity. The cursor was only allowed to move inside the grey area. A trial ended when the cursor reached the target or when it hit the boundary of the grey region.

In order to minimise eye movements during the trials, the participants were instructed to fixate their gaze on the target at the beginning of each trial, and to start moving the joystick afterwards [19].

Error trials: In these trials, the subject lost the control of the cursor when it was located at a randomly assigned distance from the center of the screen, within the area delimited by the green half-circles depicted in Fig. 1. When this happened, the cursor moved perpendicularly to its direction at the moment of the error onset, until the trial ended. The side to which it deviated was randomly assigned.

Subjects were instructed to keep their gaze fixed on the target and to bring the joystick back to the resting position when recognising that the control over the cursor was lost.

Jittered feedback: With the intention of masking the onset of the errors, in these trials the cursor jittered perpendicularly to the direction of the movement.

Preprocessing: The data were resampled from 1000 Hz to 250 Hz for the electrophysiological analyses and to 25 Hz for the time-locked classification. In addition, a Butterworth filter of order 4 was applied to bandpass the data between 1 and 10 Hz. Then the data were segmented into correct and error trials. To epoch the correct trials, we considered the trials in which the participants successfully guided the cursor to the target and extracted a 1.5 s interval beginning with the cursor crossing the horizontal midline of the screen depicted in Fig. 1. The error trials were segmented using a 1.5 s interval starting 0.5 s before the error onset. For the electrophysiological results, a CAR filter was additionally applied.

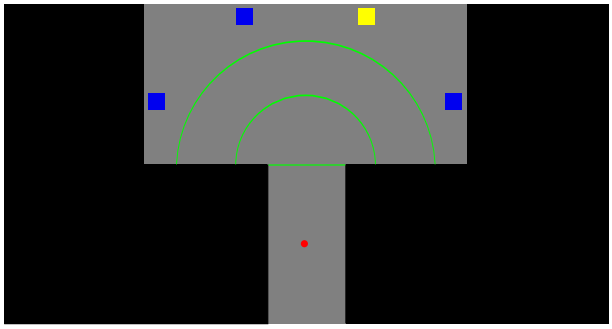

Figure 1: Experimental protocol: a possible setup at the beginning of a trial. The green half-circles delimit the region in which the errors occur. The green horizontal line represents the onset of the correct trials. The green elements are invisible to the subjects.

Outliers rejection: Box-and-whisker diagrams were used to reject outliers [20]. For each channel, the variance of the voltage during correct and error trials was calculated. The lower and upper quartiles, Q1 and Q3, of the channels' variances were used to calculate the interval $[\mathrm{Q1} - k(\mathrm{Q3} - \mathrm{Q1}),\ \mathrm{Q3} + k(\mathrm{Q3} - \mathrm{Q1})]$, with $k = 3$. Channels whose variance lied outside this interval were excluded.

To remove outlier trials, correct and error trials were treated separately. The variance of the voltage at FCz in correct and error trials was used to calculate two intervals, using the procedure described for the channels' rejection. Correct and error trials whose variance of the voltage at FCz lied outside the respective interval were excluded. Additionally, trials whose variance of the voltage at FCz was smaller than 2 µV were also excluded because they reflected problems with the electrode during the recording. On average, 5.64% of the trials were excluded.

Time-locked classification: The raw data were resampled to 25 Hz, bandpass-filtered and segmented as described above. The amplitudes of each channel at each time point of correct and error trials were used as features for training a shrinkage LDA classifier [21], which was tested using 10 times 5-fold cross validation. When classifying correct trials against error trials, training and testing sets were composed of 70% correct trials and 30% error trials. When classifying masked errors against unmasked errors, training and testing sets were balanced.

RESULTS

Electrophysiological analyses: Fig. 2 shows the average signal in error trials (red curve) and correct trials (green curve) at channel FCz for the 8 subjects. The shaded areas represent the 95% confidence interval of the average curves. In the averaged error signal, a sharp negative peak appears at 192 ms after the onset of the error ($t = 0$). It is followed by a pronounced positive peak at 300 ms. Finally, a broader negativity appears, peaking at 592 ms after the error onset. Fig. 2 depicts also the grand

Published by Verlag der TU Graz
Graz University of Technology

 DOI: 10.3217/978-3-85125-533-1-52

average ErrP (black curve). Fig. 3 depicts the grand average ErrP signal at different scalp positions. Electrodes over the central regions of the scalp show ErrPs with higher peak amplitudes.

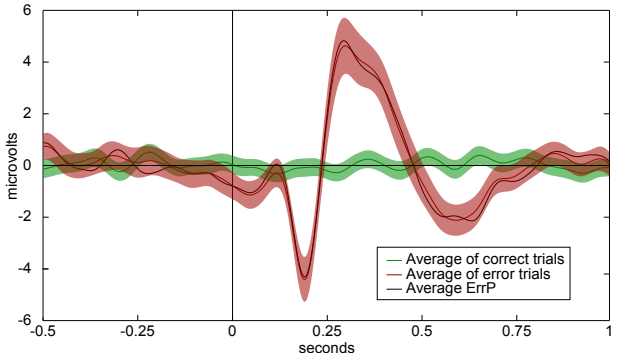

Figure 2: Grand average correct and error signals at channel FCz. The shaded areas represent the 95% confidence interval of the average curves. The black curve represents the grand average ErrP.

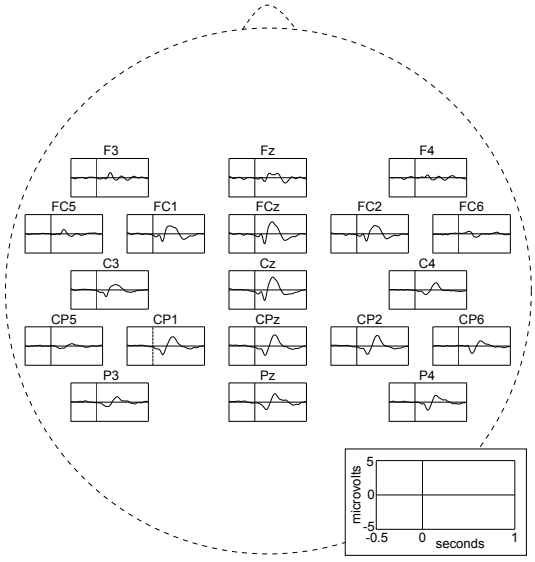

Figure 3: Grand average ErrP at different channels. The diagram on the bottom right indicates the axes' scale of the labeled plots.

Masked and unmasked errors: The grand average correct and error signals, masked and unmasked, are shown in Fig. 4. The averaged unmasked error signal presents a first negative peak 184 ms after the error onset, a positive peak at 316 ms and a broader negativity that peaks at 572 ms. The averaged masked error signal presents a first negative peak at 196 ms, followed by a positive peak at 348 ms and a broader negativity that peaks at 600 ms. The averaged masked error signal is delayed in comparison to the averaged unmasked error signal, when time-locked to the error onset. The peaks of the averaged masked error signal have a lower amplitude than the ones in the averaged unmasked error signal.

Fig. 5 displays the averaged correct and error signals, masked and unmasked, for each subject individually. The first negativity of the grand average error signal, masked and unmasked, is not present in the error signals of all the participants. A delay in the masked error signal in comparison with the unmasked error signal is present in the signals of the majority of the subjects. Subject 5 does not display ErrPs at channel FCz after CAR filtering.

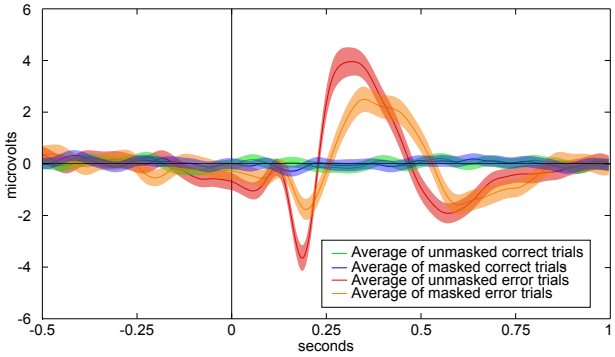

Figure 4: Grand average correct and error signals, masked and unmasked, at channel FCz. The shaded areas represent the 95% confidence interval of the average curves.

Time-locked classification: Both masked and unmasked trials were considered to classify correct trials against error trials. Tab. 1 shows the percentages (mean and standard deviation) of successfully recognised correct and error trials for each subject and their average. Tab. 1 also shows the Cohen-κ coefficient for each subject and their average. We obtained an average of 94.3% recognition rate for correct trials and of 80.3% for error trials. The average Coehen's κ coefficient obtained was of 0.76.

We also tried to classify masked errors against unmasked errors but the results obtained were at chance level (50%), as shown in Tab. 2.

DISCUSSION

We presented results on the electrophysiology of interaction ErrPs and compared errors with masked and unmasked onset. In our study, the ErrP displayed a very similar shape to the error signal because the correct signal was not associated with any event. The masked error signals were delayed in comparison to the unmasked ones, when time-locked to the error onset. We assume that this is due to subjects taking longer to recognise masked errors. The first negative and positive peaks in the masked error signals presented lower amplitudes than in the corresponding peaks in the unmasked error signals. This occurred either due to a variability of the moment in which subjects recognised the error in masked trials or due to

Published by Verlag der TU Graz
Graz University of Technology

 DOI: 10.3217/978-3-85125-533-1-52

a change in the cursor's direction causing more surprise in unmasked trials than in the masked ones, in which the participants were used to some instability in the feedback.

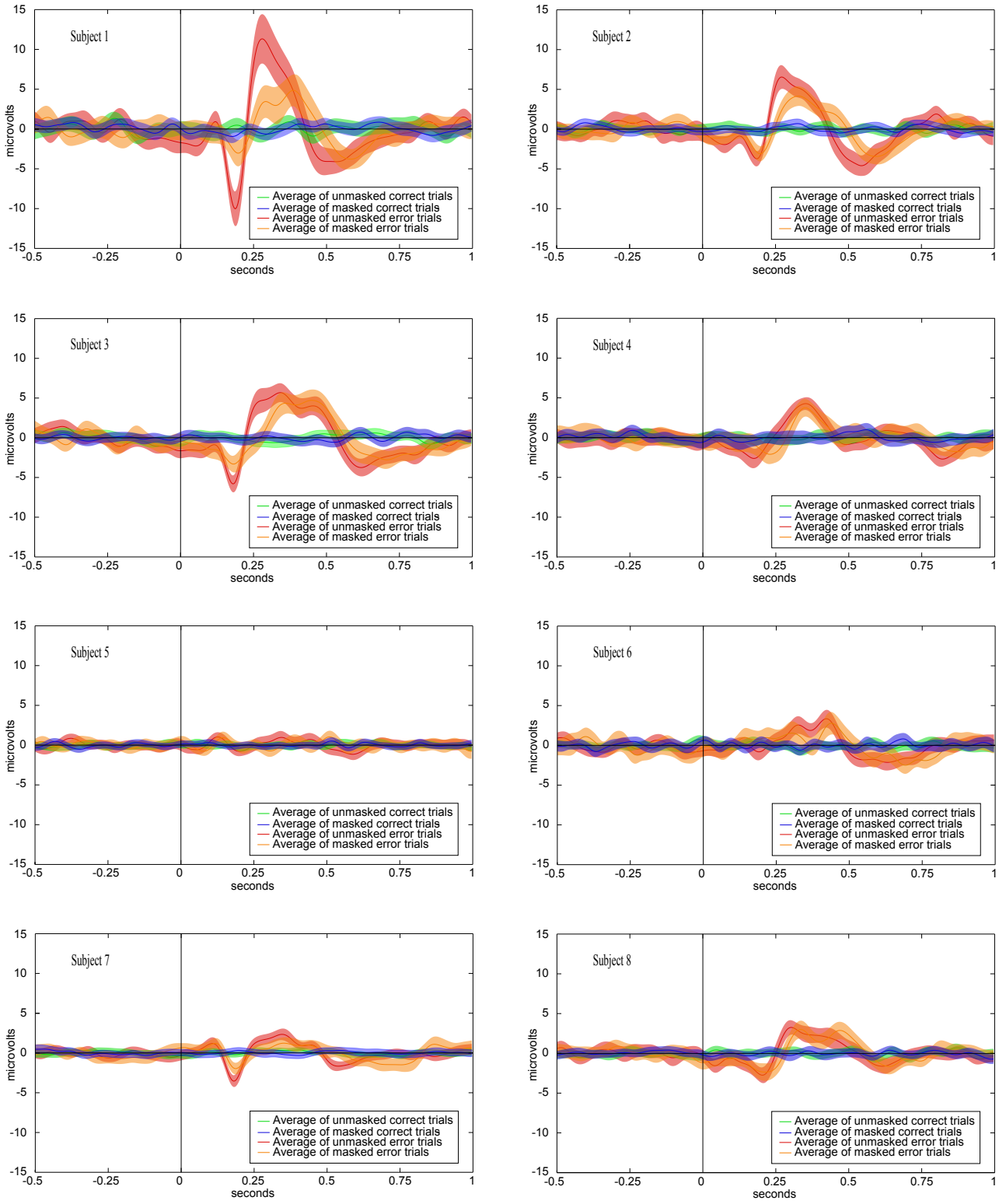

Figure 5: Average of correct and error signals, masked and unmasked, at channel FCz and for each subject. The shaded areas represent the 95% confidence interval of the mean curves.

Published by Verlag der TU Graz
Graz University of Technology

 DOI: 10.3217/978-3-85125-533-1-52

Table 1: Percentages (mean and standard deviation) of successfully classified correct and error trials and Cohen-κ coefficient.

Subject	Correct (%)	Error (%)	κ
1	98.4 ± 1.4	91.9 ± 5.6	0.91 ± 0.04
2	99.1 ± 1.4	87.5 ± 7.3	0.89 ± 0.06
3	95.0 ± 3.2	81.2 ± 7.1	0.78 ± 0.06
4	93.4 ± 3.2	82.1 ± 8.4	0.76 ± 0.08
5	90.3 ± 4.1	68.7 ± 11.0	0.60 ± 0.12
6	92.0 ± 3.9	77.3 ± 9.9	0.70 ± 0.10
7	92.3 ± 3.8	77.6 ± 10.5	0.71 ± 0.11
8	93.7 ± 3.0	76.1 ± 9.6	0.71 ± 0.09
Average	94.3 ± 4.3	80.3 ± 11.0	0.76 ± 0.13

Table 2: Percentages (mean and standard deviation) of successfully classified masked and unmasked error trials.

Subject	Masked (%)	Unmasked (%)
1	64.9 ± 13.1	68.8 ± 15.7
2	63.2 ± 12.1	54.4 ± 17.6
3	65.8 ± 15.9	70.1 ± 13.6
4	51.3 ± 16.0	62.1 ± 14.1
5	68.4 ± 15.9	68.1 ± 13.4
6	66.4 ± 13.3	55.9 ± 15.3
7	51.0 ± 14.7	55.5 ± 15.3
8	41.9 ± 17.7	41.1 ± 13.8
Average	59.1 ± 17.4	59.5 ± 17.4

CONCLUSION

We investigated interaction ErrPs with masked and unmasked onset. The masked error signals were delayed in comparison to the unmasked ones, when time-locked to the error onset. The first negative and positive peaks in the masked error signals presented lower amplitudes than the corresponding peaks in the unmasked error signals. We obtained good classification rates for correct trials against error trials using time domain features. Nevertheless, our classification results for masked errors against unmasked errors were at chance level.

ACKNOWLEDGEMENTS

The authors would like to thank M.K. Höller for the help during the experiment's preparation. This work was supported by the ERC consolidator grant 681231 "Feel Your Reach".

REFERENCES

[1] Millán JdR, Rupp R, Müller-Putz GR, Murray-Smith R, Giugliemma C, Tangermann M et al. Combining brain—computer interfaces and assistive technologies: State-of-the-art and challenges. Frontiers in Neuroscience, 2010; 4:161.

[2] Hajcak G, Moser JS, Holroyd CB, Simons RF. The feedback-related negativity reflects the binary evaluation of good versus bad outcomes. Biological Psychology, 2006; 71(2):148–154.

[3] Chavarriaga R, Sobolewski A, Millán JdR. Errare machinale est: the use of error-related potentials in brain-machine interfaces. Frontiers in Neuroscience, 2014; 8:208.

[4] Schalk G, Wolpaw JR, McFarland DJ, Pfurtscheller G. EEG-based communication: presence of an error potential. Clinical Neurophysiology, 2000; 111(12):2138–2144.

[5] Ferrez PW, Millán JdR. You are wrong!: Automatic detection of interaction errors from brain waves. In Proc. IJCAI'05, San Francisco, USA, 2005, 1413–1418.

[6] Ferrez PW, Millán JdR. EEG-based brain-computer interaction: Improved accuracy by automatic single-trial error detection. In Proc. NIPS 2007, Vancouver, Canada, 2007, 441–448.

[7] Ferrez PW, Millán JdR. Error-related EEG potentials generated during simulated brain-computer interaction. IEEE Transactions on Biomedical Engineering, 2008; 55(3):923–929.

[8] Ferrez PW, Millán JdR. Simultaneous real-time detection of motor imagery and error-related potentials for improved BCI accuracy. In Proc. of the 4th International Brain-Computer Interface Workshop and Training Course, Graz, Austria, 2008, 197-202.

[9] Blumberg J, Rickert J, Waldert S, Schulze-Bonhage A, Aertsen A, Mehring C. Adaptive classification for brain computer interfaces. In Proc. EMBC 2007, Lyon, France, 2007, 2536–2539.

[10] Llera A, van Gerven MA, Gómez V, Jensen O, Kappen HJ. On the use of interaction error potentials for adaptive brain computer interfaces. Neural Networks, 2011; 24(10):1120–1127.

[11] Galán F, Nuttin M, Lew E, Ferrez PW, Vanacker G, Philips J, Millán JdR. A brain-actuated wheelchair: Asynchronous and non-invasive brain—computer interfaces for continuous control of robots. Clinical Neurophysiology, 2008; 119(9):2159–2169.

[12] Kreilinger A, Kaiser V, Rohm M, Rupp R, Müller-Putz GR. BCI and FES training of a spinal cord injured end-user to control a neuroprosthesis. Biomed Tech, 2013; 58.

[13] Doud AJ, Lucas JP, Pisansky MT, He B. Continuous three-dimensional control of a virtual helicopter using a motor imagery based brain-computer interface. PloS one, 2011; 6(10):1–10.

[14] Kreilinger A, Neuper C, Müller-Putz GR. Error potential detection during continuous movement of an artificial arm controlled by brain–computer interface. Med Biol Eng Comput, 2012; 50(3):223–230.

Published by Verlag der TU Graz
Graz University of Technology

 DOI: 10.3217/978-3-85125-533-1-52

[15] Kreilinger A, Hiebel H, Müller-Putz GR. Single versus multiple events error potential detection in a BCI-controlled car game with continuous and discrete feedback. IEEE Transactions on Biomedical Engineering, 2016; 63(3):519–529.

[16] M. Spüler, C. Niethammer. Error-related potentials during continuous feedback: using EEG to detect errors of different type and severity. Frontiers in Human Neuroscience, 2015; 9:155.

[17] Omedes J, Iturrate I, Chavarriaga R, Montesano L. Asynchronous decoding of error potentials during the monitoring of a reaching task. In Proc. SMC2015, Hong Kong, China, 2015, 3116–3121.

[18] Omedes J, Iturrate I, Minguez J, Montesano L. Analysis and asynchronous detection of gradually unfolding errors during monitoring tasks. Journal of Neural Engineering, 2015; 12(5):056001.

[19] Sailer U, Flanagan JR, Johansson RS. Eye–hand coordination during learning of a novel visuomotor task. Journal of Neuroscience, 2005; 25(39):8833–8842.

[20] Tukey JW. Exploratory Data Analysis: Past, Present, and Future. Princeton University, Princeton, USA (1993).

[21] Peck R, Van Ness J. The use of shrinkage estimators in linear discriminant analysis. IEEE Trans. Pattern Anal. Mach. Intell.,1982; 4(5):530–537.

Published by Verlag der TU Graz
Graz University of Technology

Proceedings of the
7th Graz Brain-Computer Interface Conference 2017 DOI: 10.3217/978-3-85125-533-1-53

ONLINE CLASSIFICATION ACCURACY IS A POOR METRIC TO STUDY MENTAL IMAGERY-BASED BCI USER LEARNING: AN EXPERIMENTAL DEMONSTRATION AND NEW METRICS

F. Lotte[1], C. Jeunet[1,2,3]

[1]Inria Bordeaux Sud-Ouest / LaBRI, Talence, France
[2]Inria Rennes Bretagne Atlantique / Irisa, Rennes, France
[3]EPFL, Geneva, Switzerland

E-mail: fabien.lotte@inria.fr

ABSTRACT: While promising for many applications, Electroencephalography (EEG)-based Brain-Computer Interfaces (BCIs) are still scarcely used outside laboratories, due to a poor reliability. It is thus necessary to study and fix this reliability issue. Doing so requires to use appropriate reliability metrics to quantify both signal processing and user learning performances. So far, Classification Accuracy (CA) is the typical metric used for both aspects. However, we argue in this paper that CA is a poor metric to study how well users are learning to use the BCI. Indeed CA is notably unspecific, discrete, training data and classifier dependent, and as such may not always reflect successful EEG pattern self-modulation by the user. We thus propose new performance metrics to specifically measure how distinct and stable the EEG patterns produced by the user are. By re-analyzing EEG data with these metrics, we indeed confirm that CA may hide some learning effects or hide the user inability to self-modulate a given EEG pattern.

INTRODUCTION

While they are very promising for numerous applications, such as assistive technology or gaming, Electroencephalography (EEG)-based Brain-Computer Interfaces (BCIs) are still scarcely used outside laboratories [1]. This is mostly due to their poor reliability, as they often recognize erroneous mental commands from the user. One of the main current challenges of the community is thus to improve BCI reliability [1]. This is currently addressed at different levels, such as trying to design more robust EEG signal processing algorithms, or trying to improve BCI user training approaches, which have been shown to be inappropriate and a major cause of poor performances, both in theory and in practice [1, 3, 8]. Improving these different aspects requires to measure this reliability and thus BCI performances. Indeed such performance metrics could identify what are the limitations of a given algorithm or training approach, which is a necessary first step towards fixing these limitations [1].

User performance metrics are particularly useful for studying and improving Mental Imagery (MI) BCI user training. Appropriate performance metrics could indeed help to understand what users have successfully learned or still need to improve, which can then be used to guide them, i.e., to provide them with appropriate training tasks and feedback. In EEG-based BCI, the most used metric is Classification Accuracy (CA), i.e., the percentage of mental commands that were correctly recognized by the BCI [11, 12]. CA, together with other machine learning evaluation metrics [11, 12], have been successfully used to quantify the decoding performance of the BCI, i.e., how well the BCI recognizes the users' commands. However, CA is also used to study BCI user learning, i.e., how well users can modulate/self-regulate their EEG signals to control the BCI, and how much they learn to do so. For instance, CA is typically used to study how different feedbacks impact BCI user training [5], or how different psychological factors impact BCI user learning and performances [4].

In this paper, we argue and demonstrate that CA alone, as used in online MI-BCI, is not enough to study BCI user learning and performances. Indeed, this metric is notably unspecific, discrete as well as classifier and training data dependent, among other. In order to fully understand BCI user skill acquisition, alternative or additional metrics are thus necessary. Therefore, in this paper, we also propose new, simple and computationally efficient metrics to quantify various aspects of MI-BCI skill acquisition and compare them with the classically used online CA. We show that using online (or simulated online) CA as metric may actually hide several relevant aspects of BCI skill acquisition. In particular, online CA may miss user learning effects or fail to identify that a mental task performed is actually no different than rest EEG. Our new metrics can overcome these limitations.

This paper is organized as follows: The next section presents the material and methods, and notably how online CA is measured, and what its limitations are, as well as the new metrics we propose. It also presents the data set on which these measures are compared. Then the Results section compares the performances estimated with all metrics, which are then discussed in the Discussion section. The last section concludes the paper.

Published by Verlag der TU Graz
Graz University of Technology

 DOI: 10.3217/978-3-85125-533-1-53

MATERIALS AND METHODS

Classification accuracy and its limitations

As indicated before, CA is the most used metric to quantify BCI performances. Typically, the classifier is trained on the EEG signals from the trials of the first BCI runs (calibration runs) and applied to classify the users' EEG signals from the trials of the subsequent runs. CA is defined as the percentage of these EEG trials that were correctly classified [11]. From the classification results, we can also obtain a more detailed information on the performances from the Confusion Matrix (CM), which informs about how many trials from each class were estimated to be from each one of the possible classes. The CM is defined as follows for a two class problem:

Table 1: Confusion matrix for two classes

		Estimated class	
		Class 1	Class 2
Real Class	Class 1	a	b
	Class 2	c	d

Here, the number in row i, column j is the number of trials from class i that was classified as belonging to class j. Thus, a and d correspond to correct classifications (the real and estimated classes are the same), and c and b to erroneous classifications. CA (in %) can thus be computed as $\frac{a+d}{a+b+c+d} \times 100$. From there we can also estimate the CA of each class, e.g., $\frac{a}{a+b} \times 100$ is the percentage of trials from class 1 that were correctly classified.

This CA metric is very useful to quantify the decoding performance of a BCI [11]. However, when it comes to studying how well users can voluntarily modulate their EEG signals to control the BCI, we argue that such metric actually suffers from many limitations.

First, CA is unspecific: it only provides the global performance, but not what is (in)correctly classified, nor why it is so. Then, CA is a discrete measure: a trial is either correctly classified or not, there is no middle ground. As such, even if the user produces a stronger EEG modulation than before, but not strong enough to make the trial correctly classified, CA will not change.

CA is also strongly classifier and training data dependent. Changing the classifier type, its parameters, or the amount and/or quality of the training data will change the CA, irrespectively of how well users can modulate their EEG activity. Therefore variations of CA might not always reflect users' proficiency at BCI control. Classifiers are also sensitive to non-stationarities, and thus would lead to poor CA when applied on EEG data from a different distribution than that of the calibration runs. This is likely to happen if users are trying out various strategies or are learning. When based on a discriminative classifier such as Linear Discriminant Analysis (LDA), the most used classifiers for BCI [1], CA does not reflect how well a given mental command can be recognized but rather how distinct the mental commands are from each other. Therefore, if users are unable to modulate their EEG signals for one class (e.g., left hand MI), they may still obtain very high CA as long they can modulate their EEG for the other class (e.g., right hand MI), since the EEG signals from the two classes are distinct.

This leads to a last limitation: in BCI, CA usually considers the MI EEG signals only, but not the rest EEG signals. As illustrated just before, this prevents us from identifying whether the user's EEG patterns during MI are actually any different from rest EEG. For all these reasons, CA may not be able to reveal some important aspects of BCI user performance and BCI user learning, which thus calls for new metrics to quantify these aspects. This is what we propose in the following sections.

New Performance metrics

To address some of the limitations mentioned above, a possible approach (not new in itself but typically not used to study BCI user learning) would be to perform Run-Wise Cross-Validation (RWCV). The idea is to use CV to estimate offline the CA of each run. With RWCV, the trials from the current run are divided into K parts, K-1 parts being used for training the classifier, and the last part for testing it, the process being repeated K times, and the obtained CA averaged over the K testing parts. This thus also provides class-specific CV accuracies, as done with the standard CA. We will assess this approach in this paper. Since training and testing are performed on each run, and for different parts of each run, this makes RWCV CA much less sensitive to training data and to non-stationarities. This metric remains non-specific and discrete though, and still ignores the background EEG. It is also computationally expensive.

To further improve on the metrics mentioned above, we thus need metrics that are also specific, continuous, that consider rest EEG signals and that are computationally cheap. To go towards more specific metrics, we can first consider that the goal of BCI user training is typically defined as to enable users to produce stable and distinct EEG patterns, so that these patterns can then be recognized by the classifier. As such, it would make sense to design a set of metrics dedicated to estimating how stable and distinct the EEG patterns for each MI task actually are. A stable pattern would be a pattern that is not changing dramatically between trials, and thus with a small variance. A distinct pattern would be both 1) a pattern that is distinct from the rest EEG pattern, i.e., there is a specific signature to that pattern and 2) a pattern that is distinct from the EEG patterns of the other MI tasks.

Interestingly enough, metrics quantifying these various properties can be defined using distances in a Riemannian geometry framework. Indeed, Riemannian geometry offers an efficient and simple way to measure distances between covariance matrices, such matrices being increasingly used to represent EEG patterns [2, 14]. Given matrix $X_i \in \mathbb{R}^{N_c \times N_s}$ of EEG signals from trial i, with N_c the number of channels and N_s the number of samples per trial, the covariance matrix C_i of this trial is defined as $C_i = \frac{1}{N_s} X_i^T X_i$, with T being transpose. There-

Published by Verlag der TU Graz
Graz University of Technology

 DOI: 10.3217/978-3-85125-533-1-53

fore, the diagonal elements of C_i represent the EEG band power for each channel, and the off-diagonal elements, their covariations. Such spatial covariance matrices are used - implicitly or explicitly - to represent EEG signals in numerous MI-BCI designs, notably those based on the Common Spatial Patterns (CSP) algorithm, and many others [9, 14]. The Riemannian distance $\delta_R(C_i, C_j)$ between covariance matrices C_i and C_j can be defined as:

$$\delta_R(C_i, C_j) = [\sum_{i=1}^{n} \log(\lambda_i)^2]^{1/2} \quad (1)$$

where the λ_i are the eigen values of $C_i^{-1}C_j$. This Riemannian distance is particularly interesting since it is affine invariant: it is invariant to linear transformations, i.e., to variations such as normalization or channel displacement [14]. As such, the Riemannian distance has been used successfully for robust EEG signal decoding, in various kinds of BCIs [14]. In this paper, we show that this distance can also be a very relevant tool to quantify how distinct and stable the EEG patterns produced by a BCI user are. In particular, how distinct the EEG patterns from two tasks are could be quantified using the Riemannian distance between the average covariance matrices for each task. Then, the stability of a given EEG pattern can be defined using the average distance between each trial covariance matrix and the average covariance matrix for this task, which is a form of Riemannian standard deviation [14]. More formally, let us first define the Riemannian mean $\bar{C}$ of a set of covariance matrices C_i [14] as:

$$\bar{C} = \text{argmin}_C \sum_{i=1}^{N} \delta_R^2(C_i, C) \quad (2)$$

and the standard deviation σ_C of a set of matrices C_i as:

$$\sigma_C = \frac{1}{N} \sum_{i=1}^{N} \delta_R(C_i, \bar{C}) \quad (3)$$

From there we propose to define the distinctiveness *classDis* of the EEG patterns from two classes A and B as:

$$classDis(A, B) = \frac{\delta(\bar{C}^A, \bar{C}^B)}{0.5 \times (\sigma_{C^A} + \sigma_{C^B})} \quad (4)$$

where $\bar{C}^K$ and σ_{C^K} are respectively the mean and standard deviation of the covariance matrices from class K. This equation can be seen as the extension of the t-statistic to covariance matrices. Similarly, we propose to define the distinctiveness *restDis* between the EEG patterns from one class and those from the rest state as:

$$restDis(A) = \frac{\delta(\bar{C}^A, \bar{C}^{rest})}{0.5 \times (\sigma_{C^A} + \sigma_{C^{rest}})} \quad (5)$$

where $\bar{C}^{rest}$ and $\sigma_{C^{rest}}$ are respectively the mean and standard deviation of the covariance matrices of the rest EEG. Finally, we can define the stability of the EEG patterns from one MI task as being inversely proportional to the standard deviation of the covariance matrices from that task:

$$classStab(A) = \frac{1}{1 + \sigma_{C^A}} \quad (6)$$

These are simple, intuitive and computationally efficient metrics to quantify some aspects of users skills at BCI control. They are also training data and classifier independent, as well as robust to some non-stationarities given the affine invariance of δ_R. In the following, we compare them offline with CA and RWCV CA.

Data set and evaluation

To compare the performance metrics, we used the motor imagery EEG data from the experiment described in [3]. This data set comprises the EEG signals of 20 BCI-naive participants, who had to learn to do 2 MI-tasks, namely imagining left- and right-hand movements. Participants first had to complete a calibration run, without feedback, followed by 4 feedback runs. Each run was composed of 20 trials for each of the two MI tasks. At the beginning of each trial, a fixation cross was displayed. Then, after 2s, a beep sound occurred. Then, at t = 3s, the instruction appeared as an arrow the direction of which indicates the MI task to be performed, i.e., an arrow pointing left indicated a left hand MI and an arrow pointing right a right hand MI. From t = 3.250s, a feedback was provided for 4s in the shape of a bar the direction of which indicating the mental task that has been recognized and the length of which representing the classifier output.

EEG data were filtered in 8-30 Hz, using a 5th order butterworth filter. For each trial, the MI EEG segment used was the 2s long segment starting 0.5s after the cue (left or right arrow), i.e., from second 3.5 to 5.5 of each trial. For the rest EEG signals, we used the 2s long segment immediately before the cue, i.e., from second 1 to 3 of each trial. For CA and RWCV, we used 3 pairs of Common Spatial Pattern (CSP) spatial filters and a LDA classifier, as in [3]. For the standard (here simulated online) CA, we trained the CSP and LDA on the EEG data from the calibration run and used it to classify the EEG data from the 4 subsequent runs, as in [3]. For the RWCV CA, we used 4-fold CV on each run. For *classDis*, *restDis* and *classStab*, the covariance matrices for each trial were estimated using automatic shrinkage using the method from [7].

RESULTS

Average results

Figure 1 shows the average measures of distinctiveness between classes (MI tasks), i.e., CA, RWCV CA and *classDist*, for each run. CA displays some oscillations in performance, but no global learning effect. On the other hand, both RWCV CA and *classDist* reveal a clear continuous increase in distinctiveness between classes over runs. Despite the high inter-subject variability, the 2-way ANOVA *Metric*Run* (*Metric*: CA, RWCV CA, *classDist*

Published by Verlag der TU Graz
Graz University of Technology

 DOI: 10.3217/978-3-85125-533-1-53

- transformed to z-score to enable comparisons; *Run*: 2 to 5) for repeated measures showed a significant metric*run interaction [$F(1,19) = 4.432$; $p < 0.05$; $\eta^2 = 0.189$], see also Figure 2. Figure 3 shows the measures of distinctiveness per class (class-wise CA and *restDist*). Here as well, CA does not show any obvious learning, while RWCV CA shows some and *restDist* shows a continuous learning for one of the two classes. The 3-way ANOVA *Metric*Class*Run* (*Metric*: CA, RWCV CA, *classDist* (z-score); *Class*: left- vs. right-hand MI; *Run*: 2 to 5) for repeated measures showed a strong tendency towards a main effect of the metric [$F(1,19) = 3.826$; $p = 0.065$; $\eta^2 = 0.168$] but no metric*class*run interaction [$F(1,19) = 0.195$; $p = 0.664$; $\eta^2 = 0.010$]. Concerning the stability metric (*classStab*, Fig. 4), no clear learning is visible over a single session, at least on average.

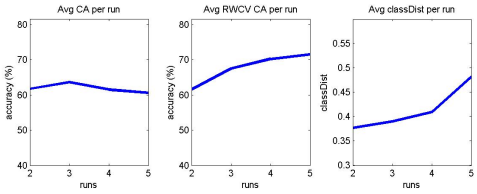

Figure 1: The average measures of distinctiveness between classes, across runs.

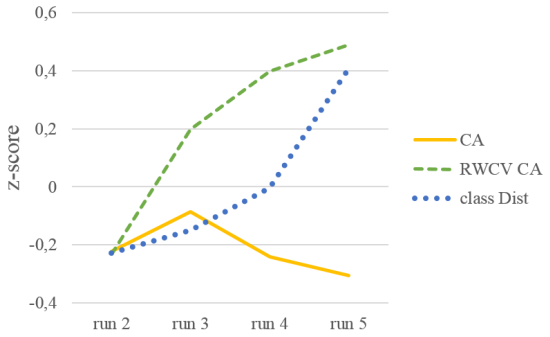

Figure 2: The z-score transformed distinctiveness measures, revealing learning with RWCV and *classDist* only.

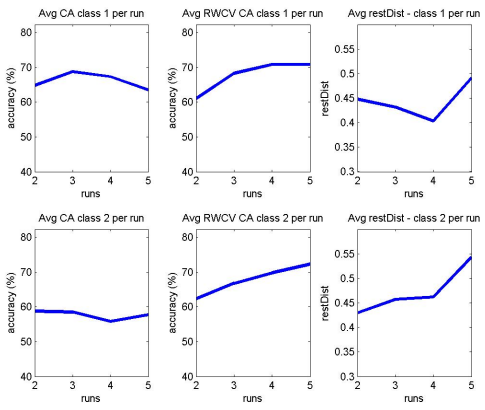

Figure 3: The average measures of class specific distinctiveness, across runs.

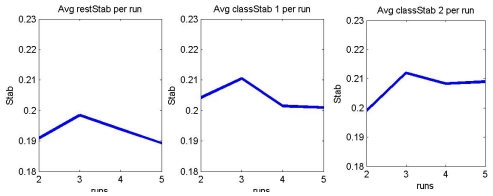

Figure 4: The average measures of stability.

Some subject specific results

As stated earlier, we observed a high inter-subject variability, therefore it is interesting to further investigate the different patterns observed in terms of metrics' evolution across the runs, for individual subjects. It will enable the analysis of the behavior of the different metrics and provide insights on their pros and cons.

For instance, all the distinctiveness measures for subject S5 could reveal a clear learning effect. However, the same metrics for subject S4 did not show any learning effect with the online CA, whereas both RWCV CA and *classDist* revealed clear learning over runs (see Fig. 5). Metrics for subject S9 (Fig. 6) revealed another interesting phenomenon. While both CA and RWCV CA did not show any learning, *classDist* did. However, *restDist* revealed that class 1 actually became increasingly more similar to rest EEG over the runs (*restDist* for class 1 sharply decreased), and thus that the increased *classDist* was probably due to the BCI discriminating rest vs right hand MI rather than left vs right MI. CA cannot identify such a phenomenon since it ignores rest EEG.

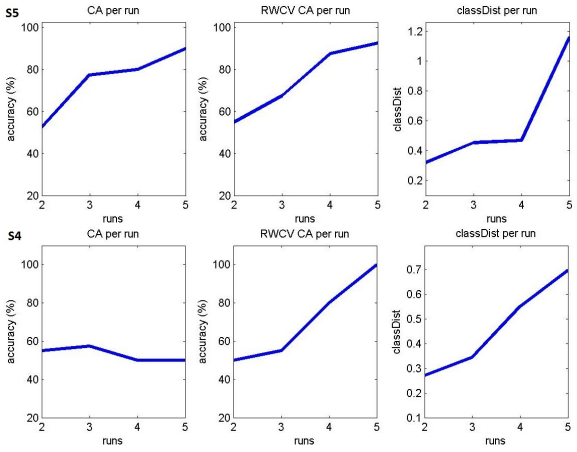

Figure 5: Examples of 2 subjects for which, either CA measured a learning effect like the other metrics (top), or did not whereas the other metrics did (bottom)

Finally, analyzes of Subject 19's data (Fig. 7) showed decreasing class discriminability with CA and *classDist*, however still revealed learning, with *restDist* continuously increasing over runs, for both classes. This could

Published by Verlag der TU Graz
Graz University of Technology

 DOI: 10.3217/978-3-85125-533-1-53

mean this subject learned to modulate his EEG signals so that they differ from rest EEG, but may have more troubles generating consistently distinct patterns between the two MI tasks. Such phenomenon has also been observed with simultaneous EEG-fMRI in [15], in which some subjects showed modulations of brain activity during MI with respect to rest signals, but no lateralization of the patterns. The *restDist* metric could thus be a cheap and easy way to identify this phenomenon in EEG.

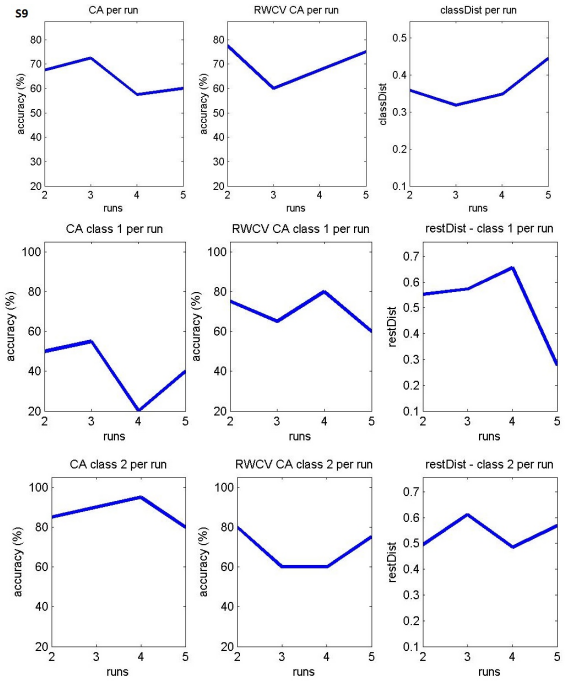

Figure 6: Subject 9, for which class 1 became like rest

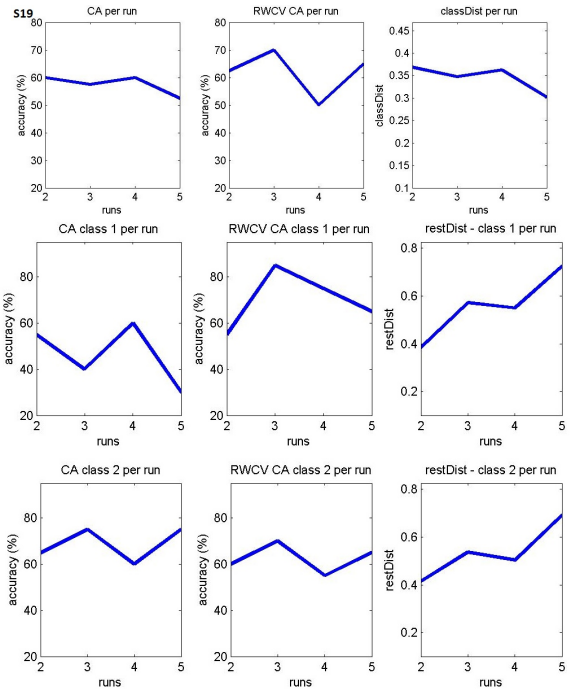

Figure 7: Subject 19 produced EEG patterns increasingly more different than rest, but not distinct from each other.

DISCUSSION

Globally, average results showed a significant metric*run interaction. This suggested that some metrics (here RWCV CA and *classDist*) revealed learning while another (CA) did not. This is all the more interesting given the fact that (1) we considered only one training session, so it is very likely that several subjects did not actually learn over such a short time and (2) the feedback was based on the CA metric. Indeed, participants were asked to make the blue bar feedback, that depended on the CA, as long as possible in the correct direction. Despite such feedback based on a possibly incomplete metric (as shown above), most of the participants showed that they were able to learn to modulate their EEG patterns, sometimes leading to metrics increase. This result is promising for the future as it suggests that with a better feedback, the ability of the participants to learn to modulate efficiently their EEG patterns, in order to improve their BCI control, could be enhanced. On the other hand, these results also suggested that different performance metrics can reveal different aspects of BCI user learning. Notably, they first showed that CA may not always reveal that users have learned to modulate their EEG patterns, whereas metrics such as RWCV CA and *classDist* can reveal such learning. They even revealed fast learning effects in several subjects, with continuous progress over runs, over a single day of training. This can have profound implications for the study of BCI user training. For instance, the present results may explain why in [6], it was concluded that most BCI studies - and notably those based on machine learning - do not actually involve human learning. Indeed, in most of the studies surveyed in [6], CA was used as the performance metric. As such, human learning might have occurred, but CA might not have been able to measure it. It thus seems necessary to re-analyse EEG data from previous studies with complementary performance metrics such as the ones proposed here, to assess whether or not human learning was actually involved. The fast learning over runs revealed by the alternative metrics also stresses the need for co-adaptive BCI systems, and explains the success of these approaches, see, e.g., [13]. Interestingly enough, these works also studied EEG changes due to BCI learning, in a univariate way at each channel, using the R^2 metric. The *restDist* metric also highlighted the need to consider rest EEG when evaluating the BCI user skills. Not doing so may prevent us from realizing that the user is not able to perform one of the MI tasks, and should thus probably be specifically trained to do so.

CONCLUSION

In this paper, we argued that CA, the most used metric to quantify BCI performance, should not be used alone to

Published by Verlag der TU Graz
Graz University of Technology

 DOI: 10.3217/978-3-85125-533-1-53

study BCI user learning. We indeed identified many limitations of CA for this purpose and proposed new metrics, based on Riemannian distance, to do so. An evaluation of these metrics indeed confirmed that online CA may hide some learning effects and cannot identify how different an MI class is from rest EEG. We therefore conclude that, when studying user learning and performance, CA should be used with care, and complemented with metrics such as the ones proposed.

Naturally, this study needs to be extended by assessing these metrics on other data sets, as well as across several sessions, to measure long-term learning as well. Nonetheless, this study and metrics open many promising perspectives. In particular it would be interesting to re-analyze the relationship between users' profile, notably neurophysiological, personality and cognitive profile, and these new performance metrics (so far done by looking for correlation with CA only [4]), which could reveal new predictors of performance, and thus new ways of improving BCI user training. In the future, these metrics could also be used as the basis to design new feedbacks, and in particular explanatory feedbacks [10]. Indeed, these metrics being based on simple distance measures, they could be computed online, using incrementally estimated average covariance matrices. In contrast, the RWCV CA metric cannot be used online, notably due to its computational cost. The *classDist*, *restDist* and *classStab* metrics could thus be provided as online feedback, to tell users whether they should improve the distinctiveness with rest, with another class, or the stability of their patterns, for instance. These concepts being abstract and unusual for BCI users, a considerable work would be needed in terms of user-centered design and human-computer interaction to find out the best ways to provide such an explanatory feedback. These metrics revealing fast learning effects, they could also be used as a cheap, possibly online way (faster and more convenient that CV) to identify when to update and retrain classifiers. Finally, it would be relevant to further refine these metrics, for instance by defining sub-metrics, for subset of EEG channels, over specific brain areas, to study brain area specific learning processes. Overall, we are convinced that BCI user training should be further studied, and we hope these new metrics could be a new way to look at these aspects.

Acknowledgments: This work was supported by the French National Research Agency with the REBEL project and grant ANR-15-CE23-0013-01, as well as by by the EPFL/Inria International Lab.

References

[1] R. Chavarriaga, M. Fried-Oken, S. Kleih, F. Lotte, and R. Scherer. Heading for new shores! overcoming pitfalls in BCI design. *Brain-Computer Interfaces*, pages 1–14, 2016.

[2] M. Congedo, A. Barachant, and A. Andreev. A new generation of brain-computer interface based on riemannian geometry. *arXiv preprint arXiv:1310.8115*, 2013.

[3] C. Jeunet, E. Jahanpour, and F. Lotte. Why standard brain-computer interface (BCI) training protocols should be changed: An experimental study. *Journal of Neural Engineering*, 13(3):036024, 2016.

[4] C. Jeunet, B. N'Kaoua, and F. Lotte. Advances in user-training for mental-imagery-based BCI control: Psychological and cognitive factors and their neural correlates. *Progress in brain research*, 2016.

[5] T. Kaufmann, J. Williamson, E. Hammer, R. Murray-Smith, and A. Kübler. Visually multimodal vs. classic unimodal feedback approach for smr-bcis: a comparison study. *Int. J. Bioelectromagn*, 13:80–81, 2011.

[6] A. Kübler, D. Mattia, H. George, B. Doron, and C. Neuper. How much learning is involved in BCI-control? In *Int. BCI Meeting*, 2010.

[7] O. Ledoit and M. Wolf. A well-conditioned estimator for large-dimensional covariance matrices. *Journal of Multivariate Analysis*, 88(2):365–411, 2004.

[8] F. Lotte and C. Jeunet. Towards improved BCI based on human learning principles. In *Proc. Int BCI Winter Conf*, 2015.

[9] L. Roijendijk, S. Gielen, and J. Farquhar. Classifying regularized sensor covariance matrices: An alternative to CSP. *IEEE Trans Neur. Syst. Rehab.*, 24(8):893–900, 2016.

[10] J. Schumacher, C. Jeunet, and F. Lotte. Towards explanatory feedback for user training in brain-computer interfaces. In *Proc. IEEE SMC*, pages 3169–3174, 2015.

[11] E. Thomas, M. Dyson, and M. Clerc. An analysis of performance evaluation for motor-imagery based BCI. *J Neur Eng*, 10(3):031001, 2013.

[12] D. E. Thompson, L. R. Quitadamo, L. Mainardi, S. Gao, P.-J. Kindermans, J. D. Simeral, et al. Performance measurement for brain–computer or brain–machine interfaces: a tutorial. *Journal of neural engineering*, 11(3):035001, 2014.

[13] C. Vidaurre, C. Sannelli, K.-R. Müller, and B. Blankertz. Machine-learning-based coadaptive calibration for brain-computer interfaces. *Neural computation*, 23(3):791–816, 2011.

[14] F. Yger, M. Berar, and F. Lotte. Riemannian approaches in brain-computer interfaces: a review. *IEEE Trans Neur. Syst. Rehab.*, 2017.

[15] C. Zich, S. Debener, C. Kranczioch, M. G. Bleichner, I. Gutberlet, and M. De Vos. Real-time EEG feedback during simultaneous EEG–fMRI identifies the cortical signature of motor imagery. *Neuroimage*, 114:438–447, 2015.

Published by Verlag der TU Graz
Graz University of Technology

Proceedings of the
7th Graz Brain-Computer Interface Conference 2017 DOI: 10.3217/978-3-85125-533-1-54

DEEP RECURRENT CONVOLUTIONAL NEURAL NETWORKS FOR CLASSIFYING P300 BCI SIGNALS

R. K. Maddula[1], J. Stivers[2], M. Mousavi[3], S. Ravindran[1], V. R. de Sa[2]

[1]Computer Science and Engineering, UC San Diego, La Jolla, CA, United States
[2]Cognitive Science, UC San Diego, La Jolla, CA, United States
[3]Electrical and Computer Engineering, UC San Diego, La Jolla, CA, United States

E-mail: desa@ucsd.edu

ABSTRACT: We develop and test three deep-learning recurrent convolutional architectures for learning to recognize single trial EEG event related potentials for P300 brain-computer interfaces (BCI)s. One advantage of the neural network solution is that it provides a natural way to share a lower-level feature space between subjects while adapting the classifier that works on that feature space. We compare the deep neural networks with the standard methods for P300 BCI classification.

INTRODUCTION

Brain-computer interfaces (BCIs) are being developed as communication methods for people with locked-in syndrome who have lost the ability to control their muscles and thus can't move, speak, or eventually even move their eyes in a well-controlled way. Electroencephalography (EEG) provides a cheap non-invasive monitoring channel with excellent temporal precision and is the most used signal for brain-computer interfaces. Classifying the EEG signals however is a difficult task as the signals are subject to poor spatial resolution, sensitivity to other electromagnetic sources as well as to the impedance of the electrode-scalp interface. The accuracy of classification algorithms for interpreting EEG data is a major barrier to the improvement of the EEG based BCI systems.

P300 based BCIs attempt to recognize a single-trial P300-like response that occurs when a subject attends to a presented rare or meaningful item. P300 responses have been studied in Cognitive Neuroscience for years and are referred to as event related potentials as they are time-locked to the presentation of the stimulus (event) [1]. Modern P300 BCIs classify the single-trial version of the event-related potential. Single-trial processing of EEG data has to date largely been most successful with very simple algorithms due to the large amounts of noise in the data and the paucity of data.

Many studies [2,3] have generally found that linear classification methods such as linear support vector machines (SVM) and linear discriminant analysis (LDA) worked better for classifying P300 BCIs than simple shallow non-linear methods such as multilayer perceptron and Gaussian kernel support vector machines. However, these classifiers treat every spatio-temporal sample equally (for example they perform identically if channel data are consistently permuted), and therefore do not benefit from the potential assumption that local temporal and spatial patterns exist in the data. By preserving the spatial organization of electrodes in the representation of the data, we could attempt to learn local spatial filters present in the data. Overall, a classifier should consider both spatial and temporal information while classifying the P300 EEG signal.

Recently deep neural networks have transformed the fields of handwriting recognition, speech recognition [4], large scale image recognition [5] and video analysis [6,7], and are rapidly transforming machine learning more generally. More recently convolutional neural nets and recurrent nets have been used in the realm of EEG signal classification. Cecotti et al.[8] used convolutional neural networks for P300 EEG classification. Mirowski et al.[9] used convolutional networks to predict epileptic seizures before they happen. Bashivan et al.[10] used a deep recurrent-convolutional network to learn representations from EEG, and demonstrated its advantages in the context of a mental load classification task. They successfully preserved the spectral, spatial, and temporal structure of the data during classification. There are multiple reasons to believe that deep learning could transform EEG processing: a) convolutional neural networks provide an intuitive and well understood way to deal with natural spatial relationships [5], b) neural networks easily allow filtering and classification to be combined in one discriminative framework, and c) recent advances in recurrent neural network (RNN) structures such as Long Short Term Memory (LSTM) [11] provide an intuitive and well understood way to deal with natural temporal relationships.

Our goal is to develop various deep learning architectures for classifying the P300 EEG signals. The proposed classifiers respect the spatial and temporal nature of the EEG signals, optimally combine their information, and naturally permit the sharing of sub-structure between tasks and between subjects. We propose a three-dimensional convolutional neural network (3D-CNN) [6,12] in conjunction with a two-dimensional convolutional neural network (2D-CNN) and LSTM to capture spatio-temporal patterns in the EEG signals We also ex-

Published by Verlag der TU Graz
Graz University of Technology

 DOI: 10.3217/978-3-85125-533-1-54

plore the use of transfer learning, where the information can be shared between different subjects [13].

Transfer learning is important in EEG analysis as due to cortical folding and other differences between people, EEG classifiers trained on one subject do not generalize as well to other subjects. However, it is time-consuming to collect training data from each new subject, so a desirable strategy is to train a "proto-classifier" with many previous subjects and then refine it with a small amount of training data from the new subject.

Our proposed method for P300 EEG signal classification is closely related to the one that is proposed by Bashivan et al.[10]. This method preserved the spatial structure of the data by transforming EEG into 2D image frames, and combined 2D-CNN and LSTM for the classification. In contrast, we propose the use of a 3D CNN in order to preserve spatio-temporal features, and also employ transfer learning to further increase classification performance.

MATERIALS AND METHODS

EEG DATASET: Data were collected from a P300 segment speller paradigm where letter segments were flashed and subjects had to mentally note which stimuli were segments from their target letter[19]. That is, targets were colored segments that form part of the desired letter and non-targets were differently colored segments that are not part of the letter. There were 10 segments total and each segment has a unique color. Subjects were cued with the colored segments at the beginning of each trial. Responses to target segments give similar P300 responses to target letters in a more common P300 BCI paradigm.

We performed experiments using two training datasets. EEG dataset 1 was recorded from 4 subjects using a 64-channel active electrode EEG system (BioSemi Active II) with a sampling rate of 512 Hz and bilaterally referenced to the average of the two mastoids. Later, the data were segmented and temporally downsampled to 128 Hz. EEG Dataset 2 was recorded from 5 subjects using the BrainVision BrainAmp 64-channel EEG system. The native sampling rate was 5 kHz, downsampled to 100 Hz for classification. Data were re-referenced to common mean (montage average reference). On both the datasets, the EEG signal is bandpass filtered with an FIR filter of length 68-taps, with passband between 2 and 35 Hz and stopband cutoffs at 0.1 and 40 Hz. Also, the signal from 150 ms to 800 ms after segment flash onset was segmented and downsampled to ten frames.

The classification task is to classify an EEG signal signal into a target class or a non target class. The target class refers to the signals collected when a target segment is flashed, while the non target class refers to the signals collected when a non target segment is flashed. The dimension of each input signal is 64 x 10 (Channels in 3D space x Time Points).

DATA PRE-PROCESSING: Our goal is to improve the detection/classification of P300 responses by learning representations from the EEG data. We preserve spatial information, by projecting the EEG data into a 2D grid as in [10]. The EEG electrodes are located in a three dimensional space over the scalp. Transforming the EEG measurements from 3D locations on the head into a 2D grid is accomplished through spatial interpolation. An azimuthal equidistant projection [14] is used to project the position of electrodes in a 2D surface. Subsequently, cubic spline interpolation [15] is applied on the resultant 2D mapping of the electrodes to obtain a 2D grid of size n x n, where n is the number of points in each row. A square with roughly 8 or 12 interpolated points on each side seems sufficient for capturing the spatial variation. For this experiment, we use 8 interpolated points on each row and column resulting in an 8 x 8 2D grid, analogous to a 2D image with pixel dimension of 8 x 8. 2D images are constructed for every time window for each trial, and are given as an input to the deep convolutional neural network. The input dimension for each signal is 10 x 8 x 8 x 1 (Time Samples x height x width x Depth).

PROPOSED MODEL ARCHITECTURES: In order to learn the inherent spatial and temporal features from an EEG signal, we use a model which combines a deep hierarchical feature extractor with the one that can learn to recognize and synthesize the temporal features.

General multilayer perceptrons have not been widely successful in EEG as the massive number of unconstrained interdependent parameters can lead to overfitting. The convolutional framework allows for successfully learning complex relationships in images without overfitting for at least two reasons: (1) Each filter is only applied to a few local inputs, and (2) each filter is learned based on multiple windows (replicated throughout the training pattern) in each labeled example. This effectively increases the amount of training data available for learning the parameters.

Moreover, human brain activity is a temporally dynamic process. Variations of the signals between time points may actually contain additional information about the underlying P300 response. Hence, Long Short Term Memory (LSTM) is adopted on top of the CNN, to learn temporal patterns as has been done for action recognition in videos [7].

Generally, convolutions are applied on 2D feature maps to compute spatial features, and later recurrent layers are used to compute temporal features. However, the 2D ConvNets do not take the temporal information into account while performing the spatial convolutions on each frame. Hence, we propose an approach based on 3D ConvNets, which initially perform spatio-temporal convolutions, to consider both spatial information in each frame and temporal information encoded in multiple contiguous frames, preserving the temporal information of the input signal.

Here are the proposed architectures to extract the spatial and temporal information from the EEG signal.

- $2D^3 - L$: Layers of 2D-CNN are stacked on top of

Published by Verlag der TU Graz
Graz University of Technology

 DOI: 10.3217/978-3-85125-533-1-54

each other, and used on each frame to extract the spatial information, while LSTM was used to extract the temporal information, on the sequence of frames.

- $3D-2D^3-L$: A 3D-CNN was used initially to extract spatiotemporal features, and then a 2D-CNN and LSTM are applied on top of the 3D CNN.

- $S(3D)-2D^3-L$: A transfer learning approach is used on $3D-2D^3-L$ architecture, where we pretain the network on a different dataset, freeze the 3D CNN layers, and train the rest of the network on the current dataset. $S(3D)$ in $S(3D)-2D^3-L$ denotes that we are sharing the weights of 3D-CNN across the subjects.

We implemented the architectures using the Keras library and Theano framework. As described in the previous section, the EEG electrode positions are projected and interpolated into an 8x8 2D square grid and a sequence of 8x8 images are extracted over the successive time windows.

$2D^3-L$ **Architecture:** Here, we combine a 2D-CNN and LSTM, as a result separately utilizing both the spatial and temporal information for the classification.

As described in the previous section, in order to account for the temporal activity, we extract 10 frames from each trial ie., EEG signal, by dividing each trial into 10 time windows, and averaging over each time window. The sequence of these images are given as input to the CNN. The input data to the CNN is of the following dimension: *Total Number of Trials* x *10 frames per each trial* x *8 width* x *8 height* x *1 depth*

The outputs of the 2D-CNN are fed into a recurrent network, where we investigate the temporal activity in the EEG signals.

During training, the input to the CNN is a fixed-size 8x8 image. The image is passed through a stack of convolutional (conv.) layers, where we use filters with a very small receptive field: 3 x 3 (the smallest size to capture the notion of left/right, up/down, center). The convolution stride is fixed to 1 pixel with rectified linear (ReLu) activation functions. In order to preserve the spatial resolution of the image, spatial padding of 1 pixel is used in each convolutional layer. Multiple convolution layers are stacked together and followed by a Max-pooling layer. Max-pooling is performed over a 2 x 2 pixel window, with stride 2. Using dataset D1, Best results were obtained by stacking 3 convolutional layers, with kernels respectively 32, 48 and 64, together, followed by a Max-Pooling layer. The dimension of the input image for each time step by the end of the 3rd Conv Layer is 8 x 8 x 64. After applying pooling, the dimension reduces to 4 x 4 x 64.

Fig. 1 illustrates the optimal CNN configuration.

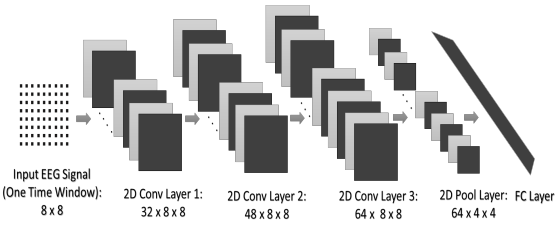

Figure 1: 2D Convolutional Neural Network for processing each temporal frame

This 2D-CNN architecture was adopted for each frame. The number of parameters in the network were reduced by sharing the parameters of the CNN over all the frames. A recurrent layer is applied on top of 2D-CNN. In order to use recurrent layers, the 3D output of 4 x 4 x 64 for each time step is converted into a 1D output of size 1024. The input dimension when training the recurrent neural network is 10 x 1024 (Time Steps x No. of Features).

RNN's provide an elegant way of dealing with sequential data that embodies correlations between data points that are close in the sequence. Though RNN's are successful in classifying many tasks such as speech recognition and text generation, they have difficulty with long term dependencies, due to the vanishing and exploding gradient problem [11], which results from propagating the gradients back through many layers. LSTMs are capable of handling the long term dependency problem; they learn when to forget previous hidden states and when to update the hidden states. We experimented (using subject D1) with various number of LSTM layers and memory cells in each layer. The best results were obtained when using a single LSTM layer with 32 memory cells.

For our implementation, we fed the extracted CNN outputs of 10 frames to the LSTM layer. The prediction of the LSTM layer at each time step was propagated up to the fully connected layer. The classification is done by averaging scores across all the frames. The outputs of the LSTM layer are fed into a fully connected layer, followed by a sigmoid layer.

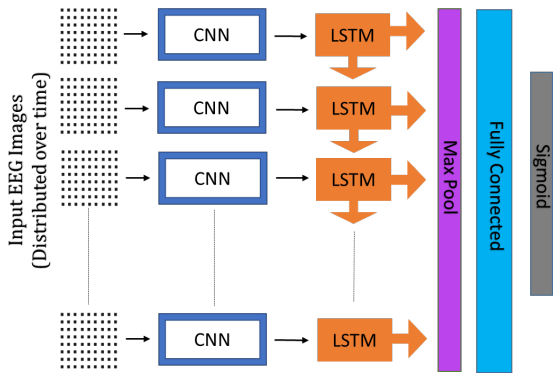

Figure 2: Overall architecture which combines 2D CNN with LSTM.

Published by Verlag der TU Graz
Graz University of Technology

 DOI: 10.3217/978-3-85125-533-1-54

We also compared using temporal convolutions instead of LSTM, in order to evaluate the performance of LSTM in extracting temporal information from a sequence of EEG images ($2D^3 - 1D$). In this model, the 2D CNN outputs across time frames are fed into a 1D CNN with 32 kernels of size 3 and a stride of 1 frame. These kernels capture different temporal patterns across multiple time frames. Fig. 2 shows the proposed $2D^3 - L$ architecture.

$3D - 2D^3 - L$ Architecture:
The 3D ConvNets are well-suited for spatio-temporal feature learning. The 3D Convolution is achieved by convolving a 3D kernel to the cube formed by stacking multiple contiguous frames together[12]. Therefore the feature maps in the convolutional layer are connected to multiple contiguous frames in the previous layer, thereby capturing the temporal information.
Initially, the multidimensional input signal, with dimension 8 x 8 x 1 x 10 (Height X Width x Depth x Time Steps) is fed into a 3D-CNN. We tried various configurations of 3D-CNN, involving different number of kernels and kernel size. Our findings indicate that using one 3D Conv layer with 24 kernels of size 3 x 3 x 3 (kernel Depth x Kernel Height x Kernel Width) is the best option. The dimensions of the signal by the end of this layer would be 8 x 8 x 24 x 10 (Height x Width x Depth x Time Steps). We used the $2D^3 - L$ architecture (Fig. 2) on top of the 3D CNN. The output of the 3D Conv layer in Figure Fig. 3 is fed into the $2D^3 - L$ network. The input for the $2D^3 - L$ network would be 10 frames of size 8 x 8 x 24. One layer of 3D-CNN with 24 kernels is followed by 3 layers of 2D-CNN with kernels 32, 48, 64 respectively for each time step.

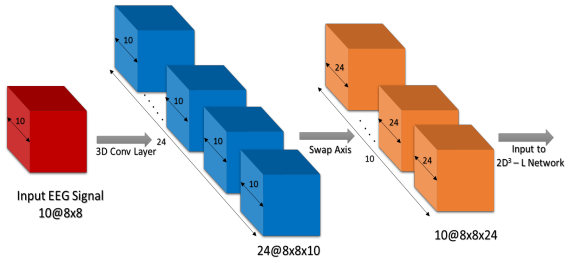

Figure 3: 3D convolutional neural network on EEG signal. Input signal (Red Cube) is of dimension 8 x 8 x 1 x 10 (Height x Weight x Depth x Time Points). The Red cube is basically formed by stacking up the 10 2D frames of size 8 x 8. A 3D -Conv layer of 24 filters with 3 x 3 x 3 size is applied (Blue cubes). The resultant output of size 8 x 8 x 10 x 24 is converted to 8 x 8 x 24 x 10 (Orange cubes). This would be the input to $2D^3 - L$ network, where 2D CNN is applied on each block of size 8 x 8 x 24, and the corresponding output of the blocks from 10 time steps is given to LSTM

Overall, the 3D-CNN helps us to extract the broad spatio-temporal features, and the 2D-CNN and LSTM find the hidden spatial and temporal features respectively.

$S(3D) - 2D^3 - L$ Architecture:
One advantage of the neural network approach is the ease in applying transfer learning where lower layer weights can be taken from a network trained on other subjects and then frozen for training of the whole network on the new subject [13].

The base network, which uses the $3D - 2D^3 - L$ architecture was initially trained on multiple subjects, and the corresponding parameters used in training the target network, which involves a fresh subject. Once the weights corresponding to the base network are copied to the target network, the 3D conv layer in the target network are frozen and do not change during the training. Only the weights corresponding to the higher layers (2D-CNN, LSTM, FC) of the target network change. We chose to freeze the CNN layers, instead of fine-tuning them, as the dataset is small and the number of parameters is large.

RESULTS

The network was trained and tested on two datasets. Dataset 1 comprises 4 subjects, while Dataset 2 comprises 5 subjects. The goal is to classify a signal as a P300 Target Signal or a Non-target signal. A split of 80% - 10% - 10% was used while dividing each fold into training, validation and testing respectively. Training is performed by optimizing the cross-entropy loss function. The network is trained using Adadelta, a variant of gradient descent which adapts over time using only first order information and has minimal computational overhead. In order to counteract possible overfitting due to the large number of weights, we used L2 Regularization penalty of 0.001 and Dropout of 20%. The architecture was the same for all subjects, where model tuning was done only on subject D1.

We compared the classification results of the proposed architectures with standards in the field - Stepwise LDA and shrinkage LDA. The shrinkage LDA algorithm uses automated shrinkage computation using the formula developed by Schaefer and Strimmer [18] based on the work of Ledoit and Wolf[17]. All tests were run with identical training/valid/test splits so that sensitive pairwise comparisons of accuracy could be made between the different algorithms. 50 different accuracy measurements were made for each network as follows: We made 5 random shuffles of the dataset and for each of these obtained 10 test sets by using an 80% train/10% validation/10% test division where each 10% of the data is used as the test set once.

Table 1: AUC measures for the proposed models on Dataset 1

	Sub. A1	Sub. B1	Sub. C1	Sub. D1
Stepwise LDA	0.67	0.65	0.69	0.65
Shrinkage LDA	0.69	0.64	0.71	0.65
$2D^3 - 1D$	0.65	0.65	0.67	0.64
$2D^3 - L$	**0.66**	**0.66**	**0.70**	**0.67**
$3D - 2D^3 - L$	**0.68**	**0.67**	**0.72**	**0.68**
$S(3D) - 2D^3 - L$	**0.69**	**0.70**	**0.72**	**0.69**

Published by Verlag der TU Graz
Graz University of Technology

 DOI: 10.3217/978-3-85125-533-1-54

Table 2: AUC measures for the proposed models on Dataset 2

	Sub. A2	Sub. B2	Sub. C2	Sub. D2	Sub. E2
Stepwise LDA	0.60	0.69	0.68	0.72	0.77
Shrinkage LDA	0.62	0.71	0.69	0.75	0.78
$2D^3 - 1D$	0.58	0.66	0.59	0.62	0.74
$2D^3 - L$	**0.61**	**0.68**	**0.62**	**0.70**	**0.76**
$3D - 2D^3 - L$	**0.64**	**0.70**	**0.67**	**0.75**	**0.76**
$S(3D) - 2D^3 - L$	**0.65**	**0.72**	**0.67**	**0.75**	**0.76**

Tab. 1 and Tab. 2 reports the Area under the ROC curve (AUC) for the baseline models and the proposed models on Dataset 1 (4 subjects) and Dataset 2 (5 subjects) respectively.

For the transfer learning in Dataset 1, we pretrain the 3D CNN network on all the subjects other than the current subject, and finally freeze the 3D convolutional layer and train the network on the current subject. For transfer learning in Dataset 2, due to the discovery of one subject (D2) with a very different "P300" signal (possibly more of an error-related potential signal), using all other subjects for transfer learning was not very successful, so one subject (E2) was used as transfer for the other subjects (A2-D2). For subject E2, all the other subjects (A2-D2) were used for transfer learning. To provide an alternate perspective, we replicated positive samples as done in [8] instead of subsampling. The first 70% was used for training, and the next 15% for validation and the last 15% for testing. The results comparing the performance of LDA with shrinkage and $S(3D) - 2D^3 - L$ are presented in Tables 3 and 4.

Table 3: Comparing AUC on Dataset 1

	Sub. A1	Sub. B1	Sub. C1	Sub. D1
Shrinkage LDA	0.67	0.58	0.7	0.59
$S(3D) - 2D^3 - L$	**0.68**	**0.69**	**0.7**	**0.7**

Table 4: Comparing AUC on Dataset 2

	Sub. A1	Sub. B1	Sub. C1	Sub. D1	Sub. E1
Shrinkage LDA	0.58	0.64	0.68	0.78	0.7
$S(3D) - 2D^3 - L$	**0.66**	**0.7**	**0.65**	**0.74**	**0.78**

DISCUSSION

We measured and compared the performance of the proposed and baseline models using a paired t-test.

On Dataset 1, Our $S(3D) - 2D^3 - L$ performed significantly better than the stepwise LDA on all the subjects, and performed significantly better (pairwise t-test) than Shrinkage LDA on subjects B1 (p = 2.32×10^{-7}) and D1 (p = 2.31×10^{-4}). The results from the $S(3D) - 2D^3 - L$ net did not differ significantly from the shrinkage LDA results on subjects A1 and C1.

On Dataset 2, $S(3D) - 2D^3 - L$ performed significantly better than $3D - 2D^3 - L$ on a few subjects and performed equally well on the other subjects. $S(3D) - 2D^3 - L$ performed better than Shrinkage (p = 6.98×10^{-4}) and Stepwise LDA (p = 5.9×10^{-3}) on subject A2. Also, it performed significantly better than stepwise LDA, (but not Shrinkage LDA) on subjects B2 (p = 2.73×10^{-5} vs Stepwise LDA) and D2(p = 6.27×10^{-5} vs Stepwise LDA). However, the shrinkage LDA performed significantly better than the $S(3D) - 2D^3 - L$ on subjects C2 (p = 8.74×10^{-4}) and E2 (p = 0.0324).

Overall, the proposed models work better than stepwise LDA and work better than the best baseline model (shrinkage LDA) on a few subjects and relatively lower on some other subjects.

The $2D^3 - L$ architecture performed numerically better than $2D^3 - 1D$ for all subjects and the difference reached statistical significance on 7 out of the 9 subjects (p- values between 3.42×10^{-11} and 0.0498). Thus it appears that LSTM did better in dealing with temporal patterns in the EEG signals compared to temporal convolution (1D-CNN) at least among the architectures we tried. The LSTM has richer temporal dynamics and can look at temporal patterns arbitrarily far back in time. 1D-CNN just looks for specific patterns in time of length up to the kernel length, while the LSTM understands and keeps track on the previous patterns and perform back-propagation through time [16].

From Tab. 1 and Tab. 2, we notice that the $3D - 2D^3 - L$ architecture performs better than the $2D^3 - L$ architecture. Moreover, the difference reaches statistical significance on 6 out of the 9 subjects (p-values between 1.17×10^{-6} and 0.0016). Even though, the performance gap is very small, it is a consistent difference. The 3D-CNN model effectively learns spatio-temporal patterns of the EEG signal.

Moreover, the transfer learning approach managed to perform better than the 3D-CNN, which states that 3D conv layer potentially learns spatio-temporal representations that are subject-independent, and the 2D-CNN and LSTM are able to deal with the intra-subject spatial and temporal patterns. The 3DConv layer captures the underlying spatial and temporal information, which are subject-independent.

Overall, the results suggest that deep learning may be used as an alternative compared to traditional machine learning techniques and that a 3D-CNN architecture is an effective model for learning the nature of P300 EEG signals.

CONCLUSION

In this work, a new approach for P300-EEG signal classification is demonstrated. As opposed to the traditional techniques, the proposed classifiers respect the inherent spatial and temporal nature of the EEG signals. This is accomplished by representing the multi-channel EEG time series as a sequence of 2D image frames. Inspired by the state-of-the-art video classification techniques, we train a deep convolutional and recurrent neural network on these sequence of 2D images. We proposed three different architectures. We discovered that using a 3D-CNN in conjunction with 2D-CNN and LSTM performed better than using 2D-CNN and LSTM. The 3D-CNN appears to most effectively model spatial and temporal information.

The best performance is obtained when using a transfer learning approach, where we pretrain a network compris-

Published by Verlag der TU Graz
Graz University of Technology

 DOI: 10.3217/978-3-85125-533-1-54

ing 3D Conv, 2D Conv and LSTM layers on different subjects, freeze the 3D Conv Layers, and perform classification training and then testing on a fresh subject. The classification performance of the proposed models are compared with common best performing classifiers in this field - Stepwise LDA and shrinkage LDA. The proposed models perform relatively better than the base line models on a few subjects. However, there is plenty of scope for improvement.
One of the benefits of the neural network approach is that spatio-temporal generalizations arise naturally. Combinations of 3D and 2D kernels could be used to optimally extract all the spatio-temporal structure that distinguishes the signals in P300 BCIs (or other temporal ERP signals). As a future direction, we will work on further increasing the performance, as improving the classification rates in BCI systems would make many more applications feasible and could improve the quality of life for those that are not able to communicate in other ways.

ACKNOWLEDGMENTS

Supported by NSF grants SMA 1041755 and IIS 1528214

REFERENCES

[1] Kutas M, McCarthy G, Donchin E. Augmenting mental chronometry: the P300 as a measure of stimulus evaluation time. Science. 1977 Aug 19;197(4305):792-5.

[2] Krusienski DJ, Sellers EW, Cabestaing F, Bayoudh S, McFarland DJ, Vaughan TM, et al. A comparison of classification techniques for the P300 Speller. Journal of neural engineering. 2006 Oct 26;3(4):299.

[3] Mirghasemi H, Fazel-Rezai R, Shamsollahi MB. Analysis of P300 classifiers in brain computer interface speller. InEngineering in Medicine and Biology Society, 2006. EMBS'06. 28th Annual International Conference of the IEEE 2006 Aug 30 (pp. 6205-6208). IEEE.

[4] Hinton G, Deng L, Yu D, Dahl GE, Mohamed AR, Jaitly N, et al. Deep neural networks for acoustic modeling in speech recognition: The shared views of four research groups. IEEE Signal Processing Magazine. 2012 Nov;29(6):82-97.

[5] Krizhevsky A, Sutskever I, Hinton GE. Imagenet classification with deep convolutional neural networks. InAdvances in neural information processing systems 2012 (pp. 1097-1105).

[6] Karpathy A, Toderici G, Shetty S, Leung T, Sukthankar R, Fei-Fei L. Large-scale video classification with convolutional neural networks. InProceedings of the IEEE conference on Computer Vision and Pattern Recognition 2014 (pp. 1725-1732).

[7] Donahue J, Anne Hendricks L, Guadarrama S, Rohrbach M, Venugopalan S, Saenko K, et al. Long-term recurrent convolutional networks for visual recognition and description. InProceedings of the IEEE conference on computer vision and pattern recognition 2015 (pp. 2625-2634).

[8] Cecotti H, Graser A. Convolutional neural networks for P300 detection with application to brain-computer interfaces. IEEE transactions on pattern analysis and machine intelligence. 2011 Mar;33(3):433-45.

[9] Mirowski PW, LeCun Y, Madhavan D, Kuzniecky R. Comparing SVM and convolutional networks for epileptic seizure prediction from intracranial EEG. InMachine Learning for Signal Processing, 2008. MLSP 2008. IEEE Workshop on 2008 Oct 16 (pp. 244-249). IEEE.

[10] Bashivan P, Rish I, Yeasin M, Codella N. Learning representations from EEG with deep recurrent-convolutional neural networks. arXiv preprint arXiv:1511.06448. 2015 Nov 19.

[11] Hochreiter S, Schmidhuber J. Long short-term memory. Neural computation. 1997 Nov 15;9(8):1735-80.

[12] Ji S, Xu W, Yang M, Yu K. 3D convolutional neural networks for human action recognition. IEEE transactions on pattern analysis and machine intelligence. 2013 Jan;35(1):221-31.

[13] Yosinski J, Clune J, Bengio Y, Lipson H. How transferable are features in deep neural networks?. In Advances in neural information processing systems 2014 (pp. 3320-3328).

[14] Snyder JP. Map projections–A working manual. US Government Printing Office; 1987.

[15] Alfeld P. A trivariate clough—tocher scheme for tetrahedral data. Computer Aided Geometric Design. 1984 Nov 1;1(2):169-81.

[16] Werbos PJ. Backpropagation through time: what it does and how to do it. Proceedings of the IEEE. 1990 Oct;78(10):1550-60.

[17] Ledoit, O. and Wolf, M. (2004). A well-conditioned estimator for large-dimensional covariance matrices. *Journal of Multivariate Analysis*, 88:365–411.

[18] Schaefer, J. and Strimmer, K. (2005). A shrinkage approach to large-scale covariance matrix estimation and implications for function genomics. *Stat. Appl. Genet. Mol. Biol.*, 4(1).

[19] Stivers, J.M. and de Sa, V.R. (2017). Spelling in parallel: towards a rapid, spatially independent BCI. Proceedings of the 7th Graz Brain-Computer Interface Conference 2017.

Published by Verlag der TU Graz
Graz University of Technology

Proceedings of the
7th Graz Brain-Computer Interface Conference 2017 DOI: 10.3217/978-3-85125-533-1-55

BRAIN ACTIVATION MAP DURING BCI COMMUNICATION IN COMPLETE LOCKED IN STATE

A. Malekshahi[1], A. Rana[1], S. Silvoni[2], N. Birbaumer[1,3], U. Chaudhary[1,3]

[1] Institute of Medical Psychology and Behavioral Neurobiology, University of Tuebingen
[2] Department of Cognitive and Clinical Neuroscience, Central Institute of Mental Health, Mannheim, Germany
[3] Wyss Center for Bio and Neuroengineering, Genéva, Switzerland

E-mail: niels.birbaumer@uni-tuebingen.de; ujwal.chaudhary@uni-tuebingen.de

ABSTRACT: Nonverbal and verbal communications are completely lost in patients with complete motor paralysis, leaving no other means of communication except brain-computer interfaces (BCIs). BCIs translate the thought to generate control signal, by which an individual can control a spelling device or external mechanical and electrical devices for communication. Recently we developed a functional near infrared spectroscopy (*f*NIRS) based auditory BCI, which was used by four patients in completely locked-in state (CLIS) to answer "yes" and "no" to known and open questions. Patients used fronto-central oxygenation concentration measured with *f*NIRS to answer "yes" and "no", while electro-encephalographic (EEG) signal was used to detect any vigilance drop during BCI sessions. Here, we evaluated frontal-central cortical activation by applying general linear model (GLM) to the *f*NIRS data and EEG signal time-frequency analysis to explore the metabolic and neuroelectric processes occurring during "yes" and "no" questions presented to CLIS patients.

INTRODUCTION

Amyotrophic lateral sclerosis may cause an individual to be in complete locked-in state (CLIS), a condition in which the patient is fully conscious and aware of their surroundings but is unable to perform any kind of movement leaving them completely paralyzed without any means of communication [1-2]. In such a scenario brain computer interface is the only remaining direct communication pathway between patient's brain and an external device [3-4].

It has been demonstrated that all of existing BCI techniques such as P300 endogenous event-related potential, slow cortical potentials (SCP) [5], extracting different features in frequency domains of the electro-encephalographic signal (EEG) [6] and subdurally implanted electrodes on the surface of the brain [6-7] do not reach a sufficient level of success for communication purposes [5]. Based on the unreliability of the aforementioned BCI, *f*NIRS based auditory BCI was used for binary communication in four Amyotrophic Lateral Sclerosis (ALS) patients in CLIS. Patients were able to successfully answer simple "yes" and "no" questions using the developed BCI [6].

Patients performed several sessions of BCI spread over weeks to learn to answer "yes" and "no" to personal and open questions, as described in Chaudhary et al. (2017) [6]. Here we present the *f*NIRS activation results and EEG time-frequency results from one of the patient.

MATERIALS AND METHODS

The Internal Review Board of the Medical Faculty of the University of Tübingen approved the experiment reported in this study and the patient's legal representative gave informed consent for the study with permission to publish the results and show the face of patients in the publication. The study was in full compliance with the ethical practice of Medical Faculty of the University of Tübingen. The clinical trial registration number is ClinicalTrials.gov Identifier: NCT02980380.

Patient

The study was performed on four patients, but here we present the results of one patient whose details are below.

Patient (Female, 76 years old, CLIS) was diagnosed with bulbar ALS in 2010. She lost speech and capability to walk by 2011. She stopped communicating with eyes in August 2014 which was confirmed by eye movement recordings. Before the brain computer interface was introduced an attempt was made to communicate with the subtle twitch of eye-lid, which proved to be unreliable. The husband and caretakers declared no communication with her since August 2014.

Instrumentation

A continuous wave (CW) based *f*NIRS system, NIRSPORT (NIRX) was used to acquire *f*NIRS data while multi-channel EEG amplifier (Brain Amp DC, Brain Products, Germany) was used to record EEG data simultaneously. EEG signal was recorded only to check the drop of vigilance based on changes of EEG signal power in the low frequency bands.

Published by Verlag der TU Graz
Graz University of Technology

 DOI: 10.3217/978-3-85125-533-1-55

The 8 sources and 8 detectors *f*NIRS optodes, and 8 EEG channels that were placed on the patient's scalp encompassing mainly primary somatosensory cortex, primary, pre-motor and supplementary motor cortex, Broca's area and dorsolateral prefrontal cortex is shown in Fig. 1.

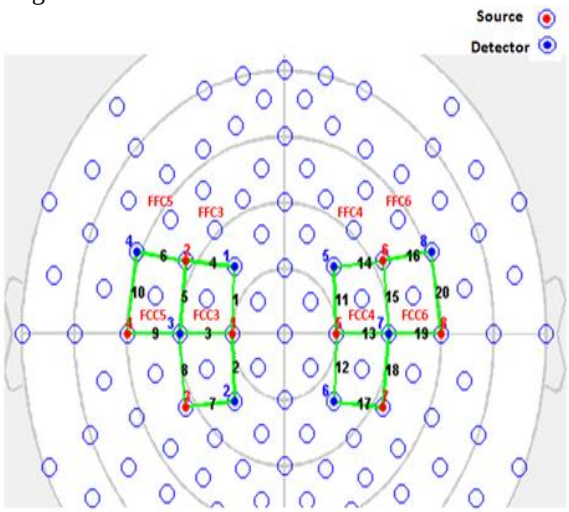

Figure 1: Source-detector layout in the fronto-central cortex with 10 source-detector pairs (channels) each on the left and right cortices and 8 EEG channels.

EEG channels locations were FFC5, FFC3, FFC4, FFC6, FCC5, FCC3, FCC4 and FCC6. Four electrodes were used to acquire the vertical and horizontal EOG, the result of EOG is presented in Chaudhary et al. (2017) [6].

Experiment Design

Patients were presented an auditory paradigm consisting of two kind of yes/no sentences: questions with known answers for training and feedback sessions (i.e. known question) and with unknown answers for the open question sessions (i.e. open question). Known questions were based on the life of patient and its answer is known by family members, caretakers and the experimenters (e.g. "Are you from Germany?"), while open questions can only be answered by the patient (e.g. "Do you have pain?").

In each training and feedback session patients listened to 10 true and 10 false known questions which are presented randomly. Patients were asked to think "ja, ja, …" (German for "yes") and "nein, nein, …" (German for "no") for 15 seconds, during the inter stimulus interval (ISI), until they heard the next sentence after an average interval of 5 seconds rest, as shown in Fig. 2. After the end of each training session, change in oxy-hemoglobin features corresponding to "yes" and "no" thinking was extracted and fed to the Support Vector Machine (SVM) classifier to differentiate between "yes" and "no" answers. After successful training (i.e. the classification accuracy of training sessions was greater than the threshold of 65%) [8] patients were presented with feedback session. During this session they were always provided with an auditory feedback of their answers at the end of the response time (i.e. "Your answer was recognized as yes" or "Your answer was recognized as no"). In this paper we performed the analysis using 16 training, 6 feedback sessions and 1 open question session performed by the patient over a period of several days.

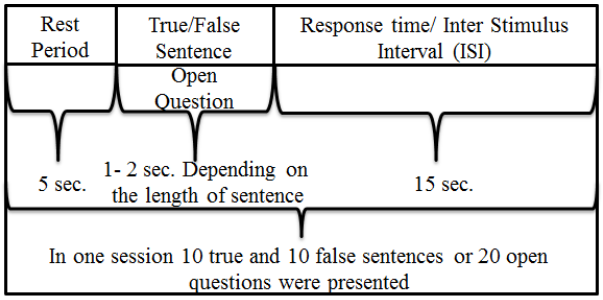

Figure 2: The auditory brain computer interface paradigm used for communication in CLIS patient.

Online fNIRS signal processing

The *f*NIRS data acquired online was normalized, filtered using a bandpass filter between 0.01-0.3 Hz and processed using the Modified Beer-Lambert law to calculate the relative change in concentration of oxy-(O_2Hb) and deoxy-hemoglobin (RHb).

The mean of relative change in O_2Hb across each channel was used as feature to train the SVM model through a 5-fold cross-validation procedure.

Since the classification accuracy as documented by (Chaudhary et al, 2017) [6] was higher for the mean of relative change in O_2Hb across each channel, the SVM model generated using O_2Hb was used to provide online feedback for known as well as open questions sessions.

EEG signal processing

Each EEG-channel was referenced to an electrode on the right mastoid and grounded to the electrode placed at Fz location of the scalp. Electrode impedances were kept below 10 kΩ and the EEG signal was sampled at 500 Hz. The signals were band pass filtered using a finite impulse response filter with a bandpass of 0.5–30 Hz and the filter order 8250 of EEGLAB [9]. As in complete locked state patients there is no eye movement [6], there is no EOG artifact contamination in EEG signal.

Offline and general linear model (GLM) analysis of fNIRS signal

Signal processing of *f*NIRS signals and the GLM analysis was done with nirsLAB (v2014.05). The *f*NIRS signal was bandpass filtered between 0.01-0.3 Hz. The Modified Beer–Lambert law was used to quantify the changes in the concentrations of O_2Hb and RHb from the absorption of near-infrared light. A statistical parametric mapping method (SPM)[10-11]was employed to extract dynamic features from hemodynamic responses and map this information to head-space models. The regressors are four conditions, "yes" question presentation, "no" question presentation,

Published by Verlag der TU Graz
Graz University of Technology

 DOI: 10.3217/978-3-85125-533-1-55

"yes" question ISI, and "no" question ISI, while the dependent variable was oxy hemoglobin (O2Hb). A canonical HRF with a time-series of stimulus onsets was convolved [11].

Offline Time-Frequency analysis of EEG signal

Offline Time-Frequency analysis of EEG signal was done using Short-Term Fourier Transform to identify low frequencies power spectra alteration during response time (ISI interval). This analysis served to exclude the slow-wave sleep state during BCI sessions.

RESULTS

In order to investigate the activated areas of brain, GLM coefficients were interpolated to elucidate activation in the fronto-central brain region of the patient during "yes" vs. "no" thinking as shown in Fig. 3. Fig. 3 shows the activation map for the change in the concentration of O_2Hb for "yes" vs. "no" responses ($p<0.05$) across the 23 sessions performed by the patient. Fig. 3 explicates significant differences between "yes" and "no" response in the left fronto-central brain region of the patient.

The GLM coefficients for "yes" and "no" response over all the sessions performed by the patient are shown in Fig. 4, which shows the *f*NIRS channels with greatest contrast between "yes" and "no" response.

Fig. 5 and Fig. 6 illustrate the time frequency decomposition of EEG signal for all EEG channels during "yes" and "no" response, respectively. Fig. 5 and Fig. 6 elucidate that the dominant frequencies during "yes" and "no" thinking are the ones in the high theta and low alpha bands.

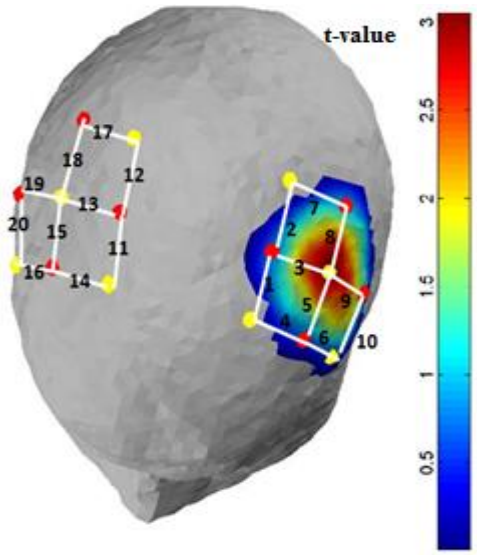

Figure 3: Activation map of change in oxy-hemoglobin across 23 sessions performed by the patient. (Contrast, "no" response > "yes" response, $p<0.05$, O_2Hb)

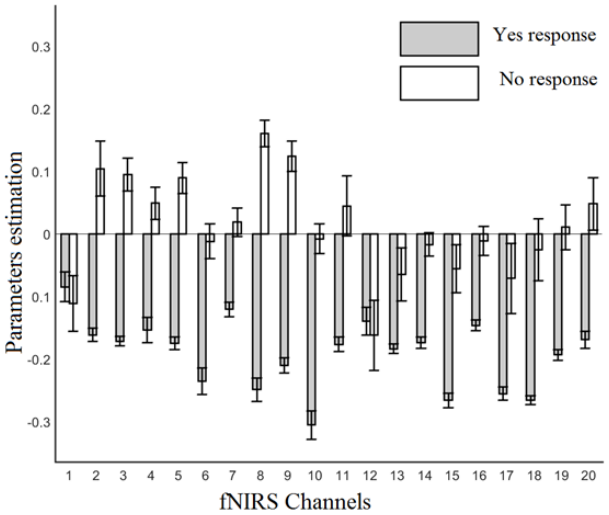

Figure 4: GLM coefficients for "yes" and "no" responses over all the sessions performed by the patient. In the Fig. y-axis is the GLM coefficient after normalization and x-axis is the *f*NIRS channels. Grey block represents the "yes" response and white block represents the "no" response.

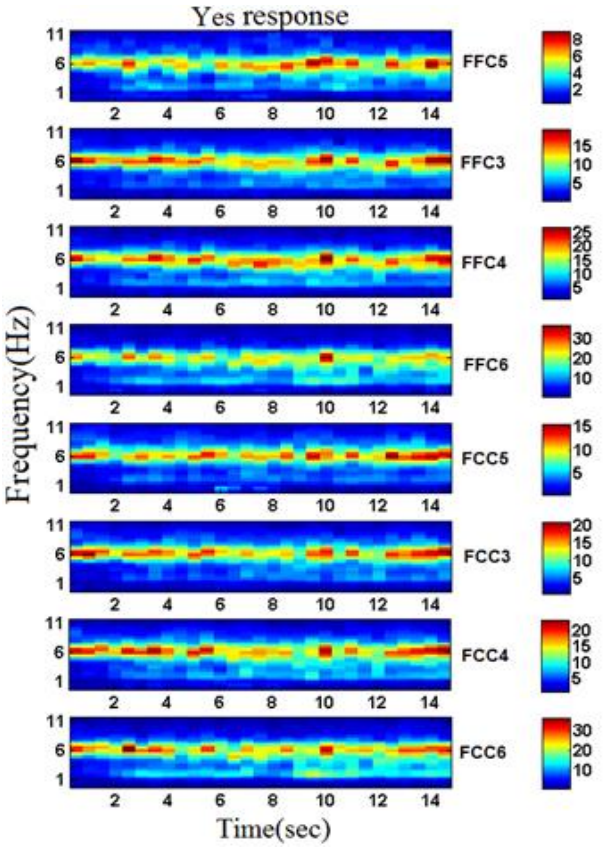

Figure 5: Time-Frequency decomposition for "yes" responses

DISCUSSION AND CONCLUSION

In patients completely motionless over years with restricted vision because of eye-muscle paralysis and drying of the cornea and likely reduced afferent input from the sensorimotor system reduced vigilance

Published by Verlag der TU Graz
Graz University of Technology

 DOI: 10.3217/978-3-85125-533-1-55

measured with EEG and a fragmented sleep-wake cycle was documented by Ramos et al. (2011) [7]and Soekadar et al. (2013) [12]. De Massari et al. (2013) [13] have shown that reduction of P300 amplitude across the BCI paradigm presentation predicted negative performance, again suggesting excessive loss and excessive variation of wakefulness and attention as a major limiting factor for BCI applications in such severely compromised patients. As it can be seen from time-frequency analysis the patient had a reduced EEG frequency band (around 6-7 Hz) compared to healthy population and almost no activity in the low frequency bands. These findings suggest that the patient was not in the sleep state, i.e., the patient was awake, mentally thinking yes or no.

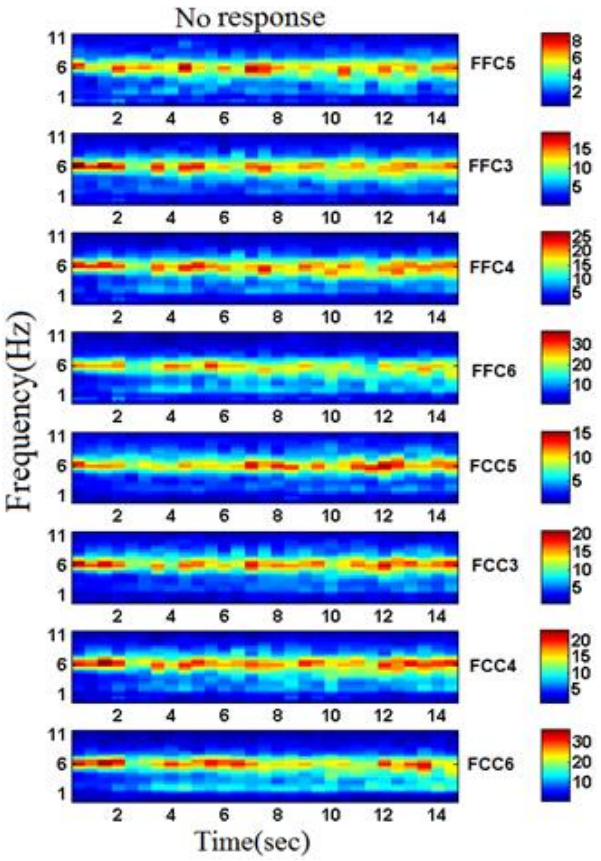

Figure 6: Time-Frequency decomposition for "no" responses

On the other hand, *f*NIRS signal showed significant difference ("no" response > "yes" response, $p<0.05$) between "yes" and "no" thinking in left hemispheres, see Fig. 3. The activation was more pronounced in the left hemisphere when compared with the right hemisphere, also shown in Fig. 4 the difference between "yes" and "no" response in the *f*NIRS channels placed on the left hemisphere of fronto-central brain region.

This suggests that in CLIS condition processing of "yes" and "no" response involves different neural substrates, in a similar manner as reported in healthy population [14]. Our result also suggests that, although the patient entered the complete locked in state from 2014, the high level cognitive functions (such as language comprehension, semantic processing and stimuli discrimination) are preserved.

Here we have presented the results from one out of four patients enrolled for this study; currently we are working on the detailed data analysis of the remaining three patients.

ACKNOWLEDGMENTS

We acknowledge the participation of all our patients because of them we have been able to shed light on the use of BCI in CLIS - ALS patients. All the researchers who were the part of team at different stages of the project, as well as our funding sources: DeutscheForschungsgemeinschaft (DFG, Kosellek), DFG BI 195/77-1, StiftungVolkswagenwerk (VW), Brain Products, Gilching and German Center of Diabetes Research (DZD) at Univ. Tuebingen, Eva and Horst KöhlerStiftung, Baden-Württernberg-Stiftung, LUMINOUS EU H2020, and Wyss center Bio and Neuroengineering, Genéva.

REFERENCES

[1] Strong MJ, Grace GM, Orange JB, Leeper HA, Menon RS, Aere C. A prospective study of cognitive impairment in ALS. Neurology. 1999;153(8):1665-70.

[2] Neary D, Snowden JS, Mann DMA. Cognitive change in motor neurone disease / amyotrophic lateral sclerosis (MND / ALS). 2000; 180: 15–20.

[3] Chaudhary U, Birbaumer N, Ramos-Murguialday A. Brain–computer interfaces for communication and rehabilitation. Nat. Rev. Neurol. 2016;12(9):513–25.

[4] Birbaumer N. Breaking the silence: Brain–computer interfaces (BCI) for communication and motor control. Psychophysiol. 2006; 43(6):517–32.

[5] Kuebler A and Birbaumer N. Brain–computer interfaces and communication in paralysis: Extinction of goal directed thinking in completely paralysed patients? Clin.Neurophysiol. 2008;119(11):2658–66.

[6] Chaudhary U, Xia B, Silvoni S, Cohen LG, Birbaumer N. Brain-Computer Interface-Based Communication in the Completely Locked-in State. PLoS Biol. 2017;15(1):e1002593.

[7] Ramos-Murguialday A, Hill J, Bensch M, Martens S, Halder S, Nijboer F, et al. Transition from the locked in to the completely locked-in state: A physiological analysis. Clin Neurophysiol. 2011;122(5):925–33.

[8] Combrisson E, Jerbi K. Exceeding chance level by chance: The caveat of theoretical chance levels in brain signal classification and statistical assessment of decoding accuracy. J. Neurosci. Methods. 2015;250: 126–136.

[9] Delorme A, Makeig S. EEGLAB: An open source toolbox for analysis of single-trial EEG dynamics including independent component analysis. J. Neurosci. Methods. 2014;134: 9–21.

[10] Ye JC, Tak S, Jang KE, Jung J, Jang J. NIRS-SPM: Statistical parametric mapping for near-infrared

Published by Verlag der TU Graz
Graz University of Technology

 DOI: 10.3217/978-3-85125-533-1-55

spectroscopy. Neuroimage. 2009;44: 428–447.
[11] Kamran MA, Jeong MY, Mannan MMN. Optimal hemodynamic response model for functional near-infrared spectroscopy. Front. Behav. Neurosci. 2015;9: 151.
[12] Soekadar SR, Born J, Birbaumer N, Bensch M, Halder S, Murguialday AR, et al. Fragmentation of slow wave sleep after onset of complete locked-in state. J Clin Sleep Med. 2013;9(9):951–3.
[13] De Massari D, Ruf CA, Furdea A et al. Brain communication in the locked-in state. Brain 2013;136(6):1989–2000.
[14] Naci L, Cusack R, Jia VZ, Owen AM. The Brain as Silent Messenger : Using Selective Attention to Decode Human Thought for Brain-Based Communication The Brain 's Silent Messenger : Using Selective Attention to Decode Human Thought for Brain-Based Communication. J Neurosci.
2013; 33(22):9385-9.

Published by Verlag der TU Graz
Graz University of Technology

Proceedings of the
7th Graz Brain-Computer Interface Conference 2017 DOI: 10.3217/978-3-85125-533-1-56

CSP-NN: A CONVOLUTIONAL NEURAL NETWORK IMPLEMENTATION OF COMMON SPATIAL PATTERNS

D. Maryanovsky[1], M. Mousavi[2], N. G. Moreno[3], V. R. de Sa[1]

[1]Cognitive Science, University of California, San Diego
[2]Electrical and Computer Engineering, University of California, San Diego
[3]Computer Science and Engineering, University of California, San Diego, La Jolla, CA, USA

E-mail: maryanovsky@gmail.com

ABSTRACT: In this paper we propose, describe, and evaluate a novel deep learning method for classifying binary motor imagery data. This model is designed to perform CSP-like feature extractions. It can be seen as a neural network with a specifically designed architecture where the latent space corresponds naturally to the features found in CSP methods. Our model allows for easy generalization from spatial filters to spatio-temporal filters. It also allows for the feature extraction and filtering stages to be optimized jointly with the classifier. This allows standard regularization methods to include the filtering stage. In addition the network provides the expressiveness and robustness of deep learning to improve upon the efficiency of CSP filtering methods.

INTRODUCTION

Motor-imagery (MI) brain-computer interfaces (BCIs) work by detecting decreases in power in the mu (7-13 Hz) and beta (13-30 Hz) frequency bands. Decreases in power in those frequencies are known to occur both prior to and during movement, as well as during imagined movement [1]. The relevant decreased power or desynchronization is spatially localized over the motor cortex. Any body part, when imagined to be moving, has a corresponding region of cortex.

Spatially discriminative mu-desynchronization is recognized using a filter that emphasizes the spatial differences between the different motor-imagery classes.

The most commonly used method is the Common Spatial Patterns, or CSP, [2] which finds a set of filters that maximizes the projected variance (power) for one class while minimizing it for the other. Applying CSPs to band-pass filtered signals can greatly emphasize the spatially segregated power differences between the different classes and is common in MI-based BCIs [2].

Let a column vector $x_t \in \mathbb{R}^C$ be the band-passed EEG signal for time t where C is the number of EEG channels on the scalp and $\mathbb{R}$ indicates the set of real numbers. The estimate of the covariance matrix for a two-class experiment can be calculated from the training data using traditional methods. Let the covariance matrix for the two classes 1 and 2 be specified as:

$$\Sigma_y \in \mathbb{R}^{C\times C} \quad y \in \{1, 2\} \tag{1}$$

CSP aims to find a projection $w \in \mathbb{R}^C$ which maximizes the variance of signals for one condition and at the same time minimizes the variance of signals of another condition. One can find w for class 1 by solving the following Rayleigh quotient:

$$R(w) = \frac{w^T\Sigma_1 w}{w^T(\Sigma_1 + \Sigma_2)w} \tag{2}$$

The solution for this problem can be found by solving the generalized eigenvalue problem given in the form:

$$\Sigma_1 w = \lambda(\Sigma_1 + \Sigma_2)w \tag{3}$$

There are C generalized eigenvectors where w_1 corresponding to the largest eigenvalue maximizes the variance for class 1 while minimizing for class 2 and w_c corresponding to the smallest eigenvalue maximizes the variance for class 2 while minimizing for class 1. It is common in the CSP algorithm to select some number (often 3) of the top and bottom eigenvectors as the discriminative spatial filters [3].

Once the CSP filters have been learned, the data are transformed according to the CSP filters, and the class bandpower is computed (via the sum of the squared filtered data, or equivalently, the variance of filtered, zero-mean data). The logarithm of this power output is often taken as the log-power is more normally distributed. These log powered features are then fed into a simple linear classifier such as linear discriminant analysis (LDA) with shrinkage, step-wise LDA, logistic regression, or linear support vector machines. These simple algorithms have been preferred because of their robustness to the large amounts of noise in, and scarcity of, EEG data. Many studies with shallow non-linear algorithms have failed to beat these simple linear algorithms However, recent advances in deep convolutional neural networks (CNNs) have transformed the fields of handwriting recognition, speech recognition, computer vision, and video analysis [4, 5], and are rapidly transforming machine learning more generally. We aim to leverage the advantages central to all of these results for the task of improving MI classification.

Published by Verlag der TU Graz
Graz University of Technology

 DOI: 10.3217/978-3-85125-533-1-56

There have been other variants on the basic CSP algorithm, some of which are reviewed in [6]. Common spatio-spectral patterns (CSSP) [7] uses the temporal structure information to improve CSP. Spectrally weighted common spatial patterns (Spec-CSP) [8] learns the spectral weights as well as the spatial weights in an iterative way. Invariant CSP (iCSP) [9] minimizes variations in the EEG signal caused by various artifacts using a pre-calculated covariance matrix characterizing these modulations. Stationary CSP (sCSP) [10] regularizes CSP filters into stationary subspaces. Local temporal common spatial patterns (LTCSP) [11, 12] uses temporally local variances to compute the spatial filters. Canonical correlation approach to common spatial patterns (CCACSP) incorporates the temporal structure of the data to extract discriminative and uncorrelated sources [13].

A neural network implementation of CSP filtering easily allows for the development of new spatio-temporal extensions to CSP. We note that these extensions may be implementable in a standard filtering pipeline, but that implementing them as part of a neural network allows for easy, quick extensions to well-studied variations of CSP, and, moreover, allows for testing novel architectures that may not be intuitive in the framework that CSPs are typically studied and used in. By considering CSP filtering as a special case of convolutional neural networks, one can quickly run through entirely novel CSP extensions, and optimize them in tandem with the classifier, simply by modifying a few canonical parameters.

Also because the CSP filters are typically trained with non-iterative algorithms, and without validation, they are prone to overfitting. Implementing both filtering and classification in one framework allows for joint monitoring and regularizing, to combat overfitting.

A major advantage of CNNs over traditional neural networks is that they are a special case of the latter. Convolutional networks are motivated by, and based on, the structure of the visual system [14–17]. Convolutional neural networks have a shared weight structure – local receptive fields are learned and the learned structure is shared throughout the input [17]. This means that each training sample provides many windows of training data for the same (shared) sets of weights which greatly increases the effective training data.

CNNs can be seen as an architectural constraint on neural networks in general, specifically, they are constrained such that they perform operations that have traditionally been used, in a non-machine learning setting, to great effect on the same task. This approach allows us to optimize the filters and classifier together, and to transparently leverage a validation set.

We hypothesize four explicit advantages to employing the CSP filtering as part of the classification network. First, early stopping or other, more advanced, deep learning regularization techniques can be used to prevent the spatial filters from overfitting. Second, the filtering and classification being optimized together may result in improved performance than performing these separately, as our filters are going to differ from CSP in that they are sensitive to classification accuracy as opposed to just class variance. Third, the CSP algorithm finds linear spatial filters whereas the neural network extension would be able to find smooth non-linear extensions. Finally, once implemented in a neural network, the network may be modified, in the common ways described in the deep learning literature, to improve on the CSP algorithm. The natural extensions to both can be leveraged to extend and strengthen the basic model described here. For example, the network's architecture can be easily extended, via weight-sharing, to allow for natural structurally-restricted spatial filters.

MATERIALS AND METHODS

EEG data were recorded from 6 healthy participants recruited from the UC San Diego student population. Participants were naive to BCI and signed a consent form approved by the University Institutional Review Board before participating in the experiment. Participants were instructed to perform kinesthetic motor imagery of their right or left hand to control a cursor to hit a target on a monitor in front of them. The cursor and the target were each represented by a circle having 2 cm diameter and colors blue and white respectively. The cursor moved discretely, one second at a time. Each trial began with the cursor at the center of the screen and the target at either end - the center was three cursor steps away from each end. After 1.5 seconds the target disappeared to minimize distraction for the participant and the cursor began moving towards or away from the target. Participants were lead to believe that they were in control of the cursor; however, in order to provide consistent cursor movements between participants, the cursor was moved based on a pre-programmed sequence. There were a total of 10 blocks and each block consisted of 20 trials [18].

Data were collected with a 64-channel EEG system (Brain Products GmbH). The electrodes were arranged based on the 10-20 international system. Data were collected at 5000 Hz sampling rate and were down-sampled to 500 Hz. Pre-processing of the data was done in MATLAB [19] and EEGLAB [20] where the data were first bandpass filtered with an FIR filter of order 500 in 1 to 200 Hz. Then clean-line [21] which is an EEGLAB plugin, was applied to remove the line noise. Then up to five channels with high power in frequencies above 60 Hz - indicating muscle artifacts - were removed. Next, the EEG on each channel was re-referenced to the common average over the remaining channels. Data were visually inspected for large muscle artifacts and less than 10% of the trials were removed. Independent component analysis (ICA) was applied and ICA components regarding muscle and eye were removed. The pre-processed data were bandpass filtered with FIR filters with 500 taps in the following eleven frequency bands: 1-3, 2-5, 4-7, 6-10, 7-12, 10-15, 12-19, 18-25, 19-30, 25-35, and 30-40

Published by Verlag der TU Graz
Graz University of Technology

 DOI: 10.3217/978-3-85125-533-1-56

Hz and epoched from 150 to 950 ms after each cursor movement.
As baseline, we used CSP in combination with regularized linear discriminant analysis (LDA). CSP is trained on data from each filter and the top 3 filters for each imagery class is selected to be passed into an LDA. Fig. 1 shows the structure of CSP+LDA classifier. We ran 3 instances of 5-fold cross-validation

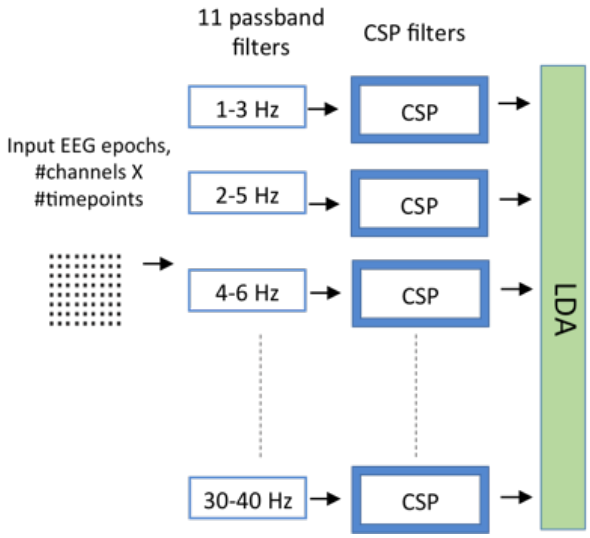

Figure 1: Conventional CSP+LDA method.

We have created two methods inspired by the success of CSPs. First we introduce a hybrid CSP/Deep Net model, which will serve as a control or reference, that learns and feeds CSPs of our eleven pass bands into a fully connected neural network with 500 hidden units. Second, we introduce the proposed model, a fully deep net with CSP-like architectures. This network's architecture has been structured such that its latent space naturally encodes for the same variance-optimizing spatial transformations described above. Similar to the hybrid net, our CSP like Neural Network, or CSP-NN, is trained on all eleven passbands of a signal.
The convolutional network computes the equivalent of a convolution of a "receptive field" with the input. It is implemented by having local connectivity between a neuron in the convolutional layer and the lower input layer. This neuron is then replicated with shifted input connectivity. The key feature is that the weights are shared between all of the neurons within a map in the layer, so that they are all forced to learn the same receptive field/kernel. At the same time many maps may be learned in parallel. These convolutional layers are commonly followed by pooling layers that combine the input from several nearby neurons within the same map. Common pooling operations are max-pooling where the maximum value of the combined inputs are output, average-pooling, where the average value of the combined inputs are output. There is also norm-pooling where the L_p norm of the combined inputs is output [22].

Hybrid CSP Net

Our hybrid model performs a standard D-dimensional CSP on each passband. treating each epoch as a data point. D is necessarily an even number, as we choose the first D/2 and last D/2 vectors of the CSP solution.The CSP filtered signals are then fed as inputs to a densely connected neural network which performs binary classification. This densely connected neural network is composed of 500 neurons fitted with hyperbolic tangent activation. We used a dropout mask with a probability of .5 in this dense layer as decided for the proposed networks discussed next. We selected binary cross-entropy as our objective function due to the binary classification nature of our network. The activations are fed into a single sigmoid output unit. The dense layer was implemented and trained in Keras [23], using Theano [24] as a backend. Fig. 2 shows the architecture of this network.

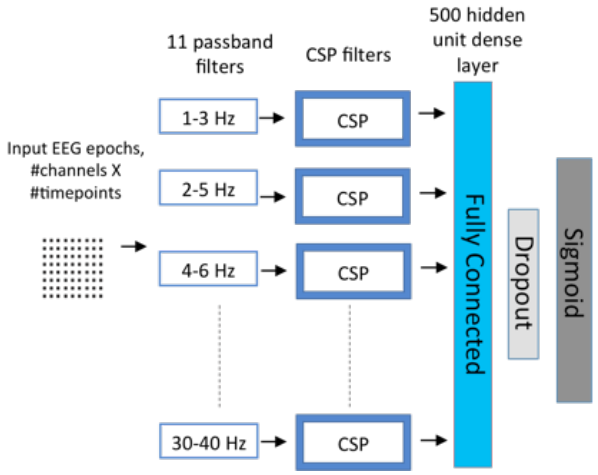

Figure 2: Structure of the hybrid CSP network.

CSP-NN

Our CSP-NN takes the 11 chosen passbands, and feeds each into one of 11 parallel 1-D convolution layers. We use D convolution kernels, where D is analogous to the number of CSP dimensions described above. Thus, we generate $11 \times D$ feature maps per data point. Each of these feature maps are element-wise squared and globally summed, analogous to the process of extracting variance in CSP, creating $11 \times D$ positive scalars. Note this operation corresponds to using norm 2 pooling instead of the commonly used max pooling, and it simulates the operation of extracting variance from CSP projections.
Interestingly, max pooling was originally motivated in the classical deep learning architectures [15, 16] motivated by complex cells and their translation invariance. However, the energy model of complex cells [25], "the de facto standard description of complex cells in primary visual cortex (Adelson and Bergen 1985)" actually models them as computing the sum of squared simple cells, and this has been found to produce a better fit [26]. These

Published by Verlag der TU Graz
Graz University of Technology

 DOI: 10.3217/978-3-85125-533-1-56

pooled output scalars are fed into a fully connected network, identical to the net used in the hybrid-model, which generates our predictions. This process is detailed below. By building a net of this architecture, and by differentiating through a global sum of squares (norm 2 pooling), we create a model that learns convolution kernels that are analogous to the CSP filter solutions found in traditional approaches. Initially, we use convolutional kernels of length one. These convolutions apply the same set of spatial weights across all time points as in the standard CSP spatial filters. Details of our models can be found in Fig. 3. We also tested kernels with some temporal sensitivity, replacing the length-1 filter with a length-T or T-degree convolution through time. These later convolutions can be said to apply a spatio-temporal filter with a T-point temporal resolution, which is analogous to common spatial temporal patterns, or CSTP filtering methods. CSTP-NN is based on sensitivity to temporal dependencies between windows of successive points. CSTP-NN is an example of a simple extension, a single parameter change in fact, to the CSP-NN that corresponds to a major class of CSP extensions in the traditional BCI literature.

The parameters learned by our proposed method code for similar features to the traditional CSP and CSTP methods. However they are not trained to maximize variance/power for one class and minimize it for the other, but aim to discover the set of kernels that provide optimal classification performance for the network as a whole. This latter advantage increases the possibility of overfitting, which we handle with a very strict early-stopping schedule as described above and detailed below. Within our method, an epoch is bandpassed into 11 separate band signals, which are concatenated into an 11 by C by T array, where C and T are number of channels and timepoints, respectively. Each level of this array is fed into one of eleven separate 1-D convolutional layers, each containing D unique feature kernels, where D is chosen to always be even, and is 6, 10, or 16 in our analysis. The length of each kernel is 1, and the width of each is equal to the number of EEG channels in our data, which is 64. These kernels are convolved through time, and are functionally similar to applying a CSP-like spatial filter to each time-point in our 11 signal bands. This yields $11 \times D$ feature maps, or filtered signals, each of which is element-wise squared and globally summed, or norm-2 pooled. This operation yields $11 \times D$ feature scalars, and is functionally similar to extracting variance of the first and last $D/2$ spatial filters in CSP. These features are concatenated and fed as an $11 \times D$ input vector into dense neural network layer, which always has 500 hidden units with hyperbolic tangent activation. This layer is fed into a single sigmoid unit. The network is trained end-to-end using stochastic gradient descent, with Nesterov momentum of .9 and training rate of .0001. We use dropout in the 500 hidden units, setting a random half of them to 0 at each training epoch. The CSP-NN, and by extension, the CSTP-NN, are both implemented in Theano [24], using the Lasagne library [27]. Again, CSTP-NN differs from CSP-NN by only a single parameter in our implementation.

The training duration was set to a maximum of 5000 epochs with early stopping. If 50 of the last 100 epochs resulted in worse validation accuracy, then early stopping was triggered, and the weights were set to those that produced the recorded best validation results. We searched over the following hyperparameters for participant 1 in the CSP-NN and kept the parameters the same for every other participant: Dropout (p = .5) vs non-dropout, learning rate, .001 vs .0001, number of kernels, 6 vs 10 vs 16 and kernel lengths, 1, 5,10, and 15. We tested hyperbolic tangent vs. rectified linear (ReLU) as activation function in the hidden layer and found that hyperbolic tangent performed better. We selected binary cross-entropy as our objective function due to the binary classification nature of our network.

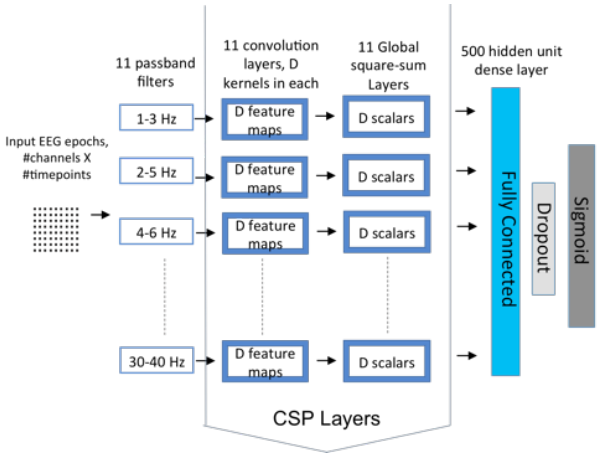

Figure 3: Structure of the CSP-NN or CSTP-NN, depending on kernel length (1 vs. > 1).

RESULTS

Results are reported for 5-fold cross-validation in Tab. 1. The rate for the baseline method, i.e. CSP+LDA, and the hybrid CSP method are reported as the average of 3 instances of 5-fold cross-validation. In each instance, the number of trials in right and left classes were balanced by dropping trials from the class with more trials.

The proposed methods, i.e. CSP-NN and CSTP-NN, were also tested in a 5-fold cross-validation scheme. We applied this cross-validation scheme to each participant individually, and we report the mean accuracy across all five folds per participant. Again, we made sure that the right and left classes were balanced. Our proposed methods outperformed on certain participants (P-2, P-3 and P-6), but underperformed on P-4. We also found that the increasing the length of the 1-D convolution also improves performance, but also increases the error bounds significantly. This is consistent with the small size of our data. We found that 16 kernels per convolution layer, as well as a kernel length, (or temporal sensitivity) of 5 produced the strongest results from among the values tried

Published by Verlag der TU Graz
Graz University of Technology

 DOI: 10.3217/978-3-85125-533-1-56

in Participant 1 (and was used for all subjects). Considering only length-1 kernel instances, the best results were found with the same parameters in Participant 1, including 16 kernels per convolution layer.

Table 1: Results - Classification accuracy. Note that * is used for CSP-NN and CSTP-NN for P-1 as results for this participant may be overfit due to parameter tuning.

ID	CSP+LDA	Hybrid NN	CSP-NN	CSTP-NN
P-1	0.8629	0.8307	0.8297*	0.8459*
P-2	0.6482	0.6381	0.7311	0.7041
P-3	0.6485	0.6553	0.6351	0.7243
P-4	0.6526	0.6571	0.6069	0.5250
P-5	0.7173	0.7104	0.7125	0.6750
P-6	0.7105	0.6970	0.7338	0.7730

The standard error among 5-fold for the results reported in Tab. 1 is at most 0.025.

DISCUSSION

The CSP-NN and CSTP-NN methods perform comparably to standard methods. It is possible that the proposed methods would have even stronger performance, with tighter error bounds, if given a larger corpus of data. Grand averages across all participants show that CSTP-NN and CSP-NN are the highest performing methods that we attempted however there is large variability between participants.

CONCLUSION

CSP-NN style approaches perform similarly to standard non end-to-end models, and can be easily extended when implemented. They can also be regularized more transparently. We find that this class of model suffers from the same dependence on large corpus of data as all CNN models, but offers a stronger method when that data is available, and we will further study the advantages and disadvantages of this class of model in the future.

ACKNOWLEDGMENTS

This work was supported by the NSF grants IIS 1219200, SMA 1041755, IIS 1528214, and UCSD FISP G2171.

References

[1] Wolpaw, Jonathan R., and Dennis J. McFarland. "Control of a two-dimensional movement signal by a noninvasive brain-computer interface in humans." Proceedings of the National Academy of Sciences of the United States of America 101, no. 51 (2004): 17849-17854.

[2] Müller-Gerking, Johannes, Gert Pfurtscheller, and Henrik Flyvbjerg. "Designing optimal spatial filters for single-trial EEG classification in a movement task." Clinical neurophysiology 110, no. 5 (1999): 787-798.

[3] Blankertz, Benjamin, Ryota Tomioka, Steven Lemm, Motoaki Kawanabe, and K-R. Muller. "Optimizing spatial filters for robust EEG single-trial analysis." IEEE Signal processing magazine 25, no. 1 (2008): 41-56.

[4] Karpathy, Andrej, George Toderici, Sanketh Shetty, Thomas Leung, Rahul Sukthankar, and Li Fei-Fei. "Large-scale video classification with convolutional neural networks." In Proceedings of the IEEE conference on Computer Vision and Pattern Recognition, pp. 1725-1732. 2014.

[5] Donahue, Jeffrey, Lisa Anne Hendricks, Sergio Guadarrama, Marcus Rohrbach, Subhashini Venugopalan, Kate Saenko, and Trevor Darrell. "Long-term recurrent convolutional networks for visual recognition and description." In Proceedings of the IEEE conference on computer vision and pattern recognition, pp. 2625-2634. 2015.

[6] Lotte, Fabien, and Cuntai Guan. "Regularizing common spatial patterns to improve BCI designs: unified theory and new algorithms." IEEE Transactions on biomedical Engineering 58, no. 2 (2011): 355-362.

[7] Lemm, Steven, Benjamin Blankertz, Gabriel Curio, and K-R. Muller. "Spatio-spectral filters for improving the classification of single trial EEG." IEEE transactions on biomedical engineering 52, no. 9 (2005): 1541-1548.

[8] Tomioka, Ryota, Guido Dornhege, Guido Nolte, Benjamin Blankertz, Kazuyuki Aihara, and Klaus-Robert Müller. "Spectrally weighted common spatial pattern algorithm for single trial EEG classification." Dept. Math. Eng., Univ. Tokyo, Tokyo, Japan, Tech. Rep 40 (2006).

[9] Blankertz, Benjamin, Motoaki Kawanabe, Ryota Tomioka, Friederike U. Hohlefeld, Vadim V. Nikulin, and Klaus-Robert Müller. "Invariant Common Spatial Patterns: Alleviating Nonstationarities in Brain-Computer Interfacing." In NIPS, pp. 113-120. 2007.

[10] Samek, Wojciech, Carmen Vidaurre, Klaus-Robert Müller, and Motoaki Kawanabe. "Stationary common spatial patterns for brain–computer interfacing." Journal of neural engineering 9, no. 2 (2012): 026013.

[11] Wang, Haixian, and Wenming Zheng. "Local temporal common spatial patterns for robust single-trial EEG classification." IEEE Transactions on Neural Systems and Rehabilitation Engineering 16, no. 2 (2008): 131-139.

Published by Verlag der TU Graz
Graz University of Technology

 DOI: 10.3217/978-3-85125-533-1-56

[12] Wang, Haixian. "Discriminant and adaptive extensions to local temporal common spatial patterns." Pattern Recognition Letters 34, no. 10 (2013): 1125-1129.

[13] Noh, Eunho, and Virginia R. de Sa. "Canonical correlation approach to common spatial patterns." In Neural Engineering (NER), 2013 6th International IEEE/EMBS Conference on, pp. 669-672. IEEE, 2013.

[14] Hubel, D., and Wiesel, T. Receptive fields, binocular interaction and functional architecture in the cat's visual cortex. Journal of Physiology, 160:106, 1962.

[15] Fukushima, Kunihiko. "Cognitron: A self-organizing multilayered neural network." Biological cybernetics 20, no. 3-4 (1975): 121-136.

[16] Fukushima, Kunihiko, and Sei Miyake. "Neocognitron: A self-organizing neural network model for a mechanism of visual pattern recognition." In Competition and cooperation in neural nets, pp. 267-285. Springer Berlin Heidelberg, 1982.

[17] LeCun, Y., Boser, B, Denker, J.S., Henderson, D., Howard, R.E., Hubbard, W., and Jackel, L.D. Handwritten digit recognition with a back-propagation network. In Advances in Neural Information Processing Systems 2, pages 396-404. Morgan Kaufmann, 1989.

[18] Mousavi, Mahta, Adam S. Koerner, Qiong Zhang, Eunho Noh, and Virginia R. de Sa. "Improving motor imagery BCI with user response to feedback." Brain-Computer Interfaces (2017): 1-13.

[19] MATLAB and Statistics Toolbox Release 2012b, The MathWorks Inc., Natick, Massachusetts, United States (2012).

[20] Delorme, Arnaud, and Scott Makeig. "EEGLAB: an open source toolbox for analysis of single-trial EEG dynamics including independent component analysis." Journal of neuroscience methods 134.1 (2004): 9-21.

[21] Available here: `http://www.nitrc.org/projects/cleanlin`

[22] Gulcehre, Caglar, Kyunghyun Cho, Razvan Pascanu, and Yoshua Bengio. "Learned-norm pooling for deep feedforward and recurrent neural networks." In Joint European Conference on Machine Learning and Knowledge Discovery in Databases, pp. 530-546. Springer Berlin Heidelberg, 2014.

[23] François Chollet. Keras. 2015. Available from: `https://github.com/fchollet/keras`

[24] Theano Development Team (2016). Theano: A Python frame-work for fast computation of mathematical expressions. arXiv e-prints, abs/1605.02688.

[25] Adelson, Edward H., and James R. Bergen. "Spatiotemporal energy models for the perception of motion." JOSA A 2, no. 2 (1985): 284-299.

[26] Vintch, Brett, J. Anthony Movshon, and Eero P. Simoncelli. "A convolutional subunit model for neuronal responses in macaque V1." Journal of Neuroscience 35, no. 44 (2015): 14829-14841.

[27] Sander Dieleman, Jan Schlüter, Colin Raffel, Eben Olson, Søren Kaae Sønderby, Daniel Nouri, et al. (2015). Lasagne: First release. [Data set]. Zenodo. `http://doi.org/10.5281/zenodo.27878`

Published by Verlag der TU Graz
Graz University of Technology

Proceedings of the
7th Graz Brain-Computer Interface Conference 2017 DOI: 10.3217/978-3-85125-533-1-57

TIKHONOV REGULARIZATION ENHANCES EEG-BASED SPATIAL FILTERING FOR SINGLE-TRIAL REGRESSION

A. Meinel[1], F. Lotte[2], M. Tangermann[1]

[1]Brain State Decoding Lab, Cluster of Excellence BrainLinks-BrainTools,
Dept. of Computer Science, Albert-Ludwigs-University, Freiburg, Germany,
[2]Inria Bordeaux Sud-Ouest / LaBRI, Talence, France
E-mail: andreas.meinel@blbt.uni-freiburg.de

ABSTRACT: Robust methods for continuous brain state decoding are of great interest for applications in the field of Brain-Computer Interfaces (BCI). When capturing brain activity by an electroencephalogram (EEG), the Source Power Comodulation (SPoC) algorithm enables to compute spatial filters for the decoding of a continuous variable. However, as high-dimensional EEG data generally suffer from low signal-to-noise ratio, the method reveals instabilities for small data sets and is prone to overfitting. We introduce a framework for applying Tikhonov regularization to SPoC by restricting the solution space of filters. Our findings show that additional trace normalization of covariance matrices is a necessary prerequisite to tune the sensitivity of the resulting algorithm. In an offline analysis on data of $N = 18$ subjects, the introduced trace normalized and Tikhonov regularized SPoC variant (NTR-SPoC) outperforms standard SPoC for the majority of individuals. With this proof-of-concept study, a generalizable regularization framework for SPoC has been established which allows for implementing different regularization strategies in the future.

INTRODUCTION

Designing electroencephalography (EEG)-based Brain-Computer Interfaces (BCIs) require translating EEG signals into messages or commands for an application, e.g. by converting EEG activity recorded during imagined hand movements into cursor movements [1]. In most current BCIs for communication and control, this is typically achieved using machine learning and classification algorithms [2]. During online use, EEG signals are then assigned to a discrete set of classes (e.g. left or right hand imagined movements).

A widely used component for effective classification of EEG signals is spatial filtering [3]. Addressing volume conduction effects, spatial filter methods estimate sources, whose signals are more different between classes than signals obtained at the sensor level. The most popular spatial filter algorithm to classify oscillatory EEG activity is the Common Spatial Pattern (CSP) algorithm [3], [4]. It aims at finding filters such that the spatially filtered signals have a variance (and thus a band power in narrow-band filtered signals) that is maximally different between classes. While the CSP algorithm proved very efficient and has become a gold standard in BCI, it is sensitive to noise, non-stationarity and limited data. To address these limitations, various regularized variants of CSP have been proposed making this algorithm effectively more robust [5], [6], [7]. Typically, these approaches inject prior knowledge into the CSP objective function, e.g. in the form of regularization terms. The regularization approaches try to guide the optimization process towards good solutions, despite noise and non-stationarities.

However, not all BCIs are based on classification methods. Several brain signal decoding problems require regression techniques to estimate continuous rather than discrete mental states. For instance, BCIs can be used to estimate continuous workload levels [8] or reaction time from oscillatory activity [9]. As for classification techniques, regression models can also significantly benefit from the use of spatial filters. Thus, Dähne et al. proposed the Source Power Comodulation (SPoC) algorithm, which can be seen as an extension of CSP to regression problems [10]. Indeed, SPoC aims at finding spatial filters such that the power of the filtered EEG signals maximally covaries with a continuous target variable.

Due to similar mathematical formulations, CSP and SPoC share a number of pros and cons. Both algorithms can deliver informative oscillatory signal features but are prone to noise, non-stationarity and limited data. However, while robust variants of CSP have been proposed based on regularization approaches [5], there are no such robust variants for SPoC. Hence, this leaves SPoC with sub-optimal performances when used on noisy data such as those encountered outside laboratories for practical BCI use. In this paper, we aim at addressing this limitation. In particular, we present a novel method to apply Tikhonov regularization to the existing SPoC algorithm. We show how this regularization approach combined with appropriate normalization can indeed outperform the basic SPoC approach. We also illustrate the impact of various regularization parameters on the resulting oscillatory components.

The reminder of this paper first presents in detail the original SPoC algorithm and the regularized variant we

Published by Verlag der TU Graz
Graz University of Technology

 DOI: 10.3217/978-3-85125-533-1-57

propose. Then it presents an evaluation of these two methods on real EEG data sets for motor performance prediction, before discussing the results.

MATERIALS AND METHODS

1) Source Power Comodulation (SPoC): Supervised spatial filtering algorithms are widely used in EEG-BCI applications. Those filters represent a linear transformation to project the multi-variate EEG data to a lower dimensional subspace. This work focuses on the Source Power Comodulation algorithm (SPoC; [10]) which optimizes a spatial filter by solving a linear regression problem.

In the following, $\mathbf{x}(t) \in \mathbb{R}^{N_c}$ describes the time course of the multivariate bandpass-filtered EEG data acquired from N_c sensors. In accordance with the generative model of the EEG [11], a spatial filter $\mathbf{w} \in \mathbb{R}^{N_c}$ describes the linear projection of the sensor space data $\mathbf{x}(t)$ to a one-dimensional source component $\hat{s}(t) = \mathbf{w}^\top \mathbf{x}(t)$. Translating $\mathbf{x}(t)$ into segments of N_e single epochs $\mathbf{x}(e) \in \mathbb{R}^{N_c \times N_s}$ with N_s sample points per epoch, then SPoC learns a spatial filter $\mathbf{w}$ such that the band-power $\Phi(e) = \mathrm{Var}[\hat{s}(e)]$ of $\hat{s}$ has maximal covariance with a given epoch-wise univariate target variable $z(e)$. Formally, this translates to maximizing the objective function

$$J_1(\mathbf{w}) = \mathrm{Cov}[\Phi(e), z(e)] = \mathbf{w}^\top \Sigma_z \mathbf{w} \qquad (1)$$

by defining a z-weighted averaged covariance matrix $\Sigma_z := \langle \Sigma(e)\, z(e) \rangle$ based on the trial-wise spatial covariance $\Sigma(e) = (N_s - 1)^{-1} \mathbf{x}(e)^\top \mathbf{x}(e)$. $\langle . \rangle$ defines the average across N_e epochs. Furthermore, a norm constraint on $\mathbf{w}$ is applied by setting $J_2(\mathbf{w}) = \mathrm{Var}[\hat{s}(e)] = \mathbf{w}^\top \Sigma_{avg} \mathbf{w} \stackrel{!}{=} 1$, where $\Sigma_{avg} = \langle \Sigma(e) \rangle$ describes the averaged covariance matrix. Overall, this translates to the Rayleigh quotient of the original SPoC$_\lambda$ formulation [10]:

$$J(\mathbf{w}) = \frac{J_1}{J_2} = \frac{\mathbf{w}^\top \Sigma_z \mathbf{w}}{\mathbf{w}^\top \Sigma_{avg} \mathbf{w}} \qquad (2)$$

Technically, maximizing $J(\mathbf{w})$ can be solved as a generalized eigenvalue problem and returns a set $\{\mathbf{w}^{(j)}\}_{j=1,..,N_c}$ of N_c spatial filters with j indexing the rank which is determined in descending order of the eigenvalues and thereby according to the covariance.

Spatial filters allow for a visual interpretation by estimating the corresponding activity pattern $\mathbf{a} = \Sigma_{avg} \mathbf{w}$ as highlighted by Haufe et al. [12].

2) Tikhonov Regularization: The SPoC objective function directly builds upon sample covariance matrices Σ_z and Σ_{avg} as stated by Eq. 2. Their estimation is very sensitive to noisy data, with small training data sets and a high dimensionality aggravating the problem. Finally, poorly estimated covariance matrices will not describe the intended neural processes well and thus mislead the spatial filter optimization. To overcome this, regularization by adding a penalty term $P(\mathbf{w})$ to the objective function's denominator is a common mitigation strategy [13], [14]. The penalty is expressed by a prior that restricts the possible solution space. In this paper, we assign a quadratic penalty term $P(\mathbf{w}) = \mathbf{w}^\top \mathbb{1} \mathbf{w} = \|\mathbf{w}\|^2$ with $\mathbb{1} \in \mathbb{R}^{N_c \times N_c}$ stating the identity matrix. As this penalty scales with the spatial filter norm, solutions with small weights are preferred. Overall, the penalty term is added to the denominator with a regularization parameter α leading to the following maximization problem:

$$J_P(\mathbf{w}) = \frac{\mathbf{w}^\top \Sigma_z \mathbf{w}}{\mathbf{w}^\top [(1-\alpha)\Sigma_{avg} + \alpha \mathbb{1}] \mathbf{w}} \qquad (3)$$

This formulation is known as Tikhonov regularization (TR, [15]) and has similarly been established for the CSP algorithm [5]. Directly solving Eq. 3 refers to SPoC with *Tikhonov regularization* (**TR-SPoC**) in this paper. In case of an extreme regularization expressed by $\alpha = 1$, the Rayleigh quotient in Eq. 3 collapses to the one of the Principal Component Analysis (PCA, [16]).

The Rayleigh quotient in Eq. 2 and 3 relates two sample covariance matrices. In order to control for their relative scaling, a normalization by the trace might be a suitable strategy [4], [17], e.g. $\Sigma'(e) = \Sigma(e)/tr(\Sigma(e))$. Trace normalization will be applied to $\Sigma(e)$ and Σ_{avg} entering Eq. 3, but not upon Σ_z as the z-weighting shall be maintained. This version of the algorithm will be stated as *normalized Tikhonov regularization* of SPoC (**NTR-SPoC**). Applying the same scheme of trace normalization to the standard SPoC algorithm (Eq. 2), will be referred to as *trace-normalized* SPoC (**TN-SPoC**).

3) Data Set for Offline Evaluation: To evaluate the introduced regularization algorithms, data of 18 subjects performing a visuomotor hand force task was used. The paradigm allowed to derive a trial-wise motor performance metric [18], [9]. Each subject completed one session with 400 trials. Within each trial, a "get-ready" interval preceded a "motor execution" phase which was initiated by a clear go-cue. EEG signals were used to predict the trial-wise reaction time (RT) of the motor task based on the time interval [-800, -50] ms prior to the go-cue. EEG activity was acquired by multichannel EEG amplifiers (BrainAmp DC, Brain Products) with a sampling rate of 1 kHz from 63 passive Ag/AgCl electrodes (EasyCap) placed according to the extended 10-20 system. After preprocessing and outlier rejection following the methods described in [9], we restricted our analysis to oscillatory features within the alpha-band frequency range of $[8, 13]$ Hz. The bandpass was realized applying a zero-phase butterworth filter of 6th order. The number of data points N_e remaining after outlier removal varied across the 18 subjects, ranging from 142 to 352 trials. In summary, the following evaluation is based upon RT as a trial-wise continuous target variable z_{true}, which we aim to predict utilizing the individual oscillatory bandpower features of the pre-go EEG activity.

Published by Verlag der TU Graz
Graz University of Technology

 DOI: 10.3217/978-3-85125-533-1-57

4) Evaluation Scheme: In an offline analysis, we evaluated the proposed algorithms NTR-SPoC and TR-SPoC w.r.t. the regularization parameter α by varying its value in the range $\{0; [10^{-8}, 10^{0}]\}$. Overall, 40 discrete, logarithmically spaced evaluation points were chosen. At each α-value the following $K = 10$-fold chronological cross-validation (CV) scheme was applied:
First, the spatial filter set $\{\mathbf{w}^{(j)}\}_{j=1,..,N_c}$ was gained on training data $\mathbf{x}_{tr}$ and the first $N_f = 4$ highest ranked components selected. Second, a linear regression model with coefficients $\{\beta_j\}_{j=0,..,N_f}$ was trained upon the bandpower features $\Phi_{j,tr} = \mathrm{Var}[\mathbf{w}_{tr}^{(j)}\mathbf{x}_{tr}]$. Finally, those coefficients were used to predict the trial-wise target variable $z_{est}(e)$ using the bandpower features $\Phi_{j,te}(e) = \mathrm{Var}[\mathbf{w}_{tr}^{(j)}\mathbf{x}_{te}](e)$ of unseen test data $\mathbf{x}_{te}$:

$$z_{est}(e) = \beta_0 + \sum_{j=1}^{N_f} \beta_j \Phi_{j,te}(e) \qquad (4)$$

In order to compare the estimated z_{est} with the true motor performance z_{true}, different metrics can be calculated [9]. For simplification, we focused on a single evaluation metric only. Per data set, the evaluation was carried out by transferring the continuous labels z_{true} into a two-class scenario according to the 50th percentile of z_{true}. This enabled the utilization of the receiver operating characteristics (ROC) curve which is calculated upon the estimated target variable z_{est} given the true two-class labels [19]. As ROC performance can be reduced to a scalar value by calculating the area under the ROC curve (AUC), we will name this metric z-AUC as it characterizes the separability of the estimated target variable z_{est}.

5) Selection of Regularization Parameter: To estimate the future performance of the proposed algorithms, we compared two alternative selection strategies in order to determine a suitable regularization parameter α_{opt} for each subject.
First, a leave-one-subject-out (LOSO) cross-validation was applied by determining the regularization parameter α_{opt} based on the grand average z-AUC across $N_{sub}-1$ subjects, calculated for the 40 evaluation points of α.
Second, α_{opt} was selected by a subject-wise nested $K = 10$-fold chronological CV. The inner CV served for estimating the individually optimal regularization parameter α_{opt} among 10 logarithmically scaled values ranging from $\alpha \in [10^{-6}, 10^{-2}]$. In comparison with the LOSO scheme, we chose fewer α values for computational reasons. The value maximizing the z-AUC metric was selected and applied to the outer CV in order to train the respective spatial filtering algorithm and the linear regression model.

RESULTS

Sensitivity to Regularization Parameter: The sensitivity of the introduced approaches TR-SPoC and NTR-SPoC in terms of the regularization parameter α is displayed in Fig. 1. For each α, the z-AUC is reported as a grand average (GA) across all 18 subjects (solid lines). For an individual subject, the impact of the regularization may depend upon the initial performances obtained with basic SPoC. Hence, we decided to separately report the performance for five good subjects (dashed lines). They were selected as the subjects with the best SPoC performance values z-AUC(SPoC) > 0.55. However, as the absolute best subject with z-AUC(SPoC) $= 0.77$ represents a very strong (positive) outlier compared to the full set of 18 subjects, it was not included into this group. (compare with Fig. 2)

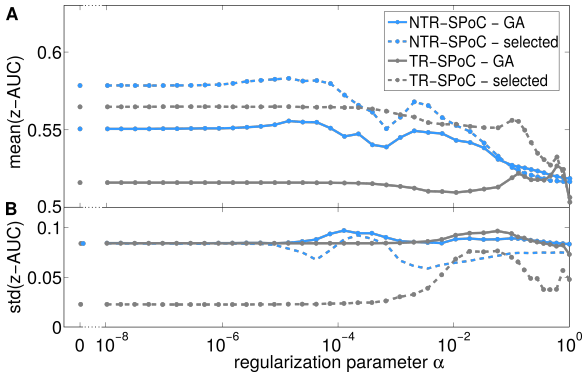

Figure 1. Sensitivity analysis wrt. the regularization strength for TR-SPoC and NTR-SPoC. (A) Averaged z-AUC performance is reported as grand average (GA) across all 18 subjects (solid line) and for five good subjects (dashed line). (B) Standard deviations of the corresponding averages are depicted. For comparison, the displayed performance at $\alpha = 0$ corresponds to the non-regularized SPoC versions.

For TR-SPoC, an increased regularization strength parameter does not affect performance within a wide range of $10^{-8} < \alpha < 10^{-3}$. While even stronger regularization with values of $10^{-1} < \alpha < 10^{0}$ sightly improves the grand average performance, it comes at the cost of a higher standard deviation (see Fig. 1(B)).
The situation looks different for NTR-SPoC as three major effects can be observed when increasing regularization strength controlled by α. Within the range $10^{-8} < \alpha < 10^{-6}$, the performance remains on a stable level. Enlarging the regularization strength to $10^{-6} < \alpha < 10^{-2}$, the performance increases (two local maxima) with best average performance obtained at $\alpha = 1.4 \cdot 10^{-5}$. Extreme regularization expressed by $\alpha > 10^{-2}$ results in a drastic drop of performance. The standard deviation of the reported performance means constantly remain on a high level, indicating that the sensitivity wrt. the regularization parameter α varies strongly across subjects.
In Fig. 1, the effect of trace normalization upon performance can be evaluated for $\alpha = 0$, which describes the absence of any regularization. Thus, the performance reported for TR-SPoC at $\alpha = 0$ corresponds to that of standard SPoC, while $\alpha = 0$ for NTR-SPoC directly

Published by Verlag der TU Graz
Graz University of Technology

 DOI: 10.3217/978-3-85125-533-1-57

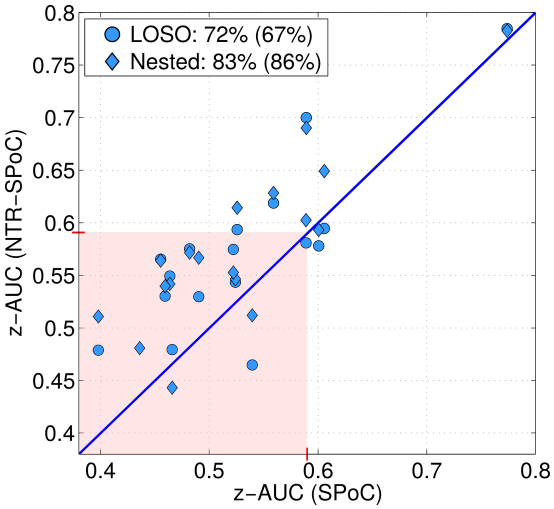

Figure 2. Performance comparison of NTR-SPoC with standard SPoC, using both LOSO and individual nested cross-validation. Each blue marker corresponds to one of the 18 subjects. For both of the selection strategies, the first number reports the percentage of subjects for which NTR-SPoC outperforms SPoC. Percentage values given in brackets are restricted to those data points located outside the red shaded area. It encloses all subjects which do not reach a threshold criterion on z-AUC for meaningful predictions.

maps to TN-SPoC. On the grand average evaluation, the performance of TN-SPoC is increased by 5 %, compared to SPoC while the corresponding standard deviations of both methods are on comparable levels.

As these intermediate results show, that NTR-SPoC effectively outperforms the non trace-normalized alternative TR-SPoC, we will restrict the evaluations in the next paragraphs to NTR-SPoC.

Individual Selection of Regularization Strength: In Fig. 2, the subject-wise performance comparison of NTR-SPoC to standard SPoC is reported for the two regularization parameter selection strategies LOSO and subject-wise nested cross-validation.

In Fig. 2, the circle-shaped markers report the individual performances obtained with LOSO. Building upon the sensitivity analysis, for 15 out of 18 subjects the regularization parameter is selected as $\alpha_{opt} = 7.9 \cdot 10^{-6}$, for the remaining three subjects it was chosen as $\alpha_{opt} = 2.4 \cdot 10^{-5}$. Those values are in good accordance with the global maximum of the grand average performance reported in Fig. 1. The diamond-shaped markers correspond to the validation by individual nested cross-validation. To compare the two selection strategies, we make use of two different group statistics. First, the overall ratio of subjects for which NTR-SPoC outperforms SPoC is provided (72 % for LOSO and 83 % for nested CV). In addition, the values in brackets consider only those individual performances which manage to cross a

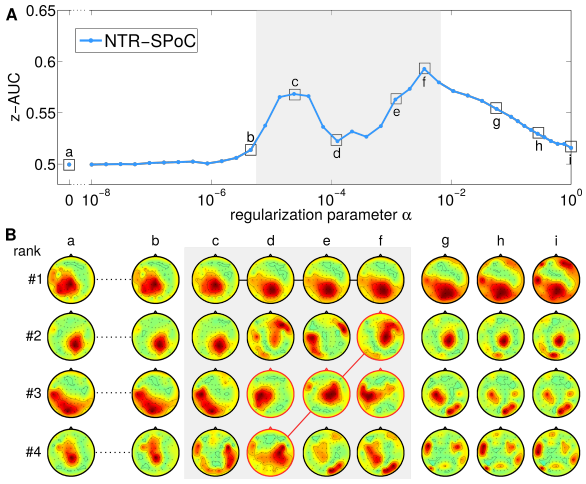

Figure 3. Effect of regularization parameter upon the performance and the spatial patterns for an exemplary subject VP9. (A) Performance of NTR-SPoC for choosing $\alpha \in [10^{-8}, 10^{0}]$. (B) Corresponding activity patterns along first four ranked components at the marked evaluation points (a)-(i).

threshold of minimum meaningful performance at z-AUC$_{th}$ = 0.59 (red shaded area). Details on how this threshold is determined have been reported in [9]. A two-sided Wilcoxon rank sum test on the full data set yields for both selection strategies that NTR-SPoC achieves statistically significant higher performances than SPoC. (The corresponding p-values obtained were $p_{\text{LOSO}} = 2.2 \cdot 10^{-2}$ and $p_{\text{Nested}} = 1.4 \cdot 10^{-3}$.)

Effect of Regularization Upon Oscillatory Components: For an exemplary subject, the effect of the regularization strength in NTR-SPoC upon the underlying first four ranked oscillatory components is depicted in Fig. 3. In (A) the z-AUC is reported for the different α values, in (B) the first four ranked patterns of the marked evaluation point (a)-(i) are shown. As the sign of a pattern $\mathbf{a}$ is arbitrary, they have been corrected to be consistent across the displayed patterns and scaled by their norm.

Consistent with the results presented in Fig. 1, three different α ranges can be identified for the selected subject. The ranges can be characterized according to two aspects, the performance (A) and the underlying spatial patterns (B).

For very small regularization values, represented by evaluation points (a) and (b), the performance as well as the spatial patterns are stable despite of increased α. In other words, NTR-SPoC is not sensitive for such small values of α. The gray shaded area in Fig. 3(A) encloses the evaluation points (c)–(f). This range is sensitive to changes of α which is revealed by performance improvements as well as rank switches among the spatial patterns (e.g. rank #4 from (d) tracked by a solid red line to (f)) or even novel patterns that appear among the top four ranks (e.g. rank #3 at position

Published by Verlag der TU Graz
Graz University of Technology

 DOI: 10.3217/978-3-85125-533-1-57

(d)). In Fig. 3(B), novel patterns are marked by a red circumference. Regularization beyond $\alpha > 10^{-2}$ ((g)–(i)) leads to a slight drop in performance. This is accompanied by an increased number of components among the first ranks, which display higher spatial frequencies in their activation patterns. The latter observation was made for most subjects and usually affected patterns of ranks 2–4.

DISCUSSION

We introduced the concept of Tikhonov regularization for the SPoC algorithm. Its performance was evaluated by applying a regression model upon the $N_f = 4$ top-ranked components. Nonetheless, this number was not optimized and thus leaves room for improvement.
As reported on the grand average of 18 subjects, the pure Tikhonov regularization of SPoC (TR-SPoC) is not detrimental for a low to medium amount of regularization. Under strong regularization the approach becomes only slightly favorable in terms of performance. However, most strongly regularized TR-SPoC components seemed to show less plausible patterns in the subjective opinion of the authors (data not shown here). Based on even a full regularization parameter sweep, an operating range has neither been observed for a linear nor a logarithmic spacing of α-values along different orders of magnitude as the Rayleigh coefficient of TR-SPoC stated in Eq. 3 is mostly insensitive to the added penalty term.
We tackled this issue by incorporating the trace normalization to the Tikhonov regularization of SPoC (NTR-SPoC). As a result, the NTR-SPoC becomes sensitive to the penalty term over a range of small regularization parameters (see Fig.1 and 3). In addition, we have shown that similar regularization parameters mostly lead to comparable performance increases. As originally proposed by Ramoser et al. [4], the trace normalization of the covariance matrices involved in Eq. 3 balances the influence of the nominator and the denominator. We have shown that NTR-SPoC can improve the performance of individuals, but have also observed that optimal operating ranges varied across subjects. As a positive side effect, the approach brings up new meaningful components. This observation is in accordance with Tikhonov regularization of the CSP algorithm [13]. However, NTR-SPoC comes at a prize, as for some individuals we observed a performance decrease. In these cases, trace normalization may unfortunately remove meaningful information. Though we did not identify a predictor yet, that could indicate, if trace normalization is useful in a new subject or not. Thus, we propose to evaluate both approaches in parallel. In the future, we aim to run the algorithms also on simulation data as this enables e.g. to control for the underlying SNR of the data. As this proof-of-concept motivated the inclusion of the trace norm, applying this to other variants of regularization will help to characterize the effect behind it.

CONCLUSION

In summary, we have presented an approach to regularize the existing SPoC algorithm using a Tikhonov regularization which favors spatial filter solutions with small norms. Our findings show that by simply adding a penalty term to the original SPoC objective function, the filter solutions are insensitive to the regularization term and performance does not improve. We applied an additional trace normalization as a remedy and observed, that it enhances the algorithm's sensitivity for the regularization. This enabled us to define a subject-specific operating range of the regularization and thus improve the achievable performance for most subjects. This proof-of-concept study opens up future research upon different regularization strategies and allows for an in-depth characterization of data sets.

ACKNOWLEDGMENT

This work was fully supported by BrainLinks-BrainTools Cluster of Excellence funded by the German Research Foundation (DFG), grant number EXC 1086. For the data analysis, the authors acknowledge support by the state of Baden-Württemberg through bwHPC and the German Research Foundation (DFG) through grant no INST 39/963-1 FUGG. For some aspects of the data analysis, the BBCI Toolbox was utilized [20].

REFERENCES

[1] Millán J. d. R, Rupp R, Mueller-Putz G, Murray-Smith R, Giugliemma C, Tangermann M, Vidaurre C, Cincotti F, Kübler A, Leeb R, Neuper C, Müller K.-R, and Mattia D. Combining brain–computer interfaces and assistive technologies: State-of-the-art and challenges. *Frontiers in Neuroscience*, 4:161, 2010.

[2] Müller K.-R, Krauledat M, Dornhege G, Curio G, and Blankertz B. Machine learning techniques for brain–computer interfaces. *Biomedical Technologies*, 49:11–22, 2004.

[3] Blankertz B, Tomioka R, Lemm S, Kawanabe M, and Müller K.-R. Optimizing spatial filters for robust EEG single-trial analysis. *Signal Processing Magazine, IEEE*, 25(1):41–56, 2008.

[4] Ramoser H, Müller-Gerking J, and Pfurtscheller G. Optimal spatial filtering of single trial EEG during imagined hand movement. *Rehabilitation Engineering, IEEE Transactions on*, 8(4):441–446, 2000.

[5] Lotte F and Guan C. Regularizing common spatial patterns to improve BCI designs: Unified theory and new algorithms. *IEEE Transactions on Biomedical Engineering*, 58(2):355–362, Feb 2011.

[6] Devlaminck D, Wyns B, Grosse-Wentrup M, Otte G, and Santens P. Multisubject learning for common spatial patterns in motor-imagery BCI. *Intell. Neuroscience*, 2011:8:8–8:8, January 2011.

Published by Verlag der TU Graz
Graz University of Technology

 DOI: 10.3217/978-3-85125-533-1-57

[7] Samek W, Kawanabe M, and Müller K.-R. Divergence-based framework for common spatial patterns algorithms. *IEEE Reviews in Biomedical Engineering*, 2014.

[8] Frey J, Daniel M, Hachet M, Castet J, and Lotte F. Framework for electroencephalography-based evaluation of user experience. In *Procedings of CHI*, pages 2283–2294, 2016.

[9] Meinel A, Castaño-Candamil S, Reis J, and Tangermann M. Pre-trial EEG-based single-trial motor performance prediction to enhance neuroergonomics for a hand force task. *Frontiers in Human Neuroscience*, 10:170, 2016.

[10] Dähne S, Meinecke F. C, Haufe S, Höhne J, Tangermann M, Müller K.-R, and Nikulin V. V. SPoC: a novel framework for relating the amplitude of neuronal oscillations to behaviorally relevant parameters. *NeuroImage*, 86(0):111–122, 2014.

[11] Parra L. C, Spence C. D, Gerson A. D, and Sajda P. Recipes for the linear analysis of EEG. *NeuroImage*, 28(2):326–341, 2005.

[12] Haufe S, Meinecke F, Görgen K, Dähne S, Haynes J.-D, Blankertz B, and Bießmann F. On the interpretation of weight vectors of linear models in multivariate neuroimaging. *NeuroImage*, 87:96–110, 2014.

[13] Samek W, Vidaurre C, Müller K.-R, and Kawanabe M. Stationary common spatial patterns for brain–computer interfacing. *Journal of Neural Engineering*, 9(2):026013, 2012.

[14] Blankertz B, Kawanabe M, Tomioka R, Hohlefeld F. U, Nikulin V. V, and Müller K.-R. Invariant common spatial patterns: Alleviating nonstationarities in brain-computer interfacing. In *Advances in Neural Information Processing Systems*, pages 113–120, 2007.

[15] Tikhonov A. N. Regularization of incorrectly posed problems. *Soviet Mathematics Doklady*, 4:1624–1627, 1963.

[16] De Bie T, Cristianini N, and Rosipal R. Eigenproblems in pattern recognition. In *Handbook of Geometric Computing*, pages 129–167. Springer, 2005.

[17] Lu H, Eng H. L, Guan C, Plataniotis K. N, and Venetsanopoulos A. N. Regularized common spatial pattern with aggregation for EEG classification in small-sample setting. *IEEE Transactions on Biomedical Engineering*, 57(12):2936–2946, Dec 2010.

[18] Reis J, Schambra H. M, Cohen L. G, Buch E. R, Fritsch B, Zarahn E, Celnik P. A, and Krakauer J. W. Noninvasive cortical stimulation enhances motor skill acquisition over multiple days through an effect on consolidation. *Proceedings of the National Academy of Sciences*, 2009.

[19] Fawcett T. An introduction to ROC analysis. *Pattern Recognition Letters*, 27(8):861–874, 2006.

[20] Blankertz B, Acqualagna L, Dähne S, Haufe S, Schultze-Kraft M, Sturm I, Uumlic M, Wenzel M. A, Curio G, and Müller K.-R. The berlin brain-computer interface: Progress beyond communication and control. *Frontiers in Neuroscience*, 10:530, 2016.

Published by Verlag der TU Graz
Graz University of Technology

Proceedings of the
7th Graz Brain-Computer Interface Conference 2017 DOI: 10.3217/978-3-85125-533-1-58

MULTI-TIMESCALE SPECTRA AS FEATURES FOR CONTINUOUS WORKLOAD ESTIMATION IN REALISTIC SETTINGS

D. Miklody[1], P. Moessmer[1], T. Dettmann[2], K. Klinkenberg[3], B. Blankertz[1]

[1]Department of Computer Science, Technische Universität Berlin, Berlin, Germany
[2]Federal Waterways Engineering and Research Institute, Karlsruhe, Germany
[3]K+S projects, Rangsdorf, Germany

E-mail: miklody@tu-berlin.de

ABSTRACT: In the real-time indication of cognitive workload in realistic settings, the main challenge in comparison to laboratory studies is the missing control of environmental variables of the participant. This introduces strong intrasubjectal/situational changes in EEG and makes most indicators built on one part of the data fail in another. We propose novel features reflecting the spatio-spectral brain state on multiple timescales as information for the workload indication. This allows the classifier to interpret the current brain state (estimated from the last 10 s) in reference to the slower changing background state (estimated from the last 10 mins). In a validation on an inland-waterway study, classification improves in a semi-realistic simulator setting from 19 % average error down to 13 %. In a corresponding real-world EEG measurement onboard a freight-ship, the improvement is less pronounced but workload estimation is possible.

INTRODUCTION

For the continuous indication of cognitive workload from electroencephalography (EEG), often averages of extracted features based on small time windows of seconds to minutes are used. The EEG features used for classification/indication are usually bandpass-filtered, spatially-filtered, spectral components, combinations of those or similar approaches[1,2,3].

While smaller windows bring the indication closer to real-time, bigger windows smooth the output and often reduce the influence of artefacts and thus improve classification accuracy[1].

While in laboratory settings cognitive workload indication can mostly be successfully performed, the transfer to realistic or semi-realistic environments remains a challenge. First of all, the participant is mostly more aware and concentrated on all of her/his actions as they have real-world effects. Also, the reduced setting of a laboratory or simulator might not elicit all the perceptual input of a real scenario and, thus, brain states might be more profound, distinct and situation-dependent in realistic situations. In addition, EEG experiments usually consist of many repetitions the data of which is then averaged to filter out unrelated signal components. This is mostly unfeasible in realistic scenarios.

With the aim to handle in particular the stronger changes in brain signals in realistic scenarios, we introduce a method that provides the classifier with the information about the recent past spectrum of the EEG. This leads to the possibility of filtering current changes out of ongoing activity.

MATERIALS AND METHODS

EEG recordings: The EEG was recorded with a BrainVision BrainAmp setup involving EasyCap ActiCaps System with 32 gel-based Ag/Ag-Cl electrodes and a sampling frequency of $f_s = 1kHz$. This amplifier setup guaranteed stable electrode impedances and high immunity to all kinds of noise and artefacts. All electrode impedances were ensured to be below 10 kOhms before recording the actual EEG.

Preprocessing & Artefact reduction: The raw EEG was low-pass filtered at 40 Hz with a Chebyshev-filter of order 10 and then downsampled to 100 Hz. After that, a PCA-based artefact reduction was performed [4]. To this end, all PCA components with a higher standard deviation than $70\,\mu V$ were removed from the original data. After this, spectrograms were built involving the Fast-Fourier-Transform (FFT) with a Hamming-window of length $500\,ms$.

Moving Average Spectrum: For moving average calculation, 2 different window-lengths were chosen: 1 min and 10 mins. These were calculated on the spectrograms with sampling frequency $f_s = 100\,Hz$.

Feature Selection: We used two different sets of feature vectors for comparison of our new approach to a common approach. From each, the spectrograms and the moving averages, 10s averages were built without temporal overlap. The first investigations

Published by Verlag der TU Graz
Graz University of Technology

 DOI: 10.3217/978-3-85125-533-1-58

were done on a feature vector x_a only containing the averages over 10s-windows of the spectrum from 3 to 20 Hz in 1 Hz bins. For the moving average spectrum approach, the 3 feature vectors of 10 s, 1 min and 10 mins - each containing Frequency x Channels - were then combined to a joint feature vector x_b.

Classification: The feature vectors were then classified in a 2-class approach involving linear discriminant analysis (LDA) with regularized shrinkage [5]. The classes were 'high' and 'low' workload according to expert ratings about the difficulty of the sailing in an inland waterway cargo ship task as described below in the section *Class labels*.

Validation: To estimate the performance of the classifier/indicator on unseen data, a cross-validation was performed with a chronological block-wise sampling. As error measures we decided for the class-wise normalized loss and the Area under Curve (AUC) of the receiver operator characteristics of the classifier output [6]. The AUC was inspected to see how well the classifier separates classes and could perform under a decision boundary shift.

Scalp Topographies: To investigate what features the classifier had actually picked, the resulting weight vectors were transformed to scalp topographies A by multiplication with the covariances of the features [7]:

$$A \propto \Sigma_X w$$

where Σ_X is the covariance matrix of the features X and w the LDA weight vector. For the classifier weights, the classifiers and the covariance were calculated on the whole dataset.

Experiments: Professional captains performed the passage of different bridges and one lock in a reference section between two locks on the river Main near Würzburg in Germany. Three captains performed several repetitions of the two bridge passages in the simulator of the Federal Waterways Engineering and Research Institute (*German* Bundesamt für Wasserbau BAW) in Karlsruhe with different water levels and travel directions. Additionally, another captain's EEG was measured while passing both locations and the part connecting them on a routine travel with the same cargo ship as in the simulator. The ship was a 186 m long push tow of 2 units (GMS 'Odeon' and GLS 'Elly').

Class labels: The labels for the workload classes "high" and "low" were chosen under consideration of expert ratings. The bridge passages under investigation were described by experts to be difficult. We chose the last 3 mins before the bridge passages in the *simulator* as "high" workload. In order to have a low workload phase to contrast this against, we chose the time window 1 min after the bridge passage as the ship was very long and took time to pass it. Also, a period of 15s after the start of each run until 4 mins after the start was used as a "low" workload time window. In the *on-board* scenario we chose longer periods of 7 mins in a similar scheme but added intermediate low workload phases to increase the available amount of data to the classifier and improve sampling over time.

RESULTS

Simulator: The classification in the simulator was in general successful with a class-wise average classification loss of 19 % for our common 10 s-window approach X_a and 13 % for the moving average based feature vector x_b, which can be seen in Table 1.

Table 1: Classification results

Subject	10s average	10s+1min+10min
SF1	26% (0.16)	19% (0.09)
SF2	13% (0.06)	11% (0.03)
SF3	18% (0.09)	10% (0.03)
Average	19% (0.10)	13% (0.05)
SF4 on-board	43% (0.41)	41% (0.34)

Class-wise normalized loss with AUC in parentheses.

We found spatial topographies that suggest neural origin as main features for classification in all participants. As we were operating in a semi-realistic environment with multiple angles of vision and the captains moving relatively freely in their chairs, eye movement, blinking, muscle and general movement artefacts were inevitable. PCA-based artefact reduction removed the strongest components which were mainly contributed to eye movements. But, as can be seen in Figure 1-4, some artefact components were most probably left in the data, discriminative of the workload and thus were used by the classifier. Strong local patterns from peripheral channels like frontal or occipital electrodes are likely to be artefacts in form of e.g. eye artefacts of SF1 or neck muscle artefacts of SF4. Still, the topographies for both x_a and x_b consisted mostly of central patterns, especially above 7 Hz. Interestingly, the classifier knowing the recent past had mostly weighted the 10 s average most strongly and often contrasted it against the recent past in form of 1 min and 10 min averages.

Published by Verlag der TU Graz
Graz University of Technology

 DOI: 10.3217/978-3-85125-533-1-58

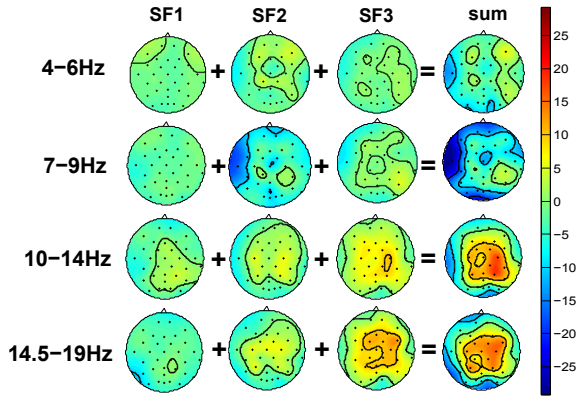

Figure 1: The scalp topographies of the classifier for feature vector x_a only containing 10 s average spectra. A positive sign represents positive weight for the class 'high' (the sign of the classifier is 'high'-'low').

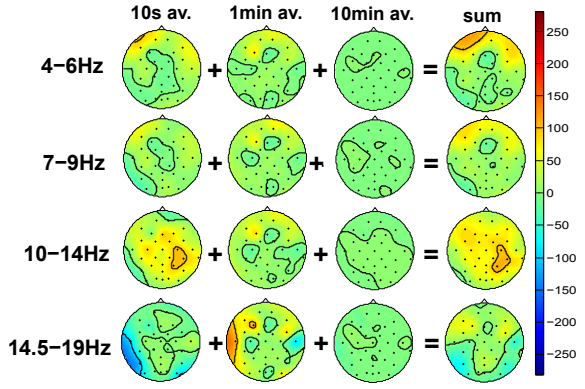

Figure 2: The scalp topographies for subject SF1 of the classifier for feature vector x_b containing 10 s, 1 min and 10 min average spectra.

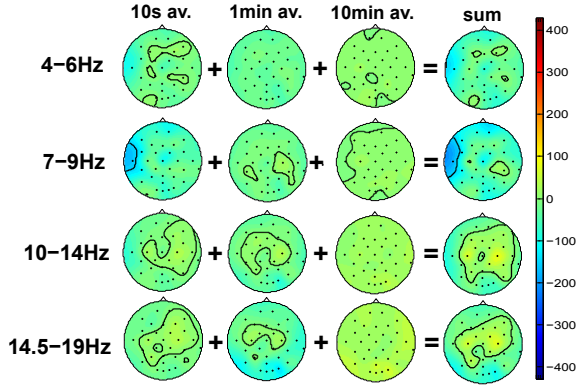

Figure 3: The scalp topographies for subject SF2 of the classifier for feature vector x_b containing 10 s, 1 min and 10 min average spectra.

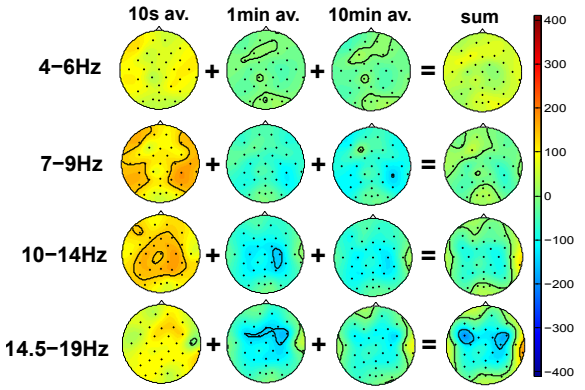

Figure 4: The scalp topographies for subject SF3 of the classifier for feature vector x_b containing 10 s, 1 min and 10 min average spectra.

In Figure 5 the Grand Average of the classifier output from a within subject block-wise cross-validation over the three subjects is shown on a map of the river Main. The classifier output interpreted as a workload indicator was in particular 'high' just in front of the bridges with an overall smooth increase and decrease.

Published by Verlag der TU Graz
Graz University of Technology

 DOI: 10.3217/978-3-85125-533-1-58

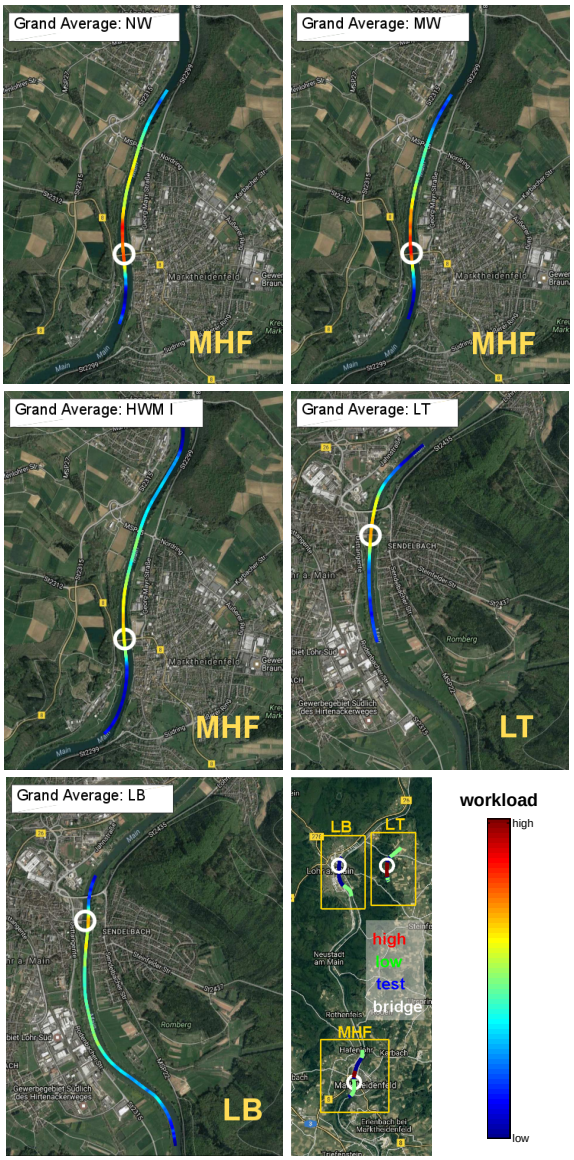

Figure 5: The workload indicator for the different scenarios in the simulator from multi-timescale feature vector x_b. The circles depict the position of the bridges. On the bottom right is an overview of the area with the two bridges and the labeling scheme. The abbreviations are as follows: *NW* low water bridge 1 - *MW* normal water bridge 1 - *HWM I* high water mark I bridge 1- *MHF* location bridge 1 - *LT* downstream bridge 2 - *LB* upstream bridge 2. *LT* is shifted horizontally on the overview map to fit into one picture.

On-Board: In the on-board data, classification worked less well in general. Classification could be performed with a class-wise averaged loss of 41% (AUC 0.34) with feature vector x_b, while the 10 s average based x_a performed with 43% (AUC 0.41), which can be examined in Table 1. The output of the multi-timescale feature vector x_b was much smoother, than that of x_a. The classifier was trained on much less samples and, also, more artefacts were visible in the spectra.

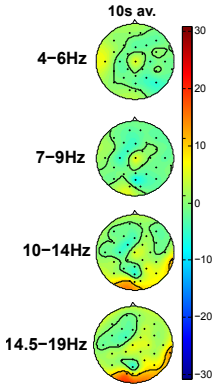

Figure 7: The scalp topography of the classifier for for subject SF4 with the 10 s only feature vector x_a. A positive sign represents positive weight for the class 'high' (the sign of the classifier is 'high'-'low').

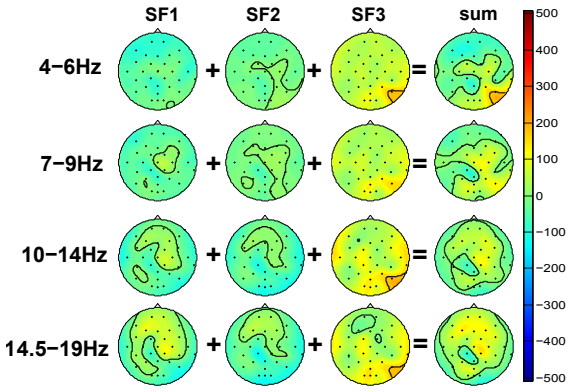

Figure 8: The scalp topography of the classifier for subject SF4 with the 10 s-1min-10 min feature vector x_b.

Published by Verlag der TU Graz
Graz University of Technology

 DOI: 10.3217/978-3-85125-533-1-58

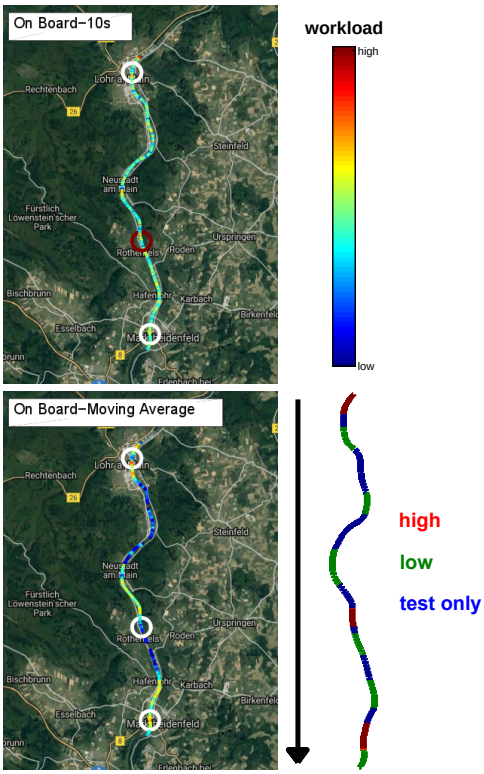

Figure 9: The workload indicator of the on-board experiment for the 10 s feature vector x_a and the multi-timescale feature vector x_b on the river Main. The upper most circle depicts bridge 2, the one in the middle the lock and the lower circle bridge 1.

DISCUSSION

Simulator data: The simulator data can be classified with a high average accuracy of 80-90 % for all of the three subjects. Scalp topographies might still include systematic movement artefacts but the connected motor activity in the brain also appears discriminative. Activity over primary sensory and motor areas of the hands could have lead to the slightly lateralized central activity in the alpha/mu-band. The workload indication within the labels was successful with high accuracies and also the overall picture of workload indication in the unmarked time spans was reasonable. Workload was "high" only in turns or close to bridges while staying "low" in between.

On-Board: Classification of the on-board data seems more challenging in general but also the much smaller amount of data has to be taken into account. Additionally, the investigation of behavior lead to very different impressions for the different time points of the trip, that were not solely connected to the bridge and lock passages. Additional communication took place, unplanned vessels crossed the way and more movement was necessary for the captain as the bridge was bigger. One big point was that the main display was mounted to the left of the captain, at which he seemed to look more frequently during sailing-induced higher workload. Accordingly, the main challenge with the on-board data of this subject seems to be the systematic motor activity connected to the observation of the display to the left of the captain. This could also be found in the scalp topographies connected to the classifier weights, as the neck muscles could have lead to the strong signals from the right occipital electrodes used for classification.

Moving average classifier: The moving average classifier improves the classification accuracy on the simulator data by 6 % on average. The scalp topographies suggest that mainly the actual 10 s-data x_a was effectively used and the 1 min and 10 mins moving averages were only slightly used, but improved the results. This supports our hypothesis that supplying the classifier with the recent past makes it more robust to experimentally unconnected temporal changes commonly exhibited in the EEG within single subjects. Compared to the simulations, more of the 10 min average was used in the on-board classification in general. All kinds of artefacts seem more pronounced for this realistic scenario. Less data is available and the class labels are probably more noisy because many more latent variables not related to the bridge and lock passage have an effect on the cognitive workload. The classifier performed slightly better than the 10 s only feature vector x_a-based.

Classifier Scalp Topographies: The topographies show in general a main effect of brain activity while more predominant artefacts are also discriminative for the classification compared to most laboratory studies. Different movement patterns and viewing directions are most probably significant of the class label, as in the high-workload phase most captains seemed to steer more and also watch the displays more frequently. This is inevitable but, additionally, the results are not fully homogeneous over subjects.

CONCLUSION

In a series of linked simulator and on-board experiments on the cognitive workload of professional inland waterway captains, we successfully performed classifications involving LDA on multi-timescale spectral features. The classifier output generalizes between situations and can be used as a linear workload indicator within our data. The workload indication in semi-realistic and realistic scenarios seems possible in general. More challenges might be raised by the step from the simulator onto the board of a real ship, as performance drops drastically here. Still, our approach involving the data of the most recent past seems to perform slightly better than a simple 10 s window feature vector in the on-board scenario and improves the results from the simulator. Sadly, the simulator data of subject SF4 could not be recorded to compare and transfer

Published by Verlag der TU Graz
Graz University of Technology

 DOI: 10.3217/978-3-85125-533-1-58

the simulator results from this subject to the on-board measurements. It was planned to also take the on-board captain to the experiments in the simulator but, due to timing issues, this was not possible. This is planned for the future and could help to measure the transferability of the indicator extracted from simulator data to more realistic on-board scenarios. Also, the amount of training data would be increased by this. As this was a simple pilot study only involving three subjects in the simulator and one on-board, results have to be carefully interpreted with this limitation in mind. Still, the differences in the results for different subjects, in particular for the topographies, could be related to different individual strategies. For example, one captain may correct his course more in the "high"-workload phase, while another might be more precise and concentrated and thus correcting his course less. Also, one captain may solve the tasks more visually while another is more focused on his sensory input and motor actions which leads to different brain activity patterns. The multi-timescale spectral feature based workload indicator has to be further investigated but first results show relevance to realistic EEG experiments.

REFERENCES

[1] Miklody D, Uitterhoeve WM, v Heel D, Klinkenberg K, Blankertz B. Maritime Cognitive Workload Assessment, in Symbiotic Interaction, Springer International Publishing, 9961, 2016.

[2] Kohlmorgen J, Dornhege G, Braun M, Blankertz B, Müller KR, Curio G, Hagemann K, Bruns A, Schrauf M, Kincses W. Improving human performance in a real operating environment through real-time mental workload detection, in Toward Brain-Computer Interfacing, MIT press, 2007.

[3] Brouwer AM, Hogervorst MA, Van Erp JB, Heffelaar T, Zimmerman PH, Oostenveld R. Estimating workload using EEG spectral power and ERPs in the n-back task, in Journal of neural engineering 2012, 9(4), 045008.

[4] Casarotto S, Bianchi AM, Cerutti S, Chiarenza GA.. Principal component analysis for reduction of ocular artefacts in event-related potentials of normal and dyslexic children, in Clinical Nneurophysiology 2004, 115(3), 609-619.

[5] Vidaurre C, Krämer N, Blankertz B,Schlögl A. Time domain parameters as a feature for EEG-based brain–computer interfaces, in Neural Networks 2009, 22(9), 1313-1319.

[6] Fawcett T. An introduction to ROC analysis, in Pattern Recognit. Lett. 2006, 27, 861–74.

[7] Haufe S, Meinecke F, Görgen K, Dähne S, Haynes JD, Blankertz B, Bießmann F. On the interpretation of weight vectors of linear models in multivariate neuroimaging, in NeuroImage 2014; 87: 96-110.

Published by Verlag der TU Graz
Graz University of Technology

Proceedings of the
7th Graz Brain-Computer Interface Conference 2017 DOI: 10.3217/978-3-85125-533-1-59

The Impact of Flow in an EEG-based Brain Computer Interface

J. Mladenović[1,2], J. Frey[1,3], M. Bonnet-Save[1], J. Mattout[2], F. Lotte[1]

[1]Inria, Bordeaux, France
[2]INSERM U1028 - CNRS UMR5292 - University Lyon 1, Lyon, France
[3]Ullo, La Rochelle, France

E-mail: jelena.mladenovic@inria.fr

ABSTRACT: Major issues in Brain Computer Interfaces (BCIs) include low usability and poor user performance. This paper tackles them by ensuring the users to be in a state of immersion, control and motivation, called state of flow. Indeed, in various disciplines, being in the state of flow was shown to improve performances and learning. Hence, we intended to draw BCI users in a flow state to improve both their subjective experience and their performances. In a Motor Imagery BCI game, we manipulated flow in two ways: 1) by adapting the task difficulty and 2) by using background music. Results showed that the difficulty adaptation induced a higher flow state, however music had no effect. There was a positive correlation between subjective flow scores and offline performance, although the flow factors had no effect (adaptation) or negative effect (music) on online performance. Overall, favoring the flow state seems a promising approach for enhancing users' satisfaction, although its complexity requires more thorough investigations.

INTRODUCTION

The Brain Computer Interface (BCI) community today's priority is to assure the system robustness and its usability. It is quite a difficult task, considering the abundant inter and intra-subject variability. The major obstacle lies in the large spectrum of sources of variability during BCI usage, ranging from (i) imperfect recording conditions e.g. environmental noise, humidity, static electricity etc. [22] to (ii) the fluctuations in the user's psycho-physiological states, due to e.g., fatigue, motivation or attention [13]. There are yet more improvements to be done for a system ready to be easily used in real life conditions [38].

BCI systems showed quite an improvement with adaptive methods, i.e. adapting the machine to the changeable brain signals of the user during a BCI task. Currently, adaptation is mainly done by using different signal processing techniques without including human factors [23]. However, if the users do not understand how to manipulate a BCI system, or are not motivated to make necessary effort for such manipulation, then they are not able to produce stable and distinct EEG patterns. In that case, no signal processing algorithm would be able to decode such signals [19]. Thus, for designing a BCI, ignoring certain information about the users, e.g. their skills, cognitive abilities and motivations, may represent one of the major drawbacks for the advancement of BCIs.

A potential improvement in BCI is to acknowledge how difficult it can be to learn to produce mental commands (a very atypical skill) without a proper feedback about the progress one has made. In every discipline, a certain feedback on ones performance is necessary to enable learning, as shown in the earliest work about Operant Conditioning and Reinforcement Learning [34]. Notably, this question was studied by behaviorists for decades on animals, using rewards e.g. food, as extrinsic motivation to promote desired behavior. As humans have more complex cognitive functions, a more effective way to promote learning is in a social context, with a tutor who would prepare and adapt a task according to the student's competences. The tutor's feedback and well organized tasks would lead the disciple to gradually build up knowledge and skills, to feel confident and to be intrinsically motivated, or to be in the Zone of Proximal Development (ZPD)[36]. Derived from cognitive developmental theories [36] and refined through instructional design theories [17, 24], intrinsic motivation is to be a substantial element for learning. Thus, it is important to carefully design the feedback if we want to encourage learning and optimal performance.

Unfortunately, for long this was not the case in BCI community, as BCI systems were improved mostly with novel machine learning techniques [23]. The result of neglecting the feedback design led to often monotonous and repetitive content, further discouraging the user, and leading to reduced skill and impaired performance [4, 18], thus highly affecting the system's accuracy. Potentially, instructional design theories could add a missing piece for designing optimal BCI feedback [19].

There have been extensive literature describing higher BCI user performance and experience using game-like feedback [31, 32]. Immersive and game-like environments attract users' attention, induce intrinsic motivation, thus promote learning and performance with less effort and frustration – for a review see [20]. Even using extrinsic motivation such as monetary reward can encourage users to perform better [18]. Some studies showed that user's belief on their performance with biased feedback induced motivation and thus higher performance [2]. Hence, sometimes it is worth to trade the system's accuracy to the perceived, subjective user's feeling of control.

Published by Verlag der TU Graz
Graz University of Technology

 DOI: 10.3217/978-3-85125-533-1-59

Keeping that into account, a way to promote efficiency and motivation while respecting the principles of instructional design leads us to the Theory of Flow introduced by Csikszentmihalyi in [7]. He was fascinated by the capacity of artists to be in a state of enjoyment while effortlessly focused on a task so immersive that one looses the perception of time, of self and of basic human needs (hunger, sleep etc.). When in the flow state, people are absorbed in an activity, their focused awareness is narrowed, they lose self-consciousness, and they feel in control of their environment. As a consequence, they often perform to the best of their capacity with a sense of automaticity and a high level of confidence. Studies report flow experience in numerous activities including rock climbing, dancing, chess, reading, etc. [7, 8].
Another pertinent element which encourages intrinsic motivation and is showed to be in relation with flow, is music [6]. Recent studies showed that music has an ergogenic effect on humans, i.e. physical enhancement while performing a physical activity [1]. In [14] was reported that Haile Gebrselassie, an athlete who broke 10 000m world record in 1998, paced his running on music he was listening to, i.e. synchronous music. There is evidence that synchronous music, as a strong motivational effect, directly enhances physical performance [33] while asynchronous (background) music induces flow when accomplishing a task [28, 27]. Most of all, background music with medium tempo (speed) has showed highest impact on flow [15].
To be in the state of flow, a task needs to have the following requirements:

- **To be immersive**, with attractive visual/audio stimuli to maintain the user's attention. The principle of preserving flow with aesthetically pleasing and ergonomic content have been researched largely in the context of human computer interaction [37] and Internet navigation, e.g. e-learning [9];
- **To adapt** the task difficulty with the user's skills, i.e. an easy task might be boring as a difficult one might be frustrating, hence finding the golden middle is the way of feeling in control and keeping the motivation. Such difficulty adaptations were found in games, to keep the gamer in flow [3], or during teaching activities [5] to improve learning and keep the student in the ZPD [36].
- **To have clear goals and immediate feedback / rewards**; aspired for educational purposes [12], so that learning becomes an enjoying and autotelic (self-rewarding) process [25].

Therefore, in order to improve BCI users' performance, learning, and experience, it seems promising to try to guide them towards the state of flow. This is what we start to explore in this paper. In particular, our research question is: *Does flow improve BCI user performance?* We chose to manipulate flow in a ludic BCI environment with 2 factors: 1) Feedback adaptation, i.e. perceived difficulty adaptation to the user skills, and 2) Asynchronous music to encourage the user. Thus, our following hypotheses are:

H1. Adapting the feedback improves flow, thus improves performance.
H2. Asynchronous music improves flow, thus improves performance.
In consonance with the Flow theory, we presented a motor imagery (MI) BCI task in an open-source 3D video game (TuxRacer [1]). We investigated the effects of these two flow factors on user's flow state as well as on user performance, i.e. classification accuracy.

MATERIALS AND METHODS

Manipulating Flow: In order to fulfill Flow theory requirements, we considered the following:

- **An immersive and ludic environment**, here the **TuxRacer** video game was adjusted for a 2-class Motor Imagery (MI) BCI. The game depicts a ski course, in which a virtual penguin, Tux – controlled by the player – slides through various slopes and has to catch as much fish as possible. With the BCI adjustments, Tux was maneuvered with kinesthetic imagination of either left or right hand, see Figure 1.
- **The adaptation** of the feedback bias, i.e. users were made to believe they performed differently from what they really did, in order to be in the flow state. If they had poor performances they were positively biased to a higher degree than if they had fairly good performances. However, when the performances were too good, then the users were slightly negatively biased, so that the task would not seem too easy. This was achieved by adaptively increasing or decreasing the classifier output, i.e. the decoding of MI commands would seem different from what it was in reality.
- **Asynchronous music** consisted of 3 songs with medium tempo (120-160 beats per min), played in the background during the BCI task. 15 persons voted on social media for songs which would motivate them while playing TuxRacer. The selected songs are "Epic" by Alexey Anisimov (113s), "Confident & Successful" by MFYM (168s) and "Acoustic Corporation" by OAP (132s), all available on Jamendo[2].
- **Clear goals with immediate audio and visual feedback**, i.e. to collect maximum points by manipulating Tux to move either left or right to catch fish. The feedback is clear – once caught, the fish disappears with a brief audio stimuli stressing that the target was reached.

Experimental design: We created a 2 (*adapt vs no-adapt*) by 2 (*music vs no-music*) mixed factorial design, i.e. a between-subject adaptation factor, and a within-subject background music factor.

Protocol: 28 healthy subjects, naive to BCI, participated in the ~2 hour-long experiment (5 women, mean age: 25.23

[1] https://extremetuxracer.sourceforge.io/
[2] https://www.jamendo.com/

Published by Verlag der TU Graz
Graz University of Technology

 DOI: 10.3217/978-3-85125-533-1-59

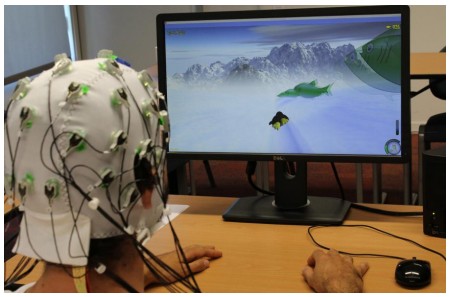

Figure 1: Participant using MI commands to play TuxRacer, e.g. imagining right hand movement to catch fish on the right.

years, SD: 2.98). The first 30 minutes consisted of (i) signing a consent form, (ii) installing of a 32 channels Brain Product LiveAmp EEG, (iii) instructions given to the user and preparation, (iv) ~10 minutes system calibration (40 trials of 7s) with the standard 2-class MI BCI (left/right hand) Graz protocol [29]. In the Graz protocol, the user was presented with arrows indicating the left or right side, to instruct the participant to imagine a left or right hand movement. Afterwards, each participant took part in 2 counterbalanced conditions of ~20mins each with TuxRacer, (a) with and (b) without background music. 3 songs were repeated to accompany the music condition of 6 runs (1 song per 2 runs). Each condition comprised of 6 $\times$ 3min-runs, with 22 trials per run (11 for left and 11 for right hand, in random order), see Figure 2. Each trial consisted in performing left/right hand MI to move Tux in order to catch fish on the left/right of the ski course, respectively. There were 7 closely arranged fish per trial, to be caught within 3 seconds. During 5-second long breaks between trials, the BCI controls were disabled so that Tux would return in a neutral position (center on the ski course) and participants could rest. The study was approved by the Inria ethics committee, COERLE (Comité opérationnel d'évaluation des risques légaux et éthiques).

Figure 2: The experiment started with ~10min calibration [29], followed by 2 conditions: either with or without music – 6 runs of 3 minutes per condition. The adapt group received an adapted (biased) feedback, contrary to the no-adapt group. Adaptation is symbolized by the magnet. Both groups were asked to fill EduFlow2 [12] questionnaires for the flow state assessment and BMRI [16] questionnaire for investigating the quality of music.

Questionnaires: Prior to the experiment, a Swedish Flow Proneness Questionnaire (SFPQ) [35] was sent to subjects to fill in at home. This 5 points Likert scale questionnaire measures flow proneness – flow as a person's trait. To estimate to which extent users were in the state of flow, they were asked to fill in the EduFlow2 questionnaire [12] after each condition (*music* or *no-music*). The EduFlow2 measures flow state through 4 dimensions: cognitive control, immersion, selflessness and autotelism – a self rewarding experience. To have a measure of the quality and motivation of the selected music, the participants also filled a dedicated questionnaire, the Brunel Music Rating Inventory (BMRI) [16].

Signal processing: The acquired EEG was band-bass filtered with a Butterworth temporal filter between 8 and 30Hz. We computed the band power using a 1s time window sliding every 1/16th s. We used a set of Common Spatial Patterns (CSP) spatial filters to reduce the 32 original channels down to 6 "virtual" channels that maximize the differences between the two class motor imagery [30]. A probabilistic SVM (Support Vector Machine) with a linear kernel was used to classify the data between left and right classes (regularization parameter C = 1). That way, the output of the SVM between 0 and 1, indicated a class recognized with a certain degree of confidence, e.g. 1 means that the right- hand class was recognized with high confidence.

Performances: The online performance corresponds to the peak accuracy of the classifier that controlled the video game, i.e. the highest classification accuracy over all trials' time windows. The offline performance was computed afterwards with a 4-folds cross validation, i.e. regarding only the data recorded during the interaction with the video game for training and testing. In other words, data recorded during the Graz protocol was not used to compute offline performances. We used a LDA (Linear Discriminant Analysis) for the offline classification, since it is less computationally demanding. Both for online and offline analyses, one accuracy score was computed over the music / no_music condition (i.e. 6 runs of 22 trials).

Game controls: The TuxRacer game was controlled *via* a virtual joystick. When a right hand movement was recognized (SVM output of 1) the virtual joystick was tilted toward the right at its maximum angle, 45 degrees. Inversely, when a left hand movement was recognized (SVM output of 0), the virtual joystick was tilted 45 degrees to the left. Between 0 and 1, the values of the virtual joystick were mapped linearly (from minus 45 degrees to 45 degrees). Thanks to this simple virtual joystick, we did not need to modify the usual input commands to the complex BCI ones in the game. Basically, the virtual joystick can act as or replace the usual computer controls, such as keys on the keyboard. Our freely available source code[3] could be used to control any (linux) joystick-based game with a BCI.

Game modifications: We designed the BCI TuxRacer game so that its timing and structure mirror that of the Graz motor imagery BCI protocol [29], but in an immersive and motivating environment. We modified the shape of the terrain, curving it alike a bobsleigh course. Consequently, by

[3] https://github.com/conphyture/LSL2joy

Published by Verlag der TU Graz
Graz University of Technology

 DOI: 10.3217/978-3-85125-533-1-59

the force of gravity, Tux would slide back to the middle of the screen between trials, when the commands were deactivated. Between trials, Tux would still be skiing towards the following trial with constant speed, enabling the users to see the next fish. We fixed the position of the fish on the ski course edges, so that the targets were equidistant from Tux at the beginning of each trial, i.e. same distance from the center of the ski course. The reason for this is to enable the user to provide equivalent potential effort for both MI classes (left/right hand). By assuring a constant speed for Tux, a race (run) always lasted 3 minutes.

Game adaptation: The *no_adapt* group was the first to participate in the experiment. Thanks to the fact that there was a correlation between the user's flow state and the performances in the control group, we empirically calculated a performance level (classifier accuracy) for which users felt most in flow. We used that value as an attractor or a quasi-flow value to lure Tux in. At each instant ($1/16^{th}$sec sliding window) we would retrieve the classifier output and add to it a value which would push Tux a half way towards our attractor. This value was determined intuitively from Flow theory, to keep the difficulty in the "golden middle". Consequently, when user performances were very poor, Tux was boosted to a higher extent towards the attractor, i.e. in this case users were helped (positively biased) more than when their performances were fairly good. However, when the performances were too good, the perceived performances were deteriorated (feedback was negatively biased). The "flow" function would then be: $f(s_i) = s_i + \frac{(a-s_i)}{2}, s_i \in [-1, 1]$, where s_i stands for user skill, which is given by the classifier output and scaled to ease the computation (-1 for left, 1 for right), for all instants i within 22 trials, ($i = 1, ..16Hz \times 66s$). Finally, $a = 0.79$ denotes the attractor for the right class ($a = -0.79$ for left class).

RESULTS

The normal distribution of all the data was verified using a Shapiro-Wilk normality test.

Flow-factor's influence on EduFlow2: We tested the effects of our mixed factorial design on each of the 4 dimensions measured by the EduFlow2 questionnaires using a Markov Chain Monte Carlo (MCMC) method [10]. The MCMC showed a significant difference between *adapt* and *no-adapt* along the 1^{st} dimension (p < 0.01). Participants in the adapt group reported higher cognitive control (mean: 5.38, SD: 0.84) compared to the no-adapt group (mean: 4.49, SD: 0.83), see Figure 3.

There was no significant difference between groups regarding their flow trait, measured with SFPQ (1-way ANOVA, p = 0.25). ANCOVA tests showed that it was not a confounding factor for neither EduFlow2 nor performances.

There was no difference between groups regarding BMRI (1-way ANOVA, p = 0.53). Mean score: 15.80, SD: 4.14 – maximum score with the questionnaire we distributed: 25.3. There was no correlation between BMRI scores and flow (p = 0.54) nor with user performance, online (p = 0.78) or offline (p = 0.20).

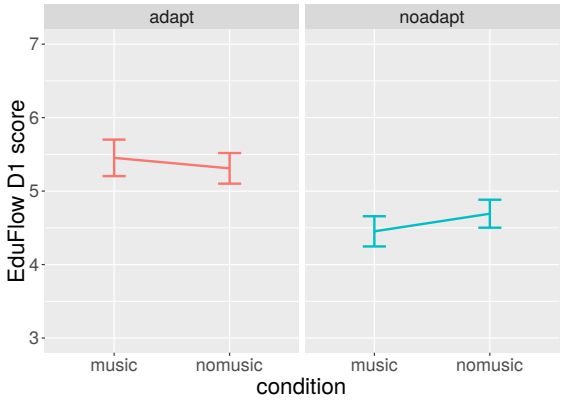

Figure 3: The EduFlow2 score (7 Likert scale) for the first dimension (cognitive control) depending on the between-subject factor *adapt* and on the within-subject factor *music*. Users were in higher cognitive control in the adapt condition (left).

Flow-factor's influence on performance: The question whether our conditions could directly improve the online performances was tested with a 2-way ANOVA. There was a significant interaction between music and adaptation (*p<0.05*). Music had a significant effect on the online performance (mean with music: 0.62, SD: 0.09, mean with no_music: 0.65, SD: 0.11, *p<0.05*) but adaptation had not (*p=0.08*), see Figure 4. A post-hoc Tukey analysis reveals that the one significant interaction occurs in the no_adapt condition, between music (mean: 0.64, SD: 0.11) and no_music (mean: 0.68, SD: 0.13) (*p<0.001*).

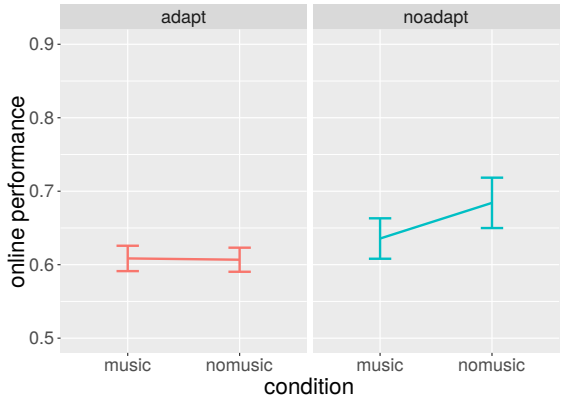

Figure 4: The peak performance during the completion of the video game depending on the between-subject factor *adapt* and on the within-subject factor *music*. In the no_adapt condition (right), users had better online performances without music.

Correlation between EduFlow2 & performance:
There was no correlation between flow (mean of all the EduFlow2 dimensions) and online performance (*p=0.12*), however there was a positive correlation between flow and offline performance (Pearson coefficient: 0.35, *p<0.01*), see Figure 5. More precisely, offline performances are significantly correlated with two dimensions of flow: the 2^{nd} – immersion (p<0.01, Pearson coefficient: 0.38) and the 4^{th}

Published by Verlag der TU Graz
Graz University of Technology

 DOI: 10.3217/978-3-85125-533-1-59

– autotelism, ($p<0.05$, Pearson coefficient: 0.32). We corrected the p-values for multiple comparisons with false discovery rate [26].

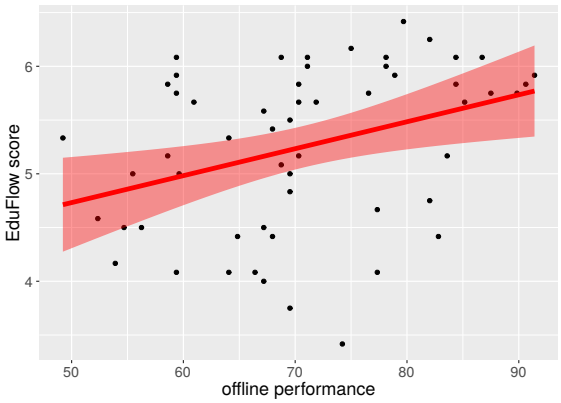

Figure 5: Positive correlation between EduFLow2 scores (mean of 4D) and offline performance (Pearson coef:0.35, *p<0.01*).

DISCUSSION

H1. validated: Adapting the task difficulty to users skill improved one dimension of flow state, cognitive control. People who faced a challenge better suited to their skill felt more in control. Thus, taking into account user's predispositions could lead to a greater user experience.

H2. in contradiction: Not only the presence of a background music had no effect on flow, but it deteriorated the online performance. Therefore, this result contradicts our second hypothesis.

Music pace mismatch. As opposed to what we expected, we could not directly improve performance by manipulating the flow factors we chose (adaptation and music). The latter could be explained by the songs we chose, since the motivational qualities of the music (measured with the BMRI questionnaire) were not very high and not correlated to any dimension of flow. Instead of picking those songs from the public domain, users may have been more motivated should they have chosen their own music. The decrease of performance in the music condition might come from the mismatch between the rhythm of the music and the pace of the game, i.e. with the pace of the imagined hands movements. Indeed, some users shared informally that they were imagining playing their musical instrument as MI commands and that the songs further disturbed their pace.

Different training environment. There was no correlation between flow state (EduFlow2) and online performances. That could be due to the differences between the calibration environment (Graz protocol) and the game, e.g. the first being minimalistic and the latter a 3D videogame. Moreover, as the calibration was done without music, maybe the performances online were better without it because the EEG signals might have changed, therefore the classifier could not recognize them anymore.

Flow increases with performances. These later assumptions are strengthened by the fact that there was a positive correlation between flow and the offline performances, when only game data was taken into consideration. The state of flow was then positively correlated with users' performance: the feeling of immersion and the autotelic experience (i.e. the completion of the task was self-rewarding) increased with the offline performance. Hence, not only encouraging a state of flow would produce BCIs more pleasing to the users, but it might also benefit the accuracy of the system. We still have to identify the direction of the correlation though: does flow state increases performances or do good performances increase flow state?

Overall, the discrepancy in our results could stress that flow is a complex phenomenon, and however beneficial to obtaining better BCI, the emerging interaction between its components should be more thoroughly investigated.

CONCLUSION

By investigating means to improve BCI user performance and usability through instructional design theories, we came across the Flow Theory. This theory, which describes an optimal user state, showed to improve performances in many fields. We hypothesized that the state of flow could benefit BCIs. In a MI BCI task, we manipulated flow by adapting the perceived difficulty and by adding a background music. We used an immersive environment, a 3D video game, TuxRacer (the modification can be found online [4]).

Our main findings show that the adaptation increases one of the dimensions of flow – cognitive control, and that user's offline performances are positively correlated with flow. In the future we could attempt to better suit the adaptation of the task to the users: it could be biased adaptively over time, across several sessions, following the progress of the user. We could also try to account for the amount of effort that the user puts into the completion of the task in order to better comprehend such complex phenomena. For example, measuring workload could facilitate the assessment of the challenge that users are facing and computationally predict the state of flow[3].

According to the literature, we chose asynchronous music with medium tempo to follow the BCI task. Unexpectedly, the background music impeded the performances of the user. This result stresses the importance of the choice of music to accompany a task. One explanation could lie in the very BCI paradigm we chose. Indeed, a motor imagery task might share similarities with actual physical activity, where it had been shown that *synchronous* music could effectively stimulate the sensory-motor cortex[11]. Hence, a future work would consist in synchronizing music to game's cues (e.g. trials sequences) or to user's motor imagery pace. Such music, generated in real time, might enhance the flow state and intrinsic motivation. Concurrently, we should verify if the user is musically educated, as in some cases users imagined playing instruments as MI commands, and because musicians elicit different brain activity in motor areas[21].

[4] https://github.com/jelenaLis/tux-modifs)

Published by Verlag der TU Graz
Graz University of Technology

 DOI: 10.3217/978-3-85125-533-1-59

Flow is not only a promising research direction to improve BCI systems, but it raises a new question: should we put all our efforts in favoring the machine accuracy, or rather the human subjective experience?

Acknowledgements: This work was supported by the French National Research Agency with the REBEL project and grant ANR-15-CE23-0013-01. The authors would like to thank Jean Heute for his help with the EduFlow questionaire.

REFERENCES

[1] Anshel, M. H. and Marisi, D. "Effect of music and rhythm on physical performance." In: *Research quarterly* 49.2 (1978), pp. 109–13.
[2] Barbero, A. and Grosse-Wentrup, M. "Biased feedback in brain-computer interfaces." In: *Journal of neuroengineering and rehabilitation* 7 (2010), p. 34.
[3] Bulitko, V. and Brown, M. "Flow Maximization as a Guide to Optimizing Performance : A Computational Model". In: *Advances in Cognitive Systems* 1 (2012), pp. 1–18.
[4] Cho, B.-H. et al. "Neurofeedback Training with Virtual Reality for Inattention and Impulsiveness". In: *CyberPsychology & Behavior* 7.5 (2004), pp. 519–526.
[5] Clement, B. et al. "Multi-Armed Bandits for Intelligent Tutoring Systems". In: *Journal of Educational Data Mining* 7.2 (2015), pp. 20–48.
[6] Croom, A. M. "Music practice and participation for psychological well-being: A review of how music influences positive emotion, engagement, relationships, meaning, and accomplishment". In: *Musicae Scientiae* 19.1 (2015), pp. 44–64.
[7] Csíkszentmihályi, M. *Beyond boredom and anxiety.* San Francisco: Jossey-Bass, 1975.
[8] Csikszentmihalyi, M. and LeFevre, J. "Optimal experience in work and leisure." In: *Journal of Personality and Social Psychology* 56.5 (1989), pp. 815–822.
[9] Esteban-millat, I. et al. "Modelling students' flow experiences in an online learning environment". In: *Computers & Education* 71 (2014), pp. 111–123.
[10] Hadfield, J. D. "MCMC methods for multi-respoinse generalized linear mixed models: The MCMCglmm R package". In: *Journal of Statistical Software* 33.2 (2010), pp. 1–22.
[11] Hardy, M. W. and Lagasse, A. B. "Rhythm, movement, and autism: using rhythmic rehabilitation research as a model for autism." In: *Frontiers in integrative neuroscience* 7 (2013), p. 19.
[12] Heutte, J. et al. "The EduFlow Model: A Contribution Toward the Study of Optimal Learning Environments". In: *Flow Experience*. Cham: Springer International Publishing, 2016.
[13] Jeunet, C. et al. "Predicting Mental Imagery-Based BCI Performance from Personality, Cognitive Profile and Neurophysiological Patterns". In: *PLoS ONE* (2015).
[14] Karageorghis, C. I. et al. "Ergogenic and psychological effects of synchronous music during circuit-type exercise". In: *Psychology of Sport and Exercise* 11.6 (2010), pp. 551–559.
[15] Karageorghis, C., Jones, L., and Stuart, D. P. "Psychological effects of music tempi during exercise". In: *International Journal of Sports Medicine* 29.7 (2008), pp. 613–619.
[16] Karageorghis, C. I., Terry, P. C., and Lane, A. M. "Development and initial validation of an instrument to assess the motivational qualities of music in exercise and sport: The Brunel Music Rating Inventory". In: *Journal of Sports Sciences* 17.9 (1999).
[17] Keller, J. M. "Development and use of the ARCS model of instructional design". In: *Journal of Instructional Development* 10.3 (1987), pp. 2–10.
[18] Kleih, S. et al. "Motivation modulates the P300 amplitude during brain–computer interface use". In: *Clinical Neurophysiology* 121.7 (2010), pp. 1023–1031.
[19] Lotte, F., Larrue, F., and Mühl, C. "Flaws in current human training protocols for spontaneous Brain-Computer Interfaces: lessons learned from instructional design". In: *Frontiers in Human Neuroscience* 7.September (2013), p. 568.
[20] Lumsden, J. et al. "Gamification of Cognitive Assessment and Cognitive Training: A Systematic Review of Applications and Efficacy". In: *JMIR Serious Games* 4.2 (2016), e11.
[21] Luo, C. et al. "Musical training induces functional plasticity in perceptual and motor networks: Insights from resting-state fMRI". In: *PLoS ONE* 7.5 (2012), pp. 1–10.
[22] Maby, E. "Technical Requirements for High-quality EEG Acquisition". In: *Brain-Computer Interfaces 2*. Hoboken, NJ, USA: John Wiley & Sons, Inc., 2016, pp. 143–161.
[23] Makeig, S. et al. "Evolving Signal Processing for Brain-Computer Interfaces". In: *Proceedings of the IEEE* 100.Special Centennial Issue (2012), pp. 1567–1584.
[24] Malone, T. W. and Lepper, M. R. *Making learning fun: A taxonomy of intrinsic motivations for learning*. 1987.
[25] Ninaus, M. et al. "Game elements improve performance in a working memory training task". In: *International Journal of Serious Games* 2.1 (2015), pp. 3–16.
[26] Noble, W. S. "How does multiple testing correction work?" In: *Nature biotechnology* 27.12 (2009), pp. 1135–1137.
[27] Pain, M. A., Harwood, C., and Anderson, R. "Pre-Competition Imagery and Music: The Impact on Flow and Performance in Competitive Soccer". In: (2011), pp. 212–232.
[28] Pates, J et al. "Effects of asynchronous music on flow states and shooting performance among netball players". In: 4 (2003), pp. 415–427.
[29] Pfurtscheller, G. and Neuper, C. "Motor imagery and direct brain-computer communication". In: *Proceedings of the IEEE* 89.7 (2001), pp. 1123–1134.
[30] Ramoser, H., Müller-Gerking, J., and Pfurtscheller, G. "Optimal spatial filtering of single trial EEG during imagined hand movement". In: *IEEE Trans Rehabil Eng* 8.4 (2000), pp. 441–446.
[31] Ron-angevin, R. "Brain–computer interface: Changes in performance using virtual reality techniques". In: 449 (2009), pp. 123–127.
[32] Scherer, R. et al. "Games for BCI Skill Learning". In: *Handbook of Digital Games and Entertainment Technologies*. Singapore: Springer Singapore, 2015, pp. 1–19.
[33] Simpson, S. D. and Karageorghis, C. I. "The effects of synchronous music on 400-m sprint performance". In: *Journal of Sports Sciences* 24.10 (2006), pp. 1095–1102.
[34] Skinner, B. F. *The behavior of organisms: an experimental analysis*. Appleton-Century, 1938. Chap. 457, p. 457.
[35] Ullén, F. et al. "Proneness for psychological flow in everyday life: Associations with personality and intelligence". In: *Personality and Individual Differences* 52.2 (2012), pp. 167–172.
[36] Vygotsky, L. S. *Mind in Society: Development of Higher Psychological Processes*. Cambridge: Harvard University Press, 1978.
[37] Webster, J., Trevino, L. K., and Ryan, L. "The dimensionality and correlates of flow in human-computer interactions". In: *Computers in Human Behavior* 9.4 (1993), pp. 411–426.
[38] Wolpaw, J. R. et al. "Brain–computer interfaces for communication and control". In: *Clinical Neurophysiology* 113 (2002), pp. 767–791.

Published by Verlag der TU Graz
Graz University of Technology

Proceedings of the
7th Graz Brain-Computer Interface Conference 2017 DOI: 10.3217/978-3-85125-533-1-60

A GUIDED TASK FOR COGNITIVE BRAIN-COMPUTER INTERFACES

J. Moser[1], M. R. Hohmann[2], B. Schölkopf[2], M. Grosse-Wentrup[2]

[1]Graduate Training Centre of Neuroscience, Tübingen, Germany
[2]Max Planck Institute for Intelligent Systems, Tübingen, Germany

E-mail: julia.moser@student.uni-tuebingen.de

ABSTRACT: Brain computer interfaces are an important tool to enable communication for patients suffering from amyotrophic lateral sclerosis. Yet most existing devices use cognitive functions that are impaired in later stages of the disease. Systems based on higher cognitive processes provide new possibilities for this field. However, many patients in the target group suffer from memory impairments. As many higher cognitive processes involve memory, this could be an interference. The present study investigates the differences between a currently existing cognitive paradigm using autobiographic memories and a new paradigm using a guided imagery story. Both are developed to be used in patients and try to target the same processes, with the new paradigm being less dependent on memory functions. Assessment of EEG- and behavioral data in healthy subjects results in two working paradigms for brain computer interface control. Higher classification accuracies and more favorable behavioral ratings are achieved by the previously existing paradigm.

INTRODUCTION

Patients suffering from the neurodegenerative disorder amyotrophic lateral sclerosis (ALS) can use brain computer interfaces (BCIs) for communication [1] [2]. Most of these BCIs are based on EEG or single-unit features from somatosensory or motor areas of cortex [3]. This is problematic for ALS patients as with the progress of the disease neurons in motor cortex, especially giant pyramidal neurons, degenerate [4]. Another class of BCIs makes use of visual evoked potentials to detect an attended or in this case preferred stimulus [3]. As this class relies on eye movement, and oculomotor dysfunction - especially dysfunction of effective pursuit - is common in ALS [5], it is also not suitable for late-stage ALS patients. Therefore, particularly for patients that reach the completely locked in stage, different classes of BCIs are needed. Until now there are no reliable BCIs for those patients available [6]. One approach are BCI systems that are based on higher cognitive functions. Hohmann et al. introduced a system that allows answering of binary questions by either thinking about a positive experience or focusing on ones breath [7] or, in a more recent version, doing mathematical calculations [8]. Making use of positive memories, however, includes a possible interference: Retrieval of autobiographic memories needs both self-referential processing and memory retrieval processes [9]. As those systems are designed to serve as communication devices for ALS patients the impact of the disease on memory processes is an important factor. A study by Mantovan et al. (2003) showed episodic memory deficits in ALS patients without dementia, with subjects having problems both in encoding and in retrieval [10]. When performing a battery of neuropsychological tests on a patient sample, nearly half of the sample showed cognitive impairments including memory, changing of judgement and reasoning and verbal fluency, as well as behavioral discontrol [11]. Those ALS patients who show cognitive impairment measured by a verbal fluency test also show frontal lobe dysfunction, as indicated by abnormalities in a PET scan [12]. Further, patients exhibit white matter changes in temporal regions, including motor pathways as well as non-motor areas including association fibres to the frontal lobe and anterior cingulate gyrus, that are accompanied by deficits in executive functions and memory [13]. In cognitively unimpaired ALS patients white matter changes were not as strong but still present [13].

These findings encourage the idea to create a BCI for which memory processes are less relevant, as well as motor and oculomotor functions, to make it usable for ALS patients in all stages of disease even when memory functions are impaired.

The system introduced by Hohmann et al. is likely to target up- and down regulation of parietal nodes in the default mode network (DMN). ALS patients even in late stages showed to be capable of modulating activity in the target region without prior training [7]. This is supported by the argument that in locked-in state patients connectivity in the DMN is not significantly different from the one in controls [14]. The DMN is associated with remembering the past, especially autobiographic remembering [15], and is also seen as the seat of self-referential processing in the brain [16] [17]. As a brain system for internal mentation the DMN is most active during spontaneous cognition including mental processes that create fantasy, imagination, daydreams and thoughts. It also takes part in self-relevant mental simulation, which means imagination of scenarios or hypothetical events [15]. Self-related thoughts correlate with an increase in spectral power mainly in the α-band (8-13 Hz), showing spatial patterns consistent with DMN modulation [16] [2]. It is proposed that the DMN consists of two systems: a sys-

Published by Verlag der TU Graz
Graz University of Technology

 DOI: 10.3217/978-3-85125-533-1-60

tem related to associations and memory retrieval, and a system related to self-relevant thoughts and self referential judgments [15]. Anatomically, the posterior cingulate cortex (PCC) is described as a critical node of the DMN [18] and the Precuneus (pC)/PCC node as possible side of interaction of the two proposed subsystems [19].
Considering these properties of the DMN, a scenario that could very well up-regulate the DMN is a guided imagery story. It is directed to the self and includes imagination and fantasy without being bound to autobiographic memory. Yet, for creating a binary BCI with external stimulation, this stimulation has to be presented simultaneously to enable subjects to make a decision. Some existing auditory BCI systems with simultaneous stimulation on both ears work with event related potentials like the N1 and P3 component and reach high accuracies even in online scenarios [20]. Studies working on decoding of auditory streams from EEG data like the one by O'Sullivan and colleagues additionally show that subjects are very well capable of following a story on one ear, when getting presented a different one on each ear [21].
In the present study this ability of selective attention is used for an auditory BCI targeting DMN activity. The task introduced by Hohmann et al., including positive memories and a math task [8], is compared to a new task including a guided imagery story and math tasks, both read to the participants simultaneously. During guided imagery a participant has to imagine for example being on a field in the sun or walking through the forest, experiencing the different tones and smells. The former will be referred to as "Memory" paradigm and the later as "Imagery" paradigm. The goal of this study is twofold: First, to find out whether the "Imagery" paradigm is suitable for a BCI system targeting DMN modulation, and second, which of the two paradigms shows a better classification performance.

MATERIALS AND METHODS

Experimental Paradigm: Participants were placed in a chair 1.25 m away from a 17" LCD screen with a resolution of 1280x1024 pixels and a 60 Hz refresh rate and were provided with Phillips SHB9250 headphones. The background of the screen was black, with a white fixation cross in the center. Subjects were briefed on the experimental procedure and the different tasks and their comprehension was assured. They performed four experimental blocks with brief intermissions in which they rated each block. Each experimental block consisted of thirty trials, in which participants were asked questions (fifteen correct and fifteen incorrect) in pseudo randomized order. The questions were binary general knowledge questions designed to be as easy as possible (e.g. "Is Christmas celebrated in December?" or "Is Berlin the capital of Italy?"). Participants indicated their answer to the questions by performing a certain task. After each question an instruction was given to remind the subject which task means "yes" and "no" (cf. Figure 1). One

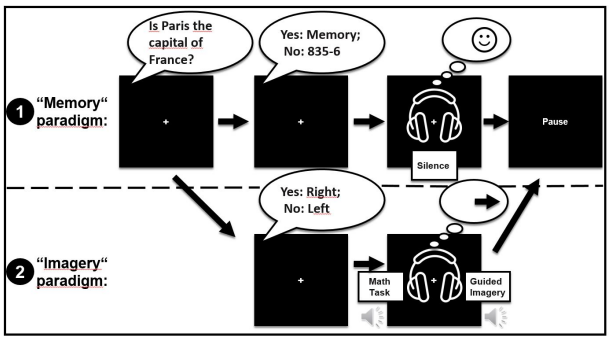

Figure 1: Example trial for the "Memory" and "Imagery" paradigm.

block lasted about 15 minutes. In two of the four blocks the task was to remember a positive experience or to subtract a number between three and nine continually from a higher number (between 800 and 850) for either "yes" or "no". The concerning numbers were named in the instructions and the task was performed in silence ("Memory" paradigm).
In the other two blocks subjects were instructed to indicate their answer by focusing on the sound on one ear while ignoring the sound on the other ear. On the right side a guided imagery story was read (based on stories published on www.hierfindichwas.de and www.planetsenior.de, accessed September 2016) and on the left side mathematical calculations (addition or subtraction of two digit numbers) were asked. The two different sounds were presented simultaneously over the whole task time ("Imagery" paradigm).
Each trial began with five seconds rest, followed by the question and instructions. The time to indicate the answer by performing the instructed task was 17 seconds, to be sure to not cut any of the auditory recordings, which were approximately 15 seconds long. The task for either "yes" or "no" stayed constant within one block but changed between blocks. The resulting different blocks with different paradigms and instructions were alternated and counterbalanced across participants. Questions remained the same for each block. After all four blocks participants got a questionnaire with all 30 general knowledge questions asked during the experiment to ensure they knew the correct answers.

Experimental Data: The study was conducted at the Max Planck Institute for Intelligent Systems in Tübingen, Germany. Ten healthy subjects (German native speakers, 5 female, 5 male) with a mean age of 34.4 $\pm$ 11.2 years took part in the experiment. All of them reported to have unimpaired hearing abilities. They received 12 Euro per hour for their participation. All participants signed a consent form to confirm their voluntary participation in ad-

Table 1: Questions (originally in German)

1) How easily could you concentrate on the task?
2) How exhausting was it to concentrate on the task?
3) How stressful was performing the task?
4) How tiring was performing the task?
5) How successful could you follow the instructions?

Published by Verlag der TU Graz
Graz University of Technology

 DOI: 10.3217/978-3-85125-533-1-60

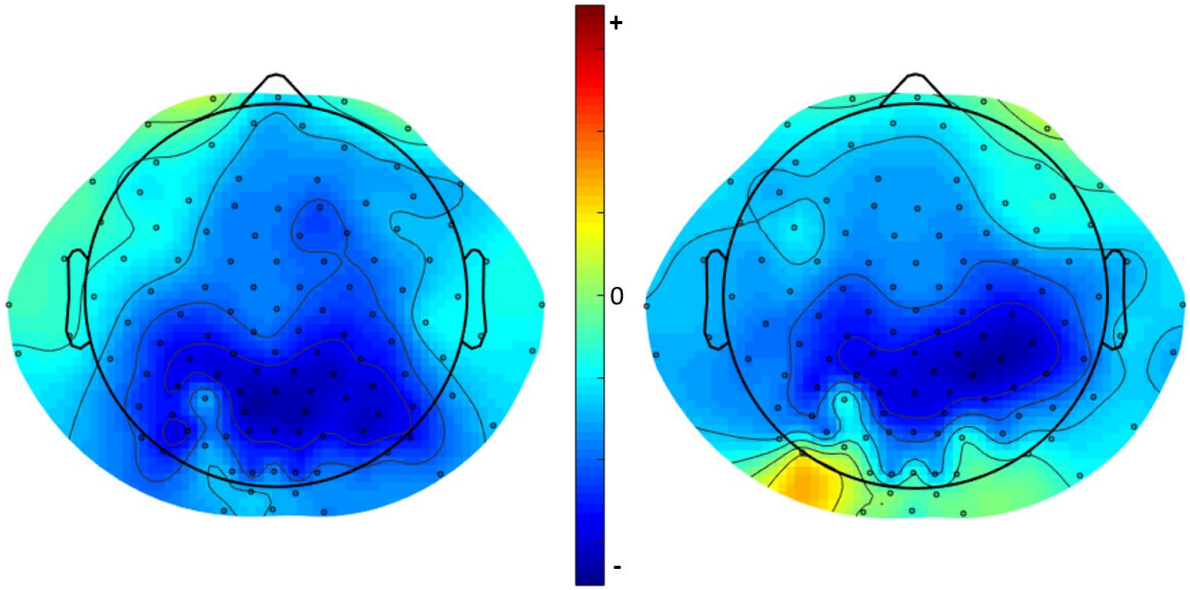

Figure 2: Left side: Encoding model for ”Memory” paradigm. Right side: Encoding model for ”Imagery” paradigm. Dark colors show the areas most relevant for classification, with the transfer learning algorithm, in arbitrary units.

vance, after being fully informed about the procedure. The study was approved by the ethics committee of the Max Planck Society. For EEG recordings a 124-channel system with a sampling frequency of 500 Hz with actiCAP active electrodes and a BrainAmp amplifier (provided by BrainProducts GmbH, Gilching, Germany) was used. Electrode placement was according to the extended 10-20 system with the left mastoid electrode as the initial reference. All recordings were converted to common average reference previous to analysis. The BCI2000 toolbox was used to implement the application [22]. Behavioral data was obtained by handing a pen and paper questionnaires to participants after each block of the experiment. The questions asked to participants are listed in Table 1. All answers could be indicated on a seven point Likert-scale, with one being the most favorable and seven the most unfavorable answer.

Data Analysis: The 17 seconds per trial in which subjects could indicate their answer to the given questions were used for EEG analysis. As previous studies [16] [7] showed that the α-frequency range is the range of most significance for modulations of the DMN, analysis was restricted to this frequency band. We used the Discrete Fourier Transform with a Hann window to compute the log-bandpower of the α-frequency band (8–13 Hz) at every channel in every trial. As the α-frequency range is not very susceptible to muscular or oculomotor artifacts, preprocessing only included the removal of electrodes that showed malfunctioning for at least one participant, reducing the feature space from 124 to 117. For obtaining optimal decoding with the relatively small number of trials recorded, we used a transfer learning technique further described by Jayaram et al. [23]. It allows to simultaneously learn decoders for all subjects while still accounting for inter-individual differences, using a linear regression model. We employed a nested cross-validation procedure, with leave-one-subject-out cross-validation for learning priors over decoders and ten-fold cross-validation to estimate decoding accuracy on each individual subject. To spatially depict the resulting encoding model, we multiplied the priors obtained by the transfer learning algorithm with the covariance matrix of the extracted features, both averaged over subjects [24]. This was plot as a topography to illustrate the areas most relevant for classification.

RESULTS

EEG Data: On average subjects achieved a decoding accuracy of 75.5% (SD 20.1%) in the ”Memory” paradigm and 64% (SD 14.7%) in the ”Imagery” paradigm. The encoding models used by the transfer learning algorithm for each paradigm are shown in Figure 2. Individual decoding accuracies can be seen in Table 2. Both paradigms classify significantly better than chance ($p < 0.001$) when tested with a permutation test with 1000 permutations of class labels. On an individual level

Table 2: Individual Accuracies

Subject	”Memory”	”Imagery”	Differences
S1	50%	63.3%	-13.3%
S2	70%	65%	5%
S3	96.7%	90%	6.7%
S4	95%	40%	55%
S5	51.7%	53.3%	-1.6%
S6	90%	51.7%	38.3%
S7	95%	83.3%	11.7%
S8	46.7%	61.7%	-15%
S9	73.3%	61.7%	11.6%
S10	86.7%	70%	16.7%
Mean	75.5%	64%	11.5%

Published by Verlag der TU Graz
Graz University of Technology

 DOI: 10.3217/978-3-85125-533-1-60

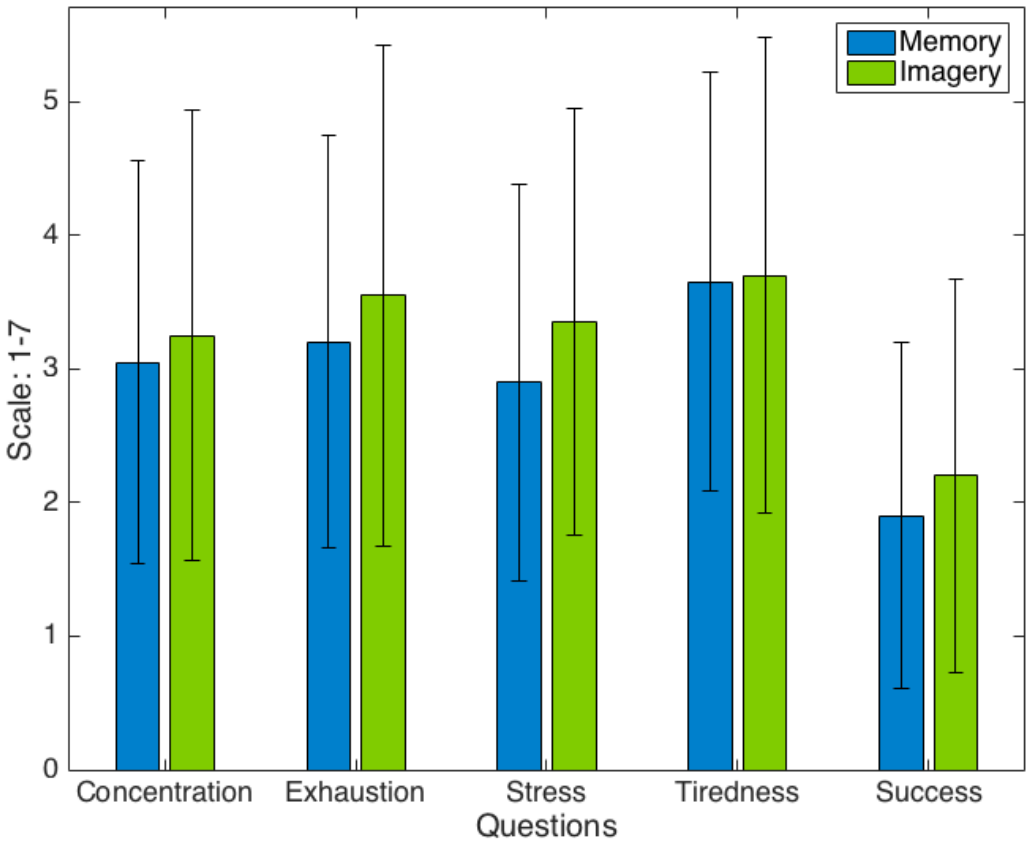

Figure 3: Mean values and standard deviations of rating data, showing a different perception of the two paradigms.

there was a high variability and some subjects did not succeed using one or the other or both paradigms while others were highly successful (Table 2). When comparing the two different paradigms in a paired permutation test with 10^4 permutations, the "Memory" paradigm achieved a better performance ($+11.5\%$), yet this difference was not significant ($p = 0.126$).

Behavioral Data: Mean rating values of each question of the pen and paper questionnaire are shown in Figure 3. Participants indicated by their ratings that they found it more difficult and more exhausting to concentrate on the "Imagery" task as well as more stressful and tiring. They also rated to have been more successful in performing the "Memory" task. Over all, the "Memory" paradigm achieved lower mean rating values (2.94, SD 0.07) compared to the "Imagery" paradigm (3.21, SD 0.59). A paired sample t-test revealed this difference to be significant ($p = 0.0167$).

DISCUSSION

Results of EEG- and behavioral data of the "Memory" paradigm and the "Imagery" paradigm lead to further support for the "Memory" paradigm to be a well functioning BCI system and introduced the "Imagery" paradigm as a new approach for classification based on DMN modulation. The "Memory" paradigm showed a better performance and was also more liked, based on participants' ratings. This pattern of results shows to be robust even when using a different approach of data preprocessing to completely omit including possible residual muscular artifacts: When performing artifact correction using an independent component analysis approach [25], instead of using the unfiltered EEG signal, the mean accuracy for classification in the "Memory" paradigm was 73.2% (SD 18%) and for the "Auditory" paradigm 60.3% (SD 8.2%). The areas weighted as being most relevant for classification by the encoding model of the transfer learning algorithm show a spatial distribution that is consistent with bandpower modulation in the pC/PCC [2]. The pC/PCC node interacts strongly with the rest of the DMN [19] and, regarding the proposition that the DMN consists of a system related to associations and memory retrieval and a system related to self-relevant thoughts and self referential judgements [15], the key role of communicating between those systems is assigned to the PCC/pC node [19]. Even though both tested paradigms appear to target the region of the PCC/pC node, there is the possibility that each of them triggers a different system of the DMN, with the "Memory" paradigm triggering system one and the "Imagery" paradigm triggering system two. This possible explanation is supported by the finding that the individual accuracies of both paradigms are not highly correlated (Pearson's $\rho = 0.315$).
A potential explanation for the differences in decoding accuracy across paradigms is provided by the over all dif-

Published by Verlag der TU Graz
Graz University of Technology

 DOI: 10.3217/978-3-85125-533-1-60

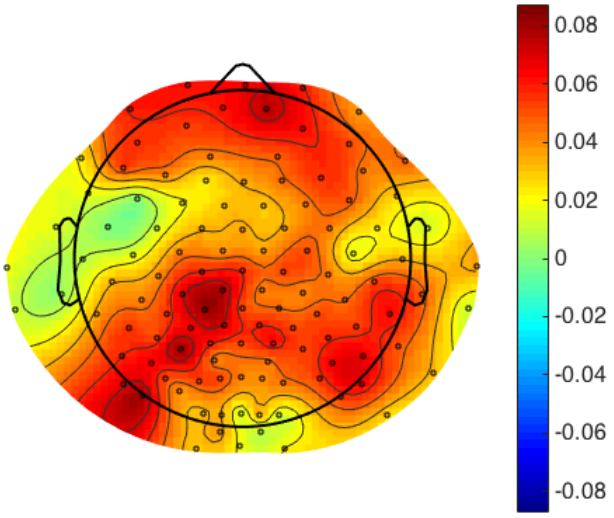

Figure 4: Baseline difference of α-power between paradigms over all participants. Approximate overlap of areas with largest differences and areas most relevant for classification.

ferences in α-power during baseline periods within each trial. The mean value of the α-log-power over all subjects and channels was -1.789 (SD 0.32) and -1.831 (SD 0.31) for the "Memory" and "Imagery" paradigm, respectively. This over all difference showed to be significant ($p = 0.031$) when tested with a paired permutation test with 10^4 permutations. The distribution of the differences over the scalp can be seen in Figure 4. These findings can be related to the research of Blankertz et al., who detected that for BCI systems based on sensorimotor rhythms (SMRs) strength of idling SMR in EEG is predictive for BCI performance.
They calculated this predictor with the maximum elevation in power spectral density compared to a noise floor over a sensorimotor area in resting state. The higher this maximum, the better the performance as it opens the possibility for a bigger difference when SMRs are attenuated [26]. Related to the current study this could mean that the over all lower α-power in the "Imagery" paradigm leaves less space for big differences due to task dependent modulations. The areas having the largest differences (Figure 4) also approximately correspond to the areas most relevant for classification. As stress is correlated negatively with α-band power [27], and participants rated the "Imagery" paradigm as more stressful, this could be the origin of the detected difference.
Nevertheless, the finding of a new paradigm working with binaural auditory stimulation supports the development of more auditory BCI systems. They could be an attractive alternative to vision based BCIs for ALS patients because, as Hill and colleagues report [20], even if vision remains intact, listening is less exhausting for most patients. Additionally, eye movements are getting more and more tiring with progressing disease. The high accuracies throughout studies support acoustic BCIs as promising tools [20] [28]. However, what should be kept in mind regarding this development is the opinion of the users. For example binaurally presented beep sounds are judged as unpleasant by participants [20] and also in the present study participants rated the paradigm presenting binaural acoustic stimuli as less appealing than the "Memory" one. Yet, the results presented here correspond to the performance and opinion of a sample of healthy subjects with no memory impairment. Until tested on an ALS patient sample, it is not clear if this pattern of results will be replicated in this special group of subjects with completely different preconditions. It is important for future research to pay attention to crucial differences between populations to be able to transfer results to target groups and develop assistive devices that can improve patients everyday life.

ACKNOWLEDGMENTS

Special thanks to Bernd Battes for his immense help with the experimental setup.

REFERENCES

[1] A. Kübler, F. Nijboer, J. Mellinger, T. M. Vaughan, H. Pawelzik, G. Schalk, et al., "Patients with ALS can use sensorimotor rhythms to operate a brain-computer interface," *Neurology*, vol. 64, no. 10, pp. 1775–1777, 2005.

[2] T. Fomina, G. Lohmann, M. Erb, T. Ethofer, B. Schölkopf and M. Grosse-Wentrup, "Self-regulation of brain rhythms in the precuneus: A novel BCI paradigm for patients with ALS," *Journal of Neural Engineering*, 2016.

[3] M. A. Lebedev and M. A. Nicolelis, "Brain–machine interfaces: past, present and future," *Trends in Neurosciences*, vol. 29, no. 9, pp. 536–546, 2006.

[4] K. Nihei, A. C. McKee, and N. W. Kowall, "Patterns of neuronal degeneration in the motor cortex of amyotrophic lateral sclerosis patients," *Acta Neuropathologica*, vol. 86, no. 1, pp. 55–64, 1993.

[5] L. Jacobs, D. Bozian, R. R. Heffner, and S. A. Barron, "An eye movement disorder in amyotrophic lateral sclerosis," *Neurology*, vol. 31, no. 10, p. 1282, 1981.

[6] M. Marchetti and K. Priftis, "Brain-computer interfaces in amyotrophic lateral sclerosis: A metanalysis," *Clinical Neurophysiology : Official Journal of the International Federation of Clinical Neurophysiology*, vol. 126, no. 6, pp. 1255–1263, 2015.

[7] M. R. Hohmann, T. Fomina, V. Jayaram, N. Widmann, C. Förster, J. Just, et al., "A cognitive brain–computer interface for patients with amyotrophic lateral sclerosis," *Progress in Brain Research*, vol. 228, pp. 221–239, 2016.

[8] M. R. Hohmann, T. Fomina, V. Jayaram, C. Förster, J. Just, M. Synofzik, et al., "An improved cog-

Published by Verlag der TU Graz
Graz University of Technology

 DOI: 10.3217/978-3-85125-533-1-60

nitive brain-computer interface for patients with amyotrophic lateral sclerosis," in *the International Brain-Computer Interface (BCI) Meeting, Asilomar, United States*, 2016.

[9] H. Kim, "A dual-subsystem model of the brain's default network: self-referential processing, memory retrieval processes, and autobiographical memory retrieval," *NeuroImage*, vol. 61, no. 4, pp. 966–977, 2012.

[10] M. C. Mantovan, L. Baggio, G. Dalla Barba, P. Smith, E. Pegoraro, G. Soraru, et al., "Memory deficits and retrieval processes in ALS1," *European Journal of Neurology*, vol. 10, no. 3, pp. 221–227, 2003.

[11] F. Portet, C. Cadilhac, J. Touchon, and W. Camu, "Cognitive impairment in motor neuron disease with bulbar onset," *Amyotrophic Lateral Sclerosis and Other Motor Neuron Disorders*, vol. 2, no. 1, pp. 23–29, 2001.

[12] S. Abrahams, L. H. Goldstein, J. J. M. Kew, D. J. Brooks, C. M. Lloyd, C. D. Frith, et al., "Frontal lobe dysfunction in amyotrophic lateral sclerosis," *Brain*, vol. 119, no. 6, pp. 2105–2120, 1996.

[13] S. Abrahams, L. H. Goldstein, J. Suckling, V. Ng, A. Simmons, X. Chitnis, et al., "Frontotemporal white matter changes in amyotrophic lateral sclerosis," *Journal of Neurology*, vol. 252, no. 3, pp. 321–331, 2005.

[14] A., Vanhaudenhuyse, Q. Noirhomme, L. J-F. Tshibanda, M-A. Bruno, P. Boveroux, C. Schnakers, et al., "Default network connectivity reflects the level of consciousness in non-communicative brain-damaged patients," *Brain : A Journal of Neurology*, vol. 133, no. Pt 1, pp. 161–171, 2010.

[15] R. L. Buckner, J. R. Andrews-Hanna, and D. L. Schacter, "The brain's default network," *Annals of the New York Academy of Sciences*, vol. 1124, no. 1, pp. 1–38, 2008.

[16] G. G. Knyazev, "EEG correlates of self-referential processing," *Frontiers in Human Neuroscience*, vol. 7, p. 264, 2013.

[17] Y. Mu and S. Han, "Neural oscillations involved in self-referential processing," *NeuroImage*, vol. 53, no. 2, pp. 757–768, 2010.

[18] M. D. Greicius, B. Krasnow, A. L. Reiss and V. Menon, "Functional connectivity in the resting brain: a network analysis of the default mode hypothesis," *Proceedings of the National Academy of Sciences*, no. 100(1), pp. 253–258, 2003.

[19] P. Fransson and G. Marrelec, "The precuneus/posterior cingulate cortex plays a pivotal role in the default mode network: Evidence from a partial correlation network analysis," *NeuroImage*, vol. 42, no. 3, pp. 1178–1184, 2008.

[20] N.J. Hill, E. Ricci, S. Haider, L. M. McCane, S. Heckman, J. R. Wolpaw, et al., "A practical, intuitive brain-computer interface for communicating 'yes' or 'no' by listening," *Journal of Neural Engineering*, vol. 11, no. 3, p. 35003, 2014.

[21] J. A. O'Sullivan, A. J. Power, N. Mesgarani, S. Rajaram, J. J. Foxe, B. G. Shinn-Cunningham, et al., "Attentional selection in a cocktail party environment can be decoded from single-trial EEG]," *Cerebral Cortex (New York, N.Y. : 1991)*, vol. 25, no. 7, pp. 1697–1706, 2015.

[22] G. Schalk, D. J. McFarland, T. Hinterberger, N. Birbaumer, and J. R. Wolpaw, "BCI2000: a general-purpose brain-computer interface (BCI) system," *IEEE Transactions on Bio-medical Engineering*, vol. 51, no. 6, pp. 1034–1043, 2004.

[23] V. Jayaram, M. Alamgir, Y. Altun, B. Scholkopf, and M. Grosse-Wentrup, "Transfer learning in brain-computer interfaces," *IEEE Computational Intelligence Magazine*, vol. 11, no. 1, pp. 20–31, 2016.

[24] S. Haufe, F. Meinecke, K. Görgen, S. Dähne, J-D. Haynes, B. Blankertz, et al., "On the interpretation of weight vectors of linear models in multivariate neuroimaging," *NeuroImage*, vol. 87, pp. 96–110, 2014.

[25] M. Grosse-Wentrup, S. Harmeling, T. Zander, J. Hill, and B. Schölkopf, "How to test the quality of reconstructed sources in independent component analysis (ICA) of EEG/MEG data," in *Pattern Recognition in Neuroimaging (PRNI), 2013 International Workshop on*. IEEE, 2013, pp. 102–105.

[26] B. Blankertz, C. Sannelli, S. Halder, E. M. Hammer, A. Kübler, K-R. Müller, et al., "Neurophysiological predictor of SMR-based BCI performance," *NeuroImage*, vol. 51, no. 4, pp. 1303–1309, 2010.

[27] N. H. A. Hamid, N. Sulaiman, S. A. M. Aris, Z. H. Murat, and M. N. Taib, "Evaluation of human stress using eeg power spectrum," in *Signal Processing and Its Applications (CSPA), 2010 6th International Colloquium on*. IEEE, 2010, pp. 1–4.

[28] N. J. Hill and B. Schölkopf, "An online brain-computer interface based on shifting attention to concurrent streams of auditory stimuli," *Journal of Neural Engineering*, vol. 9, no. 2, p. 26011, 2012.

Published by Verlag der TU Graz
Graz University of Technology

Proceedings of the
7th Graz Brain-Computer Interface Conference 2017 DOI: 10.3217/978-3-85125-533-1-61

TOWARDS ELABORATED FEEDBACK FOR TRAINING MOTOR IMAGERY BRAIN COMPUTER INTERFACES

M. Mousavi[1], V. R. de Sa[2]

[1]Department of Electrical and Computer Engineering, University of California, San Diego
[2]Department of Cognitive Science, University of California, San Diego, La Jolla, CA, USA

E-mail: mahta@ucsd.edu

ABSTRACT: Motor imagery is one common paradigm in brain computer interface (BCI) systems where the user imagines moving a part of his/her body to control a computer. Motor imagery is endogenous and requires a large amount of training for the user to be able to control the BCI. Therefore, the feedback that is provided to the user is critical to ensure informative insight into improving imagery skills. In this study, we investigate a new protocol for providing motor imagery feedback and compare it to the conventional feedback scheme. The proposed feedback focuses on 'elaborating' how the user can improve imagery as opposed to the conventional training protocols which only provide information on whether the user was 'correct' in performing imagery. Our results show that providing more easily interpretable feedback results in more efficient motor imagery training and is preferred by the users.

INTRODUCTION

Brain computer interface (BCI) systems attempt to infer certain cognitive or affective states based on neural signals collected from the brain while bypassing common neuromuscular pathways [1, 2]. One modality to collect brain signals is electroencephalography (EEG) which is popular for being non-invasive and inexpensive. Motor imagery is one common paradigm in EEG-based BCIs in which the user imagines moving a part of her/his body, such as a hand, foot, tongue, etc. Motor imagery of different body parts results in different spatial patterns of decrease in power across the scalp in mu (8-13 Hz) and beta (14-30 Hz) frequency bands [3, 4, 7, 8]. These features are used to distinguish among the imagined classes.

One of the advantages of motor imagery based BCIs is that they are endogenous [5]; they do not depend on user response to external stimulation. Endogenous BCIs have several benefits: 1) They do not require the user to have good visual or other sensory responses to respond to exogenous stimuli, 2) They do not require the computer presentation of (possibly annoying or fatiguing) stimuli, and 3) They have the potential to be used in natural asynchronous communication. However, because they are endogenous and depend on the user generating the signal, there are large individual differences in the ability to generate different discriminable motor imagery patterns for different imagined body parts. Therefore, training users to provide classifiable motor imagery signals is critical.

So far, there have been a few training methods proposed in the literature, e.g. [9–14]. Lotte et al. [15] investigated the current state-of-the-art training approaches and identified flaws in their design based on instructional design literature. They looked at the training approaches at the level of feedback provided to the user, instructions provided to her/him and the task itself. Our current study focuses on the feedback that the user receives. In traditional motor imagery BCI training, the feedback provided to the user is evaluative and corrective, where it only tells the user whether he/she has performed the task correctly and possibly with what confidence [15]. In other words, traditional motor imagery training involves giving the user feedback on the output of the classification. When classification is unsuccessful, however, this feedback does not provide any information about why it failed. For example, participants may fail to be successful at right hand vs. left hand motor imagery because they do not induce sufficient mu-desynchronization or the induced desynchronization is bilateral for both right- and left-hand motor imagery.

Motivated by work of [6] we hypothesized that providing richer feedback while users are learning motor imagery would result in faster and better learning. To do so, we decided to provide the users with not just the classification output and its confidence, but a perceivable form of features that are used by the classifier. In other words, our proposed feedback is an example of 'elaborated feedback' as described by [25], where it will provide more easily interpretable feedback and will let users evaluate their performance based on the input to the classifier.

METHODS

We recorded data from 6 healthy participants recruited from the UC San Diego student population. All participants were naive to BCI and motor imagery skills and before participating in the study, signed a consent form that was approved by UC San Diego Institutional Review Board. The demographic details of the participants (i.e., age, gender and handedness) are specified in Tab. 1.

Each participant participated in a one-session experiment consisting of 5 blocks, each consisting of 20 motor im-

Published by Verlag der TU Graz
Graz University of Technology

 DOI: 10.3217/978-3-85125-533-1-61

agery trials. Each trial began with an arrow on the screen pointing to the right or the left to specify the trial type. After 1.5 seconds, the arrow disappeared and a cross showed up in the center of the monitor and 1 second later, a term "imagery" on top of the cross appeared. Participants were instructed to begin motor imagery of the corresponding hand (depending on the direction of the arrow) for 3 seconds until the cross disappeared. The participants were instructed to imagine their action of choice so long as it involved a hand movement. Fig. 1 shows an example of the frames shown in one trial. At the end of each trial in blocks 1, 3 and 5, no feedback was provided. In blocks 2 and 4, the conventional and proposed elaborated feedback were provided which will be described next. Participants 1, 2, and 6 were shown the elaborated and conventional feedback in blocks 2 and 4 respectively. Participants 3, 4, and 5 on the other hand, were presented with the conventional feedback in block 2 and elaborated feedback in block 4. This is to balance the order of the provided feedback types.

Table 1: The demographics of participants.

Participant ID	Age	Gender	Handedness
P1	18	Female	Right
P2	18	Female	Right
P3	19	Female	Right
P4	21	Female	Right
P5	21	Male	Right
P6	18	Female	Right

We designed our experiment in python using the python-based Simulation and Neuroscience Application Platform (SNAP) toolbox [20]. In each trial, data were downsampled to 100 Hz and Laplacian filtered [19] to partially compensate for spatially distributed artifacts by subtracting the mean of the four directly neighboring channels from each channel. Next, an FIR filter of order 225 was used to calculate the average of the power in 3 seconds of motor imagery in the 8-13 Hz frequency band for the channels specified over the right and left motor cortices in Fig. 2. The average power in each channel was then normalized with respect to the sum of power in all channels specified in Fig. 2. The conventional feedback was provided as the difference between the power on the two sides and the proposed feedback protocol showed the power on both sides. In each trial, the feedback was provided as a single (static) image after the imagery period was over. Fig. 3 shows an example of the two types of feedback. Since motor imagery results in contra-lateral de-synchronization of power [7, 8] the participants were instructed to maximize the bar height on the motor imagery side.

As the power over motor cortices may be biased towards one side, we trained a threshold to be the average of the difference in the normalized power on right and left sides of the motor cortex across trials of each block. In blocks 2 and 4, the threshold that was trained with trials in blocks 1 and 3 respectively, was used to adjust for the potential bias. Therefore, the provided feedback to the participant was based on the adjusted bar heights.

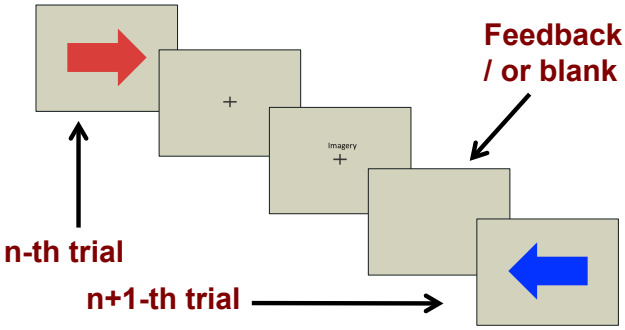

Figure 1: An example of a trial in the experiment.

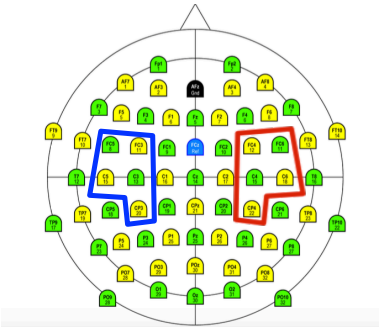

Figure 2: Electrode locations in 10-20 international system EEG cap. The selected electrodes were used to calculate power on each side of the motor cortices.

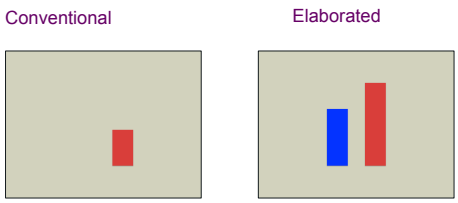

Figure 3: Types of feedback.

EEG data were recorded with a 64-channel BrainAmp system (Brain Products GmbH) located based on the international 10-20 system, as Fig. 2 shows. EMG data were also recorded with the same system through two sets of bipolar electrodes on each arm and wrist — for more details on the set-up please refer to [16]. Data were collected with sampling rate of 5000 Hz but were downsampled to 500 Hz for further processing in offline analysis. We chose 500 Hz instead of 100 Hz — which was the rate of the downsampled signal in the online experiment — to keep information in higher frequencies for the purpose of running independent component analysis (ICA) later.

MATLAB [17] and EEGLAB [18] were used for offline analysis. Data were processed in two cases: 1) without

Published by Verlag der TU Graz
Graz University of Technology

 DOI: 10.3217/978-3-85125-533-1-61

artifact removal to investigate the effect of the feedback that was provided to the participants during the experiment. 2) with artifact removal to investigate the effect of training on brain signals and to verify that the participants are not potentially using facial muscle movements to control the bar heights.

In the first case, the raw data were filtered from 8 to 13 Hz with a 500-tap FIR filter. Laplacian filter [19] was applied to partially compensate for spatially distributed artifacts by subtracting the mean of directly neighboring channels from each channel. We looked at the classifier score of each trial in blocks 2 and 4 where the feedback was present. This score is estimated as follows: first the power on each channel over motor cortices is calculated — as shown in Fig. 2. Then the power on each channel was normalized to the sum of the powers on the specified 10 channels and the average of the power on each side of the motor cortex was used as the classifier score.

We also looked at the classification rates in blocks 1, 3 and 5 where no feedback was provided. To do so, we selected three non-overlapping one-second time windows to cover 3 seconds of imagery period in each trial. Since there are 20 trials in each block, each block has a total of 60 one-second windows of imagery. Next we applied common spatial patterns (CSP) [23] to data from all 64 channels and selected the top 3 filters for each class. Linear discriminant analysis (LDA) [24] was chosen as the classifier to classify right/left imagery classes.

For the second case, we first filtered the raw data using a 500-tap FIR filter in 1 to 200 Hz. Next, we removed up to 6 noisy channels with large muscle artifacts mostly from the temporal and one from the occipital sites. Then the Cleanline EEGLAB plug-in was used to remove the line noise [21]. We removed parts of the EEG data that were suffering from large muscle artifacts; however, no information from the 3 seconds of imagery was removed. We ran independent component analysis (ICA) using the AMICA [22] EEGLAB plug-in to isolate eye and muscle artifacts. Eye and muscle artifacts from the top 30 IC components were removed. Similar analysis to the previous case were performed and the results are described next. Significance in what follows is calculated with a paired-sample two-tailed t-test with 0.05 significance level.

EMG data (4 channels, two on each hand and arm) were bandpass filtered in 10 to 200 Hz using a 500 tap FIR filter, and the line noise was removed with the Cleanline plug-in [21]. EMG data during the three seconds time interval of motor imagery were epoched into non-overlapping one second intervals and used for classification. Results are presented in the next section.

RESULTS

To investigate how the right/left classifier score changes over time, we looked at it as a function of the trial number in blocks 2 and 4. For each participant in each trial, the right/left classifier score is calculated as the ratio of the power on the corresponding side as described in the previous section. A line was fit and the slope of the line was estimated. Fig. 4 shows the slopes calculated in case one (without artifact rejection) as height of the bars in blocks 2 and 4 in separate plots based on whether conventional feedback was provided in block 2 and elaborated in block 4 or vice versa. Fig. 5 shows the same for data from case two (with artifact rejection). Note that P1, P2 and P6 show some improved performance when the elaborated feedback is provided to them — i.e., in block 2. However, they show decreased performance across the trials in block 4 — where conventional feedback was provided subsequently. P3 and P5 who were provided with conventional feedback first in block 2, show decreased performance; however, they both show improved performance during the elaborated feedback in block 4. P4 shows improved performance during both feedback types; however, the improvement is higher in the elaborated feedback block when only brain signals are considered, i.e. in Fig. 5. This shows that the proposed feedback paradigm could potentially be more effective than the conventional feedback.

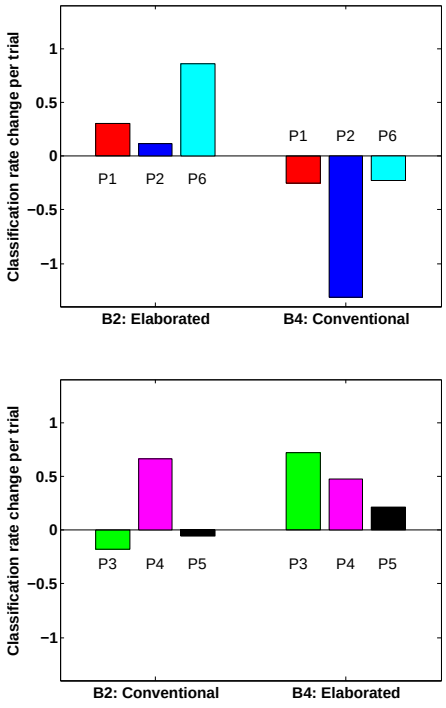

Figure 4: Percent change of classification rate per trial in data during feedback blocks, **without** artifact rejection.

To verify how the percent change in classification rates per trial (i.e. the height of the bars in Fig. 4 and Fig. 5) are different in the two elaborated and conventional feedback conditions among the 6 participants, we ran a paired-sample two-tailed t-test between the bar heights across participants. We found significant difference in both cases with p-values 0.036 and 0.006 for cases one and

Published by Verlag der TU Graz
Graz University of Technology

 DOI: 10.3217/978-3-85125-533-1-61

two respectively — i.e., with and without artifact rejection.

Classification results in no-feedback blocks — 1, 3, and 5 — are provided in tables 2a, 2b, 3a, and 3b. The training and testing were performed within each block separately and we made sure that both train and test sets were balanced and the test set was absolutely separate from the training. We ran 10-fold cross-validation while making sure that the three one second time windows from one trial will appear all in either train or test sets and the results are presented in Tab. 2a and Tab. 2b. For ease of comparison, we have included the type of feedback in blocks 2 and 4 in these tables: EF and CF stand for elaborated feedback and conventional feedback respectively. The first number in each table specifies the mean and the second number is the standard error.

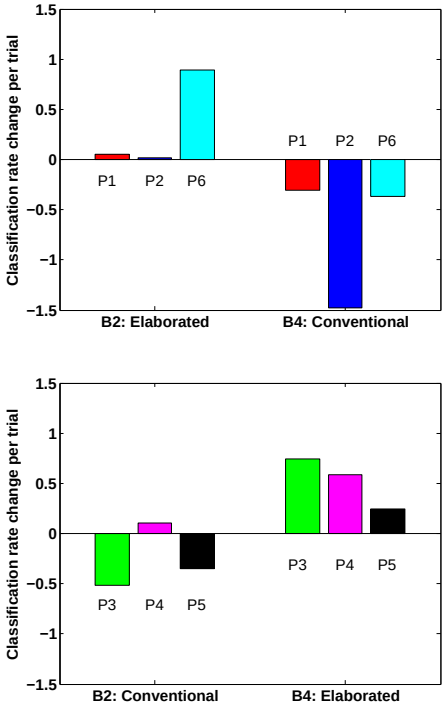

Figure 5: Percent change of classification rate per trial in data during feedback blocks, **with** artifact rejection .

Table 2a: P1, P2, P6 performances **without** artifact rejection

ID	B1	B2	B3	B4	B5
P1	0.58 / 0.048	EF	0.60 / 0.051	CF	0.37 / 0.074
P2	0.73 / 0.051	EF	0.85 / 0.058	CF	0.80 / 0.065
P6	0.75 / 0.057	EF	0.85 / 0.058	CF	0.78 / 0.043

Table 2b: P3, P4, P5 performances **without** artifact rejection.

ID	B1	B2	B3	B4	B5
P3	0.52 / 0.080	CF	0.57 / 0.037	EF	0.65 / 0.063
P4	0.82 / 0.072	CF	0.87 / 0.048	EF	1.00 / 0.000
P5	0.42 / 0.057	CF	0.57 / 0.057	EF	0.52 / 0.052

P1, P2 and P6 were provided with the elaborated feedback in block 2. P2 and P6 show improvement in block 3 compared to block 1 which can be associated with the training they received in block 2; however, this improvement is not significant. These two participants also show decreased performance in block 5 which is right after block 4 where they were provided with the conventional feedback but the decreased performance is not significant. Performance of P1 in all three blocks is below chance level which is calculated as described in [26] to be 62% with significance level of 0.05.

P3, P4 and P5 were provided with conventional feedback in block 2 and elaborated feedback in block 4. P4 shows significant improvement after being exposed to the proposed elaborated feedback in block 4; however, P3 and P5 show chance level performance in all blocks.

To make sure that the classification rates are not affected by non-brain sources including eye and muscle movements, we performed the same analysis described above with the ICA-cleaned data. In this case, we filtered each trial in 8 to 30 Hz frequency band to include both mu (8-13 Hz) and beta (14-30 Hz) frequency bands. The reason we did not include the beta band when we were classifying the non-ICA-cleaned data is that beta band is usually more contaminated with muscle artifacts. After filtering the data, non-overlapping one second time windows were selected and 10-fold cross-validation was performed — while making sure that the three one second time windows from one trial will appear all in either the train or test set — to classify right/left motor imagery in blocks 1, 3, and 5 separately. Tab. 3a and Tab. 3b show the classification results. The first number in each table specifies the mean and the second number is the standard error. For ease of comparison, we have included the type of feedback in blocks 2 and 4 in these tables: EF and CF stand for elaborated feedback and conventional feedback respectively. P3 and P4 who were provided with the conventional feedback first and proposed feedback next, both show significantly improved classification rates in block 5 compared to blocks 1 and 3. Moreover, P3 shows significantly disimproved performance after being exposed to conventional feedback in block 2. On the other hand, P1 and P5 show chance level performance in all of the blocks before and after artifact rejection. P2 and P6 do not show much difference in performance between blocks 3 and 5 after artifact rejection, which was not the case before artifact rejection. It is possible that these participants have been controlling the bars with muscle movements after elaborated feedback not brain signals. Nevertheless, this shows that the elaborated feedback was more effective for the participant to somehow (either through brain signals or muscle) control the bars. Note that since the number of samples in each class is 30, chance level calculated as described in [26] is 62% with significance level of 0.05.

Published by Verlag der TU Graz
Graz University of Technology

 DOI: 10.3217/978-3-85125-533-1-61

Table 3a: P1, P2, P6 performances **with** artifact rejection

ID	B1	B2	B3	B4	B5
P1	0.55 / 0.043	EF	0.55 / 0.056	CF	0.47 / 0.060
P2	0.82 / 0.084	EF	0.85 / 0.046	CF	0.85 / 0.052
P6	0.77 / 0.079	EF	0.85 / 0.058	CF	0.83 / 0.043

Table 3b: P3, P4, P5 performances **with** artifact rejection.

ID	B1	B2	B3	B4	B5
P3	0.68 / 0.052	CF	0.52 / 0.052	EF	0.78 / 0.071
P4	0.80 / 0.074	CF	0.82 / 0.063	EF	1.00 / 0.000
P5	0.43 / 0.051	CF	0.55 / 0.043	EF	0.55 / 0.086

Aside from EEG data, we looked at classification rate of a right/left classifier trained on EMG data in each block. Non-overlapping one second time windows were selected and 10-fold cross-validation was performed — while making sure that the three one second time windows from one trial will appear all in either the train or test set. As Tab. 4 shows, all classification rates are chance level or very close to chance level which is 62% with significance level of 0.05 except for participant 4 in block 3. However, this participant shows improved EEG classification after the elaborated feedback block in which the classification rate on EMG rate is chance level.

Table 4: EMG classification results per block.

ID	B1	B2	B3	B4	B5
P1	0.58	0.57	0.52	0.43	0.68
P2	0.32	0.60	0.57	0.55	0.40
P3	0.55	0.47	0.48	0.47	0.48
P4	0.50	0.43	0.82	0.48	0.48
P5	0.58	0.48	0.53	0.62	0.38
P6	0.52	0.33	0.63	0.68	0.57

DISCUSSION AND CONCLUSION

In this pilot study, we have explored the capability of a visually richer elaborated feedback in training motor imagery BCI and proposed a training protocol that suggests providing the participant the input to the classifier, i.e. an interpretable version of the features that are available to the classification algorithm as opposed to the classifier output. Since any classifier needs data to be trained on and our participants were all naive to motor imagery BCI, we chose to use a very simple classifier, i.e. a threshold, to minimize the effect of instability in a classifier trained with motor imagery data that is changing as the user learns how to control his/her event-related desynchronization signal. All our participants (6/6) chose the elaborated feedback in an answer to a question on the post-study questionnaire: "Which type of feedback did you like better and found more useful?". This shows that the elaborated feedback approach has the potential to replace the standard conventional feedback paradigm for motor imagery training.

Our results from offline analysis show that the elaborated feedback protocol is potentially more powerful in training motor imagery which is expected as described in [25]. In fact, our participants found the proposed feedback more 'informative' which again emphasizes this point.

One downside of the conventional feedback strategies that our proposed protocol could overcome is the need to have the first block of training with no-feedback or sham feedback as there is no data yet to train a classifier on — the conventional feedback is the output of a classifier. The issue occurs if the participant does not provide proper imagery during this time period, then the classifier is trained on 'incorrect' data. Our method provides the features to the user that later could be used to train a classifier on. We propose to use the power on the motor imagery cortices and train a threshold to compensate for biases towards either side. Even if the bias is not compensated for, the participant could still be provided with the power on two sides of motor cortices and be instructed to control the bars towards the ideal bar heights, i.e. suppressed power on left side in right hand motor imagery and suppressed power on right side in left hand motor imagery trials. Hence, our proposed elaborated feedback can function without training data.

To evaluate the elaborated feedback further, we are interested in investigating providing participants with the power on both sides of motor cortices normalized with respect to a 'baseline' time period where the participant is relaxed and not performing motor imagery. Another aspect worth investigating further is how the two approaches differ across multiple sessions and to see whether there is more significant difference between the two schemes when more time elapses between training sessions.

ACKNOWLEDGMENTS

This work was supported by the NSF grants IIS 1219200, SMA 1041755, IIS 1528214, and UCSD FISP G2171.

References

[1] Farwell, Lawrence Ashley, and Emanuel Donchin. "Talking off the top of your head: toward a mental prosthesis utilizing event-related brain potentials." Electroencephalography and clinical Neurophysiology 70.6 (1988): 510-523.

[2] Wolpaw, Jonathan R., Dennis J. McFarland, Gregory W. Neat, and Catherine A. Forneris. "An EEG-based brain-computer interface for cursor control." Electroencephalography and clinical neurophysiology 78, no. 3 (1991): 252-259.

[3] McFarland, Dennis J., Laurie A. Miner, Theresa M. Vaughan, and Jonathan R. Wolpaw. "Mu and beta rhythm topographies during motor imagery and actual movements." Brain topography 12, no. 3 (2000): 177-186.

[4] Pfurtscheller, Gert, and Christa Neuper. "Motor imagery and direct brain-computer communication." Proceedings of the IEEE 89.7 (2001): 1123-1134.

Published by Verlag der TU Graz
Graz University of Technology

 DOI: 10.3217/978-3-85125-533-1-61

[5] Nicolas-Alonso, Luis Fernando, and Jaime Gomez-Gil. "Brain computer interfaces, a review." Sensors 12.2 (2012): 1211-1279.

[6] Jeunet, Camille, Alison Cellard, Sriram Subramanian, Martin Hachet, Bernard N'Kaoua, and Fabien Lotte. "How Well Can We Learn With Standard BCI Training Approaches? A Pilot Study." In 6th International Brain-Computer Interface Conference. 2014.

[7] Pfurtscheller, Gert, C. Brunner, A. Schlögl, and FH Lopes Da Silva. "Mu rhythm (de) synchronization and EEG single-trial classification of different motor imagery tasks." NeuroImage 31, no. 1 (2006): 153-159.

[8] Pineda, Jaime A., B. Z. Allison, and A. Vankov. "The effects of self-movement, observation, and imagination on/spl mu/rhythms and readiness potentials (RP's): toward a brain-computer interface (BCI)." IEEE Transactions on Rehabilitation Engineering 8.2 (2000): 219-222.

[9] Hwang, Han-Jeong, Kiwoon Kwon, and Chang-Hwang Im. "Neurofeedback-based motor imagery training for brain–computer interface (BCI)." Journal of neuroscience methods 179.1 (2009): 150-156.

[10] Mercier-Ganady, Jonathan, Fabien Lotte, Emilie Loup-Escande, Maud Marchal, and Anatole Lécuyer. "The mind-mirror: See your brain in action in your head using eeg and augmented reality." In Virtual Reality (VR), 2014 iEEE, pp. 33-38. IEEE, 2014.

[11] Frey, Jérémy, Renaud Gervais, Stéphanie Fleck, Fabien Lotte, and Martin Hachet. "Teegi: tangible EEG interface." In Proceedings of the 27th annual ACM symposium on User interface software and technology, pp. 301-308. ACM, 2014.

[12] Neuper, Christa, and Gert Pfurtscheller. "Neurofeedback training for BCI control." Brain-Computer Interfaces. Springer Berlin Heidelberg, 2009. 65-78.

[13] Kaufmann, T., J. Williamson, E. Hammer, R. Murray-Smith, and A. Kübler. "Visually multimodal vs. classic unimodal feedback approach for SMR-BCIs: a comparison study." Int. J. Bioelectromagn 13 (2011): 80-81.

[14] J. Faller, C. Vidaurre, T. Solis-Escalante, C. Neuper and R. Scherer, "Autocalibration and Recurrent Adaptation: Towards a Plug and Play Online ERD-BCI," in IEEE Transactions on Neural Systems and Rehabilitation Engineering, vol. 20, no. 3, pp. 313-319, May 2012.

[15] Lotte, Fabien, Florian Larrue, and Christian Mühl. "Flaws in current human training protocols for spontaneous brain-computer interfaces: lessons learned from instructional design," Frontiers, 2013.

[16] Mousavi, Mahta, Adam S. Koerner, Qiong Zhang, Eunho Noh, and Virginia R. de Sa. "Improving motor imagery BCI with user response to feedback." Brain-Computer Interfaces (2017), doi: 10.1080/2326263X.2017.1303253.

[17] MATLAB and Statistics Toolbox Release 2012b, The MathWorks Inc., Natick, Massachusetts, United States (2012).

[18] Delorme, Arnaud, and Scott Makeig. "EEGLAB: an open source toolbox for analysis of single-trial EEG dynamics including independent component analysis." Journal of neuroscience methods 134.1 (2004): 9-21.

[19] McFarland, Dennis J., Lynn M. McCane, Stephen V. David, and Jonathan R. Wolpaw. "Spatial filter selection for EEG-based communication." Electroencephalography and clinical Neurophysiology 103, no. 3 (1997): 386-394.

[20] Available here: `https://github.com/sccn/SNAP`

[21] Mullen T. Nitrc: Cleanline. 2012. Available from: `http://www.nitrc.org/projects/cleanline`.

[22] Palmer, Jason A., Ken Kreutz-Delgado, and Scott Makeig. "AMICA: An adaptive mixture of independent component analyzers with shared components." Swartz Center for Computatonal Neursoscience, University of California San Diego, Tech. Rep (2012).

[23] Blankertz, Benjamin, Ryota Tomioka, Steven Lemm, Motoaki Kawanabe, and K-R. Muller. "Optimizing spatial filters for robust EEG single-trial analysis." IEEE Signal processing magazine 25, no. 1 (2008): 41-56.

[24] Blankertz, Benjamin, Gabriel Curio, and Klaus-Robert Müller. "Classifying single trial EEG: Towards brain computer interfacing." Advances in neural information processing systems 1 (2002): 157-164.

[25] Shute, Valerie J. "Focus on formative feedback." Review of educational research 78, no. 1 (2008): 153-189.

[26] Müller-Putz, Gernot, Reinhold Scherer, Clemens Brunner, Robert Leeb, and Gert Pfurtscheller. "Better than random: a closer look on BCI results." International Journal of Bioelectromagnetism 10, no. EPFL-ARTICLE-164768 (2008): 52-55.

Published by Verlag der TU Graz
Graz University of Technology

Proceedings of the
7th Graz Brain-Computer Interface Conference 2017 DOI: 10.3217/978-3-85125-533-1-62

MOREGRASP: RESTORATION OF UPPER LIMB FUNCTION IN INDIVIDUALS WITH HIGH SPINAL CORD INJURY BY MULTIMODAL NEUROPROSTHESES FOR INTERACTION IN DAILY ACTIVITIES

G.R. Müller-Putz[1], P. Ofner[1], A. Schwarz[1], J. Pereira[1], G. Luzhnica[2], C. di Sciascio[2], E. Veas[2], S. Stein[3], J. Williamson[3], R. Murray-Smith[3], C. Escolano[4], L. Montesano[4], B. Hessing[5], M. Schneiders[5], R. Rupp[5]

1 Institute of Neural Engineering, Graz University of Technology, Graz, Austria
2 Know-Center GmbH, Graz, Austria
3 IDI Group, University of Glasgow, Glasgow, United Kingdom
4 Bit&Brain Technologies, Zaragoza, Spain
5 University Hospital Heidelberg – Spinal Cord Injury Center, Heidelberg, Germany

E-mail: gernot.mueller@tugraz.at

ABSTRACT:

The aim of the MoreGrasp project is to develop a non-invasive, multimodal user interface including a brain-computer interface (BCI) for intuitive control of a grasp neuroprosthesis to support individuals with high spinal cord injury (SCI) in everyday activities. We describe the current state of the project, including the EEG system, preliminary results of natural movements decoding in people with SCI, the new electrode concept for the grasp neuroprosthesis, the shared control architecture behind the system and the implementation of a user-centered design.

INTRODUCTION

In Europe, there are 11,000 new cases of SCIs per year with a total population of 330,000 [1]. More than half of the individuals with SCI are tetraplegic, meaning that they not only suffer from paralysis of the lower but also of the upper extremities. The bilateral loss of hand function with its associated dependency on caregivers result in a tremendous decrease of quality of life and represent a major barrier for inclusion in professional and social life. Besides the burden for each affected individual, the consequences of a high SCI also have a substantial impact on the healthcare system.

Motor neuroprosthesis, systems based on functional electrical stimulation (FES), can be used to restore lost functions in particular of the grasp function. Basic grasp patterns such as the palmar or lateral grasp can be re-established by positioning FES electrodes on dedicated positions on the forearm of an end user [2]. For the control of such systems mainly the contralateral shoulder can be used, if there are enough residual voluntary movements present. This only works if the shoulder function is not restricted at all. If the shoulder control cannot be used, a BCI offers an alternative to implement a simple grasp control by the detection of imagination of movements [3, 4, 5, 6]. Most of the studies in the field are single case studies that show the feasibility of coupling BCI with FES. However, up to now no BCI-controlled neuroprosthesis has showed its successful use in the everyday life of potential end users. To overcome this situation, the European collaborative project MoreGrasp aims at the following objectives:

(O1) development of novel multimodal user interfaces based on noninvasive BCIs, which detect intentions of various hand movements from EEG using gel-less electrodes and wireless amplifiers.

(O2) development of a sophisticated noninvasive multichannel motor and sensory grasp neuroprosthesis including the integration of orientation, position and force sensors and implementation of haptic feedback as well as a closed-loop control concept for semi-autonomous operation.

(O3) implementation of the concept of personalization and user-centered design.

(O4) setup of a web-based service infrastructure by a registration and matchmaking platform for the assessment of priorities of individuals with disabilities; screening of potential users' functional, neurological and personal status with a specific evaluation toolkit; documentation of the BCI and FES performance and evaluation of the training of end users with a training toolkit.

(O5) evaluation of the novel technology with a long-term clinical study with end users in real need of a grasp neuroprosthesis to demonstrate its reliability, usefulness and impact on the end users' quality of life.

MATERALS AND METHODS

EEG Amplifier: From the EEG recording technology point of view, the MoreGrasp project final objective is to develop easy-to-use, wearable, ergonomic and comfortable systems that can be used over an extended

Published by Verlag der TU Graz
Graz University of Technology

 DOI: 10.3217/978-3-85125-533-1-62

period of time in everyday conditions. One of the main ways to increase user friendliness is to abandon gel-based electrodes. To achieve this goal, MoreGrasp is developing three EEG systems. The first two systems use water–based electrodes and will be integrated in the evaluation toolkit (32-channel amplifier) for screening and in the mobile toolkit (16-channel one) for training. Fig. 1 shows both amplifiers. They record EEG with a sampling rate of 256 Hz, 24-bit, RMS noise under 1µV, input range ±100 mV and [0,40] Hz bandwidth. The dimensions of the 16-channel amplifier are 78x72x32 mm and weighs 125g. The 32-channel version is a little bit larger (107x72x32 mm) with a weight of 164g. They are designed to be carried on the cap, or attached to the upper arm or the wheelchair. They have Bluetooth connectivity and include an inertial measurement unit (IMU) to measure motions during operation, one digital input, one photodiode input and, in the case of the 32-channel system, 2 extra ExGs inputs.

The third system will be used to evaluate the control of the final system using dry electrodes. It is still under development and will integrate as few sensors as possible placed in those locations that optimize the control of the MoreGrasp system. This cap will have the amplifier integrated within a small and light support structure. With the current prototypes, a setup and time-to-signal well under four minutes for 12 sensors is possible. Signal-to noise-ratio is not as good as water-based systems, but preliminary tests have shown that the brain processes required for MoreGrasp can be measured (motor-related cortical potentials (MRCPs), error potentials and sensorimotor rhythms). Fig. 2 shows MRCPs and ERD/S measured with the dry technology.

Figure 1: 32- and 16-channel MoreGrasp amplifiers (left). 16-channel system with the sensors and amplifier on a commercial cap (right).

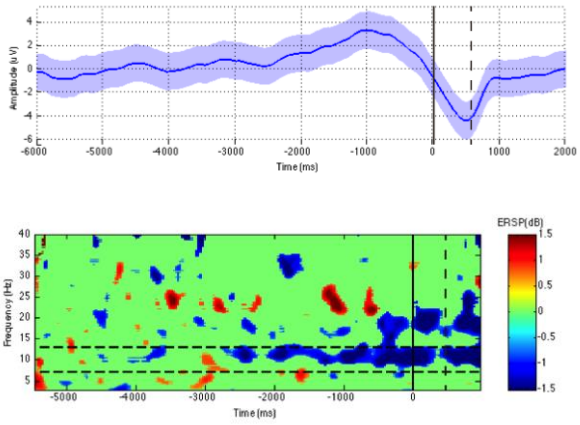

Figure 2: MRCPs measurements (top) and ERD/S (bottom) during self-paced grasping of able-bodied subjects. Results show the average EEG patterns of 10 subjects (100 trials each), measured in CP1 location. The dashed vertical line shows the EMG onset.

Decoding of natural movements with EEG:

CLASSIFICATION OF SINGLE JOINT MOVEMENTS: Based on EEG signals from 0.3 to 3 Hz, we found 6 different upper-limb movements to be discriminable with a classification accuracy of 37% in a group of 15 able-bodied subjects. The classifier sources originated mainly from premotor and primary motor areas.

CLASSIFICATION OF DIFFERENT GRASP TYPES: We conducted an EEG study in 15 able-bodied subjects to find out whether palmar, pinch and lateral grasps can be discriminated from each other and from a no-movement condition. Our results show that time-domain features located in the low frequency range provide sufficient information for classification (binary classification of 74% grasp vs. grasp).

CLASSIFICATION RESULTS IN SCI PATIENTS: Based on the previous results on able-bodied subjects [7], we conducted preliminary studies in a clinical environment with individuals with SCI (see Tab. 1). EEG was obtained from 61 channels covering frontal, central, parietal and temporal areas using active gel-based electrodes (g.tec medical engineering GmbH, Austria). The reference electrode was placed on the right mastoid, ground on AFz. We used an 8th order Chebyshev bandpass filter from 0.01 Hz to 200 Hz and sampled with 512 Hz. Power line interference was suppressed with a notch filter at 50 Hz. We downsampled the data to 32 Hz, removed artifacts based on statistical methods, and bandpass filtered the data with an 4th order zero-lag Butterworth filter from 0.3 to 3 Hz.

Table 1: Neurological and functional characteristics of the participants with SCI. EU = end user, NLI = neurological level of injury, AIS = American Spinal Injury Association (ASIA) impairment scale.

EU	NLI	AIS	Status of upper extremity motor function
P1	C3	D	rudimentary grasps
P2	C5	B	Little finger and hand function right hand
P3	C4	B	No finger function in (dominant) hand
P4	C4	C	Little index finger and thumb movements
P5	C3	D	Right: finger function, but no sensory perception Left: no motor function

GRASPS VERSUS PRONATION/SUPINATION (PARADIGM WITH ICON CUES): In this experiment, data of the 5 participants (P1-P5) were recorded while they attempted to perform two different grasp patterns and a rotation of the forearm. Recording was done using a cue-guided paradigm. At second 0 a cross appeared on the screen together with an auditory beep to get the participants'

Published by Verlag der TU Graz
Graz University of Technology

 DOI: 10.3217/978-3-85125-533-1-62

attention. At second 2 a cue indicating the type of movement was shown. This cue consisted in a hand icon in different postures, according to the movement type. The cue was on the screen for 4 seconds. As soon as the cue appeared, the participant was asked to attempt to perform the movement according to these instructions: starting from a neutral, slightly opened hand position, perform a grasp and return to the starting position. For arm rotation, participants were asked to perform a pronation followed by wrist supination.

GRASP PATTERNS VERSUS HAND OPENING (PARADIGM WITH OBJECT CUES): In this experiment, instead of the hand icons explicitly representing the movement types, objects were used as cues. Participants P3 to P5 were asked to perform/attempt the appropriate grasping action for the designated cue. The objects presented and respective instructions were:

1. **Glass** - attempt to perform palmar grasp and release
2. **Spoon** - attempt to perform lateral grasp and release
3. **Glove** - attempt to open your hand with spread fingers like putting on the glove
4. **Bush** - diverse object, just look at it and rest (not used for classification)

The EEG data from both experiments were then classified with a shrinkage regularized linear discriminant analysis (LDA) classifier using the time-lags 0, 100 and 200 ms of the EEG as input. As both experiments comprised 3 classes, we applied a 1-vs-1 classification strategy. The results were then validated with a 10-fold cross-validation.

Fig. 3 shows the classification accuracies of the icon paradigm. The maximum average classification accuracy was 53 % at 2.6 s after trial start. The classification accuracies of the object paradigm can be seen in Fig. 4. The maximum average classification accuracy was 57 % at 2.6 s after trial start. Fig. 5 and Fig. 6 show the MRCPs.

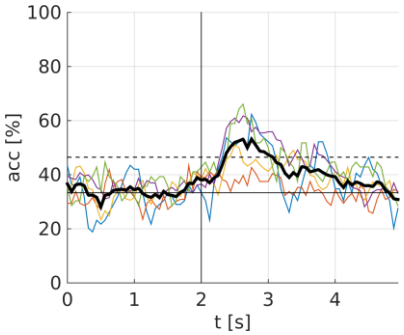

Figure 3: Classification accuracies of 5 EUs with SCI for grasps and pronation/supination (icon paradigm). The dashed line is the significance level.

New electrode concept for the grasp neuroprosthesis: Apparent disadvantages of todays grasp neuroprostheses based on a set of single surface electrodes include difficulties with daily reproduction of the desired movements and large variations in finger and thumb movements during wrist rotations due to electrode-skin shifts.

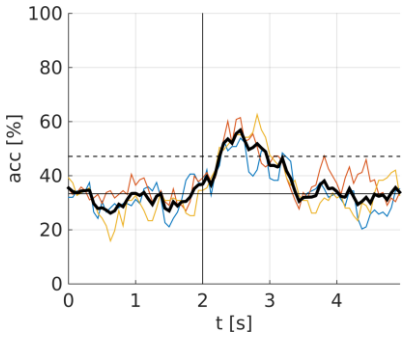

Figure 4: Classification accuracies of 3 EUs with SCI for grasps and hand open (object paradigm). The dashed line represents the significance level.

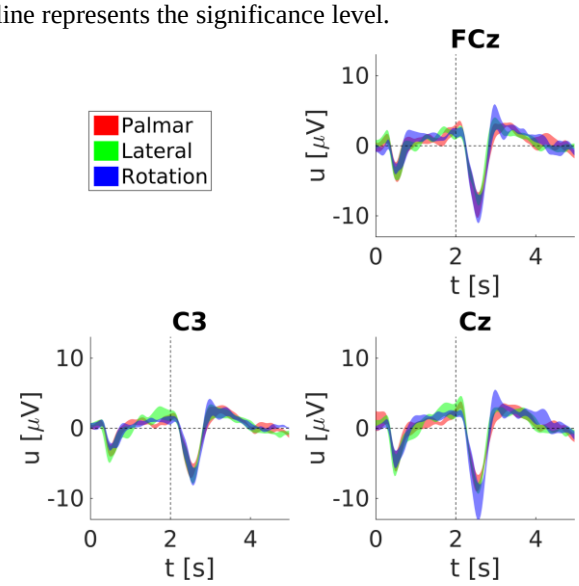

Figure 5: MRCPs evolving in the icon paradigm.

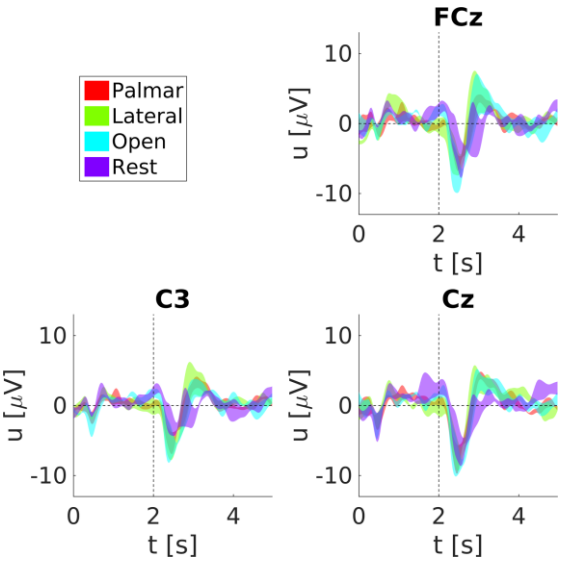

Figure 6: MRCPs evolving in the object paradigm.

In MoreGrasp, an electrode array has been developed, which consists of up to 64 electrodes integrated into a forearm sleeve (Fig. 7), which is personalized to the anatomy of each individual end user. The first prototype

Published by Verlag der TU Graz
Graz University of Technology

 DOI: 10.3217/978-3-85125-533-1-62

consists of a sleeve made from medical-grade silicon, in which an electrode array made from conductive silicon material is embedded. In the final version, the silicon array electrodes will be integrated into a textile sleeve to improve handling and comfort in particular in respect to sweating. The electrodes of the array can be electronically merged to larger electrode clusters according to context-specific demands such as varying wrist rotation angles. For measurement of the wrist angle a set of position and orientation sensors (IMUs) have been integrated in the electrode sleeve to allow for automatic adjustment of stimulation schemes (selection of electrodes, amplitudes) according to the sensor data.
With this approach, we have shown in two able-bodied subjects that dynamic electrode and skin shifts during operation can be compensated and a stable grasp pattern can be achieved.
Another important issue for users is to have feedback from the neuroprosthesis to perform fine motor tasks. Foil force sensors attached to everyday objects will allow for measurement of grip forces. Data of grip forces will be transmitted by a Low Energy (LE)-Bluetooth module to a central control unit, where a semi-autonomous grasp control can be implemented. By assignment of unique identifiers to different Bluetooth modules an automated selection of an object-dependent grasp pattern is possible. If the user moves her or his hand near the object of interest, the neuroprosthesis will automatically switch to the grasp pattern predefined for this object. By using additional FES electrodes in parts of the body with preserved sensation, e.g., the upper arm or the upper torso, electrotactile feedback about the applied grip forces will be provided to the end user.

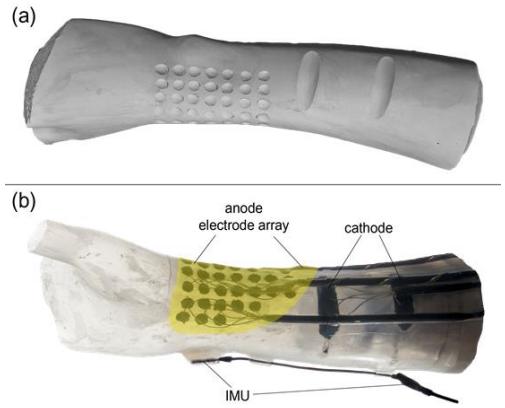

Figure 7: First prototype of a multi-electrode forearm electrode sleeve. (a) individual gypsum model of the forearm with electrode cavities, (b) prototype of personalized arm sleeve made from non-conductive medical silicon with integrated conductive silicon electrodes and cables, and Inertial Measurement Units (IMUs) for measurement of the wrist and elbow position and calculation of the wrist rotation angle.

Shared control principles: Successful FES-supported grasping requires continuous, real-time control, but existing neuroprostheses are driven by low-bandwidth, constrained input channels such as an EEG-based BCI or a shoulder position sensor. Efficient interfaces are required that maximize the control of these channels with minimum effort. Environmental sensing can be used to gather broader context about reaching and grasping tasks, and has the potential to empower users to conduct everyday tasks through the limited control channels available. Therefore, we developed a shared control architecture for the MoreGrasp project. The aim is to maximize grasping performance with minimum user effort by supporting human control processes with environmental sensing. The development of our shared control architecture was driven by the following principles: the system should be able to reason under the uncertainty of noisy and ambiguous input; to gracefully handle sensor failure; and to respond safely to emergency situations.
The proposed shared control architecture has a set of loosely coupled, configurable elements as illustrated in Fig. 8 (top panel). A sensor encoder unit estimates the probabilities of binary events such as “is the hand close enough to an object to grasp?”, “is the user activating the shoulder joystick?”, and “is the BCI indicating an intended wrist rotation?” from sensor feature vectors. A Bayesian network with binary nodes estimates the intention of the user in terms of discrete FES stimulation outcomes, and the certainty of that estimate. User feedback from this unit indicates prediction of user intentions. An action-state-machine monitors the probability of actions, and switches between activity states (e.g. “begin open grasp fully now”) when probability thresholds are crossed. Outputs affecting the estimation of intention (e.g. “the user is unlikely to release grasp 5 ms after opening it”) are fed back to the Bayesian network. User feedback from this unit indicates prediction of future actions. A continuous dynamics module generates the signals to open/close, rotate or reconfigure the hand smoothly when the action-state-machine indicates a change of state, separating the synthesis of continuous values from underlying discrete states. Direct feedback from the sleeve inertial sensing will be used for closed-loop control in this module. The “emergency stop” estimator feeds directly in here to override all pattern generation and return safely and quickly to a neutral state. The electrode pattern generator generates appropriate FES patterns across the electrode array to satisfy the continuous dynamics required.
The system is fully probabilistic between the sensor input vectors and the action-state-machine, which makes it practical to support sensors with widely-varying reliability and also to provide meaningful feedback about inferred user intentions. It is feasible to reason about the intention decoding process because of our simplifying assumptions that (i) intention can be mapped onto a set of (unknown) latent binary variables, (ii) that actions can be seen as transitions in a finite-state machine (iii) continuous closed-loop physical output can be generated from discrete internal transitions. The factorization of the decoding/control process allows different elements of behavior to be

Published by Verlag der TU Graz
Graz University of Technology

 DOI: 10.3217/978-3-85125-533-1-62

implemented by altering the Bayesian Network, without interfering with the optimization of electrode patterns or the continuous-time dynamics. Each of the pipeline elements can be developed with a significant degree of independence; for example, the electrode pattern generator can be optimized automatically without changing the sensor interpretation model. This framework is also flexible enough to support interaction spread over time. For example, a grasp may be "cued" by the BCI in advance and only executed when the probability of being close enough to an object is sufficiently high. Alternatively, the BCI could immediately issue commands, but be "locked out" by holding the shoulder joystick high to suppress control. Estimates of both local reliability (per-command) and general reliability (e.g. tiredness detection) from the BCI can be encoded as rules in the Bayesian network to support control across the full spectrum of signal quality. User feedback via electrotactile (primary) and audio/visual (secondary) channels includes the system's estimate of what the user is trying to do (intention); the certainty of that intention (reliability); and the prediction of the future action sequence that is going to occur imminently (predicted action). Simple feedback, like "countdown" style displays on LED strips or via electrotactile, can be used alongside display modes that show the uncertainty or "tension" within the inference engine.

Appraisal, Monitoring and Training Services: As has been described already, the MoreGrasp system comprises a range of complex devices and subsystems that must work in harmony to accomplish the desired task: restoring autonomy in grasp function. To benefit from it, users need to learn the skills to use it.
The consortium emphasizes adoption going beyond proof of concept, and designing a set of services to walk the user from finding out about MoreGrasp, through appraisal, training, customization of the neuroprosthesis, to a practical use.

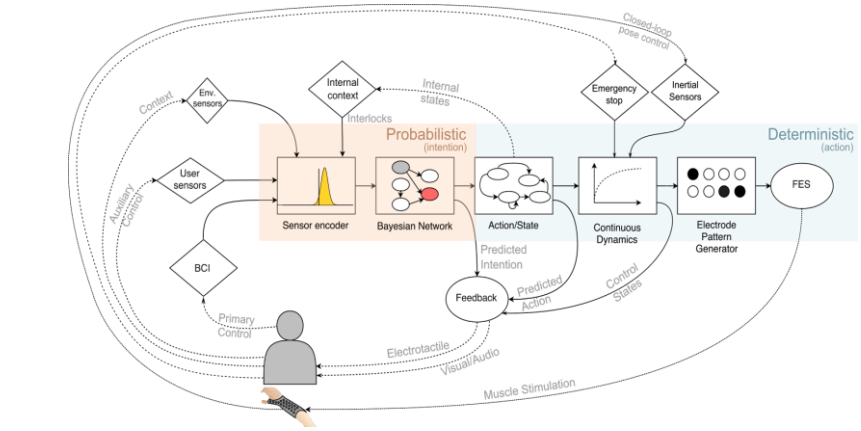

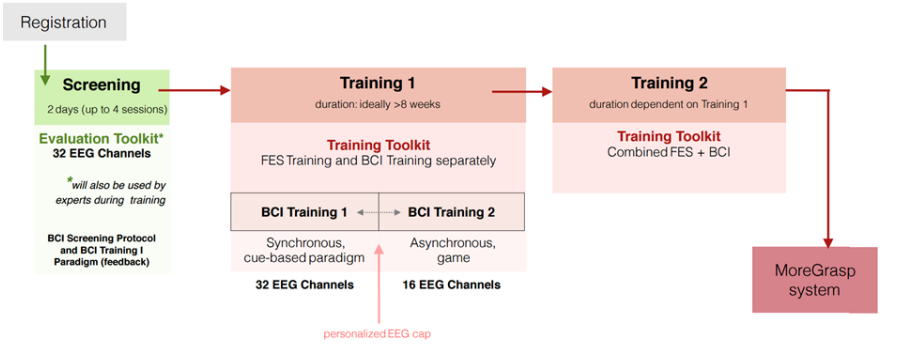

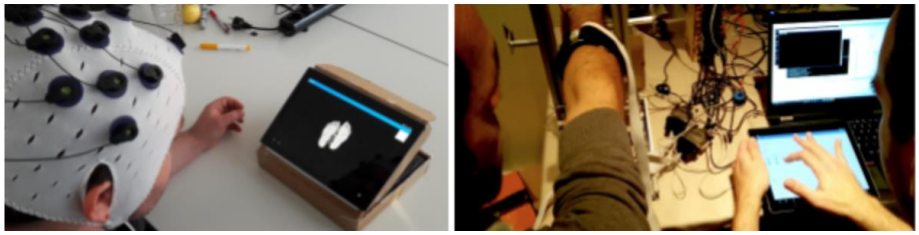

Figure 8: Shared control structure, showing the internal processing pipeline and the user in the loop. A probabilistic intention decoder is connected to a deterministic action synthesizer (top panel). MoreGrasp screening and training schemes leading to the final MoreGrasp system, including FES and BCI and respective stages of use of MET and MTT (middle panel). MET during BCI screening (lower panel, right) and MET during FES screening (lower panel, left).

Published by Verlag der TU Graz
Graz University of Technology

 DOI: 10.3217/978-3-85125-533-1-62

WEB SERVICES FOR DATA COLLECTION AND MONITORING: In the MoreGrasp approach, a potential user with SCI registers, if necessary with the help of a caregiver or relative, on the MoreGrasp registration platform (online since 03.2016). A decision maker is notified to schedule a screening visit with the potential user. He/she uses a matchmaking platform to overview the status of all registered users, filtering by medical pre-injury conditions to assign new users to a screening.
To assess if the potential user can benefit from MoreGrasp, two different screenings need to be performed: a clinical evaluation including a FES screening and a BCI screening. In both cases, an expert brings the hardware to the potential user and, with the aid of a Mobile Evaluation Toolkit, gathers the needed data, which are then used for the decision of study inclusion. A user passing the screening receives an ID and enters a training program. During the months of FES and BCI training the personalized MoreGrasp system is manufactured and is finally delivered to the end user. The systems used during screening and training collect data and seamlessly deliver it to a cloud service for analysis and personalization. These steps are represented in Fig. 8 (middle panel).
THE MOREGRASP MOBILE TOOLKIT: The MoreGrasp system consists of two subsystems: control and presentation. The control subsystem is a self-contained system with a computational unit connected to the EEG and FES systems. It includes algorithms for control, feedback, and data collection modes. A presentation subsystem was developed with interfaces for experts and caregivers to configure the control subsystem for data collection during screening and training. Both subsystems communicate over a private secure network with a proprietary protocol, optimized for streaming. There are two versions of the system with two distinct functions: evaluation (Fig. 8, lower panel) and training.
The mobile evaluation toolkit (MET) is used for evaluation (screening) mainly by experts, who visit a potential end user to acquire data about the user's condition, residual abilities and the possibility for inclusion in the MoreGrasp training programme. Two separate screening steps are carried out: Clinical/FES screening and BCI screening. The clinical screening assesses the clinical and neurophysiological condition of the potential end user as well as the degree of denervated muscles, which cannot be activated by FES. BCI screening assesses the ability of the PU to produce distinct brain patterns by the imagination of movements as a prerequisite for BCI control.
The mobile training toolkit (MTT) is used to tap the residual abilities of the user and turn them into the ability to operate a neuroprosthesis. The MTT is mainly operated by caregivers and relatives. It includes periodic training sessions for FES and BCI. The FES training aims to gradually strengthen the muscles of the end user for grasping. During the BCI training the user is expected to learn how to modulate his/her brain signals to operate the BCI.

CONCLUSION

In its current state the MoreGrasp project has created substantial basic knowledge together with various hard- and software components for a noninvasive, intuitive BCI-controlled motor and sensory grasp neuroprosthesis and the associated services for registration, evaluation and training of end users. In the next few months, a clinical proof-of-concept study will be conducted to obtain information about its impact on everyday life in end users with high SCI and to quantify their perceived changes in quality of life.

ACKNOWLEDGEMENT

This work was supported by the EU ICT Programme Project H2020-643955 MoreGrasp

REFERENCES

[1] Van den Berg ME, Castellote JM, Mahillo-Fernandez I, de Pedro-Cuesta J. Incidence of spinal cord injury worldwide: a systematic review. Neuroepidemiology. 2010 Feb 2;34(3):184-92.
[2] Rupp R, Kreilinger A, Rohm M, Kaiser V, Müller-Putz GR. Development of a non-invasive, multifunctional grasp neuroprosthesis and its evaluation in an individual with a high spinal cord injury, in Proc. EMBC'2012, San Diego, CA, USA, 2012, 1835-1838.
[3] Pfurtscheller G, Müller GR, Pfurtscheller J, Gerner HJ, Rupp R. 'Thought'–control of functional electrical stimulation to restore hand grasp in a patient with tetraplegia. Neuroscience letters. 2003 Nov 6;351(1):33-6.
[4] Müller-Putz GR, Scherer R, Pfurtscheller G, Rupp R. EEG-based neuroprosthesis control: a step towards clinical practice. Neuroscience letters. 2005 Jul 8;382(1):169-74.
[5] Rohm M, Schneiders M, Müller C, Kreilinger A, Kaiser V, Müller-Putz GR, Rupp R. Hybrid brain–computer interfaces and hybrid neuroprostheses for restoration of upper limb functions in individuals with high-level spinal cord injury. Artificial intelligence in medicine. 2013 Oct 31;59(2):133-42.
[6] Rupp R, Rohm M, Schneiders M, Kreilinger A, Müller-Putz GR. Functional rehabilitation of the paralyzed upper extremity after spinal cord injury by noninvasive hybrid neuroprostheses. Proceedings of the IEEE. 2015 Jun;103(6):954-68.
[7] Müller-Putz GR, Schwarz A, Pereira J, Ofner P. From classic motor imagery to complex movement intention decoding: The noninvasive Graz-BCI approach. Progress in brain research. 2016 Dec 31;228:39-70.

Published by Verlag der TU Graz
Graz University of Technology

Proceedings of the
7th Graz Brain-Computer Interface Conference 2017 DOI: 10.3217/978-3-85125-533-1-63

MOVEMENT DECODING FROM EEG: TARGET OR DIRECTION?

G.R. Müller-Putz, L. Peicha, P. Ofner

[1] Institute of Neural Engineering, Graz University of Technology, Graz, Austria

E-mail: gernot.mueller@tugraz.at

ABSTRACT: Arm movements have already been decoded non-invasively from electroencephalography (EEG) signals. In this study we analyzed whether the target or the movement direction of the arm can be decoded from the EEG. Ten healthy subjects executed right arm movements to one out of two targets and simultaneously received feedback on a computer screen. We then inverted the feedback movements to analyze if the EEG carries information about the target or about the movement direction. We found two groups, one encoding the target and one encoding first the movement direction followed by the target. These findings are relevant for the development of future motor neuroprostheses and non-invasive robotic arm control.

INTRODUCTION

Brain-computer interfaces (BCIs) can be used to control neuroprostheses or robotic arms. Together, these technologies allow to restore or replace basic movement function of spinal cord injured (SCI) persons. For example, in [1] a robotic arm was successfully controlled using an invasive BCI. Also non-invasive BCIs based on electroencephalography (EEG) signals can be used to restore movement function in persons with SCI. Our group demonstrated the restoration of grasp function [3], [4] and elbow function [5], [6] with a sensorimotor rhythm (SMR)-based BCI. SMR-based BCIs detect movement imagination (MI) and use it as a control signal. However, the MI itself is often not intuitive (e.g., a foot MI may be used to control the right arm). Furthermore, only the process of imagination can be detected but not the movement itself. For example, imagining squeezing a ball and playing tennis may not be distinguishable with a SMR-based BCI. However, to control a neuroprosthesis in a more natural way or even a robotic arm with its many degrees-of-freedom, more information about the movement needs to be extracted from the EEG. Interestingly, low-frequency EEG signals carry more specific information about the movement and can be used to decode even movement trajectories [7]–[9] or movement directions/targets [10]–[13]. However, the accuracy of a non-invasive movement trajectory decoder is not yet sufficient for real-time control, not to mention the decoding of imagined movement trajectories. The decoding of movement direction or movement target combined with a system which then generates the trajectory may be a more promising approach.

A general issue of studies decoding movement targets is that hand or cursor movements towards a certain target always requires a certain movement direction, i.e. movement targets correspond to movement directions. That blurs the results of such studies because it cannot be determined whether targets or movement directions are being decoded. However, that information is important when training a decoder (e.g., if targets should be shown in the training paradigm). Furthermore, in a real life application there is always a variable number of potential targets. A decoder based on the imagined or attempted movement direction would be independent on the number of targets but not a decoder based on movement targets. To investigate whether a decoder is based on targets or the movement direction, we conducted a study (here with executed movements) where subjects moved their arm to one out of two targets and received feedback on a computer screen. Then, we inverted the feedback and conducted the same number of trials to analyse whether our decoder is based on the movement direction or the movement target. We hypothesize that in case of target decoding, the classification accuracies would be above chance level. Classification accuracies below chance level would indicate the decoding of the movement direction.

MATERIALS AND METHODS

Subjects: For the experiment 10 healthy subjects (one female), all of them right-handed and with normal or corrected-to-normal vision, were recruited. None of them had participated in any prior BCI experiments. They were aged between 25 and 32 (mean 27.7 and SD of 2) years. All of them signed an informed consent.

EEG Measurement: We used 68 passive electrodes covering frontal, central, parietal and temporal areas for recording EEG signals from the scalp. An electrode cap with equidistant electrode positions was used. Also, three electrooculography (EOG) electrodes, positioned above the nasion and below the outer canthi of the eyes were used. Reference was placed on the left mastoid, ground on the right mastoid. All electrode impedances were tried to keep below 5kΩ. An 8-th order Chebyshev band-pass filter from 0.01Hz to 200Hz and a Notch filter at 50Hz was applied. Signals were sampled with

Published by Verlag der TU Graz
Graz University of Technology

 DOI: 10.3217/978-3-85125-533-1-63

512Hz using biosignal amplifiers (g.tec medical engineering GmbH, Austria). Moreover, we measured electrode positions with ELPOS (Zebris Medical GmbH, Germany). EEG, EOG and movement data (3D positions and joint angles of the right arm) were recorded with a customized TOBI Signal Server [14] and Matlab (MathWorks, Massachusetts, USA). For recording the movement data a custom made plugin for the ARMEO Spring software was used.

Experimental Paradigm: Subjects were seated in a chair and their right arm was fixed in an ARMEO Spring rehabilitation device (Hocoma, Switzerland). The ARMEO Spring is basically an exoskeleton and supports the subjects' arm from gravity to prevent muscle fatigue. With the sensors of the ARMEO Spring it is possible to keep track of the hand- and elbow position and joint angles.
For the experiment a self paced center-out reaching task was employed. Subjects moved their right arm from a starting position (about 150 degrees elbow flexion, 60 degrees shoulder flexion and 0 degree abduction in the shoulder joint (see Figure 1)) to one of two targets (red and blue) presented on a computer screen. The red and blue target were positioned in the right upper corner and in the left lower corner, respectively (see Figure 2). The final position for reaching the red target required a 100 degree flexion and 20 degree abduction in the shoulder joint and a 150 degree elbow flexion. For reaching the blue target it was a 60 degree flexion, 20 degree adduction and 30 degree internal rotation in the shoulder joint and a 150 degree elbow flexion. The computer screen also showed an arm model as a visual feedback (see Figure 2). The arm model was previously built with the software MSMS (MDDF, University of Southern California, Los Angeles, California). The model received its joint angles and coordinates from the ARMEO Spring and showed the participants their actual hand-/arm position in real time.
The experiment consisted of two conditions: (i) *normal condition* where the virtual arm on the computer screen moved exactly like the subjects' arm and (ii) *inverted condition* where the virtual arm movements were inverted to real arm movements (i.e. subjects had to move their arm to the opposite target to reach the actual target with the virtual arm).

Figure 1: Experimental setup. A subject connected with the ARMEO Spring, EEG mounted in the position in front of a screen which presents feedback to the subject.

The paradigm is shown in Figure 3. At second 0 an audio cue started a trial by either saying „Red" or „Blue". The subjects got instructed to immediately look at the specific target to avoid eye movements during the reaching phase which could have affected the classification. Three to 5 s after the trial start a beep sounded representing the go cue. The participants got instructed to start their reaching movements to the specific target 1 to 3 s after the go cue. When the virtual arm on the computer screen touched the specific target, a second beep tone sounded serving as a success cue.

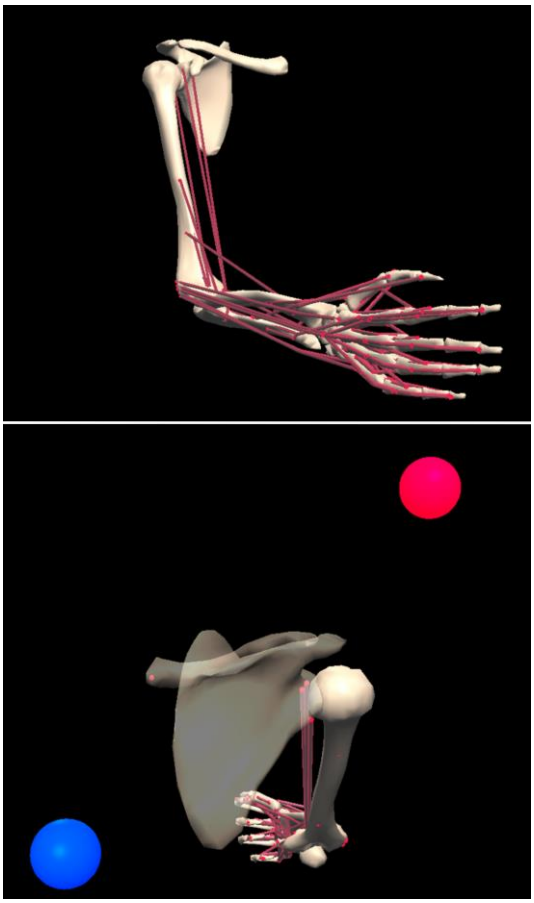

Figure 2: Upper: MSMS arm model, for giving real time feedback to the subjects. Lower: Arm model in experimental setup, i.e. first person view, transparent scapula, all joints in starting position and including both targets

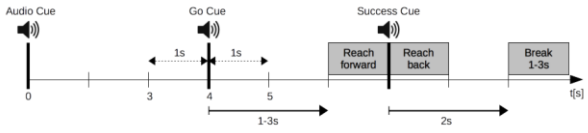

Figure 3: Paradigm and timing of a single trial.

After successfully touching a target subjects moved

Published by Verlag der TU Graz
Graz University of Technology

 DOI: 10.3217/978-3-85125-533-1-63

their arm back to the starting position. The trial ended 2 s after the success cue. After a trial, a break between 1 and 3 s followed. Each run consisted of 30 trials (15 trials for each target, randomly distributed). 12 runs were recorded - 6 for normal condition and 6 for inverted condition, always changing the condition after 2 runs. Thus, in total we recorded 180 trials - 90 trials for each condition. Additionally, we recorded 2 resting state runs and 2 runs with deliberate eye movements (not used in this work).

Signal Processing: We removed trials which were suspected to contain muscle, technical or movement artifacts. Therefore the data got filtered from 0.3Hz to 70Hz (4-th order zero-phase Butterworth filter) and trials that exceeded a threshold of 3 times the standard deviation of the absolute value, Kurtosis or joint probability were excluded from any further processing steps.
For determining the movement onset a principal component analysis (PCA) was done on the x/y/z hand position data recorded by the ARMEO Spring. We differentiated the first principal component and detected a movement onset whenever a certain threshold was crossed after the go cue. The threshold was found empirically.
For calculating the movement-related cortical potentials (MRCPs) a 0.3 Hz - 35 Hz 4-th order zero-phase Butterworth band-pass filter was applied and data segments averaged. MRCPs were calculated for both conditions and electrode positions FCz, C3, Cz and C4.
In order to discriminate between the two red and blue targets, we applied a shrinkage linear discriminant analysis (sLDA) [15] to calculate classification accuracies. A 0.3Hz - 3Hz 4-th order zero-phase Butterworth band-pass filter was applied on the raw EEG data to extract low frequency signals. Subsequently, we downsampled data to 16Hz for computational convenience. We computed the classification accuracy within the time window -2s to 2s relative to movement onset. In one analysis, we classified a moving time window of 750ms using data from all band-pass filtered EEG channels, i.e., we used all EEG data within a window of the past 750ms (12 sample points) and then moved the window one sample further. Classification accuracies were calculated using a 10x10 fold cross-validation. This analysis was separately performed for the normal and inverted condition.
In another analysis, we used the data of the normal condition as training data and the data of the inverted condition for testing in order to find out whether it was target or movement direction decoding.

RESULTS

Classification of directions: Figure 4 and 5 show the classification accuracies for the normal condition and inverted condition, respectively. Classification accuracies are scaled from 0 to 1 and time is relative to the movement onset (=0s). The significance level was 61.35% (α = 0.05, adjusted Wald interval, Bonferroni corrected for the number of shown sample points) [16]. The maximum average classification accuracies were 0.78 (normal) and 0.79 (inverted). Table 1 shows the average movement times to the targets for each condition.

Table 1: average time and standard deviation in seconds to reach red and blue target during normal and inverted condition

Target	Normal cond. [s]	Inverted cond. [s]
Red	1,20 ± 0,65	1,36 ± 0,76
Blue	1,41 ± 0,74	1,10 ± 0,65

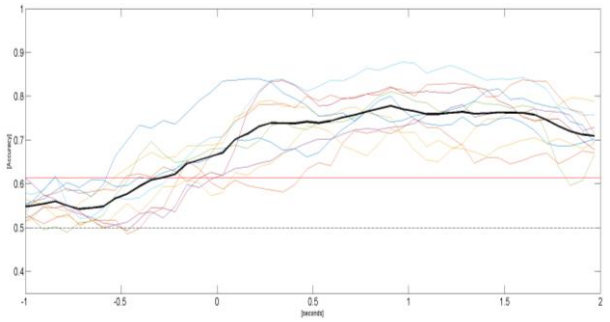

Figure 4: Cross-validated classification accuracies in the normal condition (all subjects and the grand average).

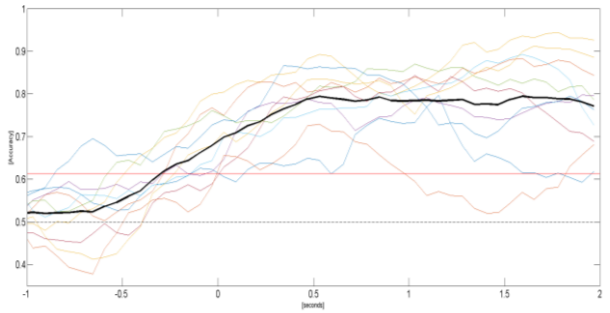

Figure 5: Cross-validated classification accuracies in the normal condition (all subjects and the grand average).

Classification (testing with inverted conditions): We trained the classifier on the normal condition and tested it on the inverted condition. Accuracies below chance level indicate movement direction decoding as hand movements were executed in the opposite direction to the target. Accuracies above chance level indicate target decoding. Two groups arose: group I shows an increasing classification accuracy after the movement onset (Figure 6); group II shows first a decrease of classification accuracy followed by an increase (Figure 7). Time is relative to the movement onset (=0s) and the significance level was 61.35%. The maximum average classification accuracies were 0.71 (group I) and 0.70 (group II).

Published by Verlag der TU Graz
Graz University of Technology

 DOI: 10.3217/978-3-85125-533-1-63

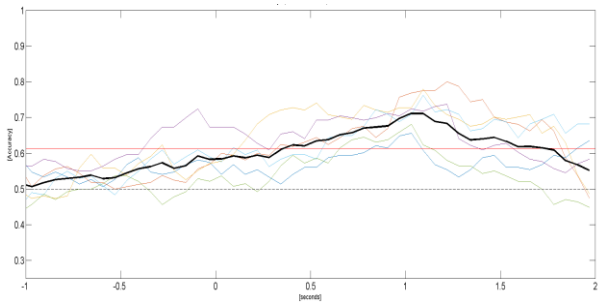

Figure 6: Classification accuracies when training on the normal condition and testing on the inverted condition (group I).

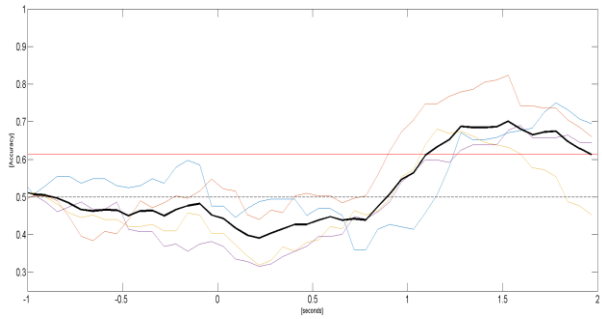

Figure 7: Classification accuracies when training on the normal condition and testing on the inverted condition (group II).

Motor related cortical potentials: Figure 8 and 9 show the MRCPs for the normal and inverted condition, respectively. The figures show the confidence intervals as determined with a bootstrap test ($\alpha = 0.05$) at the electrode positions FCz, C3, Cz and C4. In the normal condition, differences between the two targets are observable at movement onset and around the approach to the target. The inverted condition shows more distinct differences between the targets. These amplitude differences are from ca. 0.5s before movement onset up to 2s after movement onset.

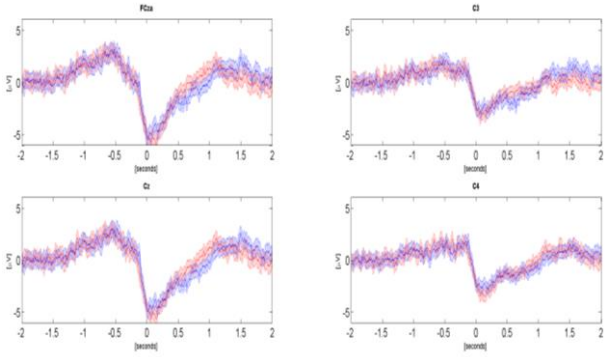

Figure 8: MRCPs evolving in the normal condition. Shown are the MRCPS for both targets (red, blue)

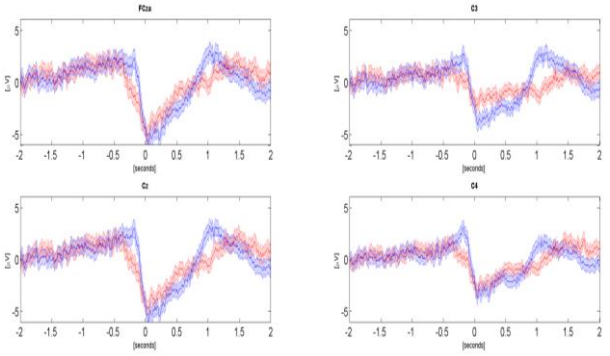

Figure 9: MRCPs evolving in the inverted condition.

DISCUSSION

We demonstrated the decoding of movements to one out of two targets from low-frequency time-domain EEG. Movements were decoded with normal and with inverted feedback. It was possible to decode the movement before movement onset, i.e. in the motor planning phase. Keeping in mind the lag introduced due to the 750ms classification time window, the classification accuracies peaked in the movement execution phase before the targets were reached. Our results are in line with other EEG studies which analyzed time-domain features during movement direction/target decoding [10], [12], [17]. However, also power modulations mostly in low-frequency bands and the high-gamma band have been shown to carry movement direction/target related information [12], [13], [18].

The motivation of our study was to analyze if low-frequency time-domain EEG signals carry information about the movement direction or the target. We did this by inverting the feedback when testing the classifier. In case of target decoding, the classifier would not be affected by the required inversion of movements and classification accuracies would still be above chance level. In case of movement direction decoding, however, the classifier would be affected and classification accuracies would be below chance level, i.e. mirrored around the chance level. Our results can be divided into two groups: in one group the decoder was mainly based on the movement targets, in the other group the decoder first decoded movement directions and then movement targets. This finding has to be considered when novel control systems for future neuroprostheses or robotic arms are developed.

Generally, classification accuracies around the time when the target was reached have to be interpreted with caution. The paradigm was designed to avoid eye movements at movement onset, but subjects may not have suppressed eye movements when approaching a target with the virtual hand as this was a visuomotor task requiring hand-eye coordination. Thus, eye movements may have happened at the end of the reaching movement and the classifier may have picked up the change of the electrical field of the eye dipole.

Published by Verlag der TU Graz
Graz University of Technology

 DOI: 10.3217/978-3-85125-533-1-63

Further analysis has to quantify this effect. Furthermore, systematic differences between the movement times of the two targets may be responsible for the successful classification. Different MRCPs may have been evolved not because of different targets but because of different movement times or movements amplitudes (MRCPs are influenced by movement parameters, e.g. movement speed [19]).

The MRCPs show a typical negative peak around movement onset [19]. The inverted feedback condition was more difficult to the subjects than the normal condition and therefore challenged more the motor planning and the movement execution. This higher difficulty probably enhanced the differences between the MRCPs in the inverted condition. The differences before movement onset correspond to the motor planning and are intrinsic. However, the amplitude differences after movement onset are either due to the execution of a motor plan which accounts for the inverted feedback (intrinsic) or due to different movement profiles (extrinsic), e.g. more correction movements. If the differences are extrinsic in nature, the same differences may evolve in the normal condition with the same altered movement profile.

We report here a study with healthy subjects. Further studies have to confirm if the same effects can be found in persons with SCI.

CONCLUSION

We show the decoding of movements to one out of two targets from low-frequency time-domain EEG. Furthermore, we found evidence that the decoding is based on movement targets but also on the movement direction.

ACKNOWLEDGEMENTS

This work was supported by the EU ICT Programme Project H2020-643955 MoreGrasp, and the ERC Consolidator Grant ERC-681231, Feel Your Reach.

REFERENCES

[1] Hochberg LR, Bacher D, Jarosiewicz B, Masse NY, Simeral JD, Vogel J, et al. Reach and grasp by people with tetraplegia using a neurally controlled robotic arm. Nature. 2012;485(7398):372–5.

[2] Collinger JL, Wodlinger B, Downey JE, Wang W, Tyler-Kabara EC, Weber DJ, et al. High-performance neuroprosthetic control by an individual with tetraplegia. Lancet. 2013; 381(9866):557–64.

[3] Pfurtscheller G, Müller GR, Pfurtscheller J, Gerner HJ, Rupp R. "Thought" – control of functional electrical stimulation to restore hand grasp in a patient with tetraplegia. Neurosci Lett. 2003; 351(1):33–6.

[4] Müller-Putz GR, Scherer R, Pfurtscheller G, Rupp R. EEG-based neuroprosthesis control: a step towards clinical practice. Neurosci Lett. 2005;382(1-2):169–74.

[5] Kreilinger A, Rohm M, Kaiser V, Leeb R, Rupp R, Mueller-Putz GR. Neuroprosthesis Control via a Noninvasive Hybrid Brain-Computer Interface. IEEE Intell Syst. 2013;28(5):40–3.

[6] Rohm M, Schneiders M, Müller C, Kreilinger A, Kaiser V, Müller-Putz GR, et al. Hybrid brain-computer interfaces and hybrid neuroprostheses for restoration of upper limb functions in individuals with high-level spinal cord injury. Artif Intell Med. 2013;59(2):133–42.

[7] Bradberry TJ, Gentili RJ, Contreras-Vidal JL. Reconstructing three-dimensional hand movements from noninvasive electroencephalographic signals. J Neurosci. 2010;30(9):3432–7.

[8] Ofner P, Müller-Putz GR. Decoding of velocities and positions of 3D arm movement from EEG. in Proc. IEEE EMBC 2012. 2012:6406–9.

[9] Ofner P, Müller-Putz GR. Using a noninvasive decoding method to classify rhythmic movement imaginations of the arm in two planes. IEEE Trans Biomed Eng. 2015;62(3):972–81.

[10] Hammon P, Makeig S, Poizner H, Todorov E, De Sa V. Predicting Reaching Targets from Human EEG. IEEE Signal Process Mag. 2008;25(1):69–77.

[11] Wang Y, Makeig S. Decoding Intended Movement from Human EEG in the Posterior Parietal Cortex. Neuroimage. 2009;47:S103.

[12] Lew EYL, Chavarriaga R, Silvoni S, Millán JDR. Single trial prediction of self-paced reaching directions from EEG signals. Front Neurosci. 2014;8:222.

[13] Robinson N, Guan C, Vinod AP, Ang KK, Tee KP. Multi-class EEG classification of voluntary hand movement directions. J Neural Eng. 2013; 10(5):056018.

[14] Breitwieser C, Daly I, Neuper C, Müller-Putz GR. Proposing a standardized protocol for raw biosignal transmission. IEEE Trans Biomed Eng. 2012; 59(3):852–9.

[15] Peck R, Van Ness J. The use of shrinkage estimators in linear discriminant analysis. IEEE Trans Pattern Anal Mach Intell. 1982;4(5):530–7.

[16] Müller-Putz GR, Scherer R, Brunner C, Leeb R, Pfurtscheller G. Better than random? A closer look on BCI results. Int J Bioelectromagn. 2008; 10(1):52–5.

[17] Waldert S, Preissl H, Demandt E, Braun C, Birbaumer N, Aertsen A, et al. Hand movement direction decoded from MEG and EEG. J Neurosci. 2008;28(4):1000–8.

[18] Loza CA, Philips GR, Hazrati MK, Daly JJ, Principe JC. Classification of hand movement direction based on EEG high-gamma activity. in Proc. IEEE EMBC 2014. 2014:6509–12.

[19] Shibasaki H, Hallett M. What is the Bereitschaftspotential? Clin Neurophysiol. 2006; 117(11):2341–56.

Published by Verlag der TU Graz
Graz University of Technology

Proceedings of the
7th Graz Brain-Computer Interface Conference 2017 DOI: 10.3217/978-3-85125-533-1-64

RANDOM VISUAL EVOKED POTENTIALS (RVEP) FOR BRAIN-COMPUTER INTERFACE (BCI) CONTROL

S. Nagel[1], W. Rosenstiel[1], M. Spüler[1]

[1]Wilhelm-Schickard-Institute for Computer Science, University of Tübingen, Tübingen, Germany

E-mail: nagels@informatik.uni-tuebingen.de

ABSTRACT: Brain-Computer Interfaces (BCIs) enable users to control devices or communicate by using brain activity only. While BCIs based on visual evoked potentials (VEPs) have been shown to achieve high performance, we present a different paradigm for BCI control: random VEP (rVEP). We designed a regression model, trained on VEPs of fully random bit codes. Afterwards, the model is able to perform a bit-wise prediction of a previously unseen stimulation sequence, which in turn can be used for BCI control. In an offline study, the model predicts unknown stimulation sequences with an average ITR of 94.5 bits per minute (bpm) and up to 281 bpm on a single-trial level. In a copy-spelling task, the model achieved an average ITR of 64.3 bpm and up to 115.5 bpm.

INTRODUCTION

Using a Brain-Computer Interface (BCI), a user is able to control a computer by brain activity without physical activity. In general, BCIs are used to restore functionalities of handicapped people, like restoring communication ability of people who are not able to communicate by muscle activity. The EEG of the brain's response to a visual stimulus, called visual evoked potential (VEP), is one commonly used method for BCI control.

For rare stimuli (less than 2 Hz) the VEP includes three major early components: C1 (60-80 ms), P1 (80-120 ms), and N1 (120–180 ms) [1]. If stimuli become more rapid, the single VEPs can no longer be determined. How the brain responds to overlapping stimuli is not entirely clear, as it could be a simple overlap of the VEPs or the brain is entrained to the stimulus frequency [2].

One of the earliest papers proposing the use of VEPs for BCI control was published by Sutter in 1984 [3]. To date, several types of stimuli were tested for BCI control, most commonly steady state VEPs (SSVEPs) or code-modulated VEPs (cVEPs). SSVEP BCIs make use of frequency modulated stimuli, and the brain's response can be interpreted, for example, by using the frequency domain. For cVEP BCIs, the stimuli are code modulated, i.e. a pseudorandom code with a low auto-correlation which is shifted for the different targets. The fastest SSVEP BCI has an information transfer rate (ITR) of 319 bits per minute (bpm) [4], whereas the fastest cVEP BCI achieves an ITR of 144 bpm [5].

Current BCIs based on VEPs have been shown to achieve high performance, but all methods are not able to interpret VEPs of arbitrary stimuli. The only study, known to us, researching VEPs of arbitrary stimuli is by Thielen *et al.* [6]. They developed a convolution model, making the assumption that the composition of VEPs induced by the parts of a decomposed modulation sequence should yield the same result as the VEP pattern induced by the modulated sequence. For this, the model was trained to predict the "single" VEPs of a decomposed modulation sequence, which in turn are composed to the predicted chain of VEPs. For an unseen modulation sequence the predicted chain of VEPs is then compared to the real measured brain's answer, in order to select one of the $6 \times 6 = 36$ targets. But the modulation sequences are not fully random, as they are composed of short and long pulses.

In this paper, we present a method to predict the bit-sequence of a fully randomly modulated stimulus and demonstrate how this can be used for BCI control based on random visual evoked potentials (rVEP).

MATERIALS AND METHODS

The rVEP BCI is based on a simple regression model, which is able to interpret the EEG signal during an arbitrary stimulation. The model uses a bit-wise prediction of the modulation sequence, which in turn can be applied for BCI control.

Bit-wise prediction: Yet, it is unclear how the VEPs are generated by the brain if the duration of two successive stimuli is lower than the duration of a single VEP (approx. 250 ms). We propose a new paradigm where sliding windows of 250 ms of the EEG data are used to predict the modulation sequence. After training, the regression model is able to predict an arbitrary and previously unseen modulation sequence by sliding the window sample-wise. A schematic representation of the rVEP prediction is illustrated in Fig. 1. For each 250 ms window of the EEG signal, the regression model predicts a real number. In order to get a bit-sequence, we defined that each predicted value above 0.5 is a boolean 1, and 0 otherwise. To get the prediction accuracy, we use the hamming distance between the predicted bit sequence and the stimulation bit sequence. Because the distances are 1's and 0's, the averaged distance of all samples corresponds to the accuracy of how much of the stimulation sequence can be predicted correctly. In short, we do an ongoing prediction of the

Published by Verlag der TU Graz
Graz University of Technology

 DOI: 10.3217/978-3-85125-533-1-64

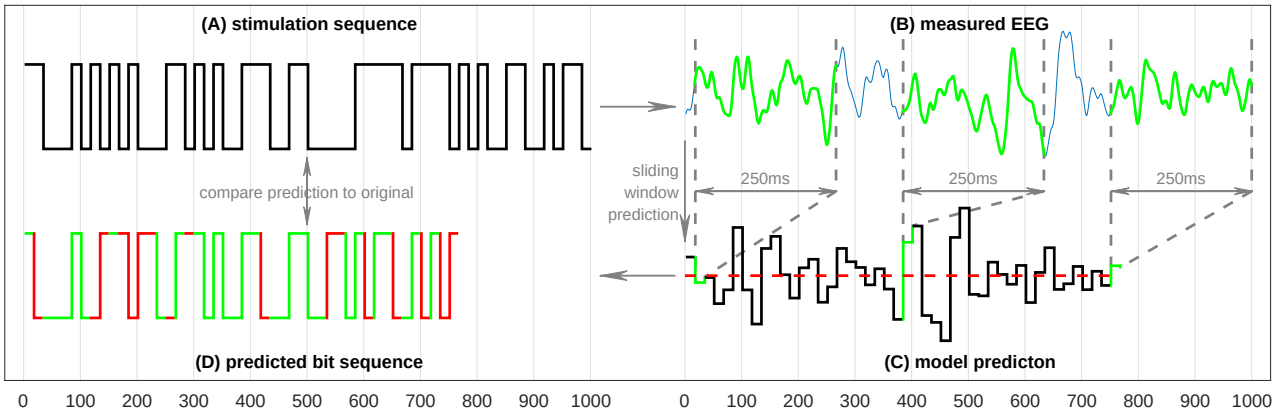

Figure 1: Schematic of the rVEP prediction. **A** Once the model is trained, an unseen (random) stimulation sequence can be used for prediction. **B** A 250ms window (highlighted in green) will be slided sample-wise over the spatially filtered EEG signal. For simplicity, it is shown bit-wise using 3 exemplary windows. **C** The trained model predicts a real number for each 250ms window (again, highlighted in green). The red dashed line indicates a value of 0.5. **D** Each value above 0.5 is interpreted as boolean 1, and as 0 otherwise. The resulting bit sequence can be compared to the stimulation sequence (match = green, mismatch = red).

modulation sequence using the following 250 ms of the EEG data after the stimulus.

BCI control: For BCI control, we need a method to choose the correct target out of others. For this, we used two methods: (1) The most obvious method is to compare the predicted bit sequence to modulation sequences of all possible targets, the one with the highest accuracy will be chosen. But the bit-wise prediction does not allow differentiation between how large (or small) the predicted real number really is, this approach wastes additional information. (2) To address this, we used a ”distance” prediction of each target. We calculated euclidean distances of predicted real numbers to the corresponding target bits and the one with the shortest distance will be chosen.

BCI design: The rVEP BCI consists of an EEG amplifier, a personal computer (PC) and a CRT Monitor, because of its near-to-zero reaction time and the resulting sharp transitions between black and white. The presentation of the stimuli are operated from the PC and synchronized with the EEG amplifier by using the parallel port. BCI2000 [7] is used as a general framework for recording the data. The visual stimuli are presented on a 17 inch CRT Monitor with a 60 Hz refresh rate and a resolution of 1280×1024 pixel. The subjects are seated approximately 80 cm in front of the monitor. To ensure synchronization of the presented stimuli with the refresh rate of the CRT monitor, DirectX (Microsoft Inc.) is used for programming the stimulation module.

A stimulus can either be black or white, which can be represented by 0 or 1 in a binary sequence. Each stimulus was modulated with a random binary sequence using a 60 Hz refresh rate. The rVEP BCI consists of 32 targets (i.e. stimuli) which are arranged as a 4×8 matrix and surrounded by 28 complementary non-target stimuli. The targets were used to select one of the 26 letters from the alphabet as well as underscore and numbers 1 to 5. A screenshot of the layout that was displayed to the subjects can be seen in Fig. 2.

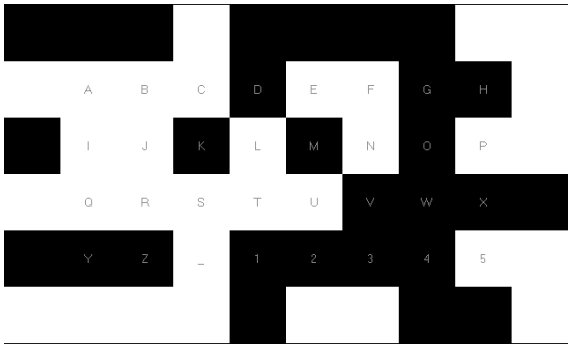

Figure 2: Screenshot of the rVEP BCI during a trial showing the target layout and non-targets.

EEG data was recorded with a g.tec g.USBamp at a samplingrate of 600 Hz and a Brainproducts Acticap system with 32 channels. Locations of the 29 EEG electrodes are depicted in Fig. 3. The ground electrode was positioned at AFz and the reference electrode at FCz. Three electrooculogram (EOG) electrodes were placed beside the left eye, right eye and at the center above the eyes. The data was notch-filtered by the amplifier at 50 Hz.

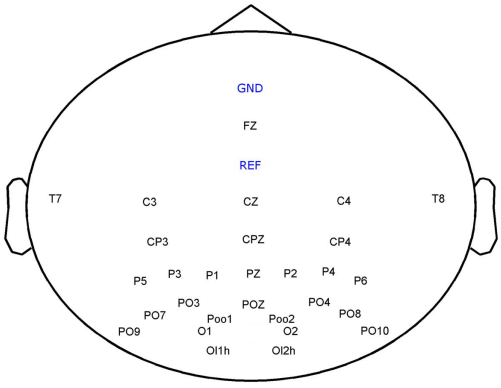

Figure 3: Location of the 29 EEG electrodes. Ground electrode (GND) was positioned at AFz and reference electrode (REF) at FCz.

Published by Verlag der TU Graz
Graz University of Technology

 DOI: 10.3217/978-3-85125-533-1-64

A spatial filter is applied to the EEG data using the Canonical Correlation Analysis (CCA) as described by Spüler *et al.* [8]. First, one needs to find the best EEG channel where the cVEP is most prominent. The EEG data of this channel is averaged over all cVEP sequence cycles and used to calculate the spatial filter. For this, each subject has to perform some cVEP trials. The spatially filtered EEG signal is used as input for the regression model.
During the training we use fully random stimulation sequences and do a regression on each 250 ms window (shifted sample-wisely) of the spatially filtered EEG data to its corresponding bit modulated at the time the window starts (see Fig. 4). We make the assumption that a fully random stimulation should be sufficient to cover most possibilities of different stimulation patterns within a window of 250 ms, provided that the random sequence is long enough. Afterwards the coefficients obtained by the regression model are used for prediction.

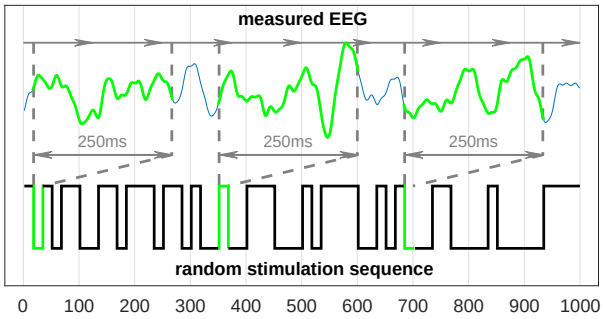

Figure 4: Training of the rVEP model. Each 250ms window of the spatially filtered EEG data will be projected to its correspondig bit (1 or 0, highlighted in green) of the corresponding random stimulation sequence.

Experiment design: To test the system, 9 healthy subjects, named S1 to S9, were recruited. All subjects had normal or corrected-to-normal vision. A summary over age, sex and vision of the subjects can be found in Tab. 1. Each subject participated in one session and completed the whole experiment. None of the subjects ever participated in another VEP EEG study.

Table 1: Subject overview. Sex and age of the subjects and if they are wearing glasses.

Subject:	S1	S2	S3	S4	S5	S6	S7	S8	S9
Sex:	w	m	m	w	w	w	w	m	m
Age:	21	19	17	18	20	19	20	22	19
Glasses:	√	×	×	×	×	√	√	×	×

The experiment was structured in three phases consisting of 16 runs in total. The first 3 runs were used for the spatial filter, the following 3 runs are the training phase of the BCI and the remaining 10 runs form the testing phase. At each run the subjects had to perform a copy-spelling task where they had to look once at each of the 32 targets in lexicographic order (A-Z, underscore, 1-5). The duration of the 32 trials was constant within each run of a phase, but varies between the three phases. At the end of a trial a target was selected, meaning that the corresponding box was highlighted in yellow for 100 ms while the rest of the matrix was darkened for the same time, to guide the subject through the experiment. During the time between the trials, called pause, the flickering continued, but the recorded EEG data was not used for training or classification. The pause between the runs amounted approximately 30 to 60 seconds.

Spatial filter phase: A cVEP modulation was used during the spatial filter phase, because random modulation is unsuitable to train a spatial filter since the EEG data has to be averaged over a static modulation in order to filter the noise. The cVEP setup was equal to the system of Spüler *et al.* [5]. For modulation of the targets we used a 63-bit binary m-sequence, because of its low auto-correlation property [9]. For each target the same m-sequence was used for modulation, but shifted circularly by 2 bits for each successive target. During each trial, the stimulation sequence was repeated 3 times. Because the length of the stimulation sequence is $63\ bit/60\ {}^{bit}/_{s} = 1.05s$, the duration of a trial is $3 \cdot 1.05s = 3.15s$. One stimulation sequence is presented during the inter-trial-pause, therefore, the subject had $1.05s$ to move on an fixate the next target. In total, the spatial filter phase consists of $3 \cdot 32 \cdot 3 = 288$ presented m-sequences, excluding the pauses.

Training phase: During the 3 runs of the training phase, each trial had a length of 5 seconds in which 300 random bits were presented. The inter-trial-pause had a length of 2 seconds during which the subject had to look at the subsequent target. Since the layout has 32 targets, the subjects have to pass 96 trials. Each trial was spatially filtered, resulting in vectors of 3000 samples (10 samples per bit). Each vector was split into windows of 150 samples (= 250 ms), shifted by 1 sample. Since the last 150 windows do not have 150 successive samples, they are excluded from the data. The resulting matrix is of size 2850×150. The vector of the corresponding random modulation sequence has also a length of 2850 samples (last 150 samples are excluded, too). The matrix and the random modulation sequence vector are used as input (predictors and observed responses, respectively) of the ridge regression model (see Fig. 4). Since the method is a proof-of-concept, we did not optimize the regression parameter λ, but it was set to its default value 1. The output of the trained model are 151 coefficients, one for each input sample and a constant term.

Testing phase: The 10 runs of the testing phase are similar to the ones of the training phase, except that a trial had a length of 2 seconds instead of 5 seconds, resulting in 320 trials (32 per run). Each test trial was spatially-filtered and split into windows of 150 samples, same procedure as for the training trials, resulting in a matrix of size 1050×150 (last 150 windows were skipped). Afterwards, the matrix was applied to the trained regression model (multiplied with the coefficients), resulting in a vector of 1050 samples, this is called the model prediction.
In order to use the model prediction p for BCI control,

Published by Verlag der TU Graz
Graz University of Technology

 DOI: 10.3217/978-3-85125-533-1-64

we used two different methods: (1) Interpret each model prediction value above 0.5 as a binary 1 and 0 otherwise. The result is a predicted binary vector b which can be compared to the binary modulation sequences s_i of all targets i. For this we used the hamming distance h_i between b and each possible s_i. The target i with the lowest h_i was selected. (2) The second method is to calculate the euclidean distance e_i between p and s_i for each target i. The target i with minimum e_i is selected.

Random bit generation: During both the training and testing phase the MT19937 [10] random generator was used for modulation of the 60 boxes. At each monitor refresh a random integer (0 or 1) is generated for each of the 60 boxes (targets and non-targets), therefore, each box's binary sequence is always random without conscious repetitions and generated with a rate of 60 bits per second, continuously. The "order" of the generated bits can be varied by an assignable random seed.

Performance Evaluation: To compare the results for the different subjects and for the different modulation types (rVEP and cVEP), the accuracy of both the model prediction and the target classifier as well as the corresponding information transfer rate (ITR) [11] were used. The ITR can be computed with the following equation:

$$ITR = \log_2 N + P \log_2 P + (1-P) \log_2 \frac{1-P}{N-1}$$

with N the number of classes and P the accuracy.

RESULTS

Although a cross-validation could be used, such a simulated online design takes into account non-stationarity effects over time that can also occur in online experiments. As such non-stationary effects don't play a role in an evaluation using a cross-validation, the evaluation used is closer to the realistic online BCI.

Bit sequence prediction: To analyze the performance of the bit sequence prediction, all 320 predicted test sequences of each subject were compared to their modulated random bit sequence. For this, the accuracies of correctly predicted bits were calculated. The results are shown in Tab. 2. On average, the regression model achieves a performance of 59.1% over all subjects, meaning that 59.1% of all $302{,}400$ bits were predicted correctly, which corresponds to an average ITR of 94.5 bits per minute (bpm). It should be noted that subject S9 achieves an average performance of 63.7%, which implies an average ITR of 197.2 bpm.

Target prediction using hamming distance: In order to use the method for an online BCI, it is required to identify the correct target. For this, we calculated the hamming distances between all possible target sequences and the predicted sequence. The one with the minimal hamming distance was chosen. Averaged over all runs and all subjects, 60.6% of all targets were predicted correctly, this is an ITR of 44.8 bpm, including the inter-trial time of 1s. Subjects S8 and S9 achieved an average performance of >90% (ITR >83 bpm). A comparison of the target prediction and the bit prediction is shown in Tab. 2. Excluding the inter-trial time, the ITR of the target prediction is 27.2 bpm lower compared to the bit prediction.

Table 2: Comparison of the bit prediction and target prediction using the hamming distance. Accuracies (P) are given in percentages of correctly predicted bits and percentages of correct classifications of the 32 targets, respectively. 60 bits are presented per second, whereas the trial duration of the target prediction amounts 2s. The Information Transfer Rates (ITR) are estimated excluding the inter-trial time.

	target prediction		**bit prediction**	
	P (%)	ITR (bpm)	P (%)	ITR (bpm)
S1	28.1	17.5	54.8	24.3
S2	78.4	95.4	60.6	116.7
S3	47.8	42.5	57.2	55.3
S4	91.6	124.9	62.9	174.5
S5	53.1	50.4	58.2	70.6
S6	52.2	49.0	58.3	72.5
S7	69.1	77.2	60.0	104.0
S8	33.1	23.1	55.9	35.6
S9	91.9	125.1	63.7	197.2
∅	60.6	67.3	59.1	94.5

Target prediction using euclidean distance: The results of the correctly predicted targets within each run of all subjects are shown in Tab. 3. Using this method, on average 66.9% of all targets were predicted correctly. This implies an average ITR of 52.6 bpm (including the inter-trial time of 1s). It is worth to note that subject S9 achieves 100% in 4 of the 10 runs with an minimum accuracy of 93.8% and an average ITR of 94.8 bpm. Excluding the inter-trial time, the ITR of the target prediction is 15.6 bpm lower compared to the bit prediction.

Table 3: Performance of each subject using the "distance" method for target prediction. Accuracies (P) are given in percentages of correct classifications of the rVEP test runs and the cVEP runs, respectively. The trial duration (T) differs for rVEP and cVEP runs. The Information Transfer Rates (ITR) are estimated including the inter-trial time of 1s.

	rVEP			**cVEP**		
	P (%)	T (sec)	ITR (bpm)	P (%)	T (sec)	ITR (bpm)
S1	31.9	2	14.4	39.2	1.05	30.0
S2	87.8	2	77.2	75.3	1.05	87.0
S3	51.6	2	32.0	53.1	1.05	49.2
S4	93.1	2	86.0	88.9	1.05	115.5
S5	59.7	2	40.6	55.2	1.05	52.4
S6	65.6	2	47.4	63.5	1.05	65.8
S7	76.9	2	61.5	47.6	1.05	41.1
S8	37.8	2	19.2	33.7	1.05	23.2
S9	97.8	2	94.8	88.5	1.05	114.7
∅	66.9	2	52.6	60.6	1.05	64.3

Published by Verlag der TU Graz
Graz University of Technology

 DOI: 10.3217/978-3-85125-533-1-64

Comparison to cVEP sequence prediction: In order to compare the rVEP BCI with other VEP BCIs, the cVEP trials of the first 3 runs were applied to the model and targets were predicted. Because each trial consists of 3 cVEP cycles, each cycle is predicted separately, meaning that each run has $3 \cdot 32 = 96$ trials. Averaged over all subjects, the accuracy is 60.6%. The results for a bit-wise prediction on the c-VEP dataset are shown in Fig. 5 for each subject, it is worth noting that subject S4 achieved an average accuracy of 66.3% of correctly predicted bits, which implies an average ITR of 281.1 bpm. The prediction of the cVEP m-sequence, can be predicted significantly better than the random sequences ($p<0.005$).
The results of the target prediction using the euclidean distance are shown in Tab. 3 including a comparison to the to the rVEP stimulation. On average, 60.6% of all targets were predicted correctly, resulting in an ITR of 64.3 bpm with an inter-trial time of 1s.

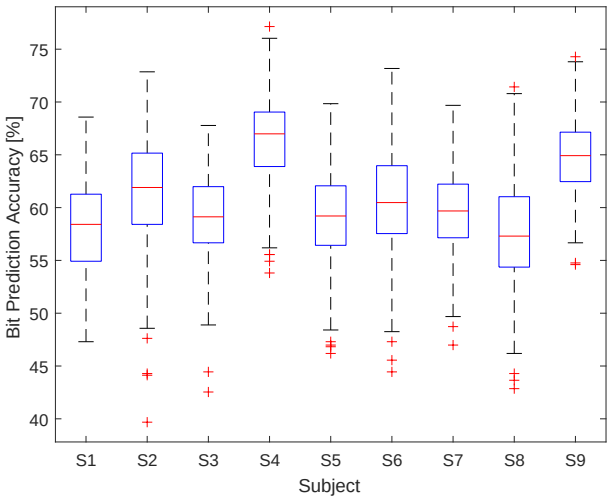

Figure 5: Prediction of the cVEP targets' modulated bit sequences. For each subject S1 to S9, the bit prediction accuracies of all 288 cVEP trials are plotted.

DISCUSSION

In this work, a novel method to classify VEPs is evaluated. While previous methods make use of special modulation codes, i.e. with a low auto-correlation, to achieve the maximum performance, we pursued a different approach. We want to address the "overlapping" VEP behavior from the ground. Since the assumption of linearity of VEP generation is investigated by several other studies [12,13], we proposed a new method based on linear ridge regression. Using random codes, we assume to cover most of the possible "overlapping" VEPs in order to predict arbitrary modulation sequences afterwards. Aside from this, the method has several advantages: trials can have an arbitrary length, phase-lock is not required (like it is for m-sequences), and the number of targets can be chosen arbitrary.
With an average ITR of 86.5 bpm, our model proves that it is possible to reconstruct arbitrary unseen (random) modulation sequences with an average accuracy of 59.1% (without repetition). Surprisingly, the prediction of the cVEP m-sequence, can be predicted significantly better with an average accuracy of 60.6% and up to an ITR of 281.1 bpm. This could be due to the low auto-correlation of the m-sequence and proves clearly that our model is also able to handle cVEP modulation, although it never has seen the m-sequence during the training phase.
As mentioned before, we loose information by using a simple threshold to construct the bit sequence. This effect can also be seen in the results of the target prediction, where the ITR is 27.2 bpm lower compared to the bit prediction. But part of this difference might also be attributed to some general problems of using ITR. By using the euclidean distance to target prediction, the ITR drops significantly less (15.6 bpm), and is therefore recommended for BCI control.
Interestingly, the variance between the subjects is very high. While two subjects achieved a poor accuracy during the whole experiment with ITRs of lower 30 bpm, two other subjects achieved average ITRs of always above 114 bpm and up to 281.1 bpm. This variance could be caused by problems during the EEG preparation and/or because of some subjects wearing glasses.
Using either the rVEP modulation or cVEP modulation, our method also performed better than the re-convolution BBVEP of Thielen *et al.* [10] which achieved an average ITR of 48.4 bpm using their early-stopping trials.

CONCLUSION

In this paper, we have introduced the rVEP BCI, a new approach to predict arbitrary VEP modulation sequences based on random sequence learning. We showed that our model was able to predict bits of fully random sequences as well as m-sequences. The model predicts random sequences with an average accuracy of 59.1% and m-sequence with an average accuracy of 60.7%. Surprisingly, the average ITR of the m-sequence prediction of S4, excluding the inter-trial time, amounts to 281.1 bpm although the model has never seen the m-sequence before. This clarifies the capability of our rVEP BCI. Also it is quite interesting why m-sequences can be predicted significantly better than random sequences, although the model was trained on random sequences. This could be due to the low auto-correlation or the amount of bit changes. We also showed that our approach can be used for BCI control with an average ITR of 64.3 bpm and up to 115.5 bpm.
In future work, the rVEP BCI will be tested in an online study. Due to the sliding window prediction, we also want to use an early-stopping method, in which a trial ends when a certain reliability-threshold is reached. Once we found a threshold the method can be applied to an asynchronous BCI, because targets will only be selected if the threshold is reached and this should only be the case if the user fixates a target. Additionally, the use of error-correcting codes could be used for stimulus modulation in order to improve the prediction.

Published by Verlag der TU Graz
Graz University of Technology

 DOI: 10.3217/978-3-85125-533-1-64

ACKNOWLEDGMENTS

This work was supported by the *Baden-Württemberg Stiftung* (GRUENS) and the *Deutsche Forschungsgemeinschaft* (DFG; SP 1533/2-1).

REFERENCES

[1] Di Russo Francesco, Teder-Sälejärvi WA, Hillyard SA (2002) In: Zani A, Proverbio AM (2003) The cognitive electrophysiology of mind and brain. Steady-state VEP and attentional visual processing. Academic press, pp 259-274.

[2] Herrmann, CS (2001) Human EEG responses to 1–100 Hz flicker: resonance phenomena in visual cortex and their potential correlation to cognitive phenomena. Experimental brain research, 137(3-4), 346-353.

[3] Sutter EE (1984) The visual evoked response as a communication channel. In: Proceedings: IEEE Symposium on Biosensors. pp. 85–100.

[4] Chen X, Wang Y, Nakanishi M, Gao X, Jung T-P, Gao S. (2015) High-speed spelling with a noninvasive brain–computer interface. Proceedings of the National Academy of Sciences of the United States of America, 112(44):E6058-E6067

[5] Spüler M, Rosenstiel W, Bogdan M (2012) Online Adaptation of a c-VEP Brain-Computer Interface(BCI) Based on Error-Related Potentials and Unsupervised Learning. PLoS ONE 7(12):e51077.

[6] Thielen J, van den Broek P, Farquhar J, Desain P (2015) Broad-Band Visually Evoked Potentials: Re(con)volution in Brain-Computer Interfacing. PloS one, 10(7):e0133797.

[7] Schalk G, Mcfarland DJ, Hinterberger T, Birbaumer N, Wolpaw JR (2004) BCI2000: A General-Purpose Brain-Computer Interface (BCI) System. IEEE Transactions on Biomedical Engineering 51:1034–1043.

[8] Spüler M, Walter A, Rosenstiel W, Bogdan M (2014) Spatial filtering based on canonical correlation analysis for classification of evoked or event-related potentials in EEG data. IEEE Transactions on Neural Systems and Rehabilitation Engineering, 22(6):1097–1103.

[9] Golomb SW (1982) Shift Register Sequences. Laguna Hills, CA: Aegan Park Press.

[10] Matsumoto M, Nishimura T (1998) Mersenne twister. A 623-dimensionally equidistributed uniform pseudorandom number generator. In: ACM Transactions on Modeling and Computer Simulation 8:3–30.

[11] Wolpaw JR, Ramoser H, McFarland DJ, Pfurtscheller G (1998) EEG-based communication: improved accuracy by response verification. Rehabilitation Engineering, IEEE Transactions on, 6(3):326–333.

[12] Capilla A, Pazo-Alvarez P, Darriba A, Campo P, Gross J (2011) Steady-state visual evoked potentials can be explained by temporal superposition of transient event-related responses. PloS ONE, 6(1):e14543

[13] Lalor EC, Pearlmutter BA, Reilly RB, McDarby G, Foxe JJ (2006) The VESPA: a method for the rapid estimation of a visual evoked potential. NeuroImage, 32(4):1549–1561

Published by Verlag der TU Graz
Graz University of Technology

Proceedings of the
7th Graz Brain-Computer Interface Conference 2017 DOI: 10.3217/978-3-85125-533-1-65

YES OR NO? – BINARY BRAIN-BASED COMMUNICATION UTILIZING MOTOR IMAGERY AND FNIRS

L.M.J. Nagels-Coune[1, 2*], D. Kurban[1*], N. Reuter[1, 3], A. Benitez[1, 2], L.K. Gossé[1], L. Riecke[1, 2], R. Goebel[1, 2, 4], B. Sorger[1, 2]

*These authors contributed equally to this work.

[1] Department of Cognitive Neuroscience, Maastricht University, Maastricht, the Netherlands

[2] Maastricht Brain Imaging Center (M-BIC), Maastricht, the Netherlands

[3] Institute of Neuroscience and Medicine (INM-1), Research Centre Jülich, Jülich, Germany

[4] Department of Neuroimaging and Neuromodeling, Netherlands Institute for Neuroscience, an institute of the Royal Netherlands Academy of Arts and Sciences (KNAW), Amsterdam, the Netherlands

E-mail: b.sorger@maastrichtuniversity.nl

ABSTRACT: Past research into motor-independent communication for the severely disabled has mainly focused on developing brain-computer interfaces (BCIs) implementing neuroelectric signals. More recently, also hemodynamic brain signals have been explored for BCI purposes. Here, we introduce a novel, straightforward, and easy-to-implement yes/no communication paradigm relying on mental imagery (mental drawing) and portable functional near-infrared spectroscopy. To hemodynamically encode answers to binary questions, participants either performed mental drawing (for encoding "yes") or did not change their mental state (for encoding "no"). Participants' answers were decoded offline using univariate and multivariate statistics. In approximately half of the participants, accuracies reached 70% or higher, which is considered a sufficient performance for binary communication BCIs. As the proposed communication technique requires relatively little cognitive capabilities, it might not only serve as a useful communication means but also as a diagnostic tool for detecting preserved conscious awareness in non-responsive patients.

INTRODUCTION

Communication is an essential element of human interaction. In the so-called 'locked-in' syndrome (LIS) [1], fully aware and conscious patients have lost the ability to naturally communicate due to severe motor paralysis. To help affected patients in this fateful condition, motor-independent communication through brain-computer interfaces (BCIs) has been suggested [2]. BCIs rely on brain signals that an individual can intentionally generate to encode an intention (e.g., to communicate a "yes" or a "no" answer). These brain signals are then measured with a functional neuroimaging method and finally decoded back into their originally intended meaning using signal-classification methods. In the field of BCI an accuracy of at least 70% is considered sufficient for a two-class communication BCI [3]. For almost 30 years now, BCI research has focused on developing communication BCIs using neuroelectric signals mainly based on noninvasive electroencephalography (EEG) [e.g., 4-6]. Though these 'classic' communication BCIs have been applied successfully in affected patients [e.g., 7,8], not all individuals achieve proficiency in EEG-based BCI control (a phenomenon referred to as 'BCI illiteracy' [9]). Thus, there is an urgent need to explore further possibilities for brain-based communication. Recently, hemodynamic brain signals as measured with functional magnetic resonance imaging (fMRI) [10-13] and functional near-infrared spectroscopy (fNIRS) [14-16] have been suggested and tested in this context. For example, our group has developed a letter speller based on differently timed mental-task performance and real-time fMRI that allows convenient back-and-forth communication of any word [17]. The robust letter speller requires almost zero pre-training or preparation time and can be of great benefit for short-term communication. However, the fMRI-based BCI approach is costly and tied to clinical or research institutions making it unsuitable for everyday-life usage. A primary need of LIS patients and their families, however, is immediate access to and frequent use of BCI communication. FNIRS is a functional neuroimaging method that relies on the same (hemodynamic, i.e., vascular) brain response as fMRI [18]. While being spatially less specific than fMRI, fNIRS is relatively easy to apply, inexpensive, safe and, most importantly, portable [19]. These factors open the possibility to transfer the developed fMRI communication paradigms to the more compact and portable fNIRS technology, making fNIRS an ideal candidate for future daily-life application. Due to its straightforward implementation it could be readily handled maybe even by the patient's care givers.

Published by Verlag der TU Graz
Graz University of Technology

 DOI: 10.3217/978-3-85125-533-1-65

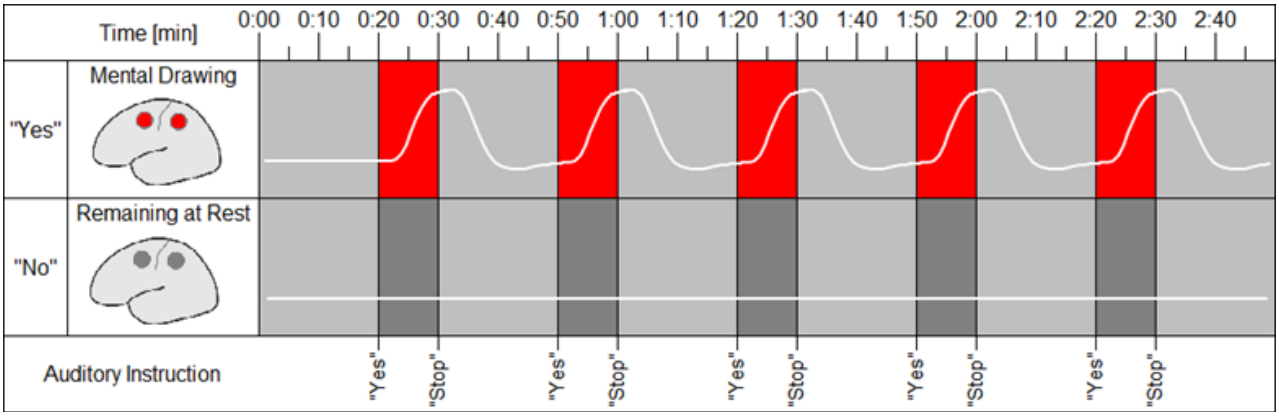

Figure 1: Encoding scheme for an answer-encoding run including expected oxyhemoglobin changes (white curve/line) in motor imagery-related brain regions. When a participant wants to encode "yes", he/she performs motor imagery causing oxygenated hemoglobin to rise. When a participant wants to encode "no", he/she stays at rest causing no relative change in oxygenated hemoglobin. Note that participants encoded the same answer five times in one run.

Here, we suggest a novel, straightforward yes/no communication procedure employing mental imagery and fNIRS. In our suggested procedure, participants performed two localizer runs, one at the beginning of the experiment and one at the end. Each of these runs consisted of twenty 10 s periods of mental-task performance that alternated with twenty-one 20 s baseline blocks, adding up to 10 min 20 s per run. Between localizer runs, six answer-encoding runs were performed, during which participants were asked to answer biographical questions (e.g., "Do you live in Maastricht?") by intentionally modulating their brain activation. For encoding "yes", participants were asked to start mental drawing as soon as "yes" was aurally presented and to halt mental-task performance as soon as "stop" was presented. For encoding "no", participants were asked to stay at rest for the whole length of the run. Each answer-encoding run consisted of five 10 s answer-encoding trials, alternated with six 20 s baseline periods, adding up to 2 min 50 s (Fig. 1). Participants' brain responses were decoded offline.

MATERIALS AND METHODS

Participants: Twenty healthy subjects (nine female, three left-handed, age = 26.0± 8.0 years [mean ± SD], all with normal or corrected-to-normal vision and reportedly normal hearing) participated in the study. Tab. 1 documents individual participants' characteristics. All participants gave written informed consent according to procedures approved by the local ethics committee and received financial compensation.

Mental-drawing paradigm: To intentionally evoke fNIRS signals, participants were instructed to: "Imagine drawing simple geometric figures (such as circles, triangles, cubes, etc.) or small contour drawings (e.g., a butterfly, star, car, tree, boat, or house) with the right hand at a comfortable but consistent speed. Imagine using a pen. This might support your imagination."

Participant preparation: Prior to the experiment, participants were familiarized with the general procedure of the study. They shortly practiced mental drawing and answer encoding until they felt comfortable (ca. 15 min). Moreover, a list of 45 binary biographical questions, simple yet unobtrusive enquiries about their lives, was provided. Six of those questions were selected by an independent experimenter: three to be answered with "yes" and "no", to assure equal distribution of answer options. After placement of the cap with the fNIRS optodes, participants were seated comfortably in a noise-dimmed cabin, which was equipped with a loudspeaker and microphone to enable verbal communication between participant and experimenter during the experiment.

Data acquisition: Self-induced hemodynamic brain signals were obtained using a NIRScout-816 system (NIRx Medizintechnik GmbH, Berlin, Germany) equipped with six detector and three source optodes (LEDs emitting wavelengths of both 760 nm and 850 nm). Sources were positioned according to the international 10-20 EEG system on FC3 (1), C3 (2) and CP3 (3) and detectors were positioned on FC5 (1), C5 (2), CP5 (3), FC1 (4), C1 (5) and CP1 (6) (Fig. 2).

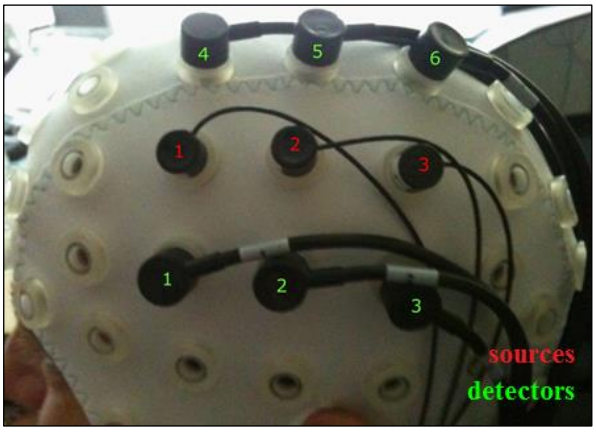

Figure 2: fNIRS optode set-up with the source optodes in red (optodes 1, 2 and 3 in the middle horizontal line) and detector optodes 1-6 in green.

This limited number of optodes was chosen to ensure clinical applicability (i.e., reasonable optode-placement time allowing for rapid bedside measurements of patients). Recorded optical signals were sampled at a rate of 12.5 Hz. Due to the limited number of sources and detectors, the optodes' montage covered a confined

Published by Verlag der TU Graz
Graz University of Technology

 DOI: 10.3217/978-3-85125-533-1-65

area above the left-hemispheric fronto-parietal (sensorimotor) cortex (Fig. 2). Auditory stimuli were presented using in-house stimulation software [20].

Subjective ratings: After each run, participants rated the experienced fNIRS comfortability according to a Likert-scale ranging from 0 (extremely uncomfortable) to 10 (extremely comfortable). We predicted that comfortability ratings would decrease over time. After completion of the experiment, the participants rated the general easiness and pleasantness of the employed mental-imagery paradigm (mental drawing) again using a Likert-scale ranging from 0 (extremely difficult/unpleasant) to 10 (extremely easy/pleasant).

Data analysis: FNIRS time series were analyzed using Satori (v0.92, Brain Innovation B.V., Maastricht, The Netherlands). During preprocessing, raw data time course values were converted to oxygenated hemoglobin (oxy-Hb) and deoxygenated hemoglobin (deoxy-Hb) values. Linear trend removal, temporal low-pass filtering (Gaussian full width at half maximum [FWHM]: 40 data points) and high-pass filtering (cut-off: 10 cycles [localizer runs] or 2 cycles [answer-encoding runs] per time course) were applied. These filtering parameters correspond approximately to a band-pass filter of 0.1-0.016 Hz for the localizer runs and 0.1-0.012 Hz for the encoding runs. The subsequent data analysis was focused on the 14 'direct-neighbor' channels (i.e., channels emerging from sources-detector combinations of close proximity; see Fig. 3). Two types of analyses were conducted: univariate general linear model (GLM) analysis and multi-channel pattern (MCP) analysis.

(1) GLM analysis. First, a single channel of interest was determined individually for each participant using the data of the first localizer run (called 'best channel' in the following). For this purpose, channel-wise (whole-run) GLM analysis was performed separately for oxy- and deoxy-Hb time series using a predictor corresponding to the motor-imagery condition and applying the statistical contrast "motor imagery vs. resting". For selecting the best channel we calculated a criterion value by averaging the obtained oxy-Hb and deoxy-Hb t-values per channel. The channel with the highest criterion value was considered the best channel and selected for further analysis. As a next step, the data of the first "yes" and "no" answer-encoding run per participant was analyzed as follows: For each of the ten trials (five "yes" and five "no" trials) the individual criterion value was calculated. Then, a mean across these ten individual criterion values was computed. This average value was used as 'cut-off' value for decoding the answers of the remaining four answer-encoding runs. Values above or below the cut-off value resulted in decoding the answer-encoding data as "yes" or "no", respectively. Encoded answers were compared post hoc to the actually intended answers given by the participant. Next to individual and group-mean single-trial (ST) accuracies, we computed multi-trial (MT) accuracies for each individual and for the group. Multi-trial accuracies were derived by integrating the five separate yes/no decisions per run using majority voting (e.g., three answers encoded as "yes" and two answers encoded as "no" were considered as a "yes" answer). Resulting single-trial accuracies were evaluated in a confusion matrix per participant using a Chi square test to assess if decoding accuracies were significantly above chance level ($p < 0.05$).

(2) MCP analysis. MCP analysis was conducted using a support vector-machine as classifier [21]. For this analysis, all channels (n = 14) were used to define the spatial features for the MCP analysis. In order to 'train' (and 'test') the classifier, means of raw values for oxy- and deoxy-Hb were estimated in a time window from 6 s to 17 s after trial onset of the mental drawing trials. This window was defined for the mental drawing trials as it corresponds to the time points where the mean hemodynamic response was expected to be the highest. For the rest conditions an 11 s time window was chosen from 11 s to 22 s after trial onset of the rest conditions, during which the mean hemodynamic response is expected to be at baseline. The single-trial data of the two localizer runs served as training data. Analysis of the six answer-decoding runs resulted in five single-trial predictions (corresponding to the five separate answer-encoding trials) per run. As in the GLM approach, each prediction was compared to the actual answer given by the participant. Again, mean single- and multi-trial accuracies were calculated individually and for the group as described above for the GLM approach. Resulting single-trial accuracies were tested for significance ($p < 0.05$) using permutation tests (10.000 permutations). For both the GLM and MCP analysis, the average sensitivity – P(yes decoded | yes encoded) – and specificity – P(no decoded | no encoded) – was calculated. Correlations were run between the single-trial and multi-trial accuracies of both approaches.

Means and SEs will be calculated with the subjective ratings.

RESULTS

GLM analysis: For each subject, a best channel could be selected based on the procedure described above (see Tab. 1 for selected channels and individual criterion values). Fig. 3 illustrates how often each channel was selected across participants. Using the GLM approach, participants' answers could be decoded correctly with an average accuracy of 64.25% on a single-trial basis (theoretical chance level being 50%). Individual single-trial accuracies varied from 35.00-95.00% (Tab. 1). In eight participants, single-trial accuracies were significantly above chance level as assessed with a Chi-Square test (Tab. 1). The classifier showed no bias, as "yes" and "no" answers were decoded respectively on 50.25% and 49.75% of the 400 trials. The average sensitivity was 65.00% and the average specificity was 65.50%. On a group level, the multi-trial accuracy was 65.00%. Individual multi-trial accuracies varied from 25.00-100.00% (Tab. 1). For the group of nine subjects with individual single-trial accuracies of 70% or higher, the average single-trial

Published by Verlag der TU Graz
Graz University of Technology

 DOI: 10.3217/978-3-85125-533-1-65

accuracy was 79.44% (SE = 2.82), whereas their average multi-trial accuracy was 84.09% (SE = 4.20). For the eleven other subjects, the average single-trial accuracy was 51.82% (SE = 2.88), whereas their average multi-trial accuracy was 47.73% (SE = 5.28).

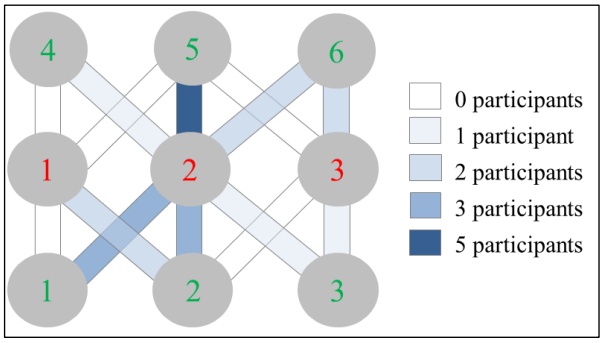

Figure 3: Frequency of best-channel selections within the GLM approach. The red and green numbers indicate source and detector optodes, respectively. Note that the most frequently selected channels correspond to brain areas [22] commonly associated with motor imagery.

MCP Analysis: Using the multi-variate approach, participants' answers could be decoded correctly from single trials with an average accuracy of 62.33%. Individual single-trial accuracies ranged from 33.33-76.67% (Tab. 1). In eleven subjects, single-trial decoding accuracies were significantly above chance level as revealed by permutation tests (Tab. 1). "Yes" and "no" answers were decoded respectively on 62.00% and 38.00% of the 600 trials. The sensitivity was 75.67% and the specificity was 51.67%. The multi-trial accuracy was 63.33% on the group level and individual multi-trial accuracies ranged from 33.33-100.00% (Tab. 1). When focusing the analysis on the ten subjects with single-trial accuracies of 70% or above, the single-trial accuracy was 72.33% (SE = 0.87), whereas the multi-trial accuracy was 85.71% (SE = 2.38). For the group of ten subjects with individual single-trial accuracies below 70%, the average single-trial accuracy was 52.33% (SE = 3.06), whereas their average multi-trial accuracy was 59.09% (SE = 7.22).

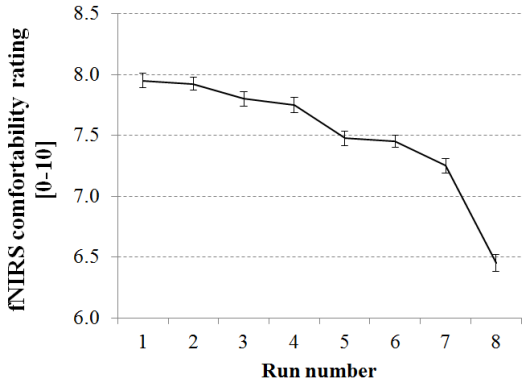

Figure 4: FNIRS comfortability ratings (group means and SEs) across runs. Values range from 0 (extremely uncomfortable) to 10 (extremely comfortable). Note that the first and eighth run were localizer runs.

Subjective ratings: FNIRS comfortability ratings were medium to high (see group means in Fig. 4). Comfortability decreased across time and dropped considerably for the last run (second localizer). Participants generally experienced the mental-drawing task as pleasant (M = 7.2, SE = .07) and easy to perform (M = 8.0, SE = .07).

Accuracy correlations: Correlations between the accuracies of the different approaches were all insignificant ($p > .05$): GLM MT and MCP MT ($r = .21$); GLM ST and MCP ST ($r = .36$).

DISCUSSION

A novel yes/no communication paradigm using mental drawing and fNIRS was tested in healthy participants. In LIS patients an fNIRS-based binary BCI has been tested recently [15,16]. However, in those studies a classifier was trained for several sessions over several days. The current approach has the potential of enabling immediate communication in the order of ca. 30 min (±15 min training; ±10 min localizer, ±6 min encoding). Of course, this should be tested using real-time decoding and in affected patients. We deem this will be successful as Naito et al. [14] found an accuracy rate above 75% in 23 out of 40 LIS patients with their fNIRS-based binary BCI using mental calculation/singing. Our results indicate that it is possible to obtain sufficiently high (≥ 70%, [3]) and reliable answer-decoding accuracies in healthy subjects by using the current paradigm and various data-analyses methods. On average, multi-trial accuracies were only marginally higher than single-trial accuracies. However, when focusing on participants reaching an accuracy of 70% or higher, there is a trend for multi-trial accuracies to be higher than single-trial accuracies in both GLM and MCP analysis. Closer inspection of these participants' data indicated relatively prominent hemodynamic responses, suggesting that the multi-trial approach is most advantageous when single-trial measurements have a sufficiently high signal-to-noise ratio.

The GLM approach might be particularly suited in the context of a communication BCI due to its simplicity. We expect that at least some LIS patients are also able to use the binary BCI presented here, as accuracies of 70% or higher were reached by approximately half the participants after a mere 15 min of training. Since our communication BCI relies on only a single fNIRS channel, preparation time can in principle (when having determined the best channel in a previous fNIRS session) be rather short. The similar sensitivity (65.00%) and specificity (65.50%) emphasizes that there is no bias to either "yes" or "no". The MCP approach might be especially useful in the context of detection of remaining consciousness in non-responsive patients because in contrast to the GLM approach, it does not require the calculation of a yes/no cut-off value. Nevertheless a localizer containing differential activity (mental imagery vs. rest) is still required to train the classifier, which might not be easily obtained in this

Published by Verlag der TU Graz
Graz University of Technology

 DOI: 10.3217/978-3-85125-533-1-65

patient group. Encouraging is the high specificity (75.67%) of this approach. In three of the four cases in which participants intentionally changed their brain states, this change was detected.

The two data-analysis approaches differ in the number of subjects reaching a level of significance (9 in the GLM vs. 11 for the MCP approach; see Tab. 1). In addition, GLM analysis accuracies do not correlate significantly with any of the MCP analysis accuracies. However, comparison of the two methods is hampered by several fundamental differences: (1) In the GLM analysis, the data from only one channel was considered, whereas all channels are considered in the MCP analysis. (2) In the MCP analysis, more single-trials could be considered, resulting in a higher chance of getting significant results. (3) Due to the fundamentally different nature of both approaches, different significance tests were employed (Chi-square vs. permutation testing).

A general shortcoming of our study, affecting both the GLM and MCP analysis accuracies, is the absence of localizer data for the "no" condition. As there was no separate localizer to identify signal characteristics while participants do not change their brain state, the training data for encoding "no" answers was selected as the time window in the end of the resting period after each task performance. Obtaining proper localizer data for the "no" condition should be done it future experiments, albeit this would be at the cost of additional measurement time.

We noted large differences between individual participants' classification accuracies: some participants performed exceptionally well whereas for others classification accuracy was at chance level. Blood pressure, respiration and heart rate are known to influence the fNIRS signal [23]. Future studies taking into account these physiological measures may filter out such influences in order to improve the contrast-to-noise ratio of the fNIRS measurements. Moreover, given the very short training period, participants with chance-level performance may be retested after providing them with additional training.

We monitored comfortability over time and measured perceived easiness and pleasantness, as it is known that subjective motivation can influence BCI performance [24, 25]. Comfortability ratings across the experimental session decreased slightly with a drop in the last run. This could be due to the fact that performing a localizer run after the answer-encoding runs was experienced as comparatively boring. Overall, application of our BCI in affected patients is encouraged by the fact that our participants gave overall positive easiness and pleasantness ratings.

Table 1: Participant characteristics, subjective rating, channel selection and classification results.

			MD SR				*GLM accuracies*		*MCP analysis accuracies*	
P	*H*	*S*	*E*	*P*	*BS*	*Crit.*	ST (%)	MT (%)	ST (%)	MT (%)
1	R	M	8	7	2-4	16.69	75.00°	75.00	53.33*	66.67
2	R	F	9	8	2-5	5.28	55.00	50.00	33.33	33.33
3	R	F	10	10	3-3	101.44	70.00	75.00	70.00*	66.67
4	R	M	9	8	2-5	313.42	95.00°	100.00	76.67*	83.33
5	R	F	8	7	1-2	291.52	75.00°	75.00	70.00*	66.67
6	L	M	4	6	2-1	44.25	60.00	75.00	56.67	50.00
7	R	F	9	9	2-2	90.16	60.00	50.00	73.33*	100.00
8	R	M	7	6	3-6	71.26	45.00	50.00	53.33	50.00
9	R	M	7	7	2-1	177.18	70.00	75.00	76.67*	83.33
10	R	F	8	9	2-5	90.60	40.00	25.00	70.00*	66.67
11	R	F	6.5	6	2-3	73.27	60.00	50.00	66.67	66.67
12	R	F	7.5	5	1-2	26.03	45.00	25.00	63.33	83.33
13	R	M	6	4	2-6	2.59	85.00°	100.00	43.33	33.33
14	R	F	9	8	2-5	85.33	55.00°	75.00	70.00*	66.67
15	R	M	10	8	2-2	44.18	75.00°	100.00	73.33*	83.33
16	R	M	8	6	2-2	49.52	85.00°	100.00	73.33*	83.33
17	R	M	9	8	3-6	35.18	65.00	50.00	56.67	83.33
18	L	M	8	8	2-6	24.08	35.00	25.00	46.67	16.67
19	L	M	8	7	2-5	114.92	50.00	50.00	50.00	33.33
20	R	F	8	7	2-1	58.75	85.00°	75.00	70.00*	50.00
Mean			7.92	7.20			64.25	65.00	62.33	63.33
SE			.07	.07			3.72	5.56	2.77	4.93

Notes. P = participant, H = handedness, R = right, L = left, S = sex, M = male, F = female, MD SR = mental drawing subjective rating, E = average easiness rating across runs, P = average pleasantness rating across runs, BS = best channel, Crit. = Criterion, ST = single trial, MT = multi-trial, ° $p < .05$ based on Chi-Square, * $p < .05$ based on permutation testing.

Published by Verlag der TU Graz
Graz University of Technology

 DOI: 10.3217/978-3-85125-533-1-65

CONCLUSION

The presented yes/no communication procedure using fNIRS and mental imagery might constitute a useful communication means for LIS patients. Moreover, as the suggested encoding paradigm requires relatively little effort from individuals, it has potential as a diagnostic means to detect preserved conscious awareness in non-responsive patients.

ACKNOWLEDGEMENT

This work was supported by the European Commission (7th Framework Programme 2007-2013, DECODER project) and the Netherlands Organisation for Scientific Research (Research talent grant 406-15-217 to L.N.-C.).

REFERENCES

[1] Plum F, Posner JB. The diagnosis of stupor and coma. Contemporary neurology series. 1972; 10(1).

[2] Wolpaw JR, Birbaumer N, Heetderks WJ, McFarland DJ, Peckham PH, Schalk G et al. Brain-computer interface technology: a review of the first international meeting. IEEE Trans Rehab Eng. 2000;8: 164-73

[3] Kubler A, Mushahwar VK, Hochberg LR, Donoghue JP. (2006). BCI meeting 2005-workshop on clinical issues and applications. IEEE Trans Rehab Eng. 2006;14(2): 131-4.

[4] Farewell LA, Donchin A. Talking off the top of your head: toward a mental prosthesis utilizing event-related brain potentials. Electroen. Clin. Neuro. 1988;70(6): 510-23.

[5] Leuthardt EC, Schalk G, Wolpaw JR, Ojemann JG, Moran DW. A brain–computer interface using electrocorticographic signals in humans. J Neural Eng. 2004;1(2): 63.

[6] Mellinger J, Schalk G, Braun C, Preissl H, Rosenstiel W, Birbaumer N, et al. An MEG-based brain-computer interface (BCI). Neuroimage. 2007;36(7): 581-93.

[7] Birbaumer N, Ghanayim N, Hinterberger T, Iversen I, Kotchoubey B, Kübler A, et al. A spelling device for the paralysed. Nature. 1999;398(6725): 297-298.

[8] Nijboer F, Sellers EW, Mellinger J, Jordan MA, Matuz T, Furdea A, et al. A P300-based brain-computer interface for people with amyotrophic lateral sclerosis. Clin Neurophysiol. 2008;119(8): 1909-16.

[9] Blankertz B, Sanelli C, Halder S, Hammer E, Kübler A, Müller KR, et al. Predicting BCI performance to study BCI illiteracy. BMC Neuroscience. 2009;10(Suppl 1): 84.

[10] Sorger B, Dahmen B, Reithler J, Gosseries O, Maudoux A, Laureys S, et al. Another kind of 'BOLD Response': answering multiple-choice questions via online decoded single-trial brain signals. Prog Brain Res. 2009;177: 275-92.

[11] Monti MM, Vanhaudenhuyse A, Coleman MR, Boly M, Pickard JD, Tshibanda L, et al. Willful modulation of brain activity in disorders of consciousness. N Engl J Med. 2010;362(7): 579-89.

[12] Bardin JC, Fins JJ, Katz DI, Hersh J, Heier LA, Tabelow K, et al. Dissociations between behavioural and functional magnetic resonance imaging-based evaluations of cognitive function after brain injury. Brain. 2011;134(3): 769-82.

[13] Naci L, Owen AM. Making every word count for nonresponsive patients. JAMA neurology. 2013;70(10): 1235-41.

[14] Naito M, Michioka Y, Ozawa K, Yoshitoshi IT, Kiguchi M, Kanazawa T. A communication means for totally locked-in ALS patients based on changes in cerebral blood volume measured with near-infrared light. IEICE trans info syst. 2007;90(7): 1028-37.

[15] Gallegos-Ayala G, Furdea A, Takano K, Ruf CA, Flor H, Birbaumer N. Brain communication in a completely locked-in patient using bedside near-infrared spectroscopy. Neurology. 2014;82(21): 1930-2.

[16] Chaudhary U, Xia B, Silvoni S, Cohen LG, Birbaumer N. Brain–Computer Interface–Based Communication in the Completely Locked-In State. PLoS biology. 2017;15(1): e1002593.

[17] Sorger B, Reithler J, Dahmen B, Goebel R. A real-time fMRI-based spelling device immediately enabling robust motor-independent communication. Curr Biol. 2012;22(14): 1333-8.

[18] León-Carrión J, León-Domínguez U. Functional near-infrared spectroscopy (fNIRS): principles and neuroscientific applications. INTECH Open Access Publisher (2012).

[19] Scholkmann F, Kleiser S, Metz AJ, Zimmermann R, Pavia JM, Wolf U, et al. A review on continuous wave functional near-infrared spectroscopy and imaging instrumentation and methodology. Neuroimage. 2014;85: 6-27.

[20] Gijsen S. BrainStim, 2015, Software available at https://github.com/svengijsen/BrainStim

[21] Chang CC, Lin CJ. LIBSVM: a library for support vector machines, 2001, Software available at http://www.csie.ntu.edu.tw/~cjlin/libsvm

[22] Koessler L, Maillard L, Benhadid A, Vignal JP, Felblinger J, Vespignani H, et al. Automated cortical projection of EEG sensors: anatomical correlation via the international 10-10 system. Neuroimage. 2009;46(1): 64-72.

[23] Bauernfeind G, Wriessnegger SC, Daly I and Müller-Putz GR. Separating heart and brain: on the reduction of physiological noise from multichannel functional near-infrared spectroscopy (fNIRS) signals. J neural eng. 2014;11(5): 056010.

[24] Nijboer F, Birbaumer N, Kübler A. The influence of psychological state and motivation on Brain–computer interface performance in patients with amyotrophic lateral sclerosis – a longitudinal study. Front Neuroprost. 2010;4.

[25] Kleih SC, Nijboer F, Halder S, Kübler A. Motivation modulates the P300 amplitude during brain–computer interface use. Clin Neurophysiol. 2010;121(7), 1023-31.

Published by Verlag der TU Graz
Graz University of Technology

Proceedings of the
7th Graz Brain-Computer Interface Conference 2017 DOI: 10.3217/978-3-85125-533-1-66

PASSIVE DETECTION OF FEEDBACK EXPECTATION: TOWARDS FLUENT HYBRID EYE-BRAIN-COMPUTER INTERFACES

Y.O. Nuzhdin[1], S.L. Shishkin[1], A.A. Fedorova[1], B.L. Kozyrskiy[1,2], A.A. Medyntsev[3], E.P. Svirin[1], O.V. Korsun[1], I.A. Dubynin[1], A.G. Trofimov[4], B.M. Velichkovsky[1,5]

[1] Department of Neurocognitive Technologies, Kurchatov Complex of NBICS Technologies, National Research Center "Kurchatov Institute", Moscow, Russia

[2] Department of Cybernetics, National Research Nuclear University MEPhI, Moscow, Russia

[3] Institute of Psychology, Russian Academy of Sciences, Moscow, Russia

[4] Department of Computer Systems and Technologies, National Research Nuclear University MEPhI, Moscow, Russia

[5] NBIC-Faculty, Moscow Institute for Physics and Technology, Moscow, Russia

E-mail: nuzhdin.urii@gmail.com, sergshishkin@mail.ru

ABSTRACT: We present a general approach to the development of an unobtrusive and fast passive brain-computer interface that could be deeply integrated with gaze based control for fluent translation of intentions into actions, as well as the results of a pilot test of its online version in 9 healthy participants. The new hybrid Eye-Brain-Computer Interface (EBCI) utilizes an electroencephalogram component presumably related to the expectation of feedback from the gaze controlled interface. Online operation of the EBCI was made possible using *Resonance*, a new platform for fast prototyping of BCIs, enabling fast synchronized processing of multimodal signals from varying hardware with scripts written in *R*. In the online mode, EBCI provided the result of 19 channel EEG classification almost immediately when gaze dwell on a screen object (a colored "ball") exceeded 500 ms time threshold. For the first time, non-random online EBCI classifier performance was demonstrated.

INTRODUCTION

Selection with gaze – Selection of an object among several different objects on a screen is one of the most fundamental user's operation in interaction with computers. This operation typically involves a gaze dwell on the same object, so automatic detection of such dwells with the eye tracking technology can be used to predict a user's command. Based on this approach, various systems for assisting paralyzed people with preserved gaze control and for helping healthy users in certain situations have been developed [1]. While these systems are serious competitors of the non-invasive brain-computer interfaces (BCIs), they all suffer from their inherent limitation known as the Midas touch problem [2]: a system that respond to a certain intentional gaze behavior, such as an intentional gaze dwell on a link to a web page, would respond in many cases to unintentional gaze behaviors, i.e. spontaneous gaze dwells used for vision or related to mind wandering. While this problem is not critical in gaze typing, it severely hinders the use of gaze based input in many other application areas. Approaches developed for solving the Midas touch problems (e.g., using long dwell time threshold or additional gaze gestures for command confirmation) requires additional efforts from the user [1, 3].

Selection with gaze plus a passive BCI – A radical solution to the Midas touch problem could be the use of a BCI that would produce "mouse clicks" only when they are required by the user: "point with your eye and click with your mind!", proposed as early as in 1996 [4]. Unfortunately, typical noninvasive BCI technologies, such as mental imagery based BCIs, are rather slow for such a task (e.g., [5]); moreover, they are based on execution of additional mental tasks that require attentional resources. A promising alternative is the use of passive BCI approach [6], here, the use of a BCI that make a click only when the gaze fixation is accompanied by an EEG pattern specific to the intention to act at the fixated location. Early attempts to implement this approach [7, 8] made use of rather long fixations (1-2 s; this is still a relatively inconvenient duration); more importantly, experimental paradigms in these studies involved elements of visual search (see the next paragraph), where strong P300 could arise and enable good classification, while the approach could fail if targets were not assigned in advance.

Communicating intention vs. communicating relevance – The gaze plus passive BCI combination is currently actively explored in the explicit visual search paradigm (e.g., [9, 10, 11]) and its applications for estimation of the implicit information's relevance to the user are also developed [12, 13]. Similarly to these tasks, communicating intention involves informing a computer about what is relevant to the user in the

Published by Verlag der TU Graz
Graz University of Technology

 DOI: 10.3217/978-3-85125-533-1-66

context of his or her current task. Both communicating intention and visual search tasks may involve single-trial analysis and immediate triggering of the interface. Both communicating intention and communicating implicit relevance use primarily individual information. Specific to the communicating intention is that the user can form his or her intention freely at any time moment, and typically can also refrain from forming an intention. Communicating intention with a BCI combined with gaze fixations can be done only if sufficient accuracy is achieved already with single-trial analysis of short EEG segments, because immediate response of the interface is needed and because group average (which can be relevant in the visual search tasks) is typically not possible. While communicating a user's intention is the most usual task for human-computer interfaces, including BCIs, specific for gaze plus passive BCI combination (if it would be successfully applied for this task) could be that it would turn intentions into computer actions in the most effortless way.

An EEG marker for the new hybrid Eye-Brain-Computer Interface (EBCI) – In our previous study [14] we recorded and compared the electroencephalogram (EEG) during gaze dwells intentionally used for control and during similar spontaneous gaze dwells (all 500 ms duration or longer). In the gaze dwells used for control, but not in the spontaneous ones, a slowly progressing negative wave was found in the occipitotemporal area, likely related to the expectation of the interface feedback. Feature extraction was oriented on using this wave as their main source. It was possible to classify the "controlling" vs. spontaneous dwells using features from 13 EEG channels and only 300 ms length epochs [14].

The problem of fast prototyping of multimodal interfaces – The new interface, the EBCI, should be able to classify the EEG synchronized with gaze events in online mode and provide a response as soon as possible when the dwell time threshold is exceeded. Creating such an interface from scratch would require a vast amount of programming work, because many computational and user interface configurations may need to be tested before finding optimal ones, while each of these configurations should be adapted for sufficiently synchronized operation together with quite different sources of data streams, the interface and the experiment control tools. A platform specifically oriented on developing multimodal interfaces could be a solution, especially if it could support high-level programming languages for more flexible, fast and inexpensive designing of highly varying configurations needed at the early stage of the development of the new types of human-machine interfaces. A number of open source software platforms for BCI prototyping have been developed ([15, 16, 17, 18, 19]; see also [20, 21] for reviews); however, as follows from the publications, online fusion of signals from different sources was either not planned by their developers or was not their primary concern.

The Resonance platform – The *Resonance* platform is developed (by Y.O.N.) specifically for supporting the development of the interfaces that need to process online data streams from different sources. The platform takes care of data and event transmissions, synchronization and recording, and running classification algorithms. An *R* package (also named *Resonance*; freely available at https://github.com/tz-lom/Resonance-Rproj ; [22]) allows not only to process data in online mode but also to apply efficiently the same *R* code offline to the recorded data for a precise reconstruction of the online processing to debug and verify the algorithms. For programming the visual part of the interface, its "behavior" in response to detected user's intentions and organization of an experiment, integration with *QML* is provided. This platform (in its earlier version) was used to create a gaze controlled game *EyeLines* for capturing EEG synchronized with gaze interaction events in [14]. Recently, it was used for the online EBCI tests using the same game [23].

The problem of the access to a ground truth in relation to EBCIs – In our first attempt to test the EBCI online [23] we found it especially difficult to obtain the ground truth when the user is given freedom in defining the ways to solve a task. Similar problems may appear in free operation using any kind of interface, yet their severity can be specific to EBCIs because both the gaze and brain components may contribute to it: gaze dwell may occur out of conscious control at a location that is already studied unconsciously as a candidate for making a click on it, and similar patterns can be expected from brain's activity that accompany preparation to the action. Indeed, our participants told us that EBCI false alarms (the events they were not going to elicit) often looked as meaningful "hints", and that in such cases it was tempting to them not to report these events as false alarms. In addition, in this preliminary study we asked to press a key for reporting a false alarm, and this instruction also could lead to the refrain from reporting because of the need to switch to a manual task from a fully non-manual one (this problem can be also observed in pure BCI and gaze control studies). Therefore, we could not evaluate the online performance of the EBCI reliably.

The aim of the current study was to test several changes in our previously developed protocol for EBCI performance evaluation: modified instruction (focus on the identity of the interface response with intention instead of its "correctness") and reporting tool (use of the EBCI instead of the keyboard for reporting deviations from intentions) in the free operation test; two new tests with fixed tasks for separate estimation of sensitivity and specificity (see details below). We also planned to get the preliminary EBCI performance estimations if the changes would turn to be successful.

METHODS

Participants – Nine healthy volunteers (four female; age 18 to 50, median 24) took part in the study after signing an informed consent.

Published by Verlag der TU Graz
Graz University of Technology

 DOI: 10.3217/978-3-85125-533-1-66

Apparatus and software were generally the same as in our previous work [23]. *Resonance* platform (see above) and specific modules controlled all aspects of the experiment. The game module (written in *QML*) implemented game logic and presented the game visual interface on a computer screen. It communicated with *EyeLink 1000* eye tracker (SR Research, Canada) to control its settings and acquire gaze data. Eye tracking data (at 500 Hz rate) were converted to dwell events with a spatial (dispersion-based) criterion: the events were generated when gaze stayed in a 2° × 2° square region for 500 ms (the dwell time threshold), and medians of X and Y coordinates during the dwell were taken as its position. When the game module received such event, it sent a message to the *Resonance* data processing module which ran an *R* script that performed synchronization of the EEG and gaze dwell events, feature extraction and classification. If classification result was positive, a "click" event was sent back to the game, typically in tens of milliseconds after exceeding the dwell time threshold. The EEG data (also at 500 Hz sampling rate) were captured by *actiCHamp* EEG amplifier with *actiCAP* active electrodes (Brain Products, Germany). Its synchronization with the eye tracking data was based on synchronization pulses sent from the eye tracker to the EEG amplifier trigger port at the beginning of each trial.

The gaze controlled game – As in our previous work [23] *EyeLines*, the gaze controlled version of the computer game Lines (also known as Color Lines), was used both for the EBCI classifier training and its online testing. In *EyeLines*, each move consists of at least two gaze "clicks": the participant had to select one of the colored balls presented in the game board with a gaze dwell on it (the selected ball was indicated by a frame around it), and then make another dwell to indicate the location where it should be moved. The game board subtended 18 × 18° on the monitor screen (Fig. 1). When 4 balls of the same color formed a line, it disappeared, and the player get a score. After each move, three new balls of randomly selected colors appeared on the board at random positions (see [14] for details).

Figure 1. *EyeLines* game board.

Classifier training – EEG data for classifier training were collected, for each participant, in four games that were played with 500 ms (or longer) gaze dwells (each game lasted 5 min). An additional element (shown left to the 7 × 7 square board in Fig. 1) was used in the game interface at this stage of experiment, as in [14, 23]: participants had to switch on the gaze based control prior to each move by fixating a special "switch-on button" (a location outside the game board). Dwells not preceded by switching control on made no effect in the game and were considered as spontaneous. 271 to 369 EEG epochs related to controlling gaze fixations (on balls and on new locations for them) were collected. In [14, 23], the "switch-on button" disappeared from time to time, to provoke more spontaneous gaze dwells. In the current study, we used EEG related to spontaneous dwells only to adjust the classifier threshold and to test the classifier. Thus, less such data were needed, and the "switch-on button" was made available to a participant during all the game. It was found in our previous study [14] that averaged EEG related to spontaneous fixations has very low amplitude. Therefore, we now decided to use EEG epochs sampled from random time instances to imitate "spontaneous" data for classifier training. The number of such epochs was equal to the number of control-related epochs for each participant.

To obtain 152 features, EEG amplitudes from 19 channels (Fz, F3, F4, Cz, C3, C4, Pz, P1, P2, P3, P4, POz, PO3, PO4, PO7, PO8, Oz, O1, O2) were averaged in 50 ms windows started at 8 time instances (+300, +320, ... +440 ms relative to dwell start), separately per channel and window. +200..+300 ms interval was used for baseline correction. No high-pass filter was used. It was shown earlier that such a procedure ensures that the features are not affected by EOG contamination [14]. Shrinkage LDA from Fieldtrip toolbox [24] (http://www.ru.nl/neuroimaging/fieldtrip) was used to train the classifier. Threshold was adjusted to obtain specificity of about 0.90 on a validation subset.

Game playing with online EBCI – After classifier training, participants played another four *EyeLines* games, now with a hybrid EBCI. Now, control was always switched on, and 500 ms gaze dwells made effects if confirmed by the EEG classifier. To compensate for the EEG classifier's misses, additional threshold was used (following a suggestion from [8]): if gaze dwell time exceeded this threshold (1000 ms), "click" was made in any case, without applying the classifier to the EEG. In the first game using the online EBCI, the rate of its positive responses was computed and used in two of the remaining three games for a "random classifier" that provided responses with this rate irrespective the current EEG data.

The participants' task in the games was almost the same in the classifier training stage and in the online EBCI stage of the experiment: they were asked just to play the game with gaze dwells only. They were told that their EEG will help to recognize their intention to click in the online EBCI stage, so there will be no "switch-on button", but sometimes their intentions will

Published by Verlag der TU Graz
Graz University of Technology

 DOI: 10.3217/978-3-85125-533-1-66

be not recognized correctly. They were also told that it is important to report each case when they notice that the selected ball is not exactly that one that they decided to select, and even cases when a "good" ball was selected when they were about to make a decision to "click" on it, but before they actually made a clear decision. Unlike in our previous study [23], the participants did not need to switch to manual tools for reporting such cases: instead, they had to deselect the ball by continuing looking on it. However, they were not aware of the difference between the real and random classifier conditions.

Online tests for sensitivity and specificity were run in the end of the experiment to obtain online classification data with well known ground truth. For these tests, a 5 × 5 board was used instead of the 7 × 7 used in the games. First, balls with random colors appeared one by one at random locations, and the participants had to set them into four lines from left to right, top to bottom (Fig. 2). This test was used to estimate online EBCI sensitivity. Then, the participant was asked to remember the locations of the balls with three colors most frequently presented at the moment. The remembering task lasted for two minutes, and then the participant had to indicate the ball locations on a paper sheet. The EBCI was on but not used intentionally, and participants were told to ignore ball selections that sometimes happened. This test was used to estimate online EBCI specificity. Two pairs of the tests, one with real and one for random classifier (in random order), were used for four participants, and a double number of them was used for another five.

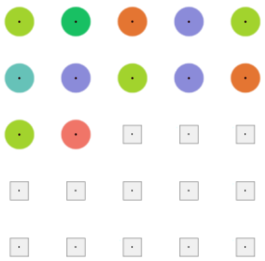

Figure 2. The board being filled with balls during a test for estimating online EBCI sensitivity.

EBCI classifier performance was estimated for ball selection in the first four games where no online EEG classification was used (Offline Performance in Games), for next four games played with online EBCI (separately for real and random classifiers, Online Performance in Games), and for the final tests (also separately for real and random classifiers, Online Performance in Tests).

Offline Performance in Games was estimated using five-fold cross-validation (the test subset did not overlap with the validation subset for threshold estimation). We computed ROC AUC, sensitivity, specificity and Youden's J index (J = sensitivity + specificity – 1; similarly to ROC AUC, it can be helpful when specificity gets higher on expense of sensitivity, and vice versa. While it is less reliable estimate than ROC AUC, its advantage is that it could be computed both for offline and online classifier performance.)

Online Performance in Games was quantified as sensitivity, specificity and J values, assuming the following meanings of the observed events: *true positives* for the gaze "clicks" with the short (500 ms) dwell time threshold (i.e., confirmed by the EEG classifier) not followed by de-selection; *true negatives* for dwells with duration between 500 ms and 1000 ms not confirmed by the EEG classifier; *false positives* for gaze "clicks" with the short (500 ms) dwell time threshold (i.e., confirmed by the EEG classifier) followed by de-selection; *false negatives* for gaze "clicks" with the long (1000 ms) dwell time threshold (spontaneous dwells of this duration are rare in playing *EyeLines* [14]).

Online Performance in Tests was also quantified as sensitivity, specificity and J values, but sensitivity and specificity were computed separately for the two tests (see above their description).

RESULTS

EBCI offline performance appeared to improve compared to our previous results: ROC AUC was 0.74 ± 0.04 ($M \pm SD$) for classification of dwells on balls (Tab. 1, second column), while, for example, in [14] it was 0.69 ± 0.09 for dwells on "switch-on button", where more prominent EEG potentials were observed comparing to dwells on balls. Among the changes in methodology that account for this improvement could be, as our additional pilot analysis suggested, the use of randomly sampled EEG epochs instead of spontaneous fixation-related data as the non-target class in classifier training.

Estimation of the EBCI online performance in games yielded, unfortunately, inconsistent results (not presented in Tab. 1): the random classifier demonstrated apparently non-random behavior. It seemed that the participants often did not reported the false positives for at least two reasons: because of not noticing the selection (especially if it appeared just before a saccade to a different location) or because of difficulty to differentiate a clearly formed decision from a decision that was yet being prepared during the dwell.

EBCI online performance in tests appeared more sensible (see Real and Rand columns in Tab. 1). Youden's J index for the random classifier did not differ from zero significantly ($p = 0.15$, according to Wilcoxon signed rank test), while for the real classifier it differed from zero ($p = 0.016$) and from random classifier J values ($Z = 2.52$, $p = 0.012$). Specificity was also significantly higher for the real classifier comparing to the random one ($Z = 2.10$, $p = 0.036$). Difference between real and random classifier for sensitivity was not significant ($Z = 1.52$, $p = 0.13$), but it was also in favor for the real classifier. Thus, although tests used to measure sensitivity and specificity were performed under different conditions, it appeared to be

Published by Verlag der TU Graz
Graz University of Technology

 DOI: 10.3217/978-3-85125-533-1-66

very likely that the significant difference in Youden's J represented non-random online performance of the EBCI. Nevertheless, online performance in tests was lower than offline performance (compare Offline and Real columns in Tab. 1). Significant decrease in online mode was observed, comparing to offline results, for Youden's J ($Z = 2.55$, $p = 0.01$) and for sensitivity ($Z = 2.55$, $p = 0.01$), while for specificity it decreased nonsignificantly ($Z = 0.18$, $p = 0.86$).

Table 1: Performance of the classifier: offline results for games and online results for tests

	AUC	**Sensitivity**			**Specificity**			**Youden's J**		
Sbj	**Offline**	**Offline**	**Real**	**Rand**	**Offline**	**Real**	**Rand**	**Offline**	**Real**	**Rand**
29	0.80	0.50	0.10	0.10	0.86	1.00	0.90	0.36	0.10	0.00
30	0.74	0.39	0.25	0.09	0.88	0.87	0.90	0.27	0.12	-0.01
32	0.74	0.42	0.15	0.08	0.88	0.85	0.86	0.30	0.00	-0.06
33	0.67	0.22	0.11	0.00	0.90	0.94	0.84	0.12	0.05	-0.16
34	0.79	0.37	0.05	0.05	0.91	0.92	0.92	0.28	-0.03	-0.03
35	0.74	0.29	0.21	0.25	0.89	1.00	0.78	0.18	0.21	0.03
36	0.75	0.36	0.30	0.23	0.87	0.80	0.73	0.23	0.10	-0.04
37	0.69	0.29	0.17	0.14	0.89	0.88	0.84	0.18	0.06	-0.02
38	0.70	0.22	0.24	0.29	0.96	0.87	0.74	0.18	0.11	0.02
M	**0.74**	**0.34**	**0.18**	**0.14**	**0.89**	**0.90**	**0.83**	**0.23**	**0.08**	**-0.03**
SD	**0.04**	**0.09**	**0.08**	**0.10**	**0.03**	**0.07**	**0.07**	**0.08**	**0.07**	**0.06**

DISCUSSION

This pilot study, for the first time, provided substantial evidence indicating that the Eye-Brain-Computer Interface based on the user's expectation of gaze controlled interface feedback may function in online mode. However, there were several issues in this study that should be resolved in future work:

(1) Online performance in this study was lower than in offline modeling. This could be related to unfavorable testing conditions. In the previous study [14] we found that the EEG marker for the gaze dwell used to send a command degrades along controlling gaze dwells that closely followed each other. Although it was not fully clear whether this was indeed a result of close positioning of the controlling dwells in time, the same effect, if it exists, could affect the marker in many gaze dwells intentionally used for control in the *EyeLines* game, because moves are often made rather automatically, without much thinking. In the sensitivity test, the required actions could be also too automatic for developing a strong expectation-related activity in the EEG.

(2) Sensitivity and specificity were calculated from data obtained under different conditions. This could bias Youden's J metric if these conditions affected classifier sensitivity and specificity differently.

(3) The EEG components that are related to the completion of a visual search task rather than to freely formed intention/expectation could contaminate the online test results. The participants had to locate each new ball in the test for sensitivity and to locate the balls related to the same color in the task of specificity, so the components related to finding a target, such as the P300 wave, could arise each time the fixation on these balls started. If the classifier was sensitive to these components, the results of these tests would be biased toward higher sensitivity and lower specificity compared to what should be observed under the use of intention-related components only; if the effect on sensitivity prevailed, Youden's J would be inflated. The time courses for the intentional dwells in *EyeLines* on which the classifier was trained (both them and topographies were similar to what was observed with our earlier studies with *EyeLines*, see Fig. 4 and Fig. 7 in [14]) were different from what is specific to the P300, however, this could not guarantee that classifier was completely insensitive to the P300 in tests.

All these issues imply that better methodology must be designed for EBCI testing. Issue (3) is especially important to resolve to finally prove if the expectation based EBCI is selectively sensitive to the user's intention. For assessing prospects for practical application, other challenging factors should be included into tests, such as saliency of relevant and irrelevant objects [25]. It is also evident that EBCI performance improvement is strongly needed. As suggested by our preliminary results, this may become possible with finding more adequate feature sets [26] and classifiers [14] for the EBCI.

If its further development will be successful, the expectation based EBCI could practically implement the idea of Grey Walter who proposed, as early as in 1960s, to use the expectation-related activity in the EEG for "the direct cerebral control of machines", "by-passing the operant effector system" [27].

ACKNOWLEDGEMENTS

This work was supported by the Russian Science Foundation, grant 14-28-00234.

REFERENCES

[1] Majaranta P, Bulling A. Eye tracking and eye-based human–computer interaction. In: Fairclough SH,

Published by Verlag der TU Graz
Graz University of Technology

 DOI: 10.3217/978-3-85125-533-1-66

Gilleade K (Ed.). Advances in Physiological Computing: Human–Computer Interaction Series. Springer, London 2014, pp. 39–65

[2] Jacob RJ. The use of eye movements in human-computer interaction techniques: what you look at is what you get. ACM Trans. Inf. Syst. 1991;9: 152-169

[3] Velichkovsky B, Sprenger A, Unema P. Towards gaze-mediated interaction: collecting solutions of the "Midas touch problem," in Proc. INTERACT'97, Chapman and Hall, London, UK, 1997, 509-516

[4] Velichkovsky BM, Hanse JP. New technological windows into mind: there is more in eyes and brains for human-computer interaction, in Proc. CHI '96, 1996, 496-503

[5] Zander TO, Gaertner M, Kothe C, Vilimek R. Combining eye gaze input with a brain–computer interface for touchless human–computer interaction. Int. J. Hum. Comput. Interact. 2010;27: 38-51

[6] Zander TO, Kothe C. Towards passive brain–computer interfaces: applying brain–computer interface technology to human–machine systems in general. J. Neural Eng. 2011:8:025005

[7] Ihme K, Zander TO. What you expect is what you get? Potential use of contingent negative variation for passive BCI systems in gaze-based HCI, in Proc. ACII'11, 2011, 447-456

[8] Protzak J, Ihme K, Zander TO. A passive brain-computer interface for supporting gaze-based human-machine interaction, in Proc. UAHCI'13, 2013, 662-671.

[9] Brouwer AM, Reuderink B, Vincent J, van Gerven MA, van Erp JB. Distinguishing between target and nontarget fixations in a visual search task using fixation-related potentials. J. Vis. 2013;13:17.

[10] Finke A, Essig K, Marchioro G, Ritter H. Toward FRP-based brain-machine interfaces–single-trial classification of fixation-related potentials. PLoS ONE. 2016;11:e0146848.

[11] Ušćumlić M, Blankertz B. Active visual search in non-stationary scenes: coping with temporal variability and uncertainty. J. Neural Eng. 2016;13:016015

[12] Jangraw DC, Wang J, Lance BJ, Chang SF, Sajda P. Neurally and ocularly informed graph-based models for searching 3D environments. J. Neural Eng. 2014;11(4):046003

[13] Golenia J, Wenzel M, Blankertz B. Live demonstrator of EEG and eye-tracking input for disambiguation of image search results. In: Blankertz B, Jacucci G, Gamberini L, Spagnolli A, Freeman J (Ed.). Symbiotic Interaction. LNCS, vol 9359. Springer, Cham, 2015, pp. 81-86

[14] Shishkin SL, Nuzhdin YO, Svirin EP, Trofimov AG, Fedorova AA, Kozyrskiy BL and Velichkovsky BM. EEG negativity in fixations used for gaze-based control: Toward converting intentions into actions with an Eye-Brain-Computer Interface. Front. Neurosci. 2016;10:528

[15] Schalk G, McFarland DJ, Hinterberger T, Birbaumer N, Wolpaw JR. BCI2000: a general-purpose brain-computer interface (BCI) system. IEEE Trans. BME. 2004;51(6):1034-1043

[16] Renard Y, Lotte F, Gibert G, Congedo M, Maby E, Delannoy V, ... Lécuyer A. OpenViBE: An open-source software platform to design, test, and use brain–computer interfaces in real and virtual environments. Presence: teleoperators and virtual environments. 2010;19(1):35-53

[17] Venthur B, Dähne S, Höhne J, Heller H, Blankertz, B Wyrm: A brain-computer interface toolbox in python. Neuroinformatics. 2015;13(4):471-486

[18] Breitwieser C. TiD--Documentation of TOBI Interface D. arXiv:1507.01313. 2015 July 6

[19] Lee MH, Fazli S, Kim KT, Lee SW. Development of an open source platform for brain-machine interface: openBMI. In Proc. 4th Int. Winter Conf. on BCI, 2016

[20] Brunner C, Andreoni G, Bianchi L, Blankertz B, Breitwieser C, Kanoh SI, Kothe CA, Lécuyer A, Makeig S, Mellinger J, Perego P. BCI software platforms. In Towards Practical Brain-Computer Interfaces. Springer, Berlin 2012, pp. 303-331

[21] Torniainen J, Henelius A. A short review and primer on online processing of multiple signal sources in human computer interaction applications. arXiv:1609.02339. 2016 Sep 8

[22] Nuzhdin YO. 2016. [A library for data processing in a brain-computer interface.] Lomonosov-2016. Moscow, Russia, pp. 78-80 (in Russian) https://lomonosov-msu.ru/archive/Lomonosov_2016/data/8342/uid73990_be24b87706be48e2ea8263b7d53dd62a7822e46b.pdf

[23] Nuzhdin YO, Shishkin SL, Fedorova AA, Trofimov AG, Svirin EP, Kozyrskiy BL, Medyntsev AA, Dubynin IA, Velichkovsky BM. The expectation based Eye-Brain-Computer Interface: An attempt of online test. Proc. BCIforReal'17, Limassol, Cyprus, 2017, pp. 39-42

[24] Oostenveld R, Fries P, Maris E, Schoffelen JM. (2011). FieldTrip: open source software for advanced analysis of MEG, EEG, and invasive electrophysiological data. Comput. Intell. Neurosci. 2011:156869

[25] Wenzel MA, Golenia J-E and Blankertz B. Classification of eye fixation related potentials for variable stimulus saliency. Front. Neurosci. 2016;10:23

[26] Shishkin SL, Kozyrskiy BL, Trofimov AG, Nuzhdin YO, Fedorova AA, Svirin EP, Velichkovsky BM. Improving eye-brain-computer interface performance by using electroencephalogram frequency components. Bull. RSMU. 2016;2:36–41

[27] Walter WG. Expectancy waves and intention waves in the human brain and their application to the direct cerebral control of machines. Electroenceph. Clin. Neurophysiol. 1966;21:616

Published by Verlag der TU Graz
Graz University of Technology

Proceedings of the
7th Graz Brain-Computer Interface Conference 2017 DOI: 10.3217/978-3-85125-533-1-67

VISUAL INPUT AFFECTS THE DECODING OF IMAGINED MOVEMENTS OF THE SAME LIMB

P. Ofner[1], P. Kersch[1], G. R. Müller-Putz[1]

[1]Institute of Neural Engineering, Graz University of Technology, Graz, Austria

E-mail: gernot.mueller@tugraz.at

ABSTRACT: A better understanding how movements are encoded in electroencephalography (EEG) signals is required to develop a more natural control for motor neuroprostheses. We decoded imagined hand close and supination movements from seven healthy subjects and investigated the influence of the visual input. We found that motor imagination of these movements can be decoded from low-frequency time-domain EEG signals with a maximum average classification accuracy of $57.3 \pm 5.0\%$. The simultaneous observation of congruent hand movements increased the classification accuracy to $64.1 \pm 8.3\%$. Furthermore, the sole observation of hand movements yielded discriminable brain patterns ($61.9 \pm 5.5\%$). These findings show that for low-frequency time-domain EEG signals, the type of visual input during classifier training affects the performance and has to be considered in future studies.

INTRODUCTION

Understanding the encoding of movements in the human brain is paramount for the development of a new and more intuitive control of motor neuroprostheses. Our group already restored movement function in persons with spinal cord injury (SCI) with motor neuroprostheses [1, 2, 3, 4] based on functional electrical stimulation (FES) [5, 6]. However, the control of FES via a non-invasive brain-computer interface (BCI) is in general unintuitive and unnatural. The BCI requires subjects to learn the expression of brain patterns which can be unrelated to the actual restored movement (e.g. imagination of foot movement to control the hand). Furthermore, the imagined movements are usually repetitive movements and not single movements. These BCIs are usually based on sensorimotor rhythms (SMR) extracted from electroencephalography (EEG) signals. However, newer research suggests that more details of movements can be decoded from low-frequency EEG signals [7, 8, 9, 10]. Furthermore, our group decoded six single movements (elbow extension/flexion, pronation/supination, hand open/close) of the upper limb from low-frequency time-domain signals [11]. This is of special interest in the context of neuroprosthesis control as, e.g., persons with SCI may then imagine or attempt one of these single movements to control a motor neuroprosthesis more naturally. However, as there are no overt movements causing a change in the sensory feedback, the visual input (here: movement observation) becomes potentially more important and may have an impact on the decoding performance. In fact, a sole observation of another movement is known to interfere with the execution of a movement [12], and affects brain rhythms [13, 14]. Furthermore, the visual system can partly substitute the somatosensory system [15]. This point is of special interest because we speculate that the decoding of movements from EEG may depend on a closed loop between the motor cortex and the spinal cord, i.e. proprioceptive feedback may partly be responsible for the modulation of low-frequency EEG signals which is then decoded with a BCI. In this work, we analysed if the lack of varying sensory feedback during motor imagination (MI) can be partly substituted by visual input which in turn may improve the classification accuracy. We hypothesize that the simultaneous observation of hand movements which correspond to imagined movements improves the classification accuracy. As a control condition, we used abstract visuals.

MATERIALS AND METHODS

Subjects: Seven healthy and right-handed subjects participated in the study. They were aged between 20 and 28 years. Three of them were female. The subjects received payment for their participation.

Paradigm:

The subjects sat in a comfortable chair in front of a horizontal computer screen which was used to give instructions and visual input to the subjects. The right arm was positioned under the computer screen (see Fig. 1). We instructed the subjects to perform kinesthetic motor imagery (MI) [14] of closing the right hand (CLOSE) or rotating the right arm (SUPINATION) while observing a movie showing a congruent realistic or an abstract movement. The realistic visual input (RVI) was pre-recorded from a human arm performing the movements while the abstract visual input (AVI) was an animation of a circle turning into an ellipse (see Fig. 2). The circle narrowed either from the top and bottom corresponding to CLOSE or from the left and right side corresponding to SUPINATION. Additionally to CLOSE and SUPINATION, we recorded a REST condition where we showed a picture (realistic or abstract) instead of a movie. In

Published by Verlag der TU Graz
Graz University of Technology

 DOI: 10.3217/978-3-85125-533-1-67

REST subject were instructed to not perform any MI. However, REST was not further analysed in this work. To disentangle the effect of MI and the observation of visual input, we employed a movement observation condition. In this condition, subjects were instructed to omit any MI while observing the movie (OBS). Thus, we had three types of conditions: CLOSE/SUPINATION/REST (movement condition), AVI/RVI (visual input condition) and MI/OBS (mental task condition) (see Fig. 3). Fig. 4 shows the sequence of one trial. At the beginning of one trial, the subjects were informed on a computer screen whether MI has to be performed synchronously to the upcoming movie or whether the movie should only be observed. When the movie appeared, it immediately started to play for 2 seconds, paused then and finally disappeared at the end of the trial, i.e. every MI or observation lasted 2 seconds. The movie was either an RVI or AVI type and the movement shown was either CLOSE, SUPINATION or REST. The initial frames of the movies were exactly the same (AVI) or indistinguishable (RVI). After the movie stopped playing, a 1.5 s long idle period followed and then the trial ended. Subsequent to one trial, an inter-trial interval with a random duration of 1.5 - 2.5 s followed. We used a block design to record the trials and runs. Each block exclusively comprised 3 AVI or 3 RVI runs and the blocks where arranged as follows: RVI/AVI/AVI/RVI. Before the first RVI and AVI run, respectively, we additionally recorded a training run. This two training runs were used to familiarize the subjects with the paradigm and were not further evaluated. At the beginning, middle and end of a recording, we also recorded runs in which subjects performed eye movements or rested. However, those runs were not further used in this work. Each run comprised 11 trials per CLOSE/SUPINATION class and 5 trials per REST class. Thus, in total we recorded 66 trials (CLOSE/SUPINATION) and 30 trials (REST) for each RVI/AVI and MI/OBS condition.

Figure 1: Subjects observed or performed MI according to real visual input or abstract visual input. The right hand was under the computer screen.

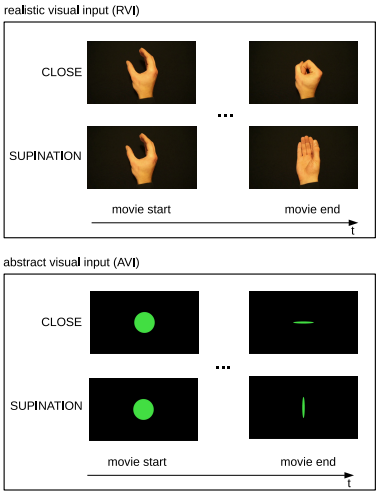

Figure 2: Subjects observed movements or performed MI with real visual input or abstract visual input.

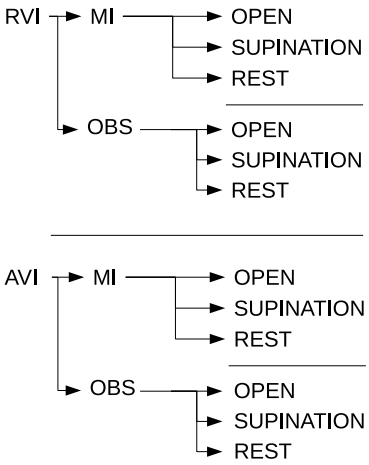

Figure 3: Types of conditions. Subjects perceived real (RVI) or abstract visual input (AVI). They performed MI of CLOSE/SUPINATION/REST or observed (OBS) CLOSE/SUPINATION/REST.

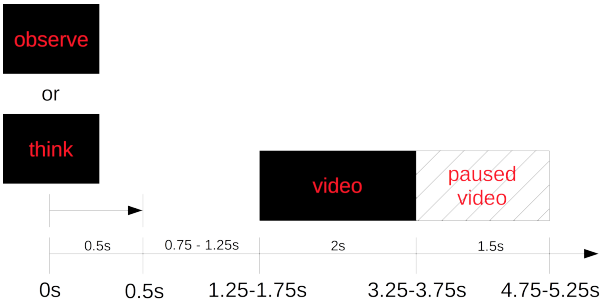

Figure 4: Trial sequence. An instruction was shown at second 0 for 500 ms to inform the subject if a MI has to be performed synchronously to the upcoming movie ("think") or if the movie should only be observed ("observe"). Subsequently, a movie appeared after a random interval and started to play.

Published by Verlag der TU Graz
Graz University of Technology

 DOI: 10.3217/978-3-85125-533-1-67

Recording: We recorded 61 EEG channels covering frontal, central, parietal and temporal areas of the head as well as 3 EOG channels placed above the nasion and the outer canthi of the eyes. Signals were recorded with active electrodes and biosignal amplifiers (g.tec medical engineering GmbH, Austria) with the reference placed on the right mastoid and ground on AFz. We applied an 8th-order Chebyshev bandpass filter from 0.01 Hz to 200 Hz and sampled the signals at 512 Hz. Furthermore, a notch filter at 50 Hz suppressed line noise.

Preprocessing: First, EEG channels were visually inspected and noisy or defective channels were removed. To prepare the data for an independent component analysis (ICA), we band-pass filtered with a zero-lag 4th-order Butterworth filter from 0.3 Hz to 70 Hz. Then we calculated the median absolute deviation (MAD) for each channel using data only from trials (i.e. not from inter-trial intervals) and marked EEG samples as artefact contaminated if they exceeded a threshold of 7.41 times the MAD (corresponding to 5 times the standard deviation for normally distributed data) of the respective channel. All samples which were not marked as artefact contaminated were subjected to an Extended Infomax ICA [16] implemented in EEGLAB [17] (which was applied using the first n principal components explaining 99 % of the variance of the data). ICA components corresponding to eye movements and muscle artefacts were marked as artefact contaminated. The above mentioned sample-based MAD method was solely used to detect transient artefacts which can impair an ICA. However, for the actual classification we used EEGLAB to detect artefact contaminated trials with: (1) amplitudes above/below -80 μV and 80 μV, respectively; (2) trials with abnormal joint probabilities; (3) trials with abnormal kurtosis. The methods (2) and (3) used 4 times the standard deviation of their respective statistic as a threshold to detect artefacts.
Finally, we applied a 0.3 Hz to 3 Hz zero-lag 4th-order Butterworth band-pass filter the original (unfiltered) EEG data to extract low-frequency time-domain features from the EEG, and removed independent components and trials previously marked as artefact contaminated.

Classification: We classified the two classes CLOSE and SUPINATION in each RVI/AVI and MI/OBS condition. We used a shrinkage linear discriminant analysis (sLDA) [18, 19] and a sliding window. In more detail, we used the time lags -200 ms to 200 ms in 100 ms time intervals relative to the center of the sliding window as an input to the sLDA classifier (i.e. 5 time lags). We moved this window over the trials (from -1 s to 3 s in 62.5 ms time steps relative to the start of the movie) and report the classification accuracies associated to the center point of the sliding window. The classification results were validated with a 10x10-fold cross-validation at each classification time step.

Topoplots: To calculate the topoplots, we first interpolated removed channels. Then, we calculated the difference between the average scalp potentials (monopolar) of CLOSE and SUPINATION for each RVI/AVI and MI/OBS condition at each time point within a trial (using a time resolution of 62.5 ms). Afterwards, we took the absolute value of each channel value and time averaged over the movie period of 2 s. Finally, we averaged over subjects.

RESULTS

Classification Accuracies: Fig. 5 shows the classification accuracies of CLOSE vs SUPINATION for all conditions. Classification accuracies were calculated from -1 s to 3 s relative to movie start with a time resolution of 1/16 s. The significance level with respect to a single subject is 64 % ($\alpha = 0.05$, adjusted Wald interval [20, 21], Bonferroni corrected for the time duration in Fig. 5). Five subjects exceeded the significance level between 0 s and 2 s in the RVI-MI condition, 6 in RVI-OBS, 4 subjects in AVI-MI, and no subject in AVI-OBS. RVI yielded higher classification accuracies than AVI, and MI yielded higher classification accuracies than OBS, c.f. Table 1. We conducted a two-way repeated measure ANOVA with 2 factors - RVI/AVI (visual input) and MI/OBS (mental task) - and compared the classification accuracies at the time point of maximal average classification accuracy. The visual input main effect was significant ($F(1,6) = 8.25$, $p = 0.03$), i.e. the classification accuracy increase between AVI and RVI was significant. The mental task main effect ($F(1,6) = 0.79$, $p = 0.41$) and the interaction effect ($F(1,6) = 0.04$, $p = 0.84$) were not significant. The sphericity assumption was tested with Mauchly's test and was not violated ($p = 0.57$).

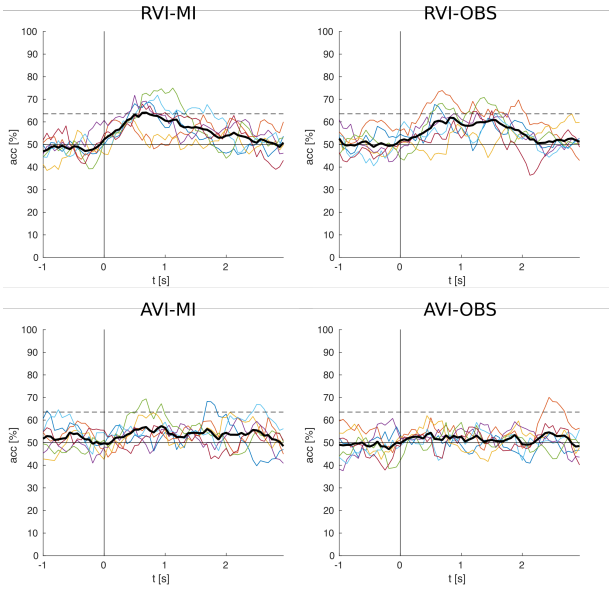

Figure 5: Classification accuracies for RVI/AVI and MI/OBS conditions. Shown are the individual subjects' accuracies and the grand average in bold. At second 0 the movie started to play for 2 seconds. The horizontal solid line is the chance level, the dashed line is the significance level on a single subject basis.

Published by Verlag der TU Graz
Graz University of Technology

 DOI: 10.3217/978-3-85125-533-1-67

Table 1: Maximum average classification accuracies with standard deviations and times relative to the movie start

	RVI-MI	RVI-OBS	AVI-MI	AVI-OBS
max acc [%]	64.1	61.9	57.3	54.4
std dev [%]	8.3	5.5	5.0	4.3
time [t]	0.69	0.81	0.94	0.50

We also analysed the classification accuracy of MI vs OBS with RVI. For this purpose, we aggregated CLOSE and SUPINATION trials in the RVI-MI and RVI-OBS conditions and classified these two conditions, see Fig. 6. The significance level with respect to a single subject is 60 %.

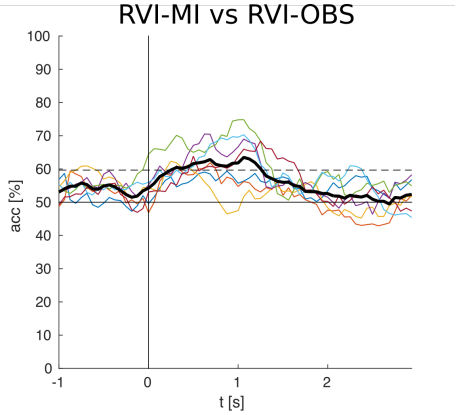

Figure 6: Classification accuracy of MI vs OBS with RVI. Shown are the individual subjects' accuracies, the grand average in bold, the chance level (horizontal solid line), and the significance level (dashed line).

Topoplots: Fig. 7 shows the topoplots where a prominent central pattern is observable for motor imagery during real visual input (RVI-MI).

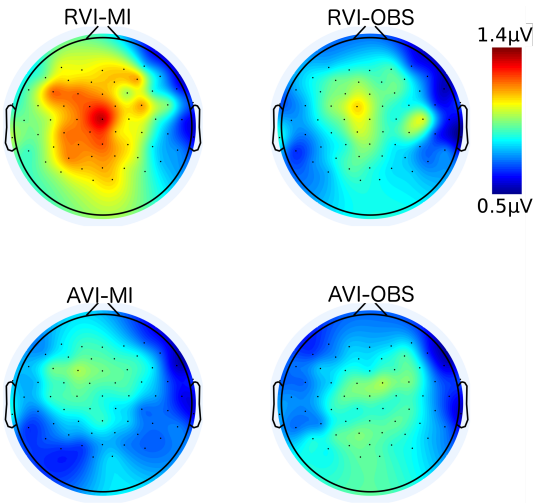

Figure 7: Topoplots. Shown are subject averaged absolute differences between the CLOSE and SUPINATION scalp potential maps. All plots have the same scale (blue is the minimum, red the maximum).

DISCUSSION

We showed the classification of two MIs from the same upper limb based on low-frequency time-domain EEG signals. Importantly, the MIs were not repetitive as in classical SMR-based BCIs but single ones, which are closer to ordinary movements. Furthermore, the MIs corresponded closely to movements which currently could be restored with a motor neuroprosthesis [6]. Some subjects reached a significant classification accuracy when observing abstract visual input. This indicates that the analysed imagined movements can be decoded even in the absence of any realistic visual input. This is in line with [22, 23], where imagined hand movements were decoded from the frequency-domain of EEG. Furthermore, consistent with our initial hypothesis, the results show that the classification accuracy can be increased when serving realistic visual input. Perhaps by substituting the somatosensory feedback at the somatosensory cortex with forwarded input from the visual system as in [15]. However, in our experiment there was no dedicated phase to incorporate the observed hand in ones own body schema.

In a practical setup, we cannot simply present realistic visual input to improve the classification accuracy because that would require knowledge about the indented movement before it was classified. The idea is rather to bootstrap the classification, i.e. presenting realistic visual input in the initial training of the classifier when no feedback is provided yet (open-loop). If the classifier performance is on an acceptable performance level, the subject can then be trained with actual feedback (closed-loop). A principle which has been applied in invasive studies [24, 25] with a robotic arm. However, their the idea was rather to obtain kinematic data for decoder calibration than observing human movements. A robotic arm is different to a human arm, however the boundary between abstract and realistic visual feedback is probably not sharp but continuous and the robotic arm may have been perceived similar to an human arm. Further studies could investigate if the presentation of a human hand is advantageous to a robotic arm in the open-loop classifier training. However, in the context of motor neuroprostheses, movement function is restored without using a robotic arm and this question does not arise.

Most surprisingly, the sole observation of hand movements yielded classification accuracies comparable to MI (c.f. RVI-MI and RVI-OBS). Movement observation has been reported to modulate brain rhythms [13, 14] (with respect to a no-movement condition). In this work, we show for the first time (to the best of our knowledge) that the observation of different movements of the same limb can be decoded from low-frequency time-domain EEG signals. In the context of motor neuroprosthesis control,

Published by Verlag der TU Graz
Graz University of Technology

 DOI: 10.3217/978-3-85125-533-1-67

this raises the question if the discriminability in RVI-MI is solely due to the simultaneously observed movement. The classification accuracies in AVI-MI indicate that a classification is basically possible, regardless of the visual input. Furthermore, the results show that MI and movement observation are discriminable during real visual input. However, it can not be answered in this study whether the classification accuracy *increase* is (1) solely due to movement observation or (2) whether the neural correlate of MI is modulated by the movement observation in a way which increases the discriminable information or (3) a combination of both. Nevertheless, the open-loop/closed-loop training approach may still work even when the increase of classification accuracy is solely due to the movement observation. Thus, the impact of this finding on the open-loop/closed-loop training has to be investigated in forthcoming studies. If the observation of movements has activated the mirror neuron system which in turn facilitated the classification is debatable. Mirror neurons fire only when observing meaningful movements. However, in our study no interaction of the movement with the environment was given, i.e. the observed movements were non-goal-directed and should not have activated the mirror neuron system.

The amount of discriminative information in the 4 different conditions is also reflected in the topoplots. The RVI-MI topoplot shows the largest amplitude differences between CLOSE and SUPINATION, followed by RVI-OBS and then the two AVI conditions. The observed RVI patterns are widespread. However, central motor areas are pronounced the most, showing that the discriminative information is indeed encoded in brain signals. Interesting is that RVI-MI has a more amplified pattern than RVI-OBS but similar classification accuracies. This may be due to a more stable pattern during the video sequence (topoplots are averaged over the whole movie period as opposed to the classification accuracies). This indicates that the discriminative information is encoded differently between MI and movement observation.

CONCLUSION

We show the classification of two imagined movements of the same upper limb and show that the classification accuracy can be increased if the movement is simultaneously observed in a video. Furthermore, we show that also the sole observation of movement videos yields discriminable brain patterns.

ACKNOWLEDGEMENTS

This work is supported by the European ICT Programme Project H2020-643955 "MoreGrasp" and the ERC Consolidator Grant ERC-681231 "Feel Your Reach".

REFERENCES

[1] G. R. Müller-Putz, R. Scherer, G. Pfurtscheller, and R. Rupp, "EEG-based neuroprosthesis control: a step towards clinical practice," *Neurosci Lett*, vol. 382, pp. 169–174, 2005.

[2] G. Pfurtscheller, G. R. Müller, J. Pfurtscheller, H. J. Gerner, and R. Rupp, ""Thought"-control of functional electrical stimulation to restore handgrasp in a patient with tetraplegia," *Neurosci Lett*, vol. 351, pp. 33–36, 2003.

[3] A. Kreilinger, V. Kaiser, M. Rohm, R. Leeb, R. Rupp, and G. Müller-Putz, "Neuroprosthesis control via noninvasive hybrid brain-computer interface," *IEEE Intell Syst*, vol. 28, no. 5, pp. 40–43, 2013.

[4] M. Rohm, M. Schneiders, C. Müller, A. Kreilinger, V. Kaiser, G. R. Müller-Putz, and R. Rupp, "Hybrid brain-computer interfaces and hybrid neuroprostheses for restoration of upper limb functions in individuals with high-level spinal cord injury," *Artif Intell Med*, vol. 59, no. 2, pp. 133–142, 2013.

[5] R. Rupp and H. J. Gerner, "Neuroprosthetics of the upper extremity - clinical application in spinal cord injury and challenges for the future," *Acta Neurochir. Suppl.*, vol. 97, no. Pt 1, pp. 419–426, 2007.

[6] R. Rupp, M. Rohm, M. Schneiders, A. Kreilinger, and G. Muller-Putz, "Functional rehabilitation of the paralyzed upper extremity after spinal cord injury by noninvasive hybrid neuroprostheses," *Proceedings of the IEEE*, vol. 103, pp. 954–968, June 2015.

[7] T. J. Bradberry, R. J. Gentili, and J. L. Contreras-Vidal, "Reconstructing three-dimensional hand movements from noninvasive electroencephalographic signals," *J Neurosci*, vol. 30, pp. 3432–3437, 2010.

[8] P. Ofner and G. R. Müller-Putz, "Decoding of velocities and positions of 3d arm movement from eeg," in *EMBC, 2012 Annual International Conference of the IEEE*, pp. 6406–6409, 2012.

[9] Y. Gu, K. Dremstrup, and D. Farina, "Single-trial discrimination of type and speed of wrist movements from eeg recordings," *Clin Neurophysiol*, vol. 120, no. 8, pp. 1596–1600, 2009.

[10] M. Jochumsen, I. K. Niazi, D. Taylor, D. Farina, and K. Dremstrup, "Detecting and classifying movement-related cortical potentials associated with hand movements in healthy subjects and stroke patients from single-electrode, single-trial eeg," *J. Neural Eng.*, vol. 12, no. 5, p. 056013, 2015.

[11] P. Ofner, A. Schwarz, J. Pereira, and G. R. M, "Movements of the same upper limb can be classified from low-frequency time-domain eeg signals," in *6th International BCI Meeting, Asilomar*, 2016.

Published by Verlag der TU Graz
Graz University of Technology

 DOI: 10.3217/978-3-85125-533-1-67

[12] J. M. Kilner, Y. Paulignan, and S. J. Blakemore, "An interference effect of observed biological movement on action," *Current Biology*, vol. 13, pp. 522–525, 2003.

[13] S. Cochin, C. Barthelemy, B. Lejeune, S. Roux, and J. Martineau, "Perception of motion and qeeg activity in human adults," *Electroencephalogr Clin Neurophysiol*, vol. 107, pp. 287–295, 1998.

[14] C. Neuper, R. Scherer, M. Reiner, and G. Pfurtscheller, "Imagery of motor actions: differential effects of kinesthetic versus visual-motor mode of imagery on single-trial eeg," *Brain Research Cognitive Brain Research*, vol. 25, pp. 668–677, 2005.

[15] S. Shokur, J. E. O'Doherty, J. A. Winans, H. Bleuler, M. A. Lebedev, and M. A. L. Nicolelis, "Expanding the primate body schema in sensorimotor cortex by virtual touches of an avatar," *PNAS*, vol. 110, no. 37, pp. 15121–15126, 2013.

[16] T. W. Lee, M. Girolami, and T. J. Sejnowski, "Independent component analysis using an extended infomax algorithm for mixed sub-gaussian and super-gaussian sources," *Neural Comput*, vol. 11, no. 2, pp. 417–441, 1999.

[17] A. Delorme and S. Makeig, "Eeglab: an open source toolbox for analysis of single-trial eeg dynamics including independent component analysis," *J Neurosci Methods*, vol. 134, no. 1, pp. 9–21, 2004.

[18] B. Blankertz, S. Lemm, M. Treder, S. Haufe, and K.-R. Müller, "Single-trial analysis and classification of erp components - a tutorial," *Neuroimage*, vol. 56, no. 2, pp. 814–825, 2011.

[19] R. Peck and J. V. Ness, "The use of shrinkage estimators in linear discriminant analysis," *IEEE Trans Pattern Anal Mach Intell*, vol. 4, no. 5, pp. 530–7, 1982.

[20] G. R. Müller-Putz, R. Scherer, C. Brunner, R. Leeb, and G. Pfurtscheller, "Better than random? a closer look on bci results," *International Journal of Bioelectromagnetism*, vol. 10, no. 1, pp. 52–55, 2008.

[21] M. Billinger, I. Daly, V. Kaiser, J. Jin, B. Z. Allison, and G. R. Müller-Putz, *Towards Practical Brain-Computer Interfaces*, ch. Is it significant? Guidelines for reporting BCI performance, pp. 333–354. Springer, Berlin Heidelberg, 2012.

[22] A. Vučković and F. Sepulveda, "Delta band contribution in cue based single trial classification of real and imaginary wrist movements," *Med Biol Eng Comput*, vol. 46, no. 6, pp. 529–539, 2008.

[23] A. Vučković and F. Sepulveda, "A two-stage four-class bci based on imaginary movements of the left and the right wrist," *Med Eng Phys*, vol. 34, no. 7, pp. 964–971, 2012.

[24] L. R. Hochberg, D. Bacher, B. Jarosiewicz, N. Y. Masse, J. D. Simeral, J. Vogel, S. Haddadin, J. Liu, S. S. Cash, P. van der Smagt, and J. P. Donoghue, "Reach and grasp by people with tetraplegia using a neurally controlled robotic arm," *Nature*, vol. 485, pp. 372–375, 2012.

[25] J. L. Collinger, B. Wodlinger, J. E. Downey, W. Wang, E. C. Tyler-Kabara, D. J. Weber, A. J. C. McMorland, M. Velliste, M. L. Boninger, and A. B. Schwartz, "High-performance neuroprosthetic control by an individual with tetraplegia," *Lancet*, vol. 381, no. 9866, pp. 557–564, 2013.

Published by Verlag der TU Graz
Graz University of Technology

Proceedings of the
7th Graz Brain-Computer Interface Conference 2017 DOI: 10.3217/978-3-85125-533-1-68

Sparse Bayesian Learning for Multiclass Classification with application to SSVEP- BCI

V. P. Oikonomou[1], G. Liaros[1], S. Nikolopoulos[1], I. Kompatsiaris[1]

[1]Information Technologies Institute, Centre for Research and Technology Hellas, CERTH-ITI, 6th km Charilaou-Thermi Road, 57001 Thermi-Thessaloniki, Greece

E-mail: {viknmu,geoliaros,nikolopo,ikom}@iti.gr

ABSTRACT: Sparse Bayesian Learning (SBL) is a basic tool of machine learning. In this work, multiple linear regression models under the SBL framework (namely MultiLRM), are used for the problem of multiclass classification. As a case study we apply our method to the detection of Steady State Visual Evoked Potentials (SSVEP), a problem we encounter into the Brain Computer Interface (BCI) concept. The multiclass classification problem is decomposed into multiple regression problems. By solving these regression problems, a discriminant feature vector is learned for further processing. Furthermore by adopting the kernel trick the model is able to reduce its computational cost. To obtain the regression coefficients of each linear model, the Variational Bayesian framework is adopted. Extensive comparisons are carried out between the MultiLRM algorithm and several other competing methods. The experimental results demonstrate that the MultiLRM algorithm achieves better performance than the competing algorithms for SSVEP classification, especially when the number of EEG channels is small.

INTRODUCTION

Brain Computer Interface (BCI) is a communication system that allows a connection between the brain and the computer[1, 2, 3]. The basic goal of a BCI system is to help people, suffering from neuromuscular disorders, to establish a communication channel between their brain and external environment without using "traditional" pathways. The brain responses can be measured by adopting various acquisition modalities such as functional Magnetic Resonance Imaging (fMRI), functional Near-Infrared Spectroscopy (fNIRS) and electroencephalography (EEG). From the above acquisition modalities, the EEG signal is the most frequently used because of its noninvasiveness, its high temporal resolution, ease of acquisition, and cost effectiveness compared to other brain activity monitoring modalities. In the literature, there exists several BCI modalities which are characterized with respect to various brain responses such as sensorimotor responses, event-related potentials and visual-evoked potentials[4, 5, 6, 7, 8, 9, 10, 11, 12]. From the above modalities, SSVEP BCI systems have attracted special interest due to lower training requirements and higher information transfer rates (ITR)[12].

A SSVEP is the brain's response evoked in occipital and occipital - parietal areas of the brain by a visual stimulus flashing at a fixed frequency [10]. SSVEP responses normally include the fundamental frequency of the visual stimulus as well as its harmonics. SSVEP BCI systems detect the different frequency components corresponding to the visual stimuli and translate them into commands. The detection of SSVEP responses is achieved by using an EEG pattern recognition algorithm. Due to frequency characteristics of SSVEPs, power spectrum density analysis (PSDA)-based methods such as fast Fourier transform (FFT) were widely used for frequency detection. Also, Support Vector Machines (SVMs) and the Linear Discriminant Analysis (LDA) are used to detect SSVEPs. A comparison between the above approaches is presented in [13].

Others algorithms used for SSVEP detection are based on Canonical Correlation Analysis (CCA) methodology and its extensions [14]. The CCA-based approaches are multichannel techniques which consider a fixed set of ideal templates. However, in cases where the signal is of small duration the template is not able to represented it well. Furthermore, their performance is deteriorated when we have a small number of EEG channels. A situation which is present when new, low cost and wireless EEG acquisition devices are used such as Emotiv device[15]. To alleviate the above problems we can use the Multivariate Linear Regression (MLR) approach [16], since the MLR does not use templates. In addition, it is not strongly depended by the multichannel nature of the signal. However, the MLR approach is based on least squares problem formulation and hence lacks robustness to the outliers while it can not handle situations where the problem is ill - posed. On the other side, Sparse Bayesian Learning (SBL)[17] is a robust technique that can successfully solve the aforementioned problems of the MLR approach. Furthermore, SBL has been successfully applied to classify event-related potentials (ERP)[4].

In this work, we propose a method, named MultiLRM, for SSVEPs classification. The multiclass classification of SSVEPs is decomposed into multiple regression models. When using a regression model an important issue is how to determine its order. Estimating the proper order is very important since models of small order may lead

Published by Verlag der TU Graz
Graz University of Technology

 DOI: 10.3217/978-3-85125-533-1-68

to underfitting, while large order values may become responsible for data overfitting. SBL framework provides an elegant solution to this problem due to the constraints that are imposed on the model through sparse priors. After learning the regression coefficients, the predictive distribution of each regression model is used to create new discriminant features helping the subsequent classification.

MATERIALS AND METHODS

Let $\mathcal{X}$ be a matrix of size $M \times P$ containing the samples from one EEG trial, where M is the number of channels and P the number of time samples. In our analysis we construct a feature vector from one EEG trial by concatenating the P temporal points from M channels into one vector $\mathbf{x}$. Let $\mathbf{x}_1, \mathbf{x}_2, \cdots, \mathbf{x}_N \in \Re^D$ be a set of EEG trials (feature vectors), where $D = M \times P$ the feature vector dimension and N is the number of training samples. It is worth noting that D is generally high compared to N in the context of BCI applications. The classes are represented by adopting the 1-of-K coding scheme, where K is the number of classes. More specifically, for a training sample $\mathbf{x}_i$ belonging to class m, its label is specified as:

$$\mathbf{y}_i = [y_1, y_2, \cdots, y_K], \text{ where } y_j = \begin{cases} 1, & \text{if } j = m \\ 0, & \text{otherwise} \end{cases}$$

The above formulation provides us with the indicator matrix $\mathbf{Y} = [\mathbf{y}_1, \mathbf{y}_2, \cdots, \mathbf{y}_N]^T, \in \Re^{N \times K}$. Assuming that each column of matrix $\mathbf{Y}$ can be expressed as a linear combination of feature vectors, we obtain the following K regression models:

$$\mathbf{y}_k = \mathbf{X}\mathbf{w}_k + \mathbf{e}_k, k = 1, \cdots, K \tag{1}$$

The above assumption leads us to K regression models where each regression model learns the labels of one class versus the rest. To obtain an estimate for the model parameters $\mathbf{w}_k$ we will resort to the framework of Sparse Bayesian Learning. But before that it is needed to provide relevant information related to Eq. (1). The vector $\mathbf{y}_k \in \Re^N$ contains 0's and 1's, with the n-th element being 1 if the n-th feature vector belongs to class k. The matrix $\mathbf{X} \in \Re^{N \times D}$ contains the EEG sampes (feature vectors) $\mathbf{x}_i, i = 1, \cdots, N$ and $\mathbf{e}_k$ denotes the noise of the model following a Gaussian distribution with zero mean and precision (inverse variance) β_k. Finally, the $\mathbf{w}_k \in \Re^D$ is a vector containing the model parameters.

Sparse Bayesian Learning: Since we make the assumption of independence between the K regression models, we can treat them independently. Our goal is to infer/learn the model parameters $\mathbf{w}_k$ and then use them to make predictions about the class labels of unseen EEG samples. For the remaining of this subsection we will omit the subscript k. In our study, we adopt a probabilistic view of model analysis, and more specifically a bayesian setting of the model through priors distributions. These types of models can be treated by using the bayesian evidence framework or the variational bayesian (VB) framework[17]. In our approach, we follow the VB framework since it provides us the ability to use prior (and hyperprior) distributions over all model parameters.

Sparsity is a very helpful property since processing is faster and simpler in a sparse representation where few coefficients reveal the information we are looking for. Hence, sparse priors help us to determine the model order in an automatic way and to reduce the complexity of the model. A natural choice for the prior distribution is the ARD prior [18, 19]. More specifically, the parameter vector $\mathbf{w}$ is treated as a random variable with Gaussian prior of zero mean and variance a_i^{-1} for each element in the vector $\mathbf{w}$:

$$p(\mathbf{w}|\mathbf{a}) = \prod_{i=1}^{D} N(0, a_i^{-1}), \tag{2}$$

where D is the length of the vector $\mathbf{w}$.

The overall precision (inverse variance) β of the noise follows a Gamma distribution: $p(\beta) = Gamma(\beta; b, c) = \frac{1}{\Gamma(c)} \frac{\beta^{(c-1)}}{b^c} \exp\left\{ -\frac{\beta}{b} \right\}$, where b and c are the scale and the shape of the Gamma distribution, respectively. We use the Gamma distribution for the noise components for two reasons: first, this distribution is conjugate to the Gaussian distribution, which helps us in the derivation of closed form solutions, and second it places the positivity restriction on the overall variance and the scaling parameters. Each parameter a_i, which controls the prior distribution of the parameters $\mathbf{w}$, follows a Gamma distribution, so the overall prior over all a_i is a product of Gamma distributions given by: $p(\mathbf{a}) = \prod_{i=1}^{D} Gamma(a_i; b_a, c_a)$. So, the overall prior over model parameters $\{\mathbf{w}, \mathbf{a}, \beta\}$ is given by: $p(\mathbf{w}, \mathbf{a}, \beta) = p(\mathbf{w}|\mathbf{a}) \prod_{i=1}^{D} p(a_i) p(\beta)$. The likelihood of the data is given by:

$$p(\mathbf{y}|\mathbf{w}, \beta) = \frac{\beta^{\frac{N}{2}}}{(2\pi)^{\frac{N}{2}}} \cdot \exp\left\{ -\frac{\beta}{2} (\mathbf{y} - \mathbf{X}\mathbf{w})^T (\mathbf{y} - \mathbf{X}\mathbf{w}) \right\} \tag{3}$$

To apply the VB methodology[17] we need to define an approximate posterior based on one factorization over the parameters $\{\mathbf{w}, \mathbf{a}, \beta\}$. In our study we choose the following factorization: $q(\mathbf{w}, \mathbf{a}, \beta) = q(\mathbf{w}|\mathbf{a}) \prod_{i=1}^{D} q(a_i) q(\beta)$.

Applying the VB methodology, and taking into account the above factorization, the following posteriors are obtained:

$$q(\mathbf{w}) = N(\hat{\mathbf{w}}, \mathbf{C}_{\mathbf{w}}), \tag{4}$$

$$q(\beta) = Gamma(\beta; b', c'), \tag{5}$$

$$q(\mathbf{a}) = \prod_{i=1}^{D} Gamma(a_i; b_{a_i}^{'}, c_{a_i}^{'}), \tag{6}$$

Published by Verlag der TU Graz
Graz University of Technology

 DOI: 10.3217/978-3-85125-533-1-68

where

$$\mathbf{C_w} = (\hat{\beta}\mathbf{X}^T\mathbf{X} + \hat{\mathbf{A}})^{-1}, \quad (7)$$

$$\hat{\mathbf{w}} = (\hat{\beta}\mathbf{X}^T\mathbf{X} + \hat{\mathbf{A}})^{-1}\hat{\beta}\mathbf{X}^T\mathbf{y}, \quad (8)$$

$$\frac{1}{b'_{a_i}} = \frac{1}{2}(\hat{w}_i^2 + \mathbf{C_w}(i,i)) + \frac{1}{b_a}, \quad (9)$$

$$c'_{a_i} = \frac{1}{2} + c_a, \quad (10)$$

$$\hat{a}_i = b'_{a_i}c'_{a_i}, \quad (11)$$

$$\frac{1}{b'_\beta} = \frac{1}{2}(\mathbf{y} - \mathbf{X}\mathbf{w})^T(\mathbf{y} - \mathbf{X}\mathbf{w}) + tr(\mathbf{X}^T\mathbf{X}\mathbf{C_w}) + \frac{1}{b}, \quad (12)$$

$$c'_\beta = \frac{N}{2} + c, \quad (13)$$

$$\hat{\beta} = b'_\beta c'_\beta, \quad (14)$$

In the above equations the matrix $\hat{\mathbf{A}}$ is a diagonal matrix with the mean of parameters a_i in its main diagonal. The Eqs. (7) - (14) are applied iteratively until convergence. Given a feature vector $\mathbf{x}$, the full predictive distribution is given by: $p(y|\mathbf{x}) = \int\int p(y|\mathbf{x},\mathbf{w},\beta)p(\mathbf{w},\beta)d\mathbf{w}d\beta$. However, the above integration over both $\mathbf{w}$ and β is intractable. But we can approximate the predictive distribution by $p(y|\mathbf{x}) = \int\int p(y|\mathbf{x},\mathbf{w},\hat{\beta})q(\mathbf{w})d\mathbf{w}$. The above integration results in a Gaussian distribution $p(y|\mathbf{x}) = \mathcal{N}(\mathbf{x}^T\hat{\mathbf{w}}, \hat{\beta}+\mathbf{x}^T C_\mathbf{w}\mathbf{x})$. In our analysis we use the predictive mean $\mathbf{x}^T\hat{\mathbf{w}}$ as a new feature. More specifically, when a new unseen feature vector $\mathbf{x}$ is provided, the K predictive means are calculated, constructing the new discriminant feature vector, and then the k-nearest-neighbour (k-NN) algorithm is applied to perform the classification.

Kernel approach: It is worth to note here that the regression models of Eq. (1) can be easily kernelized [20]. Instead of working on the original feature space described from the following equation $\mathbf{y}_k = \mathbf{X}\mathbf{w}_k + \mathbf{e}_k = \sum_{n=1}^{D} w_{kn}\mathbf{x}_n + \mathbf{e}_k$, we can work on kernel feature space by applying the kernel trick. In that case each regression model is described by $\mathbf{y}_k = \sum_{n=1}^{N} w'_{kn}k(\mathbf{x},\mathbf{x}_n) + \mathbf{e}_k = \mathbf{X}'\mathbf{w}'_k + \mathbf{e}_k$ where the matrix $\mathbf{X}'$ is a $N \times N$ symmetric matrix with elements $X_{nm} = k(\mathbf{x}_n,\mathbf{x}_m)$, $k(\cdot)$ is the kernel function and $\mathbf{w}'_k \in \Re^N$ is the new vector of regression coefficients. Now in these regression models we can apply the same bayesian analysis procedure described in the previous subsection. It is worth to note here that the kernel method can be useful in high dimensional settings, even if we only use a linear kernel. More specifically, to compute the regression coefficients $\mathbf{w}_k$ into the original feature space (primal variables) the computational cost is $O(D^3)$, while in the kernel feature space is $O(N^3)$[20]. When $D >> N$, as it is the case for the SSVEP analysis, the computational cost of working into the original feature space is considerable compared to the computational cost of kernel feature space.

RESULTS

In order to validate the performance of the proposed classification algorithm for SSVEP classification, we use the EEG dataset described in [14]. In this dataset a 12-target visual stimuli were presented on a 27-inch LCD monitor. Ten healthy subjects with normal or corrected-to-normal vision participated in this study. EEG data were recorded with 8 electrodes covering the occipital area. For each subject, the experiment consisted of 15 blocks. In each block, subjects were asked to gaze at one of the visual stimuli indicated by the stimulus program in a random order for 4s, and complete 12 trials corresponding to all 12 targets. Data epochs, comprising eight-channel SSVEPs, were extracted according to event triggers generated by the stimulus program. All data epochs were down-sampled to 256Hz. The EEG data have been band-pass filtered from 6Hz to 80Hz with an infinite impulse response (IIR) filter using the filtfilt() function in MATLAB. As indicated in [14] a latency delay of 0.135ms in the visual system is considered. The experiments have been performed using the EEG processing toolbox[21].

The goal of a SSVEP pattern recognition algorithm is to to take as input one EEG trial, $\mathcal{X}$, and assign it into one of K(=12) classes where each class corresponds to a stimulation frequency $f_k, k = 1,\cdots,K$. CCA-based algorithms compare the EEG trial with reference signals in order to make the decision. The reference signals could be purely artificial such as sines and cosines or they could be constructed by using EEG trials. On the other side, methods, such as the MLR approach and the MultiLRM, do not need reference signals and are based on the linear regression model. In addition, for the MultiLRM approach we can use its kernelized version in order to reduce the computational cost.

In our study we compared the proposed algorithm with four algorithms reported in the literature. More specifically, the standard CCA, the individual template based CCA (itCCA), the combination method of standard CCA and itCCA (CombitCCA)[14], and the MLR approach [16] are used. In addition, a PCA-based preprocessing step was performed before using the MLR as described in [16]. For MultiLRM approach we use uniformative priors over a_i and β (i.e. $b_a = b = 10^6$,$c_a = c = 10^{-6}$) and the linear kernel. Also, for the MLR and the MultiLRM, the number of neighborhoods in k-NN classifier was set to five. Finally, for each method (except classical CCA), the performance of each classifier was evaluated using a leave-one-out cross-validation scheme.

The mean accuracy over all subjects for each method is provided in Fig. 1. At first we calculate the accuracy using all available channels of the occipital area (8 channels). The results are shown in Fig. 1(a). We can observe that when the duration of the trial is small enough ($\leq$0.5sec) the MultiLRM approach provides us with higher accuracy compared to others methods. Furthermore, McNemar's test analysis [22] has shown that the differences in classification accuracy are significant at 5% significance level (MultiLRM vs CompitCCA: $p = 4.8 \cdot 10^{-4}$, MultiLRM vs MLR: $p = 1 \cdot 10^{-3}$).

Published by Verlag der TU Graz
Graz University of Technology

 DOI: 10.3217/978-3-85125-533-1-68

If the duration of the trial becomes larger($\geq$1sec) the CombitCCA approach presents the higher accuracy. This could be explained due to spatial filtering that it is performed inside this method. Furthermore, we can observe that MultiLRM and MLR approaches presents similar behaviour (with MultiLRM being slightly better) and clearly these two approaches achieve higher accuracy than itCCA and CCA when the duration of trial is small ($\leq$2secs), while the itCCA outperforms the above two approaches in larger trials duration ($>$2secs).

We have performed two additional analyses related to the number of channels. In the first experiment we have used 3 channels, the channel Oz and two other channels, which are based close to O1 and O2. In the second experiment we have used 2 channels where we have excluded the Oz from the previous 3 channels. The above settings correspond to devices such as the EPOC Emotiv [15] where very few channels in the occipital area are available. In both aforementioned experiments the MultiLRM approach presents the higher accuracy among all approaches. In addition we can observed in Figs. 1(c) and (e) that the performance of MultiLRM is considerably better when the trial duration is small ($\leq$2secs). Furthermore, we can observe that CombitCCA deteriorates significantly at these two experiments. This is expected since the spatial filters do not work sufficiently well when we have small number of channels. Finally, McNemar's test analysis, at 0.5sec, has shown that the differences in classification accuracy are significant at 5% significance level (MultiLRM vs CompitCCA: $p = 5 \cdot 10^{-6}$, MultiLRM vs MLR: $p = 3 \cdot 10^{-8}$ for 3 channels, MultiLRM vs CompitCCA: $p = 2 \cdot 10^{-4}$, MultiLRM vs MLR: $p = 1 \cdot 10^{-11}$ for 2 channels).

Furthermore in our study we compared the above methods by using the Information Transfer Rate (ITR)[10]. The ITR is a measure that takes into account, besides classification accuracy, the number of classes and the trial duration, which is needed, to achieve a particular classification. The results for the channel configuration (8, 3 and 2 channels) are reported in Fig. 1 (b),(d) and (f) for various values of trial duration. In the case of 8 channels, when the trial duration is 4 secs, we can observe that all methods present similar ITRs (around 1 bps). However, the interesting point is the behaviour of the methods when the trial duration is short ($\leq$ 1.5secs). We can observe that at 0.5sec the MultiLRM approach presents the best ITR values ($\sim$4bps) among all methods, all trials duration and all channels configuration. In addition by examining the results in the case of fewer channels (3 and 2 channels) the superiority of MultiLRM approach is terms of ITR measure is evident. To summarize, the MultiLRM approach presents the best performance in terms of ITR measure and among various channels configuration. Furthermore, when using accuracy as the comparison measure, we can see that the MultiLRM approach is superior to other methods when a small number of channels is used (2 or 3 channels).

CONCLUSION

In this work we propose a new method for SSVEP classification under the SBL framework. More specifically, our approach is able to handle multiclass classification problems by adopting multiple regression models and constructing a new discriminant vector of features. The MultiLRM approach has been used in order to study the detection of SSVEP responses in the field of BCI. The proposed method has shown superior performance, compared to other well - known methods of the SSVEP literature, in cases where the trial duration is small and we have few recordings channels. Furthermore, its kernelized version gives us a way to reduce the computational cost of the procedure when the method is applied in SSVEP-BCI problems. In future communications we intent to provide various versions of the MultiLRM by introducing dependencies between the linear models either by assuming a common covariance for the noise or by treating carefully the priors over the regression coefficients. Also, it would be useful to incorporate techniques for kernel learning.

ACKNOWLEDGEMENTS

This work is part of project MAMEM that has received funding from the European Union's Horizon 2020 research and innovation programme under grant agreement No 644780.

REFERENCES

[1] J. R. Wolpaw, N. Birbaumer, D. J. McFarland, G. Pfurtscheller, and T. M. Vaughan, "Brain computer interfaces for communication and control," *Clinical Neurophysiology*, vol. 113, no. 6, pp. 767 – 791, 2002.

[2] G. Pfurtscheller, R. Leeb, C. Keinrath, D. Friedman, C. Neuper, C. Guger, and M. Slater, "Walking from thought," *Brain Res.*, vol. 1071, no. 1, p. 145–152, 2006.

[3] N. Hill, T. Lal, M. Schroder, T. Hinterberger, B. Wilhelm, F. Nijboer, U. Mochty, G. Widman, C. Elger, B. Scholkopf, A. Kubler, and N. Birbaumer, "Classifying eeg and ecog signals without subject training for fast bci implementation: Comparison of nonparalyzed and completely paralyzed subjects," *IEEE Trans. Neural Syst. Rehab. Eng.*, vol. 14, p. 183–186, 2006.

[4] Y. Zhang, G. Zhou, J. Jin, Q. Zhao, X. Wang, and A. Cichocki, "Sparse bayesian classification of eeg for brain-computer interface," *IEEE Transactions on Neural Networks and Learning Systems*, vol. PP, no. 99, pp. 1–1, 2015.

[5] P. Herman, G. Prasad, T. M. McGinnity, and D. Coyle, "Comparative analysis of spectral ap-

  Published by Verlag der TU Graz
Graz University of Technology

 DOI: 10.3217/978-3-85125-533-1-68

proaches to feature extraction for eeg-based motor imagery classification," *IEEE Transactions on Neural Systems and Rehabilitation Engineering*, vol. 16, pp. 317–326, Aug 2008.

[6] A. Schlögl, F. Lee, H. Bischof, and G. Pfurtscheller, "Characterization of four-class motor imagery eeg data for the bci-competition 2005," *Journal of neural engineering*, vol. 2, no. 4, p. L14, 2005.

[7] C. Guan, M. Thulasida, and W. Jiankang, "High performance p300 speller for brain-computer interface," in *IEEE Int Workshop Biomed. Circuits Syst*, pp. 13–16, 2004.

[8] F. Piccione, F. Giorgi, P. Tonin, K. Priftis, S. Giove, S. Silvoni, G. Palmas, and F. Beverina, "P300-based brain computer interface: reliability and performance in healthy and paralysed participants," *Clinical neurophysiology*, vol. 117, no. 3, pp. 531–537, 2006.

[9] L. Citi, R. Poli, C. Cinel, and F. Sepulveda, "P300-based bci mouse with genetically-optimized analogue control," *IEEE Transactions on Neural Systems and Rehabilitation Engineering*, vol. 16, no. 1, pp. 51–61, 2008.

[10] S. Gao, Y. Wang, X. Gao, and B. Hong, "Visual and auditory brain computer interfaces," *IEEE Transactions on Biomedical Engineering*, vol. 61, pp. 1436–1447, May 2014.

[11] G. Bin, X. Gao, Y. Wang, B. Hong, and S. Gao, "Vep-based brain-computer interfaces: time, frequency, and code modulations (research frontier)," *IEEE Computational Intelligence Magazine*, vol. 4, pp. 22–26, November 2009.

[12] M. Nakanishi, Y. Wang, Y. Wang, Y. Mitsukura, and T. Jung, "A high-speed brain speller using steady-state visual evoked potentials," *International Journal of Neural Systems*, vol. 24, no. 06, p. 1450019, 2014.

[13] V. Oikonomou, G. Liaros, K. Georgiadis, E. Chatzilari, K. Adam, S. Nikolopoulos, and I. Kompatsiaris, "Comparative evaluation of state-of-the-art algorithms for ssvep-based bcis." arXiv:1602.00904, February 2016.

[14] M. Nakanishi, Y. Wang, Y. Wang, and T. Jung, "A comparison study of canonical correlation analysis based methods for detecting steady-state visual evoked potentials," *PLoS ONE*, p. e0140703, October 2015.

[15] "Emotiv." https://www.emotiv.com, 2016.

[16] H. Wang, Y. Zhang, N. R. Waytowich, D. J. Krusienski, G. Zhou, J. Jin, X. Wang, and A. Cichocki, "Discriminative feature extraction via multivariate linear regression for ssvep-based bci," *IEEE Transactions on Neural Systems and Rehabilitation Engineering*, vol. 24, pp. 532–541, May 2016.

[17] C. M. Bishop, *Pattern Recognition and Machine Learning (Information Science and Statistics)*. Springer, October 2007.

[18] D. J. MacKay, "Bayesian interpolation," *Neural Computation*, vol. 4, pp. 415–447, 1992.

[19] M. E. Tipping, "Sparse Bayesian Learning and the Relevance Vector Machine," *Journal of Mach. Learn. Research*, vol. 1, pp. 211–244, 2001.

[20] K. P. Murphy, *Machine Learning: A Probabilistic Perspective*. MIT Press, 2012.

[21] G. Liaros, V. Oikonomou, K. Georgiadis, E. Chatzilari, K. Adam, S. Nikolopoulos, and I. Kompatsiaris, "eeg-processing-toolbox." https://github.com/MAMEM/eeg-processing-toolbox, 2016.

[22] A. Agresti, *Categorical data analysis*. Wiley series in probability and statistics, Hoboken (N.J.): J. Wiley, 2002.

Published by Verlag der TU Graz
Graz University of Technology

 DOI: 10.3217/978-3-85125-533-1-68

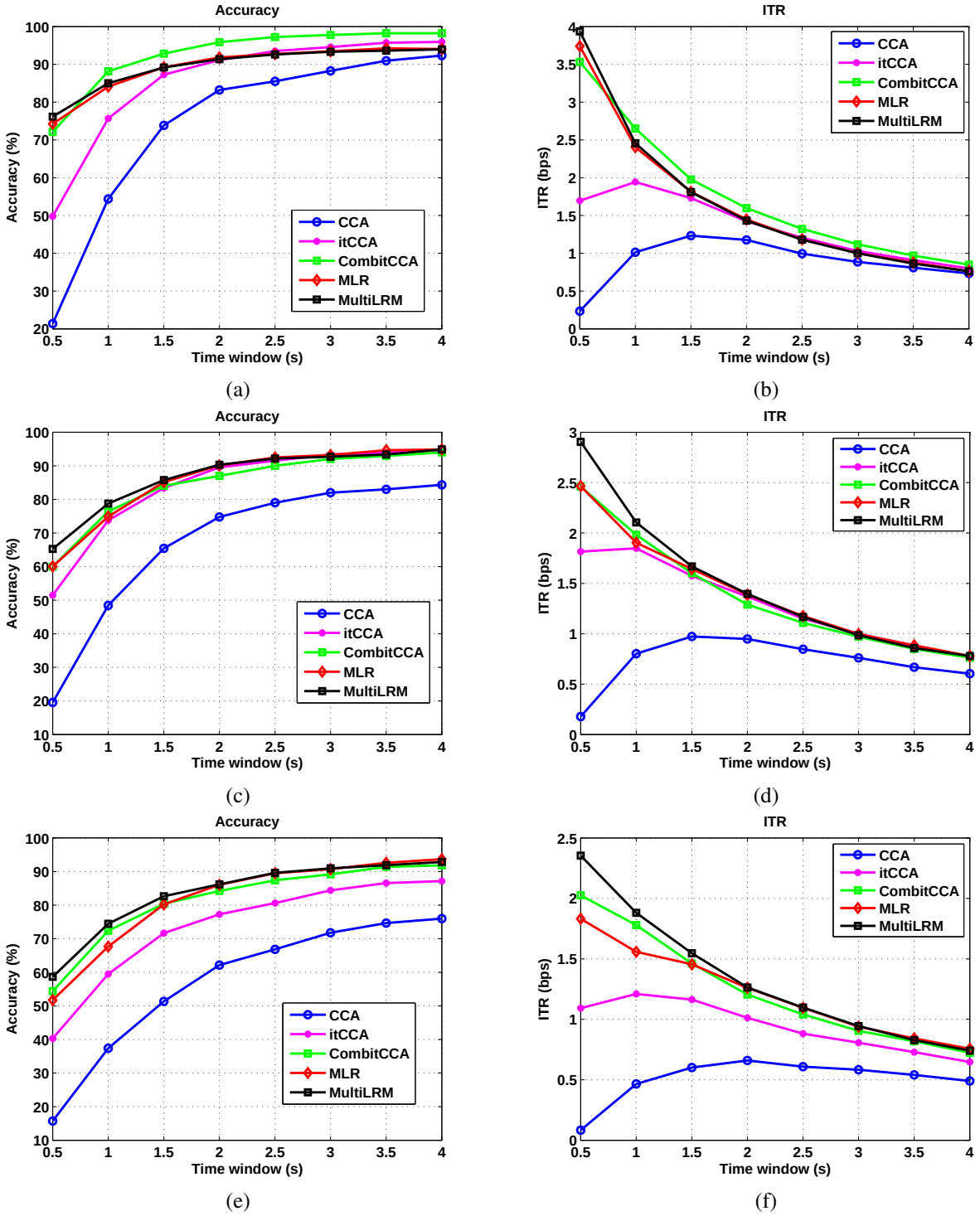

Figure 1: Mean Accuracy and Information Transfer Rate using 8 channels (a,b) using 3 channels (c,d) and using 2 channels (e,f).

Published by Verlag der TU Graz
Graz University of Technology

Proceedings of the
7th Graz Brain-Computer Interface Conference 2017 DOI: 10.3217/978-3-85125-533-1-69

VIBRO-TACTILE EVOKED POTENTIALS FOR BCI COMMUNICATION OF PEOPLE WITH DISORDERS OF CONSCIOUSNESS AND LOCKED-IN SYNDROME

R. Ortner[1,3], R. Spataro[2], J. Scharinger[3], B.Z. Allison[1], A. Heilinger[1], C. Guger[1]

[1] Guger Technologies OG, g.tec medical engineering GmbH, Graz, Austria
[2] ALS Clinical Research Center, University of Palermo, Italy
[3] Department of Computational Perception, Johannes Kepler University (JKU), Linz, Austria

E-mail: ortner@gtec.at

ABSTRACT: In this publication, data of a vibro-tactile P300 BCI are shown. The tool serves for two tasks: for assessment of consciousness in people with disorders of consciousness (DOC) and locked-in syndrome (LIS), and for communication to provide YES/NO answers. Results from one patient, classified in unresponsive wakefulness state and two LIS patients are compared to three healthy controls. The shape of the event related potentials and differences between healthy controls and patients are investigated. We discuss which evoked potentials result in successful communication and provide online results of communication tests for all participants.

INTRODUCTION

Brain-computer interfaces (BCIs) have provided communication for severely disabled users for many years [1]. The P300 speller is the preferred BCI control strategy for these users, since it provides a high information transfer rate and requires very limited training [2]. Most of these systems use a visual P300 speller, providing the whole alphabet plus numbers and/or additional control commands with only one classifier output. However, visual P300 spellers require sight and gaze control [3], although there are attempts to reduce the need for gaze control [4]. P300 BCIs could also be designed with auditory [5] or tactile stimuli [6].

Consciousness has two clinical dimensions: wakefulness and awareness [7,8]. A disorder of consciousness (DOC) results from interference with either or both of these systems [7]. In the unresponsive wakefulness state (UWS), people show complete unawareness of themselves and the environment, but show sleep-wake cycles with some preservation of autonomic brain-stem functions [9]. Patients in the minimally conscious state (MCS) show limited but clearly discernible evidence of consciousness of self or environment [10], but are unable to communicate. The correct classification of UWS and MCS is a challenge. Schnakers and colleagues compared the accuracy of diagnosis between the clinical consensus versus a neurobehavioral assessment [11]. Out of 44 patients diagnosed VS based on the clinical consensus of the medical team, 18 (41 %) were found to be in MCS following standardized assessment with the Coma Recovery Scale-Revised (CRS-R). BCI-based assessment could help overcome the limitations of tests based on observable behavior.

Locked-In Syndrome (LIS) patients have full consciousness but limited or no voluntary muscle control. This can include losing the ability to control gaze. A tactile BCI could also provide communication for these users.

In 2014, we introduced our tactile P300 BCI and tested it with healthy controls and LIS patients [12,13]. Now, we compare data from one patient classified UWS and two LIS patients to data from three healthy controls. The aim of this publication is: to compare the event related potentials (ERPs) of patients vs. healthy controls to explore signals that could be used for assessment of consciousness and for communication. Assessment tests with two and three vibro-tactile stimulators are presented. Accuracy plots are calculated, which show how well a linear discriminant analysis (LDA) classifier can separate the EEG patterns after different kinds of stimulation. The ERPs are averaged and discussed. Furthermore, each participant performed an online test to simulate real-time communication ability.

MATERIALS AND METHODS

Participants: Three patients and three healthy users were recorded for this publication (see Tables 1 and 2). P1 was diagnosed before the test as UWS, and P2 and P3 as LIS patients. The patients' tests were done at the University of Palermo, the healthy controls were assessed in Schiedlberg, Austria. All sessions were approved by the local ethical committee. Informed consent was obtained either from the participants or their legal representatives if patients were not capable. All healthy participants performed two sessions. P1 performed three sessions, while P2 and P3 one session each.

Published by Verlag der TU Graz
Graz University of Technology

 DOI: 10.3217/978-3-85125-533-1-69

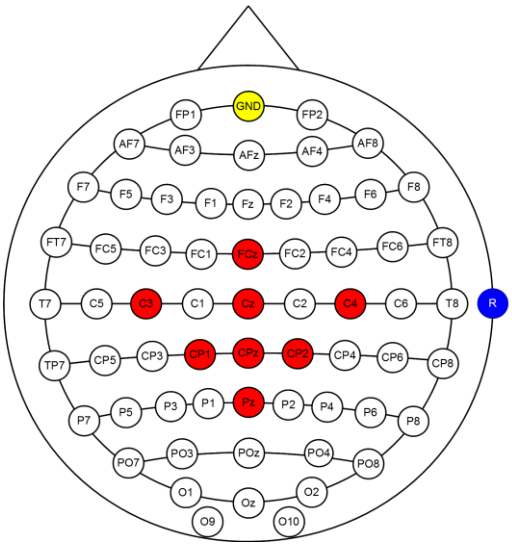

Figure 1: Acquired EEG positions. The red spots mark the positons of eight active EEG electrodes. The reference was placed on the right earlobe (blue), the ground electrode at FPz (yellow).

Paradigms: Three kinds of paradigms were tested: vibro-tactile assessment with 2 tactors (VT2), vibro-tactile assessment with 3 tactors (VT3) and a communication test. During the VT2 paradigm, the left and right wrists are randomly stimulated with a vibro-tactile stimulator for 100 ms each. One stimulator delivers 87.5 % of the stimuli, and the other stimulator presents only 12.5 % of the stimuli. The subject is verbally instructed to silently count 15 stimuli on the hand that receives the less probable target stimuli, which is called the target hand. The number of presented non-target stimuli is 7*15=105. During each run, the subject performs this task four times, with the target hand selected randomly each time, which results in a recording time of 2.5 min. The resulting data are analyzed to provide two figures: the averaged ERPs of target and nontarget trials; and an accuracy plot, showing how well the ERPs can be separated.

During the VT3 paradigm, in addition to tactors on the left and right hands, one tactor is placed to the back or shoulder of the subject as a distracter. The distracter receives 75 % of the stimuli, while the left and right wrist each receives 12.5 % of the stimuli. Then, the subject is instructed through earplugs to count stimuli to the target hand (15 targets, 7*15 non-targets), which is either the left or right hand. During each run, the subject performs this task four times, with the target hand selected randomly each time, resulting in a recording time of 2.5 min. This run results in the same kind of accuracy plot and averaged ERPs. Furthermore, an LDA classifier is created that will be used in the communication test.

The communication test is an online evaluation to see if the tool could be used for answering simple YES-NO questions. The positions of the vibro-tactile stimulators are the same as in the VT3 paradigm. Five questions are asked to the participant, in which the correct answer is known beforehand. For example: “Were you born in Austria?” The experimenter instructs the participant to answer YES by counting the stimuli on the left hand, or answer NO by counting the stimuli on the right hand. After asking a question, the system presents 30 stimuli to the left hand, 30 stimuli to the right hand and 180 stimuli to the distracter, in randomized order. The classifier generated in the VT3 run is used to analyze all those presented stimuli. The system can convey YES if the left hand was classified as target hand, or NO if the right hand was classified as target, and it provides no output if the distracter was classified as target. After the five questions were answered, the number of correctly answered questions is counted. A communication test is considered successful only if 4 or 5 out of 5 total questions were answered correctly.

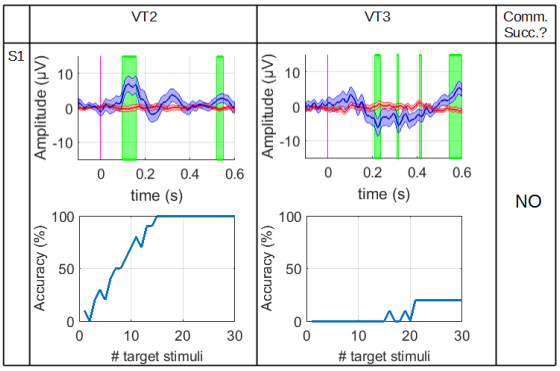

Figure 2: Results of P1, Session 1. Left and middle column top show the averaged EPs of VT2 and VT3. The bottom rows show the accompanying accuracy plot. In the right column one sees that the communication test was not successful.

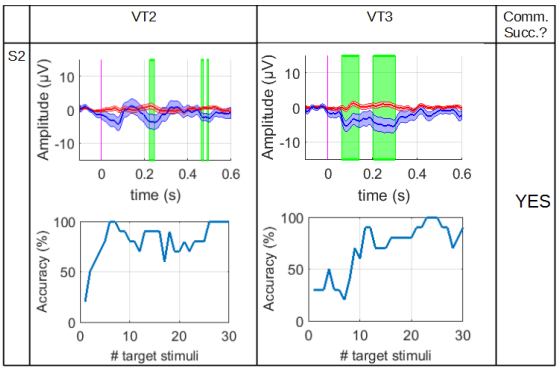

Figure 3: Results of P1, Session 2.

Signal processing: EEG data were acquired from eight sites (Fig. 1) using a g.USBamp and g.LADYbird active electrodes with a sample rate of 256 Hz. Data segments of -100 ms to 600 ms around each stimulus are extracted. To calculate the accuracy plot (see the bottom rows of Figures 2-8), the following procedure is repeated ten times, and the results are averaged into one single plot.

The target and nontarget trials are randomly assigned into two equal sized pools. One pool is used to train a classifier, and the other pool is used to test the classifier. The classifier is tested on an increasing number of

Published by Verlag der TU Graz
Graz University of Technology

 DOI: 10.3217/978-3-85125-533-1-69

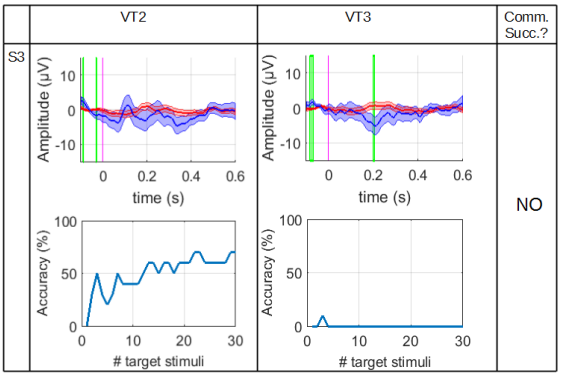

Figure 4: Results of P1, Session 3.

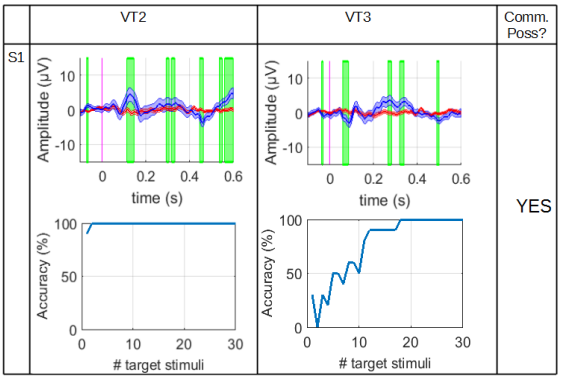

Figure 5: Results of P2, Session 1.

averaged stimuli out of the test pool. At first, it is tested on only one target and seven nontarget stimuli. If the classifier detected the target stimulus correctly, the resulting accuracy is 100 %; otherwise, it is 0 %. This process is repeated for two averaged target stimuli and 14 averaged nontarget stimuli, for three nontarget stimuli and 21 target stimuli, and so on until the full test pool is used. This produces a plot of 30 single values (for 30 target stimuli in the test pool), each one either 100 % or 0 %. The averaging of 10 single plots results in values ranging from 0 % to 100 %. Increasing the number of averaged stimuli will increase the accuracy if the subject follows the task, because this averaging reduces random noise in the data. An accuracy significantly beyond the chance level of 12.5 % shows that the subject can direct attention to the task of counting target stimuli for most or all of a run.

The ERPs from target and nontarget trials are averaged for all channels separately. Each trial is baseline corrected before averaging, using the time segment 100 ms before stimulus onset. For each sample point, a Kruskal Wallis test ($p<0.05$) is done to find statistical differences between target and nontarget trials. The top parts of Figures 2-8 show the averaged ERPs of site Cz. The thick red line presents the averaged nontarget trials. The thin red lines above and below it presents the standard error. The averaged target trials and their standard error are plotted in blue. The magenta vertical line shows the trigger time. Green areas mark areas in which the target vs. nontarget lines differ significantly.

Experimental procedure: Each session consisted of three runs in pseudorandom order: A VT2 assessment run, a VT3 assessment run and communication run.

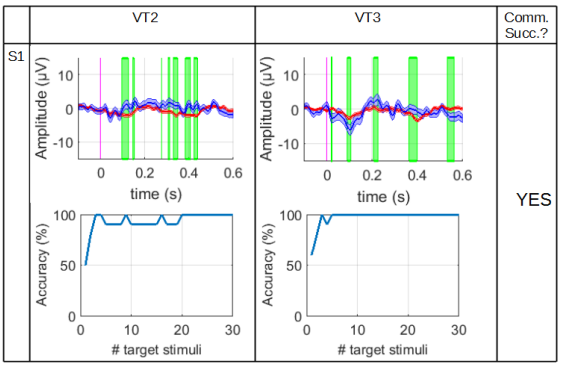

Figure 6: Results of P3, Session 1.

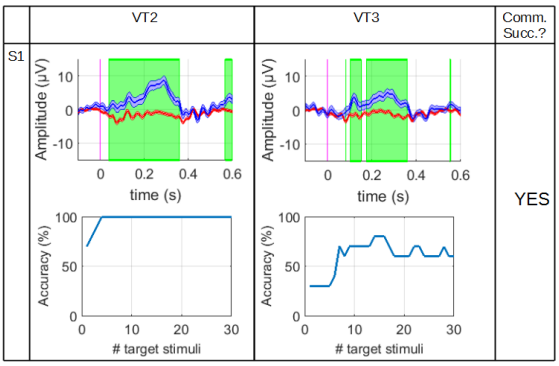

Figure 7: Results of H3, Session 1.

RESULTS

Results from patients: Table 2 and Figures 2-6 present results from patients. In each figure, the first column represents the results of the VT2 run, the second column the result of the VT3 run and the third column shows the result of the communication run (successful or not). In session 1, P1 attained 100% accuracy during the VT2 assessment but poor accuracy in VT3, and did not successfully communicate (Figure 2). P1 was able to successfully communicate in session 2, with accuracy of 80% or more in both the VT2 and VT3 runs (Figure 3). In session 3, his VT2 assessment yielded only modest accuracy, and the VT3 assessment attained 0% accuracy (Figure 4).

The two locked-in patients were both able to communicate, with high accuracy in both VT2 and VT3 (see Figures 5 and 6).

Results from healthy controls: Table 1 summarizes results from healthy controls. Figures 7 and 8 focus on a notable result, which is that H3's second communication attempt was not successful. Also, the accuracy from the preceding VT3 is worse than in other results from the healthy controls. Otherwise, the healthy subjects performed very well.

DISCUSSION

All six participants were able to communicate via vibro-tactile stimulation in at least in one session. All ERPs of the healthy subjects showed a P300 peak.

Published by Verlag der TU Graz
Graz University of Technology

 DOI: 10.3217/978-3-85125-533-1-69

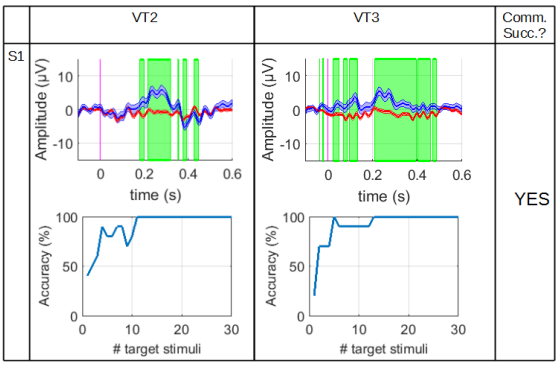

Figure 8: Results of H3, Session 2.

Only one of the patients, P2, exhibited a small P300 in the VT2 condition only. Nonetheless, classification was often accurate, indicating that other ERP components contributed heavily to classification for most patients.

P1 showed a negative deflection in all three sessions. In session 2 only, this deflection produced a stable long-lasting significant difference between target and nontarget stimuli. In sessions 1 and 3, the significant areas are much shorter, and communication was not successful. The absence of activity that reflects voluntary stimulus processing in sessions one and three may be consistent with the previous classification of UWS. Thus several tests on different days should be conducted before reaching a final decision about a patient's status.

Visual inspection of the ERPs shows that the P300 was generally not the main signal that differed between targets vs. nontargets. In most patient data, the normative P300 is not apparent. Thus, it seems that ERPs before and after the P300 probably contribute substantially to effective classification.

The observation that the ERPs of the patients did not show a P300 but still could be used for communication is consistent with earlier publications. In an auditory oddball experiment, Lulé and colleagues [14] show that classification relied largely on a negative deflection. Another study [15] presented LIS patient with a large negative deflection in a vibro-tactile oddball experiment.

Notably, H3 failed in the communication test during the first session. Although his ERPs show a high amplitude P300 during VT3 (Figure 7), the accuracy plot resulting from VT3 showed only 60% of accuracy across 30 target stimuli. Therefore, the accuracy plot provides a useful measure of target vs. nontarget separability when looking at averaged ERPs could be misleading. Nevertheless, in addition to the accuracy plots, we chose an approach of performing online communication involving real questions. This validated the practicability of our device to be used for patients with DOC and LIS.

Table 1: Healthy subjects and their results

ID	Session #	Sex/ Age	VT2 (%)	VT3 (%)	Comm success.?
H1	1	f	100	90	Yes
	2	26	100	100	Yes
H2	1	f	100	100	Yes
	2	36	100	80	Yes
H3	1	m	100	60	No
	2	33	100	100	Yes

The results also support the general approach of assessing users with VT3 prior to communication. In all results from both patients and healthy users, accuracy during the VT3 run effectively predicted the likelihood of successful communication. This is reasonable, as the communication runs are similar to the VT3 assessment runs in many ways.

As with other P300 BCIs, our approach required very little time to train the classifier. Collecting data to train the VT3 paradigm took 2.5 minutes. More training data could improve classifier performance. However, when working with severely disabled patients, longer training times could cause fatigue and ultimately provide worse results. Worse, patients with UWS or related conditions could end wakefulness during a session, meaning that effective communication is no longer possible that session.

The VT2 runs are not used for communication. Those runs are intended as an initial assessment of consciousness as well as a way to familiarize each user with the system.

CONCLUSION

This publication showed that DOC and LIS patients could use a vibro-tactile paradigm for communication. This result further supports the nascent consensus that BCI technology could be helpful for assessment of awareness in these patients and for communication.

Table 2: Patients and their results

ID	Session #	Sex	Age	Diagnosis	Disease Duration (months)	Clinicial Description	VT2 (%)	VT3 (%)	Communication successful?
P1	1	m	19	TBI	12	UWS	100	0	No
	2						80	80	Yes
	3						60	0	No
P2	1	f	76	ALS	145	LIS	100	90	Yes
P3	1	f	68	ALS	89	LIS	95	100	Yes

Published by Verlag der TU Graz
Graz University of Technology

 DOI: 10.3217/978-3-85125-533-1-69

Even users who do not have a robust P300 in the paradigms used here could attain good performance based on other ERP differences. The simplicity and low cost of a noninvasive EEG-based BCI makes this technology very promising for these groups of patients, compared to fMRI or invasive electrodes. More data will be needed though to show the reliability for all groups of potential users.

REFERENCES

[1]Wolpaw JR, Birbaumer N, McFarland DJ, Pfurtscheller G, Vaughan TM, Brain–computer interfaces for communication and control. Clinical Neurophysiology 2002:113:767–791

[2]Guger C, Daban S, Sellers E, Holzner C, Krausz G, Carabalona R., et al., How many people are able to control a P300-based brain–computer interface (BCI)? Neuroscience Letters 2009:462:94–98. doi:10.1016/j.neulet.2009.06.045

[3]Brunner P, Joshi S, Briskin S, Wolpaw J, Bischof H, Schalk, G, Does the "P300"speller depend on eye gaze? Journal of neural engineering 2010:7:56013.

[4]Aricò P, Aloise F, Schettini F, Riccio A, Salinari S, Babiloni, F et al., GeoSpell: an alternative P300-based speller interface towards no eye gaze required. International Journal of Bioelectromagnetism 2011:13:152–153.

[5]Halder, S., Rea, M., Andreoni, R., Nijboer, F., Hammer, E. M., Kleih, S. C., et al.. An auditory oddball brain–computer interface for binary choices. Clinical Neurophysiology, 2010:121(4):516–523.

[6]Brouwer A.-M, Van Erp JB, A tactile P300 brain-computer interface. Frontiers in Neuroscience, 2010:4:19.

[7]Bernat JL, Chronic disorders of consciousness. The Lancet, 2006:367(9517):1181–1192.

[8]Posner, J. B., & Plum, F. (2007). *Plum and Posner's diagnosis of stupor and coma* (Vol. 71). OUP USA.

[9]Ashwal S, Cranford R, Bernat J, et al. The multi-society task force on PVS. Medical aspects of the persistent vegetative state (1), N Engl J Med, 1994:330:1499–1508.

[10]Laureys S, Owen AM, Schiff ND. Brain function in coma, vegetative state, and related disorders. The Lancet Neurology, 2004:3(9), 537–546.

[11]Schnakers C, Vanhaudenhuyse, A, Giacino J, Ventura M, Boly M, Majerus S, et al. Diagnostic accuracy of the vegetative and minimally conscious state: Clinical consensus versus standardized neurobehavioral assessment. BMC Neurology, 2009:9(1):35.

[12]Ortner R, Lugo Z, Noirhomme Q, Laureys S, Guger C, A tactile Brain-Computer Interface for severely disabled patients, in: Haptics Symposium (HAPTICS), 2014 IEEE. pp. 235–237.

[13]Lugo ZR, Rodriguez J, Lechner A, Ortner R, Gantner IS, Laureys S, et al.. A vibrotactile P300-based BCI for consciousness detection and communication. Clin EEG and Neurosci. 2014:45(1):14-21.

[14]Lulé D, Noirhomme, Q, Kleih S, Chatelle C, Halder S, Demertzi A, et al. Probing command following in patients with disorders of consciousness using a brain–computer interface Clinical Neurophysiology, 2013:124: 101–106

[15]Lugo ZR, Rodriguez J, Lechner A, Ortner R, Gantner I.S, Laureys S, et al. A vibrotactile P300-based BCI for consciousness detection and communication. Clin EEG and Neurosci. 2014:45:14-21

Published by Verlag der TU Graz
Graz University of Technology

Proceedings of the
7th Graz Brain-Computer Interface Conference 2017 DOI: 10.3217/978-3-85125-533-1-70

CORRELATIONS OF MOTOR ADAPTATION LEARNING AND MODULATION OF RESTING-STATE SENSORIMOTOR EEG ACTIVITY

O. Özdenizci[1], M. Yalçın[1], A. Erdoğan[2], V. Patoğlu[1], M. Grosse-Wentrup[3], M. Çetin[1]

[1]Faculty of Engineering and Natural Sciences, Sabancı University, Istanbul, Turkey
[2]Department of Physical Medicine & Rehabilitation, Northwestern University, Rehabilitation Institute of Chicago, Chicago, IL, United States
[3]Empirical Inference Department, Max Planck Institute for Intelligent Systems, Tübingen, Germany

E-mail: oozdenizci@sabanciuniv.edu

ABSTRACT: There exists a variety of electroencephalogram (EEG) based brain-computer interface (BCI) assisted stroke rehabilitation protocols which exploit the recognized nature of sensorimotor rhythms (SMRs) during motor movements. For novel approaches independent of motor execution, we investigate the changes in resting-state sensorimotor EEG with motor learning, resembling the process of post-stroke recovery. In contrast to the neuroimaging studies based on visuomotor tasks, we study motor learning during an actual physical motor adaptation learning experiment. Based on analysis of EEG data collected throughout a force-field adaptation task, we observed a spectral power increase of resting SMRs across subjects. The modulation across resting-states in an early adaptation phase of the motor task was further shown to predict individual motor adaptation performance measures.

INTRODUCTION

Over the last few decades, EEG activity of the human sensorimotor cortex is widely targeted as a biomarker in BCI-assisted stroke rehabilitation protocols to support motor restoration and induce neural plasticity $[1-3]$. In general, these approaches utilize congruent haptic feedback of neurally decoded movement intent through SMRs, by a rehabilitation robot $[4-6]$, and were shown to support modulation of SMRs during training and enhance post-stroke recovery [7]. Stroke recovery involves a form of motor learning, which has also motivated studies aimed at gaining insights into the neural processes underlying human motor behavior [8]. In this context, various brain imaging studies focus on analyzing recorded neural data during motor learning experiments $[9, 10]$. However, motor learning related sensorimotor activity changes in the resting brain, independent of motor execution, are yet to be studied.

Within this scope, several pieces of previous work have studied the concept of visuomotor learning $[11-13]$. However visuomotor tasks generally require learning of an underlying mapping between the actual motor task space and the visual feedback environment. Hence as a confounding factor, this further incorporates separate processing of different visual mapping aspects into the learning process $[14, 15]$. We argue that such neuroimaging studies should dissociate learning of an underlying visual mapping from the pure motor learning process. Conventionally in motor rehabilitation literature, motor learning is studied either in the form of motor adaptation or skill learning [16], particularly with force-field adaptation tasks $[17, 18]$. Accordingly, we investigate resting-state sensorimotor EEG changes with pure motor learning during a force-field adaptation task performed within an actual physical environment using a robotic setup, without a separate artificial visual feedback environment.

Based on statistical analysis of experimental data from twenty-one healthy subjects, we observed an increase of resting-state α-band (8–14 Hz) sensorimotor activity across subjects throughout motor learning. Moreover, regression analysis demonstrates that the amount of the observed increase in sensorimotor activity across resting stages in an early adaptation phase of the motor task is predictive of individual motor adaptation learning performances. Finally we discuss how these motor learning related changes in resting-state EEG can be exploited in future BCI-assisted stroke rehabilitation protocols.

MATERIALS AND METHODS

Subjects and Experimental Data: Twenty-one right handed healthy subjects (14 male, 7 female; mean age 23.8 ± 3.1) participated in this study. All subjects were naive to the force-field adaptation task. Before the experiments, all participants gave their informed consent after the experimental procedure was explained to them in accordance with guidelines set by the research ethics committee of Sabancı University. Throughout the experiments, the robotic setup recorded data at 500 Hz sampling rate and a 64-channel EEG was recorded at 512 Hz sampling rate, using active EEG electrodes and a BioSemi ActiveTwo amplifier (Biosemi Inc., Amsterdam, The Netherlands). Electrodes were placed according to the 10-20 system. All data were re-referenced to common average reference offline.

Published by Verlag der TU Graz
Graz University of Technology

 DOI: 10.3217/978-3-85125-533-1-70

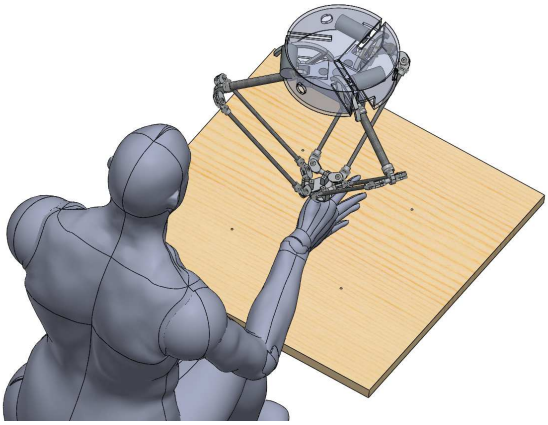

Figure 1: Illustration of the task workspace. Four target locations are placed on the board at the northeast, northwest, southeast, and southwest positions with equal distances of 200 mm from the center.

Study Design: Participating subjects performed a force-field adaptation task under simultaneous EEG recordings. The goal of the task was learning to perform planar center-out reaching movements under an unknown force-field, as straightly as possible. During the experiments, subjects sat in front of a horizontally placed board constructing the task workspace. Subjects were holding a handle, henceforth referred to as an end-effector, with their right hands that was suspended from above onto the board. The end-effector was attached to a 3 degrees-of-freedom modified delta robot which had constrained motion on z-axis and was only capable of two-dimensional movements that were restricted to fall within a circle with a radius of 200 mm. Idle starting position of the end-effector corresponded to the center of this circle. There were four target locations placed on the circle at the northeast, northwest, southeast, and southwest positions. The target locations were indicated with holes over the board containing LEDs inside. An illustration of the task workspace is provided in Fig. 1.

Before the experiments, all subjects performed a preflight phase of eight trials (i.e., reaching movements) without any force-field to get familiar with the task workspace and trial flow. As part of the force-field adaptation task, each subject performed 200 trials in total, which were divided into three blocks of 40, 80, and 80 trials. Within each of these blocks, there were equal number of trials per target location.

In order to investigate the changes in resting-state sensorimotor activity with motor adaptation learning, alongside the force-field adaptation task, five-minute resting-state EEG recordings were performed throughout the experiment. First resting-state recording was performed before the force-field adaptation task, second recording after the first block of 40 trials and a third resting-state recording after completion of the force-field adaptation task. During these recordings, subjects were placed approximately 1.5 meters in front of a computer screen and instructed to relax with eyes open, looking at a fixation cross displayed in the middle of the screen. Resting-state recordings were performed with subjects' eyes open to construct a baseline condition for the force-field adaptation task that involved visual processing [19]. Same experimental setup and data were also presented and used in our previous work for different analyses [20, 21].

Force-Field Adaptation Task: The task involved two-dimensional center-out reaching movements within the task workspace, while a velocity dependent external force-field was applied to the end-effector by the robotic setup to disturb subjects' motions. Specifically, end-effector velocity vector $\vec{v}$ was multiplied with a constant matrix $\mathbf{B}$, representing the viscosity of the imposed environment, to compute $\vec{f} = \mathbf{B}\vec{v}$ at each time point, where $\vec{f}$ represented the forces that the robotic setup is programmed to produce on the end-effector as the subject performed reaching movements. The constant matrix $\mathbf{B}$ was the same as in [22].

Throughout the experiments, subjects performed 200 trials with a randomized order of 50 trials for each of the four target locations. At the beginning of each trial, the target location was indicated with a blinking LED light. As the subject reached for the target location using the end-effector and then moved back to the starting position, a calculated *score* within a range of 0–100 was read out to the subject through a speaker. The *score* in each trial indicated how straight the movement trajectory was in the corresponding trial. To calculate the *score*, we first computed the sum of perpendicular distances of each point on the movement trajectory to the ideal path (i.e., straight line from center to target) [23]. Secondly, this sum served as an input variable to a sigmoid function, indicating a gradually diminishing increase [24]. Third, the value of the sigmoid function was multiplied by the elapsed time of the trial as a penalty on the *score*. At the end of each trial, the subjects were informed about their movement performance by inversely mapping this value to a range of 0–100; a higher *score* denoting a faster and more straight reaching movement. Aim of the subjects was to increase the *score* throughout trials.

Resting-State Sensorimotor EEG Processing: For all analyses in this study, from the 64-channel EEG data recorded during the experiments, we only used the C3, CP3, C4, and CP4 electrodes that are known to mainly represent sensorimotor activity of the brain [25 – 28]. As each resting-state five-minute time-series data constituted a high dimensional matrix (4 channels x 153600 samples), we implemented dimensionality reduction in the temporal domain. Specifically, we transformed EEG data of each electrode into the spectral domain and computed log-bandpowers in four main frequency bands; θ-band (4–7 Hz), α-band (8–14 Hz), β-band (15–30 Hz), and γ-band (55–85 Hz). We computed resting-state log-bandpowers using an FFT in conjunction with a Hann window spanning the whole five-minute resting phase. This analysis resulted in resting-state powers in four main frequency bands and four electrodes for each subject.

Published by Verlag der TU Graz
Graz University of Technology

 DOI: 10.3217/978-3-85125-533-1-70

Changes in Resting Sensorimotor Activity: We used a Wilcoxon signed-rank test to investigate if there is a significant frequency-specific change in the resting-state sensorimotor activity across subjects from first to the second resting-state with an early adaptation, or from first to third resting-state throughout the complete adaptation period. In particular, for all frequency bands and four electrodes separately, differences of bandpower values between first and second resting-state recordings, and first and third resting-state recordings were computed and was used to test the null hypothesis of zero median across twenty-one subjects.

Relation with Motor Adaptation Learning: Resting-state sensorimotor activities that showed significant power changes across subjects were further inspected on whether these changes are related with the motor adaptation learning process. As trial-to-trial variability in performance is not of interest in this context, individual rate-based motor adaptation learning metrics were quantified from the feedback *scores* for each subject. Specifically, in order to represent an early motor adaptation learning performance in the first block of 40 trials, where the initial exposure to the force-field occurs, the ratio of average *scores* of the first ten trials over average *scores* of the last ten trials of the first block is computed. Similarly to represent the complete adaptation period, the ratio of average *scores* of the first ten trials over average *scores* of the last ten trials of the whole experiment is computed. A smaller value of these metrics indicates greater motor adaptation in the corresponding time period. These measures served as the dependent variables in separate multivariate linear regression models, where the changes in resting sensorimotor activity were used to predict learning performance in the corresponding time period.

Before regression analyses, we checked all subjects' performance measures and EEG features on whether it exceeded three standard deviations of the median across subjects, as an outlier rejection criterion. The differences of the four electrode powers between the first and the second resting-state blocks served as the independent variables to the regression model to predict early motor adaptation learning rates using a leave-one-subject-out cross-validation protocol. Similarly the differences between first and third resting-state EEG features were used to predict the complete adaptation learning metrics.

Statistical Significance Testing: To quantify the strength of a prediction model, the correlation coefficient between actual and predicted performance measures was computed. Significance of this correlation was tested with a permutation test. To test the null-hypothesis of zero correlation, we randomly permuted the assignment of performance measures to EEG features across subjects 10,000 times and estimated the frequency at which the prediction model achieved a higher correlation coefficient than with the true assignment of EEG features to performance measures as the *p*-value.

RESULTS

Obtained *p*-values of the Wilcoxon signed-rank tests on potential frequency-specific changes of resting-state electrode bandpowers across subjects from first to the second resting-state with early adaptation, or from first to third resting-state with complete adaptation, are given in Tab. 1. In particular, we observe a significant increase of α-powers across twenty-one subjects in all four electrodes (C3, CP3, C4, and CP4) located over sensorimotor areas (i.e., SMRs) with early adaptation. Moreover, this across-subjects increase in SMR activity is preserved in C3 and CP4 electrodes, but not still statistically significant in CP3 and C4 ($p = 0.06$) after the experiment, with complete adaptation. We do not consider the other two statistically significant *p*-values obtained by the electrode C3 as notable due to lack of consistency. For all four electrodes, resting-state α-power levels of all subjects and the mean across subjects are presented in Fig. 2, mainly showing an increase of α-powers resulting in the significant *p*-values of Tab. 1.

Subjects explicitly show motor adaptation learning effects in terms of the feedback *score* metric they are provided (see Fig. 3a). In particular, we observe that most of the adaptation occurs in the first block of 40 trials with the initial exposure to the force-field. Investigating the relation between the observed resting-state α-power changes and individual adaptation rates, the early adaptation linear regression model shows statistically significant results. Specifically, the differences of the four electrode α-powers between the first and the second resting-state blocks (i.e., through early adaptation) of the subjects were found predictive of individual early adaptation learning rates, which span a wide range of performance measures across subjects ($\rho = 0.55, p < 0.01$, see Fig. 3b and 3c). On the other hand, difference of α-powers between the first and third resting-state recordings was not able to predict the complete adaptation learning rate metrics ($\rho = -0.30, p > 0.05$).

Table 1: *p*-values of the Wilcoxon signed-rank test on observed changes of bandpower activity in the early or complete adaptation phases across subjects. Colored cells indicate statistically significant results ($p \leq 0.05$).

Bandpower	Adaptation	C3	CP3	C4	CP4
θ-band	Early	0.01	0.37	0.90	0.15
	Complete	0.76	0.47	0.56	0.98
α-band	Early	0.03	0.01	0.04	0.05
	Complete	0.02	0.06	0.06	0.05
β-band	Early	0.84	0.52	0.76	0.33
	Complete	0.04	0.06	0.09	0.66
γ-band	Early	0.47	0.82	0.68	0.59
	Complete	0.41	0.18	0.16	0.45

Published by Verlag der TU Graz
Graz University of Technology

 DOI: 10.3217/978-3-85125-533-1-70

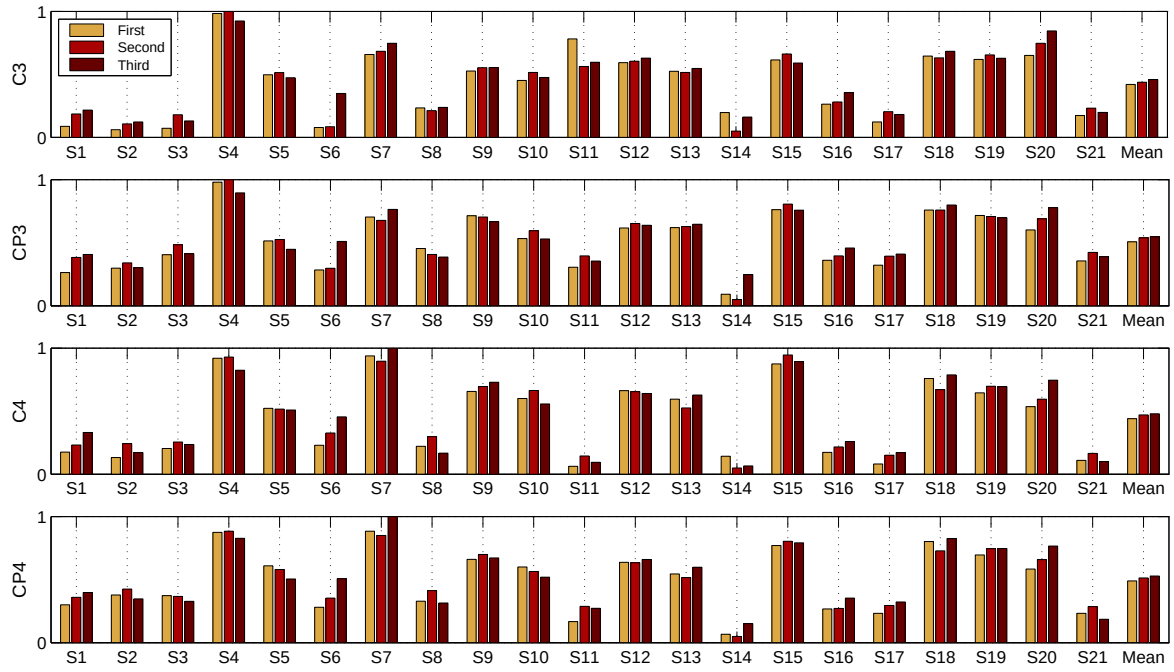

Figure 2: Normalized α-power levels of the four electrodes during three resting-state recordings of all subjects. Mean α-powers across subjects are presented at the rightmost slot.

DISCUSSION

In this study, we investigate resting-state changes in sensorimotor EEG activity throughout motor adaptation learning by a force-field adaptation task. The task was performed within an actual physical environment to discard any visual mapping confounders that potentially exist in most visuomotor task based neuroimaging studies. Subjects showed apparent motor performance increases throughout the task. We observed explicit increase in resting-state α-powers across subjects both after an early adaptation and after the adaptation was complete. Moreover, the changes in resting α-power was found predictive of individual measures of distinct adaptation rates during an early adaptation time period of the experiment.

We hypothesize that the observed SMR-power increase across subjects, which is mostly evident after an early adaptation, is likely to indicate a cortical reorganization of the SMR activity. Even though there exist a variety of studies indicating the relation of SMRs and human motor behavior, a non-invasive neuroimaging based evidence on resting activity modulations was not reported with a pure motor learning task before. While the continuity of these resting-state changes for longer durations is not established on one hand, on the other hand, these results can be further exploited in novel stroke-rehabilitation paradigms

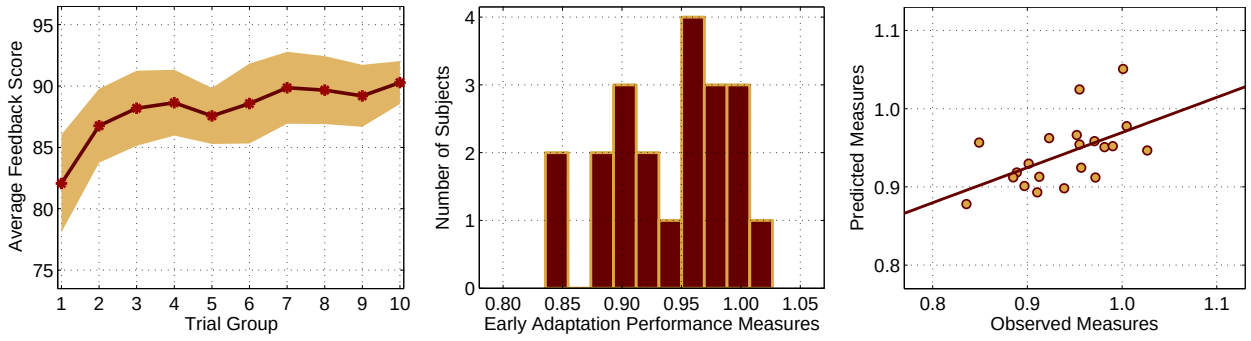

(a) (b) (c)

Figure 3: (a) Average subject feedback *scores* learning curve. Trial groups represent the sequential order of the 200 trials grouped in 20 trials each. Each point on the red curve represents an average *score* of 20 trials. Shaded region indicates the standard deviation. (b) Distribution of the early adaptation performance measures used in regression across subjects. (c) Observed versus predicted performance measures of the early adaptation regression model ($\rho = 0.55, p < 0.01$). One dot represents one subject.

Published by Verlag der TU Graz
Graz University of Technology

 DOI: 10.3217/978-3-85125-533-1-70

that can potentially incorporate neurofeedback [29] or stimulation based alterations of the electrical activity of the brain [30, 31] by subject specific SMR localization. With a similar approach, several studies have previously focused on BCI-based sensorimotor training to improve motor behavior during a reaction-time task [27] or a joystick-based cursor-movement task [28]. Nevertheless, it is important to note that the evidence presented here is not sufficient to claim that modulating such brain activity ensures an increase in motor learning performance [32]. The present work solely focuses on investigating SMR activity, however we have recently studied EEG correlates of motor adaptation learning in a broader range of brain regions both during resting-state and movement preparation phases with a different analysis approach on this collected data [33]. These evidences can potentially be exploited in mentioned novel BCI-assisted stroke rehabilitation protocols.

ACKNOWLEDGMENTS

This work was partially supported by the Scientific and Technological Research Council of Turkey under Grant 115M698, and by Sabancı University Internally-funded Research Projects (IRP).

REFERENCES

[1] Daly JJ, Wolpaw JR. Brain–computer interfaces in neurological rehabilitation. The Lancet Neurology. 2008;7(11):1032–1043.

[2] Grosse-Wentrup M, Mattia D, Oweiss K. Using brain–computer interfaces to induce neural plasticity and restore function. Journal of Neural Engineering. 2011;8(2):025004.

[3] Ushiba J, Soekadar SR. Brain–machine interfaces for rehabilitation of poststroke hemiplegia. Progress in Brain Research. 2016;228:163–183.

[4] Gomez-Rodriguez M, Peters J, Hill J, Schölkopf B, Gharabaghi A, Grosse-Wentrup M. Closing the sensorimotor loop: haptic feedback facilitates decoding of motor imagery. Journal of Neural Engineering. 2011;8(3):036005.

[5] Meyer T, Peters J, Brötz D, Zander TO, Schölkopf B, Soekadar SR, Grosse-Wentrup M. A brain–robot interface for studying motor learning after stroke, in Proc. IEEE/RSJ International Conference on Intelligent Robots and Systems, 2012, 4078–4083.

[6] Ang KK, et al. A randomized controlled trial of EEG–based motor imagery brain–computer interface robotic rehabilitation for stroke. Clinical EEG and Neuroscience. 2014:1550059414522229.

[7] Ramos-Murguialday A, Broetz D, Rea M, Laer L, Yilmaz O, Brasil FL, Liberati G, Curado MR, Garcia-Cossio E, Vyziotis A, Cho W, Agostini M, Soares E, Soekadar S, Caria A, Cohen LG, Birbaumer N. Brain–machine interface in chronic stroke rehabilitation: A controlled study. Annals of Neurology. 2013;74(1):100–108.

[8] Krakauer JW. Motor learning: its relevance to stroke recovery and neurorehabilitation. Current Opinion in Neurology. 2006;19(1):84–90.

[9] Taubert M, Lohmann G, Margulies DS, Villringer A, Ragert P. Long–term effects of motor training on resting–state networks and underlying brain structure. NeuroImage. 2011;57(4):1492–1498.

[10] Wu J, Srinivasan R, Kaur A, Cramer SC. Resting–state cortical connectivity predicts motor skill acquisition. NeuroImage. 2014;91:84–90.

[11] Meyer T, Peters J, Zander TO, Schölkopf B, Grosse-Wentrup M. Predicting motor learning performance from electroencephalographic data. Journal of NeuroEngineering and Rehabilitation. 2014;11(1).

[12] Pollok B, Latz D, Krause V, Butz M, Schnitzler A. Changes of motor–cortical oscillations associated with motor learning. Neuroscience. 2014;275:47–53.

[13] Meinel A, Castano-Candamil S, Reis J, Tangermann M. Pre–trial EEG–based single–trial motor performance prediction to enhance neuroergonomics for a hand force task. Frontiers in Human Neuroscience. 2016;10.

[14] Sailer U, Flanagan JR, Johansson RS. Eye–hand coordination during learning of a novel visuomotor task. The Journal of Neuroscience. 2005;25(39):8833–8842.

[15] Scheidt RA, Conditt MA, Secco EL, Mussa-Ivaldi FA. Interaction of visual and proprioceptive feedback during adaptation of human reaching movements. Journal of Neurophysiology. 2005;93(6):3200–3213.

[16] Krakauer JW, Mazzoni P. Human sensorimotor learning: adaptation, skill, and beyond. Current Opinion in Neurobiology. 2011;21(4):636–644.

[17] Patton JL, Mussa-Ivaldi FA. Robot–assisted adaptive training: custom force fields for teaching movement patterns. IEEE Transactions on Biomedical Engineering. 2004;51(4):636–646.

[18] Gandolfo F, Mussa-Ivaldi FA, Bizzi E. Motor learning by field approximation. Proceedings of the National Academy of Sciences. 1996;93(9):3843–3846.

[19] Barry RJ, Clarke AR, Johnstone SJ, Magee CA, Rushby JA. EEG differences between eyes–closed and

Published by Verlag der TU Graz
Graz University of Technology

 DOI: 10.3217/978-3-85125-533-1-70

eyes–open resting conditions. Clinical Neurophysiology. 2007;118(12):2765–2773.

[20] Ozdenizci O, Yalcin M, Erdogan A, Patoglu V, Grosse-Wentrup M, Cetin M. Resting–state EEG correlates of motor learning performance in a force–field adaptation task, in Proc. 24th IEEE Signal Processing and Communications Applications Conference, 2016, 2253–2256.

[21] Ozdenizci O, Yalcin M, Erdogan A, Patoglu V, Grosse-Wentrup M, Cetin M. Pre–movement contralateral EEG low beta power is modulated with motor adaptation learning, in Proc. IEEE International Conference on Acoustics, Speech and Signal Processing, 2017.

[22] Shadmehr R, Mussa-Ivaldi FA. Adaptive representation of dynamics during learning of a motor task. The Journal of Neuroscience. 1994;14(5):3208–3224.

[23] Malfait N, Shiller DM, Ostry DJ. Transfer of motor learning across arm configurations. The Journal of Neuroscience. 2002;22(22):9656–9660.

[24] Leibowitz N, Baum B, Enden G, Karniel A. The exponential learning equation as a function of successful trials results in sigmoid performance. Journal of Mathematical Psychology. 2010;54(3):338–340.

[25] Neuper C, Scherer R, Wriessnegger S, Pfurtscheller G. Motor imagery and action observation: modulation of sensorimotor brain rhythms during mental control of a brain–computer interface. Clinical Neurophysiology. 2009;120(2):239–247.

[26] Pichiorri F, Fallani FDV, Cincotti F, Babiloni F, Molinari M, Kleih S, Neuper C, Kübler A, Mattia D. Sensorimotor rhythm–based brain–computer interface training: the impact on motor cortical responsiveness. Journal of Neural Engineering. 2011;8(2):025020.

[27] Boulay C, Sarnacki W, Wolpaw JR, McFarland DJ. Trained modulation of sensorimotor rhythms can affect reaction time. Clinical Neurophysiology. 2011;122(9):1820–1826.

[28] McFarland DJ, Sarnacki WA, Wolpaw JR. Effects of training pre–movement sensorimotor rhythms on behavioral performance. Journal of Neural Engineering. 2015;12(6):066021.

[29] Ozdenizci O, Meyer T, Cetin M, Grosse-Wentrup M. Towards neurofeedback training of associative brain areas for stroke rehabilitation, in Proc. Sixth International Brain-Computer Interface Conference, 2014.

[30] Nitsche MA, Schauenburg A, Lang N, Liebetanz D, Exner C, Paulus W, Tergau F. Facilitation of implicit motor learning by weak transcranial direct current stimulation of the primary motor cortex in the human. Journal of Cognitive Neuroscience. 2003;15(4):619–626.

[31] Lotze M, Braun C, Birbaumer N, Anders S, Cohen LG. Motor learning elicited by voluntary drive. Brain. 2003;126(4):866–872.

[32] Weichwald S, Meyer T, Ozdenizci O, Schölkopf B, Ball T, Grosse-Wentrup M. Causal interpretation rules for encoding and decoding models in neuroimaging. NeuroImage. 2015;110:48–59.

[33] Ozdenizci O, Yalcin M, Erdogan A, Patoglu V, Grosse-Wentrup M, Cetin M. Electroencephalographic identifiers of motor adaptation learning. Journal of Neural Engineering. 2017.

Published by Verlag der TU Graz
Graz University of Technology

Proceedings of the
7th Graz Brain-Computer Interface Conference 2017 DOI: 10.3217/978-3-85125-533-1-71

A Gaze-Independent Audiovisual Brain-Computer Interface and its Application in Awareness Detection

Jiahui Pan[1,2], Yuanqing Li[1]

[1]School of Automation Science and Engineering, South China University of Technology, Guangzhou, China
[2]School of Software, South China Normal University, Guangzhou, China

E-mail: auyqli@scut.edu.cn

ABSTRACT: Awareness detection in patients with DOC is a challenging task, which is commonly addressed through behavioral observation scales. In this study, we proposed a gaze-independent audiovisual brain computer interface (BCI) for patients with disorders of consciousness (DOC). Semantically congruent and incongruent audiovisual number stimuli were presented one by one to evoke event-related potential (ERP) components. Subjects were instructed to selectively attend to the congruent audiovisual stimuli (target) whereas ignoring the incongruent audiovisual stimuli (nontarget). Ten healthy subjects first participated in the experiment to evaluate the system. The results demonstrated the audiovisual BCI system outperformed the corresponding auditory-only and visual-only systems. Multiple ERP components including the P300, N400 and LPC were observed in the audiovisual condition, which enhanced the discriminability between the brain responses for target and nontarget stimuli. This system was then applied to detect the awareness in eight patients with DOC. The results demonstrated the command following as well as number recognition in three of the eight patients. Therefore, this gaze-independent audiovisual BCI system might be used as a supportive bedside tool for awareness detection in patients with DOC.

INTRODUCTION

A potential application of Brain-computer interfaces (BCIs) is in awareness detection for patients with disorders of consciousness (DOC), such as vegetative state (VS) and minimally conscious state (MCS). Currently, the clinical diagnosis of DOC patients is generally based on behavioral scales such as the JFK Coma Recovery Scale-Revised (CRS-R), which rely on overt motor responses to external stimuli at the time of observation [1]. However, these patients are usually deprived of the capacity to make normal physical movements [2]. As a consequence, the clinical misdiagnosis rates have been relatively high, ranging from 37%-43% in VS and MCS patients [3]. Recently, several BCI paradigms have been presented for patients with DOC [4, 5, 6, 7]. In our previous study [7], we developed a visual hybrid BCI combining P300 and SSVEP to detect awareness in eight patients with DOC (4 VS, 3 MCS and 1 LIS) and successfully demonstrated command following in three patients (1 VS, 1MCS and 1 LIS). However, BCI-based awareness detection in patients with DOC is still in its infancy. The performance of the BCIs designed for these patients is generally poor because the patients' cognitive ability is considerably lower than that of healthy subjects. Furthermore, there existed big differences of EEG signals between the patients with DOC and healthy individuals because of severe brain injuries in these patients. One possible solution is to develop novel BCIs to improve awareness detection.

For BCI-based awareness detection, an important issue is the modality of stimulation. To date, most BCI studies have focused on unimodal (e.g., auditory-only or visual-only) stimuli. Compared to unimodal stimuli, congruent multisensory stimuli may cause additional neuronal activities and result in faster behavioral responses and more accurate perception/recognition [8]. However, multisensory stimulus paradigms have barely received attentions in the field of BCIs [9]. In this study, we focused on the potential benefits of audiovisual stimuli for the improvements of BCI performance. Since the patients with DOC lack the control of gaze movements, this study proposed a gaze-independent audiovisual BCI for their awareness detection. Specifically, the stimuli included semantically congruent and incongruent audiovisual numbers (25% congruent vs. 75% incongruent). Furthermore, all the audiovisual stimuli were presented one-by-one, this made the paradigm completely gaze-independent. With this study we aimed at (1) developing and validating a novel gaze-independent audiovisual BCI using semantically congruent and incongruent audiovisual stimuli; and (2) testing if this BCI system could serve as a supportive bedside tool for detecting covert conscious awareness in patients with DOC.

MATERIALS AND METHODS

Subjects Ten healthy subjects (nine males; mean age $\pm$ SD, 29 $\pm$ 2 years) and eight patients with severe brain injuries (seven males; five VS and three MCS; mean age $\pm$ SD, 42 $\pm$ 12 years; see Tab. 1) from a local hospital participated in this experiment. None of the patients had a history of impaired visual and auditory acuity. This s-

Published by Verlag der TU Graz
Graz University of Technology

 DOI: 10.3217/978-3-85125-533-1-71

tudy was approved by the Ethical Committee of the General Hospital of Guangzhou Military Command of People's Liberation Army, which complies with the Code of Ethics of the World Medical Association (Declaration of Helsinki). Written informed consent was obtained from the patients' legal surrogates. The eight patients attended a CRS-R assessments in the week before the experiment, with the CRS-R scores presented in Tab. 1.

GUI and audiovisual paradigm The GUI used in this study is illustrated in Fig. 1. A visual button was set at the center of a 22-inch LED monitor. Two loudspeakers were placed behind the monitor to present auditory stimuli. The visual stimuli consisted of 10 visual numbers $(0, 1, \cdots, 9)$, whereas the auditory stimuli included 10 spoken numbers ($(0, 1, \cdots, 9$; 22 kHz, 16 bit). The intensities of sounds were adjusted by equalizing the root mean square power across all sound files. Each stimulus presentation (300 ms) included a pair of the visual and spoken numbers which could be semantically congruent (such as a visual number 8 and a spoken number 8) or incongruent (such as a visual number 5 and a spoken number 6). Furthermore, there was a 700-ms interval between two consecutive stimulus appearances. Note that all the audiovisual stimuli are presented one-by-one with the visual stimuli appeared in the same location of the screen. This made the paradigm a gaze-independent one.

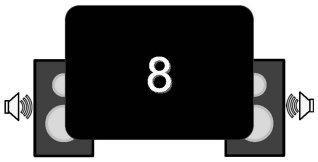

Figure 1: GUI of the audiovisual BCI.

Experimental procedures
The healthy subjects participated in Experiment I, whereas the patients with DOC participated in Experiment II. Experiment I contained three sessions in a random order, corresponding to the visual (V), auditory (A) and audiovisual (AV) stimulus conditions, respectively. In each session, there were first a calibration run of 10 trials for training the support vector machine (SVM) model and then a evaluation run of 40 trials. Note that we collected a small training data set for each subject, because this BCI system was designed mainly for patients with DOC who are easily fatigued during the experiment.
The experimental procedure of one trial of the audiovisual session is illustrated in Fig. 2. Four pairs of audiovisual stimuli were first constructed, in which one pair of audiovisual stimuli were semantically congruent and the other three pairs were semantically incongruent. Under the condition of semantic congruency/incongruency, these visual stimuli and auditory stimuli were pseudo-randomly chosen from the visual and spoken numbers $(0, 1, \cdots, 9)$. Each trial began with the visual and auditory presentation of the task instructions, which lasted 8 s. The instruction was "Count the number of times that the congruent audiovisual stimulus pairs appeared." Following the instruction, the four audiovisual stimulus pairs constructed as above were presented one by one for 8 times in a random order. Specifically, four number buttons flashed from appearance to disappearance in a random order. When a number button appeared, a spoken number was presented for 300 ms simultaneously. The subject was instructed to count the appearances of the congruent audiovisual stimuli (target) while ignoring the incongruent audiovisual stimuli (nontarget). After 32 s, a feedback result determined by the BCI algorithm appeared in the center of the monitor. If the result was correct, a positive audio feedback of applause was given for 4 s to encourage the subject. Otherwise, no feedback was presented and the screen was blank for 4 s.

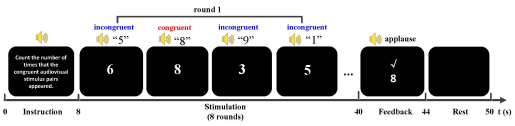

Figure 2: Procedure of one trial in the audiovisual condition.

For the visual and auditory sessions, the experimental procedure was similar to that for the audiovisual session with the following two exceptions. First, the instruction was "Focus on the target number (e.g., 8), and count the number of times that the target number is presented"; Second, there were visual-only stimuli for the visual session and auditory-only stimuli for the auditory session.
Experiment II contained an audiovisual session in which the procedure of each trial was the same as that for the audiovisual session of Experiment I. Eight patients participated in this experiment, which included a calibration run of 10 trials and an online evaluation run of 40 trials. Because the patients were subject to fatigue, the calibration and evaluation runs were divided into five blocks each of which contained 10 trials and was conducted on a separate days. Using EEG data from the calibration run, we trained a SVM classifier for the first evaluation block. For each of the later blocks, the classification model was updated using the data from the previous block. For example, we used the data from Block 2 to update the SVM model and then began the evaluation Block 3. During the experiment, the experimenters and families explained the instructions repeatedly so that the patient paid attention to the audiovisual target stimuli. The patient was carefully observed by an experienced doctor to ensure task engagement. Additionally, the break between two consecutive trials was extended to at least 10 s depending on the patient's level of fatigue.
Data acquisition A NuAmps device (Neuroscan, Compumedics Ltd, Victoria, Australia) was used to collect scalp EEG signals. Each patient wore an EEG cap (LT 37) with Ag-AgCl electrodes. The EEG signals were

Published by Verlag der TU Graz
Graz University of Technology

 DOI: 10.3217/978-3-85125-533-1-71

Table 1: Summary of patients' clinical status.

Patient	Age	Gender	Clinical Diagnosis	Etiology	Time Since Onset (months)	CRS-R score (subscores) Before the experiment
VS1	34	M	VS	ABI	2	5 (1-1-1-1-0-1)
VS2	55	M	VS	TBI	5	7 (1-1-2-2-0-1)
VS3	41	M	VS	CVA	1	6 (1-1-1-1-0-2)
VS4	48	M	VS	ABI	3	6 (1-1-2-1-0-1)
VS5	22	M	VS	TBI	18	5 (1-1-1-1-0-1)
MCS1	53	F	MCS	ABI	3	9 (1-3-2-1-0-2)
MCS2	37	M	MCS	TBI	4	8 (1-3-1-1-0-2)
MCS3	38	M	MCS	TBI	2	9 (1-3-2-1-0-2)

ABI, anoxic brain injury; CRS-R, coma recovery scale-revised; CVA, cerebrovascular accident; and TBI, traumatic brain injury; JFK CRS-R subscales: Auditory, visual, motor, oromotor, communication, and arousal functions.

referenced to the right mastoid. The EEG signals used for analysis were recorded from 32 electrodes placed at the standard positions of the 10-20 international system. The impedances of all electrodes were kept below 5 k Ω. The EEG signals were amplified, sampled at 250 Hz and band-pass filtered between 0.1 Hz and 30 Hz.

Data processing We performed the same online analysis for each session in Experiments I and II. In the following, we illustrated the online detection in an audiovisual session, as an example. For each trial of the calibration and evaluation runs, the EEG signals were first filtered between 0.1 and 20 Hz. We extracted an epoch (0-900 ms after the stimulus-onset) of the EEG signals for each channel and each stimulus appearance. This EEG epoch was down-sampled by a rate of 5 to obtain a data vector consisting of 45 data points. We concatenated the vectors from all 30 channels to obtain a new data vector, which corresponded to a stimulus appearance. Second, we constructed a feature vector for each audiovisual stimulus pair by averaging the data vectors across the 8 appearances in a trial. Third, we trained an SVM classifier using the feature vectors with labels from the calibration data. Finally, for each online trial, the SVM classifier was applied to the four feature vectors corresponding to the four audiovisual stimulus pairs, and four SVM scores were obtained. The detection result in this trial was determined as the audiovisual stimulus pair corresponding to the maximum of the SVM scores.

We performed ERP analysis using data from the evaluation run in each session of Experiment I. Specifically, for each trial, after band-pass filtering (0.1-20 Hz), the EEG epochs of each channel were extracted from 100 pre-stimulus to 900 ms post-stimulus, and baseline corrected using the data of the interval of 100 ms pre-stimulus. For artifact rejection, the epochs were discarded from averaging if the potential exceeded 60 μV in any one of channels. ERPs responses were extracted by time-locked averaging the EEG signal across 40 trials in the evaluation run for each of the stimulus conditions.

We also compared the ERPs for the target and nontarget stimuli to illustrate the effectiveness of our audiovisual BCI paradigm. Specifically, statistical analysis of the ERP components were conducted as follows [10]. First, based on the averaged ERP waveforms extracted above, the ERP components and their corresponding time windows were selected for all conditions. The width of the time window for each ERP component was 200 ms, referring to existing references such as [11]. Then, peak latency of each component was computed separately for each subject/condition individually. The latencies of maximum peaks were individually computed to ensure that each individual component's peak was enclosed in its corresponding time window. Next, mean amplitudes of these components were computed using a small window (50 ms in this study) surrounding the peak maximum. Finally, amplitude differences between targets and non-targets were tested with two-way repeated measures analyses of variance (ANOVA) on stimulus condition (the AV, V, and A conditions) and electrode site ("Pz", "Cz", and "Fz") as within-subjects factors for each of the ERP components. Post-hoc t-tests (Tukey-corrected for multiple comparisons) were further performed when necessary. Results were considered significant when p values were below 0.05.

For each session, the accuracy was calculated as the ratio of the number of all correct responses (hits) among the total number of presented trials. We used a binomial test based on Jeffreys' Beta distribution to calculate the significant level in a four-class paradigm as described below [12]:

$$\lambda \approx \left\{ a + \frac{2(N-2m)z\sqrt{0.5}}{2N(N+3)} \right\} + z\sqrt{\frac{a(1-a)}{N+2.5}}, \quad (1)$$

where N is the number of trials, m is the expected number of successful trials, a is the expected accuracy (0.25 in this study), λ is the accuracy rate, and z is the z-score based on the standard normal distribution. Given a significance level of 0.05 for a one-sided test, z is 1.65. Using (1), we could obtain the accuracy rate λ corresponding to the significance level, which is 37.3% for 40 trials.

Published by Verlag der TU Graz
Graz University of Technology

 DOI: 10.3217/978-3-85125-533-1-71

RESULTS

Results for healthy subjects Ten healthy subjects participated in Experiment I. Tab. 2 summarized the online classification accuracies for all healthy subjects. Among the AV, V and A conditions, the A one exhibited the lowest online accuracy for each healthy subject. The audiovisual online accuracies for nine of the ten healthy subjects were better than or equal to the visual-only online accuracies. The average online accuracy across all subjects were 92%, 84.75%, and 74.75% for the AV, V and A conditions, respectively, as shown in Tab. 2. A one-way repeated measures ANOVA was conducted to test the effect of stimulus condition on the online accuracy. The analysis revealed that the stimulus condition exerted a significant effect ($F(2, 27) = 7.849$, $p \leq 0.01$). Furthermore, Post-hoc Tukey-corrected t-tests indicated that the online average accuracy was significantly higher for the AV condition than for the V or A condition (all $p \leq 0.05$ corrected).

Table 2: Online accuracies for healthy subjects.

Subject	Accuracy (%)		
	A	V	AV
H1	75	80	90
H2	70	85	85
H3	55	85	85
H4	87.5	87.5	92.5
H5	70	80	90
H6	82.5	90	100
H7	67.5	80	100
H8	80	90	85
H9	82.5	87.5	97.5
H10	77.5	82.5	95
Average	74.75±0.09	84.75±0.04	92±0.06

We compared the brain responses evoked by the target and nontarget stimuli in the AV, V and A conditions in our ERP analysis. The group average ERP waveforms from 0 to 900 ms post-stimulus at the "Fz", "Cz", and "Pz" electrodes are shown in Fig. 3(a). Three ERP components P300, N400, and LPC were observed. We further determined the time windows for these ERP components (P300 window: 300-500 ms; N400 window: 500-700 ms; and LPC window: 700-900 ms). A two-way ANOVA showed no significant interaction between factors of stimulus condition and electrode site on each of the ERP components. The electrode site had no significant effect for each of the ERP components. However, the analysis demonstrated a significant main effect of stimulus condition (the audiovisual, visual-only, and auditory-only conditions) on each of the ERP components (P300: $F(2,63)=7.928$, $p \leq 0.01$; N400: $F(2,63)=8.708$, $p \leq 0.01$; LPC: $F(2,63)=12.557$, $p \leq 0.01$). Furthermore, Post-hoc Tukey-corrected t-tests revealed the following: (i) For the P300 component, the amplitude differences between target and non-target were stronger in the AV condition than in the A condition ($p \leq 0.01$ corrected). (ii) For the N400 component, the amplitude differences between target and non-target were stronger in the AV condition than in the V or A condition (all $p \leq 0.05$ corrected). (iii) For the LPC component, the amplitude differences between target and non-target were stronger in the AV condition than in the V or A condition (all $p \leq 0.01$ corrected).

We further evaluated the discriminative features in the AV, V and A conditions using point-wise running t-tests (two-tailed) for target vs. nontarget responses. It follows from Fig. 3(b) that there were more discriminative features within certain time windows, such as 300-500 ms, 500-700 ms, and 700-900 ms, for the AV condition than for the V and A conditions.

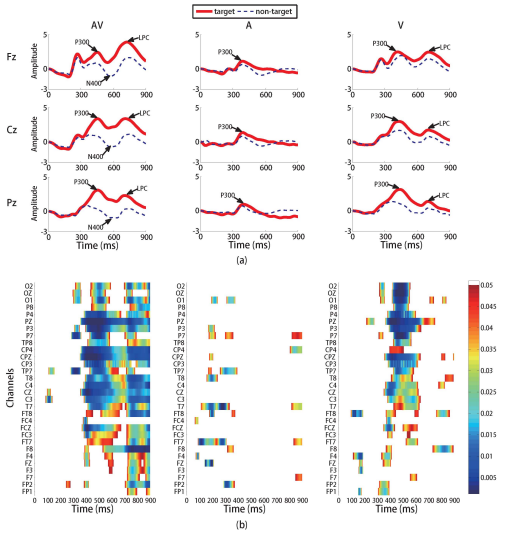

Figure 3: ERP waveforms and comparison results in the audiovisual (AV), visual-only (V) and auditory-only (A) conditions. (a) Average ERP waveforms of all healthy subjects from the "Fz", "Cz", "Pz" electrodes. The solid and dashed curves correspond to the target and nontarget stimuli, respectively. (b) Point-wise running t-tests compared target with nontarget responses across all healthy subjects for 30 electrodes. Significant differences were plotted when data points met an alpha criterion of 0.05 with a cluster size larger than seven.

Patients' results Eight patients participated in Experiment II, with the online results for the patients presented in Tab. 3. Three of the eight patients (VS4, MCS2, and MCS3) achieved accuracies (ranging from 40 to 45%) that were significantly higher than the chance level 25% (accuracy $\geq$37.3% or $p \leq 0.05$, binomial test). For patients VS1, VS2, VS3, VS5, and MCS1, the accuracies were not significant (i.e., $\leq$37.3%; ranging from 22.5 to 35%).

For the eight patients with DOC, the ERP waveforms were calculated. Specifically, the ERP waveforms from 0 to 900 ms post-stimulus were obtained by averaging the EEG channel signals across all 40 trials. Fig. 4 shows the average EEG signal amplitudes of the electrodes "Fz", "Cz" and "Pz" for the eight patients; the solid red and the

Published by Verlag der TU Graz
Graz University of Technology

 DOI: 10.3217/978-3-85125-533-1-71

dashed blue curves correspond to the target and the nontarget stimuli, respectively. For the three patients (VS4, MCS2, and MCS3) whose accuracies were significantly higher than the chance level, a P300-like component is apparent in each target curve, whereas the N400 and LPC responses were not apparently evoked as in the healthy controls. For the other five patients (VS1, VS2, VS3, VS5, and MCS1), none of the P300, N400, and LPC components were observed.

Among the five patients who were determined to be entirely vegetative based on repeated behavioral JFK CRS-R assessments, two patients (VS2 and VS4) progressed to MCS during the experiment. Furthermore, the patient VS4 subsequently emerged from MCS after the experiment. The patients MCS2 and MCS3 subsequently emerged from their conditions and showed motor-dependent behavioral communication two months after the experiment. Other patients (VS1, VS3, VS5, and MCS1) remained clinically unchanged at follow-up.

Table 3: Online accuracy of each patient.

Subject	Trials	Hits	Accuracy	p-value
VS1	40	11	27.5%	$p = 0.7150$
VS2	40	9	22.5%	$p = 0.7150$
VS3	40	12	30%	$p = 0.4652$
VS4	40	16	**42.5%**	$p = 0.0106$
VS5	40	13	32.5%	$p = 0.2733$
MCS1	40	14	35%	$p = 0.1441$
MCS2	40	16	**40%**	$p = 0.0285$
MCS3	40	18	**45%**	$p = 0.0035$

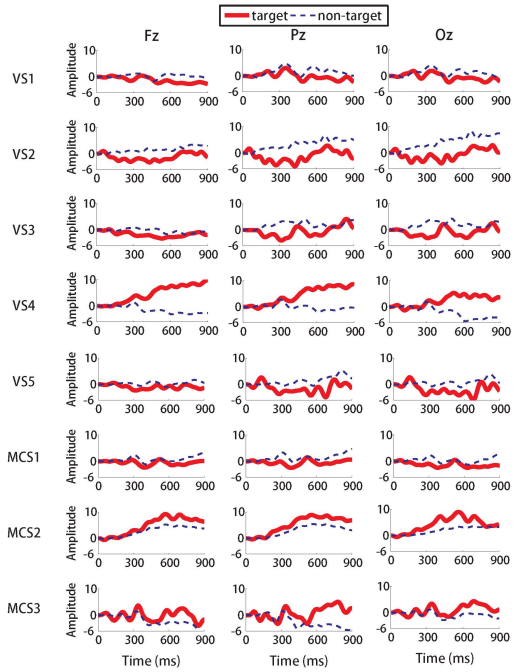

Figure 4: ERPs waveforms from the "Fz", "Cz" and "Pz" electrodes for the eight patients with DOC. The solid red curves correspond to the target stimuli, and the dashed blue curves correspond to the nontarget stimuli.

DISCUSSION

In this study, we proposed a novel audiovisual BCI system using semantically congruent and incongruent audiovisual stimuli of numbers. All the audiovisual stimuli were presented in a serial manner, which made the BCI system gaze-independent. With respect to classification accuracy, the experimental results for ten healthy subjects demonstrated that the audiovisual BCI system outperformed the corresponding visual-only and auditory-only BCI systems. Furthermore, we applied the proposed audiovisual BCI for awareness detection in patients with DOC. Among the eight DOC patients (5 VS, 3 MCS) involved in the experiment, three (1 VS, 2 MCS) achieved accuracies significantly higher than the chance level (Tab. 3). To some extent, these results demonstrated both command following and residual number recognition ability in these three patients.

Here, our paradigm was different from the classic 'oddball' paradigms. The stimuli in our paradigm included semantically congruent and incongruent audiovisual numbers (25% congruent and 75% incongruent audiovisual stimuli), which were presented one by one. Using this paradigm, our experimental results for healthy subjects showed that two main ERP correlates of semantic processing (N400 and LPC) as well as the P300 were elicited in the audiovisual condition. As shown in Fig. 3(a), the ERP responses to semantic processing first included a negative shift (N400) with a latency of 500-700 ms at electrodes "Fz", "Cz" and "Pz" for semantically incongruent stimuli (nontarget). Then, a following positive peak (LPC) during 700-900 ms was observed for semantically congruent stimuli (target) at electrodes "Fz", "Cz" and "Pz". These results are consistent with previous reports on semantic processing [13, 14]. In our ERP analysis for the healthy subject, a stronger P300 response was recorded in the AV condition than in the A condition, and both N400 and LPC responses were stronger in the AV condition than in the V and A conditions. Furthermore, as shown in Fig. 3(b), in several time windows corresponding to the P300, N400 and LPC components, the difference between the target and nontarget responses was greater for the AV condition than for the V and A conditions. This enhanced difference was useful for improving the performance of the BCI (see Tab. 2).

As previously mentioned, misdiagnosis rates based on behavioral observation scales such as CRS-R are relatively high. BCIs can be used as a supportive bedside tool to assess patients' residual cognitions. For instance, if awareness is detected in a VS patient using a BCI system, we may conclude that the patient possesses the cognitive functions associated with the experimental task and that a misdiagnosis might occur. In this study, the experiment results showed that one VS patient (VS4) was able to perform the BCI experimental task with a significant accuracy. This result corroborates previous fMRI ([15]) and EEG ([16]) data that some patients who meet the behavioral criteria for VS might have residual cogni-

Published by Verlag der TU Graz
Graz University of Technology

 DOI: 10.3217/978-3-85125-533-1-71

tive functions and even consciousness. In fact, according to the behavioral CRS-R assessments, this VS patient progressed to MCS one month after the experiment and further emerged from MCS three months later. This behavioral observation supports our BCI assessment result for this VS patient.

References

[1] R. T. Seel, M. Sherer, J. Whyte, D. I. Katz, J. T. Giacino, A. M. Rosenbaum, F. M. Hammond, K. Kalmar, T. L.-B. Pape, R. Zafonte *et al.*, "Assessment scales for disorders of consciousness: evidence-based recommendations for clinical practice and research," *Archives of physical medicine and rehabilitation*, vol. 91, no. 12, pp. 1795–1813, 2010.

[2] A. Demertzi, A. Vanhaudenhuyse, M.-A. Bruno, C. Schnakers, M. Boly, P. Boveroux, P. Maquet, G. Moonen, and S. Laureys, "Is there anybody in there? detecting awareness in disorders of consciousness," 2008.

[3] C. Schnakers, A. Vanhaudenhuyse, J. Giacino, M. Ventura, M. Boly, S. Majerus, G. Moonen, and S. Laureys, "Diagnostic accuracy of the vegetative and minimally conscious state: clinical consensus versus standardized neurobehavioral assessment," *BMC neurology*, vol. 9, no. 1, p. 35, 2009a.

[4] D. Lulé, Q. Noirhomme, S. C. Kleih, C. Chatelle, S. Halder, A. Demertzi, M.-A. Bruno, O. Gosseries, A. Vanhaudenhuyse, C. Schnakers *et al.*, "Probing command following in patients with disorders of consciousness using a brain–computer interface," *Clinical Neurophysiology*, 2012.

[5] G. Muller-Putz, D. Klobassa, C. Pokorny, G. Pichler, H. Erlbeck, R. Real, A. Kubler, M. Risetti, and D. Mattia, "The auditory p300-based ssbci: A door to minimally conscious patients?" in *Engineering in Medicine and Biology Society (EMBC), 2012 Annual International Conference of the IEEE*. IEEE, 2012, pp. 4672–4675.

[6] D. Coyle, A. Carroll, J. Stow, A. McCann, A. Ally, and J. McElligott, "Enabling control in the minimally conscious state in a single session with a three channel bci." The 1st international DECODER Workshop, 2012, pp. 25–28.

[7] J. Pan, Q. Xie, Y. He, F. Wang, H. Di, S. Laureys, R. Yu, and Y. Li, "Detecting awareness in patients with disorders of consciousness using a hybrid brain–computer interface," *Journal of neural engineering*, vol. 11, no. 5, p. 056007, 2014.

[8] M. Gondan, B. Niederhaus, F. Rösler, and B. Röder, "Multisensory processing in the redundant-target effect: a behavioral and event-related potential study," *Perception & Psychophysics*, vol. 67, no. 4, pp. 713–726, 2005.

[9] M. E. Thurlings, A.-M. Brouwer, J. B. Van Erp, and P. Werkhoven, "Gaze-independent erpbcis: augmenting performance through location-congruent bimodal stimuli," *Frontiers in systems neuroscience*, vol. 8, 2014.

[10] F. Perrin, C. Schnakers, M. Schabus, C. Degueldre, S. Goldman, S. Brédart, M.-E. Faymonville, M. Lamy, G. Moonen, A. Luxen *et al.*, "Brain response to one's own name in vegetative state, minimally conscious state, and locked-in syndrome," *Archives of Neurology*, vol. 63, no. 4, pp. 562–569, 2006.

[11] C. C. Duncan, R. J. Barry, J. F. Connolly, C. Fischer, P. T. Michie, R. Näätänen, J. Polich, I. Reinvang, and C. Van Petten, "Event-related potentials in clinical research: guidelines for eliciting, recording, and quantifying mismatch negativity, p300, and n400," *Clinical Neurophysiology*, vol. 120, no. 11, pp. 1883–1908, 2009.

[12] Q. Noirhomme, D. Lesenfants, F. Gomez, A. Soddu, J. Schrouff, G. Garraux, A. Luxen, C. Phillips, and S. Laureys, "Biased binomial assessment of cross-validated estimation of classification accuracies illustrated in diagnosis predictions," *NeuroImage: Clinical*, vol. 4, pp. 687–694, 2014.

[13] M. Liotti, M. G. Woldorff, R. Perez, and H. S. Mayberg, "An erp study of the temporal course of the stroop color-word interference effect," *Neuropsychologia*, vol. 38, no. 5, pp. 701–711, 2000.

[14] F. Perrin and L. Garcıa-Larrea, "Modulation of the n400 potential during auditory phonological/semantic interaction," *Cognitive Brain Research*, vol. 17, no. 1, pp. 36–47, 2003.

[15] M. M. Monti, A. Vanhaudenhuyse, M. R. Coleman, M. Boly, J. D. Pickard, L. Tshibanda, A. M. Owen, and S. Laureys, "Willful modulation of brain activity in disorders of consciousness," *New England Journal of Medicine*, vol. 362, no. 7, pp. 579–589, 2010.

[16] D. Cruse, S. Chennu, D. Fernández-Espejo, W. L. Payne, G. B. Young, and A. M. Owen, "Detecting awareness in the vegetative state: electroencephalographic evidence for attempted movements to command," *PloS one*, vol. 7, no. 11, p. e49933, 2012b.

Published by Verlag der TU Graz
Graz University of Technology

Proceedings of the
7th Graz Brain-Computer Interface Conference 2017 DOI: 10.3217/978-3-85125-533-1-72

IMPLANTED BRAIN-COMPUTER INTERFACE SIGNAL STABILITY OVER TIME

E.G.M. Pels[1], E.J. Aarnoutse[1], S. Leinders[1], Z.V. Freudenburg[1], M.P. Branco[1], M.A. van den Boom[1], T. Denison[2], M.J. Vansteensel[1], N.F. Ramsey[1]

[1] Brain Center Rudolf Magnus, Department of Neurology & Neurosurgery, University Medical Center Utrecht, Utrecht, The Netherlands

[2] Department of Neuromodulation, Medtronic, Minneapolis, MN

E-mail: E.pels-2@umcutrecht.nl

ABSTRACT: In recent years, implanted BCIs gained increasing interest. Relying on subdural or intracortical electrodes, these systems carry the advantage of brain signals gathered at the source. Successes in this field have been reported in controlling robotic arms, intended for severe paralysis or arm amputation, and recently also for replacing communication. A prerequisite for long-term use of implantable BCIs is that there is no decrease in signal quality over time. In this paper we examined the signal stability of a fully implanted BCI system for communication over a period of 12 months. Three different tasks were used to investigate signal stability since implantation, all of which show a stable and decodable signal, indicating that the implanted electrodes are durable and information transfer is preserved for at least 12 months. These findings suggest that ECoG-based BCI systems are robust and can be used at home for long-term in patients that need them.

INTRODUCTION

For people with severe paralysis and communication problems, assistive technologies are an important part of their lives, particularly for people suffering from locked-in syndrome (LIS). LIS is characterized by the loss of all voluntary movement, resulting in quadriplegia and the loss of speech. LIS can be divided into three categories, *classic* LIS, where only vertical eye movement and eye blinks remain, *incomplete* LIS, which is the same as *classic* LIS, but with additional voluntary movement other than vertical eye movements, and *complete* LIS, which is LIS without any voluntary movement. In all variants cognition is intact and people are aware of their surroundings [1]. The causes of LIS are very diverse and include brainstem stroke, trauma and motor neuron diseases like amyotrophic lateral sclerosis (ALS). The latter affects about 5 in 100.000 people and especially late-stage ALS patients on invasive ventilation may progress into LIS. The ability to communicate is correlated with quality of life in people with LIS [2], [3]. Current methods for communication mainly rely on residual motor control such as eye-movements or minimal movement of a finger [4]. When also that last motor function fails, communication becomes almost impossible and a BCI becomes one of the last remaining options.

Since the beginning of BCI-research, non-invasive, mostly EEG-based, BCIs have promised to be a replacement for communication in patients [5], [6]. However, the clinical application is only slowly realized and for LIS-patients, EEG-BCI performance is lower than for less severely paralyzed people [7]. Recently, functional near-infrared spectroscopy (fNIRS) was used to enable complete locked-in patients to communicate [8]. However, the application of such a device at the patients' home is currently not an option as experts need to setup the system.

Implantable *BCIs*, utilizing the brain signal recorded with electrodes on or in the brain, have the potential to become a useful solution to the daily obstacles of people suffering from LIS, due to their high signal quality and potential 24/7 availability. The promises of implantable BCIs have been investigated and demonstrated in a laboratory setting [9]–[11] but recently, the first successful independent home-use of an implantable BCI by an ALS-patient was described by our group [12]. We showed high spelling performance and user-satisfaction, bridging the gap between research and the application of implantable BCIs at home. The system was implanted in November 2015 and is still used at home by the patient. In order to allow the current patient, as well as future users, to use the system with high accuracy for an even longer period of time, the long-term stability of the measured ECoG signal is important. Long-term use of an ECoG-based BCI has not been tested before and signal recordings have mainly been done in epilepsy patients or patients receiving, experimental, closed-loop Deep Brain Stimulation (DBS). Sillay and colleagues showed long-term stability of impedance in both subdural and depth electrodes, indicating a stable tissue-electrode contact a prerequisite for good signal recordings [13].

Here we report on the signal stability of a fully implanted BCI system, the Utrecht NeuroProsthesis (UNP) during a period of 12 months, and conclude that implanted BCIs can be a long-term solution for LIS-patients.

Published by Verlag der TU Graz
Graz University of Technology

 DOI: 10.3217/978-3-85125-533-1-72

MATERIALS AND METHODS

The implanted system: The UNP consists of two four-electrode ECoG-strips connected to an implanted amplifier/transmitter device (the device; Activa® PC+S Medtronic) by subcutaneous leads. The strips are placed subdurally over the left sensorimotor hand area and on top of the left prefrontal cortex. Both locations were preoperatively determined by functional MRI. Here we only report on data collected by the strip placed on the left sensorimotor hand area. The device was implanted in the left thorax and filters and amplifies the signal before it sends it wirelessly to a computer outside the body. Outside the body, the signal is received by a receiver module connected to a Windows tablet running custom software based on the BCI2000 platform [14] for signal processing and translation. For a complete lay-out of the implant see figure 1.

Patient: For this study a locked-in patient (58-year-old female) who suffers from late-stage ALS was implanted with the UNP.

Tasks and data acquisition: Shortly after implantation, the best performing bipolar electrode pair within the strip was selected based on the correlation of the high frequency band (HFB) power (65-95Hz) with a screening task (expressed as R^2) measured at a sampling rate of 200Hz. The screening task consisted of alternated blocks of attempted movement of the right hand (finger tapping) and rest. At home, weekly repetitions of the screening task enabled us to track the R^2 values over time, as an indication of signal stability.

Additionally, we did regular baseline/rest measurements in order to follow the raw signal over time. For this we used a baseline task, in which the patient had to look at a screen with a blue circle for 3 minutes and think of nothing in particular. Data were recorded with a sampling frequency of 200Hz and HFB-power was calculated for each run using multitaper time-frequency transformation based on multiplication in the frequency domain (average power over 65-95Hz, 1Hz bin, Hanning window) [15].

Finally, in order for the patient to learn to control her brain signal we used a one-dimensional continuous cursor control task (cursor task). For this task the patient controlled the vertical speed of a cursor travelling from the left side of the screen to the right (horizontal speed was fixed), using attempted movement to steer the cursor up and rest to lower the cursor in order to hit a target on the right side. The cursor task was performed regularly after implantation, allowing us to follow the usability of the control signal over time. Data for the cursor task were recorded in the energy-saving mode of the device, this means that bandwidth filtering on HFB was done on the device with 5Hz sampling frequency. For each repetition of this task, following an initial calibration run to acquire offset and gain values for that day, a 5 minute run was done. The amount of trials varied during the year as feedback time was reduced from 6 to 2 seconds. Therefore, the amount of total trials in a 5 minute run was between 26 and 47 during the year. The score was calculated as the percentage of correct target hits. Besides the score, we report here the average power during the baseline (down) trials, as transmitted by the implanted device. For all tasks, data acquisition and stimulus presentation were done on the BCI2000 software running on a separate research laptop.

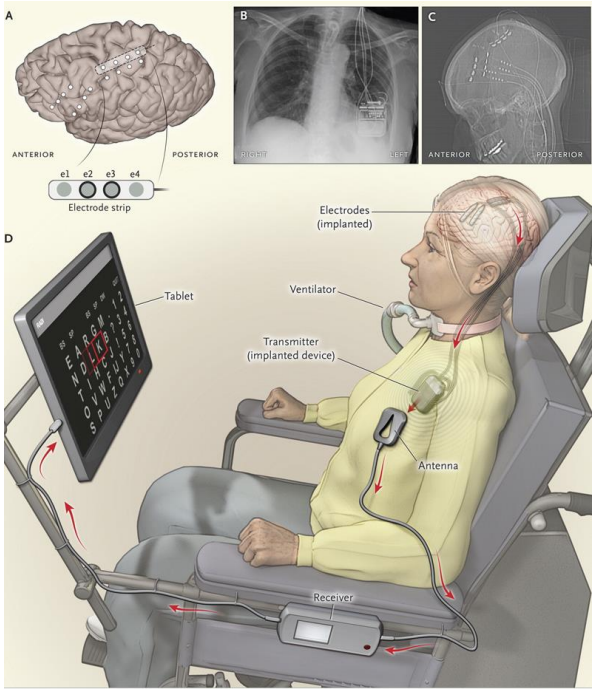

Figure 1: Electrode Placement and System Setup in the Brain–Computer Interface System. Panel A shows the contact points of the electrode strips, which are indicated by white dots, over the sensorimotor and dorsolateral prefrontal cortex; the positions of electrodes were based on postoperative computed tomographic (CT) scans merged with the pre-surgical MRI. Electrodes e2 and e3 on the electrode strip were chosen for brain–computer interface feedback. Panel B shows a postoperative chest radiograph displaying the transmitter device (Activa® PC+S, Medtronic), which was placed subcutaneously in the chest, and wires leading to the electrodes. Two of four wires were connected to the device. Panel C shows the postoperative CT scan with the locations of four electrode strips. The dots on the four wires are connectors. Panel D shows the components of the brain–computer interface system, including the transmitter, receiving antenna, receiver, and tablet. (Copyright © 2016, Massachusetts Medical Society)

RESULTS

The results of the screening task showed a stable R^2 for the bipolar pair used from 0.88 just after implantation to 0.86 one year after implantation (Figure 2).

After an initial 21% decrease of HFB power 8 weeks post-surgery, mean baseline/rest HFB power was stable and remained so for the following year. The cause for the fluctuation of 8.8% (relative Std) in mean HFB power during that year, which was also apparent in the rest periods of the cursor task (down trials; 5.7%), is uncertain but possibilities include biological factors such

Published by Verlag der TU Graz
Graz University of Technology

 DOI: 10.3217/978-3-85125-533-1-72

as, temperature, level of fatigue and circadian rhythm.
The average performance on the cursor task over 12 months with sensorimotor control was 91 ± 6%, which is significantly above chance (50%, $p<0.001$).

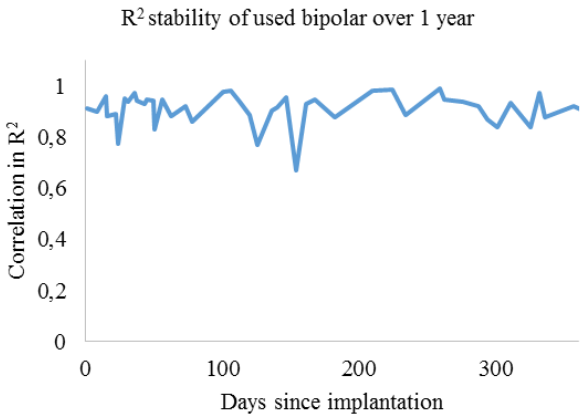

Figure 2: R^2 values of the bipolar pair used for brain-computer interface control (HFB power), measured frequently with the screening task for one year.

DISCUSSION

Here we show that a fully implantable, ECoG-based BCI system can be used by a late-stage ALS-patient at home for over a year. Twice weekly visits during a year and regular visits after that year show that the signal measured is stable and can be used for BCI-control.
This is the first study to show long-term ECoG-BCI control-signal stability. Earlier ECoG-BCI studies have mainly been performed with epilepsy patients, who were temporarily implanted with ECoG electrodes. In these patients, the time constraints of the clinical procedure generally does not allow for long-term BCI measurements. Available data did indicate, however, that ECoG-based BCI performance is good for multiple days when calibrating or using adaptive algorithms [16], [17]. In 2009, Blakely and colleagues showed robust BCI control over the course of 5 days without the need of retraining or adaptive algorithms [18].
Long-term ECoG measurements have been performed before for other purposes than BCI. Earlier studies with implanted electrodes in non-human primates show that most signal changes occur in the first months and that relevant motor system frequencies (beta and gamma bands) are detectable over the course of 24 months [19]. Additionally, in humans, long-term ECoG recordings have been done in patients receiving experimental closed-loop DBS as a treatment for epilepsy or Tourette's syndrome [13], [20], concurrent with our results that signal transfer is maintained for long-term.
A stable and robust BCI control signal for long-term use is important as it ensures availability of a BCI for patients who are likely to need the device for years. Additionally, it is also needed for reducing, or even to circumvent, the need for (re)calibration, making the system faster to start up and easier to use. Importantly, the current results suggest that there is no indication that in the future signal quality will decrease.

CONCLUSION

In conclusion these data indicate that implanted ECoG electrodes provide a durable signal quality and information transfer is preserved over the course of at least 12 months. These results demonstrate that long-term ECoG signal quality suffices for meeting the needs of late-stage ALS patients for a reliable communication device for home use.

REFERENCES

[1] E. Smith and M. Delargy, "Locked-in syndrome," *Br. Med. J.*, vol. 330, no. February, pp. 3–6, 2005.
[2] M.-A. Bruno, J. L. Bernheim, D. Ledoux, F. Pellas, A. Demertzi, and S. Laureys, "A survey on self-assessed well-being in a cohort of chronic locked-in syndrome patients: happy majority, miserable minority.," *BMJ Open*, vol. 1, no. 1, p. e000039, 2011.
[3] M.-C. Rousseau, K. Baumstarck, M. Alessandrini, V. Blandin, T. Billette de Villemeur, and P. Auquier, "Quality of life in patients with locked-in syndrome: Evolution over a 6-year period.," *Orphanet J. Rare Dis.*, vol. 10, p. 88, 2015.
[4] L. Snoeys, G. Vanhoof, and E. Manders, "Living with locked-in syndrome: an explorative study on health care situation, communication and quality of life.," *Disabil. Rehabil.*, vol. 35, no. 9, pp. 713–8, 2013.
[5] J. R. Wolpaw and E. W. Wolpaw, *Brain-Computer Interfaces: Principles and Practice*. Oxford University Press, 2012.
[6] E. W. Sellers, T. M. Vaughan, and J. R. Wolpaw, "A brain-computer interface for long-term independent home use.," *Amyotroph. Lateral Scler.*, vol. 11, no. 5, pp. 449–455, 2010.
[7] A. Kübler and N. Birbaumer, "Brain-computer interfaces and communication in paralysis: Extinction of goal directed thinking in completely paralysed patients?," *Clin. Neurophysiol.*, vol. 119, no. 11, pp. 2658–2666, 2008.
[8] U. Chaudhary, B. Xia, S. Silvoni, L. G. Cohen, and N. Birbaumer, "Brain-Computer Interface-Based Communication in the Completely Locked-In State," pp. 1–25, 2017.
[9] P. R. Kennedy, M. T. Kirby, M. M. Moore, B. King, and A. Mallory, "Computer control using human intracortical local field potentials.," *IEEE Trans. Neural Syst. Rehabil. Eng.*, vol. 12, no. 3, pp. 339–44, 2004.
[10] L. R. Hochberg, D. Bacher, B. Jarosiewicz, N. Y. Masse, J. D. Simeral, J. Vogel, S. Haddadin, J. Liu, S. S. Cash, P. van der Smagt, and J. P. Donoghue, "Reach and grasp by people with

Published by Verlag der TU Graz
Graz University of Technology

 DOI: 10.3217/978-3-85125-533-1-72

tetraplegia using a neurally controlled robotic arm," *Nature*, vol. 485, no. 7398, pp. 372–375, 2012.

[11] M. J. Vansteensel, D. Hermes, E. J. Aarnoutse, M. G. Bleichner, G. Schalk, P. C. Van Rijen, F. S. S. Leijten, and N. F. Ramsey, "Brain-computer interfacing based on cognitive control," *Ann. Neurol.*, vol. 67, no. 6, pp. 809–816, 2010.

[12] M. J. Vansteensel, E. G. M. Pels, M. G. Bleichner, M. P. Branco, T. Denison, Z. V. Freudenburg, P. Gosselaar, S. Leinders, T. H. Ottens, M. A. Van Den Boom, P. C. Van Rijen, E. J. Aarnoutse, and N. F. Ramsey, "Fully Implanted Brain–Computer Interface in a Locked-In Patient with ALS," *N. Engl. J. Med.*, vol. 375, no. 21, p. NEJMoa1608085, 2016.

[13] K. A. Sillay, P. Rutecki, K. Cicora, G. Worrell, J. Drazkowski, J. J. Shih, A. D. Sharan, M. J. Morrell, J. Williams, and B. Wingeier, "Long-term measurement of impedance in chronically implanted depth and subdural electrodes during responsive neurostimulation in humans," *Brain Stimul.*, vol. 6, no. 5, pp. 718–726, 2013.

[14] G. Schalk, D. J. McFarland, T. Hinterberger, N. Birbaumer, and J. Wolpaw, "BCI 2000: A General-Purpose Brain-Computer Interface(BCI) System," *IEEE Trans. Biomed. Eng.*, vol. 51, no. 6, pp. 1034–1043, 2004.

[15] R. Oostenveld, P. Fries, E. Maris, and J. M. Schoffelen, "FieldTrip: Open source software for advanced analysis of MEG, EEG, and invasive electrophysiological data," *Comput. Intell. Neurosci.*, vol. 2011, 2011.

[16] E. C. Leuthardt, G. Schalk, J. R. Wolpaw, J. G. Ojemann, and D. W. Moran, "A brain-computer interface using electrocorticographic signals in humans.," *J. Neural Eng.*, vol. 1, no. 2, pp. 63–71, 2004.

[17] G. Schalk, "Two-dimensional movement control using electrocorticographic signals in humans," *J Neural Eng*, vol. 5, no. 1, pp. 75–84, 2008.

[18] T. Blakely, K. J. Miller, S. P. Zanos, R. P. N. Rao, and J. G. Ojemann, "Robust, long-term control of an electrocorticographic brain-computer interface with fixed parameters.," *Neurosurg. Focus*, vol. 27, no. July, p. E13, Jul. 2009.

[19] E. Ryapolova-Webb, P. Afshar, S. Stanslaski, T. Denison, C. de Hemptinne, K. Bankiewicz, and P. a Starr, "Chronic cortical and electromyographic recordings from a fully implantable device: preclinical experience in a nonhuman primate.," *J. Neural Eng.*, vol. 11, no. 1, p. 16009, 2014.

[20] J. B. Shute, M. S. Okun, E. Opri, R. Molina, P. J. Rossi, D. Martinez-Ramirez, K. D. Foote, and A. Gunduz, "Thalamocortical network activity enables chronic tic detection in humans with Tourette syndrome," *NeuroImage Clin.*, vol. 12, pp. 165–172, 2016.

Published by Verlag der TU Graz
Graz University of Technology

Proceedings of the
7th Graz Brain-Computer Interface Conference 2017 DOI: 10.3217/978-3-85125-533-1-73

EVENT-RELATED POTENTIALS IN EXTERNALLY AND INTERNALLY-DRIVEN TARGET SELECTION: A PRELIMINARY STUDY

J. Pereira[1], A. I. Sburlea[1], G. R. Müller-Putz[1]

[1]Institute of Neural Engineering, Graz University of Technology, Graz, Austria

E-mail: gernot.mueller@tugraz.at

ABSTRACT: In this study we investigated the cue-locked (P300 and later event-related potentials components) and response-locked electroencephalography (EEG) phenomena associated to externally and internally-driven target selection. For that we designed a novel paradigm, that aimed to separate the selection of motor goals according to the respective task rules from the actual programming of the upcoming motor response. Our paradigm also made possible the estimation of the onset of a self-paced reach-and-grasp movement imagination for better capturing the associated movement-related cortical potentials (MRCPs). Our preliminary results indicate that differences between the externally and internally-driven conditions are present in the cue-locked event-related potentials, but not in the response-locked MRCPs. Our study contributes for a better understanding of the neurophysiological signature of movement-related processes, including both perception and actual motor planning, which are so extensively used in brain-computer interfaces (BCIs).

INTRODUCTION

Movement planning consists in all the movement-related processes that happen before the actual movement initiation. This broad definition of movement planning includes not only the processes that define how the movement will look like, e.g. in trajectory, but also the cognitive processes that allow us to decide on motor goals [1]. Wolpert and Landy defended that movement planning is a decision-making process, where both sensory and motor decisions are integrated [2]. In a narrower perspective, Wong et al. proposed to limit motor planning to the processes that allow the translation of the abstract definition of a motor goal to the concrete movement specifications [1]. Perception/cognition and motor planning are then linked at the moment when the motor goal is defined. For example, if we want to grasp a glass, we first observe the environment and rely on attention to locate the glass (target). Only then we decide on how we will reach it. The selection of the target is usually dependent on task rules, which are encoded in the prefrontal cortex [3]. These rules can be externally or internally-driven (e.g. *I will pick the wine glass because I intend to drink wine.*) and their application is critical to the definition of the motor goal. Undoubtedly, understanding the processes that lead to the final course of action, including the definition of motor goals, is of great interest not only for basic neuroscience but also for research fields which rely on the neurophysiological signature of movement-related processes, like in brain-computer interfaces (BCIs) research [4]. Studies on event-related potentials (ERPs) show that there is a modulation of ERPs later components, like the P300, as a function of complexity of cognitive control prior to motor tasks [5]. The explanation that only attention is modulating these ERP components started to be questioned. To elucidate the P300's role in information processing, Nieuwenhuis et al. integrated evidence to suggest that the P300 reflects the response of the locus coeruleus-norepinephrine system to the outcome of decision-making responses [6]. Another interesting component of the ERP is the positive slow wave, which emerges after the P300, and has been associated to decision-making prior to the preparation of a response [7]. Recently, our group showed that the presence of motor goals is modulated in the EEG time-domain signals in the delta band around movement onset [8]. These slow EEG fluctuations, when associated with motor tasks (e.g. movement execution or imagination) are known as movement-related cortical potentials (MRCPs) [9]. We now aim to investigate goal-directed movements when several targets are presented simultaneously and in two main conditions: in the internally-driven conditions the subjects decide which of the five or two possible targets will be their motor goal and in the externally-driven condition the subjects just have one option. After selecting their target according to the task rule, the participants imagined a single reach-and-grasp movement. In a novel paradigm, we aim to separate the target selection from actual motor planning. Further, we decided on a self-paced motor imagery task since we will later investigate new methods for movement detection for BCI control. In this paper we present and discuss the results obtained, in respect to the cue-locked (P300 and later ERP components) and response-locked (MRCPs) potentials. We study these two phenomena since the first are thought to mainly reflect stimulus processing, while the second reflect the upcoming motor response.

Published by Verlag der TU Graz
Graz University of Technology

 DOI: 10.3217/978-3-85125-533-1-73

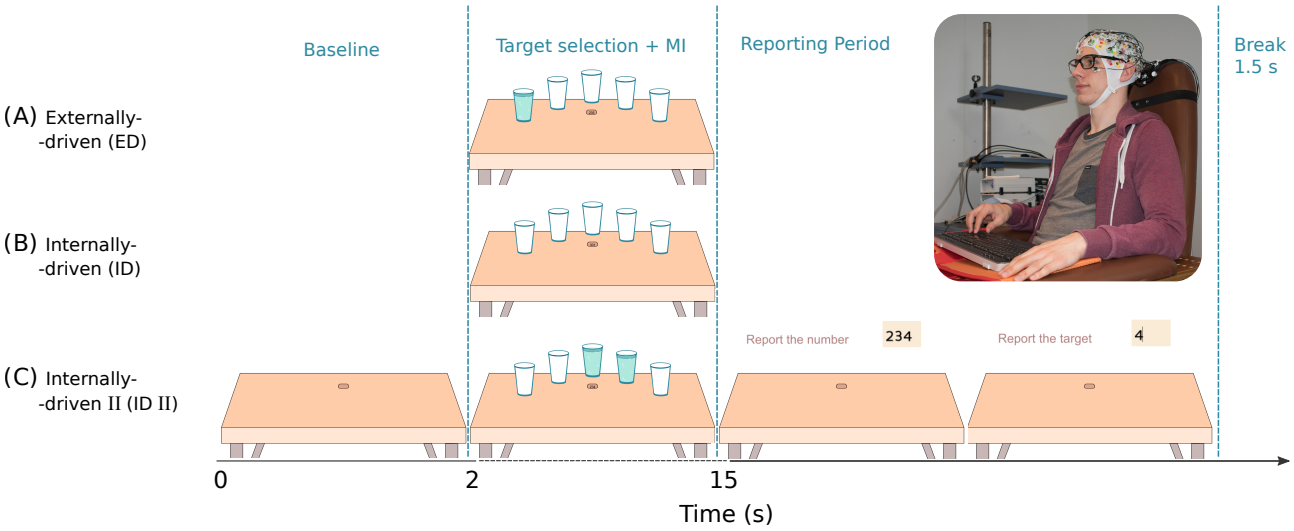

Figure 1: Trial representation. Each trial consisted of a baseline period, followed by one of the three conditions: (A) externally-driven, (B) internally-driven or (C) internally-driven II. This was followed by a reporting period, where subjects were asked to report (1) the number that was shown in the scroller (center of the virtual table) when they started the reach-and-grasp movement imagination (MI) and (2) the target of the MI.

MATERIALS AND METHODS

Participants: Six healthy participants (age 24 $\pm$ 3.3 years, 1 male) took part in this study. Participants gave their informed consent and the study was conducted in accordance with the protocol approved by the ethics committee of the Medical University of Graz. Subjects had normal or corrected-to-normal vision and no history of neurological or psychiatric disorders. All subjects were right-handed. Subjects sat in a comfortable chair, in a shielded room, facing the computer monitor that was placed at a distance of 130 cm in front of them. Their arms were supported in both armrests. Additionally, a wireless keyboard was placed in front of them, at the same level as their arms.

Conditions and Paradigm: Participants were instructed to perform a reach-and-grasp movement imagination task. After the end of each trial, there was a reporting period in which they used the keyboard. Participants performed three different conditions that were shown in a randomly alternated order, but with the same frequency. An average of 68 trials per condition were recorded, separated into runs. The trials had a variable duration dependent on the subject, due to the presence of a reporting period, and were followed by breaks of 1.5 seconds. All cues were presented on the monitor. Fig. 1 represents one trial in the three experimental conditions. Each trial began with a two-second baseline, followed by a cue that indicated one of the three conditions. In all conditions, five glasses showed up at second 2 in addition to a scroller that showed consecutive numbers every 750 ms. This scroller was positioned in the center of the screen. In the externally-driven (ED) condition, represented in Fig. 1.A, one glass was filled with water. In this condition, the subjects knew that the target of their reach-and-grasp movement imagination (MI) was the glass filled with water. In the internally-driven (ID) condition, Fig. 1.B, all glasses were empty and subjects were instructed to chose one of the five possible targets. In the second internally-driven (IDII) condition, Fig. 1.C, two of the five glasses had water and subjects were instructed to chose one of them. The glasses which had water in both ED and IDII conditions were pseudo-randomly positioned and all positions were covered with the same frequency. We instructed the participants to select the target as soon as they saw the glasses. After selecting their target according to the condition rule, subjects were asked to perform the imagination of a reach-and-grasp to the selected glass, as if it was positioned in front of them. At the moment they felt the urge to start the MI, they were instructed to memorize the number that was on the scroller and perform the reach-and-grasp movement imagination. Inspired by Libet's clock experiments [10], we used the reported numbers to estimate the time when the participants perceived the urge of performing the movement imagination. Later, we time-locked the data to this event. Subjects had 13 seconds to select the target and perform the self-paced movement imagination. At the end of the trial, as showed in Fig. 1, there was a reporting period in which subjects reported the number they memorized (from now on called "reported number") and the target they selected from 1 to 5. Fig. 1 also shows an example of a correct reporting for the IDII condition. After a break of 1.5 s, a new trial started. Subjects were asked to keep their gaze in the center of the monitor and specifically to avoid moving their eyes towards the selected target during the trial. Moreover, subjects were asked to minimize blinks and muscular artifacts. During the reporting period, those artifacts were allowed. All subjects performed reach-and-grasps to a real glass at the beginning of the experiment and practised the MI task.

Published by Verlag der TU Graz
Graz University of Technology

 DOI: 10.3217/978-3-85125-533-1-73

EEG Recordings: EEG and electrooculography (EOG) signals were recorded using 64 active actiCAP electrodes (BrainProducts GmbH, Germany). Reference was placed on the right mastoid and ground on AFz. Three EOG electrodes were placed above the nasion and below the outer canthi of the eyes. Biosignals were sampled at 1kHz using two 32-channel BrainAmp amplifiers (Brain Products GmbH, Germany). For the recordings and time-synchronization we used the lab streaming layer (LSL) framework.

EEG Processing: Raw data were first inspected visually and noisy channels were removed. We excluded the trials in which participants reported an incorrect scroller number and/or target number according to the task rules. After bandpass filtering (1-70 Hz, zero-phase 4th order Butterworth), we epoched the data from 0 to 13 s in respect to the start of the trial and we used EEGLAB [11] to: (1) find values outside an interval between -200 μV and 200 μV, (2) reject trials with abnormal joint probabilities and/or (3) abnormal kurtosis. A threshold of 5 times the standard deviation was used for each statistic. On average, 25 trials were discarded per subject. After rejecting those trials, we applied principal component analysis (PCA) for dimensionality reduction and retained components that explained 99 % of the variance of the data. We then used independent component analysis (ICA) on the PCA-compressed EEG and EOG data using the extended Infomax algorithm [12]. We marked the independent components that corresponded to ocular artifacts. In the unfiltered data, after rejecting the aforementioned artefactual trials, we used the weights of the ICA to back-project the non-artefactual components into the channel-space. ERPs were locked to the cues which distinguished the three different conditions (i.e. second 2 in Fig. 1). Individual averages were collapsed to calculate the grand-average cue-locked ERPs and topographical maps of the scalp ERPs distribution were obtained. We analysed the MRCPs as response-locked EEG neural correlates of movement intention. After bandpass filtering from 0.1 to 3 Hz with a 4th order zero-phase Butterworth filter, we time-locked the trials to the correspondent reported numbers and computed the grand-averaged MRCPs, separately for the three conditions.

RESULTS

Cue-locked ERPs and their topographical maps at time windows of interest for the three different conditions are depicted in Fig. 2.A and Fig. 2.B, respectively. For all conditions, the P300 positive deflection starts around 260 ms after the cue and peaks at 340 ms. While the peak latency is the same among conditions, the amplitude is different between the ID or IDII and the ED condition. As shown by Fig. 2.B, the differences between the internally (both ID and IDII) and externally-driven (ED) conditions are first more central distributed (200-300 ms) and then more parietal (300-400 ms). P300 amplitudes then decrease until 500 ms after the cue, followed by a slow positive component, which is stronger in the ED condition. These differences are seen in the centroparietal electrodes, according to the maps in Fig. 2.B. Fig. 3.A shows the grand-average MRCPs at electrodes FCz, C3, Cz, C4, CP3, CPz and CP4 for the three conditions and Fig. 3.B shows the respective topographical distribution around the reported number. The self-paced MI was preceded by a negativity that started at around one second before the reported number. The negative peak was higher in the midline electrodes (FCz and Cz) at 900 ms after the reported number. No differences were observed among the three conditions around this event.

DISCUSSION

Using a novel paradigm, we investigated the cue-locked and response-locked EEG phenomena associated to externally and internally-driven target selection. In a preliminary analysis, our results indicate that differences between the externally and internally-driven conditions are present in the cue-locked, but not in the response-locked ERPs (MRCPs). Specifically, the P300 and the following slow ERP components are different among the conditions. The P300 is associated to stimulus processing [13], which is present in all three conditions. Furthermore, there was the need of mapping a rule to the presented stimuli, but this rule varied in complexity among the conditions. The necessity of target selection was limited to the two internally-driven conditions (ID and IDII) which indicates a higher demand in these conditions when comparing to the externally-driven condition. As suggested by Niewenhuis et al., later ERP components encode processes of guiding the future response in the service of task demands and rules [6]. While it could be argued that an increase in task demand is due exclusively to the different number of targets available (1 in the ED against 2 or 5 in the IDII and ID, respectively), we found no differences between the IDII and ID conditions. For that reason, our first results indicate that increased amplitudes are associated to a higher demand caused by the need of target selection in both internally-driven conditions. But an important question arises: are the observed differences strictly related to the upcoming motor response? It would be interesting to know whether the need of motor planning directly influences these components by introducing a condition where no motor task is necessary.

Published by Verlag der TU Graz
Graz University of Technology

 DOI: 10.3217/978-3-85125-533-1-73

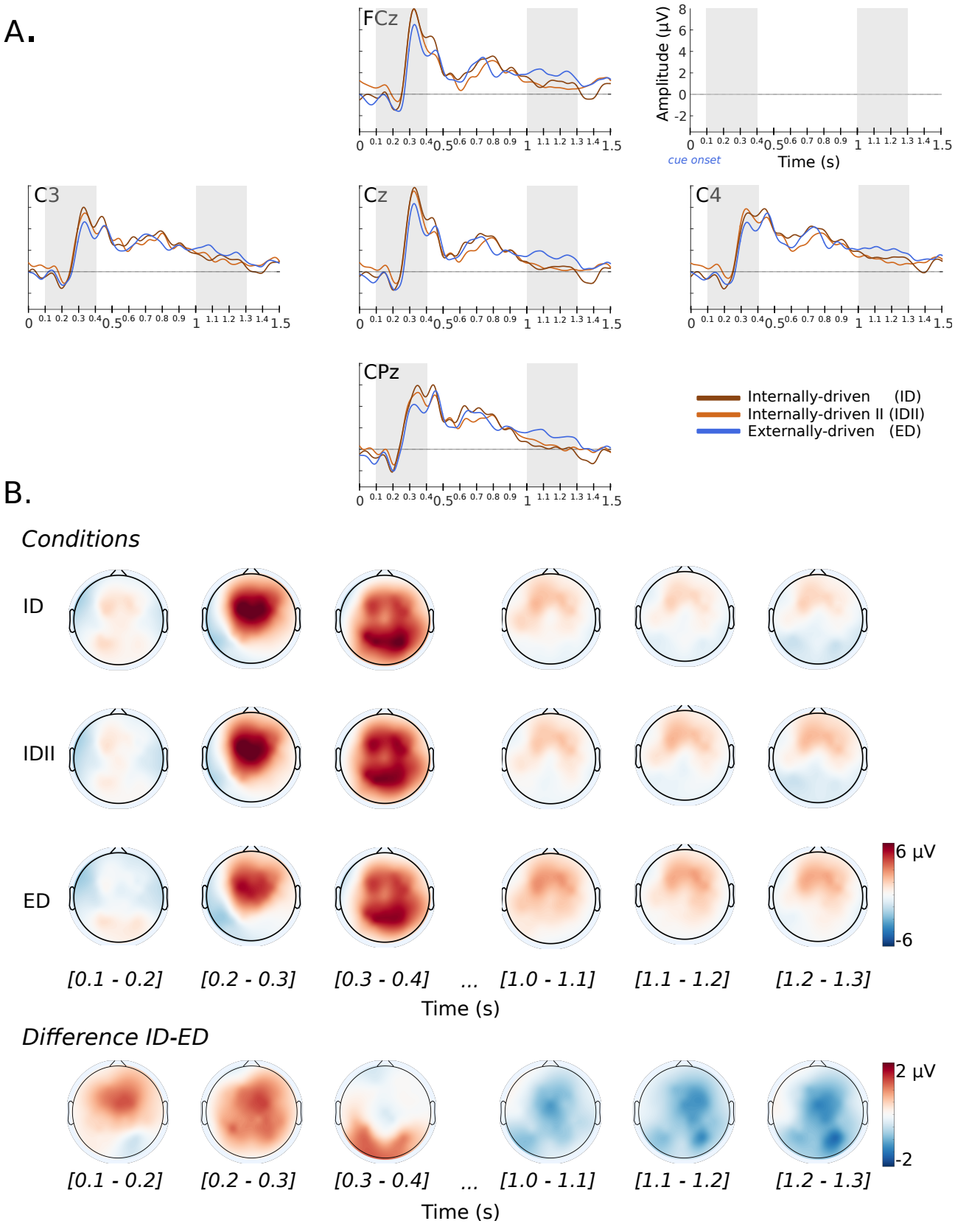

Figure 2: Results of the ERP analysis. (A) Cue-locked grand-average waveforms for electrodes FCz, C3, Cz, C4 and CPz. (B) Topographical maps in the time windows of interest. The first three rows show the topoplots for the three conditions and the last row shows the differences between the internally-driven (ID) condition and the externally-driven (ED) condition. Differences between IDII and ED are not shown since they are similar to the ID vs. ED differences here plotted.

Published by Verlag der TU Graz
Graz University of Technology

 DOI: 10.3217/978-3-85125-533-1-73

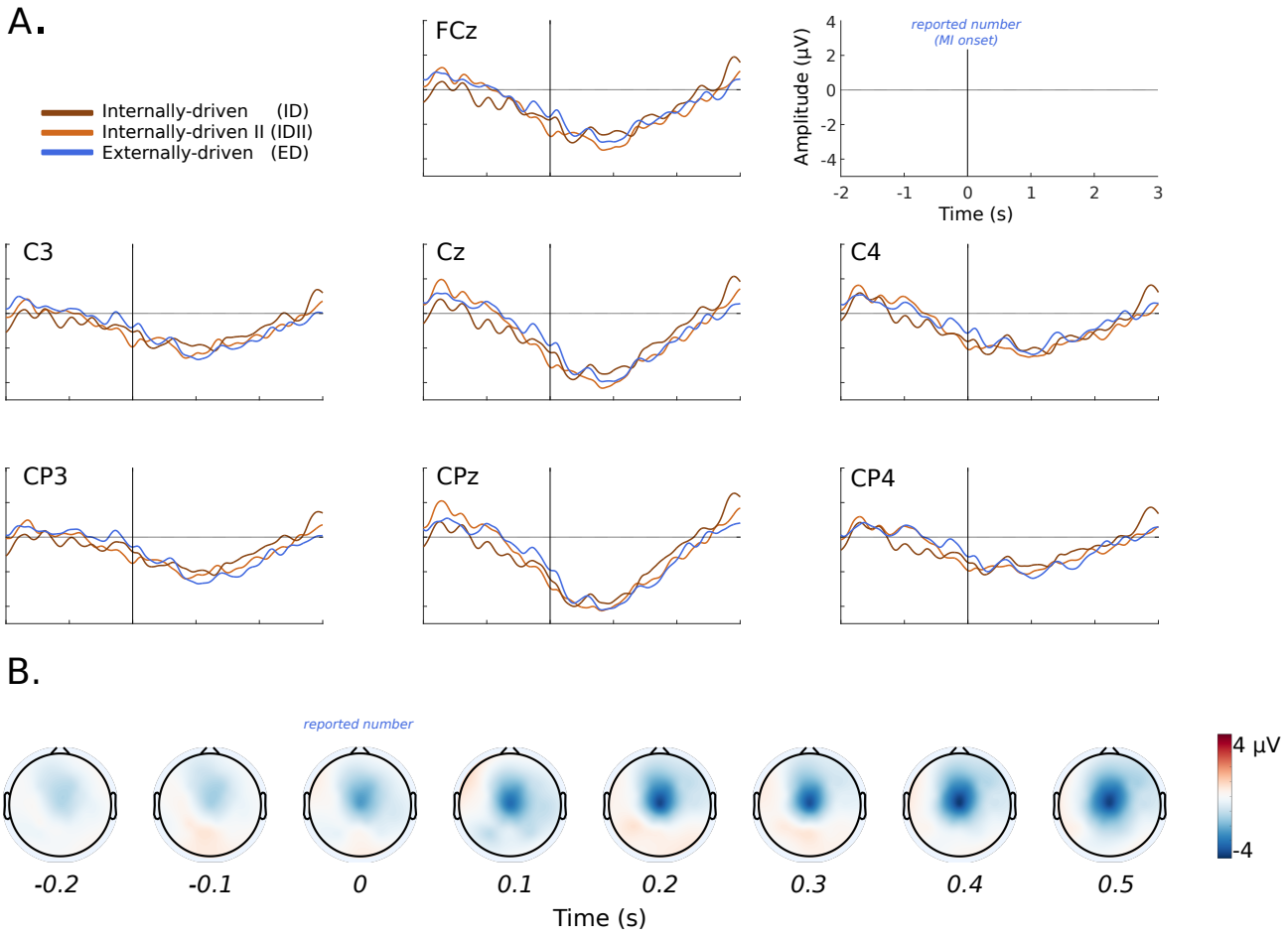

Figure 3: Grand-average movement-related cortical potentials in respect to the imagery onset (i.e. reported number). (A) Time-domain signals for electrodes FCz, C3, Cz, C4, CP3, CPz and CP4 separately for the three different conditions. (B) Topographical maps of the EEG activity around movement onset.

Internally-driven processes have been linked to the more frontal areas of the brain: fronto-striatal circuits, dorsolateral prefrontal cortex and sensorimotor area (SMA) [14]. We found out that the differences in amplitudes between the conditions are first mainly frontally distributed (higher for the internally-driven conditions) and then located in more parietal areas. The role of parietal areas in visuomotor transformations has been extensively studied [15]. Claiming exactly which brain areas contribute to the observed differences would be premature at this early stage, but the topographical distribution of the ERP components suggest the involvement of the same brain regions. With regard to the MRCPs, internally and externally-driven conditions did not differ in respect to both amplitude and latency of the negativity observed when time-locking the trials to the reported number. Participants were instructed to select their target as soon as they saw the five glasses. Since the motor goal had been previously decided according to the task rules, at the time the participants felt the urge to start the imagination, only the pure movement preparation (i.e. the abstract kinematics [1]) was necessary. These processes were the same for all the conditions but they were then dependent on the spatial location of the motor goal (i.e. position of the selected glass), which will then define the trajectory of the reach. Since a motor goal was always present, no differences were expected due to the experimental conditions. Differences can be expected depending on the target location, since low-frequency time-domain signals contain information about movement direction [4]. It is also important to mention that in our paradigm the MRCPs were not closely related (in time) to the cue-locked ERPs, since the minimum time between cue and reported number was 3.4 seconds out of all recorded trials. An interesting discussion point is then whether in paradigms in which cue and response are very close in time there is an accumulation of these two cue-locked and response-locked events. Given the nature of the self-paced task (movement imagination), we included the scroller and the reporting period to obtain a time-locking event for motor imagery. Data time-locked to this event can later be used to train a model for movement detection intention which is then tested in a pseudo-online manner. We preferred memorization to an actual motor task (e.g. key press at the end of the task) since there is the high chance that an additional motor task interferes with the motor imagery task, making the observed pattern questionable. Further, we could use this intermediate task to separate target selection from the ac-

Published by Verlag der TU Graz
Graz University of Technology

 DOI: 10.3217/978-3-85125-533-1-73

tual motor task. To determine the consistency of the EEG phenomena observed we will measure more participants and conduct the appropriate statistical analysis to access the significancy of our results. Behavioural analysis still needs to be performed, specifically to investigate the interaction between the response times (i.e. time between the cue presentation and the reported number marking the MI start) and the type of condition.

CONCLUSION

In this study we analysed the event-related potentials (cue-locked and response-locked) associated to target selection in a self-paced motor imagery task. Our first results show that differences between internally and externally-driven target selection are present in cue-locked but not response-locked ERPs. In the future we will analyse more subjects and conduct a careful statistical analysis to assess the significance of the results. Further, the paradigm that we implemented allows for a more accurate determination of a time-locking event in movement imagination tasks, which can be important for single-trial movement detection of self-paced movements.

ACKNOWLEGMENTS

This work was supported by the EU ICT Programme Project H2020-643955 *MoreGrasp*, and the ERC Consolidator Grant ERC-681231, *Feel Your Reach*.

REFERENCES

[1] Wong AL, Haith AM, Krakauer JW. Motor planning. The Neuroscientist. 2015 Aug 1;21(4):385-98.
[2] Wolpert DM, Landy MS. Motor control is decision-making. Current opinion in neurobiology. 2012 Dec 31;22(6):996-1003.
[3] Wallis JD, Anderson KC, Miller EK. Single neurons in prefrontal cortex encode abstract rules. Nature. 2001 Jun 21;411(6840):953-6.
[4] Müller-Putz GR, Schwarz A, Pereira J, Ofner P. From classic motor imagery to complex movement intention decoding: The noninvasive Graz-BCI approach. Progress in brain research. 2016 Dec 31;228:39-70.
[5] Lu M, Doñamayor N, Münte TF, Bahlmann J. Event-related potentials and neural oscillations dissociate levels of cognitive control. Behavioural Brain Research. 2017 Mar 1;320:154-64.
[6] Nieuwenhuis S, Aston-Jones G, Cohen JD. Decision making, the P3, and the locus coeruleus–norepinephrine system. Psychological bulletin. 2005 Jul;131(4):510.
[7] García-Larrea L, Cézanne-Bert G. P3, positive slow wave and working memory load: a study on the functional correlates of slow wave activity. Electroencephalography and Clinical Neurophysiology/Evoked Potentials Section. 1998 Apr 30;108(3):260-73.
[8] Pereira J, Ofner P, Schwarz A, Sburlea AI, Müller-Putz GR. EEG neural correlates of goal-directed movement intention. NeuroImage. 2017 Jan 25.
[9] Birbaumer N, Elbert T, Canavan AG, Rockstroh B. Slow potentials of the cerebral cortex and behavior. Physiological Reviews. 1990; 70:1-41.
[10] Libet B, Gleason CA, Wright EW, Pearl DK. Time of conscious intention to act in relation to onset of cerebral activity (readiness-potential). Brain. 1983 Sep 1;106(3):623-42.
[11] Delorme A, Makeig S. EEGLAB: an open source toolbox for analysis of single-trial EEG dynamics including independent component analysis. Journal of neuroscience methods. 2004 Mar 15;134(1):9-21.
[12] Lee TW, Girolami M, Sejnowski TJ. Independent component analysis using an extended infomax algorithm for mixed subgaussian and supergaussian sources. Neural computation. 1999 Feb 15;11(2):417-41.
[13] Duncan-Johnson CC. P300 latency: A new metric of information processing. Psychophysiology. 1981 May.
[14] Thut G, Hauert CA, Viviani P, Morand S, Spinelli L, Blanke O, Landis T, Michel C. Internally driven vs. externally cued movement selection: a study on the timing of brain activity. Cognitive Brain Research. 2000 Jun 30;9(3):261-9.
[15] Jeannerod M, Arbib MA, Rizzolatti G, Sakata H. Grasping objects: the cortical mechanisms of visuomotor transformation. Trends in neurosciences. 1995 Jul 31;18(7):314-20.

Published by Verlag der TU Graz
Graz University of Technology

Proceedings of the
7th Graz Brain-Computer Interface Conference 2017 DOI: 10.3217/978-3-85125-533-1-74

BCI-ASSISTED TRAINING FOR UPPER LIMB MOTOR REHABILITATION: ESTIMATION OF EFFECTS ON INDIVIDUAL BRAIN CONNECTIVITY AND MOTOR FUNCTIONS

M. Petti[1,2], F. Pichiorri[2], J. Toppi[1,2], L. Astolfi[1,2], F. Cincotti[1,2] and D. Mattia[2]

[1] Dept. of Computer, Control and Management Engineering, Sapienza University of Rome
[2] Neuroelectrical Imaging and BCI Lab., Fondazione Santa Lucia IRCSS, Rome, Italy

E-mail: manuela.petti@uniroma1.it

ABSTRACT: The aim of the study is to quantify individual changes in scalp connectivity patterns associated to the affected hand movement in stroke patients after a 1-month training based on BCI-supported motor imagery to improve upper limb motor recovery. To perform the statistical evaluation between pre- and post-training conditions at the single subject level, a resampling approach was applied to EEG datasets acquired from 12 stroke patients during the execution of a motor task with the stroke affected hand before and after the rehabilitative intervention. Significant patterns of the network reinforced after the training were extracted and a significant correlation was found between indices related to the reinforced pattern and the clinical outcome indicated by clinical scales.

INTRODUCTION

In neuroscience, the concept of brain connectivity is crucial to understand how communication between cortical regions is organized or re-organized in presence of a brain injury or brain disease [1], [2]. Group analysis studies are commonly performed when the aim is to evaluate the relevant differences between experimental conditions and/or the consistency of a treatment effect and how the differences or effects might affect the functional brain network configuration.

As such, this approach holds some limitations related to the unavoidable heterogeneity in the experimental group and further, specific effects that a given brain lesion has on neural networks (e.g. stroke) at the single patient level might be hidden. Thus, there is the need to provide measures that might account for individual pathological network configuration associated with different level of patient's impairment.

In this study, an approach based on the use of the resampling was applied to evaluate the brain network reorganization in each individual patient who underwent a rehabilitative training after stroke. Indeed typically a statistic comparison of two patient's conditions cannot be performed as the amount of data collected in an EEG recording session (multi-trial EEG dataset) are entirely used to obtain an unique connectivity estimation. To overcome this limitation, in the present work we applied jackknife approach [3] to multi-trials EEG data, thus generating a distribution of datasets out of a single observation (ie, single patient). These datasets can be then subjected to connectivity estimation to obtain a distribution of the connectivity estimator in each of the patient experimental condition as described below. We used motor task-related EEG data recorded on subacute stroke patients in two recording sessions: one preceding and one following a rehabilitative intervention based on motor imagery with the support of Brain Computer Interfaces (BCI) [2]. The BCI training in [2] lasted one month, with 3 weekly session in which patients were asked to perform motor imagery of the stroke affected hand to control a specifically designed BCI system. Control features for BCI were selected from a screening session among electrodes from sensorimotor strip on the affected hemisphere only, at frequencies relevant for sensorimotor activation (mainly beta). The patterns underlying the attempted movement of the paralyzed hand obtained before and after the intervention from each stroke patients were compared, in order to describe the individual significant connectivity changes induced by the BCI-assisted training. Connectivity matrices were also analyzed by means of a graph theory approach, and a correlation analysis was performed to test the existence of a relationship between the organization of brain networks (graph-theory derived indices) and the functional outcome measures specific for the upper limb motor function.

MATERALS AND METHODS

Partial Directed Coherence

As a frequency-domain version of Granger causality [4], PDC reveals the existence, the direction and the strength of a functional relationship between any given pair of signals in a multivariate data set.

In this study we used the squared formulation of PDC due to its higher accuracy and stability [5].

Resampling approach: Jackknife

To achieve a distribution of connectivity estimations allowing a comparison between conditions, in this study we exploited a resampling approach. Given an EEG dataset characterized by a certain number of trials, Jackknife performs leave-*N*-out on trials, where *N* is a percentage of trials to be randomly excluded from the

Published by Verlag der TU Graz
Graz University of Technology

 DOI: 10.3217/978-3-85125-533-1-74

estimation. Repeating the procedure for *K* replications, we can obtain *K* datasets to be subjected to connectivity estimation. Here, we set the parameters to the following values: *K* = 200 replications, percentage of excluded trials *N* = 50%.

Experimental design

EEG signals were acquired from 12 subacute stroke patients (mean age, 62.1 ± 9.9 years; time from the event: 1.75 ± 1.21 months; 6 left/6 right affected hemisphere). All the patients underwent standard motor rehabilitation and a newly proposed add-on intervention based on a BCI-assisted upper limb motor imagery training [2]. Immediately before and after the training intervention, the patients were subjected to two screening sessions (PRE and POST) including clinical assessment and EEG recordings during the attempt of a simple movement (grasping) by the hand affected by the motor deficit. The clinical assessment included the evaluation of the upper limb function by means of *Fugl-Meyer Assessment* (FMA, upper limb section).

Signal processing

After data preprocessing (down-sampling at 100 Hz with anti-aliasing filter, band pass filtering (1-45 Hz), and artifact rejection), we obtained for each patient and each condition (PRE and POST) an EEG dataset consisting of approximately 60 artifact-free trials related to the motor task. Then we applied the jackknife method. Brain connectivity was estimated from 29 channels by means of PDC. The achieved estimations were averaged within 5 frequency bands defined for each patient according to Individual Alpha Frequency [6]: theta [IAF-6;IAF-2], alpha [IAF-2;IAF+2], beta1 [IAF+2;IAF+11], beta2 [IAF-11;IAF+20] and gamma [IAF+20;IAF+35].

Once the patterns distributions were obtained for each patient, condition and frequency band, we performed the statistical comparison between PRE and POST conditions. In particular, to evaluate the effects of the rehabilitative intervention, we focused on the pattern that was significantly reinforced for each patient in the POST with respect to the PRE session (POST vs PRE). To perform this comparison, we used a nonparametric test: the values in the POST pattern above the thresholds related to the percentile of 97.5% of the PRE distribution, were considered significantly reinforced. The PRE vs POST comparison (inverse condition) was also tested as control.

To summarize the properties of the reinforced networks we computed some binary graph indices able to evaluate the network organization [7].

- Characteristic Path Length

$$L = \frac{1}{n}\sum_{i\in N} L_i = \frac{1}{n}\sum_{i\in N}\frac{\sum_{j\in N, j\neq i} d_{ij}}{n-1} \quad (1)$$

where L_i is the average distance between node i and all other nodes and d_{ij} is the distance between node i and node j.

- Clustering Coefficient

The binary directed version of Clustering Coefficient is defined as follows:

$$C = \frac{1}{n}\sum_{i\in N} C_i = \frac{1}{n}\sum_{i\in N}\frac{t_i}{(k_i^{out}+k_i^{in})(k_i^{out}+k_i^{in}-1)-2\sum_{j\in N} g_{ij}g_{ji}} \quad (2)$$

where t_i represents the number of triangles involving node i, k_i^{in} and k_i^{out} are the number of incoming and outcoming edges of nodes i respectively and g_{ij} is the entry ij of adjacency matrix.

- Smallworldness

A network G is defined as small-world network if $L_G > L_{rand}$ and $C_G >> C_{rand}$ where L_G and C_G represent the characteristic path length and the clustering coefficient of a generic graph and L_{rand} and C_{rand} represent the correspondent quantities for a random graph. On the basis of this definition, small-worldness can be defined as follows:

$$S = \frac{C_G / C_{rand}}{L_G / L_{rand}} \quad (3)$$

A network is said to be a small world network if S>1.

Correlation analysis

As a last step of the analysis, we performed Pearson's correlation (significance level 0.05) between the above defined neurophysiological indices extracted from the reinforced networks and the functional scale (FMA).

For the clinical measure, to account for the high inter-subject variability in terms of degree of the impairment, and for the consequent different level of recovery, we computed the parameter "effectiveness" [8], defined as follows:

$$Eff_{FMA} = \frac{FMA_{POST} - FMA_{PRE}}{Score_{\max} - FMA_{PRE}} * 100 \quad (4)$$

where $Score_{max}$ is the maximum score that can be reached in FMA scale.

RESULTS

Fig. 1 shows the connectivity pattern reinforced at the end of the rehabilitative training obtained for a representative patient with a stroke in the left hemisphere: the pattern in the motor-related frequency band (beta1) shows a higher involvement of channels over the motor areas of the affected (left) hemisphere during the attempt to move the right hand.

Results of the Pearson correlation computed between graph measures extracted from the connectivity pattern and the clinical indices across the 12 stroke patients are reported in Table I and in Fig. 2. Such results show that the properties of the functional network reinforced after the training are significantly correlated with the clinical outcome selectively in beta1 band.

Published by Verlag der TU Graz
Graz University of Technology

 DOI: 10.3217/978-3-85125-533-1-74

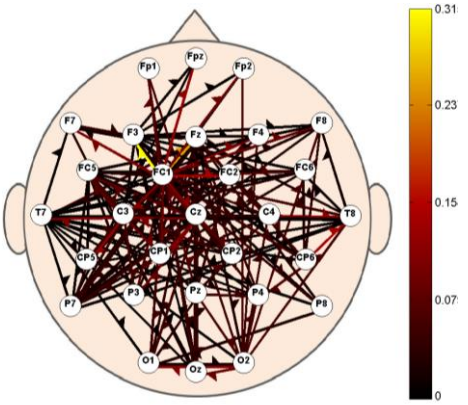

Figure 1: Reinforced connectivity pattern obtained in beta1 band (typical of sensory-motor rhythms) for a representative patient with lesion in the left hemisphere. The scalp is seen from the above, with the nose pointing to the upper part of the page. The effective connections between scalp electrodes (29 channels: Fp1, Fpz, Fp2, F7, F3, Fz, F4, F8, FC5, FC1, FC2, FC6, T7, C3, Cz, C4, T8, CP5, CP1, CP2, CP6, P7, P3, Pz, P4, P8, O1, Oz, O2) are represented by arrows whose color and diameter code for the corresponding PDC values.

Table 1: Results of the Pearson correlation computed between graph indices extracted from the reinforced pattern of motor task and the clinical recovery (effectiveness of Fugl-Meyer Assessment). Significances are highlighted in bold.

	THETA	ALPHA	BETA1	BETA2	GAMMA
	Smallworldness				
p	0.607	0.519	**0.001**	0.597	0.123
R	0.166	0.207	**0.822**	0.170	0.471
	Path Length				
p	0.468	0.653	**0.007**	0.764	0.151
R	-0.232	-0.145	**-0.735**	-0.097	-0.441
	Clustering				
p	0.390	0.368	**0.013**	0.350	0.093
R	0.274	0.286	**0.691**	0.296	0.507

In particular, the direct correlation between these neurophysiological measures and the clinical indices informs that the patients with higher clinical recovery show a better organization of the reinforced network related to the motor function (high clustering, low path length, high smallworldness). The PRE vs POST comparison performed as control returned no significant results.

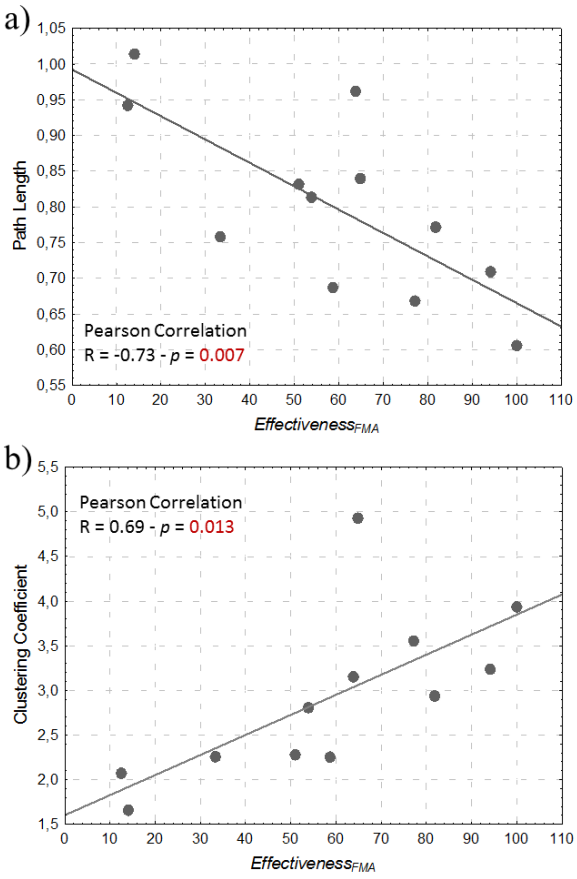

Figure 2: a) Scatter plot obtained between Path Length and the clinical recovery (effectiveness of Fugl-Meyer Assessment) in beta1 band; b) scatter plot obtained between Clustering and the clinical recovery measure in beta1 band.

DISCUSSION

In the present work, we performed a statistical evaluation of the individual brain network reorganization following a rehabilitative training in a population of subacute stroke patients. To perform the single-patient statistical comparison between the two conditions (pre- and post- intervention), jackknife was applied to multi-trial EEG datasets. The comparison between the 2 distribution of data set relative to PRE and POST sessions (POST vs PRE) revealed that the properties of the brain networks associated to attempted movements were reinforced as a function of the functional improvement (FMA effectiveness) observed after the BCI-assisted rehabilitation training.

The correlation between normalized indices of the network properties (clustering, path length, smallworldness) and the normalized index of the functional recovery (FMA effectiveness) suggests that patients with higher level of functional motor recovery show a better organization of the reinforced network such as high clustering, low path length, high smallworldness. Consistently, such correlation was specific for motor-related frequency band (beta 1) while

Published by Verlag der TU Graz
Graz University of Technology

 DOI: 10.3217/978-3-85125-533-1-74

no similar results were achieved for any other frequency band (Table I).

To assess the clinical recovery, we computed the effectiveness parameter, one of the most used rehabilitation impact indices [8]. One limit in applying such effectiveness parameter resides in the possible underestimation of clinical improvement in moderate versus severe stroke.

Although these are encouraging findings, the small patients sample (n=12) and the high variability within the group limits their interpretation. Future studies including a larger patient sample subjected to a stratification according to the clinical impairment at baseline, are thus needed.

In a previous study, [2], we showed that BCI-supported motor imagery training can significantly improve the upper limb motor outcome in a population of subacute stroke patients.

The current study represents a first step forward as it addressed i) the need of single patient estimation of connectivity networks to better isolate efficacy of treatment with respect to the high inter-individual variability in stroke population and ii) the estimation of task –related reorganizational scalp connectivity patterns changes (with respect to the resting state network), thus targeting the main outcome of the rehabilitative intervention described in [2], i.e. upper limb motor recovery.

An important aspect to discuss is related to the connectivity estimation performed with EEG sensor time series. It is known that this procedure can lead to the detection of spurious connections due to the mixing effects caused by volume conduction [9]. In this study we performed a statistical comparison between two experimental conditions that represents a way to mitigate these effects. Furthermore, in view of clinical application scalp EEG analysis can represent a more suitable procedure with respect to the use of method for solving the inverse problem that needs to take into account the presence of brain lesions. Altogether, the presented results show the feasibility of the procedure in a study aimed at capturing intervention-related variations in patients' physiological activity, in challenging conditions characterized by high individual variability.

CONCLUSION

In conclusion, the proposed procedure provided quantifiable measures of brain networks changes after a BCI-based training at the single subject level; such measures correlate significantly with the variations captured behaviourally by functional scales commonly used in the clinical practice

ACKNOWLEDGEMENT

This work was funded in part by Sapienza University of Rome - Progetti di Ateneo 2015 (C26A15N8LZ) and by the Italian National Ministry of Health (Translational Research Program).

REFERENCES

[1] A. Baldassarre, L. E. Ramsey, J. S. Siegel, G. L. Shulman, and M. Corbetta, "Brain connectivity and neurological disorders after stroke," *Curr. Opin. Neurol.*, vol. 29, no. 6, pp. 706–713, Dec. 2016.

[2] F. Pichiorri, G. Morone, M. Petti, J. Toppi, I. Pisotta, M. Molinari, S. Paolucci, M. Inghilleri, L. Astolfi, F. Cincotti, and D. Mattia, "Brain-computer interface boosts motor imagery practice during stroke recovery: BCI and Motor Imagery," *Annals of Neurology*, vol. 77, no. 5, pp. 851–865, May 2015.

[3] J. W. Tukey, "Bias and confidence in not quite large samples," *The Annals of Mathematical Statistics*, vol. 29, no. 2, pp. 614–623, Jun. 1958.

[4] C. W. J. Granger, "Investigating Causal Relations by Econometric Models and Cross-spectral Methods," *Econometrica*, vol. 37, no. 3, pp. 424–438, Agosto 1969.

[5] L. Astolfi, Cincotti F, Mattia D, Marciani MG, Baccalà LA, De Vico Fallani F, Salinari S, Ursino M, Zavaglia M, Babiloni F, "Assessing cortical functional connectivity by partial directed coherence: simulations and application to real data," *IEEE Trans Biomed Eng*, vol. 53, no. 9, pp. 1802–1812, Sep. 2006.

[6] W. Klimesch, "EEG alpha and theta oscillations reflect cognitive and memory performance: a review and analysis," *Brain Res. Brain Res. Rev.*, vol. 29, no. 2–3, pp. 169–195, Apr. 1999.

[7] M. Rubinov and O. Sporns, "Complex network measures of brain connectivity: Uses and interpretations," *NeuroImage*, vol. 52, no. 3, pp. 1059–1069, Settembre 2010.

[8] S. Shah, F. Vanclay, and B. Cooper, "Efficiency, effectiveness, and duration of stroke rehabilitation," *Stroke*, vol. 21, no. 2, pp. 241–246, Feb. 1990.

[9] F. van de Steen, L. Faes, E. Karahan, J. Songsiri, P. A. V. Sosa, and D. Marinazzo, "Critical comments on EEG sensor space dynamical connectivity analysis," *arXiv:1607.03687 [q-bio, stat]*, Jul. 2016.

Published by Verlag der TU Graz
Graz University of Technology

Proceedings of the
7th Graz Brain-Computer Interface Conference 2017 DOI: 10.3217/978-3-85125-533-1-75

THE PROMOTŒR: A SUCCESSFUL STORY OF TRANSLATIONAL RESEARCH IN BCI FOR MOTOR REHABILITATION

F. Pichiorri[1], E. Colamarino[1,2], F. Cincotti[1,2] D. Mattia[1]

[1] Neuroelectrical Imaging and BCI Laboratory, Fondazione Santa Lucia, IRCCS, Rome, Italy
[2] Department of Computer, Control, and Management Engineering "Antonio Ruberti", Sapienza University of Rome, Rome, Italy

E-mail: f.pichiorri@hsantalucia.it

ABSTRACT: Several groups have recently demonstrated in the context of randomized controlled trials (RCTs) how sensorimotor Brain-Computer Interface (BCI) systems can be beneficial for post-stroke motor recovery. Following a successful RCT, at Fondazione Santa Lucia (FSL) a further translational effort was made with the implementation of the Promotœr, an all-in-one BCI-supported MI training station. Up to now, 25 patients underwent training with the Promotœr during their admission for rehabilitation purposes (in add-on to standard therapy). Two illustrative cases are presented. Though currently limited to FSL, the Promotœr represents a successful story of translational research in BCI for stroke rehabilitation. Results are promising both in terms of feasibility of a BCI training in the context of a real rehabilitation program and in terms of clinical and neurophysiological benefits observed in the patients.

INTRODUCTION

Several groups have recently demonstrated in the context of randomized controlled trials (RCTs) how sensorimotor Brain-Computer Interface (BCI) systems can be beneficial for post-stroke motor recovery [1]–[3]. At Fondazione Santa Lucia (FSL) we demonstrated in a RCT that an EEG-based BCI-supported Motor Imagery (MI) training can improve motor rehabilitation of the upper limb in subacute stroke patients with clinically relevant benefits as well as neurophysiological signs of increased activation of the affected hemisphere [4]. A further translational effort was made at FSL with the implementation of an all-in-one BCI-supported MI training station, namely the Promotœr, which is currently employed in add-on to standard therapy in patients admitted for rehabilitation. In this paper we will briefly retrace the path of BCIs for stroke rehabilitation at FSL, from prototype design, through clinical validation, to actual use in everyday practice as a possible successful example of translationality in BCI research. Furthermore, 2 case reports of training with the Promotœr will be presented.

MATERALS AND METHODS

The prototype in [4] was developed with continuous involvement of rehabilitation experts and endowed with strong rehabilitation principles such as: an ecological feedback for correct hand MI performance, selective reinforcement of correct brain activation (i.e. enhancement of affected hemisphere activation), continuous assistance of an expert therapist during the BCI training (the therapist is indeed part of the training setting receiving feedback of the patient's brain activity on a dedicated screen). Inputs on acceptability from professionals and patients were collected first in the form of a proof-of-principle study [5] and continuously throughout the experimentation.

Subsequently we conducted a RCT in 28 subacute patients [4]. Fourteen patients received the BCI supported hand MI training across four weeks, while 14 performed the MI training without the BCI support. At completion of training, the BCI group had a significantly greater improvement in Fugl-Meyer Assessment (FMA) scores that was clinically relevant. This improvement was accompanied by a significant increase of EEG motor-related oscillatory activity over the lesioned hemisphere only in the target group.

The continuous interaction with the clinical counterpart and the experience gathered in the RCT prompted us to implement an all-in-one BCI-supported MI training station, which we called Promotœr, for its main aim to *promote motor* recovery after stroke. The Promotœr comprises a computer, a commercial wireless EEG/EMG system, a screen for the therapist feedback (EEG and EMG activity monitoring) and a screen for the ecological feedback to the patient (a virtual hand performing the imagined movement in successful trials). Two Promotœr are currently installed in a rehabilitation ward at Fondazione Santa Lucia (Fig. 1).

During training with the Promotœr, the patient is seated on a chair (or wheelchair) with arms resting on a pillow. A visual representation of the forearms and hands is given on a dedicated screen, adjusted in size, shape and position as to resemble the patient's own hands. The patient is asked to perform MI of affected hand (timing

Published by Verlag der TU Graz
Graz University of Technology

 DOI: 10.3217/978-3-85125-533-1-75

of exercise is provided via a spotlight on the screen enlightening the target hand and reinforced verbally by the therapist). During MI, the therapist is provided with continuous feedback of the patient's brain activity on a dedicated screen; in brief, desynchronization occurring on electrodes placed above the affected sensorimotor area at sensorimotor relevant frequencies (BCI control features) is represented by a cursor moving towards a target (with speed proportional to the desynchronization). In successful trials (i.e. when the cursor reaches the target) the patient receives a positive reward represented by the visual representation of the affected hand moving accordingly with the imagined movement; otherwise, no visual feedback is represented on the patient's screen. Along the whole session, the therapist is allowed to monitor the patient's EEG and EMG activity (recorded from forearm muscles) in order to ensure complete relaxation and to guide/encourage him/her during the exercise.

Training sessions are carried out with the assistance of the same therapist in charge of the standard treatment for each patient, thus encouraging a further integration of our approach within the specific rehabilitation program of each patient. Before and after training, patients undergo a neurophysiological assessment in a similar way as described in [4] but with reduced number of EEG electrodes (31 positions vs 61). The aim of the screening is twofold: a) to extract EEG features for BCI training b) to evaluate the expected reinforcement of MI induced brain activation in the affected hemisphere (pre – post training). During the neurophysiological assessment, 30 trials of MI of affected hand are performed, randomized with 30 trials of rest of equal duration. BCI training is conducted with 8 electrode positions (vs 31), personalized according to the initial screening session: control features are selected among electrodes placed above the affected sensorimotor area (4 electrodes) and the montage is completed with the 4 homologous electrodes on the contralateral hemiscalp.

Figure 1: Training session with the Promotœr. The patient is seated on a wheelchair with arms resting on a pillow. A visual representation of the forearms and hands is given on a dedicated screen, resembling the patient's own hands. The patient is asked to perform MI of affected hand and the therapist is provided with continuous feedback of the patient's EEG and EMG activity (recorded from forearm muscles).

RESULTS

Up to now, 25 patients completed training with the Promotœr during their admission for rehabilitation purposes (in add-on to standard therapy). Of these, 21 suffered from ischemic or haemorrhagic unilateral stroke, while the remaining four had other type of acquired brain injury resulting in motor impairment of the upper limb. Twelve patients were in the subacute phase (< 6 months from the event) while 13 where chronic. In total, approximately 300 BCI training sessions were carried out. No drop-outs in the scheduled training program were observed, while two patients did not perform the post- training neurophysiological assessment (for being discharged beforehand or moved to another hospital).

We will present the cases of two patients (A and B). Patient A is a 77 years-old woman; she suffered from an ischemic stroke in the territory of the right middle cerebral artery and was admitted to FSL for rehabilitation with severe left hemiparesis. She started training with the Promotœr approximately one month from the event, performing 11 training session across one month of admission. Control features were selected according to the pre- neurophysiological screening (Fig. 2, left panel) on the right hemisphere, on the central line (C2) at frequency of 13-14 Hz. At the end of the training, the neurophysiological assessment was repeated showing an increased activation on the right hemisphere at EEG frequencies employed for BCI control (Fig. 2 right panel). A significant increase in upper limb FMA score was observed after training (from 31 to 46, i.e. above the threshold of Minimal Clinically Important Difference of 7 points).

Patient B is a 20 years-old man who had a traumatic haemorrhage in the left hemisphere with severe right hemiparesis and motor aphasia (initial upper limb FMA of 9). He was attending FSL outpatient service for rehabilitation and started training with the Promotœr approximately one year from the event, performing 22 training session across two months of admission. Control features were selected according to the pre-neurophysiological screening (Fig. 3, left panel) on the left hemisphere, on the central line (C1) at frequency of 9-10 Hz. At the end of the training, the neurophysiological assessment was repeated showing an increased activation on the left hemisphere at EEG frequencies employed for BCI control (Fig. 3 right panel). Clinical assessment of upper limb function did not show a relevant improvement, however a reduction in upper limb pain was reported.

Published by Verlag der TU Graz
Graz University of Technology

 DOI: 10.3217/978-3-85125-533-1-75

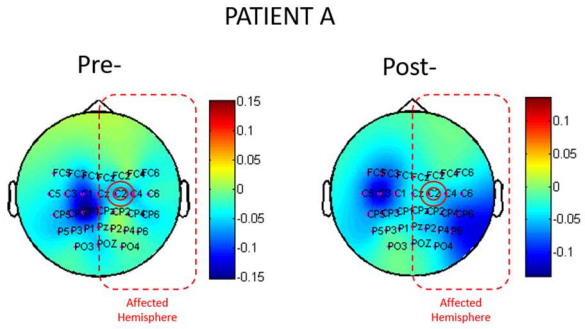

Figure 2: Pre- and Post- training neurophysiological assessment in representative patient A. Statistical maps of Rsquare values of Rest vs- left hand motor imagery at 13-14 Hz (frequency employed for BCI control; electrodes used for BCI training are circled in red).

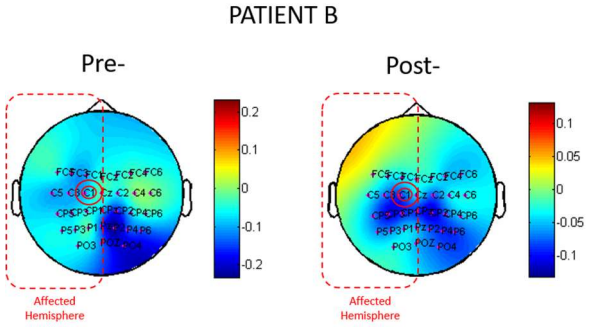

Figure 3: Pre- and Post- training neurophysiological assessment in representative patient B. Statistical maps of Rsquare values of Rest vs- right hand motor imagery at 9-10 Hz (frequency employed for BCI control; electrodes used for BCI training are circled in red).

DISCUSSION

The story of BCIs for post-stroke motor rehabilitation of the upper limb at FSL started within the TOBI project in 2008 (www.tobi-project.org). During the development and testing of our system, we fostered continuous involvement of rehabilitation experts, which resulted in a RCT on subacute patients supporting the efficacy of our approach [4]. A further translational effort led us to implement the Promotœr, a dedicated all-in-one station for BCI supported MI-training of the upper limb, which is currently used in the clinic outside any specific research program.

In this preliminary report, we are able to confirm some of the main results of the RCT [4].

First, a large number of patients/sessions with virtually no drop-out: it is indeed possible to integrate BCI technology in the real rehabilitation program of (mainly stroke) patients. Though anecdotal, general impressions from patients are enthusiastic, as they are extremely motivated to carry on the training sessions with the Promotoer.

Similarly, the close interaction with the clinical rehabilitation team is running smoothly, confirming a high acceptance of the approach among rehabilitation professionals [5].

The representative Patient A was a subacute stroke patient (thus comparable with the RCT population) showing a clinically relevant improvement of upper limb function accompanied by a reinforcement of sensorimotor related activity on the affected hemisphere (specific for the EEG feature employed in the training).

These confirmative results have some important implications. Since in the Promotœr we were able to simplify the setting (e.g. reducing the number of EEG electrodes for both training and Pre- Post- assessment) and maintain the main principles of the original system [4], we are now optimistic about the feasibility of a larger, multi-centric RCT to extend our results beyond our own institution. In this perspective, the challenges to prove the efficacy of our approach on a large scale are partially shared with other post-stroke rehabilitation strategies: a solid clinical trial design with proper randomization and proper sham/control conditions; a reliable follow-up evaluation to establish the duration of the effects. Other important aspects to take into consideration in view of a multi-centric RCT are strictly related to the BCI approach: the reliability of the system; the reproducibility of some operator dependent procedures such as features selection.

Furthermore, the possibility to extend our approach to chronic patients and patients with central nervous system lesions from different etiology (as for Patient B) paves the way for possible novel applications.

Patient B was in the chronic phase, with a severe, stabilized motor impairment. We were able to show an increase in sensorimotor related activity on the affected hemisphere throughout the training (specific for the EEG feature employed in the training). The subjective report of upper limb pain reduction along the training sessions is promising in terms of possible new applications.

CONCLUSION

The Promotœr represents a successful story of translational research in BCIs for stroke rehabilitation [6]. Though restricted to our institution, this experience allowed us as a BCI laboratory to be fully integrated in the clinic and receive daily inputs from rehabilitation experts. On one hand, the positive experience with the Promotœr prompts us to pursue a further clinical validation in a large, multi-centric RCT. On the other hand, everyday interaction with the clinical team extends our views beyond the specific intended application (e.g. spasticity or pain) which might apply not only to our approach, but to the use of BCIs in rehabilitation in general [7], [8].

ACKNOWLEDGEMENT

We thank Dr. Marco Secci for technical support in training with the Promotœr.

This work was funded in part by the Sapienza University of Rome - Progetti di Ateneo 2015 (C26A15N8LZ).

Published by Verlag der TU Graz
Graz University of Technology

 DOI: 10.3217/978-3-85125-533-1-75

REFERENCES

[1] A. Ramos-Murguialday *et al.*, “Brain-machine interface in chronic stroke rehabilitation: A controlled study: BMI in Chronic Stroke,” *Ann. Neurol.*, vol. 74, no. 1, pp. 100–108, Jul. 2013.

[2] N. Mrachacz-Kersting *et al.*, “Efficient neuroplasticity induction in chronic stroke patients by an associative brain-computer interface,” *J. Neurophysiol.*, p. jn.00918.2015, Dec. 2015.

[3] K. K. Ang *et al.*, “Facilitating effects of transcranial direct current stimulation on motor imagery brain-computer interface with robotic feedback for stroke rehabilitation,” *Arch. Phys. Med. Rehabil.*, vol. 96, no. 3 Suppl, pp. S79-87, Mar. 2015.

[4] F. Pichiorri *et al.*, “Brain-computer interface boosts motor imagery practice during stroke recovery,” *Ann. Neurol.*, Feb. 2015.

[5] G. Morone *et al.*, “Proof of principle of a brain-computer interface approach to support poststroke arm rehabilitation in hospitalized patients: design, acceptability, and usability,” *Arch. Phys. Med. Rehabil.*, vol. 96, no. 3 Suppl, pp. S71-78, Mar. 2015.

[6] F. Pichiorri, N. Mrachacz-Kersting, M. Molinari, S. Kleih, A. Kübler, and D. Mattia, “Brain-computer interface based motor and cognitive rehabilitation after stroke – state of the art, opportunity, and barriers: summary of the BCI Meeting 2016 in Asilomar,” *Brain-Comput. Interfaces*, vol. 0, no. 0, pp. 1–7, Oct. 2016.

[7] A. Riccio *et al.*, “Interfacing brain with computer to improve communication and rehabilitation after brain damage,” *Prog. Brain Res.*, vol. 228, pp. 357–387, 2016.

[8] A. Remsik *et al.*, “A review of the progression and future implications of brain-computer interface therapies for restoration of distal upper extremity motor function after stroke,” *Expert Rev. Med. Devices*, vol. 13, no. 5, pp. 445–454, 2016.

Published by Verlag der TU Graz
Graz University of Technology

Proceedings of the
7th Graz Brain-Computer Interface Conference 2017 DOI: 10.3217/978-3-85125-533-1-76

PEANUT: Personalised Emotional Agent for Neurotechnology User-Training

L. Pillette[1,2], C. Jeunet[1,3], B. Mansencal[2], R. N'Kambou[4], B. N'Kaoua[3], F. Lotte[1,2]

[1]Potioc Project Team, Inria Bordeaux Sud-Ouest / University of Bordeaux / CNRS, Talence, France
[2]LaBRI, University of Bordeaux / CNRS / Bordeaux-INP, Talence, France
[3]Handicap, Activity, Cognition, Health, University of Bordeaux , Bordeaux, France
[4]Department of Computer Sciences, UQAM, Montreal, Quebec, Canada

E-mail: lea.pillette@inria.fr

ABSTRACT: Mental-Imagery based Brain-Computer Interfaces (MI-BCI) are neurotechnologies enabling users to control applications using their brain activity alone. Although promising, they are barely used outside laboratories because they are poorly reliable, partly due to inappropriate training protocols. Indeed, it has been shown that tense and non-autonomous users, that is to say those who require the greatest social presence and emotional support, struggle to use MI-BCI. Yet, the importance of such support during MI-BCI training is neglected. Therefore we designed and tested PEANUT, the first Learning Companion providing social presence and emotional support dedicated to the improvement of MI-BCI user-training. PEANUT was designed based on the literature, data analyses and user-studies. Promising results revealed that participants accompanied by PEANUT found the MI-BCI system significantly more usable.

INTRODUCTION

Brain-Computer Interfaces (BCI) are neurotechnologies which enable users to control external applications using their brain-activity alone [22], often measured using ElectroEncephaloGraphy (EEG). In this paper, we focus more specifically on Mental-Imagery based BCI (MI-BCI) with which commands are sent using mental-imagery tasks (imagining movements for instance). Because they enable users to control devices or applications without moving, MI-BCI are extremely promising in various fields ranging from assistive technologies (e.g. wheelchairs or neuroprosthetics) to video games [15].

Nevertheless, some important issues inherent to MI-BCI make it so that these technologies are not reliable enough for applications such as navigation and control, therefore preventing them from being widely used outside laboratories. Among these issues, some are due to hardware limitations (the electrodes are sensitive to noise) and others to software issues (brain-signal processing algorithms are still imperfect). Though, the issue we will focus on here, which is rather little explored [13], concerns the users themselves. Indeed, before being able to use an MI-BCI, users have to learn how to produce brain patterns that the computer will be capable of discriminating. However, the literature [14] as well as experimental results [7] suggest that current MI-BCI training protocols

Figure 1: A participant taking part in a BCI training process. Along the training PEANUT (on the left) provides the user with social presence and emotional support adapted to his performance and progression.

are theoretically and practically inappropriate for acquiring skills. Therefore, understanding and improving MI-BCI skill-acquisition is essential to make BCI accessible. Previous research results [8] suggest that users with specific personality profiles face difficulty when learning to use an MI-BCI. More specifically, highly tense and non-autonomous people (based on the "tension" and "self-reliance" dimensions of the 16 PF5 psychometric questionnaire [2]) experience the greatest difficulties.
Indeed, the MI-BCI training process does lack aspects of utmost importance for learning: social presence and emotional support [9]. In "Distance Learning" applications (i.e., learning without a teacher or classmates, using a computer for instance) [19], the absence of social presence and emotional support has been efficiently compensated by the use of learning companions [16, 11]. Learning companions are virtual or physical characters that can speak and have facial/bodily expressions. They provide the learner with different kinds of interventions, such as support or empathy, in order to overcome the lack of social interactions and emotional support. Despite their potential to improve MI-BCI user-training, both in terms of performance and user-experience, the use of a social presence and an emotional support as provided by a Learning Companion has never been explored in this context.
Thus, the object of this work was to design, implement

Published by Verlag der TU Graz
Graz University of Technology

 DOI: 10.3217/978-3-85125-533-1-76

and validate the first learning companion dedicated to improving MI-BCI user-training. We called this companion PEANUT for *Personalised Emotional Agent for Neurotechnology User-Training*. PEANUT is a physical and anthropomorphic character providing interventions to the user in between two BCI trials. Such interventions consist in pronouncing an encouraging sentence, and displaying corresponding facial expressions of emotions.
In the following sections, we will describe the different steps which led to the companion's appearance and intervention design. Finally, we introduce the experiment dedicated to validate PEANUT's efficiency in improving MI-BCI user-training before proposing a general discussion and presenting future work.

DESIGNING PEANUT

Designing a learning companion requires to identify an appropriate appearance and intervention content, due to their impact on the user's motivation, experience and learning [1]. Thus, our design was based on the literature and a couple of user-studies.

Defining the physical appearance of PEANUT
First, we focused on the appearance of PEANUT. The literature guided our choice towards the use of a physical companion, increasing social presence in comparison to a virtual one [5]. Also, anthropomorphic features seem to facilitate social interactions [3]. Moreover, for the companion to be relevant, the combination of physical characteristics, personality/abilities, functionalities and learning function had to be consistent.
Since PEANUT's functions are simple and it is unable to interact with the user (PEANUT can talk, but cannot receive input from the BCI user), we chose to propose a cartoon-like character with anthropomorphic child-like shapes. Thus, we used the voice of a child to record PEANUT's interventions (which also enabled us not to associate PEANUT with a gender).
Regarding PEANUT's face, we asked a designer to create three styles of faces expressing each of these eight emotions: Trust, Joy, Surprise, Admiration, Boredom, Sadness, Anger and a Neutral expressions. We wanted the faces to be cartoon-like, so that they fit the body and complied with the recommendations from the literature. Prior to the experiment, an online user-survey in which 96 people gave their opinion on the different faces design expressing the different emotions was led. It enabled us to select the style of face that would fit the most the requirements from the literature. Interestingly, the results indicated that the presence of eyebrows could influence positively the expressiveness of a cartoon face.

Defining the Behaviour of PEANUT
Second, we concentrated on the content of PEANUT's interventions. One intervention corresponds to the association of a sentence and a facial expression. Sentences were selected from the following five main categories, elaborated through recommendations from the literature [10, 23, 21, 6], with respect to subject's MI-BCI performance and progression, i.e. the context of intervention.

- Temporal interventions, related to the temporal progress of the experiment [10] (ex. "I am happy to meet you", when starting the first session)
- Effort-related interventions, focusing on the fact that learning is the goal, and intended to minimise the importance of current performance while promoting long-term learning [23]. (ex. "Your efforts will be rewarded")
- Empathetic interventions, which aim at letting users know that their companion understands that they are facing a difficult training process [21]. (ex. "Don't let difficulties discourage you")
- Performance/results and progression associated interventions, which were designed to motivate users by focusing on the abilities they had already acquired [6]. (ex. "You are doing a good job!")
- Strategy-related interventions which aim at encouraging people to keep the same strategy when progression was positive or to change strategy when it was negative/neutral. (ex. "You seem to have found an efficient strategy")

Then, we also explored different sentences' characteristics, e.g., exclamatory or declarative (ex. "You are doing good!" or "You are doing good."); and personal (second person) or non-personal (third person) mode (ex. "You are doing good!" or "These results are good!"). To determine which characteristics the intervention should have depending on the context (performance & progression), we led an online user survey with 104 persons. The study consisted in an online questionnaire giving users similar instructions and mental imagery tasks as the ones given during actual BCI training. Simulated performances (since the surveyed users were not actually using a BCI) were displayed and were evolving positively, neutrally or negatively given the group the user was randomly assigned to. After the situation was introduced, two different intervention sentences were displayed on screen Users were asked to rate each of them (on a Likert scale ranging from 1 to 5) based on five criteria: appropriate, clear, evaluative, funny, motivating.
The results of these questionnaires revealed that users facing a negative progression should only be provided with declarative personal interventions and those facing a neutral progression with either declarative or exclamatory personal interventions. Results also revealed that participants showing a positive progression should be provided with declarative non-personal sentences (when the goal was to give clear information about the task) or exclamatory personal sentences (when the goal was to increase motivation) (see also Figure 2). One should add that

Published by Verlag der TU Graz
Graz University of Technology

 DOI: 10.3217/978-3-85125-533-1-76

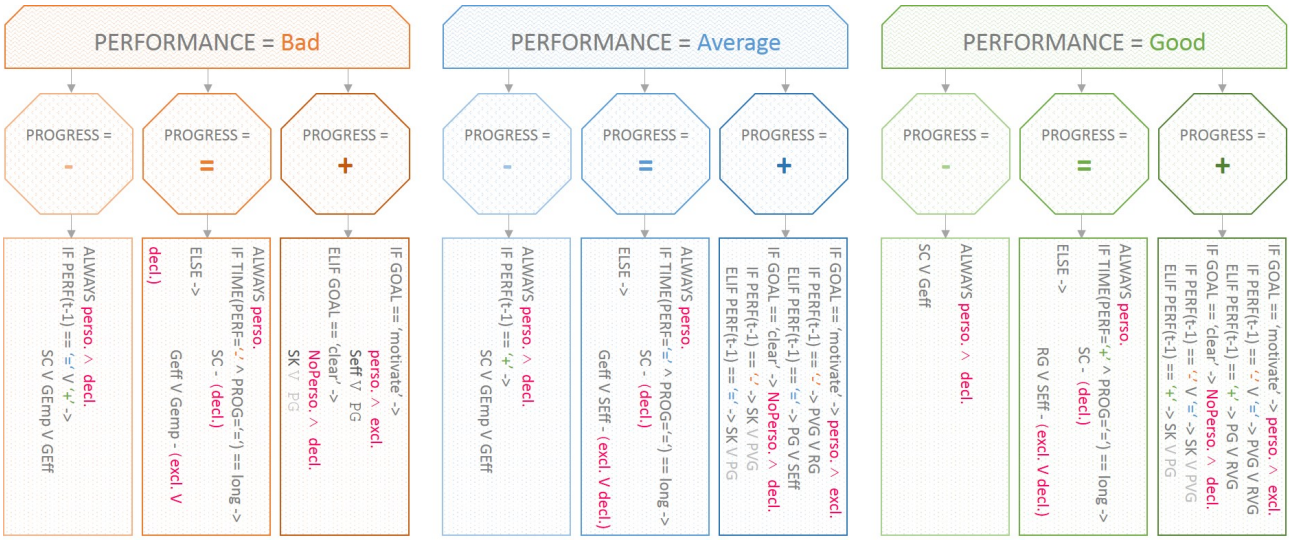

Figure 2: PEANUT's rule tree. Depending on performance and progression ("-"=negative, "="=neutral", "+"=positive), a set of rules is determined. Type of sentences: "perso." for personal, "NoPerso." for non-personal ; Mode of the sentence: "decl." for declarative, "excl." for exclamatory. Interventions: "GEff" for general effort, "SEff" for support effort, "GEmp" for general empathy, "SK" for strategy keep, "SC" for strategy change, "RG" for results good, "RVG" for results very good, "PG" for progress good, "PVG" for progress very good. Moreover, "∧" sign represents the logical operator "and" while "∨" sign represents the logical operator "or".

when an exclamatory sentence was used for the intervention, the emotion displayed through PEANUT's facial expressions was made more intense than for an equivalent declarative sentence. We could then translate these various results into rules, and more precisely into the the rule tree presented in Figure 2. This rule tree enables the system to select one specific rule (i.e., an intervention content - sentence & expression - and style) with respect to the context (performance and progression).

In particular, we determined a bad, average and good performance according to the 25th and 75th percentile of each user performance at the first run. Similarly, we determine a negative, neutral or positive progression according to the 25th and 75th of the user progression during the first session. Progression was estimated as the slope of the regression line of the user performance over the last 10 trials.

Implementation of PEANUT

Users' EEG signals were first measured using a g.tec gUSBAmp (g.tec, Austria) and processed online using OpenViBE 0.19.0 [18]. OpenViBE provided users with a visual feedback about the estimated mental task, and computed users' performances which were then transmitted to a home-made software, the rule engine using the Lab Streaming Layer (LSL) protocol. The rule engine processed performance measures received from OpenViBE to compute progression measures and browsed the Rule Tree described in Figure 2 in order to select an appropriate intervention for PEANUT (sentence and facial expression) with respect to the context. The selected intervention was then transmitted to an Android smartphone application by WiFi, which enunciated the sentence and animated PEANUT's facial expression.

VALIDATION OF THE EFFICIENCY OF PEANUT TO IMPROVE BCI USER-TRAINING

Once the companion created, the next step consisted in studying its efficiency to improve MI-BCI user-training both in terms of performance and user-experience.

Participants

Our study included twenty MI-BCI-naive participants (10 women; aged 21.05±1.64), and was conducted in accordance with the relevant guidelines for ethical research according to the Declaration of Helsinki. This study was approved by Inria's ethics committee, the COERLE. All participants signed an informed consent form at the beginning of the experiment and received a compensation of 50 euros.

Our experiment comprised 2 participant groups, which determined the support they would receive throughout the MI-BCI training sessions: no learning companion (*control group*) or a learning companion adapted to their MI-BCI performance & progression, i.e., PEANUT (*experimental group*). As the control group, we used the results obtained from 10 subjects in a previous experiment [8]. This experiment used the same protocol, but without PEANUT. Among the 18 participants of this previous study, 10 were selected so that they matched, as far as possible, the characteristics of the participants from

Published by Verlag der TU Graz
Graz University of Technology

 DOI: 10.3217/978-3-85125-533-1-76

the experimental group in terms of gender and initial MI-BCI performance. Furthermore, tension and self-reliance scores were comparable for the two groups.

Experimental Protocol

Before the first session, participants were asked to complete a validated psychometric questionnaire, the 16 PF-5 [2], that enabled us to compute their tension and self-reliance scores. Each participant took part in 3 sessions, on 3 different days. Each session lasted around 2 hours and was organised as follows: EEG cap setup, five runs during which participants had to learn to perform three MI-tasks (around 60 min, including breaks between the runs), removing the EEG cap and debriefing. The MI-tasks (i.e., left-hand motor imagery, mental rotation and mental subtraction) were chosen according to Friedrich et al. [4], who showed that these tasks were associated with the best performance on average across participants. During each run, participants had to perform 45 trials (15 trials per task, presented in a random order), each trial lasting 8s. At t=0s, an arrow was displayed with a left hand pictogram on the left (*L-HAND* task), the subtraction to be performed at the top (*SUBTRACTION* task) and a 3D shape on the right (*ROTATION* task). At t=2s, a "beep" announced the coming instruction and one second later, at t=3s, a red arrow was displayed for 1.250s. The direction of the arrow informed the participant which task to perform, e.g., an arrow pointing to the left meant the user had to perform a *L-HAND* task. In order to stress this information, the pictogram representing the task to be performed was also framed with a white square until the end of the trial. Finally, at t=4.250s, a visual feedback was provided in the shape of a blue bar, the length of which varied according to the classifier output. Only positive feedback was displayed, i.e., the feedback was provided only when there was a match between the instruction and the recognised task. The feedback lasted 4s and was updated at 16Hz, using a 1s sliding window. During the first run of the first session (i.e., the calibration run, see next Section), no real feedback could be provided, since the classifier has not been calibrated yet for this user. Thus, in order to limit biases with the other runs, e.g., EEG changes due to different visual processing between runs, the user was provided with a sham feedback, i.e., a blue bar randomly appearing and varying in length, irrespectively of the user's actual EEG (this feedback was based on the data from a previous user), as in [4]. A gap lasting between 3.500s and 4.500s separated each trial.

The *experimental group* was accompanied by PEANUT during the training, from the second run of session 1 (after the calibration run). PEANUT intervened every 6 ± 2 trials (the exact trial during which PEANUT intervened was randomly selected in that interval), during the inter-trial interval. PEANUT's interventions were adapted to participants' performance during the first session, and to their performance and progression during the second and third sessions.

EEG Recordings & Signal Processing

The EEG signals were recorded using 30 active scalp electrodes (F3, Fz, F4, FT7,FC5, FC3, FCz, FC4, FC6, FT8, C5, C3, C1, Cz, C2, C4, C6, CP3, CPz, CP4, P5, P3, P1, Pz, P2, P4, P6, PO7, PO8, 10-20 system), referenced to the left ear and grounded to AFz. EEG data were sampled at 256 Hz.

In order to classify the 3 mental imagery tasks on which our BCI is based, the following EEG signal processing pipeline was used. First, EEG signals were band-pass filtered in 8-30Hz, using a Butterworth filter of order 4. Then EEG signals were spatially filtered using 3 sets of Common Spatial Pattern (CSP) filters [17].

The CSP algorithm aims at finding spatial filters whose resulting EEG band power is maximally different between two classes. To provide a participant-specific feedback, each set of CSP filters was optimised during a calibration run (i.e., the first run of the first session) to discriminate EEG signals for a given class from those for the other two classes. We optimised 2 pairs of spatial filters for each class, corresponding to the 2 largest and lowest eigen values of the CSP optimisation problem for that class, thus leading to 12 CSP filters. The band power of the spatially filtered EEG signals was then computed by squaring the signals, averaging them over the last 1 second time window (with 15/16s overlap between consecutive time windows) and log-transforming the result. These resulted in 12 band-power features that were fed to a multi-class shrinkage Linear Discriminant Analysis (sLDA) [12], built by combining three sLDA in a one-versus-the-rest scheme. As for the CSP filters, the sLDA were optimised on the EEG signals collected during the calibration run, i.e., during the first run of the first session. To reduce between session variability, the sLDA classifiers' biases were re-calculated after the first run of sessions 2 and 3, based on the data from this first run, as in [4]. The resulting classifier was then used online to differentiate the 3 MI-tasks during the 3 sessions.

The sLDA classifier output (i.e., the distance of the feature vector from the LDA separating hyperplane) for the mental imagery task to be performed was used as feedback provided to the user. In particular, if the required mental task was performed correctly (i.e., correctly classified), a blue bar with a length proportional to the LDA output and extending towards the required task picture was displayed on screen and updated continuously.

This processing pipeline led to a total of 64 classification outputs per trial (16 per second for 4 seconds). OpenViBE thus computed the user's performance for this trial as the rate of correct classification outputs among these 64 outputs, and sent it to the rule engine (which in turn computed progression measures).

Variables & Factors

We studied the impact of the group (no companion, companion) on participants' MI-BCI performance, with respect to the session and participant's profile (tension and

Published by Verlag der TU Graz
Graz University of Technology

 DOI: 10.3217/978-3-85125-533-1-76

self-reliance scores). MI-BCI performance was assessed in term of mean classification accuracy (mean performance measured over all the windows of the feedback periods from all the different runs). We also evaluated the impact of the group on MI-BCI usability, with respect to MI-BCI performance. MI-BCI usability was assessed using a questionnaire focusing on 4 dimensions: learnability/memorability (LM), efficiency/effectiveness (EE), safety and satisfaction.

Results

First of all, statistical tests (t-tests) revealed no significant differences between the two groups in terms of tension, autonomy or initial cross validation performances on the calibration. This ensures the two groups are comparable. Therefore, we analysed each group's MI-BCI performance in term of mean classification accuracy, for this 3-class BCI (thus with a chance level of 33%). The group with no companion obtained 51.65% $\pm$ 3.78 and the group with the companion obtained 50.85% $\pm$ 7.94 mean classification accuracy. An ANOVA did not find any significant difference between the mean performance of the two groups [F(2,18)=-0.29, p=0.777] though their variance is significantly different [F(2,18)=4.737, p=0.043] (see Figure 3).

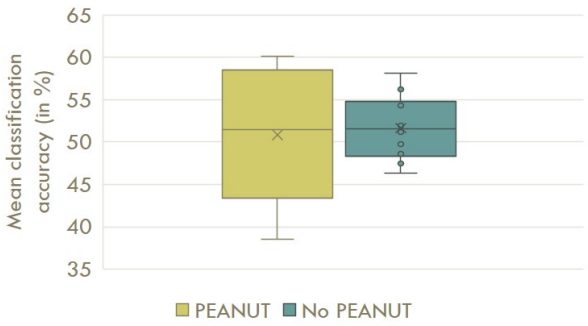

Figure 3: Mean classification accuracy per users group.

The subtantial difference of variability between the two groups might suggest that PEANUT had a beneficial effect on some participants and a detrimental effect on some others. However, this is only an hypothesis, and the number of participants included in the study does not allow us to identify the characteristics of those benefiting (or not) from PEANUT.

Finally, we analysed the influence of the group on usability scores. We performed four one-way ANCOVAs (one per dimension) with the Group as factor, the usability score for the target dimension as dependent variable and the mean classification accuracy as co-variable, since better classification accuracy is likely to lead to better perceived efficiancy, irrespectively of the condition. Results revealed a main effect of the group on the learnability/memorability (LM) dimension [D(1,18)=6.073; p$\leq$0.05, η^2=0.263]: participants who were provided with a companion considered the system's learnability/memorability to be higher than those with no companion (see Figure 4).

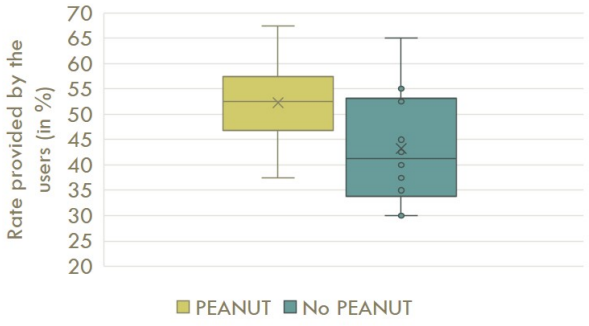

Figure 4: LM scores with respect to users' group.

DISCUSSION & CONCLUSION

In this paper, we introduced PEANUT, the first learning companion dedicated to MI-BCI user-training. The strength of this companion is its design: a combination of recommendations from the literature and of user-studies. PEANUT was validated in a relatively large MI-BCI study (20 participants, 3 sessions per participant), with two conditions: one control group with no learning companion and one experimental group with a learning companion whose behaviour was adapted to users' performance and progress. The higher variance in terms of performance in the group with PEANUT might suggest that PEANUT had a beneficial influence on some participants' performance but a detrimental one on others, although this hypothesis remains to be formally tested. This is in accordance with some previous studies indicating a differential effect of learning companion depending on sex and previous knowledge [1]. Nonetheless, this study also revealed that using PEANUT has a significant impact on user-experience. Indeed, participants who used PEANUT found it was easier to learn and memorise how to use the MI-BCI system than participants who had no learning companion. This confirmed that carefully designing PEANUT based on literature from educational psychology and user-centered design methods substantially benefited MI-BCI training user-experience.

In the future, PEANUT's behavior could be improved by adapting its interventions to the user's profile and state (frustration, overload, joy, boredom, etc.). We also plan to have PEANUT providing cognitive support, i.e., help to guide users towards the acquisition of specific skills. In order to be able to provide such support in an appropriate way, we first have to define a cognitive model of MI-BCI user-training, i.e., a model describing the factors impacting MI-BCI performance. Such a cognitive support, also known as explanatory feedback, is recom-

Published by Verlag der TU Graz
Graz University of Technology

 DOI: 10.3217/978-3-85125-533-1-76

mended by the educational psychology literature to ensure efficient training [20]. It would also be interesting to define more refined performance metrics and user state measures in order to provide more specific/adapted interventions, possibly further improving the support.
Overall, we are working towards providing a better cognitive and emotional feedback to MI-BCI users thanks to the use of learning companions. We hope that such companions could become broadly used tools for MI-BCI user-training in order to push BCI performance and usability much further. In this view, we designed and implemented PEANUT for a low cost, using only open-source and free software. We hope this work will contribute to make MI-BCI more widely accessible technologies.

Acknowledgements: This work was supported by IdEx Bordeaux and the French ANR with the REBEL project and grant ANR-15-CE23-0013-01.

REFERENCES

[1] A. L. Baylor and K. Yanghee. Pedagogical agent design: The impact of agent realism, gender, ethnicity, and instructional role. In *Proc ICITS*, pages 592–603. Springer, 2004.

[2] R. B. Cattell and H. E. Cattell. Personality structure and the new fifth edition of the 16pf. *Educ Psych Measur*, 55(6):926–37, 1995.

[3] B. R. Duffy. Anthropomorphism and the social robot. *Robotics and autonomous systems*, 42(3):177–190, 2003.

[4] E. V. Friedrich, C. Neuper, and R. Scherer. Whatever works: A systematic user-centered training protocol to optimize brain-computer interfacing individually. *PloS one*, 8(9):e76214, 2013.

[5] E. Hornecker. The role of physicality in tangible and embodied interactions. *interactions*, 18(2):19–23, 2011.

[6] P. A. Jaques, R. M. Vicari, S. Pesty, and J.-F. Bonneville. Applying affective tactics for a better learning. In *ECAI*, volume 16, page 109, 2004.

[7] C. Jeunet, E. Jahanpour, and F. Lotte. Why standard brain-computer interface (BCI) training protocols should be changed: an experimental study. *Journal of neural engineering*, 13(3):036024, 2016.

[8] C. Jeunet, B. N'Kaoua, S. Subramanian, M. Hachet, and F. Lotte. Predicting Mental Imagery-Based BCI Performance from Personality, Cognitive Profile and Neurophysiological Patterns. *PLoS ONE*, 10(12):20, 2015.

[9] D. W. Johnson and R. T. Johnson. An educational psychology success story: Social interdependence theory and cooperative learning. *Educational researcher*, 38(5):365–379, 2009.

[10] W. L. Johnson and P. Rizzo. Politeness in tutoring dialogs:"run the factory, that's what i'd do". In *International Conference on Intelligent Tutoring Systems*, pages 67–76. Springer, 2004.

[11] B. Kort, R. Reilly, and R. W. Picard. An affective model of interplay between emotions and learning: Reengineering educational pedagogy-building a learning companion. In *Proc ICALT*, 2001.

[12] F. Lotte and C. Guan. Learning from other subjects helps reducing brain-computer interface calibration time. In *Proc ICASSP*, 2010.

[13] F. Lotte and C. Jeunet. Towards improved BCI based on human learning principles. In *Proc Int BCI Winter Conf*, pages 1–4, 2015.

[14] F. Lotte, F. Larrue, and C. Mühl. Flaws in current human training protocols for spontaneous brain-computer interfaces: lessons learned from instructional design. *Front Hum Neurosc*, 7(568), 2013.

[15] J. Millán, R. Rupp, G. Müller-Putz, R. Murray-Smith, C. Giugliemma, M. Tangermann, et al. Combining brain-computer interfaces and assistive technologies: State-of-the-art and challenges. *Frontiers in Neuroprosthetics*, 4:161, 2010.

[16] R. Nkambou, J. Bourdeau, and R. Mizoguchi. *Advances in intelligent tutoring systems*, volume 308. Springer, 2010.

[17] H. Ramoser, J. Muller-Gerking, and G. Pfurtscheller. Optimal spatial filtering of single trial EEG during imagined hand movement. *IEEE Trans Rehab Eng*, 8(4):441–446, 2000.

[18] Y. Renard, F. Lotte, G. Gibert, M. Congedo, E. Maby, V. Delannoy, O. Bertrand, and A. Lécuyer. OpenViBE: An open-source software platform to design, test and use brain-computer interfaces in real and virtual environments. *Presence: teleoperators and virtual environments*, 19(1):35–53, 2010.

[19] L. Sherry. Issues in distance learning. *Int J Educ Telecom*, 1(4):337–365, 1996.

[20] V. Shute. Focus on formative feedback. *Review of Educational Research*, 78(1):153–189, 2008.

[21] E. Um, J. Plass, E. Hayward, B. Homer, et al. Emotional design in multimedia learning. *Journal of Educational Psychology*, 104(2):485, 2012.

[22] J. Wolpaw and E. Wolpaw. *Brain-computer interfaces: principles and practice*. Oxford University Press, 2012.

[23] B. P. Woolf, I. Arroyo, D. Cooper, W. Burleson, and K. Muldner. Affective tutors: Automatic detection of and response to student emotion. In *Advances in Intelligent Tutoring Systems*, pages 207–227. Springer, 2010.

Published by Verlag der TU Graz
Graz University of Technology

Proceedings of the
7th Graz Brain-Computer Interface Conference 2017 DOI: 10.3217/978-3-85125-533-1-77

NO TRAINING, SAME PERFORMANCE!? – A GENERIC P300 CLASSIFIER APPROACH

Andreas Pinegger[1], Gernot R. Müller-Putz[1]

[1] Institute of Neural Engineering, Graz University of Technology, Graz, Austria

E-mail: a.pinegger@tugraz.at

ABSTRACT: One of the main goals of modern brain-computer interfaces (BCIs) is that they should be simple and intuitive to use. Long-lasting training and learning periods are demotivating for the intended user. Therefore, the training should be reduced to a minimum. This particularly applies to P300-based BCIs, which are known as highly accurate and robust.
In this paper, we evaluated an approach that uses a generic classifier for P300 spelling instead of the usual personalized classifier, which users have to train before they can use the P300-based BCI. The generic classifier was calculated using the training data of 18 persons and evaluated with the data of 7 persons. Results were compared to the results achieved with personalized classifiers. We found that the generic classifier achieved comparable results regarding the effectiveness and efficiency. Therefore, our approach seems to be an appropriate, zero training alternative to personalized classifiers.

INTRODUCTION

The electroencephalogram (EEG) can be used to establish a noninvasive communication or control channel between the human brain and a computer, a so-called brain-computer interface (BCI) [1].
A very prominent BCI application is the P300 speller [2]. This type of BCI is mainly based on the positive component of an event-related potential (ERP) that appears approximately 300ms after a rare stimulus occurred among frequently occurring stimuli.
P300-based BCI provide high accuracies in combination with low illiteracy rates. Therefore, they are often used for communication and control systems. Various applications (e.g., speller [3], Brain Painting [4], music composer [5], and web browser [6]) are implemented.
Prior using such an application, training of a classifier is required. Normally, the training is performed by copy-spelling 5-10 predefined symbols and takes between 5 and 10 minutes. However, the question is, whether this training is really necessary.
Different approaches are proposed to avoid or reduce the training of the classifier. Kindermans et al. introduced a probabilistic zero training framework for ERPs [7]. They report high accuracies after a certain number of sequences. A sequence is defined as all rows and columns of the P300 matrix flashed once. However, the accuracy is still poor, when the number of sequences is limited to 3 or 4.
Lu et al. introduced a subject-independent model, learned offline from EEG of a pool of subjects, to capture common P300 characteristics [8]. They compared the learned model with a subject-specific classification model and a cross-subject model. Results indicate that this approach delivers high classification accuracies (on average approx. 84%) in combination with zero training. The number of sequences was defined with ten. No statement was given regarding the accuracies achieved with a lower number of sequences.

We asked whether the measured ERP during a P300 spelling task is stable enough to use a generic classifier. Consequently, the aim of this paper is to evaluate the power of a generic classifier (GC). The GC was calculated with the training data of eighteen P300 BCI users. The shrinkage regularized linear discriminant analysis (sLDA) was used for classification. Blankertz et al. suggested to use this method as a new standard for classifying ERPs [9]. The GC was evaluated with the data of seven users regarding the efficiency, in terms of highlighting sequences that are needed to reach certain accuracy. Effectiveness was investigated by recalculating the results of a prior study [10] with the GC: seven users had to spell four words and to control a multimedia player and a web browser with the P300 BCI. The accuracies of the online measurements and the offline simulations were compared.

MATERALS AND METHODS

Data acquisition:
The EEG data were acquired with a tap water-based biosignal amplifier (Mobita, TMSi, Oldenzaal, the Netherlands). Data were taken from six scalp electrodes (Fz, Cz, Pz, PO7, PO8, Oz) placed according to the extended international 10-20 system. A sampling rate of 250 Hz was used. The signal processing was performed in Matlab (MathWorks, Natick, USA). The EEG signal was filtered between 0.1 and 60 Hz with a 4^{th} order Butterworth band pass filter. These filter settings were chosen to compare the results of this evaluation to the results of a prior study [10].

Published by Verlag der TU Graz
Graz University of Technology

 DOI: 10.3217/978-3-85125-533-1-77

Generic training data generation:
Eighteen healthy volunteers (5 female, mean age: 29.39, SD:12.71 years) performed a standard P300 classifier training procedure: the participants were seated in a comfortable chair approximately 60 cm away from a computer screen showing the P300 stimulation matrix, see Fig. 1. The training was performed with fifteen highlighting flashes per row and column. Each highlighting had a duration of 50 ms and the time between flashes was set to 125 ms. The task of the participants was to copy-spell five characters out of a 6 x 6 matrix filled with letters and numbers. The characters were "H3P5FU", which were equally distributed over the matrix. Elements of the matrix were highlighted with famous faces [11].

Figure 1 – P300 stimulation matrix with letters and numbers. Rows and columns were highlighted with the face of Albert Einstein.

Test data generation:
Data from the study presented in [10] were used as test data. Seven participants (1 female, mean age 25.29, SD:2.75) performed a training, hereinafter called personal training, two copy-spelling tasks, a multimedia player, and a web browser control task with the same data acquisition system, which we used to gather the training data. None of the seven participants participated in the generic training data generation measurements and the data were acquired at least half a year later than the training data. In [10] the personal training setup and signal processing were the same as described for the generic training data generation, except the word ‘’BRAIN’’ was spelled.
The copy-spelling tasks consisted of spelling 4 words with 5 letters each. The participants were advised to spell the German words ‘’SONNE’’ (engl. ‘’sun’’), ‘’BLUME’’ (engl. ‘’flower‘‘), ‘’TRAUM‘‘ (engl. ‘’dream’’), and ‘’KRAFT’’ (engl. ‘’force’’). Between the second and the third word additional tasks, see below, were performed. The users were instructed not to correct wrongly spelled letters. The matrix was the same for training and copy-spelling.
The multimedia player task was to control a multimedia player to look at pictures. The minimal number of selections was 10 and the maximum number was 15. The participants were advised to correct misclassifications. The web browser task was to look for ‘’BCI’’ in Google and to select and read the Wikipedia webpage about BCI. The minimal number of selections was 9 and the maximum number was 18. The participants were advised to correct misclassifications. The P300 matrices for the multimedia player and the web browser task were different, cf. [6].

Generic classifier creation:
The generic training data of the eighteen volunteers were divided into epochs of approximately 800 ms (204 samples) after stimulus onset. The epochs were averaged per channel and row or column. Afterwards, the data were downsampled by the factor of 12 to reduce the number of features per channel. The data of each channel were concatenated to receive one feature vector per row and column. Thus, ten target feature vectors (2 vectors * 5 characters) and fifty non-target feature vectors (10 vectors * 5 characters) were available per volunteer.
In sum, 180 target feature vectors and 900 non-target feature vectors were used to train a generic sLDA classifier.

Generic classifier evaluation:
The GC was evaluated with the test data described before. We compared the accuracies calculated with the personalized classifier (PC), i.e., the classifier trained with data from the personal training, and the GC, respectively. PC accuracies for every flashing sequence were calculated per participant by a leave-one-letter-out cross validation of the personal training data. The same personal training data were classified with the GC. Accuracies per sequence and participant were calculated to evaluate the efficiency of the GC. The efficiency is high when a small number of sequences suffice to achieve high accuracy, i.e. above 70%. This is the proposed minimal level of sufficient accuracy for BCIs, cf. [12-15].
Additionally, we compared the online accuracies of the different tasks with simulated accuracies calculated with the GC to investigate the effectiveness of the GC.

RESULTS

The spatial GC weight distribution is shown in Fig. 2. To highlight only important weights, absolute values below 0.2 are not shown.
Fig. 3 shows the average accuracies and confidence intervals of the GC and the PC using the training data of [10]. The confidence intervals show no significant differences. Interestingly, the GC on average showed better classification accuracies after sequence 13: the accuracies of the GC stayed stable at 100% or 2.9% above the PC accuracies. The proposed minimal level of

Published by Verlag der TU Graz
Graz University of Technology

 DOI: 10.3217/978-3-85125-533-1-77

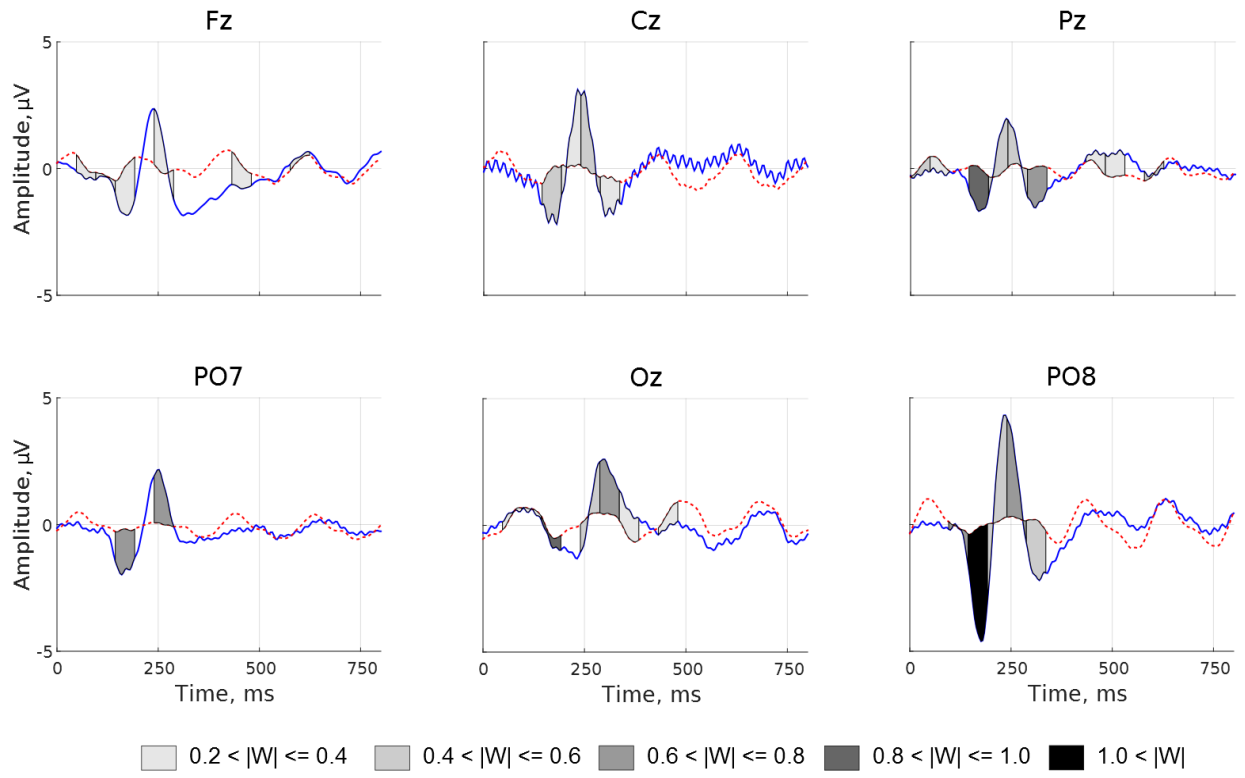

Figure 2 – The graphs show the averaged EEG data of 18 participants after targets stimulations (blue solid lines) and non-target stimulations (red dashed lines). Additionally, the weights of the GC are represented by different gray tone areas. Due to the downsampling of the signals, weights are shown as areas.

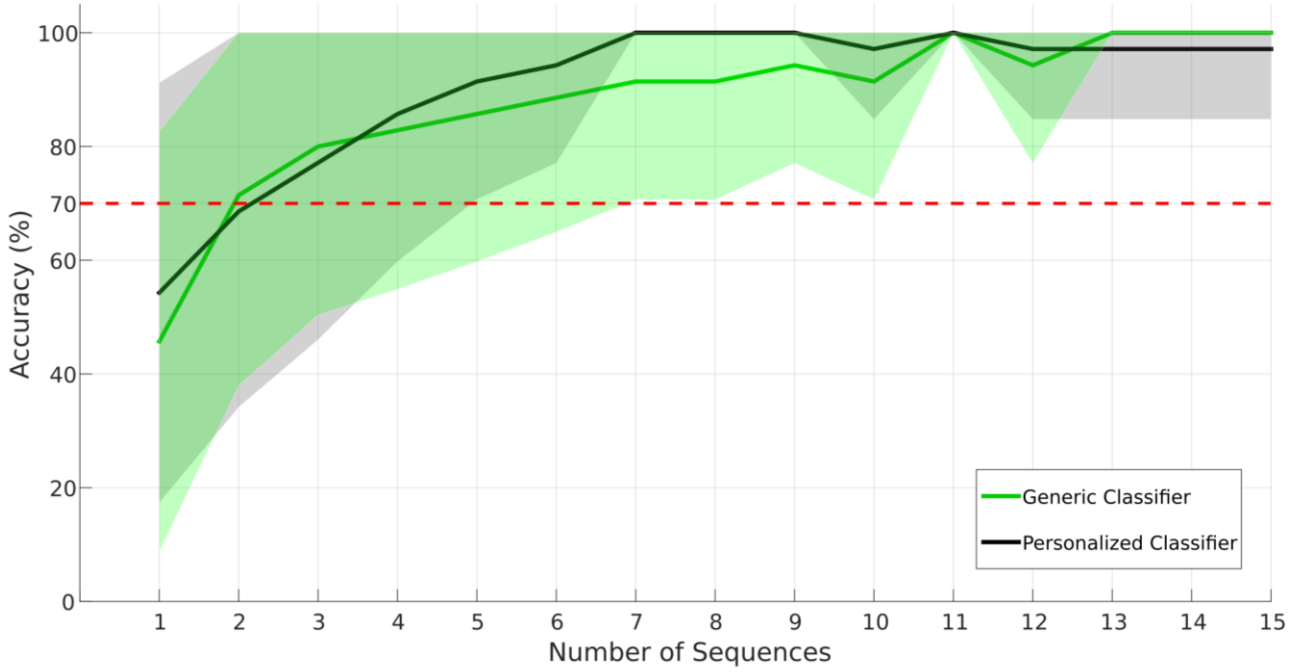

Figure 3 – Average (N=7) accuracies achieved with a certain number of sequences. The accuracies for the personal classifier were calculated with a leave-one-letter-out cross validation. Gray and green areas indicate the confidence intervals (CI) for proportions. The red dashed line indicates the minimal level of sufficient accuracy.

Published by Verlag der TU Graz
Graz University of Technology

 DOI: 10.3217/978-3-85125-533-1-77

Table 1 – Offline (simulated) accuracies of the copy-spelling tasks using the generic classifier (GC) and the personalized classifier (PC). Different results are marked in bold. Sp1, Sp2…Spelling run 1, 2; MMP…Multimedia player; WB…Web browser.

Part.	Sequ.	GC accuracies in %						PC accuracies in %					
		Sp1	MMP	WB	Sp2	Av.	SEM	Sp1	MMP	WB	Sp2	Av.	SEM
1	8	100	100	81.8	**100**	**95.5**	10.4	100	100	**90.9**	90	95.2	10.7
2	8	100	90	**100**	80	92.5	13.2	100	**100**	90.9	**100**	**97.7**	7.5
3	9	100	100	100	100	100	0.0	100	100	100	100	100	0.0
4	10	80	91.7	88.9	80	83.9	18.4	**100**	91.7	**100**	**90**	**95.4**	10.4
5	11	70	**100**	66.7	**80**	**79.2**	20.3	**80**	64.3	**73.3**	70	71.9	22.5
6	13	100	100	**100**	100	**100**	0,0	90	100	90	100	95.0	10.9
7	14	100	100	100	**100**	**100**	0.0	100	100	100	90	97.5	7.8

sufficient accuracy (70%) was reached by the GC on average after 2 (71.4%) and by the PC after 3 (77.1%) sequences. However, the lower limits of the confidence intervals exceeded this level after 5 sequences (PC) and 7 sequences (GC), respectively, see Fig. 3.

The GC evaluation showed comparable results between the PC and GC, see Tab. 1. Differences are marked in bold. On average the GC outperformed the PC four times (range 0.3 – 7.3%) and the PC outperformed the GC two times (5.2% and 11.5%, respectively).
The average accuracies are far above the level of sufficient accuracy (70%).

DISCUSSION AND CONCLUSION

We showed that it is possible to use a P300-based BCI with zero training and high accuracies using a generic classifier. The results indicate that in terms of efficiency and effectiveness both classifiers are about equal. Moreover, the simulated GC spelling results partly outperformed the PC results.
The comparison of the accuracies for a defined number of sequences, see Fig. 3, shows that in case of a small number (between 1 and 4) no differences were detectable. For a medium number (between 5 and 10), the PC achieved better results than the GC. Finally for a large number (above 12), the GC outperformed the PC. However, the confidence intervals overlap most of the time and to make a more accurate statement more data must be taken into account.
During the spelling and control tasks the participants used a defined number of flashing sequences, see Tab. 1 second column. Comparing the averaged results indicates that participants (P2, P4) who used a medium number of sequences (between 8 and 10) would achieve better results with the PC. On the other hand, participants (P5, P6, and P7) who used a large number of sequences (above 10) would achieve higher accuracies with the GC.

One limitation of this comparison is that the presented online results were achieved with an SWLDA classifier and the simulated results were achieved with an sLDA classifier. Another limitation is that the GC was evaluated with data obtained by the same setup regarding the biosignal acquisition system, the signal processing etc. as the training data. It might be reasonably assumed that using a different biosignal acquisition system requires an adapted generic classifier.

Lu et al. also reported high P300 spelling accuracies using a generic classifier [8]. However, they performed two similar sessions with ten participants spelling the same 41 characters twice and performed a two-fold cross validation. No information was given regarding the time between the sessions and they did not evaluate the efficiency of their subject-independent model. We trained the GC with the data from different users and tasks than we evaluated it. In addition, we used different matrix sizes, cf. [6]. Finally, we used only six electrodes instead of eight in [8].

The next step would be to test the GC online with a representative number of people. In addition, it is conceivable to adapt the GC to a person by recalculating the GC with data of the actual user. Our results indicate that it should be sufficient to use a high number of sequences at the beginning to achieve almost 100% accuracy with the GC. This data can be used to recalculate the GC and adapt it to a person. Subsequently, the number of stimulation sequences can be reduced afterwards.

ACKNOWLEDGMENTS

This paper only reflects the authors' views, and funding agencies are not liable for any use that may be made of the information contained herein. The research leading to these results has received funding from the European Community's, Seventh Framework Programme FP7/2007-2013, BackHome project grant agreement number 288566.

Published by Verlag der TU Graz
Graz University of Technology

 DOI: 10.3217/978-3-85125-533-1-77

REFERENCES

[1] J Millàn, R Rupp, GR Müller-Putz, R Murray-Smith, C Giugliemma, M Tangermann, C Vidaurre, F Cincotti, A Kübler, R Leeb, C Neuper, K-R Müller, and D Mattia. Combining brain-computer interfaces and assistive technologies: state-of-the-art and challenges. Frontier in Neuroscience, vol. 4, p. 12, 2010.

[2] LA Farwell and E Donchin. Talking off the top of your head: toward a mental prosthesis utilizing event-related brain potentials. Electroence-phalography and Clinical Neurophysiology, vol. 70, pp. 510–523, 1988.

[3] E Donchin, KM Spencer, and R Wijesinghe. The mental prosthesis: assessing the speed of a P300-based brain-computer interface. IEEE Transactions on Neural Systems and Rehabilitation Engineering, vol. 8, pp. 174–179, 2000.

[4] J Münßinger, S Halder, S Kleih, A Furdea, V Raco, A Hösle, and A Kübler. Brain painting: first evaluation of a new brain-computer interface application with ALS-patients and healthy volunteers. Frontiers in Neuroprosthetics, vol. 4, p. 182, 2010.

[5] A Pinegger, SC Wriessnegger, and GR Müller-Putz. Sheet music by mind: Towards a brain-computer interface for composing. in Engineering in Medicine and Biology Society (EMBC), 2015 37th Annual International Conference of the IEEE, pp. 1053–1056, Aug 2015.

[6] S Halder, A Pinegger, I Käthner, SC Wriessnegger, J Faller, JBP Antunes, GR Müller-Putz, and A Kübler. Brain-controlled applications using dynamic P300 speller matrices. Artificial Intelligence in Medicine, vol. 63, no. 1, pp. 7 – 17, 2015.

[7] P-J Kindermans, M Tangermann, K-R Mueller, and B Schrauwen. Integrating dynamic stopping, transfer learning and language models in an adaptive zero-training ERP speller. Journal of Neural Engineering, vol. 11, 2014.

[8] S Lu, C Guan, and H Zhang. Unsupervised brain computer interface based on intersubject information and online adaptation. IEEE Transactions on Neural Systems and Rehabilitation Engineering, vol. 17, no. 2, pp. 135–145, 2009.

[9] B Blankertz, S Lemm, M Treder, S Haufe, and K-R Müller. Single-trial analysis and classification of ERP components – a tutorial. NeuroImage, vol. 56, pp. 814–825, 2011.

[10] A Pinegger, SC Wriessnegger, J Faller, and GR Müller-Putz. Evaluation of different EEG acquisition systems concerning their suitability for building a brain-computer interface: case studies. Frontiers in Neuroscience, 2016.

[11] T Kaufmann, SM Schulz, C Grünzinger, and A Kübler. Flashing characters with famous faces improves ERP-based brain-computer interface performance. Journal of Neural Engineering, vol. 8, no. 5, 2011.

[12] J Perelmouter, N Birbaumer. A binary spelling interface with random errors. IEEE Transactions on Rehabilitation Engineering. 2000;8:227–232.

[13] A Kübler, B Kotchoubey, J Kaiser, JR Wolpaw, N Birbaumer. Brain-computer communication: unlocking the locked in. Psychological Bulletin. 2001;127:358–375.doi:10.1037/0033-2909.127.3.358.

[14] F Nijboer, A Furdea, I Gunst, J Mellinger, DJ McFarland, N Birbaumer, et al. An auditory brain-computer interface (BCI). Journal of Neuroscience Methods. 2008;167(1):43–50. doi:10.1016/j.jneumeth.2007.02.009.

[15] A Furdea, S Halder, DJ Krusienski, D Bross, F Nijboer, N Birbaumer, et al. An auditory oddball (P300) spelling system for brain-computer interfaces. Psychophysiology. 2009;46:1–9. doi:10.1111/j.1469-8986.2008.00783.x.

Published by Verlag der TU Graz
Graz University of Technology

Proceedings of the
7th Graz Brain-Computer Interface Conference 2017 DOI: 10.3217/978-3-85125-533-1-78

APPROACHES TO ZERO-SHOT STIMULUS DECODING IN ECOG FOR POTENTIAL BCI APPLICATIONS

C. Ratto[1], C. Caceres[1], M. Roos[1], K. Rupp[2], G. Milsap[2], N. Crone[3], and M. Wolmetz[1]

[1] The Johns Hopkins University Applied Physics Laboratory, Laurel, MD, United States
[2] Dept. of Biomedical Engineering, Johns Hopkins University, Baltimore, MD, United States
[3] Department of Neurology, Johns Hopkins University, Baltimore, MD, United States

E-mail: christopher.ratto@jhuapl.edu

ABSTRACT: Most Brain-Computer Interface (BCI) work has focused on detecting specific sensory or motor information, but BCIs are beginning to be applied to more abstract domains like covert speech and communication of semantic thought. One potential approach to decoding more abstract information is linear zero-shot classification via semantic attributes, which is computationally efficient and may facilitate real-time processing. In this work, several variations of this model are applied to electrocorticography (ECoG) data recorded during a picture-naming task with nine patients. Performances of encoding and decoding models are compared, and results are discussed in the context of BCI applications.

INTRODUCTION

Sensory and motor information can be understood and encoded in terms of physical functions and attributes, and brain-computer interface (BCI) applications typically utilize models based on these characteristics, e.g. limb motion [1] or speech [2]. These approaches are not applicable in more abstract domains, such as lexical semantics and conceptual thought. However, words or concepts can be decomposed into sets of meaningful attributes [3], so one can study how those attributes are encoded in the brain. For example, the concept of "lettuce" might be encoded with heavy weight on the attributes "green," "edible," and "plant" and low weight on the attributes "black," "manmade," and "hard."

By using machine learning methods to derive these decompositional models from neural data, e.g. functional magnetic resonance imagery (fMRI), a better understanding of how more abstract concepts are represented in the human brain has been achieved [4, 5, 6, 7]. Stimuli can be represented by their constituent semantic attributes, and mappings can be learned between each attribute and the observed neural responses. In the same way, stimuli can be recovered by induction after applying the mapping to novel neural data.

While this approach has been a boon for studying how abstract representations are semantically *encoded* in neural activations, there are clear advantages for neural *decoding* applications as well. Semantically decoding neural signals in this manner allows for the classification of novel classes of stimuli. This process, coined *zero-shot* classification [5], differs from traditional pattern recognition, in which models are tested on new data from the same classes used to train the model. In zero-shot classification, models are tested on data from *new* classes that were *not* used to train the model. Zero-shot classification has been successfully demonstrated in several applications such as computer vision [8] and target detection [9].

Zero-shot classification on neural signals would allow for BCIs to handle novel stimuli more robustly. In previous work [10], it was demonstrated that zero-shot classification of recognized objects was possible from electrocorticography (ECoG) at high levels of performance on par with whole-brain fMRI [4]. Demonstrations of reliable neural decoding performance from electrophysiological responses like this suggest a viable path to BCIs for more abstract domains. For example, zero-shot decoding could potentially be used to classify and/or semantically annotate novel stimuli that produce P300 responses [11], such as anomalous images [12] or frames of video [13]. Furthermore, communication BCIs, such as those used by locked-in individuals [14], could potentially use zero-shot classification to decode conceptual thought as opposed to individual characters.

While promising, applications of zero-shot decoding to ECoG are new and not well-explored. The mapping between semantic attributes and neural features may be learned as an *encoding model*, i.e. a map from attributes to neural features [4, 10], or as a *decoding model*, *i*.e. direct prediction of attributes from neural signals [5, 6], but the efficacy of these approaches have not been compared. The mapping is often assumed to be linear, and typically learned by either least-squares [4] or ridge regression [5, 6, 10] to limit the possibility of overfitting. Support vector machines (SVMs) have been used for classifying neural data in past studies of human-computer interaction [15], as well as in zero-shot classification for computer vision [8]. However SVMs have not yet been investigated for zero-shot ECoG decoding. In this paper, we build on the encoding model described by our group in [10] to compare different approaches to zero-shot decoding in ECoG.

Published by Verlag der TU Graz
Graz University of Technology

 DOI: 10.3217/978-3-85125-533-1-78

MATERIALS AND METHODS

The experiments carried out for this work utilized ECoG recordings collected during a picture-naming task. Data was recorded from 9 patients with intractable epilepsy (2 female, 31-44 years old) during inpatient monitoring for pre-surgical localization of their ictal onset zone and eloquent cortex. All patients provided informed consent according to a protocol approved by the Johns Hopkins Medicine Institutional Review Boards.

The stimulus set was originally reported in [4], and the data collection paradigm and analyses were originally reported in [10]. White line drawings of objects were briefly presented on a black background, and a white fixation cross was shown between stimuli. Each image was shown for one second, with a rest interval varying randomly between 3.5 and 4.5 seconds. Participants were instructed to name the image as soon as possible, or pass when necessary. Six blocks of data were collected per patient, with all 60 objects being shown in pseudo-random order within each block. ECoG signals were sampled at 1000 Hz, digitized, and recorded using the BlackRock Neuroport system.

The stimuli consisted of line drawing representations of 60 nouns from 12 semantic categories as listed in Tab. 1. Each of the 60 nouns was uniquely mapped to a vector of $P = 218$ semantic attributes originally used in [5]. The attributes were generated by crowdsourcing answers to a series of 218 questions via Amazon Mechanical Turk. All 218 questions were asked of 1,000 different objects, including all 60 of the objects included in this study. Questions probed a variety of semantic properties, including size, usage, composition, and category, with answers on an ordinal scale $[-1, -0.5, 0, 0.5, 1]$. It was empirically determined that regression models tended to perform better when the vector of attributes for a given noun was normalized to unity length.

A high-level illustration of the neural feature extraction process is shown in Fig. 1. After data collection, excessively noisy channels were discarded,

Table 1: List of stimulus nouns and their categories.

Category	Nouns
Animals	bear, cat, cow, dog, horse
Body parts	arm, eye, foot, hand, leg
Buildings	apartment, barn, church, house, igloo
Building parts	arch, chimney, closet, door, window
Clothing	coat, dress, pants, shirt, skirt
Furniture	bed, chair, desk, dresser, table
Insects	ant, bee, beetle, butterfly, fly
Kitchen Utensils	bottle, cup, glass, knife, spoon
Manmade Objects	bell, key, refrigerator, telephone, watch
Tools	chisel, hammer, pliers, saw, screwdriver
Vegetables	carrot, celery, corn, lettuce, tomato
Vehicles	airplane, bicycle, car, train, truck

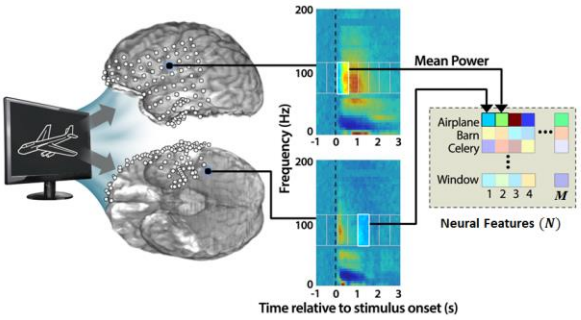

Figure 1. Illustration of neural feature extracton from ECoG recordings, adapted from [10].

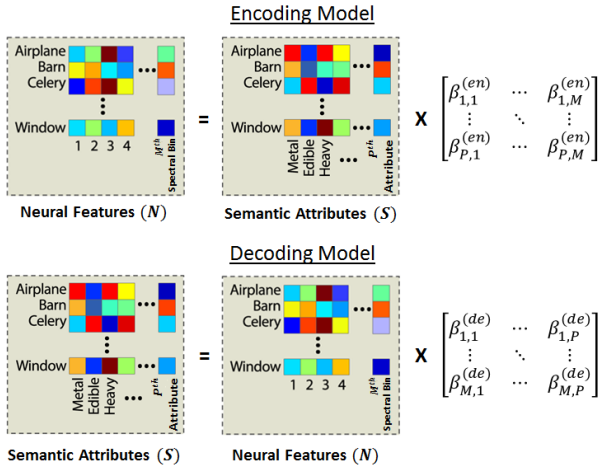

Figure 2: Illustration of encoding (top) and decoding (bottom) models, adapted from [10].

and the signals that were retained were spatially filtered using local common-average referencing. Signals were then low-pass filtered, resampled to 256 Hz, and time-gated from stimulus onset to one second post stimulus onset. Features were extracted from the FFT spectrogram by integrating over 12 octaves with center frequencies spaced by half-octaves beginning at 2 Hz and time offsets of 250 and 500 ms post-stimulus. Because the number of electrodes varied per subject, the number of potential ECoG features varied as well. Features were down-selected by ranking them according to their stability over stimulus presentation, which has precedence in similar studies [4, 5, 6]. The stability of a particular neural feature was calculated by averaging all pairwise Pearson correlations between responses in blocks of trials. Up to 200 of the most stable neural features were considered.

The collected ECoG features and the accompanying semantic attributes for each stimulus can be used to learn an encoding or decoding model. The manner by which these models relate the neural and semantic features to one another are illustrated in Fig. 2.

Let $\boldsymbol{s}$ be a P-dimensional vector of semantic attributes, and $\boldsymbol{n}$ be an M-dimensional vector of neural features. The *encoding model* takes the form of a linear mapping of $\boldsymbol{s}$ onto each n_m, for $m = 1,2,\dots,M$:

$$\hat{n}_m = \boldsymbol{s}^T \boldsymbol{\beta}_m^{(en)} \qquad (1)$$

The parameter vector $\boldsymbol{\beta}_m^{(en)}$ consists of the regression coefficients for encoding the mth feature. In prior work,

Published by Verlag der TU Graz
Graz University of Technology

 DOI: 10.3217/978-3-85125-533-1-78

$\boldsymbol{\beta}_m^{(en)}$ was learned using ridge regression [10], and the same is done here since the model output $\hat{n}_m$ is continuous-valued. The ridge regression solution for $\boldsymbol{\beta}_m^{(en)}$ is given by

$$\boldsymbol{\beta}_m^{(en)} = \left(\boldsymbol{S}^T\boldsymbol{S} + \lambda^{(en)}\boldsymbol{I}\right)^{-1}\boldsymbol{S}^T\boldsymbol{n}_m, \quad (2)$$

where $\boldsymbol{S}$ is the $T \times P$ matrix of semantic attributes, where T is the total number of trials used to train the model, $\boldsymbol{n}_m$ is the $T \times 1$ vector of values of the mth neural feature (normalized to zero-mean, unit-variance), and $\lambda^{(en)}$ is a regularization parameter determined empirically by grid search amongst five values between 1 and 10.

Conversely, the *decoding model* takes the form of a linear mapping of $\boldsymbol{n}$ onto each s_p, for $p = 1,2,\dots,P$:

$$\hat{s}_p = \boldsymbol{n}^T\boldsymbol{\beta}_p^{(de)}, \quad (3)$$

The parameter vector $\boldsymbol{\beta}_p^{(de)}$ consists of the regression coefficients for decoding the pth attribute. The ridge regression solution for $\boldsymbol{\beta}_p^{(de)}$ is given by

$$\boldsymbol{\beta}_p^{(de)} = \left(\boldsymbol{N}^T\boldsymbol{N} + \lambda^{(de)}\boldsymbol{I}\right)^{-1}\boldsymbol{N}^T\boldsymbol{s}_p, \quad (4)$$

where $\boldsymbol{N}$ is the $T \times M$ matrix of neural features, $\boldsymbol{s}_p$ is the $T \times 1$ vector of values of the pth attribute, and $\lambda^{(de)}$ is a regularization parameter determined empirically by grid search amongst five values between 100 and 1000.

The discrete-valued output $\hat{s}_p$ suggests that a classifier may be more appropriate than regression for learning the decoding model. As suggested by [8], a linear SVM is also used to learn $\boldsymbol{\beta}_m^{(de)}$. For a binary problem where $s_p \in [-1,1]$, the SVM solves the following optimization problem, which maximizes the margin between the classes:

$$\boldsymbol{\beta}_p^{(de)} = \arg\min_{\boldsymbol{\beta}}\left\{c\sum_{t=1}^{T}\max\left[0,1 - s_p(\boldsymbol{\beta}^T\boldsymbol{n}_t)\right]^2 + \|\boldsymbol{\beta}\|^2\right\} \quad (5)$$

To train the SVM, the elements of $\boldsymbol{s}$ were re-quantized to $[-1,0,1]$ by combining the [-0.5, 0, 0.5] responses. Re-quantization casts the original attribute values as simple answers: *no*, *don't know*, and *yes*. The `liblinear` software package was used to train three *one-versus-one* SVM classifiers to discriminate each pair of values [16]. Tuning parameters $c = \{1, 10, 100\}$ were considered, with per-class weighting according to the number of training samples. Voting amongst the three classifiers is used at test to predict $\hat{s}_p$. To assess the effect of modifying the attributes in this manner, ridge regression was also applied to the re-quantized attributes in another version of the decoding model.

After learning the mapping between neural features and attributes, a novel stimulus can be decoded by a distance-based classifier in neural space (if an encoding model was used) or semantic space (if a decoding model was used). Let the cosine distances resulting from the encoder output be denoted as

$$d_\phi^{(en)} = \frac{\hat{\boldsymbol{n}} \cdot \boldsymbol{n}_\phi}{\|\hat{\boldsymbol{n}}\| \cdot \|\boldsymbol{n}_\phi\|}, \quad (6)$$

where $\boldsymbol{n}_\phi$ is the output of the trained encoder applied to $\boldsymbol{s}_\phi$, the true attribute vector for noun ϕ, and $\hat{\boldsymbol{n}} = [\hat{n}_1, \hat{n}_2, \dots, \hat{n}_M]^T$. Therefore, neural decoding by means of an encoding model takes the form of

$$\hat{\phi}^{(en)} = \arg\min_{\phi}\left\{d_\phi^{(en)}\right\}. \quad (7)$$

Similarly, neural decoding by means of a decoding model takes the form of

$$d_\phi^{(de)} = \frac{\hat{\boldsymbol{s}} \cdot \boldsymbol{s}_\phi}{\|\hat{\boldsymbol{s}}\| \cdot \|\boldsymbol{s}_\phi\|}, \quad (8)$$

$$\hat{\phi}^{(de)} = \arg\min_{\phi}\left\{d_\phi^{(de)}\right\}, \quad (9)$$

where $\boldsymbol{s}_\phi$ is the decoder output and $\hat{\boldsymbol{s}} = [\hat{s}_1, \hat{s}_2, \dots, \hat{s}_P]^T$.

RESULTS

Experiments were conducted to assess performance of zero-shot stimulus prediction using four different modeling approaches: *Ridge Encoder*, *Ridge Decoder*, *Ridge Decoder Re-Quantized Attributes*, and *SVM Decoder with Re-Quantized Attributes*. The zero-shot problem was simulated by employing leave-one-noun-out cross-validation; feature selection and training were performed using 59 of the 60 nouns, and one noun was held out for testing. Therefore, the number of trials used to train the models was $T = 6 \times 59 = 354$ per subject. Two options for testing were compared: predicting from the average ECoG feature vector over all 6 trials, and predicting from single trials. Performance was measured via the *mean rank accuracy* (MRA). The MRA represents the average rank accuracy (RA) of the zero-shot test class, taken across the full set of 60 nouns ranked according to the cosine distance,

$$MRA = \frac{1}{60}\sum_{\phi=1}^{60} RA_\phi, \quad (10)$$

where RA_ϕ is the relative (percentage) rank of the test noun ϕ within a ranked list of potential classes,

$$RA_\phi = 100 \times \left(\frac{60 - r_\phi}{59}\right), \quad (11)$$

and r_ϕ is the rank of $d_\phi^{(en)}$ (if an encoding model was used) or $d_\phi^{(de)}$ (if a decoding model was used). The MRA could also be calculated on a per-category basis by averaging the MRA of all nouns within the same category.

The per-noun and per-category MRAs were tested for significance using a Monte Carlo procedure. A total of 1,000 null encoding and decoding models were trained for each subject by permuting the rows of $\boldsymbol{S}$, and the maximum MRA was calculated over all choices of M and $\lambda^{(en)}$ or $\lambda^{(de)}$. The p-values for the MRAs achieved by the alternative models were then computed using the distribution of the MRAs achieved by the null models.

The observed *per-noun* MRAs of the four decoding approaches are summarized in Tab. 2 and Tab. 3. The reported values represent maximum performance over all numbers of neural features and choices of regularization/tuning parameters that were considered. Tab. 2 summarizes the performance for decoding block-averaged neural responses, and Tab. 3 summarizes the performance of decoding single-trial neural responses.

The MRA for block-averaged neural features were

Published by Verlag der TU Graz
Graz University of Technology

 DOI: 10.3217/978-3-85125-533-1-78

Table 2: *Per-noun* MRA using *block-averaged* neural features at test. Boldface indicates significance at $p < 0.01$, italics indicates significance at $p < 0.05$, and the highest performance per subject is underlined.

	Ridge Encoder	Ridge Decoder	Ridge Decoder w/ Requant	SVM Decoder w/ Requant
S1	***84.11***	***79.19***	***80.08***	***75.25***
S2	***83.92***	***79.75***	***78.33***	***77.33***
S3	*65.64*	*62.86*	*62.47*	60.79
S4	***66.69***	***65.69***	***64.47***	*62.81*
S5	***68.17***	***67.42***	***67.58***	***65.93***
S6	***67.14***	***70.81***	***70.11***	*64.19*
S7	***67.31***	***69.67***	***69.47***	*64.07*
S8	***75.61***	***73.00***	***72.36***	***71.03***
S9	***87.69***	***82.75***	***81.75***	***80.58***

Table 3: *Per-noun* MRA using *single-trial* neural features at test. Boldface indicates significance at $p < 0.01$, italics indicates significance at $p < 0.05$, and the highest performance per subject is underlined.

	Ridge Encoder	Ridge Decoder	Ridge Decoder w/ Requant	SVM Decoder w/ Requant
S1	***74.80***	***71.07***	***71.17***	***64.05***
S2	***75.70***	***72.65***	***71.81***	***70.82***
S3	*57.55*	*56.31*	*55.77*	54.99
S4	***59.15***	***57.86***	***57.13***	*56.80*
S5	***60.13***	***60.62***	***60.58***	***57.75***
S6	***59.13***	***61.74***	***61.59***	57.15
S7	***65.07***	***66.19***	***65.38***	*60.16*
S8	***64.15***	***62.28***	***61.81***	***61.18***
S9	***80.63***	***76.65***	***75.56***	***73.09***

Table 4: *Per-category* MRA using *block-averaged* neural features at test. Boldface indicates significance at $p < 0.01$, italics indicates significance at $p < 0.05$, and the highest performance per subject is underlined.

	Ridge Encoder	Ridge Decoder	Ridge Decoder w/ Requant	SVM Decoder w/ Requant
S1	***80.54***	***79.17***	***79.86***	***73.87***
S2	***82.19***	***79.63***	***79.19***	***78.31***
S3	***62.99***	***62.99***	***62.83***	***61.33***
S4	***65.55***	***65.12***	***64.42***	***63.18***
S5	***64.77***	***67.01***	***66.09***	***67.03***
S6	***66.52***	***70.63***	***70.46***	***64.79***
S7	***68.79***	***70.13***	***69.96***	***65.49***
S8	***70.18***	***73.34***	***73.36***	***70.92***
S9	***82.23***	***81.99***	***81.22***	***80.59***

Table 5: *Per-category* MRA using *single-trial* neural features at test. Boldface indicates significance at $p < 0.01$, italics indicates significance at $p < 0.05$, and the highest performance per subject is underlined.

	Ridge Encoder	Ridge Decoder	Ridge Decoder w/ Requant	SVM Decoder w/ Requant
S1	***72.39***	***70.63***	***70.77***	***63.37***
S2	***74.16***	***72.65***	***72.31***	***70.41***
S3	***56.52***	***56.00***	***55.85***	***55.34***
S4	***58.56***	***58.01***	***57.81***	***57.16***
S5	***58.50***	***59.48***	***59.25***	***57.55***
S6	***58.87***	***61.79***	***61.78***	***57.77***
S7	***66.47***	***66.55***	***66.01***	***60.63***
S8	***62.11***	***62.37***	***62.04***	***60.97***
S9	***76.48***	***75.84***	***75.34***	***72.63***

higher than single-trial MRA because averaging repeated trials mitigates noise. Performance varied within 5% MRA for most subjects. For all but one subject, S2, the Ridge Encoder/Decoder MRA was significant at $p < 0.01$. For most of the subjects (S1-S4, S8, and S9 for block-average and single trial decoding, S5 for block-average decoding only) the Ridge Encoder also yielded the highest MRA and is consistent with performance in similar fMRI studies, e.g. [4]. For the other subjects (S5 for single-trial decoding, S6 and S7 for both types of decoding), the Ridge Decoder was slightly better and re-quantizing the attributes did not significantly affect performance.

The *per-category* MRA, for both block-averaged and single-trial neural features at test, is summarized in Tab. 4 and Tab. 5, respectively. All per-category MRAs were significant at $p < 0.01$. For each subject, the highest per-category MRA tended to be no more than 5% less than the highest per-noun MRA. For three subjects, the Ridge Decoder performed best, and the Ridge and SVM Decoders with Re-Quantized Attributes were each best for one subject.

The RA of each noun was analyzed by comparing the results of the best-performing (S1) and worst-performing (S3) subjects. Those results are illustrated in Fig. 3 and Fig. 4, respectively. The nouns are listed in descending order of RA by the Ridge Encoder. Note that the performance of the three decoder models does not follow the same trend as the performance of the encoder model. In fact, some of the nouns that are decoded poorly by the Ridge Encoder (e.g., *hand* and *foot* for S1, *fly* and *bed* for S3) are actually decoded with much higher RA by the three decoder models.

DISCUSSION

For a majority of subjects, zero-shot stimulus prediction via an encoding model was superior to decoding models for ECoG signals recorded primarily from temporal and basal occipital regions. The difference in MRA between the encoding model and the best decoding model was within 5%. A possible explanation may be that the encoding model is more robust. The semantic attributes used to fit the encoding model are deterministic, while the ECoG features used to fit the decoding model are noisy.

The SVM Decoder was the worst performing model for most subjects and yielded less significant MRAs, suggesting that it makes several incorrect assumptions about the decoding problem. One might be the training

Published by Verlag der TU Graz
Graz University of Technology

 DOI: 10.3217/978-3-85125-533-1-78

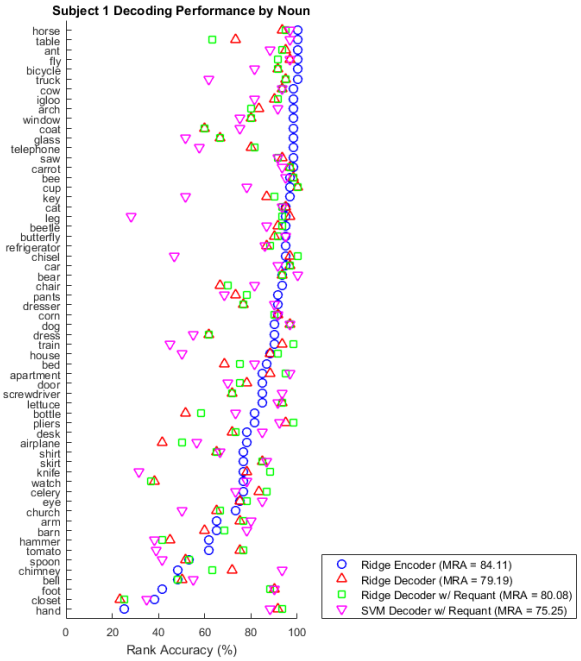

Figure 3: Per-noun RA using block-averaged neural features for S1 (best performer). Nouns are listed in order of descending RA by the Ridge Encoder.

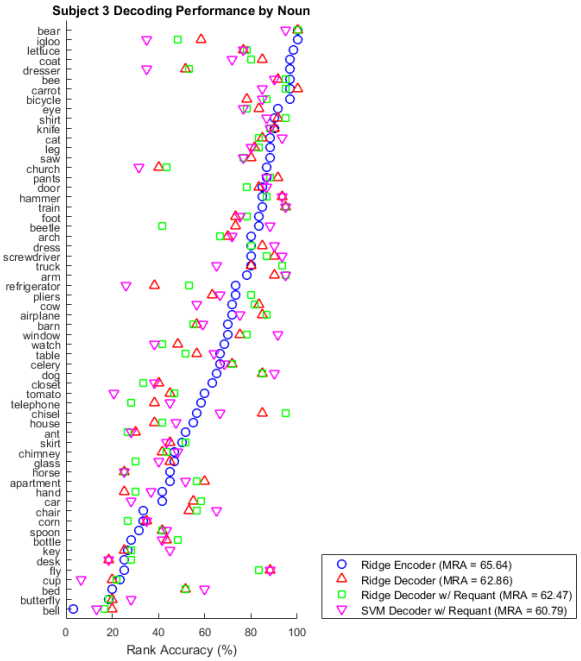

Figure 4: Per-noun RA using block-averaged neural features for S3 (worst performer). Nouns are listed in order of descending RA by the Ridge Encoder.

set size. In [8], the SVM was applied to visual features extracted from a set of 75,489 images belonging to 57 classes – a much larger data set than what was considered in this study. It is possible that the smaller training set may be bolstered by use of a kernel function, but this introduces another tuning parameter which would need to be optimized for each attribute to avoid overfitting.

The SVM also assumes the training set is balanced between classes, so that maximizing the margin minimizes the classification error. However, of the 218 attributes, only 50 had reasonable balance between the re-quantized classes $s = -1, s = 0,$ and $s = 1$. We attempted to soften this assumption by weighting the SVM cost parameter (c) proportionally to the size of each class, but the effect was negligible. One could soften the balanced-class assumption further by optimizing c for each attribute, but that was not explored in this study.

Several aspects of this work suggest that some form of a semantic BCI may be viable. First, we demonstrated that the semantic zero-shot learning approach to semantic decoding can be fruitfully applied to ECoG using encoding or decoding models. As pointed out in [5], "It is intractable to collect neural training images for every possible word in English, so to build a practical neural decoder we must have a way to extrapolate to recognizing words beyond those in the training set." Our study only focused on the ability to classify among 60 zero-shot nouns, and the problem will become more difficult as the scale increases to more classes, especially when the attribute-to-noun mapping is ambiguous or completely unknown. In such cases, simply outputting the most highly-weighted semantic attributes may still be useful for communicating a novel word or concept.

One issue that would need to be addressed is collection of adequate training data, which can be time consuming and costly. But efforts in fMRI demonstrating how voxel-wise models can be built from large datasets of activity elicited by natural stimuli, like movies and stories, suggests these might be more economical strategies for collecting training data [17, 18]. Furthermore, efforts in large-scale pattern classification using semantic hierarchies to trade specificity for accuracy suggest a potential avenue towards robust classification of a wide variety of novel classes [19].

Another obstacle that must be overcome in developing a practical semantic BCI is consistency in real-time decoding performance. While the highest MRAs were achieved when averaging across multiple trials, there was a modest drop (< 10%) in performance when decoding nouns or categories from single trials. In addition, our encoding model did not account for temporal variability in semantic processing, as our features were extracted from fixed time windows post stimulus onset. However, the superior performance observed for the encoding model implies that accurate real-time decoding may be possible by cross-correlating a recorded neural signal against a pre-computed lookup table of signals predicted from various combinations of attributes.

CONCLUSION

Four approaches to zero-shot stimulus prediction were compared for predicting recognized objects from ECoG signals evoked during a picture-naming task. All four approaches attempt to learn a mapping between neural

Published by Verlag der TU Graz
Graz University of Technology

 DOI: 10.3217/978-3-85125-533-1-78

features and semantic attributes, but differ in what they consider to be the direction of the mapping and in how the mapping is learned from training data. Performance was relatively consistent from subject to subject between the four approaches, though in most cases the Ridge Regression Encoding model yielded the best performance. These results represent an initial step toward realizing semantic BCI, and suggest that the next generation of neuroimaging technologies paired with the algorithms demonstrated here could help new BCI applications to come to fruition.

REFERENCES

[1] Anderson NR, Blakely T, Schalk G, Leuthardt EC, Moran DW. Electrocorticographic (ECoG) correlates of human arm movements. Experimental Brain Research 2012; 223(1): 1-10

[2] Martin D, Brunner P, Holdgraf C, Heinze HH, Crone NE, Rieger J, et al. Decoding spectrotemporal features of overt and covert speech from the human cortex. Frontiers in Neuroengineering 2014; 7(14)

[3] Rosch E. Principles of Categorization. In: Cognition and Categorization, Erlbaum Associates, Hillsdale NJ, 1978, pp. 27-48

[4] Mitchell TM, Shinkareva SV, Carlson A, Chang K-M, Malave V, Manson R, et al. Predicting Human Brain Activity Associated with the Meanings of Nouns. Science 2008; 320(5880): 1191-1195

[5] Palatucci M, Pomerleau D, Hinton GE, Mitchell TM, Zero-shot learning with semantic output codes, in Proc. NIPS, Vancouver, Canada, 2009.

[6] Sudre G, Pomerleau D, Palatucci M, Wehbe L, Fyshe A, Salmelin R, et al. Tracking neural coding of perceptual and semantic features of concrete nouns. NeuroImage. 2012; 62(1): 451-463

[7] Pereira F, Botvinick M, Detre G. Using Wikipedia to learn semantic feature representations of concrete concepts in neuroimaging experiments. Artificial Intelligence 2013; 194: 240-252

[8] Burlina P, Schmidt AC, Wang I-J. Zero shot deep learning from semantic attributes, in Proc. ICMLA, Miami, USA, 2015.

[9] Colwell KA, Collins LM. Attribute-driven transfer learning for detecting novel buried threats with ground-penetrating radar, in Proc. SPIE Defense + Security, Baltimore, USA, 2016

[10] Rupp K, Roos M, Milsap G, Caceres C, Ratto C, Chevillet M, et al. Semantic attributes are encoded in human electrocorticographic signals during visual object recognition. NeuroImage 2017; 148: 318-329

[11] Fazel-Rezai R, Allison BZ, Guger C, Sellers EW, Kleih SC, Kubler A. P300 brain computer interface: current challenges and emerging trends, Frontiers in Neuroengineering 2012; 5(14)

[12] Sajda P, Pohlmeyer E, Wang J, Parra L, Christoforou C, Dmochoski J, et al. In a blink of an eye and a switch of a transistor: cortically coupled computer vision. Proc. IEEE 2010; 98(3): 462-478

[13] Khosla D, Bhattacharyya R, Tasinga P, Huber DJ. Optimal detection of objects in images and videos using electroencephalography (EEG), in Proc. SPIE Defense, Security, and Sensing, Orlando, USA, 2011

[14] Vansteensel M, Pels EGM, Bleichner MG, Branco MP, Denison T, Freudenburg ZV, et al. Fully Implanted Brain-Computer Interface in a Locked-In Patient with ALS, N Engl J Med 2016; 375: 2060-2066

[15] Quitadamo LR, Cavrini F, Sbernini L, Riillo F, Bianchi L, Seri S, et al. Support vector machines to detect physiological patterns for EEG and EMG-based human–computer interaction: a review. Journal of Neural Engineering 2017; 14(4)

[16] Fan R-E, Chang K-W, Hsieh C-J, Wang X-R, Lin C-J. LIBLINEAR: A library for large linear classification. Journal of Machine Learning Research 2008; 9: 871-1874

[17] Huth AG, Nishimoto S, Vu AT, Gallant JL. A continuous semantic space describes the representation of thousands of object and action categories across the human brain. Neuron 2012; 76(6): 1210-1224

[18] Wehbe L, Murphy B, Talukdar P, Fyshe A, Ramdas A, Mitchell T. Simultaneously uncovering the patterns of brain regions involved in different story reading subprocesses. PLoS ONE 2014: 9(11)

[19] Deng J, Krause J, Berg A, Fei-Fei L. Hedging your bets: optimizing accuracy-specificity trade-offs in large scale visual recognition, in Proc. IEEE CVPR, Providence, USA, 2012

Published by Verlag der TU Graz
Graz University of Technology

Proceedings of the
7th Graz Brain-Computer Interface Conference 2017 DOI: 10.3217/978-3-85125-533-1-79

THE BRAINHACK PROJECT: ARTS MEETING BCI TECHNOLOGY

Angela Riccio[1], Aleksander Väljamäe[2], Jurre Ongering[3], Lucas Evers[3], Veronica Alfano[4], Sabine Roeser[4], Pavel Smentana[5], Mairéad Hurley[6], Irene Ingardi[7], MarcBoonstra[3], Louis Miguel Girao[7], Donatella Mattia[1] and Febo Cincotti[1,8]

[1]Neuroelectrical Imaging and BCI lab, Fondazione Santa Lucia, Roma
[2]School of Digital Technologies, Tallinn University
[3] Waag Society, Amsterdam
[4]Delft University of Technology, Delft
[5]T.S.R.ACT, Prague
[6]Science Gallery, Dublin
[7]Artshare, Aveiro
[8]Sapienza University of Rome, Italy

E-mail: a.riccio@hsantalucia.it

ABSTRACT: BrainHack is a Coordination and Support Action project funded by the European Commission with the goal of engaging the international artistic community experimenting with Brain Computer Interface (BCI) technologies and link it to the BCI scientific community. In this paper we reported on BrainHack activities, focused on two hackathons. The hackathons involved participants with a wide range of artistic and scientific backgrounds, successfully achieving the purpose of encouraging knowledge exchange in a multidisciplinary environment and creating a meeting point between Art and BCI technology. However some limits were identified in the scientific aspects of some of the projects, due to the obstacles encountered when dealing with BCI technology within a limited interval of time. Suggestions to go beyond such limits were inspired by the results of the interviews performed with participants, mentors and guest speakers.

INTRODUCTION

Studies on brain computer interface (BCI) published in the last decades were mostly focused on clinical applications. Within clinical applications, effort was made in developing BCI for providing new channels of communication for severely disabled persons [1], [2] and on rehabilitation, to improve motor function after stroke [3], [4]. Recently the reliability of EEG-based BCI systems improved, together with the interest of scientists in developing applications for healthy users.

Such applications aimed at enhancing human functions, allowing the monitoring of users' workload in operational contexts [5]–[7], decoding car drivers' error-related brain signals [8] or monitoring subjects affective/cognitive states [9]. Furthermore the interest in designing BCI applications related to the creation and the experience of Art has significantly grown [10]. Indeed, monitoring persons' affective cognitive state can be used to influence an application to modify an artistic environment (e.g. modifying animations and musifications) expressing users' emotions.

Within this approach BCI has been used to create music performance, modifying music in response of performer's and listener's affective state [11] or to perform collaborative sonification [12]. Brain-to-brain coupling between performer/s and spectator/s was also used as means of controlling audio-visual creative outputs [13]. Furthermore BCI was used to allow people with severe motor disability to express themselves through painting [14].

BrainHack is a Coordination and Support Action project funded by the European Commission, under the Horizon 2020 FET Open program (http://hackthebrain-hub.com). The main goal of BrainHack is to engage/organize the international artistic community experimenting with BCI technologies and link it to the BCI scientific community, to bring together interdisciplinary groups of artists, scientists (and developers) to mutually exchange knowledge on applications and implications of neuro-technology, to investigate if and how these groups develop new relevant insights, and to encourage discussion and reflection around ethical issues related to (artistic) applications of BCI.

BrainHack activities are centered around three hackathons over two years. Hackathons are problem-focused computer programming events, where people with different background collaborate intensively in a short period of time (usually 3-4 days) to develop an idea and make it a prototype. Within the BrainHack project hackathons represent an environment where ideas and knowledge are exchanged between artists and scientists: a collaboration space supporting the creation of new concepts. Results of an hackathon would be the production of codes, hardware, sculptures, wetware prototypes or speculative prototypes.

In this paper we will report about two hackathons which were organized by the BrainHack consortium. We will

Published by Verlag der TU Graz
Graz University of Technology

 DOI: 10.3217/978-3-85125-533-1-79

also report about the methods which were applied to evaluate the hackathons and to collect insights for the next ones.

MATERIALS AND METHODS

Hackathons

BrainHack consortium organized two (out of the three) hackathons in 2016. The third one will be held in Dublin (Science Gallery) in June 2017.

The first one took place in Amsterdam (Medieval Waag Society building), between the 24th and the 26th of June, and was titled "Hack yourself better (or worse)".

Participants had access to the FabLab and Open Wetlab facilities in the Waag building. FabLabs are digital fabrication laboratory, equipped with a range of digital manufacturing technologies, allowing people to turn their ideas into products. The Open Wetlab is a space for bio-art, bio-design and biotechnology.

The second hackathons was held in Prague, between the 2nd and the 4th of December 2016.

During both the hackathons, participants had access to a range of technologies: G-Tec g.Nautilus (g.tec medical engineering GmbH, Austria), SmartBCI (Novatech EEG), Open BCI (http://openbci.com/), Neurosky Mindwave http://store.neurosky.com/pages/mindwave), TMSI Mobita(http://www.tmsi.com/products/systems/item/mobita), Emotive Epoc (http://emotiv.com/epoc/), Necomimi(http://www.necomimi.com/), Muse(www.choosemuse.com).

A pre-event was organized one-month before each of the two hackathons, consisting in an event which lasted one evening and was aimed at stimulating participants' involvement and boosting their knowledge.

During the hackathons, participants worked in teams, and were involved in the implementation of a project in which art met BCI technology. Mentors with various backgrounds, supported them in planning and developing the projects. Mentors' backgrounds were cognitive scientists, neuroscientists, software developers, programmers, mathematicians, physicists, visual artists and film creators. Also scientists working in BCI field, neuroscientists, and experts in the connection between Art and Science, gave lectures during the three-day hackathons, in order to provide to participants an overview on the state of art in their respective fields.

Jury evaluation

A jury composed of experts in BCI research, neuroscience, art, philosophy and ethics was established. They evaluated the teams projects scoring them from 1 to 5, within 4 criteria: *i*) Artistic value (weight 40%), *ii*) Scientific value (weight 30%), *iii*) Level of maturity (weight 10%), *iv*) Novelty (Weight: 20 %).

Hackathon evaluation

In order to perform an evaluation of the hackathon, consortium members administered a structured (open) interview to mentors.

The interview was structured in different points regarding *i)* the importance of mentors' expertise in supporting participants during the hackathons, *ii)* the competences that the participants had and the competences that they developed during the hackathons, *iii)* which different expertise the hackathons would havebenefitted from among both the participants and the supervisors, *iv)* the awareness of participants about what they were working on and *v)* the quality of the interaction of the participants within and between the groups.

Ethics

Consortium members also conducted interviews about ethics. The interviews were aimed at gaining insight about the ethical aspects of BCI technologies, particularly regarding the role of Art in such field. The topics of privacy, intellectual autonomy, free will, personal identity, and technological determinism were addressed [15].

RESULTS

Hackathons participants

Sixty-two people attended the hackathon in Amsterdam. Eleven of them were consortium members and 53 people were an active part of the teams working at the projects. Within the participants the backgrounds of 37 of them were categorized as "scientist and/or developer expert" or "other" and 25 of them were categorized as "artists and developer expert". Artists background varied from fashion design, speculative design, media arts and sculpture. Scientists and developers backgrounds included philosophy, commercial BCI development, medical science, neuroscience and computer science. Eleven teams working at 11 projects were created.

Forty-seven people with a wide range of different backgrounds attended the Prague hackathon. Within the participants 16 of them were "software developer", 6 of them were artists, and 3 defined their background as in the between of Art and science, 11 were psychologists, 3 neuroscientists and 7 were classified as having "others background".

Interview

Four mentors were interviewed during the two hackathons. Their backgrounds were scientists/developers, neuroscientists and BCI experts. They were all very satisfied of the hackathon experience and of the role that they covered in the event. Results of the interviews showed that they considered their expertise relevant in supporting the participants in *i*) the initial process of brainstorming and creating a framework *ii*) merging technical processes, hardware and software, *iii*) clarifying computer science and

Published by Verlag der TU Graz
Graz University of Technology

 DOI: 10.3217/978-3-85125-533-1-79

programming concepts, *iv*) applying neurophysiology concepts to obtain BCI control.
Two mentors reported that the participants were initially unaware about science limitations i.e. what can be achieved with scientific methods in a limited time slot. In their opinion, during the hackathon, participants gained a greater awareness about "*the limitation of science*", and it was indeed one of the most valuable competence that the participants gained .
On the interaction between participants with different backgrounds, all the mentors reported that participants' backgrounds were complementary and allowed them to learn from each other, within and between the groups.
Mentors underlined as important factors for teams success *i)* the balance across members backgrounds (stated from all the interviewees) *ii)* the quality of the initial brainstorming on intention and ideas about the projects (stated from 2 interviewees). Weakness identified by the mentors were *i)* the low number of participants with an expertise in computer graphics, graphic design and visualization of data, to design accessible interfaces and highlight both the artistic and the scientific parts of the projects (stated from 1 interviewees) *ii*) the restricted number of participants with a background of neurophysiology applied to BCI (stated from 3 interviewees).

Projects
Seven teams participated at the Prague hackathon, each developing its own project. In a total of six projects 4 were dealing with the classification of attention/concentration and two with the classification of emotions. Artistic products in projects focused on concentration were *i*) virtual reality, visual and auditory animation based on theta activity, *ii*) sonification and virtual reality environment based on frontal alpha and beta and on theta activity in parietal lobe, *iii*) a sculpture representing a kinetic worm moving on the basis of frontal alpha modulation, *iv*) an environmental (visual and auditory) change aimed at maintaining high level of concentration, monitored classifying frontal lobe 12-18 Hz.
In the two projects dealing with emotions, it was developed *i*) a real-time video mirror to reflect the emotional state of the person (beta levels) and *ii)an* emotion detection device using frontal alpha asymmetry to influence the brightness of some LEDs, inserted in a polystyrene sculpture representing a head.
Advisory board members noted that almost everyone (except 1 team) described the EEG signals which were classified and half of the teams did it adequately in depth. Three teams used a standard, scientific tools to induce emotions (affective pictures database) and one project had scientific and real-life potential. However some of the projects did not go beyond the traditional applications, and advisory board members noted a lack of knowledge of neuroscience state of art.

Ethics
Fifteen interviews about ethics were conducted with hackathon mentors, guest speakers, and participants. Interesting patterns of convergence and divergence emerged. There was a good deal of disagreement about to what extent BCI technologies can provide us with a new kind of self-insight or self-awareness; many interviewees have mentioned the paradoxical way in which Art can teach lessons (about curiosity, about critical thinking) by refusing to teach overt lessons; there has been a fascinating discussion about the fact that field-based constraints can actually generate creativity, with the caveat that overcoming those constraints through collaboration can also be extremely fruitful.

DISCUSSION

In this paper we reported about the BrainHack project objectives. Two hackathons were organized within the project, which involved a total of 109 participants organized in 17 teams. Methods utilized to obtain feedback and ethics insight collection, were reported.
The hackathons attracted people with different backgrounds. Artists' backgrounds varied from fashion design to performance, speculative design, media arts, sculpture and design. Scientists had a background varying from philosophy, commercial BCI development, medical science, neuroscience and computer science. Therefore hackathons successfully achieved the purpose of involving people with different expertise, encouraging the knowledge exchange in a multidisciplinary environment and creating a meeting point between Art and BCI technology. Also the members of the advisory board underlined the positive results of the hackathons in terms of multidisciplinary, and quality of some of the projects developed.
However some limits were identified in the scientific aspects of some projects. Mentors noted that working on a project dealing with BCI in a limited interval of time (3-days hackathon), presents some weakness in identifying the features to be extracted to train the classifier, and obtain an online feedback (mentor interview).
In order to improve the hackathons quality, the following solutions were identified. Given the complexity of transferring BCI methodology to Art, e.g. using the online classification of cognitive emotional states, a starting point would consists in concentrating introductory lectures on neurophysiology and BCI methodologies, and in increasing the number of mentors with this background.
Also participants could be encouraged to identify and communicate their interests in advance (topics on which they would like to work), so that pre-existing algorithms could be shared by the hackathon organizer on a common platform. Such algorithms could be used by the participants, who would have more time for working on a final product, without focusing too long on details

Published by Verlag der TU Graz
Graz University of Technology

 DOI: 10.3217/978-3-85125-533-1-79

CONCLUSION

From the ethical insight obtained by interviewing participants, mentors and speakers, about the interaction between Art and BCI, it can be speculated that because artists are not bound by the same practical limitations as are scientists, Art can function as a testing ground that explores the risks of new technologies without incurring their negative consequences: when an artwork elicits strong emotional reactions, it can spark public debate about controversial topics. Is there an ethical imperative to use the aesthetic realm in this way? How do we balance this imperative with the ideal of artistic freedom? Some Hackathon artists saw their role as entirely amoral, while some implied that Art's very detachment from moral duties is what enables those who encounter it to live a good life. For example, Art themed around BCI technology can increase audiences' capacity for empathizing with the disabled and/or expand ideas of "the human" to better account for disabled individuals.

ACKNOWLEDGMENT

This work has been supported by EU-funded FET-Open SCA project "BrainHack" (GA: 686987).

REFERENCES

[1] F. Schettini*et al.*, "Assistive Device With Conventional, Alternative, and Brain-Computer Interface Inputs to Enhance Interaction With the Environment for People With Amyotrophic Lateral Sclerosis: A Feasibility and Usability Study," *Arch. Phys. Med. Rehabil.*, vol. 96, no. 3, Supplement, pp. S46–S53, Mar. 2015.

[2] A. Riccio*et al.*, "Hybrid P300-Based Brain-Computer Interface to Improve Usability for People With Severe Motor Disability: Electromyographic Signals for Error Correction During a Spelling Task," *Arch. Phys. Med. Rehabil.*, vol. 96, no. 3, Supplement, pp. S54–S61, Mar. 2015.

[3] F. Pichiorri*et al.*, "Brain–computer interface boosts motor imagery practice during stroke recovery," *Ann. Neurol.*, vol. 77, no. 5, pp. 851–865, May 2015.

[4] G. Morone*et al.*, "Proof of principle of a brain-computer interface approach to support poststroke arm rehabilitation in hospitalized patients: design, acceptability, and usability," *Arch. Phys. Med. Rehabil.*, vol. 96, no. 3 Suppl, pp. S71-78, Mar. 2015.

[5] T. O. Zander and C. Kothe, "Towards passive brain–computer interfaces: applying brain–computer interface technology to human–machine systems in general," *J. Neural Eng.*, vol. 8, no. 2, p. 025005, 2011.

[6] B. Blankertz*et al.*, "The Berlin Brain-Computer Interface: Progress Beyond Communication and Control," *Front. Neurosci.*, vol. 10, p. 530, 2016.

[7] P. Aricò, G. Borghini, G. Di Flumeri, A. Colosimo, S. Pozzi, and F. Babiloni, "A passive brain-computer interface application for the mental workload assessment on professional air traffic controllers during realistic air traffic control tasks," *Prog. Brain Res.*, vol. 228, pp. 295–328, 2016.

[8] H. Zhang, R. Chavarriaga, Z. Khaliliardali, L. Gheorghe, I. Iturrate, and J. d R. Millán, "EEG-based decoding of error-related brain activity in a real-world driving task," *J. Neural Eng.*, vol. 12, no. 6, p. 066028, Dec. 2015.

[9] A.-M. Brouwer, T. O. Zander, J. B. F. van Erp, J. E. Korteling, and A. W. Bronkhorst, "Using neurophysiological signals that reflect cognitive or affective state: six recommendations to avoid common pitfalls," *Front. Neurosci.*, vol. 9, p. 136, 2015.

[10] A. Nijholt and C. S. Nam, "Arts and Brain-Computer Interfaces (BCIs)," *Brain-Comput. Interfaces*, vol. 2, no. 2–3, pp. 57–59, Apr. 2015.

[11] J. Eaton, D. Williams, and E. Miranda, "The Space Between Us: Evaluating a multi-user affective brain-computer music interface," *Brain-Comput. Interfaces*, vol. 2, no. 2–3, pp. 103–116, Apr. 2015.

[12] G. Leslie and T. Mullen, *MoodMixer: EEG-based Collaborative Sonification.* 2011.

[13] P. Zioga, P. Chapman, M. Mae, and F. Pollick, "A Hypothesis of Brain-to-Brain Coupling in Interactive New Media Art and Games Using Brain-Computer Interfaces," in *Serious Games*, 2015, pp. 103–113.

[14] E. M. Holz, L. Botrel, T. Kaufmann, and A. Kübler, "Long-term independent brain-computer interface home use improves quality of life of a patient in the locked-in state: a case study," *Arch. Phys. Med. Rehabil.*, vol. 96, no. 3 Suppl, pp. S16-26, Mar. 2015.

[15] S.Roeser, V.Alfano and C. Nevejan "The Role of Art in Emotional-Moral Reflection on Risky and Controversial Technologies: The Case of BNCI" (in press).

Published by Verlag der TU Graz
Graz University of Technology

Proceedings of the
7th Graz Brain-Computer Interface Conference 2017 DOI: 10.3217/978-3-85125-533-1-80

DISCRETE MOTOR IMAGERIES CAN BE USED TO ALLOW A FASTER DETECTION

S. Rimbert[1,2,3], O. Avilov[4,1,2,3], and L. Bougrain[2,1,3]

[1]Neurosys team, Inria, Villers-lès-Nancy, F-54600, France
[2]Artificial Intelligence and Complex Systems, Université de Lorraine, LORIA, UMR 7503, Vandœuvre-lès-Nancy, F-54506, France
[3]Neurosys team CNRS, LORIA, UMR 7503, Vandœuvre-lès-Nancy, F-54506, France
[4]Electronic Dept., National Technical University of Ukraine "Igor Sikorsky Kyiv Polytechnic Institute", Kyiv, Ukraine

E-mail: sebastien.rimbert@inria.fr

ABSTRACT: Motor imagery (MI) modulates the neural activity within the primary sensorimotor areas of the cortex and can be observed through the analysis of electroencephalographic (EEG) recordings. It is particularly interesting for Brain-Computer Interface (BCI) applications. In most MI-based BCI experimental paradigms, subjects realize continuous motor imagery (CMI), i.e. a repetitive and prolonged intention of movement, for a few seconds. The system detects the movement based on the *event-related desynchronization* and the *event-related synchronization* features in electroencephalographic signal. Currently, improving efficiency such as detecting faster a motor imagery is an important issue in BCI to avoid fatigue and boredom. The purpose of this study is to show the difference, in term of classification, between a discrete motor imagery, i.e. a single short MI, and a CMI. The results of experiments involving 16 healthy subjects show that a BCI based on DMI is as effective as a BCI based on CMI and could be used to allow a faster detection.

INTRODUCTION

Motor imagery (MI) is the ability to imagine performing a movement without executing it [1]. According to Jeannerod [2], MI represents the result of conscious access to the content of the intention of a movement, which is usually performed unconsciously during movement preparation [3]. MI has two different components, namely the visual-motor imagery and the kinesthetic motor imagery (KMI) [4]. KMI generates an *event-related desynchronization* (ERD) and an *event-related synchronization* (ERS) in the contralateral sensorimotor area, which is similar to the one observed during the preparation of a real movement (RM) [5]. More precisely, compared to a resting state taken before a motor imagery, several power modulations are observed in in the alpha (8-12 Hz) and in the beta (18-25 Hz) bands of the electroencephalographic signal measured over the sensorimotor area corresponding to the body part involved in the motor imagery. Firstly there is a gradual power decrease in the alpha and in the beta bands, called ERD. Secondly, a low power level is maintained during the movement. Finally, from 300 to 500 milliseconds after the end of the motor imagery, there is a power increase called ERS or post-movement beta rebound with a duration of about one second. Although several studies showed an activity uniquely in the contralateral area [6], other studies showed that ERD and ERS are also in the ipsilateral area [7].

Emergence of ERD and ERS patterns during and after a MI has been intensively studied in the *Brain-Computer Interface* (BCI) domain [8] in order to define detectable commands for the system. Hence, a better understanding of these processes could allow for the design of better interfaces between the brain and a computer system. Additionally, they could also play a major role where MI are involved such as rehabilitation for stroke patients [9], monitoring consciousness during general anesthesia [10] or the recovery of the motor capacity after neurological damage. For example MI training is a promising approach in facilitating paretic limb recovery.

Currently, most of the paradigms based on MIs require the subject to perform the imagined movement several times for a predefined duration of a few seconds. In this study, such a task is commonly referred to as a continuous motor imagery (CMI). However, first the duration of the experiment is long. Second a succession of flexions and extensions generate an overlapping of ERD and ERS patterns making the signal less detectable. In fact, one simple short MI, referred in this article as a discrete motor imagery (DMI), could be more useful for two reasons. Firstly, a DMI could be used to combat fatigue and boredom for BCI users improving ERD and ERS production [11]. Secondly, the ERD and ERS generated by the DMI could be detectable at a higher quality and more rapidly compared to a CMI. This was found in a previous study that established a relationship between the duration of the MI and the quality of the ERS extracted [12]. It also showed that a brief MI (i.e. a 2-seconds MI) could be more efficient then a sustained MI. Our main hypothesis is that a DMI generates robust ERD and ERS patterns

Published by Verlag der TU Graz
Graz University of Technology

 DOI: 10.3217/978-3-85125-533-1-80

which could be detectable by a BCI system. Results indicate that a DMI produces a robust ERS and is as detectable as a CMI.

MATERIALS AND METHODS

Participants: 16 right-handed healthy volunteer subjects took part in this experiment (9 men and 7 women, from 19 to 43 years old). They had no medical history which could have influenced the task such as diabetes, peripheral neuropathology, renal insufficiency, anti-depressant treatment or motor problem. All subjects gave their agreement and signed an information consent form approved by the ethical INRIA committee before participating. This experiment follows the statements of the WMA declaration of Helsinki on ethical principles for medical research involving human subjects [13].

Real movement: The first task consisted of an isometric flexion of the right index finger on a computer mouse. A low frequency beep indicated when the subject had to execute the task. The right-click is recorded as a trigger and has allowed to know exactly when the participant executes the RM.

Discrete imagined movement: The second task was a DMI of the previous real movement. A low frequency beep indicated when the subject has to execute the task.

Continuous imagined movement: The third task was a CMI during four seconds of the real movement of the first task. More precisely, the subject imagined several (around four) flexions and extensions of the right index finger. This way, the DMI differed from the CMI by the repetition of the imagined movement. For this task, two beeps, respectively with low and high frequencies, separated by a four second delay, indicated the beginning and the end of the CMI.

Protocol: Each of the three tasks introduced in section corresponds to a session. The subjects completed three sessions during the same day. All sessions were split into several runs. Breaks of a few minutes were planned between sessions and between runs to avoid fatigue. Before each session, the task was described, and the subject practiced the tasks. At the beginning of each run, the subject was told to relax for 30 seconds. Condition 1 corresponded to RMs was split into 2 runs of 50 trials. Conditions 2 and 3 corresponded to discrete and continuous imagined movements, respectively, was split into 4 runs of 25 trials. Thus, 100 trials were performed by subjects for each task. Each experiment began with condition 1 as session 1. Conditions 2 and 3 were randomized to avoid possible bias cause by fatigue, gel drying or another confounding factor. For conditions 1 and 2, the timing scheme of a trial was the same: one low frequency beep indicated the start followed by a rest period of 12 seconds. For condition 3, a low frequency beep indicated the start of the MI to do during 4 seconds, followed by a rest period of 8 seconds. The end of the MI is announced by a high frequency beep (Fig. 1).

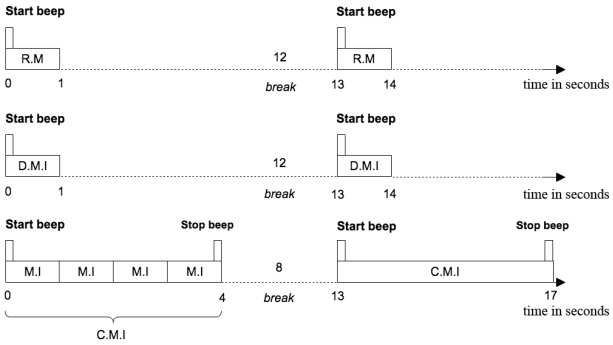

Figure 1: Timing schemes of a trial for each task: Real Movement (RM, top); Discrete Motor Imagery (DMI, middle); Continuous Motor Imagery (CMI, bottom). The DMI and CMI sessions are randomized.

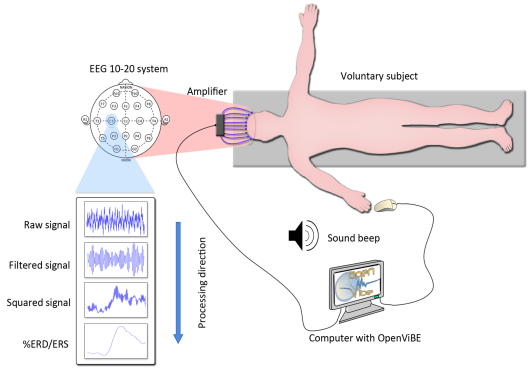

Figure 2: Schematic representation of the experiment. A low frequency beep indicates the start of the (real or imagined) movement. A high frequency beep indicates the end of the continuous imagined movement. Depending on the task, the subject presses or imagines pressing the button of the mouse.

Behavioral data: A custom-written scenario for OpenViBE [14] was designed to automate the generation of beeps, and to record triggers and EEG signals. The triggers corresponding to the right-click allowed us to detect potential behavioral errors. All non realized movement were removed from the analysis. For all three tasks, we used a fixed preparatory period duration in which the subjects could anticipate the GO signal.

EEG data: EEG signals were recorded through the OpenViBE platform with a commercial REFA amplifier developed by TMS International. The EEG cap was fitted with 9 passive electrodes re-referenced with respect to the common average reference across all channels over the extended international 10-20 system positions to cover the primary sensorimotor cortex. The selected electrodes are FC3, C3, CP3, FCz, Fz, CPz, FC4, C4, CP4. No additional filtering was used during the recording. Skin-electrode impedances were kept below 5 kΩ. Incorrect trials were removed from the analyses.

ERD/ERS patterns: To evaluate more precisely the modulation produced by the tasks, we computed the ERD/ERS% using the “band power method” [5] with

Published by Verlag der TU Graz
Graz University of Technology

 DOI: 10.3217/978-3-85125-533-1-80

a matlab code. First, the EEG signal is filtered between 8-30 Hz (Alpha+Beta) for all subjects using a 4th-order Butterworth band-pass filter. Then, the signal is squared for each trial and averaged over trials. Then it is smoothed using a 250-millisecond sliding window with a 100 ms shifting step. We have chosen a specific sliding window because the nature of the real and imagined movement, as well as the components ERD/ERS that underline them, require a short window. Finally, the averaged power computed for each window was subtracted and then divided by the averaged power of a baseline corresponding to 2 seconds before each trial. Finally, the averaged power computed for each window was subtracted and then divided by the averaged power of a baseline corresponding 2 seconds before each trial. This transformation was multiplied by 100 to obtain percentages. This process can be summarized by the following equation:

$$ERD/ERS\% = \frac{\overline{x^2} - \overline{BL^2}}{\overline{BL^2}} \times 100 \ , \qquad (1)$$

where $\overline{x^2}$ is the average of the squared signal over all trials and samples of the studied window, $\overline{BL^2}$ is the mean of a baseline segment taken at the beginning of the corresponding trial, and ERD/ERS% is the percentage of the oscillatory power estimated for each step of the sliding window. It is done for all channels separately.
ERD and ERS are difficult to observe from the EEG signal. Indeed, an EEG signal expresses the combination of activities from several neuronal sources. One of the most effective and accurate techniques used to extract events is the average technique [15]. We decided to use this technique to represent the modulation of power of the Alpha+Beta rhythms for three tasks (Real Movement, Discrete Motor Imagery and Continuous Motor Imagery).

Common Spatial Pattern: We used the algorithm called Common Spatial Pattern (CSP) to extract motor imagery features from EEG signals; this generated a series of spatial filters that were applied to decompose multi-dimensional data into a set of uncorrelated components [16]. These filters aim to extract elements that simultaneously maximize the variance of one class, while minimizing the variance of the other one.

Feature extraction and linear discriminant analysis: We trained a linear discriminant classifier to distinguish the features of motor imageries from the ones of a resting state. We applied the common spatial pattern algorithm to obtain 3 pairs of linear combinations from the 8-30 Hz filtered EEG signals. Then for each linear combinations we computed the logarithm of the variance for a studied window. We considered a 2 seconds window taken 3 seconds before the GO signal for the resting state. The 1 second window before the GO signal is not taken into consideration because the beep can generate an audio ERP and the subject usually prepares the movement in advance. So it not really a resting state. The features of a DMI is computed from 0.2 to 1 second after the GO signal (Fig. 5, Tab. 1). The features of a CMI is computed from 0.2 to 3 seconds after the GO signal (Fig. 5, Tab. 1).

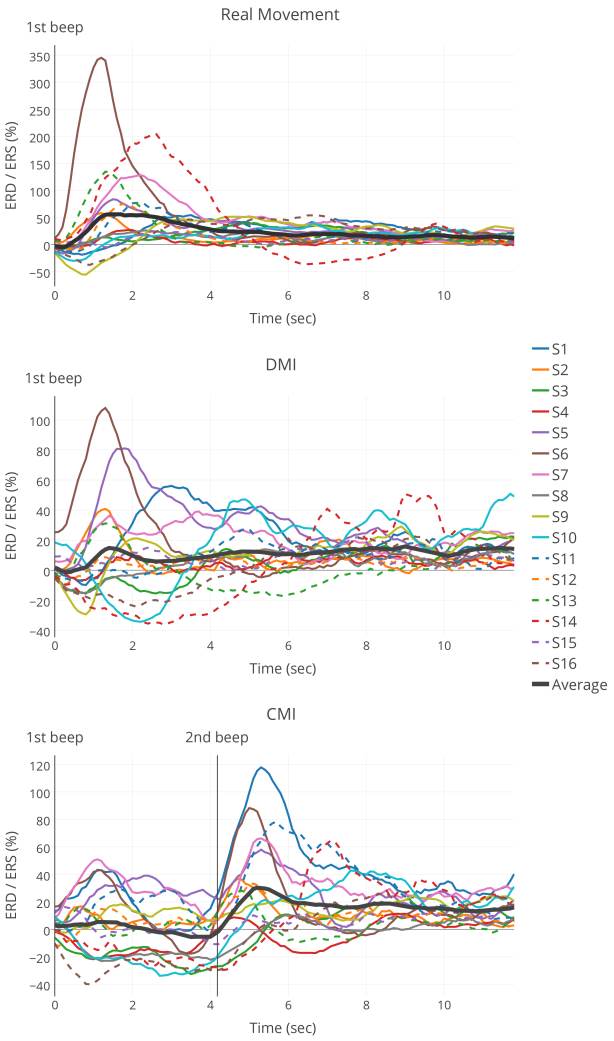

Figure 3: Grand average ERD/ERS% curves (in black, Average) estimated for the RM, the DMI and the CMI within the alpha + beta band (8-30 Hz) for electrode C_3. The average for each subject is also presented. A first beep indicated the start of the (real or imagined) movement. A second beep indicated the end of the continuous imagined movement.

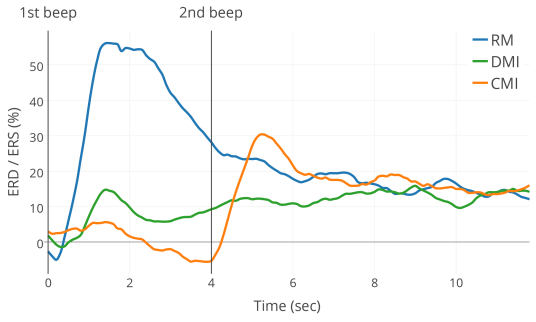

Figure 4: Grand average ERD/ERS% curves estimated for the RM (blue), the DMI (green) and the CMI (orange) within the alpha + beta band (8-30 Hz) for electrode C_3. A first beep indicated the start of the (real or imagined)

Published by Verlag der TU Graz
Graz University of Technology

 DOI: 10.3217/978-3-85125-533-1-80

movement. A second beep indicated the end of the continuous imagined movement.

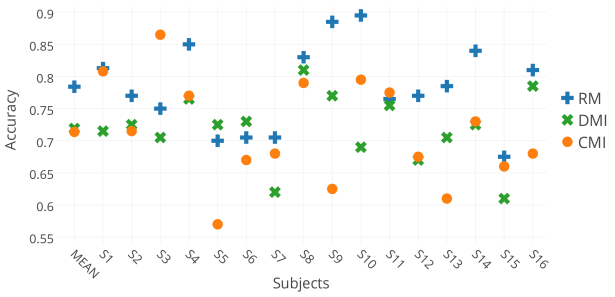

Figure 5: Accuracies obtained by linear discriminant analyses for the 3 conditions (RM, CMI and DMI). The features of a RM and DMI are computed from 0.2 to 1 second after the GO signal. The features of a CMI are computed from 0.2 to 3 seconds after the GO signal.

Table 1: Grand average accuracies obtained by linear discriminant analyses for the 3 conditions (RM, CMI and DMI) and 3 frequency bands (alpha, beta and alpha + beta).

	Frequency Bands		
	Alpha	**Beta**	**Alpha+Beta**
	8-12 Hz	18-25 Hz	8-30 Hz
RM	75,3 ± 6,17	73,8 ± 6,1	**78,4 ± 6,67**
DMI	70,4 ± 5,5	71,2 ± 3,6	71,9 ± 5,4
CMI [0.2-3s]	68,8 ± 5,6	71,2 ± 6	71,4 ± 8,15
CMI [0.2-1s]	68,1 ± 5,25	68,4 ± 5,8	70,625 ± 6,1

RESULTS

To prove the usability of a DMI in BCI-domain, firstly we computed ERD and ERS patterns to study the relative power (8-30 Hz) for the electrode C3. Secondly, we verified the detectability of a DMI in calculating classification rate.

ERD and ERS modulation: To verify if a DMI generates ERD and ERS patterns which could be detectable by a CMI, we studied the relative power (8-30 Hz) for the electrode C3. Electrode C3 is suitable for monitoring right hand motor activity. A grand average was calculated over the 16 subjects. We used a Friedman's test to analyze whether ERS were significantly and respectively different during the three conditions. Due to eyes-closed experiment, the alpha band is disturbed (confirmed by the time-frequency analysis) and not considered for this study. Consequently values corresponding to the desynchronization during the real and imagined movements will appear smaller. Moreover a visual inspection of time-frequency analysis shown modulations of alpha + beta power between 8-30 Hz for all the 16 subjects (Fig. 3).

ERD and ERS modulation during/after a real movement: The ERD/ERS% averages (Fig. 4) indicate that one second after the cue, the power in the 8-30 Hz band increases by around 60%, reaches its maximum and returns to the baseline 7 seconds after. The evolution from ERD to ERS is rapid (less than one second) and should be linked to the type of movement realized by the subjects. Interestingly, each subject (except Subject 9 and Subject 16) has the same ERD/ERS% profile (i.e. a strong rebound) after the real movement (Fig. 3).

ERD and ERS modulation during/after a discrete motor imagery: The ERS post-DMI reaches 18% which is weaker compare to the other tasks (Fig. 4). Some subjects (S1, S2, S5, S6, S10) have a stronger robust ERS produced by DMI while others have no beta rebound. Some subjects (S9, S10, S15) have a strong ERD after the task (Fig. 3). This variability between subjects could explain the weakness of the ERS post-DMI. The presence of ERD and ERS during/after a DMI suggest that a DMI could be used in BCI-domain.

ERD and ERS modulation during/after a continuous motor imagery: During the CMI, the subjects imagined several movements in a time window of 4 seconds. Fig. 4 shows a global decrease of activity during the CMI and stronger modulation in 8-30 Hz after the CMI. The results of the grand average shows a low desynchronization during this time window. It is interesting to note that some subjects (S7, S9, S11) have no desynchronization during the CMI task and could have a negative effect on the classification phase. Other subjects (S2, S15) have a different profile which shows that a first ERS is reached one second after the beginning of the CMI, then the power increases and decreases again, being modulated during 3 seconds. Indeed, this global ERD can be considered as the concatenation of several ERDs and ERSs due to the realization of several MIs. The variability between subjects during this period could also have a negative effect on the classification rate.

Detection results: Discrete motor imageries generate robust ERD and ERS (see previous section). In this section, we will study if they are detectable enough to have a faster detection in BCI than using continuous motor imageries. For each subject, 4 runs of 25 trials were available. The process of the cross validation consisted in using trials of 3 runs for train classifier and 1 run for test it. Four permutations were possible and we averaged accuracies obtain by the 4 classifiers on their testing run for a better evaluation. This method of cross validation was chosen because of its proximity to online condition. Figure 5 presents the accuracy for each subject and the mean accuracy. The mean accuracy for RM, DMI and CMI are respectively 78,4%, 71,9% and 71,4%. The detection of real movement is easier than the one of motor imageries. The difference between the two motor imageries is not statistically significant at a level of 5%. The precision of the ME is 0,78 (22% of false positive) and the recall is 0.79. The precision of the DMI is 0.71 (29% of false positive) and the recall is 0.74. The precision of the CMI is 0,73 (27% of false positive) and the recall is 0,68. Interestingly, some subjects (S5, S6, S9, S16) have a better

Published by Verlag der TU Graz
Graz University of Technology

 DOI: 10.3217/978-3-85125-533-1-80

detection for the DMI task. In Tab. 1, we computed the grand average of accuracies for the three conditions (RM, DMI and CMI) for three frequency bands (alpha, beta and alpha + beta). It appears that the 8-30 Hz frequency band increases the classification rate. Furthermore, the comparison of the classification rate between a DMI and a CMI on the same period (0.2s-1s) shows an equivalence.

DISCUSSION

The subjects carried out voluntary movements, DMI and CMI of an isometric flexion of the right hand index finger. Results show that the power in the 8-30 Hz band is modulated during the three tasks. The comparison between ERSs suggests that subjects on average have a stronger ERS during a CMI than a DMI. However, this is not the case for all subjects. Furthermore, the detection rate for a DMI is as effective as for a CMI.

EEG system: It is well established that a large number of electrodes allows having a good estimation of the global average potential of the whole head [17]. Although we focused on specific electrodes, our results were similar by using method of the derivation, which corresponded with the literature. We chose to study C3 without derivation because we are interested in designing a minimal system to detect ERD and ERS during general anesthesia conditions.

ERD/ERS modulation during real movements: The results are coherent with previous studies describing ERD/ERS% modulations during motor actions. The weakness of the ERD can be linked to the instruction that was focused more on the precision than the speed of the movement [18]. However, although some subjects were making efforts to do a voluntary movement, we must consider that an isometric flexion movement on a mouse is a movement setting in the subject's memory. This can have an impact on the low ERD amplitude. We also showed that the rebound starts before the click. Since a mouse click, is a really fast movement, we expect that the beta rebound will appear fast as well [19].

ERS modulation during motor imageries: The results show that the ERS is lower after a DMI or a CMI than after a real movement, which has been already been demonstrated previously [20]. However, the novelty is the beta rebound is stronger on average after a CMI than DMI for a few subjects.

ERD modulation during continuous motor imagery: When the subjects performed the CMI, the ERD was highly variable during the first 4 seconds. For some subjects, our hypothesis is there are some intern-ERD and intern-ERS into this period. The difficulty is that the CMI involves several MI, that are not synchronized across trials, unlike the DMI which starts and ends at roughly the same time for each trial, due to the cue. Normally, for continuous real movement, the ERD was sustained during the execution of this movement [21]. However, in our data it is possible to detect several ERDs during the 4 seconds of CMI where the subject performed 4 MIs. This assumes that the ERD and ERS components overlap in time when we perform a CMI. Several studies already illustrate the concept of overlap of various functional processes constituting the beta components during RMs [22]. Moreover, the beta rebound generated by a median nerve stimulation is reduced when the stimulation is made during different types of real or imagined hand movements [23], [24]. However, even if the components cancel each other out in the signal, it does not mean that the operation of the underlying processes are similarly affected. This interpretation assumes implicitly that the components are combining each other, which means that the temporal superposition of an ERD and an ERS would result in an intermediate amplitude signal. This could explain why the ERD during a CMI could be less detectable and more varied than the ERD during a DMI. To validate this hypothesis, we plan to design a new study to explore how two fast-successive movements (or MIs) can affect the signal in the 8-30 Hz frequency band.

Detection rate: We showed that the detection of a real movement was easier than discrete and continuous motor imageries but we could discuss about the weakness of the classification rate for the three task. Usually, a real movement has often a high classification rate and it is not the case in this study. However, it is important to remind that the subject performed real movement, DMI and CMI of an isometric flexion of the right hand index finger. The rapidity and the precision of the three tasks could be linked with the low classification rate. One limitation of this study is that all trials of a type had the same length and was not randomized within a block.

Establishing a link between the ERD/ERS users profiles and the detection rate: Our study shows results which could allow to understand more differences, in term of ERD and ERS, between subjects. Indeed, we showed that for a same task (RM, DMI and CMI), for some subjects a strong ERS appeared whereas for some others, no ERS appeared. We observed the same phenomenon for ERD. It could be interesting to establish a link between the particular ERD/ERS users profiles and the detection rate. The importance of BCI users profiles, especially for patients with severe motor impairments has already been established by other studies [25]. This is why, we expect designing an adaptive BCI based on the specific motor activity of the motor cortex. More subjects are necessary to precise this BCI user profile.

CONCLUSION

This article examined the modulation of power (8-30 Hz) in EEG during a real movement, a discrete motor imagery (DMI) and a continuous motor imagery (CMI). We showed that during a real voluntary movement corresponding to an isometric flexion of the right hand index finger a low ERD appeared, and was followed by a rapid and powerful ERS. Subsequently, we showed that the ERD and ERS components were still modulated by both a DMI and a CMI. The ERS is present in both cases

Published by Verlag der TU Graz
Graz University of Technology

 DOI: 10.3217/978-3-85125-533-1-80

and shows that a DMI could be used in BCI domain. The classification results show no any difference between a CMI and a DMI and confirm that a DMI could have a future impact in BCI-domain to save time and avoid fatigue.

REFERENCES

[1] L. Avanzino, A. Giannini, A. Tacchino, E. Pelosin, P. Ruggeri, and M. Bove, "Motor imagery influences the execution of repetitive finger opposition movements, Neuroscience Letters, vol. 466, no. 1, pp. 11–15, 2009.

[2] M. Jeannerod, "Mental imagery in the motor context, Neuropsychologia, vol. 33, no. 11, pp. 1419–32, Nov 1995.

[3] M. Lotze and U. Halsband, Motor imagery, "JPhysiol Paris, vol. 99, no. 4-6, pp. 386–95, Jun2006.

[4] C .Neuper, R. Scherer, M. Reiner, and G. Pfurtscheller, "Imagery of motor actions:Differential effects of kinesthetic and visual motor mode of imagery in single-trial EEG, Cognitive Brain Research, vol. 25, no. 3, pp. 668 – 677, 2005.

[5] G. Pfurtscheller and F. H. Lopes da Silva, "Event-related eeg/meg synchronization and desynchronization: basic principles, Clin Neurophysiol, vol. 110, no. 11, pp. 1842–57, Nov 1999.

[6] G. Pfurtscheller and C. Neuper, "Motor imagery and direct brain-computer communication, Proceedings of the IEEE, vol. 89, no. 7, pp. 1123 –1134, July 2001.

[7] S. Fok, R. Schwartz, M. Wronkiewicz, C. Holmes, J. Zhang, T. Somers, D. Bundy, and E. Leuthardt, "An eeg-based brain computer interface for rehabilitation and restoration of hand control following stroke using ipsilateral cortical physiology. Conf Proc IEEE Eng Med Biol Soc, vol. 2011, pp. 6277–6280, 2011.

[8] E. W. W. Jonathan Wolpaw, Ed., Brain-Computer Interfaces: Principles and Practice. Oxford university press, 2012.

[9] A. J. Butler and S. J. Page, "Mental practice with motor imagery: evidence for motor recovery and cortical reorganization after stroke. Arch Phys Med Rehabil. , vol. 87, pp. S2–11, dec. 2006.

[10] Y. Blokland, J. Farquhar, J. Lerou, J. Mourisse, G. J. Scheffer, G.-J. van Geffen, L. Spyrou, and J. Bruhn, "Decoding motor responses from the eeg during altered states of consciousness induced by propofol, Journal of Neural Engineering, vol. 13, no. 2, p. 026014, 2016.

[11] M. Ahn and S. C. Jun, "Performance variation in motor imagery brain-computer interface: a brief review. J Neurosci Methods, vol. 243, pp. 103–110, Mar 2015.

[12] E. Thomas, J. Fruitet, and M. Clerc, "Investigating brief motor imagery for an erd/ers based bci. Conf Proc IEEE Eng Med Biol Soc, vol. 2012, pp. 2929–2932, 2012.

[13] A. World Medical, "World medical association declaration of helsinki: ethical principles for medical research involving human subjects. J Postgrad Med, vol. 48, no. 3, pp. 206–208, Jul-Sep 2002, kIE:KIE Bib: human experimentation.

[14] Y. Renard, F. Lotte, G. Gibert, M. Congedo, E. Maby, V. Delannoy, O. Bertrand, and A. Lécuyer, "Openvibe: An opensource software platform to design, test and use brain-computer interfaces in real and virtual environments, Presence : teleoperators and virtual environments, vol. 10, no. 1, 2010.

[15] R. Quiroga and H. Garcia, "Single-trial event-related potentials with wavelet denoising, Clinical Neurophysiology, vol. 114, no. 2, pp. 376–390, 2003.

[16] B. Blankertz, R. Tomioka, S. Lemm, M. Kawanaba, and K. Muller, "Optimizing spatial filters for robust EEG single-trial analysis [revealing tricks of the trade], IEEE Signal processing magazine, 2008.

[17] J.Dien, "Issues in the application of the average reference: review, critiques, and recommendations, "Behavior Research Methods, vol. 30, p. 34, 1998.

[18] B. Pastotter, F. Berchtold, and K.-H. T. Bauml, "Oscillatory correlates of controlled speed-accuracy tradeoff in a response-conflict task, Hum Brain Mapp, vol. 33, no. 8, pp. 1834–49, Aug 2012.

[19] L. M. Parkes, M. C. M. Bastiaansen, and D. G. Norris, "Combining eeg and fmri to investigate the post-movement beta rebound, Neuroimage, vol. 29, no. 3, pp. 685–96, Feb 2006.

[20] A. Schnitzler, S. Salenius, R. Salmelin, V. Jousmaki, and R. Hari, "Involvement of primary motor cortex in motor imagery: a neuromagnetic study. Neuroimage, vol. 6, no. 3, pp. 201–208, Oct 1997.

[21] N. Erbil and P. Ungan, "Changes in the alpha and beta amplitudes of the central eeg during the onset, continuation, and offset of long-duration repetitive hand movements. Brain Res, vol. 1169, pp. 44–56, Sep 2007.

[22] B. E. Kilavik, M. Zaepffel, A. Brovelli, W. A. MacKay, and A. Riehle, "The ups and downs of beta oscillations in sensorimotor cortex. Exp Neurol, vol. 245, pp. 15–26, Jul 2013.

[23] G. Pfurtscheller, M. Woertz, G. Muller, S. Wriessnegger, and K. Pfurtscheller, "Contrasting behavior of beta event-related synchronization and somatosensory evoked potential after median nerve stimulation during finger manipulation in man. Neurosci Lett, vol. 323, no. 2, pp. 113–116, Apr2002.

[24] S. Salenius, A. Schnitzler, R. Salmelin, V. Jousmaki, and R. Hari, "Modulation of human cortical rolandic rhythms during natural sensorimotor tasks, NeuroImage, vol. 5, no. 3, pp. 221–228, 1997.

[25] J. Hohne, E. Holz, P. Staiger-Salzer, K.-R. Muller, A. Kuber, and M. Tangermann, "Motor imagery for severly motor-impaired patients: Evidence for brain-computer interfacing as superior control solution, PLOS ONE, vol. 9, 2014.

Published by Verlag der TU Graz
Graz University of Technology

Proceedings of the
7th Graz Brain-Computer Interface Conference 2017 DOI: 10.3217/978-3-85125-533-1-81

MEASURING THE QUALITY OF 3D VISUALIZATIONS USING EEG: A TIME-FREQUENCY APPROACH

F. Shahbazi Avarvand[1], S. Bosse[1], G. Nolte[2],
T. Wiegand[1,3], W. Samek [1]

[1]Department of Video Coding & Analytics, Fraunhofer Heinrich Hertz Institute, Berlin, Germany
[2]Department of Neurophysiology and Pathophysiology, University Medical Center Hamburg-Eppendorf, Hamburg, Germany
[3]Image Communication Group, Technische Universität Berlin, Berlin, Germany

E-mail: forooz.shahbazi@hhi.fraunhofer.de, wojciech.samek@hhi.fraunhofer.de

ABSTRACT: In this study we have assessed the quality of experience objectively when vertical disparity is introduced in the stereoscopic presentation of images. Four different conditions including a cube in 2D and the same cube in 3D with and without vertical disparities are compared based on the EEG signals recorded from 17 subjects. Two different vertical disparity levels are studied. Event-related potentials (ERPs) corresponding to four conditions are compared in time-frequency domain. The results show an increase in beta power of the occipital region for the images with vertical disparity compared to the 3D image with no vertical disparity. An increase in beta power in this region correlates with an increase in the level of attention which in our case is caused by the vertical disparity component in the stereoscopic images.

INTRODUCTION

Stereoscopic imaging technologies are used since almost two centuries for inducing the illusion of visual depth by providing images from horizontally slightly shifted focal points to the two eyes of the observer [1]. In recent years, this technique became popular again in various application domains and is used to create or increase the impression of greater realism and immersion e.g. for entertainment, as in movies or computer games, or in data visualization. New application scenarios in virtual and augmented reality environments are in reach with the advent of market-ready head mounted displays such as the Oculus Rift. The imaging systems' quality experienced by the user is crucial for the success of these applications. One aspect driving the quality of experience for systems based on stereoscopy is visual comfort that can be severely impaired e.g. by accommodation/vergence conflicts, excessive binocular parallax, dichoptic errors and other factors [2]. As for most multimedia signals and their impairments, unfortunately, no reliable objective computational model is currently available. Therefore, assessing the perceived quality of imaging systems relies on behavioral tests. These tests are typically carried out as psychophysical judgment experiments, during which a subject has to rank the quality of a set of test stimuli by giving an overt response. Thus, the outcome of these tests is the result of a cognitive process of the subject. This leads to different drawbacks of this method: The ratings are highly variable across subjects and prone to subjective factors as bias, expectations and strategies. As such tests are exhaustive for the subject, participants' ratings may become unreliable over time and the duration of psychophysical quality assessment test should not take longer than 30 minutes [3]. Moreover, it is very difficult, if not impossible, to integrate this kind of behavioral procedure in real-time assessment of perceived quality.

To overcome these limitations, brain activity recordings for directly monitoring the users cognitive state have shown promising results recently. Electroencephalography (EEG) in particular is one of the easiest and most mobile devices to record brain signals and has been used to study neural correlates of perceived quality of multimedia, such as audio [4] and 2D [5, 6, 7, 8] and 3D video [9]. [10] and [11] provide a comprehensive overview on approaches to assessing perceived quality physiologically.

If the two focal points in a stereoscopic imaging system are not aligned vertically, vertical disparities occur alongside horizontal disparities. While the latter serve as depth cue, vertical disparities commonly cause visual discomfort experienced by the observer that can ultimately even lead to physical pain. In this paper we address the assessment of visual discomfort caused by vertical disparities using EEG. For that the brain signals recorded for two amounts of vertical disparity are compared to no vertical disparity and a 2D image on channel level in time-frequency domain. More detailed analysis of this data set with a focus on the ERP components is presented in [12]. The next section describes the experimental setup and explains the event-related potentials (ERPs) which are studied in time-frequency domain. The results show significant differences in time-frequency domain, more precisely larger beta power for occipital region in vertical disparity conditions. The results and discussion are presented in more details in the last two sections.

Published by Verlag der TU Graz
Graz University of Technology

 DOI: 10.3217/978-3-85125-533-1-81

METHODS

Experimental Setup: In an objective approach we have studied EEG features caused by the vertical disparity in stereoscopic images. The vertical disparity is simulated for a 3D image of a cube in which the right camera is shifted upwards relative to the left one. Two conditions are simulated in this way while the amount of vertical disparity in one condition (3D-2) is 40 % less than the other condition (3D-3). The cube is presented to the subjects in four different conditions in two categories of 2D and 3D, i.e. three images in 3D including two different 3D images with vertical disparity levels and one 3D image without vertical disparity. The same cube is also presented in 2D shown in Figure 1 a).

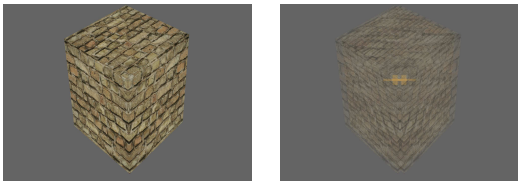

Figure 1: a) The cube is presented in 2D and in three different 3D conditions (3D, 3D-2 and 3D-3). b) A cross in 3D is presented in between the epochs as a pause interval. The cross is projected on the cube in this figure to show its exact location relative to the center of the cube.

Each image is presented randomly for 120 trials (epochs) for 4 seconds and between the images a cross is presented in 3D for an interval of 3 seconds. This interval is implemented for subjects to be able to rest their eyes and it helps to reduce the amount of ocular artifacts.
In Figure 1 b), the cross is projected on the cube to visualize the exact position of it relative to the cube. To keep the subjects attentive they were asked to do a task: they were supposed to press a button when an image of a cat was shown. 120 images of a dog (80%) and a cat (20%) appeared randomly among other stimuli between two fixation crosses. If the subject successfully hit the target image (cat) by a minimum 90% accuracy he/she was rewarded by 5 € extra. All subjects were rewarded for their participation by 8.5 € per hour. The horizontal angle of view is 20.76 degrees while the distance between the subject and the screen is 280 cm. The subjects wear 3D polarized glasses during the experiment. According to a previous study [13] polarized passive glasses tend to be more comfortable than the active shutter glasses. The experiment was conducted in a dimly lit and silent room. The 3D screen is JVC 3D LCD Monitor (model number: GD-463D10E). EEG signals are recorded by an actiCap from Brain Products GmbH with 64 active electrodes (Fp1,2, F1 to F8, FC2 to FC6, T7 and T8, C1 to C6, Cz, Tp7, Tp9 and Tp10, Pz, P1 to P8, PO3 and PO4, POz, PO7 to PO10, O1 and O2, Oz, AF3, AF4, AF7, AF8, FT7 to FT10, FC3 and FC4, CP3 and CP4, CPz, VEOG) and the impedance of electrodes was kept below 10 KΩ. 21 subjects have been recorded out of which 4 data sets have been excluded due to the low signal-to-noise values and high number of rejected trials. The data from 17 subjects, 6 male and 11 female, with the average age of 25.83 is analyzed. All subjects have been checked to have normal or corrected to normal vision and are tested for their 3D vision and gave informed consent. We have received a permission for the experiment in accordance with the declaration of Helsinki from the IRB of Technische Universität Berlin (TU Berlin).

Pre-processing of EEG data: EEG data is low-pass filtered below 30 Hz during the analysis besides the filter applied by the EEG amplifier hardware at 0.016 Hz. FCz was selected as the original reference electrode during the experiment and the data is re-referenced to the common average for the analysis. Muscle artifacts are removed from the data by removing the trials with the variance larger than a threshold. The baseline in the time interval between -200 ms, i.e. 200 ms before the stimulus onset and the stimulus onset is subtracted from the time course of each epoch. Ocular artifacts are removed by regression through projecting out part of the data which is correlated with EOG electrodes. For this purpose a short measurement was conducted before the experiment in which the subject was supposed to blink when a circle appeared on the screen. Meanwhile the vertical ocular activity was measured by an electrode underneath the right eye (VEOG) and Fp2. The horizontal ocular activity of the subjects was also recorded in a similar approach in which the subject was supposed to follow a circle on the screen which moved from the right end to the left end of the screen and vice versa. The difference between two electrodes, i.e. F7 and F8 is estimated as the horizontal component while the difference between Fp2 and VEOG is estimated as the vertical component. Part of the EEG data which is correlated with these two components is then projected out from the data. For more details on the method please refer to [14]. In an additional step epochs in which the difference between maximum and minimum amplitude exceeds 70 μV are rejected.

Event-related potentials: Part of the responses in EEG signals are phased-locked with the stimulus however with a very low signal to noise ratio due to the non-phase locked activities which are considered as noise when the focus is on the event-related potentials (ERP). EEG data is averaged over all trials to cancel out all non-phase-locked activities and therefore to increase the signal-to-noise ratio. The time window of this average is selected between 200 ms before the stimulus onset and 900 ms after that because the brain activity appeared not to be affected by the stimuli after 900 ms anymore. The BBCI toolbox, which is a Matlab-based toolbox [15], is used for the ERP analysis.
The ERP components might vary for different conditions both in amplitudes and latencies of the peak. Different conditions are ideally differentiable from each other based on their different ERP components. We have stud-

Published by Verlag der TU Graz
Graz University of Technology

 DOI: 10.3217/978-3-85125-533-1-81

ied ERP components in time-frequency domain to extract the features correlated with different conditions.

Statistical tests: To verify the significance of the differences between time-frequency analysis results of different conditions a combination of Jackknife re-sampling method and the student's t-test is applied.
One alternative would be a student's t-test between data sets of ERPs of 17 subjects for two classes. However since the signal-to-noise ratios of single subject ERPs are low, we have taken another approach. As it is described in [16], Jackknife re-sampling test in combination with a one sample Student's t-test is applied. Jackknife is performed as follows: the averaged ERP of each single subject is left out each time and the grand average ERP is estimated by averaging over the rest of subjects (16 subjects in 17 iterations). The differences between the absolute values of wavelet transformed ERPs are then estimated for each two conditions and each iteration and a one sample t-test is applied to test the null hypothesis that the mean of the distribution is zero. Note that in this case the t values i.e., t, should be corrected to t_c

$$t_c = \frac{t}{(n-1)} \tag{1}$$

where n is the number of subjects. The proof of this adjustment is provided in [16].
Another issue to be considered is the correction for the problem of multiple comparison. The correction is applied as it is suggested in [17] for controlling the false discovery rate (FDR). The p-values are sorted and c is estimated as

$$c = \sum_{i=1}^{N} \frac{1}{i} \tag{2}$$

where N is the number of all samples. In the case of time-frequency analysis it will be the number of p-values of all time and frequency points. For the largest i where

$$P_i \leqslant \frac{i \times q}{N \times c} \tag{3}$$

P_i is selected (q is the desired false detection rate which is usually set to 0.05.) and if P_i is larger than the significant threshold of Bonferroni, it will be replaced as the new significance level. Otherwise the level will be set to the Bonferroni level. All p-values are then compared to the new significance level.

RESULTS

EEG signals are averaged over all trials for single subjects in the interval between -200 ms and 900 ms after the baseline correction is applied. To increase the signal-to-noise ratio of single subjects ideally we average over all subjects given that subjects are consistent enough. To verify the consistency the ERPs on channel O2 for single subjects averaged over all epochs for condition 2D in Figure 2 are compared to each other and to the ERP of the grand averaged data, i.e., the ERP average over all subjects shown in the thick red curve in the same Figure. It is shown that the peaks in single subject curves have slight differences in amplitude and peak latencies which correspond to normal differences between subjects and therefore we found them consistent enough to be averaged. We have also checked the scalp topographies of single subjects for intervals of 50 ms starting from -200 ms up to 900 ms and observed strong similarities between subjects' topographies. Therefore in the following analysis we only focus on the grand averaged data.
We are interested to figure out how the corresponding differences between conditions shown in Figure 3 are behaving in different frequency ranges. For this reason, we have applied wavelet transformation to the ERP signals averaged over all epochs for single subjects and for each condition. The absolute values are then averaged over all subjects to be studied in the time frequency domain. The wavelet window applied in our analysis is a Morlet window. The baseline correction is applied to the wavelet transformation of averaged ERP of each subject by subtracting the mean of the absolute value of wavelet transformed data in the interval of -200 ms and 0 ms from the absolute value of the rest of the wavelet transformed data. In Figure 4 differences of the absolute values (second row) of wavelet transformations for each two conditions are plotted together with the p-values (first row) corresponding to each time point and frequency point. The statistical test is performed as it is described in Section Statistical Tests using Jackknife and student's t-test. The significance threshold (alpha) is corrected according to the FDR method for the time frequency window to consider the problem of multiple comparisons.

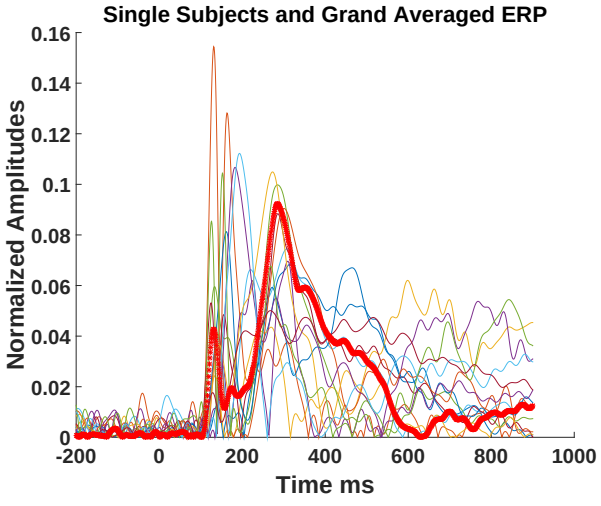

Figure 2: ERPs averaged over all epochs for each subject on channel O2 and condition 2D are plotted in the time interval between -200 ms and 900 ms. The thick line in red shows the grand average ERP, i.e. the average over all subjects. The absolute value of the curves are normalized by their norms. Single ERPs have different amplitudes and differences in latencies but in general they are consistent enough to be averaged over subjects.

Published by Verlag der TU Graz
Graz University of Technology

 DOI: 10.3217/978-3-85125-533-1-81

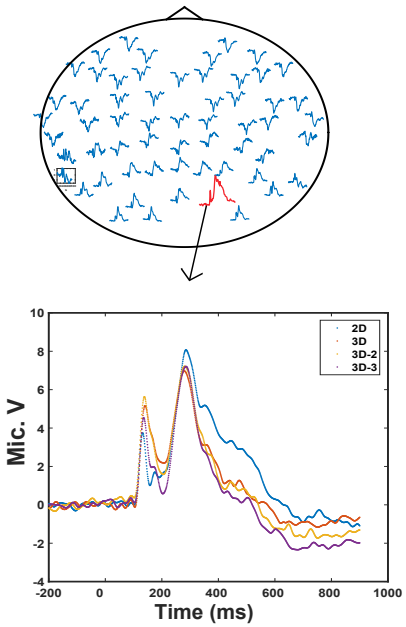

Figure 3: ERPs of grand average corresponding to each channel are plotted on the scalp in the top figure. On the bottom, ERps of channel O2 are compared between conditions.

Except for the condition 2D and 3D-3, the comparisons between 2D and 3D, 3D and 3D-2 as well as 3D and 3D-3 all show significant differences in the frequency band between 14 Hz and 17 Hz starting very early (almost 22 ms) after the stimulus onset up to 150 ms. This effect is shifted towards 200 ms for the comparison between 3D and 3D-2 and 3D and 3D-3 in the same frequency band. The brain activities in the frequency of interest (Beta band) in the occipital region, i.e. O2 channel in our analysis, are reported to be correlated with the level of attention in previous studies [18, 19, 20]. According to these studies, an increase in the attention caused the beta power in the occipital cortex to increase. In Figure 4.a the power in 3D is subtracted from the power in 2D which shows larger power values for 2D compared to 3D. This means the attention level in condition 2D was higher for subjects than in 3D. Figure 4.c shows higher power for 3D-2 than 3D and Figure 4.d shows higher beta power for 3D-3 compared to 3D. Logically the amount of information which is presented to the subjects in 3D-2 and 3D-3 is higher due to the vertical disparity simulated in these two conditions. In 3D-3 most of the subjects reported that the vertical disparity was very strong and noticeable. Since this parameter changes the stimuli to be a less normal stimuli it is expected to observe higher amount of attention in this condition compared to 3D which is confirmed by the results as well. However, what surprises us in the first glance is the higher attention level in 2D compared to 3D. It was expected that the depth information in 3D increases the attention level in the subjects in contrast to our results. Our hypothesis in this case is that this effect is caused by a change in the dimensionality of presentation in the 2D condition. As it was mentioned before, a three dimensional cross is presented before the stimulus onset in all conditions. In the case of 2D stimulus, there is a switch from a three dimensional cross to a two dimensional cube which might be the reason of higher attention level in 2D. However the 3D condition follows a three dimensional cross and therefore no switching is happening in the dimensionality of the cross and the cube and therefore less increase in the attention level is observed.

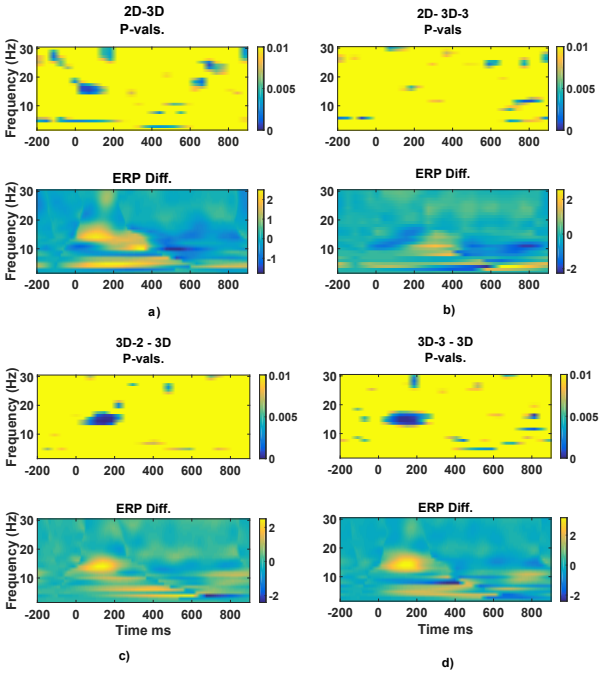

Figure 4: Time frequency analysis on the differences between conditions: Each figure contains two plots. The plot on the second row shows the difference between the absolute values of wavelet transformations for two conditions and the plot on the first row shows the corresponding p-values.

CONCLUSION

In this study the simulated vertical disparity in stereoscopic images was the focus of an objective test for the quality of experience. Time frequency analysis of ERP components has shown a significant increase in the beta band power in 3D-2 and 3D-3 compared to the 3D condition. In previous studies the increased occipital beta power has been linked to the increase in the attention level. An increased attention level in 3D-3 and 3D-2 compared to 3D was observed which sounds reasonable due to extra unexpected amount of information in these two conditions due to the vertical disparity component. We suggest that an increase in the occipital beta power can be extracted from the data as a feature correlated with an increase in the vertical disparity of stereoscopic images even before the subjects show first signs of visual fatigues. However we have also observed an increase in the beta power for 2D compared to 3D. This increase in attention can be explained by the change in the dimensionality

Published by Verlag der TU Graz
Graz University of Technology

 DOI: 10.3217/978-3-85125-533-1-81

of the cross presented before the cube in 2D. Since the cross is presented in 3D in all pause intervals, the switch happening between the three dimensional cross and the two dimensional cube has been probably the reason of higher attention for 2D condition than the 3D condition in spite of our expectation for a higher attention in 3D than 2D.
In future work we will investigate multimodal [21] and deep [22] approaches for quality assessment of stereoscopic images.

ACKNOWLEDGMENT

This research was partially funded by the German Research Foundation (DFG, SFB938/Z3 and TRR-169).

References

[1] C. Wheatstone, "Contributions to the Physiology of Vision.Part II. On Some Remarkable, and Hitherto Unobserved, Phaenomena of Binocular Vision,(Continued).," *Proc. R. Soc. London*, vol. 6, pp. 138–141, 1850.

[2] M. Lambooij, W. IJsselsteijn, M. Fortuin, and I. Heynderickx, "Visual Discomfort and Visual Fatigue of Stereoscopic Displays: A Review," *J. Imaging Sci. Technol.*, vol. 53, no. 3, pp. 030201, 2009.

[3] ITU-R Recommendation BT.500-13, "Methodology for the subjective assessment of the quality of television pictures," Tech. Rep., International Telecommunication Union, Geneva, Switzerland, 2012.

[4] A. K. Porbadnigk, M. S. Treder, B. Blankertz, J.-N. Antons, R. Schleicher, S. Möller, G. Curio, and K.-R. Müller, "Single-trial analysis of the neural correlates of speech quality perception.," *J. Neural Eng.*, vol. 10, no. 5, pp. 056003, 2013.

[5] S. Bosse, L. Acqualagna, A. K. Porbadnigk, B. Blankertz, G. Curio, K.-R. Müller, and T. Wiegand, "Neurally informed assessment of perceived natural texture image quality," in *IEEE Int. Conf. Image Process. (ICIP)*, 2014, pp. 1987–1991.

[6] L. Acqualagna, S. Bosse, A. K. Porbadnigk, G. Curio, K.-R. Müller, T. Wiegand, and B. Blankertz, "EEG-based classification of video quality perception using steady state visual evoked potentials (SSVEPs)," *J. Neural Eng.*, vol. 12, no. 2, pp. 026012, 2015.

[7] S. Bosse, L. Acqualagna, A. K. Porbadnigk, G. Curio, K.-R. Müller, B. Blankertz, and T. Wiegand, "Neurophysiological assessment of perceived image quality using steady-state visual evoked potentials," *Proceedings of SPIE*, vol. 9599, pp. 959914, 2015.

[8] S. Scholler, S. Bosse, M. S. Treder, B. Blankertz, G. Curio, K.-R. Müller, and T. Wiegand, "Toward a direct measure of video quality perception using EEG.," *IEEE Trans. Image Process.*, vol. 21, no. 5, pp. 2619–29, 2012.

[9] J. Frey, A. Appriou, F. Lotte, and M. Hachet, "Classifying EEG Signals during Stereoscopic Visualization to Estimate Visual Comfort," *Comput. Intell. Neurosci.*, vol. 2016, 2016.

[10] S. Bosse, K.-R. Müller, T. Wiegand, and W. Samek, "Brain-Computer Interfacing for Multimedia Quality Assessment," in *IEEE Int. Conf. on Systems, Man, and Cybernetics (SMC)*, 2016, pp. 002834–002839.

[11] U. Engelke, D. P. Darcy, G. H. Mulliken, S. Bosse, M. G. Martini, S. Arndt, J.-N. Antons, K. Y. Chan, N. Ramzan, and K. Brunnstrom, "Psychophysiology-Based QoE Assessment: A Survey," *IEEE Journal of Selected Topics in Signal Processing*, pp. 1–1, 2016.

[12] F. Shahbazi Avarvand, S. Bosse, K-R. Müller, R. Schäfer, G. Nolte, T. Wiegand, and W. Samek, "Objective quality assessment of stereoscopic images with vertical disparity using EEG," *Journal of Neural Engineering*, 2017.

[13] A. S. Malik, R. N. H. R. Khairuddin, H. U. Amin, M. L. Smith, N. Kamel, J. M. Abdullah, S. M. Fawzy, and S. Shim, "EEG based evaluation of stereoscopic 3d displays for viewer discomfort," *BioMedical Engineering OnLine*, vol. 14, no. 1, pp. 21, 2015.

[14] L. C. Parra, C. D. Spence, A. D. Gerson, and P. Sajda, "Recipes for the linear analysis of EEG," *NeuroImage*, vol. 28, no. 2, pp. 326 – 341, 2005.

[15] B. Blankertz, L. Acqualagna, S. Dähne, S. Haufe, M. Schultze-Kraft, I. Sturm, M. Uščumlic, M. A. Wenzel, G. Curio, and K.-R. Müller, "The berlin brain-computer interface: Progress beyond communication and control," *Frontiers in Neuroscience*, vol. 10, pp. 530, 2016.

[16] R. Ulrich and J. Miller, "Using the jackknife-based scoring method for measuring lrp onset effects in factorial designs," *Psychophysiology*, vol. 38, no. 5, pp. 816–827, 2001.

[17] C. R. Genovese, N. A. Lazar, and T. Nichols, "Thresholding of statistical maps in functional neuroimaging using the false discovery rate," *NeuroImage*, vol. 15, no. 4, pp. 870 – 878, 2002.

[18] M. Gola, M. Magnuski, I. Szumska, and A. Wróbel, "EEG beta band activity is related to attention and attentional deficits in the visual performance of elderly subjects," *International Journal of Psychophysiology*, vol. 89, no. 3, pp. 334–341, 2013.

Published by Verlag der TU Graz
Graz University of Technology

 DOI: 10.3217/978-3-85125-533-1-81

[19] A. Wróbel, A. Ghazaryan, M. Bekisz, W. Bogdan, and J Kamiński, "Two streams of attention-dependent beta activity in the striate recipient zone of cat's lateral posterior–pulvinar complex," *Journal of Neuroscience*, vol. 27, no. 9, pp. 2230–2240, 2007.

[20] A. Wróbel, "Beta activity: a carrier for visual attention," *Acta Neurobiol Exp*, vol. 60, no. 2, pp. 247–260, 2000.

[21] S. Dähne, F. Bießmann, W. Samek, S. Haufe, D. Goltz, C. Gundlach, A. Villringer, S. Fazli, and K. R. Müller, "Multivariate machine learning methods for fusing multimodal functional neuroimaging data," *Proceedings of the IEEE*, vol. 103, no. 9, pp. 1507–1530, 2015.

[22] I. Sturm, S. Lapuschkin, W. Samek, and K.-R. Müller, "Interpretable deep neural networks for single-trial EEG classification," *Journal of Neuroscience Methods*, vol. 274, pp. 141–145, 2016.

Published by Verlag der TU Graz
Graz University of Technology

Proceedings of the
7th Graz Brain-Computer Interface Conference 2017 DOI: 10.3217/978-3-85125-533-1-82

BRAIN-COMPUTER INTERFACES AND AUGMENTED REALITY: A STATE OF THE ART

H. Si-Mohammed[1], F. Argelaguet[1], G. Casiez[2], N. Roussel[1], A. Lécuyer[1]

[1] Inria, France
[2] Université Lille 1, Villeneuve d'Ascq, France

E-mail: {hakim.si-mohammed ; ferran.argelaguet}@inria.fr

ABSTRACT: This paper reviews the state of the art of using Brain-Computer Interfaces (BCIs) in combination with Augmented Reality (AR). First it introduces the field of AR and its main concepts. Second, it describes the various systems designed so far combining AR and BCI categorized by their application field: medicine, robotics, home automation and brain activity visualization. Finally, it summarizes and discusses the results of the survey, showing that most of the previous works made use of P300 or SSVEP paradigms with EEG in Video See-Through systems, and that robotics is a main field of application with the highest number of existing systems.

INTRODUCTION

Research in the field of BCIs has gained more and more popularity over the past few decades. BCIs have been used in a wide variety of applications, rehabilitation [3], robotics [7], entertainment [24] or in association with different input modalities: gaze trackers or electromyography systems. They have also extensively been used in Virtual Reality contexts [27], and more recently with Augmented Reality [22, 30], which is itself gaining more interest nowadays.

Brain-Computer Interfaces and Augmented Reality are two fields that can be combined for interaction and/or visualization purpose. On the one hand, AR-based systems usually rely on Head Mounted Displays (HMD) equipped with cameras, that can be used in scenarios requiring hands-free interaction [9]. BCI paradigms can provide such means of input, either to interact with virtual [16] or real objects [36]. On the other hand, BCIs can take advantage of AR in order to interact with the real world. AR can also provide interesting ways of displaying feedback by integrating it in the real world environment. This feedback is important for a BCI-based system to enable users to access and modulate their cerebral activity [26, 32].

Despite this, combining BCIs and AR is not an easy task. Many constraints have to be taken into consideration. First, at the hardware level, both technologies can require head mounted devices that cannot easily be worn at the same time and, if worn, it is necessary to make sure that they do not interfere. BCIs use very low amplitude signals and are thus very noise-sensitive. Then, software constraints have also to be taken into account. It is for instance necessary to have a middleware or an intermediary agent in order to synchronize between them and to combine inputs. Finally, recording brain activity in the context of AR where users are generally free to move may also be difficult as muscle activity provokes artifacts in the BCI recordings [17].

This paper aims to give an overview of the state of the art of systems combining BCIs and AR. Section **2** introduces the field of augmented reality, highlighting some of its most important concepts. Section **3** reviews existing BCI-AR applications, by categorizing them according to their application field. Section **4** summarizes and discusses the results of our survey. Finally, section **5** is a general conclusion.

INTRODUCTION TO AUGMENTED REALITY

Definition of Augmented Reality

Augmented Reality relates to the integration of virtual objects and information in the real world in real-time [40]. According to Azuma [5] three characteristics define an AR system: (1) the combination of real and virtual content, (2) the real-time interaction, (3) the 3D registration of the virtual content in the real environment. Contrarily to Virtual Reality where the user is immersed in a completely virtual world, AR mixes virtual and real content, ideally, making them appear to coexist in the same space [5].

Milgram and Kishino [31] established a continuum ranging from complete virtuality to complete reality. Between them, exist different combinations of real and virtual environments, depending on the level of each one in the scene (see Figure 1).

In the scope of this paper, only visual AR applications are considered.

Types of Augmented Reality

Augmented Reality is generally divided between: (1) Video See-Through (VST) AR: in which real images are

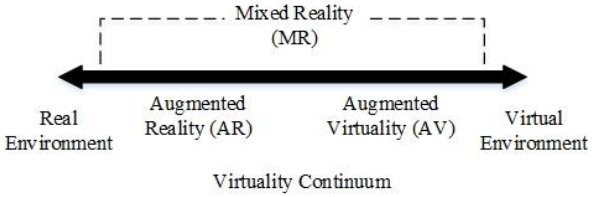

Figure 1: Representation of Milgram and Kishino Virtuality continuum of mixing real and virtual environments (from [31]).

Published by Verlag der TU Graz
Graz University of Technology

 DOI: 10.3217/978-3-85125-533-1-82

shot by the camera of a device (tablet, phone, etc.) before being visualized through a screen, augmented with virtual information; (2) Optical See-Through (OST) AR: in which the virtual content is directly displayed in front of the user's eyes onto a semi-transparent screen (e.g., Microsoft Hololens); and (3) Projective AR (a.k.a. Spatially Augmented Reality): in which virtual content is projected into a real environment object [4].

Tracking and Registration

An essential part of any AR system, is the ability to collocate virtual and real objects, which is known as registration. Afterward, tracking allows to properly render the change in virtual objects according to the position of the camera and thus, ensuring their credible integration into the real world [40]. Registration of virtual elements can be done using fiducial markers placed in the real environment, through pattern recognition techniques to identify real objects or with active sensors [5]. One popular way of achieving the tracking, consists in using the Simultaneous Localization And Mapping (SLAM) algorithms [8] related to the resolution of the problem of enabling a robot to simultaneously discover its surroundings and infer its position [37]. Originally designed for robots' navigation [14], it has been adapted for use in AR [13] as it allows the tracking of objects in unknown environments [8].

Interaction

Interaction is a major challenge for AR as it is necessary to provide the user with means to act on the virtual elements [40] and to manipulate them. However, being in the context of wearable computers, new ways of interaction, different from mouse and keyboard, have to be employed. So far, this has mainly been done through voice commands and hand gesture recognition [21] (as with Microsoft's Hololens), gaze tracking [20] or with physical buttons [34] (as with Google Glasses). BCIs could particularly contribute to AR-based systems interaction means, especially on visual selection tasks that can be done via SSVEP or P300 for example [19, 25].

APPLICATIONS COMBINING AR AND BCIs

In theory, combining AR and BCI could potentially be applied to most topics where BCIs can, e.g. assisting disabled people, entertainment, sports. There are different reasons why to combine AR and BCI. First, from a BCI point of view, AR offers new ways to integrate feedback in real world environment, thus, bringing new interaction possibilities and enhancing the user experience. Second, from an AR point of view, BCIs offer new hands-free paradigms for interaction with physical and virtual objects as well as new physiological information about the user's mental state, allowing to create more adaptive scenarios.

This section presents the state of the art of combined BCI and AR systems, categorized according to their application fields which are: (1) medicine; (2) robotics; (3) home automation; (4) brain activity visualization.

Medicine

Three main types of applications combining AR and BCIs for medicine can be identified: (1) surgeons aid or training, (2) psychological treatments and (3) disabled people assistance.

An attempt to aid surgeons during operation is the work of Blum et al. [9] who developed a Video See-Through Head Mounted Display (VST HMD) AR system granting "X-ray Superman-like vision" to surgeons in order to let them have more in-depth vision of patients under surgery. The goal of this application was to combine a BCI with a gaze-tracker, the latter selecting the area where to zoom-in and the former being used to control the level of zoom. The main utility of using a BCI in this context, is that surgeons act in a totally hands-free context, as their hands are sterilized and hence, cannot be used to interact with the AR-System [9]. However, their final setup relied on EMG instead of EEG.

When it comes to help surgeons, this can either be done by providing them with tools to use during operations [9], or to provide ways for them to train before to operate. This has been done by Barresi et al. who developed a prototype called BcAR [6]. They combined BCIs and AR feedback in order to train surgeons for Human-Robot-Interaction based surgeries. In BcAR, surgeons train for robot-assisted laser microsurgery. They have to manipulate a "retractable" scalpel represented by a haptic arm. AR feedback, displayed through a Video See-Through Head Mounted Display (VST HMD), is used to show them their attention level – measured through the BCI – represented by the length of the scalpel, so that they can adapt it (see Figure 2 (a)). The goal of the system is to teach surgeons keep their concentration during the whole time of the operation. Another therapy that has been enhanced by combining AR and BCI is the "exposure therapy". To cure patients from phobias and anxiety, Acar et al. developed an EEG based system to help patients overcome their fear [1]. The AR system consisted of a smartphone, displaying a camera view augmented with the entity the user feared (such as insects), to help them confront it. EEG was measured in order to determine the efficiency of this AR-enhanced exposure therapy. As stated before, BCIs and AR can also be combined in order to enhance psychological therapies. Correa-Agudelo et al. [12] developed ViLimbs, a computer screen based AR-BCI for phantom limb pain treatment. In this system, a patient is placed in front of a wide screen displaying a facing camera stream. Thanks to a fiducial marker placed on the beginning of the missing limb, the patient has an image of himself with both arms, allowing him to move the missing one from painful positions. It is hence, an enhanced version of the mirror therapy. Brain and muscle activity are used to determine user's motion intent to allow him to move his virtual limb. Despite using EEG, authors' prototype relied 80% on myoelectric signals and far less on Motor Imagery [12]. A last kind of medical application combining BCIs and AR is about assistive technologies, particularly electric wheelchair control. This has been explored by Borges et al. [10] who are designing an

Published by Verlag der TU Graz
Graz University of Technology

 DOI: 10.3217/978-3-85125-533-1-82

Figure 2: examples of applications combining AR and BCIs (a) Surgeon laser microsurgery training [6]; (b) Home automation system to control a lamp using P300 [36]; (c) TEEGI, brain activity visualization puppet [18] (d) MindMirror: brain activity visualization [30].

environment to allow disabled people to safely learn how to drive a wheelchair. Among different modalities to drive the wheelchair, they designed an SSVEP-based solution to control the direction. The goal of AR in this system was to be able to provide different driving scenarios by integrating virtual obstacles to the real world scene while still ensuring users' safety.

Robotics

BCIs and AR have particularly been used in the field of Robotics: (1) to explicitly steer or control a robot agent or (2) to manipulate a robotic arm. It is possible through AR, to provide a first-person view of the real world, augmented with contextual visual commands. This has been demonstrated by works like Escolano et al. who developed a P300-based AR system to control a mobile robot [15]. The robot was in a different room, equipped with a camera displaying a first-person view on a computer screen, augmented with a P300 menu to control it. A similar work had also been done by Gergondet et al. [19] who proposed a system to steer a robot using SSVEP. Their system allowed users to control a robot equipped with a camera displaying the augmented robot's view on a computer screen. But in this case, the menu consisted on four flickering commands. In addition to merely steer the robot, it was possible to select different speeds. Petit et al. developed a robot navigation system to allow users to interact with a robot [33]. Thanks to a fiducial marker placed on the user's VST HMD, the user can make the robot come towards him. Then, a body part selection happens with fiducial markers placed on different parts of the user's body beginning to flicker so that they can be selected through SSVEP for the robot to interact with.

BCIs and AR have also been used to control robotic arms through goal selection (shared control) rather than step-by-step control. This has notably been done by Lenhardt and Ritter [25] who have used a P300 oddball paradigm in order to make a robotic arm move real objects on a table. The objects were 5 cubes tagged with AR markers that had 3D virtual numbers appearing on top of them when seen through a VST HMD. The numbers were highlighted in a random order to elicit a P300 response when the user wanted to select one of them. When an object was selected, a grid appeared on the table. Each case representing a possible target destination that was also selected through the P300 paradigm. After the selection of both target object and destination, the robotic arm performed the motion. Another robotic arm control project has been achieved by Martens et al. They designed a robotic arm for two tasks [29]. The first consisted to select and move objects through P300 paradigm. The 'stones' to move were augmented when seen through a VST HMD so that the user could focus on the stimuli. The second task was to control the robotic arm to insert a key in a keyhole and was done through the augmentation of the HMD view with four SSVEP commands. Lampe et al. have used Motor Imagery (MI) for the purpose of controlling a robotic device present in a different location than the user [23]. The robot was equipped with two cameras, one for hand view and the other for the scene view, and both displayed on a computer screen. Whenever a selectable object entered the field of view, it was augmented so that the user could select the object to grasp through MI, and the robotic arm autonomously grabbed it. In this case, three commands were sent through Motor Imagery: *left*, *right*, to select which object to grasp, and *confirmation*. These commands respectively corresponding to left or right finger tapping and toe clenching.

Home automation

Another application is the ability to control smart environments, whether it is to provide comfort automated mechanisms or assistive control to manipulate home appliances. In this case, combining BCIs and AR is achieved through mainly two different strategies: (1) direct interaction [36], (2) indirect interaction through a robot agent [22].

The first strategy has been used by Takano et al. in a P300-based AR-BCI system to control multiple devices at home [36]. They tagged house appliances with AR markers which, when seen-through an Optical See-Through (OST HMD), make a control panel appear over them. The P300 paradigm is then used to select the command to execute (see Figure 2 (b)).

Indirect interaction has been proposed by Kansaku et al. [22], with a system that allows users to control a distant robot in a house environment through brain activity. The robot was equipped with a camera displaying a video stream of its environment where appliances were tagged with fiducial markers. When one of them entered the robot's field of view, a control panel was displayed, allowing users to control it.

Brain activity visualization

BCIs can also be useful for brain activity visualization purpose. Whether it is (1) for neurofeedback or (2) for pedagogic reasons, AR can offer a natural way to display how the brain works and integrate it in real life context.

The notion of neurofeedback is an essential part of the

Published by Verlag der TU Graz
Graz University of Technology

 DOI: 10.3217/978-3-85125-533-1-82

training for BCI use [28]. Neurofeedback has been provided in AR either by projecting it on real life objects [18], or displaying it directly on the representation of the user [30]. Mercier-Ganady et al. [30] developed an application called MindMirror using AR for the purpose of neurofeedback. The system consisted of a smart mirror - a LCD Screen with a facing camera - displaying the user in a somehow X-Ray vision way (see Figure 2 (d)) showing him/her the activated areas of his/her brain through EEG measurement. More precisely, the system displayed the distribution of the electrical potential over the surface of the virtual brain. Frey et al. developed a projected AR system called Teegi [18]. It consists on a tangible figurine on the head of which, the recorded EEG of the user is displayed (see Figure 2 (c)). The goal of Teegi was educational as it was designed for people to understand how EEG works.

Research studies

Some works do not totally fall in one of these categories. They are proof of concepts and feasibility/research studies. It is the case for the system of Faller et al. who developed a proof of concept of SSVEP-based BCI to control a virtual character augmented on a real table [16]. Their system included a VST HMD device, and the users' goal was to make the character move through a series of points represented by flickering checkerboards. Another feasibility study was performed by Uno et al. who wanted to determine the effect of an uncontrolled real space background on the performance of a P300-based BCI [39]. Their preliminary results showed no effect of real space background on the selection accuracy, thus encouraging the use of combined AR-BCI applications. Chin et al. developed a prototype in which users could reach and grasp virtual objects augmented on a real table [11]. The user's hands were augmented with virtual ones that he could control through Motor Imagery. The whole scene was displayed on a computer screen and no impact of AR was found on MI performance. Another type of applications has made use of fNIRS in the context of wearable devices. Afergan et al. developed a fNIRS-based BCI called Phylter [2]. Used in combination with Google Glasses, their system helped prevent the user from getting flooded by notifications. It was passively analyzing user's cognitive state to determine whether or not he/she could receive notification. The decision was based on the level of cognitive workload of the user determined after training the classifier on different user's states. Still using fNIRS-based BCIs, Shibata et al. presented a prototype of a Google Glass application called Zero Shutter Camera [35] which consisted on a passive photo trigger, based on user's mental workload. The system took the predicted user mental state as input and automatically triggered a camera snapshot at 'special moments' estimated when user's mental workload was above a threshold determined through training.

DISCUSSION

Table 1 summarizes the previous works combining AR and BCIs according to the BCI paradigm, the type of AR display and the brain sensing technology used. This table shows first that most of the time augmentation is done either through computer screens or HMDs, and that only a few number used Optical See-Through AR. The reason

Table 1: Overview of previous systems combining AR and BCIs. **CS**: Computer Screen; **VST**: Video See-Through; **HMD**: Head Mounted Display; **OST**: Optical See-Through; **HA**: Home Automation; **PoC**: Proof of Concept; **M**: Medicine; **BAV**: Brain Activity Visualization; **SAR**: Spatially Augmented Reality. **N.A**: Proof of concept, no AR implemented. **M.W:** Mental Workload.

Work	*BCI paradigm*	*AR type*	*AR display*	*BCI sensor*	*Field*	*Objective*
Escolano et al. [15]	P300	VST	CS	EEG	Robotics	Robot steering
Lenhardt et al.[25]	P300	VST	HMD	EEG	Robotics	Robotic arm control
Takano et al. [36]	P300	OST	HMD	EEG	HA	Direct HA
Kansaku et al. [22]	P300	VST	CS	EEG	HA	Indirect HA
Uno et al. [39]	P300	VST	CS	EEG	PoC	Feasibility study
Martens et al. [29]	P300/SSVEP	VST	HMD	EEG	Robotics	Robotic arm control
Broges et al. [10]	SSVEP	N.A	N.A	EEG	M	Wheelchair control
Gergondet et al. [19]	SSVEP	VST	CS	EEG	Robotics	Robot steering
Petit et al. [33]	SSVEP	VST	HMD	EEG	Robotics	Robot steering
Faller et al. [16]	SSVEP	VST	HMD	EEG	PoC	Virtual char. control
Lampe et al. [23]	MI	VST	CS	EEG	Robotics	Robotic arm control
Chin et al. [11]	MI	VST	CS	EEG	PoC	Virtual hand grasping
Correa et al. [12]	MI/EMG	VST	CS	EEG	M	Phantom Pain therapy
Blum et al. [9]	EMG	VST	HMD	EEG	M	Surgeons assistance
Barresi et al. [6]	Concentration	VST	HMD	EEG	M	Surgeons training
Acar et al. [1]	Raw data	VST	Smartphone	EEG	M	Phobia therapy
Mercier et al. [30]	Raw data	VST	CS	EEG	BAV	Neurofeedback
Frey et al. [18]	Raw data	SAR	Puppet	EEG	BAV	Education
Afergan et al. [2]	MW	OST	HMD	fNIRS	PoC	Proof of Concept
Shibata et al. [35]	MW	OST	HMD	fNIRS	PoC	Proof of Concept

Published by Verlag der TU Graz
Graz University of Technology

 DOI: 10.3217/978-3-85125-533-1-82

for this may be that the first solution is convenient for prototyping and the second very intuitive, enabling more mobility for users. However, if screen-based AR clearly prevents users from moving, the state of BCIs development so far, also prevents them from moving with HMDs due to the risk of muscle artifacts. As combining AR and BCI is relatively new, the question of mobility did not seem to be discussed in most of the papers using HMDs. But, the development and improvement of BCI technology, notably developing filtering methods to efficiently remove muscle artifact is a prerequisite for using BCIs as AR interaction tool to its full potential. The second observation that can be made is that the majority of works has made use of EEG. A reason may be the real-time nature of AR interaction, for which the time resolution of EEG seems more appropriate than fNIRS for example. Regarding BCI paradigms, although a number have been considered, SSVEP and P300 paradigms are the most used ones. This popularity could be due to the graphical aspect of the augmentation, as AR is based on displaying graphical virtual elements on the users' field of view, hence, vision-based paradigms are well suited for selection tasks. However, it is important to explore more deeply the effect of AR on BCI performances, not only from the system point of view but also in terms of users' cognitive load as evolving in a AR context may be more cognitively demanding. In addition, most of the works were still at the stage of prototypes. They made use of intermediary computers to translate brain activity and integrate it in the interaction. If SSVEP seems rather robust to synchronization issues, P300 is probably more sensitive to jitter. Using intermediary computer between BCI and AR device might introduce a bias and decrease P300 performances. A solution to this, could be to develop all-in-one wearable devices, powerful enough to directly process mental activity, this would dispense from the use of external intermediary agent and reduce the risk of desynchronization. Besides, it could be interesting to explore other BCI paradigms in AR context. Covert Attention [38] for instance could be interesting to study as AR implies elements in the whole field of view of users with no limitation to the screen's borders. It is noticeable from Table 1 that most of the works relied on active BCI paradigms (including reactive). They were mostly used for manipulation and voluntary control of physical or virtual objects. Passive BCIs have for their part, mostly been used for gathering neurophysiological information about the user to determine his mental state. Such passive paradigms could be more deeply studied in future works.

Finally, it seems necessary to consider AR-BCI systems from a Human-Computer Interaction perspective to evaluate and improve them. In addition, more and other fields of application could study and benefit from combining AR and BCIs in the future. Examples include: entertainment and gaming, rehabilitation, education, or communication and videoconferences.

CONCLUSION

This paper presented the state of the art of combining Brain-Computer Interaction an Augmented Reality. It first introduced the field of AR which can be divided into Optical See-Through, Video See-Through and Projected AR. Then it presented the previous works combining AR and BCIs in the fields of medicine, robotics, home-automation, brain activity visualization as well as proofs of concept or feasibility studies. Our survey showed that most of the previous works made use of P300 or SSVEP paradigms in VST setups, that EEG was the most employed brain sensing technology and that robotics was the field with the highest number of applications. Combining AR and BCIs seems useful in scenarios favoring hands-free interaction, but there is little doubt that future works will explore this combination in many more application fields, and that new interaction techniques will be designed as well as new feedback modalities will be invented, taking advantage from both technologies.

REFERENCES

[1] Acar D, Miman M, Akirmak OO. Treatment of anxiety disorders patients through eeg and augmented reality. European Social Sciences Research Journal. 3, 2 (2014), 18–27.

[2] Afergan D, Hincks SW, Shibata T, Jacob RJK. Phylter: a system for modulating notifications in wearables using physiological sensing. International Conference on Augmented Cognition (2015), 167–177.

[3] Ang KK, Guan C. Brain-computer interface in stroke rehabilitation. Journal of Computing Science and Engineering. 7, 2 (2013), 139–146.

[4] Azuma R, Baillot Y, Behringer R, Feiner S, Julier S, MacIntyre B. Recent advances in augmented reality. IEEE CGA. 21, 6 (2001), 34–47.

[5] Azuma RT. A survey of augmented reality. Presence: Teleoperators and virtual environments. 6, 4 (1997), 355–385.

[6] Barresi G, Olivieri E, Caldwell DG, Mattos LS. 2015. Brain-Controlled AR feedback design for user's training in surgical HRI. IEEE SMC. (2015), 1116–1121.

[7] Bi L, Fan XA, Liu Y. EEG-based brain-controlled mobile robots: a survey. IEEE Trans. on Human-Machine Systems. 43, 2 (2013), 161–176.

[8] Billinghurst M, Clark A, Lee G. A survey of augmented reality. Foundations and Trends Human–Computer Interaction. 8, 2–3 (2015), 73–272.

[9] Blum T, Stauder R, Euler E, Navab N. Superman-like X-ray vision: towards brain-computer interfaces for medical augmented reality. IEEE ISMAR (2012), 271–272.

[10] Borges LR, Martins FR, Naves ELM, Bastos TF, Lucena VF. Multimodal system for training at distance in a virtual or augmented reality environment for users of electric-powered wheelchairs. IFAC-PapersOnLine. 49, 30 (2016), 156–160.

Published by Verlag der TU Graz
Graz University of Technology

 DOI: 10.3217/978-3-85125-533-1-82

[11] Chin ZY, Ang KK, Wang C, Guan C. Online performance evaluation of motor imagery BCI with augmented-reality virtual hand feedback. Annual Int. Conf. of the IEEE EMBC. 138632, (2010), 3341–3344.
[12] Correa-Agudelo E, Hernandez AM, Ferrin C, Gomez JD. ViLimbs: Improving Phantom Limb treatment through multisensory feedback. Extended Abstracts ACM CHI. 2, (2015), 1313–1318.
[13] Davison AJ, Reid ID, Molton ND, Stasse O. MonoSLAM: Real-time single camera SLAM. IEEE Trans. on Pattern Analysis and Machine Intelligence. 29, 6 (2007).
[14] Dissanayake MWMG, Newman P, Clark S, Durrant-Whyte HF, Csorba M. A solution to the simultaneous localization and map building (SLAM) problem. IEEE Trans. on Robotics and Automation. 17, 3 (2001), 229–241.
[15] Escolano C, Antelis JM, Minguez J. A telepresence mobile robot controlled with a noninvasive brain–computer interface. IEEE SMC. 42, 3 (2012), 793–804.
[16] Faller J, Allison BZ, Brunner C, Scherer R, Schmalstieg D, Pfurtscheller G, Neuper C. A feasibility study on SSVEP-based interaction with motivating and immersive virtual and augmented reality. arXiv preprint arXiv:1701.03981. (2017).
[17] Fatourechi M, Bashashati A, Ward RK, Birch GE. EMG and EOG artifacts in brain computer interface systems: A survey. Clinical Neurophys. 118, 3 (2007), 480–494.
[18] Frey J, Gervais R, Fleck S, Lotte F, Hachet M. Teegi: tangible EEG interface. ACM UIST. (2014), 301–308.
[19] Gergondet P, Druon S, Kheddar A, Hintermüller C, Guger C, Slater M. Using brain-computer interface to steer a humanoid robot. IEEE ROBIO. (2011), 192–197.
[20] Höllerer, T. and Feiner, S. 2004. Mobile augmented reality. Telegeoinformatics: Location-Based Computing and Services. Taylor and Francis Books Ltd., London, UK. 21, (2004).
[21] Irawati S, Green S, Billinghurst M, Duenser A, Ko H. An Evaluation of an Augmented Reality Multimodal Interface Using Speech and Paddle Gestures. In Advances in Artificial Reality and Tele-Existence. Lecture Notes in Computer Science, vol 4282. Springer, Berlin 2006, Heidelberg.
[22] Kansaku K, Hata N, Takano K. My thoughts through a robot's eyes: An augmented reality-brain-machine interface. Neuroscience Research. 66, 2 (2010), 219–222.
[23] Lampe T, Fiederer LDJ, Voelker M, Knorr A, Riedmiller M, Ball T. A brain-computer interface for high-level remote control of an autonomous, reinforcement-learning-based robotic system for reaching and grasping. ACM IUI. (2014), 83–88.
[24] Lécuyer A, Lotte F, Reilly RB, Leeb R, Hirose M. Slater M. Brain-computer interfaces, virtual reality, and videogames. Computer. 41, 10 (2008), 66–72.
[25] Lenhardt A, Ritter H. An augmented-reality based brain-computer interface for robot control. Lectures Notes in Computer Science, 6444 LNCS, PART 2 (2010), 58–65.
[26] Lotte F. On the need for alternative feedback training approaches for BCI. Berlin Brain-Computer Interface Workshop (2012).
[27] Lotte F, Faller J, Guger C, Renard Y, Pfurtscheller G, Lécuyer A, Leeb R. Combining BCI with virtual reality: towards new applications and improved BCI. Towards Practical Brain-Computer Interfaces. Springer. (2012), 197–220.
[28] Lotte F, Jeunet C. Towards improved BCI based on human learning principles. Int. Winter Conf. on BCI. (2015), 1–4.
[29] Martens N, Jenke R, Abu-Alqumsan M, Kapeller C, Hintermüller C, Guger C, Peer A, Buss M. Towards robotic re-embodiment using a Brain-and-Body-Computer Interface. IEEE/RSJ IROS. (2012), 5131–5132.
[30] Mercier-Ganady J, Lotte F, Loup-Escande E, Marchal M, Lécuyer A. The Mind-Mirror: See your brain in action in your head using EEG and augmented reality. IEEE VR. (2014), 33–38.
[31] Milgram P, Kishino F. A taxonomy of mixed reality visual displays. IEICE Trans. on Information and Systems. 77, 12 (1994), 1321–1329.
[32] Neuper C, Pfurtscheller G. Neurofeedback training for BCI control. BCIs. Springer. (2009) 65–78.
[33] Petit D, Gergondet P, Cherubini A, Meilland M, Comport AI, Kheddar A. Navigation assistance for a bci-controlled humanoid robot. IEEE CYBER. (2014), 246–251.
[34] Schall G, Mendez E, Kruijff E, Veas E, Junghanns S, Reitinger B, Schmalstieg D. Handheld Augmented Reality for underground infrastructure visualization. Personal and Ubiquitous Comp. 13, 4 (2009), 281–291.
[35] Shibata T, Peck EM, Afergan D, Hincks SW, Yuksel BF, Jacob RJK. Building Implicit Interfaces for Wearable Computers with Physiological Inputs : Zero Shutter Camera and Phylter. ACM UIST. (2014), 89–90.
[36] Takano K, Hata N, Kansaku K. Towards intelligent environments: An augmented reality-brain-machine interface operated with a see-through head-mount display. Frontiers in Neuroscience. 5, APR (2011), 1–5.
[37] Thrun S, Leonard JJ. Simultaneous localization and mapping. Springer handbook of robotics. Springer. (2008), 871–889.
[38] Tonin L, Leeb R, Sobolewski A, del R Millán J. An online EEG BCI based on covert visuospatial attention in absence of exogenous stimulation. Journal of neural engineering. 10, 5 (2013), 56007.
[39] Uno K, Naito G, Tobisa Y, Yoshida L, Ogawa Y, Kotani K, Jimbo Y. Basic investigation of Brain–Computer Interface combined with augmented reality and development of an improvement method using the nontarget object. Electronics and Communications in Japan. 98, 8 (2015), 9–15.
[40] Zhou F, Duh HBL, Billinghurst M. Trends in augmented reality tracking, interaction and display: A review of ten years of ISMAR. IEEE ISMAR (2008), 193–202.

Published by Verlag der TU Graz
Graz University of Technology

Proceedings of the
7th Graz Brain-Computer Interface Conference 2017 DOI: 10.3217/978-3-85125-533-1-83

PREDICTION OF CONSCIOUSNESS RECOVERY IN UNRESPONSIVE WAKEFULNESS SYNDROME BY A VIBROTACTILE P300-BCI

R. Spataro[1], A. Heilinger[2], B. Allison[3], V. La Bella[1] and C. Guger[2]

1 Department of Experimental Biomedicine and Clinical Neurosciences, ALS Clinical Research Center, University of Palermo, Palermo, Italy;
2 Guger Technologies OG, g.tec Medical Engineering GmbH, Schiedlberg, Austria
3 Cognitive Science Department, University of California at San Diego, Gilman Drive, La Jolla, CA, USA.

E-mail: rossellaspataro@libero.it

ABSTRACT: The clinical evaluation of the disorders of consciousness (DOC) is challenging, leading to a high rate of misdiagnosis. Herein, we aimed to evaluate somatosensory responsiveness in Unresponsive Wakefulness Syndrome (UWS) patients using a vibrotactile P300-based BCI and explore its predictive role on consciousness recovery.
Methods: 10 UWS patients were enrolled and participated in a BCI session including two vibrotactile paradigms (i.e. VT2 and VT3). All patients were followed up for six months after the BCI assessment. A correlation analysis was used to evaluate whether the VT2 and VT3 Accuracy rates were associated with the clinical outcome.
Results: Four UWS patients showed clear responsiveness at the vibrotactile paradigms. Accuracy rates showed no correlation with clinical variables.
At 6-months follow-up, the clinical outcome expressed as Coma Recovery Scale-Revised (CRS-R) scores, strongly correlated with the VT2 and VT3 Accuracy rates.
Conclusions: somatosensory discrimination can be detected in UWS patients and might play a predictive role in the recovery of consciousness.

INTRODUCTION

In the clinical practice, the Disorders of Consciousness (DOC) are assessed by the bedside administration of behavioral tools, aiming to collect verbal or motor responsiveness to the environment. Unresponsive Wakefulness Syndrome (UWS) is a disorder of consciousness characterized by spontaneous eye opening without consistent behavioral responses to external stimuli. When reproducible signs of awareness are detected, the clinical condition is defined as Minimally Conscious State (MCS). However, the behavioral assessment of awareness has objective limitations, leading to up to 30-40% of diagnostic errors[1]. In the last decades, several EEG-based protocols have been applied to the detection of consciousness, with the aim of increase the diagnostic accuracy of the DOC. These approaches included BCIs, mostly based on auditory evoked potentials[2]. The Event-related potentials evoked by the violation of local and global auditory regularity have been proposed as a marker of consciousness[3].
In preliminary studies, a vibrotactile P300-based BCI was used to detect command following, and to allow communication in healthy subjects and patients with locked-in syndrome/complete locked-in syndrome (LIS/CLIS),[4,5].
In the present research, we used two different vibrotactile BCI paradigms to explore awareness in UWS patients, and evaluate the predictive role of somatosensory discrimination on the recovery of consciousness.

MATERALS AND METHODS

Participants

We enrolled 10 patients (8 males, 2 females) affected by UWS (Coma Recovery Scale-Revised [CRS-R] $\leq$ 6). Three patients had a traumatic brain injury, seven a non-traumatic disease (Table 1). Mean age was 53.3 years (SD= 25.1), median disease's duration was 62 (IQR 45-260) days since disease's onset. Clinical characteristics of the patients are shown in Table 1. Behavioral responsiveness was repeatedly assessed using CRS-R. Written informed consent was obtained from the legal guardians of the patients. All procedures were approved by our Ethics Committee.

Hardware

The mindBEAGLE system® (g.tec, Austria) provided the hardware and software platform for all recordings, stimulus presentation and real-time data analysis. It has been validated for assessment of consciousness and communication on healthy subjects, DOC patients, and locked-in patients[6]. The system includes a laptop with installed software, three vibrotactile stimulators, two in-ear headphones, one g.USBamp biosignal amplifier with 16 channels and 24 Bit ADC resolution and one EEG cap with 16 g.LADYbird active electrodes. The EEG is sampled with 256 Hz and filtered between 0.1-

Published by Verlag der TU Graz
Graz University of Technology

 DOI: 10.3217/978-3-85125-533-1-83

30 Hz. Data were recorded from Fz, C3, Cz, C4, CP1, CPz, CP2, PZ for the P300 paradigms.

Experimental procedure
All the experiments were performed in the ward by a trained physician, with the patients lying in bed.
To prepare each session, the experimenter mounted first the electrode cap on the participant's head according to the International 10-20 system. A small amount of electrode gel was then placed under each electrode to establish a good connection between each electrode and the corresponding scalp region (for scalp electrodes) or earlobe (for the earlobe clip electrodes).
One earbud in each of the participant's ears, as well as one vibrotactile stimulator on each of three locations: the left wrist, right wrist, and the right ankle.
A system check was performed to ensure that the electrodes were providing high quality data and that the earbuds and stimulators were both operating correctly. Then, the experimenter provided the instruction to the patient in the subject's mother tongue.

Assessment
This study presents two of mindBEAGLE's assessment paradigms for evoking potentials (EP) like the P3 response:

Vibro-tactile stimulation with two tactors (VT2): In this paradigm, the left and right wrist are randomly stimulated with a vibrotactile stimulator for 100 ms each. One stimulator delivers 87,5% of the stimuli which are used for distraction. The other stimulator delivers 12,5% of the stimulation thereby evoking a P300 response. The subject is verbally instructed to count the stimuli silently on the hand that receives the less probable target stimuli. Afterward, 480 trials are presented to the subject in a random order where 12.5% of all trials (60 trials) are stimulation on the target hand. During each run, the subject performs this task four times whereby the location of the target hand is selected in a random order.

Vibro-tactile stimulation with three tactors (VT3): A third tactor was added to the VT2 paradigm whereby the number of 480 trails presented to the subject stayed the same. The positions were on the left, right wrist and one tactor placed on the foot or the back as an additional distractor. The distractor receives 75.% of the stimuli (360 trials) while the left and right wrist each receives 12,5% (120 trials, 60 trials per hand) of the stimuli. The subject is instructed through earplugs to count stimuli to the target hand which is either the left or right wrist. Afterward, 120 trials are presented to the subject in a random order where 12.5% of all trials are stimuli on the target hand, 12.5% of all trials are stimuli on the non-target hand, and 75% of all stimuli are on the distractor. During each run, the subject performs this task four times whereby the location of the target hand is selected in a random order.

Table 1 | Clinical Characteristics and Classification Accuracy results of the patients.

Patient	Gender	Age	Diagnosis	Disease Duration (days)	VT2 Classification Accuracy	VT3 Classification Accuracy
1	M	19	TBI	360	80	80
2	M	19	TBI	300	30	10
3	F	36	TBI	60	45	10
4	M	34	HBI	240	20	30
5	M	91	STROKE	49	30	0
6	M	82	SDH	64	20	0
7	M	61	HBI	45	50	60
8	M	66	STROKE	180		
9	F	65	ME	35	50	50
10	M	60	HBI	45	0	15

TBI: Traumatic Brain Injury, HBI: Hemorrage Brain Injury, ME: meningoencefalitis

Published by Verlag der TU Graz
Graz University of Technology

 DOI: 10.3217/978-3-85125-533-1-83

Signal Processing and Classification

The raw EEG data and the stimulation time points are recorded during each run with a sample rate of 256. The EEG data is filtered between 0.1 and 30 Hz. Data segments from -100 ms to 600 ms from each stimulation point are created. The data are classified using linear discriminant analysis (LDA). To evaluate the classification, a classification accuracy is created ranging from 0% to 100% averaged over 30 trials.

To calculate the classification accuracy, the following procedure is repeated ten times and the results are averaged over 30 trials: The target and nontarget trials are randomly assigned into two equal sized pools. One pool is used to train a classifier, and the other pool is used to test the classifier. The classifier is tested on an increasing number of averaged stimuli out of the test pool. At first, it is tested on only one target and seven nontarget stimuli. If the classifier detected the target stimulus correctly, the resulting accuracy is 100 %; otherwise, it is 0 %. This process is repeated for two averaged target stimuli and 14 averaged nontarget stimuli, for three nontarget stimuli and 21 target stimuli, and so on until the full test pool is used. This produces 30 single values (for 30 target stimuli in the test pool), each one either 100 % or 0 %. The averaging of 10 single results in values ranging from 0 % to 100 %. Increasing the number of averaged stimuli will increase the accuracy if the subject follows the task, because this averaging reduces random noise in the data. An accuracy significantly beyond the chance level of 12.5 % shows that the subject can direct attention to the task of counting target stimuli for most or all of a run.

For the calculation of the EPs, the system compares the data segments from -100 ms to 600 ms from the target and non-target stimuli. The data are extracted, baseline corrected and averaged. Trials with an amplitude above 100 μV are rejected. A Kruskal-Wallis-Test was performed that presents areas under the curve with significant differences between targets and non-targets as green-shaded ($p<0.05$). An example for such an elicited Evoked Potential response can be seen in Figure 1. Results from Patient 1 and Patient 9 are shown.

Data Analysis and Statistics

We divided the patients into two groups according to the Accuracy rates. Patients with an Accuracy rate equal or greater than 4 x class probability (4 x 12.5 % = 50) were considered responsive, while patients with lower Accuracy rates were dubbed as unresponsive. Continuous variables were compared using the Mann–Whitney U test. The Spearman rank correlation coefficient was used to evaluate if the neural correlates of somatosensory discrimination were associated with the behavioral assessment of consciousness, expressed as CRS-R scores, at six months following the investigation.

RESULTS

Patients n. 1, 7 and 9 showed responsiveness at both VT2 and VT3 paradigms, patient n. 8 obtained a positive score only at VT2.
Overall, the patients obtained higher Accuracy rates at VT2 than VT3 (p 0.018 T-Test Paired).
Responsive patients didn't differ from unresponsive patients in age (Mann-Whitney U Test [MWUT], VT2: p=0.9, VT3: p= 0.6), disease's duration (MWUT, VT2: p=0.9, VT3: p=0.6) and CRS-R (MWUT, VT2: p= 0.4, VT3: p=0.18).
At 6-months follow-up, Patients n. 2 and 5 had died. Patients n. 1 and 7 evolved to an MCS, whereas Patient 9 recovered full consciousness. Correlation analysis showed a strong association between the VT2 and VT3 Accuracy rates and the 6-months CRS-R scores (VT2: rs = 0.77, p 0.004, VT3: rs = 0.85, p 0.01) but not with age (rs =0.23, p 0.5) and disease's duration (rs =0,1, p 0.7).

DISCUSSION

We aimed to detect neural signatures of consciousness in UWS patients using two vibrotactile P300-based BCI paradigms. Results demonstrated that a considerable proportion of UWS patients shows neural signatures of volitional behavior. The two paradigms allowed us to explore discrimination of an infrequent stimulus along a regular stimulation (VT2) and left/right somatosensory localization and suppression of irrelevant stimuli (VT3). Overall the patients obtained higher scores at VT2 than VT3, as a consequence of the different complexity of the mental tasks.
However, six-months follow-up showed that the Accuracy levels at both VT2 and VT3 paradigms correlate with the recovery of detectable behavioral responses.
This evidence fosters the importance of integrating neurophysiological approaches into clinical evaluation of the DOC. EEG-based quantitative measures of cortical responsiveness represent a non-invasive and easily repeatable diagnostic tool, which provides also prognostic information.

Published by Verlag der TU Graz
Graz University of Technology

 DOI: 10.3217/978-3-85125-533-1-83

REFERENCES

[1] Giacino JT, Fins JJ, Laureys S, Schiff ND. Disorders of consciousness after acquired brain injury: the state of the science. Nature Review 2014; 10: 99-114.
[2] Lulè D, Noirhomme Q, Kleih S, Chatelle C, Haldr S, Demertzi A et al. Probing command following in patients with disorders of consciousness using a brain-computer interface. Clinical Neurophysiology 2013; 124: 101-106
[3] Bekinschtein T, Dehaene S, Rohaut B, Tadel F, Cohen L, Naccache L. Neural signature of the conscious processing of auditory regularities. Proc Natl Acad Sci USA, 2009., vol. 106 (pg. 1672-77)
[4] Ortner R, Lugo Z, Noirhomme Q, Laureys S, Guger C, A tactile Brain-Computer Interface for severely disabled patients, in Haptics Symposium (HAPTICS), 2014 IEEE. pp. 235–237 10.1109/HAPTICS.2014.6775460
[5] Guger C, Spataro R, Allison B, Heilinger A, Ortner R, Cho W and La Bella V. Locked-in patients: Assessment and communication with vibrotactile and motor imagery brain-computer interface tools
Original Research, Front. Neurosci. – Neuroprosthetics, submitted, 2017.
[6] Spataro R, Allison B, Guger C, La Bella V. Communication in CLIS ALS patients using a vibrotactile P300 and motor imagery-based brain-computer interface. Amyotrophic Lateral Sclerosis and Frontotemporal Degeneration, 2016; 17: 264–277

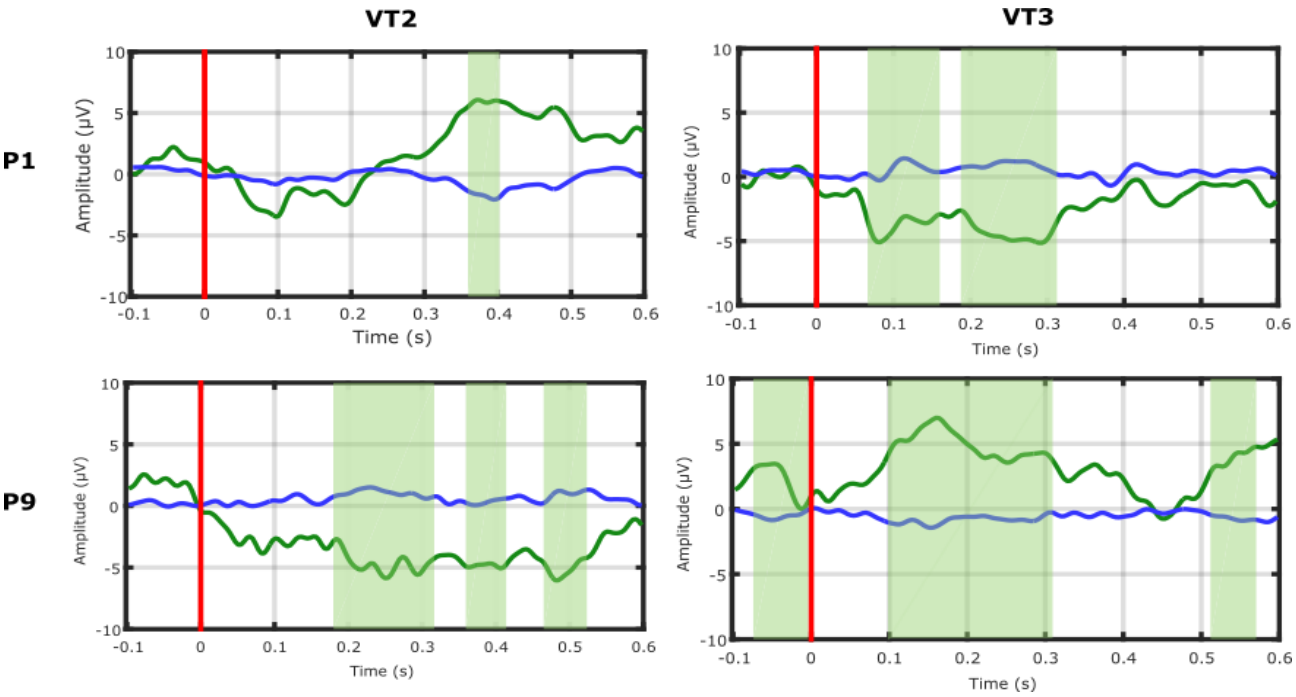

Figure 1:| The elicited Evoked Potential responses from Patient P1 and P9 from the Cz electrode position. In the left column the EPs from the vibro-tactile 2 paradigm (VT2) can be seen, in the right column the Eps elicited from the vibro-tactile 3 paradigm (VT3) can be seen.

Published by Verlag der TU Graz
Graz University of Technology

Proceedings of the
7th Graz Brain-Computer Interface Conference 2017 DOI: 10.3217/978-3-85125-533-1-84

SPATIAL FILTERING OF EEG AS A REGRESSION PROBLEM

Martin Spüler[1]

[1]Department of Computer Engineering, Eberhard Karls University Tübingen, Tübingen, Germany

E-mail: spueler@informatik.uni-tuebingen.de

ABSTRACT: In the field of Brain-Computer Interfaces (BCIs), Electroencephalography (EEG) is a widely used, but very noisy method. To improve signal-to-noise ratio (SNR) of the recorded signals, spatial filtering is commonly applied. This paper concentrates on spatial filtering methods to enhance the SNR of evoked- or event-related potentials (ERPs). While methods like Canonical Correlation Analysis (CCA) or xDAWN have been shown to provide good spatial filters, this paper introduces an alternative view on spatial filtering, showing that spatial filtering can be seen as a regression problem. It is shown how regression methods can be used to construct spatial filters and their use is evaluated on an EEG dataset containing error-related potentials (ErrPs), showing that classification accuracy is significantly improved using regression-based spatial filtering. As arbitrary regression methods can be used for construction of spatial filters, non-linear spatial filters can be constructed and new approaches, like deep learning, can be used for spatial filtering.

INTRODUCTION

A Brain-Computer Interface (BCI) allows a person to control a computer by using only his brain activity, without the need for muscle control [1]. While its main goal is to enable communication in paralyzed patients [2], it is also used in other fields like rehabilitation of stroke patients or the detection of mental states. As Electroencephalography (EEG) is a relatively cheap and non-invasive method, it is commonly used to measure the brain activity for the use with BCI. However, EEG is a rather noisy technique, which makes it difficult to correctly interpret the recorded brain signals.

One commonly used method to improve the signal-to-noise-ratio (SNR) of EEG, is the use of spatial filters. Spatial filters can be seens as mathematical operation, which mixes the signal from the EEG electrodes in a way that the signal of interest is enhanced, while noise or artifactual components are reduced. This can be implemented by a linear transformation matrix W_s that transforms the raw input signal X_r into the spatially filtered signal X_s.

$$X_s = W_s \cdot X_r \tag{1}$$

The general question is, how to find an optimal W_s that enhances the signal while reducing the noise.

There are basic spatial filters like common average referencing (CAR) or Laplacian spatial filters [3], which can be applied for any type of EEG signal and whithout any training process. There are also more sophisticated, data-driven methods for the creation of spatial filters like common spatial patterns (CSP) [4], whitening [5], xDAWN [6] or canonical correlation analysis (CCA) [7], which are optimized on a specific dataset and therefore need data to be trained. Depending on the type of BCI, different spatial filtering methods can be applied. For BCIs in which classification is done in the frequency domain, e.g., motor-imagery BCIs, CSP can be used to improve the SNR of selected oscillations. If classification is done in the time domain, to detect evoked- or event related potentials like in the popular P300 speller [8], methods like whitening, xDAWN or CCA can be used. It should be noted that CCA is also often used in SSVEP and c-VEP BCIs, where it is used as a method for combined spatial filtering and classification [9, 10] or used solely for spatial filtering in combination with a different method for classification [11].

In the course of this paper, only spatial filter for time-domain classification will be considered. Unsurprisingly, data-driven spatial filter work better than basic spatial filters [7], but a clear comparison of the three methods is missing. In [7] whitening and CCA were compared on five different datasets with CCA yielding the better results on average, although whitening performed exactly the same on some datasets. Roy and colleagues [12] found that CCA performed slightly better than xDAWN in a test on workload EEG data, but the difference was not significant. Iwane and colleagues [13] compared CCA and xDAWN of data containing error-related potentials, and also showed CCA to have better results, but again, the difference was not significant.

As an alternative to the previously mentioned methods, this paper describes how spatial filtering can be seen as a regression problem and how arbitrary regression methods can be used to construct spatial filters. As all previously used spatial filtering methods create linear filters, it is of special interest that the use of regression methods also allows the construction of non-linear spatial filters.

METHODS

In this section, it is explained first, how Canonical Correlation Analysis (CCA) can be used for spatial filtering.

Published by Verlag der TU Graz
Graz University of Technology

 DOI: 10.3217/978-3-85125-533-1-84

Based on this method, it is shown how spatial filtering can be seen as regression problem and how regression methods can be used to design spatial filters. At last, different spatial filtering methods are evaluated on an EEG dataset containing error-related potentials (ErrPs).

CCA for spatial filtering

CCA is a multivariate statistical method developed by H. Hotelling [14]. When having two datasets, which may have some underlying correlations, CCA can be used to find linear transformations for these two datasets, which maximize the correlation between the transformed datasets. Assuming there are two multidimensional datasets X and Y and their transformed datasets $x = W_x^T X$ and $y = W_y^T Y$, CCA can be used to find the two transformations W_x and W_y, which maximize the correlation between x and y by solving

$$\max_{W_x, W_y} \rho(x, y) = \frac{W_x^T X Y^T W_y}{\sqrt{W_x^T X X^T W_x \cdot W_y^T Y Y^T W_y}} \quad (2)$$

The process of using CCA for spatial filtering was previously described in [7]. To use CCA for spatial filtering, one needs to make a distinction between one-class problems and two-class problems, because the process of creating a spatial filter is slightly different in both cases.

For one-class problems (e.g. c-VEPs or SSVEPs), the classification is based on properties of the potential, like the time delay (c-VEP) or the frequency (SSVEP). For two-class problems (e.g. P300 or ErrP), the presence of such a potential is classified, if such a potential is found or not.

As signal-to-noise ratio (SNR) of single-trial EEG data is usually low, a common method to improve SNR is to average over multiple trials. The idea behind using CCA for spatial filtering is to find a linear transformation that maximizes the correlation between the recorded signal and the average evoked response, thereby improving the SNR of the transformed signal on a single-trial basis.

For the application of CCA, X is the raw EEG data and Y is the waveform of the average evoked response. CCA is then applied to find W_x and W_y, with W_x being used as spatial filter.

In the case of a one-class problem, we have k trials with EEG data, each consisting of a $n \times m$ matrix with n being the number of channels and m being the number of samples. For the application of CCA, all trials are concatenated to a new matrix X with new dimensions $n \times (k \cdot m)$. To obtain Y, first the average waveform of the evoked potential R is generated by averaging over all k trials, then R is replicated k times, to obtain a $n \times (k \cdot m)$ matrix $Y = [RR \dots R]$. Since R does not necessarily has to contain all n channels, also a subset of $n_s \leq n$ channels can be used, so that Y has dimensions $n_s \times (k \cdot m)$. Regardless of the channelsubset used in R and Y, respectively, all n channels should be used in X, since this achieved better performance in previous, unpublished offline experiments.

For two-class problems, CCA is used similarly. Assume we have the EEG data X_1 containing all trials without the evoked potential and X_2 containing all trials with the evoked potential. For X_1 and X_2, Y_1 and Y_2 are obtained in the same way as for a one-class problem. Then X and Y are generated by concatenating $X = [X_1 X_2]$ and $Y = [Y_1 Y_2]$ and CCA is applied on X and Y to find W_X, which can be used as a spatial filter.

Regression for spatial filtering

A regression tries to predict a variable y_i based on a vector x_i, with x_i having n dimensions. In the case of a least-squares regression, the squared difference between the actual variable y_i and the prediction $\hat{y}_i$ is minimized

$$\min_w \sum_{i=1}^{m} (y_i - \hat{y}_i)^2 \quad (3)$$

For an optimal prediction, the goal is to find a set of weights w which minimize the above equation.

$$\hat{y}_i = \sum_{j=1}^{n} x_{ij} w_j \quad (4)$$

Regarding the use of regression for spatial filtering, it should be noted that the raw EEG signal consists of the ERP signal plus a lot of noise. A good spatial filter transforms the raw EEG signal in a way that the noise is reduced while keeping the ERP signal. As the averaged EEG signal contains the (nearly) noise-free ERP signal, we want to find a transformation, so that the transformed signal is very similar to the noise-free ERP signal. Using the notation of the regression described above, we want to find a set of weights w, which minimizes the difference between the noise-free ERP signal y and the spatially filtered EEG signal $\hat{y}$.

When applying a regression to find a spatial filter matrix W, the first step is the same step as for CCA, where X is created as a concatenation of the single-trial EEG data and Y is the concatenation of the (noise-free) averaged potentials, with Y_c being a vector containing a concatenation of the averaged potential at EEG channel c and X_c being the concatenation of the raw signal at channel c.

After that, a regression method is used for each channel c to find a transformation w_c that minimizes the distance between the spatially filtered signal $\hat{Y}_c$ and the average potential Y_c.

$$\min_{w_c} ||Y_c - \hat{Y_c}|| \quad (5)$$

$$\min_{w_c} ||Y_c - w_c X|| \quad (6)$$

By concatenating the w_c of all channels, a quadratic filter matrix W can be obtained, which can be multiplied with the raw EEG signal to obtain a spatially filtered signal. Essentially, arbitrary regression methods can be used to find the spatial filter weights w_c for each channel c. As the above formulation only considers linear regression methods, it is important to note, that also non-linear

Published by Verlag der TU Graz
Graz University of Technology

 DOI: 10.3217/978-3-85125-533-1-84

methods can be used in which w_c is not a vector, but a function that is optimized.

$$\min_{w_c} ||Y_c - w_c(X)|| \quad (7)$$

Thereby also kernel methods or deep learning methods could be applied to find an optimal spatial filter function.

Evaluation on EEG dataset

To test the spatial filtering methods, we used data collected in a previous study [15], which contained error-related potentials (ErrPs). The subjects had to use a P300 speller [8] and if the BCI detected the wrong letter, the user should recognize the error and an ErrP should be elicited by the erroneous feedback. By detecting the ErrP, the wrong letter could be deleted and thereby the detection of ErrPs serves as an error correction system. EEG was recorded from electrodes F3, Fz, F4, T7, C3, Cz, C4,T8, CP3, CP4, P3, Pz, P4, PO7, PO8, Oz with a g.USBamp amplifier (an internal 0.5-30 Hz order eight Chebyschev bandpass filter was active) and digitised at 256 Hz. Ground and reference electrodes were placed at the left and right mastoid, respectively. We kept the impedance of all electrodes below 10 kΩ , in most cases below 5 kΩ. Impedance was measured before and after every session.

The 23 participating subjects were split into 3 different groups. H1 was drawn from the student population (N = 9, four female, mean age = 24.6 (SD $\pm$2.3), range $20-28$), all right-handed). H2 comprised a second group of elderly subjects age-matched to the group of participants with motor impairment(N = 8, two female, mean age = 45 (SD $\pm$5.2), range $39-52$). Group A2 (N = 6, one female, mean age = 51.2, SD $\pm$10.2, range $36-63$) includes 5 individuals diagnosed with ALS and one individual with Duchenne muscular dystrophy (participant A2u).

To evaluate the benefit of the different spatial filtering methods, we used the ErrP data from the above mentioned study, which consisted of 2 sessions per subject. To simulated the online case, we used the same data for training and testing the classifier as was used online. The training data consisted on average of 294 trials per subject (SD $\pm$45), while the test data consisted on average of 217 trials per subject (SD $\pm$78). After the display of the letter (at t=0 ms), the interval t=100-800ms was used as input for classification. After spatial filtering the raw EEG data, the data was bandpass filtered in the range of 0.5-16 Hz (by fast Fourier transform (FFT), removal of unwanted frequency bands, followed by inverse FFT). Subsequently the data was downsampled to 32 Hz. Thereafter, linear trends were removed from the EEG data and the data was scaled by centering and mapping the absolute maximum value to $\pm$1. All 16 channels were used as input for classification. As classifier we used a Support Vector Machine (SVM) with the LibSVM [16] implementation (RBF-Kernel with default parameters $\gamma = 1/(2\sigma)$ and $C = 1$). Due to the imbalanced classes (more correct trials than erroneus ones), we used a weighted SVM [17] with $w_{-1} = 0.3$.

Table 1: Classification accuracies on the ErrP dataset using different methods for spatial filtering: no spatial filtering (none), canonical correlation analysis (CCA), ridge regression (RR), linear support vector regression (lSVR) and support vector regression with an RBF-kernel (rSVR)

Subj.	none	CCA	RR	lSVR	rSVR
H1a	79.2 %	84.0 %	82.2 %	79.5 %	78.9 %
H1b	81.8 %	89.5 %	87.7 %	86.8 %	81.8 %
H1c	82.8 %	93.6 %	91.7 %	88.7 %	84.4 %
H1d	64.3 %	75.9 %	73.8 %	69.7 %	67.0 %
H1e	66.7 %	79.3 %	78.4 %	78.7 %	65.8 %
H1f	77.6 %	87.1 %	79.7 %	87.0 %	74.6 %
H1g	77.1 %	87.0 %	82.3 %	86.7 %	74.0 %
H1h	65.0 %	80.8 %	80.3 %	73.4 %	61.1 %
H1i	62.4 %	81.0 %	77.0 %	73.0 %	71.2 %
mean	**73.0 %**	**84.2 %**	**81.5 %**	**80.5 %**	**73.2 %**
H2j	76.4 %	100 %	100 %	100 %	100 %
H2k	60.4 %	68.9 %	59.5 %	60.4 %	59.5 %
H2l	93.4 %	93.4 %	92.9 %	82.5 %	81.5 %
H2m	75.6 %	100 %	100 %	100 %	100 %
H2n	81.6 %	84.0 %	84.4 %	86.0 %	80.8 %
H2o	78.0 %	87.0 %	85.3 %	79.1 %	72.9 %
H2p	62.1 %	80.3 %	76.8 %	74.2 %	59.6 %
H2q	79.6 %	84.1 %	76.6 %	76.6 %	76.6 %
mean	**75.9 %**	**87.2 %**	**84.4 %**	**82.3 %**	**78.9 %**
A2s	63.8 %	81.5 %	82.3 %	66.9 %	61.5 %
A2t	80.0 %	92.0 %	91.5 %	93.0 %	84.5 %
A2u	76.6 %	87.3 %	78.5 %	78.5 %	78.5 %
A2v	75.0 %	78.6 %	79.7 %	79.7 %	79.7 %
A2w	82.4 %	80.7 %	77.3 %	79.8 %	74.0 %
A2x	63.7 %	78.3 %	78.3 %	73.3 %	72.0 %
mean	**73.6 %**	**83.1 %**	**81.3 %**	**78.5 %**	**75.0 %**
mean	**74.2 %**	**85.0 %**	**82.5 %**	**80.6 %**	**75.6 %**

For the different spatial filter methods, we evaluated classification accuracy without any spatial filter, when using CCA for spatial filtering and when using three different regression methods. We usedthe MATLAB implementation of a ridge regression with a regularization parameter of $\lambda = 0.0001$ and a support vector regression with default paramters. To also test a non-linear regression, we evaluated the support vector regression with an RBF kernel using the LibSVM [16] implementation with default parameters.

RESULTS

The detailed results for the classification accuracy on the ErrP dataset with different spatial filtering methods can be seen in Table 1. While the average accuracy without spatial filtering is 74.2 %, it could be improved to 85.0 % by using CCA for spatial filtering, which is significantly better ($p < 0.001$, Wilcoxon ranksum test). Using ridge regression for the creation of a spatial filter resulted in an average accuracy of 82.5 %, which is not significantly lower than CCA ($p > 0.05$). Using support vector regression for spatial filter creation results in an average accu-

Published by Verlag der TU Graz
Graz University of Technology

 DOI: 10.3217/978-3-85125-533-1-84

racy of 80.6 % when using a linear kernel and 75.6 % with an RBF kernel. Results with linear kernel are not signficantly different to CCA($p > 0.05$), but results with RBF kernel are significantly worse ($p < 0.005$).

DISCUSSION AND CONCLUSION

In this paper, it was described how spatial filtering of EEG can be seen as regression problem and how arbitrary regression methods can be used for the construction of spatial filters. Three different regression methods were tested and compared to CCA on an EEG dataset containing error-related potentials. Classification accuracy was highest when using CCA for the construction of spatial filters, but performance with linear regression methods was not significantly worse. Using a non-linear support vector regression with an RBF-kernel resulted in significantly lower performance.

Based on the presented results it should be discussed what the benefits of using a regression method for spatial filtering are, or if there are any at all. Although performance difference to CCA was not significant, the results give a hint that when in doubt, better use CCA. Also from a theoretical standpoint, CCA seems to be better suited. As CCA uses two transformation matrices W_x and W_y, W_x is used as spatial filter and W_y transforms the averaged potential to a subspace containing different ERP components. With this last step, CCA bears similarity to principal component analysis (PCA). The spatial filter generated by CCA thereby does not try to increase the SNR on EEG sensor level, but separates the average ERP into (uncorrelated) components and improve the SNR for those components. On the other hand, regression tries to increase SNR on EEG sensor level. As neighboring sensors are correlated, regression-based spatial filters deliver some redundant information and thereby the spatial filter created by CCA might be better for classification as components are uncorrelated and thereby contain less redundant information.

The most interesting thing about using regression methods for spatial filtering is the possibility to use non-linear methods. So far, all spatial filtering methods used in EEG signal processing are linear methods. Being able to use arbitrary regression methods for spatial filtering means that also kernel methods or artificial neural networks and deep learning can be used for the creation of spatial filters. But why should non-linear spatial filters be superior to linear filters, as the results in this paper rather point in the other direction? The signal recorded at the EEG sensors is generally considered to be a linear mixture of electrical sources in the brain and artefactual/noise sources [18]. As spatial filters are trying to eliminate noise sources, it is basically a reversal of this mixture process and if the mixture is a linear process, a linear spatial filter should be able to yield optimal results. However, this is only true under certain assumptions: that all sources are stationary and that there are equal or less sources than we have channels. If a source is moving, the influence of the source on the sensors depends non-linearly on its position and therefore non-linear filters might be better to remove those sources. If there are more sources than sensors (and assuming some independence between the sources) the sources can not be perfectly reconstructed and hence, non-linear methods might achieve better results in reconstructing and removing these sources. So, it depends on the assumptions one makes about EEG if non-linear spatial filter can provide better results than linear filters.

A further argument that questions the use of non-linear spatial filters (or spatial filtering in general) is that classifiers can also integrate spatial filtering. Assuming an optimal spatial filter function $s(x)$, the raw EEG data x_r and a classification method that always finds an optimal classifier. If this method is trained on the spatially filtered data $x_s = s(x_r)$ it would return a function $g(x)$, so that $g(x_s)$ is the optimal classification result. But as the classification method always finds the optimal classifier, it would return the function $f(x) = g(s(x))$ if it is trained on the raw EEG data. Thereby, if one has a classification method that always gives the optimal classifier, spatial filtering is obsolete and a non-linear classifier would be able to also learn a non-linear spatial filtering. However, this is a rather theoretical remark. As this and previous papers [5, 6, 7, 12, 13] have shown, for classifiers commonly used in BCI applications spatial filtering always improves results. It should also be noted that an optimal classifier is only able to learn spatial filtering when trained on the raw EEG data, i.e. time-domain features. If there is a feature extraction step, like power spectrum estimation, an optimal classifier can not learn the spatial filtering anymore. While SSVEP is a good example where evoked potentials are often classified in the frequency domain, a classification of event-related potentials in the frequency domain can also be used if there is no clear stimulus onset, as it was shown for such asynchronous classification that ErrPs [19] and P300s [20] can be reliably detected based on power spectral features. In these cases a spatial filter could be trained on ERP data and then applied before power spectral estimation.

Coming back to the question if non-linear spatial filtering can improve results compared to linear spatial filtering, the results presented in this paper should be seen merely as a proof-of-concept to demonstrate that non-linear spatial filtering is possible. In future work, different non-linear methods like neural networks should be tested to evaluate if non-linear spatial filtering can improve results compared to what linear spatial filters can offer. As linear regression did not provide better results than CCA, CCA is still being recommended for the creation of spatial filters as it is easy to use and already implemented in all major frameworks like R, Python or MATLAB.

ACKNOWLEDGMENTS

This work was supported by the *Deutsche Forschungsgemeinschaft* (DFG; grant SP 1533/2-1).

Published by Verlag der TU Graz
Graz University of Technology

 DOI: 10.3217/978-3-85125-533-1-84

REFERENCES

[1] J. R. Wolpaw, N. Birbaumer, W. J. Heetderks, D. J. McFarland, P. H. Peckham, G. Schalk, and et al. Brain-computer interface technology: A review of the first international meeting. *IEEE Transactions on Rehabilitation Engineering*, 8:164–173, 2000.

[2] A. Kübler, F. Nijboer, J. Mellinger, T.M. Vaughan, H. Pawelzik, G. Schalk, D.J. McFarland, N. Birbaumer, and J.R. Wolpaw. Patients with ALS can use sensorimotor rhythms to operate a brain-computer interface. *Neurology*, 64(10):1775–1777, 2005.

[3] D J McFarland, L M McCane, S V David, and J R Wolpaw. Spatial filter selection for EEG-based communication. *Electroencephalography and clinical neurophysiology*, 103(3):386–94, September 1997.

[4] Y. Wang, S. Gao, and X. Gao. Common spatial pattern method for channel selelction in motor imagery based brain-computer interface. In *Engineering in Medicine and Biology Society, 2005. IEEE-EMBS 2005. 27th Annual International Conference of the*, pages 5392–5395. IEEE, 2006.

[5] J. Farquhar and N. J. Hill. Interactions between pre-processing and classification methods for event-related-potential classification. *Neuroinformatics*, 11:175–192, 2013.

[6] B. Rivet, A. Souloumiac, V. Attina, and G. Gibert. xDAWN algorithm to enhance evoked potentials: application to brain-computer interface. *IEEE transactions on bio-medical engineering*, 56(8):2035–43, August 2009.

[7] M. Spüler, A. Walter, W. Rosenstiel, and M. Bogdan. Spatial filtering based on canonical correlation analysis for classification of evoked or event-related potentials in eeg data. *IEEE Transactions on Neural Systems and Rehabilitation Engineering*, 22(6):1097–1103, 2014.

[8] L. A. Farwell and E. Donchin. Talking off the top of your head: toward a mental prosthesis utilizing event-related brain potentials. *Electroencephalogr Clin Neurophysiol*, 70(6):510–523, December 1988.

[9] G. Bin, X. Gao, Z. Yan, B. Hong, and Sh. Gao. An online multi-channel SSVEP-based brain-computer interface using a canonical correlation analysis method. *Journal of Neural Engineering*, 6(4):046002, 2009.

[10] G. Bin, X. Gao, Y. Wang, Y. Li, B. Hong, and S. Gao. A high-speed BCI based on code modulation VEP. *Journal of Neural Engineering*, 8(2):025015, 2011.

[11] M. Spüler, W. Rosenstiel, and M. Bogdan. Online adaptation of a c-VEP brain-computer interface (BCI) based on error-related potentials and unsupervised learning. *PloS one*, 7(12):e51077, 2012.

[12] R. Roy, S. Bonnet, S. Charbonnier, P. Jallon, and A. Campagne. A comparison of erp spatial filtering methods for optimal mental workload estimation. In *Engineering in Medicine and Biology Society (EMBC), 2015 37th Annual International Conference of the IEEE*, pages 7254–7257. IEEE, 2015.

[13] F. Iwane, R. Chavarriaga Lozano, I. Iturrate, and J. Millán. Spatial filters yield stable features for error-related potentials across conditions. In *2016 IEEE International Conference on Systems, Man, and Cybernetics*, number EPFL-CONF-223780, 2016.

[14] H. Hotelling. Relations between two sets of variates. *Biometrika*, 28(3/4):321–377, 1936.

[15] M. Spüler, M. Bensch, S. Kleih, W. Rosenstiel, M. Bogdan, and A. Kübler. Online use of error-related potentials in healthy users and people with severe motor impairment increases performance of a P300-BCI. *Clinical Neurophysiology*, 123(7):1328–1337, 07 2012.

[16] C. Chang and C. Lin. *LIBSVM: a library for support vector machines*, 2001. Software available at http://www.csie.ntu.edu.tw/ cjlin/libsvm.

[17] Y. Tang, Y. Zhang, N. Chawla, and S. Krasser. SVMs modeling for highly imbalanced classification. *Systems, Man, and Cybernetics, Part B: Cybernetics, IEEE Transactions on*, 39(1):281–288, 2009.

[18] A. Delorme, J. Palmer, J. Onton, R. Oostenveld, and S. Makeig. Independent eeg sources are dipolar. *PloS one*, 7(2):e30135, 2012.

[19] M. Spüler and C. Niethammer. Error-related potentials during continuous feedback: using eeg to detect errors of different type and severity. *Frontiers in human neuroscience*, 9:155, 2015.

[20] T. Krumpe, C. Walter, W. Rosenstiel, and M. Spüler. Asynchronous p300 classification in a reactive brain-computer interface during an outlier detection task. *Journal of neural engineering*, 13(4):046015, 2016.

Published by Verlag der TU Graz
Graz University of Technology

Proceedings of the
7th Graz Brain-Computer Interface Conference 2017 DOI: 10.3217/978-3-85125-533-1-85

COMPARISON OF SPEED, ACCURACY, AND USER FRIENDLINESS BETWEEN SSVEP-BASED BCI AND EYETRACKER

P. R. Stawicki[1], F. W. Gembler[1], A. Saboor[1], I. Volosyak[1]

[1]Rhine-Waal University of Applied Sciences, 47533 Kleve, Germany

E-mail: ivan.volosyak@hochschule-rhein-waal.de

ABSTRACT: This article intends to compare two rivaling technology tools that could reestablish communication for people with severe disabilities. One of the tested technologies, steady state visual evoked potentials (SSVEPs)-based Brain-Computer Interface (BCI), detects patterns in brain activity. Eye-tracking devices, on the other hand, measure the eye position, blinks, saccades, fixation paths, and other eye-specific parameters. Both methods can be used to interpret the users intent allowing control of spelling applications. Accuracy and speed of these two control methods are compared. A graphical user interface (GUI) with 30 targets (letters of the alphabet and special characters) was developed implementing each of the two technologies. Nine participants (two female) completed the phrase "RHINE WAAL UNIVERSITY" with both technologies. As expected, the achieved ITR with the eye-tracking device was significantly higher (91.8 bpm compared to 38.2 bpm for the SSVEP-based BCI). However, the eye tracking did not work for all of the participants, in this case the SSVEP-based interface can offer an alternative. The optimal interface needs to be customized individually.

INTRODUCTION

A brain-computer interface (BCI) can be seen as a specific type of Human-Cumputer Interaction (HCI) device. BCI can be defined as system that replaces, restores, enhances, supplements, or improves natural central nervous system output [1], or more general, as a device that communicates with other devices (or adjust the communication between them) via the brain signals [2]. The most common BCI approaches are the event-related desynchronization/synchronization (ERD/ERS) [27], steady state visually evoked potential (SSVEP) [28, 29, 16], and the P300 event-related potential (ERP) [3]. This article focuses on BCIs based on SSVEPs, neural responses which are evoked by repetitive visual stimuli (e. g. flickering boxes on a computer screen).

Though SSVEP-based BCIs have shown to be fast and reliable [4, 5], its dependency on eye gaze could exclude patients with lack of oculomotor control from using such systems and they therefore compete with other healthcare applications based on gaze direction. Another control method that also depends on gaze direction is eyetracking. Eye trackers are devices that compute the gaze direction; the calculated gaze coordinates can be used to classify objects the user is interested in. Typically, the eye movements are tracked by utilizing infrared technology and a high-resolution camera. Meanwhile commercial eye-tracking devices have become a valuable tool in augmentative communication [6].

Eye-tracking devices are generally considered more practical than SSVEP-based BCIs as they are faster and the required setup is much simpler; usually only the short calibration is necessary. However, some studies suggest that the performance gap between the two technologies might be smaller than expected. Kishore et al. compared the two methods using a head-mounted display (HMD) as a means of controlling gestures of a humanoid robot [7]. They found that both methods are appropriate for usage in immersive settings, but results for the eye tracker were surprisingly poor (two out of ten participants did not succeed in triggering gestures of a controlled robot using the eyetracker). It was stated though, that there were technological differences in this setup. Kosmyna and Tarpin-Bernard tested eye tracking in combination with different BCI paradigms in a gaming setup. Though they stated that the combination of eye tracking and SSVEP was slightly slower, it was more accurate than the pure Eye-Tracker [8].

One major obstacle with the eye tracking technology is the so called "Midas touch-problem" (see e. g. [9]). Usually the activation of a selected target object is based on dwell times; the user has to focus on a target object for an extended period. But the system cannot differentiate intentional from unintentional fixation, which can easily lead to false classifications. Another disadvantage is that any visual correction such as glasses or contact lenses can reflect the infrared (IR) light and thus make the readings inaccurate (optical eye trackers use the reflection of IR light for pupil recognition). Suefusa and Tanaka compared the eye-tracking with SSVEP when dealing with small targets [10]. They found that for short selection times the SSVEP-based BCI had higher information transfer rates (ITRs) then the eye-tracking interface for small size (square, 20 mm) targets. They suggested also that for small screen sizes (e. g. smartphone, tablets) BCI can be a better choice then eye-tracking.

The implementation of SSVEP-based BCIs as spelling interfaces has been a major research field in the BCI community. An important issue preventing a broader

Published by Verlag der TU Graz
Graz University of Technology

 DOI: 10.3217/978-3-85125-533-1-85

use of BCIs is so-called BCI illiteracy (also synonymously called BCI deficiency), basically describing the fact that a BCI cannot detect the intentions of the user accurately [11]. That also takes into account the situations, if the classification accuracy cannot surpass a certain threshold of e. g. 70% [12]. The BCI literacy rate is defined reciprocally as the percentage of users who are able to achieve effective control over the BCI.

Meanwhile, a high number of targets can be implemented using SSVEP-based BCIs. Higher number of visual stimuli generally allow higher information transfer rates (ITRs). Hwang et al. developed a SSVEP-based BCI spelling system adopting a QWERTY-style LED keyboard [13]. Such multi target applications can also be implemented on computer screens using the frequency approximation method [14]. Up to 84 simultaneously flickering targets can be controlled utilizing this method [15].

This allows a direct comparison of the two technologies. In this respect, the reliability, speed and user friendliness of each system was investigated. Each technology was tested using a custom-made graphical user interface (GUI) utilizing 30 targets (letters of the alphabet and additional characters).

MATERIALS AND METHODS

Participants: Nine users (two female) with a mean age 23.8 years participated in the study, all students or employees of the Rhine-Waal University of Applied Sciences in Kleve. Participants were asked not to wear spectacles if their vision was sufficient to identify the individual targets, this was necessary because the extra IR reflection would lead to misreadings of the gaze coordinates. This study was conducted in accordance with the Declaration of Helsinki. All participants (healthy adult volunteers) gave written informed consent prior to the experiment. Information needed for the further analysis was stored anonymously, and cannot be traced back to the participants. No financial reward was granted for participation. This research was approved by the Ethical Review Board of the Medical Faculty of the University Duisburg-Essen (reference 16-6955-BO).

Hardware: Participants were seated in front of a LCD screen (BenQ XL2420T, resolution: 1920×1080 pixels, vertical refresh rate: 120 Hz) at a distance of about 60 cm. The used computer system operated on Microsoft Windows 7 Enterprise running on an Intel processor (Intel Core i7, 3.40 GHz).

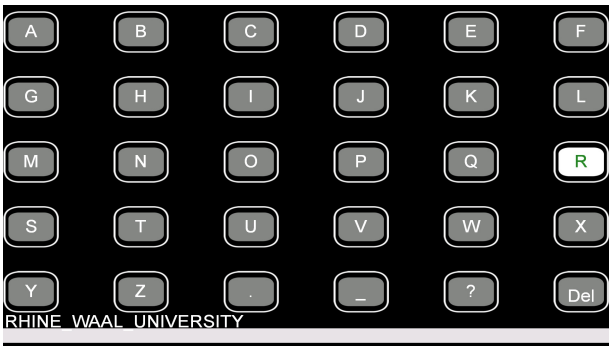

Figure 1: The Graphical User Interface. A participant was spelling the word “RHINE WAAL UNIVERSITY”.

For the BCI experiment, standard Ag/AgCl electrodes were used to acquire the signals from the surface of the scalp. The ground electrode was placed over AF_Z, the reference electrode over C_Z, and the eight signal electrodes were placed over $P_Z, PO_3, PO_4, O_1, O_2, O_Z, O_9$ and O_{10} in accordance with the international system of EEG electrode placement. Standard abrasive electrolytic electrode gel was applied between the electrodes and the scalp to bring impedances below $5\,k\Omega$. An EEG amplifier, g.USBamp (Guger Technologies, Graz, Austria), was utilized.
The sampling frequency was set to 128 Hz. During the EEG signal acquisition, an analogue band pass filter (between 2 and 30 Hz) and a notch filter (around 50 Hz) were applied directly in the amplifier.

Signal Acquisition: The minimum energy combination method (MEC) [16] was used for SSVEP signal classification. To detect the signal-to-noise ratio (SNR) of a specific frequency in the spatially filtered signals the SSVEP power estimations for all N_f frequencies were normalized into probabilities,

$$p_i = \frac{\hat{P}_i}{\sum_{j=1}^{N_f} \hat{P}_j} \text{ , with } \sum_{i=1}^{N_f} p_i = 1\,, \qquad (1)$$

where $\hat{P}_i$ is the ith power estimation, $1 \leq i \leq N_f$.
Further, in order to increase the difference between probabilities, a Softmax function was aplied:

$$p'_i = \frac{e^{\alpha p_i}}{\sum_{j=1}^{j=N_f} e^{\alpha p_j}} \text{ with } \sum_{i=1}^{i=N_f} p'_i = 1\,, \qquad (2)$$

with $\alpha = 0.25$.
All classifications were performed online on the basis of the hardware synchronization of the EEG amplifier (g.USBamp); the new EEG data were transferred to the PC in blocks of 13 samples (101.5625 ms with the sampling rate of 128 Hz). The classification was performed with a blockwise increasing time window (up to 160 blocks) [5, 16].
If the ith stimulation frequency had the highest probability p'_i and exceeded certain predefined thresholds β_i the corresponding target was classified. The thresholds

Published by Verlag der TU Graz
Graz University of Technology

 DOI: 10.3217/978-3-85125-533-1-85

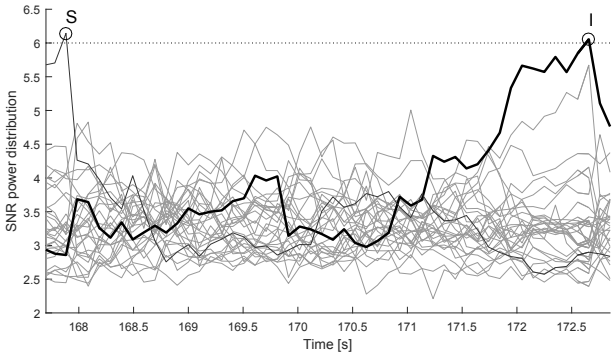

Figure 2: Thirty SNR values (equivalent to the number of flickering targets) for one participant (# 1) during spelling of the word "RHINE WAAL UNIVERSITY". The black line represents the SNR value of the frequency of the relevant box with the letter "I" and the threshold value (in this case 6) The SNR values representing the previous selection (letter S) is marked.

Figure 3: Path of the Eye-movement from the letter "S" to the letter "I" for participant # 1. The participant was spelling the word "RHINE WAAL UNIVERSITY". Before the selection of the letter "I" the eye tracker (TheEyeTribe) recorded several gaze positions across the path from "S" to "I", when the eye focused sufficiently long (2 seconds) on the desired box, the letter was selected.

of the SSVEP GUI were determined in a short calibration session where the user was asked to spell a short word of free choice. After each classification the classifier output was rejected for 914 ms (9 blocks). During this gaze shifting period, the targets did not flicker and the user could change her or his focus to another target unhindered (please also refer to [16] for more details). In this study the minimal classification time window was set to 2 seconds, same to the dwell time of the eye tracking interface.

This minimal time window is based on our previous studies that implemented this frequency approximation method [15, 17]. We have observed that a certain time (greater then the minimal 800 ms for SSVEP response [16]) is needed until the desired stimulation frequency can be detected in the EEG signal, in other words, the brain response to this duty cycle needs longer time windows.

In the frame-based stimulus approximation method a varying number of frames is used in each cycle [14, 15]. The stimulus signal at frequency f is generated by

$$\text{stim}(f, i) = \text{square}[2\pi f(i/\text{RefreshRate})], \qquad (3)$$

where $\text{square}(2\pi ft)$ generates a square wave with frequency f and i is the frame index.

E. g., the black/white reversing interval for the approximated frequency 17 Hz includes 17 cycles of varying length (three or four frames). By using the formula above, the one-second stimulus sequence of 17 Hz can be generated: (*4 4* 3 4 3 4 3 4 3 4 3 4 3 4 3 4 3 *4 4* 3 4 3 4 3 4 3 4 3 4 3 4 3). For the online spelling task with the SSVEP GUI approximated frequencies between 6.1 and 11.8 Hz (logarithmically distributed resolution, as suggested in our previous research [17]) were used to avoid overlapping in the 2-nd harmonics.

The Eye-Tracker (TheEyeTribe, Kopenhagen, Denmark) with the sizes $20 \times 1.9 \times 1.9$ cm, sampling rate 30 Hz, connected through USB 3.0 port to the PC was used for tracking the users gaze coordinates. For each participant a short (below 1 minute) eye tracking calibration run took place (9 point matrix) with the provided software.

Software:

The spelling interface displayed 30 buttons which were arranged into 5 rows (see Fig. 1). For the SSVEP system each box flickered, using the aforementioned frame-based stimulus approximation method. Any desired character could be selected in a single step. Each box was outlined by a frame which determined the maximum size a box could reach. The box sizes varied between 130×90 and 170×120 pixels, mirroring the current SNR power distribution of the corresponding frequency. For the eye-tracking system the box size mirrored the duration of the total gaze position frames over the box during the dwell time (longer gazing time on a box = bigger box). In order to further increase the user friendliness, every command classification was followed by an audio feedback with the name of the selected command or the letter spelled.

Experimental Setup: After signing the consent form, each participant was prepared for the EEG recording. Participants were asked to complete spelling tasks for both devices in random order. Initially users participated in a familiarization run, spelling the word "KLEVE" and a word of their own choice (e. g. their first name). Afterwards, they were instructed to spell the phrase "RHINE WAAL UNIVERSITY" (name of our University). The spelling phase ended automatically when the phrase was spelled correctly. In case a user was not able to execute a desired classification within a certain time frame, or if repeated false classifications occurred, the experiment was stopped manually. Spelling errors were corrected via the "delete" button. Information needed for the further analysis was stored anonymously during the experiment. After the test phase the participants completed a post-questionnaire, answering questions regarding the preferred spelling application. The entire session took on

Published by Verlag der TU Graz
Graz University of Technology

 DOI: 10.3217/978-3-85125-533-1-85

Table 1: Results of the spelling performance. The phrase "RHINE WAAL UNIVERSITY" was spelled with the SSVEP, and Eye-Tracker interface, respectively. For each system one participant was not able to gain sufficient control. These two participants (3 and 9) were excluded from the calculation of the corresponding mean values.

	SSVEP				**Eye**			
Subject	Time [s]	Acc. [%]	ITR [bpm]	character/min	Time [s]	Acc. [%]	ITR [bpm]	character/min
1	184.133	81.82	35.91	10.75	62.867	100.00	98.35	20.04
2	188.906	78.38	36.47	11.75	64.796	100.00	95.42	19.45
3	N/A	N/A	N/A	N/A	107.111	86.21	59.43	16.24
4	91.711	100.00	67.41	13.74	56.063	100.00	110.28	22.47
5	431.641	73.33	17.36	6.26	60.125	100.00	102.83	20.96
6	200.180	83.87	32.39	9.29	70.890	95.65	86.39	19.47
7	114.359	100.00	54.06	11.02	61.242	100.00	100.96	20.57
8	156.914	95.65	39.03	8.79	75.563	95.65	81.05	18.26
9	276.859	86.21	22.99	6.28	N/A	N/A	N/A	N/A
Mean	205.588	87.41	38.20	9.74	69.832	97.19	91.84	20.18
SD	107.309	10.07	16.10	2.62	16.280	4.85	16.02	1.34

average about 35 minutes for each user. Participants had the opportunity to opt-out of the study at any time.

RESULTS

The overall BCI performance for both tested spelling applications is given in Table 1. Provided are the time T needed to complete the task, the command accuracy P and the commonly used information transfer rate (ITR) in bits/min:

$$B = \log_2 N + P \log_2 P + (1-P) \log_2 \left[\frac{1-P}{N-1} \right], \quad (4)$$

where B represents the number of bits per trial. The overall number of possible choices (N) was 30.
The accuracy P was calculated based on the number of correct command classifications divided by the total number of classified commands C_n. To obtain ITR in bits per minute, B is multiplied by the number of command classifications per minute. To obtain the average command classification time, the total time needed for the spelling task, T, was divided by C_n.

DISCUSSION

As can be seen in Table 1, BCI performance varied considerably between participants. While most participants performed better with the eye tracking GUI, not all were able to use it.
The average accuracy achieved with the SSVEP interface (87%) was significantly lower than the accuracy of the Eye-Tracking device (97%). A paired Student's t-test (with unpooled variances) revealed a statistically significant difference between the mean accuracies t(10) = 2.475, p¡0.05. Further, participants reached a mean ITR of 38.2 bpm with the SSVEP-based BCI and 91.8 bpm with the Eye-Tracking device, respectively. However, for each of the interfaces, one participant did not gain sufficient control.
Except for subject 9, all participants achieved better performance with the Eye-Tracking system.

Some users stated that the SSVEP interface was the more exhausting one. The comparably low accuracy also caused frustration for some participants. In addition to that, the time the user had to focus their gaze at a target was generally larger for the SSVEP GUI. The average command classification time (including the gaze shifting period) was 7.3 seconds for the SSVEP GUI, which is considerably longer than the mean classification times for the eye tracking system (on average 5.9 seconds). The importance of the of appropriate time window length has already been discussed e. g. in [18].

The obtained performance with the SSVEP GUI is quite promising; a mean ITR of 29.82 bpm was achieved. These results indicate the potential use of noninvasive SSVEP-based BCIs as a standalone high-speed communication tool. Though multitarget BCIs usually allow higher speed, slightly worse BCI accuracies have been previously reported with a higher number of stimuli [15]. The literacy rate is generally higher with BCIs implementing a low number of visual stimuli; some larger BCI studies with only four targets reported that even all users were able to gain control over the application [4, 5, 19]. Higher classification accuracies can be achieved with fewer targets [15]. Low target SSVEP-based BCI are therefore more suitable for hybrid systems, which combine input signals of different brain patterns, or biosignals such as eye gaze (see e. g. [20, 21, 22, 23, 24]).

Reliability of such systems could be improved further e. g. through user specific parameter setup [5].

While speed attracts much attention in development of BCI application, high accuracies are the priority for control applications and also tend to provide the highest literacy rate. This is especially relevant as demographic factors influence BCI performance, e. g. elderly people are slightly poorer BCI performers [25]. Eye tracking devices, on the other hand, may be affected by the ethnicity

Published by Verlag der TU Graz
Graz University of Technology

 DOI: 10.3217/978-3-85125-533-1-85

(e. g. asian origin) or physiology (e. g. ptosis of the eyelid) factors of the participant [26].
Further tests with brain-injured patients are desirable, as results might differ from findings of this study. In future our focus lies on further development of low target SSVEP-based BCIs and data fusion with eye tracking devices.

CONCLUSION

The presented study compares performance of an SSVEP-based BCI with an Eye-Tracking device. These two communication technologies were tested with nine healthy participants in order to explore the speed and accuracy of each system.
Though all participants achieved reliable control over at least one of the tested systems; both the SSVEP-BCI system as well as the system based on Eye-Tracking could not interprete the user intend accurately in all cases. The comparison of mean values for literate participants shows that ITR as well as classification accuracy was significantly higher for the Eye-Tracking device. The results demonstrate, however, that each of the devices has its advantages and disadvantages, and should be chosen for each user individually.

ACKNOWLEDGEMENT

This research was supported by the European Fund for Regional Development under Grant GE-1-1-047. The authors thank the participants and student assistants: Aya Rezeika, Frederike Oetker, Linh-Nga Tran, Mariya Kamenshchikova, Mihaly Benda for their help during the study.

REFERENCES

[1] C. Brunner, N. Birbaumer, B. Blankertz, C. Guger, A. Kübler, D. Mattia, J. del R. Millán, F. Miralles, A. Nijholt, E. Opisso, N. Ramsey, P. Salomon, and G. R. Müller-Putz. BNCI Horizon 2020: towards a roadmap for the BCI community. Brain-Computer Interfaces, vol. 2, no. 1, pp. 1–10, 2015.

[2] J. B. Van Erp, F. Lotte, and M. Tangermann. Brain-computer interfaces: beyond medical applications. Computer-IEEE Computer Society-, vol. 45, no. 4, pp. 26–34, 2012.

[3] B. He, S. Gao, H. Yuan, and J. R. Wolpaw. Brain-Computer Interfaces. In He B., (ed.) Neural Engineering, pp. 87–151, Boston, MA: Springer US, 2013.

[4] C. Guger, B. Z. Allison, B. Großwindhager, R. Prückl, C. Hintermüller, C. Kapeller, M. Bruckner, G. Krausz, and G. Edlinger. How many people could use an SSVEP BCI? Frontiers in neuroscience, vol. 6, pp. 1–6, 2012.

[5] F. Gembler, P. Stawicki, and I. Volosyak. Autonomous parameter adjustment for SSVEP-based BCIs with a novel BCI wizard. Frontiers in Neuroscience, vol. 9:474, 2015.

[6] I. S. MacKenzie and K. Tanaka-Ishii. Text entry systems: Mobility, Accessibility, Universality. Morgan Kaufmann, 2010.

[7] S. Kishore, M. González-Franco, C. Hintemüller, C. Kapeller, C. Guger, M. Slater, and K. J. Blom. Comparison of SSVEP BCI and Eye Tracking for Controlling a Humanoid Robot in a Social Environment. Presence: Teleoperators and Virtual Environments, vol. 23, no. 3, pp. 242–252, 2014.

[8] N. Kos' Myna and F. Tarpin-Bernard. Evaluation and comparison of a multimodal combination of BCI paradigms and Eye-tracking in a gaming context. IEEE Transactions on Computational Intelligence and AI in Games (T-CIAIG), pp. 150–154, 2013.

[9] R. J. Jacob. Eye Tracking in Advanced Interface Design, Virtual environments and advanced interface design. pp. 258–288, 1995.

[10] K. Suefusa and T. Tanaka. Visually Stimulated Brain-Computer Interfaces Compete With Eye Tracking Interfaces When Using Small Targets. In 2014 36th Annual International Conference of the IEEE Engineering in Medicine and Biology Society, pp. 4005–4008, Aug 2014.

[11] I. Volosyak, D. Valbuena, T. Lüth, T. Malechka, and A. Gräser. BCI Demographics II: How many (and what kinds of) people can use an SSVEP BCI? IEEE Trans. Neural Syst. Rehabil. Eng., vol. 19, no. 3, pp. 232–239, 2011.

[12] J. Fernandez-Vargas, H. U. Pfaff, F. B. Rodríguez, and P. Varona. Assisted closed-loop optimization of SSVEP-BCI efficiency. Frontiers in neural circuits, vol. 7, 2013.

[13] H.-J. Hwang, J.-H. Lim, Y.-J. Jung, H. Choi, S. W. Lee, and C.-H. Im. Development of an SSVEP-based BCI spelling system adopting a QWERTY-style LED keyboard. Journal of neuroscience methods, vol. 208, no. 1, pp. 59–65, 2012.

[14] Y. Wang, Y.-T. Wang, and T.-P. Jung. Visual stimulus design for high-rate SSVEP BCI. Electronics letters, vol. 46, no. 15, pp. 1057–1058, 2010.

[15] F. Gembler, P. Stawicki, and I. Volosyak. Exploring the Possibilities and Limitations of Multitarget SSVEP-based BCI Applications. In 2016 38th Annual International Conference of the IEEE Engineering in Medicine and Biology Society (EMBC), pp. 1488–1491, Aug 2016.

[16] I. Volosyak. SSVEP-based Bremen-BCI interface – boosting information transfer rates. J. Neural Eng., vol. 8, no. 3, p. 036020, 2011.

[17] P. Stawicki, F. Gembler, and I. Volosyak. Evaluation of Suitable Frequency Differences in SSVEP-Based BCIs. In Symbiotic Interaction, pp. 159–165, Springer, 2015.

Published by Verlag der TU Graz
Graz University of Technology

 DOI: 10.3217/978-3-85125-533-1-85

[18] I. Volosyak, H. Cecotti, and A. Gräser. Steady-State Visual Evoked Potential Response - Impact of the Time Segment Length. In Proc. on the 7th international Conference on Biomedical Engineering BioMed2010, Innsbruck, Austria, February 17 –19, pp. 288–292, 2010.

[19] P. Stawicki, F. Gembler, and I. Volosyak. Driving a Semiautonomous Mobile Robotic Car Controlled by an SSVEP-based BCI. Computational Intelligence and Neuroscience, Hindawi, vol. 2016, no. 5, 2016.

[20] T. Malechka, T. Tetzel, U. Krebs, D. Feuser, and A. Graeser. sBCI-Headset-Wearable and Modular Device for Hybrid Brain-Computer Interface. Micromachines, vol. 6, no. 3, pp. 291–311, 2015.

[21] Y.-H. Liu, S.-H. Wang, and M.-R. Hu. A Self-Paced P300 Healthcare Brain-Computer Interface System with SSVEP-Based Switching Control and Kernel FDA + SVM-Based Detector. Applied Sciences, vol. 6, no. 5, p. 142, 2016.

[22] M. H. Chang, J. S. Lee, J. Heo, and K. S. Park. Eliciting dual-frequency SSVEP using a hybrid SSVEP-P300 BCI. Journal of neuroscience methods, vol. 258, pp. 104–113, 2016.

[23] C. Brennan, P. McCullagh, G. Lightbody, L. Galway, D. Feuser, J. L. González, and S. Martin. Accessing Tele-Services Using a Hybrid BCI Approach. In: Rojas I., Joya G., Catala A. (eds) Advances in Computational Intelligence. pp. 110–123. Cham: Springer International Publishing, 2015.

[24] P. McCullagh, C. Brennan, G. Lightbody, L. Galway, E. Thompson, and S. Martin. An SSVEP and Eye Tracking Hybrid BNCI: Potential Beyond Communication and Control. In: Schmorrow D., Fidopiastis C. (eds) Foundations of Augmented Cognition: Neuroergonomics and Operational Neuroscience. pp. 69–78, Springer, 2016.

[25] F. Gembler, P. Stawicki, and I. Volosyak. A Comparison of SSVEP-Based BCI-Performance Between Different Age Groups. Advances in Computational Intelligence, pp. 71–77, Springer, 2015.

[26] P. Blignaut and D. Wium. Eye-tracking data quality as affected by ethnicity and experimental design. Behavior Research Methods, vol. 46, no. 1, pp. 67–80, 2014.

[27] G. Pfurtscheller and C. Neuper. Future prospects of ERD/ERS in the context of brain–computer interface (BCI) developments. Progress in brain research, vol. 159, pp. 433–437, 2006.

[28] G. R. Müller-Putz, R. Scherer, C. Brauneis, and G. Pfurtscheller. Steady-state visual evoked potential (SSVEP)-based communication: impact of harmonic frequency components. Journal of neural engineering, vol. 2, no. 4, p. 123, 2005.

[29] G. R. Muller-Putz and G. Pfurtscheller. Control of an electrical prosthesis with an SSVEP-based BCI. IEEE Transactions on Biomedical Engineering, vol. 55, no. 1, pp. 361–364, 2008.

Published by Verlag der TU Graz
Graz University of Technology

Proceedings of the
7th Graz Brain-Computer Interface Conference 2017 DOI: 10.3217/978-3-85125-533-1-86

SPELLING IN PARALLEL: TOWARDS A RAPID, SPATIALLY INDEPENDENT BCI

J.M. Stivers[1], V.R. de Sa[1]
[1] Cognitive Science Department, University of California, San Diego

E-mail: jstivers@ucsd.edu

ABSTRACT: BCI Spellers for end-users utilize numerous different techniques, but many require that stimuli in different areas of the screen be foveated for best performance. Spatial independence, however, is of considerable value for patients suffering from locked-in syndrome, which significantly attenuates their capacity for voluntary movements. To this end, we have designed a 10-segment library of letter subsets, which combinatorially create the letters of the alphabet. Segments can thus be centrally presented, allowing letters to be cued in parallel while maintaining the spatial independence of RSVP-style spellers. A 68% segment-classification accuracy yields a reasonably rapid speller, with several avenues for maximizing accuracy and information transfer rate.

INTRODUCTION

Neurodegenerative diseases have an increasingly significant impact on public health as life expectancies and treatment strategies improve. Locked-in syndrome (LIS) in particular – whether caused by injury or illness – poses significant challenges for patient and healthcare professionals. While the inability to communicate needs or discomforts can have a deleterious effect on one's health, the lack of social interaction can also pose a significant issue. P300 BCI spellers are a popular technique for ameliorating these challenges. In the original P300 system developed by Farwell and Donchin [1] the user observes a screen with a grid of symbols; individual rows and columns are flashed pseudo-randomly and the user is told to count the times their target symbol flashes. Due to the large size of the letter grid and the small size of the flashed letters, eye movements must be made to the vicinity of the desired letter.

This can be a problem for late-stage ALS patients who – even if they have some residual voluntary eye movement capacity – are not always able to make voluntary gaze shifts to direct overt attention [2,3]. To address this issue, rapid serial visual presentation (RSVP) spellers have been developed, which serially present whole letters flashed in the center of the screen [4,5]. While alleviating the problem of eye movements, the lack of simultaneously flashed items results in less combinatorial efficiency and a lower information transfer rate for these systems [5]. In this paper we describe preliminary experiments to develop a hybrid system with the benefits of combinatorial efficiency as well as centrally presented stimuli. As segments occur in many letters, we have the combinatorial advantage of one flash probing for many letters.

MATERIALS AND METHODS

Segment Library: Our stimuli or segment library was similar to the work of Minett et al. [6], wherein Chinese stroke-based text systems are used as the basis of a BCI. Since English letters are not composed of a series of ordinal strokes, a new system needed to be designed. Moreover, since our segments would by definition be arbitrary, it was important to design segments that are both simple to visualize, yet sufficiently distinct to allow easy comparison. To this end, we projected all 26 letters of the English alphabet onto a 7x5 grid of circular nodes, using a derivative of the scoreboard font. This allowed us to reduce the spatial complexity of characters into more general elements.

Our speller used a 10-segment library (Fig. 1) of letter subsets as query stimuli. Each segment consisted of 2-5 contiguous nodes on the 7x5 grid. The segments were assigned a specific color, which – along with their positions on the grid – was invariant. The color-segment mapping allowed participants to identify segments either through their colors or their relative spatial positions, minimizing the difficulty in making a correct discrimination. Not all nodes were contained within a segment; said independent nodes were colored white (see Fig 1).

Relative to a given letter, segments could be classified as "targets" or "non-targets", based on whether they are subsections of that letter (Figure 1). As most letters are made of a unique combination of segments, the responses to individual stimulations can be used to predict the target letter probabilistically via Bayesian inference. With our current library, O and D cannot be discriminated purely through segments, which could be a challenge in a standalone system. Language modeling and other techniques (see "Output-Letter Checks", Discussion) can easily resolve this shortcoming.

Experimental Paradigm: At the start of each block, the participant was assigned a random letter of the alphabet. For this initial test of the system, we excluded I, V, X, and Y from the list of potential targets due to their

Published by Verlag der TU Graz
Graz University of Technology

 DOI: 10.3217/978-3-85125-533-1-86

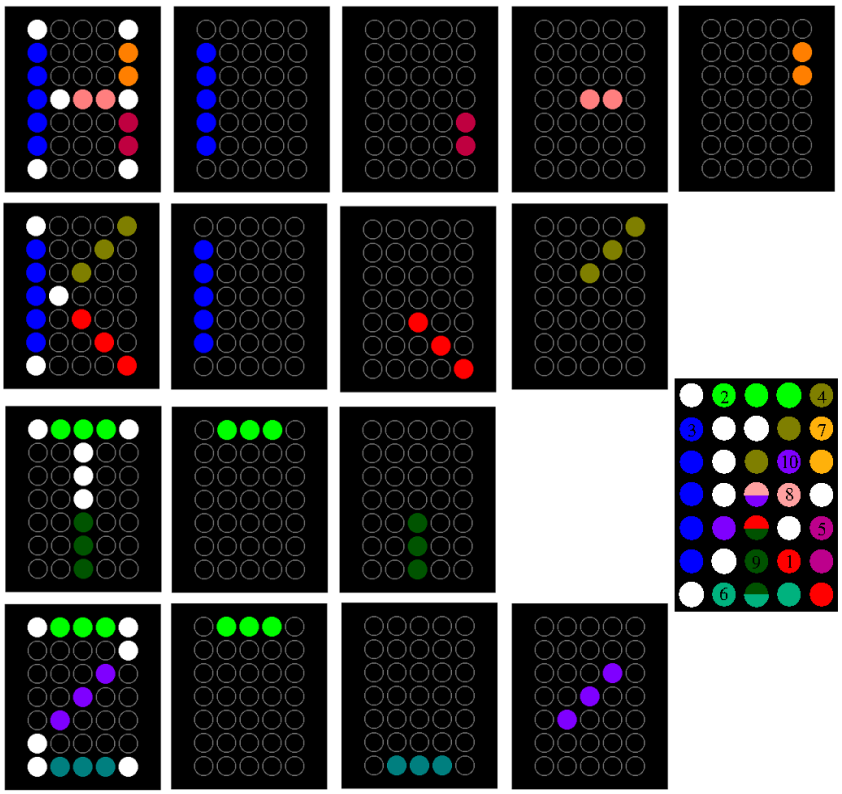

Figure 1: The segment library consists of 10 unique, invariant letter subsets. Each letter can be spelled with its own combination of segments. Depending on the letter to be spelled, component segments are deemed 'targets', whereas all others are 'non-targets'.

unique morphologies. The target letter was displayed for 2.5 seconds, with the component segments colored appropriately. This served to inform the subject of their target letter and target segments (shape and color). Afterwards, individual segments were presented serially, with a stimulus duration of 390 ms, and an inter-stimulus interval of 180 ms (total stimulus onset asynchrony 570 seconds).

The experiment consisted of an offline "training" phase, wherein data were collected to train a classifier, and an online "testing" phase, wherein the users' responses were analyzed and fed back to the system in real time. During the training phase, target segments were presented 30% of the time, and a total of 30 segments were presented before a block ended. During the analysis of the testing phase, stimuli were flashed until a) a letter was identified by the segment model or b) a total of 30 segments had been presented. During the experiment, incorrect letter selections were not a block-stopping criterion, in order to acquire more data for pseudo-online analysis.

Data Collection and Analysis: Data were collected from 6 undergraduates (4 Female, 1 Left-handed, mean age 19.5.) Stimulus presentation and timing were coordinated via the Simulation and Neuroscience Application Platform (SNAP, SCCN). The subjects' EEG data were collected using a BrainAmp (BrainVision) 64-channel active electrode system. Data were collected at 5 kHz. The marker and data streams were synchronized via LabRecorder, a Lab Streaming Layer derivative. Offline data analysis was performed using EEGLAB v 13.6.5b[7]. Data were downsampled to 500 Hz. For the topographic plots, the Artifact Subspace reconstruction designed by Christian Kothe [8] (clean_rawdata, EEGLAB) was used to clean artifactual data, and data were bandpass filtered from .1 to 5 Hz using EEGLABs hamming window sinc FIR filter (implemented in pop_eegfiltnew, EEGLAB). For visualizing plotted traces (Figure 2), data were re-referenced to the mastoids, and bandpass filtered from .1 to 10 Hz using the same filter.

Classifier: To train the classifier, class means were specified using 5 windows (100ms length) from 300ms to 800ms post-stimulus. For training of the classifier, data were downsampled to 100 Hz and bandpass filtered from .1 to 5 Hz using BCILABs [9] built-in FFT filter. The FFT filter has a much shorter length; beneficial for online filtering of 100 Hz downsampled data. LDA with automated shrinkage determination [10] as implemented in BCILAB was used. Due to the 30% target rate, a random subset of the nontarget trials were used to train to the classifier, in order to avoid erroneous solutions derived from imbalanced training classes. While the exact number of target trials (and thus nontarget trials) used for training varied slightly between subjects, about 320 trials for each class were used as training data.

Segment Model: During the online phase, a probability vector keeps track of the probabilities given to each possible letter of the alphabet. At the beginning of a block, the system assumes a uniform probability over all letters. In an end-user's speller application, this can be replaced with the probability mass function for initial letters in the language of the user; future letters can be initialized by a conditional probability function conditioned on the previous character.

Given the responses and results of the trained classifier on the serially presented segments, the model updates the letter probabilities based on the classifier response. In the case of a "target" decision by the classifier:

$$P(l\,|\text{"}target\text{"}, seg) = \frac{P(\text{"}target\text{"}|seg,l) \times P(l)}{P(\text{"}target\text{"}|\,seg)}$$

where P("*target*"|*seg*,*l*) = target segment hit rate for letters (*l*) with segment *seg* in them and
P("*target*"|*seg*,*l*) = target segment false alarm rate

Published by Verlag der TU Graz
Graz University of Technology

 DOI: 10.3217/978-3-85125-533-1-86

for letters (*l*) without segment *seg* in them, P(*l*) is the prior probability for letter *l* before receiving the response to the flashed segment *seg*.
P("*target*"|*seg*) is the normalizing factor that keeps the total probabilities over all letters summed to 1.

Likewise in the case of a "non-target" decision by the classifier:

$$P(l|\text{"}nontarget\text{"},seg) = \frac{P(\text{"}nontarget\text{"}|seg,l) \times P(l)}{P(\text{"}nontarget\text{"}|seg)}$$

where P("*nontarget*"|*seg*,*l*) = target miss rate for letters (*l*) with segment *seg* in them and P("*nontarget*"|*seg*,*l*) = *target correct rejection rate* for letters (*l*) without segment *seg* in them.

P(*l*|*seg*) = P(*l*|"*target*",*seg*)when a target is detected and P(*l*|"*nontarget*",*seg*) when the classifier declares a non-target. These can be updated in parallel for all letters. Letter selection can be based on P(*l*|*seg*) exceeding a given threshold (e.g. 0.5) or P(l_1|*seg*) being more than a threshold above P(l_2|*seg*) where $l_1$is deemed the most probable letter, and $l_2$the second most probable. For these experiments, we used this latter rule with threshold of .2.

Note that for the purposes of these analyses (and the segment selection discussed below), we assume that the hit rates are the same for all segments that are present in the letters and the false alarm rate is also the same for all segments that are not present in the letters. For this work, we assumed a hit rate of 65% and a false alarm rate of 35%. This is very close to what was observed in the training data.

Given the letter probabilities and the mapping of segments to letters as well as estimates of the false-alarm and miss rates, the expected information gain acquired by receiving the response to each flashed segment can be computed. Segments are chosen to maximize:

$$E_{seg}(KL(P(\text{"}targ\text{"}|seg)P(l|\text{"}targ\text{"},seg) + P(\text{"}nontarg\text{"}|seg)P(l|\text{"}nontarg,seg),P(l))$$

That is, we maximize the expected Kullback-Leibler divergence between the expected letter probabilities after the response and the current letter probabilties.

Table 1: Per-subject global segment accuracy (acc), as well as class confusion performance (T/F – True, False; P/N – Positive, Negative) from the online testing phase.

	acc	TP	TN	FP	FN
S1	0.628	0.625	0.630	0.370	0.375
S2	0.664	0.639	0.675	0.325	0.361
S3	0.692	0.647	0.718	0.282	0.353
S4	0.712	0.740	0.697	0.303	0.260
S5	0.723	0.689	0.740	0.260	0.311
S6	0.597	0.559	0.615	0.385	0.441

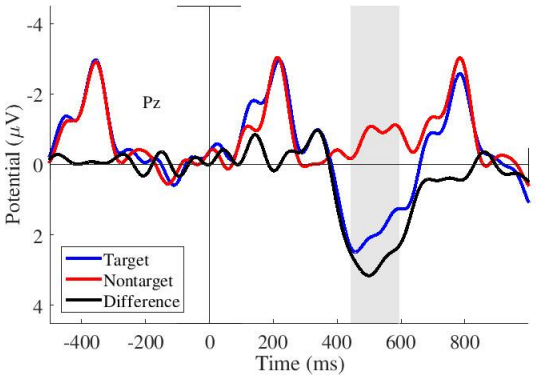

Figure 2: Grand average traces for the target (blue) and nontarget (red) classes, with the difference in black. Shaded regions reflect regions of significant difference between classes (p < .01, without correction).

Note that in the case of ties, the segment with the lowest index was selected. This does not hold true, however, if said segment was presented within the last two trials. Instead, the segment with the next lowest index was chosen.

Pseudo-Online Letter Selection: To probe the 21x25 class letter selection accuracy (Table 2), we decided to merge each subject's offline and online data, roughly doubling the number of blocks evaluated. As the experimental design between the offline and online phase is – to the participant – identical, this should be a reasonable approach. For training the pseudo-online classifier, we balanced the classes by splitting nontargets trials into two disjoint sets, and trained these sets separately, using all target-class trials. Using the same classifier, we split the data into 10 folds, using 2 folds of the data for testing.

Classifier outputs were yielded for each trial, reflecting P("*target*"|*seg*) vs P("*nontarget*"|*seg*). As each nontarget trial was in the test set twice, and each target trial was in the test set four times, the classifier outputs for each given trial are averaged. Then, seperately for each block, classifier outputs are fed into the segment model to infer the expected target. Table 2 reflects selections made a) when P(l_1|*seg*) more than .2 P(l_2|*seg*) or b) at end of a block, where P(l_1|*seg*) is selected as the model's output.

RESULTS

Offline analyses: Comparing responses from the target class (class 1) and the nontarget class (class 2), we see the expected significant difference in subject responses at Pz, averaged across all subjects (Figure 2). While the onset time of this stimulus is significantly longer than the 300ms that lends its name, it is not an unreasonable onset latency for a visual task [11]. A distinct N2 can be seen for the time-locked stimulus, as well as for the prior and subsequent letter stimulations. The N2 appearing at a typical latency improves our confidence in our observed high-latency P3. Fig, 2 also hints at a potential issue for the current system. The offset latency of the positive-

Published by Verlag der TU Graz
Graz University of Technology

 DOI: 10.3217/978-3-85125-533-1-86

trending difference wave is – relative to stimulus onset – later than the onset of the following stimulus.

The per-subject topographic plots show an interesting trend. Excluding subject 4, all show a positive-amplitude posterior signal, reflecting a higher class 1 response amplitude consistent with a P300. The low amplitude of signal shown in Subject 6's (S6) plots may explain the poor classification results (Table 1). S4 shows a significantly different response pattern, relative to all other subjects. While some very posterior, positive-trending activity can be noticed in windows 2-4, its spatial pattern is distinct, with no immediately apparent dipole.

Online analyses: As seen from Table 1 the true negative rate was equal to or greater than true positive rate for most subjects. The one exception – S4 – also possessed a unique spatial pattern in their [target - nontarget] class responses (Fig. 3). S6 also has a somewhat unique topography; the differences between the class means appear attenuated in this subject. This could explain the uniquely poor classification results for S6.

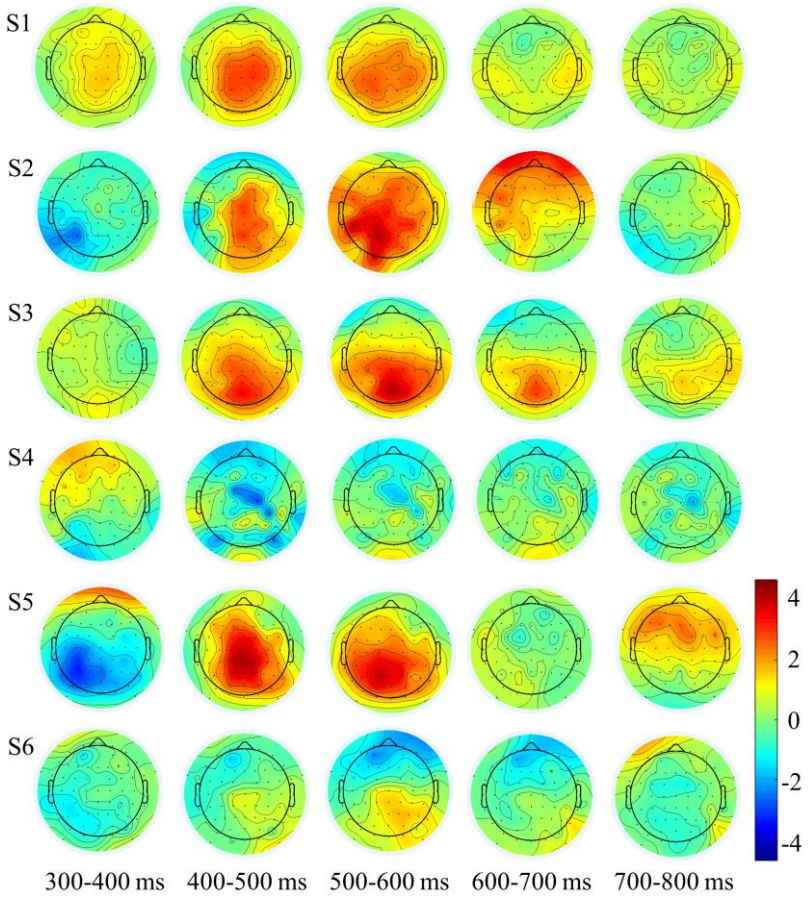

Figure 3: Per-subject topographic plots for the offline phase. Each row of plots is a scrolling average (100 ms window, 100 ms step between plots) extending from 300 ms to 800 ms. Due to the planar depiction of the 3-D electrode locations, electrodes further down the head extend beyond the head model.

Of the actual online blocks using the threshold method, 61.4% ended with the segment model outputting a potential letter. Of those output letters, 31.7% matched the blocks target. Letter selection accuracies could be improved by increasing the threshold for selection of an "output letter". Implemented along with more segment presentations per target, correct target accuracy could increase dramatically.

Pseudo-Online Results: As can be seen from Table 2, the incorrectly selected output-letters tend to share common characteristics. Sums along the columns – especially relative to diagonals – reflect high false selection rates for a given letter. Of the 261 letters selected output by the model, 88 (33.7%) matched the target letter for their given block.

We can see from this array (Table 2) that dense-segment letters – particularly B, E, G, and R – suffer from poor selection accuracies. Erroneous outputs tend to share many shape characteristics with the true target, however, and each of said letters shares at least 2 segments. Longer trials or a more conservative threshold could lead to increases in ITR, even at the cost of increasing time.

DISCUSSION

Spatially independent spellers pay a non-trivial cost as they restrict themselves to specific regions of the visual field [3,5]. In many cases this cost must be assessed, as directing overt attention towards a target is not feasible for all end-use scenarios [2]. Moreover, BCIs that require accurate eye movements must compete with eye trackers that overcome many of an EEG BCI's shortcomings. Our system was designed with patients suffering from LIS in mind. A high information transfer rate despite the spatial independence is nevertheless important, especially when designing a channel of communication.

The classifier's discrimination of subject responses benefits from the distinct class-specific posterior potential, which we believe to be a P300. In this case of S5, however, no significant posterior response is elicited. Despite this, the online accuracy of the subject is slightly above the rest of the participant cohort's average. It is possible that the anterior negativity present in the second and third windows nevertheless allows the classes to be discriminated. Alternatively, the ocular activity in the prefrontal channels, or other artefactual sources may be responsible. The 5 Hz lowpass attenuates most of the muscle activity, but it is also possible that unconscious reflexes elicited in some class-specific manner could be driving classification. These peripheral signals should be more salient in the topographic plots, however, so we

Published by Verlag der TU Graz
Graz University of Technology

 DOI: 10.3217/978-3-85125-533-1-86

find this unlikely. Increasing single-segment classification is an obvious goal moving forward. A Markov Chain, coding previous trial class as state could be fruitful, as the duration of the subjects' responses to targets are longer than the SOA. This would be especially useful if stimulus rates grow faster than 2 Hz; with a 300 ms SOA, the onsets of the preceding P3 (here, latency 500 seconds) and the subsequent N200 would overlap.

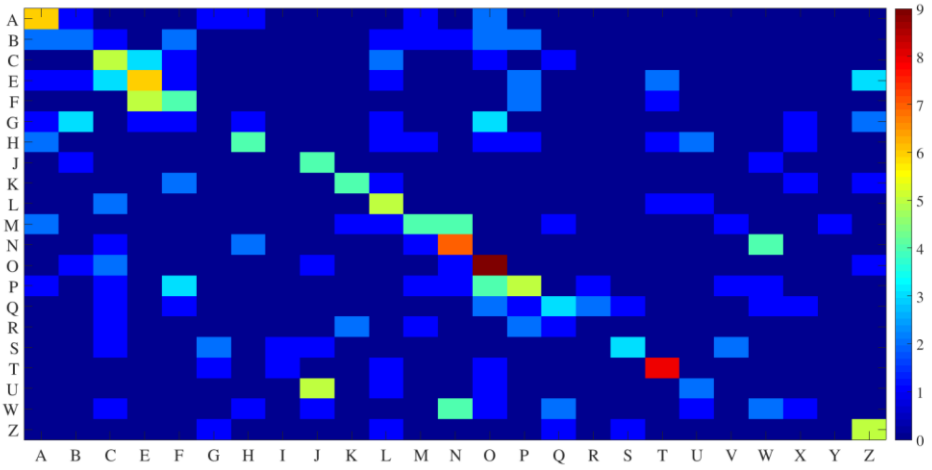

Figure 4: Visualization of the confusion matrix shown in table 2. Rows represent the target letter for a given block, whereas columns represent the letter output by the segment model. Thus, (1,1)/ (A,A) is the sum of all A's output by the segment model while A was the target.

Output-Letter Checks: Letter selection accuracies could be improved by increasing the threshold for selection of an "output letter". We have previously tested output letter feedback via full letter presentations. These presentations can either be timed identically to the segment stimuli, or the output-letter checks can be flashed with longer preceding and anteceding inter-stimulus intervals. Preliminary tests on small numbers of trials suggest that both yield responses distinct from the segments. This is not surprising, as while the segments are subsets of letters, the complete letter arrays are – by design – relatively complex images [11].

Consequently, a second independently-trained classifier will be the most appropriate implementation. It is possible that responses to these flashed "test letters" would be more like an error-related response than a P300

Table 2: This confusion matrix reflects all output-letters selected by the segment model. The rows correspond to target stimulus, and the columns correspond to classifier output. 'Blocks' reflects the number of time a given letter was a target. Shaded version in Fig. 4.

	A	*B*	*C*	*E*	*F*	*G*	*H*	*I*	*J*	*K*	*L*	*M*	*N*	*O*	*P*	*Q*	*R*	*S*	*T*	*U*	*V*	*W*	*X*	*Y*	*Z*	*Blocks*
A	6	1	0	0	0	1	1	0	0	0	0	1	0	2	0	0	0	0	0	0	0	0	0	0	0	12
B	2	2	1	0	2	0	0	0	0	0	1	1	1	2	2	0	0	0	0	0	0	0	0	0	0	14
C	0	0	5	3	1	0	0	0	0	0	2	0	0	1	0	1	0	0	0	0	0	0	0	0	0	13
E	1	1	3	6	1	0	0	0	0	0	1	0	0	0	2	0	0	0	2	0	0	0	0	0	3	20
F	0	0	0	5	4	0	0	0	0	0	0	0	0	0	2	0	0	0	1	0	0	0	0	0	0	12
G	1	3	0	1	1	0	1	0	0	0	1	0	0	3	0	0	0	0	0	0	0	0	1	0	2	14
H	2	0	0	0	0	0	4	0	0	0	1	1	0	1	1	0	0	0	1	2	0	0	1	0	0	14
J	0	1	0	0	0	0	0	0	4	0	0	0	0	0	0	0	0	0	0	0	0	1	0	0	0	6
K	0	0	0	0	2	0	0	0	0	4	1	0	0	0	0	0	0	0	0	0	0	0	1	0	1	9
L	0	0	2	0	0	0	0	0	0	0	5	0	0	0	0	0	0	0	1	1	0	0	0	0	0	9
M	2	0	0	0	0	0	0	0	0	1	1	4	4	0	0	1	0	0	0	0	1	0	0	1	0	15
N	0	0	1	0	0	0	2	0	0	0	0	1	7	0	0	0	0	0	0	0	0	4	0	0	0	15
O	0	1	2	0	0	0	0	0	1	0	0	0	1	9	0	0	0	0	0	0	0	0	0	0	1	15
P	1	0	1	0	3	0	0	0	0	0	0	1	1	4	5	0	1	0	0	0	1	1	0	0	0	19
Q	0	0	1	0	1	0	0	0	0	0	0	0	0	2	1	3	2	1	0	0	0	1	1	0	0	13
R	0	0	1	0	0	0	0	0	0	2	0	1	0	0	2	1	0	0	0	0	0	0	0	0	0	7
S	0	0	1	0	0	2	0	1	1	0	0	0	0	0	0	0	0	3	0	0	2	0	0	0	0	10
T	0	0	0	0	0	1	0	1	0	0	1	0	0	1	0	0	0	0	8	0	0	0	0	0	0	12
U	0	0	0	0	0	0	0	0	5	0	1	0	0	1	0	0	0	0	0	2	0	0	0	0	0	9
W	0	0	1	0	0	0	1	0	1	0	0	0	4	1	0	2	0	0	0	1	0	2	1	0	0	14
Z	0	0	0	0	0	1	0	0	0	0	1	0	0	0	0	1	0	1	0	0	0	0	0	0	5	9

Published by Verlag der TU Graz
Graz University of Technology

 DOI: 10.3217/978-3-85125-533-1-86

response.

Furthermore, given the letter selection frequency in the 30-trial online blocks, a larger maximum trial cap is an obvious change going forward. As the discrimination difficulty and input fatigue make the task somewhat strenuous, brief breaks may be necessary as blocks lengthen. Current, trials last no longer than 20 seconds, and responses may grow increasingly non-stationary due to fatigue if that duration significantly increases.

One advantage of the segment speller is that errors tend to be to visually similar letters (letters with similar subsets of segments) as opposed to neighboring letters in the grid for standard P300 grid and hexagonal spellers. This means that perfect selection of letters may not be necessary for typed words to be readable, as replacing letters by visually similar ones can still be quite legible.

An important question to consider is whether the combinatorial advantage of using segments justifies the increase in task difficulty. The complexity of the oddball task increases significantly when moving from letters to segments, and the chances of misidentification also increase. Moreover, task difficulty has been shown to attenuate P3 amplitude [12], especially that of the more frontal P3a [13]. It is possible that the high latency, posterior distribution of our responses is a consequence of this difficult categorization task. Consequently, future experiments could compare responses to an easier oddball task, to help contextualize the data.

CONCLUSION

The online classification of target vs nontarget segments proved possible for all subjects, with an average segment accuracy of 68%. The segment model – designed to probabilistically infer the target letter based on segment classification – outputs a target 61.4% of the time. Of these output targets, the correct letter was selected 31.7% of the time. As only 30 segments could be queried per target letter, we expect a longer selection block paired with a higher threshold should significantly improve final letter accuracy and rate.

ACKNOWLEDGEMENTS

This study would not have been possible without the support of our funding agencies. This work was supported by the NSF grants SMA 1041775 and IIS 1528214.

REFERENCES

[1] Farwell, L. A., & Donchin, E. (1988). Talking off the top of your head: toward a mental prosthesis utilizing event-related brain potentials. *Electroencephalography and clinical Neurophysiology*, *70*(6), 510-523.

[2] Cohen, B., & Caroscio, J. (1982). Eye movements in amyotrophic lateral sclerosis. *Journal of neural transmission. Supplementum*, *19*, 305-315.

[3] Brunner, P., Joshi, S., Briskin, S., Wolpaw, J. R., Bischof, H., & Schalk, G. (2010). Does the 'P300'speller depend on eye gaze?. *Journal of neural engineering*, *7*(5), 056013.

[4] Orhan, U., Hild, K. E., Erdogmus, D., Roark, B., Oken, B., & Fried-Oken, M. (2012, March). RSVP keyboard: An EEG based typing interface. In *Acoustics, Speech and Signal Processing (ICASSP), 2012 IEEE International Conference on* (pp. 645-648). IEEE.

[5] Chennu, S., Alsufyani, A., Filetti, M., Owen, A. M., & Bowman, H. (2013). The cost of space independence in P300-BCI spellers. *Journal of neuroengineering and rehabilitation*, *10*(1), 82.

[6] Minett, J. W., Zheng, H. Y., Fong, M. C., Zhou, L., Peng, G., & Wang, W. S. (2012). A Chinese text input brain–computer interface based on the P300 speller. *International Journal of Human-Computer Interaction*, *28*(7), 472-483.

[7] Delorme, A., & Makeig, S. (2004). EEGLAB: an open source toolbox for analysis of single-trial EEG dynamics including independent component analysis. *Journal of neuroscience methods*, *134*(1), 9-21.

[8] Kothe, C. A. E., & Jung, T. P. (2014). *U.S. Patent Application No. 14/895,440*.

[9] Kothe, Christian Andreas, and Scott Makeig. "BCILAB: a platform for brain–computer interface development." *Journal of neural engineering* 10.5 (2013): 056014.

[10] Ledoit, O., & Wolf, M. (2004). A well-conditioned estimator for large-dimensional covariance matrices. *Journal of multivariate analysis*, *88*(2), 365-411.

[11] Polich, J., Ellerson, P. C., & Cohen, J. (1996). P300, stimulus intensity, modality, and probability. *International Journal of Psychophysiology*, *23*(1), 55-62.

[12] Johnson, R., & Donchin, E. (1980). P300 and stimulus categorization: two plus one is not so different from one plus one. *Psychophysiology*, *17*(2), 167-178.

[13] Baur, N., Metzner, M. F., & Śmigasiewicz, K. (2014). The hard oddball: Effects of difficult response selection on stimulus-related P3 and on response-related negative potentials. *Psychophysiology*, *51*(11), 1089-1100.

[14] Kim, K. H., Kim, J. H., Yoon, J., & Jung, K. Y. (2008). Influence of task difficulty on the features of event-related potential during visual oddball task. *Neuroscience letters*, *445*(2), 179-183.

Published by Verlag der TU Graz
Graz University of Technology

Proceedings of the
7th Graz Brain-Computer Interface Conference 2017 DOI: 10.3217/978-3-85125-533-1-87

USING RECURRENT NEURAL NETWORKS FOR P300-BASED BRAIN-COMPUTER INTERFACES

O. Tal, D. Friedman

The Advanced Reality Lab, The Interdisciplinary Center, Herzliya, Israel

Contact: doronf@idc.ac.il

ABSTRACT: P300-based spellers are one of the main methods for electroencephalogram (EEG)-based brain-computer interface, and the detection of the target event with high accuracy is an important prerequisite. The rapid serial visual presentation (RSVP) protocol is of high interest because it can be used by patients who have lost control over their eyes. In this study we wish to explore the suitability of recurrent neural networks (RNNs) as a machine learning method for identifying the target letter in RSVP data. We systematically compare RNN with alternative methods such as linear discriminant analysis (LDA) and convolutional neural networks (CNN). Our results indicate that RNN does not have any advantages in single subject classfication. However, we show that a network combining CNN and RNN is superiour in transfer learning among subjects, and is significantly more resilient to temporal noise than other methods.

INTRODUCTION

Neural networks have recently been shown to achieve outstanding performance in several machine learning domains such as image recognition [15] and voice recognition [12]. Most of these breakthroughs have been achieved with CNNs [16], but some promising results have also been demonstrated by using RNNs for tasks such as speech and handwriting recognition [11, 10], usually when using the long short-term memory (LSTM) architecture [13]. CNNs are feed forward networks that implement receptive fields. RNNs, on the other hand, contain directed cycles and are thus able to "remember" the previous activation state of the network, which makes them especially suitable for learning sequences.

There have been some studies on using "deep neural networks" for P300 classification [5, 19]. The results reported, despite some success, do not show the same dramatic progress achieved by 'deep learning' methods as compared to the previous state of the art; while in areas such as image or voice recognition 'deep' neural networks have resulted in classification accuracy exceeding other methods by far, this has not yet been the case with EEG in general and P300 detection specifically. The small number of samples typically available in neuroscience (or BCI) is most likely one of the main reasons. In addition, the high dimensionality of the EEG signal, the low signal to noise (SNR) and the existence of outliers in the data, pose other difficulties when trying to use neural networks for BCI tasks (see [18]). The main question in this research is whether the RNN model, and particularly LSTM, can enhance the accuracy of P300-based BCI systems and if so, under what conditions.

BACKGROUND

P300-based BCI systems can recognize a taregt stimulus out of a set of stimuli, typically letters and numbers, by examining the subject's EEG data. The first system that used the P300 effect was presented by [8] and since then different versions of P300 based BCI systems were suggested. One example of such a paradigm is the P300 rapid serial visual presentation (RSVP) speller. In this paradigm letters are presented one after the other in a random order, and the subject is asked to pay attention only to one of the letters, reffered to as the *target* (e.g., by counting them silently).

There are a lot of methods for identifying the target letter for a BCI task. Blankertz et al. [4] suggest to select the time interval with maximal separation between the target and non target samples, average their electro-potential value and use shrinkage LDA to classify these features. Using this method has a drawback due to the low complexity of LDA model [6]. The winner of the BCI competition III: dataset II used an ensemble of support vector machines (SVM) [21], and other methods include hidden Markov model, k-nearest neighbours, and more [6].

More recently, given the success of 'deep' neural networks [15], there have been several attempts to apply 'deep learning' for BCI related tasks. Cecotti and Graser [5] were the first to use CNNs for a P300 speller. In their work, they train an ensemble of CNN-based P300 classifiers to identify the existence of P300. Manor and Geva [19] used CNN for the RSVP P300 classification task and suggested a new spatio-temporal regularization method, which have shown improvement in the performance.

Unlike feed forward network models such as CNN and multi-layer perceptron (MLP), the RNN architecture allows directed cycles within the network, which enable

Published by Verlag der TU Graz
Graz University of Technology

 DOI: 10.3217/978-3-85125-533-1-87

the model to "memorize past events". LSTM [13] is a type of RNN, which includes a special node that can be described as a differentiable memory cell. The specific architecture of LSTM enables it to overcome some of the weakness of simple RNNs [3].
There are several reasons why LSTM is a good candidate for modelling the P300 pattern. First, RNN and LSTM have shown success when modeling time series for tasks such as handwriting and speech recognition [11, 10, 28]. Second, RNN is known to have the capability to approximate dynamical systems [17], which makes it a natural candidate for modelling the dynamics of EEG data. Another motivation is that RNN can be seen as a powerful form of hidden Markov models (HMM), which have been shown to classify EEG successfully [23, 20, 6]; RNNs can be seen as HMMs with an exponentially large state space and an extremely compact parametrization [24].
LSTM was already used for analysing EEG data for emotion detection [22] and a phenomena called behavioral microsleeps [7]. Bahshivan et al. [2] modeled inter-subject EEG features for identifying cognitive load by using convolutional LSTM. Their representation of the input was a "video" comprised of topographic scalp maps in three different band powers over time. One of the major differences between their work and ours is that we use the original signal without any feature extraction (such as band power), and we focus specifically on P300 speller data.

MATERIALS AND METHODS

We compared the performance of LSTM based methods with other methods on a dataset from a RSVP P300 speller study [1]. We used average prediction across 10 trials to measure the P300 speller accuracy as applied in [1].
The dataset includes 55 channels of EEG recordings from 11 subjects. Each subject is presented with 10 repetitions of 60 to 70 sets of 30 different letters and symbols. In total there are approximately 20,000 samples for each subject where 1/30 of them are supposed to contain a P300 wave. While the original experiment contains 3 different settings (interval of 116ms with/without colors and 83ms with color), we used the experiment setting of 116ms intervals with letters in different colors. For more detail, see [1].
In addition to the filters applied in [1], all models that we used share the same pre-processing stage of downsampling the input frequency from 200Hz to 25 Hz. The result is that each learning sample is a matrix of 55 channels with 25 time samples each, or $55 * 25 = 1375$ features. Each sample thus covers exactly 1 second around the target event, at times [-200,800] ms.
The models evaluated in this experiment are:

- LDA - A common method used in P300 classification for BCI [1, 4]. Here we used a simplified version; unlike [1] we use all the timestamps as features, and we are using a non-shrinkage version of LDA.
- CNN (Fig.1a) – The CNN model we use is similar to the one used in [5]. The first layer is composed of 10 spatial filters, each of size $55 * 1$ – the number of channels. The second layer contains 13 different temporal filters with size of $1 * 5$. Each one of the temporal filters processes 5 subsequent time stamps without overlapping. The third and fourth layers are simple fully connected layers followed by a single cell with a sigmoid activation function that emits a scalar.
- LSTM large/small (Fig.1b) – LSTM large/small are both composed of single LSTM layers with 100 and 30 hidden cells in each, correspondingly. Both models end with a single cell with a sigmoid activation layer that emits a scalar.
- LSTM-CNN large/small Fig.1c – The model has CNN as a first layer (the spatial domain layer) and LSTM as the second layer for the temporal domain. The first convolutional layer is the same as in the CNN model. Unlike the CNN model, the temporal layer is an LSTM layer with 100/30 hidden cells. The last layer contains a single cell with a sigmoid activation layer that emits a scalar.

In order to examine the power of each method in modelling the inter-subject and intra-subject variance we have conducted the following experiments:

1. Training and testing on each subject's data separately in order to explore intra-subject generalization.
2. Training and testing on all the different subjects data combined in order to investigate the impact of larger amounts of data.
3. Training on all subjects expect one. We conduct this experiment in order to explore the performance of a model that was trained off-line, on different subjects, and then applied to a new subject, with or without additional calibration, as a test of transfer learning.
4. Testing different models when introducing temporal noise.

A highly desired property from BCI systems is tolerance to a small degree of noise in the stimuli onset time, and this is the objective of the fourth experiment. In order to evaluate the resistance to such noise, we use a model trained on the original stimuli onset (i.e, noise level = 0ms) and evaluate its performance on different stimuli onset: noise levels of -120ms,-80ms,-40ms, +40ms, +80ms, and 120ms. We conducted this experiment using 10-fold cross validation in order to be able to get statistically significant results. This last experiment was conducted only on the CNN and LSTM-CNN models and

Published by Verlag der TU Graz
Graz University of Technology

 DOI: 10.3217/978-3-85125-533-1-87

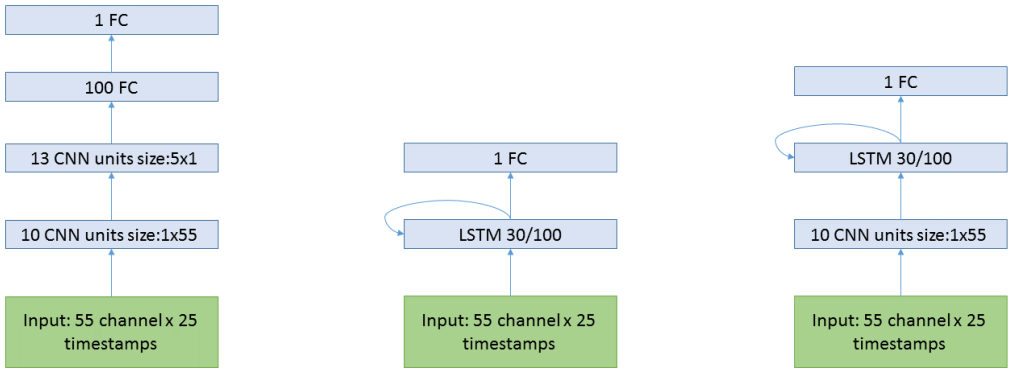

(a) CNN model (b) LSTM model (c) CNN-LSTM model

Figure 1: Schematic diagrams of the neural networks evaluated. FC stands for fully connected layers.

used data from all subjects (as in experiment 2 described above).

For all the experiments, the different models were trained using the RMSProp [26] optimizer: first for 30 epochs with a learning rate of 0.001 and then continued training for additional 30 epochs with a learning rate of 0.00001.

RMSProp [26] is a stochastic gradient descent (SGD) method. Unlike simple SGD, the method adapts a different learning rate for each parameter separately by applying a moving average across the magnitude of the past gradients, and then re-scaling the learning by this past gradient. We decided to use RMSProp since it is said to be robust and fast [27, 14, 25].

RESULTS

Tab. 1 summarizes the results of the different experiments; all results are based on an average of 10 consecutive trials to detect the target letter, as in [1]. The results for training and testing on the same subject indicate that LSTM is inferior (82%), and even the LSTM-CNN combined model performs less than the the simple LDA method (86 and 93% in the LSTM-CNN models and 96% using LDA) . A possible advantage for LSTM only becomes apparent with larger amounts of data – when training and testing on all the subjects together (Tab. 1). The large LSTM model performs poorly – 77%; we suspect that this is due to the large number of trainable parameters – 62501 ("over-fitting"); this is why we introduced CNN as a first layer and reduced the number of hidden LSTM cells.

Tab. 2 summarizes the results per single subject. There is a significant difference among subjects, across the different models. For example subject *fat* results in higher accuracy than *icn* regardless of the tested model. Eventually, the best network method - using training on other subjects and recalibration with a combined CNN-LSTM large model, is able to boost the results of the worse subject to 86%.

Tab. 3 is aimed at estimating learning across subjects – it provides the detailed results when training the models on all subjects except one, and then testing on that subject. In the second stage, we continue training the model on the rest $3/4$ of the **test subject's** data using a smaller learning rate (0.0001 using RMSProp) for 30 epochs – this is presented in columns *CNN and LSTM-CNN all except one fine tune* . The results indicate that the LDA accuracy is much poorer than those of the CNN and LSTM-CNN models (65% as opposed to 84%); i.e., the neural networks are superior under these conditions of inter-subject variability. When we allow calibrating the model for each subject, we achieve an average accuracy of 97% for both CNN and LSTM-CNN; there is no standard method for similarly re-calibrating an LDA algorithm, so we do not have an equivalent comparison.

Resistance to temporal noise is displayed in Tab. 4. In this test we also see that LDA accuracy drops significantly. Both CNN and the combined LSTM-CNN seems to overcome such noise; the LSTM-CNN model results in 4% or 5% when adding or removing 40ms to the original stimuli onset, and a t-test indicates that this difference is statistically significant ($p < 0.05$).

A possible explanation can be seen when looking at the two models' saliency map (Fig. 2). In order to investigate the "attention", or the sensitivity of the LSTM model, and compare it to the CNN model, we used a technique suggested by [9] and draw the absolute gradient of the neural network with respect to the input.

If $f(x_1, ..., x_n)$ is a differentiable, scalar-valued function, its gradient is the vector whose components are the n partial derivatives of f, which is a vector-valued function. In our case of $f(x|\theta)$ is the neural network with fixed weights θ and input x. The partial derivatives of $f(x|\theta)$ with respect to x can be interpreted as "how changing each value of x will change the prediction score". This gradient should not be confused with the gradient used for training, where the goal is to optimize the model parameters θ when x is fixed.

Published by Verlag der TU Graz
Graz University of Technology

 DOI: 10.3217/978-3-85125-533-1-87

Table 1: Average accuracy across all experiments; x marks experiments that were not performed.

model	number of parameter	accuracy per subjects	accuracy all subjects	all but one	all but one after fine tuning
LDA	1375	0.96	0.79	0.65	x
LSTM large	62501	0.82	0.77	x	x
LSTM small	10351	0.86	0.9	x	x
CNN	7924	0.98	0.92	0.84	0.97
LSTM-CNN large	49041	0.93	0.9	x	x
LSTM-CNN small	5511	0.89	0.93	0.84	0.97

Table 2: Average accuracy per subject comparing all models.

subject	LDA	LSTM large	LSTM-CNN large	CNN	LSTM small	LSTM-CNN small
fat	1.00	0.98	0.98	0.98	1.00	0.95
gcb	0.91	0.82	0.88	0.92	0.74	0.75
gcc	1.00	0.84	0.92	1.00	0.92	0.97
gcd	0.97	0.80	0.90	1.00	0.76	0.93
gcf	1.00	0.92	0.94	0.95	0.97	0.95
gcg	0.94	0.74	0.96	0.96	0.80	0.87
gch	0.97	0.93	0.96	0.97	0.97	0.96
iay	0.94	0.62	0.92	0.98	0.75	0.86
icn	0.94	0.62	0.86	0.98	0.77	0.77
icr	0.93	0.97	0.98	0.98	0.98	0.98
pia	0.97	0.82	0.94	1.00	0.77	0.81
mean	0.96	0.82	0.93	0.98	0.86	0.89

In the case of P300 prediction, x is a matrix of $C \times T$ (C - number of channels, T - number of time steps) and $f(x|\theta)$ is the neural network where θ is the model's weights after training. The gradient $\nabla f(x|\theta)$ (see Eq.1) is a matrix with the same size as the input x, where the amplitude of each cell reflects its impact on the function value. Cells with high absolute value can be interpreted as the cells that have a significant influence on the prediction function.

$$\nabla f\left(x|\theta\right) = \begin{bmatrix} \frac{\partial f(x|\theta)}{\partial x(c_1,t_1)} & \dots & \frac{\partial f(x|\theta)}{\partial x(c_1,t_T)} \\ \dots & \dots & \dots \\ \frac{\partial f(x|\theta)}{\partial x(c_C,t_1)} & \dots & \frac{\partial f(x|\theta)}{\partial x(c_C,t_T)} \end{bmatrix} \quad (1)$$

The results displayed in Fig.2a and Fig. 2b show the average absolute gradient across all the *target* samples of a single cross validation test data: the warm colors correspond to high gradient values, indicating that the model is more sensitive to change in these input features. We can see the sensitivity of the CNN model spreads across the recording relatively evenly as opposed to the LSTM-CNN which is focused around the 250ms and 450ms time-stamps.

Table 4: Accuracy when introducing temporal noise. The best results are boldfaced when the differences are statistically significant.

Noise	CNN	LSTM_CNN	LDA
-120	0.058	0.044	0.016
-80	0.275	0.299	0.016
-40	**0.825**	**0.864**	**0.565**
40	**0.848**	**0.896**	**0.608**
80	0.335	0.390	0.260
120	0.042	0.042	0.059

DISCUSSION

In this work we examined using LSTM neural networks for the task of the BCI task of P300 speller. Despite its temporal nature, no version of LSTM investigated in this work has shown a significant advantage compared to the CNN model suggested by [5]. LSTM results improved with large amounts of data from multiple subjects, and superior results are obntained with a combined CNN-LSTM model; moreover, we have shown that this combined model is significantly more robust to temporal noise in the stimuli onset. We also show that the sensitivity of the LSTM based model is much more focused on the area between 250ms to 450ms than CNN based model, which is in line with our expectation from

Published by Verlag der TU Graz
Graz University of Technology

 DOI: 10.3217/978-3-85125-533-1-87

Table 3: Accuracy when training and testing on different subjects.

subject	LDA all except one	CNN all except one	CNN all except one fine tune	SMALL LSTM-CNN all except one	SMALL LSTM-CNN all except one fine tune
fat	0.94	1.00	1.00	0.98	1.00
gcb	0.43	0.83	0.91	0.86	0.92
gcc	0.79	0.98	0.98	0.95	0.97
gcd	0.66	0.80	0.99	0.83	0.97
gcf	0.68	0.89	0.98	0.79	0.98
gcg	0.52	0.81	0.94	0.77	0.90
gch	0.87	0.97	0.97	0.97	0.99
iay	0.48	0.69	0.98	0.67	0.97
icn	0.44	0.58	0.92	0.61	0.95
icr	0.63	0.81	1.00	0.89	1.00
pia	0.77	0.87	0.96	0.91	0.97
mean	0.65	0.84	0.97	0.84	0.97

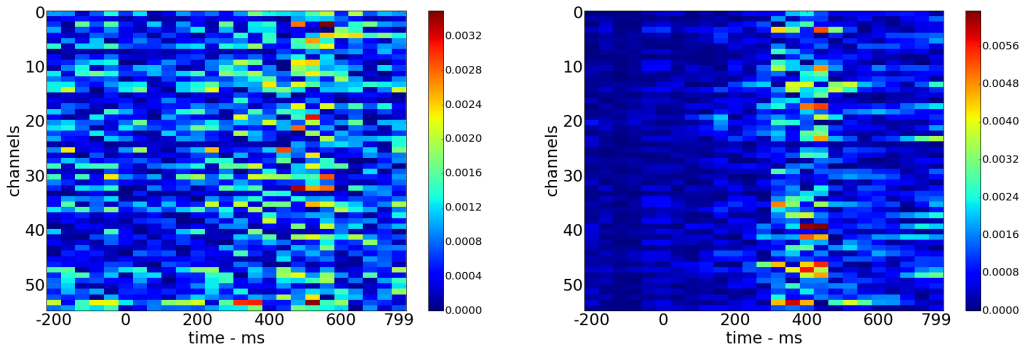

(a) CNN

(b) LSTM-CNN

Figure 2: Average gradient in target samples, comparing CNN and LSTM-CNN.

the P300 ERP. To conclude – in the dataset we have explored a simple algorithm such as LDA performed extremely well when trained and tested on the same subject, but additional experiments involving cross-subject training and temporal noise expose the possible advantages of 'deep' networks, and especially the LSTM-CNN combined method.

REFERENCES

[1] L. Acqualagna and B. Blankertz., "Gaze-independent BCI-spelling using rapid serial visual presentation (rsvp)," *NeuroImage*, vol. 124, pp. 901–908, 2013.

[2] P. Bashivan, "Learning representations from EEG with deep recurrent-convolutional neural networks." *arXiv*, vol. 1511.06448, 2015.

[3] Y. Bengio, P. Simard, and P. Frasconi, "Learning long-term dependencies with gradient descent is difficult," *IEEE Transactions on Neural Networks*, vol. 5, no. 2, pp. 157–166, 1994.

[4] B. Blankertz, "Single-trial analysis and classification of erp components—a tutorial," *NeuroImage*, vol. 50, pp. 814–825, 2011.

[5] H. Cecotti and A. Graser, "Convolutional neural networks for p300 detection with application to brain-computer interfaces," *IEEE transactions on pattern analysis and machine intelligence*, vol. 33, pp. 433–445, 2011.

[6] F. Cincotti, A. Scipione, A. Timperi, D. Mattia, A. Marciani, J. Millan, S. Salinari, L. Bianchi, and F. Bablioni, "Comparison of different feature classifiers for brain computer interfaces," in *Neural Engineering, 2003. Conference Proceedings. First International IEEE EMBS Conference on*. IEEE, 2003, pp. 645–647.

[7] P. Davidson, R. Jones, and M. Peiris, "Detecting behavioural microsleeps using eeg and lstm recur-

Published by Verlag der TU Graz
Graz University of Technology

 DOI: 10.3217/978-3-85125-533-1-87

rent neural networks," in *Proc. Int. Conf. IEEE Eng. Med. Biol. Soc*, vol. 27, 2005, pp. 5754–5757.

[8] L. A. Farwell and E. Donchin, "Talking off the top of your head: toward a mental prosthesis utilizing event-related brain potentials," *Neural Computation*, vol. 70, pp. 510–523, 1988.

[9] A. Graves, *Supervised Sequence Labelling*. Berlin, Heidelberg: Springer Berlin Heidelberg, 2012, pp. 5–13.

[10] A. Graves, M. Liwicki, H. Bunke, J. Schmidhuber, and S. Fernández, "Unconstrained on-line handwriting recognition with recurrent neural networks," in *Advances in Neural Information Processing Systems*, 2008, pp. 577–584.

[11] A. Graves, A.-r. Mohamed, and G. Hinton, "Speech recognition with deep recurrent neural networks," in *2013 IEEE international conference on acoustics, speech and signal processing*. IEEE, 2013, pp. 6645–6649.

[12] G. Hinton, L. Deng, D. Yu, G. E. Dahl, A.-r. Mohamed, N. Jaitly, A. Senior, V. Vanhoucke, P. Nguyen, T. N. Sainath *et al.*, "Deep neural networks for acoustic modeling in speech recognition: The shared views of four research groups," *IEEE Signal Processing Magazine*, vol. 29, no. 6, pp. 82–97, 2012.

[13] S. Hochreiter and J. Schmidhuber., "Long short-term memory," *arXiv*, vol. 9.8, pp. 1735–1780, 1997.

[14] A. Karpathy and L. Fei-Fei, "Deep visual-semantic alignments for generating image descriptions," in *Proceedings of the IEEE Conference on Computer Vision and Pattern Recognition*, 2015, pp. 3128–3137.

[15] A. Krizhevsky, I. Sutskever, and G. E. Hinton, "Imagenet classification with deep convolutional neural networks," in *Advances in neural information processing systems*, 2012, pp. 1097–1105.

[16] Y. LeCun, "Gradient-based learning applied to document recognition." *Proceedings of the IEEE*, vol. 86, pp. 2278–2324, 1998.

[17] X.-D. Li, J. K. Ho, and T. W. Chow, "Approximation of dynamical time-variant systems by continuous-time recurrent neural networks," *IEEE Transactions on Circuits and Systems II: Express Briefs*, vol. 52, no. 10, pp. 656–660, 2005.

[18] F. Lotte, M. Congedo, A. Lécuyer, F. Lamarche, and B. Arnaldi, "A review of classification algorithms for eeg-based brain–computer interfaces," *Journal of neural engineering*, vol. 4, no. 2, p. R1, 2007.

[19] R. Manor and A. B. Geva, "Convolutional neural network for multi-category rapid serial visual presentationBCI," *Frontiers in computational neuroscience*, vol. 9, 2015.

[20] B. Obermaier, C. Guger, C. Neuper, and G. Pfurtscheller, "Hidden markov models for online classification of single trial eeg data," *Pattern recognition letters*, vol. 22, no. 12, pp. 1299–1309, 2001.

[21] A. Rakotomamonjy and V. Guigue, "BCI competition iii: dataset ii-ensemble of svms for BCI p300 speller," *IEEE transactions on biomedical engineering*, vol. 55, no. 3, pp. 1147–1154, 2008.

[22] M. Soleymani, S. Asghari-Esfeden, M. Pantic, and Y. Fu, "Continuous emotion detection using eeg signals and facial expressions," in *2014 IEEE International Conference on Multimedia and Expo (ICME)*. IEEE, 2014, pp. 1–6.

[23] S. Solhjoo, A. M. Nasrabadi, and M. R. H. Golpayegani, "Classification of chaotic signals using hmm classifiers: Eeg-based mental task classification," in *Signal Processing Conference, 2005 13th European*. IEEE, 2005, pp. 1–4.

[24] I. Sutskever, G. E. Hinton, and G. W. Taylor, "The recurrent temporal restricted boltzmann machine," in *Advances in Neural Information Processing Systems*, 2009, pp. 1601–1608.

[25] C. Szegedy, V. Vanhoucke, S. Ioffe, J. Shlens, and Z. Wojna, "Rethinking the inception architecture for computer vision," in *Proceedings of the IEEE Conference on Computer Vision and Pattern Recognition*, 2016, pp. 2818–2826.

[26] T. Tieleman and G. Hinton, "Lecture 6.5-rmsprop: Divide the gradient by a running average of its recent magnitude," *COURSERA: Neural networks for machine learning*, vol. 4, no. 2, 2012.

[27] K. Xu, J. Ba, R. Kiros, K. Cho, A. C. Courville, R. Salakhutdinov, R. S. Zemel, and Y. Bengio, "Show, attend and tell: Neural image caption generation with visual attention." in *ICML*, vol. 14, 2015, pp. 77–81.

[28] J. Yue-Hei Ng, M. Hausknecht, S. Vijayanarasimhan, O. Vinyals, R. Monga, and G. Toderici, "Beyond short snippets: Deep networks for video classification," in *Proceedings of the IEEE Conference on Computer Vision and Pattern Recognition*, 2015, pp. 4694–4702.

Published by Verlag der TU Graz
Graz University of Technology

Proceedings of the
7th Graz Brain-Computer Interface Conference 2017 DOI: 10.3217/978-3-85125-533-1-88

A SSVEP BCI BASED ON CANONICAL CORRELATION ANALYSIS

L. Talevi[1], V. Mondini[1], A.L. Mangia[1], M. Lannocca[1], A. Cappello[1]

[1] Department of Electrical, Electronic and Information Engineering (DEI), University of Bologna, Cesena, Italy

E-mail: valeria.mondini3@unibo.it

ABSTRACT: Canonical correlation analysis (CCA) is one of the most popular methods in the field of Brain Computer Interfaces (BCIs) based on steady-state visual evoked potentials (SSVEPs). The efficacy of the method has been widely proved, and several variations have been proposed. However, most of the approaches still consider only the first canonical correlation as a feature for classification, which can leave some important information behind. Notably, if the signal shows phase transitions, its informative content can be diffused over more than one coefficient. We show here that considering the first two canonical correlations, instead of the largest one only, can significantly improve classification accuracy without increasing computational load, and that an adjunctive pre-processing step with sinc-windowing can further enhance the results.

INTRODUCTION

A Brain-Computer Interface (BCI) is a system creating a direct communication channel between the brain and the outside [1]. EEG-based BCIs can be based on slow cortical potentials (SCPs), event-related desynchronization/synchronization (ERD/ERS), event-related potentials (like P300), or steady-state evoked potentials (SSVEPs) [2]. Among these, SSVEP-based systems are appealing for their high accuracy and information transfer rate (ITR), due to the high signal-to-noise ratio of SSVEPs even without user training [2]. SSVEPs are periodic evoked potentials induced by repetitive visual stimulations at frequencies greater than 6Hz [3]. If two or more targets (LEDs, squares, symbols) flicker at different frequencies, an analysis of the frequency content of SSVEPs can lead to conclude which stimulus the user is gazing at.

An intuitive and commonly used frequency detection approach is the one based on *power spectral density analysis* (PSDA). In PSDA methods, power values are evaluated from the spectrum at the target stimulation frequencies, and used for classification. Recently, the application of Canonical Correlation Analysis (CCA) was proposed in the field of SSVEP BCIs [3]. The efficacy of the method has been widely proved by several studies (e.g. [4], [5]). Furthermore, its superiority to PSDA both in terms of computational load and accuracy has been shown [6], [7], so several variations of CCA have been proposed [8]–[18].

In this work, we present a SSVEP BCI based on the classical CCA method. However, we introduce here two variations in i) the pre-processing of the signals and ii) the composition of the feature vector. We show that both modifications can significantly improve classification accuracy, without an excessive increase of the computational load.

MATERIALS AND METHODS

EEG recording: The EEG was recorded from 8 electrodes (PO7, PO3, O1, POz, Oz, PO4, O2, PO8) positioned according to the international 10-20 layout. The signals were acquired using the Brainbox EEG-1166 amplifier (Braintronix), with 256Hz sample frequency and a 50Hz notch filter on.

The BCI system: The online BCI system was implemented using LabVIEW, for a better synchronization of the signal recording and the stimulus presentation modules. SSVEP stimulation was provided through two blue LEDs, emitting lights flickering at two different frequencies, f_1 and f_2. A NI MyDAQ device controlled the behavior of the LEDs, which were arranged around the screen of the PC running the software (Figure 1). We chose the LED stimulus implementation to provide accurate and stable flickering frequencies, avoiding any operating system control delay and independently from the screen refreshing rate.

The implemented software was organized into three modules: *training* (T), *validation* (V) and *free mode* (F). During T and V, a yellow square appeared on the screen indicating the LED to gaze at. This permitted to deduce the true class label to train (T module), validate (V module) and use (F module) the underlying system classifier. During both T and V, the stimulus was presented in the form of subsequent trials. Each trial was composed by a *preamble*, a *stimulus* and a *break* period. During the *preamble*, the yellow square appeared near the target LED, then both lights started flickering (*stimulus*), and the trial ended with a *break* period where the squares disappeared and the LEDs shut off. No feedback was provided to the user during T module, while in V the recognized target was highlighted at the end of each trial. Both in T and V, the target sequence presentation was balanced and in random order.

The *free mode* module F was designed to simulate a real operating condition. During F, both the LEDs

Published by Verlag der TU Graz
Graz University of Technology

 DOI: 10.3217/978-3-85125-533-1-88

continuously flickered, while a square appeared near the one recognized by the classifier, as a continuous feedback for the user (Figure 1).

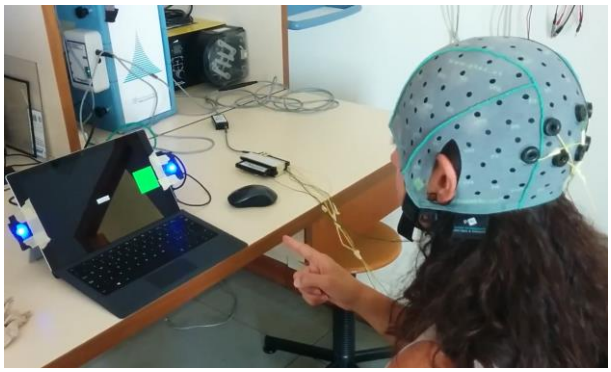

Figure 1: Operation of the system in *free mode* (F).

Signal processing: In all the three modules (T, V and F), 1.5s-long epochs (no overlapping) were processed by the software in three steps: i) sinc-windowing, ii) CCA analysis and iii) SVM training/classification.
First of all, the EEG segments were convolved with an adequately modulated sinc function (sinc-windowing) to perform a high-Q band-pass filtering around the two main stimulation frequencies, f_1 and f_2, and N_{harm} harmonic frequencies. As it is known, the inverse Fourier transform of an ideal rectangular band-pass filter, centered on f_0 and with M bandwith, is:

$$rect\left(\frac{f-f_0}{M}\right)+rect\left(\frac{f+f_0}{M}\right)\xrightarrow{F^{-1}}2Msinc(Mt)\cos(2\pi f_0 t) \quad (1)$$

where f is the frequency and F^{-1} is the inverse Fourier transform. Thus, the extraction of f_1 and f_2 components and their N_{harm} harmonics was performed with a convolution of the signals and the following function:

$$h(t)=2Msinc(Mt)\left(\sum_{n=1}^{N_{harm}}\cos(2\pi n f_1 t)+\cos(2\pi n f_2 t)\right) \quad (2)$$

with M bandwidth and N_{harm} number of considered harmonics. A preliminary analysis suggested using M=2Hz and N_{harm}=3.
After sinc-windowing, canonical correlation analysis (CCA) was performed for feature extraction. CCA is a multivariate statistical method [19] revealing the underlying correlation between two sets of data. Notably, given two sets of variables $\mathbf{X} \in \mathbb{R}^{pxt}$ and $\mathbf{Y} \in \mathbb{R}^{qxt}$ (p≤q), CCA finds two corresponding sets **U=AX** and **V=BY**, called *canonical variables*, so that the correlation between each pair (*Ui*,*Vi*) is maximized:

$$\rho_i=\frac{cov(U_i,V_i)}{\sqrt{var(U_i)var(V_i)}} \quad (3)$$

while every pair (U_i,V_j), (U_i,U_j) and (V_i,V_j) is uncorrelated if i≠j. The p resulting ρ_i are called *canonical correlations*, and are a measure of similarity between the two sets of data.

The use of CCA in the field of SSVEP-based BCIs was first introduced by Lin et al [3], which proposed to perform *k* CCAs - one for each stimulation frequency f_k - between the set of acquired EEG signals in **X** and a set $\mathbf{Y_k}$ of pure SSVEP responses. Each set $\mathbf{Y_k}$ is composed as follows:

$$\boldsymbol{Y}_k=\begin{pmatrix}\cos(2\pi f_k t)\\ \sin(2\pi f_k t)\\ \cos(2\pi 2 f_k t)\\ \sin(2\pi 2 f_k t)\\ \vdots\\ \cos(2\pi N_{harm} f_k t)\\ \sin(2\pi N_{harm} f_k t)\end{pmatrix} \quad (4)$$

with f_k stimulation frequency and N_{harm} number of considered harmonics. Even though every CCA generates multiple correlation coefficients, usually only the largest one is considered. After performing CCA between each set $\mathbf{Y}_k$ and the recorded signals in **X**, the segment is assigned to the frequency f_k showing the largest canonical correlation.
The efficacy of the CCA method in the SSVEP-based BCI field has been widely proved [4], [5] and many variations were proposed [8]–[18]. However, most approaches consider only the first canonical correlation as a feature for classification, which can leave some important information behind. Moreover, usually the CCA method is employed without any pre-filtering of the incoming signals (the only exceptions are [17], [18], using IIR filter banks).
In the present work, we decided to implement the standard CCA method proposed by Lin et al [3] with two slight variations: i) convolution of the signals with the above introduced sinc-windowing function (Equation 2) and ii) consideration of the two largest canonical correlations instead of the largest one only. The rationale behind this is that, if EEG shows phase transitions, the information can be diffused over more than one coefficient. We further hypothesize that, if the largest canonical correlation is mainly referred to the sine (cosine) at a certain frequency, then the second largest correlation will probably be linked to the cosine (sine) at the same frequency. We therefore decided to consider, for each frequency f_k, the square root of the sum of squares of the largest two canonical correlations:

$$r_k=\sqrt{\rho_{k1}^2+\rho_{k2}^2} \quad (5)$$

If it is true that the second canonical correlation ρ_{k2} holds an information content complementary with respect to ρ_{k1}, then this combination of the two should incorporate a more complete information regarding the investigated frequency f_k., thus increasing the completeness of the feature and, hopefully, the achievable accuracy.
The values of r_1 and r_2 were extracted, for each EEG segment, from the two CCAs between **X** and $\mathbf{Y_1}$ and **X** and $\mathbf{Y_2}$. The data were finally used to train and use a linear SVM classifier, for which we chose a soft margin parameter c=2.

Published by Verlag der TU Graz
Graz University of Technology

 DOI: 10.3217/978-3-85125-533-1-88

Experimental paradigm and subjects: Four healthy volunteers (age 25 to 27, three females and a male) took part in the system test. All participants had normal or corrected to normal vision. The flickering frequencies for the two LEDs, f_1=12Hz and f_2=17Hz, were selected beforehand and were the same for all subjects. We chose these frequencies to exploit the SSVEP peak responses without harmonics overlapping. During the experiment, participants seated in a comfortable chair, approximately 60cm distant from the PC monitor.

Each volunteer underwent one *training* (T) and four *validation* (V) repetitions. Throughout the entire experiment, the system considered 1.5s-long epochs for feature extraction. Each training (T) was composed by 16 trials with 6s stimulus duration, so a total of 16*6/1.5=64 elements composed the training set. Each validation (V) was composed by 24 trials with 4.5s stimulus duration, so a total of 24*4.5/1.5=72 elements composed each test set.

System evaluation: We computed the online classification accuracy for each subject and *validation* repetition. To evaluate the influence of the two proposed variations (sinc-windowing and feature composition) on classification accuracy, all data were re-analyzed to test all the possible combinations. We therefore tested our method against i) sinc-windowing + CCA with classical feature extraction (first canonical correlation) ii) no sinc windowing and CCA with the proposed feature extraction and iii) no sinc-windowing and CCA with classical feature extraction.

Just for the sake of comparison, we repeated simulations also with a PSDA-based method. In this case, we composed the feature vector by using the periodogram-estimated powers in 2Hz-large bins around f_1, f_2 and N_{harm} respective harmonics.

Each accuracy was compared to chance level [20] via confidence intervals (α=0.05). As regards the comparisons between methods, to account for the fact that multiple data came from the same subject (i.e. the samples could not be assumed to be completely independent), we ran the evaluations as post-hoc tests of a repeated measures ANOVA. The ANOVA design included both the factors "method" (the within-subject factor) and "subject", thus considering all dependencies among data. The post-hoc analyses were performed through Fisher's LSD. A preliminary Kolmogorov-Smirnov test confirmed the normality of data distributions, which justified the use of parametric statistical tests.

The computation times for the presented procedure and PSDA were also evaluated and compared trough a paired t-test, and the proportion of time required for sinc-windowing was further investigated.

The average and peak information transfer rate (ITR) [21] were finally computed according to:

$$ITR(bit/min) = \frac{60}{T}\left(log_2(N) + plog_2(p) + (1-p)log_2\left(\frac{1-p}{N-1}\right)\right) \quad (6)$$

where N=2 is the number of choices, p is classification accuracy and T is the epoch duration (1.5s).

RESULTS

The classification accuracies obtained for the five methods are detailed in Table 1 for each subject and *validation* repetition, and summarized in Figure 2. The chance level at α=0.05 for our experimental setup was 61.25%, so all the obtained accuracies were significantly higher than chance, with the only exception of PSDA. The results of the post-hoc comparisons between each pair of methods are detailed in Table 2.

Table 1: Detailed accuracies (each subject and validation repetition) for the five methods.

		sinc+CCA (sumsq)	sinc+CCA (first)	only CCA (sumsq)	only CCA (first)	PSDA
S1	val_1	97.2	97.2	94.4	94.4	77.8
	val_2	95.8	91.6	94.4	91.6	76.4
	val_3	98.6	98.6	97.2	97.2	88.9
	val_4	100	100	98.6	93.1	87.5
S2	val_1	88.9	84.7	91.7	84.7	70.8
	val_2	87.5	79.2	83.3	80.6	65.3
	val_3	80.6	75.0	72.2	68.1	47.2
	val_4	94.4	94.4	93.1	90.3	68.1
S3	val_1	87.5	84.7	81.9	81.9	69.4
	val_2	86.1	83.3	86.1	83.3	66.7
	val_3	93.1	90.3	93.1	87.5	61.1
	val_4	86.1	88.9	86.1	80.6	59.7
S4	val_1	81.9	76.4	72.2	69.4	63.9
	val_2	75.0	75.0	79.2	77.8	65.3
	val_3	84.7	80.6	86.1	79.2	66.7
	val_4	80.6	80.6	80.6	76.4	69.4
Average		**88.6**	**86.3**	**86.9**	**83.5**	**69.0**
Peak		**100**	**100**	**98.6**	**97.2**	**88.9**

Table 2: p-values from the post-hoc tests between each pair of methods.

	sinc+CCA (sumsq)	sinc+CCA (first)	only CCA (sumsq)	only CCA (first)	PSDA
sinc+CCA (sumsq)	-	p<0.01 **	p=0.11	p<0.001 ***	p<0.001 ***
sinc+ CCA (first)	-	-	p=0.53	p<0.01 **	p<0.001 ***
only CCA (sumsq)	-	-	-	p<0.001 ***	p<0.001 ***
only CCA (first)	-	-	-	-	p<0.001 ***

Published by Verlag der TU Graz
Graz University of Technology

 DOI: 10.3217/978-3-85125-533-1-88

The implemented method performed significantly ($p<0.001$) better with respect to standard CCA method with no sinc-windowing. The accuracy improvement occurred indeed in almost every subject and session, with an average improvement of 5.1% and a peak improvement of 12.5%. As regards the influence of the single factors we can observe that the consideration of the first two canonical variables significantly outperforms the consideration of the largest only, both in the sinc-windowing ($p<0.01$) and no-sinc-windowing ($p<0.001$) condition. As regards the PSDA method, this confirmed to perform significantly worse ($p<0.001$) than any CCA variation.
As regards computation times, our CCA-based method confirmed to be significantly ($p<0.001$) faster with respect to PSDA, with an average time per operation of approximately the half (110µs against 239µs). As concerns sinc-windowing, it contributed for approximately a third on average (35µs) with respect to the total time of each operation (110µs).
As regards the information transfer rate of the presented system, we obtained a peak ITR of 40bits/min and an average ITR of 20.12bits/min. We don't detail the ITRs for each subject and *validation* to avoid repetition, but they can be easily computed from Table 1.

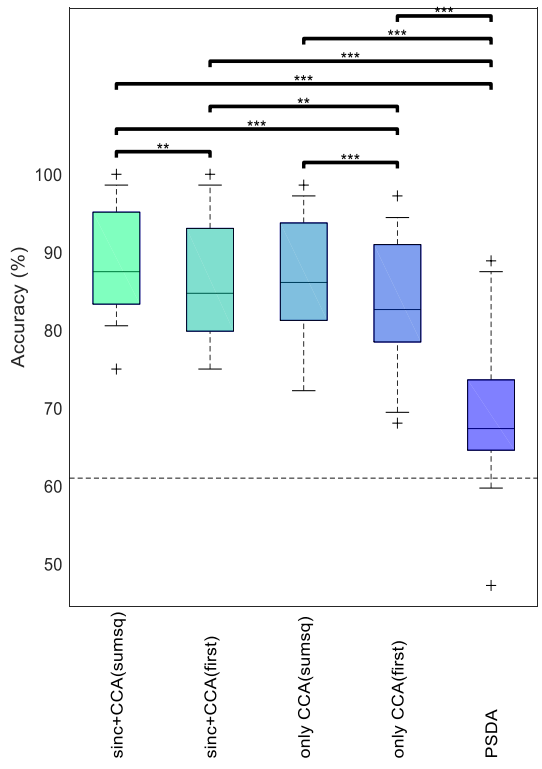

Figure 2: A box-plot showing the classification accuracy distributions for the five methods. The double star ** indicates a p-value<0.01, while triple star *** a p-value<0.001. The horizontal, dashed line marks the chance level (α=0.05).

DISCUSSION

Our results show how the consideration of two canonical correlations instead of using the largest one only, significantly improves the achievable accuracy without increasing computational load. The described effect is probably due to the fact that, since the canonical variables U_i are uncorrelated, the second canonical variable U_2 will contain information which are in quadrature with those contained in the first canonical variable U_1. So, if U_1 is mainly explained e.g. by the sine at a certain frequency, then U_2 will be mainly explained by the cosine at the same frequency. Then, taking the previously described combination of the largest correlations will include a more complete information.
Although Table 1 and 2 suggest that the consideration of two canonical correlations improves the performances regardless of sinc-windowing, we still retain that a pre-processing step is important. We indeed hypothesize that the positive influence of sinc-windowing may emerge depending on both the subject and the set of stimulation frequencies. To give an example, if a subject showed an enhanced peak near one of the stimulation frequencies, independently from the stimulation condition (e.g. if the subject showed an enhanced spontaneous alpha rhythm and one of the selected frequencies was in the alpha range), then the adjunctive role of a narrow-band filtering would be enhanced. Since sinc-windowing only affects the total computation time for approximately one third, we think it is reasonable to keep and recommend this feature in future implementations. However, further data are required to confirm the importance of its role.
As regards the comparison with PSDA, our results confirm the ones in literature [6], [7], which indicate the superiority of CCA both in terms of accuracy and computational load.
As regards the performances of our system in absolute terms, it is difficult to compare ITRs because most of the recent studies implement more than 2 classes, which drastically increases ITR. The most recent 2-class BCI based on SSVEPs found in literature is the one in [22], which reports a *peak* accuracy of 89.9% and a *peak* ITR of 10.30bits/min. Since our *average* accuracy and ITR were of 88.6% and 20.12bits/min, we think we can say our results are at least in line with the reported ones. A multi-class implementation of the presented paradigm could lead to an improvement in ITRs too.

CONCLUSION

In the present work we implemented a 2-class SSVEP-based BCI system. The system was based on CCA analysis, and our results indicate that considering two canonical correlations instead of the largest one only can significantly improve accuracy without increasing the computational load. An additional narrow-band filtering permits to gain an average 5.1% and a peak of 12.5% accuracy with respect to classical CCA. Even though this is only a 2-class paradigm, it can be easily extended to multi-class to improve ITR. An advantage of the

Published by Verlag der TU Graz
Graz University of Technology

 DOI: 10.3217/978-3-85125-533-1-88

presented system is that it remains quite simple, light and fast, since it only performs sinc-windowing of the incoming signals, followed by a CCA feature extraction and SVM classification. We think taking low computational costs and simple procedures is an important aspect, especially to favor the spread of low-cost and high-portability devices.

REFERENCES

[1] L. F. Nicolas-Alonso e J. Gomez-Gil, «Brain Computer Interfaces, a Review», *Sensors*, vol. 12, n. 2, pagg. 1211–1279, gen. 2012.

[2] S. Amiri, A. Rabbi, L. Azinfar, e R. Fazel-Rezai, «A review of P300, SSVEP, and hybrid P300/SSVEP brain-computer interface systems,[w:] Brain-Computer Interface Systems–Recent Progress and Future Prospects, 2013», *DOI*, vol. 10, pag. 56135.

[3] Z. Lin, C. Zhang, W. Wu, e X. Gao, «Frequency recognition based on canonical correlation analysis for SSVEP-based BCIs», *IEEE Trans. Biomed. Eng.*, vol. 54, n. 6, pagg. 1172–1176, 2007.

[4] G. Bin, X. Gao, Z. Yan, B. Hong, e S. Gao, «An online multi-channel SSVEP-based brain–computer interface using a canonical correlation analysis method», *J. Neural Eng.*, vol. 6, n. 4, pag. 046002, 2009.

[5] Y. Zhang, P. Xu, T. Liu, J. Hu, R. Zhang, e D. Yao, «Multiple Frequencies Sequential Coding for SSVEP-Based Brain-Computer Interface», *PLOS ONE*, vol. 7, n. 3, pag. e29519, mar. 2012.

[6] Q. Wei, M. Xiao, e Z. Lu, «A comparative study of canonical correlation analysis and power spectral density analysis for ssvep detection», in *Intelligent Human-Machine Systems and Cybernetics (IHMSC), 2011 International Conference on*, 2011, vol. 2, pagg. 7–10.

[7] G. Hakvoort, B. Reuderink, e M. Obbink, «Comparison of PSDA and CCA detection methods in a SSVEP-based BCI-system», 2011.

[8] Y. Zhang *et al.*, «Multiway Canonical Correlation Analysis for Frequency Components Recognition in SSVEP-Based BCIs», in *Neural Information Processing*, 2011, pagg. 287–295.

[9] J. Pan, X. Gao, F. Duan, Z. Yan, e S. Gao, «Enhancing the classification accuracy of steady-state visual evoked potential-based brain–computer interfaces using phase constrained canonical correlation analysis», *J. Neural Eng.*, vol. 8, n. 3, pag. 036027, 2011.

[10] Y. Zhang, G. Zhou, J. Jin, M. Wang, X. Wang, e A. Cichocki, «L1-Regularized Multiway Canonical Correlation Analysis for SSVEP-Based BCI», *IEEE Trans. Neural Syst. Rehabil. Eng.*, vol. 21, n. 6, pagg. 887–896, nov. 2013.

[11] M. H. Chang e K. S. Park, «Frequency recognition methods for dual-frequency SSVEP based brain-computer interface», in *Engineering in Medicine and Biology Society (EMBC), 2013 35th Annual International Conference of the IEEE*, 2013, pagg. 2220–2223.

[12] Y. U. Zhang, G. Zhou, J. Jin, X. Wang, e A. Cichocki, «Frequency recognition in SSVEP-based BCI using multiset canonical correlation analysis», *Int. J. Neural Syst.*, vol. 24, n. 04, pag. 1450013, 2014.

[13] M. Nakanishi, Y. Wang, Y.-T. Wang, Y. Mitsukura, e T.-P. Jung, «Enhancing unsupervised canonical correlation analysis-based frequency detection of SSVEPs by incorporating background EEG», in *Engineering in Medicine and Biology Society (EMBC), 2014 36th Annual International Conference of the IEEE*, 2014, pagg. 3053–3056.

[14] Y. Wang, M. Nakanishi, Y.-T. Wang, e T.-P. Jung, «Enhancing detection of steady-state visual evoked potentials using individual training data», in *Engineering in Medicine and Biology Society (EMBC), 2014 36th Annual International Conference of the IEEE*, 2014, pagg. 3037–3040.

[15] Y. Zhang, G. Zhou, J. Jin, X. Wang, e A. Cichocki, «SSVEP recognition using common feature analysis in brain–computer interface», *J. Neurosci. Methods*, vol. 244, pagg. 8–15, apr. 2015.

[16] P. Yuan, X. Chen, Y. Wang, X. Gao, e S. Gao, «Enhancing performances of SSVEP-based brain–computer interfaces via exploiting inter-subject information», *J. Neural Eng.*, vol. 12, n. 4, pag. 046006, 2015.

[17] X. Chen, Y. Wang, S. Gao, T.-P. Jung, e X. Gao, «Filter bank canonical correlation analysis for implementing a high-speed SSVEP-based brain–computer interface», *J. Neural Eng.*, vol. 12, n. 4, pag. 046008, 2015.

[18] M. R. Islam, T. Tanaka, M. Nakanishi, e M. K. I. Molla, «Frequency recognition of steady-state visually evoked potentials using binary subband canonical correlation analysis with reduced dimension of reference signals», in *Acoustics, Speech and Signal Processing (ICASSP), 2016 IEEE International Conference on*, 2016, pagg. 769–773.

[19] H. Hotelling, «Relations between two sets of variates», *Biometrika*, vol. 28, n. 3/4, pagg. 321–377, 1936.

[20] G. Mueller-Putz, R. Scherer, C. Brunner, R. Leeb, e G. Pfurtscheller, «Better than random: A closer look on BCI results.», *Int. J. Bioelectromagn.*, vol. 10, n. EPFL-ARTICLE-164768, pagg. 52–55, 2008.

[21] P. Yuan, X. Gao, B. Allison, Y. Wang, G. Bin, e S. Gao, «A study of the existing problems of estimating the information transfer rate in online brain–computer interfaces», *J. Neural Eng.*, vol. 10, n. 2, pag. 026014, 2013.

[22] E. C. Lalor *et al.*, «Steady-state VEP-based brain-computer interface control in an immersive 3D gaming environment», *EURASIP J. Appl. Signal Process.*, vol. 2005, pagg. 3156–3164, 2005.

Published by Verlag der TU Graz
Graz University of Technology

Proceedings of the
7th Graz Brain-Computer Interface Conference 2017 DOI: 10.3217/978-3-85125-533-1-89

EEG-BASED GRAPH THEORY INDICES TO SUPPORT THE CLINICAL DIAGNOSIS OF DISORDERS OF CONSCIOUSNESS

J. Toppi[1,2], L. Astolfi[1,2], M. Risetti[2], R. Formisano[2], D. Mattia[2]

[1] Department of Computer, Control and Management Engineering, Sapienza University of Rome, Italy

[2] Neuroelectrical Imaging and Brain Computer Interface Laboratory, Fondazione Santa Lucia IRCCS, Rome, Italy

E-mail: jlenia.toppi@uniroma1.it

ABSTRACT: Severe acquired brain injury often leads to a disorder of consciousness (DOC) which can be classified in vegetative state (VS) or minimally consciousness state (MCS) according to its severity. While the standardized Coma Recovery Scale Revised (CRS-R) is considered the gold-standard for the diagnosis of DOCs, fluctuations in the level of awareness and/or operator-dependence variation may hinder diagnostic accuracy (up to 40% of misdiagnosis for VS). Here we aimed at providing reliable EEG-based indices extracted from resting state networks that can corroborate clinical diagnosis with high level of accuracy, even in absence of behavioral signs of consciousness. Advanced methodologies for connectivity estimation and graph theory were applied to EEG resting state data from 15 DOC patients (2 groups: 6 VS and 9 MCS). Indices describing the global properties of the resting networks and the information flows between anterior and posterior brain regions resulted significantly different between the two groups. Moreover, they allowed the discrimination between VS from MCS with accuracy above 80%. These findings boost the role of EEG synthetic indices as valuable and reliable tool to support DOC clinical diagnosis.

INTRODUCTION

Disorders of Consciousness (DOCs) after severe acquired brain injury include, in the acute phase, coma and in the post-acute phase, vegetative state (VS) and minimally conscious state (MCS). The VS is a condition that follows coma, when the patient recovers vigilance (eyes opening), but not awareness, defined as the ability to interact with the surroundings, in spite of eyes opening and partial recovery of the sleep-wake circadian cycle [1]. More recently, the European Task Force has introduced the definition of "unresponsive wakefulness syndrome" (UWS) [2] to replace the term "vegetative state," although it has not been universally accepted [3]. Here, we will use the term VS/UWS. The MCS has been described as a condition in which the patient recovers eye tracking ability or fluctuating commands, while remaining unable to communicate [4].

The current gold-standard in diagnosis of DOC patients is the JFK Coma Recovery Scale Revised (CRS-R) which allows the clinical assessment of residual visual, auditory, motor, verbal functions, patients' communication ability and awareness [5]. Reliance on behavioral assessment presents however, significant challenges and may lead to a misdiagnosis up to 40% (in VS) with evident impact on DOCs assistance and rehabilitation [6].

In light of this, several studies investigating neuroelectrical and hemodynamical brain signals at rest and during batteries of auditory, visual and tactile stimuli have been conducted in DOC patients in order to isolate quantitative markers of awareness independently of behavior [7]–[9]. The most promising studies appears to be those based on the analysis of alterations in DOC resting state networks, particularly in the so-called Default Mode Network, with respect to healthy subjects [10].

Hemodynamical and neuroelectrical measures have recently gained growing interest as a tool that may—in perspective—support the diagnosis of patients with different DOC by circumventing the need for behavioral responses. The networks defined by the statistical relationship between different signals (and their properties at different frequencies) can be seen as indirect correlates of the information processing by the patient's brain.

EEG shows invaluable advantages with respect to other neuroimaging techniques, both at the theoretical and at the practical level: it allows to capture the dynamics of brain connectivity and its spectral distribution, by keeping it viable to handle severely disabled patients even with bedside testing, being therefore eligible for routine clinical application.

Previous studies have identified markers derived from a combination of connectivity estimators and graph theory able to classify MCS patients from VS/UWS and healthy subjects with an accuracy slightly above chance [11], [12].

In this study, we employed Partial Directed Coherence, as spectral multivariate connectivity estimator [13] combined with asymptotic statistic method to assess patterns of connectivity [14] and graph theory to extract EEG indices describing the topology of

Published by Verlag der TU Graz
Graz University of Technology

 DOI: 10.3217/978-3-85125-533-1-89

resting state networks in DOC [15]. As such, the combination of these computational methods was demonstrated to provide accurate, reliable and repeatable patterns in different experimental conditions and under different levels of signals quality [16]. The aim was to provide EEG-based indices to accurately discriminate/classify between different DOCs.

MATERALS AND METHODS

Participants: Fifteen patients were included in the study (age: 50±16 years, 8 males; lesions: 5 left, 5 right, 5 bilateral; etiology: 7 stroke and 8 traumatic brain injury). All the patients were recruited at the post coma unit of the Neurorehabilitation Hospital "Fondazione Santa Lucia," Rome, Italy. According to their CRS-R scores, patients were divided in two groups: 6 VS/UWS and 9 MCS. No significant differences between the two groups were found in terms of age, gender, and lesion site. One MCS subject was excluded from the analysis because of the presence of artifacts in EEG traces.

Scalp EEG recordings: All patients were subjected to an experimental session including EEG recordings during 2 minutes of eyes-closed resting condition (19 electrode cap, positioned according to 10-20 International System as used in clinical routine, reference on both earlobes and ground at left mastoid, sampling frequency of 250 Hz, g.USBamp amplifier, Guger Technologies, Austria).

Connectivity Analysis and graph theory: EEG signals were downsampled to 100 Hz and band pass filtered at 1–45 Hz. EEG traces were segmented in epochs of 1s length and then subjected to PDC estimation.

PDC is a is a full multivariate spectral measure used to determine the directed influences between pairs of signals in a multivariate dataset. Let us suppose that the following multivariate autoregressive (MVAR) process is an adequate description of the dataset Y:

$$\sum_{k=0}^{p} A(k)Y(t-k) = E(t) \qquad (1)$$

Where Y(t) is the data vector in time, E(t) = [e1(t),…,eN(t)]T is a vector of multivariate zero-mean uncorrelated white noise processes, A(1),A(2),…,A(p) are the NxN matrices of model coefficients, and p is the model order. PDC can be computed as follows [13]:

$$\pi_{ij}(f) = \frac{\left|A_{ij}(f)\right|^2}{\sum_{m=1}^{N}\left|A_{mj}(f)\right|^2} \qquad (2)$$

where $A_{ij}(f)$ represents the frequency version of the ij entry of matrix A.

The estimated PDC values were averaged in five frequency bands: delta (1–3 Hz), theta (4–7 Hz), alpha (8–12 Hz), beta (13–25 Hz), and gamma (26–40 Hz).

PDC significance was assessed against null-case by means of asymptotic statistics approach with a significance level of 5%. Such approach allows to derive the probability distribution of the null-case squared PDC estimator (the χ^2 distribution), by knowing its asymptotic variance [14], [16].

To compute indices describing the main local and global properties of the investigated patterns, we adopted measures derived from a graph theoretical approach [17], computed on the adjacency matrix *G* resulting from the assessment procedures [15]. In particular, we considered the following indices: i) ant/post asymmetry, anterior density, ant/post influence for describing the involvement of anterior areas with respect to the posterior ones, ii) inter-hemispheric connections, left/right divisibility, left/right modularity for describing the information exchange between left and right hemispheres [16] iii) clustering, global efficiency, local efficiency, path length for characterizing the global properties of the network such as the efficiency in communication or the tendency to create clusters [17].

Statistical analysis and classification: An independent samples t-test was performed (significance level 0.05, corrected by means of False Discovery Rate) between the indices extracted from VS/UWS and MCS networks. To check whether such indices were able to characterize each individual patient, we built a support vector machine (SVM) classifier with linear kernel, using as features the indices resulted as statistically different between VS/UWS and MCS. The classifier was built for each couple of indices and each frequency band. We employed a leave-one-out cross-validation approach, testing one subject each time. The corresponding classifier training was performed on two groups of patients of the same size. As a performance parameter, we computed the percentage of subjects whose state has been correctly classified.

Finally, the brain connectivity indices were correlated (Spearman correlation, $p<0.05$) with the clinical (CRS-R) scores. False discovery rate correction was used to correct for multiple correlations.

RESULTS

As reported in Fig. 1, (panel a), we found significantly higher values of ant/post asymmetry, ant/post influence, and anterior density in MCS patients with respect to VS/UWS as estimated in delta band of frequency. The ant/post asymmetry and ant/post influence indices were also significantly different between VS/UWS and MCS, in favor of MCS, in the theta band of frequency (Fig.1, panel a). Altogether, these results indicated a *lower* functional involvement of the frontal regions in VS/UWS patients as indicated by negative values of these indices in that experimental group. No significant differences were found between the two groups as for the indices of functional interhemispheric communication, namely the inter-hemispheric connections, left/right divisibility, left/right modularity (Fig.1, panel b) in both delta and theta bands. Regarding global properties of the resting state networks (Fig.1, panel c), we found significantly higher values of clustering coefficient and local efficiency and lower values of path length in MCS with respect to VS/UWS only in delta band.

Published by Verlag der TU Graz
Graz University of Technology

 DOI: 10.3217/978-3-85125-533-1-89

Table1 - Classification accuracy obtained using as features graph indices derived from DOC's resting state connectivity networks in delta band. A SVM classifier with linear kernel and three support vectors was built for comparing VS/UWS and MCS for each combination of graph indexes (reported on x- and y-axis). Classification accuracies above 70% were highlighted in bold.

	Ant/Post Asym	Ant Density	Ant/Post Infl	IHC	L/R div	L/R mod	Clust	Glob Eff	Loc Eff	Path Length
Ant/Post Asym	---	68,9	**78,5**	**73,7**	**78,8**	**73,4**	**81**	68,4	**82**	**82,8**
Ant Density	---	---	58,8	**76,4**	68,6	66,7	**70,7**	**79,3**	59,1	69,6
Ant/Post Infl	---	---	---	**78,5**	**75,5**	**75,3**	**72,7**	**73,5**	**74,7**	**73,3**
IHC	---	---	---	---	61,9	49	69	**70**	58,2	50,6
L/R_div	---	---	---	---	---	26	50,1	48,9	69,3	69,8
L/R_mod	---	---	---	---	---	---	43,2	42,4	56,5	39,4
Clust	---	---	---	---	---	---	---	63,4	51,5	64,5
Glob Eff	---	---	---	---	---	---	---	---	41,9	46,1
Loc Eff	---	---	---	---	---	---	---	---	---	54,8
Path Length	---	---	---	---	---	---	---	---	---	---

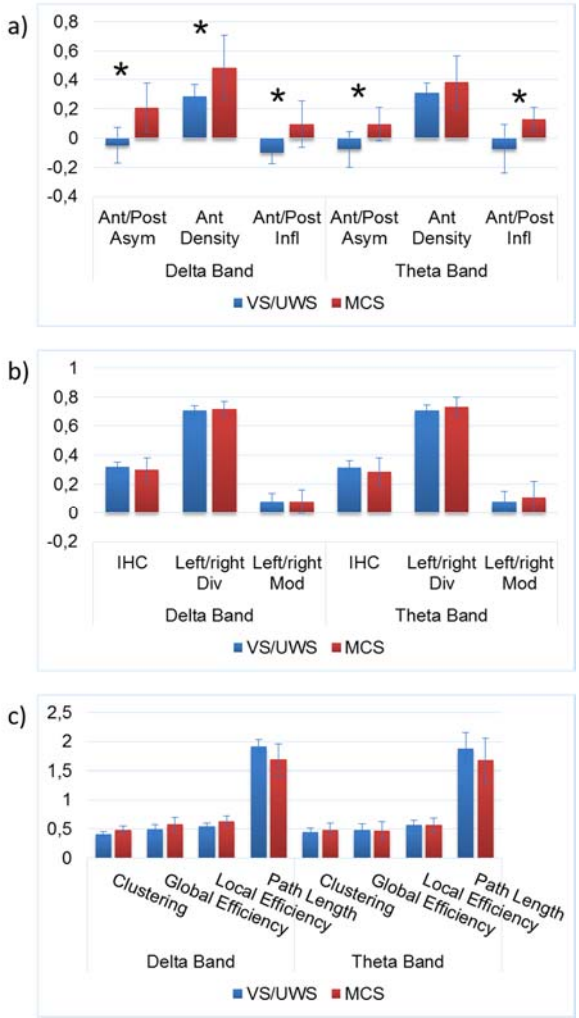

Figure 1: Bar diagrams reporting results related to the graph indices extracted separately for VS/UWS and MCS in delta and theta bands. Indices are grouped as follows: anterior/posterior (panel a), left/right (panel b), global indices (panel d). P-values associated to the statistical comparison between VS and MCS are reported for each index (independent samples t-test). In bold, values related to an alpha = 5% ($P < 0.05$).

No significant differences were found in the other bands for all the three groups of indices.

All the graph indices were used, in couples, as features to feed the SVM classifier. We built a classifier for each pair of indices (45 pairs in total) and two frequency bands (delta and theta). Results are reported in Table1. In particular, we found that accuracy above 70% was obtained only when the couple included indices such as those relative to functional communication between anterior and posterior areas and to the global properties of the networks. Worth of note are the accuracies above 80% obtained considering as features the ant/post asymmetry and tree global indices (clustering, local efficiency and path length). The accuracy obtained in theta band resulted lower than that in delta band.

Regarding the results of the Spearman correlation between the CRS-R scores and the ant/post asymmetry in the delta band. A significant positive correlation ($R=0.6$, $p=0.024$) between the ant/post asymmetry index and the CRS-r scores was observed only in the delta band.

No statistical correlations were found for the other indices in all frequency bands.

DISCUSSION

In this paper we aimed at providing quantitative and reliable indices extracted from EEG resting state networks, to discriminate VS/UWS from MCS in order to corroborate the clinical/behavioral diagnosis of DOC patients.

According to our findings, the main differences found between VS/UWS and MCS can be quantified by 2 classes of indices: i) those describing the relationship between anterior and posterior areas of the brain and ii) those describing global properties of resting state networks such as efficiency and tendency to create clusters. In particular, VS/UWS's resting state networks present a reduced connectivity in frontal regions of the brain and a decrease in the communication flows going from the anterior to the posterior regions with respect to MCS. This is in line with previous studies pointing out in VS/UWS patients a deactivation of areas related to Default Mode Networks (including anterior cingulate cortex and medial pre-frontal cortex) and a reduction of the fronto-parietal connections [18], [19]. Furthermore, resting state networks in MCS were characterized by higher communication efficiency and higher tendency to

Published by Verlag der TU Graz
Graz University of Technology

 DOI: 10.3217/978-3-85125-533-1-89

organize their structure in clusters with respect to VS/UWS as underlined by the significant differences in clustering, local efficiency and path length indices. Finally, most of the significant results were found in slow frequency bands (delta and theta), which have been related to cognitive tasks [20] and to different unconsciousness levels [21]. Overall, we speculate that this could reflect a global *deterioration* of the resting state networks in VS/UWS patients.

Previous EEG studies based on graph theory indices extracted from connectivity networks at rest, have already pointed out the distinctive aspects of DOCs' brain networks with respect to healthy subjects also providing correlations of resting state networks with the degree of behavioral responsiveness or hidden awareness in DOCs [22]. However, the characterization of DOC's resting state networks has been made only on the basis of global indices, such as clustering and path length, which give information about general properties of the networks. In this paper, we firstly confirmed what already found in terms of global properties of DOCs' networks. Then, we provided information about the spatial reorganization of DOCs' resting state netwroks induced by the brain injury. In particular, we employed indices describing the level and direction of information flow between anterior and posterior areas and between the two hemispheres. Regarding the global indices, we found results similar to those in [22] even considering a reduced number of electrodes (19 instead of 32). The simplification of the experimental setup without any loss of accuracy in the DOCs characterization is an important issue which has to be addressed if we are interested in employing such indices in the clinical diagnosis of DOCs.

Notably, the ant/post asymmetry index values appear to vary as function of the CRS-R scores. As yet, the same set of indices (in couple) was also reliable in 2-class discrimination analysis, that is VS/UWS and MCS were classified with up to 80% of accuracy. This finding further strengthens the relevance that such surrogate measure of the consciousness disorders might have to improve clinical diagnosis of DOC patients.

Once our findings would be confirmed in a larger group of patients we will move from a supervised approach where the classifier is trained on the basis of the results of CRS-R scale to an unsupervised approach entirely data driven in order to remove the dependence of the results on the diagnosis provided by CRS-R scale.

CONCLUSION

Our findings, if confirmed in a larger group of DOC patients, indicate how surrogate measures of consciousness disorders based on EEG might allow to improve the accuracy of the gold-standard clinical instruments for diagnosis. This can be achieved with just few minutes of EEG signal recording without requiring any voluntary contribution by the patient, provide that these findings are confirmed in a larger cohort of DOCs.

REFERENCES

[1] S. Ashwal, "Medical aspects of the persistent vegetative state (1). The Multi-Society Task Force on PVS," *N. Engl. J. Med.*, vol. 330, no. 21, pp. 1499–1508, May 1994.

[2] S. Laureys *et al.*, "Unresponsive wakefulness syndrome: a new name for the vegetative state or apallic syndrome," *BMC Med.*, vol. 8, p. 68, 2010.

[3] R. Formisano, F. Pistoia, and M. Sarà, "Disorders of consciousness: A taxonomy to be changed?," *Brain Inj.*, vol. 25, no. 6, pp. 638–639, 2011.

[4] R. Formisano *et al.*, "Vegetative state, minimally conscious state, akinetic mutism and Parkinsonism as a continuum of recovery from disorders of consciousness: an exploratory and preliminary study," *Funct. Neurol.*, vol. 26, no. 1, pp. 15–24, 19 2011.

[5] J. T. Giacino, K. Kalmar, and J. Whyte, "The JFK Coma Recovery Scale-Revised: measurement characteristics and diagnostic utility," *Arch Phys Med Rehabil*, vol. 85, no. 12, pp. 2020–2029, Dec. 2004.

[6] K. Andrews, L. Murphy, R. Munday, and C. Littlewood, "Misdiagnosis of the vegetative state: retrospective study in a rehabilitation unit," *BMJ*, vol. 313, no. 7048, pp. 13–16, Jul. 1996.

[7] H. Erlbeck, R. G. L. Real, B. Kotchoubey, D. Mattia, J. Bargak, and A. Kübler, "Basic discriminative and semantic processing in patients in the vegetative and minimally conscious state," *Int. J. Psychophysiol.*, vol. 113, pp. 8–16, Mar. 2017.

[8] R. G. L. Real *et al.*, "Information processing in patients in vegetative and minimally conscious states," *Clin. Neurophysiol.*, vol. 127, no. 2, pp. 1395–1402, Feb. 2016.

[9] M. M. Monti, J. D. Pickard, and A. M. Owen, "Visual cognition in disorders of consciousness: From V1 to top-down attention," *Hum. Brain Mapp.*, vol. 34, no. 6, pp. 1245–1253, Jun. 2013.

[10] Y. Hannawi, M. A. Lindquist, B. S. Caffo, H. I. Sair, and R. D. Stevens, "Resting brain activity in disorders of consciousness: a systematic review and meta-analysis," *Neurology*, vol. 84, no. 12, pp. 1272–1280, Mar. 2015.

[11] Y. Höller *et al.*, "Connectivity biomarkers can differentiate patients with different levels of consciousness," *Clin. Neurophysiol.*, vol. 125, no. 8, pp. 1545–1555, Aug. 2014.

[12] L. Pollonini *et al.*, "Information communication networks in severe traumatic brain injury," *Brain Topogr.*, vol. 23, no. 2, pp. 221–226, Jun. 2010.

[13] L. A. Baccalá and K. Sameshima, "Partial directed coherence: a new concept in neural structure determination," *Biol. Cybern.*, vol. 84, pp. 463–474, May 2001.

[14] K. Sameshima, D. Y. Takahashi, and L. A. Baccalá, "On the Statistical Performance of Connectivity Estimators in the Frequency Domain," in *Brain Informatics and Health*, vol. 8609, Cham: Springer International Publishing, 2014, pp. 412–423.

[15] J. Toppi *et al.*, "How the statistical validation of functional connectivity patterns can prevent erroneous definition of small-world properties of a brain connectivity network," *Comput. Math. Methods Med.*, vol. 2012, p. 130985, 2012.

[16] J. Toppi, D. Mattia, M. Risetti, R. Formisano, F. Babiloni, and L. Astolfi, "Testing the Significance of Connectivity Networks: Comparison of Different Assessing Procedures," *IEEE Trans. Biomed. Eng.*, vol.

Published by Verlag der TU Graz
Graz University of Technology

 DOI: 10.3217/978-3-85125-533-1-89

63, no. 12, pp. 2461–2473, Dec. 2016.

[17] M. Rubinov and O. Sporns, "Complex network measures of brain connectivity: uses and interpretations," *Neuroimage*, vol. 52, no. 3, pp. 1059–1069, Sep. 2010.

[18] J. S. Crone *et al.*, "Altered network properties of the fronto-parietal network and the thalamus in impaired consciousness," *NeuroImage Clin.*, vol. 4, pp. 240–248, 2014.

[19] A. Soddu *et al.*, "Resting state activity in patients with disorders of consciousness," *Funct. Neurol.*, vol. 26, no. 1, pp. 37–43, Mar. 2011.

[20] M. Kawasaki, K. Kitajo, and Y. Yamaguchi, "Fronto-parietal and fronto-temporal theta phase synchronization for visual and auditory-verbal working memory," *Front. Psychol.*, vol. 5, Mar. 2014.

[21] B. Molaee-Ardekani, L. Senhadji, M.-B. Shamsollahi, E. Wodey, and B. Vosoughi-Vahdat, "Delta waves differently modulate high frequency components of EEG oscillations in various unconsciousness levels," *Conf. Proc. Annu. Int. Conf. IEEE Eng. Med. Biol. Soc. IEEE Eng. Med. Biol. Soc. Annu. Conf.*, vol. 2007, pp. 1294–1297, 2007.

[22] S. Chennu *et al.*, "Spectral signatures of reorganised brain networks in disorders of consciousness," *PLoS Comput. Biol.*, vol. 10, no. 10, p. e1003887, Oct. 2014.

Published by Verlag der TU Graz
Graz University of Technology

Proceedings of the
7th Graz Brain-Computer Interface Conference 2017 DOI: 10.3217/978-3-85125-533-1-90

UTRECHT NEUROPROSTHESIS: FROM BRAIN SIGNAL TO INDEPENDENT CONTROL

M.A. van den Boom[1], M. Vermaas[1], E.J. Aarnoutse[1], S. Leinders[1], E. G. M. Pels[1], Z.V. Freudenburg[1], M.P. Branco[1], M.J. Vansteensel[1], N.F. Ramsey[1]

[1] Brain Center Rudolf Magnus, Department of Neurology and Neurosurgery, UMC Utrecht

E-mail: M.A.vandenBoom-4@umcutrecht.nl

ABSTRACT: Recently a locked-in ALS patient was equipped with the Utrecht NeuroProsthesis (UNP), a fully implantable electrocorticography (ECoG)-based BCI system. The UNP system translates the neuronal activity from this patient to a control signal that is used to make selections within a graphical user interface (GUI) and speller application. This paper describes the current architecture of the UNP system from brain signal to GUI and speller control.

INTRODUCTION

Due to severe paralysis, patients with Locked-In Syndrome (LIS) are no longer able to communicate with the outside world independently. Although their cognition is still intact, LIS patients do not have the ability to move or speak anymore. Using assistive technology, LIS patients may use eye movements to control (communication) devices. As an alternative, BCI solutions are occasionally used to employ brain activity for control. Our BCI system is the first fully implanted ECoG-based system, where electrode strips are placed - subdurally - directly on the cortical surface and connected to a transmitter device inside the chest. Because the electrodes are permanently implanted, caretaker assistance for using the system only involves placing an antenna over the implanted transmitter and connecting it to the computer. In addition, brain potentials are measured directly from the cortex so we can record brain activity with a high spatial and high temporal resolution. Over the past 1.5 years we have developed a signal processing pipeline and GUI to allow the patient to control the UNP independently. By means of this pipeline and GUI, the patient is now able to alert her caregiver, spell sentences and practice tasks to improve control [1]. The UNP-system employs brain driven 'clicks' as the primary input to the GUI. Input by means of brain clicks was chosen since this would provide the most robust control for the patient. The aim of this paper is to describe the features and architecture of the UNP system that the patient currently uses.

MATERIALS AND METHODS

The UNP system was implanted in a 58-year-old locked-in patient who suffers from late stage Amyotrophic Lateral Sclerosis (ALS). A subdural four-electrode strip (Resume®, Medtronic, 4mm electrode diameter, 1cm inter-electrode distance) was placed over the hand region of the left motor cortex, which activates on attempted hand movements [2]. The electrode strip is connected to a left infraclavicular, subcutaneously placed amplifier and transmitter device (Activa® PC+S, Medtronic). The Activa® device can process and amplify signals from each bipolar electrode pair on a single strip. We selected the electrode pair showing the strongest responses in high frequency band power (HFB, 65-95 Hz) during attempted hand movement. For the UNP, we configured the Activa® S to transmit power in two frequency bands: Beta power (center frequency 20Hz) and Gamma power (center frequency 80Hz) from the selected electrode pair at a rate of 5Hz. During use of the system, an antenna is placed on the chest over the device to receive the amplified and converted signal. The received signal is forwarded to a signal decoding computer (Microsoft Surface Pro 4 Tablet), which runs both a signal processing pipeline and GUI implemented on the BCI2000 platform [3]. The tablet running the pipeline and GUI is placed in front of the patient. She currently uses attempted hand movements to control the UNP-system.

RESULTS

The signal processing pipeline consists of six consecutive filters: Time smoothing, Z-transformation, Linear classification, Escape sequence, Threshold classification and Click translation (see Fig. 1). Each filter takes one or more input channels, manipulates or interprets the channels and sends output to the next filter or to the application. At the beginning of the pipeline, each of the two frequency bands is received on a separate channel, the Beta power on one channel and the Gamma power on another.

Time Smoothing: The incoming power signal from each channel is smoothed over time by taking the average over the current and previous 5 samples (a smoothing window of 1.2 seconds). Time smoothing is applied to deal with the noisy and spiky characteristics of ECoG measured brain signals.

Z-Transformation: The smoothed signal from each channel is taken from the previous step and normalized by subtracting the mean and division by the standard

Published by Verlag der TU Graz
Graz University of Technology

 DOI: 10.3217/978-3-85125-533-1-90

deviation of that channel. This normalization step stabilizes slow amplitude trends in the signal (i.e. different days or parts of the day). Initially, the mean and standard deviation were based on a 30 second pre-run calibration. However, since the amplitude and deviation of the signal proved to be stable over a longer period of time, a fixed mean and standard deviation are currently used.

Linear Classification: The normalized (z-scored) Beta and Gamma signals from the previous step are combined into a single control signal by subtracting the low frequency (Beta) channel from the high frequency (Gamma) channel.

Escape Sequence: The incoming signal proceeds through this filter without modification. This filter specifically detects long periods of sustained activity produced by the user, and, if detected, it outputs an 'escape' trigger directly to the GUI. The duration is currently set to 5.6 seconds of sustained activity.

Threshold Classification: The control signal from the linear classification is converted to a binary signal based on a threshold value. For every incoming sample the filter will output a '1' if the control signal is above the threshold, or a '0' if below the threshold.

Click Translation: The incoming binary signal is converted to clicks. This filter buffers the incoming samples and sends out a single click if a pre-defined number of consecutive '1'-samples is received from the previous filter (currently set to 5 samples). After sending out a click, the filter sets a refractory period of 3.6 seconds where no clicks can be made.

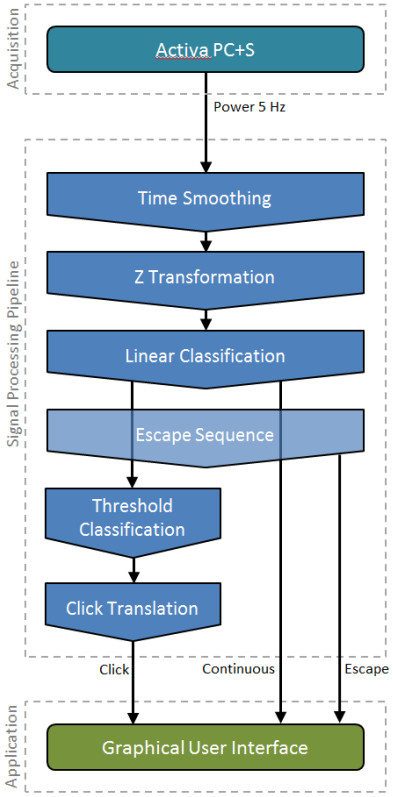

Figure 1: Overview of the processing pipeline. When click-control is required to control the GUI, the signal will pass through all six filters. If continuous-control is required then only the first four are enabled, skipping the Threshold Classification and Click translation steps.

The GUI connects at the end of the pipeline. By making (brain) clicks, the patient can navigate through the GUI menus (see Fig. 2).

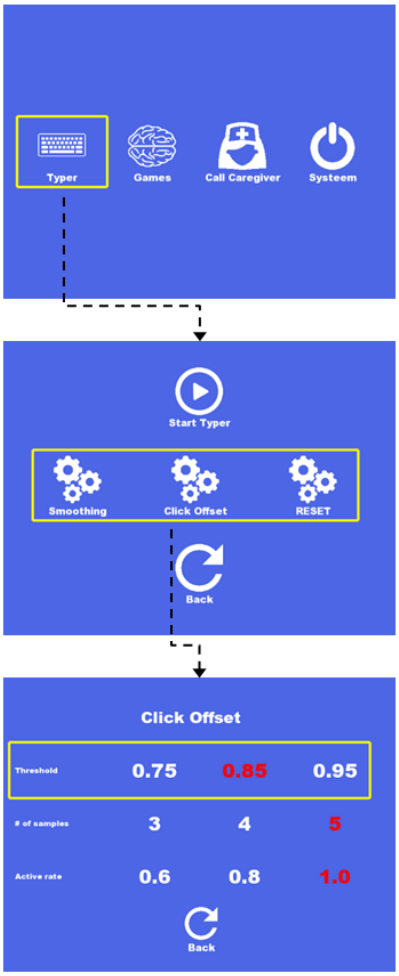

Figure 2: The GUI, showing the start menu, the speller menu and the speller click settings menu. Each menu in the GUI consists of icons organized in rows and columns. A selection rectangle will loop from top to bottom over each row. The patient can select a row by making a (brain-)click. When a row is selected a selection rectangle will loop from left to right within the row, allowing the patient to click an icon in the row. If no icon is clicked, the selection will revert back to row selection. If an icon is clicked, the selection rectangle will stay there for 3 seconds, requiring the patient to make another click within that time to confirm that option.

Over the past 1.5 years, several features were introduced into the pipeline and GUI to help the patient use the UNP.

Practice Games: A number of research tasks/games have been developed and are performed regularly in

Published by Verlag der TU Graz
Graz University of Technology

 DOI: 10.3217/978-3-85125-533-1-90

order to improve control over the (spelling) system. These tasks allowed us to find the optimal parameters for control and allow her to gain control over her brain activity. Normally these tasks are started by the researcher during home visits. However, since these tasks provided a good mean of practice for signal control, we included them in the GUI, allowing her to practice independently.

Spelling: The patient is able to start spelling software by choosing the 'Typer' icon in the GUI. When the patient chooses to start spelling in the menu, Tobii Dynavox Communicator 5 is started and takes focus on the tablet. The Tobii software is set to work in a similar way as the GUI, but instead shows a letter matrix for spelling and only single clicks have to be made. Clicks coming from the pipeline are relayed by the GUI to clicks in the Tobii application, allowing her to spell and pronunciate letter, words and sentences.

Optimizing pipeline parameters: As soon as the tablet is switched on, the pipeline is booted automatically with standard parameter values (e.g. a smoothing window of five samples). The standard parameter values were calculated from research task data. However, in certain circumstances, the user may wish to change these settings, for example to make clicking easier. In order to facilitate such changes, the UNP allows the patient to set some of the parameters values herself through the GUI (see Fig 2). For the speller (Tobii) and practice tasks she is able to set the smoothing window and various click parameters.

Escape: The escape sequence accommodates the need for the patient to stop what she is doing in the GUI and/or call for care. As soon as the escape sequence is made (keeping the control signal high for 5.6 seconds), the GUI shows a popup menu asking her if she wants to call the caregiver using audio, stop what she is doing or continue what she was doing. This feature allows her to always signal her caregiver, and from any place within the GUI and speller.

Continuous control: The UNP system has two control modes, a click control mode and a continuous control mode. The mode for click control involves all six filters. The patient uses this mode to navigate the menus, practice click-based tasks and use the spelling software. The mode for continuous control only uses the first four filters and is currently used in only one of the practice games. In this mode the amplitude of the signal controls the vertical position of a ball on the screen. The GUI can automatically switch modes in the pipeline depending on the tasks or program she is using.

DISCUSSION AND CONCLUSION

The UNP-system allows the patient to communicate using speller software and brain-clicks. In addition to spelling, the pipeline and GUI allow the patient to alert the caregiver, practice tasks to improve control signal regulation and fine-tune parameter settings independently. The patient has reported good user satisfaction with the implantable BCI system [1], and uses it on a regular basis without help from the research team. Although the system provides in a number of needs, improvements can be made. For example, the spelling speed could be improved by allowing her to experiment with the click refractory period and the number of consecutive above-threshold samples required for a click. In the coming period, we will work on further fine-tuning the system. The input of the participant is invaluable in this process, since only a system that fully meets the wishes and needs of the end-users will be interesting for further development and commercialization and eventually become available for the people who need it.

REFERENCES

[1] Vansteensel MJ, Pels EGM, Bleichner MG, Branco MP, Denison T, Freudenburg ZV, et al. Fully Implanted Brain–Computer Interface in a Locked-In Patient with ALS. *New England Journal of Medicine. 2016; 375*(21): 2060–2066.

[2] Bouton CE, Shaikhouni A, Annetta NV, Bockbrader MA, Friedenberg DA, Nielson DM, et al. Restoring cortical control of functional movement in a human with quadriplegia. *Nature 2016;533*:247–250.

[3] Schalk G, McFarland DJ, Hinterberger T, Birbaumer N, Wolpaw JR. BCI2000: a general-purpose brain-computer interface (BCI) system. *IEEE Trans Biomed Eng 2004;51*:1034–1043.

Published by Verlag der TU Graz
Graz University of Technology

Proceedings of the
7th Graz Brain-Computer Interface Conference 2017 DOI: 10.3217/978-3-85125-533-1-91

EVALUATION OF BCI RESEARCHERS' OPINIONS REGARDING THE FUTURE OF BCIS: RESULTS OF BCI ROADMAP QUESTIONNAIRE 2014

M.J. Vansteensel[1], E.J. Aarnoutse[1], G. Kristo[1], N.F. Ramsey[1]

[1] Department of Neurosurgery, Brain Center Rudolf Magnus, University Medical Center Utrecht, BCI, Str 4.205, PO Box 85060, 3508 AB Utrecht, The Netherlands

E-mail: m.j.vansteensel@umcutrecht.nl

ABSTRACT: The field of Brain-Computer Interface (BCI) research has seen a steep expansion during the last years, and interesting progress has been made in all different aspects of the BCI pipeline. Despite that, BCIs are not yet widely used by either the diseased or healthy target populations. In the current study, we asked BCI researchers worldwide to fill out a questionnaire about how they see the future of BCI research, what hurdles need to be taken for BCIs to become available and widely used applications, and the research that is needed to accomplish this. The data reveal that researchers foresee that real BCI applications will appear on the market in the coming years, but that important improvements are needed in especially the hardware, performance and user friendliness of BCIs.

INTRODUCTION

Since the pioneering work on brain-computer interfaces (BCIs) in the late sixties and early seventies of the previous century [1,2], BCI research has seen a fast growth. The new insights gained as a result of that have led to the BCI field currently recognizing several types of application scenarios, each with their own target populations [3,4], ranging from applications to *replace* lost brain function (e.g. BCI-control of communication devices) to tools that *enhance* the daily functioning of healthy people (e.g. BCI-driven detection of attention lapses for airline pilots). Despite these developments, BCIs seem to remain largely a laboratory tool and are hardly available on the market. As a result, only a very limited number of patients and healthy people use BCIs in home, work or clinical settings.

In order to make sure that potential end-users, in time, will start to benefit from BCIs, it is important to identify the most promising BCI applications and target groups, and to signal topics that need more attention. To this purpose, a group of European BCI stakeholders (i.e. the BNCI Horizon2020 project, funded within the European Commission's Framework Programme 7) worked on the development of a roadmap for the BCI field [5], between November 2013 and May 2015. As part of this project, the consortium approached BCI researchers worldwide with the request to fill out a questionnaire, asking them about their view on the current status and the future of their field. A summary of the findings was presented in one of the Appendices of the BNCI Horizon2020 roadmap. Here, we present the results of the questionnaire in more detail.

MATERALS AND METHODS

Approach: In May 2014, the BCI researchers' questionnaire was sent to 3291 BCI researchers by email, followed by two reminders to non-responding researchers before the first round was closed in July 2014. A second round ran from December 2014 until January 2015.

Questionnaire: The questionnaire contained three sections:

1) Respondents. Here, researchers were asked to answer a list of multiple choice questions on e.g. their education, lab size, and BCI research focus, with the purpose to characterize the respondents.
2) Near future. In this section, researchers were asked to shortly describe a BCI application that they considered feasible within the near future, and assign it to one of the BCI scenarios (*replace, restore, enhance, improve, supplement and research tool*). Then, they were presented with a list of potential bottlenecks and a list of possible research directions. For each item, they had to indicate to what extent it applied to the BCI application they just described, on a five-point rating scale that ranged from strongly agree to strongly disagree.
3) Far future. Here, respondents were asked to think out of the box and into the far future, and shortly describe a potential killer application or major research breakthrough, for both non-invasive and implanted BCIs.

Data analysis: Data analysis was performed separately for each section.

1) Respondents. Numbers of selections of multiple choice items were computed as percentages of the total number of respondents.
2) Near future. The described BCI applications were evaluated for clarity and correctness of assignment to the application scenarios and re-assigned if necessary. Ratings were labeled with weights, i.e. 'not applicable' with 0, 'totally disagree' with 1, 'disagree' with 2, 'neutral' with 3, 'agree' with 4, and 'totally agree' with 5. Subsequently, the ratings given by the respondents to each of the

Published by Verlag der TU Graz
Graz University of Technology

 DOI: 10.3217/978-3-85125-533-1-91

bottlenecks/research direction statements were used to compute, per statement, a center of mass (COM). COM values >3.5 indicated that most respondents agreed/strongly agreed with a statement, whereas COM values <2.5 indicated disagreement or strong disagreement. Values between 2.5 and 3.5 indicated not particularly relevant or irrelevant.

3) Far future. Incomplete and unclear answers were excluded from analysis. The other statements were used to assemble a list of numbered codes (topics). The final list covered all issues described by the respondents. Subsequently, each statement was annotated with one or more codes of the list. Finally, for each code, the number of instances among all statements on non-invasive and implanted BCIs was counted.

RESULTS

Respondents: In total, the questionnaire was filled out by 298 respondents, mostly from Europe, North-America and Asia. Almost 90% of them worked with non-invasive BCIs, the rest on implantable BCIs. The percentage of respondents working on implantable BCIs in North-America (26%) was substantially larger than in Europe and Asia (both < 10%).

Near future: The 298 respondents described and rated 363 BCI applications, of which 317 were included in the analysis. Most of the applications were related to *replacing* lost central nervous system (CNS) output, followed by tools to *improve* lost CNS output (Table 1). Over 80% of the applications were suggested to be developed using a non-invasive BCI approach.

Bottleneck statements that respondents considered most relevant for their non-invasive applications were those related to insufficient system performance (COM>3.5 for 6 out of 6 BCI scenarios, i.e. *replace, restore, enhance, improve, supplement* and *research tool*), the unawareness of end-users about BCIs (COM>3.5 for 5/6 scenarios), the complexity of BCI systems (COM>3.5 for 5/6 scenarios), and the fact that wishes and needs of end-users are not met sufficiently (COM>3.5 for 4/6 scenarios).

Table 1: Number of respondents describing an implanted and non-invasive solution for applications within the six BCI scenarios in the Near future section.

Scenario	Implanted	Non-invasive	Total
Replace	21	83	104 (33%)
Restore	6	11	17 (5%)
Improve	9	75	84 (26%)
Enhance	3	47	50 (16%)
Research	4	19	23 (7%)
Supplement	1	38	39 (12%)
Total	44 (14%)	273 (86%)	317

For *replace* applications with an implanted BCI approach, respondents agreed (COM>3.5) that durability and performance are insufficient, and that there is insufficient evidence of system performance, durability and the risk/benefit ratio for end-users. Also here, respondents agreed that end-users are insufficiently aware of BCIs.

Research directions considered most relevant for non-invasive applications were related to sensors and signal processing techniques to improve system performance, clinical trials to demonstrate system performance and identification of the wishes and needs of end-users. For implanted BCIs to *replace* CNS function, all research directions of the list received a COM rating of more than 3.5, indicating agreement/strong agreement with each of these.

Far future: In total, 169 and 178 far future statements, for non-invasive and implanted BCIs respectively, were included in the analysis. Statements were used to define a list of topics, and were subsequently labelled according to this list. Each statement received one or more label. Topics most often addressed in the statements were 'user friendliness' and 'hardware: sensors'. Both these topics occurred most often in the non-invasive out-of-the-box statements. For implanted BCI out-of-the-box statements, 'communication and environmental control for patients' and 'prostheses and artificial limbs for patients' were referred to most often. In addition, 'accuracy and reliability of signal processing and decoding' was often addressed.

DISCUSSION

Here, we describe the view of BCI researchers about the future of their field, as determined by the responses to the BCI researcher's questionnaire. Most respondents of the questionnaire worked on non-invasive approaches, which may not be surprising because of the practical difficulties associated with implanted BCI research, such as the limited number of available subjects and the access to the required medical context. Interestingly, our data showed a difference between North-America and Europe/Asia in the balance between non-invasive and implanted BCI research, which has been described before [6], and which may be related to a different perception or different regulations regarding implants. The percentages of researchers working on non-invasive (89%) and implanted (11%) BCIs corresponded largely with the percentages of applications using these respective approaches (86% vs 14%) that were described in the Near future section. This indicates that the opinion of the respondents about the bottlenecks and requirements for future research is based on actual expertise and knowledge of these issues, which subscribes to the validity of the results of this questionnaire.

There was quite some consistency about the bottlenecks and research directions that were considered relevant for the six non-invasive BCI application scenarios. One of the most important hurdles seems to be system performance. In fact, for 75% of the described non-

Published by Verlag der TU Graz
Graz University of Technology

 DOI: 10.3217/978-3-85125-533-1-91

invasive applications, the respective respondent indicated that (long-term) system performance is not yet good enough. Moreover, system complexity and the insufficient incorporation of the needs and wishes of end users needs to be addressed. Also for implanted BCIs to replace CNS function, system performance, as well as durability, needs to be improved. Moreover, respondents indicated that more data on performance, durability and the risk-benefit ratio are needed.

Interestingly, for both non-invasive and implanted BCI application descriptions, respondents indicated that potential users are unaware of BCIs. This finding does not agree with other studies involving healthy and disabled end-users, which showed that 50-80% of the interviewed potential end-users were aware of BCIs [7-9]. Whether this discrepancy reflects an inclusion bias of the respective studies, or whether our respondents underestimated the BCI-awareness of potential end-users remains to be determined.

When BCI researchers were asked to think out of the box and into the far future, and describe a killer application or major research breakthrough within the non-invasive BCI field, they most often referred to 'user-friendliness', indicating that systems have to become easy-to-use (in any environment), as well as wearable and durable. It is unlikely that the respondents of the questionnaire considered implanted BCIs more user-friendly than their non-invasive counterparts. Rather, the stage of the implanted BCI research field may be viewed as too premature to consider user-friendliness. Most out-of-the-box statements on implanted BCIs referred to *replacing* lost CNS function, indicating that a major breakthrough is needed to apply neuroscientific knowledge into actual BCI applications for patients.

Limitations of the current study include the limited number of respondents, which may be caused by the length and the relative complexity of the questionnaire, and a potential bias towards European BCI researchers. Despite that, several of our results correspond to previous reports, suggesting that the outcome of this questionnaire and the identified topics reasonably reflect the view of the BCI research field.

CONCLUSION

We conclude that BCI researchers are quite optimistic about the feasibility of BCIs becoming real and available applications for patients and healthy end users. However, more research is needed to solve several crucial issues related to hardware, performance and user friendliness before these products adequately meet the wishes and needs of the end-users and can eventually penetrate the market.

REFERENCES

[1] Fetz EE. Operant conditioning of cortical unit activity. Science 1969;163: 955-958.

[2] Vidal JJ. Toward direct brain-computer communication. Annu. Rev. Biophys. Bioeng. 1973:2: 157-180.

[3] Wolpaw JR, Winter Wolpaw E. Brain-computer interfaces-principles and practice. Oxford University Press, Inc (2012).

[4] Brunner C, Birbaumer N, Blankertz B, Guger C, Kübler A, Mattia D, et al (2015) BNCI Horizon 2020: towards a roadmap for the BCI community. Brain Comput. Interfaces 2015:2: 1-10.

[5] BNCI Horizon 2020 Roadmap 2015, http://bnci-horizon-2020.eu/images/bncih2020/Roadmap_BNCI_Horizon_2020.pdf

[6] Berger TW, Chapin JK, Gerhardt GA, McFarland DJ, Principe JC, Soussou WV, et al. WTEC Panel Report on International assessment of research and development in brain-computer interfaces (2007).

[7] Ahn M, Lee M, Choi J, Jun SC. A review of brain-computer interface games and an opinion survey from researchers, developers and users. Sensors 2014:14: 14601-14633.

[8] Lahr J, Schwartz C, Heimbach B, Aertsen A, Rickert J, Ball T. Invasive brain-machine interfaces: a survey of paralyzed patients' attitudes, knowledge and methods of information retrieval. J. Neural Eng. 2015:12: 043001.

[9] Collinger JL, Boninger ML, Bruns TM, Curley K, Wang W, Weber DJ. Functional priorities, assistive technology, and brain-computer interfaces after spinal cord injury. J. Rehabil. Res. Dev. 2013:50: 145-160.

Published by Verlag der TU Graz
Graz University of Technology

Proceedings of the
7th Graz Brain-Computer Interface Conference 2017 DOI: 10.3217/978-3-85125-533-1-92

HEADGEAR FOR MOBILE NEUROTECHNOLOGY: LOOKING INTO ALTERNATIVES FOR EEG AND NIRS PROBES

A. von Lühmann[1,2], S. Soekadar[3], K.-R. Müller[1,4], B. Blankertz[2]

[1] Machine Learning Group, Berlin Institute of Technology, Berlin, Germany
[2] Neurotechnology Group, Berlin Institute of Technology, Berlin, Germany
[3] Applied Neurotechnology Lab, University Hospital of Tübingen, Tübingen, Germany
[4] Dept. of Brain and Cognitive Engineering, Korea University, Seoul, Korea

E-mail: vonluehmann@bimos.tu-berlin.de

ABSTRACT: Brain-computer interfaces are now entering real-life environments. Particular hybrid systems using more than one input signal, e.g. electroencephalography (EEG) and functional near-infrared spectroscopy (fNIRS), offer a broad spectrum of applications in basic research and clinical neuroscience. Here, we provide an overview of recent EEG-electrode and fNIRS-optode approaches that aim to improve usability. We include our new multi-function clip-on design that allows the use of conventional gel-based ring electrodes with water. For EEG electrode approaches (conventional gel, solid gel, new custom water-based) we compared impedances and frequency response over multi-hour recordings. While the water-based solutions showed comparable performance in terms of signal quality, applicability and comfort, solid-gel electrodes on hairy skin required additional contact pressure. Overall, however, all tested EEG electrode types were well compatible with concurrent fNIRS recordings using a novel hybrid fNIRS/EEG headgear, paving the way for cognitive workload experiments under real-life conditions.

INTRODUCTION

In the past years, electroencephalography (EEG) and (continuous wave) functional near-infrared spectroscopy (NIRS) have significantly advanced towards higher miniaturization and mobility. While EEG allows assessing brain electric activity with high time- but low spatial precision, NIRS measures the metabolic (oxygen-dependent) activity of brain areas with high spatial but lower temporal precision. In general, this new generation of wearable hardware enables new approaches in many domains related to neuroscience and neurotechnology, such as in diagnostic medicine, cognitive science, psychology and brain-computer-interfaces (BCIs).

In non-invasive BCI, traditional approaches provide an active communication interface, e.g. for severely impaired or locked-in patients. Taking advantage of the recent trends in wearable instrumentation, BCI research increasingly focuses on domains beyond these applications [1] [2]. Amongst them are exoskeletons [3], [4], rehabilitation and mobility aids as well as adaptive neurotechnology research [5], [6] and neuroergonomics [7]: These BCIs aim to improve work environments, efficiency and security while advancing the understanding of brain function in everyday life scenarios. However, taking non-invasive neurotechnology further out of the lab and into everyday-life environments bears several multidisciplinary challenges.

I. *New instrumentation* needs to fulfill requirements w.r.t. size, power consumption, weight and cost while maintaining high acquisition performance in single wireless devices and body sensor networks
II. *Signal and analysis approaches* have to face lower signal to noise ratios (SNR), and increased influence of non-stationarities due to environmental influences and physiological artifacts, while further progressing with respect to robustness and overall accuracy / performance.
III. *Usability*: To achieve a wider adoption of neurotechnology outside of the laboratory, ergonomic aspects such as user-friendliness, preparation and set up times play a key role. Here, the interface between acquisition hardware and user is subject to research and developments. This includes headgear and fixation concepts as well as EEG electrodes and fNIRS optodes.

One way of tackling these challenges is by jointly using EEG and NIRS, for instance in *hybrid BCIs* [2], [8]. These bi- or multimodal systems exploit shared and complementary information in the acquired signals and use their respective strengths with respect to spatial and temporal resolution and artifacts to improve performance [9], [10]. Both technologies are relatively low cost and can be miniaturized and integrated in portable / wearable devices. We did this in our Mobile Modular Multimodal Biosignal Acquisition (M3BA) architecture [11], designed to tackle many of the challenges in mobile and out-of-the lab BCI. The M3BA modules are wireless miniaturized hardware for joint acquisition of EEG, fNIRS, electrocardiography (ECG) / electromyography (EMG) and accelerometer signals. We now integrated two modules into a new headset for mobile hybrid-BCI based experiments towards out of the lab scenarios. For headgear in mobile and life-like scenarios, optimization of usability and ergonomics of electrode

Published by Verlag der TU Graz
Graz University of Technology

 DOI: 10.3217/978-3-85125-533-1-92

and optode solutions are crucial. Several non-traditional solutions have been presented in both research and industry in the past years [12] [13].

In this paper, we present results of our evaluation and work towards practical and user-friendly electrode/optode solutions for mobile EEG-NIRS based neurotechnology applications. We present a custom water-based open electrode design concept that enables the cost effective and easy upgrade of gel-based AgCl ring electrodes to water-based electrodes, allowing full integration into existing gel-based technology, such as the EasyCAP ring electrode products. We provide evaluation results of impedance measurements using different new electrode types and characterize the so far outstanding frequency response of solid-gel electrodes from [14] in a new epidermis-based experimental setup. Furthermore, we briefly discuss our developments in the field of spring-loaded and flexible NIRS optode holders.

MATERALS AND METHODS

Here, we categorize and summarize (without claim of completeness) existing solutions for EEG-electrodes and NIRS-optodes and our new approaches (see fig. 1, new approaches encircled in blue). We then present methods conducted for evaluation.

Traditional EEG electrodes

In EEG, a standard solution is the use of head caps made from stretch fabric with wet or dry electrodes at positions specified by the 10-20 (or 10-5) system. Conventional wet electrodes are usually based on AgCl material with an electrolyte (NaCl) based gel that also acts as a buffer, reducing motion and shift artifacts. Because a second person is required for the application of gel and hair cleaning after the measurements, usability of conventional wet gel electrodes is not optimal.

Dry electrodes are usually active (including built-in pre-ampliers), need no further preparation and rely on direct contact to skin. Different numbers and shapes of pins for skin-contact / hair penetration are available. They have higher impedances and thus show lower SNR and need a relatively high contact pressure that many users perceive as unpleasant over time. Furthermore, they are more prone to movement artifacts.

When there is no or little hair, sticky electrodes can be directly applied to the skin and provide good signal quality. Due to hair on the head, this type of electrodes is, however, usually not suitable for EEG.

With these electrode types, integration of BCI into everyday life and combination with wearable equipment seems not feasible. To achieve this, other solutions are more promising

Recent EEG electrode approaches

To perform EEG measurements in / around the ear, dry or wet electrodes in the ear [15] and sticky C-shaped electrodes around the ear [16] were proposed. For on-scalp measurements, many recent solutions focus on wet alternatives to sticky gel, such as non-adhesive new solid gel electrodes [14] and water-based electrodes. The latter combine sponges, pressed up wool

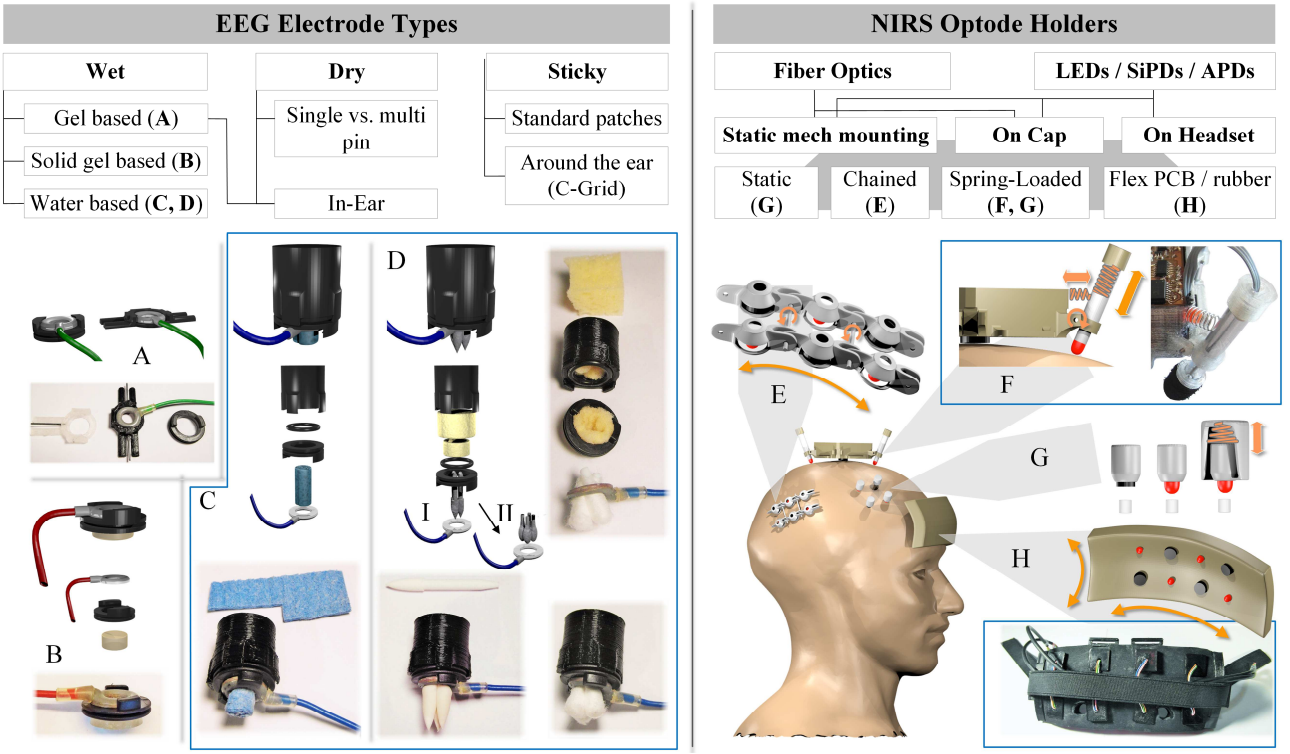

Figure 1: Strategies for (wet) EEG electrodes and NIRS optode attachment, our approaches encircled in blue. A: conventional gel ring electrode; B: ring electrode with solid-gel from [14], C/D: our new water-based adapter for EasyCAP ring electrodes. C: with rolled sponge/pressed cotton similar to [17], D: In a new approach with sponge and soft synthetic felt brush pen tips (I) or cotton bud heads (II). E: chain-link optode holders as in [21]; F: our spring-loaded open-NIRS design [24]; G: conventional, as in [19]; H: flexible PCB (as in [22]) / rubber mat (our M3BA headset).

Published by Verlag der TU Graz
Graz University of Technology

 DOI: 10.3217/978-3-85125-533-1-92

or rolled-up cotton [17] soaked in a NaCl dilution with AgCl electrodes and have been successfully applied in BCI applications [18].

Novel Developments

In a new water-based approach, we developed an easy-to-apply upgrade for EasyCAP ring-electrodes enabling a variety of applications. The electrodes can either be directly attached to a headset or to a 10-20 cap and allow traditional use with gel (fig. 1A), solid-gel (fig. 1B) and our custom water-based solutions:
Core of the invention is a 3D-printed clip-on reservoir for standard Easycap B10 series ring-electrode holders. The electrode is used upside-down, with its surface facing up towards the reservoir. The reservoir is clipped onto the holder with an O-ring seal. When used with cut and rolled sponge cloth (fig. 1C) stuck through the center of the electrode and a water based NaCl-shampoo solution, the resulting electrodes can be used similarly to [17] and TMSI water-electrode products. However, rolled cotton or sponge cloth creates a single contact surface that is more likely to be obstructed from direct skin contact by dense hair. Fig. 1D I) and II) show another new approach using our clip-on design. The reservoir is filled with sponge material soaked with the water based NaCl-shampoo solution. Either contact to the scalp is established with three synthetic felt brush-pen tips (fig. 1D I) or three cotton bud heads with hollow tubes (fig. 1D II). Similar to multi-pin dry electrodes, these soft pins can pass obstructing hair more easily. While being far more comfortable than solid dry metal pins and enabling direct (water-based) conduction, they offer only minimal surface for evaporation of water.

NIRS optode Approaches

In continuous wave NIRS, solutions depend on the optode architecture: many older instrument generations use rather heavy and bulky fiber optics to transfer light from the emission/detection hardware to the scalp. These are usually not suited for wearable equipment. Newer generations, few of which also support mobile applications, integrate LEDs and photo diodes into the optodes that are then attached directly to the scalp. They can be statically attached (fig. 1G) on stretch fabric caps similar to EEG [19], mechanical headsets or static mechanical mounting structures that do not allow the subject to move [20]. For wearable headset applications, chain link holders (fig 1.E) [21] for the whole head and flexible PCB / rubber mat pads for the forehead (fig 1H) [22] as well as forehead-covering headsets (e.g. [23]) were proposed.

Here, we implemented 4 NIRS emitters and detectors each, resulting in 10 channels (with 3.5cm optode distances), into a stretchy rubber mat piece with 3D printed mechanical holders for the user's forehead (fig 1H). The patch can easily be integrated into a headset and is the most convenient solution for non-haired regions, while at the same time blocking ambient light from the regions of interest.

Optical NIRS signals are prone to optode movements resulting in artifacts that are hard to distinguish from physiological changes in signals. Spring-loaded solutions (fig. 1F/G) can remedy this partly, but are mechanically more sophisticated. For headset-based optode attachment on hairy regions, we developed a double-spring-loaded optode solution (see fig. 1F). It ensures fast and easy perpendicular placement and accessibility of hair for preparation (for details please refer to the openNIRS project, [24]).

Experiment I: Evaluation of electrode impedances

To evaluate and compare the electrode-to-skin impedances of traditional gel (Abralyt 2000, EasyCAP), Mg and Ca based solid-gel and the new water-based electrode approaches, we conducted the following experiment. Two electrodes of each type (A, B, C, DI and DII) were applied to hairy regions of the head on 10-20 positions AF7/8, F1/2, C3/4, P5/6, AFz, Fpz and Oz on an EasyCAP. Impedances were measured using a commercially available signal amplifier (BrainAmp®, BrainProducts, Gilching, Germany), with a gel-based electrode reference on the left mastoid for A, C, DI, DII and a solid gel-based electrode reference on the right earlobe for B. Impedances were measured repeatedly every 30 min. over the course of 4 hours.

Experiment II: a) solid-gel impedances frequency response, b) solid-gel electrode impedances

Frequency responses and DC-characteristics of AgCl electrodes in a NaCl solution (gel- or water-based) are well known. Toyama et al. evaluated and compared their new solid-gel electrodes in several ways [14] and reported impedances and signals comparable to those from conventional paste-based recordings, but no frequency response. To enable a comparison of conventional gel and solid gel electrode frequency characteristics in the EEG-Spectrum over time, we now performed an experiment repeatedly measuring the

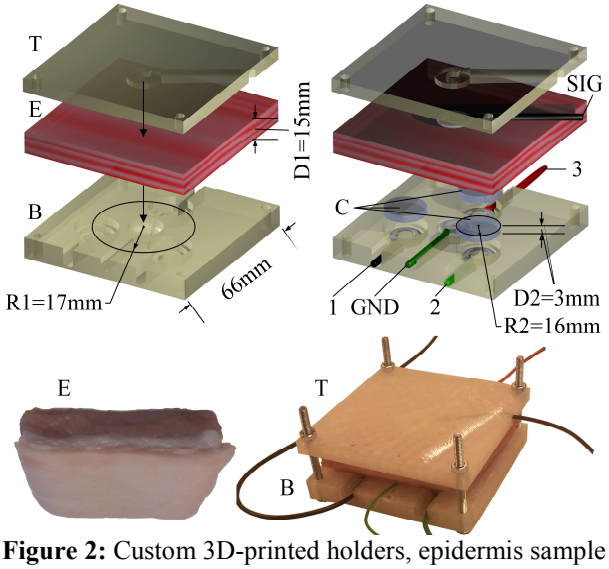

Figure 2: Custom 3D-printed holders, epidermis sample (E) with thickness D1, sine signal (SIG) and ground electrode (GND). Measurement electrodes (1, 2, 3) placed equidistantly (R1) to GND, to each other and to SIG; are covered by cylindrical conductive volumes (C) with defined radius (R2) and thickness (D2): Solid gel based on Mg (electrode 1), solid gel based on Ca (electrode 2), conventional electrolyte gel (electrode 3).

Published by Verlag der TU Graz
Graz University of Technology

 DOI: 10.3217/978-3-85125-533-1-92

frequency responses of both the Mg/Ca based solid-gel and sticky paste (Abralyt 2000) together with conventional AgCl ring electrodes.

To enable a realistic, but controlled, close to real-life measurement scenario that includes interaction of the materials with skin/tissue over longer periods of time, we designed a custom 3D-printed holder. It allows precise positioning of the electrodes and electrolyte material on an epidermis-based phantom using a tissue sample of pork belly with 15 mm thickness and conventional AgCl EEG ring electrodes (see figure 2). Two 3D-printed holders (T, B) fixate the electrodes on the epidermis sample (E) at defined positions. An adjustable sine current is impressed into the tissue between a centered signal electrode (SIG) and a consumer load electrode (GND) that is connected to signal generator ground via a 150 Ω resistance. Signal measurement electrodes (1, 2, and 3) are placed equidistantly (R1= 17 mm) around the center GND electrode, furthermore equally distant from each other and from the signal (SIG) electrode. Between the measurement ring electrodes and the epidermis surface, cylindrical volumes with radius (R2) 16mm and height (D2) 3mm are filled with the conductive materials that are to be investigated: Mg based solid gel pads (electrode 1), Ca based solid gel pads (electrode 2) and standard abrasive electrolyte gel (EasyCAP Abralyt 2000) (electrode 3).

We performed three experiments at a constant room temperature of 23±1 °C, using three epidermis samples over the course of 4 hours. The impedance and frequency dependent attenuation of each channel (1-3) were measured within intervals of 30 minutes using a 100 mV_{pp} offset free sine signal in the range of 1-200 Hz with the following frequency steps: 1-50 Hz in 1 Hz steps, 50-200 Hz in 10 Hz steps.

Signals were generated with an Agilent Technology DSO-X 2014A device and acquired at all electrodes using a National Instruments USB-6003 data acquisition card. For each step in the frequency spectrum, 2 s were sampled with 1 kHz / 16 Bit resolution. From the datasets, average AC root mean square values and spectral power in the target frequency using FFT (Hamming window) were calculated for each frequency and each channel. Attenuation factors for the overall frequency response [dB] were calculated using the ratio of signal powers measured at the electrodes. The ADC's quantization limit and the maximum signal amplitude of 100 mV yielded a precision of the attenuation measurements of 0,026 dB. Tissue property influences that are assumed to be equal for all measurement channels as well as homogeneous changes over the course of the experiment (such as changes in moisture level and conductance), are minimized by pointwise subtraction: The differences $\Delta Att_{Mg/Ca}$ between frequency responses of the electrolyte gel $A_E(f)$ and of the solid gel electrodes ($A_{Mg}(f)$ and $A_{Ca}(f)$ respectively), depict deviations between the responses of both types.

$$\Delta Att_{Mg/Ca}\,[dB] = A_{Mg/Ca}(f) - A_E(f)\,[dB]. \quad (1)$$

Offsets of the average ΔAtt frequency responses, being all in the same order of magnitude, were then removed for better comparability, as they are based on constant tissue inhomogeneities between the electrode pairs.

RESULTS

Electrode impedances: Experiment I and IIb

The new designed reservoir-clip water electrode adapters (fig 1C and 1D I/II) were successfully applied in impedance measurement experiments and showed comparable EEG signal quality to that acquired with conventional gel. Figure 3 EI shows the impedances of all three water electrode types over the course of 4 h compared to gel. All three types showed impedances around 10 kΩ without additional preparation. Over the timecourse of the experiment, impedances dropped further below 10 kΩ.

The impedances of the solid gel electrodes showed poor performance on hairy regions in experiment I when no additional manual pressure was applied and were discarded from the set of data. Figure 3 EIIb shows the impedances of the Ca- and Mg-based solid gel electrodes measured in the epidermis probe

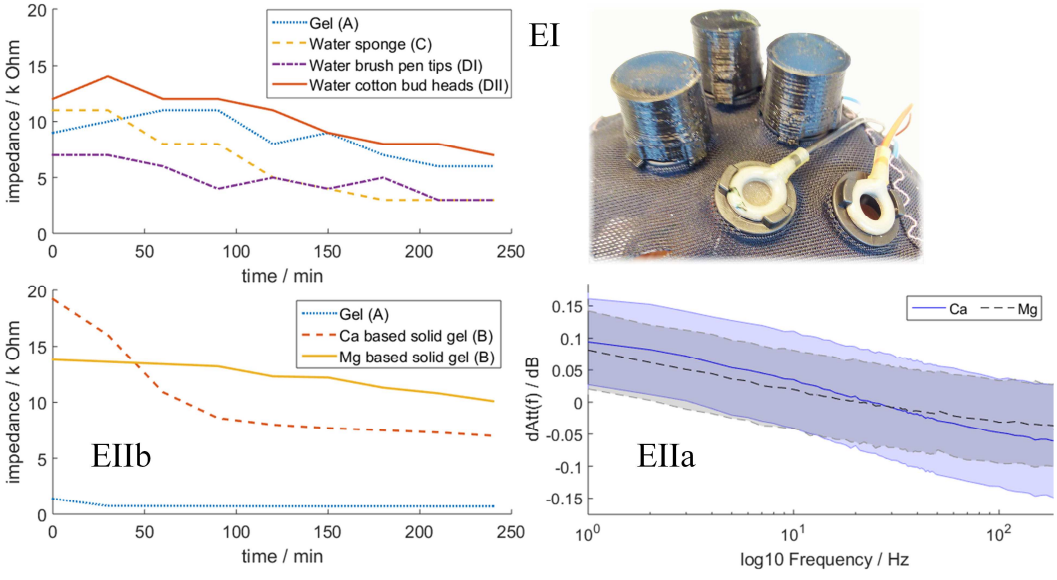

Figure 3:
EI: Water vs. gel based electrode impedances and all 5 electrode types on EasyCap
EIIb: Solid gel vs. gel based electrode impedances
EIIa: grand average ΔAtt_{Mg} and ΔAtt_{Ca} over all three experiments and timepoints. Shaded bars: average standard deviation of ΔAtt(f) over all timepoints.

Published by Verlag der TU Graz
Graz University of Technology

 DOI: 10.3217/978-3-85125-533-1-92

Experiment IIb. These exemplify the solid-gel performance when applied directly on skin for longer time periods. Here, 14 kΩ and 19 kΩ were initially measured for the Mg-based and the Ca-based solid-gel respectively. Both impedances then further decreased significantly towards 8 kΩ (Ca) and 11 kΩ (Mg) over the timecourse of the experiment.

Solid gel frequency response: Experiment IIa

The average attenuation of the sine signal by the tissue was approx. -3 dB for all electrode types. Figure 3 EIIa shows the grand average delta frequency responses (all experiments and timepoints) for both solid-gel materials over the 4 hour experiments (blue solid and black dashed line). We observed a continuous change in the relative offsets of the delta frequency responses over the whole time-course. The grand average delta responses were roughly equal to the single responses measured at the midterm of the experiments. To depict the offset-shift of delta frequency responses relative to midterm over time, shaded bars show the 3-experiment average of the delta responses' standard deviation using the attenuation factors of all measured time points for a respective frequency bin. The measurements show negligible differences between the time-average frequency response of the electrolyte gel and both solid-gel materials over the range of 1-200 Hz. Over all time points, the delta frequency responses of both materials deviate less than ±0.06 dB from the average, which is only a little bit more than twice the measurements' precision bound of 0.026dB. Over the whole time-course, the maximum difference between the reference electrolyte's frequency response and Ca- and Mg- based solid gel responses was less than 0.31 dB and 0.24 dB, respectively.

DISCUSSION

All new water-based approaches (cotton bud heads, sponge cloth and brush pen tips) competed well with conventional gel electrodes and none excelled the others with respect to impedances and signal quality. While the new water-based types were easy to set up and comfortable to wear, reduction in their preparation time was not noteworthy. However, depending on the user's residual functional capability, they can decrease or obviate the need for support by a second person.

The solid-gel electrodes did not perform well on hairy regions without additional (manual) pressure. In the epidermis-based experiments however, they showed coinciding impedance results (range and time-courses) with those measured by Toyama et al. [14]. While the preparation of solid-gel electrodes required the least amount of time, the design and pressure of an optimized headset seems necessary. The frequency response evaluation results indicate that the time-averaged solid gel frequency responses deviate less than 0.155 dB (1.8%, Ca) and 0.11 dB (1.3%, Mg) from the conventional electrolyte over the range of 1-200Hz. While the attenuation is constant over all frequencies, the time courses of the attenuation offsets showed a total change of <0.31 dB for Ca and <0.24 dB for Mg based solid gel over the course of 4 hours. These offsets over time are likely due to the decline of solid gel electrode impedance over time in the experiment.

The set-up was designed symmetric and with equidistant electrode positions to enable a maximum comparability between the three measurement channels. However, despite the careful selection of tissue samples with minimal natural inhomogeneities, the exact impact of these tissue inhomogeneities on attenuation differences in the measurement channels cannot be determined completely. Thus, the acquired data can only be used for pessimistic upper bound estimates of the differences in the material's frequency responses.

However, we consider these upper bound estimates to be a good indicator that the solid-gel electrodes can be used for biopotential/EEG measurements leading to results comparable with conventional electrolyte gel.

CONCLUSION & OUTLOOK

Fusing the results of our work on hybrid EEG-NIRS acquisition and electrode/optode technology allowed us to design a new stand-alone hybrid EEG-fNIRS headset utilizing two M3BA modules and one rechargeable LiPo battery (up to 10 hours continuous acquisition), resulting in 9 EEG, 10 NIRS and 3 EMG/ECG channels and two 3D accelerometer signals (see figure 4). The headset weighs 150 g and can be worn on top of an additional EEG cap to enable change in number and standardized positions of electrodes, if desired. It enables the use of all electrode and optode solutions discussed in this paper and exemplifies one of several

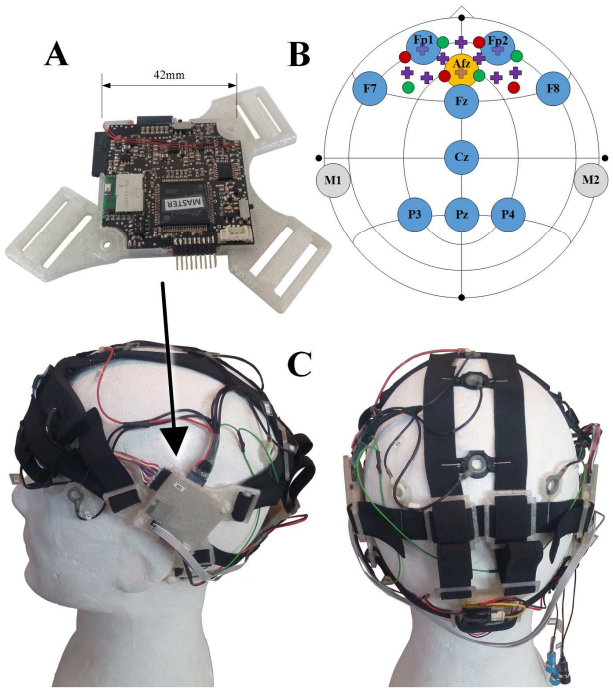

Figure 4: New hybrid EEG-NIRS M3BA headset. A: M3BA module in custom holder. B: channel placement. Blue: 10-20 EEG electrode positions; orange: GND; grey: linked mastoid reference; red/green: NIRS emitters/detectors; purple: NIRS channels. C: Headset.

Published by Verlag der TU Graz
Graz University of Technology

 DOI: 10.3217/978-3-85125-533-1-92

alternatives for new mobile experiments. In this layout, the headset's channel placement was chosen to enable acquisition of frontal/parietal alpha/theta EEG power and metabolism, frontal asymmetries (in both the EEG spectrum and NIRS oxygenation signal), Error Potentials and Event Related Potentials. We will soon apply it in mobile cognitive workload detection experiments that are currently in preparation.

REFERENCES

[1] B. Blankertz, L. Acqualagna, S. Dähne and others, "The Berlin Brain-Computer Interface: Progress Beyond Communication and Control," *Frontiers in Neuroscience,* vol. 10, 21 November 2016.

[2] G. Müller-Putz, R. Leeb, M. Tangermann and others, "Towards Noninvasive Hybrid Brain-Computer Interfaces: Framework, Practice, Clinical Application, and Beyond," *Proceedings of the IEEE,* vol. 103, no. 6, pp. 926-943, 2015.

[3] N.-S. Kwak, K.-R. Müller and S.-W. Lee, "A lower limb exoskeleton control system based on steady state visual evoked potentials," *Journal of Neural Engineering,* vol. 12, no. 5, p. 056009, 2015.

[4] S. Soekadar, M. Witkowski and C. Gómez, "Hybrid EEG/EOG-based brain/neural hand exoskeleton restores fully independent daily living activities after quadriplegia," *Science Robotics,* vol. 1, no. 1, p. eaag3296, 2016.

[5] K.-R. Müller, M. Tangermann, G. Dornhege and others, "Machine learning for real-time single-trial EEG-analysis: From brain-computer interfacing to mental state monitoring," *Journal of neuroscience methods,* vol. 167, no. 1, pp. 82-90, 2008.

[6] T. O. Zander and C. Kothe, "Towards passive brain-computer interfaces: applying brain-computer interface technology to human-machine systems in general," *Journal of neural engineering,* vol. 8, no. 2, p. 025005, 2011.

[7] R. Parasuraman, "Neuroergonomics: Brain, Cognition, and Performance at Work," *Current Directions in Psychological Science,* vol. 20, no. 3, pp. 181-186, 2011.

[8] G. Pfurtscheller, B. Allison, G. Bauernfeind and others, "The hybrid BCI," *Frontiers in Neuroscience,* vol. 4, no. 3, 2010.

[9] S. Fazli, J. Mehnert, J. Steinbrink and others, "Enhanced performance by a hybrid NIRS-EEG brain computer interface," *Neuroimage,* vol. 59, no. 1, pp. 519 - 529, 2012.

[10] S. Dähne, F. Biessmann, W. Samek and others, "Multivariate Machine Learning Methods for Fusing Multimodal Functional Neuroimaging Data," *Proceedings of the IEEE,* vol. 103, no. 9, pp. 1507-1530, 2015.

[11] A. von Lühmann, H. Wabnitz, T. Sander and others, "M3BA: A Mobile, Modular, Multimodal Biosignal Acquisition architecture for miniaturized EEG-NIRS based hybrid BCI and monitoring," *IEEE Trans. on Biomedical Engineering,* vol. in print, 2016.

[12] C. Grozea, C. Voinescu and S. Fazli, "Bristle-sensors - low-cost flexible passive dry EEG electrodes for neurofeedback and BCI applications," *Journal of neural engineering,* vol. 8, no. 2, p. 025008, 2011.

[13] F. Popescu, S. Fazli, Y. Badower and others, "Single Trial Classification of Motor Imagination Using 6 Dry EEG Electrodes," *PloS one,* vol. 2, no. 7, p. e637, 2007.

[14] S. Toyama, K. Takano and K. Kansaku, "A non-adhesive solid-gel electrode for a non-invasive brain-machine interface," *Frontiers in Neurology ,* vol. 3, 2012.

[15] D. Looney, P. Kidmose, C. Park and others, "The In-the-Ear Recording Concept: User-Centered and Wearable Brain Monitoring," *IEEE Pulse,* vol. 3, no. 6, pp. 32-42, 2012.

[16] S. Debener, R. Emkes, M. De Vos and others, "Unobtrusive ambulatory EEG using a smartphone and flexible printed electrodes around the ear," *Scientific reports,* vol. 5, p. 16743, 2015.

[17] I. Volosyak, D. Valbuena, T. Malechka and others, "Brain–computer interface using water-based electrodes," *Journal of Neural Engineering,* vol. 7, no. 6, p. 066007, 2010.

[18] V. Mihajlovic, G. Garcia Molina und J. Peuscher, „To what extent can dry and water-based EEG electrodes replace conductive gel ones?: A Steady State Visual Evoked Potential Brain-computer Interface Case Study," in *ICBE 2011: Int. Conf. on Biomed. Eng.*, Venice, 2011.

[19] S. K. Piper, A. Krueger, S. P. Koch and others, "A wearable multi-channel fNIRS system for brain imaging in freely moving subjects," *NeuroImage,* vol. 85, pp. 64-71, 2014.

[20] S. Coyle, T. Ward and C. Markham, "Brain-computer interface using a simplified functional near-infrared spectroscopy system.," *Journal of Neural Engineering,* vol. 4, pp. 219-226, 2007.

[21] J. Safaie, R. Grebe, H. Moghaddam and others, "Toward a fully integrated wireless wearable eeg-nirs bimodal acquisition system," *Journal of Neural Engineering,* vol. 10, no. 5, p. 056001, 2013.

[22] K. Izzetoglu, S. Bunce, M. Izzetoglu and others, "Functional near-infrared neuroimaging," *IEMBS '04. 26th Ann. Int. Conf. of the IEEE,* vol. 2, pp. 5333-5336, 2004.

[23] M. Kiguchi, H. Atsumori, I. Fukasaku and others, "Note: Wearable near-infrared spectroscopy imager for haired region," *Review of Scientific Instruments,* vol. 83, p. 056101, 2012.

[24] A. von Lühmann, C. Herff, D. Heger and others, "Towards a wireless open source instrument: functional Near-Infrared Spectroscopy in mobile neuroergonomics and BCI applications," *Frontiers in Human Neuroscience,* vol. 9, no. 617, 2015.

Published by Verlag der TU Graz
Graz University of Technology

Proceedings of the
7th Graz Brain-Computer Interface Conference 2017 DOI: 10.3217/978-3-85125-533-1-93

HOME USED, PATIENT SELF-MANAGED, BRAIN-COMPUTER INTERFACE FOR TREATMENT OF CENTRAL NEUROPATHIC PAIN IN SPINAL CORD INJURY: FEASIBILITY STUDY

M.K.H. Al-Taleb[1,3], M. Purcell[2], M. Fraser[2], A. Vuckovic[1]

[1] Biomedical Engineering Research Division, University of Glasgow, Glasgow, United Kingdom
[2] Queen Elizabeth National Spinal Injuries Unit, Queen Elizabeth University Hospital, Glasgow, United Kingdom
[3] Wasit University, Wasit, Iraq

E-mail: Aleksandra.Vuckovic@glasgow.ac.uk

ABSTRACT: Central Neuropathic Pain (CNP) is a frequent chronic condition in people with spinal cord injury (SCI). In a previous study, we showed that using laboratory brain-computer interface (BCI) technology for neurofeedback training, it is possible to reduce pain in SCI people who suffered from CNP for many years. In this study, we show initial results from 12 people with SCI and CNP who practiced neurofeedback on their own using our portable BCI, consisting of a wearable EEG headset (Emotiv, EPOC, USA) and a computer tablet. Eight participants showed a positive initial response to neurofeedback and seven learned how to use portable BCI on their own at home. In this paper, we present a portable BCI and discuss the main challenges of training lay people, patients and their caregivers, to use a custom designed BCI application at home.

INTRODUCTION

Brain-computer Interface has been a focus of multidisciplinary research for almost two decades, and most of its applications have been designed for patients. Yet with the exception of BCI spellers for nearly locked in people [1] and brain painting BCI [2], there is no reported application of BCI that patients can use at home on their own, though several studies explored priorities of potential BCI home users, including patients with SCI [3] . There are several consumer BCI systems in the research phase or on the market [4], but their applications are mainly for gaming or improving the concentration of the able-bodied population. Furthermore, consumer BCI applications typically do not involve EEG recording during training allowing post hoc analysis, so it is hard to check user's actual performance.

It is reasonable to assume that the main users of consumer BCI systems are people who like technical innovations [4]. The experience of these people might not necessarily be directly transferable to patients who may have a physical or cognitive disability, belong to an older age group and possibly do not share a passion for technical innovations.

With the advent of portable and inexpensive EEG [4], it became possible to organize feasibility pragmatic studies, on a larger number of participants to observe how lay people, with mild to severe physical impairments and with average consumer technical literacy use BCI on their own. Due to the nature of participants, it is equally important to understand the attitude of their caregivers towards an unconventional assistive/rehabilitation device.

In this paper, we present, to the best of our knowledge, the first pragmatic (not directly controlled by a researcher) feasibility study of neurofeedback treatment of SCI patients based on [5], using BCI technology in a home environment. We present the main components of custom-made software for portable BCI and the effect of training on pain. The main focus of the paper is however patients' experience of using the BCI system on their own.

MATERIALS AND METHODS

Patients: Twelve patients (54±9, 2F) with chronic SCI and with previously diagnosed CNP were included in the study (Table 1). Paraplegic and tetraplegic adult patients, with complete or incomplete injury, were included in the study. Americal Spinal Injury Association (ASIA) impairment scale level A-D corresponds to the different levels of severity of motor and sensory impairments [6]. The level of injury C (cervical) correspond to tetraplegia while T (thoracic) and L (lumbar) to paraplegia (Table 1).

Exclusion criteria were the patients' inability to understand the task, epilepsy or any self-reported mental health problem. Minimum computer literacy and Internet access were required. Patients were asked to try not to change their regular pain medications (pregabalin or amitryptiline) throughout the study as this could influence the outcome. Only patients with CNP equal to or greater than 4 on the Visual Numerical Scale VNS (0=no pain, 10=worst pain imaginable) were included in the study. All patients signed the informed consent. Ethical permission was obtained from the local

Published by Verlag der TU Graz
Graz University of Technology

 DOI: 10.3217/978-3-85125-533-1-93

national healthcare service Ethical Committee.

BCI software: Custom-made software was created in visual C++.net. It consisted of three main parts: raw EEG data collected through a wireless communication with the headset, signal processing following the algorithm described in [5], and a graphical user interface. The graphical user interface had three screens (Fig.1). It consisted of the main screen for neurofeedback training, pain diary screen and screen for setting system parameres. Control buttons on the main screen were color coded to enable persons with mild vision problems to easily recognize different commands.
Electronic pain diary (in VNS units) had to be filled out before the start of training and before logging off. EEG signal was recorded during training and the experimenter could remotely access patients' EEG to upload the data if patients allowed access.

Neurofeedback training: Prior to taking portable BCI home for neurofeedback training, patients had up to four 30 min long neurofeedback pre-training sessions using a laboratory device usbamp (Guger Technologies, Austria) following protocol [5]. The EEG sampling frequency was 256 samples/s, the right ear served as a reference and the left ear as a ground. The impedance was set prior to the EEG recording to a value under 5kΩ. At the very beginning, a 2 min EEG was recorded to serve as a baseline for subsequent neurofeedback. Training was provided from C4, located over the primary motor cortex, which is an area typically targeted by neuromodulatory treatments of CNP [7]. Patients were presented with a graphical user interface (GUI) showing three bars. The bars changed size and color, to either red or green (Fig .2). Patients were instructed to "do whatever necessary to make bars green". Three bars represented the theta, alpha and higher beta (20-30 Hz) band relative power. Relative power was calculated as a power of a chosen frequency band divided by a power in 2-30 Hz band. The bars representing theta and beta band had a green color when the relative power was 10% or more, below the baseline value, otherwise, they had a red color. A bar representing the alpha band had a green color when the power was 10% or more, above the baseline value, otherwise was red. Chosen features were based on our study defining markers of CNP [8]. Four sessions for the initial assessment of the effect of neurofeedback on pain were chosen based on the literature [9]. A subset of patients, who reported a reduction in pain of at least a 1 grade on the VNS and in addition reported sensations such as tingling or pleasant heat during neurofeedback pre-training, were included in the 2nd part of the study, using BCI at home. In the previous study [5] it was noticed that these sensations often precede the reduction of pain. Because patients were not informed about these sensations prior to training, this served as a quick "anti-placebo" test.

Questionnaires and Communication with Patients:

Upon arrival at the laboratory, the purpose of the study was explained to patients. A semi-structured interview was either audio recorded or notes were taken by two experimenters. After briefly demonstrating how the BCI system works, on the first session, they were asked to complete a custom-made questionnaire on the "Perceived usefulness of a device for a home-based treatment of central neuropathic pain", a validated questionnaires "Brief Pain Inventory" [10] and "Neuropathic pain symptoms inventory" [11]. Patients were contacted after one week and after one month by either phone, SMS, email or Skype, and some visited the laboratory. Volunteers who completed the study have been asked to finally complete the "Brief Pain Inventory" and a custom-made questionnaire: "Neuropathic system users questionnaire".

Educating patients to use portable BCI: on each session, following neurofeedback pre-training with usbamp, patients and their caregivers were trained to use the EPOC headset and a custom made software. Tuition consisted of three parts: training to adequately moisten the electrodes and to place the headset on the right location of the head, training to use Emotiv proprietary software to check the electrode-skin impedance and training to use a custom designed BCI software. The headset was tilted back compared to the recommended use by Emotiv, so that the electrode locations F3 and F4 were located approximately at locations C3 and C4 (or for smaller heads between C3 and C1 and between C4 and C2). To find the right location, patients were instructed to imagine a vertical line coming from their ears and to place the device in such a way that one long EEG electrode is placed just to the front of that line and the other long electrode just to the back, as shown in Fig. 2. The electrode just behind the vertical red line was used for neurofeedback training. A photo of a patient wearing the headset was also taken on the patient's smartphone.
Following this, patients were taught how to use a GUI to check the color-coded electrode impedance (Emotiv proprietary software). They were instructed to add saline and press the electrodes gently, aiming for the green colour to appear on all electrodes. The electrode from which neurofeedback training was provided was labeled with a sticker so that patients could be sure that it always had good contact. In order to assure a good tight contact between a headset and the head, in particular, a good contact of the reference electrodes, patients were given an elastic band to wrap around the head to prevent the headset from slipping. EPOC EEG has a sampling frequency of 128 samples/s and two references at P3 and P4 (in the case of this application they were placed over parietal lobes close to ears) for CMS/DRL noise cancellation. As the last step, patients and caregivers were trained to use the custom-made software. Before they got a portable BCI to take home, they had to demonstrate to the experimenter that they were capable of doing all three steps on their own (placing EEG headset, impedance check, neurofeedback training). Two manuals were provided to patients: a proprietary EPOC headset manual and a custom-made manual explaining how to correctly place the headset

Published by Verlag der TU Graz
Graz University of Technology

 DOI: 10.3217/978-3-85125-533-1-93

for the purpose of neurofeedback training and how to use the custom-made software. Patients were offered as many sessions as needed to learn to use the portable BCI. Neurofeedback protocol with portable BCI followed the same rules as the one with 'usbamp', previously described. They were asked to use BCI for three months, at least once a week and were offered to keep it following that period.

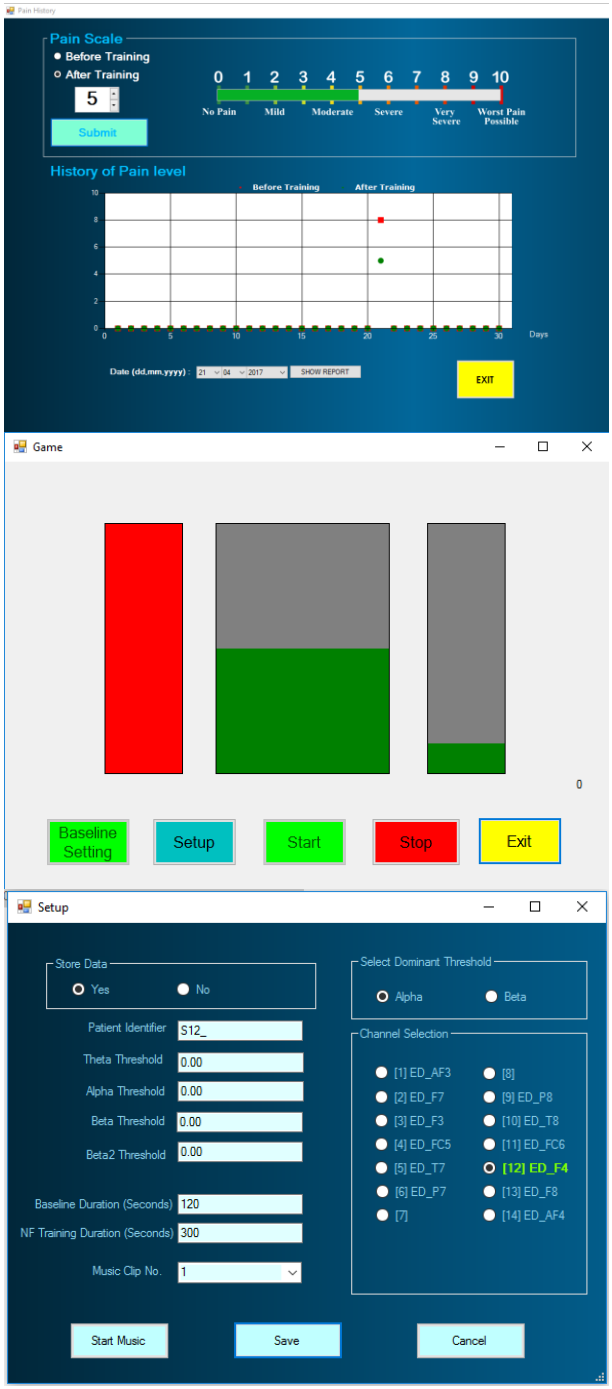

Figure 1. Main screens. Upper: Pain diary; Middle: Neurofeedback GUI; Lower: System parameteres

RESULTS

Information about patients is provided in Table. 1, while information about training is provided in Table. 2. In Table. 2, the first column to the left shows the intensity of pain as measured by VNS for each patient before and after the first few assessment sessions. Column 'Min pain' is the minimum intensity of pain reported while using BCI at home. Column "Nr AS" shows the number of assessment/education sessions, column "Nr SS" shows the number of additional support sessions requested by a patient, after starting to use BCI at home. These sessions were in addition to regular checks-ups after a week and a month. Column "Diff" shows the patient' perceived difficulty of using a portable BCI (1=very easy, 10=extremely difficult), the average value shown in Table. 3. Finally, the last column shows how long patients used the system for. The only person who considered BCI difficult to use (Diff=7) gave up after trying to use it for a month.

Fig. 3 shows one example of EEG Power Spectrum Density (PSD) taken from a home based neurofeedback session of one representative patient. The blue colour represents PSD during 2 min long EEG baseline recording while the red color represents PSD during 5min long neurofeedback sub-session. The patient was successfully reducing theta and higher beta power and to a lesser degree was increasing the power of the alpha band. This example shows that patients can successfully use the system on their own and that they are capable of simultaneously increasing and decreasing EEG power in different frequency bands.

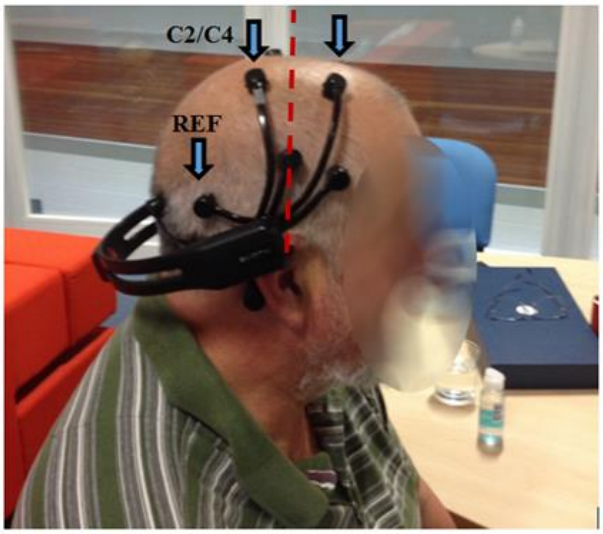

Figure 2. An example of correct placement of the headset. Long EEG electrodes normally placed frontally, tilted to the central area are marked with arrows. A reference electrode in the parietal region is also marked with an arrow. Electrode for neurofeedback training has an approximate location between C2/C4.

Published by Verlag der TU Graz
Graz University of Technology

 DOI: 10.3217/978-3-85125-533-1-93

Patient demographic. Seven patients were paraplegic and five were tetraplegic. Three tetraplegic patients had an injury that prevented them from using their hands, so they required a caregiver to help them with using the headset. One of them gave up after the first session, due to ill health, one patient and a caregiver were interested in using BCI but the patient had no response to neurofeedback and one patient had a supportive caregiver and a response to neurofeedback.

Table 1. Information about patients

	Age/gender/	Injury level	ASIA	Years since injury
P1.	62 M	L3/L4	D	9
P2.	51 M	T6/T7	D	7
P3.	56 F	T5	D	3
P4.	64 M	T4	A	7
P5.	66 M	L3	D	5
P6	59 M	C2	B	5
P7.	59 M	C2	A	7
P8.	50 M	C3/C5	D	3
P9.	54 F	T5	A	7
P10.	35 M	C4	D	15
P11.	42 M	C2	A	1
P12.	49 M	T6	B	1

Table 2. Information about pain level and the number of support sessions. Nr AS: the number of assessment and training sessions, Nr SS: number of additional support sessions. Diff: estimated difficulty of using portable BCI.

	Pain before/ after initial assessment	Min pain	Nr AS	Nr SS	Diff	Home use (months)
P1.	10/8	1	2	/	2	10
P2.	7/5	2	1	/	2	7
P3.	7/5	5		4	7	1
P4.	7/5	3	3		3	3
P5.	5/4	4	3		2	3
P6	8/8	8	1	-	-	-
P7.	5/3	2	2		2	2
P8.	5/5	5	3	-	-	-
P9.	5/5	5	2	-	-	-
P10.	5/3	2	2		1	2
P11.	5/5	5	3	-	2	-
P12.	8/4	2	3	1	1	1

Only two out of 9 patients who could use their hands brought a caregiver to the laboratory, to learn how to use BCI so that they could help at home as required, two of these patients lived on their own. All patients had at least a secondary school education. Four patients were employed, three retired and five stopped working after injury. All patients lived in areas within an hour drive of the hospital.

Pain descriptors: Central neuropathic pain was present in all patients below the level of injury and all patients had pain on their feet and below their knees. The pain was described with standard descriptors of CNP i.e. extremely hot (burning) or extremely cold (freezing), stinging or as a tightrope (in patients who also had pain at the level of injury). All patients first started feeling tingling, pleasant warmth and reduction of pain in feet. The effect of neurofeedback training was assessed using the VNS and also the total body area affected by pain. Fig. 4 shows an example of body maps affected by pain before and after 3 months of training, showing that pain was completely reduced in the upper body.

Patients' expectations: Prior to demonstrating a portable BCI, experimenters asked patients about their expectation prompting them to describe the preferred weight, and size of the device and the expected usage pattern. The majority expected a small and robust device that could fit into a handbag. The most frequent questions to the experimenter were, how long should they wear the headset for? Could they do daily activities wearing the headset? And should they use the device constantly? The last question indicates that lay people, in general do not have a good understanding of how BCI works, i.e. that it requires some sort of feedback and that it is used intermittently.

BCI usage pattern: Three patients used the device almost daily while most patients used it at least once a week. Although they were advised to use the device for 30 min, P2 used it much shorter while still reporting benefits. Most patients used the device in the evening when they had more time. Similar to our previous study [5], 5 patients who used BCI reported that they could bring themselves into the 'traning' state without using the device, by simply imagining doing it. For example, a patient who worked in a call center wearing headphones said that he imagined that the headphones were the EEG headset and that helped him to imagine training and experience less pain.

Communication with patients: most patients preferred SMS or the Internet and two used Skype messenger. We offered to all patients video Skype support (the tablet computer had a camera) but only one patient used it. The laboratory in which patients were recruited was situated within the Spinal Injuries Unit, thus four patients preferred coming to the laboratory for a check-up or for additional assistance with BCI. This indicates that people like having personal contact although electronic communication is less time-consuming.

Perceived usefulness of portable BCI: At the end of the first demonstration session patients were asked to answer a set of questions shown in Tables 3 and 4. Table 3 shows perceived usefulness and ease of use of BCI. On average, all patients believed that they could understand the main purpose of the device and that it would not be hard for them and their caregivers to use it. They also showed a strong belief towards the potential usefulness of the device.

Attitude towards using a novel technology: Table 4 showed that all participants had a positive attitude towards novel technologies. There was no stigma about wearing a gadget on the head in front of family and friends. Patients were also asked to choose one or more of the following attributes of a new product which is most important to them when deciding to buy a device: price, aesthetics (looks), size, new features, size of letters

Published by Verlag der TU Graz
Graz University of Technology

 DOI: 10.3217/978-3-85125-533-1-93

and symbols, friends and family already having the device, it is novel (only a few people have it), easy to relate to something they already have, technical support. The most frequently selected answers were "price" and "new features", followed by "technical support" and "size".

Technical issues with EEG headset: Three headsets frames broke and two patients asked for replacement sponges for the EEG electrodes. The most frequent issues were loose electrodes falling out from their sockets and difficulty achieving good electrode-skin contact. Occasionally slipping of the headset was reported due to loosening of the frame (after prolonged use) or due to long hair. This was resolved by wrapping an elastic band around the headset.

Technical issues with the custom made software: Patients mostly complained of the small size of a warning message at the end of the baseline EEG recording. Some patients initially forgot to complete to pain diary to allow them to start training or log out. A major problem was that there was no electronic evidence of neurofeedback performance, which could be compared from one day to another.

Other issues affecting the study: The main issue affecting the use of BCI was a change of daily routine, caused by e.g. unrelated health problems, travels, pressure sores which required bed rest, moving home and a change of caregiver. Due to the headset design, it was inevitable that the location of electrode varies from one session to another, possibly influencing its performance. Another factor influencing the study was a negative opinion of a trusted authority such as a general practice doctor (" We do not really know what the device is doing").

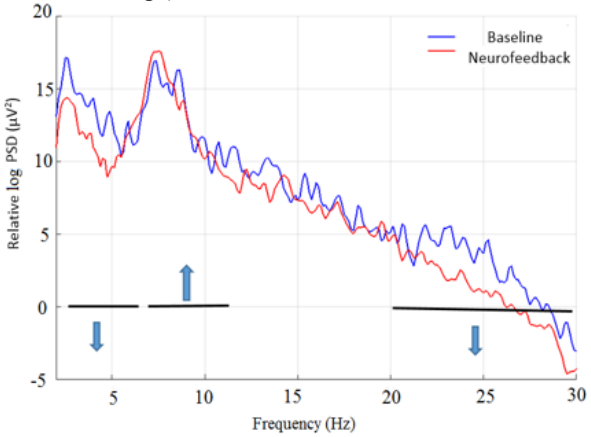

Figure 3 PSD as a function of frequency during baseline and during NF training of a representative patient during home use of BCI. Theta and higher beta band power was decreased and alpha power was increased during neurofeedback training

DISCUSSION

This feasibility study shows that lay people with a mixed social background are capable of using BCI technology on their own or with the help of their caregivers. Although there are published studies on SCI patients views of BCI technology, this is the first study in which SCI people actually used BCI on their own. Kubler et al. [12] suggested a model of user centered design with three main parameters: efficiency, effectiveness and satisfaction. In the context of this study, effectiveness could be expressed as a reduction of pain, efficiency as the number of sessions required to learn neurofeedback and time to setup the system. Although we did not use validated questionnaires for patient satisfaction as suggested in [12] we believe that custom made questionnaires (Tables 3 and 4) and semi-structured interviews cover the areas such as usefulness, expected functionality, usage pattern and patient's appearance while using a device.

Table 3: Perceived usefulness and the ease of use of a portable BCI. Question 3 contains two statements, but it was assumed that all people who attended the training were interested in having a device.

Questions	Range	Average
1.In your opinion, how easy is it to understand the main purpose of the EEG-tablet system?	1 very easy 10 very hard	2.1±0.7
2. How easy do you feel that it is to use this device on a daily basis?	1 very hard 10 very easy	8.0±1.7
3. I would like to have this device but I am not sure if my caregiver and I would understand how to use it	1 very false 10 very true	1.0±0.0
4. Please rate how much you feel convinced that the device might help reducing your pain?	1 not at all 10 very much convinced	7.9±0.7

Table 4: Attitude towards using a novel technology.

Questions	Range	Average
1. Please rate how you would feel if other people would see you wearing the device at home	1 very embarrassed 10 very amused	8.7±1.7
2. Please rate how you would feel if other people would know that you are using the device at home	1 very embarrassed 10 very amused	8.3±2.2
3. Please rate your attitude towards using a novel technology (e.g. computers, phones, other gadgets)	1 extreme avoidance 10 extreme excitement	8.4±1.0

From patients' perspective,the largest problem was to ensure that the training electrode was always close to C4 location because the headset was not designed to be used over the central area.

Published by Verlag der TU Graz
Graz University of Technology

 DOI: 10.3217/978-3-85125-533-1-93

Another problem was that the initial measurement of the impedance was the only check of signal quality because patients were not familiar with the morphology of EEG and could not check the raw EEG signal. A post-hoc analysis of EEG signals recorded during neurofeedback, indicated that most of the time patients were getting an EEG signal of a reasonable quality.

While we did not have a control group, from the initial set of 12 patients we selected for home based BCI study, only people who, based on our previous experience, had additional self-reported sensations (tingling, pleasant warmth) accompanying the reduction in pain. About two-thirds of patients in this study experienced a reduction of pain. Neurofeedback is a technique which requires training and some people who did not experience a reduction of pain did not learn how to control their brainwaves within 4 training sessions. We showed that people who used BCI at home achieved a larger reduction in pain with a prolonged use [5].

While for a patient, self-manged therapy is essential to have highly motivated participants, it was possible that placebo effect to some extent contributed to the reduction in pain because of patients' high expectation of the BCI. However, the main aim of this study was to test if an average adult with no previous knowledge of BCI, who may possibly need the assistance of a caregiver, could use BCI at home. We believe that this study provides some useful information for future developers of consumer EEG headsets.

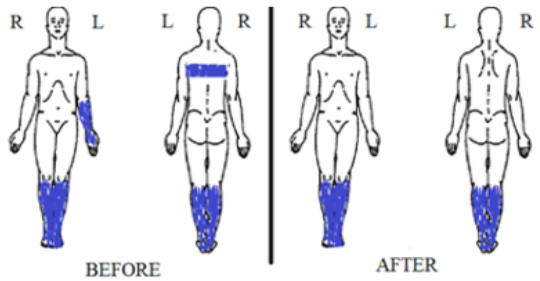

Figure 4 . Body diagram showing the location of pain in one representative patient before and after practicing neurofeedback at home for 3 months. The diagram provides an additional information to VNS.

CONCLUSIONS

The study demonstrates the feasibility of home-based patient and caregiver managed BCI therapy for CNP. The results of this study should encourage other researchers to take BCI from labs and hospitals to patients' homes and should inform the developers of wearable consumer BCI devices

REFERENCES

[1] Sellers EW, Vaughan TM, Wolpaw JR. A brain-computer interface for long-term independent home use. Amyotroph Lateral Scler. 2010;11:449-55.

[2] Holz EM, Botrel L, Kaufmann T, Kübler A. Long-term independent brain-computer interface home use improves quality of life of a patient in the locked-in state: a case study. Arch Phys Med Rehabil. 2015;96(3 Suppl):S16-26.

[3] Huggins JE, Moinuddin AA, Chiodo AE, Wren PA. What would brain-computer interface users want: opinions and priorities of potential users with spinal cord injury. Arch Phys Med Rehabil. 2015 Mar;96(3 Suppl):S38-45

[4] Mihajlovic V, Grundlehner B, Vullers R, Penders J.Wearable, wireless EEG solutions in daily life applications: what are we missing? IEEE J Biomed Health Inform. 2015 Jan;19(1):6-21.

[5] Hassan MA, Fraser M, Conway BA, Allan DB, Vuckovic A.The mechanism of neurofeedback training for treatment of central neuropathic pain in paraplegia: a pilot study.BMC Neurol. 2015 Oct 13;15:200.

[6] Marion RJ, Barros T, Biering-Sorensen F, Burns SP, Donovan WH, Graves DE, Haak M, Hudson LM, Priebe MM. International standards for neurological classification of spinal cord injury. J Spinal Cord Med 2013; 26:50–56

[7]Boldt I, Eriks-Hoogland I, Brinkhof MW, de Bie R, Joggi D, von Elm E. Non-pharmacological interventions for chronic pain in people with spinal cord injury. Cochrane Database Syst Rev. 2014; 11:CD009177.

[8] Vuckovic A, Hasan MA, Fraser M, Conway BA, Nasseroleslami B, Allan DB. Dynamic oscillatory signatures of central neuropathic pain in spinal cord injury. J Pain. 2014;15:645-55

[9] Jensen MP, Gertz KJ, Kupper AE, Braden AL, Howe JD, Hakimian S, Sherlin LH.Steps toward developing an EEG biofeedback treatment for chronic pain.Appl Psychophysiol Biofeedback. 2013 Jun;38(2):101-8

[10] Cleeland CS, Ryan KM. Pain assessment: global use of the Brief Pain Inventory.Ann Acad Med Singapore. 1994 Mar;23(2):129-38.

[11] Bouhassira D, Attal N, Fermanian J, Alchaar H, Gautron M, Masquelier E, Rostaing S, Lanteri-Minet M, Collin E, Grisart J, Boureau F.Development and validation of the Neuropathic Pain Symptom Inventory.Pain. 2004 Apr;108(3):248-57.

[12]Kübler A, Holz EM, Riccio A, Zickler C, Kaufmann T, Kleih SC, Staiger-Sälzer P, Desideri L, Hoogerwerf EJ, Mattia D. The user-centered design as novel perspective for evaluating the usability of BCI-controlled applications. PLoS One. 2014;9:e112392

ACKNOWLEDGEMENTS

This work was supported by Inspire Foundation UK, and by Higher Committee for Education Development, Iraq.

Published by Verlag der TU Graz
Graz University of Technology

Proceedings of the
7th Graz Brain-Computer Interface Conference 2017 DOI: 10.3217/978-3-85125-533-1-94

IMPROVING CLASSIFICATION PERFORMANCE OF A BCI SYSTEM BY SHIFTING RAPID SERIAL VISUAL PRESENTATION

Dong-Ok Won[1], Han-Jeong Hwang[2], Klaus-Robert Müller[1,3], and Seong-Whan Lee[1]

[1]Department of Brain and Cognitive Engineering, Korea University, Seoul, Republic of Korea
[2]Department of Medical IT Convergence Engineering, Kumoh National Institute of Technology, Gumi, Republic of Korea
[3]Department of Computer Science, Berlin Institute of Technology, Berlin, Germany.

E-mail: sw.lee@korea.ac.kr

ABSTRACT: Most of event-related potential (ERP)-based brain-computer interface (BCI) spellers are limited practical value for paralyzed patients with severe oculomotor impairments. Recently, a gaze-independent BCI speller was proposed that uses rapid serial visual presentation (RSVP), but it is difficult to recognize targets because of the rapid presentation of characters. We developed two ERP-based BCI spellers using RSVP with motion, and non-motion stimulation. We evaluated the effect of the two different stimulus conditions on the performance of the speller system with eight participants. The stimulation methods that employ motion stimulation inside the foveal vision demonstrate not only gaze-independence but also higher performance than method that uses non-motion stimulation (73.61±22.57% for non-motion RSVP, 92.36±11.09% for motion RSVP). The performance of the different stimulation methods was susceptible to ERP latency and amplitudes. As a result, motion-type RSVP stimulation condition (i.e., motion RSVP) had shorter latency and higher amplitudes than the non-motion RSVP stimulation condition. It is expected that the proposed motion RSVP stimulation method could be used for developing a gaze independent BCI system with high performance.

INTRODUCTION

A brain-computer interface (BCI) uses brain signals instead of muscles to control external devices such as an exoskeleton, robot arm, or communication system [1, 2]. Electroencephalography (EEG) signals have a good temporal resolution, can be recorded non-invasively, and enable real-time control, and its associated equipment is portable and inexpensive [3]. One of the most widely studied BCI systems is EEG-based BCI, which can monitor conscious electrical brain activity and detect distinct patterns that are generated by the brain. After the EEG signal is digitized, it can be processed via digital signal processing algorithms to convert it into a real-time control signal [5]. Several EEG-based BCIs have been categorized according to the type of brain activity used for BCIs, for example, P300, steady-state visual evoked potential, event-related (de)synchronization, and slow cortical potential.

The EEG-based speller is a typical application of BCI systems, which enables the user to write on a screen without muscle movements. Many BCI studies have shown that BCI spelling systems can be implemented using event-related potentials (ERPs). The ERP based speller (or P300 speller) devices acquire neural activity generated by user attention to a target speller. Accordingly, the ERP-based speller recognizes user's intentions. ERPs distinguish attention and non-attention (target and non-target). The conventional ERP-based speller consists of a 6 × 6 symbol matrix. The row and columns alternately flicker in a random order, where the user concentrates on the target symbol. These conventional spellers can achieve excellent performance.

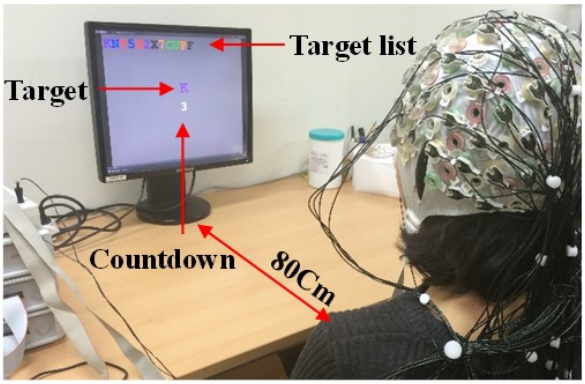

Figure 1: Experimental environment setup.

Recently, some studies based on ERP based spellers have considered gaze-independence [4-6]. Gaze-independence means that there is no involvement of eye movements for controlling BCIs. Several studies solve gaze-independence issues with other sensory activities, such as auditory and tactile activity. However, these activities not only generate weaker signals than visual stimuli but also are constrained to a limited num-

Published by Verlag der TU Graz
Graz University of Technology

 DOI: 10.3217/978-3-85125-533-1-94

(a)

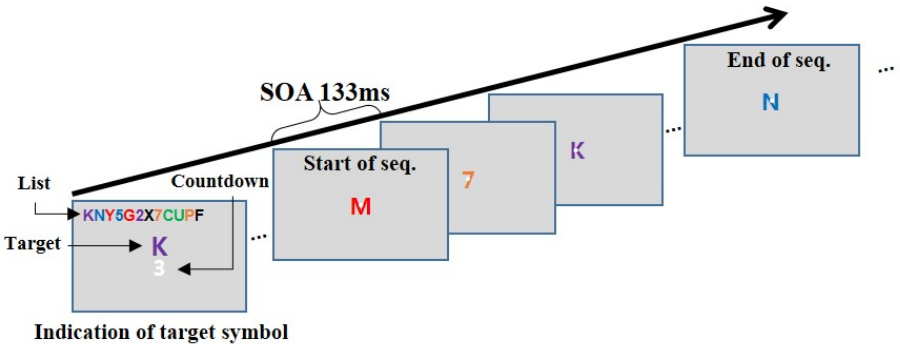

(b)

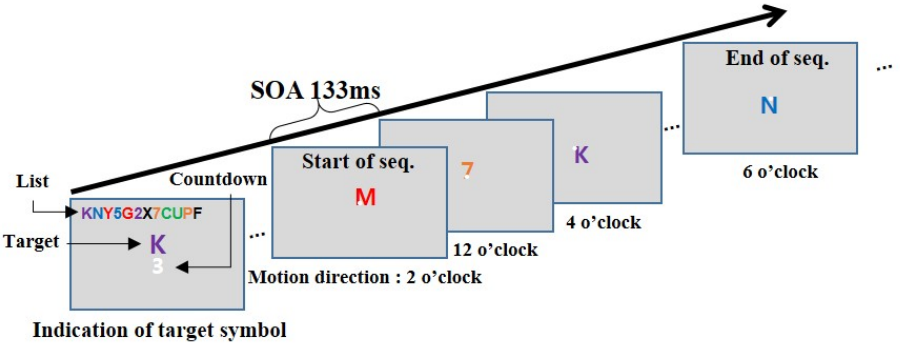

Figure 2: Experimental visual stimuli presentation setup (a) S-RSVP paradigm, (b) M-RSVP paradigm.

ber of targets. Other current visual ERP-based gaze-independent spellers have been successfully implemented using visual stimuli paradigms such as the covert attention paradigm, rapid serial visual presentation (RSVP) paradigm, and motion-onset visually evoked potentials (mVEPs) paradigm [4-6]. The RSVP-based speller is implemented using RSVP visual stimuli [6]. In RSVP, targets (e. g., symbols or pictures) are presented one-by-one in the same location of a display. The RSVP characteristic not only made it difficult to recognize targets but also cause visual discomfort.

In the present study, we proposed a gaze-independent speller with more easily recognized targets and less visual fatigue than one that uses conventional RSVP speller (e.g., requirements of low luminance and contrast) [6]. We proposed a novel visual oddball paradigm using RSVP and shifting (motion) stimuli. We implemented a gaze-independent speller that utilizes standard RSVP (S-RSVP) and motion RSVP (M-RSVP). Whenever the M-RSVP stimulus presentations start, all the symbols are presented center position with one-by-one [5]. The motion characters were moved one of the six directions within the near-central visual field (i.e., the 2, 4, 6, 8, 10, and 12 o'clock directions). The visual stimuli moved within the near-central visual field and the participants focused on the central point. Finally, we evaluated the ERP patterns and the classification performance for different gaze independent systems (i.e., S-RSVP and M-RSVP).

MATERIALS AND METHODS

A. Subjects: The experiment included 8 participants (6 males and 2 females; mean = 24.73±5.53 years). All participants had no history of visual disorders and corrected-to-normal or normal vision. The experiments were conducted in accordance with the principles described in the Declaration of Helsinki. This study was approved by the Institutional Review Board of Korea University [1040548-KU-IRB-15-163-A-1].

Red Group	Blue Group	Green Group	Orange Group	Magenta Group	Black Group
A	B	C	D	E	F
G	H	I	J	K	L
M	N	O	P	Q	R
S	T	U	V	W	X
Y	Z	-	1	2	3
4	5	6	7	8	9

Figure 3: Characters in each of the color and direction groups.

Published by Verlag der TU Graz
Graz University of Technology

 DOI: 10.3217/978-3-85125-533-1-94

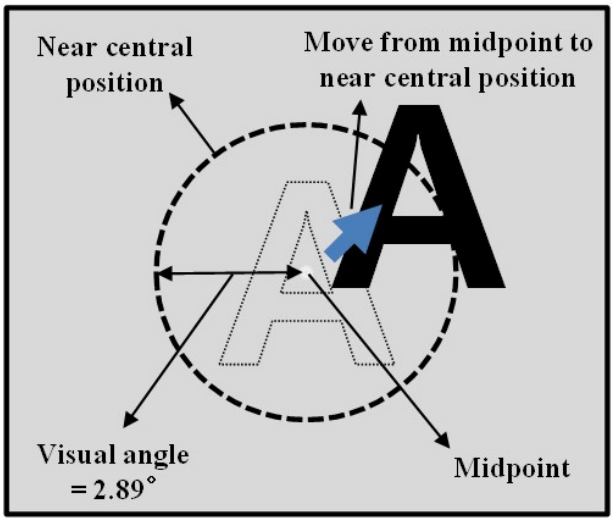

Figure 4: Motion stimulus during one presentation of the M-RSVP sequence.

B. Experimental stimuli and paradigm: Two different RSVP spellers were employed: the S-RSVP without motion stimulus, the M-RSVP with motion stimulus. We used 36 character symbols (i. e. the 26 letters of the English alphabet (A-Z), nine numerals (1-9), and the hyphen "-" used to separate different words). These characters were divided into the same six color groups in the spirit of [6] as follows: Red: A, G, M, S, Y, and 4; Blue: B, H, N, T, Z, and 5; Green: C, I, O, U, and 6; Orange: D, J, P, V, 1, and 7; Magenta: E, K, Q, W, 2, and 8; and Black: F, L, R, X, 3, and 9, as shown in Fig. 3. Thus, the target stimulus can be detected for the user by only using direction and color (e.g., the 2 o'clock direction consisted of the G, H, I, J, K, and L characters with red, blue, green, orange, magenta, and black, respectively).
The RSVP sequence (consisting of 36 symbols) was randomly shuffled before the presentation. We used a stimulus onset asynchrony (SOA) of 133 ms without an intersequence interval. The screen background was a static gray color [5]. The participants fixated on a point in the center of the monitor. The participants were asked to direct their attention toward the target and silently count whenever they found it. M-RSVP characters were divided into six directions (i.e. 12, 2, 4, 6, 8, and 10 o'clock). The measured visual angle of the disk area of the M-RSVP speller was 2.89 ◦ for all the subjects. In this design, the motion stimulation was entirely presented in foveal regions, as shown in Fig. 4 [6].

C. EEG Acquisition: During the experiments for all conditions, EEG data was recorded at a 1000 Hz sampling rate and 63 electrodes were attached using the international 10-20 system along with BRAINAMP amplifiers and an actiCap active electrode (Brain Products, Germany). The Fp1-2, AF3-4, Fz, F1-10, FCz, FC1-6, FT7-8, Cz, C1-6, T7-8, CPz, CP1-6, P7-8, Pz, P1-10, POz, PO3-4, PO7-10, Oz, and O1-2 electrodes were used. The EOG was recorded under the subject's left eye [22]. The reference was located on the ridge of the participant's nose, and the ground was located at AFz. The impedances of all electrodes were kept under 10 kΩ. The experiment paradigm was implemented in Psychtoolbox (http://psychtoolbox.org/). The participants were seated in a comfortable chair at a distance of about 80 cm from the screen and asked to fixate on a point at the center of the monitor. The participants were asked to direct their attention toward the target and silently count whenever they found it without movement (e. g. without head or eye movements). There were two sessions, a training session and an off-line test session. In the training session, participants had to copy-spell the predefined word "KNY5G2X7CUPF" (12 characters). In the test session, participants had to spell the predefined word "BSQH-DRT94WJEM36I1" (18 characters) for off-line classification. These predefined words are quite balanced combinations of the six color for equitable evaluation. For all speller conditions, the sequences flashed one-by-one for 36 symbols and the participants focused (and counted) when the target symbol flashed. A break of 3 s was given between sequences (i. e. countdown), as shown in Fig. 2. The participants were able to take a rest during that time. The participants paid attention to 10 sequences of target symbols, which consisted of one-by-one flashes of 36 symbols. In this study, the data analyzes were conducted off-line and this experiment had no feedback.

D. Data analysis: For pre-processing, all EEG data was downsampled to 100 Hz and bandpass filtered at 0.5-30 Hz with a Chebyshev filter in off-line analysis. We used the BBCI toolbox (http://bbci.de/toolbox) for data analysis and classification was performed using MATLAB (MathWorks, Natick, MA, USA). The EEG data contained physiological artifacts (e.g., eye and head movements). We computed an independent component analysis for all 63 EEG electrodes using a temporal decorrelation source separation algorithm [5]. We computed the correlations of the independent components with related EOG channels (Fp1, Fp2, F9, F10, and under left eye) and determined a conservative threshold (more than two standard deviations) for rejecting ICs as EOG-contaminated data [4]. We then rejected artifacts based on a min-max criterion (i. e. a min-max voltage difference $> 75\mu V$) [5]. For classification, the data was epoched from -233 to 800 ms based on the stimulus onset in all conditions. We selected a pre-stimulus interval (-233 to 0 ms) for baseline correction. For off-line classification analysis, the most discriminative intervals were subject-dependent from 100 to 800 ms. The five selected discriminative intervals were selected using a well-established heuristic method using signed r-squared values ($sgn - r^2$) [5]. We obtained five feature in each channel. So, we can used a feature dimension of 315 (63 electrode channels x 5 time windows). We used a regularized linear discriminant analysis with shrinkage of the covariance matrix for off-line classification [5]. The performance calculated classification accuracy (chance level

Published by Verlag der TU Graz
Graz University of Technology

 DOI: 10.3217/978-3-85125-533-1-94

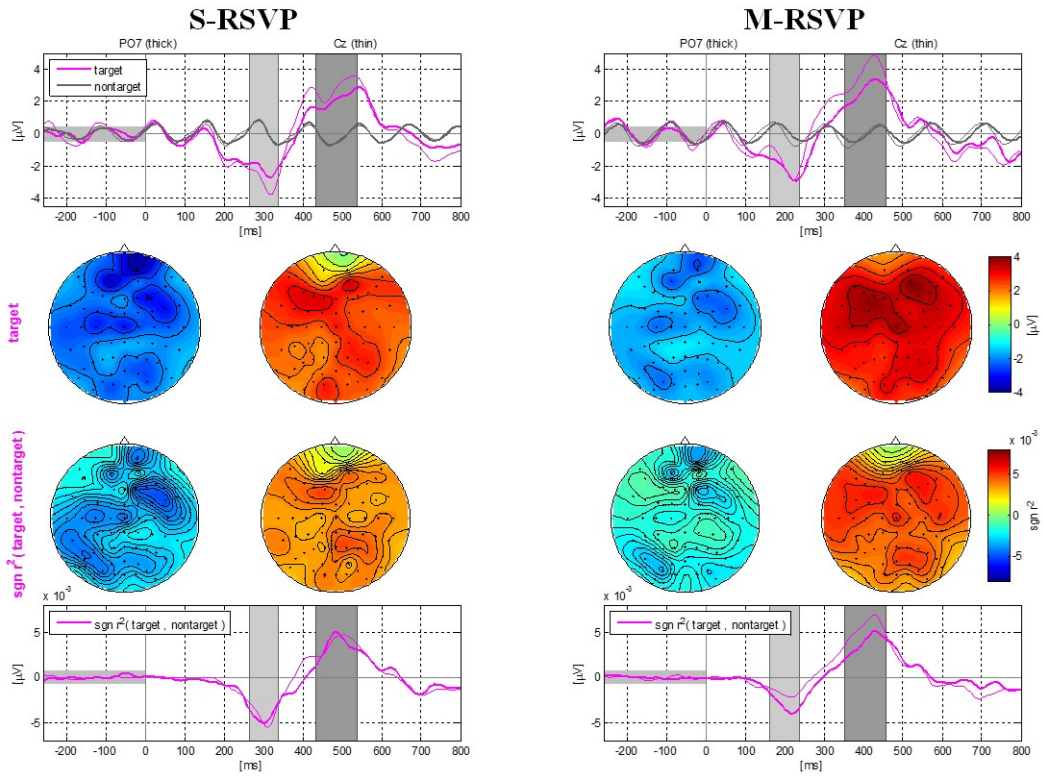

Figure 5: Grand average ERPs for the targets and non-targets in S-RSVP (first column), M-RSVP (second column). The light gray and dark gray shadows represent the N200 (S-RSVP: 265-335 ms and M-RSVP: 165-235 ms) and P300 (S-RSVP: 435-535 ms and M-RSVP: 355-455 ms) signals, respectively.

= 1/36 (2.78) %). Finally, user-intended character was determined by selecting maximum classifier output value that was averaged across the sequences.

RESULTS

The ERPs of the oddball paradigm (i. e. the target and non-target tasks) were similar with other results reported in the literature [4]. The most obvious ERP components were the N200 and P300 amplitudes from 150-350 ms and 350-550 ms based on the stimulus onset, respectively (Fig. 5). The N200 of the target and non-target tasks was a distinguishable channel located around PO7 [5]. The P300 of the target and non-target tasks was a distinguishable channel located around Cz [5]. In this study, the ERPs showed N200 and P300 components for each PO7 and Cz (Fig. 5).

We obtained the average ERP response as well as the $sgn - r^2$ values between target and non-target (Fig. 5). For all conditions, we used the PO7 and Cz electrode for the N200 and P300 components, respectively. In the S-RSVP condition, the ERP response appeared the N200 (amplitude: -2.711 μV and latency: 315 ms) and P300 (amplitude: 3.593 μV and latency: 530 ms). In the M-RSVP condition, the ERP response appeared the N200 (amplitude: -2.902 μV and latency: 225 ms) and P300 (amplitude: 4.848 μV and latency: 425 ms). Table 1 shows the classification accuracies of each subject and their mean accuracies for the 1^{st}, 6^{th}, and 10^{th} stimulus sequences. The M-RSVP condition achieved higher accuracy than the S-RSVP condition on all sequences. In addition, a Wilcoxon signed-rank test for the classification accuracy of M-RSVP conditions was significantly higher than S-RSVP condition on the 6^{th}, 8^{th}, 9^{th}, and 10^{th} sequences ($p < 0.05$), but no significant differences were found between the accuracies of S-RSVP and M-RSVP on the other sequences (i. e., 1^{st}, 2^{nd}, 3^{rd}, 4^{th}, 5^{th}, and 7^{th} sequence).

DISCUSSION

In this study, we implemented two RSVP BCI speller to achieve gaze-independence. We obtained (using 10 off-line stimulus sequences) mean classification accuracies of 73.61±22.57% and 92.36±11.09% respectively for the S-RSVP and M-RSVP conditions. We demonstrated that the M-RSVP speller system achieved easier target recognition and higher accuracy than the S-RSVP speller. Fig. 5 shows the differences in amplitude and latency between the S-RSVP and M-RSVP conditions. Also, the last line of Fig. 5 shows the $sgn - r^2$ values in the S-RSVP and M-RSVP. The M-RSVP has higher $sgn - r^2$ value than the S-RSVP condition. Moreover,

Published by Verlag der TU Graz
Graz University of Technology

 DOI: 10.3217/978-3-85125-533-1-94

Table 1: The classification accuracy for each subject.

	First sequence		Six sequence		Last sequence	
	S-RSVP(%)	M-RSVP(%)	S-RSVP(%)	M-RSVP(%)	S-RSVP(%)	M-RSVP(%)
Sub. 1	45.00	29.44	95.00	79.44	100	94.44
Sub. 2	25.00	38.89	70.00	86.11	88.89	100.0
Sub. 3	39.44	20.55	76.67	93.33	88.89	100.0
Sub. 4	22.78	11.11	36.11	83.89	38.89	94.44
Sub. 5	29.44	57.22	57.22	87.78	61.11	94.44
Sub. 6	38.89	93.33	93.33	94.44	94.44	100.0
Sub. 7	20.55	57.22	57.22	83.33	66.67	88.89
Sub. 8	11.11	39.44	39.44	45.56	50.00	66.67
Mean±SD	29.03±11.40	33.75±11.17	65.62±22.26	81.74±15.46	73.61±22.57	92.36±11.09

The M-RSVP has shorter latency then the S-RSVP condition. The high $sgn-r^2$ value and short latency have respect to higher target/non-target discrimination. The ERP latency could be affected by stimulus evaluation and response production [4]. And the different cognitive task conditions could be reflected in the latency and amplitude characteristics of ERPs (i. e., shorter latencies and larger amplitudes corresponded with the easier task). In this study, we can see the M-RSVP latency shorter than the S-RSVP. Therefore, the M-RSVP is easier task than S-RSVP. As a result, the M-RSVP performance is higher than that of S-RSVP. In addition, the standard deviations of classification accuracies over all subjects are shown to be more stable for M-RSVP than S-RSVP (Table 1). Further investigations are necessary in order to compare between the latency distributions across trials in S- and M-RSVP, as well as on amplitude distributions.

All the gaze-independent visual spellers that present the stimuli in the near central location were successfully implemented. The M-RSVP uses the main characteristic of RSVP. This paradigm, which presents all the stimuli in a nearly central position, is mainly processed by the foveal region of the retina. However, the motion stimuli could be affected by slight eye movements in healthy participants. Unfortunately, we did not directly evaluate saccades analytically using an eye tracker. Therefore, we indirectly showed that little eye movement was induced during the experiment using EOGs. In order to further investigate whether saccade or micro-saccade has influenced the performance, we analyzed the relationship between saccades and brain signals using gamma-band EEG responses [7-8]; the spectrogram analysis results verified that no significant EOG interferences.

We were only able to successfully improve the accuracy of the gaze-independent speller using motion RSVP. In future studies, we will include an attempt to improve BCI performance with spectral features using non-linear regression techniques.

CONCLUSION

In the present study, a novel BCI paradigm that combines the RSVP paradigm with motion stimuli was proposed and compared with the S-RSVP speller. We were able to successfully design stimulus for the ERP pattern using M-RSVP. We improved the accuracy of the RSVP-based gaze-independent speller system using the motion stimuli conditions. Thus, this study demonstrates that it is beneficial for designers to adopt motion stimuli in RSVP-based BCI spellers for practical applications. Consequentially, we suggest an M-RSVP system for practical gaze-independent applications.

ACKNOWLEDGEMENTS

This research was supported by the MSIP(Ministry of Science, ICT and Future Planning), Korea, under the “SW Starlab” (IITP-2015-1107) supervised by the IITP(Institute for Information & communications Technology Promotion).

REFERENCES

[1] Wolpaw JR, Birbaumer N, McFarland DJ, Pfurtscheller G, Vaughan TM. Brain-computer interfaces for communication and control. Clinical Neurophysiology, 2002;113(6):767-791.

[2] Wolpaw JR. Brain-computer interfaces as new brain output pathways. The Journal of Physiology, 2007;579(3):613-619.

[3] Mason MF, Norton MI, Van Horn JD, Wegner DM, Grafton ST, Macrae CN. Response to Comment on “Wandering Minds: The Default Network and Stimulus-Independent Thought”. Science, 2007;317(5834):43-43.

[4] Liu Y, Zhou Z, Hu D. Gaze independent brain-computer speller with covert visual search tasks. Clinical Neurophysiology, 2011;122(6):1127-1136.

[5] Acqualagna L, Blankertz B. Gaze-independent BCI-spelling using rapid serial visual presentation (RSVP). Clinical Neurophysiology, 2013;124(5):901-908.

[6] Schaeff S, Treder MS, Venthur B, Blankertz B. Exploring motion VEPs for gaze-independent communication. Journal of Neural Engineering, 2012;9(4):045006.

[7] Martinez-Conde S, Macknik SL, Troncoso XG, Hubel DH. Microsaccades: a neurophysiological analysis. Trends in Neurosciences, 2009;32(9):463-475.

[8] Schwartzman DJ, Kranczioch C. In the blink of an eye: The contribution of microsaccadic activity to the induced gamma band response. International Journal of Psychophysiology, 2011;79(1):73-82.

Published by Verlag der TU Graz
Graz University of Technology

Proceedings of the
7th Graz Brain-Computer Interface Conference 2017 DOI: 10.3217/978-3-85125-533-1-95

Enhanced CSP Spatial filtering for Improved Motor Imagery BCI Performance by Integrating the Sensation-induced Neurophysiological Prior

Lin Yao[1], Mei Lin Chen[1], Xinjun Sheng[2], Natalie Mrachacz-Kersting[3], Xiangyang Zhu[2], Dario Farina[4], Ning Jiang[1]

[1] Department of Systems Design Engineering, University of Waterloo, Waterloo, Canada
[2]State Key Lab of Mechanical System and Vibration, Shanghai Jiao Tong University, Shanghai, China
[3]Center for Sensory-Motor Interaction, the Faculty of Medicine, Aalborg University, Aalborg, Denmark
[4]Department of Bioengineering, Imperial College London, London, UK

E-mail: ning.jiang@uwaterloo.ca

ABSTRACT:

In this work, the idea of the sensation-induced neurophysiological prior was introduced to facilitate motor imagery (MI) classification. Covariance matrix of MI without Prior, with stimulus-induced Neurophysiological Prior, and with regularization, were separately constructed to extract spatial filter via Common Spatial Pattern (CSP). It has been shown that the MI BCI performance was significantly higher in MI with Neurophysiological Prior condition than other two with $p<0.05$, while there showed no significant difference between MI without Prior and MI with regularization. Integration of the externally induced neurophysiological prior has the benefit of helping CSP spatial filter extraction, and improve the classification performance of BCI users.

INTRODUCTION

Brain-computer Interface (BCI) provides a non-muscular communication and control channel between the user's thoughts and the external world, providing a promising channel for completely locked-in patient to re-interact interact with society [1]. Through mentally performing imagined movement of one's own limbs (e.g., left or right hand), their subjective motor intention can be decoded by translating the brain signals induced by the motor imagery (MI) [2], [3]. This is done without the need for external stimulus, such as visual stimuli in P300 and Steady-state visual evoked potential (SSVEP) based BCI system [4], [5]. MI based independent BCI has received enormous interest [6]–[9], and provided a new avenue for stroke neurorehabilitation [10], [11]. However, numerous experimental evidence has shown that a significant portion of individuals cannot successfully use MI-based BCI system. This phenomenon has been called "BCI-illiteracy" problem, where BCI control does not work for roughly 15%–30% of users [12]–[15].

There is extensive interest in further improving MI performance and reducing the number of BCI-illiterate users. Machine learning algorithms on MI detection has largely improved through several BCI competition, and the Common Spatial Pattern (CSP) is currently most widely used in MI detection [7], [8]. However, recent studies have reported gains in accuracy of approximately 5% when using CSP extensions and optimized spatial-spectrum filtering based on mutual information [9]. Some users still fail to reach the acceptable level of accuracy, which is often set to 70%, even with the state-of-the art algorithms [16], [17]. Other techniques shown to help subjects achieve greater BCI control include training the subject to modulate rhythmic activity [18], and coadaptating the subject with the machine [19] have all been shown to help more subjects to achieve BCI control. Recently, the idea of utilizing tactile stimulation for calibration and training subjects has shown to be a promising way to facilitate MI decoding [15]. Because of the similarity between vibration induced oscillatory activation and MI induced brain dynamics, and the fact that subjects were able to produce much more consistent brain acitivation patterns after receiving real tactile stimulation, we hypothesize that the neurophysiological prior induced by tactile sensation would help to improve MI decoding. In this study, the feasibility of this objectively induced neurophysilogical prior will be investigated.

MATERIALS AND METHODS

Subjects

Five healthy subjects participated in this experiment (two female, all right handed, average age 23.2±1.5 years). This study was approved by the Ethics Committee of the Shanghai Jiao Tong University, Shanghai, China. All participants signed an informed consent form before participation.

EEG Recording and Somatosensory Stimulation

EEG signals were recorded using a SynAmps2 system (Neuroscan, U.S.A.). A 64 channel quick-cap was used to collect 62 channel EEG signals, and the electrodes were placed according to the extended 10/20 system. The reference electrode was located on the vertex, and the ground electrode was located on the forehead. An analog bandwidth filter of 0.5 Hz to 70 Hz and a notch filter of 50 Hz were applied to the raw signals. Signals were digitally sampled at 250 Hz.

In this experiment, mechanical stimulation was applied to the wrist extensor tendons. The vibration motor (Pico Vibe 9mm Vibration Motor, Precision Microdrives Ltd., typical normalized amplitude 6 G) was

Published by Verlag der TU Graz
Graz University of Technology

 DOI: 10.3217/978-3-85125-533-1-95

used for wrist tendon stimulation. The vibrator was enclosed in a rubber case and sewn in an elastic band. This was done to isolate it from the skin on the subject's wrist to avoid any injection of leakage current to the hand. The vibration frequency was 110 Hz. The amplitude of vibration and stimulation positions were individually adjusted such that the subject could properly sense it.

Experimental Protocol

The experiment comprised of two sections. In the first section, the subject performed only left and right hand MI tasks, and in the second section vibration stimuli were applied to the subject's left and right wrist tendons and the subject's task was to passively feel the stimulation. In the first section, the subject's task was to perform MI according to a given cue. A total of 120 trials were performed by the subjects in 3 runs. At the beginning of each trial, a fixation '+' appeared in the center of the screen. At the 1st second, a vibration burst with the same intensity stimulated both hands to alert the user of the subsequent task. The vibration pulse lasted 200 ms. Then at the 3rd second, a red cue pointing either left (L-MI) or right (R-MI) was presented visually on the computer monitor. This cue was superimposed on the fixation '+' and lasted for 1.5 s. Subjects were instructed to perform the mental task after the appearance of the cue arrow. The mental task continued until the 8th second when the fixation '+' disappeared. Next there was a relaxation time period lasting for about 1.5 s, during which subjects relaxed and could blink. Finally a random time period of about 0 to 2 s was inserted after the relaxation period to further avoid subject's adaptation. In the second session, the subject's task was to feel the vibration sensation according to a given cue. A total of 120 trials were also performed by the subjects in 3 runs. The timing of the trial was the same, except that at 3.6 s, vibrations were only applied to the left or right tendon of the wrist until the 8th second when the fixation '+' disappeared.

Algorithm with Neurophysiological Prior

Spatial filter technology was adopted for reducing the high dimensional feature space and enhancing the feature discrimination between different mental tasks. The spatial filters were calculated based on the common spatial pattern (CSP), which has been extensively explored in MI-based BCI literature. Mathematically, it is realized by simultaneous diagonalization of the covariance matrices for the two classes. The bandpass filtered EEG signal is represented as X_k with dimensions M × N, where M is the number of recording electrodes, and N is the number of sample points, and k is the trial index. The spatial covariance of the EEG can be obtained from

$$C_k = \frac{X_k X_k^T}{trace(X_k X_k^T)} \quad (1)$$

where X_k^T denotes the transpose of the matrix X_k, and $trace(X_k X_k^T)$ is the sum of the diagonal elements of the matrix $X_k X_k^T$.

$$C_l = \sum_{k \in S_l} C_k \quad (2)$$

$$C_r = \sum_{k \in S_r} C_k \quad (3)$$

$$M_l = \sum_{k \in V_l} C_k \quad (4)$$

$$M_r = \sum_{k \in V_r} C_k \quad (5)$$

where S_l and S_r are the two index sets for left and right hand MI respectively, and V_l and V_r are the two index sets for left and right hand vibration stimulation respectively. C_l and C_r are the estimated covariance of left and right MI respectively, and M_l and M_r are the estimated covariance of the left and right hand vibration stimulation respectively.

$$C_l^P = (1-\beta)C_l + \beta M_l \quad (6)$$

$$C_r^P = (1-\beta)C_r + \beta M_r \quad (7)$$

$$C_l^N = (1-\beta)C_l + \beta I \quad (8)$$

$$C_l^N = (1-\beta)C_r + \beta I \quad (9)$$

The covariance with sensation-induced neurophysiological prior will be C_l^P and C_r^P, for contrast, C_l^N and C_r^N will be regularized covariance, β is the parameter for the regulariztion, with the range between 0 to 1, and selected among {0:0.1:1}.

Three sets of the spatial filter will be extracted based on the following augmented generalized decomposition problem:

$$(C_l + C_r)W = \lambda C_l W \quad (10)$$

$$(C_l^P + C_r^P)W = \lambda C_l^P W \quad (11)$$

$$(C_l^N + C_r^N)W = \lambda C_l^N W \quad (12)$$

The rows of W are called spatial filters; the columns of $W^{-1}$are spatial patterns. For the *k-th* trial, the filtered signal $Z_k = W X_k$ are uncorrelated. In this work, the log variance of the first three rows and last three rows of Z_k (corresponding to the three largest and three smallest eigenvalues), are chosen as feature vectors, and linear discriminative analysis (LDA) is selected as the classifier. The training set of LDA was only based on motor imagery dataset.

We attempted to give a view considering the nonstationary property of the data by performing a cross validation with a ten-fold chronological split. The 60 trials of each MI task were temporally sorted, and divided into ten partitions, each of which contained temporal information similar to actual BCI use. Difference Spatial filters were extracted from the above condition in the divided training set, i.e. without prior (equation 10), with neurophysiological prior (equation 11) and with regularization (equation 12).

RESULTS AND DISCUSSION

Fig. 1 compares the MI performance when the CSP spatial filters were extracted in different condition. One way ANOVA with repeated measure indicated that there was a significant difference among the three conditions ($F(2,8)=14.6$, $P<0.05$), and post-hoc comparison showed that the MI with Neurophysiological Prior was significant greater than other two conditions, and no significance difference was found between MI without Prior and MI with Regularization. It can be noted that two of the five subjects, the performance were around 60% with traditional method but it improved with the proposed method and surpassed the 70% accuracy level.

Published by Verlag der TU Graz
Graz University of Technology

 DOI: 10.3217/978-3-85125-533-1-95

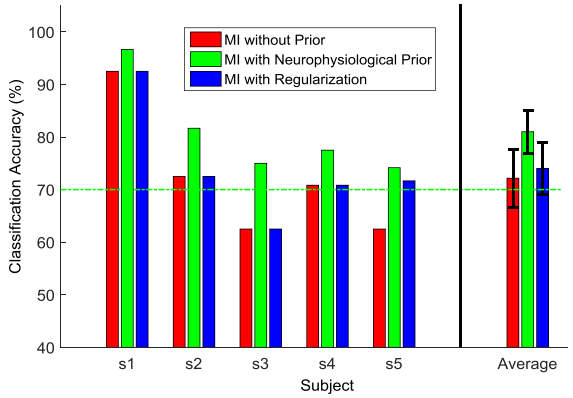

Figure 1. Classification accuracy across subjects. Red bar indicates the MI discrimination accuracy without Prior; the green bar indicates the MI with Neurophysiological Prior; the blue bar indicates the MI with regularization. Green line indicates the 70% accuracy.

The results have shown that the sensation-induced neurophysiological prior provides a way to help CSP spatial filters extraction, the induced prior has the characteristics of easy to induce, stable and less likely to be influenced by subject's internal state, such as attention, stress, which affect MI mental effort.

Through pre-experiment recording session of the real vibration sensation, it would also provide a way to evaluate the potential BCI performance of subjects [15] and provide guidance to subjects in order to better use MI based BCI system.

As the BCI performance is the result of a cumulation of BCI-specific and user-specific factors, this current offline analysis only focused on the algorithm part of CSP with stimulus-induced Neurophysiological Prior. This approach provided a potential way to further improve MI-based BCI performance.

CONCLUSION

Motor Imagery BCI performance can be further improved by integrating the stimulus sensation-induced neurophysiological prior. The stimulus-induced oscillatory dynamics facilitate the extraction of CSP spatial filters, which resulted an improved MI performance. This proposed method has the potential to further improve BCI performance.

ACKNOWLEDGMENT

We thank all volunteers for their participation in the study. This work is supported by the University Starter Grant of the University of Waterloo (No. 203859), the National Natural Science Foundation of China (Grant No. 51421092).

REFERENCES

[1] J. J. Daly and J. R. Wolpaw, "Brain-computer interfaces in neurological rehabilitation," *Lancet Neurol.*, vol. 7, no. 11, pp. 1032–1043, 2008.

[2] G. Pfurtscheller, C. Neuper, and others, "Motor imagery activates primary sensorimotor area in humans.," *Neurosci. Lett.*, vol. 239, no. 2–3, p. 65, 1997.

[3] G. Pfurtscheller and C. Neuper, "Motor imagery and direct brain-computer communication," *Proc. IEEE*, vol. 89, no. 7, pp. 1123–1134, 2001.

[4] F. Nijboer, E. W. Sellers, J. Mellinger, M. a Jordan, T. Matuz, a Furdea, S. Halder, U. Mochty, D. J. Krusienski, T. M. Vaughan, J. R. Wolpaw, N. Birbaumer, and a Kübler, "A P300-based brain-computer interface for people with amyotrophic lateral sclerosis.," *Clin. Neurophysiol.*, vol. 119, no. 8, pp. 1909–16, Aug. 2008.

[5] M. Cheng, X. Gao, S. Gao, and D. Xu, "Design and implementation of a brain-computer interface with high transfer rates," *Biomed. Eng. IEEE Trans.*, vol. 49, no. 10, pp. 1181–1186, 2002.

[6] B. Blankertz, K.-R. Muller, G. Curio, T. M. Vaughan, G. Schalk, J. R. Wolpaw, A. Schlogl, C. Neuper, G. Pfurtscheller, T. Hinterberger, and others, "The BCI competition 2003: progress and perspectives in detection and discrimination of EEG single trials," *Biomed. Eng. IEEE Trans.*, vol. 51, no. 6, pp. 1044–1051, 2004.

[7] B. Blankertz, K.-R. Muller, D. J. Krusienski, G. Schalk, J. R. Wolpaw, A. Schlogl, G. Pfurtscheller, J. R. Millan, M. Schroder, and N. Birbaumer, "The BCI competition III: Validating alternative approaches to actual BCI problems," *Neural Syst. Rehabil. Eng. IEEE Trans.*, vol. 14, no. 2, pp. 153–159, 2006.

[8] M. Tangermann, K.-R. Müller, A. Aertsen, N. Birbaumer, C. Braun, C. Brunner, R. Leeb, C. Mehring, K. J. Miller, G. R. Müller-Putz, and others, "Review of the BCI competition IV," *Front. Neurosci.*, vol. 6, 2012.

[9] J. Meng, L. Yao, X. Sheng, D. Zhang, and X. Zhu, "Simultaneously optimizing spatial spectral features based on mutual information for EEG classification," vol. 62, no. 1, pp. 227–240, 2015.

[10] N. Mrachacz-Kersting, N. Jiang, A. J. T. Stevenson, I. K. Niazi, V. Kostic, A. Pavlovic, S. Radovanovic, M. Djuric-Jovicic, F. Agosta, K. Dremstrup, and D. Farina, "Efficient neuroplasticity induction in chronic stroke patients by an associative brain-computer interface," *J. Neurophysiol.*, vol. 115, no. 3, pp. 1410–1421, Mar. 2016.

[11] F. Pichiorri, G. Morone, M. Petti, J. Toppi, I. Pisotta, M. Molinari, S. Paolucci, M. Inghilleri, L. Astolfi, F. Cincotti, and D. Mattia, "Brain-computer interface boosts motor imagery practice during stroke recovery," *Ann. Neurol.*, vol. 77, no. 5, pp. 851–865, 2015.

[12] C. Guger, G. Edlinger, W. Harkam, I. Niedermayer, and G. Pfurtscheller, "How many people are able to operate an EEG-based brain-

Published by Verlag der TU Graz
Graz University of Technology

 DOI: 10.3217/978-3-85125-533-1-95

computer interface (BCI)?," *IEEE Trans. Neural Syst. Rehabil. Eng.*, vol. 11, no. 2, pp. 145–7, Jun. 2003.

[13] B. Z. Allison, C. Brunner, V. Kaiser, G. R. Müller-Putz, C. Neuper, and G. Pfurtscheller, "Toward a hybrid brain--computer interface based on imagined movement and visual attention," *J. Neural Eng.*, vol. 7, no. 2, p. 26007, 2010.

[14] B. Blankertz, C. Sannelli, S. Halder, E. M. Hammer, A. Kübler, K.-R. Müller, G. Curio, and T. Dickhaus, "Neurophysiological predictor of SMR-based BCI performance.," *Neuroimage*, vol. 51, no. 4, pp. 1303–9, Jul. 2010.

[15] L. Yao, J. Meng, X. Sheng, D. Zhang, and X. Zhu, "A novel calibration and task guidance framework for motor imagery BCI via a tendon vibration induced sensation with kinesthesia illusion.," *J. Neural Eng.*, vol. 12, no. 1, p. 16005, Dec. 2015.

[16] V. Kaiser, G. Bauernfeind, A. Kreilinger, T. Kaufmann, A. Kübler, C. Neuper, and G. R. Müller-Putz, "Cortical effects of user training in a motor imagery based brain--computer interface measured by fNIRS and EEG," *Neuroimage*, vol. 85, pp. 432–444, 2014.

[17] F. Pichiorri, F. D. V. Fallani, F. Cincotti, F. Babiloni, M. Molinari, S. C. Kleih, C. Neuper, A. Kübler, and D. Mattia, "Sensorimotor rhythm-based brain--computer interface training: the impact on motor cortical responsiveness," *J. Neural Eng.*, vol. 8, no. 2, p. 25020, 2011.

[18] A. J. Doud, J. P. Lucas, M. T. Pisansky, and B. He, "Continuous three-dimensional control of a virtual helicopter using a motor imagery based brain-computer interface," *PLoS One*, vol. 6, no. 10, p. e26322, 2011.

[19] C. Vidaurre, C. Sannelli, K.-R. Müller, and B. Blankertz, "Co-adaptive calibration to improve BCI efficiency," *J. Neural Eng.*, vol. 8, no. 2, p. 25009, 2011.

Published by Verlag der TU Graz
Graz University of Technology

Proceedings of the
7th Graz Brain-Computer Interface Conference 2017 DOI: 10.3217/978-3-85125-533-1-96

APPLYING PASSIVE BRAIN-COMPUTER-INTERFACES IN AUTONOMOUS DRIVING: A CASE OF TAKING OVER CONTROL

X. Zhang[1,2], T.O. Zander[1,2]

[1]Biological Psychology and Neuroergonomics, Technical University of Berlin, Berlin, Germany
[2]Team PhyPA, Biological Psychology and Neuroergonomics, Technical University of Berlin, Berlin, Germany

E-mail: xixie.zhang@googlemail.com

ABSTRACT: This paper communicates the research plan for a dissertation in the field of Passive Brain-Computer Interfaces. The main aim is the detection of a driver's mental state in real time and its use in autonomous driving. One example of this is embedded in the context of driver taking over control of the automated vehicle. A offline experiment in laboratory as well as both an online and offline experiment in a driving simulator will be conducted. This paper proposes an experiment planning as well as materials and methods to be used. The conduction of experiments and data analysis are pending. The outcome of these studies is expected to contribute to the design of the driver-vehicle-interaction in autonomous driving by identifying driver's mental states during mode transition.

INTRODUCTION

In recent years, autonomous driving has become one of the hot topics in research and engineering, which aims at minimizing the workload of drivers and optimizing the traffic situation. However, in most countries the human drivers are still responsible for anything that happens while autonomously driving [1]. Therefore, the autonomous driving systems designed by most research institutes or technology companies at the moment are not fully automated, that is to say, when the system cannot handle some situations or when the automated system is performing some errors, the driver must be able to take over control. For example, driving along a highway could be automated, but once an urgent traffic situation occurs, the driver is required to take over control. When the car drives autonomously, the driver's attention might probably be distracted to secondary tasks other than driving, as a result, a signal given by the system for takeover might be missed, or might surprise the driver. This could be dangerous during driving. Hence, it is of great importance to monitor the driver's mental state during autonomous driving.

Passive Brain-Computer Interfaces (passive BCIs) provide a new perspective on the use of BCI technology and have proven to be one of the most promising approaches for monitoring user's mental state, utilizing real-time brain signal decoding [2]. It could provide valuable information about the users' intentions, situational awareness and emotional states to the technical system. This allows the technical system to better adapt to the user and thus enhances the human-machine interaction performance, leading to neuroadaptive technology [3].

In the context of autonomous driving, passive BCI is considered as a promising method to improve the driver-vehicle interaction. It enables the real-time detection of driver's mental state like fatigue, workload, and degree of relaxation [4], which could provide essential information regarding drivers' state to the car. Combining with other sensor data, the car could adapt to individual aspects of the driver and make decisions accordingly. As passive BCIs do not rely on directed or even conscious actions of the driver [2, 4], the car could gain an additional stream of information about subjective situational interpretation of the driver while in autonomous driving mode. Furthermore, thanks to the improvements on dry electrodes, it is now of great convenience to apply a dry electrodes system in BCI research and its applicability in the context of a running vehicle has also been validated, based on the evaluation of BCI classification accuracy, amplitude and temporal structures of ERPs as well as features in the frequency domain [5].

During autonomous driving, knowing the actual state of the driver and communicating it to the car is crucial, especially in the process of take-over control during autonomous driving. Ensuring that the driver is able to take over control of the automated system properly is one of the major issues in highly automated driving. For example, the detection of whether the driver is in a relaxed state or mentally stressed before takeover, whether the driver fully concentrates on driving or is distracted by other driving-unrelated tasks, and whether the driver is experiencing drowsiness or is totally awake, is relevant information to design a communication from the car to the driver informing the need to take over. Besides, the detection of whether the transmitted signal from the automated system has really been perceived by the driver or was ignored, is also an important issue in autonomous driving. More abstract, from a human factors perspective, it is important that the driver possesses situational awareness [6]. It is important that the car is "aware" about the drivers' situation in order to

Published by Verlag der TU Graz
Graz University of Technology

 DOI: 10.3217/978-3-85125-533-1-96

communicate important information in an appropriate and secure way. Based on former studies, drivers tend to show higher drowsiness and less workload with vehicle automation, and more involved with the in-vehicle entertainment, affording less visual attention to the road ahead [7]. Thus in the presented workplan, mental workload, attention, and perception of stimulus will be examined, which are influential factors on driver's situational awareness while driving. They are all recognizable by EEG and their detections could provide helpful information to the vehicle to improve the interaction of driver and vehicle.

Detection of mental workload with EEG has been studied by many researchers (e.g. [8-11]) and some EEG features have been proven to be relevant to mental workload, like ERPs and variation of spectral power in theta and alpha band. However, there are few studies on detection of mental workload in driving, especially in online analysis. Kohlmorgen et al. detected real-time mental workload in drivers operating under real traffic conditions using EEG-based system [12]. They created a system which is able to measure the level of mental workload in real time and mitigate the workload induced by the influx of information from the car's electronic systems, ultimately to detect and avoid stressful situations for drivers. Lei also detected driver's mental workload by EEG in real time and used the result to adapt a secondary task allocated to driver [13]. With the information on driver's mental workload, the system can better know about driver's state before take over and can thus adapt the take over request to it.

Distraction is fatal in driving and found to be one of the main causes for car accidents. Although there are already many physiological methods tracking user's attention (e.g. eye tracking, measuring heart rate), EEG is also an important way to investigate attention, as it could reflect cognitive processing more directly [4]. Many studies (e.g. [14-16]) have found alpha activity as an indicator of attention allocation. Wang et al. [17] also proposed a model to recognize distracted and concentrated EEG epochs with a self-organizing map and found frontal and left motor components relevant to distracted driving. However, there's still less application in online study for driving so far.

ERP could also be used to detect missed stimulus [18]. If a typical ERP sequence is detected, the participant should have responded adequately to the stimulus. If a pending response is not accompanied by an ERP, the participant might have missed to detect the stimulus. In the context of take over control of automated driving, ERP could also be used to detect whether a transmitted request to take over is perceived or missed by the driver, which could provide significant information to the system.

Hypotheses: Mental states like mental workload, attention, and perception of stimulus could be monitored in real time by means of passive BCIs, in driving-like tasks in laboratory as well as in a simulated take-over context in autonomous driving.

MATERALS AND METHODS (IN PLAN)

In the whole experiment process, three studies for detection of mental workload, attention and perception of stimuli will be conducted. In the following parts, I'll present the detailed design for detection of mental workload both in laboratory and in a driving simulator. The experiments for attention and perception of stimuli will soon be developed. The experiment procedure for detection of mental workload is illustrated in Figure 1.

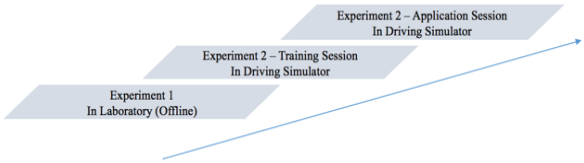

Figure1: Procedure of two experiments for detection of mental workload in laboratory and in driving simulator.

Experiment 1

Laboratory. This experiment will be conducted in a well-controlled laboratory with a screen presenting corresponding task.

Experimental Design. 12 participants will perform two tasks at the same time. The primary task is to monitor an automated system, which might pause at some time point and needs to be controlled by the participants, similar to the context of take-over control in autonomous driving. The Critical Tracking Task [19] will be employed as primary task, which requires the participants to control a bar by pressing the left and right key to bring the bar back to the central line (see Fig. 2). During the monitoring phase, the bar stays in the central automatically and participants need to take action only when a signal for take-over is delivered. Simultaneously, the participants will perform a secondary task – an auditory n-back task [20] – to induce different mental workload levels. A series of numbers will be presented at a time with intervals of 3 second in a randomly ordered sequence. As each new item being presented, participants are required to say out loud the number n items back in the current sequence. For high mental workload level, numbers are two-digit numbers from 10-99 and each time a 3-items-back number should be recalled. For low mental workload level, the numbers are digits from 0-9 and each time one item back. Conductions of different mental workload levels are separated in different blocks and each will be performed 40 times with a counterbalanced sequence (see Fig. 3). Each block lasts 60s and there'll be a brief pause after each block and a longer break after every 20 blocks.

Published by Verlag der TU Graz
Graz University of Technology

 DOI: 10.3217/978-3-85125-533-1-96

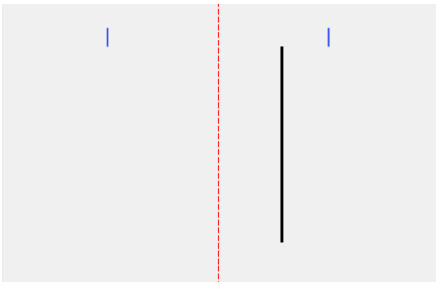

Figure 2: Appearance of Critical Tracking Task. While monitoring, the bar stays always in the central line. From some time point on, it will move away from the central line and participants need to bring it back by pressing the left/right key.

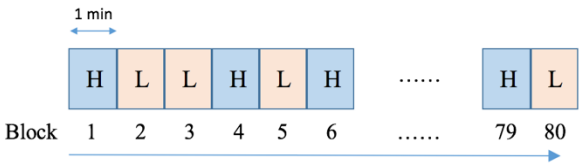

Figure 3: Experiment procedure for two mental workload levels in Experiment 1. H – High mental workload, L – Low mental workload. The sequence of H/L blocks is counterbalanced.

Materials. The data will firstly be collected using a 64 active Ag/AgCl electrodes mounted according to the extended 10–20 system to examine which electrode positions are relevant to the corresponding mental states and to identify the underlying cortical sources. Based on these results, the experiment will be successively conducted with a BrainVision LiveAmp system of a reduced number of dry electrodes.

Analysis. In order to discriminate between different mental workload levels, we'll employ following method to classify two mental workload levels. There are two parts of this analysis method for EEG data: feature extraction and classification. The feature extraction consists of four steps: removal of artifact, bandpass filtering in most discriminative frequency band, spatial filtering, and computing the power spectral in the selected frequency band. Classifiers will be chosen from linear (LDA, rLDA) methods and classification accuracy will be estimated by cross-validation. Furthermore, the performance of primary task including reaction time and deviation of the bar will also be analyzed to investigate the influence of mental workload on take-over performance.

Experiment 2

Driving Simulator. This experiment is based on a high fidelity static driving simulator of the Department of Psychology and Ergonomics at Technical University of Berlin, which consists of steering wheel, gas/brake pedals and other control elements. A driving scenario will be projected in front of the participants and they could also use the side mirrors as well as the rearview mirror. This driving simulator is partly automated with Advanced Driver Assistance Systems such as Adaptive Cruise Control.

Take-over situation. The vehicle is driving automatically on a highway and is going to drive off at the next exit. The driver is engaged in different non-driving tasks and he/she will then be informed of the need to take over control of the vehicle and to drive off the highway.

Experimental Design. In this experiment, there are two sessions, including training session and application session. In both sessions, 12 participants will perform two tasks simultaneously. The primary task is to monitor the automatically driving vehicle in the simulator, and at some time point participants will be informed to take over control of it. At the same time, the participants need to perform secondary tasks. The secondary tasks used to induce different mental workload levels are listening to voice recordings from speeches and answering relevant questions (high mental workload) and listening to some quiet classical music (low mental workload). The procedure of tasks in the training session is the same as in Experiment 1, while each block lasts longer (2 min) and there're be 20 blocks in total. The recorded EEG data in this session will then be trained. In the application session, real-time estimation of driver's mental workload level based on classification trained before will enable the system adapt to the driver and give corresponding information to the driver.

Materials. The data collection will be accomplished using the BrainVision LiveAmp system with active dry electrodes, as stated in Experiment 1.

Analysis. The data collected in training session will be analyzed as stated in Experiment 1. Classifier for distinguishing different mental workload levels will be trained. In the following application session, the best performing classifier will then be applied and the outputs represent estimated level of workload. Corresponding adaptation or feedback will thus be given from the system back to the driver, in order to make take-over more proper and safer.

OUTLOOK

The results obtained from the experiments above will be discussed and conclusions will be formulated. Significant real-time detections of different levels of mental workload, attention as well as perception of stimuli by means of passive BCIs are to be expected, thus providing important information to the vehicle and ensuring the driver-vehicle-interaction more secure and comfortable. It should be confirmed that passive BCIs could be applied in autonomous driving situations to detect drivers' real-time states.

REFERENCES

[1] Beiker SA. Legal aspects of autonomous driving. Santa Clara L. Rev., 2012, 52: 1145.

[2] Zander TO, Kothe C. Towards passive brain–computer interfaces: applying brain–computer interface technology to human–machine systems in general. Journal of neural engineering, 2011, 8(2): 025005.

[3] Zander TO, Krol LR, Birbaumer NP, Gramann K. Neuroadaptive technology enables implicit cursor

Published by Verlag der TU Graz
Graz University of Technology

 DOI: 10.3217/978-3-85125-533-1-96

control based on medial prefrontal cortex activity. Proceedings of the National Academy of Sciences, 2016: 201605155.

[4] Blankertz B, Tangermann M, Vidaurre C, Fazli S, Sannelli C, Haufe S, et al. The Berlin brain–computer interface: non-medical uses of BCI technology. Frontiers in neuroscience, 2010, 4: 198.

[5] Zander TO, Andreessen LM, Berg A, Bleuel M, Pawlitzki J, Zawallich L, et al. Evaluation of a dry EEG system for application of passive Brain-Computer Interfaces in autonomous driving. Frontiers in Human Neuroscience, 2016. accepted.

[6] Baumann MRK, Rösler D, Krems JF. Situation awareness and secondary task performance while driving. International Conference on Engineering Psychology and Cognitive Ergonomics. Springer Berlin Heidelberg, 2007: 256-263.

[7] Jamson AH, Merat N, Carsten OMJ, Lai FC. Behavioural changes in drivers experiencing highly-automated vehicle control in varying traffic conditions. Transportation research part C: emerging technologies, 2013, 30: 116-125.

[8] Sterman MB, Mann CA. Concepts and applications of EEG analysis in aviation performance evaluation. Biological psychology, 1995, 40(1): 115-130.

[9] Berka C, Levendowski DJ, Lumicao MN, Yau A, Davis G, Zivkovic VT, et al. EEG correlates of task engagement and mental workload in vigilance, learning, and memory tasks. Aviation, space, and environmental medicine, 2007, 78(5): B231-B244.

[10] Brouwer AM, Hogervorst MA, Van Erp JB, Heffelaar T, Zimmerman PH, Oostenveld R. Estimating workload using EEG spectral power and ERPs in the n-back task. Journal of neural engineering, 2012, 9(4): 045008.

[11] Borghini G, Astolfi L, Vecchiato G, Mattia D, Babiloni F. Measuring neurophysiological signals in aircraft pilots and car drivers for the assessment of mental workload, fatigue and drowsiness. Neuroscience & Biobehavioral Reviews, 2014, 44: 58-75.

[12] Kohlmorgen J, Dornhege G, Braun M, Blankertz B, Müller KR, Curio G, et al. Improving human performance in a real operating environment through real-time mental workload detection. Toward Brain-Computer Interfacing, 2007: 409-422.

[13] Lei S. Driver mental states monitoring based on brain signals. 2011.

[14] Schubert R, Tangermann M, Haufe S, Sannelli C, Simon M, Schmidt EA, et al. Parieto-occipital alpha power indexes distraction during simulated car driving. International journal of psychophysiology, 2008, 69(3): 214.

[15] Jensen O, Bahramisharif A, Oostenveld R, Klanke S, Hadjipapas A, Okazaki YO, et al. Using brain–computer interfaces and brain-state dependent stimulation as tools in cognitive neuroscience. Frontiers in psychology, 2011, 2: 100.

[16] Brouwer AM, Van Erp J, Heylen D, Jensen O, Poel M. Effortless passive BCIs for healthy users. International Conference on Universal Access in Human-Computer Interaction. Springer Berlin Heidelberg, 2013: 615-622.

[17] Wang YK, Chen SA, Lin CT. An EEG-based brain–computer interface for dual task driving detection. Neurocomputing, 2014, 129: 85-93.

[18] Venthur B, Blankertz B, Gugler MF, Curio G. Novel applications of BCI technology: psychophysiological optimization of working conditions in industry. Systems Man and Cybernetics (SMC), 2010 IEEE International Conference on. IEEE, 2010: 417-421.

[19] Petzoldt T, Bellem H, Krems JF. The critical tracking task: a potentially useful method to assess driver distraction?. Human factors, 2014, 56(4): 789-808.

[20] Mehler B, Reimer B, Dusek JA. MIT AgeLab delayed digit recall task (n-back). Cambridge, MA: Massachusetts Institute of Technology, 2011.

Published by Verlag der TU Graz
Graz University of Technology